Pediatr Radiol (2016) 46 (Suppl 1):S1–S372
DOI 10.1007/s00247-016-3579-x

ABSTRACTS

IPR 2016

The International Pediatric Radiology
7th Conjoint Meeting & Exhibition

IPR 2016: PEDIATRIC IMAGING ACROSS THE GLOBE

May 15-20, 2016
Fairmont Hotel. Chicago, Illinois, United States
NEW **– Radiographer Program**
May 17-19, 2016

Presented by
The Society for Pediatric Radiology (SPR)
The European Society of Paediatric Radiology (ESPR)

Supported by
African Society of Paediatric Imaging (AfSPI)
Asian and Oceanic Society for Paediatric Radiology (AOSPR)
Sociedad Latino Americana de Radiología Pediátrica (SLARP)
The World Federation of Pediatric Imaging (WFPI)

Jointly provided by the American College of Radiology

This supplement was not sponsored by outside commercial interests; it was funded by the Societies' own resources.

TABLE OF CONTENTS

WELCOME MESSAGE

Dear friends and colleagues,

International Pediatric Radiology (IPR) a collaborative initiative of the SPR and the ESPR had its origin in Toronto in 1987 and has raised the global visibility of pediatric radiology. Carrying on this great tradition, the 7th IPR Congress will convene in Chicago.

Chicago – the heart of US cities is the perfect venue. The Fairmont Hotel, located walking distance from world-class museums, Chicago Symphony Orchestra, theatre, music, Lake Michigan, parks and of course, shopping, will offer a unique opportunity to renew old friendships, to establish new, and to liaise professionally. The social program will make the most of Chicago's historic and architectural heritage.

The scientific program will include world-renowned speakers, sunrise workshops, keynote lectures with scientific sessions, posters, and the ever-popular Laurent Garel-hosted game show. This year for the first time we will feature a separate radiographer's program with content specifically targeted for pediatric radiology technologists and radiographers.

IPR 2016 kicks off on Sunday the 15th of May and will run through Friday the 20th of May.

We look forward to seeing you in Chicago!

James S. Donaldson, MD, FACR
SPR, Co-President IPR

Karen Rosendahl, MD, PhD
ESPR, Co-President IPR

IPR ORGANIZATION

IPR Co-Presidents
James S. Donaldson, MD, FACR, SPR President and IPR Co-President (USA)
Karen Rosendahl, MD, PhD, ESPR Congress Committee Chair and IPR Co-President (Norway)

Categorical Course Directors
Michael J. Callahan, MD, SPR (USA)
Stein M. Aukland, MD, PhD, ESPR (Norway)

Sunrise Workshop Directors
Mary R. Wyers, MD, SPR (USA)
Samuel Stafrace, MD, MRCP (UK), FRCR,FRCP Edin., ESPR (Qatar)

Radiographer Program Directors
Laura Gruber, MBA, RT(R), RDMS, RVT (USA)
Graciano Paulo, Professor (Portgual)

Meeting Curriculum Organizers
Maria Argyropoulou, MD (Neuroradiology Session)
Thomas Augdal, MD (Radiographer Program)
Dianna M.E. Bardo, MD (3D Session)
Alex M. Barnacle, BM, MRCP, FRCR (Interventional Radiology Session)
Johan Blickman, MD, PhD (Radiographer Program)
Sylvain Breton, MD (Radiographer Program)
Taylor Chung, MD (MR Protocol Session & Cardiovascular Session)
Mervyn D. Cohen, MBChB, MD, MRCP, FRCR (ALARA Session)
Brian D. Coley, MD, FACR (Hands-On US & US Protocol Session)
Kassa Darge, MD, PhD (Hands-On US)
Jerry R. Dwek, MD (Musculoskeletal Session)
Donald P. Frush, MD, FACR (ALARA Session)
Laurent Garel, MD, FRCPC (IPR Olympics Session)
R. Paul Guillerman, MD (CT Protocol Session)
Roger Harned, MD, FACR (Interventional Radiology Session)
Jeffrey C. Hellinger, MD, MBA (3D Session)
Thierry A. G. M. Huisman, MD (Neuroradiology Session)
Geetika Khanna, MD, MS (Oncology/Nuclear Medicine Session)
Todd Lehkamp, RT(R), CV (Radiographer Program)
Helen R. Nadel, MD, FRCPC (Oncology/Nuclear Medicine Session)
Charlotte M. Nusman, PhD (Musculoskeletal Session)
Lil-Sofie Ording Muller, MD, PhD (Musculoskeletal Session)
Øystein E. Olsen, MD, PhD (MR Protocol Session)
Catherine M. Owens, MBBS, FRCR (CT Protocol Session & Cardiovascular Session)
Manish N. Patel, DO (Interventional Radiology Session)
Dean Pekarovic, BSc (Radiographer Program)
Philip Petit, MD (MR Protocol Session)
Andrew Phelps, MD (US Protocol Session)
Louise Rainford, PhD (Radiographer Program)
Cynthia K. Rigsby, MD, FACR (Cardiovascular Session)
Ian Robinson, MBChB, FRANZCR (Hands-On US & US Protocol Session)
Donna Rolin, BSBA, ARRT, CRT (R)(F) (Radiographer Program)
Rija M. Seuri, MD (CT Protocol Session)
Dennis W. W. Shaw, MD (Neuroradiology Session)

Stephen F. Simoneaux, MD (Radiographer Program)
Anne Smets, MD (Oncology/Nuclear Medicine Session)
Erich Sorantin, MD (CT Protocol Session)
Samuel Stafrace, MD, MRCP (UK), FRCR, FRCP Edin. (US Protocol Session)
Peter J. Strouse, MD, FACR (Reviewing for Pediatric Radiology Session)
Shreyas S. Vasanawala, MD, PhD (MR Protocol Session)
Sjirk J. Westra, MD (CT Protocol Session)

SPR – Abstract Review Committee – Papers
James S. Donaldson, MD, FACR, Chair
Lorna P. Browne, MD
Dorothy I. Bulas, MD, FACR, FAAP
Christopher I. Cassady, MD, FAAP
Teresa Chapman, MD, MA
Taylor Chung, MD
Brian D. Coley, MD, FACR
Jonathan R. Dillman, MD, MSc
Lynn A. Fordham, MD, FACR
Donald P. Frush, MD, FACR
Roger Harned, MD
Mark Hogan, MD
Nadja Kadom, MD
Bernadette Koch, MD
Rajesh Krishnamurthy, MD
Neha Kwatra, MD
David Larson, MD, MBA
John MacKenzie, MD
M. Beth McCarville, MD
Robert Orth, MD, PhD
John Racadio, MD
Cynthia K. Rigsby, MD, FACR
Maura Ryan, MD
Jonathan Samet, MD
Richard Shore, MD
Keith Strauss, MSc
Peter J. Strouse, MD, FACR
Alexander J. Towbin, MD
Andrew T. Trout, MD
Teresa Victoria, MD, PhD
Stephan D. Voss, MD, PhD

SPR – Abstract Review Committee – Scientific Exhibits/Posters
Nadja Kadom, MD, Chair
Sarah S. Milla, MD, Vice Chair
Aparna Annam, DO
Anjum Bandarkar, MD
Mark Bittman, MD
Sarah Bixby, MD
Madhan Bosemani, MBBS
Maria Calvo-Garcia, MD
Michael D'Alessandro, MD
Kassa Darge, MD, PhD
Steven Don, MD

R. Paul Guillerman, MD
C. Matthew Hawkins, MD
Thierry A.G.M. Huisman, MD
Douglas Jamieson, MD
J. Herman Kan, MD
Geetika Khanna, MD, MS
Rajesh Krishnamurthy, MD
Neha Kwatra, MD
Maria Ladino-Torres, MD
Jonathan Loewen, MD
Craig Mitchell, DO, MA
Jonathan Murnick, MD, PhD
Helen Nadel, MD
Srikala Narayanan, MBBS
Daniel J. Podberesky, MD
Janet R. Reid, MD
Douglas Rivard, DO
Ashley Robinson, MBChB
Susan E. Sharp, MD
Manrita Sidhu, MD
Stephen F. Simoneaux, MD
Aylin Tekes-Brady, MD
Alexander J. Towbin, MD
Jason Tsai, MD
Nghia (Jack) Vo, MD
Arash Zandieh, MD

ESPR-Abstract Review Committee-Papers
Karen Rosendahl, MD, PhD, Chair
Owen Arthurs, FRCR, PhD, Vice Chair
Ignasi Barber, MD
Rutger A. J. Nievelstein, MD, PhD

***ESPR-Abstract Review Committee-Scientific Exhibits*/ Posters**
Amaka Offiah, MBBS, PhD, Chair
Lil-Sofie Ording Muller, MD, PhD, Vice Chair
Maria Argyropolou, MD
Claudio Granata, MD
Philippe Petit, MD

Radiographer Abstract Committee
Laura Gruber, MBA, RT(R), RDMS, RVT, Co-Chair
Graciano Paulo, Professor, Co-Chair
Thomas Augdal, MD
Johan G. Blickman, MD, PhD
Todd Lehkamp, RT(R), CV
Dean Pekarovic, BSc
Louise Rainford, PhD
Donna Rolin, BSBA, ARRT, CRT (R)(F)
Stephen F. Simoneaux, MD
Abbey Studer, BS, BA, MBA

Annual Banquet Entertainment Provided By
Ashok Panigrahy, MD

Medical IT Director
Neil Johnson, MD

Assistant Medical IT Director
Alexander J. Towbin, MD

CONTINUING MEDICAL EDUCATION

Accreditation Statement:
This activity has been planned and implemented in accordance with the accreditation requirements and policies of the Accreditation Council for Continuing Medical Education through the joint providership of the American College of Radiology and the Society for Pediatric Radiology.The American College of Radiology is accredited by the ACCME to provide continuing medical education for physicians.

Credit Designation Statement:
The American College of Radiology designates this activity for a maximum of *36.75 AMA PRA Category 1 Credit(s)*™. Physicians should claim only the credit commensurate with the extent of their participation in the activity.

Technologists:
The American College of Radiology is approved by the American Registry of Radiologic Technologists (ARRT) as a Recognized Continuing Education Evaluation Mechanism (RCEEM) to sponsor and/or review Continuing Medical Educational programs for Radiologic Technologists and Radiation Therapists. The American College of Radiology designates this educational activity as meeting the criteria for up to 36.75 Category A credit hours of the ARRT.

The American Medical Association has an agreement of mutual recognition of Continuing Medical Education (CME) credits with the European Union of Medical Specialists (UEMS), the accreditation body for European countries. Physicians interested in converting *AMA PRA Category 1 Credit*™ to UEMS-European Accreditation Council for Continuing Medical Education CME credits (ECMECs) should contact the UEMS at mutualrecognition@uems.eu.

MAINTENANCE OF CERTIFICATION
Select sessions during the Categorical Course, as well as designated sessions on Friday meet the ABR's criteria for a self-assessment (SAM) activity in the ABR Maintenance of Certification (MOC) Program.

OBJECTIVES
The 7th International Pediatric Radiology Conjoint Meeting & Exhibition will provide pediatric and general radiologists with an opportunity to do the following:

1. Summarize the most current information on state of the art pediatric imaging and the practice of pediatric radiology.
2. Describe and apply new technologies for pediatric imaging.
3. Describe and apply basic principles for implementing quality and safety programs in pediatric radiology.
4. Discuss trends in research concerning the care and imaging of pediatric patients.
5. Identify common challenges facing pediatric radiologists, and possible solutions.
6. Evaluate and apply means of minimizing radiation exposure during diagnostic imaging and image guided therapy.

At the conclusion of the experience, participants should have an improved understanding of the technologies discussed, increasing awareness of the costs and benefits of diagnostic imaging in children and of ways to minimize risks, and an improved general knowledge of pediatric radiology worldwide.

DISCLOSURE
In compliance with ACCME requirements and guidelines, the ACR has developed a policy for review and disclosure of potential conflicts of interest, and a method of resolution if a conflict does exist. The ACR maintains a tradition of scientific integrity and objectivity in its educational activities. In order to preserve this integrity and objectivity, all individuals participating as planners, presenters, moderators and evaluators in an ACR educational activity or an activity jointly sponsored by the ACR must appropriately disclose any financial relationship with a commercial organization that may have an interest in the content of the educational activity.

The following planners, presenters, abstract authors, evaluators have disclosed no financial interests, arrangements or affiliations in the context of this activity:

Presenters
Catherine S. Adamsbaum, MD
Adina L. Alazraki, MD
Savvas Andronikou, MBBCH, FCRad, FRCR (Lond), PhD (UCT), PhD (Wits)
Mehrak Anooshiravani, MD
Oewn J. Arthurs, FRCR, PhD
Fred E. Avni, MD, PhD
Paul Babyn, MD
Susan Back, MD
Ignasi Barber, MD
Kimberly Bauer, AAS, (RT), (R)
Ellen C. Benya, MD
M. Ines Boechat, MD, FACR
Micheál A. Breen, MBBChBAO (Hons), BMedSc, MRCPI, FFRRCSI
Herve J. Brisse, MD, PhD
Lorna P. Browne, MD

Nuno Canto-Moreira, MD, PhD
Christopher I. Cassady, MD, FAAP
Jean-François Chateil, MD, PhD
Gulraiz Chaudry, MBChB, FRCR
Nancy A. Chauvin, MD
Govind Chavhan, MD, DABR
Jung-Eun Cheon, MD, PhD
Lorraine Chisari, RDMS, RVT
Steve Y. Cho, MD
Jeanne S. Chow, MD
Pierluigi Ciet, MD, PhD
Susan L. Cohn, MD
Heike Elisabeth Daldrup-Link, MD, PhD
Jie Deng, PhD
Eline Deurloo, MD, PhD
Mohan Doss, PhD, MCCPM
Monica Epelman, MD
Joanna J. Fairhurst, MRCP, FRCR
Shane J. Foley, PhD
Marcelo Galvez, MD
Cristian J. Garcia, MD
Catherine Garel, MD
Michelle Garza, AS
Fernando M. Gómez, MD, PhD
Süreyya Burcu Görkem, Assitant Professor
Claudio Granata, MD
Jared Green, MD
Richard B. Gunderman, MD, PhD
Katharine Halliday, MBChB, FRCS, FRCR.
Kathy Lynne Hamer, MEd, RT
Zoltan Harkanyi, MD
Christine Harris, RT, MR
Mary Patricia Harty, MD
Manraj K.S. Heran, MD, FRCPC
Therese Herlihy, BSc, MPH, MSC, Pg.Dip.UTL
James E. Hickey, RT, (R)(CT)(MR)
Franz Wolfgang Hirsch, Prof.
Thierry A.G.M. Huisman, MD
Paul D. Humphries, MRCP FRCR
Juan C. Infante, MD
Douglas H. Jamieson, MB ChB FRCPC
Diego Jaramillo, MD, MPH
Jacob L. Jaremko, MD, PhD, FRCPC
Stanley T. Kim, MD
Paul K. Kleinman, MD
Steven J. Kraus, MD MS
Rajesh Krishnamurthy, MD
Supika Kritsaneepaiboon, MD
Kamlesh U. Kukreja, MD
Wendy Wai Man Lam, MB, BS, FRCR
Tal Laor, MD
Charlotte de Lange, MD, PhD
Maarten H. Lequin, MD,PhD
Philipp C. Lurz, MD, PhD
Mario Maas, MD, PhD, Professor
Robert MacDougall, MSc
Andrea Magistrelli, MD

Gurdeep S. Mann, MRCP (UK), FRCR
Robert Marterer, MD
Beth McCarville, MD
Kieran McHugh, MB, FRCR, FRCPI
Jonathan P. McNulty, PhD, Dip (MRI), BSc (Hons) Radiography
Patricia L. Mecca, BS, RT (R), (MR),(CT)
James S. Meyer, MD
James W. Murakami, MD
Jaishree Naidoo, FCRad diag (SA)
Jennifer L. Nicholas, MD, MHA
Rutger A.J. Nievelstein, MD, PhD
Aikaterini Ntoulia, MD
Amaka Offiah, MBBS, PhD
Øystein E. Olsen, MD PhD
Ximena Ortega, MD
Crystal Parenti, DMS
Marguerite T. Parisi, MD, MS
Anne Paterson, MBBS, MRCP, FRCR
Dean Pekarovic, BSc
Philippe Petit, MD
Tiina H. Pöyhiä, MD, PhD
Laura Poznick, AAS, RDMS
Sanjay P. Prabhu, MBBS
Louise A. Rainford, PhD
Ashley J. Robinson, FRCR, FRCPC
Derek Roebuck, FRANZCR
Emily A. Rogers, MS, CCLS
Johannes Roth, MD, FRCPC, RhMSUS
Erin Rudzinski, MD
Maura E. Ryan, MD
Beth K. Ryan, MEd, CCLS
Jonathan D. Samet, MD
Joana Santos, PhD
Pierre Schmit, MD
Aurelio Secinaro, MD
Raija M. Seuri, MD
Susan E. Sharp, MD
Dennis W. W. Shaw, MD
Sergio Sierre, MD
Cicero Silva, MD
V. Michelle Silvera, MD
Marni R. Slavik, JD
Thomas Slovis, MD
Michael R. Slovis, JD
Ethan A. Smith, MD
Antonio Soares Souza, MD
Kushaljit S. Sodhi, MD, PhD, FICR
Gloria A. Soto Giordani, MD
John D. Strain, MD
George A. Taylor, MD
Andrew M. Taylor, MD
Aylin Tekes-Brady, MD
Mahesh Thapa, MD
Ben Thurlow, BSc, MSc
Paolo Toma, MD
Christopher C. Tomlinson, MBA, CRA
Fabio M. Triulzi, MD

Pierre-Hugues Vivier, MD, PhD
Thekla von Kalle, Priv.-Doz.
Stephan D. Voss, MD, PhD
Arastoo Vossough, PhD, MD
Jacqueline M. Wameling, BS, CCLS IV
Chris Young, MRS, RRA, RT(R)

Planning Committee
Maria Argyropoulou, MD
James S. Donaldson, MD, FACR
Jerry R. Dwek, MD
Roger Harned, MD, FACR
Charlotte M. Nusman, PhD
Manish N. Patel, DO
Ian Robinson, BSc, MBChB, FRANZCR
Dennis W. Shaw, MD
Anne Smets, MD
Mary R. Wyers, MD

Planning Committee/Presenter
Stein M. Aukland, MD, PhD
Alex M. Barnacle, BM, MRCP, FRCR
Johan G. Blickman, MD, PhD
Michael J. Callahan, MD
Mervyn Cohen, MBChB, MD, MRCP, FRCR
Kassa Darge, MD, PhD
Donald P. Frush, MD, FACR
Laurent Garel, MD, FRCPC
Laura Gruber, MBA, RT(R), RDMS, RVT
Geetika Khanna, MD, MS
Helen R. Nadel, MD, FRCPC
Lil-Sofie Ording Muller, MD, PhD
Catherine M. Owens, FRCR, PhD
Graciano Paulo, Professor
Karen Rosendahl, MD, PhD
Stephen F. Simoneaux, MD
Samuel Stafrace, MD, MRCP (UK), FRCR, FRCP Edin
Peter J. Strouse, MD, FACR

Staff
Angela R. Davis, CAE

Reviewer
John Amodio, MD

The presenters and content reviewers listed below have disclosed the following relevant financial relationships. Potential conflicts have been resolved.

Planning Committee with Disclosures
Brian D. Coley, MD, FACR – Royalties and Editor, Elsevier

Presenters with Disclosures
Jonathan R. Dillman, MD, MSc – Grant, Siemens Medical Solutions USA
Scott E. Fraser, PhD - Varocto Inc. - IP/Owner/Founder and ChroMed - Owner/Founder
Richard E. Heller, III, MD, MBA – Advisor – OCA Ventures
Neil D. Johnson, MBBS, FRANZCR, M.Med – Grant – Philips Healthcare
Michael E. Katz, MD – Aris Radiology – Medical Director, Pediatric Imaging
Cynthia H. McCollough, PhD – Grant – Siemens Healthcare
Arnold C. Merrow, MD - Amirsys/Elsevier - Pediatrics Lead Author/Consultant, Royalties/Fees
Peter S. Moskowitz, MD - Center for Professional & Personal Renewal – Owner, Honoraria/Fees
Daniel J. Podberesky, MD - Member & Professional Speaker Bureau - Toshiba America Medical Systems, GE – Travel Reimbursement, Siemens – Travel Reimbursement, Philips – Travel Reimbursement, Guerbet – Consultant, Honoraria and Travel Reimbursement, Amirsys – Author, Royalties
Christina L. Sammet, PhD, DABR – Global Informatics Advisory Board – Bayer Healthcare
Alexander J. Towbin, MD – Grant & Consultant – Guerbet, Grant – Siemens, Shareholder – Merge Healthcare, Consultant – Applied Radiology, Author & Royalties - Elsevier
Andrew T. Trout, MD – Advisory Board & Travel Reimbursement – Philips Healthcare
Shreyas S. Vasanawala, MD, PhD – Research – GE Healthcare, Founder/Stock Options - Arterys

Planning Committee/Presenter with Disclosures
Taylor Chung, MD – Travel Reimbursement – Philips Healthcare
Cynthia K. Rigsby, MD, FACR – Research – Siemens

Reviewer with Disclosures
Angela Shah - Spouse/Partner - Cook Medical, Bard PV, IMARC Research - Consultant

ACKNOWLEDGEMENTS

As the Host Society, The Society for Pediatric Radiology gratefully acknowledges the exhibitors and promotional supporters of the 7th International Pediatric Radiology Conjoint Meeting & Exhibition.

Agfa HealthCare Corp.
Alexion Pharmaceuticals, Inc.
AppliedMedTech
Bayer
GE Healthcare
Guerbet LLC
Hitachi
Imorgon Medical, LLC
Kubtec Digital Ray
LMT Medical Systems
NeoCoil
Philips Healthcare
QGenda
SealCath LLC
Siemens Healthcare
Toshiba America Medical Systems
Wolters Kluwer
ZONARE

As of February 1, 2016

PROGRAM-AT-A-GLANCE

7th International Pediatric Radiology Conjoint Meeting & Exhibition
Chicago, Illinois, United States

Categorical Course: Sunday, May 15-Thursday, May 19, 2016 • **Annual Meeting:** Monday, May 16-Friday, May 20, 2016
Radiographer Program: Tuesday, May 17-Thursday, May 19, 2016

	Sunday, May 15	Monday, May 16	Tuesday, May 17	Wednesday, May 18	Thursday, May 19	Friday, May 20
6:00 AM		REF FUN RUN				
7:00		CONTINENTAL BREAKFAST (7:00-8:30 am)	CONTINENTAL BREAKFAST (6:45-8:30 am)	CONTINENTAL BREAKFAST (6:45-8:30 am)	CONTINENTAL BREAKFAST (6:45-8:30 am)	CONTINENTAL BREAKFAST (6:45-8:30 am)
7:30			CONCURRENT SUNRISE SESSIONS (7:00-8:20 am)	CONCURRENT SUNRISE SESSIONS (7:00-8:20 am)	CONCURRENT SUNRISE SESSIONS (7:00-8:20 am)	REVIEWING FOR PEDIATRIC RADIOLOGY (7:00-8:15 am)
8:00		CATEGORICAL COURSE				US PROTOCOL SESSION (7:15-8:15 am)
8:30			CATEGORICAL COURSE (8:30-10:00 am) NEW-RADIOGRAPHER PROGRAM BEGINS (8:30-10:00 am)	CATEGORICAL COURSE (8:30-11:00 am) RADIOGRAPHER PROGRAM (7:50-11:00 am)	CATEGORICAL COURSE (8:30-10:20 am) RADIOGRAPHER PROGRAM (8:30-9:00 am)	CONCURRENT SPECIAL SESSIONS (8:30 am-12:30 pm)
9:00						
9:30		BREAK (9:10-9:30 am)				
10:00	REGISTRATION OPENS	CONCURRENT SCIENTIFIC SESSIONS (9:40-11:40 am)	BREAK & EXHIBITS (10:00-10:20 am)			
10:30			CONCURRENT SCIENTIFIC SESSIONS (10:25-11:55 am) RADIOGRAPHER PROGRAM (10:25-11:55 am)		BREAK & EXHIBITS (10:20-10:50 am)	
11:00				BREAK & EXHIBITS (11:00-11:30 am)	CONCURRENT SCIENTIFIC SESSIONS (10:55-11:55 am) RADIOGRAPHER PROGRAM (10:55-11:55 am)	
11:30						
12:00 PM		LUNCH ON OWN OR 3D RWE OR CT PROTOCOL SESSION (11:45 am-1:00 pm)	LUNCH AT THE MID AMERICA CLUB (12:00-1:40 pm) *Registered attendees only; must bring conference badge*	CONCURRENT SCIENTIFIC SESSIONS (11:35 am-1:15 pm) RADIOGRAPHER PROGRAM (11:35 am-1:05 pm)	SPR MEMBERS' BUSINESS MEETING OR ESPR GENERAL ASSEMBLY OR LUNCH ON OWN (12:00-1:00 pm)	
12:30						
1:00	WELCOME & OPENING CEREMONY	NEUHAUSER/LEFÈBVRE LECTURE (1:10-2:15 pm)				
1:30			CATEGORICAL COURSE (1:50-4:20 pm)	jSPR/JESPeR LUNCH (1:30-2:30 pm) MR PROTOCOL SESSION (1:30-2:30 pm)	RADIOGRAPHER PROGRAM (12:50-2:20 pm) CATEGORICAL COURSE (1:10-2:20 pm)	
2:00						
2:30		CATEGORICAL COURSE (2:15-3:15 pm)			BREAK & EXHIBITS (2:20-2:50 pm)	
3:00				TOURS OF LURIE CHILDREN'S (2:00-5:00 pm)		
3:30		BREAK & EXHIBITS (3:15-3:45 pm)			CONCURRENT SCIENTIFIC SESSIONS (2:55-4:40 pm) RADIOGRAPHER PROGRAM (2:55-5:30 pm)	
4:00	CATEGORICAL COURSE BEGINS (1:30-6:10 pm)	CONCURRENT SCIENTIFIC SESSIONS (3:50-4:40 pm)				
4:30			BREAK & EXHIBITS (4:20-4:50 pm)			
5:00						
5:30		AWARDS CEREMONY (4:45-6:15 pm)	RADIOGRAPHER PROGRAM (4:40-6:10 pm) CONCURRENT SCIENTIFIC SESSIONS (4:50-6:00 pm)		CONCURRENT SCIENTIFIC SESSIONS (4:45-5:25 pm)	
6:00						
6:30		WELCOME RECEPTION (6:30-7:45 pm)			ANNUAL RECEPTION & DINNER (7:30-11:00 pm) *Separate fee applies*	
7:00						
7:30						
8:00						

MEETING SPACE

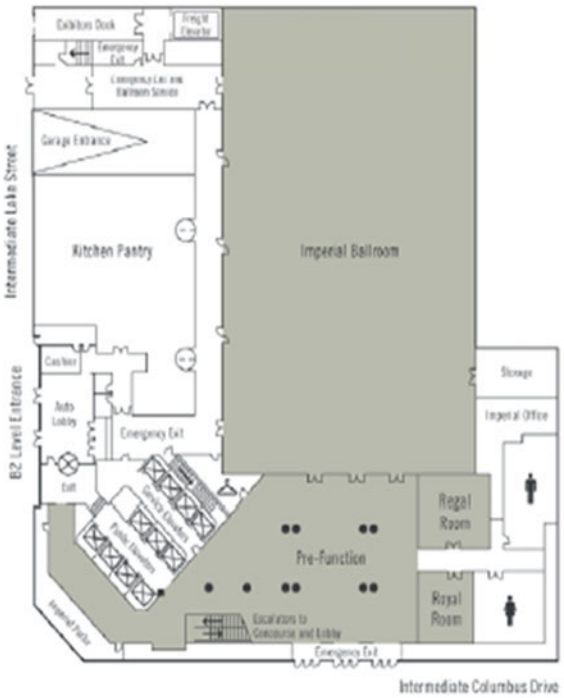

B2 Level

2nd Level

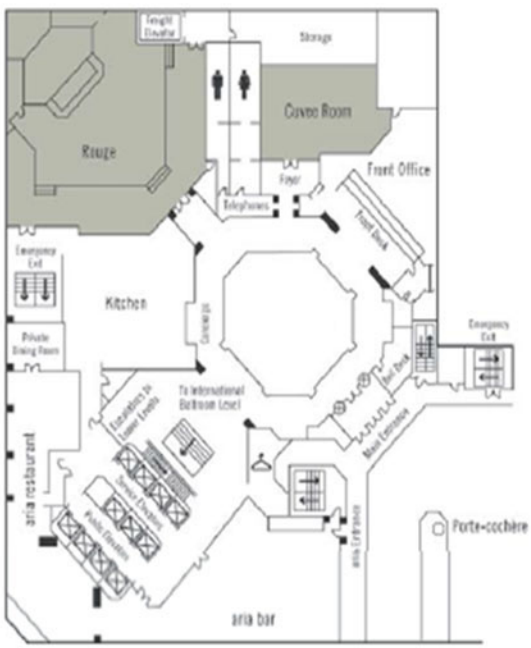

Lobby Level

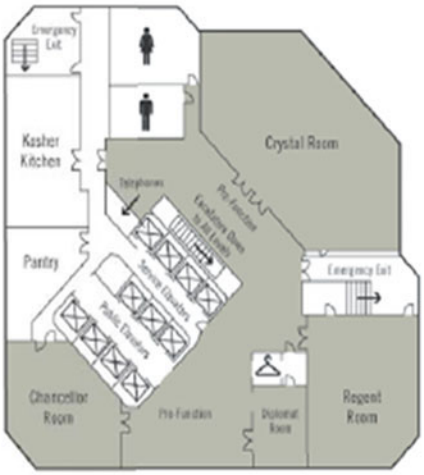

3rd Level

SPR GENERAL INFORMATION

Mission Statement
The Society for Pediatric Radiology is dedicated to fostering excellence in pediatric health care through imaging and image-guided care.

SITES OF PREVIOUS MEETINGS

1991 & IPR'91	Stockholm, Sweden
1992	Orlando, Florida
1993	Seattle, Washington
1994	Colorado Springs, Colorado
1995	Washington, D.C.
1996 & IPR'96	Boston, Massachusetts
1997	St. Louis, Missouri
1998	Tucson, Arizona
1999	Vancouver, British Columbia, Canada
2000	Naples, Florida
2001 & IPR'01	Paris, France
2002	Philadelphia, Pennsylvania
2003	San Francisco, California
2004	Savannah, Georgia
2005	New Orleans, Louisiana
2006 & IPR'06	Montreal, Quebec, Canada
2007	Miami, Florida
2008	Scottsdale, Arizona
2009	Carlsbad, California
2010	Boston, Massachusetts
2011 & IPR'11	London, England
2012	San Francisco, California
2013	San Antonio, Texas
2014	Washington, D.C.
2015	Bellevue, Washington

FUTURE MEETINGS

2017	May 16-20, 2017	Vancouver, British Columbia, Canada
2018	May 15-19, 2018	Nashville, Tennessee
2019	April 30-May 4, 2019	San Francisco, California

SPR OFFICERS, DIRECTORS AND COMMITTEES 2015–2016

Board of Directors
Brian D. Coley, MD, FACR, Chair
James S. Donaldson, MD, FACR, President
Diego Jaramillo, MD, MPH, President-Elect
Peter J. Strouse, MD, FACR, 1st VP
Taylor Chung, MD, 2nd VP
Christopher I. Cassady, MD, FAAP, Secretary
Michael J. Callahan, MD, Secretary-Elect
Molly E. Dempsey, MD, Treasurer
Stephen F. Simoneaux, MD, Treasurer-Elect and SCORCH President
Kassa Darge, MD, PhD
Edward Y. Lee, MD, MPH
Cynthia K. Rigsby, MD, FACR
M. Beth McCarville, MD
Daniel J. Podberesky, MD
Mary R. Wyers, MD
Donald P. Frush, MD, FACR, Past President & Image Gently Alliance Liaison
Sue C. Kaste, DO, ex officio
Richard A. Barth, MD, FACR, ex officio
Marta Hernanz-Schulman, MD, ACR Commission Liaison
Robert C. McKinstry, MD, PhD, SCORCH President (10/2013-10/2015)
Benjamin H. Taragin, MD, Web Editor
Gisela Mercado-Dean, MD, AAP Liaison
M. Ines Boechat, MD, WFPI Liaison

Abdominal Imaging
Daniel J. Podberesky, MD, Chair
Sudha A. Anupindi, MD
Lauren W. Averill, MD
Mark E. Bittman, MD
Lee K. Collins, MD
Jonathan R. Dillman, MD
Arthur B. Meyers, MD
Martha M. Munden, MD
Lena Nassif Naffaa, MD
Hansel J. Otero, MD
Ethan A. Smith, MD
Kristen B. Thomas, MD
Andrew T. Trout, MD

Bylaws
Brian D. Coley, MD, FACR, Chair
Richard A. Barth, MD, FACR
George S. Bisset III, MD, FACR
Christopher I. Cassady, MD, FAAP
James S. Donaldson, MD, FACR
Edward Y. Lee, MD, MPH
Cynthia K. Rigsby, MD, FACR

Cardiac Imaging
Dianna M. E. Bardo, MD, Chair
Lorna P. Browne, MB BS
Mark R. Ferguson, MD
S. Bruce Greenberg, MD
Eric Hoggard, MD
Joshua Q. Knowlton, MD
Prakash M. Masand, MD
Cynthia K. Rigsby, MD, FACR
Laureen M. Sena, MD
Mike Seed, MBBS
Suraj D. Serai, PhD
Gauri S. Tilak, MD

Child Abuse
Sabah Servaes, MD, Chair
Stephen D. Brown, MD
Arabinda K. Choudhary, MBBS, MRCP, FRCR
Stephen Done, MD
Laura L. Hayes, MD
Jeannie K. Kwon, MD
Bradley A. Maxfield, MD
Kenneth L. Mendelson, MD
Joelle Moreno (Attorney)
Sandeep Narang, MD
Michael D. Rubin, MD
Dana S. Schwartz, MD
Daniel M. Schwartz, MD
Terry J. Vaccaro, MD
Gregory A. Vorona, MD

Clinical Practices Steering Committee
Michael J. Callahan, MD, Chair
Christopher I. Cassady, MD, FAAP, Chair
Dianna M. E. Bardo, MD
Taylor Chung, MD
Kassa Darge, MD, PhD
Jerry R. Dwek, MD
Monica Epelman, MD
Judy A. Estroff, MD
Mary Patricia Harty, MD
Ramesh S. Iyer, MD

Geetika Khanna, MD, MS
Beth M. Kline-Fath, MD
Beverley Newman, MD, FACR
Manish N. Patel, MD
Daniel J. Podberesky, MD
Sabah Servaes, MD
Dennis W. Shaw, MD
Sjirk J. Westra, MD

Contrast-Enhances Ultrasound Task Force
Kassa Darge, MD, PhD, Chair
Susan Back, MD
Carol Barnewolt, MD
Dorothy I. Bulas, MD, FACR, FAAP
Jamie Coleman, MD
Jonathan R. Dillman, MD
Lynn A. Fordham, MD
Mary Beth McCarville, MD
Harriet Joan Paltiel, MD
Frank M. Volberg, MD

CT
Sjirk Westra, MD, Chair
R.Paul Guillerman, MD, Vice Chair
Jonathan R. Dillman, MD
Kara G. Gill, MD
Thaddeus W Herliczek, MD, MS
John D. MacKenzie, MD
Pallavi Sagar, MD
Karuna V. Shekdar, MD
Jacqueline A. Urbine, MD
Dayna M. Weinert, MD
Sheila C. Berlin, MD, Advisory

Education - Curriculum
Diego Jaramillo, MD, MPH, Chair
Sarah S. Milla, MD, Vice Chair
Michael J. Callahan, MD
Christopher I. Cassady, MD, FAAP
Taylor Chung, MD
Molly E. Dempsey, MD
Angelisa M. Paladin, MD
Bruce R. Parker, MD
Sanjay Prabhu, MD
Janet R. Reid, MD
Manrita K. Sidhu, MD
Stephen F. Simoneaux, MD
Peter J. Strouse, MD, FACR

Fellowship Program Director
Jane E. Benson, MD, Chair

Fetal Imaging
Beth M Kline-Fath, MD, Chair
Dorothy I. Bulas, MD, FACR, FAAP
Lucia Carpineta, MD, CM
Kimberly A. Dannull, MD
Nilesh Desai, MD
Judy A. Estroff, MD
Katrina S. Hughes, MD
S.Pinar Karakas, MD
Mariana L. Meyers, MD
Erika Rubesova, MD
Gaurav Saigal, MD
Chetan C. Shah, MD
Gayathri Sreedher, MD

Laura J. Varich, MD
Teresa Victoria, MD, PhD

Finance
Stephen F. Simoneaux, MD, Chair
Richard A. Barth, MD, FACR
Molly E. Dempsey, MD
James S. Donaldson, MD, FACR
Diego Jaramillo, MD, MPH
Avrum Nathaniel Pollock, MD, FRCPC
Matthew D. Schmitz, MD
Randheer Shailam, MD
Peter J. Strouse, MD, FACR
Dayna M. Weinert, MD

History
Alan Schlesinger, MD, Historian
N. Thorne Griscom, MD, Consultant

Honors
Donald P.Frush, MD, FACR
Richard A. Barth, MD, FACR
Sue C. Kaste, DO

Informatics
Alexander J. Towbin, MD, Chair
Karen Blumberg, MD, FACR
Michael L. Francavilla, MD
Safwan Halabi, MD
C. Matthew Hawkins, MD
Neil D. Johnson, MD
Nadja Kadom, MD
Summer L. Kaplan, MD
David B. Larson, MD, MBA
Peter A. Marcovici, MD
Takashi Sato, MD
Narendra Shet, MD
Keith S. White, MD

Interventional
Manish N Patel, DO, Chair
Leah E. Braswell, MD
John J. Crowley, MD
Kari L. Hayes, MD
Jared R. Green, MD
Craig M. Johnson, MD
Shellie C. Josephs, MD
Janice McDaniel, MD
Els Nijs, MD
Jeremiah J. Sabado, MD

Judiciary
Richard B. Gunderman, MD, FACR, Chair
Richard A. Barth, MD, FACR
Stephen D. Brown, MD
Charles D. Williams, MD

MR
Taylor Chung, MD, Chair
Govind B. Chavhan, MD, DABR
Jesse Courtier, MD
Robert J. Fleck, MD
Michael S. Gee, MD, PhD
Mai-Lan Ho, MD
Geetika Khanna, MD, MS
Michael M. Moore, MD

Thang Ngo, MD
Unni K. Udayasankar, MD
Shreyas S. Vasanawala, MD, PhD
Matthew J. Winfeld, MD

MSK
Jerry R. Dwek, MD, Chair
Lauren W. Averill, MD
Murray J. Bartlett, MBBS
Nancy A. Chauvin, MD
Kirsten Ecklund, MD
Michael F. Fadell, MD
R. Paul Guillerman, MD
Munire Gundogan, MD
Siddarth Jadhav, MD
Tal Laor, MD
Archana Malik, MD
Arnold C. Merrow, MD
Arthur B. Meyers, MD
Jie C. Nguyen, MD
Kamaldine Oudjhane, MD, MSc
Shawn E. Parnell, MD
Amisha Shah, MD
Mahesh M. Thapa, MD
Sai G. Yarram, MD

Neuroradiology
Dennis W. Shaw, Chair
Mariaem M. Andres, MD
Timothy Ni. Booth, MD
Thangamadhan Bosemani, MD
Charles R. Fitz, MD
S. Srinivas Ganapathy, MD
Carolina V. Guimaraes, MD
Saurabh Guleria, MD
Thierry A.G. M. Huisman, MD
Arzu Kovanlikaya, MD
Jason N. Nixon, MD
Raghu H. Ramakrishnaiah, MD
Diana P. Rodriguez, MD
Nancy K. Rollins, MD
Gaurav Saigal, MD

Newborn
Judy A. Estroff, MD, Chair
John B. Amodio, MD
Evelyn Y. Anthony, MD
Thangamadhan Bosemani, MBBS
John A. Cassese, MD
Ellen M. Chung, MD
Pamela Deaver, MD
Luis Goncalves, MD
Emily M. Janitz, DO
David W. McDonald, MD
Richard Parad, MD
Kalyan C. Tatineny, MD

Nominating
Brian D. Coley, MD, FACR, Chair
Ronald Cohen, MD
Scott Dorfman, MD
Monica Epelman, MD
Beth Kline-Fath, MD
Janet R. Reid, MD
Alan Schlesinger, MD

Nuclear Medicine
Helen Nadel, MD
Deepa R. Biyyam, MB, BS
Hedieh Eslamy, MD
Lena Nassif Naffaa, MD
Sara M. O'Hara, MD
Victor J. Seghers, MD, PhD
Sabah Servaes, MD
Kalyan C. Tatineny, MD
S. Ted Treves, MD
Esben S. Vogelius, MD

Oncology
Geetika Khanna, MD, MS, Chair
Adina L. Alazraki, MD
Kiery A. Braithwaite, MD
Kara Gill, MD
Sue C. Kaste, DO
M. Beth McCarville, MD
Ajaykumar C. Morani, MD
Edward Richer, MD
Susan E. Sharp, MD
Thomas Laurence Slovis, MD
Stephan D. Voss, MD, PHD

Physician Resources
Rebecca L. Hulett-Bowling, MD, Chair
Summer Kaplan, MD
Brooke S. Lampl, DO
Janice D. McDaniel, MD
Gisela Mercado-Deane, MD
Sosamma Methratta, MD
Debra J. Pennington, MD
Avrum N. Pollock, MD, FRCPC
Mitchell L. Simon, MD
Kristen Barry Thomas, MD

Public Policy
Richard M. Benator, MD, FACR, Chair
Aparna Annam, DO
Evelyn Y. Anthony, MD
Richard A. Barth, MD, FACR
Steven L. Blumer, MD
Kate A. Feinstein, MD, FACR
Michael L. Francavilla, MD
Donald P. Frush, MD, FACR
Marta Hernanz-Schulman, MD, FACR
Susan D. John, MD, FACR
Michael E. Katz, MD, FACR
Megan B. Marine, MD
Debra J. Pennington, MD
Matthew D. Schmitz, MD
Jonathan Swanson, MD
David W. Swenson, MD

Publications
Ethan A. Smith, MD, Chair
Andrew T. Trout, MD, Vice Chair
Johan G. Blickman, MD, PhD
Michael J. Callahan, MD
Christopher I. Cassady, MD, FAAP
Matthew R. Hammer, MD
Ashok Panigrahy, MD
Srikala Narayanan, MD
Pooja Thakrar, MD
Teresa Victoria, MD, PhD

Website Editorial Committee
Benjamin H. Taragin, MD, Chair and Web Editor
Peter A. Marcovici, MD, Assistant Web Editor
Amy R. Mehollin-Ray, MD, Assistant Web Editor

Representatives
Dorothy I. Bulas, MD, FACR, FAAP, Academy of Radiology Research
C. Matthew Hawkins, MD, ACR Council Steering Committee
Maria-Gisela Mercado-Deane, MD, AAP
Susan E. Sharp, MD, SNMMI

SPR PAST PRESIDENTS, AWARDEES & EDWARD B. NEUHAUSER LECTURERS

Past Presidents
1958 59 Edward B. Neuhauser, MD*
1959 60 Frederic N. Silverman, MD*
1960 61 John F. Holt, MD*
1961 62 Arthur S. Tucker, MD*
1962 63 John W. Hope, MD*
1963 64 R. Parker Allen, MD
1964 65 Edward B. Singleton, MD*
1965 66 J. Scott Dunbar, MD*
1966 67 Harvey White, MD*
1967 68 M.H. Wittenborg, MD*
1968 69 David H. Baker, MD
1969 70 John A. Kirkpatrick, Jr., MD*
1970 71 Norman M. Glazer, MD*
1971 72 Bertram R. Girdany, MD*
1972 73 Donald H. Altman, MD
1973 74 Hooshang Taybi, MD*
1974 75 John L. Gwinn, MD*
1975 76 Lawrence A. Davis, MD*
1976 77 Marie A. Capitanio, MD
1977 78 John P. Dorst, MD*
1978 79 Bernard J. Reilly, MB, FRCP (C)
1979 80 Walter E. Berdon, MD
1980 81 Andrew K. Poznanski, MD
1981 82 N. Thorne Griscom, MD
1982 83 Virgil R. Condon, MD
1983 84 Jerald P. Kuhn, MD
1984 85 Lionel W. Young, MD
1985 86 John C. Leonidas, MD*
1986 87 Derek C. Harwood Nash, MD, DSc*
IPR ‘87 Denis Lallemand, MD (ESPR)
1987 88 Beverly P. Wood, MD
1988 89 John ‘F. O’Connor, MD*
1989-90 E.A. Franken, Jr., MD
1990-91 Donald R. Kirks, MD
IPR ‘91 Hans G. Ringertz, MD, PhD (ESPR)
1991 92 William H. McAlister, MD
1992 93 M. B. Ozonoff, MD
1993 94 Joanna J. Seibert, MD
1994 95 Eric L. Effmann, MD
1995-96 Kenneth E. Fellows, MD
IPR ‘96 Paul S. Thomas, MD (ESPR)
1996-97 Diane S. Babcock, MD
1997-98 Charles A. Gooding, MD
1998-99 Robert L. Lebowitz, MD
1999-00 Thomas L. Slovis, MD
2000-01 Janet L. Strife, MD
IPR’01 Francis Brunelle, MD (ESPR)
2001-02 Bruce R. Parker, MD
2002-03 Richard B. Towbin, MD
2003-04 David C. Kushner, MD
2004-05 Stuart A. Royal, MS, MD
2005-06 George A. Taylor, MD

IPR'06 Richard Fotter, MD (ESPR)
2006-07 Marilyn J. Goske, MD
2007-08 Marta Hernanz-Schulman, MD
2008-09 M. Ines Boechat, MD
2009-10 Neil D. Johnson, MBBS
2010-11 Dorothy I. Bulas, MD, FACR
IPR'11 Catherine M. Owens, MD (ESPR)
2011-12 Donald P. Frush, MD, FACR
2012-13 Sue C. Kaste, DO
2013-14 Richard A. Barth, MD, FACR
2014-15 Brian D. Coley, MD, FACR

*Deceased

GOLD MEDALISTS

1988	Frederic N. Silverman, MD
1989	John L. Gwinn, MD
1990	John F. Holt, MD
1991	John A. Kirkpatrick, Jr., MD
1991	Bernard J. Reilly, MB, FRCP
1992	Edward B. Singleton, MD
1993	Hooshang Taybi, MD
1994	Walter E. Berdon, MD
1994	J. Scott Dunbar, MD
1995	Guido Currarino, MD
1995	Derek C. Harwood Nash, MD, DSc
1996	Andrew K. Poznanski, MD
1996	Beverly P. Wood, MD
1997	N. Thorne Griscom, MD
1997	John F. O'Connor, MD
1998	William H. McAlister, MD
1999	E. Anthony Franken, MD
2000	Eric L. Effmann, MD
2001	Giulio J. D'Angio, MD
2002	David H. Baker, MD
2003	Brinton B. Gay, Jr., MD
2003	William H. Northway, Jr., MD
2004	Diane S. Babcock, MD
2004	Virgil R. Condon, MD
2005	Jerald P. Kuhn, MD
2005	Thomas L. Slovis, MD
2006	Robert L. Lebowitz, MD
2006	John C. Leonidas, MD
2007	Leonard E. Swischuk, MD
2008	Barry D. Fletcher, MD
2009	Charles A. Gooding, MD
2010	Janet L. Strife, MD
2011	Carol M. Rumack, MD
2012	Marilyn J. Goske, MD
2013	Stuart A. Royal, MS, MD
2014	David C. Kushner, MD, FACR
2015	George A. Taylor, MD, FACR, FAIUM, FSRU
2016	Jennifer K. Boylan, MA

PIONEER HONOREES

1990	John Caffey, MD
1991	M.H. Wittenborg, MD
1992	Edward B. Singleton, MD
1993	Frederic N. Silverman, MD
1994	John P. Dorst, MD
1995	E.B.D. Neuhauser, MD
1996	Edmund A. Franken, MD
1996	Kazimierz Kozlowski, MD
1996	M. Arnold Lassrich, MD

1997	Arnold Shkolnik, MD
1998	Heidi B. Patriquin, MD
1998	William H. Northway, Jr., MD
2000	Jerald P. Kuhn, MD
2001	Diane S. Babcock
2001	Fred E. Avni, MD, PhD
2003	Walter E. Berdon, MD
2004	G.B. Clifton Harris, MD
2005	Rita L. Teele, MD
2006	Robert L. Lebowitz, MD
2007	Carol M. Rumack, MD
2008	Paul S. Babyn, MD
2009	Kenneth E. Fellows, MD
2010	David K. Yousefzadeh, MD
2011	Massoud Majd, MD
2012	George S. Bisset, III, MD
2013	Barry D. Fletcher, MD
2014	Diego Jaramillo, MD, MPH
2015	William E. Shiels, DO*
2016	Mary R. Wyers, MD

*Deceased

PRESIDENTIAL RECOGNITION AWARDS

1999	David C. Kushner, MD
2000	Paul K. Kleinman, MD
2001	Neil D. Johnson, MBBS
2001	Christopher Johnson
2002	Jennifer K. Boylan, MA
2002	Thomas L. Slovis, MD
2003	Danielle K.B. Boal, MD
2003	Marta Hernanz-Schulman, MD
2004	Kenneth L. Mendelson, MD
2005	Taylor Chung, MD
2005	J. A. Gordon Culham, MD
2005	Shi-Joon Yoo, MD
2006	L. Christopher Foley, MD
2007	Donald P. Frush, MD, FACR
2008	Mary K. Martel, PhD
2008	Connie L. Mitchell, MA, RT(R)(CT)
2008	Harvey L. Neiman, MD
2009	Karen S. Schmitt
2010	Richard A. Barth, MD
2011	Kimberly E. Applegate, MD, MS, FACR
2011	Keith Strauss, MS, FACR
2012	David C. Kushner, MD, FACR
2012	Stuart A. Royal, MS, MD
2013	Alan E. Schlesinger, MD
2014	Richard M. Benator, MD, FACR
2015	Cynthia K. Rigsby, MD, FACR
2016	Vicente Gilsanz, MD, PhD

HONORARY MEMBERS

1985	Jacques Sauvegrain, MD
1987	Bryan J. Cremin, MD
1987	Ole A. Eklof, MD
1987	Clement C. Faure, MD
1987	Andres Giedion, MD
1987	Denis Lallemand, MD
1987	Arnold Lassrich, MD
1987	Ulf G. Rudhe, MD
1998	Frederic N. Silverman, MD
1989	John L. Gwinn, MD
1990	John F. Holt, MD

1990	Richard G. Lester, MD
1991	Gabriel L. Kalifa, MD
1991	Javier Lucaya, MD
1991	John P. Masel, MD
1991	Noemi Perlmutter Cremer, MD
1991	Hans G. Ringertz, MD
1991	John A. Kirkpatrick, Jr., MD
	Bernard J. Reilly, MB, FRCP(C)
1992	Edward B. Singleton, MD
1992	Donald R. Kirks, MD
1992	Beverly P. Wood, MD
1993	Hooshang Taybi, MD
1992/94	Walter E. Berdon, MD
1994	Marie A. Capitanio, MD
1994	Edmund A. Franken, Jr., MD
1994	John C. Leonidas, MD
1994	William H. McAlister, MD
1994	Andrew K. Poznanski, MD
1994	J. Scott Dunbar, MD
1995	David H. Baker, MD
1992/95	Derek C. Harwood Nash, MD, DSc
1995	N. Thorne Griscom, MD
1995	Guido Currarino, MD
1996	Francis O. Brunelle, MD
	Lloyd L. Morris, MD
1996	Heidi B. Patriquin, MD
1997	John F. O'Connor, MD
	Theodore E. Keats, MD
1998	Rita L. Teele, MD
1998	H. Ted Harcke, MD
1999	J. Bruce Beckwith, MD
2000	Joseph Volpe, MD
2001	Ulrich V. Willi, MD
2001	Henrique M. Lederman, MD
2001	Mutsuhisa Fujioka, MD
2002	Eric J. Hall, DSc, FACR, FRCR
2002	Walter Huda, PhD
2003	Michael R. Harrison, MD
2004	Lee F. Rogers, MD
2005	Carden Johnston, MD, FAAP, FRCP
2006	Alan B. Retik, MD
2007	Robert R. Hattery, MD
2008	Professor Hassen A. Gharbi
2009	Dolores Bustelo, MD
2009	Pedro A. Daltro, MD, PhD
2009	Cristian Garcia, MD
2009	Antônio Soares de Souza, MD
2010	Stephen Chapman, MD
2011	Catherine M. Owens, MBBS
2011	Madan M. Rehani, PhD
2012	Harvey L. Neiman, MD, FACR
2013	Savvas Andronikou, MBBCh, FCRad, FRCR, PhD
2014	Timothy M. Cain, MBBS
2015	In-One Kim, MD
2015	Professor Guy Sebag (posthumously)
2016	Bernard F. Laya, DO

SINGLETON-TAYBI AWARD

2006	Corning Benton, Jr., MD
2007	Michael P. D'Alessandro, MD
2007	Janet R. Reid, MD
2008	Dorothy I. Bulas, MD, FACR, FAAP
2009	Lane F. Donnelly, MD
2010	Wilbur L. Smith, Jr., MD
2011	Ralph S. Lachman, MD, FACR

2012	Alan Daneman, MD
2013	Lisa H. Lowe, MD, FAAP
2014	Robert H. Cleveland, MD
2015	Stephen F. Simoneaux, MD
2016	Michael A. DiPietro, MD

John A. Kirkpatrick Young Investigator Award

This award is given to the author of the best paper presented by a Resident or Fellow at the SPR meeting. Beginning in 1995, the award became known as the John A. Kirkpatrick Young Investigator Award.

1993	Philipp K. Lang, MD
1993	Stephanie P. Ryan, MD
1994	Sara O'Hara, MD
1995	Philipp K. Lang, MD
1996	Fergus V. Coakley, MB, FRCR
1997	Ronald A. Alberico, MD
1998	Laura J. Varich, MD
1999	A. E. Ensley, BS
1999	R.W. Sze, MD
2000	S. H. Schneider, MD
2001	Valerie L. Ward, MD
2002	Ricardo Faingold, MD
2003	Andrea Doria, MD
2004	Nina M. Menezes, PhD
2005	Lena Naffaa, MD
2006	Courtney A. Coursey, MD
2007	Ashley J. Robinson, MBChB
2008	Hee Kyung Kim, MD
2009	Conor Bogue, MD
2010	Albert Hsiao, MD, PhD
2011	Ethan A. Smith, MD
2012	Saivivek Bogale, MD
2013	Emma Raver, BA
2014	Aarti Luhar, MD
2015	Ashish Parikh, MD PGY-5

WALTER E. BERDON AND THOMAS L. SLOVIS AWARDS - 2014

Best Clinical Research Paper
Catlin, M, Bohl, D, Blickman, J. "A randomized controlled trial: child life services in pediatric imaging", *Pediatric Radiology,* 2014.

Best Basic Science Paper
Tsai, A, McDonald, A, Rosenberg, A, Gupta, R, Paul K. Kleinman. "High-resolution CT with histopathological correlates of the classic metaphyseal lesion of infant abuse", *Pediatric Radiology,* 2014

2015 recipients will be announced at the meeting. For a list of prior recipients, please visit the SPR website.

THE SPR RESEARCH AND EDUCATION FOUNDATION AWARDS

The SPR Research and Education Foundation is dedicated to promoting research and scholarship in pediatric radiology. The SPR Board of Directors has supported research through grants since 1990. The Foundation was established in 1994 with an initial donation from the Society's reserves.

The Jack O. Haller Award for Excellence in Teaching

2005	Alan Daneman, MD
2006	William R. Cranley, MD and John F. O'Connor, MD
2007	Cindy R. Miller, MD
2008	Sara J. Abramson-Squire, MD
2009	Michael A. DiPietro, MD
2010	George A. Taylor, MD
2011	Paul K. Kleinman, MD
2012	Richard I. Markowitz, MD
2013	Gary L. Hedlund, DO
2014	Tal Laor, MD
2014	Carrie B. Ruzal-Shapiro, MD

2015	Laura Z. Fenton, MD
2016	Melvin Senac, MD

The Heidi Patriquin International Fellowship

2005	Luy Lyda, MD, Angkor Hospital for Children, Siem Reap, Cambodia
2006	Hakima Al-Hashimi, MD Salmaniya Medical Complex, Manama, Bahrain
2006	Pannee Visrutaratna, MD, Chiang Mai University, Chiang Mai, Thailand
2006	Juana Maria Vallejo, MD, Clinica del Country, Bogota, Colombia
2007	Nathan David P. Concepcion, MD, St. Luke's Medical Center, Quezon City, Philippines
2008	Rolando Reyna Lopez, MD, Hospital Santo Tomas, Panama City, Panama
2009	Ahmed Mussa Jusabani, MD, Kilimanjaro Christian Medical Centre, Moshi Town, Tanzania
2010	Omolola Mojisola Atalabi, MD, College of Medicine, University of Ibadan, Nigeria
2011	Kushaljit Singh Sodhi, MD, Postgraduate Institute of Medical Education and Research (PGIMER), Chandigarh, India)
2012	Wambani Sidika Jeska, MBchB, Kenyatta National Hospital, Nairobi, Kenya
2012	Yocabel Gorfu, MD, Addis Ababa University, Addis Ababa, Ethiopia
2013	Regina Nava, MD, St. Luke's Medical Center, Quezon City, Philippines
2013	Olubukola Abeni Omidiji, MBBS, University of Lagos, Lagos, Nigeria
2014	Nneka I. Iloanusi, MBBS, University of Nigeria Teaching Hospital, Enugu, Nigeria
2014	Beatrice Mulama, MBChB, M.Med, Kenyatta National Hospital, Nairobi, Kenya
2015	Nasreen Mahomed, MBBCh, University of the Wiwatersand, Johannesburg, Gauteng
2015	Waseem Akhtar Mirza, MBBS, The Aga Khan University, Karachi, Pakistan
2016	Daniel Zewdneh Solomon, MD, Addis Ababa University, Addis Ababa, Ethiopia
2016	Vikas Yadav, MD, Christian Medical College, Vellore, Tamilnadu, India

Pilot Awards - 2015

"Understanding Cardiac Biomechanics in Congenital Heart Disease: A Serial Imaging Study of Single Ventricle Pediatric Patients using Cardiac MRI" - Ramkumar Krishnamurthy, PhD, et al. Texas Children's Hospital

"Enhancing Safety and Quality of Medical X-ray Imaging" Steven Don, MD, St. Louis Children's and Robert D. MacDougall, M.Sc., Boston Children's Hospital

Seed Grants - 2015

"Shear Wave Sonoelastography for the Noninvasive Evaluation of Hepatic Fibrosis in the Pediatric Population" - Shannon G. Farmakis, MD, St. Louis University School Of Medicine

"Imaging Utilization in the Diagnosis Of Appendicitis in Children in the United States: Analysis Of Trends, Costs And Outcomes" - Hansel J. Otero, MD, Et Al. Children's National Medical Center

Fellow Award - 2015

"Structural and Functional Connectivity of the Attention Network: Identifying Imaging Biomarkers of Attention Impairment in Pediatric Concussions and Neuroplasticity after Cognitive Training" - University of California in San Francisco - Alireza Radmanesh, MD, et al. University of California in San Francisco

2016 recipients will be announced at the meeting. For a list of prior recipients, please visit the SPR website.

Previous Neuhauser Lectures

1997	S. Steven Potter, PhD, Cincinnati, Ohio "Homeobox Genes and Pattern Formation (Master Genes)"
1998	Roy A. Filly, MD, San Francisco, California "Fetal Thoracic Surgery"
1999	Harold A Richman, PhD "Child Abuse: From a Radiologist's Discovery to a Major Issue of Public Policy. What Have We Wrought?"
2000	William D. Lyman, PhD, Detroit, Michigan "Prenatal Molecular Diagnosis and Fetal Therapy"
2001	Jerry R. Dwek, MD, Columbus, Ohio "Médecins Sans Frontiéres/The Doctors Without Borders Experience – Afghanistan"
2002	Eric J. Hall, DSc, FACR, FRCR, New York, New York "Lessons We Have Learned From Our Children: Cancer Risks From Diagnostic Radiology"
2003	Jeffrey A. Towbin, MD, Houston, Texas "Molecular Cardiology: Laboratory to Bedside" Bruce R. Rosen, MD, PhD, Boston, Massachusetts "New Advances in MRI: A Guide for the Practicing Pediatric Radiologist"

2005	Bruce R. Korf, MD, PhD, Birmingham, Alabama "Pathobiology and Management of NF1 in the 'Genomic Era'"
2006	Richard M.J. Bohmer, MD, MPH "Evolution, Innovation and the Changing Nature of Healthcare Delivery"
2007	Nogah Haramati, MD "21st Century Radiology: Growth and Development of Our Workflows and Processes"
2008	Emanuel Kanal, MD, FACR, FISMRM, AANG MR Technology: Where Are We, Where Are We Going?
2009	Roberta G. Williams, MD "Cardiology and Radiology: Partners in Producing Healthy Adults with Congenital Heart Disease"
2010	Regina E. Herzlinger, PhD "The Economic Basis of Change in Healthcare"
2011	Sanjiv Gambhir, MD, PhD "Molecular Imaging"
2012	William R. Hendee, PhD "Past and Future Patient Benefits of Radiologist/Physicist Collaboration"
2013	James R. Downing, MD "The Pediatric Cancer Genome Project – Implications for Clinical Medicine
2014	Robert Pearl, MD "The Future of American Medicine – The Impact of Health Care Reform"
2015	Robert Gillies, PhD "Radiomics and Radiogenomics"

For a list of Neuhauser Lecturers prior to 1997, please visit the SPR website.

SPR 2016 HONOREES

SPR 2016 Gold Medalist

The Gold Medal of The Society for Pediatric Radiology is our most distinguished honor. The SPR Medal is awarded to pediatric radiologists who have contributed greatly to the SPR and our subspecialty of pediatric radiology as a scientist, teacher, personal mentor and leader.

Jennifer K. Boylan, MA

This is the 24th year that Jennifer Boylan has been the public face of The Society for Pediatric Radiology (SPR) as well as our conscience, visionary, and advocate. To understand what she has meant to the SPR, one needs to know a little of our history. Prior to 1992, the SPR was really a mom and pop organization of several hundred pediatric radiologists. In the 1980s, the secretary ran the show with whatever resources available and a renewable term for as long as he/she could take it. The only administrative support was the staff assistant for the secretary. There were few committees and the entire focus was the annual meeting. The president made suggestions for the meeting and the secretary did the contracting, planning, and, with the treasurer, the financing. The current 5-year line of succession to the Presidency and then Chairman of the Board was started in the late 1980s to insure continuity with society- educated officers. We were dramatically increasing in size and the IPR began in 1987. All of this led to a culture change with diversification of responsibilities and innumerable chores being thrown at our only administrator, the secretary. It was a recipe for disaster but this was avoided when in the summer of 1992 the SPR contracted with the RSNA for administrative services and they assigned Jennifer to us.

She and I began at the same time – Jennifer as Executive Secretary and me as the new Society Secretary. It is hard to imagine how she put up with this brash radiologist from Detroit who called every morning at the tick of 8 a.m. Chicago time (9 a.m. Detroit time) with all sorts of questions and requests. But this is Jennifer, outwardly calm, tactful, and self -assured. She took her coat off, got her coffee and without a missed beat, jumped in with fantastic ideas and solutions for us to move forward. She was always inventive and positive. She coordinated the new roles of the Society secretary, president, and chairman of the board and developed instant rapport with our new meeting planner, Karen Schmitt. Karen and Jennifer worked with the Board to expand the 3-day meeting into a 5-day meeting composed of scientific papers and a formal course.

Most importantly, she guided us through the organization and legal aspects to form the SPR Foundation (1994), implemented the first Informatics Committee and coordinated the first Campaign for Children (2001). She correctly perceived our Society as the advocate for children's imaging and led us to be focused not only on our academics but more extensive external role. In 2001, the potential problems of radiation and CT surfaced. As Chairman of the Board, I was determined to do something to help us all understand the problem but the Board was uncertain. It was Jennifer who led the way at our Board meeting when she said, "let's do it, we can make a difference". This was enough to convince the Board of our leadership role and she planned The ALARA Conference 3 months later in Chicago (August 2001). She helped coordinate a meeting of scientific experts of diverse specialties and for the first time demonstrated to both the public and radiologic societies the advocacy role of the SPR.

It was Jennifer, looking out for our interest that organized moves of our administrative infrastructure from the RSNA to IMM (2000) and to the ACR (2005) insuring that we had the proper administrative resources to carry out all our functions to help children. Since 2000, she has been the Executive Director of the SPR and the SPR Research and Education Foundation.

In many ways, the very distillation of Jennifer's many attributes is her role in the Alliance for Radiation Safety in Pediatric Imaging, more familiar as the Image Gently Alliance. Image Gently originated in The Society for Pediatric Radiology, but its vision has grown into an organization with international impact and acclaim. Most remarkable is how something with a proclamation so profound and powerful arose from a simple, harmonious and reverberating whisper… *Image Gently*. These two words were Jennifer's imprimatur, her voice on what was to call the new venture. This carefully crafted phrase gave breath, vibrancy and life to the formative Alliance. Jennifer's hand is more than leadership although she adeptly displayed this leadership. All of her talents and skills graced the Image Gently Alliance. A perfect mixture of vision, wisdom, diplomacy, conviction, humanism, passion, all tempered with common sense and a style that always let everyone feel equal in responsibility and equal in success … what a remarkable gift. Together with Marilyn Goske, the chair and creator of the Alliance concept and strategy, there was a shared and complementary skill set that made Image Gently a phenomenon. Marilyn adds, "Jennifer Boylan is just an exceptional woman. Not only is she organized, incredibly intelligent and savvy, but she is also creative. It was she who coined the name 'Image Gently' for the first CT campaign. We are forever indebted as the phrase perfectly captured the thoughtful and positive tone we wished to establish for this new initiative. Jennifer's energy propelled the campaign forward to help make it the worldwide movement it is today." More than leadership, Jennifer's role in Image Gently is really a legacy.

Through all this, Jennifer has maintained the "old" feeling of a mom and pop organization. We are still family. Once in the first year or two with us, I was startled when she said "I need to take this emergency call from my daughter's principal". Clearly whatever we were doing was not important and I made her promise to call me back about Emma. Well Emma (about 5 years old) decided not to go to school that day and after getting off the bus, she took off to explore the neighborhood. Emma like Jennifer is an independent soul and thought she could plan her day. Luckily, one of her classmate's mother saw her wandering about and brought her to the principal.

When I was distraught at the untimely death of my friend Jack Haller and looking for a way to honor him, it was Jennifer who had the best of suggestion – The Haller Teaching Award. She always was there for the SPR and its members.

Sharing family experiences and often just talking about problems brings people closer together. The many fortunate SPR members who had the opportunity to work with Jennifer view her as friend and part of their family as well as a superb colleague.

And what is a more fitting tribute now than to simply say "Thank you for all you have done." No one in this organization has touched so many in so many different ways. She has pointed us in the right direction, wagged at us when necessary and simply always had an open mind, moreover open hands and heart whenever we needed it. The story doesn't end here, and for this we are also grateful and look forward to the new tapestry you will help us to weave for the children we all care for.

Thomas L. Slovis, MD, FACR, FAAP and Donald P. Frush, MD, FACR, FAAP

SPR 2016 Pioneer Honoree

Pioneer Honorees were first acknowledged in 1990 as a means to honor certain physicians who made special contributions to the early development of our specialty.

Mary R. Wyers, MD

Mary R. Wyers, MD has earned the 2016 Society for Pediatric Radiology Pioneer Award in recognition of her commitment to and success with advancing the SPR website which strengthened the ability of the SPR to meet its educational, research and clinical goals. Mary's efforts have had a profound impact on those who visit the website and have benefitted the vast majority of the SPR membership.
Mary received her MD degree from Washington University School of Medicine where she went on to complete a Diagnostic Radiology residency and a Pediatric Radiology fellowship at the Mallinckrodt Institute of Radiology. It was at Mallinckrodt that Mary had the pleasure of working alongside Drs. Gary Shackelford and Bill McAlister who have served as her career mentors. Following fellowship, Mary joined the faculty of the former Children's Memorial Hospital, now Ann & Robert H. Lurie Children's Hospital of Chicago, and over the past 15 years has advanced her pediatric radiology career at Lurie Children's.

Education through technology has always been Mary's primary academic interest. During the time when the transition from film to digital imaging was taking place, Mary supervised the digitization of the Children's Memorial Hospital departmental film-based teaching file. She incorporated these cases into a digital teaching file that she developed using Medical Imaging Resource Center (MIRC) a free software program created and supported by the RSNA. This teaching file has grown into a collection of over 1000 cases and associated educational modules based on the educational curriculum endorsed by the SPR.

Mary's most significant contributions to the SPR began when she was named the Society's website editor in 2007. During that time of digital technology explosion, she helped direct the SPR website redesign that created a more user-friendly web environment with improved organizational content. Features that Mary worked to initiate during her time as SPR website editor include the popular unknown case of the month that linked the SPR website to the pediatric radiology digital teaching file that she created, and the addition of subspecialty committee pages that have fostered communication between the subspecialty committees and the SPR membership. With her input, these subspecialty pages have grown to include committee generated expert educational material and protocols.
Whether through education, communication or availability of information, every SPR member has benefitted from the website that Mary has worked so diligently to advance.

In 2015, Mary was elected to the SPR Board of Directors, she has been the sunrise session co-organizer for two recent SPR meetings, and she has also served the SPR as a valued reviewer for Pediatric Radiology. She has also been involved with the ABR as a Board Examiner and MOC Committee member, and with the RSNA on its MIRC and Education Exhibit Committees.

On a day-to-day basis, Mary can consistently be seen teaching medical students, residents and fellows. For her outstanding educational efforts, the Lurie Children's pediatric radiology fellows awarded her the 2014 Teacher of the Year Award.

Mary and her husband Stephan are the proud parents of three boys, Alec, Henry and Adrian who bring daily joy into their lives.

Gary Shackelford writes, "Mary's eagerness to learn, her delightful manner in working with colleagues, and her compassion for patients and their parents have all served her well during her distinguished career. Her long-standing commitment to the SPR website exemplifies an understanding that the process of learning is continuous".
The SPR membership and the children we serve have been touched by Mary's passion and commitment to improving the SPR website and we gladly bestow upon her the 2016 SPR Pioneer Award.

Cynthia K. Rigsby, MD, FACR

SPR 2016 Presidential Recognition Award

The Society bestows Presidential Recognition Awards on members or other individuals whose energy and creativity have made a significant impact on the work of the Society and its service to its members.

Vicente Gilsanz, MD, PhD

This year's Presidential Recognition Award goes to Dr. Vicente Gilsanz for his contributions to our specialty and Society as a pediatric radiologist and scientist. Science and research lead to improved diagnostic and treatment methods for children and ultimately advance our specialty of pediatric radiology. Dr. Gilsanz epitomizes the physician-scientist who as a pediatric radiologist has spent his career committed to research.

After completing his fellowship in pediatric radiology at Boston Children's Hospital, he was on staff for a short stay at the Hospital Infantil in Madrid, Spain, his native country. But the sun of Southern California was brighter - as was the allure of Ines Boechat who would become his wife - so after only a short time home in Spain, he moved to Los Angeles where he joined the faculty at the University of Southern California and the medical staff at the Children's Hospital of Los Angeles. He has spent his entire clinical and productive research career there.

During the early years of his career, Dr. Gilsanz focused on clinical pediatric radiology publishing on a wide variety of diseases. He became focused on bone development and carried out a series of experiments in rabbits that explored the effects of diet on bone density. This led to studies assessing bone density of boys and girls of different ethnicities through puberty – these studies are now used as the classic reference standards. The next 20 years were spent studying the effects of various disease states and drugs therapies on bone density leading to publication of an additional 100 papers, 17 book chapters and a text book.

He began using cross-sectional imaging to segment and quantify subcutaneous and visceral fat. The rediscovery of metabolically active brown fat on CT PET scans launched his more recent area of interest. Dr. Gilsanz has developed MR and CT techniques to identify and quantify brown fat in children and he was the first to recognize the relationship between brown fat and muscle mass. He has investigated the effects of pediatric disease states on brown fat stores and the implications for the child in the future. He is internationally recognized for these studies.

Dr. Gilsanz has published 208 peer reviewed research papers, 332 abstracts, 16 book chapters and one text book. He has received numerous awards and honors. Since 1993, he has been awarded 10 million dollars in federal funds, primarily from the NIH. He has successfully mentored numerous pediatric radiology fellows and 12 research assistants who subsequently were accepted into medical school. After 37 years Dr. Vicente Gilsanz shows no signs of slowing down and continues to pursue his academic interests.

A source of pride for Vicente are the many accomplishments of his wife Ines Boechat, an SPR Past President, the founding President of the World Federation of Pediatric Imaging (and many, many more accomplishments.) Vicente is proud of his three children, Paola, Diego and Monica. There is no doubt their team and partnered approach has benefited all of their highly successful careers.

The SPR has made science and research a high priority through the establishment of the Research and Education Foundation that now has a balance of over 3 million dollars. It is timely and fitting that we honor an accomplished colleague and scientist as we embark on the second phase of the Campaign for Children. It is through this campaign that we hope to launch the careers of future researchers and educators from our society.

It is a rare individual who is both a pediatric radiologist and an internationally acclaimed scientist whose research is as high quality and impactful as Dr. Gilsanz'. The SPR is honored to have him among our ranks and he is a role model to us all.

James S. Donaldson, MD, FACR

SPR 2016 Honorary Member

The Society extends Honorary Membership to individuals outside of pediatric radiology who have made outstanding contributions to the care of children.

Bernard F. Laya, DO

It is a privilege to chronicle the life and career of Dr. Bernard F. Laya who is the recipient of the 2016 SPR honorary membership in recognition of his outstanding academic achievements and international leadership in pediatric radiology.

Bernie was born and raised in the Philippines where he attended school from preschool to college. He took up and finished Bachelor of Science in Biology in the University of Santo Tomas which holds the oldest extant university charter in the Philippines and in Asia. On his first year in medical school in the same university, he and his family migrated to the United States of America. He finished his medical degree from the University of Health Sciences College of Osteopathic Medicine in Kansas City, Missouri. After his medical internship at the Pacific Hospital of Long Beach in California, he proceeded and finished residency in Diagnostic Radiology at the Ohio University, Grandview Hospital in Dayton, Ohio. Immediately after residency, he moved on to a fellowship in Pediatric Radiology at the combined program of the Cleveland Clinic Children's Hospital and of Children's Hospital and Medical Center of Cincinatti in Ohio, USA. He practiced as pediatric radiologist at The Children's Medical Center where he remained as active staff in 2004.

Guided by his vision and motivated by patriotism, Dr. Laya went back to the Philippines and started his radiology career in the country at St Luke's Medical Center in Quezon City in 2004. The beginning of his journey in the center was not easy, to say the least, as he was initially unpopular with the local radiologists who doubted his intentions. But slowly and persistently, he showed and I witnessed as a Radiology resident why he came back. He simply wanted to share his knowledge, expertise, time and skills. He started with the residents by giving a lecture series on pediatric radiology. He is a very effective speaker. Each time after listening to his lecture, I am always motivated to read more on the topic he discussed. It is not a surprise that Bernie is a favorite speaker on pediatric radiology and has given over 100 lectures in the Philippines and internationally.

His generosity extended beyond radiologists and St Luke's. Bernie also spent time, mingled and became friends with the clinicians especially the pediatricians in St Luke's and in nearby hospitals. In 2006, he was able to formally set up a Pediatric Radiology Fellowship at St. Luke's Medical Center, which is the only formal multimodality pediatric radiology fellowship in the country.

Aside from teaching and mentoring, two of Bernie's other passions are research and writing, which he also unselfishly shares with his Filipino colleagues, fellows and residents. He devotes much time and energy in these fields and has consistently been given recognition and awards both in the Philippines and abroad since 2006 up to the present. He authored or co-authored 30 peer-reviewed articles and has written chapters for 5 pediatric radiology textbooks. He is on the Editorial board of the Journal of American Osteopathic College of Radiology, Asian Oceanean Forum for Pediatric Radiology, and has reviewed articles for the European Journal of Radiology and Pediatric Radiology Journal. His field of interest is childhood neuroimaging and chest imaging, quality and safety in medical imaging and medical education. For his interest and experience on childhood tuberculosis (TB), Dr. Laya was elected as the lead radiologist on the TB initiatives of the world federation of pediatric imaging (WFPI).

Dr. Bernard F. Laya is a Professor of Radiology and is currently the Associate Dean for Student and Faculty Affairs at St. Luke's College of Medicine – William H. Quashia Memorial in the Philippines. Concurrently, he is also the Director of Radiology at St. Luke's Medical Center-Global City, and Head of Pediatric Radiology at St. Luke's Medical Center-Quezon City, Philippines. He is a Board Member of the World Federation of Pediatric Medical Imaging (WFPI) and the Asian Oceanic Society for Pediatric Radiology (AOSPR). He is a Program Committee member in pediatric radiology for Radiological Society of North America (RSNA) and Asian Oceanic School of Radiology.

I can go on enumerating Dr Laya's lengthy achievements but to me his greatest accomplishment is his being a mentor because he continuously inspires those lucky enough to be under his care. He is effective because he knows how to listen. No matter how busy he is, he gives us, his mentees his full attention. He guides and helps us find direction, but never pushes us. He is always accessible, criticizes constructively, and points out areas that need improvement; always focusing on the mentee's behavior and never on one's character. He is supportive, unceasingly encourages us to learn and improve. And he cares, not just with our works and careers but more importantly with our personal lives. To paraphrase a quote by William Arthur Ward: "The mediocre mentor tells. The good mentor explains. The superior mentor demonstrates. The great mentor inspires."

Congratulations Dr. Laya for this very well-deserved and befitting award.

Maricar Paguia, MD

SPR 2016 Singleton-Taybi Award

The Singleton-Taybi Award is given in honor of Edward Singleton and Hooshang Taybi, in recognition of their personal commitment to the educational goals of the SPR. Initiated in 2006, the Award is presented annually to a senior member of the SPR whose professional lifetime dedication to the education of medical students, residents, fellows, and colleagues has brought honor to him/her and to the discipline of pediatric radiology.

Michael A. DiPietro, MD

Michael DiPietro grew up in upstate New York. He attended Union College (Schenectady, NY) and received his MD at SUNY, Upstate Medical Center in Syracuse (1974). Mike completed a residency in pediatrics at Children's Hospital of Pittsburgh (1976) where he also spent 6 months each as a trainee in both pediatric pathology and pediatric radiology. At Pittsburgh, Mike was exposed to many great pediatric radiologists who had a profound impact on his career, including John Caffey, Bert Girdany and Lionel Young. Mike did his residency in radiology at Yale (1980) and fellowship in pediatric radiology at Boston Children's Hospital (1982). Mike joined the faculty at C.S. Mott Children's Hospital of the University of Michigan in 1982 where he has worked since. At Michigan, Mike was mentored by Jack Holt. Fittingly, Mike is now the John F. Holt Collegiate Professor of Radiology.
Mike's contributions to medical education at all levels have been and continue to be exemplary:

Medical students – Mike served the Director of Medical Student Education for the Department of Radiology from 2003 to 2013. He served over three decades as director of medical student rotations in the Section of Pediatric Radiology. Mike has been active in preclinical medical student education and curriculum development, serving on medical school Curriculum Committee and Curriculum Strategic Planning Committees. The best testament to Mike's skill and dedication as an educator of medical students is the constant gravitation of students to his work station – Mike teaches via the Socratic method – the students are engaged and active participants in the work.

Radiology Residents –Mike has had a profound impact on many residents considering a career in pediatric radiology. I was once one such a resident, a visitor from another program. Mike's enthusiasm and dedication were one of the factors that excited me about a career in pediatric radiology.

Pediatric Radiology Fellows – Mike actively engages the fellows and seeks to ensure that each fellow achieves a well-rounded training. Similar to the medical students and residents, but at a higher level, our fellows often gravitate to Mike for instruction, advice and mentoring. His critical, thoughtful approach and his dedication to always doing what is best for the patient make Mike an ideal role model for all pediatric radiology trainees.

Radiologists – Mike has lectured in many CME courses, national meetings and as a visiting professor at many institutions. Throughout his career, Mike has been considered an international expert on the use of ultrasound in children. He is at his best in hands-on ultrasound workshops. Mike pioneered the use of ultrasound for examination of the spinal cord in children, particularly in the diagnosis or exclusion of a tethered spinal cord. Currently, he is doing extraordinary and meticulous work on brachial plexus ultrasound. Mike served as chair of the Neurosonography (1992-1994) and Pediatric (2003-2005) Sections of the American Institute of Ultrasound in Medicine. Since 1991, Mike has been active as one of the founders and co-directors of the Society for Musculoskeletal Ultrasound, actively working on the planning of the annual international society meeting and contributing to the education content.

Clinical Physicians – Mike is also board certified in Pediatrics, in part accounting for his dedication to teaching our clinical brethren. He has long extolled the value of ultrasound in children and the new applications that could be applied in clinical practice. Mike has actively participated in the American Association of Pediatrics (AAP) and previously served as the chair of the Radiology Section (2004-2008). He has regularly participated in lectures and teaching sessions at the AAP meetings aimed at educating the general pediatrician and pediatric subspecialist about pediatric radiology. Every interdepartmental conference which Mike attends is a better conference with him there. Mike has the uncanny ability to ask the right questions to learn from a case. If he doesn't know the answer and wants to learn, he asks the question. If he thinks others in the room can learn from his query, he asks the question (even if he already knows the answer).

Technologists – Mike realizes that our imaging technologists are a critical component to excellence in imaging and patient care. More so than any radiologist that I have witnessed in my career, Mike takes time to educate the technologists on how to perform their work better and thus better assist us, the radiologists, in producing the highest quality work possible.

Mike has received innumerable awards recognizing his clinical and educational excellence. Mike was awarded the Jack O. Haller Award for Excellence in Teaching in 2009 by the SPR. Mike is one of only ten members of the University of Michigan Medical School faculty that are members of both the medical school's League of Clinical Excellence and the League of Educational Excellence (an inaugural member). Mike received an award for "Lifetime Achievement in Clinical Care" from the medical school in 2012. In 2014, we were privileged to inaugurate the Michael A. DiPietro, MD Lectureship in Pediatric Radiology in Mike's honor. The lectureship will focus on speakers who share Mike's enthusiasm for teaching of pediatric radiology.

It would be remiss not to briefly mention one of Mike's other loves, music. Mike plays bassoon in two orchestras, one being the University of Michigan Life Sciences Orchestra. It should come as no surprise that Mike won the "Spirit of the LSO" award for his contributions. Mike has served on the doctoral dissertation committee for several music students. Mike has many, many interests outside of radiology and in addition to music – history of Pediatric Radiology, history of our department, travel, dogs (specifically, West Highland Terriers), trains, Star Trek, Star Wars. Residents who meander into one of these topics during readout receive additional education. More importantly, he is genuinely interested in learning about the residents, their backgrounds and their interests.

Mike's greatest contributions are without documentation. Concepts of "life-long learning," "teachable moments" and "teaching by example" embody Mike's approach to pediatric radiology. Mike is at his best in conference, at a workstation or on a phone. Every interaction is an opportunity to teach and an opportunity to learn. For Mike, this is true regardless of the person on the other end, be it the newly minted M3 medical student or the seasoned chief of Pediatric Surgery. If you want to learn, he will teach you. The more interest you show, the more he will teach you. Time is never an issue. By constantly learning, Mike constantly seeks to be a better doctor. By constantly teaching, he seeks to make those around him better doctors and better servants to the patient. We should all strive to approach the profession of medicine with the same enthusiasm and dedication as Mike DiPietro.

Peter J. Strouse, MD, FACR

SPR CAFFEY AWARDEES

John Caffey, MD 1895–1978

Dr. Caffey was regarded throughout the world as the father of pediatric radiology. His classic textbook, "Pediatric X-Ray Diagnosis", which was first published in 1945, has become the recognized bible and authority in its field. The seventh edition of this book was completed several months before his death in 1978. It has been among the most successful books of its kind in the medical field.

Dr. Caffey was born in Castle Gate, Utah on March 30, 1895. It is interesting that he was born in the same year that Roentgen discovered the x-ray. Dr. Caffey was graduated from University of Michigan Medical School in 1919, following which he served an internship in internal medicine at Barnes Hospital in St. Louis. He spent three years in Eastern Europe with the American Red Cross and the American Relief Administration, and returned to the United States for additional training in medicine and in pediatrics at the Universities of Michigan and Columbia, respectively.

While in the private practice of pediatrics in New York City at the old Babies Hospital of Columbia University College of Physicians and Surgeons, he become interested in radiology and was charged with developing a department of pediatric radiology in 1929. He frequently expressed appreciation and admiration for the late Ross Golden, Chairman of Radiology at Columbia Presbyterian Hospital, who allowed him to develop a separate department of diagnostic radiology without undue interference, and who was always available to help and advise him.

Dr. Caffey's keen intelligence and inquiring mind quickly established him as the leader in the fields of pediatric x-ray diagnosis, which recognition became worldwide almost instantaneously with the publication of his book in 1945.

Dr. Caffey received many awards in recognition of his achievements. Outstanding among these were the Mackenzie Davidson Medical of the British Institute of Radiology in 1956, the Distinguished Service Award of the Columbia Presbyterian Medical Center in 1962, the Outstanding Achievement Award of the University of Michigan in 1965, the Howland Award of the American Pediatric Society in 1967, the Jacobi Award of the American Medical Association in 1972, and the Gold Medal Award of the American College of Radiology in 1975. He had been a member of the American Journal of Roentgenology. He was a counselor of The Society for Pediatric Radiology and was an honorary member of the European Society of Pediatric Radiology.

Dr. Caffey's contributions to the pediatric radiologic literature were many. He was instrumental in directing attention to the fact that a prominent thymic shadow was a sign of good health and not of disease, an observation that literally spelled the end to the practice of thymic irradiation in infancy. Infantile cortical hyperostosis was described by him and is called "Caffey's Disease". Dr. Caffey in 1946 first recognized the telltale radiographic changes that characterize the battered child, and his stu¬dents helped disseminate his teachings about these findings. It was Dr. Caffey who first recognized and descried the characteristic bony changes in vitamin A poisoning. He recognized and described the findings associated with prenatal bowing of the skeleton.

In 1963, 3 years after his retirement from Babies Hospital, he joined the staff of the Children's Hospital of Pittsburgh as associate radiologist and as Visiting Professor of Radiology and Pediatrics at the University of Pittsburgh School of Medicine. Although Dr. Caffey came to Children's Hospital and the University of Pittsburgh in an emeritus position, he worked daily and on weekends throughout the years he was there. In Pittsburgh, he made four major new contributions to the medical literature. He described the entity, "idiopathic familial hyperphosphatasemia". He recognized and described the earliest radiological changes in Perthes' Disease. He called attention to the potentially serious effects of shaking children, and used this as a subject of his Jacobi Award lecture. He described, with the late Dr. Kenny, a hitherto unrecognized form of dwarfism which is now known as the Caffey-Kenny dwarf. The John Caffey Society, which includes as its members pediatric radiologists who have been intimately associated with Dr. Caffey, or who have been trained by his students, was established in 1961. This society is now among the most prestigious in the field of radiology. His book and the society named in his honor will live on as important memorials to this great man.

His greatness was obvious to all who worked with him. He was warm, kind, stimulating, argumentative, and above all, honest in his approach to medicine and to x-ray diagnoses. His dedication to the truth was expressed in his abiding interest in the limitations of x-ray signs in pediatric diagnosis and in his interest in normal variation in the growing skeleton. He was concerned with the written and spoken word and was a skilled semanticist. His book and his articles are masterpieces of language and construction. He stimulated and was stimulated and loved by all who had the privilege of working with him. Radiology and Pediatrics have lost a great man, but they shall ever have been enriched by his presence.

Bertram R. Girdany, MD

Caffey Award for Best Basic Science Research Paper

2005 Quantitative Measurement of Microbubble Ultrasound Contrast Agent Flow to Assess the Efficacy of Angiogenesis Inhibitors In Vivo. McCarville B, Streck C, Li CS, Davidoff A
2006 64Cu-Immuno-PET Imaging of Neuroblastoma with Bioengineered Anti-GD2 Antibodies. Voss SD, Smith SV, DiBartolo NM, McIntosh LJ, Cyr EM, Bonab AA, et al.
2007 MR Imaging of Adenocarcinomas with Folate-Receptor Targeted Contrast Agents. Daldrup-Link HE, Wang ZJ, Meier R, Corot C
2008 Evaluation of Quality Assurance Quality Control Phantom for Digital Neonatal Chest Projection Imaging. Don S.
2009 Faster Pediatric MRI Via Compressed Sensing. Vasanawala S, Alley M, Barth R, Hargreaves B, Pauly J, Lustig M
2010 Clinical Evaluation of Readout-Segmented-EPI for Diffusion-Weighted Imaging. Bammer R, Holdsworth S, Skare S, Yeom K, Barnes P
2010 High-Resolution Motion-Corrected Diffusion-Tensor Imaging (DTI) in Infants. Skare S, Holdsworth S; Yeom K; Barnes P, Bammer R
2010 3D SAP-EPI in Motion-Corrected Fast Susceptibility Weighted Imaging (SWI). Bammer R, Holdsworth S, Skare S, Yeom K, Barnes P
2010 T1-Weighted 3D SAP-EPI for Use in Pediatric Imaging. Bammer R, Holdsworth S, Skare S, Yeom K, Barnes P
2011 An MR System for Imaging Neonates in the NICU. Tkach J, Giaquinto R, Loew W, Pratt R, Daniels B, Jones B, Donnelly L, Dumoulin C
2012 Advantages of a Nanoparticle Blood Pool Contrast Agent Over Conventional Intravascular Glomerular-Filtered Contrast Agents for Pulmonary Vascular Imaging. Annapragada A, Guillerman RP, Hoffman E, Kaczka D, Ghaghada K, Badea C
2013 Psychometric Function: A Novel Statistical Analysis Approach to Optimize CT Dose: Steven Don, MD, Mallinckrodt Institute of Radiology, St. Louis, MO, Bruce Whiting, David Politte, Parinaz Massoumzadeh, Charles Hildebolt
2014 No Longer a Holiday: Improving The Pediatric Radiology Elective for Medical Students and Pediatric Housestaff
Eddiel Hyatt, Vanderbilt University, Department of Radiology and Radiological Sciences, Nashville, TN, Cody Penrod, Sudha Singh, Jayne Seekins, DO, Amy Fleming, Melissa Hilmes, MD
2015 Gonad Shields: Good or Bad for Patient Radiation Exposure?; Summer L. Kaplan, MD, Department of Radiology, The Children's Hospital of Philadelphia, Philadelphia, PA, Dennise Magill, MS, Marc A. Felice, MS, Sayed Ali, MD, Xiaowei Zhu, MS

Caffey Award for Best Clinical Research or Education Paper

2005 Evaluation of High Resolution Cervical Spine CT in 529 Cases of Pediatric Trauma: Value Versus
Radiation Exposure. Shiran D, Jimenez R, Altman D, DuBose M, Lorenzo R
2006 Alterations in Regional O2 Saturation (StO2) and Capillary Blood Volume (HbT) with Brain Injuries and ECMO. Grant PE, Themelis G, Arvin K, Thaker S, Krishnamoorthy KK, Franceschini MA
2007 Evaluation of Single Functioning Kidneys Using MR Urography. Grattan-Smith D, Jones R, Little S, Kirsch A, Alazraki A
2008 Evaluating the Effects of Childhood Lead Exposure with Proton MR Spectroscopy & Diffusion Tensor Imaging Neuroradiology. Cecil KM
2009 Improving Patient Safety: Effects of a Safety Program on Performance and Culture in a Department of Radiology at a Children's Hospital. Donnelly L, Dickerson J, Goodfriend M, Muething S
2010 Juvenile Osteochondritis Dissecans (JOCD): Is It a Growth Disturbance of the Secondary Physis of the Epiphysis? Laor T, Wall E; Zbojniewicz A
2011 Quantitative Assessment of Blood Flow with 4D Phase-Contrast MRI and Autocalibrating Parallel Imaging Compressed Sensing. Hsiao A, Lustig M, Alley M, Murphy M, Vasanawala S
2012 Multidetector CT Pulmonary Angiography in Children with Suspected Pulmonary Embolism: Thromboembolic Risk Factors and Implications for Appropriate Use. Lee EY, Tse SK, Zurakowski D, Johnson VM, Donald TA, Boiselle PM
2013 Prospective Comparison of MRI and Ultrasound for the Diagnosis of Pediatric Appendicitis" Robert Orth, MD, PhD, Texas Children's Hospital, Houston, TX, R. Paul Guillerman, Prakash Masand, MD, Wei Zhang, George Bisset
2014 Ultrasound-Derived Shear Wave Speed Correlates with Liver Fibrosis in Children; Jonathan Dillman, M.D., Department of Radiology, Section of Pediatric Radiology, University of Michigan C.S. Mott Children's Hospital, Ann Arbor, MI, Ethan Smith, Amer Heider, Nahid Keshavarzi, Jacob Bilhartz, Jonathan Rubin
2015 Contrast Enhanced Ultrasound in the Assessment of Pediatric Solid Tumor Response to Anti-Angiogenic Therapy; Beth McCarville, MD, Department of Radiological Sciences, Division of Diagnostic Imaging, St. Jude Children's Research Hospital, Memphis, TN, Jamie Coleman, MD, Junyu Guo, PhD, Yimei Li, PhD, Xingyu Li, PhD, Fariba Navid, MD

Caffey Award for Posters

2005 3D MRI and CT in the Evaluation of Congenital Anomalies of the Aortic Arch. Dehkharghani S, Olson K, Richardson R
2006 Diffusion Weighted Imaging in Pediatric Neuroradiology: A Primer. Sagar P, Grant PE
Imaging of Suprarenal Fossa in Children: Radiological Approach and Clinico-Pathological Correlation.
Kukreja K, Restrepo R, D'Almeida M
2007 Neuroimaging of Nonaccidental Trauma: Pitfalls and Controversies. Lowe L, Obaldo RE, Fickenscher KA, Walsh I,
2008 Estimation of Cumulative Effective Doses from Diagnostic and Interventional Radiological Examinations in Pediatric Oncology Patients. Thomas KE, Ahmed BA, Shroff P, Connolly B, Chong AL, Gordon C
2009 Case Report: Multi-Modality Imaging Manifestations of the Meckel's Diverticulum in Pediatric Patients. Kotecha MK, Bellah RD, Pena AH, Mattei P
2009 Educational: MR Urography: Functional Analysis – Made Simple! Khrichenko D, Darge K
2009 Scientific: MRI Findings in the Term Infant with Neonatal Seizures. An Etiologic Approach. Rebollo Polo M, Hurteau-Miller J, Laffan E, Tabban H, Naser H, Koujok K
2010 Scientific: Dual Phase Intravenous Contrast Injection in Pediatric Body CT. Mann E, Alzahrani A, Padfield N, Farrell L, BenDavid G, Thomas K
2010 Educational: Hemangiomas Revisited: The Useful, the Unusual and the New. Restrepo R, Palani R, Matapathi U, Altman N, Cervantes L, Duarte AM, Amjad I
2010 Case Report: MRI of Congenital Urethroperineal Fistula. Mahani M, Dillman J, Pai D, Park J, DiPietro M, Ladino Torres M

2011 Scientific: Updated Estimated Radiation Dose for Pediatric Nuclear Medicine Studies. Grant F, Drubach L, Treves ST, Fahey F
2011 Educational: Button Battery Ingestion in Children: What the Radiologist Must Know. Kappil M, Rigsby C, Saker M, Boylan E
2011 Case Report: MR Imaging Features of Fetal Mediastinal and Intrapericardial Teratomas. Rubio E, Kline-Fath B, Calvo-Garcia M, Guimaraes C
2012 Case Report: Neuroimaging in Hemiplegic Migraine: Cases and Review of the Literature. Stence NV, Kedia S, Maloney JA, Armstrong-Wells J, Bernard T
2012 Educational: Primary and Secondary Amenorrhea in Pediatric Patients: From the Beginning to the End. Cortes C, Ramos Y, Restrepo R, Diaz A, Sequeira L, Lee EY
2012 Scientific: Prenatal Evaluation of Limb Body Wall Complex with Emphasis on MRI. Aguirre-Pascual E, Victoria T, Johnson A, Chauvin N, Coleman B, Epelman M
2013 Scientific Exhibit: TIEPhantom Iterative Reconstruction Technique (PIRT)-a quantitative ALARA method to test iterative reconstructions effect on image quality and dose in the pediatric population Anne McLellan, DO, Medical, Radiology, Phoenix Children's Hospital, Phoenix, AZ; James Owen, MS, Robyn Augustyn, BSRT (R)(CT), John Egelhoff, DO, John Curran, MD, Jeffrey Miller, MD, Richard Southard, MD, William Pavlicek, PhD, Richard Towbin, MDMorbidity associated with delayed treatment of cholelithiasis in pediatric patients with sickle cell disease Heather Imsande, MD, Boston Medical Center, Boston, MA
2014 Case Report: Contrast-enhanced Ultrasound of Pediatric Abdominal Visceral Trauma: Initial Data; Beatrice Dionigi, Carol Barnewolt, Jill Zalieckas, David Mooney, Harriet Paltiel, MD, Department of Surgery, Boston Children's Hospital, Boston, MA
2014 Educational Poster: The Pediatric Breast: What to do with Lumps and Bumps; Natalie Burns, University of Washington Medical Center, Seattle, WA, Habib Rahbar, Teresa Chapman
2014 Scientific Poster: Towards radiation dose reduction in MDCT with iterative reconstruction for the prenatal diagnosis of skeletal dysplasia: the minimum radiation dose required to evaluate the normal fetal bones?; Chihiro Tani, Hiroshima University Hospital, Hiroshima, Japan, Yoshinori Funama, Chikako Fujioka, Kazuo Awai
2015 Case Repot: Congenital Portocaval Shunt: A Rare Entity, Arash Zandieh, MD, Georgetown University Hospital, Washington, DC, Christabel Lee, Frank Volberg
2015 Educational Poster: Pediatric Radiology Economics and Politics in Jeopardy: A Primer, David Swenson, MD, The Alpert Medical School of Brown University, Providence, RI, Cassandra Sams
2015 Scientific Poster: Infant Bone Age Estimation Based on Fibular Shaft Length: A Validation Study, Andy Tsai, MD, PhD, Boston Children's Hospital, Boston, MA, Catherine Stamoulis, Sarah Bixby, Michael Breen, Susan Connolly, Paul Kleinman

The top candidates being considered for a Caffey Poster Award from the Scientific and Educational categories will present their work during one of the scheduled breaks in the exhibit hall.

For a list of Caffey Award papers and posters prior to 2005, please visit the SPR website.

2016 Edward B. Neuhauser/Jacques Lefèbvre Lecture
Multimodal Imaging of the Molecular, Cellular and Tissue Events Underlying Embryonic Development

Scott E. Fraser, PhD
Provost Professor
University of Southern California

Scott E. Fraser, PhD, has a long-standing commitment to quantitative biology, applying the tools of chemistry, engineering and physics to problems in biology and medicine. His personal research centers on imaging and molecular analysis of intact biological systems, with an emphasis on early development, organogenesis and medical diagnostics.

After training in physics (B.S., Harvey Mudd College, 1976) and biophysics (Ph.D., Johns Hopkins University, 1979), he joined the faculty at UC Irvine and rose through the ranks to become Chair of the Department of Physiology and Biophysics. In 1990 he moved to Caltech to serve as the Anna L. Rosen Professor of Biology and the Director of the Biological Imaging Center. He is deeply committed to interdisciplinary training and translational research, having helped found the Caltech Brain Imaging Center and the Kavli Institute of Nanoscience, as well as serving as the Director of the Rosen Center for Biological Engineering. In fall 2012, he moved to USC to take a Provost Professorship in the Dornsife College of Letters, Arts and Sciences, Children's Hospital Los Angeles, Keck School of Medicine and the Viterbi School of Engineering. He remains active in interdisciplinary research and serves as the Director of Science Initiatives as well as the Elizabeth Garrett Chair of Convergent Biosciences for the USC campuses.

ESPR GENERAL INFORMATION

The aims of the European Society of Paediatric Radiology are the following:
– to organise and bring together physicians involved in the field of paediatric imaging
– to contribute to the progress of paediatric imaging particularly within but also outside Europe
– to encourage training and education with other branches of medical imaging and paediatrics in clinical, scientific, education and research field

Past Presidents & Sites of Previous Meetings
1964 Jacques Lefebvre, Paris, France
1965 Ulf Rudhe, Stockholm, Sweden
1966 John Sutcliffe, London, England
1967 Herbert Kaufmann, Basel, Switzerland
1968 Arnold Lassrich, Hamburg, Germany
1969 Ksawery Rowinsky, Warsaw, Poland
1970 Guido Lannacone, Rome, Italy
1971 Gregers Thomsen, Copenhagen, Denmark
1972 Jacques Sauvegrain, Paris, France
1973 Roy Astley, Birmingham, UK
1974 Per-Erik Heikel, Helsinki, Finland
1975 Klaus Knapp, Madrid, Spain
1976 Ole Eklof, Stockholm, Sweden
1977 Andreas Giedion, Lucerne, Switzerland
1978 Noemi Perlmutter-Cremer, Brussels, Belgium
1979 Klaus Dieter Ebel, Cologne, Germany
1980 The Dutch Group of Paediatric Radiologists, The Hague, Netherlands
1981 Gunnar Stake, Oslo, Norway
1982 Antonin Rubin, Prague, Czechoslovakia
1983 Clement Fauré, Paris, France
1984 Gianfranco Vicchi, Florence, Italy
1985 Elizabeth Sweet, Glasgow, Scotland
1986 Javier Lucaya, Barcelona, Spain
1987 Denis Lallemand (ESPR) and Derek Harwood-Nash (SPR), Toronto, Canada
1988 Daniel Nussle, Montreux, Switzerland
1989 Noel Blake, Dublin, Ireland
1990 Helmut Fendel, Munich, Germany
1991 Hans Ringertz (ESPR) and Donald Kirks (SPR), Stockholm, Sweden
1992 Bela Lombay, Budapest, Hungary
1993 Donald Shaw, London, UK
1994 Fred Avni, Brussels, Belgium
1995 Peter Kramer, Utrecht, Netherlands
1996 Paul Thomas (ESPR) and Kenneth Fellows (SPR), Boston, USA
1997 Ulrich Willi, Lugano, Switzerland
1998 Basilos Theodoropoulos, Rhodes, Greece
1999 Jacob Bar-Ziv and Gabriel Kalifa, Jerusalem, Israel
2000 Jose Fonseca Santos, Lisbon, Portugal
2001 Francis Brunelle (ESPR) and Janet Strife (SPR), Paris, France
2002 Tore Nordshus, Bergen, Norway
2003 Paolo Tomà, Genoa, Italy
2004 Jochen Troeger, Heidelberg, Germany
2005 Veronica Donoghue, Dublin, Ireland
2006 Richard Fotter (ESPR) and George Taylor (SPR),Montreal, Canada
2007 Goya Enriquez, Barcelona, Spain
2008 Stephen Chapman, Edinburgh, UK
2009 Mithat Haliloglu, Istanbul, Turkey
2010 Jean-François Chateil, Bordeaux, France
2011 Catherine Owens (ESPR) and Dorothy Bulas (SPR), London, United Kingdom
2012 Maria Argyropoulou, Athens, Greece
2013 Éva Kis, Budapest, Hungary
2014 Rutger A. J. Nievelstein, Amsterdam, The Netherlands
2015 Michael Riccabona and Erich Sorantin, Graz, Austria

FUTURE MEETINGS

2017	May 30 – June 3, 2017	Davos, Switzerland
2018	June 18 – June 22, 2018	Berlin, Germany

Officers 2015 – 2016

President, Catherine M. Owens (London, United Kingdom)
General Secretary, Maria I. Argyropoulou (Ioannina, Greece)
Treasurer, Philippe Petit (Marseille, France)
Congress Chair/Research Committee Chair, Karen Rosendahl (Bergen, Norway)
Future Congress Chair, Jacques F. Schneider (Basel, Switzerland)
Past Congress Chair, Michael Riccabona (Graz, Austria)

COMMITTEES

Education	Rutger A. J. Nievelstein
Publications Committee	Veronica Donoghue
Research Committee	Karen Rosendahl
(includes the European Excellence Network	Erich Sorantin (Co-chair) on Paediatric Radiology)
Congress Committee	Karen Rosendahl
jESPeR Committee	Tom Anthony Watson

TASKFORCES

ABDOMEN (GI & GU)
M. Riccabona (Chair)
F. Avni
L. Blickman
B. Damasio
K. Darge
M.L. Lobo
H.J. Mentzel
A. Ntoulia
L.S. Ording-Müller
F. Papadopoulou
P. Vivier
U. Willi
P.H. Vivier

CHILD ABUSE TASK FORCE
A. Offiah (Chair)
C. Adamsbaum (Co-chair)
R. van Rijn

CT & DOSE
C.M. Owens (Chair)
E. Sorantin (Co-chair)
R.J. Nievelstein
G. Enriquez
P. Toma

MUSCULOSKELETAL
K. Rosendahl (Chair)
P. Toma (Co-chair)
C. Treguier
C. Adamsbaum
I. Barber
L.S. Ording-Müller
P. Humphries
L. Tanturri De Horatio
P. Simoni

PAEDIATRIC NEURORADIOLOGY
M. Argyropoulou (Chair)
A. Rossi (ESNR)
N. Girard (ESPR, ESNR)
J.F. Chateil
C. Adamsbaum
E. Vasquez
V. Donoghue

ONCOLOGY
A. Smets (Chair)
H. Brisse (previous chair)

Honorary Members

1964 John Caffey (USA)
1964 Lutz Schall (Germany)
1965 Sven R. Kjelberg (Sweden)
1965 Edward B. D. Neuhauser (USA)
1966 Jacques Lefebvre (France)
1973 Hardy M. Geffert (Hungary)
1973 Ksawery Rowinski (Poland)
1974 Frederic Silverman (USA)
1975 Ulf G. Rudhe (Sweden)
1979 John Kirkpatrick (USA)
1979 Arnold Lassrich (Germany)
1979 Jacques Sauvegrain (France)
1982 Clement Fauré (France)
1982 Andes Giedion (Switzerland)
1983 Eberhard Willich (Germany)
1984 Roy Astley (England)
1987 Jean Bennet (France)
1987 Ole Eklof (Sweden)
1987 Charles A. Gooding (USA)
1987 John Holt (USA)
1987 Andrew Poznanski (USA)
1987 D.C. Harwood-Nash (USA)
1987 Hooshang Taybi (USA)
1988 Herbert Kaufmann (Germany)
1989 Bryan Cremin (South Africa)
1989 Klaus D. Ebel (Germany)
1989 Helmut Fendel (Germany)
1989 Elizabeth Sweet (Scotland)
1990 Donald Kirks (USA)
1991 Alan Chrispin (England)
1991 Edmund Franken (USA)
1991 Daniel Nussle (Switzerland)
1991 Beverly Wood (USA)
1992 Walter Berdon (USA)
1993 Javier Lucaya (Spain)
1993 Wilhelm Holthusen (Germany)
1994 Noemie Perlmutter (Belgium)
1994 Hans Ringertz (Sweden)
1994 Donald Shaw (England)
1996 Robert Lebowitz (USA)
1996 Bela Lombay (Hungary)
1997 Yan Briand (France)
1997 Philip Small (England)
1997 N. Thorne Griscom (USA)
1998 Alan Daneman (Canada)
1998 Gabriel Kalifa (France)
1999 Michael Grunebaum (Israel)
1999 Paul Thomas (Ireland)
2000 Noel Blake (Ireland)
2000 Peter Kramer (Netherlands)
2000 Gunnar Stake (Norway)
2001 Janet Strife (USA)
2001 Robert Brasch (USA)
2001 Max Hassan (France)
2001 Yacob Bar-Ziv (Israel)
2002 Sven Laurin (Sweden)
2003 Aldo Pelizza (Italy)
2003 Giampiero Beluffi (Italy)
2003 Helen Carty (England)
2003 Bruce Parker (USA)

2004 Christine Hall (England)
2004 Andrzej Marcinski (Poland)
2005 Ulrich Willi (Switerland)
2005 Jean-Philippe Montagne (France)
2005 Giuseppe Farielo (Italy)
2006 Francis Brunelle (France)
2006 Laurent Garel (Canada)
2006 Morteza Meradji (Netherlands)
2006 Alan E. Oestreich (USA)
2007 Marianne Spehl (Belgium)
2007 Gabriel Benz-Bohm (Germany)
2007 Pedro A. Daltro (Brazil)
2007 Richard Fotter (Austria)
2008 Jose Fonseca-Santos (Portugal)
2008 Ingmar Gassner (Austria)
2008 Tom Slovis (USA)
2008 Rita Teele (New Zealand)
2009 Reinhart Schumacher (Germany)
2009 Nicholas Gourtsoyiannis (Greece)
2009 Ines Boechat (USA)
2009 Steve Chapman (United Kingdom)
2009 Jochen Troeger (German)
2009 Ernst Richter (Germany)
2010 Veronica Donoghue (Ireland)
2010 Freddy Avni (Belgium)
2010 François Diard (France)
2010 Paolo Toma (Italy)
2011 R. De Bruyn (United Kingdom)
2011 Goya Enriquez (Spain)
2011 Cristiàn Garcia (Chile)
2011 Paul Kleinman (USA)
2011 George Taylor (USA)
2012 Corinne Veyrac (France)
2013 Daniele Pariente (France)
2014 RosemaryArthur (Scotland)
2014 Mithat Haliloglu (Turkey)

Gold Medalists

2007 Javier Lucaya (Spain)
2008 Gabriel Kalifa (France)
2010 Ulrich Willi (Switzerland)
2011 Richard Fotter (Austria)
2012 Francis Brunelle (France)
2013 Fred Avni (Belgium)
2014 Veronica Donoghue (Ireland)
2015 Guy H. Sebag (France)

Jacques Lefebvre Awards

1977 Ringertz H. (Sweden)	The width of cranial sutures in neonates: an objective method of assessment.
1978 Garel L. (France)	Xanthogranulomatous pyelonephritis in children: 19 cases
1979 Brauner M. (France)	Metrizamide myelography in infants with brain injury to the brachial plexus
1980 Spehl-Robberech M. (Belgium)	Ultrasonic study of the pancreas in cystic fibrosis
1981 Garel L. (France)	The renal sinus: an important anatomical landmark in children
1982 Couture A. (France)	Ultrasonographic exploration of cerebral malformations
1983 Brunelle F. (France)	Percutaneous cholecystography in children
1984 Veyrac C. (France)	Ultrasound of normal and pathologic choroid plexus
1985 Avni F. (Belgium)	Utrasonic demonstration of abnormal and atypical gallbladder content in newborns
1986 Pariente D. (France)	Biliary tract involvement in children with Langerhans cell Histiocytosis
1987 Sellier N. (France)	Focal cortical dysplasia: a rare cause of epilepsy
1988 Deeg K. H. (Germany)	Pulsed Doppler sonographic measurement of normal values for the flow velocities incerebral arteries of healthy infants
1989 Winkler P. (Germany)	Major pitfalls in the Doppler examination of cerebral vascular system
1990 Garel C. (France)	Laryngeal ultrasonographic study in infants and children. Pathological findings
1991 Pracros J. P. (France)	Systemic study of superior mesenteric vessels in abdominal ultrasound

1992 Hollman A. (UK)	Colour Doppler imaging of the acute paediatric scrotum
1993 Chami M. (France)	Ultrasound contribution in the analysis of the newborn infant normal foot and club foot: preliminary study
1994 Adamsbaum C. (France)	Vermian agenesis without posterior fossa cyst
1995 Sebag G. (France)	Magnetic resonance angiography of paediatric renal transplants with quantification of allograft blood flow
1996 Rohrschneider W. (Germany)	US, CT and MR imaging. Characteristics in nephroblastomatosis: evaluation of 23 Patients
1997 Hertz-Pannier L. (France)	Non-invasive preoperative motor mapping in children with brain functional MRI
1998 Nicaise N. (Belgium)	Dynamic Gd-DTPA-enhanced T1W turbo field echo imaging: Interest in paediatricrenal evaluation
1999 Rypens F. (Belgium)	Fetal lung volume estimation by MRI: normal values and potential use
2000 Ziereisen F. (Belgium)	Doppler assessment of pulsatility index (PI) of the uterine artery in girls around puberty
2001 Lidegran M.K (Sweden)	MRI and echocardiography in assessment of ventricular function in atrially corrected transposition of the great arteries
2002 Cassart M. (Belgium)	The assessment of fetal uronephropathies by MR imaging
2003 Boddaert N. (France)	18F-Fluoro-L-Dopa PET scan of focal forms of hyerinsulinism of infancy
2004 Jourdan C. (Germany)	US evaluation of intima-media thickness (IMT) and elastic properties distensibility,stiffness and incremental modulus of elasticity of the common carotid artery as a markerof early vascular damage in children with chronic renal failure and reference values.
2005 Kellenberger C.J. (Switzerland)	Cardiovascular MRI for investigating Newborns and Infants with Congenital Heart Disease.
2006 Ou P. (France)	Magnetic resonance assessment of aortic flow dynamics and aortic arch geometry in patients with successful repair of coarctation of the aorta
2007 Sporcq C. (Belgium)	Reappraisal of the sonographic characteristics of the fetal and newborn kidney: introducing the cortico-medullary ratio
2008 Damasio M. B. (Italy)	Which is the best imaging modality to capture bone erosions in juvenile idiopathic arthritis?
2009 McDonald K. (UK)	DWI to assess chemotherapy response in solid tumors
2010 Ording-Müller L.S. (Norway)	Development of the wrist. Normal standards based on MRI for 6–15 year old
2011 Duran C. (Spain)	Voiding urosonography: normal and abnormal appearance of the urethra
2012 Vazquez J. (Spain)	External manual reduction with US assistance: a new procedure for pediatric idiopathic ileocolic intussuseption
2013 Viehweger A. (Germany)	The Gini-coefficient: A new method to assess fetal brain development
2014 Kinner S.	MR colonography with diffusion weighted imaging (DWI) in children and adolescents with inflammatory bowel disease (IBD)
2015 Shur J. (United Kingdom)	Size matters – Dose reference levels (DRL's) based on patient thickness, instead of age

Poster Awards

1994 Gomes H. (France)	Neonatal hip sonography from anatomy to sonography
1995 Schmit P. (France)	Imaging of cystic mesenchymal hamartomas of the liver. Review of 13 patients
1997 Schmit P. (France)	Congenital hepatic vascular malformations in children
1998 Brisse H. (France)	In utero MRI. Normal gyral development of the human brain
2000 Valle M. (Italy)	High-frequency ultrasound detection of the brachial plexus in newborns and infants
2001 Rohrschneider W. K (Germany)	Static dynamic MR-urography – simultaneous morphological and functional evaluation of the urinary tract
2002 Owens C.M (UK)	The utility of MRI in the assessment of symptomatic adenoidal hypertrophy and rhinosinusitis in children. pre and post medical therapy
2003 Schumacher R. (Germany)	Sonographical anatomy of the anal sphincter complex (ASC) and levator ani muscle inneonates and infants
2004 Mentzel H.-J. (Germany)	Comparison of whole body STIR MRI and 99mTc-methylene diphosphonate scintigraphy in the examination of children with suspected multifocal bone lesions
2005 Enriquez G (Spain)	Prenatal assessment of lung hypoplasia in congenital diaphragmatic hernia: correlation between volumetric MRI and biometric ultrasound measurements
2006 Sorge I. (France)	Reduction of radiotherapy in children with early stages of Hodgkin's lymphoma, Influenced by a new imaging and FDG-PET based strategy
2007 Punwani S. (UK)	Effects of reducing radiation dose on lung nodule detection
2008 Chateil J.-F. (France)	Imaging of acquired spinal cord lesions and spinal canal pathology in children
2009 Barez MG. (Spain)	Spectrum of imaging findings in the brachial apparatus anomalies
2010 Brun M. (France)	Diffusion tension imaging in attention
2011 Fonda C. (Italy)	3T arterial spin labelling (ASL) in pediatric patients
2012 Arthurs O. (UK)	Diffusion weighted MRI of the fetal brain in intrauterine growth restriction.
2013 Duran C. (Spain)	Voiding urosonography: a pictorial essay of the lower urinary tract pathology
2014 Tanase A. (France)	Ultra low dose imaging for the follow up of idiopathic scoliosis: feasibility of spinal 3D reconstructions and reproducibility of 3D parameters reproducibility- a pilot study
2015 Napolitano M. (Italy)	MR assessment of Crohn's disease activity in a paediatric population: correlation with clinical index of disease
2015 Kljucevsek D. (Slovenia)	Contrast- enhanced Ultrasound (CEUS) of bowel wall with quantitative assessment of Crohn's disease activity in child: a case report

Young Researcher Awards

2003 Brun M. (France)	Phonological Decoding in Dyslexic Children: Activation Pattern of FMRI
2004 Barnacle A.B (UK)	Image-guided percutaneous biopsy of soft tissue masses in children
2005 Raissiki M. (Greece)	Eye-lens Bismuth Shielding in Pediatric Head CT Examinations

2006 Sorge I. (Germany)	Reduction of radiotherapy in children with early stages of Hodgkin's lymphoma, influenced by a new imaging and FDG-PET based strategy
2007 Alison M. (France)	In vivo targeting of macrophagic activity with MRI contrast agent (USPIO) in an experimental model of neonatal brain lesions
2008 Herrmann J. (Germany)	Capsular arterial collateralisation after paediatric liver transplantation
2010 Arthurs O. (UK)	MR Voiding cystourethrography for vesico-ureteric reflux in unsedated infants
2011 Gupta N. (UK)	Predictors of vesicoureteric reflux in infants with UTI using NICE criteria
2012 Laborie L. B. (Norway)	Associations between femoroacetabular impingement and hip dysplasia as demonstrated radiographically. Preliminary results
2013 Lochbühler N. (Switzerland)	MRI assessment of inflammatory activity and mandibular growth following intra-articular TMJ steroid injection in children with JIA
2014 Slaar A. (The Netherlands)	A clinical decision rule for acute wrist trauma in children
2015 Shelmerdine S. (UK)	Achondroplasia: Really Rhizomelic

President's Awards

2004 Kilian A.K. (Germany)	Prenatal magnetic resonance (MR) lung volumetry of congenital diaphragmatic hernia(CDH): comparison with the clinical outcome and the necessity of extracorporealmembrane oxygenation (ECMO)
2005 Larke A. (Ireland)	MRI findings as an indication of underlying genetic lesions in congenital malformations of the brain
2007 Duran C. (Spain)	Voiding cystosonography for the study of the urethra
2008 Calder A. (UK)	Computed tomography compared with ultrasound and chest radiography in childrenwith pleural empyema
2009 Senocak E. (Turkey)	MRI and DWI findings in children with hemophagocytic lymphohistiocytosis: tendency for symmetricity
2010 Franchi-Abella S. (France)	Congenital portosystemic shunt: complications and outcome after closure: about 19 pediatric cases
2011 Punwani S. (Greece)	MRI vs. PET/CT for detection of focal splenic lesions in paediatric and adolescent lymphoma at initial staging
2012 Xenophontos P. (Greece)	Detection of primary sclerosing cholangitis (PSC)-type lesions in children with inflammatory bowel disease via MRCP: a relative risk measures analysis
2013 Pasztor G. (Hungary)	The importance of pyelectasis – report of a clinical study in progress
2014 Littooij A. S. (The Netherlands)	Whole-body MRI for staging of paediatric lymphoma: prospective comparison to an FDG-PET/CT-based reference standard
2015 C. Wieser (Austria)	Vessel flexibility index as a new marker for cardio-vascular disease – a pilot study

2016 ESPR Honorees

ESPR Gold Medal Award 2016

Professor Paolo Tomà

Professor Paolo Tomà qualified in medicine from the University of Genoa in 1976. He trained in both radiology and paediatrics in Genoa. Between 1980 and 1994 he worked as a radiologist in the department of Imaging, G. Gaslini Institute, first as a registrar – later in a more senior position. From 1992 to 1994 he was Director of the Ultrasound division. Between 1995 and 2009 he was Director of Radiology, and between 2005 and 2009 he also held the position of Director of Department of Imaging at the G. Gaslini Institute in Genoa.

Prof. Tomà was appointed Professor of Paediatric Radiology in "Radiology and Paediatric Postgraduate Schools" at Genoa University in 1990, and for the last 20 years he has mentored, inspired, and led a strong committed group of paediatric radiologists at the Gaslini Institute. Since 2010, he has held a similar position at the Bambino Gesù Hospital in Rome.

Prof. Toma has published widely on several topics, and has made major contributions within radiation protection, early screening for hip dysplasia, and within chest imaging. He has published over 200 papers in peer reviewed journals, book chapters and books and has given a substantial number of invited lectures across the world. He was President of the Italian Society of Paediatric Radiology from 1996 to 2000. He has been a member of the Editorial board in Pediatric Radiology from 2011.

Internationally, he served as Vice-President of the European Society of Paediatric Radiology (ESPR) from 1999 to 2002, as President from 2002 to 2003, as senior councillor from 2006 to 11 and as one of three Trustees for the past few years, and now one of "three wise men" supporting the ESPR Board. Indeed, Prof Toma is sage, with the gentle ability to differentiate between important and unimportant matters. Just as Dwight D. Eisenhower's principle that guided him through his hugely successful career as General and President: "What is important is seldom urgent and what is urgent is seldom important." Furthermore, he has served as a member of the ESR Subspecialties Committee from 2008 to 2011, mentored numerous young radiologists and contributed to the annual ESPR meetings over nearly four decades. His position as a leader within paediatric radiology has resulted in of the training numerous talented young Italian paediatric radiologists

Professor Karen Rosendahl

ESPR 2016 Honorary Members

Dorothy I. Bulas, MD, FACR, FAAP

Dorothy I. Bulas, MD, FACR is board certified in both pediatrics and radiology, completing her pediatric training at New York Hospital and her radiology residency at the Albert Einstein School of Medicine in NYC. She is professor of Pediatrics and Radiology at the George Washington University School of Medicine and serves as Vice Chief of Academic Affairs, Program Director of Pediatric Radiology, Section Head of Ultrasound and Fetal Imaging at Children's National Medical Center in Washington DC.

Dr. Bulas is a fellow of the American Institute of Ultrasound in Medicine, the American College of Radiology, Society of Radiologists in Ultrasound and American Association of Pediatrics. She is a past President of the Society for Pediatric Radiology helping organize the combined ESPR/SPR 2011 IPR meeting in London as co-president. She is a member of the Image Gently Steering Committee.

Dr. Bulas has been a member of the American College of Radiology Pediatric Radiology Practice Guidelines Committee, was Section Chair for Certificate of Qualification in Pediatrics for the American Board of Radiology, a member of the ACGME milestones committee for radiology residency and chaired the milestones committee for the pediatric radiology fellowship program. Since 2014 she has been the chair of the educational refresher course series at the RSNA.

Dr. Bulas's main areas of interest are fetal imaging, pediatric ultrasound, transcranial Doppler, and radiation safety. She has authored over 120 peer reviewed manuscripts, and 70 invited articles and chapters. She is an editor of the recently published "Fundamental and Advanced Fetal Imaging US and MRI". She serves as a reviewer for multiple journals and is perinatal Section Editor for the Pediatric Radiology Journal.

International outreach and education have been important focuses in her career. She has delivered over 120 national and international invited lectures. She has helped plan multiple pediatric radiology conferences in the United States as well as internationally in countries such as Poland, Russia, South Africa, Haiti, Eritrea, and Brazil**.** A founding member of the World Federation of Pediatric Imaging, Dr. Bulas is chair of the WFPI Education Committee. She is a member of the ACR and RSNA international outreach committees.

On a personal note, Dr. Bulas is married to an adult neurologist and has two sons, one graduating from medical school this year, the other working at Google. She loves to travel and enjoys many outdoor activities particularly hiking and skiing.

Professor Karen Rosendahl

Éva Kis, MD, PhD

Dr Éva Kis, MD, PhD, qualified in medicine from the Semmelweis University, Budapest in 1974. She trained in radiology, paediatrics and paediatric radiology at the same university, followed by visiting fellowships at the Kinderklinik in Heidelberg, as well as at the Hospital for Sick Children in Toronto. In 1992 she successfully defended her PhD thesis on Imaging of the developmental anomalies of the paediatric urinary tract. Between 1990 and 2014 she held the posts of Associate Professor and Head of Radiology Departments of Imaging and Paediatrics at the Semmelweis University. Between 2010 and 2014, she additionally, held the position of Director of Department of Imaging and Medical Instrumentation, Semmelweis University, Faculty of Health Sciences.

Dr Kis's major interest has been ultrasound, and in particular imaging of the urinary tract. She has written over 110 peer reviewed papers, two books and ten book chapters, and given numerous invited lectures across the world. She has been a regular reviewer for Pediatric Radiology, European Radiology, Pediatrics and Hungarian Radiology. Nationally, Dr Kis held the positions of Secretary for the Hungarian Paediatric Radiology Committee, board member of the Society of Radiologists and board member of the Ultrasound Committee.

Dr Kis attended her first ESPR meeting in Dublin 1989. In 1992 she was the secretary for the ESPR meeting in Budapest, in 2002 she organized the ECPR course in musculoskeletal radiology. Between 2005 and 2009 she was a member of the ECR Paediatric Subcommittee and in 2013 she was President of the very successful ESPR annual meeting in Budapest. She was a member of the ESPR board from 2000 to 2013. Furthermore, she is a member of the European Radiology Society and the German Paediatric Radiology Society.

During the past decades, Dr Kis has contributed hugely to global outreach, and continues her altruistic work within international outreach and education. She has undertaken periods of voluntary work in Tanzania, India, Cambodia and Malawi, and is currently an ESPR representative in the World Federation of Paediatric imaging (WFPI).

Eva is married and has two children. She loves music, travelling and being with friends. She has dedicated her professional life to the care of children and is a most worthy recipient for ESPR honorary membership!

Professor Karen Rosendahl

Catherine Mary Owens, MBBS, FRCR, FRCP

Dr Catherine Mary Owens, MBBS, FRCR, FRCP, qualified in medicine from St Bartholomew's Hospital Medical School, London in 1984. She has been a Consultant Radiologist at Great Ormond Street Hospital (GOSH) NHS Trust since 1996 and is an Honorary Reader at University College London (UCL). She has, during the past two decades, contributed significantly to the art of Paediatric Radiology, both nationally and internationally. In 2015 she was elected President of the European Society of Paediatric Radiology (ESPR), after having served as Treasurer from 2003 to 2007 and General Secretary from 2008 to 2015. During her time in office, she has revamped and improved the ESPR internal structure, facilitated research and built strong links and partnerships with the European Society of Radiology (ESR), via ESR Eurosafe, the establishment of a Research Initiative hosted by the EIBIR (European Institute of Biomedical Imaging) and with other relevant sub specialities. Since 2014 she has served as Senior Councillor in the ESR being responsible for the Subcommittee for subspecialty societies and allied health professionals.

In 2011 she hosted a successful International Congress of Paediatric Radiology (IPR) in London together with her co President Dr. Dorothy Bulas. Dr Owens' major interest is in cardiothoracic CT, with a focus for imaging the heart and lungs, and a keen research interest in diffuse lung disease and the immune compromised lung in children. She has written over 120 peer reviewed papers, 29 chapters, edited 2 books and delivered more than 160 invited lectures. Moreover, she has secured substantial funding, in excess of £5million for national and international research projects. She is subeditor of European Radiology and is on the Editorial Board of seven major international journals. She has been visiting Professor to numerous international departments including Harvard, Toronto Sick Kids, Childrens' Hospital of Philadelphia (CHOP), and Cincinnatti Childrens' Hospital.

Nationally, she built a world renowned team at GOSH, as Clinical Director for 6 years, led installation of PACS, developed state of the art body MRI and dual source CT and introduced Cardiac MR/CT to the Trust, reducing radiation burden to children. She is a Royal College of Radiology assessor for trainees and helps supervise radiology residents and radiology fellows at GOSH. She writes guidelines for the Delphi database for paediatric thoracic imaging at RCR. She is UK paediatric imaging liaison with Public Health England (PHE) previously NRPB and holds EU grants for paediatric dose reference levels via ESR where she is on the radiation Protection working group. Within Europe she is a point of contact/supervisor for the allocated ESOR scholars at GOSH. Dr Owens has a major International role as a teacher within Paediatric radiology facilitating guideline/protocol sharing to standardise and improve the care of children.

On a personal note, she has been happily married to Professor Paul Veys, Director of Bone Marrow transplantation at GOSH, for 30 years and they have 3 children: Charles, Delphine, Eloise and a much beloved dog Lara. Her work, family and friends are central to her joie de vivre, giving her the considerable energy and enthusiasm to embrace life to the full.

Professor Karen Rosendahl

SOCIAL EVENTS

SPR Research and Education Foundation Fun Run

Underwritten by Texas Children's Hospital
Monday, May 16, 2016
6:00 a.m.
Join us for a run through Millennium Park and get your day off to a great start! Runners and walkers are all welcome.
Entrance fee is $25 and includes a T-Shirt.

Welcome Reception
Monday, May 16, 2016
6:30-7:45 p.m.
Preston Bradley Room of the Chicago Cultural Center
Hors d'oeuvres and Refreshments
Business Casual Attire

Reception and Annual Banquet
Thursday, May 19, 2016
7:30-11:00 p.m.
Fairmont Hotel
Reception, Dinner and Dancing
Business Casual Attire

Activities
The Fairmont Hotel employs a full-service concierge staff who are happy to share their detailed knowledge of Chicago, Illinois and the surrounding area. You may contact them by telephone at 1-312-565-8000.

Additional information is included on the IPR website.

FULL PROGRAM SCHEDULE

For the scientific sessions, see the Author Index to view the countries represented by the Presenting Authors.

CATEGORICAL COURSE ABSTRACTS

Sunday, May 15, 2016

10:00 AM	**5:30 PM**	**Registration**
1:00 PM	**1:15 PM**	**Opening Ceremony** James S. Donaldson, MD, FACR (USA) and Karen Rosendahl, MD, PhD (Norway)
1:15 PM	**1:30 PM**	**Categorical Course Welcome** Michael J. Callahan, MD, (USA) and Stein M. Aukland, MD, PhD (Norway)
1:30 PM	**3:00 PM**	**Categorical Course: Chest** *Moderators: Paul G. Thacker, MD (USA) and Catherine M. Owens, MBBS, FRCR (UK)*
1:30 PM	*1:40 PM*	**CT or MR for Imaging of Cystic Fibrosis?** Pierluigi Ciet, MD, PhD (The Netherlands)
1:40 PM	*1:50 PM*	**Imaging Scoring Systems for Cystic Fibrosis – Helpful or Not?** Paul G. Thacker, MD (USA)
1:50 PM	*2:00 PM*	**Misplaced Central Venous Catheters in the Chest** George A. Taylor, MD, FACR (USA)
2:00 PM	*2:10 PM*	**Pre-natal Evaluation of Congenital Diaphragmatic Hernia** Catherine Garel, MD (France)
2:10 PM	*2:20 PM*	**Imaging Interstitial Lung Disease in Children: An Update** Catherine M. Owens, MBBS, FRCR (UK)
2:20 PM	*2:30 PM*	**MR Imaging Technique of the Chest for Pulmonary Nodule** Sureyya B. Gorkem, MD (Turkey)
2:30 PM	*3:00 PM*	**Q&A with RSNA Diagnosis Live™**
3:00 PM	**3:30 PM**	**Break**
3:30 PM	**4:40 PM**	**Categorical Course: Cardiovascular** *Moderators: Monica Epelman, MD (USA) and Franz Wolfgang Hirsch, MD (Germany)*
3:30 PM	*3:40 PM*	**Anatomic Causes for Renovascular Hypertension** Jung-Eun Cheon, MD, PhD (Korea)
3:40 PM	*3:50 PM*	**Role of US in Renovascular Hypertension** Ethan A. Smith, MD (USA)
3:50 PM	*4:00 PM*	**Role of CT in Renovascular Hypertension** Monica Epelman, MD (USA)
4:00 PM	*4:10 PM*	**Role of MRI in Renovascular Hypertension** Franz Wolfgang Hirsch, MD (Germany)
4:10 PM	*4:20 PM*	**Role of Angiography in Renovascular Hypertension** Derek J. Roebuck, MD (UK)
4:20 PM	***4:30 PM***	**Q&A with RSNA Diagnosis Live™**
4:40 PM	**6:10 PM**	**Categorical Course: Neuroradiology** *Moderators: Sanjay P. Prabhu, MBBS, FRCR (USA) and Nuno Canto Moreira, MD, PhD (Sweden)*
4:40 PM	*4:50 PM*	**Imaging the Premature Brain: New Knowledge** Stein M. Aukland, MD, PhD (Norway)
4:50 PM	*5:00 PM*	**Hydrocephalus: Imaging Update** Nuno Canto Moreira, MD, PhD (Sweden)
5:00 PM	*5:10 PM*	**3-D Printing for Pediatric Neuro Imaging** Sanjay P. Prabhu, MBBS, FRCR (USA)
5:10 PM	*5:20 PM*	**Abusive Head Trauma: The Role of DWI, SWI and MRS** Jean-Francois Chateil, MD, PhD (France)
5:20 PM	*5:30 PM*	**Spinal Findings in the Setting of Child Abuse** Michael A. Breen, MBBCh (USA)
5:30 PM	*5:40 PM*	**Biomechanics in Spondylolysis** Marcelo Galvez, MD (Chile)
5:40 PM	*6:10 PM*	**Q&A with RSNA Diagnosis Live™**
6:10 PM		**Adjourn**

Monday, May 16, 2016

7:00 AM	**8:30 AM**	**Continental Breakfast**
7:00 AM	**6:00 PM**	**Registration**
7:00 AM	**8:00 AM**	**AAWR Networking Breakfast**
7:50 AM	**8:00 AM**	**Welcome and Announcements** Michael J. Callahan, MD (USA) and Stein M. Aukland, MD, PhD (Norway)
8:00 AM	**8:30 AM**	**Categorical Course: CT Radiation DRLs and Dose Reporting Guidelines**
8:00 AM	*8:12 AM*	**US Perspective** Michael J. Callahan, MD (USA)
8:12 AM	*8:24 AM*	**Europe Perspective** Raija M. Seuri, MD (Finland)
8:25 AM	*8:30 AM*	**Questions and Answers**
8:30 AM	**9:10 AM**	**Categorical Course: Genitourinary Imaging** *Moderators: Jeanne S. Chow, MD (USA) and Pierre-Hugues Vivier, MD, PhD (France)*
8:30 AM	*8:40 AM*	**Current Trends in Pediatric GU Imaging: US Perspective** Jeanne S. Chow, MD (USA)
8:40 AM	*8:50 AM*	**Current Trends in Pediatric GU Imaging: European Perspective** Pierre-Hugues Vivier, MD, PhD (France)
8:50 AM	*9:00 AM*	**Current Trends in Pediatric GU Imaging: South American Perspective** Ximena C. Ortega, MD (Chile)
9:00 AM	*9:10 AM*	**Questions and Answers**
9:10 AM	**9:30 AM**	**Break**
9:40 AM	**11:40 AM**	**Scientific Session I-A: Gastrointestinal Radiology** *Samuel Stafrace, MD, MRCP (UK), FRCR, FRCP Edin. (Qatar) and Andrew T. Trout, MD (USA), Moderators*
9:40 AM	*9:50 AM*	**Ultrasound Imaging of the Spleen; Tips and Tricks to Aid Diagnosis** Samuel Stafrace, MD, MRCP (UK), FRCR, FRCP Edin. (Qatar)
9:50 AM	*11:40 AM*	***Scientific Papers***

Paper #: 001	9:50 AM	Trout	Interrater reproducibility of measured pancreatic secretory function on secretin-enhanced MRCP
Paper #: 002	9:58 AM	Alsabban	Clinical Relevance of Unsuspected MRE-detected PAD in Pediatric IBD
Paper #: 003	10:06 AM	Rosenbaum	US and MRI predictors of surgical bowel resection in pediatric Crohn's disease
Paper #: 004	10:14 AM	Dillman	Prospective Cohort Study of Ultrasound-Ultrasound and Ultrasound-MRI Agreement in the Evaluation of Pediatric Small Bowel Crohn's Disease
Paper #: 005	10:22 AM	Sasser	T2* MRI Assessment of Iron in Different Hepatic Segments in Pediatric Patients with Sickle Cell Hemoglobinopathies
Paper #: 006	10:30 AM	Tipirneni-Sajja	Assessment of Free-breathing R2*-UTE for Hepatic Iron Content Quantification in a Sedated Pediatric Cohort
Paper #: 007	10:38 AM	Khanna	MR based liver iron estimation in children: a comparison of signal intensity ratio method with T2* relaxometry
Paper #: 008	10:46 AM	Munden	Shear Wave Elastography of the Liver and Spleen, Comparison to Hemodynamics, Underlying Disease Process, and Isolating the Best Representative Segments
Paper #: 009	10:54 AM	Hartung	Ultrasound elastography with acoustic radiation force impulse (ARFI) to assess liver fibrosis and portal hypertension (HTN) in children with autosomal recessive polycystic kidney disease (ARPKD)
Paper #: 010	11:02 AM	Trout	Comparison of Gradient recalled echo (GRE) and Spin Echo-Echo planar imaging (SE-EPI) based MR Elastography of the liver in children with liver disease.
Paper #: 011	11:10 AM	Joshi	MR Elastography is a technically robust technique for assessment of hepatic stiffness in pediatric patients
Paper #: 012	11:18 AM	Joshi	Quantitative MR of the liver: Correlation between liver volume, stiffness, and fat fraction in a pediatric population
Paper #: 013	11:26 AM	Ahmad	Doppler Parameters of Hepatic Artery as Predictors of Graft Status in Children with Liver Transplant

9:40 AM	**11:40 AM**	**Scientific Session I-B: Oncology & Nuclear Medicine**	
		Govind B. Chavhan, MD, DABR (Canada) and Haemi P. Schemuth, MD (Germany), Moderators	
9:40 AM	*9:50 AM*	**Overview of Cancer Therapy Related Toxicities** Govind B. Chavhan, MD, DABR (Canada)	
9:50 AM	*11:40 AM*	***Scientific Papers***	
Paper #: 014	9:50 AM	Bagrosky	Utility of 18F-FDG PET/CT for diagnosis and staging of osseous metastatic disease in Ewing Sarcoma Family of Tumors: is there a correlation with genetic mutation or outcome?
Paper #: 015	9:58 AM	Schemuth	Detection of Pulmonary Nodules in Children with a Free Breathing MRI Technique compared to CT Scans
Paper #: 016	10:06 AM	Baheti	Imaging Features of Hepatoblastoma and Correlation with Pathological Subtype: A Single Institute Experience
Paper #: 017	10:14 AM	Caro Dominguez	Can diffusion weighted MR imaging distinguish between benign and malignant pediatric liver tumors?
Paper #: 018	10:22 AM	Tijerin Bueno	Imaging Review of DICER1 Syndrome: A Single Centre Experience
Paper #: 019	10:30 AM	Lai	PET/MRI detection of pulmonary nodules for pediatric cancer staging
Paper #: 020	10:38 AM	Rothenberg Maddocks	Pediatric head and neck sarcomas: Comparison of apparent diffusion coefficient (ADC) on diffusion weighted MR imaging and maximum standardized uptake value (SUVmax) at 18F-FDG PET/CT with histologic correlation
Paper #: 021	10:46 AM	Littooij	Correlation of whole-tumour apparent diffusion coefficient measurements with histopathological findings in nephroblastoma
Paper #: 022	10:54 AM	Martinez-Rios	Role of Diffusion Weighted Imaging in Differentiating Nephroblastomatosis from Wilm's tumour: a pilot study
Paper #: 023	11:02 AM	Semple	Can diffusion weighted imaging predict relapse in paediatric classical Hodgkin lymphoma? A pilot study.
Paper #: 024	11:10 AM	Humphries	Staging of p aediatric classical Hodgkin lymphoma (cHL) using F18-Fluorodeoxyglucose Positron emission tomography MRI (F18-FDG PET-MRI): a prospective pilot comparison to F18-FDG PET-CT reference standard.
Paper #: 025	11:18 AM	Martinez-Rios	Utility of Adult-based Ultrasound Criteria to Predict Malignancy in Pediatric Thyroid Nodules
Paper #: 026	11:26 AM	Littooij	Whole-body MRI reveals high incidence of osteonecrosis in children treated for Hodgkin lymphoma in the Euronet-PHL-C1 trial
11:45 AM	**1:00 PM**	**Lunch** *(On your own)*	
11:45 AM	**1:00 PM**	**CT Protocol Session** *(First-come, first-serve basis; lunch provided for the first 60 participants)* *Moderators: Sjirk J. Westra, MD (USA), R. Paul Guillerman, MD (USA), Catherine M. Owens, MBBS, FRCR (UK), Erich Sorantin, MD (Austria) and Raija M. Seuri, MD (Finland)*	
11:45 AM	**1:00 PM**	**3D Read with the Experts Session** *(First-come, first-serve basis; lunch provided for the first 100 participants)* *Moderators: Dianna M. E. Bardo, MD (USA) and Jeffrey E. Hellinger, MD, MBA (USA)*	

1:10 PM	**2:15 PM**	**Edward B. Neuhauser/Jacques LefèbvreLecture**	
		Multimodal Imaging of the Molecular,Cellular andTissueEvents Underlying Embryonic Development	
		Scott E. Fraser, PhD of the University of Southern California	
2:15 PM	**3:15 PM**	**Categorical Course: Whole Body Imaging**	
		Moderators: Shreyas S. Vasanawala, MD, PhD (USA) and Øystein E. Olsen, MD, PhD (UK)	
2:15 PM	*2:25 PM*	**Whole Body MR: The Basics**	
		Lil-Sofie Ording Muller, MD, PhD (Norway)	
2:25 PM	*2:35 PM*	**Whole Body MR: Pitfalls and Incidental Findings**	
		Øystein E. Olsen, MD, PhD (UK)	
2:35 PM	*2:45 PM*	**Whole Body Vascular MRI**	
		Shreyas S.Vasanawala, MD, PhD (USA)	
2:45 PM	*2:55 PM*	**Whole Body Imaging of Non-Oncologic Disorders**	
		Andrew T. Trout, MD (USA)	
2:55 PM	*3:15 PM*	**Q&A with RSNA Diagnosis Live™**	
3:15 PM	**3:45 PM**	**Break & Exhibits**	
3:50 PM	**4:40 PM**	**Scientific Session II-A: Gastrointestinal Radiology**	
		Savvas Andronikou, MBBCh, FRCR, PhD (UK) and Sudha A. Anupindi, MD (USA), Moderators	
3:50 PM	*4:40 PM*	***Scientific Papers***	
Paper #: 027	3:50 PM	Hwang	Pediatric Focal Nodular Hyperplasia: Value of Superb Micro-Vascular Imaging
Paper #: 028	3:58 PM	Fay	MRI and Malrotation: Excluding Intestinal Malrotation on Magnetic Resonance Examinations Ordered for Other Indications
Paper #: 029	4:06 PM	Andronikou	Position of nasogastric tube tip in the antrum results in better quality, speed and radiation dose of emergency upper GI contrast studies for suspected malrotation and mid-gut volvulus
Paper #: 030	4:14 PM	Guillerman	Bowel Perforation Complicating Attempted Intussusception Reduction by Air Enema: Risk Factors and the Myth of the Microperforation
Paper #: 031	4:22 PM	Schwartz	Is appendicitis less common in pediatric patients with sickle cell disease? A retrospective cohort study of a large, urban population.
Paper #: 032	4:30 PM	Pugmire	Imaging button battery ingestions and insertions in children: a 15-year single center review
3:50 PM	**4:40 PM**	**Scientific Session II-B: Cardiovascular**	
		Catherine M. Owens, MBBS, FRCR (UK) and Stanley T. Kim, MD (USA), Moderators	
3:50 PM	*4:40 PM*	***Scientific Papers***	
Paper #: 033	3:50 PM	Semple	Neonatal coronary anatomy deliniation via CT -A comparison of standard versus high pitch cardiovascular CT in neonates
Paper #: 034	3:58 PM	Zhong	Diagnostic accuracy of sub-mSv prospective ECG-triggering cardiac CT in low weight infant with complex congenital heart disease

Paper #: 035	4:06 PM	Deaver	Cardiac catheterization (CC) compared with cardiac computed tomography (CT) prior to second stage single ventricle (SV) palliation in low risk patients.
Paper #: 036	4:14 PM	Krishnamurthy	A MRI Cardiac Biomechanics Study of Segmental Strain Coupling in Single Ventricle Patients
Paper #: 037	4:22 PM	Srivaths	Assessment of intracardiac morphology and proximal coronary arteries in infants: Comparison of 64 detector CT, lower dose target mode volumetric CT, higher dose target mode volumetric CT, and retrospective EKG gated CT
Paper #: 038	4:30 PM	Zhong	Evaluation of Anomalous origin of the coronary artery from the pulmonary artery using three-dimensional steady state free precession sequence

3:50 PM	**4:40 PM**	**Scientific Session II-C: Fetal/Neonatal Imaging** *Owen Arthurs, MB BChir, FRCR, PhD (UK) and Richard A. Barth, MD, FACR, FAAP (USA), Moderators*	
3:50 PM	*4:40 PM*	***Scientific Papers***	
Paper #: 039	3:50 PM	Victoria	Right congenital diaphragmatic hernias: is there a correlation between prenatal lung volume and postnatal survival, as in isolated left diaphragmatic hernias?
Paper #: 040	3:58 PM	Garcia	Fetal lung volumes by MRI: Normal weekly values from 18 weeks through 28 weeks gestation.
Paper #: 041	4:06 PM	Goergen	The added value of MRI for the diagnosis of fetal neurological injury in survivors of monochorionic co-twin demise
Paper #: 042	4:14 PM	Cheung	Correlation with MR findings in Neonates with Hypoxic Ischaemic Encephalopathy Undergoing Cerebral Hypothermia and Subsequent Neurolodevelopmental Outcomes
Paper #: 043	4:22 PM	Cullen	Do all prenatally diagnosed bronchopulmonary malformations get smaller? Evaluation on serial fetal MRI and postnatal imaging
Paper #: 044	4:30 PM	Waelti	Neonatal congenital lung tumors: the importance of prenatal imaging as a diagnostic clue
4:40 PM		**Adjourn**	
4:45 PM	**6:15 PM**	**Awards Ceremony**	
6:30 PM	**7:45 PM**	**Welcome Reception** *Preston Bradley Room of the Chicago Cultural Center*	

Tuesday, May 17, 2016

6:30 AM	**5:00 PM**	**Registration**
6:45 AM	**8:30 AM**	**Continental Breakfast & Exhibits**
7:00 AM	**8:20 AM**	**Sunrise Sessions (concurrent)**
7:00 AM	**8:20 AM**	**Fetal Imaging** *Moderator: Christopher I. Cassady, MD, FAAP (USA)*
7:00 AM	*7:20 AM*	**Fetal Chest Imaging Update** Christopher I. Cassady, MD, FAAP (USA)
7:20 AM	*7:40 AM*	**Fetal Neuroimaging Update** Ashley J. Robinson, MB ChB, FRCR, FRCPC (Qatar)
7:40 AM	*8:00 AM*	**Post MortemImaging fromaEuropeanPerspective** Owen J. Arthurs, MB BChir, FRCR, PhD (UK)
8:00 AM	*8:20 AM*	**Post MortemImaging fromaNorthAmerican Perspective** Pat Harty, MD (USA) and Pierre Schmit, MD (Canada)
7:00 AM	**8:20 AM**	**Child Abuse** *Moderator: Catherine Adamsbaum, MD (France)*
7:00 AM	*7:25 AM*	**Evidence/Legal Issues (Europe)** Catherine Adamsbaum, MD (France)
7:25 AM	*7:50 AM*	**Inflicted Skeletal Injury: Diagnostic Challenges** Paul K. Kleinman, MD (USA)
7:50 AM	*8:15 AM*	**Different Perspectives on Follow Up** Joanna J. Fairhurst, MD (UK)
8:15 AM	*8:20 AM*	**Question and Answer**
7:00 AM	**8:20 AM**	**Oncology & Hybrid Imaging** ***Moderators:****Stephan D. Voss, MD, PhD (USA) and Paul D. Humphries, MD, FRCR (UK)*
7:00 AM	*7:20 AM*	**SPECT/CT** Helen R. Nadel, MD, FRCPC (Canada)
7:20 AM	*7:40 AM*	**PET/CT: Strategies for Integrating Diagnostic CT into the PET/CT Examination** Stephan D. Voss, MD, PhD (USA)
7:40 AM	*8:00 AM*	**PET/MR Techniques, Indications and Applications** Franz Wolfgang Hirsch, MD (Germany)
8:00 AM	*8:20 AM*	**PET/MR and Lymphoma: A Model for Quantitative Hybrid Imaging** Paul D. Humphries, MD, FRCR (UK)
7:00 AM	**8:20 AM**	**Value Added Imaging** ***Moderator: Richard E. Heller, III, MD, MBA (USA)***
7:00 AM	*7:20 AM*	**Value Added Imaging: Beyond the Platitudes** Richard E. Heller, III, MD, MBA (USA)
7:20 AM	*7:40 AM*	**Artificial Intelligence and Radiology with The Haptic Radiologist** Johan G. Blickman, MD, PhD (USA)
7:40 AM	*8:00 AM*	**24/7 Coverage** Jean-Francois Chateil, MD, PhD (France)
8:00 AM	*8:20 AM*	**Adding Value through Efficiency** John D. Strain, MD (USA)
8:30 AM	**10:00 AM**	**Categorical Course: Musculoskeletal Imaging** ***Moderators:****Mahesh M. Thapa, MD (USA) and Mario Maas, MD, PhD (The Netherlands)*
8:30 AM	*8:40 AM*	**Ultrasound-Guided Pediatric MSK Procedures** Mahesh M. Thapa, MD (USA)
8:40 AM	*8:50 AM*	**Surface Lesions of Bone in Children** James S. Meyer, MD (USA)
8:50 AM	*9:00 AM*	**Brachial Plexus Birth Injury: US Screening for Glenohumeral Joint Instability** Tiina H.Pöyhiä, MD, PhD (Finland)

9:00 AM	*9:10 AM*	**Sports Injury in the Wrist** Mario Maas, MD, PhD (The Netherlands)	
9:10 AM	*9:20 AM*	**Dynamic Gadolinium-Enhanced MRI of the Proximal Femur in Healthy Children** Diego Jaramillo, MD, MPH (USA)	
9:20 AM	*9:30 AM*	**MRI of the TMJs in Children with JIA: Cut-off Between Normality and Pathology** Thekla von Kalle, MD (Germany)	
9:30 AM	*10:00 AM*	***Q&A with RSNA Diagnosis Live™***	
8:30 AM	**9:00 AM**	**Radiographer Scientific Session: Dose & Radiation Safety** *Moderators: Stephen F. Simoneaux, MD (USA) and Graciano Paulo, Professor (Portugal)*	
		Scientific Papers	
Paper #: 01 (R) 8:30 AM		*Foley*	*A comparison of paediatric CT protocols and doses across Irish hospita ls*
Paper #: 02 (R) 8:38 AM		*Gates*	*Combined PET/Diagnostic CT exams as a means toward dose reduction in pediatric patients with lymphoma*
Paper #: 03 (R) 8:46 AM		*Santos*	*The impact of paediatric Computed Tomography tube current and tube voltage modulation intensity in organ dose and image quality*
Paper #: 04 (R) 8:54 AM		*Paulo*	*Optimisation and establishment of Diagnostic Reference Levels in paediatric plain radiography*
Paper #: 05 (R) 9:02 AM		*Santos*	*Establish and optimise dose levels for chest radiography in paediatric intensive care unit*
Paper #: 06 (R) 9:10 AM		*Paulo*	*Analysis of overexposed areas in paediatric plain radiography*
Paper #: 07 (R) 9:18 AM		*O Connor*	*An Investigation of the current status of the Alliance for Radiation Safety in Paediatric Imaging (ARSPI) Back to Basics campaign in Paediatric Projection Radiography in Ireland*
8:30 AM	**9:00 AM**	**Radiographer Back to Basics Session: Imaging Children – Immobilization and Distraction Techniques** *Moderator: Laura Gruber, MBA, RT(R), RDMS, RVT (USA)* Speaker: Michelle Garza, RT(R) (USA)	
10:00 AM	**10:20 AM**	**Break & Exhibits**	
10:25 AM	**11:55 AM**	**Scientific Session III-A: Genitourinary Radiology** *Damien Grattan-Smith, MD (USA) and Robert Marterer, MD (Austria), Moderators*	
10:25 AM	*10:35 AM*	**Intravenous Urography Through the Ages** Damien Grattan-Smith, MD (USA)	
10:35 AM	*11:55 AM*	***Scientific Papers***	
Paper #: 045	10:35 AM	Trout	Large multicenter study of the association between testicular microlithiasis and testicular neoplasia in a pediatric population
Paper #: 046	10:43 AM	Strubel	Reliability of the new Urinary Tract Dilation (UTD) classification system for the evaluation of postnatal urinary tract dilation

Paper #: 047	10:51 AM	Bruno	ARFI Evaluation of the Kidneys in Ex Premature Infants: Preliminary Results
Paper #: 048	10:59 AM	Ozkan	The reliability and accuracy of diffusion tensor imaging and tractography in kidneys : Is it a new predictible tool to understand the microstructurel changes in renal impairment at the pediatric age group ?
Paper #: 049	11:07 AM	Urquia	Functional Magnetic Resonance Urography: Adjunct Non-Contrast Angiography Increases Diagnostic Confidence in Assessment of Crossing Vessels in Pelvico-ureteric Junction Obstruction
Paper #: 050	11:15 AM	Tsai	Simultaneous Renal Parenchyma Classification and Time-Intensity Curve Estimation for Dynamic MR Urography
Paper #: 051	11:23 AM	Delgado	Relationship between Bladder Volume and Functional Results of MR Urography in Children
Paper #: 052	11:31 AM	Eichenberger	Obstruction, Flow, and Function as Relating to Functional Renal Imaging
Paper #: 053	11:39 AM	Ntoulia	Unilateral Ureteropelvic Junction Obstruction (UPJO) in Children: Evaluation of Pre-and Postoperative Imaging Findings and Correlation with Surgical Outcomes
Paper #: 054	11:47 AM	Ntoulia	Comparison of Contrast Enhanced Voiding Urosongraphy (ceVUS) using the Ultrasound Contrast Agent (Optison®) with Voiding Cystourethrography (VCUG)

10:25 AM	**11:55 AM**	**Scientific Session III-B: Informatics, Education, QI & Healthcare Policy**
		Lane F. Donnelly, MD (USA) and Nadja Kadom, MD (USA), Moderators
10:25 AM	*10:35 AM*	**The Dire State of Pediatric Radiology in Malawi: The Urgent Need to Train Future Pediatric Radiologists** Amit S. Sura, MD, MBA (USA)
10:35 AM	*11:55 AM*	***Scientific Papers***

Paper #: 055	10:35 AM	Tsai	Validation of a Novel Simulator for Teaching Radiology Residents How to Perform Brain Ultrasonography: A Pilot Study
Paper #: 056	10:43 AM	Donnelly	The Daily Readiness Huddle –A Process to Rapidly Identify Issues and Foster Improvement through Problem Solving Accountability
Paper #: 057	10:51 AM	Delgado	Intussusception simulation device, an inexpensive hands-on tool to learn pneumatic reduction technique.
Paper #: 058	10:59 AM	Otero	Imaging Utilization Patterns for the Diagnosis of Appendicitis in Stand-Alone Children's Hospitals in the United States: an update of trends and costs
Paper #: 059	11:07 AM	Simoneaux	Outside Study Interpretation: Current Practice in Children's Hospitals
Paper #: 060	11:15 AM	Reid	RadEd: Early experience with a content management system (CMS) for radiology education
Paper #: 061	11:23 AM	Breen	The Dreaded Addendum: A First Step to Reduction of Radiology Reporting Errors in Cases of Suspected Child Abuse
Paper #: 062	11:31 AM	Munden	Applying Current ACR Guidelines to the Limping Toddler: Is it Enough?
Paper #: 063	11:39 AM	Richer	To Pee or Not To Pee: A Survey of SPR Members Regarding Practice Patterns for VCUG in the Setting of

			UTI and the American Academy of Pediatrics Guidelines.
Paper #: 064	11:47 AM	Botwin	The Role of a Real-Time Electronic Dashboard in Improving Clinical Workflow for Pediatric Radiologists

10:25 AM	**11:55 AM**	**Scientific Session III-C: ALARA**
		Steven Don, MD (USA) and Rutger A. J. Nievelstein, MD, PhD (The Netherlands), Moderators
10:25 AM	*10:35 AM*	**Radiation Protection in Children: Current Status** Rutger A. J. Nievelstein, MD, PhD (The Netherlands)
10:35 AM	*11:55 AM*	***Scientific Papers***

Paper #: 065	10:35 AM	Kaplan	Gonad Shielding Increases Patient Radiation
Paper #: 066	10:43 AM	Lazarus	Accurate radiation dose monitoring in pediatric fluoroscopy: Are we measuring the correct parameter?
Paper #: 067	10:51 AM	Kaplan	Intussusception Reduction: Effect of Contrast Selection on Radiation Dose
Paper #: 068	10:59 AM	Rostad	Unnecessary Multi-pass Acquisitions are a Common Problem Leading to Increased Radiation Dose in CT Abdomen/Pelvis Examinations
Paper #: 069	11:07 AM	Andronikou	Accuracy of Non-Radiologists and Lay-People for Identifying Children with Cerebral Cortical Atrophy From Mercator map' Curved Reconstructions of the brain
Paper #: 070	11:15 AM	Tabari	Evaluati on of ultralow dose high pitch body CT in young children as a technique for evaluating pathology in awake patients
Paper #: 071	11:23 AM	Tabari	Pediatric chest CTA, comparison between exposure, measured skin dose and modeled organ and effective dose
Paper #: 072	11:31 AM	Guillerman	Improving the Yield of Bronchoscopy for Suspected Pediatric Airway Foreign Bodies with a Clinical Care Protocol Incorporating Low -Dose Airway CT
Paper #: 073	11:39 AM	Little	The Old and the New – How Time -Tested Antiscatter Grids Interact with Portable Digital Radiography Technology
Paper #: 074	11:47 AM	Tabari	Role of Adaptive Statistical Iterative Reconstruction (ASIR) in lowering radiation dose for pediatric head CT.

10:25 AM	**11:55 AM**	**Radiographer Refresher Course: The Knowledge Skills and Competences (KSC) for a Technologist/Radiographer in Pediatric Radiology**
		Moderator: Lorraine Chisari (USA)
10:25 AM	*10:45 AM*	**Education and Training of Technologists/Radiographers: The Specificity of Pediatric Radiology** Louise A. Rainford, PhD (Ireland)
10:45 AM	*11:05 AM*	**The Implementation of Evidence-Based Practice to Develop Technologists/Radiographers KSC** Graciano Paulo, Professor (Portugal)
11:05 AM	*11:25 AM*	**The Role of Our RRA/RPA (Registered Radiologist Assistant/Radiology Practitioner Assistant) in a Busy Academic Pediatric Fluoroscopy Division in a Children's Hospital in the USA** Christopher Young, MRS, RRA, RT(R) (USA) and Steven J. Kraus, MD, MS (USA)

11:25 AM	*11:55 AM*	**Panel Discussion**
12:00 PM	**1:40 PM**	**Lunch at The Mid America Club** *(All registered attendees invited)*
1:50 PM	**3:15 PM**	**IPR Olympics Panel**
		Moderator: Laurent Garel, MD, FRCPC (Canada)
		Team A: Christopher I. Cassady, MD, FAAP (USA), Katherine Halliday, MD (UK), Supika Kritsaneepaiboon, MD (Thailand) and Philippe Petit, MD (France)
		Team B: Antonio Soares Souza, MD (Brazil), Monica Epelman, MD (USA), Douglas H. Jamieson, MD (Canada) and Lil-Sofie Ording Muller, MD, PhD (Norway)
3:20 PM	**4:20 PM**	**Should the ALARA Concept and the Image Gently Campaign be Terminated?**
		Moderator: Kieran McHugh, MB, FRCR, FRCPI, DCH (UK)
3:20 PM	*3:30 PM*	**Speaking Against the Termination of the "ALARA Concept and the Image Gently Campaign"** Donald P. Frush, MD, FACR (USA)
3:30 PM	*3:40 PM*	**Speaking Against the Termination of the "ALARA Concept and the Image Gently Campaign"** Cynthia H. McCollough, PhD, FAAPM, FACR (USA)
3:40 PM	*3:50 PM*	**Speaking in Favor of the Termination of the "ALARA Concept and the Image Gently Campaign"** Mervyn D. Cohen, MD, FACR (USA)
3:50 PM	*4:00 PM*	**Speaking in Favor of the Termination of the "ALARA Concept and the Image Gently Campaign"** Mohan Doss, PhD, MCCPM (USA)
4:00 PM	*4:20 PM*	**Question & Answer**
4:20 PM	**4:50 PM**	**Break & Exhibits**
4:40 PM	**6:10 PM**	**Radiographer Refresher Course: The Full Exploitation of New Technological Features in Pediatric CT**
		Moderator: Jim E. Hickey, RT, (R)(CT)(MR) (USA)
4:40 PM	*5:00 PM*	**The Pros and Cons of Dose Modulation** Patricia L. Mecca, BS, RT (R), (MR), (CT) (USA)
5:00 PM	*5:20 PM*	**Iterative Reconstructions: The Impact on Dose and Image Quality** Shane J. Foley, PhD (Ireland)
5:20 PM	*5:40 PM*	**Tips & Tricks in CT Dose Optimization: How Low is Too Low?** Robert D. MacDougall, MSc (USA)
5:40 PM	*6:10 PM*	**Panel Discussion**
4:50 PM	**6:00 PM**	**Scientific Session IV-A: Gastrointestinal Radiology**
		Robert C. Orth, MD, MPH, PhD (USA) and Samuel Stafrace, MD, MRCP (UK), FRCR, FRCP Edin. (Qatar), Moderators
10:25 AM	*10:35 AM*	**Imaging Pediatric Appendicitis - Past, Present, and Future** Robert C. Orth, MD, MPH, PhD (USA)
10:35 AM	*11:55 AM*	***Scientific Papers***

Paper #: 075	5:00 PM	Lee	Ultrasonographic Features of Secondary Inflammation of the Appendix in Pediatric Patients.
Paper #: 076	5:08 PM	Dibble	CT versus MRI: Effectiveness following sonography in staged imaging algorithm for suspected pediatric appendicitis
Paper #: 077	5:16 PM	Otero	Rising Utilization of Magnetic Resonance Imaging in the Management of Pediatric Appendicitis in the United States: An Update Using a Large Administrative Database
Paper #: 078	5:24 PM	Gupta	Diagnostic accuracy of MR imaging for evaluation of acute appendicitis: A prime prospective study of Canadian pediatric population.
Paper #: 079	5:32 PM	Eng	Diagnostic Accuracy of MRI for Acute Appendicitis in Pediatric Patients as Compared with Adult and Obstetric Patients: A Meta-Analysis
Paper #: 080	5:40 PM	Martinez-Rios	Priority Setting in Imaging Diagnosis of Pediatric Appendicitis: Parental Preferences According to ImagingTechniques' Attributes
Paper #: 081	5:48 PM	Otero	Applicability of Emergent MRI for Suspected Pediatric Appendicitis with Equivocal Ultrasound Results

4:50 PM 6:00 PM Scientific Session IV-B:Thoracic Imaging

Mark C. Liszewski, MD (USA) and Anne Paterson, MB BS, MRCP, FRCR, FFR RSCI (UK), Moderators

10:25 AM 10:35 AM **Postnatal Management of Fetal Echogenic Lung: the Northern Ireland Perspective**
Anne Paterson, MB BS, MRCP, FRCR, FFR RSCI (UK)

10:35 AM 11:55 AM ***Scientific Papers***

Paper #: 082	5:00 PM	Mahomed	Are Chest X-ray Patterns Associated with Specific Clinical and Acute Phase Reactants in HIV-infected, HIV-Exposed-Uninfected andHIV-Unexposed Children Hospitalized with WHO Defined Severe, Very Severe Pneumonia?
Paper #: 083	5:08 PM	Sagar	Screening for pulmonary arteriovenous malformations (PAVM) in children with Hereditary Hemorrhagic Telangiectasia (HHT) by dual energy CT pulmonary angiography (DE-CTPA). Is it as good as it sounds?
Paper #: 084	5:16 PM	Zhong	Evaluation of Pediatric Tracheobronchial Anomalies with congenital heart disease using Three-dimensional Turbo Field Echo Magnetic Resonance Imaging Sequence
Paper #: 085	5:24 PM	Nguyen	Quantification of emphysema by CT in children with cystic fibrosis and comparison to pulmonary function parameters
Paper #: 086	5:32 PM	Sodhi	Rapid lung MRI as an alternative to CT scan in children with pulmonary infections
Paper #: 087	5:40 PM	White	Clearing Away the Mud: A Retrospective Review of CT Findings in Pulmonary Interstitial Glycogenosis (PIG)
Paper #: 088	5:48 PM	Lazarte	Tomographic Patterns of Pulmonary Tuberculosis in Children

4:50 PM 6:00 PM Scientific Session IV-C: Neuroradiology

Marvin D. Nelson, MD, MBA (USA) and Maarten Lequin, MD, PhD (The Netherlands), Moderators

10:25 AM 10:35 AM **History of Hydrocephalus**
Marvin D. Nelson, MD, MBA (USA)

10:35 AM 11:55 AM ***Scientific Papers***

Paper #: 089	5:00 PM	Wieselthaler	HIV and Stroke. A Retrospective Review at our Institution
Paper #: 090	5:08 PM	Andronikou	Curved reformat of the paediatric brain MRI into a 'flat-earth map' –a standardised method for demonstrating cortical surface atrophy resulting from hypoxic ischaemic encephalopathy
Paper #: 091	5:16 PM	Golriz	Network Architecture and Global Intelligence in Children with Localization-related Epilepsy
Paper #: 092	5:24 PM	Golriz	Metrics of Network Architecture Probe the Impact of Ongoing Seizures on Cognitive Development in Children with Epilepsy
Paper #: 093	5:32 PM	Starosolski	High-resolution CT Angiography and Computational Fluid Dynamics for stroke risk assessment in a mouse model of pediatric cerebrovascular disease
Paper #: 094	5:40 PM	Cullen	Variable Refocusing Flip Angle Single Shot Imaging For Faster Anesthesia-Free Brain MRI
Paper #: 095	5:48 PM	Nanwani	Does size really matter? - Role of CT measurement in identification of otherwise normal "dwarf" cochlea in pediatric cochlear implant candidates

6:00 PM Adjourn

Wednesday, May 18, 2016

6:30 AM	**1:00 PM**	**Registration**
6:45 AM	**8:30 AM**	**Continental Breakfast & Exhibits**
7:00 AM	**8:20 AM**	**Sunrise Sessions (concurrent)**
7:00 AM	**8:20 AM**	**Education** *Moderator: Rutger A. J. Nievelstein, MD, PhD (The Netherlands)*
7:00 AM	*7:20 AM*	**Training Pathways in Pediatric Radiology** Rutger A. J. Nievelstein, MD, PhD (The Netherlands)
7:20 AM	*7:40 AM*	**Incorporating New Technology in Radiology Education** Jennifer Nicholas, MD, MHA (USA)
7:40 AM	*8:00 AM*	**Simulation in Pediatric Radiology Education** Ellen C. Benya, MD (USA)
8:00 AM	*8:20 AM*	**Creating Videos in Presentations and *for Online Content*** *Mahesh M. Thapa, MD (USA)*
7:00 AM	**8:20 AM**	**Taking US Farther** ***Moderator: Mehrak Anooshiravani, MD (Switzerland)***
7:00 AM	*7:20 AM*	**How to Begin: Contrast Enhanced US** Kassa Darge, MD, PhD (USA)
7:20 AM	*7:40 AM*	**Shear Wave Elastography in Children** Mehrak Anooshiravani, MD (Switzerland)
7:40 AM	*8:00 AM*	**Skin Sonography in Children** Cristian J. Garcia, MD (Chile)
8:00 AM	*8:20 AM*	**US and Teleradiology: Do they mix?** Michael E. Katz, MD, FACR (USA)
7:00 AM	**8:20 AM**	**ER Imaging** *Moderator: Stein M. Aukland, MD, PhD (Norway)*
7:00 AM	*7:20 AM*	**Neuro Emergencies** Stein M. Aukland, MD, PhD (Norway)
7:20 AM	*7:40 AM*	**Injuries in Children Following a Fall on Outstreched Hand (FOOSH)** Amaka C. Offiah, BSc, MBBS, MRCP, FRCR, PhD, FRCPCH (UK)
7:40 AM	*8:00 AM*	**Emergent IR Procedures** Jared R. Green, MD (USA)
8:00 AM	*8:20 AM*	**Abdomen Emergencies** Andrew T. Trout, MD (USA)
7:00 AM	**8:20 AM**	**Fellows Forum** *Moderator: Arnold Carl Merrow, MD (USA)*
7:00 AM	*7:20 AM*	**The Limping Child** Gurdeep S. Mann, MRCP(UK), FRCP (Qatar)
7:20 AM	*7:40 AM*	**Imaging & Management of the Child with Pneumonia** Ian Robinson, MBChB, FRANZCR (Ireland)
7:40 AM	*8:00 AM*	**Imaging the Child with Seizures** Maura Ryan, MD (USA)
8:00 AM	*8:20 AM*	**Imaging the Child with Lumps & Bumps** Arnold Carl Merrow, MD (USA)
7:50 AM	**8:20 AM**	**Radiographer Professional Challenge Session: Image Quality Issues in Pediatrics** *Moderator: Laura Gruber, MBA, RT(R), RDMS, RVT (USA)* Speaker: Christina L. Sammet, PhD, DABR (USA)
8:30 AM	**10:00 AM**	**Radiographer Refresher Course: Communication and Novel Issues in Pediatric Imaging** *Moderator: Johan G. Blickman, MD, PhD (USA)*
8:30 AM	*8:50 AM*	**Child-life: Developmental Techniques to Facilitate Radiographer's Tasks** Emily A. Rogers, MS, CCLS (USA) and Beth K. Ryan, MEd, CCLS (USA)
8:50 AM	*9:10 AM*	**How to Communicate the Risk to Parents and Careers in Clinical Setting** Jonathan P. McNulty, PhD (Ireland)
9:10 AM	*9:30 AM*	**Facing the Challenges of Preparing the Child for Imaging Procedures** Jackie M. Wameling, BS, CCLS (USA)
9:30 AM	*10:00 AM*	**Panel Discussion**
8:30 AM	**10:00 AM**	**Categorical Course: Abdominal Imaging** *Moderators: Daniel J. Podberesky, MD (USA) and Ignasi Barber, MD (Spain)*
8:30 AM	*8:40 AM*	**Normal DW Imaging Appearances of Abdominal Organs** Govind B. Chavhan, MD, DABR (Canada)

8:40 AM	*8:50 AM*	**MR Imaging of Anorectal Malformations** Daniel J. Podberesky, MD (USA)
8:50 AM	*9:00 AM*	**Voiding Urosonography: Techniques and Pitfalls** Kassa Darge, MD, PhD (USA)
9:00 AM	9:10 AM	**Perinatal (differential) Diagnosis and Management of Abdominal Teratomas** Fred E. Avni, MD, PhD (Belgium)
9:10 AM	*9:20 AM*	**The Role of DWI for IBD MRI** Ignasi Barber, MD (Spain)
9:20 AM	*9:30 AM*	**Imaging of Congenital Urachal Abnormalities** Paul D. Humphries, MD, FRCR (UK)
9:30 AM	*10:00 AM*	**Q&A with RSNA Diagnosis Live™**

10:00 AM 11:00 AM Radiographer Scientific Session: Potpourri-Cardio/Chest/GI

Moderators: Stephen F. Simoneaux, MD (USA) and Joana R. Santos, PhD (Portugal)

Scientific Papers

Paper #: 08 (R)	10:00 AM	Mullen	An investigation of how to improve recall and awareness of radiation dose levels associated with pediatric cardiovascular interventionalprocedures
Paper #: 09 (R)	10:08 AM	Rainford	Comparison of radiation dose between centers in the aim of establishing DRLs for commonly performed pediatric cardiac interventional procedures
Paper #: 10 (R)	10:16 AM	Leloutre	Measurement of the density of bronchoceles in cystic fibrosis as an indicator of allergic broncho-pulmonary aspergillosis: preliminary study
Paper #: 11 (R)	10:24 AM	O'Connor	Clinically acceptable noise levels in paediatric chest and abdomen CT examinations
Paper #: 12 (R)	10:32 AM	O'Connor	A comparison of manual, semi-automated and automated visceral adipose tissue quantification on paedatric abdominal CT examinations
Paper #: 13 (R)	10:40 AM	Maher	The practical considerations of research scanning using ARFI elastography: A healthy pediatric liver cohort investigation.

10:00 AM 11:00 AM Categorical Course: Cardiovascular/Interventional Radiology

Moderators: Rajesh Krishnamurthy, MD (USA) and Sergio Sierre, MD, FSIR, FCIRSE (Argentina)

10:00 AM	*10:10 AM*	**Dynamic MR Lymphangiography** Rajesh Krishnamurthy, MD (USA)
10:10 AM	*10:20 AM*	**RFA, Cryo, MW and Laser for Tumor Management in Pediatric Patients** Fernando Gómez Muñoz, MD, PhD (Spain)
10:20 AM	*10:30 AM*	**Complications of Catheter Related Thrombosis in Children** Cicero J. Torres A. Silva, MD (USA)
10:30 AM	*10:40 AM*	**Embolization Procedures in Neonates and Infants** Sergio Sierre, MD, FSIR, FCIRSE (Argentina)
10:40 AM	*11:00 AM*	**Q&A with RSNA Diagnosis Live™**

11:00 AM 11:30 AM Break & Exhibits

11:35 AM	**1:05 AM**	**Radiographer Refresher Course: Reduction Stragies in Pediatric Imaging**	
		Moderator: Michelle Garza, RT(R) (USA)	
11:35 AM	*11:55 AM*	**Tips & Tricks for Dose Reduction in Digital Radiology** Kim Bauer, (RT), (R) (USA)	
11:55 AM	*12:15 PM*	**Diagnostic Reference Levels in Pediatric Imaging: The International Recommendations** Joana R. Santos, PhD (Portugal)	
12:15 PM	*12:35 PM*	**The Impact of Dose Management Systems: The Impact in Daily Practice** Lynne Hamer, MEd, RT (USA) and Christina L. Sammet, PhD, DABR (USA)	
12:35 PM	*1:05 PM*	**Panel Discussion**	
11:35 AM	**1:15 PM**	**Scientific Session V-A: Fetal/Neonatal Imaging** *Owen Arthurs, MB BChir, FRCR, PhD (UK) and Dorothy I. Bulas, MD, FACR, FAAP (USA), Moderators*	
11:35 AM	*11:45 AM*	**Fetal MRI Past, Present and Future** Dorothy I. Bulas, MD, FACR, FAAP (USA)	
11:45 AM	*1:15 PM*	***Scientific Papers***	
Paper #: 096	11:45 AM	Blask	Severe Nasomaxillary Hypoplasia on Prenatal US/MRI: An Important Marker for the Prenatal Diagnosis of Chondrodysplasia Punctata (CDP)
Paper #: 097	11:53 AM	Caro Dominguez	Are there calcifications in the parenchyma of solid organs in children with meconium peritonitis?
Paper #: 098	12:01 PM	Somcio	Low intralesional T2 signal on fetal MRI: is it pathology-specific?
Paper #: 099	12:09 PM	Yen	Correlation between maternal breakfast and fetal motion during fetal MRI
Paper #: 100	12:17 PM	Perez	Derangement of the knee in patients with congenital longitudinal deficiencies of the lower limbs: MR findings
Paper #: 101	12:25 PM	Starosolski	Ultra-High Resolution Imaging of Utero-Placental Vasculature in a Rodent Model of Pregnancy
Paper #: 102	12:33 PM	Ghaghada	In vivo Profiling of Folate Receptor Expression in Rat Placenta Using MR Molecular Imaging
Paper #: 103	12:41 PM	Dance	T1 weighted MRI of the fetus using 3D mDixon gradient echo.
Paper #: 104	12:49 PM	Rothenberg Maddocks	Fetal Coloboma and its Associations
Paper #: 105	12:57 PM	Hutchinson	Diagnostic accuracy of micro-CT for fetal heart dissection (comparison of imaging to autopsy)
Paper #: 106	1:05 PM	Prodhomme	Prenatal Intestinal Volvulus About A Series of 12 Cases: The Snail Sign of Fetal MRI The Diagnostic Clue in 9 Cases
11:35 AM	**1:15 PM**	**Scientific Session V-B: Interventional Radiology** *Josee Dubois, MD (Canada) and Stephanie Franchi-Abella, MD, PhD (France), Moderators*	
11:35 AM	*11:45 A M*	**Congenital Porto-Systemic Shunt: Role of Interventional Radiology** Stephanie Franchi-Abella, MD, PhD (France)	
11:45 AM	*1:15 PM*	***Scientific Papers***	
Paper #: 107	11:45 AM	Kaufman	Training the Pediatric Interventional Radiologist
Paper #: 108	11:53 AM	Acomb	Case Controlled Analysis of Utility of Ultrasound Guidance during Bone Biopsies

Paper #: 109	12:01 PM	Shellikeri	Evaluation of MR Overlay on live fluoroscopy for pediatric percutaneous extremity biopsies of exclusively MR visible bone lesions in the Interventional Radiology suite
Paper #: 110	12:09 PM	Li	Diffusion Tensor Imaging in Pediatric Renal Transplants: Testing A Potential Non-Invasive Alternative to Biopsy
Paper #: 111	12:17 PM	Gnannt	Peripherally Inserted Central Catheters (PICC's) in Pediatric Patients: Variables Affecting the Central Tip Position
Paper #: 112	12:25 PM	Gnannt	Ultrasound Guided Percutaneous Cholecystostomy Drains in Children: a Case Series
Paper #: 113	12:33 PM	Shellikeri	Integration of syngo iGuide navigational software with C-arm CT images for percutaneous bone biopsies in the Interventional Radiology suite at a pediatric institution
Paper #: 114	12:41 PM	Plunk	Placement of small caliber tunneled central lines via the internal jugular vein in children less than two years
Paper #: 115	12:49 PM	Towbin	Davis Intubated Ureterotomy: Treatment of Ureteral Injury/Transection
Paper #: 116	12:57 PM	Grattan-Smith	Intra-operative MRI guided, laparoscopic-assisted anorectoplasty in the treatment for imperforate anus
Paper #: 117	1:05 PM	Chennapragada	CT-guided preoperative localisation of nonpalpable lung nodules in children

11:35 AM	**1:15 PM**	**Scientific Session V-C: Musculoskeletal Imaging** *Lene Bjerke Laborie, MD, PhD (Norway) and Mahesh Thapa, MD (USA), Moderators*
11:35 AM	*11:45 AM*	**Femoroacetabular Impingement in Adolescents and Young Adults – An Update** Lene Bjerke Laborie, MD, PhD (Norway)
11:45 AM	*1:15 PM*	***Scientific Papers***

Paper #: 118	11:45 AM	Koning	Pre-Season versus Post -Season Quantitative MRI Assessment of the Elbow in Little League Baseball Players
Paper #: 119	11:53 AM	Laborie	Fetal, infant, and childhood growth and acetabular hip dysplasia at skeletal maturity: findings from a prospective study with follow-up from newborn to adult life
Paper #: 120	12:01 PM	Kammen	Clinical Update On Rapid High Resolution Two-Point DIXON Turbo Spin Echo (TSE) With Conventional TSE On 3T MR Imaging of the Pediatric Knee in 50 patients
Paper #: 121	12:09 PM	Bao	Fast comprehensive single sequence 4D pediatric knee MRI
Paper #: 122	12:17 PM	Jadhav	Arthroscopic and MRI discrepancies for chondral injuries of the knee in 329 children
Paper #: 123	12:25 PM	Ecklund	Bone Marrow Fat Content in 70 Adolescent Girls with Anorexia Nervosa: MRI/MRS Assessment
Paper #: 124	12:33 PM	Kan	Does Pre-Operative Hip Location or Post-Operative Hip Abduction Angle Better Predict Perfusion Abnormalities on Post-Operative SPICA MRI after Closed Reduction for Developmental Dysplasia of the Hip?
Paper #: 125	12:41 PM	Jaremko	Preliminary accuracy of 3D ultrasound diagnosis of infant hip dysplasia using indices of acetabular 3D shape and coverage.
Paper #: 126	12:49 PM	Golriz	Acute inflammatory neck swelling in children: which patients bene fit most from early ultrasound?
Paper #: 127	12:57 PM	McGill	An Evidence Based Medicine Approach to Paediatric Cervical Spine Trauma: Cervical Spine Plain Radiography vs. Computed Tomography
Paper #: 128	1:05 PM	Paddock	What is the value of spine, hand and foot radiographs as part of the skeletal survey for diagnosing suspected physical child abuse?

1:15 PM		**Adjourn**
1:30 PM	**2:30 PM**	**jSPR/JESPeR Lunch**
1:30 PM	**2:30 PM**	**MR Protocol Session** *(First-come, first-serve basis; lunch provided for the first 60 participants)* *Moderators: Taylor Chung, MD (USA), Shreyas S.Vasanawala, MD, PhD (USA), Øystein E.Olsen, MD, PhD (UK) and Philip Petit, MD (France)*
2:00 PM	**5:00 PM**	**Lurie Children's Hospital Tours** ***(Optional;Pre-registrationRequired)***

Categorical Course – SAM Eligible | Categorical Course | Sunrise Session - Concurrent
Radiographer Program | Friday half-day Session | Scientific Session - Concurrent

Thursday, May 19, 2016

6:30 AM	**5:30 PM**	**Registration**
6:45 AM	**8:30 AM**	**Continental Breakfast & Exhibits**
7:00 AM	**8:20 AM**	**Sunrise Sessions (concurrent)**
7:00 AM	**8:20 AM**	**MSK** *Moderator: Tal Laor, MD (USA)*
7:00 AM	*7:20 AM*	**Imaging the Patellofemoral Joint in Children** Tal Laor, MD (USA)
7:20 AM	*7:40 AM*	**Painful Hip** Lil-Sofie Ording Muller, MD, PhD (Norway)
7:40 AM	*8:00 AM*	**Langerhans Cell Histiocytosis from Head to Foot** Jonathan D. Samet, MD (USA)
8:00 AM	*8:20 AM*	**Soft Tissue Lesions** Philip Petit, MD (France)
7:00 AM	**8:20 AM**	**Research Forum** *Moderator: Heike E. Daldrup-Link, MD, PhD (USA)*
7:00 AM	*7:20 AM*	**Translational Research in Pediatric Radiology** Heike E. Daldrup-Link, MD, PhD (USA)
7:20 AM	*7:40 AM*	**Clinical Research: How to Begin** Karen Rosendahl, MD, PhD (Norway)
7:40 AM	*8:00 AM*	**Basic Statistics for the Radiologist** Geetika Khanna, MD, MS (USA)
8:00 AM	*8:20 AM*	**Proper Measurement Techniques** Øystein E. Olsen, MD, PhD (UK)
7:00 AM	**8:20 AM**	**Career Growth in Pediatric Radiology** *Moderator: Peter S. Moskowitz, MD (USA)*
7:00 AM	*7:30 AM*	**Personal Survival in Times of Chaos: Life Coaching Strategies for Self-Renewal and Work-Life Balance** Peter S. Moskowitz, MD (USA)
7:30 AM	*7:55 AM*	**Leading as a Pediatric Radiologist** Richard B. Gunderman, MD, PhD (USA)
7:55 AM	*8:20 AM*	**Healthy Career Growth** Fred E. Avni, MD, PhD (Belgium)
7:00 AM	**8:20 AM**	**Head Scratchers: Cases from Around the World Uniting WFPI** *Moderator: Paolo Toma', MD (Italy) and M. Ines Boechat, MD FACR (USA)*
7:00 AM	*7:15 AM*	**Challenging Cases Europe** Paolo Toma', MD (Italy)
7:15 AM	*7:30 AM*	**Challenging Cases US** Juan C. Infante, MD (USA)
7:30 AM	*7:45 AM*	**Challenging Cases Asia** Wendy W. Lam, MBBS, FRCR (Hong Kong)
7:45 AM	*8:00 AM*	**Challenging Cases South America** Gloria A. Soto, MD (Chile)
8:00 AM	*8:15 AM*	**Challenging Cases South Africa** Jaishree Naidoo, FCRad diag (SA) (South Africa)
8:15 AM	*8:20 AM*	**Questions and Answers**
8:30 AM	**9:20 AM**	**Categorical Course: Imaging in Infectious Disease/WFPI** *Moderators: Paul S. Babyn, MD (Canada) and Rutger A. J. Nievelstein, MD, PhD (The Netherlands)*
8:30 AM	*8:40 AM*	**Africa** Savvas Andronikou, MBBCh, FRCR, PhD (South Africa)
8:40 AM	*8:50 AM*	**Asia** Kushaljit Singh Sodhi, MD, PhD, FICR (India)
8:50 AM	*9:00 AM*	**North America** Paul S. Babyn, MD (Canada)
9:00 AM	*9:10 AM*	**Europe** Rutger A. J. Nievelstein, MD, PhD (The Netherlands)
9:10 AM	*9:20 AM*	**Questions and Answers**
8:30 AM	**9:00 AM**	**Radiographer New Horizon Session: The Role of Hybrid Imaging in Pediatrics** *Moderator: Laura Gruber, MBA, RT(R), RDMS, RVT (USA)* Speaker: Ben Thurlow, BSc, MSc (UK)
9:20 AM	**10:20 AM**	**Categorical Course: Medical Negligence Trial: The Many Roles of a Pediatric Radiologist, A Mock Trial** *Moderator: Thomas L. Slovis, MD, FACR (USA)* Panel: Michael R. Slovis, JD (USA), Marni R. Slavick, JD (USA) and George A. Taylor, MD, FACR (USA)
10:20 AM	**10:50 AM**	**Break & Exhibits**

10:55 AM	**11:55 PM**	**Scientific Session VI-A: Fetal Neonatal – GI Intussusception**	
		Christopher I. Cassady, MD, FAAP (USA) and Charlotte de Lange, MD, PhD (Norway), Moderators	
10:55 AM	*11:05 AM*	**Fetal MR: From Infancy to Adolescence** Christopher I. Cassady, MD, FAAP (USA)	
11:05 AM	*11:55 AM*	***Scientific Papers***	
Paper #: 129	11:05 AM	Kaplan	Normal values for size of ovaries, testes, uterus, and breast buds at birth.
Paper #: 130	11:13 AM	Ayyala	Fetal Intracranial MRI In Complicated Monochorionic Multiple Gestations Undergoing In Utero Therapy
Paper #: 131	11:21 AM	Palathinkal	Sonography and Neuromotor Outcomes in Prematurity
Paper #: 132	11:29 AM	Farley	Experience with Institutional Imaging Guidelines for Intussusception at a Regional Children's Hospital: Compliance and Outcomes
Paper #: 133	11:37 AM	Solomon	Reducing by three-quarter the surgical laparotomy rate for intussusception with the introduction of US-guided hydrostatic reduction
Paper #: 134	11:45 AM	Han	The usefulness of second time cranial ultrasonography in predicting the significant white matter injury of premature neonates

10:55 AM	**11:55 PM**	**Scientific Session VI-B: Thoracic Imaging**	
		Claudio Granata, MD (Italy) and Alexander J. Towbin, MD (USA), Moderators	
10:55 AM	*11:05 AM*	**Abdominal Manifestations of Cystic Fibrosis** Alexander J. Towbin, MD (USA)	
11:05 AM	*11:55 AM*	***Scientific Papers***	
Paper #: 135	11:05 AM	Mahomed	Computer Aided Diagnosis (CAD4WHOKids) for WHO Endpoint Consolidation on Chest X-Ray in Children
Paper #: 136	11:13 AM	Amaxopoulou	Magnetic Resonance Imaging of Congenital Lung Lesions
Paper #: 137	11:21 AM	Mahomed	Chest X-ray Findings in Children Hospitalized with WHO Defined Severe, Very Severe Pneumonia in a High HIV Prevalence Setting in the Era of Bacterial Conjugate Vaccines
Paper #: 138	11:29 AM	Lam	Diagnosis of secondary pulmonary lymphangiectasia in congenital heart disease: a novel role for chest ultrasound.
Paper #: 139	11:37 AM	Binkovitz	Imaging Findings of Nuss Bar Migrations: A Retrospective Review
Paper #: 140	11:45 AM	Zandieh	Thoracic CTA in Children with Hemoptysis: Imaging Findings and Implications for Appropriate Use

10:55 AM	**11:55 PM**	**Scientific Session VI-C:MR Contrast Agents**	
		Dennis W. W. Shaw, MD (USA) and Thekla von Kalle, MD (Germany), Moderators	
10:55 AM	***11:05 AM***	**Gadolinium Contrast: Stability, Inertia and Toxicity** *Dennis W. W. Shaw, MD (USA)*	
11:05 AM	*11:55 AM*	***Scientific Papers***	
Paper #: 141	11:05 AM	**Ro**sendahl	Fifty shades of enhancement: timing of post gadolinium images strongly influences the degree of pathology on wrist MRI in children with Juvenile Idiopathic Arthritis.
Paper #: 142 the	11:13 AM	Annapragada	A Nanoparticle Contrast Agent Does Not Penetrate Placental Barrier
Paper #: 143	11:21 AM	Albers	Utility of Gadolinium Use in the Imaging Follow-Up of Non-enhancing Primary CNS Neoplasms in Children
Paper #: 144	11:29 AM	Hackenbroch	Safety of gadoterate meglumine in over 1,600 children included in the prospective observational SECURE study.

Paper #: 145	11:37 AM	Roebel	Evaluation of Potential Gadolinium Deposition in the Abdomen of Children Following Administration of Gadoxetate Disodium
Paper #: 146	11:45 AM	Brown	NSsaFe study: Observational study on the incidence of nephrogenic systemic fibrosis in patients with renal impairment following gadoterate meglumine administration

10:55 AM	**11:55 AM**	**Radiographer Scientific Session: Informatics, Education, QI & Healthcare Policy**	
		Moderators: Stephen F. Simoneaux, MD (USA) and Louise A. Rainford, PhD (Ireland)	
		Scientific Papers	
Paper #: 14 (R)	10:55 AM	Head	The Benefits of an Online MRI Safety Awareness Training Module in a Hospital Setting: "Just Log In"
Paper #: 15 (R)	11:03 AM	Butler	Disclosure of radiation risks in paediatric CT-radiographer's practice and viewpoint.
Paper #: 16 (R)	11:11 AM	Pokorney	Non -Contrast Dynamic Angiography with Arterial Spin Labeling: Preliminary Experience in Children With CINEMA
Paper #: 17 (R)	11:19 AM	Rainford	An investigation of radiology practitioners' and radiographers' opinion of benefit-risk communication and parental consent for pediatric imaging procedures
Paper #: 18 (R)	11:27 AM	Gruber	Improving the Operational Efficiency of Pediatric MR Suites; A multi-year journey
Paper #: 19 (R)	11:35 AM	Grehan	An investigation of the challenges of continuing professional development in the "specialist" field of pediatric radiography
12:00 PM	**1:00 PM**	**Lunch**	
12:00 PM	**1:00 PM**	**SPR Members' Business Meeting**	
12:00 PM	**1:00 PM**	**ESPR General Assembly**	
1:10 PM	**2:20 PM**	**Categorical Course: Oncological Imaging**	
		Moderators: Stephan D. Voss, MD, PhD (USA) and Eline E. Deurloo, MD, PhD (The Netherlands)	
1:10 PM	*1:20 PM*	**Secondary Malignancies and the Role of Surveillance Imaging in Pediatric Oncology** Stephan D. Voss, MD, PhD (USA)	
1:20 PM	*1:30 PM*	**Whole Body MRI in Lymphoma** Claudio Granata, MD (Italy)	
1:30 PM	*1:40 PM*	**Staging of Wilms Tumor** Geetika Khanna, MD, MS (USA)	
1:40 PM	*1:50 PM*	**Guidelines for Imaging and Staging of Neuroblastic Tumors** Hervé J. Brisse, MD, PhD (France)	
1:50 PM	*2:00 PM*	**Chest Tumors in Children Beyond Lymphoma** Eline E. Deurloo, MD, PhD (The Netherlands)	
2:00 PM	*2:20 PM*	**Q&A with RSNA Diagnosis Live™**	

12:50 PM	**2:20 PM**	**Radiographer Refresher Course: Ultrasound Developments in Pediatric Imaging**
		Moderator: Johan G. Blickman, MD, PhD (USA)
12:50 PM	*1:10 PM*	**Looking into Joints** Crystal Parenti, RDMS (USA)
1:10 PM	*1:30 PM*	**Clinical Indications for New Ultrasound Technological Features** Therese Herlihy, BSc, MPH, MSC, Pg.Dip.UTL (Ireland)
1:30 PM	*2:20 PM*	**The Role of Radiographer in Ultrasound (The European and USA Model)** Therese Herlihy, BSc, MPH, MSC, Pg.Dip.UTL (Ireland) and Johan G. Blickman, MD, PhD (USA)
2:20 PM	**2:50 PM**	**Break & Exhibits**
2:55 PM	**4:40 PM**	**Scientific Session VII-A: Neuroradiology**
		Maria Argyropoulou, MD (UK) and Alok Jaju, MD (USA), Moderators
2:55 PM	*3:05 PM*	**Imaging Findings in the Encephalopathy of Prematurity** Maria Argyropoulou, MD (UK)
3:05 PM	*4:40 PM*	***Scientific Papers***

Paper #: 147	3:05 PM	Lequin	Arterial Spin Labeling: a normative value pediatric database
Paper #: 148	3:13 PM	Curran	Amide Proton Transfer MRI Assessment of Brain Tumors: Preliminary Experience in Pediatric Patients
Paper #: 149	3:21 PM	Stamler	The Diagnostic Yield of Head Ultrasound in Outpatient Infants Presenting with Benign Macrocrania
Paper #: 150	3:29 PM	Sergeant	Can MRI face the challenges of cerebellar mutism?
Paper #: 151	3:37 PM	Pratt	Can cranial Doppler ultrasound be used as a problem-solving tool in neonates with equivocal cerebral sinovenous thrombosis?
Paper #: 152	3:45 PM	Webb	Incidence of Venous Sinus Thrombosis and Blunt Cerebrovascular Injury in Pediatric Temporal Bone Fracture
Paper #: 153	3:53 PM	Alt inok	Evaluation of Arcuate Fascicules in Patients with Language Delay and Autism
Paper #: 154	4:01 PM	Valdez	MRI Signal Intensity Characteristics of the Hemorrhagic Quintana Subdural Collections in Children
Paper #: 155	4:09 PM	Cornejo	3 Tesla Multi-transmit Fetal Brain MRI: Preliminary Experience
Paper #: 156	4:17 PM	Kline-Fath	Twin Twin Transfusion Syndrome and Cerebral Pathology: A Comparison of Fetal MRI and Ultrasound
Paper #: 157	4:25 PM	Faingold	Assessment of Cerebral Per fusion in Infants with Hypoxic Ischemic Encephalopathy with Dynamic Color Doppler Sonography

2:55 PM	**4:40 PM**	**Scientific Session VII-B: Cardiovascular Imaging**
		Cynthia K. Rigsby, MD, FACR (USA) and *Susan C. Shelmerdine, MBBS, FRCR (UK), Moderators*
2:55 PM	*3:05 PM*	**4D Flow MRI: Current State and Future Perspectives** Michael Markl, PhD (USA)
3:05 PM	*4:40 PM*	***Scientific Papers***

Paper #: 158	3:05 PM	Shelmerdine	Pediatric Radiology: What Does it Take to get published?
Paper #: 159	3:13 PM	Geiger	Visualization of altered pulmonary artery hemodynamics following TOF repair by 4D flow MRI
Paper #: 160	3:21 PM	Geiger	Flow-sensitive 4D MRI for the Follow-up of Pediatric Patients with Marfan Syndrome: Early Risk Stratification of Progressive Aortic Disease

Paper #: 161	3:29 PM	Geiger	Serial Analysis of Aortic Hemodyna mics in Patients with Repaired Aortic Coarctation by 4D flow MRI
Paper #: 162	3:37 PM	Lai	Feasibility of Non-Anesthesia Neonatal and Young Infant Cardiac Magnetic Resonance Imaging
Paper #: 163	3:45 PM	Deaver	Low Dose Dynamic CTA for Pulmonary Vein Obstruction in Children: A Technical Innovation
Paper #: 164	3:53 PM	Masand	Peri-coronary fat sign on multidetector computed tomographic angiography (MDCTA): A new sign to determine presence and length of intramural course of anomalous aortic origin of the coronary artery (AAOCA)
Paper #: 165	4:01 PM	Nelson	Cardiac catheterization (CC) compared with cardiac MRI (CMR) prior to second stage single ventricle (SV) palliation in low risk patients.
Paper #: 166	4:09 PM	Dillman	Effect of Stage 3 Fontan Operation on Liver Stiffness in Children with Single Ventricle Physiology
Paper #: 167	4:17 PM	Browning	High Takeoff of Coronary Arteries: Incidental finding or Ischemic Predisposition?
Paper #: 168	4:25 PM	Dodd	Inter and Intra-Observer Variability in the Volumetry of Single Ventricle Hearts using a Standardized Approach to Segmentation on MRI

2:55 PM **4:40 PM** **Scientific Session VII-C: Musculoskeletal Imaging**

Amaka Offiah, MBBS, PhD (UK) and Jonathan D. Samet, MD (USA), Moderators

2:55 PM ***3:05 PM*** **MSK Diagnoses: Inflicted, Infected and Inadvertent**

Amaka Offiah, MBBS, PhD (UK)

3:05 PM ***4:40 PM*** ***Scientific Papers***

Paper #: 169	3:05 PM	Clarke	Post Mortem CT as an adjunct to ra diographic skeletal survey in the assessment of sudden unexpected death in infancy and childhood
Paper #: 170	3:13 PM	Hutchinson	Diagnostic accuracy of perinatal post mortem magnetic resonance imaging: single reporter experience
Paper #: 171	3:21 PM	Kriss	Incidence and location of abusive skeletal injuries in infants and children: does perpetrator handedness matter?
Paper #: 172	3:29 PM	Healey	Ischiofemoral impingement in children and adolescents: MRI evaluation
Paper #: 173	3:37 PM	Laor	Incorrect Diagnosis of Distal Radius Buckle Fractures in Children
Paper #: 174	3:45 PM	Stein	The Effect of Scapular Position on MRI Measurements of Glenohumeral Dysplasia Caused by Brachial Plexus Birth Palsy
Paper #: 175	3:53 PM	Miron	Evaluation of Adductus Foot Deformations in Infants Using Ultrasound: A Longitudinal Study
Paper #: 176	4:01 PM	Tsai	Finite Element Analysis of the Classic Metaphyseal Lesionof Infant Abuse: Preliminary Experience
Paper #: 177	4:09 PM	Lindsay	Extended Field of View MR Imaging for suspected osteomyelitis in very young children:Is it useful?
Paper #: 178	4:17 PM	Golriz	Modern American Scurvy – Experience with Vitamin C Deficiency at a Large Children's Hospital
Paper #: 179	4:25 PM	Parikh	Evaluation of Femoral Head Viability in the Post-Operative Pediatric Patient

2:55 PM	**5:30 PM**	**Radiographer Hands-On Ultrasound Session** *(limited space; pre-registration required)*	
4:00 PM	**5:30 PM**	**Radiographer Refresher Course: Talking About MRI** *Moderator: Christopher C. Tomlinson, MBA, CRA (USA)*	
4:00 PM	*4:20 PM*	**Advanced MRI Techniques in Pediatrics** Chris Harris, RT (R) (MR) (USA)	
4:20 PM	*4:40 PM*	**Optimizing MRI Protocols for Pediatric Imaging** Jie Deng, PhD, DABMP (USA)	
4:40 PM	*5:00 PM*	**Safety in MRI: What We All Should Know** Jonathan McNulty, PhD (Ireland)	
5:00 PM	*5:30 PM*	**Panel Discussion**	
4:45 PM	**5:25 PM**	**Scientific Session VIII-A: Interventional Radiology** *Stephanie Franchi-Abella, MD (France) and Charles A. James, MD, FACR (USA), Moderators*	
3:05 PM	*4:40 PM*	***Scientific Papers***	
Paper #: 180	4:45 PM	Gupton	Comparative analysis of anterior and posterior contrast injection approaches for shoulder arthrograms
Paper #: 181	4:53 PM	Hernandez	Endovascular management of portal venous complications after pediatric liver transplantation: a
Paper #: 182	5:01 PM	Kaye	The Role of Portal Venous Embolization as an Adjunct to Hepatectomy by Helping Prevent Post-Resection Liver Failure
Paper #: 183	5:09 PM	Cleveland	Tract embolization for ultrasound-guided percutaneous liver biopsies in a pediatric population: Does what we use matter?
Paper #: 184	5:17 PM	Hayatghaibi	Pediatric Outpatient Ultrasound-Guided Liver Biopsies: Does Decreasing Post-Biopsy Observation Period Time Impact Complication Rates?
4:45 PM	**5:25 PM**	**Scientific Session VIII-B: Tumor-Mass Imaging** *Jonathan R. Dillman, MD, MSc (USA) and Oystein E. Olsen, MD, PhD (UK), Moderators*	
3:05 PM	*4:40 PM*	***Scientific Papers***	
Paper #: 185	4:45 PM	Ahyad	Incidental splenic masses detected during MRI evaluation for iron overload in children.
Paper #: 186	4:53 PM	Pillay	Limited Chest MRI for Detecting Intrathoracic Lymphadenopathy in Children with Suspected Pulmonary Tuberculosis
Paper #: 187	5:01 PM	Alford	MR Imaging of Tumor Associated Macrophages In Pediatric Patients with Malignant Lymphomas and Sarcomas
Paper #: 188	5:09 PM	Cruz Romero	N-Myc Gene Amplification on Pediatric Neuroblastomas
Paper #: 189	5:17 PM	Lai	Streamlining PET/MRI Workflow in Pediatric Oncologic Imaging
4:45 PM	**5:25 PM**	**Scientific Session VIII-C: Cardiothoracic Imaging** *Maria Pilar Garcia-Peña, MD (Spain) and In-One Kim, MD (Republic of Korea), Moderators*	
3:05 PM	*4:40 PM*	***Scientific Papers***	
Paper #: 190	4:45 PM	El Jalbout	Association between carotid artery non invasive elastography and BMI as an indicator of early changes of cardiovascular diseases in children
Paper #: 191	4:53 PM	Krishnamurthy	Free-breathing Reduced Field of View (ZOOM) Black Blood Imaging in P ediatric Cardiac MRI
Paper #: 192	5:01 PM	Suther	Image quality assessment of 3T MR coronary angiography (3D SSFP) in patients operated for transposition of the great arteries with three qualitative methods
Paper #: 193	5:09 PM	Gullberg	Optimizing contrast enhanced thoracoabdominal CT in Lidegran children during extracorporeal membrane oxygenation (ECMO).
Paper #: 194	5:17 PM	Ezon	Lessons learned from patient-specific 3D printing of pulmonary atresia with major aortopulmonary collaterals (MAPCAS) for surgical planning
5:25 PM		**Adjourn**	
7:30 PM	**11:00 PM**	**Annual Reception & Dinner** *(Registration required; additional fee applies)*	

Friday, May 20, 2016

6:45 AM	**12:30 PM**	**Registration**
6:45 AM	**8:30 AM**	**Continental Breakfast**
7:00 AM	**8:15 AM**	**Reviewing for *Pediatric Radiology*** *Moderator: Peter J. Strouse, MD, FACR (USA)*
7:00 AM	*7:15 AM*	**Overview of the Review Process** Øystein E. Olsen, MD, PhD (UK)
7:15 AM	*7:25 AM*	**Title/Abstract/Introduction/Key Words** Anne Paterson, MBBS, MRCP, FRCR (UK)
7:25 AM	*7:35 AM*	**Materials & Methods/Results** Geetika Khanna, MD, MS (USA)
7:35 AM	*7:45 AM*	**Discussion/References/Tables Figures** Cynthia K. Rigsby, MD, FACR (USA)
7:45 AM	*8:00 AM*	**From a Reviewer's Perspective: How I Approach a Review** Andrew T. Trout, MD (USA)
8:00 AM	*8:15 AM*	**How to Make Your Reviews Most Helpful to the Editors** Peter J. Strouse, MD, FACR (USA)
7:15 AM	**8:15 AM**	**US Protocol Session** *(First-come, first-serve basis)* *Moderators: Andrew Phelps, MD (USA), Brian D. Coley, MD, FACR (USA),Samuel Stafrace, MD, MRCP (UK), FRCR, FRCP Edin. (Qatar) and Ian Robinson, MBChB, FRANZCR (Ireland)*
8:30 AM	**12:30 PM**	**Special Sessions (Concurrent)** Unless indicated otherwise, the half day sessions are SAM applicable
8:30 AM	**12:30 PM**	**Musculoskeletal: Imaging in JIA** *Moderators: Lil-Sofie Ording Muller, MD, PhD (Norway) and Charlotte M. Nusman, PhD (The Netherlands)*
		Part 1 – Anatomy vs. Pathology on Imaging
8:30 AM	*9:00 AM*	**Scoliosis: What You Need to Know** Nancy A. Chauvin, MD (USA)
9:00 AM	*9:30 AM*	**Sacroiliac Joint** Jacob L. Jaremko, MD, PhD, FRCPC (Canada)
9:30 AM	*10:00 AM*	**Knee Joint** Mario Maas, MD, PhD (The Netherlands)
10:00 AM	*10:15 AM*	**Discussion**
10:15 AM	***10:30 AM***	**Break**
		Part 2 – Inflammation
10:30 AM	*11:20 AM*	**US in JIA** Paul D. Humphries, MD, FRCR (UK) and Johannes Roth, MD, FRCPC, RhMSUS (Canada)
11:20 AM	*11:50 AM*	**Osteomyelitis/CRMO** Diego Jaramillo, MD, MPH (USA)
11:50 AM	*12:15 PM*	**Update on International Recommendations in JIA-Imaging** Karen Rosendahl, MD, PhD (Norway)
12:15 PM	*12:30 PM*	**Discussion**
12:30 PM		**Adjourn**
8:30 AM	**12:30 PM**	**Oncology & Nuclear Medicine**
		Part 1 *Moderators: Hervé J. Brisse, MD, PhD (France)* ***and*** *Helen R. Nadel, MD, FRCPC (Canada)*
8:35 AM	*8:45 AM*	**Neuroblastoma: Image Defined Risk Factors** Hervé J. Brisse, MD, PhD (France)
8:45 AM	*9:00 AM*	**Image Defined Risk Factor and the New International Neuroblastoma Risk Group Staging System (INRGSS)** Susan L. Cohn, MD (USA)
9:00 AM	*9:10 AM*	**Neuroblastoma: Radionuclide Imaging/Therapy** Adina L. Alazraki, MD (USA)
9:10 AM	*9:20 AM*	**Retinoblastoma Imaging Update** Hervé J. Brisse, MD, PhD (France)
9:20 AM	*9:30 AM*	**Pediatric Soft Tissue Sarcomas** Beth McCarville, MD (USA)
9:30 AM	*9:40 AM*	**SPECT-CT** Susan E. Sharp, MD (USA)
9:40 AM	*9:50 AM*	**Hybrid Imaging in the Era of Personal Oncogenomics** Helen R. Nadel, MD, FRCPC (Canada)
9:50 AM	*10:00 AM*	**Thyroid Carcinoma - Imaging and Therapy** Marguerite T. Parisi, MD, MS (USA)
10:00 AM	*10:10 AM*	**Pediatric Oncologic Interventions - American Approach** Kamlesh U. Kukreja, MD (USA)
10:10 AM	*10:20 AM*	**Pediatric Oncologic Interventions - European Approach** Fernando Gómez Muñoz, MD, PhD (Spain)
10:20 AM	*10:30 AM*	**Discussion**
10:30 AM	**10:45 AM**	**Break**

		Part 2 Moderators: *Øystein E. Olsen, MD, PhD (UK) and Geetika Khanna, MD, MS (USA)*
10:45 AM	*10:55 AM*	**Limitations of RECIST in Pediatric Oncology** Kieran McHugh, MB, FRCR, FRCPI, DCH (UK)
10:55 AM	*11:05 AM*	**Pediatric Lymphoma-PET Imaging** Steve Yoon-Ho Cho, MD (USA)
11:05 AM	*11:15 AM*	**Hepatoblastoma Update** Alexander J. Towbin, MD (USA)
11:15 AM	*11:25 AM*	**Advances in Pediatric Bone Tumor Assessment** Philippe Petit, MD (France)
11:25 AM	*11:35 AM*	**DWI** Øystein E. Olsen, MD, PhD (UK)
11:35 AM	*11:45 AM*	**Whole Body MRI for Cancer Staging** Heike E. Daldrup -Link, MD, PhD (USA)
11:45 AM	*11:55 AM*	**PET-MR** Geetika Khanna, MD, MS (USA)
11:55 AM	*12:05 PM*	**Late Effects** Eline E. Deu rloo, MD, PhD (The Netherlands)
12:05 PM	*12:15 PM*	**Imaging in Bone Marrow Transplant Patients** Ethan A. Smith, MD (USA)
12:15 PM	*12:30 PM*	**Questions and Answers**
12:30 PM		**Adjourn**
8:30 AM	**12:30 PM**	**Cardiovascular Session** *Moderators: Catherine M. Owens, MBBS, FRCR (UK) and Cynthia K. Rigsby, MD, FACR (USA)*
8:30 AM	*8:55 AM*	**Basic CMR Physics** Taylor Chung, MD (USA)
8:55 AM	*9:15 AM*	**CMR Techniques** Taylor Chung, MD (USA)
9:15 AM	*9:40 AM*	**Basic CT Physics** Christina L. Sammet, PhD, DABR (USA)
9:40 AM	*10:00 AM*	**CT Techniques** Aurelio Secinaro, MD (Italy)
10:00 AM	*10:10 AM*	**Discussion**
10:10 AM	**10:25 AM**	**Break**
10:25 AM	*10:40 AM*	**MRI for Assessment of Left-to-Right Shunts** Lorna P. Browne, MD (USA)
10:40 AM	*10:55 AM*	**MRI for Postoperative Assessment of Tetralogy of Fallot** Andrew Taylor, MD, MRCP, FRCR (UK)
10:55 AM	*11:10 AM*	**MRI for Iron Imaging** Cynthia K. Rigsby, MD, FACR (USA)
11:10 AM	*11:30 AM*	**MRI for Assessment of Myocarditis** Phillip C. Lurz, MD, PhD (Germany)
11:30 AM	*11:45 AM*	**Imaging of Pulmonary Hypertension** Catherine M. Owens, MBBS, FRCR (UK)
11:45 AM	*12:00 PM*	**Coronary Imaging**

		Aurelio Secinaro, MD (Italy)
12:00 PM	*12:15 PM*	**Newborn CTA** Rajesh Krishnamurthy, MD (USA)
12:15 PM	*12:30 PM*	**Discussion**
12:30 PM		**Adjourn**
8:30 AM	**12:30 PM**	**Hands-On Ultrasound Session (Non-SAM Session)** *Moderators: Brian D. Coley, MD, FACR (USA), Ian Robinson, MBChB, FRANZCR (Ireland) and Kassa Darge, MD, PhD (USA)*
8:30 AM	**9:40 AM**	**Session 1: Bowel Imaging** Andrea Magistrelli, MD (Italy)
9:40 AM	**10:50 AM**	**Session 2: Ultrasound Elastography in the Pediatric Population** Jonathan R. Dillman, MD, MSc (USA)
10:50 AM	**11:05 AM**	**Break**
11:05 AM	**11:40 AM**	**Session 3: Contrast Enhanced Voiding Urosonography (ceVUS)** Part 1: Oral Presentations
11:05 AM	*11:15 AM*	**How to Do ceVUS: A Step-by-Step Approach** Kassa Darge, MD, PhD (USA)
11:15 AM	*11:20 AM*	**Case Demonstration: ceVUS in Daily Practice** Susan Back, MD (USA)
11:20 AM	*11:25 AM*	**Intrarenal Reflux in ceVUS: Additional Detail** Zoltan Harkanyi, MD (Hungary)
11:25 AM	*11:30 AM*	**Safety: ceVUS with Intravesical Contrast** Aikaterini Ntoulia, MD (UK)
11:30 AM	*11:35 AM*	**Comparative Case Demonstration** Jeanne S. Chow, MD (USA)
11:35 AM	*11:40 AM*	**In Vitro Demonstration of ceVUS: What and How?** Kassa Darge, MD, PhD (USA)
11:40 AM	*12:30 PM*	Part 2: In Vitro Demonstration and Hands-On Practice Kassa Darge, MD,PhD (USA), Aikaterini Ntoulia, MD, PhD (UK), Susan Back, MD (USA) and Laura Poznick, ASS, RDMS (USA) ***Station 1: In-vitro ceVUS Simulation*** Kassa Darge, MD, PhD (USA) and Susan Back, MD (USA) ***Station 2: US Contrast Preparation for ceVUS*** Laura Poznick, AAS, RDMS (USA) ***Station 3: Hands-On Imaging Microbubbles*** Laura Poznick, AAS, RDMS (USA) ***Station 4: Hands-On Imaging Microbubbles*** Aikaterini Ntoulia, MD (UK)
12:30 PM		**Adjourn**
8:30 AM	**12:30 PM**	**Interventional Radiology** *Moderators: Manish N. Patel, DO (USA) and Alex M. Barnacle, BM, MRCP, FRCR (UK)*
8:30 AM	*9:00 AM*	**Sclerotherapy of Slow Flow Orbital Malformations** James W. Murakami, MD (USA)

9:00 AM	*9:30 AM*	**Bleomycin Sclerotherapy** Gulraiz Chaudry, MD, MBChB, MRCP, FRCR (USA)
9:30 AM	*10:00 AM*	**Pediatric Stroke Update** Manraj K. S. Heran, MD, FRCPC (Canada)
10:00 AM	*10:15 AM*	**Discussion**
10:15 AM	**10:30 AM**	**Break**
10:30 AM	*11:00 AM*	**The Underestimated Role of Ablation Techniques in Pediatic Interventional Oncology: What They Could Offer in Children** Fernando Gómez Muñoz, M D, PhD (Spain)
11:00 AM	*11:30 AM*	**Advanced MSK/IR Intervention** Neil D. Johnson, MD (USA)
11:30 AM	*12:15 PM*	**Paediatric IR Tips and Tricks** Alex M. Barnacle, BM, MR CP, FRCR (UK) and Derek J. Roebuck, MD (UK)
12:15 PM	*12:30 PM*	**Discussion**
12:30 PM		**Adjourn**
8:30 AM	**12:30 PM**	**Neuroradiology** *Moderators: Maria Argyropoulou, MD (UK), Dennis W. Shaw, MD (USA) and Thierry A. G. M. Huisman, MD (USA)*
8:30 AM	*9:00 AM*	**Neuroimaging Updates on Neonatal Hypoxic Ischemic Injury and Hypothermia** Fabio M. Triulzi, MD (Italy)
9:00 AM	*9:30 AM*	**Fetal MRI of the Central Nervous System and Beyond** Catherine Adamsbaum, MD (France)
9:30 AM	*10:00 AM*	**New Imaging Concepts in Central Nervous System Neoplasms** Maarten H. Lequin, MD, PhD (The Netherlands)
10:00 AM	*10:20 AM*	Questions and Answers
10:20 AM	**10:40 AM**	**Break**
10:40 AM	*11:10 AM*	**Update on Soft Tissue Vascular Anomalies in the Pediatric Head and Neck** Aylin Tekes-Brady, MD (USA)
11:10 AM	*11:40 AM*	**What You Should Know About Accidental and Non-Accidental Head Injury** V. Michelle Silvera, MD (USA)
11:40 AM	*12:10 PM*	**Arterial Spin Labeling in Pediatric Neuroradiology** Arastoo Vossough, MD, PhD (USA)
12:10 PM	*12:30 PM*	**Questions and Answers**
12:30 PM		**Adjourn**

Sunday, May 15, 2016

CHEST

CT or MR for Imaging of Cystic Fibrosis?

Pierluigi Ciet MD, PhD (The Netherlands)

Cystic fibrosis (CF) lung disease is monitored at regular intervals to guide therapy and to prevent or reduce the progressive lung damage. CF lung disease monitoring has changed in the last decade. Nowadays, computed tomography (CT) is considered the most sensitive method to monitor CF lung disease in early and advanced stages. The main disadvantage of CT is that it exposes patients to ionizing radiation. Therefore, CT protocols for CF are usually low or ultra-low dose. Despite this low radiation dose, it restricts the use of chest CT for short and long-term follow-up, especially in children, who are more sensitive to radiation than adults. Magnetic Resonance Imaging (MRI), as radiation free technique, has been introduced as an alternative to CT. To date, MRI has been directly compared to CT in few studies, using various MRI sequences, and with discordant results. From these studies, MRI seems almost comparable to CT with regard to the detection of large morphological changes (i.e. bronchiectasis and consolidation), but still less sensitive in the assessment of lung's periphery and to detect trapped air. At the same time, MRI is superior to CT when it comes to the assessment of functional changes, such as altered pulmonary perfusion, pulmonary ventilation or for the quantification of pulmonary inflammation. This presentation gives an overview of our 10-year experience in CT and MR imaging for CF lung disease. It provides a brief state-of-the-art review of CT and MR protocols for CF, and outlines the advantages and the disadvantages of each techniques.

Imaging Scoring Systems for Cystic Fibrosis-Helpful or Not?

Mantosh Rattan, MD (USA)

Cincinnati Children's Hospital Medical Center

Imaging has traditionally been an important tool in the evaluation of lung disease in patients with cystic fibrosis. The use of imaging provides useful insights into the role of imaging biomarkers in the improvement of care for patients with a chronic disease.

Scoring systems allow for the conversion of an image interpretation (which may be relatively subjective) into a more objective numerically based instrument. Data can then be analyzed for statistical significance, used to create a database of normative values to provide a standard of reference, and ultimately facilitate prognostication based on a disease score which would otherwise be impossible (or at least much more difficult) with traditional textual based imaging reports. There are a number of studies that have demonstrated that higher lung disease scores on CT in childhood predict more severe disease later in life. Numerically based disease scoring systems also provide value in that they allow for demonstration of change over time, which may help to determine appropriate timing for interval surveillance.

The principal goal of cystic fibrosis research is realization of a cure. Imaging will continue to play an essential role in disease monitoring and will undoubtedly be of chief importance in demonstration of the absence of disease once cure is ultimately achieved. This discussion will focus on the usefulness of imaging based disease scoring systems as well as the potential impact that implementation of these systems may have on routine patient care and cystic fibrosis research.

Misplaced Central Venous Catheters in the Chest

George A. Taylor, MD, FACR (USA)

The use of central venous catheters is commonplace in children for hyperalimentation, intravenous drug therapy, hemodialysis and volume administration. Despite the use of image guidance with fluoroscopy and ultrasound during placement, arterial misplacement occurs in up to 2.2% of attempted insertions. This presentation will review the common radiographic signs suggestive of unintentional arterial misplacement of vascular catheters. These include leftward curvature of the vertical portion of the catheter, left-sided catheter tip position, lack of catheter crossover on the frontal radiograph, as well as exaggerated anterior angulation of the catheter on the lateral chest radiograph. The utility of a lateral chest radiograph will be emphasized in confirming normal and suboptimal placement of venous catheters.

Neonates with congenital diaphragmatic hernia are another cohort of patients that are at high risk for misplacement of venous catheters. The resultant alterations in vascular and hepatic anatomy can result in incorrectly placed umbilical venous catheters (UVC) in up to 52% of infants. Most common locations for suboptimally placed UVC's include the contralateral chest (27%), abdominal intrahepatic location (16.7%) and the umbilical vein (8.3%). One study found that 30% of radiographic reports were inadequate regarding the location of the catheter tip, and in 9%, the location of the catheter tip was reported incorrectly. This presentation will review normal and suboptimal placement of UVC's in this population, and will detail the underlying anatomic alterations responsible for suboptimal placement.

Prenatal Evaluation of Congenital Diaphragmatic Hernia

Catherine Garel, MD (France)

Congenital diaphragmatic hernia (CDH) results from a diaphragmatic defect with subsequent ascension of abdominal organs into the thorax. Most CDH are left-sided and posterolateral. A sac is usually absent. CDH are very uncommonly bilateral. The aims of prenatal imaging are: - to diagnose the hernia, - to evaluate the prognosis, - to follow-up during pregnancy, particularly in case of prenatal therapy.

The diagnosis of left CDH is usually assessed by ultrasonography (US) and is mostly based on indirect findings: mediastinal shift with visibility in the hemi thorax of bowel loops and/or stomach and/or left liver. Ascension of the liver results in displacement of the umbilical vein and hepatic vessels. In right CDH, the herniated liver may be mistaken for lung. The diaphragmatic defect is better depicted by MRI, which also clearly shows the herniated organs and the amount of normal lung. CDH should be differentiated from eventration, which carries a better prognosis.

The prognosis depends on associated findings, present in 30-50% of cases and partly searched for by US. The main prognostic factor is pulmonary hypoplasia, accounting for CDH being lethal in 30–40% of cases. Lung volume is evaluated indirectly by US (LHR, lung-to-head ratio) and directly by MRI. Both observed (o) LHR and lung volumes are compared to expected (e) values for gestational age. The prognosis is poor in case of herniated liver with LHR<1, LHRo/LHRe<25% and o/e lung volume <25%.

In intermediate and severe types, transient fetal tracheal occlusion may be performed during the third trimester.

Imaging Interstitial Lung Disease in Children: An Update

Catherine M. Owens, MBBS, FRCR (UK)

Diffuse interstitial lung disease in children is different from interstitial lung disease in adults, and a distinct entity.

The childhood interstitial lung disease (ChILD) classification, devised in 2010, separates the relevant conditions into those confined to infants, and those not specific to infants.

Those conditions not specific to infants contains conditions related to systemic diseases (including connective tissue diseases and depositional / storage disorders), and also conditions occurring in children with primary and secondary immunodeficiency.

In this lecture we briefly review normal lung growth and development, briefly discuss our preferred technique for imaging the lungs with computed tomography (CT) and present the radiological appearances of selected childhood interstitial lung diseases. We use cases from our institution, and emphasize more recently recognised conditions including

pleuroparenchymal fibroelastosis (PPFE) and filamin A (FLNA) deficiency related lung disease.

MR Imaging Technique of the Chest for Pulmonary Nodules
Sureyya B. Gorkem, MD (Turkey)

MDCT is currently the primary cross-sectional imaging modality of choice because of its well-established accuracy and wide availability for detection and characterization of pulmonary nodules. Although MDCT can yield highly accurate information in children, it is associated with potentially harmful ionizing radiation exposure. The effort to reduce radiation exposure due to MDCT is particularly important to pediatric patients because they are more radiosensitive and thus have higher risk than adults of development of neoplasms from ionizing radiation exposure. Because of this concern, MRI is an attractive alternative imaging modality for evaluating thoracic disorders in the pediatric population. In both adult and pediatric literature encouraging results have been reported for detection of pulmonary nodules larger than 3 mm in diameter by use of fast imaging techniques. Especially 3D or 2D gradient recalled echo (GRE) and T2-weighted fast spin-echo (FSE) or T2-weighted HASTE sequences are mostly in use for detection of pulmonary nodules. Although lung MRI has some disadvantages including low proton density in parenchyma, magnetic susceptibility differences between air and soft tissue and motion artifacts due to cardiac pulsation and respiratory motion, sequence improvements may aid to identify pulmonary nodules. For the pediatric patients whom need multiple imaging studies for follow-up of pulmonary nodules, lung MRI as a first-line cross-sectional imaging study in lieu of MDCT should be considered. This presentation is designed to provide a brief review about current MR imaging technique of the chest for pulmonary nodules in children.

CARDIOVASCULAR

Anatomic Causes of Renovascular Hypertension in Children
Jung-Eun Cheon, MD, PhD (Korea)

Renovascular disease or renal artery stenosis is an unusual but important cause of hypertension in children because it is potentially curable with angioplasty or surgery. Fibromuscular dysplasia (FMD), an idiopathic angiopathy characterized by non-inflammatory fibrodysplastic narrowing of medium sized arteries, is the most common cause of renal artery stenosis in children. Numerous pediatric disorders such as neurofibromatosis type I, Takayasu arteritis, or moyamoya disease, have been associated with renal artery stenosis. The lesions that occur in patients with these disorders are frequently multiple and complex with long-segment stenosis and have abnormalities of other vessels (aorta cerebral, intestinal or iliac). In children without comorbid conditions, renal artery stenosis shows different pattern. It is usually single and focal, and commonly located in branch arteries or accessory renal arteries. The purpose of this presentation is to provide a brief review of renovascular disease in children focused on its anatomic causes. A clear understanding of anatomic causes of renovascular hypertension in children has great potential to lead to optimal management in pediatric patients with clinically suspected renovascular hypertension.

Role of US in Renovascular Hypertension
Ethan A. Smith, MD (USA)

Pediatric hypertension is different from that seen in adults; up to 85% of children have an identifiable cause for their hypertension. Vascular abnormalities account for between 5 and 10% of pediatric hypertension. Children with renovascular hypertension present clinically with markedly elevated blood pressure, often refractory to multiple medications. Pediatric renovascular hypertension can be idiopathic, but is also associated with a variety of syndromes, including neurofibromatosis type 1 and William's syndrome. In patients with suspected renovascular hypertension, imaging is employed to confirm the diagnosis, to characterize the renovascular abnormality and to guide therapy. Ultrasound with Doppler is the most frequently used initial imaging test, but has historically been thought to be unreliable due to suboptimal sensitivity and specificity. More recent investigations have demonstrated that renal ultrasound with Doppler may perform better than previously thought. Findings that may indicate a renovascular cause for hypertension include abnormal arterial waveforms with a prolonged acceleration index (*parvus et tardus*), increased peak systolic velocities in the main renal artery, low resistive indices (<0.5), or asymmetric renal size. Importantly, renal ultrasound may reveal a non-vascular cause for pediatric hypertension, such as an adrenal mass. The role of ultrasound with Doppler in the diagnosis of pediatric hypertension is evolving. Although catheter based digital subtraction angiography remains the gold standard imaging test in clinically suspected renovascular hypertension, renal ultrasound with Doppler is a reasonable initial test, as it may guide the further diagnostic work up or reveal a non-vascular cause for the patient's hypertension.

Role of CT in Renovascular Hypertension
Monica Epelman, MD (USA)

Hypertension may be primary (e.g. essential) or secondary. In pediatric patients, secondary hypertension occurs more commonly than essential hypertension. Renovascular disease is the third most common cause of pediatric hypertension, following coarctation of the aorta and renal parenchymal disease. The precise incidence of pediatric renovascular disease is unknown, but is estimated to account for 5 to 25% of the cases, while in adults, renovascular hypertension is found only in approximately 1% of the cases. The best choice of imaging modality for evaluation of pediatric renovascular hypertension remains controversial. Historically, the standard of care for the evaluation of renovascular hypertension has been ultrasound, renal scintigraphy, and digital subtraction angiography. Based on its high accuracy reported in adults, renal computed tomography angiography (CTA) with pediatric appropriate low dose radiation techniques, is an alternative imaging option in the assessment of renovascular hypertension in children. Key advantages of renal CTA is that it is a non-invasive, three dimensional angiographic technique which can be performed rapidly, at low cost and in the majority of instances without sedation. This presentation is designed to illustrate by examples these advantages and to provide an overview of renal CTA findings in the most common childhood renovascular diseases.

Role of MRI in Renovascular Hypertension
Franz Wolfgang Hirsch, MD (Germany)

The Magnetic Resonance Angiogram (MRA) is an important alternative to the CTA and the DSA. It is mainly used for children, when ionizing radiation should be avoided. The spatial resolution of the MRA is slightly lower than the resolution of the CTA, and well below the resolution of the DSA. Nevertheless, the sensitivity and specificity of the MRA is just as high as in the CTA for vessels ≥2 mm diameter (90-100%). There are no comparative data from CTA and MRA for smaller intrarenal vascular changes in children, however.

Renal arteries can be presented with the MR both with and without contrast agent. The conventional techniques with time-of-flight (TOF) or spin-labeling are not so sensitive with renal arteries. Newer techniques without contrast agent (NC-MRA) are based on fast-steady-state-gradient protocols. These are axially acquired, and allow secondary reconstructions in any plane. Unfortunately, however, the sequences only allow a small field of view.

The most experience is with children with contrast-enhanced-MRA (CE-MRA) of the renal arteries. It also allows much larger FOVs than with the NC-MRA, down to the iliac arteries, which is important when accessory renal arteries from the iliac vessels should also be displayed.

The indications for a renovascular imaging with magnetic resonance tomography are identical to the CTA: renal hypertension caused by fibromuscular dysplasia (FMD), by Takaysu arteritis (TA), and children with vascular stenosis due to neurofibromatosis type 1 (NF1). Another indication is the search for extrinsic obstructive accessory renal arteries as a cause of hydronephrosis.

Role of Angiography in Renovascular Hypertension
Derek J. Roebuck, MD (UK)

Digital subtraction angiography (DSA) remains crucial in the diagnosis of children with suspected renovascular hypertension. A large proportion of treatable arterial disease in these patients involves lesions of small vessels that are currently difficult to detect with non-invasive imaging. It is mandatory to perform a test with high sensitivity for these lesions because the long-term morbidity of hypertension is very significant. Most children with renovascular hypertension will undergo endovascular treatment at the same procedure as diagnostic angiography.
DSA is best performed under general anesthesia. Involvement of the abdominal aorta, celiac trunk and superior and inferior mesenteric arteries is not unusual in children with renovascular disease. These vessels may be best assessed with a rotational aortogram, which also allows evaluation of the number and origins of the renal arteries. Selective renal angiography in various projections is essential for the accurate diagnosis of intrarenal arterial lesions. Various indirect signs of arterial pathology may be helpful, especially the presence of collateral circulation to or within the kidney.
Although DSA provides images with extremely high spatial and temporal resolution, it has important deficiencies. These include the detection of abnormalities of the arterial wall (such as wall thickening and inflammation and the presence of webs), failure to detect stenoses due to the projectional nature of the technique, and poor assessment of the functional significance of a lesion. Various supplementary techniques, such as pressure measurements, intravascular ultrasound or optical coherence tomography, and renal vein renin sampling, may mitigate these problems to some extent.

NEURORADIOLOGY

Imaging the Premature Brain: New Knowledge
Stein M. Aukland, MD, PhD (Norway)

Premature birth has major effects on the newborn brain and imaging is of great importance. Performing Magnetic Resonance Imaging (MRI) in a premature is a challenge and in acute decision- making, cerebral Ultrasonography (cUS) is still the modality of choice. Whether cUS or MRI is the best prognostic tool is debated and so is the frequency and the timing of imaging.
Serial cUS detects most abnormalities associated with abnormal neurodevelopmental outcome but cerebellar hemorrhage, small cortical infarcts and hypoglycemic parenchymal injurymay be missed. MRI scanning at gestational age week 30 has been proposed, but the value is uncertain. Near-term MRI as a predictor of outcome is a routine in some institutions, but long-term follow- up studies for evaluation of this screening are lacking. In extremely preterm, abnormalities detected on late cUS and near-term MRI are associated with outcome and term-equivalent age may be the best time-point for scanning these newborns. Several studies have compared the value of serial cUS and near- term MR, but no strong conclusions are drawn. Advanced MRI as Diffusion Weighted Imaging may assess disease severity and evaluate the effect of treatment and patterns at MR spectroscopy may reflect subtle White Matter pathology.
In this lecture, I will focus on imaging in the newborn period, as a prognostic tool; the choice between cUS and MRI, serial imaging vs. near-term imaging. A brief update on the most common imaging findings and their value for the diagnostic and prognostic work-up will also be given.

Hydrocephalus: Imaging Update
Nuno Canto Moreira, MD, PhD (Sweden)

The concept of hydrocephalus is not consensual but it may be defined as a disorder of cerebrospinal fluid (CSF) flow that results in the enlargement of ventricles.
This is not a disease but instead a complex secondary process that usually follows an obstruction to CSF-flow in the ventricles or at the brain convexity. Overproduction of CSF, abnormal vascular behaviour or genetic factors may also induce hydrocephalus, by mechanisms that are not fully understood in all cases.
Regardless of the cause, the management of hydrocephalus is still quite standard and is the most common set of procedures done in children by neurosurgeons.
As an entity that often demands multiple interventions over time, with a major impact on healthcare, the importance of understanding the key-points in hydrocephalus by radiologists cannot be over-emphasised.

For this short presentation we shall focus on some relevant topics:
1) Main concepts on the pathophysiology of hydrocephalus
2) MR protocols for the investigation of hydrocephalus in children
3) How to diagnose a hydrocephalus by imaging
4) The consequences of hydrocephalus on the paediatric brain
5) Can we to distinguish hydrocephalus from a benign enlargement of CSF spaces (BESS)?
6) Treatment and major complications
7) Future trends

3-D Printing for Pediatric Neuro Imaging
Sanjay P. Prabhu, MBBS, FRCR (USA)

3D printed models are being increasingly used in medicine to help referring clinicians plan and simulate complex surgical procedures and enable patient and trainee education about complex structural abnormalities and implications of treatment plans. Radiologists are being called upon to be at the center of this process of creating 3D printed models, as an accurate patient-specific model depends upon carefully planned and high quality imaging studies. The role of 3D printing in neurosurgical procedures involving the pediatric brain, head and neck and spine is still being defined. This presentation gives an overview of optimized workflows required to deliver high quality prints from neuroimaging studies based on a novel "on-demand" in house 3D printing service developed over the last 2 years. The need for detailed image planning, overview of segmentation techniques and multimodality overlays to print different parts of the anatomy and technical requirements including printer selection, personnel training, software requirements and quality control to produce accurate 3D models will be emphasized in this presentation. The utility of 3D printing for planning complex pediatric neurosurgical procedures including endovascular treatment and surgical resection of complex cerebrovascular lesions, epileptogenic focus resection, craniofacial and skull base surgery and spinal procedures like complex scoliosis correction will be highlighted. The presentation will also review the benefits of 3D printing specific to pediatric patients and potential pitfalls to watch out for while setting up a 3D print service including start- up costs and reimbursement challenges.

Abusive Head Trauma: The Role of DWI, SWI and MRS
Jean-Francois Chateil, MD, PhD (France)

Brain injuries are a major cause of morbidity and mortality in abused children under 2 years of age. In emergency, CT remains the initial examination in suspected head trauma, but MRI is indicated to better depict the parenchymal lesions when CT is equivocal or discordant with clinical signs, or to give more details about pericerebral spaces or parenchymal lesions; MRI is also particularly useful for follow-up. In addition to T1- and T2-weighted sequences, diffusion-weighted imaging (DWI) is mandatory, especially in the initial phase of trauma, to look for hypoxic-ischemic

changes. Hypoxic lesions are seen as restriction of water diffusion in relation with cytotoxic edema; it could be focal, cortical and sub-cortical or more diffuse; associated basal ganglia lesions are of poor prognosis. Progression of the lesions can be seen after the acute onset during the first days. DWI is also useful to depict axonal lesions, with a lower fraction of anisotropy and fibers disruption seen with tractography during follow-up. Susceptibility-weighted imaging (SWI) is more sensitive than T2* for small hemorrhages and is considered as the best tool to depict a bleed. It appears as a hyposignal within the brain parenchyma. SWI also helps to characterize intracranial extra-axial hemorrhages (subarachnoid, subdural) but also within the spinal canal. Associated retinal hemorrhages may also be seen with SWI. MR spectroscopy (MRS) is useful at the acute phase to assess hypoxic lesions, when high relative concentration of lactate, compared to creatine and N-acetylaspartate (NAA), is obvious.

Spinal Findings in the Setting of Child Abuse
Michael A. Breen, MBBCh (USA)

Abusive head trauma is the most common etiology of traumatic brain injury in infants. Mortality ranges between 15 and 25% with significant neurological deficits in the majority of survivors. Spinal injuries have been under recognized in abusive head trauma in the past but changes in autopsy protocols, more frequent use of computed tomography (CT) and magnetic resonance imaging (MRI) of the spine and the emerging use of fluorine 18-labeled sodium fluoride positron emission tomography (18F-Na-F PET) have led to an increased awareness of the association of spinal injuries with abusive head trauma.
Spinal fractures are seen radiographically in 10% of infants with a positive skeletal survey and may be the only indication of skeletal injury on these studies. Advanced imaging techniques such as CT, MRI and 18F-NaF often demonstrate additional spinal fractures in these children. Children with spinal fractures are at significantly greater risk for intracranial injury than those without spinal fracture.
MRI also commonly demonstrates ligamentous injuries; particularly at the craniocervical junction; and spinal subdural hematomata in abused children. This presentation is designed to provide a brief review of the pathophysiology of spinal injuries in abusive head trauma. We will review the imaging characteristics and techniques used for detection of spinal fractures on radiographs and skeletal surveys, CT, MRI and 18F-NaF studies. The MRI appearance of spinal ligamentous injuries and spinal subdural hematoma seen in abusive head trauma will be reviewed.

Biomechanics in Spondylolysis
Marcelo Galvez, MD (Chile)

The Spondylolysis fractures is a defect of the interarticularis parts of the lumbar spine, having a major tendency of cases in L4 and L5 due to the fact of carrying more load from the upper body. This condition can be cause by fatigue of pars interarticularis because of repetitive trauma done to the lumbar spine. This injury has a higher incidence in activities that includes repetitive movements or high-impact sports such as tennis, soccer or gymnastic. It is has been also suggest a hereditary condition to form thin lumbar vertebral bones that has much to do with the occurrence of spondylolysis. But the principal question to be answered is to know if some characteristics of each person as pelvic incidence, sacral slope, inter-facet region with trapezoidal shape or slip percentage, can significantly affect the loads distribution of lumbar spines, to reach the presence of spondylolysis fractures the worst case scenario. In other words, to predict the structure failure for particular biomechanical patients factors. Finite element analysis has been an excellent tool in order to study biomechanical loads and motion. The construction 3D lumbar spine of patient specific characteristic may study the geometry facts that may cause abnormal loads creating spondylolysis formation. With FEA simulation, complex personalized structures can be model to create biomechanical test to find the causes of the failure and compare virtual structure treating result such as surgical intervention scenarios to predict events and evaluate consequences.

Monday, May 16, 2016

CT RADIATION DRLS AND DOSE REPORTING GUIDELINES
US Perspective
Michael J. Callahan, MD (USA)

The term diagnostic reference level (DRL) was initially established by the International Commission on Radiological Protection about 20 years ago. A DRL should be considered a safety guideline to identify unusually high radiation doses for common medical imaging procedures, and not an optimization target. DRLs can serve as a reference for radiology practices to compare their radiation doses to aggregate dose data previously accumulated locally, regionally or nationally. Traditionally, the DRL process involves determination of a 75th percentile of aggregated dose data. Institutions who have a mean or median exposure above the DRL for a group of patients should strongly consider modifying their CT protocols. Although the United States (U.S.) has unique challenges related to the creation of national DRLs, the U.S. lags behind its European counterparts in the generation of large-scale data for the creation of DRLs, particularly in children. Recently, the American College of Radiology's Dose Index Registry has provided a nationwide resource for aggregate CT patient dose data by which DRL data may be obtained for both adults and children. In 2013, the Quality Improvement Registry for CT Scans in Children (QuIRCC) provided diagnostic reference ranges for pediatric abdominal CT studies as a function of patient body width. This presentation will provide a brief overview of the use of DRLs in the U.S., focusing on the unique challenges related to the effective implementation and maintenance of DRLs for pediatric CT studies.

Europe Perspective
Raija M. Seuri, MD (Finland)

The European Guidelines on DRLs for Paediatric Imaging is published in 2016. The PiDRL project to establish the Guideline was initiated by EU, led by ESP, accompanied by other professional organizations, e.g. ESPR and EFOMP. The PiDRL Guidelines include the European DRLs for the most common pediatric examinations. It also introduces the principles how to establish national and local DRLs, and how the reference levels should be used.
The European DRLs are based on existing national DRLs. Though many countries have NDRLs for pediatric radiography, only a few have established DRLs for CT examinations, and most of them only for head and chest CT.
According to the PiDRL Guidelines the DRLs are based on actual patient dose values collected from representative organizations including all types of radiological practices. Also the dose values compared to the DRLs should be collected from clinical examinations; phantom measurements have their role in the technical QA.
Dose quantities used should be easily available from the console. Both $CTDI_{vol}$ and DLP are recommended quantities for DRLs. SSDE may be used in the future, when the automatic software able to manage also the use of TCM is available. According to the Guidelines the different sizes of children are managed by using recommended weight groups or a DRL curve.
Comparing dose levels is a way to increase our awareness of the level of optimization in our own unit, hospital and country.

GENITOURINARY IMAGING
Current Trends in Pediatric GU Imaging: US Perspective
Jeanne S. Chow, MD (USA)

In this presentation we will tour the Americas and highlight the current innovative and exciting trends and trendsetters in pediatric uroradiology. We will focus on the practical new clinical and technological innovations

happening in the field that are useful to all pediatric radiologists, not just those who specialize in genitourinary imaging. The topics will include the new imaging methods which provide more robust visual and functional information of the urinary tract, how consensus and collaboration have provided improved care for our patients, and hopefully spark creative interest for further research in our field.

Current Trends in Pediatric GU Imaging: European Perspective
Pierre-Hugues Vivier, MD, PhD (France)

Genitourinary tract explorations are extremely frequent in a pediatric radiology department. However, the number of examinations has decreased due to a decreasing number of indications. For example, recent literature suggests to limit the screening for vesico-ureteric reflux. The use of ionizing radiations has dramatically decreased in this setting, in line with the ALARA principle. New techniques, such as contrast-enhanced voiding contrast-enhanced voiding urosonography, allow partial replacement of classical radiological examinations. New Doppler techniques offers substantial refinements for a better evaluation of tissular vascularisation. MRI challenges scintigraphy for urinary obstruction evaluation.
A new trend in European uroradiology corresponds to the publication of recommendations every year since 2008 by the uroradiology taskforce of the European Society of Pediatric Radiology. The goal is to try to standardize practices in Europe. Also, the taskforce collaborated with European pediatric urologists and nephrologists to elaborate a pediatric radiological thesaurus.

Current Trends in Pediatric GU Imaging: South American Perspective
Ximena C. Ortega, MD (Chile)

The malformations of the urinary system constitute one of the major challenges of the pediatric radiology. The early diagnosis allows timely interventions ensuring better anatomical and functional results. Magnetic Resonance Imaging has contributed significantly to the diagnosis because the resolution of the images with no radiation, outlining alterations of position, shape and size of the kidney, ureteropelvic junction, ureter and bladder. In countries with no legal pregnancy interruption, fetal imaging have become in an important tool to address delivery according the necessity for immediate or deferred urologic intervention, helping also to plan complementary images, deciding for whom, when and how to perform an ultrasound, X-Ray or CT examination. After birth, MRI can also give us functional information using contrast dynamic studies. This approach, having the focus in the earliest precise diagnosis is rewriting the history of genitourinary pathology, as a continuous process from the fetal life to the childhood. This class highlights those pathologies where the early notice can make the difference.

WHOLE BODY IMAGING

Whole Body MR: The Basics
Lil-Sofie Ording Muller, MD, PhD (Norway)

New Magnetic Resonance Imaging (MRI) techniques, combined coils and moving table tops has made it possible to perform whole body MRI (WBMRI) to search for multifocal pathology, like malignancies, inflammatory- and metabolic lesions. Historically, radiography and bone-scintigraphy have been used for these purposes, however, at the cost of ionizing radiation and low spatial resolution and tissue contrast. As radiation protection is particularly important during childhood and puberty the WBMRI technique has been embraced for clinical use although to date, it's precision, accuracy and clinical validity in children is not determined.
The protocol in WBMRI varies with the clinical query, however there are some 'core' sequences that are most often included. A water sensitive fat-supressed sequence is typically performed. STIR, or T2 DIXON are preferred techniques due to the homogenous fat-suppression. Spin echo T1 sequence, increases the specificity, particularly for findings in the bone marrow. The common scan plane is coronal with additional planes being added depending on the indication. In 2004 Takahara et al. discovered that coherent motions during breathing did not influence the assessment of water diffusivity on diffusion weighted MRI, as previously thought. Development of diffusion weighted imaging with body background suppression, the DWIBS-technique which, with the use of parallel imaging, echo planar diffusion and STIR fat-suppression, made it possible to also perform diffusion weighted imaging as part of the WBMRI-protocol.
This presentation will provide a brief overview of technical aspects, main indications and the rationale behind the choice of sequences for the most common queries for WBMRI.

Whole Body MR: Pitfalls and Incidental Findings
Øystein E. Olsen, MD, PhD (UK)

"Whole-body MRI" commonly means relatively low-resolution short-tau inversion recovery (STIR) MRI, often with coronal acquisitions only. But some studies add planes (e.g. sagittal STIR of the spine) or sequences (e.g. diffusion-weighted imaging [DWI]) depending on indication(s).
It follows that one cannot talk about some well-defined advantages and disadvantages of "whole-body MRI"; that depends on what we use it for and how we define the term. However, in broad terms pitfalls may be:

A. Failure to detect significant abnormalities
1. Due to biology
Embryonal tumours (small round blue cell tumours) are the neoplasms most commonly seen in childhood. These are membrane-rich water-poor, which presumably explains why they may not have very high signal intensity on STIR.
Relatively small lymph nodes involved in lymphoma. These have high signal intensity (and restricted water diffusion) just like non-neoplastic lymph nodes.
2. Due to technique
Motion artefact causes difficulties with interpretation typically in the mediastinum (cardiac pulsation), liver (breathing) and mesentery/retroperitoneum (peristalsis)
Partial voluming phenomena increase with increasing slice thickness. A single-plane scan does not mitigated these
Inappropriate imaging planes, e.g. axial or coronal images of the spine; coronal images of the chest, abdomen pelvis

B. Failure to correctly classify observations as normal

Striking focal signal variability (both on STIR and DWI) is normal with no age-related pattern. DWI highlights normal lymphoid and neural tissue. Such lack of specificity reflects the nature of MRI.

Whole Body Vascular MRI
Shreyas S. Vasanawala, MD, PhD (USA)

Some pediatric vascular diseases are systemic and thus may benefit from imaging large regions of the body. These include vasculitides, collagen-vascular diseases, vascular malformations, and venous thromboses. While coverage of these large regions by CT increases radiation dose and makes timing of image acquisition relative to contrast injection more challenging, MRI can overcome these issues. This presentation will cover practical aspects of whole body MRI for vascular diseases, including choice of contrast agent and optimization of imaging protocol.

Whole Body Imaging of Non-Oncologic Disorders
Andrew T. Trout, MD (USA)

Whole body MRI allows imaging of large areas of anatomy without radiation exposure. As such, whole body MRI is gaining substantial traction as the imaging modality of choice for whole body screening,

particularly in the pediatric and young adult population. Screening of patients with tumor predisposition syndromes is a major application of whole body MRI and there are ongoing studies of the value of whole body MRI in staging and follow-up of known malignancy. Beyond oncology, however, there are opportunities to leverage the large field of view and tissue contrast provided by whole body MRI. Such opportunities include, but are not limited to:
Vascular imaging – vascular malformations, vasculopathies, assessment of venous patency
Imaging of systemic and multifocal infection
Imaging of systemic and multifocal inflammatory processes
This talk will discuss whole body MR protocols and techniques for imaging of non-oncologic indications and how those techniques might differ from tumor screening exams. The talk will also review the current state of knowledge with regard to whole body MR for non-oncologic indications. Clinical cases will serve to introduce discussion of non-oncologic indications for whole body MR and whole body MR imaging techniques.

Tuesday, May 17, 2016

MUSCULOSKELETAL IMAGING

Ultrasound-Guided Pediatric MSK Procedures

Mahesh M. Thapa, MD (USA)

Ultrasound guided pediatric MSK procedures
In this brief, 10-min session, we will be discussing ultrasound guided arthrograms and steroid injections of the following joints: shoulder, elbow, hip, knee, tibio-talar, and subtalar. We will also mention other procedures we utilize ultrasound for, such as tendon sheath and bursal injections. Finally, we will finish by discussing ultrasound guided foreign body removal. In addition to the step by step instructions, we will mention our preferred tools and medication. Proper needle visualization techniques and approaches will also be discussed.

Surface Lesions of Bone in Children

James S. Meyer, MD (USA)

Surface lesions of the bone may arise in any location ranging from the endosteal surface to the fibrous tissue immediately superficial to the periosteum. These lesions are termed: endosteal when arising from the inner cortex; intracortical when arising from within the cortex; subperiosteal when between the cortex and periosteum; or periosteal when arising from the periosteum. For some lesions, the more general terms parosteal or juxtacortical are used when the lesions are located next to the outer cortex and originate from periosteum or adjacent ligaments, tendons, or fascia. Paracortical is an even more general term that covers lesions where the site of origin is so uncertain that it may range from the endosteum to the periosteum.
This presentation will provide a concise review of the imaging appearances and differential considerations for benign and malignant bone surface lesions of neoplastic, infectious, and traumatic etiologies.

Brachial Plexus Birth Injury: US Screening for Glenohumeral Joint Instability

Tiina H. Pöyhiä, MD, PhD (Finland)

In brachial plexus birth injury (BPBI) the imbalance of the developing muscle leads to progressive posterior subluxation (PS) of a humeral head. Permanent BPBI carries a high risk for shoulder instability during the first year of life. Early detection of PS allows the possibility of early treatment. US is a fast and reliable tool for dynamic investigation of shoulder instability and detection of PS of the humeral head. US study is performed using an 8-10 MHz linear transducer. Young infants are lying on their side, and 1-year-olds may be seated. A parent supports the child and holds the studied hand in the proper position. A posterior axial approach with the upper arm of the patient adducted and the elbow flexed to 90° is used for the visual detection of PS of the humeral head and for the static evaluation of joint congruency in maximal internal and external rotation as well as for the dynamic evaluation of the joint. The humeral ossification center is normally located ventral to the posterior margin of the scapula (the posterior scapular line). In posterior displacement, the center of the humeral head is located posterior to scapular axis. For confirmation and severity assessment of subluxation the α-angle should be assessed. It is measured between the line along the posterior margin of the scapulae and the line drawn tangentially to the humeral head and posterior edge of the glenoid. The α-angle>30° means PS.
This presentation provides a brief review of the pathology and describes US examination of the PS in BPBI.

Sports Injury in the Wrist

Mario Maas, MD, PhD (The Netherlands)

Sports injuries are increasingly seen in the pediatric population, with the early onset of intensive training programs in many Olympic Sports. A shift from primarily Musculoskeletal radiology to pediatric Radiology, as key player in the radiological arena is encountered. This means that the awareness on typical sports related injuries, like overuse injuries of bone (stress reaction, stress fracture) or soft tissue (muscle injury, tendon overuse injury) in pediatric radiologists needs to be present. Knowledge on biomechanics of sports is mandatory to understand the sports-specific injuries that will occur, yet this is not enough.. Since patient empowerment and sheared decision making already is mainstay in the elite sports management, the radiologist dealing with injury of the elite pediatric athlete needs to be part of the medical team and needs to feel responsible for this position. Since Musculoskeletal radiologists are key players in this field for many years, close interaction between the two subspecialties is beneficial for the patient.
In this 10 min presentation I will provide our experiences as IOC center of excellence in working as a team when managing the adequate diagnostics for the injured athlete. Illustrations of sports specific injuries in the pediatric population will enhance the transfer of knowledge. Dealing with future challenges on this topic will start by building a bridge between Musculoskeletal and Pediatric Radiology

Dynamic Gadolinium-Enhanced MRI of the Proximal Femur in Healthy Children

Diego Jaramillo, MD, MPH (USA)

The proximal femoral epiphysis is supplied by the medial and lateral circumflex arteries, which form anastomotic rings at the base of the neck and at the femoral head-neck junction. Once the vessels penetrate the epiphysis, they supply vascular canals within the epiphyseal cartilage. These canals are non-anastomotic spaces that contain vessels and surrounding loose areolar tissue, and in turn are surrounded by cartilage. Once the epiphyseal ossification center develops, a capillary network develops within the bone. The epiphyseal vessels supply blood and nutrients to the proximal femoral physis, and the metaphyseal vessels participate in the process of chondrocyte apoptosis during endochondral ossification.
Following the administration of gadolinium, these vascular canals are visible in 3 phases as the contrast travels through the 3 spaces: a vascular phase, a canalicular phase which lasts 5 to 10 min, and a cartilage In infants and young children, following the intravenous administration of gadolinium. After the appearance of the secondary center of ossification., the arrangement of the vascular canals changes from parallel to radial, as the canals converge towards the ossified epiphysis.
The area that enhances most briskly is the metaphyseal spongiosa, related to endochondral ossification. The cambium layer of the periosteum, related to membranous ossification has a slower enhancement, but it becomes increasingly prominent with time. The metaphyseal marrow enhances more than the epiphyseal marrow, and the cartilage of the physis

and epiphysis enhances the least.

MRI of the TMJs in Children with JIA: Cut-off Between Normality and Pathology
Thekla von Kalle, MD (Germany)

MRI of the TMJs in children with JIA. Cut-off between normality and pathology. Arthritis of the temporomandibular joint (TMJ) is common in children and adolescents with Juvenile Idiopathic Arthritis (JIA). Early treatment is warranted to prevent severe growth disturbances and joint deformities. As TMJ arthritis is often clinically silent, MRI with contrast-enhancement has been considered to be the most reliable method to assess early signs of inflammation.
However, the depiction of the special developmental and anatomical characteristics of the TMJ as well as its reaction to inflammatory diseases are to date not completely understood. One of the open questions is the differentiation between normal synovial findings and mild signs of synovitis. In this context, it is of utmost importance to clearly define the MR characteristics of a normal TMJ as a basis for the assessment of minor pathological changes.
This presentation summarizes the current knowledge on anatomy and MR imaging of the components of a normal TMJ, including age dependent variations. It discusses the minimum requirements of image quality and spatial resolution, the best image orientation, as well as the advantages of fat suppression and subtraction analysis in contrast-enhanced imaging. And it presents the available data on a possible cut-off between normality and pathology.

Wednesday, May 18, 2016

ABDOMINAL IMAGING

Normal DW Imaging Appearances of Abdominal Organs
Govind B. Chavhan, MD, DABR (Canada)

Diffusion weighted imaging (DWI) is emerging as an essential sequence for abdominal imaging in various pathologic conditions. It is important to know the appearance of normal abdominal organs on DWI to be able to correctly interpret any abnormality. Signal intensity of any tissue or organ on DWI is determined by overall water molecule mobility (diffusion) in that tissue as well as T2 relaxation time of the tissue. The spleen has highest signal intensity on diffusion weighted (high b-value) image in the upper abdomen followed by gallbladder and kidneys. The spleen turns hypointense on ADC map suggesting true diffusion restriction while gallbladder remains bright suggesting T2-shine through. Kidneys remain slightly hyperintense on ADC map suggesting mild degree of T2-shine through reflecting its high T2- relaxation time. Liver and pancreas show intermediate signal on diffusion weighted image as well as ADC map. Similar to spleen, other lymphoid tissues including normal lymph nodes and spinal cord show diffusion restriction. Signal intensity of a normal spleen and spinal cord can be used as reference to assess diffusion restriction in other organs and tissues. In well-distended small bowel loops, normal jejunal wall may show hyperintensity while ileal wall usually does not show signal on high b-value images. Normal ovarian stroma and testicular parenchyma show diffusion restriction while the endometrium shows T2-shine through. In this presentation, normal signal intensity of abdominal organs and tissues on DWI will be illustrated and basis for the appearance will be discussed.

MR Imaging of Anorectal Malformations
Daniel J. Podberesky, MD (USA)

Anorectal malformations (ARM) are a diverse spectrum of congenital malformation involving the anus and rectum. These malformations can range in severity, with an overall incidence of approximately 1 in 5000 newborns, and a slight male predominance. Associated anomalies are found in approximately 50% of patients with congenital ARM, and primarily involve the gastrointestinal, genitourinary, skeletal, nervous, and cardiovascular systems. Imaging has long played a vital role in the evaluation and management of patients with ARM. In order to accomplish a successful postoperative outcome, a detailed preoperative imaging assessment is frequently required. This assessment includes determination of the level and type of malformation, the presence and level of fistula, the developmental state of the levator sling and sphincter complex, and the presence of associated anomalies. In the postoperative ARM patient, accurate imaging is often required for identification of postoperative complications, potential reopertative planning, and predicting morbidity and quality of life. Contrast enemas, voiding cystourethrograms, distal high-pressure colostograms, renal, pelvic, and spine ultrasounds, abdominal and sacral radiographs, and CT all play roles in the imaging evaluations of these complex patients. Recently, MRI is increasingly being utilized by radiologists in the diagnostic work-up of ARM patients prenatally, before definitive surgical repair, and postoperatively. MRI is ideally suited to answer many of the clinical questions that arise in this patient population given its lack of ionizing radiation, multiplanar imaging capabilities, and excellent intrinsic contrast resolution. In this presentation, a brief overview of MRI techniques and imaging examples in ARM will be reviewed.

Voiding Urosonography: Techniques and Pitfalls
Kassa Darge, MD, PhD (USA)

Contrast enhanced voiding urosonography (ceVUS) is a radiation free and more sensitive modality for the diagnosis of vesicoureteric reflux (VUR). It entails the intravesical administration of ultrasound contrast agents (UCA) which are composed of microbubbles. Currently, 2 UCA are used for pediatric ceVUS. These are the sulphur hexafluoride-phospholipid (SonoVue®/Lumason®) and the perfluorocarbon-album (Optison®) based UCAs. The first step for introducing ceVUS is to have one of these UCAs on the pharmacy formulary. For the intravesical administration a bladder catheter is necessary. The examination can be performed in the US or fluoroscopy suite by appropriately trained sonographer or pediatric radiologist. It is important to prepare each UCA according to its package insert. The UCA is injected into a normal saline bag and the infusion connected to the catheter with a 3-way-stop-cock. It is important to ensure that normal saline from vacuum-sealed glass containers is not used. The low mechanical index (MI) contrast specific modality is used for scanning. Under sonographic monitoring the bladder is filled with the infusion until homogenous distribution of the microbubbles is attained. A high concentration of UCA can cause dorsal acoustic shadowing and obliterate the view of the retrovesical space. The kidneys are scanned in supine, prone or both positions, alternating between the right and left one. It is helpful to use the dual scan option and ensure for the contrast part adequate background subtraction by appropriate selection of the MI. A 5 level grading system for grading VUR in ceVUS.

Perinatal (differential) Diagnosis and Management of Abdominal Teratomas
Fred E. Avni, MD, PhD (Belgium)

A larger number of teratomas is detected during the fetal life due to systematic obstetrical US examinations (After birth, teratomas will rather be detected due to symptoms related to the tumoral volume). The sacro-coccygeal location represents over 40% of the teratomas that may develop in the fetus or even after birth. They will develop inside and/or outside the fetus. Duplex ultrasound (helped by color Doppler) allows the detection and characterization of the tumor. The larger the tumor, the more difficult its assessment. Fetal MR imaging will provide useful complementary information regarding the tumoral extent and complications. The most usual sonographic presentation would be a large abdomino-pelvic mass with extra fetal

extension. The mass is usually cystic but with localized more echogenic areas.
The differential diagnosis should include cystic lymphangioma, cloacal complex and hydrocolpos for cystic lesions; pelvic neuroblastoma and rhabdomyosarcoma for echogenic solid lesions.
Most fetuses with SCT will have an uneventful course. Still, close obstetrical and US follow-up is mandatory as some tumors will grow rapidly or even bleed. Heart failure may occur.
Besides SCT, teratoma may develop in the retroperitoneal space, but rarely in utero. These tumors may mimic ovarian cysts and retroperitoneal lymphangioma. Fetal MRI and postnatal imaging are mandatory in order to evaluate these masses.
Antenatal diagnosis allows an optimized management at birth. Surgery is performed at birth as soon as possible in order to remove the entire tumor including the coccyx. Recurrence rate is high especially for immature tumors.

The Role of DWI for IBD MRI
Ignasi Barber, MD (Spain)

Magnetic resonance (MR) enables accurate assessment of inflammatory bowel disease (IBD) in children, and free breathing diffusion-weighted imaging (DWI) has been investigated in the assessment of bowel inflammation. Studies have usually compared the DWI findings with conventional MR findings in determining disease activity among patients with IBD. Special interest has been given to the correlation between DWI and dynamic contrast enhanced MR (DCE-MR).
Using DWI the bowel segments with active inflammation are detected as those containing high signal intensity given the restricted diffusion in the bowel wall. Evaluation of DWI can be based on visual evaluation but a quantitative assessment using the ADC values is also feasible.
It has been demonstrated that DWI can differentiate actively inflamed small bowel loops and colon from normal ones. It has also been demonstrated that DWI might be helpful for colonic evaluation when MR is obtained without oral or rectal preparation. Based on preliminary published results DWI could be used to enhance detection of diseased bowel segments and assess treatment response, and it could potentially replace post contrast imaging in IBD patients
This presentation is designed to provide a brief review of the present role of DWI for IBD MR.

Imaging of Congenital Urachal Abnormalities
Paul D. Humphries, MD, FRCR (UK)

Under normal circumstances, during the 4th-6th week of fetal life the allantois and superior end of the bladder undergo regression, transforming into a fibrous band, known as the urachus or median umbilical ligament. With an incidence of approximately 1:150,000, all or part of the allantois and superior bladder apex remain patent, resulting in a urachal fistula, umbilical urachal sinus, vesicourachal diverticulum or urachal cyst. Urachal cysts are the most common manifestation, accounting for approximately 30% of all urachal abnormalities. Urachal fistula is rare, accounting for approximately 15%.
Patients are often asymptomatic, however clinical manifestations can be extremely variable. A patent urachal fistula presents in the neonatal period with umbilical discharge, which may be persistent or intermittent. The most common sequela of a urachal cyst is infection, which can present with non-specific features and the diagnosis may be delayed owing to this. Other sequelae include acute haemorrhage, rupture, fistula formation and malignant degeneration.
Ultrasound is frequently the initial imaging modality used for the evaluation of urachal abnormalities, with cross sectional imaging reserved for complicated cases or where there is uncertainty. The relative merits of CT vs MRI will be discussed.

CARDIOVASCULAR/INTERVENTIONAL RADIOLOGY

Dynamic MR Lymphangiography
Rajesh Krishnamurthy, MD (USA)

MR techniques have been used to evaluate lymphatic system morphology and function in a wide array of conditions including lymphedema, generalized lymphatic anomaly, lymphatic vessel leakage, and before microsurgical reconstruction of lymphatic vessels. Previous MR techniques for CCL using heavily T2 weighted sequences or digital contrast injection have limitations: inability to distinguish edema from small lymphatics, variable opacification of CCL, venous contamination, lack of functional or dynamic information like reflux or collateralization and artifacts related to breathing and peristalsis. dMRL is a novel technique for mapping the CCL after intranodal injection of gadolinium contrast, and provides rapid, selective opacification of the CCL, reliable visualization of the thoracic duct and cisterna chyli, and dynamic imaging of lymphatic transit without venous contamination. dMRL is a useful tool for evaluation of both anatomy and function, and helps direct patient management by demonstrating a range of pathology involving the CCL. Potential applications include assessment of severity and extent of CCL obstruction, determination of the distribution and adequacy of collateral pathways, screening for the presence of lymphangiectasia and chylolymphatic reflux, and guidance for MR guided interventions involving the thoracic duct. The use of MR as the imaging technique eliminates potential risks related to radiation. Since conventional gadolinium based contrast agents are used for injection, in contrast to lipid based contrast oils, it is safe in congenital heart disease patients with right to left shunts.

RFA, Cryo, MW and Laser for Tumor Management in Pediatric Patients
Fernando Gómez Muñoz, MD, PhD (Spain)

Local ablation techniques are widely used in adults for the treatment of both benign and malignant lesions. These techniques include radiofrequency ablation, percutaneous cryoablation, microwave ablation, interstitial laser thermotherapy, percutaneous ethanol injection, and irreversible electroporation. In some cases, these techniques are included in the algorithms of treatment of oncological diseases at the same level as more aggressive techniques such as surgical resection; in others they represent an alternative to surgery in patients who are not candidates for resection due to high anesthetic risk or other circumstances. Local ablation can be carried out with curative or palliative intent, either alone or in combination with systemic (immunotherapy or chemotherapy) or locoregional therapies (radiotherapy or chemoembolization). The effect of systemic chemotherapy may be enhanced by the physiological changes produced by thermal ablation. Furthermore, ablation can sometimes be used as a complement to surgery, individualizing the treatment for each lesion in a single patient. These treatments have been applied to tumors located in almost every organ in the human body including the liver, kidney, lung, musculoskeletal system and pancreas. Although thermal ablation is widely regarded as the treatment of choice for osteoid osteoma in extraspinal location, the use of these techniques still remains exceptional in children with malignancy. Ablative techniques are feasible and promising treatments for certain pediatric tumors, large multicenter prospective trials will be needed to establish its efficacy.

Complications of Catheter Related Thrombosis in Children
Cicero J. Torres A. Silva, MD (USA)

The purpose of this presentation is to describe the spectrum of complications arising from catheter-related thrombosis in the pediatric population. Thrombosis is uncommon in children, but its complications can potentially be devastating. At least 50% of pediatric thrombosis cases are attributed to central venous catheters (CVC). Rates of CVC-related thrombosis are highest in those critically ill and in neonates. Acute complications usually occur in the setting of thrombus dislodgement and migration (thromboembolism). Chronic complications, including post-thrombotic

syndrome and isolated venous occlusion, are often mild. Umbilical venous catheter-related thrombosis involves the portal system. Acute complications are rare due to compensatory blood flow from the hepatic artery. The most common long-term complication is left hepatic lobe atrophy; portal hypertension occurs less often, in the setting of thrombus propagation from the left into the main portal vein. Umbilical arterial catheter-related thrombosis may affect of the aorta and its abdominal branches, resulting in necrotizing enterocolitis, hypertension, renal failure, or limb compromise. Peripheral arterial catheter-related complications are usually minor.

Embolization Procedures in Neonates and Infants
Sergio Sierre, MD, FSIR, FCIRSE (Argentina)

There has been a tremendous growth in pediatric vascular interventions and currently transcatheter embolization is a common procedure in pediatric tertiary centers. Vascular Interventional Radiology in Pediatrics differs from adult vascular interventions in several aspects. Despite anatomical and technical issues, endovascular techniques used in children for diagnostic and therapeutic purposes have achieved significant clinical and technical success rates in the pediatric population.
Embolotherapy has demonstrated its effectiveness in a wide range of indications in neonates and pediatric patients with current available materials and equipment, particularly thanks to the availability of small size diagnostic catheters and microcatheters.
Special consideration must be given to the choice of sedation or general anesthesia, to the maintenance of temperature control, to fluid balance, contrast dose, equipment selection and radiation safety.
Embolization in neonates and infants should be performed by dedicated and specifically trained physicians, with knowledge of the pediatric pathology and experience in the management of the specific considerations related to this age group. A multidisciplinary discussion, management and follow-up is essential for this continuous evolution of endovascular techniques in Pediatrics.
This presentation will briefly describe and discuss some of the more frequent indications for embolization treatment in Pediatrics, highlighting particular clinical and technical issues related to this age group.

Thursday, May 19, 2016

IMAGING IN INFECTIOUS DISEASE/WFPI

Africa
Savvas Andronikou, MBBCh, FRCR, PhD (UK)

Making the diagnosis of pulmonary TB (PTB) in children can be difficult, as microbiological confirmation is not often achieved. Diagnosis is therefore often based on clinical features in combination with chest X-ray findings. Recently, imaging diagnosis using novel mediastinal ultrasound techniques and fast magnetic resonance imaging has been proposed and shows promise, but the chest X-ray remains the most frequently used and available diagnostic imaging tool in children.
Chest X-ray is able to demonstrate large lymphadenopathy of the hilar and para-tracheal regions on the frontal view, and large subcarinal lymphadenopathy on the lateral view, but wide inter-observer variability has been reported for radiologists' and clinicians' interpretations of these. This may reflect the lack of standardized imaging criteria for diagnosis as well as radiologists objectives for achieving sensitivity rather than specificity. Establishment of size criteria for diagnosing lymphadenopathy and diagnostic chest X-ray criteria for PTB are needed to enable standardized interpretation. Similar to the template of images used for asbestosis scoring or for bone age determination, a guiding template of chest X-ray images for PTB are needed for standardized diagnosis.
This talk will demonstrate examples of the novel imaging techniques and discuss the obstacles to implementation of these. It will also make proposals for diagnostic imaging criteria as well as provide a proposed template of example images and a standardized reporting template.

Asia
Kushaljit Singh Sodhi, MD, PhD, FICR (India)

Despite significant progress in prevention and treatment, infectious diseases remain an important source of morbidity and mortality, particularly in immunocompromised persons and developing countries. Bacterial, fungal, and parasitic pathogens can affect and involve any body system. Asian countries have been for long a hot spot for infectious diseases.
Nearly half of all deaths caused by infectious diseases each year can be ascribed to just three diseases: tuberculosis, malaria, and AIDS. Other common infections include typhoid, hepatitis, leptospirosis, diarrhoeal diseases, amoebiasis, cholera, dengue, brucellosis, hookworm, influenza, filariasis, Japanese encephalitis and echinococcal infections. Tuberculosis remains a worldwide public health problem, particularly in the third world countries. Nearly 5, 00,000 deaths annually are reported due to this disease. We shall be laying special emphasis on different radiological patterns of tuberculosis. Fungal infections predominate in immunocompromised hosts. Mucormycosis and aspergillosis are characterized by angioinvasiveness and are associated with high morbidity and mortality among immunocompromised patients. Amongst the parasitic infections, neurocysticercosis, toxoplasmosis, echinococcosis, malaria, and schistosomiasis, deserve a special mention.
Modern imaging techniques are used to define the anatomic region involved, diagnose complete disease spectrum, and its various complications and thus help in better management of these patients. This particular course is targeted to provide a brief review of the common infections seen in children in the asian sub continent and would include their patterns of involvement, imaging characteristics and radiological techniques used for their detection.

North America
Paul S. Babyn, MD (Canada)

Health care-associated infections (HAIs) cause considerable morbidity and mortality to hospitalized patients. A HAI occurs when a patient acquires an infection as a result of receiving healthcare. Multinational point prevalence studies demonstrate a HAI rate of around 8-10%. HAIs can occur in any patient and most commonly include urinary tract, respiratory tract, surgical site (wounds) device related and blood stream infections. They are the most common complications affecting patients in hospital, and involve bacterial (with or without antibiotic multi-resistance) and viral infections. This talk will review the commonly affected patients, imaging findings and workup of these patients as well as discuss the role of the imaging department in infection prevention.

Europe
Rutger A. J. Nievelstein, MD, PhD (The Netherlands)

Infectious diseases in children are common and still cause significant morbidity and mortality, even in the developed countries of Europe. Although the prevalence of the different causative pathogens in Europe will differ from other continents, infections by atypical pathogens (including mycobacterial, fungal and parasitic infections) are increasingly besides the more common bacterial and viral infections. This is most likely related to the increasing international travel and migration, but a compromised immunity due to medical treatment (f.i. chemotherapy, stem cell transplantation) and multi-drug resistant pathogens are an growing medical problem. Imaging plays an important role in establishing the cause, source, and involved body region as well as in monitoring the treatment response. In this short lecture, an overview will be given of hot topics in pediatric infection and related imaging strategies from a European perspective.

ONCOLOGICAL IMAGING

Secondary Malignancies and the Role of Surveillance Imaging in Pediatric Oncology

Stephan D. Voss, MD, PhD (USA)

Second malignancies occur with increased frequency in childhood cancer survivors, with second cancers accounting for up to 50% of non-recurrence related mortality. There is increasing evidence that exposure to ionizing radiation from diagnostic imaging studies can result in increased risks of malignancy. These risks are increased in children due to long latency periods following early exposure to ionizing radiation and longer life expectancy, increasing susceptibility to cumulative biologic effects. Survivors of childhood cancers are frequently subjected to a large number of routine surveillance imaging tests, leading to repeated exposure to ionizing radiation, increased risks of contrast administration and anesthesia, and in many instances little improvement in overall outcome as a result in routine surveillance imaging. This presentation will review strategies and data regarding routine surveillance imaging in a number of pediatric malignancies, concluding that many routine surveillance imaging investigations may be unnecessary, particularly in patients with low stage low risk disease.

Whole Body MRI in Lymphoma

Claudio Granata, MD (Italy)

Hodgkin lymphoma and non-Hodgkin lymphoma account for 15% of malignancies in children. Staging is fundamental for treatment and prognosis. Current protocols recommend the use of F-fluoro-2-deoxy-D-glucose positron emission tomography (FDG-PET)/computed tomography (CT) for staging and assessment of response to therapy. However, FDG-PET/CT causes high ionizing radiation exposure, which is of particular concern in children with cancer for the risk of radiation-induced secondary malignancies.

Whole-body MRI (WB-MRI) is a radiation-free technique, which is increasingly proposed as possible alternate method for staging and response assessment in lymphoma. Until now, there is no standardized technique for performing WB-MRI. The most common sequences are STIR and T1W FSE. Recently, diffusion-weighted imaging (DWI) with apparent diffusion coefficient (ADC) has been proposed to increase the detectability of the lesions.

A few recent studies verified the agreement between FDG-PET/CT and WB-MRI findings at initial staging. Good agreement with STIR and T1W FSE imaging was reported in limited series. An improved agreement was reported with WB-DWI in small series, whereas other studies did not confirm the additional value of DWI.

The prognostic value of both interim and end of treatment reassessment with FDG-PET/CT is presently studied in clinical trials: similarly, the prognostic role of WB-MRI in interim and end of treatment response assessment is investigated in some pilot studies.

WB-MRI could become a radiation-free alternative to FDG-PET/CT. However, there is still a strong need for large prospective studies to better validate its role.

This presentation briefly reviews the role, techniques and findings of WB-MRI in children with lymphoma.

CT vs. MRI for Staging of Wilms Tumor

Geetika Khanna, MD, MS (USA)

Wilms tumor is the second most common solid tumor, outside the central nervous system, in children. In the Children's Oncology Group series, Wilms tumor accounts for about 80% of pediatric renal tumors followed by renal cell carcinoma. Favorable histology Wilms tumor is far more common than anaplastic Wilms tumor. The role of imaging at baseline is to confirm the organ of origin, evaluate local staging (capsular invasion, rupture, vascular invasion), evaluate for synchronous contralateral lesions, and evaluate for distant metastasis. Lung followed by liver are the most common sites of metastasis. The speaker will provide an update on the trends in imaging of pediatric renal tumors across North America and Europe. Key imaging findings for staging will be illustrated with discussion on the role of CT vs. *MRI. Controversies in surveillance imaging will be highlighted.*

Guidelines for Imaging and Staging of Neuroblastic Tumors

Hervé J. Brisse, MD, PhD (France)

Neuroblastic tumors (neuroblastoma, ganglioneuroblastoma, ganglioneuroma) are the most common extracranial solid tumors occurring in children. The International Neuroblastoma Staging System (INSS) is based on the extent of tumor removal and therefore is not suitable for pre-treatment risk classification of patients with localized disease. The International Neuroblastoma Risk Group (INRG) Project proposed a new staging system (INRGSS, Monclair T. et al. J Clin Oncol 2009) including two stages of localized disease dependent on whether Image Defined Risk Factors (IDRF) are present or not. IDRF are surgical risk factors detected on imaging that make total tumor excision risky or difficult at diagnosis. An international consensus report was subsequently published (Brisse HJ et al. Radiology 2011) to optimize imaging and uniform reporting for staging and facilitate comparison of risk-based clinical trials. The recommended imaging method for primary tumor analysis is MRI (with or without contrast), or CT-scan (with contrast) if MRI is not available. Mandatory imaging methods for distant metastases depiction are ^{123}mIBG scintigraphy (or SPECT-CT), liver imaging (US, MRI or CT) and chest X-ray (CT if abnormal CXR only). Bone scan (^{99m}Tc-MDP) or ^{18}FDG-PET-CT is mandatory if the primary tumor is not mIBG-avid. Equivocal skeletal uptake requires additional imaging methods. Brain imaging is not required unless neurological symptoms are present. According to the INRGSS, localized tumors are classified L1 or L2 dependent on whether IDRF are present or not. Stages M and Ms are disseminated disease (comparable to INSS stages 4 and 4S, respectively).

Chest Tumors in Children Beyond Lymphoma

Eline E. Deurloo, MD, PhD (The Netherlands)

A wide spectrum of malignancies (primary or metastatic) and benign lesions can occur in the pediatric chest, originating from lungs, mediastinum or chest wall. They have to be differentiated from benign, mainly congenital or infectious, lesions.

Differential diagnosis is guided by location and characterisation, patient age and clinical presentation.

Imaging plays a crucial role in the diagnosis of a thoracic tumor. It is initiated by clinical symptoms and starts with a chest x-ray. Further imaging with ultrasound, CT and/or MR is necessary to better localize and characterize the mass.

Imaging is urgent in case of suspicion of compression of the airway, superior vena cava or spinal cord.

Primary pulmonary tumors are extremely rare in children and are made up of carcinoid tumors, pleuropulmonary blastoma and carcinoma. Pulmonary metastases from other tumors are much more frequent. Primary lung tumors are usually discovered when non-specific symptoms and/or radiographic abnormalities persist or fail to respond to therapy.

The mediastinum is the most common location for intrathoracic tumors in children. Most mediastinal masses in children are malignant. The mediastinum can be divided into 3 compartments in which specific tumors may arise: tumors in the anterior mediastinum are mainly of thymic, lymphatic or germ cell origin; middle mediastinal

masses are usually of lymphoid origin, and the majority of posterior mediastinal masses are neurogenic.
Malignant chest wall masses can originate from bone or soft tissues. They are identical to soft tissue and bone tumors elsewhere in the body and include Ewing sarcoma/PNET, and rhabdomyosarcoma.

SCIENTIFIC PAPERS

Authors are listed in the order provided. An author listed in bold identifies the presenting author.

Paper #: 001

Interrater reproducibility of measured pancreatic secretory function on secretin-enhanced MRCP

Andrew Trout, *Radiology, Cincinnati Children's Hospital Medical Center, Cincinnati, OH, andrew.trout@cchmc.org;* Daniel Wallihan, Maisam Abu-El-Haija

Disclosures: Andrew Trout has indicated a relationship with Philips Healthcare, Advisory Board. All other authors have disclosed no financial interests, arrangements or affiliations in the context of this activity.
Purpose or Case Report: Exocrine secretory function is an important measure of pancreatic sufficiency in patients with chronic pancreatitis. Secretin-enhanced magnetic resonance cholangiopancreatography (MRCP) provides a non-invasive way to assess exocrine function. A study of adult patients previously defined normal secreted volume in response to secretin as 112±50 mL (Mensel B. AJR. 2014). While normative values are not yet known for children, if secretin-enhanced MRCP is to be a viable technique for assessment of exocrine function, there should be minimal interrater variability of measured secretory function. The purpose of this study was to assess interrater variability in measured exocrine pancreatic secretion by secretin-enhanced MRCP.

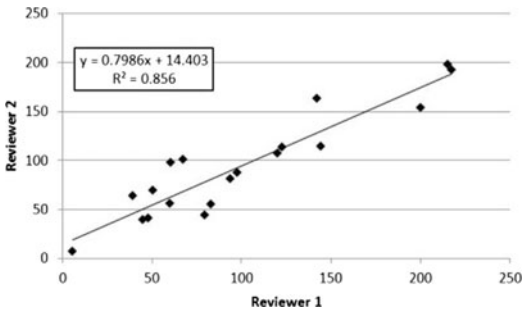

Methods & Materials: Pediatric and young adult patients with suspected pancreatic disease underwent secretin-enhanced MRCP including coronal fat-saturated single shot fast spin echo sequences acquired before and after secretin administration. Secreted volume was calculated as the difference in enteric (gastric and small intestinal) fluid volume between the pre- and post-secretin images. Enteric fluid volume was calculated by summing the volume of fluid on each imaging slice which was in turn calculated by multiplying slice thickness by the area (cm^2) of fluid signal. The area of fluid signal was measured by thresholding the images to include only pixels with fluid signal (ImageJ v1.48 k 2013, National Institutes of Health) with the same threshold applied to both the pre- and post-secretin images. Secreted fluid volume was independently measured by two reviewers who each independently selected thresholds and drew regions of interest. Measured secreted volumes were compared using paired t-tests and Spearman's correlation with bias between measurements determined by Bland-Altman analysis.

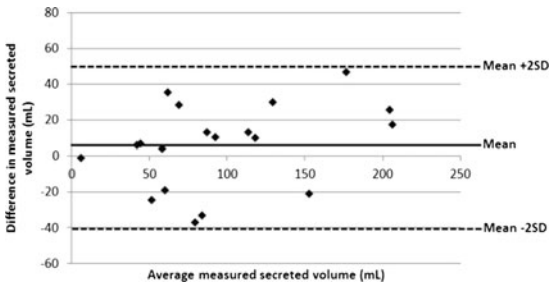

Results: 19 patients (mean age 13.2 y, range: 0.6-25.3y) were included in this study. Measured secreted fluid volumes were highly correlated between reviewers (r=0.93, Figure 1). Mean secreted volumes measured by reviewers 1 and 2 were 99.6 and 93.9 mL (p=0.23) with a bias between measurements of 5.7 mL (95%CI:-40-51.5 mL, Figure 2).
Conclusions: Measurement of secreted fluid volume on MRCP in response to secretin administration is highly reproducible with a bias of less than 10 mL between reviewers. This difference is small in comparison to the range of secreted volumes in adult patients and suggests MRCP is a technically viable means to non-invasively assess pancreatic exocrine function.

Paper #: 002

Clinical Relevance of Unsuspected MRE-detected PAD in Pediatric IBD

Zehour Alsabban, *The Hospital for Sick Children/University of Toronto, Toronto, ON, Canada, zehour.alsabban@sickkids.ca;* Nicholas Carman, Sebastian King, Rahim Moineddin, Ryan Lo, Jacob Langer, Thomas Walters, Anne Griffiths, Peter Church, Mary-Louise Greer, MBBS

Disclosures: Thomas Walters has indicated a relationship with Janssen Canada: Speakers bureau, Consultant Abbvie Canada: Speakers bureau, Consultant. All other authors have disclosed no financial interests, arrangements or affiliations in the context of this activity.
Purpose or Case Report: Increasingly, perianal fistulae (PAF) and abscesses (PAA) are identified on Magnetic Resonance Enterography (MRE) in pediatric inflammatory bowel disease (PIBD). Not all perianal disease (PAD) is clinically suspected, creating a clinical dilemma regarding additional imaging and/or treatment. The purpose of this study was to assess clinical relevance of these findings, correlating PAD on MRE with clinical evidence of PAD.

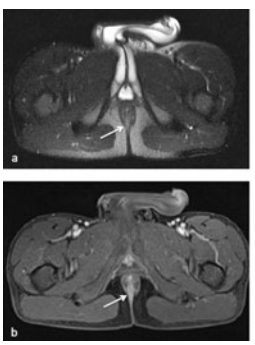

Figure 1: 15 year-old male with MRE showing a 6 o'clock transsphincteric fistula (arrows).

(a) Axial T2 HASTE fat suppressed (FS)

(b) Axial post-gadolinium T1 VIBE FS

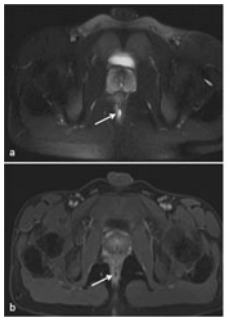

Figure 2: 17 year-old male with smal volume perianal abscess on MRE.

(a) Axial T2 HASTE FS demonstrating 8 o'clock T2 hyperintense fluid collection (arrow).

(b) Axial post gadolinium T1 VIBE fat suppressed image showing rim-enhancement of the collection (arrow).

Methods & Materials: This research ethics board approved retrospective study identified patients ≤18 years having MRE and pelvic magnetic resonance imaging (PMR) within a 6-month period over 2 years 2011–2013, for known or clinically suspected IBD. Exclusions were interval surgical intervention (except Seton), and non-standard/non-diagnostic MRI. Two pediatric radiology fellowship-trained readers experienced with MRI, blinded to clinical data, reviewed MRI for number, type and length of PAF and number and volume of PAA. Where discrepant, a consensus read was performed. MRE were paired with the gold standard PMR closest in ≤6 months and compared for PAD. MRE with PAD (MRE+) were classified as true or false positive (TP, FP).

Clinical data captured independently by gastroenterology and surgical fellowship-trained researchers experienced in PIBD, included presence of PAF, fissures, PAA, skin tags and PAD activity, with patients classified as clinically positive or negative for PAD if PAF and/or PAA were detected. Clinical outcomes were recorded.

Diagnostic statistics for sensitivity, specificity, positive and negative predictive values (PPV, NPV) were calculated using MRE+ consensus data.

		MRE (validated with PMR)		
		+ N=58 (MRE TP)	- N=4 (MRE FP)	
Clinically Evident PAD	+ N=24	TP = 24	FP = 0	PPV = 100%
	- N=38	FN = 34	TN = 4	NPV = 10.5%
		SENSITIVITY 41.4%	SPECIFICITY 100%	

Table 1: Comparison of all positive MRE vs. clinically detected perianal disease

(MRE=Magnetic resonance enterography, PMR = pelvic MRI, PAD= Perianal Disease, N=Number, P/NPV= Positive/Negative Predictive Values, TP = True Positive, TN = True Negative, FP = False Positive, FN = False Negative)

Results: Ninety-four patients (male:female 61:33) had 108 MRE and 131 PMR, median age at initial MRI 14.1 years (5.3-18.6 years), a majority with Crohn's disease. After excluding 16 MRE for lack of clinical data ≤6 months, 77 patients and 80 PMR/MRE pairs remained, with 62 MRE+ (58 TP and 4 FP) compared with clinical data.

Sensitivity was 41.4%, specificity 100%, PPV 100%, and NPV 10.5.%. (Table 1) False negative (FN) PAA average volume was 0.85 ml vs. TP 3.5 ml, and PAF average lengths were similar, FN 2.9 cm vs. TP 2.8 cm. The 34 FN studies were in 31 patients, 9 later developing clinically evident PAD.

Conclusions: MRE increasingly detects PAD not always clinically evident. Recognizing the natural history of PIBD, continued monitoring for PAD requiring intervention is warranted when detecting PAD on MRE. The high FN vs. low FP also suggests a low threshold for imaging if PAD is clinically suspected.

Paper #: 003

US and MRI predictors of surgical bowel resection in pediatric Crohn's disease

Daniel Rosenbaum, MD, *Radiology, NewYork-Presbyterian Hospital/Weill Cornell Medical Center, New York, NY, dgr2001@med.cornell.edu;* David Biko, MD, Sudha Anupindi

Disclosures: All authors have disclosed no financial interests, arrangements or affiliations in the context of this activity.

Purpose or Case Report: To identify imaging features of the terminal ileum (TI) on short-interval bowel ultrasound (US) and MR enterography (MRE) in children with Crohn's disease (CD) requiring subsequent surgical bowel resection compared with those managed by medical therapy alone, and to correlate imaging features with histopathology.

Methods & Materials: This retrospective study evaluated patients with CD undergoing short-interval bowel US and MRE (within 2 months of one another), as well as subsequent ileocecectomy or endoscopy within 3 months of imaging. Imaging appearance of the TI on both modalities was compared between surgical patients and those managed with medical therapy, with the following parameters assessed: bowel wall thickness (BWT), mural stratification, vascularity, fibrofatty proliferation, abscess, fistula, and stricture on bowel US; BWT, T2 ratio, enhancement pattern, mesenteric edema, fibrofatty proliferation, abscess, fistula, and stricture on MRE. Imaging findings in surgical patients were correlated with location-matched histopathologic scores of inflammation and fibrosis using a scoring system adapted from the Simple Endoscopic Score for Crohn's Disease.

Results: Twenty-two surgical patients (mean age 16.5 years; M/F: 13/9) and 20 non-surgical patients (mean age 14.8; M/F: 8/12) were included in final analysis. Surgical patients demonstrated significantly increased bowel wall thickness (p=0.01), loss of mural stratification (p=0.02), and increased fibrofatty proliferation (p=0.04) on bowel US, as well as increased bowel wall thickness (p=0.02), increased T2 ratio (p=0.03), increased mesenteric edema (p=0.001), and stricture (p=0.005) on MRE. Nineteen of 22 ileocecectomy specimens showed severe inflammation and 21/22 showed severe fibrosis, with specimen homogeneity limiting meaningful correlation with imaging findings.

Conclusions: Children with CD requiring surgical bowel resection demonstrate multiple imaging features on US and MRE traditionally associated with both active inflammation and chronic fibrosis, findings corroborated by histopathology. These features may potentially serve as imaging biomarkers of medical therapy refractoriness in determining which patients will progress to surgery.

Paper #: 004

Prospective Cohort Study of Ultrasound-Ultrasound and Ultrasound-MRI Agreement in the Evaluation of Pediatric Small Bowel Crohn's Disease

Jonathan Dillman, MD, MSc, *Cincinnati Children's Hospital Medical Center, Cincinnati, OH, jonathan.dillman@cchmc.org;* Ethan Smith, MD, Ramon Sanchez, Michael DiPietro, Soudabeh Fazeli, Matthew Davenport

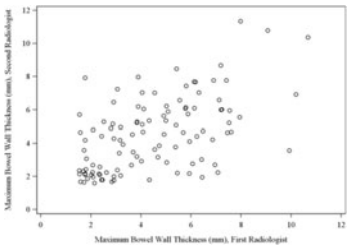

Disclosures: Johnathan Dillman has indicated a relationship with Siemens Medical Solutions USA as a Primary Investigator. All other authors have disclosed no financial interests, arrangements or affiliations in the context of this activity.

Purpose or Case Report: To prospectively assess US-US and US-MRE inter-radiologist agreement in pediatric small bowel Crohn's disease.

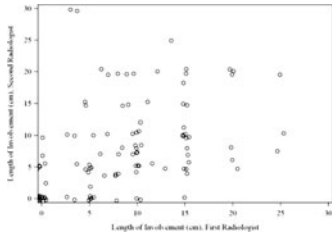

Methods & Materials: IRB approval and informed consent/assent were obtained for this HIPAA-compliant prospective cohort study of children with newly diagnosed distal small bowel Crohn's disease (July 2012 to December 2014). Enrolled subjects (*N*=29) underwent two small bowel US examinations performed by blinded independent radiologists both before and at multiple time points after initiation of medical therapy (231 unique ultrasound examinations, in total); 134 US examinations were associated with concurrent MRE. The MRE examination was interpreted by a third blinded radiologist. The following was documented on each examination: involved length of ileum (cm); maximum bowel wall thickness (mm); amount of bowel wall and mesenteric Doppler signal; presence of stricture, penetrating disease, and/or abscess. Inter-radiologist agreement was assessed with single-measure three-way mixed model intra-class correlation coefficients (ICC) and prevalence-adjusted, bias-adjusted kappa statistics (κ). Numbers in brackets are 95% confidence intervals.

Results: US-US agreement was moderate for involved length (ICC: 0.41 [0.35-0.49]) (Figure 1a); substantial for maximum bowel wall thickness (ICC: 0.67 [0.64-0.70]) (Figure 1b); moderate for bowel wall Doppler signal (ICC: 0.53 [0.48-0.59]); slight for mesenteric Doppler signal (ICC: 0.25 [0.18-0.42]); and moderate to almost perfect for stricture (κ: 0.54), penetrating disease (κ: 0.80), and abscess (κ: 0.96). US-MRE agreement was moderate for involved length (ICC: 0.42 [0.37-0.49]); substantial for maximum bowel wall thickness (ICC: 0.66 [0.65-0.69]); and substantial to almost perfect for stricture (κ: 0.61), penetrating disease (κ: 0.72), and abscess (κ: 0.88).

Conclusions: US-US agreement was similar to US-MRE agreement for assessing pediatric small bowel Crohn's disease. Discrepancies in US-US and US-MRE reporting question the utility of US as an accurate, reproducible radiologic biomarker for assessing response to medical therapy and disease-related complications.

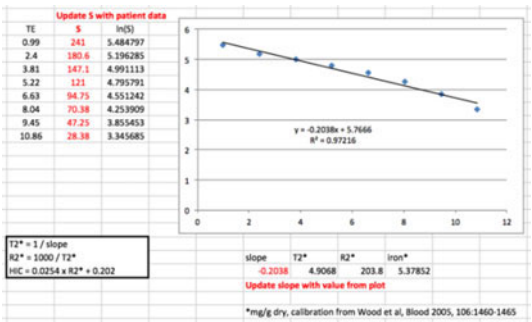

Paper #: 005

T2* MRI Assessment of Iron in Different Hepatic Segments in Pediatric Patients with Sickle Cell Hemoglobinopathies

Hampton Sasser, MD Candidate, *Radiology and Radiological Science, Medical University of South Carolina, Charleston, SC, sasserh@musc.edu;* Heather Collins, Anil Rao, MBBS, DMRD, DNB

Disclosures: All authors have disclosed no financial interests, arrangements or affiliations in the context of this activity.

Purpose or Case Report: To evaluate if there is a variation in hepatic iron concentration (HIC) between liver segments when assessing iron overload in pediatric patients with sickle cell hemoglobinopathies.

Methods & Materials: This is a retrospective analysis of abdomen MRI studies following IRB approval. T2* weighted gradient recalled echo (GRE) serial axial images of the liver were acquired with same time of repetitions (TR) and increasing echo times (TE). Same sized region of interest (ROI) circles were placed on all Couinaud liver segments. T2* was calculated as the negative inverse value of the slope got by plotting natural logarithmic ROI values with TE values. HIC was calculated for each of the Couinaud segments using R2* (R2*=1000/T2*) and an equation formulated by Wood et al. (2005) as follows: HIC=(R2* x 0.0254)+0.202 (Sample Figure). The mean HIC values of all patients for each of liver segments (Table 1) were compared and analyzed statistically for variance using a two tailed ANOVA test with Sidak correction. A Pearson correlation was conducted to identify associations between ferritin levels and HIC for each segment and a mean of all segments combined. All analyses were considered significant at $p<0.05$ values.

Table 1: Mean values and standard deviation of HIC (in mg/g dry weight of liver tissue)

Liver segments	Mean	Std. Deviation
seg1	10.0964	6.41755
seg2	11.0083	7.62852
seg3	10.1209	7.03515
seg4a	11.2591	7.88266
seg4b	10.7479	7.35574
seg5	9.4606	8.42875
seg6	9.5382	7.95831
seg7	11.9168	8.74154
seg8	11.8698	8.14229

Results: There were 47 abdomen MRI studies done in 26 patients (11 female, 15 males; age range 5–19 years; mean age 14 years). Overall, there was no significant main effect of liver segment on hepatic iron content, $F(152.39, 65.23)=2.34$, $p=.10$, $\eta_p^2=0.05$. Ferritin levels positively correlated (Table 2) with HIC in all the liver segments and also with the overall mean value of all segments combined, r (45)=.545, $p<.001$.

Conclusions: No significant differences in HIC between liver segments were found indicating that ROI estimation of HIC in a single liver segment is sufficient to assess hepatic iron burden. HIC positively correlates with serum ferritin levels.

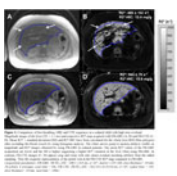

Table 2: Correlation values between ferritin and HIC for all segments and the segment mean (mean value of all segments combined).

	seg1	seg2	seg3	seg4a	seg4b	seg5	seg6	seg7	seg8	Segment Mean
Pearson Correlation	.634**	.417**	.507**	.454**	.482**	.491**	.451**	.458**	.397**	.545**
p-value (2-tailed)	.000	.004	.000	.001	.001	.000	.001	.001	.006	.000
Sample size	47	47	47	47	47	47	47	47	47	47

2: Correlation value between ferritin and HIC for all segments and the segment mean (mean value of all segments combined).

	seg1	seg2	seg3	seg4a	seg4b	seg5	seg6	seg7	seg8	Segment Mean
Pearson Correlation	.634**	.417**	.507**	.454**	.482**	.491**	.451**	.458**	.397**	.545**
p-value (2-tailed)	.000	.004	.000	.001	.001	.000	.000	.001	.006	.000
Sample size	47	47	47	47	47	47	47	47	47	47

Paper #: 006

Assessment of Free-breathing R2*-UTE for Hepatic Iron Content Quantification in a Sedated Pediatric Cohort

Aaryani Tipirneni-Sajja, *Diagnostic Imaging, St. Jude Children's Research Hospital, Memphis, TN, aaryani.sajja@stjude.org;* Beth McCarville, MD, Axel Krafft, Ralf Loeffler, Ruitian Song, Chris Goode, Gail Fortner, Jane Hankins, Claudia Hillenbrand

Disclosures: All authors have disclosed no financial interests, arrangements or affiliations in the context of this activity.
Purpose or Case Report: Quantification of hepatic iron content (HIC) using R2*-MRI is an alternative to liver biopsy. R2* is usually obtained from breath-hold multi-gradient-echo images (BH-GRE); HIC is calculated from R2* using liver biopsy calibrations. However, in children who require sedation or cannot hold their breath, GRE images contain degrading respiratory motion artifacts that introduce errors in HIC estimation. Here, we propose a free-breathing (FB) ultra-short echo time (UTE) R2* acquisition that reduces erroneous R2*-based HIC assessment introduced by physiological motion.
Methods & Materials: 27 sedated patients (age, 6.7±3.8 years) with iron overload (IO) were scanned at 1.5T using both FB-GRE and FB-UTE sequences. Further, FB exams were compared to standard BH-GRE in a non-sedated IO patient to test for potential R2* deviation in FB scans. R2* maps were obtained for all sequences by fitting a monoexponential decay to the signal. To calculate mean liver R2*, whole liver ROIs were drawn and blood vessels were excluded via histogram analysis. The mean and standard deviation (SD) of R2* values extracted from FB-GRE and FB-UTE were analyzed using linear regression and Bland-Altman plots.

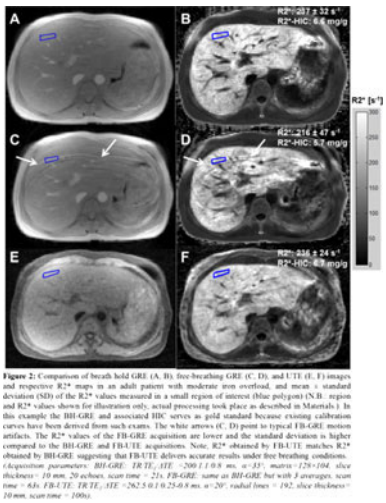

Figure 2: Comparison of breath hold GRE (A, B), free-breathing GRE (C, D), and UTE (E, F) images and respective R2* maps in an adult patient with moderate iron overload, and mean ± standard deviation (SD) of the R2* values measured in a small region of interest (blue polygon) (N.B. region and R2* values shown for illustration only, actual processing took place as described in Materials.). In this example the BH-GRE and associated HIC serves as gold standard because existing calibration curves have been derived from such exams. The white arrows (C, D) point to typical FB-GRE motion artifacts. The R2* values of the FB-GRE acquisition are lower and the standard deviation is higher compared to the BH-GRE and FB-UTE acquisitions. Note, R2* obtained by FB-UTE matches R2* obtained by BH-GRE suggesting that FB-UTE delivers accurate results under free breathing conditions. *(Acquisition parameters: BH-GRE: TR/TE, ΔTE: ~200/1.1/0.8 ms, α=35°, matrix=129×104, slice thickness= 10 mm, 20 echoes, scan time = 21s. FB-GRE: same as BH-GRE but with 3 averages, scan time = 63s. FB-UTE: TR/TE, ΔTE =262.5/0.1/0.25-0.8 ms, α=20°, radial lines = 192, slice thickness= 10 mm, scan time = 100s).*

Results: All FB-GRE images of sedated children had motion artifacts and inferior image quality compared to FB-UTE images; the artifacts appeared more pronounced with increasing HIC. As an example, Fig. 1 shows FB-GRE and FB-UTE images and respective R2* maps of a sedated child. Barely any artifacts are visible in FB-UTE images. The non-sedated patient (Fig. 2) also displayed motion artifacts for FB-GRE images and a lower mean liver R2* and higher SD than the standard BH-GRE and FB-UTE suggesting that artifacts are the main cause for this observed R2* underestimation. Overall, we consistently found lower mean R2* values for FB-GRE, with a 2-fold higher SD compared to FB-UTE (Fig. 3).
Conclusions: R2* is underestimated for FB-GRE most likely due to motion artifacts which primarily arise from bright subcutaneous fat signal. Artifacts become more visible with increasing HIC as the contrast between artifacts and dark liver tissue increases. Furthermore, R2* underestimation and SD become greater towards high IO which introduces a strong bias in high HIC estimates. In contrast, FB-UTE had barely any motion artifacts as radial sampling is intrinsically insensitive to motion. We conclude that FB-UTE with its excellent image quality is a viable method for accurate R2*-HIC assessment in sedated children and patients who cannot breath-hold.

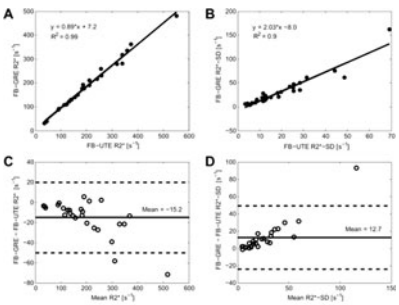

Figure 3: Linear regression (A, B) and Bland-Altman (C, D) analysis between mean R2* values and R2*-SDs obtained using FB-GRE and FB-UTE acquisitions in sedated patients. For regression plots, the equations and correlation coefficients (R^2) are included and for Bland-Altman plots, mean bias is included. The FB-GRE acquisition, as expected, underestimates mean R2* values and produces a higher SD compared to FB-UTE.

Paper #: 007

MR based liver iron estimation in children: a comparison of signal intensity ratio method with T2* relaxometry

Swapnil Bagade, MD, **Geetika Khanna,** *Radiology Associates, St. Francis Hospital, Hartford, CT, khannag@mir.wustl.edu*

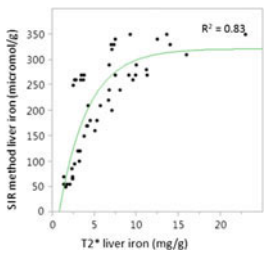

Disclosures: All authors have disclosed no financial interests, arrangements or affiliations in the context of this activity.
Purpose or Case Report: MR evaluation of liver iron concentration is standard of care in children with predisposition to iron overload. T2* relaxometry is the standard of care for MR based liver iron estimation. However, this technique is not available in all institutions. The signal intensity ratio (SIR) method developed by Gandon, et al. is easy to

implement and has a web-based formula for liver iron estimation. The purpose of our study was to:

1. Determine correlation between liver iron concentration (LIC) estimated by SIR and T2* methods 2. To assess the accuracy of LIC quantification by SIR method using T2* as the reference standard.

Methods & Materials: This is a retrospective, IRB approved, HIPAA compliant study. Radiology information system was queried to identify subjects <25 years of age who had MRI for LIC between December 2011-October 2014. All subjects underwent LIC estimation using the SIR and T2* methods in the same visit. The SIR method measures the ratio of liver to muscle signal intensity in 5 gradient echo (GRE) sequences. The T2* method uses a multiecho T2 GRE sequence. LIC was estimated by SIR method by reader 1 and T2* method by reader 2. The readers were blinded to all clinical information and other sequences. Spearman's rank correlation coefficient was used to assess the association between the two methods. The accuracy of LIC estimated by the SIR method was determined using T2* as reference standard.

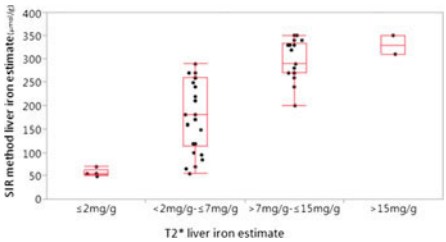

Results: 51 MRIs were performed on 37 children (21F), age 3–22 years with following disorders: sickle cell 30, Blackfan Diamond 3, bone marrow transplant 2, and thalassemia major 2. T2* based LIC was 1.4-23 (median 4.5) mg/g dry weight of liver.

The Spearman's rank correlation coefficient between the two methods was 0.83 (P<0.01) (Fig 1). 5/5 subjects with LIC <2 mg/g were accurately classified as mild iron overload, and 2/2 with LIC >15 mg/g were accurately classified as major iron overload by the SIR method. 9/14 (64%) subjects with LIC in 2-7 mg/g range were accurately classified as moderate iron overload by SIR method, while 5 (36%) were underestimated by the SIR method. 18 subjects had LIC in 7-15 mg/g range, and all were accurately classified as either intermediate (10) or major (8) iron overload by SIR method (Fig 2).

Conclusions: There is good correlation between the SIR method and T2* relaxometry for LIC estimation. While severity of LIC is accurately determined in patients with <2 mg/g or >7 mg/g of liver iron, the classification is less accurate in the intermediate range.

Paper #: 008

Shear Wave Elastography of the Liver and Spleen, Comparison to Hemodynamics, Underlying Disease Process, and Isolating the Best Representative Segments

Martha Munden, MD, *Pediatric Radiology, Texas Children's Hospital, Houston, TX, mmmunden@texaschildrens.org;* Alexander Dodd, Wei Zhang, Daniel Leung

Disclosures: All authors have disclosed no financial interests, arrangements or affiliations in the context of this activity.

Purpose or Case Report: The purpose of the study is to determine the utility of shear wave elastography (SWE) of the liver and spleen compared to sonographic characteristics, hemodynamic parameters, disease entity and to assess the most representative liver segment for shear wave sampling in the pediatric patient.

Methods & Materials: The study was approved by institutional IRB and informed consent was obtained. A prospective cohort of healthy patients (n=24) and those with known liver disease (n=23) were analyzed. Results of SWE values of the liver (segments 5–8), SWE of the spleen were compared and correlated with ultrasound morphology (UM), underlying disease entity and hemodynamic parameters [Congestion Index of the portal vein (CI), portal hypertension index (PHI)].

The Spearman correlation coefficients were calculated of each of the 5 (4 liver segments, 1 spleen) regions to CI, PHI, and UM, and as normal vs known liver disease. The means and standard deviations of the shear wave values were summarized and compared using UM, disease vs no disease groupings, using the Wilcoxon Rank test. P value<0.05 was considered significantly different. For the correlation of shear wave values of liver to spleen, the Spearman and Pearson correlation coefficients were calculated.

Results: Segment 5 had the highest correlation coefficient with the ultrasound morphology grading system (Spearman: 0.64, p value<0.0001), segment 8 was next (Spearman: 0.46, p value: 0.0027). When all normal livers were grouped against known liver disease, segments 5 (1.1 m/s+/-0.2 vs 1.4 m/s +/-0.4) again showed the most significant difference with segment 8 (1.2 m/s +/-0.2 vs 1.7 m/s +/-0.7) next with P values of <0.0001 for segment 5 and 0.0032 for segment 8.

The Pearson Correlation Coefficient for comparing shear wave of liver and spleen showed a linear but negative correlation.

Shear wave measurements of segments 5–8 of the liver did not correlate well with CI or PHI. Of disease entities, those who had undergone a Fontan procedure with single ventricle physiology had the highest overall stiffness with cystic fibrosis the second highest.

Conclusions: SW elastography does correlate liver elasticity with known underlying liver disease and with abnormal sonographic characteristics. Segments 5 and 8 provided the highest correlation. No correlation was found with hemodynamic parameters.

Of the various underlying disease states, those having undergone a prior Fontan procedure with single ventricle physiology had the highest stiffness.

Paper #: 009

Ultrasound elastography with acoustic radiation force impulse (ARFI) to assess liver fibrosis and portal hypertension (HTN) in children with autosomal recessive polycystic kidney disease (ARPKD)

Erum Hartung, MD, *Children's Hospital of Philadelphia, Philadelphia, PA, hartunge@email.chop.edu;* Kassa Darge, MD, PhD

Disclosures: All authors have disclosed no financial interests, arrangements or affiliations in the context of this activity.

Purpose or Case Report: To evaluate if liver and spleen stiffness measured by ARFI can distinguish (1) ARPKD children from healthy controls, and (2) ARPKD children with and without clinical signs of portal HTN (presence/absence of splenomegaly or thrombocytopenia).

Methods & Materials: Children ≤21 y/o with ARPKD (n=11) and controls (n=11) were compared cross-sectionally. Stiffness of the right and left liver lobes and spleen were evaluated using a Siemens Acuson S3000 ultrasound scanner to measure shear wave velocity (SWV) in m/s (mean of 10 measurements per site). Splenomegaly was defined as sagittal spleen length >90th %ile for height based on published norms. Thrombocytopenia was defined as platelets <150 K/uL. Liver and spleen SWV were compared in (1) ARPKD vs. controls; and (2) ARPKD children with vs. without signs of portal HTN, using Wilcoxon rank sum test. Receiver operating characteristic (ROC) analysis was used to determine if liver and spleen SWV can distinguish between these groups.

Results: SWV in the right and left liver lobes (RLL and LLL) and spleen were significantly higher in ARPKD vs. controls [RLL 1.70 m/s (IQR 1.57, 2.67) vs. 1.29 m/s (IQR 1.02, 1.40)(P=0.0007); LLL 2.32 m/s (IQR 1.77, 3.23) vs. 1.06 m/s (IQR 0.96, 1.27)(P=0.0001); spleen 3.27 m/s (IQR 2.83, 3.74) vs. 2.66 m/s (IQR 2.36, 2.88)(P=0.03)](Figure 1). Liver and spleen SWV were higher in ARPKD children with splenomegaly vs. those without [RLL 2.49 m/s (IQR 1.95, 3.04) vs. 1.57 m/s (IQR

1.49,1.58)(*P*=0.01); LLL 3.01 m/s (IQR 2.37, 3.29) vs. 1.77 m/s (IQR 1.64, 1.83)(*P*=0.006); spleen 3.67 m/s (IQR 3.32, 3.85) vs. 2.83 m/s (IQR 2.17, 2.88)(*P*=0.006)]. Liver and spleen SWV were also higher in ARPKD children with thrombocytopenia vs. those without [RLL 2.67 m/s [IQR 2.25, 3.04] vs. 1.58 m/s (IQR 1.49, 1.69)(*P*=0.006); LLL 3.23 m/s [IQR 2.80, 3.29] vs. 1.80 m/s (IQR 1.64, 1.83)(*P*=0.006); spleen 3.74 m/s [IQR 3.60, 3.85] vs. 2.86 m/s (IQR 2.17, 3.02)(*P*=0.006)](Figure 2). ROC analysis showed high AUC for RLL, LLL, and spleen SWV to differentiate ARPKD vs. controls [AUC (95%CI): 0.92 (0.80-1.00), 1.00 (1.00-1.00), and 0.76 (0.53-1.00) respectively]; ARPKD children with vs. without splenomegaly [AUC (95%CI): 0.92 (0.77,1.00), 0.91 (0.72-1.00), and 0.94 (0.81-1.00)]; and ARPKD children with vs. without low platelets [AUC (95%CI) 1.00 (1.00-1.00) for all 3 sites](Figure 3).

Conclusions: Liver and spleen stiffness measured by ARFI can distinguish children with ARPKD from healthy controls, and can detect presence of portal hypertension in children with ARPKD.

Figure 1: Box plots of ARFI shear wave velocity (stiffness) in **(A)** liver and **(B)** spleen in ARPKD children compared to healthy controls. * P=0.0007, ** P=0.0001, ‡ P=0.03

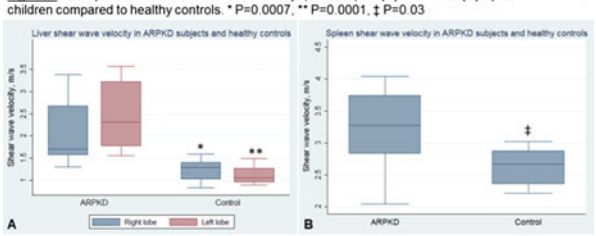

Figure 2: Box plots of ARFI shear wave velocity (stiffness) in the liver and spleen in ARPKD children without and with signs of portal HTN. **(A)** Liver and **(B)** spleen SWV in children without and with and splenomegaly. **(C)** Liver and **(D)** spleen in children without and with thrombocytopenia. *P=0.01, **P=0.006

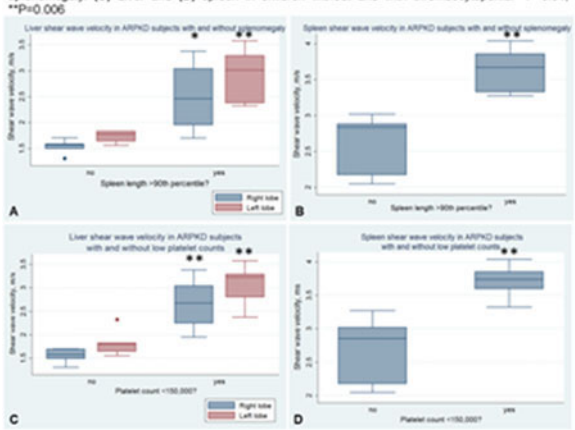

Figure 3: ROC curves to explore cut-offs of liver and spleen shear wave velocities (stiffness) to differentiate **(A)** ARPKD children vs. controls; **(B)** ARPKD children with and without splenomegaly; **(C)** ARPKD children with and without low platelets. ROC areas (AUC) with corresponding 95% confidence intervals are shown below each curve.

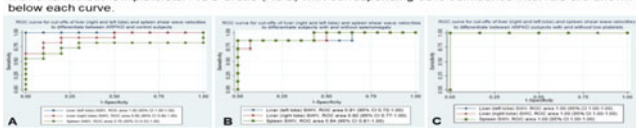

Paper #: 010

Comparison of Gradient recalled echo (GRE) and Spin Echo-Echo planar imaging (SE-EPI) based MR Elastography of the liver in children with liver disease.

Suraj Serai, PhD, **Andrew Trout,** *Radiology, Cincinnati Children's Hospital, Cincinnati, OH, andrew.trout@cchmc.org;* Jonathan Dillman, M.D., M.Sc., Kevin Glaser, Richard Ehman

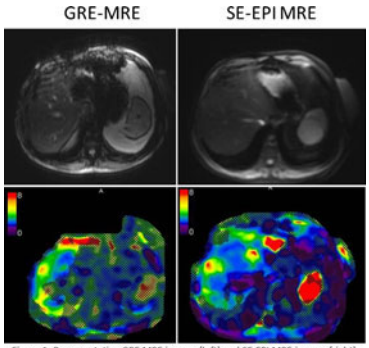

Figure 1: Representative GRE MRE images (left) and SE-EPI MRE images (right). Top row shows the magnitude images and bottom row shows the respective elastograms.

Disclosures: Andrew Trout has indicated a relationship with Philips Healthcare, Advisory Board. Kevin Glaser has indicated a relationship with Resoundant, Inc. Richard Ehman has indicated a relationship with Resoundant Inc as researcher. Johnathan Dillman has indicated a relationship with Siemens Medical Solutions USA as a Primary Investigator. All other authors have disclosed no financial interests, arrangements or affiliations in the context of this activity.

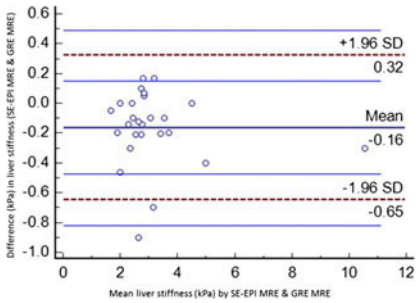

Purpose or Case Report: Magnetic Resonance Elastography (MRE) primarily has been performed using a gradient echo sequence (GRE). GRE MRE, however, has two main limitations in a pediatric population where non-alcoholic fatty liver disease is a major cause of liver fibrosis: 1) Breath holds can be inconsistent, resulting in poor image quality, and 2) Signal loss in the deep liver in obese patients can result in undersampling possibly leading to erroneous stiffness values. Spin-echo echo planar imaging (SE-EPI) is an alternative means of performing MRE that has higher SNR and is faster (Figure 1). The aim of this study was to compare GRE and SE-EPI MRE in a pediatric population.

Methods & Materials: 26 patients referred for clinical liver MRE were imaged using both GRE and SE-EPI MRE on a 1.5T MR scanner (HDx, GE Healthcare, Waukesha, USA) using an 8-channel torso coil and identical active driver amplitudes. GRE MRE was acquired in 4 breath holds of 15 s each and SE-EPI MRE was acquired in a single breath hold of 15 s. Four axial slices through the liver were obtained in each subject. MR elastogram maps were generated using a multimodal direct inversion (MMDI) algorithm (Mayo Clinic; Rochester, MN) with liver stiffness calculated as a mean of the means for stiffness measured on each slice (kPa). Pearson correlation and Bland-Altman difference plots were generated to assess agreement between techniques. Area of the sampled regions of interest was also recorded and compared with a 2-sample paired *t*-test (two-tailed).

Results: Mean patient age was 13.8 years (range: 0.7-19.8 years), and 57% were boys. Mean liver stiffness was 3.2±0.9 kPa by GRE MRE and 3.1±1.0 kPa by SE-EPI MRE. Sampled areas were 9,445±5,177 cm^2 for GRE MRE and 1,1973±4,533 cm^2 for SE-EPI MRE (p=0.001). When compared, all stiffness values but one fell within 95% agreement with the line of equality with an ICC value of 0.99 (95% CI: 0.976-0.995, p<0.001) (Figure 2). Bland-Altman analysis demonstrates a bias of -0.16 kPa between techniques with all but one value falling within 95% prediction limits (Figure 3). The outlier reflected an obese patient

(BMI=35) in whom GRE MRE under-sampled the liver giving a stiffness value of 3.1±1.0 kPa versus 2.2±0.8 kPa for SE-EPI MRE.
Conclusions: There is strong agreement in measured hepatic stiffness between GRE and SE-EPI MRE with a bias of less than 0.2 kPa between techniques. SE-EPI MRE has the advantage of sampling a larger area of the liver and can be performed in a single breath hold.

Paper #: 011

MR Elastography is a technically robust technique for assessment of hepatic stiffness in pediatric patients

Madalsa Joshi, MD, *Radiology, Cincinnati Children's Hospital Medical Center, Cincinnati, OH, madalsa.joshi@cchmc.org;* Alexander Towbin, MD, Daniel Podberesky, Suraj Serai, PhD, Jonathan Dillman, M.D., M.Sc., Stavra Xanthakos, Rohit Kohli, Andrew Trout

Disclosures: Alexander Towbin has indicated a relationship with Merge as a shareholder, Guerbet as anunrestricted grant/ consultant, Elsevier as an author and Applied Radiology as a consultant. Daniel Podberesky has indicated a relationship with Philips Healthcare. Andrew Trout has indicated a relationship with Philips Healthcare, Advisory Board. Johnathan Dillman has indicated a relationship with Siemens Medical Solutions USA as a Primary Investigator. All other authors have disclosed no financial interests, arrangements or affiliations in the context of this activity.
Purpose or Case Report: To determine the rate of success of MR elastography of the liver in a pediatric population and identify the reasons for unsuccessful examinations.
Methods & Materials: Imaging records were searched for patients 18 years of age and younger, who underwent MR elastography of the liver between January 1, 2011 and August 5, 2015. MR elastography examinations were performed on one of two scanner platforms (different vendors, both 1.5T) using gradient recalled echo pulse sequences. Imaging reports were reviewed for the frequency of failed MR elastography acquisitions. Unsuccessful examinations were investigated further to determine the causative factor(s) resulting in failure, and to determine if a subsequent successful examination had been performed.
Results: A total of 449 examinations were performed on 356 unique patients during the study period. The mean age of the patient population was 12.6 ±3.6 years (range 0.1-18 years). The success rate for MRI elastography was 96% (431/449) with 18 failed examinations (4%, mean age=11.4 years, range=2.3-17.3 years). The reasons for examination failure included in order of decreasing frequency: large body habitus causing difficulties in paddle positioning (n=6), hepatic iron overload (n=4), patient inability to tolerate the MRI (n=3), patient motion/inability to follow breathing instructions (n=3), artifact from implanted hardware (n=1), and technical (hardware/software) malfunction (n=1). Eight of the 18 patients underwent repeat examinations, 6 (75%) of which were successful. Changes which yielded successful studies on repeat imaging included improved paddle positioning in patients with large body habitus (n=2), slice selection away from the hardware causing artifact (n=1), scanning the patient with sedation (n=1), proper functioning of hardware/software (n=1), and improved breath holding (n=1).
Conclusions: MR elastography of the liver is a technically robust, non-invasive method for evaluating liver stiffness in pediatric patients. Failure of MR elastography examinations is infrequent and largely reflects patient specific factors, some of which can be mitigated with careful technique.

Paper #: 012

Quantitative MR of the liver: Correlation between liver volume, stiffness, and fat fraction in a pediatric population

Madalsa Joshi, MD, *Radiology, Cincinnati Children's Hospital Medical Center, Cincinnati, OH, madalsa.joshi@cchmc.org;* Alexander Towbin, MD, Jonathan Dillman, M.D., M.Sc., Daniel Podberesky, Suraj Serai, PhD, Stavra Xanthakos, Rohit Kohli, Andrew Trout

Disclosures: Alexander Towbin has indicated a relationship with Merge as a shareholder, Guerbet as anunrestricted grant/ consultant, Elsevier as an author and Applied Radiology as a consultant. Daniel Podberesky has indicated a relationship with Philips Healthcare. Andrew Trout has indicated a relationship with Philips Healthcare, Advisory Board. Johnathan Dillman has indicated a relationship with Siemens Medical Solutions USA as a Primary Investigator. All other authors have disclosed no financial interests, arrangements or affiliations in the context of this activity.
Purpose or Case Report: MRI allows the assessment of liver stiffness (elastography), hepatic fat fraction, and liver volume in a single test. The purpose of this study was to determine the relationship between liver volume, stiffness, and fat fraction in a pediatric population. Specifically, we hypothesized that measured liver volume would increase with increasing fat content and decrease with increasing stiffness.
Methods & Materials: The reports for all quantitative MR examinations of the liver performed over 3 years, 8 months in patients less than 18 years of age were reviewed and liver stiffness (mean of means for four adjacent axial slices in kPa), liver volume, and hepatic fat fraction were extracted. Limited MR examinations had been performed at 1.5 T, and included an MR elastography sequence, in and opposed phase imaging for calculation of hepatic fat fraction, and an axial fat-suppressed T2 weighted sequence for determination of liver volume based on manual segmentation. The electronic medical record was reviewed for clinical information including age, sex, weight, and underlying diagnosis. Unadjusted and adjusted relationships between variables were assessed using Pearson correlation and multiple linear regression.
Results: A total of 449 MR elastography examinations were performed in 356 unique patients (mean age=12.7±3.6 years) during the study period. Based on univariate analysis, there was a significant positive correlation between liver volume and both patient age (r=0.52, p<0.0001) and hepatic fat fraction (r=0.57, p<0.0001). There were significant negative correlations between liver volume and mean liver stiffness (r=-0.10, p=0.03) and between hepatic fat fraction and liver stiffness (r=-0.26, p<0.0001). When adjusted for age, gender, and other variables, a 1% increase in hepatic fat fraction was associated with a 62 mL increase in liver volume (p<0.0001); and a 1 year increase in age was associated with a 111 mL increase in liver volume (p<0.0001). On average, female gender was associated with a 144 mL decrease in liver volume compared to males (p=0.02). In the adjusted analysis, the relationship between liver stiffness and volume reversed suggesting an interplay between variables with a 1kPa increase in mean liver stiffness associated with a 59 mL increase in liver volume (p=0.04).
Conclusions: Liver volume is significantly associated with hepatic fat fraction and liver stiffness, with increases in each accounting for measurable increases in liver volume.

Paper #: 013

Doppler Parameters of Hepatic Artery as Predictors of Graft Status in Children with Liver Transplant

Tahani Ahmad, MD, *IWK Health Center, Halifax, NS, Canada, tahani1523@yahoo.com;* Govind Chavhan, MD, Yaron Avitzur, Rahim Moineddin, Kamaldine Oudjhane, MD, MSc

Disclosures: All authors have disclosed no financial interests, arrangements or affiliations in the context of this activity.
Purpose or Case Report: To assess the clinical utility of hepatic artery Doppler parameters in evaluating graft status in children with liver transplant and to determine pediatric-specific ranges/cut off values of hepatic artery flow velocity (HAV) that portends complications
Methods & Materials: A retrospective review of the transplant database at tertiary pediatric hospital was performed for all children (289) who underwent liver transplantation between February1998- September 2014. The operative reports, clinical notes, laboratory results, pathological findings and ultrasound records were reviewed at three time points (day 3, month 3 and 1 year post-operative). Basic descriptive data and

statistical analysis including T test, ROC, Chi-squared test and Fisher exact test were performed as appropriate to assess the correlation between hepatic artery velocity and intrahepatic resistive index (RI) on one hand with liver function tests (LFT) and graft status (rejection, biliary or vascular complications) on the other hand.
Results: Of 120 children (54 girls and 66 boys; mean age of 3 years and 2 months) enrolled, 70/120 had satisfactory graft status at the 1-year follow-up. Clear cut off value for HAV that can predict graft status was not identified. However, velocities between 50 cm/s and 200 cm/s were associated with normal graft status (p=0.0658). Vascular and biliary complications in the immediate post-operative period were more frequent at velocities 200–300 cm/s (p-value 0.0024). There was positive association between RI and graft status (p=0.0308) and values below 0.5 were associated with vascular complications (p=0.0116). There is no significant association between the liver function test and the Doppler parameters apart from a positive correlation between HA velocity at month-3 and the GGT (p-value 0.0410).
Conclusions: HAV between 50 and 200 cm/s and RI (0.5- 0.8) are likely associated with normal graft status in children. These values should be used as an assist to the constellation of the ultrasonic findings and the clinical picture in pursuing a timely appropriate clinical decision

Paper #: 014

Utility of $^{18F\text{-}FDG}$ PET/CT for diagnosis and staging of osseous metastatic disease in Ewing Sarcoma Family of Tumors: is there a correlation with genetic mutation or outcome?

Elizabeth Lio, MD, Laura Fenton, MD, **Brian Bagrosky,** *Department of Radiology, Children's Hospital Colorado, University of Colorado Denver, Denver, CO, brian.bagrosky@childrenscolorado.org;* Brian Greffe, Mark Lovell, Billie Carstens

Disclosures: All authors have disclosed no financial interests, arrangements or affiliations in the context of this activity.
Purpose or Case Report: The Ewing sarcoma family of tumors (ESFT) includes skeletal ES, extraosseous ES, primitive neuroectodermal tumor and Askin (chest wall) tumor. Studies stratifying ESFT by subtype or genetic mutation and correlative FDG uptake are lacking. We have encountered ES patients with osseous metastatic disease diagnosed by MRI that is subtle or negative by $^{18F\text{-}FDG}$ PET/CT (PET/CT). Our goals include comparing primary and osseous metastatic disease maximum SUV on PET/CT, evaluating ESFT subtypes for EWSR FLI 1 mutation and correlating these with outcome.
Methods & Materials: Following IRB approval, the electronic medical record was reviewed for patients with ESFT and PET/CTs from 10/2010-2/2015. All PET/CTs and concurrently obtained MRI exams were reviewed. Patients were stratified by ESFT subtype and genetic mutation. Outcomes were assessed using statistical analysis with one way ANOVA, α=0.05.
Table 1. Primary tumor SUV

Variable	EWSR1/ERG (n=4)	Non-type 1 (n=7)	Not detected (n=2)	Type 1 (n=10)	Pval
Primary	5.1 (3, 7.2)	4.2 (2.7, 5.8)	5 (2, 8)	4.9 (3.6, 6.2)	0.89

Results: 47 patients were identified (2–23 years old at diagnosis; 26 male), with a total of 181 PET/CTs. 23 patients had PET/CT scans at diagnosis. Primary tumor SUV max ranged from 1.4 to 17.2 (mean 6.8, median 5.6). 25 had metastatic disease. Metastatic disease SUV max ranged from 0.5 to 13.9 (mean 4.6, median 4.8). 12 PET/CTs were limited by diffuse increased bone marrow uptake secondary to growth colony stimulating factor administration. MRI aided in confirming false positive PET/CTs in 3 patients. 40 patients were tested for genetic mutations (18 type 1 EWSR FLI 1, 11 non-type 1 EWSR FLI 1 and 11 EWSR1/ERG). Differences in primary tumor glucose uptake were not statistically different among genetic tumor types (Table 1). Outcome analysis revealed 19 disease-free, 5 in treatment, 18 deceased and 5 lost to follow-up. Time to death for patients with type 1 tumors was not significantly different from time to death for patients with other tumor types; p=0.96 (Figure 1). Glucose uptake by the primary tumor and 2 largest metastases were not significant predictors of time to death; p=0.57, 0.43 and 0.78, respectively.

Figure 1. Time to death by tumor genetics

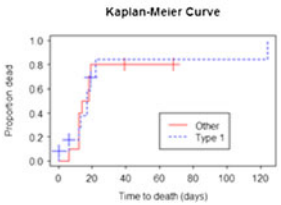

Conclusions: There was no difference in primary tumor glucose uptake or time to death between ESFT subtypes. Unlike prior literature suggests, PET/CT may not be sensitive for all osseous metastases. The SUV max range for metastatic disease in ESFT is significantly lower than the primary tumor. In several patients, focal FDG avidity worrisome for metastatic disease was excluded by concurrent MRI. Future research evaluating whole body MRI and PET/CT would be helpful.

Paper #: 015

Detection of Pulmonary Nodules in Children with a Free Breathing MRI Technique compared to CT Scans

Haemi Schemuth, *Department of Diagnostic and Interventional Radiology and Neuroradiology, University Clinic Essen, Essen, Germany, haemi.schemuth@uk-essen.de;* Selma Sirin, Bernd Schweiger, Juliane Goebel, Sonja Kinner

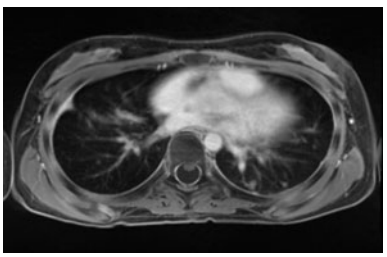

Disclosures: All authors have disclosed no financial interests, arrangements or affiliations in the context of this activity.
Purpose or Case Report: In children with malignancies CT scans still are the main diagnostic tool to assess pulmonary metastases, but carry a radiation burden. Breathhold MRI scans are especially challenging in this age group. Thus we evaluated a new radial imaging acquisition technique without the need of breath holds for the detection of pulmonary nodules.

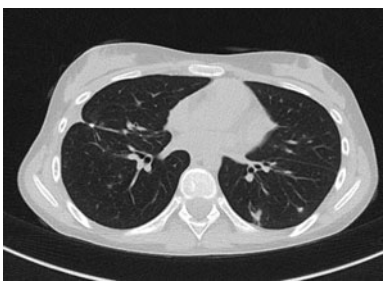

Methods & Materials: 22 oncologic patient (age 1–14, median 5.2 years) who underwent a staging chest CT as well as a MRI (cervical, thoracic, abdominal) were included. A free breathing chest MRI with a radial vibe sequence (StarVIBE, Siemens, Erlangen, Germany) was acquired after contrast (3 mm slice thickness). StarVIBE MRIs were evaluated separately by two radiologists in consensus concerning i) presence/absence of pulmonalry nodules and ii) largest diameter of the present nodules (<3 mm, 3-6 mm, 6-10 mm, >10 mm). Chest CT (slice thickness 3 mm) served as reference standard.
Results: All eleven of 22 patient presenting with pulmonary nodules in the CT scan were correctly identified with MRI. There were no false positive findings. Numbers of pulmonary lesions per patient in the CT ranged from 0 to 20. A total of 84 nodules were detected by the CT (<3 mm: 21, 3-6 mm: 40, 6-10 mm: 13, >10 mm: 10), while MRI detected 72 nodules (<3 mm: 18, 3-6 mm: 31, 6-10 mm: 13, >10 mm: 10) with a sensitivity of 86% for the MRI in total (<3 mm: 86%, 3-6 mm: 78%, 6-10 mm: 100%, >10 mm: 100%).
Conclusions: Free-breathing pulmonary MRI with a radial vibe sequence proved feasible and shows promising results in children to detect pulmonary lesions, even when they are smaller than 3 mm. As discrimination of patients with and without lesions was correct, it should be considered to be used as a screening tool to lower the radiation burden.

Paper #: 016

Imaging Features of Hepatoblastoma and Correlation with Pathological Subtype: A Single Institute Experience

Akshay Baheti, MD, *Seattle Children's Hospital, Seattle, WA, akshaybaheti@gmail.com;* A. Luana Stanescu, MD, Teresa Chapman, MD

Disclosures: All authors have disclosed no financial interests, arrangements or affiliations in the context of this activity.

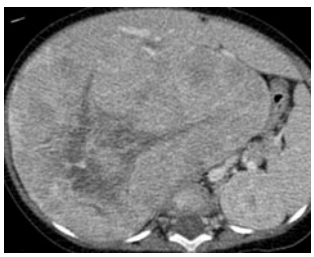

Purpose or Case Report: Specific tumor subtypes of hepatoblastomas correlate with patient prognosis. Small cell undifferentiated (SCUD) subtype is high-risk, while pure fetal subtype has better prognosis,with studies suggesting chemotherapy may not be needed after surgical resection. With the International Childhood Liver Tumors Study Group(SIOPEL) guidelines advocating neoadjuvant chemotherapy prior to resection in all cases, true tumor classification is usually based on a limited biopsy sample,and imaging may assist in more specifically identifying patient populations requiring neoadjuvant chemotherapy. The purpose of the study was to see whether imaging features of hepatoblastoma correlate with tumor pathology.
Methods & Materials: This was an IRB-approved HIPAA compliant retrospective study. Imaging and clinicopathologic data of 35 patients (26 males; mean age: 17 months; range: 0–113 months) with hepatoblastomas treated at our institute between 2000 and 2015 were reviewed. 3 radiologists in consensus reviewed the baseline CTs available in 24 patients.

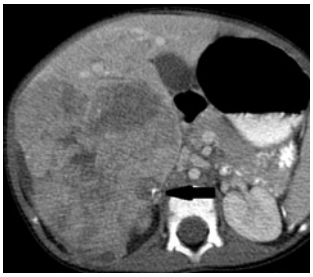

Results: On baseline CT (n=24), tumors were predominantly large (mean size 10.3 cm), solitary (16/23), and well-circumscribed (20/23). SCUD tumors (n=3) were lobulated, heterogeneous, hypoattenuating, lacked calcifications, and had enhancing septations. Two-thirds had necrosis ranging from 20 to 60% of the tumor. Pure fetal subtype (n=2) demonstrated none to minimal necrosis, fine reticular septations (2/2), and a central scar (1/2). Epithelial tumors with both fetal and embryonal differentiation (n=10) also demonstrated more internal architecture in the form of a central scar (4/10) or a reticular lacy pattern of fine septations (n=2), were often iso-hyperattenuating (6/10), lacked calcifications, and demonstrated none or minimal (<10%) necrotic component. Mixed epithelial and mesenchymal tumors (n=9) were relatively more heterogeneous in appearance, had calcifications (4/9), were iso/hypoattenuating (9/9), and had necrosis (4/9) ranging from 10 to 25% necrosis. Calcifications were fine, coarse or curvilinear. At the time of last follow-up, 5 patients had expired (2 having SCUD), 27 were alive and 3 lost to follow-up.
Conclusions: Hepatoblastomas with SCUD were more necrotic on CT imaging, whereas pure fetal and mixed fetal and embryonal tumors had overlapping features. Mixed epithelial and mesenchymal tumors demonstrate calcifications at baseline and were relatively more heterogeneous. Awareness of these imaging features, correlated

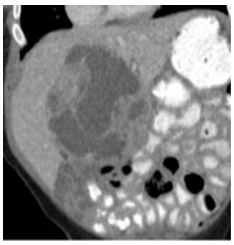

Paper #: 017

Can diffusion weighted MR imaging distinguish between benign and malignant pediatric liver tumors?

Pablo Caro Dominguez, Fellow, *Diagnostic Imaging Department, The Hospital for Sick Children, University of Toronto, Toronto, ON, Canada, pablocaro82@hotmail.com;* Govind Chavhan, MD

Disclosures: All authors have disclosed no financial interests, arrangements or affiliations in the context of this activity.
Purpose or Case Report: To determine whether qualitative and quantitative diffusion weighted imaging (DWI) can be used to differentiate and characterize pediatric liver lesions.
Methods & Materials: 371 consecutive abdominal MRI reports performed from January 2010 to May 2015 were reviewed searching for focal hepatic lesions and complete liver examination including DWI. Only first available exam and a maximum of two separate lesions per patient were included.
MRI studies were reviewed by 2 pediatric radiologists blinded to clinical details and diagnosis. Liver lesions were evaluated qualitatively to note

diffusion restriction. ADC values were obtained by drawing region of interest on ADC map.

Pathology reports were reviewed for final diagnosis of lesions. In those without pathology, combination of clinical, laboratory and imaging features along with follow up was used for final diagnosis.

Results: 112 focal hepatic lesions in 89 children (38 boys, 51 girls; mean age 10.1 years; range-10 months-18 years) were included, of which 95 lesions were benign and 17 malignant. Pathology was available in 40 lesions.

Interobserver agreement was almost perfect for both qualitative (kappa-0.8735) and quantitative (ICC-0.96) assessment.

All malignant lesions showed qualitative diffusion restriction. Most benign lesions were not restricted except abscess and two FNH. However, studies with these 2 FNH were suboptimal in quality from artifacts. Excluding abscesses, there was significant association of restriction with malignancy and non-restriction with benignancy (Fisher's exact test p-<0.0001).

Mean ADC values of malignant lesions (0.92, SD 0.32) were lower than benign lesions excluding abscesses (1.16, SD 0.52) (student's t-test, p-0.0148). However, there was significant overlap of ADC between benign and malignant lesions with wide range for each diagnosis (Table 1). Even though increase in ADC value decreased odds of the lesion being malignant, ADC values alone are not a powerful predictor of malignancy (p 0.0453). ROC analysis revealed an AUC of just 0.658 for prediction malignancy.

Conclusions: Qualitative diffusion restriction in pediatric hepatic lesions excluding abscess, is a strong predictor of malignancy and can be used to differentiate between benign and malignant lesions.

Even though malignant lesions demonstrated significantly lower ADC values than benign lesions, quantitative diffusion cannot be reliably used at this stage to differentiate them because of significant overlap and wide ranges of ADC values in hepatic lesions.

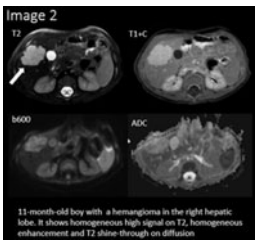

Paper #: 018

Imaging Review of DICER1 Syndrome: A Single Centre Experience

Marta Tijerin Bueno, Fellow, *Hospital for Sick Children/University of Toronto, Toronto, ON, Canada, tijerinradiologist@gmail.com;* Alejandro De La Puente Gregorio, Claudia Martinez-Rios, MD, David Malkin, Mary-Louise Greer, MBBS

Disclosures: All authors have disclosed no financial interests, arrangements or affiliations in the context of this activity.

Purpose or Case Report: To determine the spectrum of abnormalities associated with DICER1 syndrome.

To review imaging studies performed in oncologic staging and surveillance.

To delineate the screening protocol used in those with positive genetic testing.

Methods & Materials: This research ethics board approved retrospective study evaluated genetically confirmed or suspected DICER1 pediatric patients referred to our tertiary institution between 2004 and 2015.

Patients with tumors such as pleuropulmonary blastoma (PPB) or pineoblastoma (PNB) in isolation with no other features of DICER1 spectrum were excluded.

Subject	Imaging Findings
1	• pineoblastoma • thyroid nodules
2	• cystic nephroma • pineal cyst
3	• no findings
4	• pleuropulmonary blastoma • thyroid cysts
5	• renal high grade sarcoma
6	• ovarian juvenile granulosa cell tumor
7	• cystic nephroma • thyroid cysts • ovarian embryonal rhabdomyosarcoma
8	• no findings
9	• pleuropulmonary blastoma • thyroid nodules and cysts
10	• pineoblastoma • thyroid nodules • renal cysts
11	• pleuropulmonary blastoma
12	• pleuropulmonary blastoma

Figure 1. Spectrum of DICER1-related pathology, benign and malignant, in patient cohort.

Modality type and timing was captured and imaging analyzed to determine what related to staging; to treatment e.g. screening for infection, line insertions; and to cancer predisposition screening.

Results: There were 12 patients (5 male and 7 female) with mean age at presentation of 4.6 years (range 14 days to 8 years). We included all patients with a confirmed genetic diagnosis (10) and strong clinical history (2) whose parents did not consent to genetic testing.

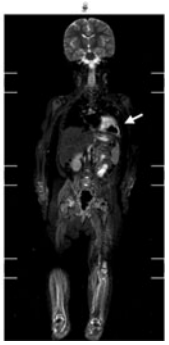

Figure 2. 23-month-old female presented with developmental delay. Genetic testing was DICER1 positive. First surveillance study performed was a Whole Body MRI using coronal STIR with fat suppression demonstrated a complex solid and cystic mass in the left hemithorax, confirmed to be a pleuropulmonary blastoma on surgical pathology.

During the study period, our patients underwent 619 imaging studies (139 x-rays, 186 ultrasounds, 99 CTs and 195 MRIs). This included oncologic staging and follow-up, and surveillance imaging, some elements suspended during active cancer treatment.

The screening protocol for additional tumors in those with known malignancies, and at risk for neoplasia but with no known tumors, started as early as 14 days old, the youngest age at first malignancy being 1 year.

Screening initially consisted of a chest x-ray, abdominal and neck ultrasound and dedicated brain MRI. Novel technique whole body MRI was introduced during the study period, performed simultaneous to the brain MRI, substituting the chest x-ray, to minimize ionizing radiation.

DICER1 related pathology included malignant lesions in 75% of patients: 4 PPB, 2 PNB, 2 ovarian sex cord stromal tumors and 1 renal sarcoma. No patient had >1 malignancy during the study period.

Benign lesions in 83% of patients included: 2 cystic nephromas, 3 thyroid nodules, 3 thyroid cysts, 1 renal cyst and 1 pineal cyst.

Two subjects, confirmed with DICER1, who were relatives of index cases, had no tumors.

Conclusions: Given the high incidence of neoplasia in DICER1 and early age at first presentation, early screening of at risk patients is critical, as is awareness of the types of DICER1-related tumors.

The current DICER1 screening protocol used in our institution includes an abdominal and neck ultrasound, and whole body and brain MRI.

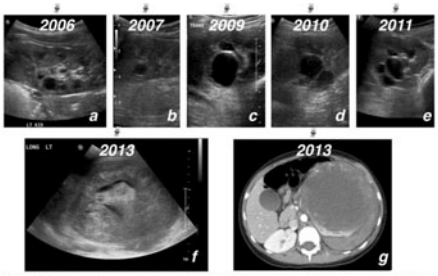

Figure 3. Sonographic images (a-f) of sequential abdominal ultrasounds performed as a screening in a 2 year-old female with a renal cyst followed since 2006. The cystic lesion was increasing in size and getting more complex, finally becoming a large renal sarcoma at the age of 8 seen in (g) axial enhanced abdominal CT.

Paper #: 019

PET/MRI detection of pulmonary nodules for pediatric cancer staging

Lillian Lai, MD, *Lucile Packard Children's Hospital, Stanford University, Radiology, Stanford, CA, lmlai@stanford.edu;* Anne Muehe, Andrew Quon, Samantha Holdsworth, Valentina Taviani, Arun Rangaswami, Ranjana Advani, Neyssa Marina, Heike Daldrup-Link

Disclosures: All authors have disclosed no financial interests, arrangements or affiliations in the context of this activity.

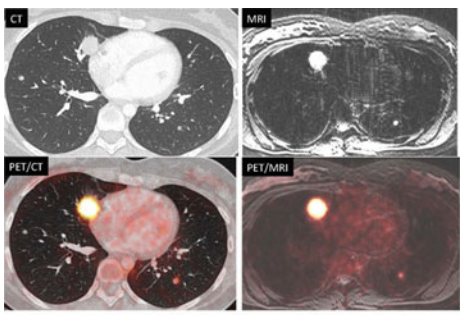

Figure 1: 16 year-old female with primary nasopharyngeal carcinoma with lung metastases, demonstrated by the FDG-avid nodules on CT, PET/CT, MRI, and PET/MRI. (Because of slice selection, small right non FDG-avid nodule on CT is not seen on the MRI.)

Purpose or Case Report: Our goal is to establish PET/MR as an imaging approach that would provide equal sensitivities compared to standard clinical CT and ^{18}F-FDG PET/CT for clinically relevant pulmonary nodules ≥3 mm in size for initial and subsequent staging of pediatric solid tumors.
Methods & Materials: In this IRB-approved, HIPAA compliant prospective study, we performed 7 "one stop" PET/MRI scans of the primary tumor and whole body in 5 pediatric patients with lymphoma, bone sarcoma or nasopharyngeal carcinoma. Scans were performed on a GE Signa 3T PET/MR scanner 2-3 days after intravenous (IV) ferumoxytol (5 mg Fe/kg) and 2 h after IV ^{18}F-FDG (2–3 mBq/kg). Lungs were evaluated with T2-FSE (TR 6000 s/TE 65 ms) sequences with simultaneous PET-data acquisition. Two experienced reviewers assessed the presence, size, and FDG-avidity of nodules on CT, PET/CT, MRI, and PET/MRI. Sensitivity of PET/CT and PET/MRI included all lung nodules seen on PET plus the respective modality (CT or MRI). Imaging follow-up or histopathology was used as a standard of reference. Tumor staging was considered positive for lung metastases if an FDG-avid lung nodule was identified with an FDG-avid primary lesion, and results among modalities were compared using Cohen's k statistics.
Results: Standard of reference revealed 12 nodules 1-2 mm in size, 15 nodules 3-4 mm in size, and 23 nodules ≥5 mm. Sensitivity for detection of all nodules was 50/50 (100%) for both CT and PET/CT, and 20/50 (40%) for MR and PET/MRI. Sensitivity for FDG-avid nodules was 22/50 (44%) for PET/CT and 17/50 (34%) for PET/MRI. The majority of missed nodules on MRI and PET/MRI were 1-2 mm, which is usually not resected, but some nodules ≥3 mm were also missed. When considering clinically significant nodules ≥3 mm, sensitivity was 38/38 (100%) for CT and PET/CT and 20/38 (53%) for MR and PET/MR. Overall sensitivity for FDG-avid nodules ≥3 mm was 22/38 (58%) for PET/CT and 17/38 (45%) for PET/MRI, with missed nodules on PET/MRI possibly due to PET/MR alignment, inferior MR resolution, or artifacts. For overall tumor staging results, there was excellent agreement among all modalities with a k of 1.0.
Conclusions: MR and PET/MRI provide inferior sensitivity compared to standard clinical CT and ^{18}F-FDG PET-CT for the detection of clinically relevant lung nodules with diameters ≥3 mm. We plan to continue to accrue more patients, improve MR resolution and alignment with PET, and evaluate the value of FDG-tumor uptake in differentiating benign versus malignant lesions.

Paper #: 020

Pediatric head and neck sarcomas: Comparison of apparent diffusion coefficient (ADC) on diffusion weighted MR imaging and maximum standardized uptake value (SUV max) at 18F-FDG PET/CT with histologic correlation

Alexis Rothenberg Maddocks, MD, *Radiology, The Children's Hospital of Philadelphia, Bryn Mawr, PA, Alexis.Rothenberg@gmail.com;* Karuna Shekdar, Lisa States

Disclosures: All authors have disclosed no financial interests, arrangements or affiliations in the context of this activity.
Purpose or Case Report: Several studies have demonstrated the inverse relationship between apparent diffusion coefficient (ADC) on diffusion weighted MR imaging (DWI) and maximum standardized uptake value (SUV max) at 18F-FDG PET/CT in the context of head and neck sarcomas in the adult population though their evaluation in the pediatric population has not been widely assessed. The purpose of this study is to investigate the potential correlation of ADC assessed by DWI and glucose metabolism determined by standardized uptake value at 18F-FDG PET/CT in pediatric head and neck sarcomas.
Methods & Materials: We retrospectively reviewed a cohort of pediatric patients with head and neck sarcomas who had pre-treatment evaluation with MR and 18FDG PET/CT performed within 1 month of one another between 2010 and 2015. Cases without adequate DWI were excluded. Available imaging in the selected cases was independently reviewed by 2 pediatric neuro-radiologists, and 1 pediatric/nuclear medicine radiologist. The primary lesion SUV max on 18FDG PET/CT and ADC values on MR DWI imaging (6 on 1.5 T and 7 on 3.0 T) were measured. In the course of our study we also assessed ADC values and SUV max in enlarged lymph nodes. Clinical charts were reviewed.
Results: There were 13 patients ranging in age from 4 months to 22 years 11 months with confirmed head and neck sarcomas. The histologic distribution of the sarcomas included 5 Ewing sarcoma, 3 embryonal rhabdomyosarcoma, 2 alveolar rhabdomyosarcoma, 1 synovial cell sarcoma, 1 undifferentiated sarcoma and 1 metastatic liposarcoma to the left mandible/masticator space. There was an inverse correlation between SUV max and ADC values with lower pretreatment ADC values correlating with higher SUV max. The ADC values varied with histologic type and primary lesion heterogeneity. Complementary information was obtained from ADC values and SUV max in enlarged lymph nodes that led to lymph node biopsy valuable in guiding therapy.
Conclusions: This preliminary study is one of the first to study the relationship between SUV and ADC in pediatric head and neck sarcomas. The inverse correlation of these two quantitative imaging parameters elicits the association of metabolic activity and tumor cellularity. Pretreatment ADC and SUV max comparison may be helpful in predicting outcome and selecting high risk patients for more aggressive therapy. Further studies are needed in the pediatric population to investigate the possible complementary role of ADC and PET/CT in staging, management and treatment response.

Paper #: 021

Correlation of whole-tumour apparent diffusion coefficient measurements with histopathological findings in nephroblastoma

Annemieke Littooij, M.D., *Radiology, University Medical Centre Utrecht, Utrecht, Netherlands, alittooij@hotmail.com;* Neil Sebire, Øystein Olsen

Disclosures: All authors have disclosed no financial interests, arrangements or affiliations in the context of this activity.

Purpose or Case Report: To explore the potential correlation of whole-tumour apparent diffusion coefficient parameters with histopathological findings in nephroblastoma

Methods & Materials: Children (n=52) with histopathologically proven nephroblastoma underwent diffusion-weighted MRI before preoperative chemotherapy. Of these, 25 underwent an additional MRI after preoperative chemotherapy, shortly before resection. The whole-tumor specimen was available for pathological review. An experienced reader performed the whole-tumour ADC measurements of all lesions, excluding non-enhancing areas. Median ADC before preoperative treatment (ADC_{pre}), after preoperative treatment (ADC_{post}) and the shift in median ADC were analysed. An experience pathologist reviewed the postoperative specimens.

Results: ADC_{pre} (0.945×10^{-3} mm^2/s; SD 0.232; range 0.641- 1.416×10^{-3}) was significantly lower than ADC_{post} (1.310×10^{-3} mm^2/s; SD 0.343; range 0.781-1.951×10^{-3}, p<0.001). ADC_{pre} showed a moderate correlation with proportion blastema subtype in the selected population of 25 patients (r=-0.410, p=0.042).

ADC_{pre} and ADC_{post} showed moderate correlation with proportion stromal subtype at histopathology (r=0.401, p=0.003 and 0.579, p=0.002, respectively). By receiver-operator characteristics analysis, the optimal threshold of ADC_{post} for detecting stromal subtype was 1.362×10^{-3} mm^2/s with sensitivity and specificity of 100% and 78.9% respectively.

Conclusions: Whole-tumour ADC markers in nephroblastoma are correlated with stromal subtype histopathology, however differentiation between epithelial and blastema predominant types is challenging because both subtypes show marked diffusion restriction.

Paper #: 022

Role of Diffusion Weighted Imaging in Differentiating Nephroblastomatosis from Wilm's tumour: a pilot study

Claudia Martinez-Rios, MD, *The Hospital for Sick Children, Toronto, ON, Canada, claudia.martinez-rios@sickkids.ca;* Marta Tijerin Bueno, Fellow, Rahim Moineddin, Armando Lorenzo, Marta Wilejto, Gino Somers, Ronald Grant, Mary-Louise Greer, MBBS

Disclosures: All authors have disclosed no financial interests, arrangements or affiliations in the context of this activity.

Purpose or Case Report: To evaluate the utility of diffusion weighted imaging (DWI) to differentiate nephroblastomatosis (NR) from Wilm's tumor (WT)

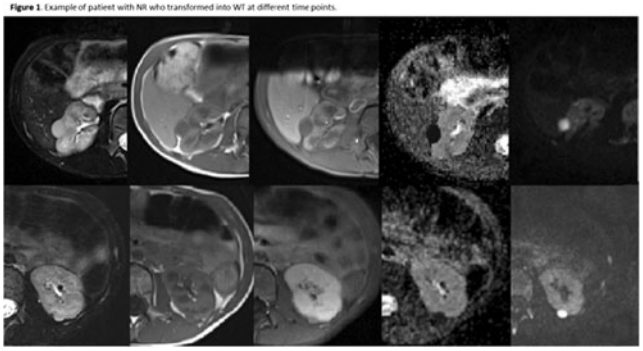

Figure 1. Example of patieet with NR who transformed into WT at different time points.

Methods & Materials: This retrospective pilot study was approved by our REB and informed consent waived. Our cohort consisted of 20 baseline lesions in 6 children [3 females; mean 7.9 years (2–13.4)] having abdominal magnetic resonance imaging (MRI) for assessment of renal lesions excluding other than NR and WT. By consensus two readers evaluated MRI data sets in a blinded, randomized fashion. Multiple regions of interest were drawn over renal lesions and normal kidneys in control and cohort MRI to obtain mean ADC values. Gold standard was histopathology and clinical outcome. Statistical analyses included t-test, sensitivity (Sen), specificity (Spec), positive and negative predictive values (PPV and NPV) at a 95% confidence interval (CI)

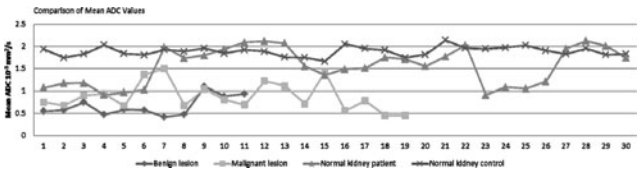

Results: ADC values from 30 lesions, 20 on baseline and 10 follow-up MRI were included. Diagnoses were 8 WT; 7 NR-2 transforming into WT; and 5 non-specific, on follow-up diagnosed as WT. Lesion characteristics evolved on conventional sequences and DWI. Control group ADC values were higher [1.8×10^{-3} mm^2/sec; range 1.6-2.1] versus (vs.) cohort lesion-free kidneys [1.5×10^{-3} mm^2/sec; range 0.9-2.1] (P<0.0001), vs. NR [0.6×10^{-3} mm^2/sec; range 0.4-1.0] (P<0.0001), and vs. WT [0.9×10^{-3} mm^2/sec; range 0.4-1.4] (P<0.0001). NR vs. WT ADC values showed a statistically significant difference (P=0.03). Six extrarenal WT vs. renal WT had higher ADC values [1.01×10^{-3} mm^2/sec; range 0.6-1.4 vs. 0.7×10^{-3} mm^2/sec; range 0.4-1.4] but not different (P=0.08). Baseline non-specific lesions had ADC values of 0.7×10^{-3} mm^2/sec (range 0.4-0.9) vs. follow-up MR diagnoses of WT [0.9×10^{-3} mm^2/sec; range 0.4-1.4] (P=0.23), not statistically significant but trending upward, compared with essentially stable NR ADC values on follow-up. Baseline vs. follow-up MRI compared with the gold standard had a Sen 58.8% (CI: 32.9-81.6) vs. 75% (CI: 34.9-96.8), same Spec 100% (CI: 29.2-100), PPV 100% (CI: 69.1-100) vs. 100% (CI: 54–100), and NPV 30% (CI: 6.7-65.2) vs. 60% (CI: 14.6-94.7), respectively

Conclusions: ADC values from NR and WT are different, and while absolute ADC values don't definitely identify transformation of NR into WT, there is an upward trend warranting further prospective lesion analysis. Qualitatively, lesion delineation is equal to or greater on DWI vs. conventional sequences

Paper #: 023

Can diffusion weighted imaging predict relapse in paediatric classical Hodgkin lymphoma? A pilot study.

Thomas Semple, MBBS, BSc, *University College London Hospital, London, United Kingdom, tsemple@doctors.org.uk;* Gemma Price, Stephen Daw, Owen Arthurs, FRCR, PhD, Paul Humphries, MRCP, FRCR

Disclosures: All authors have disclosed no financial interests, arrangements or affiliations in the context of this activity.

Purpose or Case Report: A small number of paediatric patients with classical HL (cHL) relapse following primary therapy, with increased morbidity. This pilot study aims to assess the ability of apparent diffusion coefficient (ADC) analysis to predict disease relapse following first line treatment for paediatric cHL, which could enable treatment modification during primary therapy.

Methods & Materials: The cancer registry data of a tertiary referral paediatric haemato-oncology centre was retrospectively reviewed from 2007 to 2015 to identify cHL patients who relapsed following

standardised risk and response adapted treatment and compared with matched controls who did not relapse.
Clinically acquired anonymized MRI images were used for retrospective review, which did not require ethical approval. Individual nodal group volumes were contoured on ADC maps for each patient at initial staging and at early response assessment (ERA), blinded to relapse status, using Osirix. Histographic analysis was performed using Image J.
Tenth centile ADC (10^cADC) was evaluated as a biomarker, analysed on an individual basis for relapse patients and between relapse and non-relapse patients. IBM SPSS version 23 was used for statistical analysis.
Results: Three relapse cHL patients (1 male, 2 female, mean age 17.3 ±2 years) were gender and stage matched to 3 controls (mean age 11.6 ±6 years). Twelve nodal sites were evaluated in relapse patients and 4 in control patients.
The mean 10^cADC of all nodes was lower at staging in patients who relapsed ($0.88\times10^{-6}mm^2/s$) compared to those who did not ($1.32\times10^{-6}mm^2/s$; $p<0.01$). There was no statistical difference for ERA 10^cADC between groups.
There was no statistical difference between staging or ERA 10^cADC for relapsing nodes and non-relapsing nodes within patients who relapsed.
Conclusions: 10^cADC at staging in cHL may be a useful biomarker for disease relapse although this requires confirmation with a larger population.

Paper #: 024

Staging of paediatric classical Hodgkin lymphoma (cHL) using F^{18}-Fluorodeoxyglucose Positron emission tomography MRI (F^{18}-FDG PET-MRI): a prospective pilot comparison to F^{18}-FDG PET-CT reference standard

Paul Humphries, MRCP FRCR, *Radiology, Great Ormond Street Hospital for Children and University College London Hospital, London, United Kingdom, p.humphries@ucl.ac.uk;* Leon Menezes, Deena Nerriman, Stephen Daw

Disclosures: All authors have disclosed no financial interests, arrangements or affiliations in the context of this activity.
Purpose or Case Report: Paediatric cHL patients are currently treated using risk adaptive therapy based on anatomical disease staging and metabolic activity using F^{18}-FDG PET-CT. Reduction in diagnostic radiation burden is possible using newly available PET-MRI systems, however it is imperative to preserve accurate staging to ensure correct treatment group allocation. This pilot study evaluates the diagnostic accuracy of PET-MRI for the initial staging of paediatric cHL.
Methods & Materials: This ERB approved prospective study recruited patients referred for clinical PET-CT as part of staging investigations for suspected or proven cHL between February 2015 and July 2015. Following written informed consent and using the same F^{18}-FDG injection that had been administered for PET-CT, each patient underwent PET-MRI, comprising whole body T2 imaging, DIXON T1 attenuation correction sequences and whole body diffusion weighted imaging.
PET-CT was used as the reference standard. PET-CT was reviewed by a Nuclear Medicine (NM) physician and PET-MRI reviewed by a second NM physician and radiologist in consensus. Each study was independently prospectively staged using 20 nodal sites and 8 extra-nodal sites per patient, with SUV_{max} and mean apparent diffusion coefficient (ADC_{mean}) recorded for the most avid node/focus of extra-nodal disease at each site. Statistical analysis was performed for disease involvement, overall staging, SUV_{max} measurements between the two modalities and to assess the relationship between ADC_{mean} and SUV_{max}, using IBM SPSS (version 23).
Results: Eleven patients (7 male, 4 female, 8-20 year, mean 14.9 years) were recruited. Patient numbers per disease stage was as follows: Stage 1 (1), Stage 2 (7), Stage 3 (2), Stage 4 (1). PET-MR was concordant with PET-CT for staging in each patient.
Forty-seven nodal sites were involved on the PET-CT reference standard. PET-MR identified all of these sites and also identified one site not demonstrated on PET-CT (sensitivity 100%, specificity 78%; positive predictive value 98%; negative predictive value 99% for nodal disease involvement).
There was one patient with extra-nodal involvement, with multiple lesions within the pelvis on PET-CT. PET-MRI identified this disease but showed a greater number of lesions (13 vs 7).
PET-MR SUV_{max} measurements showed no significant difference to those on PET-CT (PET-MR mean disease SUV_{max} 8.1 (2.6-15.1), PET-CT mean disease SUV_{max} 7.6 (2.4-13.6), p 0.45).
There was a significant inverse linear relationship identified between ADC_{mean} and SUV_{max} (Pearson correlation coefficient logADC_{mean}/log SUV_{max} -0.47, p 0.001).
Conclusions: In this study, PET-MRI was highly accurate for the staging and identification of nodal disease in paediatric cHL compared to PET-CT. The simultaneous acquisition of ADC and SUV using PET-MRI will allow further investigation of the clinical impact of the relationship between ADC_{mean} and SUV_{max} demonstrated in this study. Further patient recruitment is needed to assess PET-MR accuracy for extra-nodal disease involvement, given that there was only one case in this cohort.

Paper #: 025

Utility of Adult-based Ultrasound Criteria to Predict Malignancy in Pediatric Thyroid Nodules

Claudia Martinez-Rios, MD, *The Hospital for Sick Children, Toronto, ON, Canada, claudia.martinez-rios@sickkids.ca;* Lydia Bajno, Alan Daneman, Rahim Moineddin, Danielle CM van der Kaay, Jonathan Wasserman

Disclosures: All authors have disclosed no financial interests, arrangements or affiliations in the context of this activity.
Purpose or Case Report: Individual ultrasound (US) features have limited ability to distinguish benign from malignant thyroid nodules. Several systems have been developed to integrate features and to improve diagnostic accuracy. None have been validated in children, in whom the likelihood of malignancy is 2-5× higher than adults. We evaluated the utility of two adult-based US malignancy stratification risk approaches for assessment of thyroid nodules in children
Methods & Materials: This retrospective study comprised 124 children (40 males:84 females, average age 13.6 years (range 3-17) who had thyroid US. 3 pediatric radiologists evaluated the US in a blinded, randomized fashion using the American Thyroid Association (ATA) risk stratification method and the Thyroid Image Reporting and Data System (TIRADS). Readers diagnostic confidence was scored using a 5-point Likert scale. The reference standard was histopathology or cytology and clinical outcome
Results: We assessed 124 nodules: 71 benign, 52 malignant and 1 indeterminate. The ATA system classifies nodules based on US **patterns** associated with suspicion for malignancy. 36/52 (69%) malignant nodules were scored as high suspicion and 6/52 (11%) as intermediate. The overall likelihood of malignancy for High, Intermediate, Low, Very Low, and Benign categories was 75%, 43%, 14%, 10% and 0% respectively. TIRADS assigns an increasing likelihood of malignancy based on the **number** of suspicious US features within a nodule. Nodules were classified as TIRADS 2, 3, 4a, 4b, 4c, and 5 with frequencies of malignancy of 0%, 0%, 13.5%, 13.5%, 61.5% and 11.5% respectively. Reviewers reported greater confidence scoring malignant nodules than with benign (mean of 4.3 vs. 3.6 on the Likert scale), although this difference was not significant. Confidence in assessment did not vary between assignment of TIRADS score and ATA class. US features of malignancy in our study: partial/absent halo 49 (94%), ill-defined or

spiculated margins 43 (83%), solid 42 (81%), hypoechoic 32 (62%), microcalcifications 37 (71%), and taller than wide 8 (15%). Non-ATA/TIRADS features included: nodular hypervascularity 43 (83%), and abnormal lymph nodes 20 (38%)
Conclusions: The ATA and TIRADS classifications are similar in their test characteristics, although both demonstrate regions of overlap between benign and malignant lesions. Results from this study define the US features of malignancy in children and advocate for a more specific classification in children

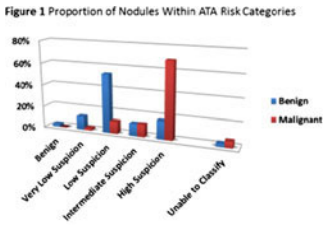

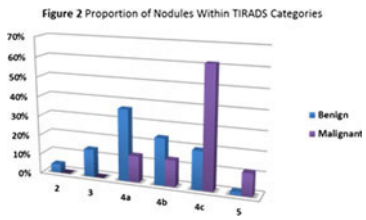

Paper #: 026

Whole-body MRI reveals high incidence of osteonecrosis in children treated for Hodgkin lymphoma in the Euronet-PHL-C1 trial

Annemieke Littooij, M.D., *Radiology, University Medical Centre Utrecht, Utrecht, Netherlands;* Thomas Kwee, Jonathan Verbeke, Claudio Granata, MD, Auke Beishuizen, Charlotte de Lange, Floriana Zennaro, Rutger Nievelstein, MD, PhD

Disclosures: All authors have disclosed no financial interests, arrangements or affiliations in the context of this activity.
Purpose or Case Report: To determine the incidence of osteonecrosis in children treated for Hodgkin lymphoma using whole-body magnetic resonance imaging (MRI).

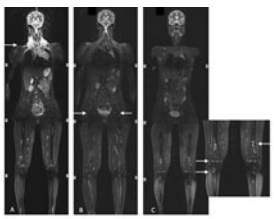

Figure 1 Coronal STIR images of a 15-year-old girl with stage II Hodgkin lymphoma (a) illustrate the development of osteonecrosis in both femora and proximal tibia diagnosed during response assessment after 2 cycles of OEPA chemotherapy (b,c)

Methods & Materials: Ethical committee approval and informed consent were obtained for this prospective study. Pediatric patients with newly diagnosed Hodgkin lymphoma who were enrolled in the EuroNet-PHL-C1 trial (Table 1) were eligible for inclusion. Whole-body MRI (including T1-weighted and T2-weighted short inversion time inversion recovery [STIR] sequences) was performed before start, after 2 cycles of vincristine, etoposide, prednisone and doxorubicin (OEPA), and after completion of chemotherapy. Whole-body MRI scans were evaluated for geographic areas of decreased signal on T1-weighted images with increased signal on T2-weighted STIR images, consistent with osteonecrosis.

Table 1 Treatment of overview for the three treatment groups (TG) according to the Euronet-PHL-C1 trial

TG-1	Stage IA/B, IIA with bulk <200 cm^3 and/or ESR<30 mm/hr	2x OEPA
TG-2	Stage 1E A/B, IIE A, IIB or IIIA and Stage IA/B, IIA with bulk>200 cm^3 and/or ESR>30 mm/hr	2x OEPA, Consolidation treament with 2x COPDAC
TG-3	Stage IIE B, IIIE A, IIIB or IVA/B	2x OEPA, consolidation treatment with 4x COPDAC

Results: A total of 24 patients (mean age 14.8 years, 12 girls) were included. Osteonecrosis was diagnosed in 10 patients (41.7%, 95% confidence interval: 22.0 - 61.4%) during therapy response assessment. In 9 patients osteonecrosis was detected after 2 cycles of OEPA. Epiphyseal involvement of long bones was seen in 4 of 10 children (Figure 1). None of the patients with osteonecrosis had any signs of bone collapse at the times of scanning.
Conclusions: Whole-body MRI demonstrates osteonecrosis to be a common finding during therapy response assessment of pediatric Hodgkin lymphoma in the Euronet-PHL-C1 trial. Detection of early epiphyseal osteonecrosis could allow for treatment before bone collapse and joint damage may occur.

Paper #: 027

Pediatric Focal Nodular Hyperplasia: Value of Superb Micro-Vascular Imaging

Sook Min Hwang, *radiology, Samsung Medical Center, Seoul, Korea (the Republic of), okanagan@naver.com;* So-Young Yoo, Woo Kyoung Jeong, Tae Yeon Jeon, MD, Ji Hye Kim

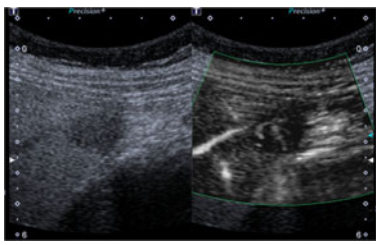

Disclosures: All authors have disclosed no financial interests, arrangements or affiliations in the context of this activity.
Purpose or Case Report: To investigate the value of superb microvascular imaging (SMI), a novel Doppler US technique that can visualize low velocity microvascular flow, for assessing pediatric focal nodular hyperplasia (FNH).
Methods & Materials: All ten FNH lesions (mean size 4 cm, range 1 ~ 10 cm) in 7 patients (all female, mean age 12, range 2 ~ 17 years) examined by both Color Doppler imaging (CDI) and SMI during US examination were enrolled. Diagnosis of FNH was made by means of MR, CT imaging findings or biopsy. Single lesion was found in 4 patients including two with absent portal vein, while multiple lesions were present in 3 patients who had undergone chemotherapy. Spoke-wheel vascular pattern (the central vessel radiating from the center to the periphery), a highly specific finding of FNH, was evaluated in each lesion and assigned

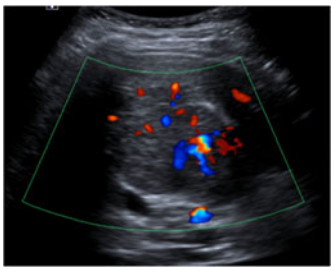

as definite, equivocal, absent according to visual assessment by consensus of two radiologists on CDI and SMI, respectively.
Results: All FNHs appeared as an iso- or slightly hypoechoic lesion. Spoke-wheel pattern was more frequently and more clearly visualized with SMI (definite 6, equivocal 3, absent 1) compared with CDI (definite 2, equivocal 2, absent 6). In five FNHs (5/10, 50%), SMI demonstrated spoke-wheel pattern which was not visualized on CDI.
Conclusions: Our preliminary study shows that SMI, with its greater ability to demonstrate spoke-wheel pattern than CDI, can be a promising, noninvasive adjunctive technique for diagnosing FNH in children.

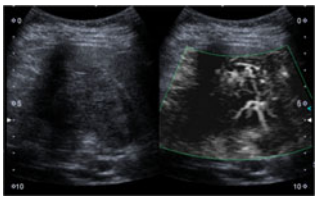

Paper #: 028

MRI and Malrotation: Excluding Intestinal Malrotation on Magnetic Resonance Examinations Ordered for Other Indications

Jill Fay, *Montefiore Medical Center, New York, NY;* Victoria Chernyak, Benjamin Taragin

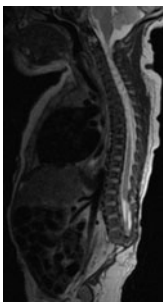

Disclosures: All authors have disclosed no financial interests, arrangements or affiliations in the context of this activity.
Purpose or Case Report: Children with vomiting or need for percutaneous gastrostomy placement frequently undergo upper gastrointestinal series (UGI) to exclude intestinal malrotation. UGI requires radiation exposure, which may contribute to increased risk of subsequent malignancies. Anatomical imaging findings indicative of malrotation can be evaluated on cross-sectional imaging. The goal of our study is to evaluate ability to exclude malrotation based on pediatric magnetic resonance (MRI) exams performed for non-related indications.
Methods & Materials: This retrospective study included patients ≤21 years, who had MRI of the chest, spine, or abdomen between the years of 2006 and 2014, and also had UGI performed within 10 years of the MRI date. A pediatric radiologist reviewed images from UGI to determine intestinal rotation for each case. Then, two attending radiologists (a pediatric radiologist and an adult abdominal radiologist) independently reviewed the MRI images. The following questions were assessed on each case:
1. Is the duodenum retroperitoneal?
2. Is the duodenojejunal junction in the left upper quadrant?
3. Is the superior mesenteric artery to the left of the superior mesenteric vein?
4. Is the cecum in the right lower quadrant?

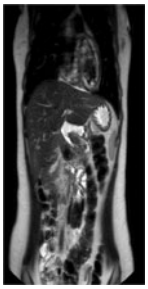

The questions were answered as "yes", "no" or "unclear". Numbers of cases with all four questions answered as "yes" ("4-YES") were tabulated for each radiologist. Kappa statistics was used to estimate interobserver agreement for cases with "4-YES".
Results: The study included 109 MRIs (15 [13.8%] chest, 41 [37.6%] spine, and 53 [48.6%] abdomen) done on 109 patients (46 [42.2%] males, mean age 10.2 [±6.9] years. Of the 109 studies, 4 (3.7%) had abnormal rotation and 105 (96.3%) had normal rotation as confirmed by UGI. For the pediatric radiologist, 71 (65.1%) of 109 cases were "4-YES". For the adult abdominal radiologist, 65 (60.0%) of 109 cases were "4-YES". Interobserver agreement for "4-YES" was moderate (k=0.57, 96%CI 0.40-0.73). For both readers, 0 (0%) of "4-YES" cases had malrotation.
Conclusions: Normal anatomy can be confirmed on 60-65% of MRIs performed for non-related indications, excluding intestinal malrotation and potentially eliminating the need for UGI. When MRI can confidently exclude malrotation by answering "yes" to these four questions pertaining to normal anatomy, UGI and radiation exposure may be avoided.
Paper #: 029

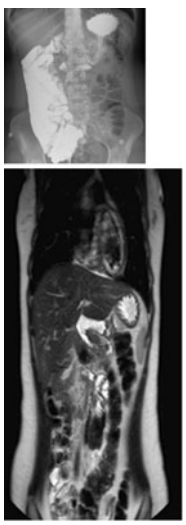

Position of nasogastric tube tip in the antrum results in better quality, speed and radiation dose of emergency upper GI contrast studies for suspected malrotation and mid-gut volvulus

Savvas Andronikou, MBBCh, FCRad, FRCR, PhD, *Paediatric Radiology, University of Bristol, Bristol, United Kingdom, docsav@mweb.co.za;* Sarah Athur

Disclosures: All authors have disclosed no financial interests, arrangements or affiliations in the context of this activity.
Purpose or Case Report: Emergency upper GI contrast studies are indicated to diagnose malrotation / volvulus in newborns and children with bile-stained vomiting. The study can be expedited using indwelling nasogastric tubes (NGT). A fundal position of the NGT tip may cause pooling of contrast in the fundus allowing trickling into the duodenum and jejunum, contaminating visualization of the duodenal C-loop. This may prolong procedures with increased radiation doses, require patient repositioning, affect image quality and result in gastro-oesophageal reflux.
Aim: To compare UGIS through fundal placed and antral placed NGT's in neonates and children with suspected malrotation / volvulus with regard to quality, time of procedure, radiation dose and complications.
Methods & Materials: Emergency UGIS in neonates and children with suspected malrotation / mid-gut volvulus reviewed 6 months retrospectively on PACS regarding NGT position (fundal / antral), quality (diagnostic / non-diagnostic), time taken (start and end time), radiation dose (DAP and CTDI), lateral re-positioning and gastro-oesophageal reflux. Radiologist reports were reviewed.
Results: 58 UGIS were reviewed from 6 months (9.6procedures / month). NGT was fundal in 50 and antral in 8. 17 (29%) were 'contaminated' and a further 10 (17%) had trickling of contrast without 'contaminating' the field i.e. 47% had trickling and or contamination. Fundal tubes had contamination in 16 (32%), and a further 10 (20%) had trickling without contamination. Only 1 (13%) antral tube had contamination and trickling. Reports, however, indicated only 4 cases (7%) required repeating. 19 cases (33%), including these 4, were considered non-diagnostic on review. Average time for fundal tubes was 5.9 min and 2.75 for antral tubes. Overall average radiation dose was D.A.P 24.868 and E.D 0.505 (range DAP 0.024- 124.800/ E.D 0.01-2.598). Average radiation dose for fundal tubes was D.A.P 24.986/ E.D 0.505 and for antral tubes D.A.P 24.043/ E.D 0.478. Lateral repositioning during the procedure was performed in 39 cases, 36 of which were fundal tubes (fundal 72%; antral 37%). Reflux was occurred in 13 cases, 11 fundal (22%) and 2 antral (25%).
Conclusions: Antral placed tubes during UGIS resulted in higher quality images, faster studies, lower doses and required less repositioning. Despite only 4 reports recommending repeat imaging, UGIS images on PACS indicated that 33% were non-diagnostic.

Paper #: 030

Bowel Perforation Complicating Attempted Intussusception Reduction by Air Enema: Risk Factors and the Myth of the Microperforation

R. Guillerman, *Texas Children's Hospital, Houston, TX, rpguille@texaschildrens.org;* Farahnaz Golriz, MD, Robert Orth, MD, PhD, Wei Zhang, John Hicks, Lane Donnelly, MD

Disclosures: Robert Orth has indicated a relationship with General Electric as a fellow. All other authors have disclosed no financial interests, arrangements or affiliations in the context of this activity.
Purpose or Case Report: To determine the safety and effectiveness of air enema intussusception reduction performed with and without a rectal balloon.

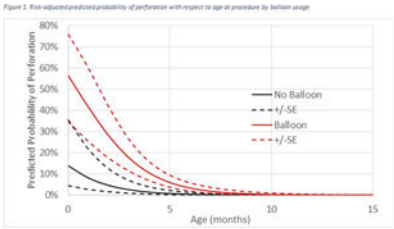

Methods & Materials: A retrospective review was conducted of all ileocolic intussusceptions managed by air enema reduction from January 2008 to July 2015 at a large children's hospital. Univariate analysis with Fisher's exact test for categorical variables and Wilcoxon rank test for continuous variables was performed. Multivariate logistic regression was applied to identify risk factors for bowel perforation and unsuccessful reduction. Odds ratios (OR) for bowel perforation and unsuccessful reduction were calculated, and a risk-adjusted predictive probability plot was generated.
Results: 521 patients (male:female 324:197; median age 15 months; range 2 months-14 years) underwent 581 air enema reduction attempts. The success rate of the initial attempts at reduction was 86% (214/246) using an inflated rectal balloon and 80% (220/275) not using a balloon (p=0.0056). Delayed re-attempts at reduction were performed in 60 cases with a success rate of 63% (28/44) using a balloon and 31% (5/16) not using a balloon (p=0.04). Bowel perforation occurred in 9 patients (mean age: 4 months; range: 2-8 months), requiring needle decompression of tension pneumoperitoneum in 8 patients. The perforation site was non-necrotic bowel in 8 patients (with extensive bowel tears requiring ileocolic resection in 5), and necrotic bowel in 1 patient. Eight perforations occurred with use of a balloon, 3 of these during delayed re-attempts. None of the perforated cases had lead point masses. Adjusting for other risk factors, a higher risk of perforation was associated with younger age (p=0.001) and use of a rectal balloon [OR=8 (CI: 0.94-68); p=0.057], but not with the number of reduction attempts (p=0.36). The rate of successful reduction was not associated with age (p=0.18), but was associated with use of a balloon (P=0.005). A risk-adjusted predicted probability plot of perforation with respect to age (Figure 1) shows increased perforation risk in patients less than 10 months of age, and very low perforation risk after 10 months of age regardless of balloon catheter use.
Conclusions: Use of an inflated rectal balloon increases the success rate of air enema intussusception reduction but is associated with a higher risk of bowel perforation in young infants. In contrast to previous animal model data, the resultant perforations are often large and necessitate extensive resection of non-necrotic bowel.

Paper #: 031

Is Appendicitis Less Common In Pediatric Patients With Sickle Cell Disease? A Retrospective Cohort Study of A Large, Urban Population

Carly Schwartz, MD, *Montefiore Medical Center, Bronx, NY, carlysschwartz@gmail.com;* Benjamin Taragin, Moonseong Heo, Netta Blitman, Kerry Morrone, Mark Liszewski

Disclosures: All authors have disclosed no financial interests, arrangements or affiliations in the context of this activity.
Purpose or Case Report: Patients with sickle cell disease (SCD) often experience acute abdominal pain related to vasoocclusion, and symptoms may mimic acute appendicitis (AA). Antal et al. found that the incidence of AA in patients with SCD was significantly lower than the national incidence, but point out that this comparison could be confounded by a lower incidence of AA in the nonwhite population. We investigate whether the incidence of AA differs between pediatric patients with SCD and those without, utilizing study and control groups taken from the same large urban population.
Methods & Materials: A retrospective cohort study was conducted at the Children's Hospital at Montefiore. The SCD study group included patients with hemoglobin SS (HbSS), hemoglobin SC (HbSC), and sickle cell-β thalassemia (HbS-β) disease aged 0-21 years, and first seen between 01/01/2001 and 12/31/2014, with at least one additional clinical encounter within 24 months. The control group included patients without SCD aged-21 years first seen between 01/01/2011 and 12/31/2011, with at least one

additional clinical encounter within 24 months. Patients with prior appendectomy were excluded. Demographic data was collected and incidence of AA was determined, with initial clinic visit defining the start point, and last clinic note or admission for AA defining the endpoint. Statistical significance was assessed utilizing an exact test based on binomial distribution.

Table 1 Incidence of Appendicitis in Patients with Sickle Cell Disease and Controls

	SCD Group (HbSS, HbSC, and Sickle Cell-β Thal)	HbSS Cohort	HbSC Cohort	Sickle Cell-β Thal Cohort (includes SBO and SB+)	Control Group
Number of patients	1064	759	246	59	115,109
Cases of Appendicitis	2	1	1	0	343
Patient years followed	6,979	5,006	1579	394	321,376
Cases of appendicitis per 10,000 patient-years	2.9 (p=0.044)*	2.0 (p=0.062)*	6.3 (p=0.997)*	0 (p=1.000)*	10.7

Results: The SCD group included 1,064 patients followed for 6,979 patient-years. The control group included 115,109 patients followed for 321,376 patient-years. Incidence of AA was significantly lower in the SCD group compared to controls (2.9 cases/10,000 patient-years vs. 10.7 cases/10,000 patient-years; p=0.044) [Table 1]. Subgroup analysis revealed a lower incidence of AA in patients with HbSS disease compared to controls that approached but did not achieve statistical significance (2.0 cases/10,000 patient-years vs. 10.7 cases/10,000 patient-years; p=0.062) [Table 1].

Conclusions: Patients with SCD had a significantly lower incidence of AA than controls taken from the same large urban population. The biological basis for this is unknown, but AA should be viewed as an uncommon cause of acute abdominal pain in patients with SCD.

Paper #: 032

Imaging button battery ingestions and insertions in children: a 15-year single center review

Brian Pugmire, M.D., *Cincinnati Children's Hospital Medical Center, Cincinnati, OH, bpugmire42@gmail.com;* Scott Pentiuk, Alessandro de Alarcon, Catherine Hart, Tom Lin, Andrew Trout

Disclosures: Andrew Trout has indicated a relationship with Philips Healthcare, Advisory Board. All other authors have disclosed no financial interests, arrangements or affiliations in the context of this activity.

Purpose or Case Report: Ingested or inserted button/disk batteries pose a significant health risk, particularly if they lodge in the esophagus. In this study we report a comprehensive review of all patients with confirmed button battery ingestions/insertions imaged at our institution in the last 10 years.

Methods & Materials: Radiology reports inclusive of the last 15 years were searched for the terms "battery" and "batteries." Only cases of battery ingestion/insertion confirmed by endoscopy or imaging for which images were available were reviewed. Each case was reviewed in detail for: types of imaging performed, imaging findings (including battery location and size), patient demographics, clinical history, and management.

Results: A total of 276 cases of button battery ingestions/insertions were reviewed. 62% of patients were male and the mean age was 52.3 ±4.6 months (range 9–211). All patients were imaged with radiography, 21 with fluoroscopy (7.6%), and 4 with CT (1.4%). On initial radiographs, batteries were present in the stomach in the majority of cases (n=169, 61.2%) with fewer batteries in the esophagus (n=27, 9.8%), colon (n=24, 8.7%) small bowel (n=15, 5.4%), nasal cavity (n=6, 2.2%), and external ear canal (n=1, 0.3%). In 33 cases (11.2%) the battery was in the abdomen, but a more precise location could not be determined.

Batteries retained in the esophagus were significantly larger on average than those which had passed distally (22.1±3.3 mm vs. 13.7±1.6 mm, p<0.0001). The smallest battery to be retained in the esophagus measured 12 mm, but the vast majority (n=25, 92.6%) were ≥20 mm. The proximal esophagus was the most common site of esophageal impaction (n=9, 33.3%).

Retrieval was attempted in 97 patients (35.1%) including 96.2% of cases of esophageal batteries and 36.7% of cases of gastric batteries. Mucosal injury was seen on endoscopy in 71 patients (73% of all endoscopies) including 100% of endoscopies for esophageal batteries. Seven patients (2.5%) had serious clinical complications (e.g. esophageal perforation, tracheoesophageal fistula) following battery ingestion.

Conclusions: Button battery ingestions/insertions in children are an important health risk. Larger batteries (>20 mm) are more likely to lodge in the esophagus and batteries in the esophagus are more likely to cause tissue injury. Radiography is the mainstay of diagnosis; fluoroscopic studies and advanced imaging may be necessary in some cases. The rate of serious complications is low, but morbidity in these cases is substantial.

Paper #: 033

Neonatal coronary anatomy deliniation via CT - A comparison of standard versus high pitch cardiovascular CT in neonates

Thomas Semple, MBBS, BSc, *The Royal Brompton Hospital, London, United Kingdom, tsemple@doctors.org.uk;* M Sriharan, O Lazoura, I Castellano, Catherine Owens, M Rubens, SPG Padley, E Nicol

Disclosures: All authors have disclosed no financial interests, arrangements or affiliations in the context of this activity.

Purpose or Case Report: We sought to design a high-pitch, non-gated cardiac CT protocol that would allow evaluation of both cardiac and extra-cardiac structures, including the coronary arteries, in a neonatal population, referred for congenital heart disease assessment and compare it to a standard pitch protocol in an equivalent cohort.

Methods & Materials: Twenty-nine high pitch scans were compared with 31 age, sex, weight, and dosimetrically (CTDIvol)-matched standard pitch scans. All were performed at 80 kV. The quality and visualisation of both cardiac and extra-cardiac structures were scored by consensus between two trained, blinded observers. Image quality and radiation doses were compared.

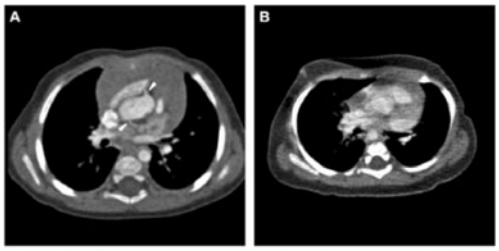

Figure 1. Example of no motion artefact (A) and excessive motion artefact (B). Both images are at the level of coronary sinuses, however, the motion artefact in B precludes identification of the origins and course of the coronary arteries. These are well visualised in A (arrowheads)

Results: The high pitch protocol better demonstrated the pulmonary veins (p=0.03) and all coronary segments (all p<0.05) except the distal right coronary artery (p=0.10), with no significant difference in the visualisation of the remaining cardiac or extra-cardiac structures. Both contrast and signal to noise ratios were improved, with significantly less streak (P<0.01) and motion (P<0.01) artefacts. The high pitch acquisition resulted in a small, but significant, increase in DLP (13.0 mGy.cm [9.0 to 17.3] vs. 11.0 mGy.cm [9.0 to 13.0]; p=0.05).
Conclusions: In neonates, a high pitch protocol improves coronary artery and pulmonary vein delineation compared with the standard pitch protocol. Thus allowing a more comprehensive assessment of congenital heart disease, whilst obviating the need for either patient sedation or heart rate control. There was a small increase in radiation burden, but this is mitigated by potentially avoiding invasive assessment of these structures preoperatively.

Paper #: 034

Diagnostic accuracy of sub-mSv prospective ECG-triggering cardiac CT in low weight infant with complex congenital heart disease

Yumin Zhong, MD,PhD, Diagnositic Imaging Center, Shanghai Children's Medical Center, *Shanghai, China, zyumin2002@yahoo.com;* Aimin Sun, Wei Gao

Disclosures: All authors have disclosed no financial interests, arrangements or affiliations in the context of this activity.
Purpose or Case Report: To explore the clinical value and evaluate the diagnostic accuracy of sub-mSv low-dose prospective ECG-triggering cardiac CT in low weight infants with complex congenital heart disease (CHD).

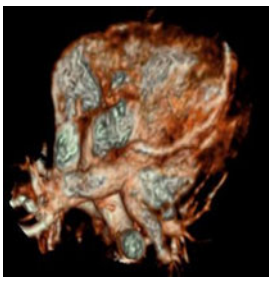

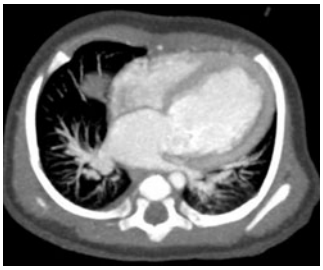

Methods & Materials: A total of 102 consecutive infant patients (53 boys and 49 girls with mean age of 2.93±2.41 m and weight less than 5 kg) with complex CHD were prospectively enrolled. Scans were performed on a 64-slice high definition CT scanner with low dose prospective ECG-triggering mode and reconstructed with 80% adaptive statistical iterative reconstruction (ASIR) algorithm. All studies were performed during free breathing with sedation. The subjective image quality was evaluated by 5-point grading scale and interobserver variability was calculated. The objective image noise (standard deviation, SD) and contrast to noise ratio (CNR) was calculated. The effective radiation dose from the prospective ECG-triggering mode was recorded and compared with the virtual conventional retrospective ECG-gating mode. The detection rate for the origin of coronary artery was calculated. 81 patients had surgery and their preoperative cardiac CT findings were compared with the surgical results for assessing the diagnostic accuracy.
Results: Heart rates were 70–161 beats per minute (bpm) with mean value of 129.19±14.52 bpm. The effective dose of 0.53±0.15 mSv in the prospective ECG-triggering cardiac CT was lower than the calculated value in a conventional retrospective ECG-gating mode (2.00±0.35 mSv) ($p<0.001$). The mean CNR and SD were 28.19±13.00 and 15.75 ±3.61HU, respectively. The image quality scores were 4.31±0.36 and 4.29±0.41 from reviewer 1 and 2 respectively with an excellent agreement between them (*Kappa*=0.85). The detection rate for the origins of the left and right coronary arteries was 96% and 90%, respectively. Comparing to the surgery reports, diagnostic accuracy of 95% (77/81) for extracardiac defects and 91% (74/81) for intracardiac defects were achieved.
Conclusions: Prospective ECG-triggering cardiac CT with sub-mSv effective dose provides excellent imaging quality and high diagnostic accuracy for low weight infants with complex CHD.

Paper #: 035

Cardiac catheterization (CC) compared with cardiac computed tomography (CT) prior to second stage single ventricle (SV) palliation in low risk patients.

Pamela Deaver, MD, *Department of Radiology, Texas Children's Hospital, Houston, TX, pamela.deaver@gmail.com;* Christine Nelson, Luis De Leon, Dhaval Parekh, Shireen Hayatghaibi, MPH, Wei Zhang, Lauren Kane, Rajesh Krishnamurthy

1f. Post Operative and Long term Outcomes					
		CC (N = 65)	CT (N = 7)	P-Value CC versus CT	
Did the patient have any post op complications?	Yes	27 (42)	7 (41)	1.0000	
No unplanned Post Op Procedures within 30 days?	Yes	5 (7.7)	0(0)	0.5782	
O2 Saturations >75% at discharge?	Yes	63 (97)	15 (88)	0.1884	
ICU Discharge at POD 4?	Yes	50 (77)	8 (47)	0.0329	
Hospital Discharge by day POD 7?	Yes	30 (46)	6 (35)	0.5843	
Clinically Well at 3-10 months post op?	Yes	63 (97)	17 (100)	1.0000	
Change in Ventricular Function by Echo at 3-10 months post op clinic follow-up?	Yes	5 (7.7)	2 (13)	0.6199	
Deceased?	Yes	1 (1.5)	1 (6.3)	0.3580	
Transplant?	Yes	0(0)	0(0)		

Disclosures: All authors have disclosed no financial interests, arrangements or affiliations in the context of this activity.
Purpose or Case Report: CC is often used prior to second stage palliation for functional SV patients. The study hypothesis is that CT is a safer, less expensive and equally effective alternative to CC by comparing diagnostic accuracy, procedural morbidity and costs, operative morbidity, and clinical outcome between the two groups.

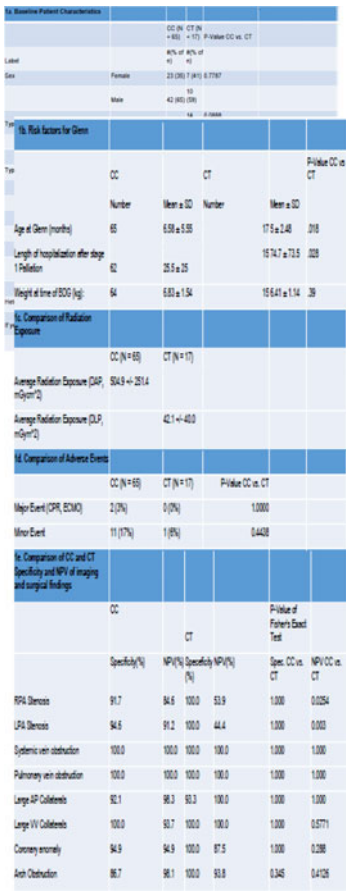

1a. Baseline Patient Characteristics				
		CC (N = 65)	CT (N = 17)	P-Value CC vs. CT
Label		#(% of n)	#(% of n)	
Sex	Female	23 (35)	7 (41)	0.7767
	Male	42 (65)	10 (59)	
Type				

1b. Risk factors for Glenn					
Type	CC		CT		P-Value CC vs CT
	Number	Mean ± SD	Number	Mean ± SD	
Age at Glenn (months)	65	6.58 ± 5.55		17.6 ± 2.48	.016
Length of hospitalization after stage 1 Palliation	62	25.5 ± 25		19.74.7 ± 73.5	.028
Weight at time of BDG (kg)	64	6.83 ± 1.54		15 6.41 ± 1.14	.39
Post					

1c. Comparison of Radiation Exposure		
	CC (N = 65)	CT (N = 17)
Average Radiation Exposure (DAP, mGycm^2)	504.9 +/- 251.4	
Average Radiation Exposure (DLP, mGycm^2)	42.1 +/- 40.0	

1d. Comparison of Adverse Events			
	CC (N = 65)	CT (N = 17)	P-Value CC vs. CT
Major Event (CPR, ECMO)	2 (3%)	0 (0%)	1.0000
Minor Event	11 (17%)	1 (6%)	0.4428

1e. Comparison of CC and CT Specificity and NPV of imaging and surgical findings						
	CC		CT		P-Value of Fisher's Exact Test	
	Specificity(%)	NPV(%)	Specificity (%)	NPV(%)	Spec. CC vs. CT	NPV CC vs. CT
RPA Stenosis	91.7	84.6	100.0	53.9	1.000	0.0254
LPA Stenosis	94.5	91.2	100.0	44.4	1.000	0.003
Systemic vein obstruction	100.0	100.0	100.0	100.0	1.000	1.000
Pulmonary vein obstruction	100.0	100.0	100.0	100.0	1.000	1.000
Large AP Collaterals	92.1	96.3	93.3	100.0	1.000	1.000
Large VV Collaterals	100.0	93.7	100.0	100.0	1.000	0.5771
Coronary anomaly	94.9	94.9	100.0	87.5	1.000	0.288
Arch Obstruction	86.7	96.1	100.0	93.8	0.345	0.4126

Methods & Materials: After IRB approval, a retrospective review of all patients undergoing a bidirectional Glenn at our institution from 2007 to 2014 was performed. A low-risk population, comprising 74% of all patients undergoing pre-Glenn evaluation, was isolated by excluding patients with severe atrioventricular (AV) regurgitation, severe ventricular dysfunction, aortic obstruction, pulmonary hypertension, pulmonary vein stenosis, or large collaterals. Clinical characteristics, diagnostic findings, procedural morbidity and costs, operative data, post-operative morbidity and outcomes were assessed. End-points included specificity and negative predictive value (NPV) of imaging findings, adverse events at imaging, procedural costs, peri-operative morbidity, length of hospital stay after Glenn, and clinical outcome, including progression to cardiac transplant or death. Continuous variables were compared via the Wilcoxon rank test, while categorical variables were compared via the Fisher's exact test.
Results: Eighty-two low risk patients underwent evaluation, with 65 in the CC group and 17 in the CT group. Both groups were similar in patient characteristics (Table 1a). Patient characteristics indicating a higher risk Glenn procedure were similar in both groups (Table 1b). There was a higher incidence of adverse events with CC, though this was not statistically significant (Table 1d). There was no significant difference in diagnostic specificity or NPV for evaluation of the pulmonary veins, aorta, systemic veins, or collaterals. The NPV of CC for pulmonary arterial stenosis exceeded that of CT, though both CC and CT were equally specific (Table 1e). There was no significant difference in bypass time, length of intubation, thoracostomy duration, or post-operative morbidity. ICU duration was longer in the CT group, though overall length of hospital stay was no different (Table 1f). Procedural cost and radiation exposure data is being gathered.
Conclusions: Low risk SV patients undergoing pre-Glenn evaluation by CC or CT have similar diagnostic accuracy for major targets in SV, surgical morbidity and long-term outcomes, with a higher rate of procedural morbidity with CC compared to CT.

Paper #: 036

A MRI Cardiac Biomechanics Study of Segmental Strain Coupling in Single Ventricle Patients

Ramkumar Krishnamurthy, Ph.D., *Texas Children's Hospital, Houston, TX, rxkrish1@texaschildrens.org;* Cory Noel, MD, Jeffrey Jacot, Zili Chu, PhD, Rajesh Krishnamurthy

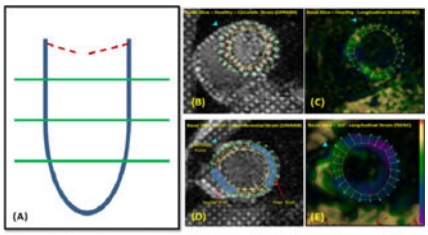

Figure 1: Schematic representation of SPAMM and fSENC images is presented in this figure. Three short axis slices at basal, mid-cavity and apical location of the ventricles is obtained (A). An external post-processing software is used to obtain the circumferential (B, D) and longitudinal (C, E) strain from the short axis slices. Representative images at mid-systole is shown for an asymptomatic volunteer (B, C) and a patient with a single left ventricular morphology (C, E). Strain is obtained along the cardiac cycle and analyzed.

Disclosures: All authors have disclosed no financial interests, arrangements or affiliations in the context of this activity.
Purpose or Case Report: Ventricular dysfunction in single ventricular (SV) patients after total cavopulmonary connection (TCPC) is the most important risk factor for morbidity and mortality, and cardiac MR biomechanics have thrown new light on predisposing factors for SV failure. In normal 2 ventricular hearts, there is favorable ventricular interdependence, while this has not been well studied in SV[1–3]. The purpose of this study is to understand changes in regional ventricular biomechanical indices in SV, when coupled or uncoupled to a dysfunctional ventricle.

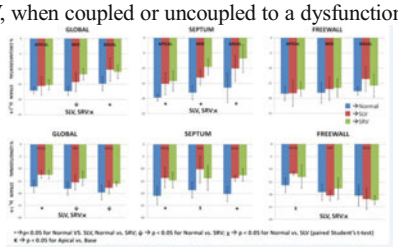

Figure 2: Bar plots showing th longitudinal (ε_{ll}) and circumferential (ε_{cc}) strain in a pediatric single ventricle population. We demonstrate a significant reduction in both ε_{cc} and ε_{ll}. The septum is the most affected with negligible differences observed in free wall. Also, there is a significant difference observed from apex to base globally for both single systemic ventricle patients, while the free wall ε_{ll} shows a significant increase.

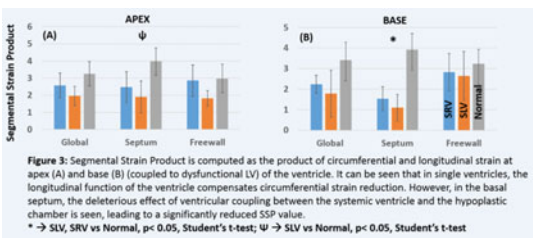

Figure 3: Segmental Strain Product is computed as the product of circumferential and longitudinal strain at apex (A) and base (B) (coupled to dysfunctional LV) of the ventricle. It can be seen that in single ventricles, the longitudinal function of the ventricle compensates circumferential strain reduction. However, in the basal septum, the deleterious effect of ventricular coupling between the systemic ventricle and the hypoplastic chamber is seen, leading to a significantly reduced SSP value.
* → SLV, SRV vs Normal, p< 0.05, Student's t-test; Ψ → SLV vs Normal, p< 0.05, Student's t-test

Methods & Materials: We performed a prospective, IRB approved study of 15 SV (8 SRV age: 11.4 +/- 2.3; 7 SLV age: 12.7 +/- 4.2 years) and 9 normal (age: 11.8 +/- 3) subjects. All SV were asymptomatic, and status post TCPC. Strain information was acquired at two short axis slices at basal (coupled to dysfunctional ventricle), and apical (uncoupled) locations in all 18 subjects in a 1.5T MRI scanner (Philips Acheiva) using: a) Complementary Spatial Modulation of Magnetization (CSPAMM)[4] images: ε_{cc}; and b) Fast-Strain Encoded (fSENC)[5] images: ε_L. Global, free-wall and septal ε_{cc} and ε_L were calculated using Diagnosoft™ at both locations. and a segmental strain product (SSP) was calculated as ($\varepsilon_{cc} * \varepsilon_L$ /100).

Results: Strain values of SLV and SRV subjects significantly different from normals.
Strain at the septal location is significantly reduced in SV patients.
Circumferential strain of the SV progressively decreased from apex to base, while the longitudinal strain increased.
SSP lower for SV compared to normal at apex and base
SSP is significantly reduced at the basal septum - pointing to deleterious effect of ventricular coupling between the systemic ventricle and the dysfunctional ventricle.
Septal SSP is significantly lower in SLV compared to SRV, while there is no difference in ε_{cc} or ε_L.

Conclusions: SV biomechanics is affected by deleterious ventricular coupling related to the hypoplastic chamber. SSP brings out difference between SLV and SRV, which is otherwise not apparent from global or regional strain analysis, and may serve as unique biomarker.

References
1. Fogel et al., Circulation 1998;98:330
2. Kaneko et al., JASE. November 2012, Vol 25, No. 11, 1222
3. Petko et al., Congenit Heart Dis. 2012;7:1
4. Noel et al., JCMR 2014, 16(Suppl 1):P111

Paper #: 037

Assessment of intracardiac morphology and proximal coronary arteries in infants: Comparison of 64 detector CT, lower dose target mode volumetric CT, higher dose target mode volumetric CT, and retrospective EKG gated CT

Keshav Srivaths, *Pediatric Radiology, Texas Childrens hospital, Houston, TX, lvsrivat@txch.org;* Prakash Masand, MD, Siddharth Jadhav, M.D., Farahnaz Golriz, M.D, Wei Zhang, Rajesh Krishnamurthy

Disclosures: All authors have disclosed no financial interests, arrangements or affiliations in the context of this activity.
Purpose or Case Report: Low dose CT angiography (CTA) is now performed in infants for evaluation of extra-cardiac vasculature. It is used for evaluating intracardiac and coronary morphology in neonates and infants, and retrospective EKG gating with higher radiation is used to evaluate small structures. The aim of this study is to compare CTA image quality using ungated 64 detector CT (64D), low dose target mode prospective EKG gated volumetric CT (LT), higher dose target mode prospective EKG gated volumetric CT (HT), and retrospective EKG gated volumetric CT (R) in infants for structures like ventricles, valvular structures, aortic root, and coronaries.

	Total	64	HT	LT	R	
Label	n	Mean±SD	Mean±SD	Mean±SD	Mean±SD	*P*
kVp	49	107±9.85	100±.	80±.	93.9±9.61	<.0001
mA	49	231±84.4	180±44.7	71.4±17.5	155±64.8	<.0001
mAs	49	113±40.7	63±15.7	28.6±6.99	64.3±32.2	<.0001
CTDI	48	15±5.04	12.8±7.05	1.61±0.35	16.8±8.27	<.0001
DLP	48	134±36.3	38.8±19.7	14.8±5.45	72.5±56.7	<.0001
mSv	48	5.25±1.3	1.48±0.74	0.57±0.22	2.75±2.15	<.0001
RCA grade	49	0.06±0.24	1.4±0.89	0.71±0.83	1.15±0.8	0.0004
LCA Grade	49	0.41±0.62	1.4±0.89	0.93±0.73	1.62±0.51	0.0004
LAD grade	49	0.35±0.49	1.4±0.55	0.71±0.83	1.46±0.66	0.0006
LCx grade	49	0.24±0.56	1±0.71	0.57±0.65	1.23±0.73	0.0018
Ao root grade	49	1.24±0.44	1.6±0.55	1.43±0.51	1.77±0.44	0.034
Ao valve grade	49	0.35±0.49	1.4±0.55	0.64±0.84	1.54±0.52	0.0002
Mitral valve	49	0.53±0.62	1.6±0.55	1±0.68	1.31±0.75	0.0072
LV grade	49	1.24±0.44	1.8±0.45	1.57±0.51	1.69±0.48	0.036

Methods & Materials: This IRB approved retrospective study in infants aged 0-1 year involved 17 patients scanned by 64D using a GE Lightspeed CT, 14 with LT, 5 with HT, and 13 with R. LT, HT and R were performed on a Toshiba 320 detector CT. Choice of technique for each patient was determined by indication. Visualization of imaging targets (left ventricle, mitral valve, aortic valve, proximal segments of the right (RCA), left main, left anterior descending (LAD) and circumflex (LCx) coronary arteries was graded on a 3-point scale (excellent 2, good 1, poor 0) customized by 2 observers blinded to the technique and clinical indication. Evaluation was restricted to the proximal coronaries. Average scores of image quality for each imaging target, and interobserver variability were calculated.
Results: There was excellent agreement between the two readers for all targets (average Kappa=0.81). There was no significant difference in image quality scores for structures between HT and R. The ungated 64D studies received the lowest scores for all structures, being lower than the other 3 techniques except ventricular assessment (LV). LT scores were superior to 64D for all structures except LV. LT fared worse than HT and R for all structures except aortic root and LV. Average effective radiation dose for

each technique were 5.25 +/- 1.3, 0.57 +/- 0.22, 1.48 +/- 0.74, and 2.75 +/- 2.15 for 64D, LT, HT, and R respectively (P<.001).
Conclusions: HT offers comparable image quality to R for evaluation of intracardiac structures and proximal coronaries in infants with less radiation. LT has the lowest radiation exposure of all techniques, and provides comparable image quality to HT or R for intracardiac morphology and aortic root, but fares poorly for valvular structures and coronaries. Target mode volumetric imaging improves image quality with less radiation in pediatric cardiovascular imaging.

Paper #: 038

Evaluation of Anomalous origin of the coronary artery from the pulmonary artery using three-dimensional steady state free precession sequence

Yumin Zhong, MD,PHD, *Diagnostic Imaging Center, Shanghai Children's Medical Center, Shanghai, China, zyumin2002@yahoo.com;* Aimin Sun, Wei Gao

Disclosures: All authors have disclosed no financial interests, arrangements or affiliations in the context of this activity.
Purpose or Case Report: Anomalous origin of the coronary artery from the pulmonary artery is a rare congenital anomaly. Anomalous origin of the left coronary artery from the pulmonary artery (ALCAPA) is most common and anomalous origin of the right coronary artery (ARCAPA) is extremely rare. ALCAPA or ARCAPA is associated with early infant mortality and sudden death in adults. Cardiac computed tomography (CT) and magnetic resonance imaging (MRI) has allowed noninvasive evaluation of the coronary anatomy by direct visualization of the origin of the left or right coronary artery from the pulmonary artery.
Purpose: To define diagnostic accuracy of three-dimensional steady state free precession sequence (3D-SSFP) to detect this anomaly.
Methods & Materials: Eighteen cases from January 1, 2007 to December 31, 2014 were retrospectively reviewed. In 18 patients, age ranged from 3.7 to 141 months; the median age was 6.9 months. A 3D-SSFP (3D Balanced turbo field echo (3D B-TFE) sequence with navigator respiratory compensation were performed on 18 patients to evaluate coronary artery anatomy and 2D-SSFP and late gadolinium enhancement (LGE)were performed on15 cases to evaluate the cardiac function and cardiac tissue characterization. Seventeen patients underwent surgery
Results: Fifteen cases were made correct diagnosis by 3D-BTFE, Left coronary artery arose from left posterior wall of main pulmonary artery in 14 cases and left coronary artery arose from right posterior wall in 1 cases. There were no positive results of LGE in 15 cases. Surgery results of 17 cases demonstrated that 16 cases were ALCAPA and one case was ARCAPA. The diagnostic accurate rate was 88%.
Conclusions: 3D-SSFP is a very useful MRI sequence for demonstrating ALCAPA or ARCAPA anomalies in congenital heart disease. MRI can supply helpful information for preoperative strategies.

Paper #: 039

Right congenital diaphragmatic hernias: is there a correlation between prenatal lung volume and postnatal survival, as in isolated left diaphragmatic hernias?

Teresa Victoria, MD PhD, *Children's Hospital of Philadelphia, Philadelphia, PA, victoria@email.chop.edu;* William Peranteau, Ann Johnson, Alan Flake, Beverly Coleman, N Adzick, Holly Hedrick

Disclosures: All authors have disclosed no financial interests, arrangements or affiliations in the context of this activity.

Purpose or Case Report: MRI lung volume ratio Observed versus Expected (O/E) is a strong prenatal indicator of postnatal survivor in the fetus with an isolated left congenital diaphragmatic hernia (L-CDH). We evaluated O/E and the ratio of the herniated intrathoracic liver in predicting outcome in the fetus with an isolated Right CDH (R-CDH).
Methods & Materials: Following IRB approval, we reviewed all fetal MR studies of isolated R-CDH from 2005 through 2014. Inclusion criteria: diagnostic MRI studies of fetuses with isolated R-CDH with available postnatal follow-up. Left lung volume (LV), right lung volume (RV), total lung volume (TLV) and observed/expected lung volume (O/E LV) based on gestational age (GA) were calculated. Chart review was used to determine survival and use of ECMO. Percentage of herniated liver (intrathoracic liver/total liver volume) was also plotted against survival and postnatal ECMO use.
Results: There were 31 fetuses referred for R-CDH during the time period of the study. Of these, 8 were excluded (3 had additional lung lesions, 3 with inadequate MR studies, 2 with no hernia). Of the 23 cases that met criteria, avg maternal age: 31 yo ±7.6; average GA at the time of MR imaging: 25 weeks±4.7; avg GA at delivery: 37±weeks 2.3. Findings in addition to herniated liver: intrathoracic bowel only (2/23); herniated gallbladder and bowel (21/23); pleural fluid at the apex of the right hemithorax (22/23). There were 15/23 survivors (65%), mortality of 35%. Mean O/E in survivors: 26±10; in non-survivors: 21±5. Percentage herniated liver in survivors: 35%±13; in non-survivors: 38%±9. ECMO use was 7/15 survivors (47%) and 2/8 of non-survivors (25%). Neither O/E MR lung volumes nor percentage of herniated intrathoracic liver showed correlation with survival or ECMO use (p>0.05).

FIGURE 1. Comparison survival of Left vs Right isolated CDH fetuses with respect to O/E MRI lung volumes. Data from L-CDH survival comes from a previously published manuscript [1].

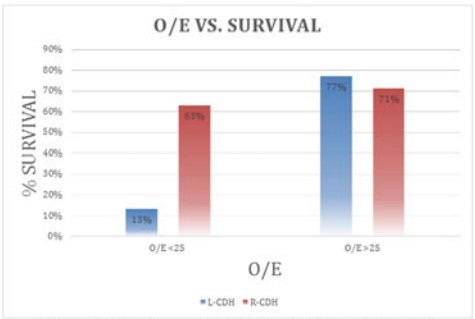

1. Victoria T, Bebbington MW, Danzer E, Flake AW, Johnson MP, Dinan D, Adzick NS, Hedrick HL (2012) Use of magnetic resonance imaging in prenatal prognosis of the fetus with isolated left congenital diaphragmatic hernia. Prenat Diagn 32:715-723.

Conclusions: Unlike L-CDH, MR O/E lung volume does not predict postnatal outcome with respect to survival or ECMO use. Caution must be exercised when counseling parents carrying a fetus with isolated R-CDH. In addition, treatment planning and possible fetal intervention may not be guided solely by the calculated O/E ratio.

Paper #: 040

Fetal lung volumes by MRI: Normal weekly values from 18 weeks through 28 weeks gestation.

Jacquelyn Garcia, D.O., *UT Health Science Center Houston, Houston, TX, jacquelyn.r.garcia@uth.tmc.edu;* Amy Mehollin-Ray, M.D., Kiara Blough, Wei Zhang, Mariana Meyers, MD, Christopher Cassady, MD

Disclosures: All authors have disclosed no financial interests, arrangements or affiliations in the context of this activity.

TFLV Analysis – MEANS Procedure	Comparison to Rypens Formula – T-Test						
GA (Weeks)	N	Mean (ml)	SD	Median	Rypens FLV (ml)	*P*-value*	95% CI
18	13	11.1	2.2	10.9	12.8	0.0165	-3.029 to -0.371
19	27	12.4	2.5	12.5	15	0.0001	-3.589 to -1.611
20	32	15.5	3.9	15.4	17.4	0.0097	-3.306 to -0.494
21	43	17.4	5.0	17.0	20	0.0005	-3.992 to -1.208
22	52	20.4	4.9	20.0	22.8	0.0009	-3.764 to -1.036
23	56	24.1	6.1	24.3	25.9	0.0314	-3.434 to -0.166
24	45	27.8	7.6	26.7	29.2	0.2231	-3.683 to 0.883
25	47	31.6	7.2	31.0	32.9	0.2221	-3.414 to 0.814
26	31	34.8	6.7	36.5	36.8	0.1069	-4.458 to 0.458
27	33	40.3	10.2	40.6	40.9	0.7376	-4.217 to 3.017
28	40	48.8	15.8	46.5	45.4	0.1813	-1.653 to 8.453

*Bolded values are statistically significant.

Purpose or Case Report: MRI is increasingly used for evaluation of both maternal and fetal structures, including volumetric organ analysis. Insufficient development of the lungs correlates with poor neonatal outcome. Since fetal MRI is frequently performed for conditions that may impair fetal lung growth, it is important to establish robust normal reference values for fetal lung volume (FLV). Although previous studies have reported normal FLV ranges (Rypens F et al. Radiology 2001;219:236–41), a larger patient population covering an earlier gestational age range is needed in order to establish more accurate normal FLV reference values particularly early in pregnancy when termination may be an option. Therefore the objective of this study is to establish normal FLV reference ranges from 18 to 28 weeks at 1-week intervals.

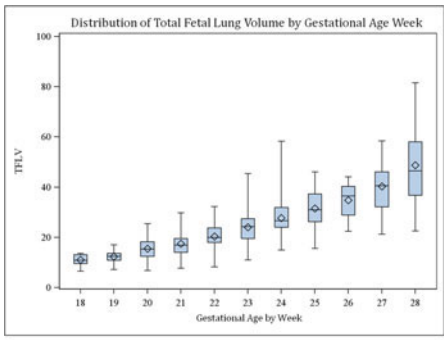

Figure 1. Distribution of total fetal lung volume (TFLV) by gestational age grouped by week. Each boxplot is composed of a diamond representing the mean; lower, middle and upper lines of each box representing the 25th, 50th and 75th percentiles, respectively; and lower and upper bars representing the 5th and 95th percentiles, respectively. Mean total fetal lung volume showed an increase at each gestational age week interval.

Methods & Materials: After IRB approval, patients were retrospectively identified from a database of fetal MR exams performed at two tertiary fetal centers. Exclusion criteria included: exams with technical limitations (pitch greater than 1, fetal motion); fetal diagnoses that may impair fetal lung growth (lung malformation, congenital diaphragmatic hernia, omphalocele, skeletal dysplasia); oligo- or anhydramnios; intrauterine growth restriction; and patients with a discrepancy between established delivery date and US dating. Fetal lung volumes were measured in at least 2 planes either manually or using a separate workstation, with the values averaged, in fetuses from 18 to 28 weeks gestation.
Results: 419 patients were included. The data was analyzed using the MEANS procedure provided by SAS. The normal total FLV (TFLV) increased throughout gestational age, with a weekly increase in mean TFLV from 18 weeks through 28 weeks gestation (Figure 1). There was also a gradual increase in the range of normal TFLV each week, creating a broader range of normal TFLV with advancing gestational age. Means were then compared to expected TFLV as generated by the formula proposed by Rypens et al. using a one-sample *t*-test, which showed that mean TFLV from 18 weeks to 23 weeks was significantly lower than those predicted by formula (Table 1), while mean TFLV from 24 weeks to 28 weeks was not statistically different.
Conclusions: This study provides weekly reference ranges for normal FLV beginning at 18 weeks. We propose that between 18 weeks and 23 weeks, these values could be used in place of FLV generated by the Rypens et al. formula. FLV remains an important fetal MRI measurement frequently used in prenatal counseling and delivery planning.

Paper #: 041

The added value of MRI for the diagnosis of fetal neurological injury in survivors of monochorionic co-twin demise

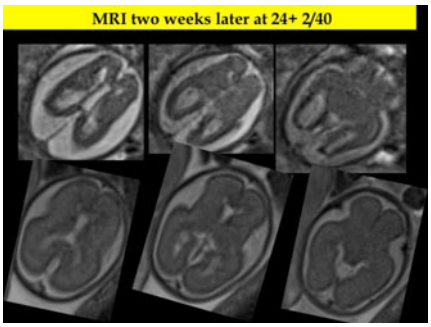

Stacy Goergen, MD, *Monash University, Departments of Surgery and Medical Imaging, Southern Clinical School, Clayton, VIC, Australia, Stacy.Goergen@gmail.com;* Mark Teoh, Alice Robinson, Andrew Edwards

Disclosures: All authors have disclosed no financial interests, arrangements or affiliations in the context of this activity.
Purpose or Case Report: Monochorionic diamniotic (MCDA) twin pregnancies complicated by demise of one of the twins are known to be associated with increased risk of adverse neurodevelopmental outcome in the survivor. We aimed to determine the additional diagnostic benefit of obstetric MRI (OMRI) following tertiary ultrasound (TUS), in the diagnosis of cerebral abnormalities in monochorionic diamniotic (MCDA) twin pregnancies affected by co-twin demise (CD).

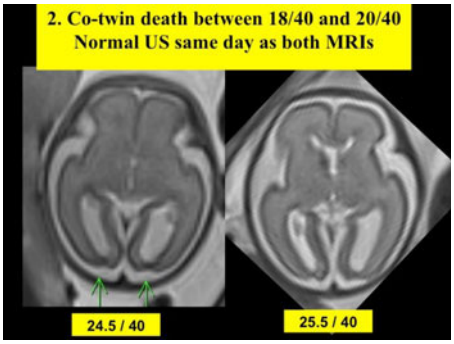

Methods & Materials: All women with MCDA twin pregnancies complicated by co-twin demise who were referred to us for OMRI after tertiary ultrasound performed at our institution between January 2007 and September 2014 were candidates for inclusion in this study. All patients had tertiary ultrasound evaluation of the surviving fetus prior to OMRI. OMRI was performed on a Siemens Avanto 1.5T scanner using an 8 channel torso and 8 channel spine array coils. The fetal head was evaluated using multiplanar T2 TSE, T1, True FISP, diffusion, and gradient echo sequences.

Results: OMRI was performed in 16 women with MCDA twin pregnancies complicated by CD. In 6, CD followed SFLP and in 10, CD was spontaneous and unassociated with documented TTTS. OMRI was performed at 21-32/40 (median=25/40). In the 6 cases of treated TTTS, 3 fetuses had brain abnormalities on OMRI not detected on TUS (dural sinus thrombosis, reduced cerebellar diameter and germinolytic cysts). In 10 pregnancies affected by SCD, 5 of 10 surviving fetuses had normal TUS and OMRI. Of the other 5, 1 had intraventricular haemorrhage diagnosed by OMRI but not ultrasound, 3 had severe hemispheric ischaemic injuries undiagnosed or incompletely characterized by TUS, and 1 had a morphologically normal cerebellum, but with cerebellar biometry below the 5th centile not detected by TUS.
Conclusions: Obstetric MRI added clinically relevant diagnostic information not provided by US in 50% of MCDA fetuses surviving demise of a co-twin. MRI should be routine in this situation to assist with counseling regarding neurodevelopmental prognosis for the survivor.

Paper #: 042

Correlation with MR findings in Neonates with Hypoxic Ischaemic Encephalopathy Undergoing Cerebral Hypothermia and Subsequent Neurolodevelopmental Outcomes

Kenneth Cheung, MBBS, *Department of Radiology, Queen Mary Hospital, Hong Kong, Hong Kong, knnth.c@gmail.com;* Janice IP, Lee-yuen Ko, Martin Law, Wendy Lam

Disclosures: All authors have disclosed no financial interests, arrangements or affiliations in the context of this activity.

Purpose or Case Report: Hypoxic ischaemic encephalopathy (HIE) arising from perinatal insult remains an important disease burden with potential profound morbidity and mortality. Cerebral hypothermia is increasingly utilised as a treatment option. Magnetic resonance (MR) imaging has been proven to be the gold standard in detection of subtle abnormalities from hypoxic injury. Our hospital is a local tertiary neonatal unit with a predominantly Asian population. This study demonstrates local experience in key MR findings of neonates undergoing cerebral hypothermia for HIE, and their potential values for predicting subsequent neurodevelopmental outcomes.
Methods & Materials: Cohort study was performed on 15 cases of neonates with documented HIE undergoing cerebral hypothermia. MRI brain was performed for quantification of degree and extent of hypoxic damage. Grading of MR signal intensity changes of key regions of the neonatal brain was reviewed by a paediatric radiologist and a paediatric neurologist. Subsequent long term follow-up by paediatric neurologists was made for monitoring of developmental progress.
Results: Posterior limb of internal capsule (PLIC) abnormalities are shown to be associated with poor overall outcomes (p=0.02) and fine motor outcomes (p=0.011). Combined PLIC abnormalities and moderate to severe basal ganglia and thalami (BGT) abnormalities are associated with poor outcomes (p=0.03), with patients developing spastic quadriplegia and gross motor delay with dystonic posturing. Association with overall adverse outcome was of borderline clinical significance (p=0.06). Abnormalities of central, interhemispheric fissures or of the white matter abnormalities are not specific in prediction of subsequent neurological outcomes.
Conclusions: MR findings in neonates undergoing cerebral hypothermia for HIE is an important tool for prediction of neurodevelopmental outcomes. Cerebral hypothermia therapy does not alter the predictive value of brain signal abnormalities with subsequent neurodevelopmental outcomes. PLIC abnormalities are predictive of poor overall and fine motor outcomes. Combined PLIC and BGT abnormalities are also associated with poor outcomes. Further studies are warranted for elucidation of correlation of cortical and white matter abnormalities and long term neurodevelopmental outcomes.

Paper #: 043

Do all prenatally diagnosed bronchopulmonary malformations get smaller? Evaluation on serial fetal MRI and postnatal imaging

Thomas Cullen, *Stanford University, Palo Alto, CA, cullen.tom@gmail.com;* Katherine Wong, Richard Barth, Diego Jaramillo, MD, MPH, Erika Rubesova, MD

Disclosures: All authors have disclosed no financial interests, arrangements or affiliations in the context of this activity.
Purpose or Case Report: Bronchopulmonary malformations (BPM) are diagnosed with increasing frequency prenatally. Although management is variable, they have usually good prognosis. They are believed to decrease in size during pregnancy based on rare ultrasound studies and case reports. BPM tend to be isoechogenic to the lung in the 3rd trimester and therefore difficult to evaluate. The purpose of this study was to measure lesion size on early and late fetal MRI and postnatal imaging to evaluate their growth pattern.
Methods & Materials: IRB approved, retrospective analysis was performed between 2009 and 2015 to evaluate all patients who underwent fetal MRI and ultrasound examinations in early (22-31 weeks gestational age (GA)) and late third trimester (31-37 weeks GA) at our institution for lung mass. 42 patients met criteria for this study. 33 patients underwent follow-up imaging within the first 5 months of life, 29 of whom underwent surgical excision. Excised lesions were categorized by dominant pathologic appearance. In non-surgical patients (13) radiologic diagnosis was determined by review of the postnatal CTA or 3rd trim. MRI by three experienced radiologists, blinded to the initial interpretation.

Volumes of the lesions were calculated using maximum dimensions in three planes. Ultrasounds performed the same day as the late 3rd trim. MRI were reviewed to determine the visibility of the BPM. Z-test was used to compare proportions of growth patterns.

Table 1: Percentage of BPM subtypes which increased in size, comparing volumes in early to late prenatal (above) and late prenatal to postnatal periods (below)..

Early vs. Late Prenatal Imaging			
	Total	Increased	%
Type 1 CPAM	9	2	22.22
Type 2 CPAM	6	3	50
Sequestration	13	5	38.46
Hybrid lesion	5	1	20
CLO	7	2	28.57
Bonchogenic cyst	2	1	50
	42	14	33.33
Late vs Postnatal Imaging			
	Total	Increased	%
Type 1 CPAM	7	5	71
Type 2 CPAM	3	3	100
Sequestration	8	5	62.5
Hybrid lesion	5	4	80
CLO	4	4	100
Bonchogenic cyst	2	2	100
	29	23	79.31

Results: 19 of the 42 BPMs (45%) were not visualized on late third trimester ultrasounds. All the lesions were seen on late 3rd trimester MRI. From early to late fetal MRI, BPM increased in size as follows: 22% type 1 CPAM (9), 50% type 2 CPAM (6), 38% sequestrations (SQ) (13), 20% hybrid lesions (5), 28% lobar overinflations (CLO)(7), 50% of bronchogenic cysts (BC). From late to postnatal imaging lesions increased as follows: 71% type 1 CPAM, 100% type 2 CPAM, 63% SQ, 80% hybrid lesions, 100% of CLO and BC. In total, 33% of lesions increased from early to late fetal MRI ($p<0.01$) and 79% increased late fetal MRI to postnatal imaging ($p<0.01$).

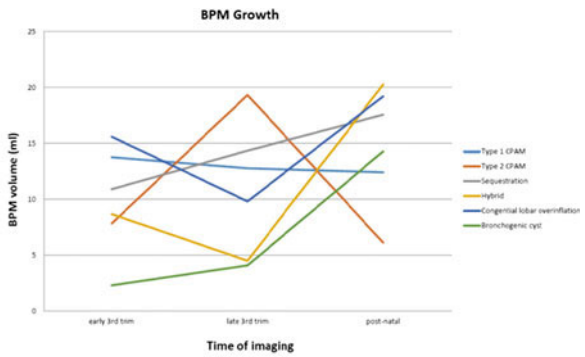

Figure 1: BPM volume growth patterns by subtype on prenatal and postnatal imaging.

Conclusions: Bronchopulmonary malformations present a prognostic challenge. MRI can assess BPM, which are difficult to visualize on third trimester ultrasound. Some BPM grow prenatally and/or postnatally. It is important to recognize the growth pattern of the subtypes of BPM to help identifying any atypical prenatal lesions such as rare fetal malignant lung masses and to improve parental counseling.

Paper #: 044

Neonatal congenital lung tumors: the importance of prenatal imaging as a diagnostic clue

Stephan Waelti, *Radiology, CHU Sainte-Justine, Montreal, QC, Canada, stephan.l.waelti@bluewin.ch;* Laurent Garel, Dorothée Dal Soglio, Françoise Rypens, Chantale Lapierre, Josée Dubois, MD

Disclosures: All authors have disclosed no financial interests, arrangements or affiliations in the context of this activity.

Purpose or Case Report: Primary lung masses in neonates are mainly linked to various developmental abnormalities. Congenital lung tumors are much rarer, such as the cystic pleuro-pulmonary blastoma, the fetal lung interstitial tumor, the congenital peribronchial myofibroblastic tumor and the congenital fibrosarcoma.

The differentiation between bronchopulmonary malformations and lung tumors is often challenging postnatally because of the lack of specific imaging features.

Objectives:

To establish distinctive diagnostic features between bronchopulmonary malformations and congenital lung tumors and, accordingly, to contribute to the management of congenital lung lesions in newborns and infants.

Methods & Materials: The congenital lung lesions seen pre and postnatally over 10 years in our mother-child institution were retrospectively reviewed.

The following parameters were recorded: imaging features in the fetus and at birth, time of detection of abnormalities in utero (mid 2nd trimester, 3rd trimester, not visible prenatally), clinical symptoms at birth, treatment, pathology and follow-up.

Results: Among the 135 congenital lung lesions, there were 4 congenital lung tumors (3% of overall cases), 2 pleuro-pulmonary blastomas and 2 fetal lung interstitial tumors.

Contrary to the developmental pulmonary abnormalities, where the lesions were conspicuous on mid 2nd trimester ultrasound, there was no visible lung lesion on the 20-22 WGA ultrasound in the 4 cases of pulmonary tumors.

The 2 pleuro-pulmonary blastomas were cystic, the 2 fetal lung interstitial tumors solid, both on prenatal and neonatal imaging.

Conclusions: The timing of conspicuity in utero is a key differential diagnostic feature between bronchopulmonary malformations, pleuro-pulmonary blastomas and fetal lung interstitial tumors. In our material of congenital lung lesions, neonatal lung lesions that were not present on mid 2nd trimester ultrasound proved to be tumors.

At birth, a cystic lung lesion in the context of a normal 22 WGA ultrasound is diagnostic of pleuro-pulmonary blastoma.

Conversely, a solid neonatal lung lesion associated with a normal mid 2nd trimester ultrasound makes fetal lung interstitial tumor the most likely diagnosis.

According to the few reported cases of fetal peribronchial myofibroblastic tumor, a solid pulmonary lesion already depicted in the 2nd trimester that continues to grow in the 3rd trimester could also correspond to a congenital peribronchial myofibroblastic tumor, especially if associated with early hydrops fetalis.

Paper #: 045

Large Multicenter Study of the Association between Testicular Microlithiasis and Testicular Neoplasia in a Pediatric Population

Andrew Trout, *Radiology, Cincinnati Children's Hospital Medical Center, Cincinnati, OH, andrew.trout@cchmc.org;* Jeanne Chow, MD, Erin McNamara, Kassa Darge, MD, PhD, Raul Ramirez, Martha Munden, MD, Sarah Rothan, Oscar Navarro, Marta Tijerin Bueno, Kevin Bove, Kudakwashe Chikwava, Amer Heider, John Hicks, Gino Somers, Bin Zhang, Jonathan Dillman, M.D., M.Sc.

Disclosures: Andrew Trout has indicated a relationship with Philips Healthcare, Advisory Board. Johnathan Dillman has indicated a relationship with Siemens Medical Solutions USA as a Primary Investigator. All other authors have disclosed no financial interests, arrangements or affiliations in the context of this activity.
Purpose or Case Report: To retrospectively define in a large pediatric population the association between testicular microlithiasis and testicular neoplasia.
Methods & Materials: Retrospective multicenter study of scrotal ultrasounds performed between January 2000 and April 2014 in subjects <18 years of age. All unique subject scrotal ultrasound reports from each institution were reviewed for mention of microlithiasis. For subjects with serial exams, the most recent exam performed was included in the analysis. All exams mentioning microlithiasis were reviewed by site-specific investigators to confirm the presence of ≥5 punctate calcifications in the testicle on a single image. The presence of testicular germ cell and stromal tumors were determined for subjects with and without microlithiasis through review of institutional pathology and imaging databases. The risk of testicular neoplasia in the context of microlithiasis was expressed in terms of odds ratios with (A-OR) and without adjustment (U-OR) for fixed study site (institution) effects by logistic regression.
Results: The study population included 37,863 unique subjects with confirmed microlithiasis in 1,097 (2.9%). Mean subject age was 11.1±4.7 years for subjects with microlithiasis and 9.1 ±5.9 years for subjects without (p<0.0001). 139 subjects (0.37%) had germ cell tumors (86 malignant, 63 benign) and 34 subjects (0.09%) had stromal tumors. Malignant germ cell tumors were present in 2.8% of subjects with microlithiasis and 0.12% without for an A-OR of 22.37 (95%CI: 13.35-37.49) and an U-OR=17.26 (95%CI: 11.8-25.25), p<0.0001. Benign germ cell tumors were present in 1.4% of subjects with microlithiasis and 0.13% without for an A-OR of 10.97 (95%CI: 5.74-20.99) and an U-OR=10.61 (95%CI: 5.7-19.72), p<0.0001. Stromal tumors were observed in 0.46% of subjects with microlithiasis and 0.079% without for an A-OR=6.39 (95%CI: 2.21-18.44) and an U-OR of 5.8 (95%CI: 2.1-16), p<0.01.
Conclusions: This large, multicenter study confirms that there is a significant, strong association between testicular microlithiasis and testicular neoplasia, particularly malignant germ cell tumors. Children with microlithiasis have approximately 22X greater odds of having a malignant germ cell tumor than children without microlithiasis. This reinforces the need for a large prospective study assessing the risk of developing testicular neoplasia in children with incidentally identified diffuse microlithiasis.

Paper #: 046

Reliability of the New Urinary Tract Dilation (UTD) Classification System for the Evaluation Of Postnatal Urinary Tract Dilation

Naomi Strubel, MD, *Radiology, New York University School of Medicine, New York, NY, naomi.strubel@nyumc.org;* Shailee Lala, Lynne Pinkney, James Babb, Nancy Fefferman, MD

Disclosures: All authors have disclosed no financial interests, arrangements or affiliations in the context of this activity.
Purpose or Case Report: To evaluate the reliability of the UTD classification system

Table A. Cross-tabulation of results summarizing inter-reader agreement. There are three distinct reader pairs: score 1 is the score from the arbitrarily designated first reader in each pair and score 2 is from the remaining reader in each pair. Numbers in red denote instances of disagreement.

Score 1	Score 2			
0	1	2	3	
0	66	26	9	5
1	27	49	20	4
2	10	22	51	19
33	3	3	22	51

Methods & Materials: This IRB approved, retrospective study included 129 renal ultrasound examinations performed from May 2010 - May 2015 in patients less than 6 months of age for the clinical indication of prenatal hydronephrosis identified by key word search in PACS. Three pediatric radiologists independently reviewed each study for the following: anterior posterior renal pelvic diameter (APRPD), central calyceal dilation (CCD), peripheral calyceal dilation (PPD), renal parenchymal appearance (PA), renal parenchymal thickness (PT), ureteral abnormality, and bladder abnormality. Readers assigned each study a UTD category (normal, UTD P1, UTD P2, UTD P3). Inter-rater percent agreement for individual criteria and overall UTD categorization was assessed.
Results: There was overall good inter-reader agreement in assessment of individual criteria (APRPKD, PA, PT, ureter, and bladder) ranging from 85.3 to 96.1% for 3 reader pairs. Inter-reader agreement for CCD and PCD was slightly lower, ranging from 69.0 to 97.7%. Inter-reader agreement for overall risk assesment ranged from 50.4 to 67.4%. Agreement across 3 readers was 48.8% for CCD, 64.3% for PCD, and 37.2% for overall risk stratification.
Conclusions: The new UTD classification system is intended to guide clinical management of postnatal urinary tract dilation. For it to be widely accepted and useful, users need to apply it with precision and accuracy. Poor agreement for categorization of risk assessment among our experienced readers suggests that further clarification of the system or training for users is necessary for its optimal use in clinical practice.

Paper #: 047

Arfi Evaluation of the Kidneys In Ex Premature Infants: Preliminary Results

Costanza Bruno, *radiplogy, policlinico gb rossi, Verona, Italy, costanza_bruno@libero.it;* Salvatore Minniti

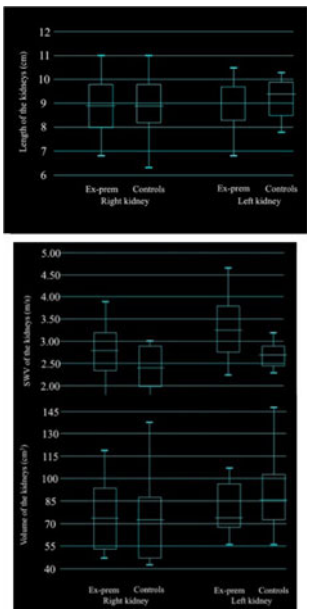

Disclosures: All authors have disclosed no financial interests, arrangements or affiliations in the context of this activity.
Purpose or Case Report: To establish whether, in the school-aged children, any relationship exists between prematurity and US and ARFI findings
Methods & Materials: 20 patients born preterm (gestational age: 28.5+/-3.3 W; age range: 8+/-1.1 ys) were compared with 20 healthy controls.
Length and volume were measured for each kidneys.
A mean SWV was calculated for each kidney from nine measurements obtained at the upper, middle and lower third
An overall SWV for the two kidneys was also calculated. The statistical significance of the difference found between the two groups was evaluated by means of the Mann–Whitney test.
Results: Non statistically significant difference was found between the two groups when considering the length of the two kidneys and the volume as well. The mean SWV of the two kidneys of ex premature infants was statistically higher than the mean SWV of healthy controls (3.02+/-0.60 m/s vs. 2.56+/-0.37 m/s; $p<0.01$); the difference existing between the SWV of left kidneys between the two groups was statistically significant too (3.30+/-0.66 m/s vs. 2.73+/-0.27 m/s; $p<0.01$). No statistical significant difference was found between the SWV of the right kidneys of the two groups (2.70+/-0.65 m/s vs. 2.40+/-0.51).
Conclusions: Prematurity is associated to a statistically significant difference in the overall SWV of the two kidneys probably reflecting an early damage due to the reduced number of nephrons present at birthz.

Paper #: 048

The Reliability And Accuracy Of Diffusion Tensor Imaging And Tractography In Kidneys: Is It A New Predictible Tool To Understand The Microstructurel Changes In Renal Impairment At The Pediatric Age Group?

Mehmet Ozkan, **Fellow**, *Dr. Sami Ulus Research and Training Hospital, Ankara, Turkey, bozkan04@gmail.com;* Robert Marterer, Sebastian Tschauner, Utku Yildirim

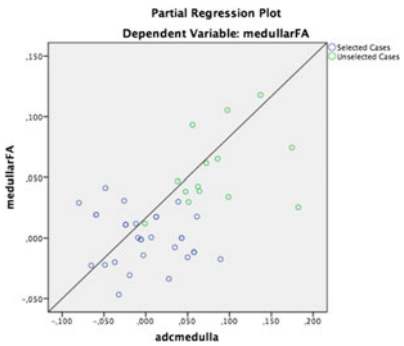

Disclosures: All authors have disclosed no financial interests, arrangements or affiliations in the context of this activity.
Purpose or Case Report: **Background:** Diffusion tensor imaging (DTI) provides information about the microstructure of renal tissue and is becoming increasingly useful in the evaluation of relationship between renal structure and function.

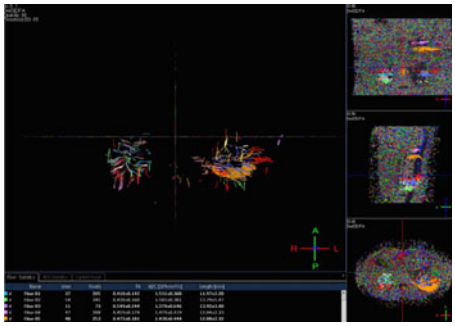

Objectives : To investigate whether DTI allows assessment of renal impairment and pathology in patients with decreased renal functions at the pediatric age group.
Methods & Materials: This study was approved by the institutional ethical review committee, and written informed consent was obtained. Thirty-two patients and 15 healthy children were enrolled in this study. For DTI, a respiratory- triggered coronal EPI sequence was performed (TR, 1400 ms; TE, 76 ms; diffusion direction, 6; NEX, 4; b values, 0 and 600 s/mm2; slices thickness, 6 mm, with no intersection gap). Regions of interest were placed in the medulla and cortex to measure DTI parameters of microstructure. Cortical and medullary mean, axial and radial diffusivity, fractional anisotropy (FA) were analysed. Siemens 1.5T machine were used and Trackvis program to evaluate the fiber tracking.
Results: In healthy subjects group, the cortical FA values were lower than the medullary FA values. ADC cortex showed positive correlation with the ADC medulla values (p=0,041, r=0,499) and negative correlation with the FA cortex values (p=0,028, r=-0,533) (Figure 1). The eGFR values were negatively correlated with the adc medulla values (p=0,049, r=-0,484) in the healthy subjects and positively correlated with the λ1 medulla values (p=0,027, r=0,385). Additionally in the patient group, the age was positively correlated with FA cortex values (p=0,018,r=0,411) and adc medulla values (p=0,007, r=0,461). However, the medullar FA values were negatively correlated with the medullar ADC values (p=0,038, r=-0,363). Tractography of healthy volunteers showed a radial arrangement which converges into the pyramids where as the renal insufficiency patients had irregular patterns of arrangements and architectural distortion in the observed ones (Figure-2a, b).

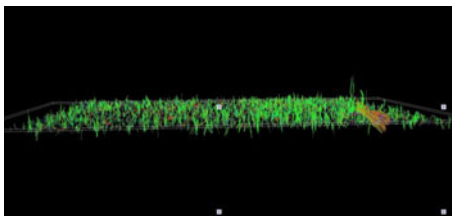

Conclusions: Renal DTI is a promising diagnostic tool in the assessment of microstricturel changes within the correlation of eGFR. Therefore it gives an estimation of arrangement of tracts extending from the renal medulla and diffusion of water molecules. This study enlights the usage of DTI in renal pediatric kidneys but in needs of validation at larger cohort groups within the histopatologic biopsies.

Paper #: 049

Functional Magnetic Resonance Urography: Adjunct Non-Contrast Angiography Increases Diagnostic Confidence in Assessment of Crossing Vessels in Pelvico-ureteric Junction Obstruction

Arlen Urquia, *Evelina London Children's Hospital, London, United Kingdom, urquia.arlen@gmail.com;* James Carmichael

Disclosures: All authors have disclosed no financial interests, arrangements or affiliations in the context of this activity.

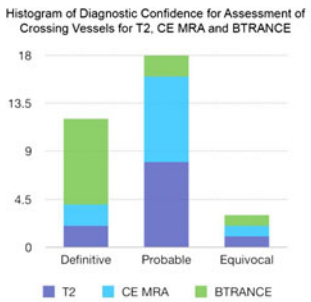

Purpose or Case Report: To evaluate diagnostic confidence in detection of crossing vessels by Functional Magnetic Resonance Urography (fMRU), in children with pelvico-ureteric junction obstruction (PUJO) by comparison of three sequences. At our institution, our protocol supplements the standard fMRU technique of a rapid 3d gradient echo sequence (e-THRIVE, Phillips) with:
1) 3d T2 weighted TSE (VISTA, Phillips).
2) ECG gated and respiratory compensated flow-in labelled balanced steady state free precession (bSSFP) (b-TRANCE, Phillips).

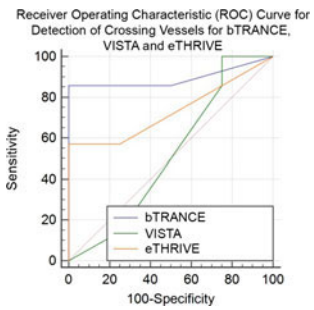

The standard fMRU 3d gradient echo sequence used for functional assessment has limited spatial and contrast resolution due to the demanding requirement for high temporal resolution. Our additional non-contrast b-TRANCE technique aims to provide improved angiographic data.
We compared the diagnostic accuracy of the three sequences against crossing vessel presence at pyeloplasty.
Methods & Materials: A retrospective analysis of 11 patients (total 33 sequences) with known PUJO who underwent fMRU prior to pyeloplasty. The presence of crossing vessel was recorded at time of pyeloplasty.
Data from the angiographic phase of eTHRIVE, VISTA and b-TRANCE sequences were anonymised. The 33 sequences were randomised and evaluated for a crossing vessel with a 5 point scale of diagnostic confidence:
1. Definitely present, 2. Probably present, 3. Equivocal, 4. Probably not present, 5. Definitely not present.
We assessed the sensitivity, specificity, negative predictive value and ROC curves for each sequence to compare diagnostic performance. A Mann–Whitney test was used to compare the diagnostic confidence of each sequence.
Results: The b-TRANCE correctly identified crossing vessels in 6 cases (86% sensitivity, 75% specificity, negative predictive value 75%), VISTA in 6 cases (86% sensitivity, 25% specificity, negative predictive value 50%), and eTHRIVE in 4 cases (57% sensitivity, 75% specificity, negative predictive value 50%).
As expected for sample size, differences in area under ROC curves between sequences did not reach significance, however a clear trend of improved diagnostic performance was observed for the b-TRANCE sequence.
The b-TRANCE sequence gave significantly improved diagnostic confidence compared to eTHRIVE, p=0.03. The mean acquisition time of b-TRANCE was 4.2 mins.
Conclusions: Detection of crossing vessels in PUJO can be improved by the addition of non-contrast angiographic b-TRANCE, with an acceptable time cost.

Paper #: 050

Simultaneous Renal Parenchyma Classification and Time-Intensity Curve Estimation for Dynamic MR Urography

Andy Tsai, **MD**, **PhD**, *Radiology, Boston Children's Hospital, Boston, MA;* Frederick Grant, Jeanne Chow

Disclosures: All authors have disclosed no financial interests, arrangements or affiliations in the context of this activity.
Purpose or Case Report: To introduce an expectation-maximization (EM) algorithmic framework for partitioning the kidney into its various subparts while simultaneously estimating the time-intensity curves associated with each of these subparts for computer assisted evaluation, analysis, and quantification of dynamic MR urography (MRU) data.
Methods & Materials: Analysis was performed on dynamic excretory component of MRU, employing the enhancement and excretory phases of intravenous gadolinium in conjunction with T1-weighted images. The image processing problem of simultaneous tissue segmentation and time-intensity curve estimation was formulated by viewing it as an incomplete-data problem. Specifically, the acquired MRU data were viewed as the incomplete data, the segmentation class labels were judiciously introduced as the hidden data, and the time-intensity curves served as the quantities to be estimated. Posing this problem in this fashion with probabilistic modeling of the observed data and the class labels, the E-step iteratively computed the class labels while the M-step utilized a maximal likelihood estimator to iteratively calculate the various time-intensity curves.
Results: Experiments on patients who underwent MRU demonstrated that this algorithm was fast and effective in accurately accomplishing the two tasks of renal parenchyma segmentation and time-intensity curve estimation. The algorithm was able to accurately label the kidney into its various subparts (renal cortex, renal medulla, and renal pelvis). The estimated time-intensity curves accurately reflected the transit of contrast through the various subparts of the kidneys.
Conclusions: Feasibility of using a computer algorithm to automatically segment the kidney while providing information about the cortical, medullary, and excretory phases within each subpart of the kidney was demonstrated. The segmentation results may be useful in objectively

assessing the anatomic/structural integrity of the kidneys, while the time-intensity curves may play an important role in quantifying the functionality of the kidneys.

Paper #: 051

Relationship between Bladder Volume and Functional Results of MR Urography in Children

Jorge Delgado, *Radiology, Children's Hospital of Philadelphia, Philadelphia, PA, delgadoj@email.chop.edu;* Maria Bedoya, Dmitry Khrichenko, Robert Carson, Ann Johnson, Kassa Darge, MD, PhD

Disclosures: All authors have disclosed no financial interests, arrangements or affiliations in the context of this activity.
Purpose or Case Report: In many centers, for functional MR urography (fMRU) in children a bladder catheter is placed. This is more stringent in those that will be sedated deeply, those with megaureters or high-grade vesicoureteral reflux. The reason for trying to drain the bladder during the post-contrast dynamic series is to avoid potential reduction or delay in the contrast washout similar to nuclear medicine studies. The purpose of this study was to assess during fMRU if the bladder was being drained and, if not, the effect of distention on the contrast transit times.
Methods & Materials: A retrospective review of our fMRU database was performed. Inclusion criteria were the presence of a bladder catheter, the absence of duplex kidney or ectopic ureteral insertion, and the availability of the calyceal (CTT) and renal (RTT) transit times of the right and/or left kidneys. The size of the Foley catheter had been selected according to age. The bladder filling was qualitatively evaluated during the post-contrast dynamic series. This was defined subjectively as empty (no or minimal fluid within the bladder), partially full (bladder without distention and non-round shaped) or full (bladder distended and round shaped). The urinary tract pathology (ureteropelvic or ureterovesical junction obstruction), ureteropelvic angle, pelvicalyceal dilation (PCD) grade, corticomedullary differentiation (CMD) and cortical thinning were recorded.

Table 1. Baseline characteristics and differences in the transit times between different degrees of bladder filling.

	Empty bladder (32 PUU)	Partially full bladder (68 PUU)	Full bladder (61 PUU)	p-value
Gender (M/F)	11/21	32/36	33/28	0.19
Mean age	9.65	6.18	7.32	0.04*
Urinary tract pathology **	26/6	51/17	52/9	0.35
Median uretropelvic angle (IQR)	26 (16)	29 (19)	26 (13)	0.77
CMD (normal/ decreased)***	31/1	59/9	58/3	0.12
Cortical thinning (yes/no)	4/28	15/53	9/52	0.40
Median CTT in seconds (IQR)	139 (39.50)	130 (40.00)	139 (39.00)	0.98
Median RTT in seconds (IQR)	170 (74.75)	184 (103.75)	170 (108.50)	0.73

*=significant; ** Ureteropelvic or ureterovesial junction obstruction; *** CMD=corticomedullary differentiation

Results: Inclusion criteria were met by 94 children, 46 boys and 48 girls with a mean age of 6.85 years (range: 0.09 - 17.59 years) with 161 pelviureteral units (PUU) (78 right PUU, 83 left PUU). The bladder was empty in 32 PUU. However, despite the presence of a bladder catheter in 68 and 61 PUUs i.e. 80%, the bladder was partially full or full, respectively. No differences in the bladder filling between gender, pelviureteric angle, pelvicalyceal dilation, CMD and cortical thinning were found (p>0.12) (Table 1). A difference in the bladder filling between the ages was found. No differences in the bladder filling and the CTT and RTT were detected even taking the PCD grade into consideration (p>0.73) (Table 1).
Conclusions: Bladder drainage during fMRU was inadequate. The degree of bladder filling did not appear to influence the transit times. This raises the question if the use of bladder catheter is justified or not? Actual bladder volume measurements with correlation to maximum bladder capacity may need to be carried out to further evaluate the relationship of bladder distention and transit times.

Paper #: 052

Obstruction, Flow, and Function as Relating to Functional Renal Imaging

André Eichenberger, MD BSEE, *Children's University Hospital Zürich, Zürich, Switzerland, aceichenberger@gmail.com*

Disclosures: All authors have disclosed no financial interests, arrangements or affiliations in the context of this activity.
Purpose or Case Report: A theory is developed that describes the mechanism by which functional renal imaging (FRI) assigns a property called "function" to an obstructed kidney. The theory elucidates the association between obstruction, flow, and function.
Background: There are three common beliefs held about FRI: 1) obstruction reduces flow; 2) flow is an appropriate measure of renal function; and 3) renal function measured by FRI positively correlates with flow. According to the Patlak method, tracer amount is estimated by integration over time of the product of flow and tracer density. Curiously, FRI measures neither tracer density nor flow within tubular structures. The disparity between the theoretical Patlak method and applied FRI results in an ambiguous assessment of flow and renal function.
Methods & Materials: The kidney is modeled as an autoregulated and partially collapsed elastic tubular structure equivalent to a Starling resistor. FRI is modeled semi-quantitatively to illustrate the dependency of function on both renal volume and flow. Additionally, obstruction is equated to ureteral resistance. The theory predicts that during steady state excretion function is a measure only of volume. Moreover, during transient hyperexcretion, function is a measure of volume as well as a measure of variable flow.
Results: During steady state conditions, no correlation is found between obstruction and flow, as well as no correlation between function and flow. During increasing pelvic pressure, flow is greater in an obstructed than in a non-obstructed kidney. The arbitrary measurement of function is the result of indeterminate flow and ureteral resistance. A re-interpretation of data acquired by both MR Urography and scintigraphy verifies that, on average, ureteral resistance uniquely determines function.
Conclusions: Function is a measure only of obstruction. Neither flow nor function evaluates the true performance of an autoregulated kidney. Functional imaging is based on misconceptions - functional imaging muddles the definitions of obstruction, flow and function. Clinical evaluations of obstructive uropathy may be misguided. The use of FRI should be reconsidered.

Paper #: 053

Unilateral Ureteropelvic Junction Obstruction (UPJO) in Children: Evaluation of Pre- and Postoperative Imaging Findings and Correlation with Surgical Outcomes

Aikaterini Ntoulia, MD, PhD, *Children's Hospital of Philadelphia, Philadelphia, PA, ntouliaa@email.chop.edu;* Dmitry Khrichenko, Melkamu Adeb, Leslie LeCompte, Dana Weiss, Kassa Darge, MD, PhD

Disclosures: All authors have disclosed no financial interests, arrangements or affiliations in the context of this activity.
Purpose or Case Report: To evaluate the pre- and postoperative imaging findings in children with unilateral Ureteropelvic Junction (UPJ) Obstruction and contralateral normal kidney who underwent surgical treatment.
Methods & Materials: We retrospectively reviewed medical records of children with surgically corrected unilateral UPJ obstructed kidneys from 2006 to 2013. In all cases preoperative ultrasound (US) and functional MR urography (fMRU) findings were analyzed and correlated to surgical results. Serial postoperative US scans were evaluated for resolution of obstruction.

Figure 1

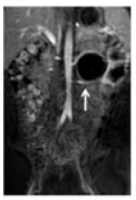

Crossing vessel causing UPJ obstruction.
Two left main renal arteries arising from the abdominal aorta. The lower vessel crosses anteriorly to the left renal pelvis entering to the lower pole of the kidney, causing dilation of the pelvicalyceal system at the level of the uretero-pelvic junction.

Results: 68 children, 41 boys and 27 girls, mean age 4.2 years (6 days-22.8 years) at the time of fMRU were included. 36 children (52.9%) underwent fMRU for antenatal and 32 children (47.1%) for postnatal pelvicalyceal dilation. fMRU findings in kidneys with UPJO were compared with the contralateral normal ones (Table 1). Surgery was performed at mean age of 5.5 years (1.5 months–22.8 years): open pyeloplasty (n=17), laparoscopic (n=9) and robotic-assisted dismembered pyeloplasty (n=34), nephrectomy (n=3), UPJ balloon dilation (n=4), and ureterolysis (n=1). The UPJO was a result of intrinsic ureteral narrowing (n=41), crossing vessel (n=16), ureteral kinking (n=7), atresia (n=3) and fibroepithelial polyp (n=1). Follow-up US scans were performed over a mean time period of 1.8 years (6 months–7 years) and revealed resolution (n=19), improvement (n=42), stability (n=4) and worsening (n=3) of pelvicalyceal dilation. Urinary tract infection (n=10) and stone formation (n=3) were the most commonly encountered long-term problems.

Table 1

Morphological findings	Kidney with UPJO	Normal Kidney
Cortical parenchymal thinning (n (%)	27/34 (79.41%)	0
Decreased cortical-medullary differentiation (n (%)	23/34 (67.6%)	0
Renal parenchymal edema (n (%)	10/34 (29.4%)	0
Cystic parenchymal changes (n (%)	5/34 (14.7%)	0
Functional results		
CTT Mean time (range)	2:23 (1:09–11:18)	1:13 (1:09–3:18)
RTT* Mean time (range)	9:13 (2:50–34:17)	2:49 (1:19–3:12)
TTP* Mean time (range)	3:44 (1:20–12:53)	1:24 (1:27–3:13)
pDRF* Mean % (range)	45.2% (6.2–61.6%)	54.9% (38.4–93.8%)
vDRF* Mean % (range)	42.65% (15.3–55.3%)	57.18% (44.7–84.7%)
vpDRF* Mean % (range)	39.43% (4.5–59.0%)	60.89% (41.0–95.5%)

CTT: Calyceal Transit Time, RTT: Renal Transit Time, TTP: Time-To-Peak and pDRF: Patlak Differential Renal Function.

*Statistical significant differences (p<0.001)

Conclusions: fMRU allows evaluation of UPJO and degree of impaired renal function. Various surgical techniques including minimally invasive ones were employed for the management of the UPJO. Pelvicalyceal dilation may remain postoperatively, although it significantly improves in the majority of cases.

Paper #: 054

Comparison of Contrast Enhanced Voiding Urosonography (ceVUS) using the Ultrasound Contrast Agent (Optison®) with Voiding Cystourethrography (VCUG)

Aikaterini Ntoulia, **MD**, **PhD**, *Department of Radiology, King's College, London, London, United Kingdom, ntouliaa@email.chop.edu;* Susan Back, MD, laura poznick, Trudy Morgan, Joanne Kerwood, Richard Bellah, Janet Reid, MD, FRCPC, Diego Jaramillo, MD, MPH, Douglas Canning, Kassa Darge, MD, PhD

Disclosures: Janet Reid has indicated a relationship with Oxford University as an editor. All other authors have disclosed no financial interests, arrangements or affiliations in the context of this activity.
Purpose or Case Report: CeVUS is a sensitive and safe method for detection of vesicoureteric reflux (VUR). The most widely used US contrast agent for ceVUS was not available in the U.S. The existing US contrast agent Optison® had not yet been evaluated for use in ceVUS. The aim of this study was to compare ceVUS with the intravesical administration of Optison® with fluoroscopic VCUG regarding diagnostic efficacy and safety.
Methods & Materials: A prospective comparative study between ceVUS and VCUG was carried out under an investigational new drug (IND) authorization by the Food and Drug Administration of the U.S. and after obtaining institutional IND and IRB approvals. The patients were referred from urology for clinically indicated VCUG. A written informed consent signed by both parents/guardians was obtained. Safety assessment included physical examination and monitoring of the heart rate and pO2 before, during and after the study. A 48-h phone follow-up was carried out using a standardized questionnaire. After bladder catheterization ceVUS was performed with an infusion of a 0.1%-0.5% suspension of the US contrast agent in normal saline. Contrast specific low MI US scan modality was used to evaluate the bladder and kidneys during bladder filling and emptying. Vesicoureteric reflux (VUR) was diagnosed when microbubbles were detected in a ureter or pelvicalyx. A standard VCUG followed at the end of the ceVUS.
Results: 31 patients were recruited and 1 excluded as it required sedation after enrollment. The remaining 30 patients, 21 females and 9 males with a mean age of 3.5 years (0.1-17.0 years) completed the study. The indications for reflux study were urinary tract infection 18 (60%), follow-up of known VUR 6 (20%), antenatal urinary tract dilation 3 (10%), dysplastic kidney 2 (6.7%) and voiding dysfunction 1 (3.3%). The safety monitoring at the time of the examination was normal in all cases. On the 48-h follow-up 1 (3.3%) of the patients had a minor adverse event, a transient dysuria, most likely due to the catheterization. The 30 patients had a total of 62 pelvi-ureteric units. Taking the VUR depicted in ceVUS and/or VCUG as the reference standard the sensitivity of ceVUS and VCUG was equal at 92.3%. The comparison of the grades of VUR was discrepant in 3/13 positive pelvi-ureteric units.
Conclusions: The intravesical use of the US contrast agent Optison® for ceVUS in children is safe. The comparison of ceVUS with VCUG demonstrated comparable results. Thus ceVUS with Optison can replace VCUG in routine practice.

Paper #: 055

Validation of a Novel Simulator for Teaching Radiology Residents How to Perform Brain Ultrasonography: A Pilot Study

Andy Tsai, **MD**, **PhD**, *Radiology, Boston Children's Hospital, Boston, MA;* Carol Barnewolt, MD, Sanjay Prabhu, Reimi Yonekura, Andrew Hosmer, Noah Schulz, Peter Weinstock

Disclosures: Andrew Hosmer has indicated a relationship.
All other authors have disclosed no financial interests, arrangements or affiliations in the context of this activity.

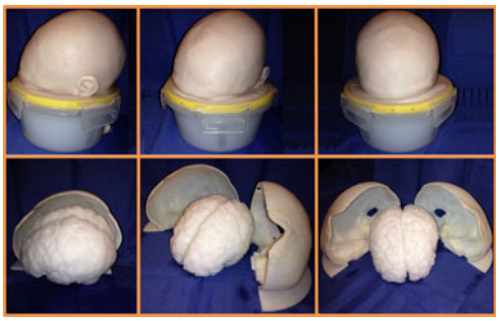

Purpose or Case Report: Historically, skills training in performing neonatal brain ultrasonography (BUS) has been limited to hours of scanning infants for lack of adequate synthetic models or alternatives. The purpose of this study was to determine the utility of using a novel simulator model for teaching radiology residents how to perform neonatal BUS.

Fig. 2

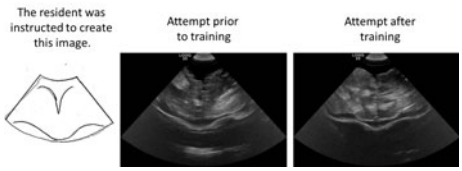

Methods & Materials: A BUS simulator (Fig. 1) was constructed using a combination of multi-modality imaging, 3D printing, material/acoustic engineering, and sculpting/molding. Radiology residents were invited to participate prior to their pediatric rotation. The study included: (1) an initial questionnaire and resident-creation of 3 coronal images using the simulator during their orientation day; (2) a subsequent 1-h BUS lecture and hands on simulator practice (<5 min per person); and (3) a follow-up questionnaire and creation of the same 3 coronal images following training. A blinded radiologist with 23 years of scanning experience scored the quality of the pre- and post-training images (Fig. 2), using metrics including degrees of deviation from vertical and horizontal planes and ability to measure predetermined landmarks. Wilcoxon rank sum test was used to compare pre- and post-training questionnaire rankings (5-point scale) and image quality scores (3-point scale).
Results: Ten residents participated. Pairwise analysis between pre- and post-training rankings showed improvement in technical knowledge (1.5/5–>3.7/5, $P<0.005$); technical confidence (1.1/5–>3.3/5, $P<0.005$); and anxiety related to performing the ultrasound (1.6/5–>3.3/5, $P<0.005$). Objective measures of image quality pre- and post-training also improved (1.7/3–>2.3/3, $P<0.005$). Mean reported value score for simulator training was high across participants (5/5)-including perceived improved scanning skills (4.8/5), enjoyment of interacting with the simulator (4.7/5), recommendation of the training to colleagues (5/5), and interest in additional practice on the simulator (4.2/5).
Conclusions: The BUS simulator model was well-received by residents with regard to technical knowledge, confidence, anxiety, and overall enjoyment. Even with limited simulator interaction, acquired image quality also improved. A novel simulator in pediatric radiology training may provide a much needed new paradigm in BUS training with a positive impact on the quality of the experience, resultant scanning skills, and ultimately on patient outcomes.

Paper #: 056

The Daily Readiness Huddle – A Process to Rapidly Identify Issues and Foster Improvement through Problem Solving Accountability

Lane Donnelly, **MD**, *Radiology, Texas Children's Hospital, Houston, TX, lfdonnel@texaschildrens.org;* Shirley Cherian, Kimberly Chua, Sam Thankachan, Alex Koroll, George Bisset

Disclosures: All authors have disclosed no financial interests, arrangements or affiliations in the context of this activity.
Purpose or Case Report: In order to provide reliable care, systems need to be in place to make sure that the system runs as designed as well as is continuously improved. We describe our Daily Readiness Huddle (DRH) and the effects of the process on problem identification and improvement.

Methods & Materials: Our DRH has four elements: clinical volume review, daily readiness assessment, problem accountability, and review of metrics. It is attended by radiologists, directors, managers, front line staff with concerns, representatives from support services (IT, Biomed), and representatives from off-site locations. Data is visually displayed on a white board (Fig 1). The daily readiness assessment uses queues to determine if anyone has concerns regarding and/or outlier data in regards to S-MESA (Safety, Methods (protocols, atypical patients), Equipment (modalities down, maintenance, IT issues), Supplies, or Associates (staffing). Through this assessment, problems are identified and categorized as "Quick Hits" (will be resolved in 24-48 h, not requiring project management) and "Complex Issues" (CIs). CIs are assigned an owner, quality support person, and report back date. There is a process flow map for CIs and a problem solving template (Figs. 2 & 3). If a CI is not resolved in 60 days it is escalated to radiology administrative leadership. "Projects" are defined as improvements that are often strategic, are anticipated to take more than 60 days, and do not necessarily arise out of identified issues. Each day the DRH summary is emailed to all radiology associates so those who are not able to attend the huddle are informed. The mean, median, and range of days to completion was tracked and

calculated for CIs and Projects during the first 6 months of implementation of this process.

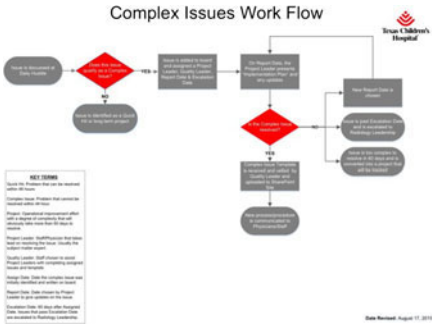

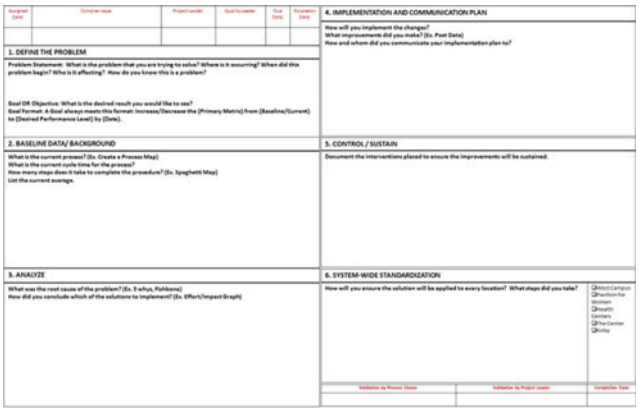

Results: During the first 6 months there have been 43 CIs resolved and 8 in progress and 21 Projects completed with 13 active or in planning. Concerning CIs, time to completion (in days) was: mean 35, median 25, and range 7-105. For Projects, time to completion (in days) was: mean 55, median 54, and range 5-138. Updated data will be presented at the meeting. Specific CI's will be illustrated.
Conclusions: The DRH process has given us a framework to rapidly identify issues, bring accountability to problem solving, and foster improvement. It has also had a positive effect on team building and coordination.

Paper #: 057

Intussusception simulation device, an inexpensive hands-on tool to learn pneumatic reduction technique

Jorge Delgado, *Radiology, Children's Hospital of Philadelphia, Philadelphia, PA, delgadoj@email.chop.edu;* Maria Bedoya, MD, Sabah Servaes, Janet Reid, MD, FRCPC, Victor Ho-Fung, MD, Nathan King

Disclosures: Janet Reid has indicated a relationship with Oxford University as an editor. All other authors have disclosed no financial interests, arrangements or affiliations in the context of this activity.
Purpose or Case Report: Pneumatic reduction (PR) remains a valuable method for treatment of ileocolonic intussusception. Trainees may have limited opportunities to learn the proper technique using the standard pneumatic reduction equipment. Our purpose is to validate an inexpensive hands-on teaching tool with video instruction for pneumatic reduction of ileocolonic intussusception.

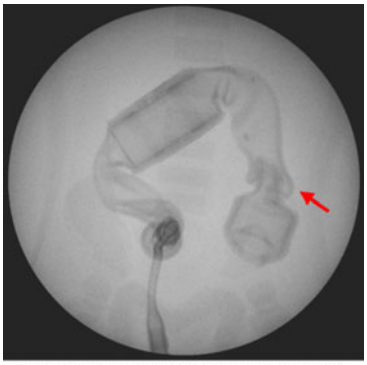

Figure 1: Fluoroscopic image of the model showing an intussusception located in the ascending colon (arrow) (prone position).

Methods & Materials: We developed an intussusception model used under fluoroscopy, consisting of a box containing an aluminum 2D skeleton (simulating radiopaque shadows of bones), a surgical rubber tube (simulating bowel and the intussusception) (Figure 1), and a fabric model (simulating the buttocks and rectum) to practice tube insertion, taping, and rectal seal. We used the standard pneumatic intussusception reduction kit on the model to simulate the procedure. The intervention consisted of pretesting, an instruction video and posttesting. Pre and post confidence questionnaires (Table 1) and pre and post skills tests (Table 2) were done. An 8 min instructional video created to demonstrate the procedure was viewed in-between pre- and posttesting. Pretest and posttest scores were statistically compared.
Results: Following IRB approval, radiology trainees (n=8) were enrolled prospectively (PGY-2=3, PGY-3=3, pediatric radiology fellows=2). The mean time between pre- and post-test was 11 days. Before completing both phases of testing, trainees witnessed on average 2 (range: 0-6) procedures and performed 0.75 (range: 0-3) intussusception reductions. Pretest and posttest confidence questionnaires and skills test (tables 1 and 2) showed improvement in their final scores (p<0.03). All trainees felt the intervention was valuable.
Conclusions: This study validates an inexpensive option for teaching PR using fluoroscopy and the standard commercial equipment. Simple instructions to build the model and the educational video will be shared. Our goal is that trainees worldwide can increase their confidence and skills performing this procedure.

Parameter (Scale 1-5; 1=Poor, 3=Average, 5=Excellent)	Median pretest score (range)	Median posttest score (range)	p-value
Assembling the IAR kit	2.5 (1-4)	5 (3-5)	0.017*
Operating fluoroscopy machine	4 (3-5)	4 (3-5)	>0.99
Operating manometer device	3.5 (1-5)	5 (3-5)	0.109
Performing rectal seal	3 (1-5)	5 (3-5)	0.016*
Identifying successful intussusceptions reduction	3 (2-4)	5 (3-5)	0.066
Total Score (Minimum score=5, maximum score=25)	15 (7-23)	23 (15-25)	0.018*

Table 1: Confidence questionnaire. Median scores and significance of the different statements. (* statistical significance p value less than 0.05)

Parameter	Median pretest score	Median posttest score (range)	p-value
Assembling of the intussusceptions air reduction kit (score: 1-4)	2 (1-4)	4 (3-4)	0.02*
Rectal tube insertion and sealing technique (score: 1-3)	2 (1-3)	3 (2-3)	0.059*
Air insufflation and monitoring under fluoroscopy (score: 1-3)	2.5 (1-3)	3 (2-3)	0.18
Acquisition of images (score: 1-3)	3 (1-3)	3 (3)	0.317
Appropriate identification of successful reduction (Yes/No)	All	All	-
Total (Minimum score=4, maximum score=14)	10 (8-14)	14 (12-14)	0.027*

Table 2: Skills test. Median scores and significance of the different parameters. (*statistical significance *p* value less than 0.05)

Paper #: 058*

Imaging Utilization Patterns for the Diagnosis of Appendicitis in Stand-Alone Children's Hospitals in the United States: an update of trends and costs

Hansel Otero, MD, *Radiology, Children's National Medical Center, Washington, DC, hotero@childrensnational.org;* Lauren Crowder

Disclosures: All authors have disclosed no financial interests, arrangements or affiliations in the context of this activity.
Purpose or Case Report: To describe the imaging utilization patterns, demographics and costs for the diagnosis of appendicitis among children's hospitals in the US over the last 10 years (2005-2014).
Methods & Materials: All patients with a primary discharge diagnosis of appendicitis included in a large administrative database of 42 pediatric institutions in the United States between 2005 and 2014 were selected. Demographics, imaging utilization, outcomes and costs were described.

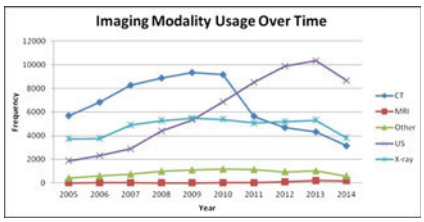

Results: Data from 96,786 children with appendicitis were analyzed. Average length of stay decreased from 5.0 days to 3.3 days); while mean total cost per hospital stay increased from $11,900 to $16,000 during the study period, respectively. Utilization of CT slightly increased between 2005 and 2007 (59.1% to 62.56%). Then, from 2007 to 2014 CT utilization decreased from 63% (*n*=8268) to 33% (*n*=3147) for a 62% decline; while the percentage of patients undergoing ultrasound increased from 25% (*n*=2886) to 61% (*n*=8648) over the same period (increase of 300%). The percentage of patients undergoing MRI during the study period increased from 0.03% (*n*=4) in 2005 to 0.99% (*n*=193) in 2014.
Imaging costs have remained relatively stable going from $3,206 in 2005 to $3,260 in 2014. However, the percentage of hospital costs related to radiology during this period decreased from 27.5% to 19.8%.
Conclusions: There has been a significant decrease in the utilization rate of CT for the diagnosis and management of pediatric appendicitis while ultrasound has continued to increase without an identifiable plateau. Imaging cost have remained stable in comparison to rising total hospital costs generating a drop in the percentage of cost related to imaging from 27.5% to 19.8%.
*Work supported by the SPR Research and Education Foundation

Paper #: 059

Outside Study Interpretation: Current Practice in Children's Hospitals

Stephen Simoneaux, *Children's Healthcare of Atlanta/Emory University, Atlanta, GA, stephen.simoneaux@choa.org*

Disclosures: All authors have disclosed no financial interests, arrangements or affiliations in the context of this activity.
Purpose or Case Report:
The purpose of this study was to determine current practice related to the interpretation of outside studies for patients at children's hospitals.
Methods & Materials: A survey was sent to all members of the Society of Chairs of Radiology at Children's Hospitals in 2014. Questions included: whether their institutions read outside studies; if not, then why not; what types of studies were read; how recent did studies have to be to get an interpretation; how many such studies were read; how studies were handled in their computer systems; billing-related issues; and, other logistical requirements. The surveys were sent electronically with two separate reminders to complete the entries.
Results: 62 respondents returned surveys (80% response rate). Eighty-seven percent of hospitals formally dictate a result for an examination of any age, with most sites reading radiographs, CT, and MRI. Many sites do not read fluoroscopy, ultrasound, nuclear medicine, including PET, and interventional procedures. Nearly all sites bill for the interpretation, either the original CPT code of the study or a consult CPT codes. Nearly all sites have experienced an increase in requests for these readings with 75% doing 6 or more per day. Less than 10% require the outside report for all cases and most sites scan the report into PACS. Nearly 80% have an official policy on outside study interpretation, some approved by the Medical Executive Committee. Ninety-seven percent allow images into PACS without an on-site dictation. Ninety-six percent require a written order for the exam to be read.
For non-reading sites, the main reasons for not doing the interpretations were: no payment, not enough staff, and no strong requests from clinical services. For these sites, nearly half reported moderate pressure to start.
Conclusions:
The interpretation of outside studies is commonplace in children's hospitals. Nearly all sites have a formal process including official policies, written orders, billing, and delineation of studies that will and will not be read. Most hospital report this practice is growing. Nearly all hospitals will allow images into PACS without a reading.

Paper #: 060

RadEd: Early experience with a content management system (CMS) for radiology education

Janet Reid, MD, FRCPC, *Children's Hospital of Philadelphia, Philadelphia, PA, reidj@email.chop.edu;* Trupti Gandhi, Parvez Kazmi, Sudha Anupindi, Michael Francavilla, MD, Lisa States

Disclosures: Janet Reid has indicated a relationship with Oxford University as an editor. All other authors have disclosed no financial interests, arrangements or affiliations in the context of this activity.
Purpose or Case Report: Education of radiology trainees has reached a critical juncture that calls for a system to filter and organize the many Internet-based learning and teaching resources available to trainees and staff radiologists. This will create a foundation that enables scientific evaluation learning pathways that are linked to quality outcomes in our future radiologists.
Methods & Materials: This first generation radiology CMS was created and populated with an array of digital learning and teaching tools created both within the host radiology department and at outside institutions. Available at point of care, it was studied from July-Oct 2015. Residents, fellows and staff radiologists completed a user preferences questionnaire regarding their use practices and suggestions for future improvements. Navigation patterns were studies through Google Analytics®.
Results: A total of 73 Survey Monkey® surveys was sent to rotating residents, fellows & staff radiologists in a large tertiary care children's hospital radiology training program; 48.6% were returned. Top 5 portals: External links; reference articles; Internal search; Imaging tools; recorded lectures. The administrative portal was also popular (conference schedules, rotations, MRI protocols, policies & procedures). Up to 35% agreed : "this site has the potential to replace Google searches for most of my regular tools and references"; "facilitates learning at the point of care"; "facilitates teaching"; and "improves my efficiency at work". Net promotor score: 9 (early positive likelihood that respondent would recommend the site to friend or colleague). Possible enhancements: automatic log in without early time-out (4); content personalized by body system and modalities (2); include tip of the day (3); conduct tutorials to maximize use of the system (2). Total avg page views: 2094; total unique page views: 1229; avg time spent on pgs: 1:16 mins (10% inc). Bounce rate (times one leaves a page) and exit rate (times one exits the site) showed decreasing trends (43-28% and 18-11% respectively) consistent with increased retention over the study interval.
Conclusions: Early experience with our first generation CMS for pediatric radiology education shows value in collating high quality materials in one location to facilitate teaching and learning. Through an iterative process that incorporates user feedback and navigation analytics, such a system shows true promise in building a next generation engine that supports best learning pathways in pediatric radiology.

Paper #: 061

The Dreaded Addendum: A First Step to Reduction of Radiology Reporting Errors in Cases of Suspected Child Abuse

Micheal Breen, MBBChBAO (Hons) BMedSc MRCPI FFRRCSI, *Department of Radiology, Boston Children's Hospital, Boston, MA, micheal.breen@childrens.harvard.edu;* Jeannette Perez-Rossello, MD, Paul Kleinman, MD

Disclosures: All authors have disclosed no financial interests, arrangements or affiliations in the context of this activity.
Purpose or Case Report: Radiology reports in cases of suspected child abuse are distinctly important medical documents. Whether trivial or substantive, errors in reports may take on special significance in care/protection and criminal court proceedings. The purpose of this study was to determine the incidence and types of addenda issued for skeletal survey(SS) reports as a first step to reduce these potentially important medical errors.

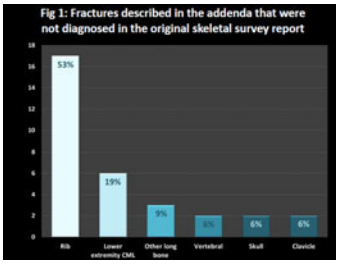

Methods & Materials: Following IRB approval, a text search was performed for addenda issued to reports of SSs done for possible child abuse between January 2005 and September 2015. All addenda were reviewed and categorized.

Results: Of 1346 SS reports, addenda were issued in 48(3.6%). 33/48(69%) of these reports were interpreted as positive before and/or after the addendum. In 16(33%), additional fractures not described in the original report were noted in the addenda. 32 additional fractures were reported in the addenda (mean no. of fractures/SS, 2; range, 1-5) (Figs 1,2). In 7/48(15%), fractures described in the original report were reinterpreted as normal in the addenda (Fig 3).
4(8%) addenda clarified right/left error. 5(10%) changed the location of a fracture described in the original report. 2 (4%) changed the language used to describe the age of a fracture. 7 (30%) addenda were issued for other/purely typographical errors. 8 (17%) made reference to additional radiographs performed after the initial skeletal survey was done and 2 (6%) referred to other imaging modalities. Consultation with a named radiologist with a special interest in child abuse was documented in 5 (10%) of addenda.
Conclusions: Our findings highlight the challenges of reporting these sensitive studies. Although an overall incidence of addenda was modest (3.6%), it is notable that 69% of addended SSs were considered to be positive (for unsuspected fractures). A prior report drawn from this same population found that only 20% of infant SSs were positive, and thus our error rate for positive surveys is likely >10%.
Measures to reduce errors include correlation with contemporaneous imaging studies and consultation with colleagues. Other steps include routine double reads of SSs and the use of a structured electronic skeletal survey reporting tool. Since easily avoidable typographical and casual non-substantive errors can, at the least be embarrassing, and at worst can create confusion and undermine a radiologist's credibility in court, a simple "time out" between the preliminary and final reports should be encouraged.

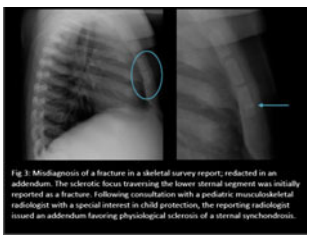

Paper #: 062

Applying Current ACR Guidelines to the Limping Toddler: Is it Enough?

Martha Munden, **MD**, *Pediatric Radiology, Texas Children's Hospital, Houston, TX, mmmunden@texaschildrens.org;* Alaina Moore

Disclosures: All authors have disclosed no financial interests, arrangements or affiliations in the context of this activity.
Purpose or Case Report: The purpose of this study was to evaluate the various etiologies of limping toddlers applying current ACR guidelines to determine if the current recommendations are sufficient.
Methods & Materials: Following IRB approval, we retrospectively reviewed all children aged 3 years and under presenting for imaging for the acute onset of a limp between January 1, 2010 and September 1, 2014. Imaging and electronic medical records were reviewed. Those excluded were children where there was no ultimate diagnosis or follow-up imaging.
Results: Of 951 patients, 698 with no revealing radiologic study or follow-up were excluded. An etiology for the limp was found for 253 patients. The most common etiology for a limp was an underlying fracture, found in 125/253 (49.4%). Soft tissue injury, joint effusions, infection and foreign body were found in 43% while more ominous etiologies including malignancy were found in the remaining patients.
Of the 125 patients with a fracture, 105 fractures were found on initial radiographs and 20 on delayed imaging. With the initial fractures, 38% involved the tibia, 10% the fibula, 27% the cuboid, 18% a metatarsal, 2% the calcaneus, and 5% the femur or hip. On those found with delayed imaging, 50% involved the tibia, 5% the fibula, 45% the cuboid or metatarsals.
Conclusions: Forty-nine% of toddlers with a limp had an underlying fracture. Of those fractures found on initial presentation, 47% involved the foot and on delayed imaging, 45% involved the foot. The ACR appropriateness criteria for a limping child gives xrays of the tibia/fibula a rating of 8 (usually appropriate) while the foot is given a rating of 5 (maybe appropriate). We feel that foot views should be included with the initial evaluation of a limping toddler.

Paper #: 063

To Pee or Not To Pee: A Survey of SPR Members Regarding Practice Patterns for VCUG in the Setting of UTI and the American Academy of Pediatrics Guidelines.

Edward Richer, **MD**, *University of Michigan, Ann Arbor, MI, richerej@gmail.com;* Barbara Pawley, MD

Disclosures: All authors have disclosed no financial interests, arrangements or affiliations in the context of this activity.
Purpose or Case Report: In 2011 the American Academy of Pediatrics (AAP) published revised guidelines for the management of urinary tract infections (UTI) in patients 2 - 24 months, including recommendations for imaging. Recommendation 1 was that renal and bladder ultrasound (RBUS) should be performed in febrile patients with UTI. Recommendation 2 was that voiding cystourethrogram (VCUG) should not be routinely performed in patients with their first febrile UTI, with exceptions in cases of positive findings on RBUS or other complex situations which might necessitate VCUG. This exhibit presents the results of a survey of SPR members in regards to their practice patterns for performance of VCUG for UTI.
Methods & Materials: An IRB waiver was obtained for this study. A short questionnaire was created and distributed via email to the list of active SPR members maintained by the Society for Pediatric Radiology. The survey was sent to 1540 members, with 353 respondents, for a response rate of 22.9%. Questions included length of time in practice, geographic practice location, practice setting, members' awareness of the AAP guidelines, types of referring clinicians, and whether or not the radiologist contacted the clinician to discuss the need for VCUG when RBUS was normal.
Results: The most common respondent was at least 15 years out of training (44%). The most common reported practice locations were the Midwest (22.6%) and the Northeast (19.1%). Most respondents were in an academic practice setting (61.3%). Most respondents (78%) reported being aware of the AAP guidelines, although when asked if they would perform a VCUG after a patient was noted to have a normal RBUS, a majority (61.6%) reported they would perform the VCUG without contacting the referring clinician regarding its necessity. Fewer than 10% of respondents reported that they routinely contacted the referring clinician in this situation, and when contacted, the referring clinician rarely cancelled the examination (12.5%).
Conclusions: While the majority of pediatric radiologists are aware of the 2011 AAP guidelines for imaging in the setting of UTI, implementation of the guidelines is not as widespread, given that most respondents would proceed with VCUG in the setting of a normal renal ultrasound. This could be explained by a variety of factors, including local practice patterns and referring clinician expectations, or other patient specific circumstances known to the radiologist at the time of examination. These factors could be elucidated with further research.

Paper #: 064

The Role of a Real-Time Electronic Dashboard in Improving Clinical Workflow for Pediatric Radiologists

Ariel Botwin, *Massachusetts General Hospital, Boston, MA, botwina@knights.ucf.edu;* Michael Gee, MD, PhD, Markus Stout, Randheer Shailam, MD

Disclosures: All authors have disclosed no financial interests, arrangements or affiliations in the context of this activity.

Table 1
Mean and standard deviation for survey responses. All questions were answered based upon a 5 point Likert scale, with 1 being strongly disagree and 5 being strongly agree.

	Mean±SD
Do you feel you are less prone to making medical errors?	3.83±0.98
Do you feel you are able to focus more on interpreting studies and performing procedures?	4.00±0.89
Do you feel that it reduces inquiries and phone calls related to protocolling?	4.67±0.52
Do you feel more prepared for upcoming exams?	4.33±1.2
Do you feel it makes you more efficient?	4.50±0.55

Purpose or Case Report: Optimizing workflow in pediatric radiology is an important part of patient care, given the numerous imaging modalities and individualized radiation dose and imaging protocols in clinical practice. We developed an electronic dashboard that interfaces with the RIS to provide a real-time reading room visual display of scheduled and in-progress exams, patient wait times, and studies requiring a radiologist protocol. This study evaluates the effectiveness and radiologist perception of a pediatric imaging electronic dashboard.
Methods & Materials: Six reading room sessions with the dashboard were compared with six sessions without the dashboard to assess dashboard effectiveness. Time between CT/MRI exam order by requesting physician and radiologist protocol entry in RIS, as well as number of phone calls received regarding unprotocoled exams, were recorded for each session. To assess radiologist perception of

the dashboard, a 5 question survey based on a 5 point Likert scale (1=strongly disagree, 2=somewhat disagree, 3=no effect, 4=somewhat agree, 5=strongly agree), was distributed to all pediatric radiologists in the department. Statistical analysis was performed using Student's *t*-test.

Results: Overall mean time between CT/MRI exam order and pediatric radiologist protocol entry was 217.8±315.9 h (n=17) with the dashboard compared with 684.9±1534.6 h (n=48) without (P=0.22, Student's t test). When selecting exams ordered and protocoled on the same day, mean time was 12.3±4.1 min with the dashboard and 27.3 ±20 min without (P=0.17, Student's t test). The dashboard was associated with a significant reduction in phone calls received by radiologists about unprotocoled CT/MR studies (mean 0±0 calls with dashboard vs 0.83±0.75, P=0.02). Overall radiologist perception was that the dashboard helps reduce interruptions related to protocolling (4.67 ±0.52) and improves efficiency (4.50±0.55). No significant effect on reducing medical errors (mean score 3.83±0.98) was reported on surveys.

Conclusions: The use of a real-time electronic dashboard resulted in improved clinical workflow in pediatric radiology, evidenced by significant reduction in phone calls about unprotocoled studies and decreased mean time to CT/MRI exam protocoling. Radiologists believe the dashboard improves overall efficiency and reduces interruptions. This suggests a role for real-time dashboard technology in pediatric radiology reading areas.

Paper #: 065

Gonad Shielding Increases Patient Radiation

Summer Kaplan, **M.D.**, *Radiology, The Children's Hospital of Philadelphia, Philadelphia, PA, kaplans2@email.chop.edu;* Christopher Edgar, Marc Felice, Dennise Magill, Michael Francavilla, MD, Xiaowei Zhu

Dose Effect of Gonad Shield Use

	No Shield	Lateral View Shield	AP View Shield
ALL FEMALES			
N	211	259	133
Mean DAP ratio*	0.182	0.244	0.118
p-value		0.002	0.001
AEC, FEMALES≥6 years old			
N	127	160	88
Mean DAP ratio	0.235	0.308	0.137
p-value		0.001	0.000
ALL FEMALES<5 years old			
N	57	45	26
Mean DAP ratio	0.155	0.197	0.072
p-value		0.356	0.092
ALL MALES			
N	265	145	205
Mean DAP ratio	0.229	0.261	0.164
p-value		0.114	0.001
ALL MALES<5 years old			
N	57	29	19
Mean DAP ratio	0.53	0.242	0.170
p-value		0.061	0.758
ALL PATIENTS<5 years old			
N	114	74	45
Mean DAP ratio	0.154	0.215	0.113
p-value		0.062	0.269

* Mean of dose are product (DAP) ratio calculated as: $\log \frac{Lateral\ \ DAP}{AP\ \ DAP}$

Disclosures: All authors have disclosed no financial interests, arrangements or affiliations in the context of this activity.

Purpose or Case Report: For decades, people have questioned the use of gonad shields, given the difficulty of accurate shield placement and potential for obscuring relevant anatomy. The 2007 ICRP Publication 103 decreased the weighting factor of the gonads to be lower than other abdominal organs, further diminishing the rationale for shielding. Radiography today is typically performed with automatic exposure control (AEC), a dose-saving technology that detects incoming photons and terminates the x-ray beam at a threshold exposure. However, when a dense object such as a gonad shield is placed over the AEC sensor, the patient dose may increase.

Methods & Materials: We retrospectively reviewed 2-view AP and lateral pelvis radiographs performed on four digital radiography units between January 1, 2013, and December 31, 2014. We included male and female patients from 0 months to 21 years old with a gonad shield in ≤1 view. Exclusion criteria were non-standard views, shield in >1 view, implanted mid-pelvic opacity, and hemipelvectomy. We compared dose from lateral or AP shielding to unshielded exams, using t-tests to assess differences in a ratio of dose area product (DAP) expressed as log(Lateral DAP/AP DAP). Male and female exams were analyzed separately.

Results: Analysis included 635 male and 616 female exams. For all girls, gonad shields increased patient dose when placed in either the lateral or the AP view. When only girls ≥6 years old with AEC in place were evaluated, the increase was larger and more significant. We do not typically use AEC for children <5 years old, and no dose increase was observed when shields were used in patients <5 years old. For boys ≥6 years old with AEC technique, shields increased dose when placed in the AP view, but not in the lateral view. However, when all male exams were considered, a significant dose increase occurred with both AP and lateral shield placement.

Conclusions: The results confirmed that female gonad shields increase dose. This effect only occurred in girls in whom AEC was used, confirming the role of AEC in increasing dose with shielding. We predicted that shielding would not increase dose in boys, because the male gonad shield should lie outside the AEC cells. However, male shields placed in the AP view did increase dose when the AEC was used. Although shielding the lateral view in boys with AEC did not increase dose, shields resulted in a net dose increase when all boys were considered.

Paper #: 066

Accurate radiation dose monitoring in pediatric fluoroscopy: Are we measuring the correct parameter?

Matthew Lazarus, **MD**, **PhD**, *Montefiore Medical Center, Bronx, NY, matthewslazarus@gmail.com;* Amichai Erdfarb, Terry Levin, MD, Eduardo Nororis, Benjamin Taragin

Disclosures: All authors have disclosed no financial interests, arrangements or affiliations in the context of this activity.

Purpose or Case Report: Fluoroscopy represents a significant source of radiation exposure in pediatric patients. Fluoroscopy time (FT) has traditionally been used as a measure of exposure. However, FT does not assess additional factors that may affect dose, such as collimation, magnification, or pulsed imaging. Modern fluoroscopic equipment allows more direct dose monitoring by measuring dose-area product (DAP). DAP, however, is

heavily affected by patient size, which may vary by up to 100 fold in children. These factors present a unique challenge in tracking radiation exposure.

Methods & Materials: Fluoroscopy studies performed in a pediatric tertiary care hospital were monitored over the course of 11 months. Patient age, FT, and DAP were recorded and compared using linear regression. Cases were then separated by study type and age category (created based on weight-doubling points on published CDC growth charts). Dose thresholds were established as >90th percentile of FT or DAP. Thresholds were also separately determined for UGI or VCUG. Cases exceeding FT or DAP thresholds were compared.

Results: A total of 575 studies (257 upper gastrointestinal studies [UGI], 139 voiding cystourethrograms [VCUG] and 179 miscellaneous studies) were evaluated. DAP correlated with age (r^2=0.30, p<0.0001) while FT demonstrated a much weaker correlation with age (r^2=0.02, p=0.0003). For all study types, DAP thresholds were: 13 μGy•m^2 for 0-3 months, 21 μGy•m^2 for 3 months-2 years, 37 μGy•m^2 for 2-8 years, 306 μGy•m^2 for 8-14 years, and 512 μGy•m^2 for >14 years; FT thresholds were 162 s, 183 s, 203 s, 239 s, and 233 s, respectively. Of the 56/575 cases that exceeded FT threshold (top 10%) and the 56/575 cases that exceeded DAP threshold, only 24 cases exceeded both FT and DAP thresholds (Cohen's κ=0.37). For UGI, 24 cases exceeded FT and 24 exceeded DAP, while only 9 exceeded both (κ=0.27). For VCUG, 13 cases exceeded FT and 13 cases exceeded DAP, while only 4 exceeded both (κ=0.17).

Conclusions: Although DAP is a more comprehensive measure of dose than FT, its correlation with patient age necessitates the use of age-stratified thresholds. The limited overlap of cases exceeding both FT and DAP thresholds indicates that FT alone is inadequate for identifying high exposure cases. We have established age and study specific DAP thresholds. Future adoption of DAP benchmarks will allow more accurate dose monitoring for children undergoing fluoroscopy.

Paper #: 067

Intussusception Reduction: Effect of Contrast Selection on Radiation Dose

Summer Kaplan, **M.D.**, *Radiology, The Children's Hospital of Philadelphia, Philadelphia, PA, kaplans2@email.chop.edu;* Sudha Anupindi, Christopher Edgar, Dennise Magill, Marc Felice, Xiaowei Zhu

Mean Values, Air vs. Liquid Contrast

	Air reduction (N=26)	Opaque Contrast Reduction (N=14)	p-value
Age (months)	1.9	1.8	0.76
Weight (kg)	11.8	11.5	0.77
Fluoroscopy time (minutes)	2.24	1.97	0.64
DAP[a] (dGy-cm^2)	1.31	2.51	0.02
$\frac{DAP}{Fluoroscopy\ \ time}$	0.64	1.46	<0.001
$\frac{DAP}{Fluoroscopy\ \ time \times Weight}$	0.06	0.13	<0.001

[a]Dose Area Product = DAP

Disclosures: All authors have disclosed no financial interests, arrangements or affiliations in the context of this activity.

Purpose or Case Report: Fluoroscopic reduction of intussusception has been performed for many decades, traditionally via hydrostatic enema using radio-opaque contrast. Pneumostatic reduction of intussusception using air enema is a more recent, but well-accepted, technique with equivalent or better success. Air enema may be safer in case of perforation and may be faster, resulting in less fluoroscopy time and lower radiation dose. Fluoroscopy units today use automatic exposure control (AEC), a dose-sparing technology that limits exposure of the image receptor plate to a set diagnostic threshold. We investigate whether pneumostatic reduction results in a lower dose than hydrostatic reduction independent of exam time, due to radio-opaque contrast covering the AEC.

Methods & Materials: We retrospectively reviewed 40 fluoroscopic enemas (26 air, 14 liquid) for intussusception reduction performed on a single digital fluoroscopy unit. We recorded the following information: dose area product (DAP), exposure, fluoroscopy time, type of contrast, age, sex, weight, month, and radiologist. We excluded ultrasound-guided reductions and fluoroscopic exams that used both air and hydrostatic contrast. The outcome measure was DAP/(fluoroscopy time x weight). Due to the relatively small numbers in each group, we confirmed results of t-tests with non-parametric Mann–Whitney U tests to assess significance.

Results: Mean DAP per minute fluoroscopy time per patient kilogram was 240% higher with hydrostatic technique than with air (p<0.001 for t-test and Mann–Whitney). Mean fluoroscopy time was higher with air, but not significantly so (p<0.05). Mean DAP was 190% higher for hydrostatic contrast reduction (p<0.05) without controlling for fluoroscopy time and patient weight. Mean patient weight and age did not differ between the groups. Given small numbers, effect of performing radiologist and month of exam could not be assessed.

Conclusions: Patient dose is higher when radiologists choose radio-opaque contrast rather than air for fluoroscopy-guided intussusception reduction. Our study did not control for individual radiologist performance, month of exam, or use of magnification, but the doses reflect routine practice in an academic pediatric hospital. All adjusted DAP values were within 2.5 standard deviations of the mean. Our results suggest that selection of air for fluoroscopic reduction of intussusception provides a significant dose savings to the patient.

Paper #: 068

Unnecessary Multi-pass Acquisitions are a Common Problem Leading to Increased Radiation Dose in CT Abdomen/Pelvis Examinations

Bradley Rostad, **MD**, *Department of Radiology and Imaging Sciences, Emory University School of Medicine, Atlanta, GA, brostad@emory.edu;* Kimberly Applegate, Tammy Kim, Sarah Milla, MD

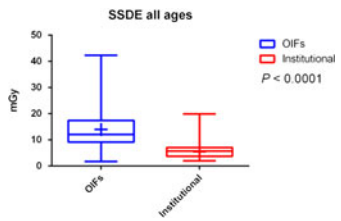

Disclosures: All authors have disclosed no financial interests, arrangements or affiliations in the context of this activity.

Purpose or Case Report: Our tertiary care pediatric hospital receives many children transferred with contrast enhanced computed tomography exams of the abdomen and pelvis (CE-CTAPs) performed at outside imaging facilities (OIFs). Many outside exams have multi-pass imaging (additional scans after an initial contrast enhanced scan). We aim to determine the prevalence of multi-pass CE-CTAPs that are uploaded to the hospital based PACS, and to compare the dose per pass to our institutional practice. Additionally, we aim to identify OIFs with high rates of multi-pass imaging which may benefit from focused practice quality improvement (PQI) efforts.

Methods & Materials: The IRB waived consent as a PQI project. The study was HIPAA compliant. Retrospective analysis was performed on

CE-CTAPs from OIFs uploaded to PACS between January 1, 2012 and December 31, 2014 with indications of abdominal/pelvic pain or related symptoms. Excluded studies were those that potentially justified multiple imaging passes: trauma, tumor/malignancy, and suspected urinary tract leak. Images and dose pages were reviewed to determine the number of passes, CTDIvol, and size-specific dose estimate (SSDE) per pass. Doses per pass of OIFs were compared to institutional performed scans submitted to the American College of Radiology Dose Index Registry (ACR-DIR).

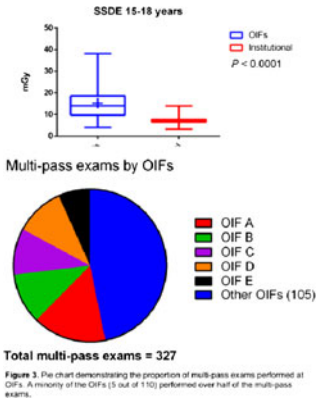

Figure 3. Pie chart demonstrating the proportion of multi-pass exams performed at OIFs. A minority of the OIFs (5 out of 110) performed over half of the multi-pass exams.

Results: There were 571 CE-CTAPs from 110 OIFs that met inclusion criteria. Mean age was 12.1 years (standard deviation 4.5 years, range 0-20 years). More than half of the CE-CTAPs were multi-pass studies: 56% had two passes, and<2% had three or more passes. Dose information could be obtained for 356 (62%) exams. The dose per pass (SSDE) for OIFs was 2.1 x higher than the dose per pass at our institution for all age categories as defined by the ACR-DIR, mean 15.2 vs. 7.1 mGy (p=<0.0001). In the largest age category from OIFs, 15-18 year olds (n=116), the 25th percentile, median, and 75th percentile were 10, 14, and 18 mGy respectively for OIFs, compared to 7, 7, and 8 mGy for institutional performed scans. More than half (53%) of the total number of multi-pass exams were performed by five (4.5%) of the 110 OIFs.
Conclusions: The majority of OIF CE-CTAPs submitted to our institution include unnecessary multi-pass acquisitions. Furthermore, the dose per pass for OIFs is higher than for institutional performed exams. Since only a few of the OIFs (4.5%) contribute to over half (53%) of the multi-pass exams, there is potential for significant improvement in dose reduction from focused PQI efforts.

Paper #: 069

Accuracy of Non-Radiologists and Lay-People for Identifying Children with Cerebral Cortical Atrophy from 'Mercator map' Curved Reconstructions of the Brain)

Savvas Andronikou, *CRICBristol*, University of Bristol, Bristol, United Kingdom, docsav@mweb.co.za; Ewan Simpson, Jade Thai, Schadie Vedajallam, Anith Chacko

Disclosures: All authors have disclosed no financial interests, arrangements or affiliations in the context of this activity.
Purpose or Case Report: Communication of bilateral, symmetric, zonal cortical brain atrophy in children with term hypoxic ischaemic injury (HII) to lay-people and legal personnel in courtrooms using text reports and cross sectional images is challenging. 'Mercator maps' (curved reconstructions from MRI) flatten out the brain surface as a map of the world is derived from a globe of the earth. Lay people and expert's ability to identify abnormal scans from 'Mercator-maps' without prior training requires evaluation before acceptance in non-medical settings. Aim: To determine the accuracy of nonradiologists (including lay people) and radiologists in detecting abnormal brain scans in children with term hypoxic ischaemic injury (HII) and cerebral cortical atrophy from Mercator map reconstructions of brain MRI, without prior training.
Methods & Materials: 'Mercator maps' from curved reformatting coronal MRI of the brain was used in 10 children (5 with previous partial prolonged hypoxic ischaemic injury at term, one with peri-Sylvian cortical dysplasia and 4 with normal MRI reports). 'Mercator maps' were demonstrated as a grid (fig 1) for viewing on a standard computer screen. Participants were conscripted from the immediate clinical and research environment to include lay-people; non-radiologist medical personel and radiologists. They were shown how a world map is derived from a globe of the earth and it was explained that 'Mercatormaps' represent flattened out brain scans designed for viewing of the whole surface of the brain. They were not trained in image interpretation or patterns of injury in HII. They were required to indicate which of the 10 'Mercator-maps' were abnormal. Sensitivity and specificity overall and for subgroups was derived by averaging the true positives and negatives; false positives and negatives.
Results: Participants (29) comprised 10 lay-people, 13 non-radiologist medical personnel (10 radiographers, 2 physicians and 1 scientist) and 6 radiologists. Overall sensitivity was 75% and specificity 83%. Lay-people had sensitivity 70% specificity 68%; non-radiologist medical sensitivity 68% and specificity 85%; radiologists sensitivity 95% and specificity 100%.
Conclusions: The high accuracy of radiologists and ability of Lay-people and non-radiologists with no training to identify bilateral symmetric zonal abnormality on 'Mercator-maps' in HII bodes well for the use of single images to demonstrate zonal cortical brain atrophy in court rooms.

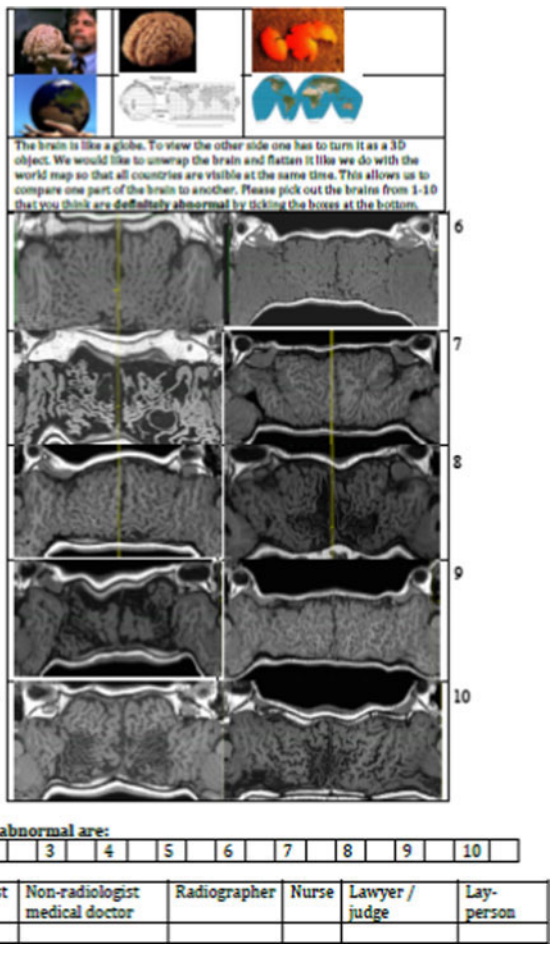

Paper #: 070

Evaluation of ultralow dose high pitch body CT in young children as a technique for evaluating pathology in awake patients

Azadeh Tabari, **MD**, *Radiology, Massachusetts General Hospital, Boston, MA, atabari@mgh.harvard.edu;* Sarabjeet Singh, MD, MMST, Sjirk Westra, Randheer Shailam, MD, Pallavi Sagar, Katherine Nimkin, Michael Gee, MD, PhD

Disclosures: All authors have disclosed no financial interests, arrangements or affiliations in the context of this activity.

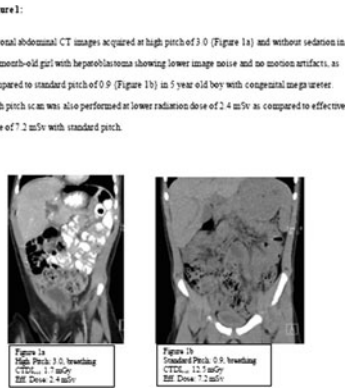

Purpose or Case Report: Due to concerns over ionizing radiation and motion degradation of image quality, infants and young children often undergo MRI with sedation. Technological innovations have enabled CT to be performed in awake children with high pitch CT {HPCT}(>2.2), in order to reduce both radiation and motion artifacts. The purpose of our study is to evaluate our initial clinical experience with high-pitch ultra low dose CT in order to assess image quality, diagnostic confidence, and dose compared with standard CT (pitch ~1).

Methods & Materials: In this retrospective IRB-approved and HIPPA compliant study, a CT database was queried to identify pediatric patients who underwent chest or abdominal HPCT. An age matched comparison group was also generated who had standard pitch (0.9-1.1) chest or abdominal CT{SPCT}. The study cohort was divided into age groups of <1, 1-4, 5-9 and ≥10 years. Subjective image quality was independently performed for lesion margins, motion artifacts and noise. Objective noise was measured and statistical analysis was performed with Student t-test

Table 1: Quantitative and radiation measurements are tabulated high pitch (>2.2) and standard pitch (0.9.1.1) pediatric body CT examinations. High pitchCT examinations were performed at 48% lower radiation dose (3.4/6.6 mGy) with diagnostically acceptable image quality.

		Standard pitch	High pitch
Number of patients		30	29
Objective measurements	Average HU values	191.2±87	155.5±94
	Standard Deviation (HU)	13.0±5.1	12.0±6.5
Radiation dose estimates	$CTDI_{vol}$ (mGy)	6.6±4.1	3.4±2.4
	DLP (mGy.cm)	242.2±179	126.6±126
	SSDE (mGy)	9.5±4.5	4.3±2.4
	SSDE (mGy)	9.5±4.5	4.3±2.4
	Eff Dose (mSv)	3.9±3.0	2.3±2.0

Results: 29 patients were identified {9.8±6.5 years, M:F13:16} who underwent HPCT {*n*=15 chest and *n*=14 abdomen} on a dual source dual energy CT (Siemens SOMATOM Definition Flash}. Most of the HPCT were performed in children >10 (*n*=15), followed by 5-9 (*n*=6), 1-4 (*n*=5) and <1 year old (*n*=3). None of the HPCT cases required sedation or anesthesia, including all 8 patients under 5 years of age and 1 case of multi-phase abdominal CT performed to evaluate a hepatic lesion. Compared with age-match SPCT controls, HPCT was associated with a 48.5% dose reduction {HPCT CTDIvol: 3.4 ±2.4 vs SPCT 6.5±4.0 mGy; *p*=0.0002 Student's *t* test). On subjective image quality, noise was graded as comparable to SPCT and, no motion artifacts were reported. Overall image quality was rated as diagnostically acceptable, including adequate resolution of small sub-centimeter lymph nodes and branch vessels/bronchi. No significant difference in noise was found with HPCT {11.9±6.5} compared to SPCT {13.0±5.1}(*p*=0.22).

Conclusions: Our preliminary clinical experience demonstrates that ultra low dose high pitch chest and abdominal CT can be performed in children and adolescents without the need for sedation and potential alternative to MRI. Radiation dose is reduced by an average of 48% with compared with CT with standard pitch.

Paper #: 071

Pediatric Chest CTA, Comparison between Exposure, Measured Skin Dose and Modeled Organ And Effective Dose

Azadeh Tabari, **MD**, *Radiology, Massachusetts General Hospital, Boston, MA, atabari@mgh.harvard.edu;* Sarabjeet Singh, MD, MMST, Kai Yang, Xiang Li, Bob Liu, Michael Gee, MD, PhD, Sjirk Westra

Disclosure: All authors have disclosed no financial interests, arrangements or affiliations in the context of this activity.

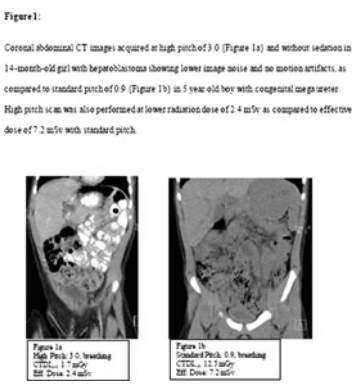

Purpose or Case Report: CT radiation dosimetry is complicated with several available dose estimation tools, including phantom-based estimates (CTDIvol), size specific dose estimates (SSDE), and model-based estimated effective dose and organ doses. In this study, compare directly measured CT surface entrance skin dose with different estimates of skin and organ radiation dose.

Methods & Materials: This prospective observational study was approved by our Institutional Review Board {IRB} and compliant with HIPAA guidelines. The study cohort included 17 consecutive children (average age 7.8±5.2 years, Male: Female 10:7) undergoing chest CT angiography from March 2004 to April 2011. Tube voltage of 80, 100 kVp was selected and Automatic Tube Current Modulation employed. Radiation dosimeters {Unfors Model TN-RD-60, Billdal, Sweden} were placed on skin at 4 locations {mid sternum, right and left nipple, and left lateral}. Radiation dose

monitoring software (Radimetrics™ Enterprise Platform, Bayer HealthCare) was used to perform Monte Carlo simulation and derive organ doses. Demographic and scan information, scanning parameters, and radiation dose, including CTDIvol effective dose as well as organ specific dose was collected. Statistical analysis was performed with Student's t-test.

Table 1:

This table demonstrates the surface radiation dose values (mGy) obtained by dose monitors placed at mid sternum (Mid), left nipple (L), right nipple (R), left lateral position (Lat) in 17 patients.

No.	Gender	Age	Lat	R	Mid	L
1	F	15	21	27.4	32.7	22.6
2	F	17	8.5	8.2	10	7.1
3	M	8	18.5	24.6	21.7	29
4	M	7	10.3	12.8	13.1	11.9
5	M	1	2.37	3.55	4.81	4.72
6	F	10	2.44	4.04	5.69	5.21
7	M	1	1.02	1.11	1.24	1.23
8	M	1	1.92	1.65	2.24	0.8
9	M	7	1.98	1.45	1.17	2.08
10	F	11	7.79	11.8	12.1	10.5
11	M	7	3.09	4	4.01	3.35
12	M	17	1.84	8.77	9.76	5.86
13	M	7	20.9	30.5	31.5	30.7
14	F	1	4.1	1.65	4.61	4.41
15	M	7	2.3	2.89	1.17	2.08
16	F	5	12.3	13.9	15.3	11.2
17	F	9	5.55	5.41	6.95	6.7

Results: The average radiation doses for the chest CTA scans, in terms of CTDIvol were 4.4±4.5 mGy and corresponding SSDE of 10.4±10.9 mGy and estimated effective dose of 0.8±1.1 mSv. Skin dosimeters reported an average of 9.0±9.8 mGy, 8.4±9.2 mGy, 8.4±9.2 mGy and 6.4±6.9 mGy for mid sternum, right nipple, left nipple and left lateral respectively. Measured dose at mid sternum was higher by 30% compared to left lateral position and only 7% more at nipples ($p<0.0008$, $p<0.02$). (Table. 1)

Monte Carlo based estimation of organ doses showed highest dose to breasts (7.7±12.0 mGy), heart (7.4±11.5 mGy), lungs (7.1±11.9 mGy), followed by solid abdominal organs, such as liver (5.8±10.4 mGy), spleen (5.8±10.4 mGy), stomach (5.5±10.3 mGy), esophagus (4.8±8.7 mGy) and least to thyroid (0.7±1.7 mGy). In individual cases, large differences were observed between measured skin doses and modelled organ doses (Figure 1).

Conclusions: Compared to CTDIvol, entrance skin dosimeters reported higher measured radiation dose at the mid sternum level. Monte Carlo based organ dose estimation showed highest dose to breasts, heart and lungs, followed by solid abdominal organs.

Paper #: 072

Improving the Yield of Bronchoscopy for Suspected Pediatric Airway Foreign Bodies with a Clinical Care Protocol Incorporating Low-Dose Airway CT

R. Guillerman, *Texas Children's Hospital, Houston, TX, rpguille@texaschildrens.org;* Farahnaz Golriz, M.D, Omar Ahmed, Wei Zhang, Carla Giannoni

Disclosures: All authors have disclosed no financial interests, arrangements or affiliations in the context of this activity.

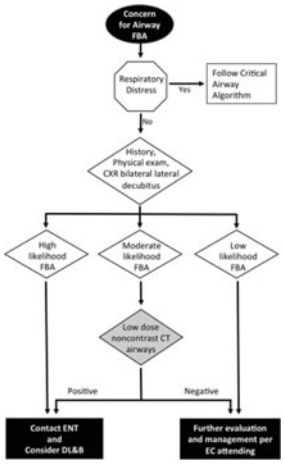

Purpose or Case Report: To determine the effectiveness of a clinical care protocol incorporating low-dose airway CT in reducing the rate of negative diagnostic laryngoscopy and bronchoscopy (DL&B) in children with suspected foreign body aspiration (FBA).

Methods & Materials: A retrospective chart review was conducted of the results of CT and DL&B exams performed from February to October 2015 at a large children's hospital following implementation of a clinical care protocol entailing selective use of low-dose airway CT in children with an intermediate likelihood of FBA on the basis of the history, physical exam and decubitus chest radiograph (CXR) findings (Figure 1). Diagnostic performance characteristics were calculated from 2×2 contingency tables.

Results: 20 patients (mean age: 26 months; range: 8 months - 8 years; M:F 14:6) with an intermediate likelihood of FBA underwent airway CT exams (volumetric noncontrast free-breathing acquisition from larynx to segmental bronchi; mean effective dose 0.8 mSv), revealing foreign bodies in 6 patients, all confirmed at DL&B. No foreign body was found in 4 patients who underwent DL&B despite negative airway CT exams, and no foreign body was found in 6 of 28 patients in the high likelihood group who underwent DL&B without preceding airway CT exams. The sensitivity, specificity, positive predictive value, and negative predictive value (with corresponding 95% confidence intervals) of airway CT for FBA in the intermediate likelihood group were 100% (54-100%), 100% (77-100%), 100% (54-100%), and 100% (77-100%), respectively. The corresponding values for CXR in the 16 patients in the intermediate likelihood group with bilateral decubitus CXR obtained prior to airway CT were 33% (1–91%), 77% (46-95%), 25% (1-81%) and 83% (52-98%), respectively. The overall negative DL&B rate for the combined intermediate and high likelihood groups following implementation of the protocol was 26%, compared to an institutional historical rate of 34% prior to implementation of the protocol. The negative DL&B rate would have been 16% for the combined intermediate and high likelihood groups and 0% for the intermediate likelihood group had management been strictly guided by the findings of airway CT.

Conclusions: Low-dose airway CT is highly sensitive and specific for airway foreign bodies, and the incorporation of low-dose airway CT into a clinical care protocol for children with suspected foreign body aspiration could greatly reduce the negative bronchoscopy rate, thereby decreasing operative risks and costs.

Paper #: 073

The Old and the New – How Time-Tested Antiscatter Grids Interact with Portable Digital Radiography Technology

Adrian Sanchez, Ph.D., Michael Baad, M.D., Kevin Little, *Department of Radiology, University of Chicago Medical Center, Chicago, IL, Kevin.Little@uchospitals.edu;* Ingrid Reiser, Zheng Feng Lu, Kate Feinstein

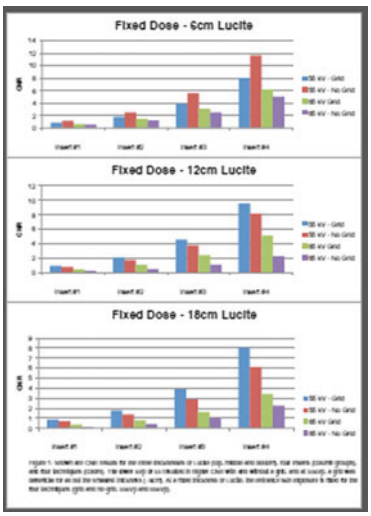

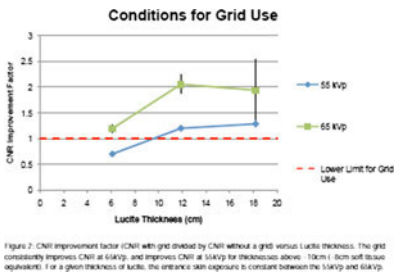

Figure 2: CNR improvement factor (CNR with grid divided by CNR without a grid) versus Lucite thickness. The grid consistently improves CNR at 65kVp, and improves CNR at 55kVp for thicknesses above ~10cm (~8cm soft tissue equivalent). For a given thickness of lucite, the entrance skin exposure is constant between the 55kVp and 65kVp.

Disclosures: All authors have disclosed no financial interests, arrangements or affiliations in the context of this activity.
Purpose or Case Report: 1) To use phantom experiments to systematically relate technique factors, patient size and antiscatter grid use to image quality in pediatric radiography with portable digital x-ray systems.
2) To determine the patient thickness beyond which antiscatter grids provide benefit for image quality with a modern portable x-ray system.
Methods & Materials: Portable x-ray systems play a crucial role in pediatric radiology, and with the advent of digital radiography (DR), the technological sophistication of these systems has increased substantially. In light of recent advancements in detector technology and image processing, we propose a reassessment of antiscatter grid use in portable DR systems. Specifically, while grids have been used for decades to improve contrast, most patient-size criteria for grid use are based on computed radiography systems or film. Determining appropriate scenarios and optimal techniques for grid use in DR is of particular importance in pediatric cases because of the increased radiation dose often applied to compensate for grid attenuation. To this end, we constructed a Lucite phantom with aluminum inserts and measured the contrast-to-noise ratio (CNR) with and without a grid for a range of phantom thicknesses and technique factors. A portable DR system (MobileDaRt Evolution, Shimadzu) was used to acquire the images. The CNR at a fixed entrance skin exposure was calculated for 6.1 cm, 12 cm, and 18.2 cm of Lucite at both 55 and 65 kVp, with and without a grid. The ratio of CNR with a grid to CNR with no grid was computed and proposed as a metric for determining conditions for appropriate grid use.
Results: The results of our phantom CNR measurements indicate a cutoff of roughly 10 cm of Lucite (8 cm of soft tissue) for deriving CNR benefit from grid use with our specific system and field size. Further, for the same additional entrance skin exposure, we observed a CNR benefit from increasing mAs but a CNR penalty from increasing kVp when using a grid. These results suggest grids may be appropriate for most pediatric patients, and that maintaining a low kVp but increasing mAs with a grid may help maintain image quality at low patient doses.
Conclusions: We have constructed a Lucite slab phantom and performed CNR measurements, determining that with our portable DR system, an approximate thickness of 10 cm of Lucite (8 cm of soft tissue equivalent) is the minimum for beneficial antiscatter grid use at 55 kVp. We also observed that a lower kVp setting produced higher CNR when using a grid.

Paper #: 074

Role of Adaptive Statistical Iterative Reconstruction (ASIR) in lowering radiation dose for pediatric head CT

Azadeh Tabari, MD, *Radiology, Massachusetts General Hospital, Boston, MA, atabari@mgh.harvard.edu;* Dhruv Singh, Sarabjeet Singh, MD, MMST, Michael Gee, MD, PhD, Sandra Rincon, Paul Caruso

Disclosures: All authors have disclosed no financial interests, arrangements or affiliations in the context of this activity.
Purpose or Case Report: Iterative reconstruction has recently shown promising results for substantial CT dose reduction. However, there are concerns about image quality at very low dose levels and careful selection of settings of the Adaptive Statistical Iterative Reconstruction (ASIR) is recommend to achieve optimal image quality. The purpose of this study was to assess the potential benefit of ASIR in low dose pediatric head CT by comparing image quality with standard dose filtered back projection (FBP).
Methods & Materials: Institutional review board approval was obtained for this study and HIPPA guidelines were followed. Study cohort was selected as all consecutive pediatric head CT performed on Discovery 750 HD (GE Healthcare) with ASIR 90%. For comparison, pediatric head CT examinations performed on scanners with standard Filtered Back Projection (FBP) was included. Patient demographics, including maximum skin-to-skin transverse head diameter, scanner information {mA, kVp} as well as radiation dose information were recorded. Effective dose was calculated as per the ICRP103 guidelines. Image quality was assessed my measuring image noise as standard deviation of HU values as well as Contrast to Noise Ratio {CNR} for grey white matter. Statistical analysis was performed with student t-test.
Results: Fifty-six children {average age 12.0±4.0, M: F 32:24} underwent head CT examinations with ASIR 90 enabled protocol as compared to 82 head CT {average age 12.7±4.7, M: F 46:36} with standard FBP reconstruction. There was no significant difference in head diameter between ASIR90% {166.6±10.5 mm} and FBP {170.5 ±22.6 mm} (p=0.07). However, there was significant reduction of radiation dose of 52% with ASIR90% {CTDIvol 14.8±10.4, DLP 272.6 ±217.9 mGy.cm, 0.5±0.4 mSv}, as opposed to FBP {CTDIvol 31.1 ±17.4, DLP 593.6±376.9 mGy.cm, 1.2±0.7 mSv} (p<0.001). Furthermore, objective image noise measure in white and grey matter with ASIR90% was found to be similar as FBP (p=0.5-0.6). In addition, contrast to noise ratio {CNR} was not affected with ASIR90%, when compared to FBP (p=0.67).
Conclusions: Pediatric head CT could be acquired at 52% lower radiation dose with Adaptive Statistical Iterative Reconstruction {ASIR90%} without affecting image noise and contrast to noise ratio.

Paper #: 075

Ultrasonographic Features of Secondary Inflammation of the Appendix in Pediatric Patients

Kwanseop Lee, **MD**, *Radiology, Hallym University Sacred Heart Hospital, Anyang-si, Korea (the Republic of), kwanseop@hallym.or.kr*

Disclosures: All authors have disclosed no financial interests, arrangements or affiliations in the context of this activity.
Purpose or Case Report: To describe the ultrasonographic findings of inflamed appendix due to secondary causes other than primary acute appendicitis and to discuss the differential findings compared with primary acute appendicitis.
Methods & Materials: We retrospectively reviewed the secondary inflamed appendix which shows more than 6 mm of maximal appendiceal diameter and color flow on Doppler US. On follow up, inflamed appendix underwent self limiting course with medical treatment. We included 53 patients group of secondary appendicitis, 38 boys and 15 girls with mean age of 6.6 years old, from May 2003 to May 2014. As the controlled group of primary appendicitis, we included 72 patients who diagnosed pathologically proven acute suppurative appendicitis, evaluated by US. For this group, 45 boys and 27 girls, mean age of 10.1 years, from June 2013 to May 2014. We analysed secondary signs of appendicitis in US such as diameter of the appendix, periappendiceal fat inflammation, lymph nodes enlargement, free fluid in right lower quadrant (RLQ) abdomen, presence of appendicolith and presence or absence of combined inflammation of bowel. US exams were performed by 25 radiologists using low frequency curved array and high frequency linear transducers and reviewed by two experienced radiologists retrospectively. For statistical analysis, Mann Whitney Wilcoxon test was used for statistical significance of continuous variable such as aximal diameter of appendix. Fisher's exact test was used statistical significance of categorical variables such as periappendiceal fat inflammation, mesenteric lymph nodes enlargement, free fluid in RLQ area, appendicolith and combined inflammation of bowel, by SPSS 22.
Results: Compared with acute appendicitis, secondary appendicitis has smaller diameter (6.49±0.64 mm vs 9.91±2.57 mm, $p<0.0001$), much less frequently shows periappendiceal fat inflammation (3.8% vs 97.3%, $p<0.0001$) and appendicolith (3.8% vs 31.9%, $p<0.0001$). Secondary appendicitis more frequently shows mesenteric lymphadenopathy (86.8% vs 20.8%, $p<0.0001$) and combined bowel inflammation (100% vs 20.8%, $p<0.0001$). Secondary inflammation of the appendix showed enlarged diameter and increased color flows as in primary acute appendicitis. But periappendiceal fat inflammation was negative or minimal in secondary inflammation of the appendix and most of all children showed combined bowel inflammation.
Conclusions: In children with inflamed appendix, conservative management and follow up US is recommended rather than appendectomy if negative periappendiceal fat inflammation and associated bowel inflammation.

Paper #: 076

CT versus MRI: Effectiveness Following Sonography in Staged Imaging Algorithm for Suspected Pediatric Appendicitis

Elizabeth Dibble, **MD**, *Diagnostic Imaging, Alpert Medical School of Brown University/Rhode Island Hospital, Providence, RI;* David Swenson, M.D., Claudia Cartagena, Thaddeus Herliczek

Disclosures: All authors have disclosed no financial interests, arrangements or affiliations in the context of this activity.
Purpose or Case Report: To compare computed tomography (CT) and magnetic resonance imaging (MRI) in the evaluation of pediatric patients with suspected appendicitis following sonography (US).
Methods & Materials: In this IRB-approved, HIPAA compliant retrospective study, we reviewed the radiology database for all CT and MRI exams performed in pediatric patients with suspected appendicitis from 1/1/11-12/31/12. US was the initial modality used to evaluate all pediatric patients with suspected appendicitis. When US findings were equivocal or when clinical assessment was discordant with US findings, patients often went on to MRI or CT. All pediatric patients (under 18 years) with US followed by MRI or CT were included. Imaging reports were reviewed. US reports were coded as positive, negative, or equivocal for appendicitis. MRI and CT reports were coded as positive or negative for appendicitis. Electronic medical records including surgical notes and pathology reports were reviewed. Sensitivity, specificity, positive predictive value (PPV), and negative predictive value (NPV) of CT and MRI for pediatric appendicitis following US were calculated.
Results: 108 patients underwent MRI for appendicitis (53 male, 55 female, mean age 13.8 years, range 5.68-17.99 years). 78 patients underwent CT for appendicitis (31 male, 47 female, mean age 14.1 years, range 2.31-17.97 years). The sensitivity, specificity, PPV, and NPV of MRI were 85%, 96.6%, 85%, and 95.6%, respectively. The sensitivity, specificity, PPV, and NPV of CT were 100%, 98.4%, 94.1%, and 100%, respectively.
Conclusions: CT and MRI are effective second-line studies to evaluate for appendicitis in a staged algorithm following US. CT had higher sensitivity, specificity, PPV, and NPV than MRI, but MRI had similar specificity and NPV as CT. MRI is nearly as effective as CT for excluding acute appendicitis in patients with equivocal US findings and does not use ionizing radiation, a particular benefit in the pediatric population.

Paper #: 077

Rising Utilization of Magnetic Resonance Imaging in the Management of Pediatric Appendicitis in the United States: An Update Using a Large Administrative Database

Hansel Otero, **MD**, *Radiology, Children's National Medical Center, Washington, DC, hotero@childrensnational.org;* Lauren Crowder

Disclosures: All authors have disclosed no financial interests, arrangements or affiliations in the context of this activity.
Purpose or Case Report: Imaging is an essential component of appendicitis management. Magnetic resonance imaging (MRI) eliminates the use of ionizing radiation and has been reported to be as accurate as computed tomography (CT) for the diagnosis of appendicitis after an inconclusive ultrasound. Emergent abdominal MRI is evolving as an alternative second-line imaging modality for suspected pediatric appendicitis. We sought to describe the basic nationwide trends of MRI adoption and utilization in the management of appendicitis in children from 2005 to 2014.
Methods & Materials: Inpatients with a primary diagnosis of acute appendicitis from January 2005 through December 2014 were identified from the Pediatric Health Information System (PHIS). PHIS is a comparative pediatric database, which contains administrative data from 45 children's hospitals in the United States.
All pediatric patients with a primary diagnosis of appendicitis and an abdominal MRI during the same encounter were initially selected from the database. Patients with incomplete demographics or financial data and those from hospitals with less than 10 cases over the study period were excluded. Demographics, cost and outcomes were compared to national averages.
Results: A total of 96,786 patients were identified with a primary diagnosis of appendicitis and complete demographic and costs data. An abdominal MRI was obtained in 746 patients and 606 from 10 different hospitals were selected for the final sample.
The number of patients undergoing MRI increased from an average of 13 cases/year in the 2005-2011 period to 172 cases/ year in the 2012-2014. For patients undergoing MRI, the average age was

10.9 years (compared to 9.9 years national average) and the average length of stay (ALoS) was 4.6 days for the study period (compared to 3.6 days national average). The average hospital cost was $20,200.9 (compared to $12,329.6 national average). The percentage of costs represented by imaging was 34.5%, which is also higher than the national average of 19.8%.
Conclusions: MRI utilization in the management of appendicitis increased substantially after 2012. However, patients undergoing MRI represent less than 1% of all cases and all come from 10 "early adopter" hospitals. The demographics of the MRI group are similar to the nationwide average but has longer ALoS and higher hospital costs. Additionally, the percentage of total hospital cost represented by imaging is higher in patients receiving MRI.

Paper #: 078

Diagnostic accuracy of MR imaging for evaluation of acute appendicitis: A prime prospective study of Canadian pediatric population.

Saima Batool, Graham Thomson, Clara Ortiz, Samarjeet Bhandal, **Priya Gupta**, *Alberta Children's Hospital, Calgary, AB, Canada, guptapriyagupta@hotmail.com*

Disclosures: All authors have disclosed no financial interests, arrangements or affiliations in the context of this activity.
Purpose or Case Report: Acute appendicitis (AA) is a frequent surgical emergency and cause of hospitalization of children worldwide. Accurate diagnosis can reduce the likelihood of associated morbidity and mortality rate. Ultrasonography (US) is the primary imaging modality for diagnosis of AA. US has limitations including operator dependence, body habitus and appendiceal position. Currently in US equivocal cases, CT is resorted to as the test of choice for diagnosis of AA.CT has higher sensitivity and specificity than US in diagnosing AA, however the frequency of use is limited in children because of ionizing radiation and contrast injection.
With recent advances and more readily available interpreter expertise, in magnetic resonance (MR) imaging, it has proved to be an excellent modality for the diagnosis of AA in pediatric population particularly with equivocal US. The purpose of this study was to determine the diagnostic accuracy of MR in AA among children and compare with surgical outcomes.
Methods & Materials: This IRB approved pilot study comprised of a prospective review of 100 children with AA compares MR with surgical outcome. Three pediatric radiology fellowship trained staff, blinded to the final pathology, reviewed MR for diagnosis of AA and attendant complications. Sensitivity (SN), specificity (SP), positive predictive value (PPV) and negative predictive value (NPV) for disease severity and complications visualized with MR were calculated.
Results: Among the 100 participants, 56% were female and 44% were male. Appendix was visualized in 83%. The periappendicular fluid was seen in 36%, fat stranding in 31% and appendicolith in 5% patients. AA was present in 39% on pathology. MR predicted acute appendicitis in 40%. The SN is 97%, SP is 98%, PPV is 97%, NPV is 98% for the severity of disease.
Conclusions: Conclusion
MR showed high diagnostic accuracy to predict disease severity and complications, equal to and at times superior to that of either US or CT as confirmed on surgery.
Clinical Relevance
MR is a reliable and accurate imaging test for diagnosing ultrasound equivocal cases of AA in the pediatric population for minimizing radiation and avoiding CT.
Ours's is the first and largest pediatric Canadian study and we hope to incorporate this as a standard step in the imaging algorithm of AA in pediatric centers through a good imaging protocol and establish the accuracy of MRI.

Paper #: 079

Diagnostic Accuracy of MRI for Acute Appendicitis in Pediatric Patients as Compared with Adult and Obstetric Patients: A Meta-Analysis

Kevin Eng, *The Hospital for Sick Children, Toronto, ON, Canada, keng@qmed.ca;* Aryan Abadeh, Carolina Ligocki, Yvonne Lee, Rahim Moineddin, Joseph Beyene, Suzanne Schuh, Andrea Doria

Disclosures: Andrea Doria has indicated a relationship with Physician's Service Incorporation as a researcher, Novonordisk Healthcare as a researcher and Bayer Healthcare as a researcher. All other authors have disclosed no financial interests, arrangements or affiliations in the context of this activity.
Purpose or Case Report: To evaluate the diagnostic accuracy of magnetic resonance imaging (MRI) for acute appendicitis in pediatric patients as compared with adult and obstetric patients.
Methods & Materials: Two reviewers independently conducted a literature search of MEDLINE (1996 - 2015), Embase (1980 - 2015), Cochrane Central Register of Controlled Trials (2015), Cochrane Database of Systematic Reviews (2005 - 2015), CINAHL (1981 - 2005), and ACP (1991 - 2015) to identify relevant articles for the diagnostic accuracy of MRI for appendicitis in children, adults, and pregnant women. Prospective or retrospective studies that used surgery/histopathology alone or in combination with clinical follow-up to evaluate the diagnostic accuracy of MRI were included. Three reviewers independently assessed the methodological and reporting quality of articles using the Quality Assessment of Diagnostic Accuracy Studies 2 (QUADAS-2) and the Standards for Reporting of Diagnostic Accuracy (STARD) scoring systems, respectively. Weighted pooled sensitivities and specificities were calculated using the bivariate linear fixed-effects model.
Results: Nine articles on children (973 patients), 9 articles on adults (720 patients), and 7 articles on pregnant women (629 patients) were selected. Weighted pooled sensitivity and specificity of MRI for diagnosis of appendicitis in studies of children was 97% (95% Confidence Interval [CI]: 94%, 98%) and 96% (CI: 94%, 98%) respectively, in studies of adults was 96% (CI: 93%, 97%) and 93% (CI: 89%, 95%) respectively, and in studies of pregnant women was 93% (CI: 83%, 98%) and 96% (CI: 94%, 97%) respectively. Sensitivity analysis was used for statistics of equivocal results in our meta-analysis. In 3 of 9 (33%) studies on children, 7 of 9 (78%) on adults, and 3 of 7 (43%) on pregnant women, the treatment of equivocal results in the calculation of sensitivity/specificity was not reported, and in the remaining studies, different approaches were used.
Conclusions: MRI had a similar sensitivity and specificity for the diagnosis of appendicitis in studies of children as compared with studies of adults and pregnant women. Upon comparison with the accuracy of ultrasound and computed tomography (CT) for diagnosis of appendicitis from a previous meta-analysis, our results show that MRI is as accurate as CT in studies of both children and adults. Thus there is evidence to consider MRI as an alternative to CT especially in pediatric and obstetric patients where exposure to ionizing radiation is most undesirable.

Paper #: 080

Priority Setting in Imaging Diagnosis of Pediatric Appendicitis: Parental Preferences According to Imaging Techniques' Attributes

Claudia Martinez-Rios, MD, *Radiology, The Hospital for Sick Children, Toronto, ON, Canada, claudia.martinez-rios@sickkids.ca;* Jennifer McKinney, Nadine Al-Aswad, Arvind Shergill, Lillian Sung, Karen Thomas, MD, Suzanne Schuh, Andrea Doria

Disclosures: All authors have disclosed no financial interests, arrangements or affiliations in the context of this activity.

US ATTRIBUTES THRESHOLD		
PAIN	FREQ	%
Mild	4	21
Mild to mod.	1	5.3
Mod. to severe	3	15.8
Severe	7	36.8
Worst pain ever	4	21
No modality change	0	0
↓ LENGTH MRI	REQ	%
20 min	10	52.6
10 min	6	31.5
No modality change	3	15.8
MRI ATTRIBUTES THRESHOLD		
IV CONTRAST	FREQ	%
1 in 1 million	6	15
1 in 300,000	3	7.5
1 in 100,000	6	15
1 in 50,000	2	5
1 in 10,000	4	10
1 in 1,000	1	2.5
1 in 500	3	7.5
No modality change	15	37.5
SEDATION	FREQ +1 h	%
1 in 100	16	40
3 in 100	5	12.5
5 in 100	4	10
7 in 100	2	5
10 in 100	2	5
No modality change	11	27.5
LENGTH, MRI ↑	FREQ	%
40 min	6	15
50 min	11	27.5
60 min	8	20
No modality change	15	37.5
NOISE	FREQ	%
Minor (80 dB)	3	7.5
Major (100 dB)	11	45
Severe (120 dB)	18	27.5
No modality change	8	20

Purpose or Case Report: Parents' preferences on imaging diagnostic tests (IDT) for evaluation of acute health care conditions are unknown. Decisions on IDT are made by clinicians upon a debatable informed consent of parents rarely aware of the IDT attributes, thus assessment of parents' preferences on IDT is paramount. The purposes of this study were to determine parents' strength of preference score of IDT (ultrasound-US, computed tomography-CT, magnetic resonance imaging- MRI) for appendicitis, to rank the factors of strength of preference for selected IDT, and to identify the probability at which respondents would give up their initial choice

Methods & Materials: Respondents (resp.) were parents of children (10 year; range 5-16) who had had an abdominal US for right lower quadrant pain. The choices of IDT and their attributes [accuracy, discomfort, radiation, oral (OC) and intravenous (IVC) contrast/allergic reactions, and sedation/complications] were explained. We compared US vs. CT and US vs. MRI. Resp. indicated their preferred IDT and confidence for the selection based on the IDT attributes using a threshold method and ranked the IDT attributes in the order of impact to their selection

Results: 50 resp. (80% mothers) participated. When comparing US vs. CT there was stronger preference for US as IDT for appendicitis (68%, P=0.02) associated with higher importance ranks for cancer risk (P<0.0001), accuracy (P=0.04), pain (P=0.3), length (P<0.0001), and lower for sedation (P=0.04), IVC (P<0.02) and OC (P=0.06). 27% and 47% of resp. said that a decrease of cancer risk from a baseline of 1/5000 to 1/10000 and 1/100000 respectively would be a factor to favour CT. When comparing US vs. MRI there was stronger preference for MRI (78%, P<0.0001) associated with higher importance ranks for accuracy (P=0.2), pain (P=0.06), length (P=0.06) and lower for noise (P<0.0001), claustrophobia (P<0.0001), IVC (P=0.06) and sedation (P=0.2). 37%, 27%, 37% and 20% of resp would not modify their IDT selection if IVC was needed, if higher risk of sedation-related complications, a lengthier or noisier MRI, respectively. There was a high confidence for selecting US (93%) and MRI (90.5%).No predictors of strength of preference (P>0.05) for the IDT related to level of education, gender, age and English as first language were seen

Conclusions: US and MRI were parents' most preferable IDTs for acute appendicitis. The risk of cancer associated with CT radiation, and equivalent accuracy with MRI were the strongest factors considered for their decisions

US ATTRIBUTES THRESHOLD		
PAIN	FREQ	%
Mild	2	5
Mild to mod.	1	2.5
Mod. to severe	↑9	22.5
Severe	12	30
Worst pain ever	8	20
No modality change	8	20
↓ CANCER RISK	FREQ	%
1 in 10,000	11	27.5
1 in 100,000	19	47.5
No modality change	10	25
CT ATTRIBUTES THRESHOLD		
↑ CANCER RISK	FREQ	%
1 in 1,000	9	47.4
1 in 500	8	42.1
No modality change	2	10.5
ORAL CONTRAST	FREQ + 1 h	%
1 tsp (5 mL)	4	21
1 tbs (15 mL)	2	10.5
1/2 cup (125 mL)	8	42
1 cup (250 mL)	4	21
2 cups (500 mL)	0	0
1 L (1000 mL)	0	0
No modality change	1	5.3
IV CONTRAST	FREQ	%
1 in 1 million	5	26.3

(continued)

1 in 300,000	1	5.3
1 in 100,000	3	15.8
1 in 50,000	1	5.3
1 in 10,000	1	5.3
1 in 1,000	0	0
1 in 500	2	10.5
No modality change	6	31.6
SEDATION	FREQ + 1 h	%
1 in 100	8	42.1
3 in 100	5	10.5
5 in 100	3	15.8
7 in 100	1	5.3
10 in 100	1	5.3
No modality change	4	21

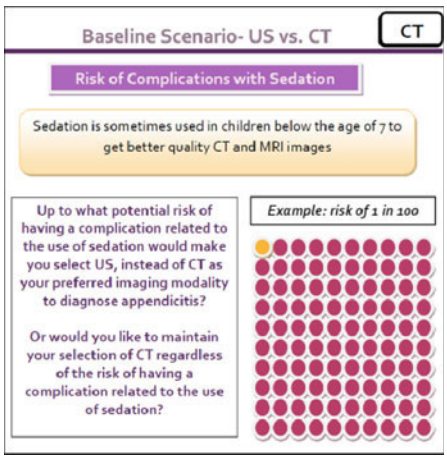

Paper #: 081

Applicability of Emergent MRI for Suspected Pediatric Appendicitis with Equivocal Ultrasound Results

James Martin, Paul Mullan, David Mathison, **Hansel Otero, MD**, *Radiology, Children's National Medical Center, Washington, DC, hotero@childrensnational.org*

Disclosures: All authors have disclosed no financial interests, arrangements or affiliations in the context of this activity.

Purpose or Case Report: BACKGROUND: Emergent abdominal MRI is evolving as an alternative second-line imaging modality for suspected pediatric appendicitis. Previous studies have demonstrated significant time delays from equivocal abdominal US to MRI. After initiation of a Fast MRI protocol, we hypothesized that abdominal MRI is a feasible and accurate tool in evaluation of suspected appendicitis in children when compared to abdominal CT.

Methods & Materials: We retrospectively reviewed children with suspected appendicitis and equivocal abdominal ultrasound results who received secondary imaging. We compared two separate groups (A) abdominal CT as second-line imaging (n=99) versus (B) MRI as second-line imaging (n=41). Group A comprises abdominal CT from the 9 month period immediately prior to MRI use from April 2014 through December 2014. Fast MRI became available in February 2015 and Group B includes all abdominal MRI for suspected appendicitis from February 2015 through September 2015. Fast MRI availability included hours of 7A to 5P Monday through Friday at a single, tertiary care children's hospital. To reflect the applicability of daytime MRI hours as above, we also compared two sub-groups of those with US completion Monday through Friday between 5A to 5P. Time of imaging completion is the timestamp of the last recorded image. No PO/IV contrast was utilized for MRI. No sedation utilized for any modality. Time of disposition is the time of the admission or discharge order.

Results: Abdominal MRI characteristics were: sensitivity 90%, specificity 97.1%, positive predictive value 90%, and negative predictive value 97.1%. Abdominal CT characteristics were: sensitivity 88%, specificity 98.6%, positive predictive value 95.7%, and negative predictive value 95.8%. Mean time from US to MRI of 3.10 h (*vs* CT 4.62 h), mean time from US to disposition of 6.12 h in the MR group (*vs* 6.83 h in CT group), and mean total length of stay (triage to disposition) of 8.23 h in the MR group (vs 9.28 h in CT group)

Conclusions: Abdominal MRI for suspected appendicitis in children has high diagnostic accuracy and utility when compared to abdominal CT. In addition, with a fast MRI protocol, abdominal MRI is both feasible and timely as second-line imaging in the evaluation of appendicitis in the emergency department setting.

Paper #: 082

Are Chest X-ray Patterns Associated with Specific Clinical and Acute Phase Reactants in HIV-infected, HIV-Exposed-Uninfected and HIV-Unexposed Children Hospitalized with WHO Defined Severe, Very Severe Pneumonia?

Nasreen Mahomed, MBBCh (Wits), FC Rad (SA), MMed (Wits), *University of Witwatersrand, Johannesburg, South Africa, nasreen.mahomed@wits.ac.za;* David Moore, Tanusha Sewchuran, Halvani Moodley, Shabier Madhi

Disclosures: All authors have disclosed no financial interests, arrangements or affiliations in the context of this activity.

Table 1 CXR pattern association with clinical parameters and acute phase reactants in HIV-infected children

HIV-infected	WHO end-point consolidation aOR (95% CT)	Other infiltrate only aOR (95% CI)	Intrathoracic Lymphadenopathy aOR (95% CI)	Chronic Lung disease aOR (95% CI)	Bilateral air trapping aOR (95% CI)	Normal chest X-ray aOR (95% CI)
Fever	1.0 (0.4-2.4)	0.7 (0.3-1.9)	0.3 (0.1-1.1)	0.3 (0.0-1.9)	0.5 (0.2-1.3)	1.0
Hypoxia	0.6 (0.2-1.7)	1.2 (0.4-3.4)	8.7 (1.0-74.9)	0.6 (0.1-4.0)	0.7 (0.2-1.3)	1.0
Tachypnea	1.0 (0.4-2.4)	1.0 (0.4-2.8)	1.7 (0.4-7.0)	0.3 (0.1-2.4)	0.8 (0.3-2.4)	0.3 (0.1-1.4)
Crackles	1.0 (0.4-2.4)	1.6 (0.6-4.4)	1.7 (0.4-7.1)	1.7 (0.1-19.8)	0.7 (0.2-2.1)	0.2 (0.1-1.3)
Malnutrition	1.0 (0.5-2.2)	1.4 (0.6-.3)	4.0 (1.2-13.9)	3.1 (0.3-30.4)	0.7 (0.3-1.9)	0.9 (0.2-4.9)

(continued)

Death within 30days of hospitalization	0.7 (0.2-2.0)	2.7 (0.9-8.3)	0.1 (0-1.0)	1.1 (0.1-13.7)	0.3 (0.1-1.6)	0.5 (0.1-5.9)
Raised CRP	2.3 (0.9-5.5)	0.4 (0.1-1.1)	0.3 (0.1-1.2)	1.9 (0.3-12.9)	0.1 (0-0.7)	1.7 (0.3-10.5)
Leucocytosis	1.3 (0.6-2.8)	0.9 (0.4-2.2)	1.1 (0.4-3.5)	1.1 (0.2-7.6)	1.1 (0.4-3.1)	1.0 (0.2-5.4)
Positive Antibiotic serum activity	0.4 (0.2-0.9)	2.3 (0.9-6.1)	0.8 (0.3-2.6)	1.5 (0.2-10.9)	0.9 (0.3-2.4)	1.6 (0.3-1.7)
PCV partially Vaccinated	1.7 (0.4-6.1)	0.3 (0.1-1.3)	1.6 (0.2-12.1)	1.0	1.3 (0.3-6.2)	0.3 (0.1-2.0)
PCV fully vaccinated	0.6 (0.2-1.9)	1.1 (0.3-3.7)	1.8 (0.4-8.7)	1.0	0.6 (0.1-3.6)	1

Purpose or Case Report: Pneumonia is the leading infectious cause of morbidity and mortality in children under 5 years globally. HIV-exposed-uninfected (HEU) infants have two to four times higher mortality compared to HIV-unexposed children in the African settings. Internationally the chest X-ray remains the most readily available and commonest imaging modality for the assessment of childhood pneumonia. The association between chest X-ray patterns and clinical and acute phase reactants have not been described in HIV-infected and HEU children.

Objective: To determine if specific chest X-ray patterns are associated with clinical parameters and acute phase reactants in HIV-infected, HEU and HIV-unexposed children.

Methods & Materials: This study was nested within the prospective PERCH study, South African site. Children hospitalized with WHO defined severe, very severe pneumonia were enrolled over 2 years (August 2011 to August 2013). Chest X-rays were interpreted by 3 radiologists independently, blinded to all clinical data, using modified WHO standardized chest X-ray interpretation criteria. The majority consensus reading was used during the data analysis phase. To determine the association between chest X-ray patterns and clinical and acute phase reactants a univariate analyses was incorporated into multivariate analyses, using a stepwise logistic regression model and adjusted odds ratios were determined.

Table 2 CXR pattern association with clinical parameters and acute phase reactants in HEU children

HEU	WHO end-point consolidation aOR (95% CI)	Other infiltrate only aOR (95% CI)	Intrathoracic Lymphadenopathy aOR (95% CI)	Chronic Lung disease aOR (95% CI)	Bilateral air trapping aOR (95% CI)	Normal chest X-ray aOR (95% CI)
Fever	1.4 (0.8-2.5)	1.6 (0.9-2.8)	1.5 (0.7-3.0)	1.8 (0.2-17.7)	0.9 (0.5-1.8)	0.4 (0.2-0.6)
Hypoxia	1.7 (0.9-3.1)	0.8 (0.4-1.4)	0.6 (0.3-1.2)	1.4 (0.1-14.3)	1.3 (0.6-2.9)	0.9 (0.5-1.6)
Tachypnea	1.1 (0.6-2.0)	1.0 (0.6-2.0)	0.9 (0.4-2.0)	0.8 (0.1-8.4)	1.7 (0.7-4.1)	0.7 (0.4-1.3)
Crackles	1.0 (0.6-1.7)	1.0 (0.6-1.7)	1.1 (0.5-2.2)	0.3 (0.1-3.7)	0.8 (0.4-1.6)	1.1 (0.6-1.9)
Malnutrition	3.0 (1.8-5.2)	0.6 (0.3-1.1)	1.0 (0.5-2.1)	2.3 (0.3-16.7)	1.2 (0.6-2.4)	0.5 (0.3-0.9)
Death within 30 days of hospitalization	0.6 (0.1-2.8)	3.2 (0.6-16.8)	1.0	1.0	1.0	0.9 (0.2-5.4)
Raised CRP	2.0 (1.1-3.7)	0.7 (0.4-1.5)	0.9 (0.4-2.2)	8.4 (0.8-90.8)	1.1 (0.6-2.5)	0.8 (0.4-1.6)
Leucocytosis	1.0 (0.6-1.8)	0.6 (0.3-1.0)	0.9 (0.5-1.9)	0.3 (0-3.5)	1.2 (0.6-2.3)	1.3 (0.7-2.2)
Positive Antibiotic serum activity	1.6 (0.9-2.8)	1.4 (0.8-2.5)	0.7 (0.4-1.5)	3.3 (0.3-32.5)	0.7 (0.4-1.4)	0.5 (0.3-1.0)
PCV partially vaccinated	0.6 (0.3-1.3)	1.7 (0.7-3.8)	2.0 (0.6-6.0)	1.0	2.4 (0.8-7.3)	1.1 (0.5-2.2)
PCV partially vaccinated	0.5 (0.2-1.2)	3.6 (1.5-8.8)	2.3 (0.7-7.6)	0.3 (0.1-10.3)	4.1 (1.3-13.4)	0.5 (0.2-1.1)

Results: From the 858 children with interpretable chest X-rays 108 (13%) were HIV- infected, 284 (33%) were HEU and 428 (50%) were HIV-unexposed. HIV-infected children with raised CRP (>40 mg/dl) had a 90% lower likelihood of bilateral air trapping (aOR 0.1; 95% CI 0.0-0.7), but no significant association with WHO end-point consolidation. HIV-infected children with hypoxia and malnutrition had a greater prevalence of intrathoracic lymphadenopathy (aOR 8.7; 95% CI 1.0-74.9) and (aOR 4.0; 95% CI 1.2-13.9) respectively. No significant association between chest X-ray patterns and fever, tachypnea, crackles, death within 30 days of hospitalization and leucocytosis in HIV-infected children were observed. HEU children with raised CRP had a 2-fold greater odds (aOR 2.0; 95% CI 1.1-3.7) for WHO end-point consolidation. HEU children with malnutrition had a 3-fold greater odds (aOR 3.0; 95% CI 1.8-5.2) for WHO end-point consolidation and conversely a 50% lower likelihood of normal chest X-rays (aOR 0.5; 95% CI 0.3-0.9). HIV-unexposed children with raised CRP had a 5-fold greater odds (aOR 4.5; 95% CI 2.8-7.3) for WHO end-point consolidation, and conversely had a 50% lower likelihood of other infiltrate only (aOR 0.5; 95% CI 0.3-0.9), 70% lower likelihood of bilateral air trapping (aOR 0.3; 95% CI 0.1-0.8) and 60% lower likelihood of normal chest X-rays (aOR 0.4; 95% CI 0.2-0.7). HIV-unexposed children with fever had a 2-fold greater odds (aOR 2.3; 95% CI 1.5-3.5) for WHO end-point consolidation and conversely a 50% lower likelihood of normal chest X-rays (aOR 0.5; 95% CI 0.3-0.7). No significant association between chest X-ray patterns and hypoxia, tachypnea, crackles and leucocytosis was observed in HEU and HIV-unexposed children.

Conclusions: HIV-unexposed children with a raised CRP had a 5-fold greater odds and HEU had a 2-fold greater odds for WHO endpoint consolidation. An association with WHO end point consolidation and raised CRP was not demonstrated in HIV-infected children. WHO end-point consolidation on chest X-ray may be used as a proxy for bacterial infection in HEU and HIV-unexposed children.

Table 3 CXR pattern association with clinical parameters and acute phase reactants HIV-unexposed children

HIV-unexposed	WHO end-point consolidation aOR (95% CI)	Other infiltrate only aOR (95% CI)	Intrathoracic Lymphadenopathy aOR (95% CI)	Chronic Lung disease aOR (95% CI)	Bilateral air trapping aOR (95% CI)	Normal chest X-ray aOR (95% CI)
Fever	2.3 (1.5-3.5)	1.0 (0.6-1.6)	1.9 (1.0-3.6)	0.8 (0.1-5.1)	1.3 (0.7-2.4)	0.5 (0.3-0.7)
Hypoxia	1.0 (0.6-1.6)	1.5 (0.8-2.9)	0.9 (0.5-1.8)	1.0	0.8 (0.4-1.4)	1.1 (0.7-1.9)
Tachypnea	1.0 (0.6-1.6)	1.3 (0.7-2.5)	1.8 (0.8-4.2)	0.5 (0.1-5.9)	1.8 (0.8-4.2)	0.6 (0.4-1.1)
Crackles	1.2 (0.8-1.9)	0.9 (0.5-1.6)	1.0 (0.5-1.7)	1.4 (0.1-13.5)	1.0 (0.5-1.9)	0.8 (0.5-1.2)
Malnutrition	1.7 (1.1-2.8)	0.9 (0.5-1.6)	0.5 (0.3-1.1)	6.8 (1.1-41.9)	1.1 (0.6-2.1)	0.7 (0.4-1.2)
Death within 30 days of hospitalization	3.1 (1.0-10.7)	0.8 (0.2-3.9)	0.6 (0.1-4.9)	1.0	0.6 (0.1-5.2)	0.5 (0.1-2.2)
Raised CRP	4.6 (2.8-7.3)	0.5 (0.3-0.9)	0.8 (0.4-1.5)	1.6 (0.3-10.4)	0.3 (0.1-0.8)	0.4 (0.2-0.7)
Leucocytosis	1.2 (0.8-1.9)	0.9 (0.6-1.5)	0.7 (0.4-1.3)	1.8 (0.3-11.2)	0.7 (0.4-1.2)	0.9 (0.6-1.4)
Positive Antibiotic serum activity	1.7 (1.1-2.5)	0.9 (0.6-1.5)	1.2 (0.7-2.2)	0.7 (0.1-4.3)	0.9 (0.5-1.7)	0.7 (0.4-1.0)
PCV partially vaccinated	1.5 (0.9-2.7)	0.5 (0.3-1.1)	1.2 (0.4-3.4)	4.7 (0.4-49.2)	1.2 (0.5-2.9)	0.8 (0.4-1.5)
PCV fully vaccinated	0.9 (0.5-1.7)	1.0 (0.5-2.0)	2.5 (0.9-6.8)	1.0	0.9 (0.4-2.3)	1.1 (0.6-2.2)

Paper #: 083

Screening for pulmonary arteriovenous malformations (PAVM) in children with Hereditary Hemorrhagic Telangiectasia (HHT) by dual energy CT pulmonary angiography (DE-CTPA); is it as good as it sounds?

Alexi Otrakji, **MD**, Mannudeep Kalra, Randheer Shailam, MD, Sjirk Westra, Katherine Nimkin, Michael Gee, Pallavi Sagar, *Radiology, Massachusetts General Hospital, Boston, MA, PSAGAR@mgh.harvard.edu*

Disclosures: All authors have disclosed no financial interests, arrangements or affiliations in the context of this activity.

Purpose or Case Report: HHT is a rare genetic disorder of vascular development that can present with PAVM. Single energy CT pulmonary angiography (SE-CTPA) is commonly used to detect PAVM. DE-CTPA is a new technique capable of material decomposition thus able to assess pulmonary perfusion. The aim of this study was to assess the performance and added value of DE-CTPA and compare the radiation doses with SE-CTPA in screening children and young adults with HHT for PAVM.

Methods & Materials: Our study included 12 patients with HHT (female:male 5:7; mean age 14±7). Of those, 5 patients (female:male 4:1; mean age 20±5) underwent SE-CTPA and 7 patients(female:male 1:6; mean age: 9±5) underwent DE-CTPA. All DE-CTPA exams were performed on dual source MDCT scanner using bolus tracking technique. Dual energy dataset generated 80 kVp, 140 kVp, weighted average, monochromatic reconstructed images at 40/60 keV and pulmonary blood volume (PBV) maps. Images were assessed for pulmonary artery enhancement, presence of PAVM, size, number, location and additional information on PBV. Radiation doses including CTDI vol, DLP, and effective estimated dose (EED) were compared with SE-CTPA. Data were analyzed using student's t-test.

Results: PAVM were detected in 3 out of 7 cases on DE-CTPA. All monochromatic images were optimal to excellent for the evaluation of vascular enhancement. PBV maps were more sensitive in detecting smaller PAVM due to enhanced lesion conspicuity from increased iodine distribution. A successful embolization of PAVM was performed later in 13 years old patient. In a case of a 3 years old, PBV was not able to detect a PAVM in the right upper lobe seen on monochromatic images, which was thought to be due to relative lung immaturity and contrast streak artifact. Radiation doses for DE-CTPA were(CTDI: 2.1±0.8 mGy; DLP: 67±23 mGy.cm; EED: 0.9±0.3 mSv). There was a significant reduction in radiation dose on DE-CTPA (p=0.02) when compared to SE-CTPA.

Conclusions: DE-CTPA is a desirable technique with the potential to increase reader confidence in confirming the presence of PAVM with relative lower radiation doses while screening children with HHT. Monochromatic images provide optimal to excellent enhancement of the pulmonary vasculature. PBV maps are complementary and play a role in better detection of PAVM, however, has artifacts the reader needs to be aware of and can be less sensitive in younger children. Further studies on DE-CTPA in HHT with larger study samples (rare syndrome) would be useful to confirm the above statistical observations.

Paper #: 084

Evaluation of Pediatric Tracheobronchial Anomalies with congenital heart disease using Three-dimensional Turbo Field Echo Magnetic Resonance Imaging Sequence

Yumin Zhong, **MD**,**PHD**, *Diagnostic Imaging Center, Shanghai Children's Medical Center, Shanghai, China, zyumin2002@yahoo.com;* Aimin Sun, Wei Gao

Disclosures: All authors have disclosed no financial interests, arrangements or affiliations in the context of this activity.

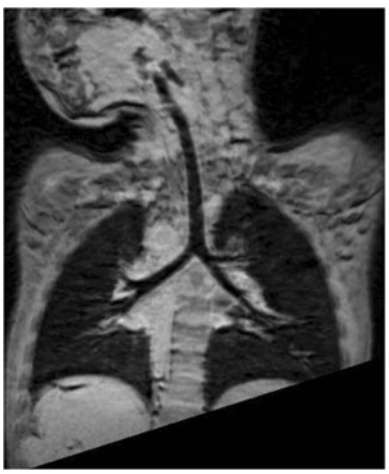

Purpose or Case Report: Tracheobronchial anomalies including tracheobronchial stenosis, tracheal bronchus, cardiac bronchus and bronchial isomerism are common in congenital heart disease. Cardiovascular anomaly is the principal extrinsic lesion causing tracheobronchial stenosis. MRI has the advantage of being non-ionizing and providing excellent soft tissue contrast for the diagnosis of congenital heart disease and tracheobronchial anomalies

Purpose: To define diagnostic accuracy of three-dimensional turbo field echo (3D-TFE) to detect tracheobronchial anomalies in patients with congenital heart disease

Methods & Materials: Sixty-eight patients with congenital heart disease from December 1, 2013 to September 31, 2014 were retrospectively reviewed. Cardiac MR was performed to provide further preoperative information about anatomy and function. In 68 patients, age ranged from 1.4 months to 134 months; the median age was 10.4 months. A 3D-TFE and 3D Balanced turbo field echo (3D B-TFE) sequences were performed on all patients to evaluate tracheobronchial anatomy. All patients also underwent multi-slice computed tomography (MSCT) either before or after MRI. Inter-modality agreement for tracheobronchial anomaly findings was tested by the kappa coefficient and the sensitivity, specificity of 3D-TFE for the detection of tracheobronchial anomalies were evaluated.

Results: Among the 68 cases, 35 cases had a normal tracheobronchial tree, 33 had tracheobronchial anomalies (1 had situs inversus bronchus, 3 had bronchial isomerism, 8 had tracheal bronchus and 25 had tracheobronchial stenosis). The predominant causes of tracheobronchial stenosis were double aortic arch, right aortic arch with mirror-image branching, right aortic arch with left aberrant subclavian artery and posterior patent ductus arteriosus (PDA) or ligament, left pulmonary artery sling enlarged left atrium. There was excellent inter-modality agreement between 3D-TFE and MSCT for the detection of tracheobronchial anomalies. The sensitivity and specificity of 3D-TFE were 90% and 84%.

Conclusions: 3D-TFE is a useful MRI sequence for demonstrating the tracheobronchial tree and diagnosing tracheobronchial anomalies in congenital heart disease. MRI can supply helpful information for preoperative strategies.

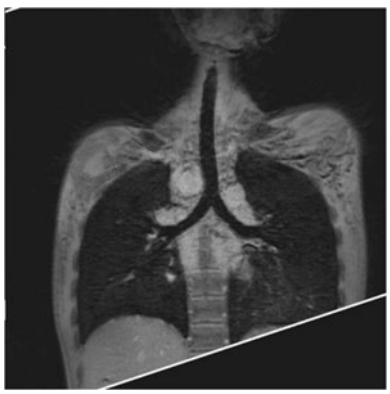

Paper #: 085

Quantification of emphysema by CT in children with cystic fibrosis and comparison to pulmonary function parameters

HaiThuy Nguyen, M.D., *Cincinnati Children's Hospital - Department of Radiology, Cincinnati, OH, haithuyn@gmail.com;* Zackary Cleveland, Alan Brody, John Clancy, Jason Woods

Disclosures: All authors have disclosed no financial interests, arrangements or affiliations in the context of this activity.

Purpose or Case Report: Cystic fibrosis (CF) has largely been considered a disease of the airways; however, recent findings in adults suggest parenchymal involvement, leading to alveolar destruction (emphysema). Emphysematous changes have been documented by chest computed tomography (CT), with increasing involvement with age, but this aspect of CF lung disease has not been systematically examined in pediatrics. The purpose of this study was to quantify the prevalence and severity of emphysema in children with CF, defined by the emphysema index (EI) on CT, to assess the trend of EI compared to age, and to correlate EI with pulmonary function by spirometry.

Methods & Materials: Emphysema index (percentage of lung pixels<-950 HU at inspiration) was calculated from 42 HRCTs performed within 1 year of 42 BALs from 35 patients from the pulmonary clinic registry from 2003 to 2015. 42 HRCTs from age- and sex-matched controls (normal findings from non-contrast chest CTs) were obtained from our radiological database. Statistical analysis comparing the mean EI of CF to control and correlating EI with age and pulmonary function were performed using two sample t-test, linear regression, and Spearman's correlation.

Results: Of the 35 patients, 57% were females (20/35) and the average age was 12.2 years old (range 0.9 - 0.8). The average age for the 42 controls was 12.1 years old (range 1.1 - 20.9). The mean EI for the CF group was 5.1%±8.2% vs. 0.3%±0.6% for the control group (p=0.001). EI increased with age, but with wide variability. There was significant negative correlation between EI and spirometric lung function parameters FEV1 (p=0.014) and FEV1/FVC (p=0.003).

Conclusions: The amount of emphysematous lung is more than 15 times greater in children with CF, than in normal controls. The wide variability in the amount of emphysema with increasing age suggests that the emphysema index may be a useful tool in identifying subgroups at greater risk for rapidly progressing CF lung disease. The emphysema index correlates with spirometric lung function parameters and may be a complementary tool to assess emerging treatments for CF.

Paper #: 086

Rapid lung MRI as an alternative to CT scan in children with pulmonary infections

Kushaljit Sodhi, MD,PhD,FICR, *PGIMER,Chandigarh, Chandigarh, India, sodhiks@gmail.com;* Niranjan Khandelwal, Akshay Saxena, Meenu Singh, Anmol Bhatia, Ritesh Agarwal, Edward Lee

Disclosures: All authors have disclosed no financial interests, arrangements or affiliations in the context of this activity.

Purpose or Case Report: To determine the diagnostic utility of a new rapid magnetic resonance imaging (MRI) protocol compared with computed tomography (CT) scan for the detection of various pulmonary and mediastinal abnormalities in children with suspected pulmonary infections. These children can thus be protected from the potential harmful effects of radiations associated with computed tomography scan.

Methods & Materials:

Seventy-five children (age range of 5 to 15 years) with clinically suspected pulmonary infections were enrolled in this prospective study, which was approved by the institutional ethics committee. All patients underwent thoracic MRI and CT scan within 48 h of each other. The sensitivity, specificity, positive predictive value(PPV), and negative predictive value (NPV) of MRI were evaluated with CT as a standard of reference. Inter-observer agreement was measured with the kappa coefficient.

Results: MRI with a new rapid MRI protocol demonstrated sensitivity, specificity, PPV, and NPV of 100% for detecting pulmonary consolidation, nodules (>3 mm), cyst/cavity, hyperinflation, pleural

effusion, and lymph nodes. The kappa test showed almost perfect agreement between MRI and CT scan in detecting thoracic abnormalities (k=0.899). No statistically significant difference was observed between MRI and CT scan for detecting thoracic abnormalities by the McNemar test (p>0.05).

Conclusions:

Rapid lung MRI is comparable to CT scan for detecting thoracic abnormalities in pediatric patients with clinically suspected pulmonary infections. As it is a radiation free modality, it should be the preferred initial cross sectional imaging modality for the radiological detection of abnormalities in these children. CT scan can thus be reserved only for cases which are normal on MRI or demonstrate clinical non-correlation.

Paper #: 087

Clearing Away the Mud: A Retrospective Review of CT Findings in Pulmonary Interstitial Glycogenosis (PIG)

Christina White, **D.O.**, *Pediatric Radiology, Children's Hospital of Colorado, Denver, CO, christina.white@childrenscolorado.org;* Jason Weinman, MD, Lorna Browne, Csaba Galambos

Disclosures: All authors have disclosed no financial interests, arrangements or affiliations in the context of this activity.

Purpose or Case Report: Pulmonary interstitial glycogenosis (PIG) is a recently described form of children's interstitial lung disease (chILD) characterized by the histologic finding of abundant glycogen-laden mesenchymal cells within the alveolar interstitium. Patients present within the first few months of life with respiratory distress. Fortunately patients with PIG have a better prognosis than many other diffuse lung diseases of infancy. The pathophysiology is poorly understood, however recent research suggests restricted diffusivity across alveolar membranes as a contributing factor. Often PIG is accompanied by alveolar simplification/immaturity, potentially complicating recognition and diagnosis.

Despite recognition of PIG as a distinct entity, only a few case reports describing imaging findings are found in the literature, with no published systematic review available. The purpose of this review is to provide a review of CT findings of PIG with histologic correlation, to aid in early diagnosis and management.

Methods & Materials: Following IRB approval, retrospective review was performed to identify pediatric patients<21 years who underwent biopsy and CT within the last 10 years at our institution. The inclusion criterion encompasses patients who had a CT within 2 months of biopsy and pathology-proven PIG. CTs were evaluated by 3 radiologists using a standardized scoring system.

Results: 13 patients met inclusion criteria (8 males, 5 females). At the time of initial pre-biopsy CT, ages ranged from 2 weeks to 5 months. Pulmonary symptoms presented at birth (n=10), by 1 month (n=1), 3 months (n=1), and 6 months (n=1). Ground glass opacities were the most common CT finding (n=13), which varied from diffuse to scattered. Cysts (n=8) were noted in many patients. Parenchymal bands (n=2), interlobular septal thickening (n=4), and architectural distortion (n=4) were less common findings.

Conclusions: The dominant CT features of PIG are ground glass opacities with cystic change. There is significant overlap of these findings with surfactant deficiency, an entity which also presents with respiratory distress in the early neonatal period. Imaging findings are helpful in differentiating PIG from other lung diseases of infancy, such as follicular bronchiolitis and neuroendocrine cell hyperplasia. Management is largely supportive in these children, though steroid administration has shown benefit in facilitating lung maturation, which often results in clinical improvement.

Paper #: 088

Tomographic Patterns of Pulmonary Tuberculosis in Children

Claudia Lazarte, **Radiologist**, *Instituto Nacional de Salud del Niño-San Borja, LIMA, Peru, claudiaisabellazarte@hotmail.com;* Carlos Ugas, Radiologist, Viky Suncion-Loescher

Disclosures: All authors have disclosed no financial interests, arrangements or affiliations in the context of this activity.

Purpose or Case Report: To determine the tomographic features in patients younger than 15 years diagnosed with pulmonary tuberculosis

Methods & Materials: Multidetector computed tomography imaging (64 multislice CT scanner) of 52 patients younger than 15 years old diagnosed with pulmonary tuberculosis were retrospectively analyzed by one independent pediatric radiologist with 10 years of experience. Diagnosis of pulmonary tuberculosis was done according to the National Program of Pulmonary Tuberculosis. All data were analyzed using SPSS 18, quantitative data expressed as mean and standard deviation and qualitative data as percentages.

Results: Of the 52 cases (Male=28 and Female=24), 80.8% of the cases showed signs of consolidation on CT, 45.2% were segmental, 35.7% were multilobar, 14.3% were lobar, and 4.8% were lobar-segmental. In the cases with lobar and lobar-segmental consolidation, 87.5% were located in the upper lobe and 12.5% in the lower lobe. Importantly the presence of cavern occurred in 71.2% of the cases. The tree-in-bud pattern was observed in 50% of cases, reaching all lobes in 50%, lower lobe in 26.9%, upper lobe in 19.2%, middle lobe in 3,9%, and bilateral in 61.5%. The 28.8% of cases had atelectasis, 60% were segmental and 40% were lobar. Milia was observed in 28.8% of cases and ground glass pattern in 36.5%. Interestingly, pulmonary nodules, hyperaeration and lung abscesses were observed in 26.9%, 42.3% and 7.7% respectively. Lymphadenopathy was seen in 92.3% of cases and 18.8% of these cases showed internal necrosis. Calcification occurred in 59.6% of cases and was located in the mediastinum in 80.6%, in the lung in 12.9% and in mediastinum-lung in 6.5%. Pleural effusion was evident in 21.2% of cases. This was most often located on the right (54.5%) than on the left lung (27.3%). Bilateral pleural effusion and pleural thickening was found in 18.2% and 5.8% respectively.

Conclusions: The presence of consolidation, tree-in-bud pattern, cavern and lymphadenopathy were predominantly observed in pediatric population with diagnosis of pulmonary tuberculosis. Surprisingly, although pleural effusion has been commonly observed in pulmonary tuberculosis, this was noted only in 21.2% of our patients.

Paper #: 089

HIV and Stroke. A Retrospective Review at our Institution

Nicky Wieselthaler, **MBChB**, **Fc Rad (diagnostic)**, *Radiology, Red Cross War Memorial Children's Hospital, Cape Town, South Africa, nicole.wieselthaler@westerncape.gov.za*

Disclosures: All authors have disclosed no financial interests, arrangements or affiliations in the context of this activity.

Purpose or Case Report: An estimated 3.2 million children have HIV infection worldwide. 91% of these children live in sub-Saharan Africa.

Stroke is a recognised complication of HIV infection. However moyamoya syndrome is a rare serious complication of HIV, with only 2 reported cases in the literature.

Methods & Materials: A retrospective review was done of all HIV positive children who presented to our institute from 2002 to the current date with a stroke. Demographics were screened for patient profile, clinical presentation, past medical history as well as standard blood and imaging work-up. Access and compliance to antiretroviral therapy (ART), duration of treatment, inclusive of CD4 counts and viral loads in relation to the timing of the stroke were specifically noted. Infarcts due to secondary aetiologies for e.g. infective causes were excluded.

Results: Nine patients with HIV vasculopathy were identified. They were subdivided into those with moyamoya syndrome (n=3) and those with ischaemic stroke (n=6). No patients had a haemorrhagic stroke, SAH or infarction due to venous thrombosis.

All the moyamoya patients presented over 5 years ago. Two of these 3 patients were assumed to have HIV encephalopathy and without neuroimaging this progressive vascular disease would not have been diagnosed. Neuroimaging supported progressive vascular disease and preceding clinically silent disease course.

The clinical profile of the children with ischaemic stroke and moyamoya syndrome was similar, such that without neuroimaging the diagnosis of moyamoya syndrome would have been missed.

Of the 6 patients who presented with ischaemic stroke all patients had involvement of the MCA territories (left n=4, right n=2), abnormal MRA was identified in 5 and 1 patient had an aneurysm. These findings comply with the literature which identified only 74 cases of stroke in HIV infected children.

Conclusions: The prevalence of moyamoya appeared to correlate with limited ART access and in children with poor viral load control. Whilst improved access to ART has correlated with improved outcomes and decreased morbidity, in the sub-Saharan setting where there is limited access to neuroimaging many children are not being identified with cerebrovascular disease.

Paper #: 090

Curved reformat of the paediatric brain MRI into a 'flat-earth map' – a standardised method for demonstrating cortical surface atrophy resulting from hypoxic ischaemic encephalopathy

Ewan Simpson, Savvas Andronikou, MBBCh, FCRad, FRCR, PhD, *CRICBristol, University of Bristol, Bristol, United Kingdom, docsav@mweb.co.za;* Schadie Vedajallam, Jade Thai, Anith Chacko

Disclosures: All authors have disclosed no financial interests, arrangements or affiliations in the context of this activity.

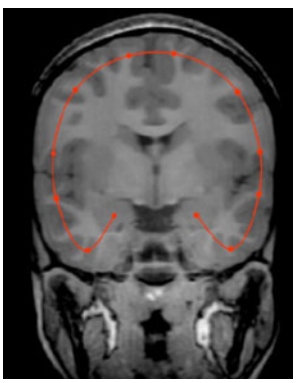

Purpose or Case Report: MRI in term hypoxic ischaemic brain injury (HII) demonstrates cortical atrophy and ulegyria in characteristic locations. Communicating bilateral zonal injury to parents and in court rooms using reports and cross-sectional images is challenging. An overview map of the brain surface generated from a curved reconstruction of MRI is ideal for such scenarios. A standardized technique is described, and cortical anatomy and zonal involvement in HII is demonstrated.

Methods & Materials: Freeware was used to describe a standardized method of curved reconstructions of the paediatric brain from 3D MRI in 10 children with cortical atrophy from term HII and 10 age-matched 'controls'. Multiple techniques were tested from various planes, different landmark slices and angles of reconstruction at various depths to the surface. Two images (from the coronal and sagittal planes) were determined to give the best overview of the watershed, peri-Sylvian and peri-Rolandic zones:

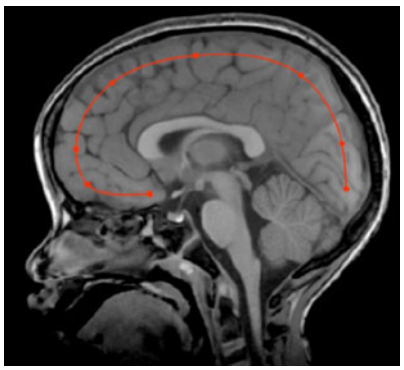

The coronal slice with foramina of Monro was selected and curved reconstruction was plotted 1-cm-deep to the cortical surface by depositing 12 cursors *(figure 1a)* for a 'Mercator-map'. The sagittal midline slice of the aqueduct of Sylvius was plotted 1-cm-deep to the cortical surface by depositing 8 cursors (*figure 1b)* for a 'scroll-map'.

Cortical anatomy was identified and watershed zones were described on both maps. 'Mercator' and 'scroll'maps were generated for 10 children with HII alongside 10 age-matched controls.

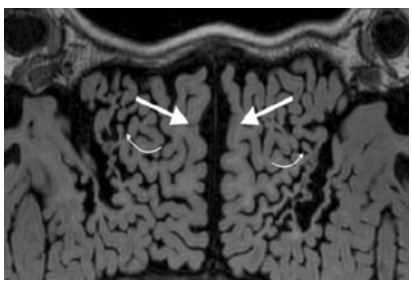

Results: ***All flat earth maps:***

Peri-Sylvian, peri-Rolandic zones and frontal lobes were better demonstrated on the 'Mercator' maps. 'Scroll' maps demonstrated lateral structures poorly but demonstrated central posterior parietal and occipital lobes better. Watershed zones were well demonstrated on both maps.

HII cases:

Localised 'bi-convex' inter-hemispheric fissure widening was present in all patients on both maps i.e. para-sagittal /para-falcine watershed atrophy (figure 2). An inter-vascular watershed band of atrophy was seen on both maps. Peri-Rolandic and peri-Sylvian atrophy was better demonstrated on Mercator maps. Ulegyria was identified in 90%.

Conclusions: Standardized curved reconstruction of the brain surface from MRI allows visualization of key cortical features of term HII on two images, 'Mercator' and 'scroll' maps, which can replace multi-slice MRI for communicating cortical findings to legal professionals and parents, and can be embedded within multimedia reports.

Paper #: 091

Network Architecture and Global Intelligence in Children with Localization-related Epilepsy

Michael Paldino, M.D., Wei Zhang, Mary Chapieski, Farahnaz Golriz, M.D, *Radiology, Texas Children's Hospital, Houston, TX, fxgolriz@texaschildrens.org;* Zili Chu, PhD

Disclosures: All authors have disclosed no financial interests, arrangements or affiliations in the context of this activity.
Purpose or Case Report: The biologic basis for intelligence rests to a significant degree on the capacity for efficient integration of information across the cerebral network. As a result of advances in computational neuroscience and MRI, network architecture of the brain is now accessible to systematic study. The clinical value of such techniques has yet to be realized, however, in large part because the physiologic meaning of network metrics has not been established in the setting of cerebral pathology. Normal rewiring of the cerebral network during development as well as the known impact of anesthesia on the MR measurement of brain networks further complicate the situation in children. We therefore sought to measure: 1. the relationship between network architecture and intelligence in the pediatric, epileptic brain; 2. the impact of anesthesia during MRI on this relationship.

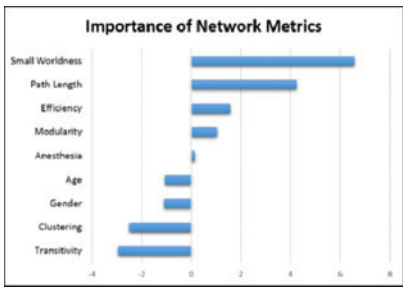

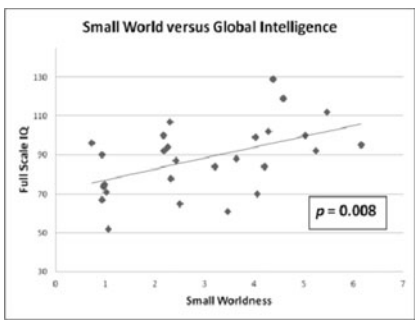

Methods & Materials: Patients were retrospectively identified with: 1. A diagnosis of localization related epilepsy; 2. Brain MRI at 3 T, including resting state functional MRI; 3. Full scale IQ measured (age-appropriate version of the Wechsler Intelligence Test) by a pediatric neuropsychologist. Resting-state time series were co-registered to a T1-weighted structural image. The cerebral cortex was parcellated into 400 gray matter network "nodes". The strength of a connection between two nodes was defined as the absolute value of the correlation between their BOLD time series. The following topological properties were calculated: clustering coefficient, transitivity, modularity, path length, small worldness, and global efficiency. A machine learning algorithm was used to: 1. measure the independent contribution of each metric to IQ after adjusting for the contribution of all other metrics; 2. model the impact of anesthesia on this contribution.

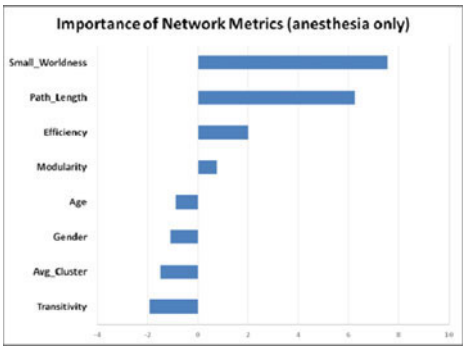

Results: 28 patients met criteria (age: 7-18 years). Path length (p=0.004) and small worldness (p=0.008) independently predicted global intelligence (Figure 1). The relationship of small worldness with IQ is depicted in figure 2. Repeating the analysis using only anesthesia patients did not alter the metrics contributing intelligence (Figure 3).
Conclusions: We report two main findings in this cohort of pediatric epilepsy patients: 1. Two metrics of network integration strongly contributed to full scale IQ; 2. these relationships to intelligence were robust to anesthesia. These findings support the physiologic relevance of imaging-based metrics of network architecture in the abnormal, developing brain.

Paper #: 092

Metrics of Network Architecture Probe the Impact of Ongoing Seizures on Cognitive Development in Children with Epilepsy

Farahnaz Golriz, M.D, *Radiology, Texas Children's Hospital, Houston, TX, fxgolriz@texaschildrens.org;* Wei Zhang, Mary Chapieski, Zili Chu, PhD, Michael Paldino, M.D.

Disclosures: All authors have disclosed no financial interests, arrangements or affiliations in the context of this activity.
Purpose or Case Report: In appropriately selected epilepsy patients who fail medical management, surgical resection of epileptogenic lesions can be curative. In suboptimal candidates, however, continued medical therapy is frequently adopted as the safer course. Ongoing seizures and/or seizure medication, however, have been shown to alter the structural framework of the cerebral network which over time could contribute to cognitive decline. As a result of advances in computational neuroscience and functional MRI, network architecture of the brain is now accessible to systematic study. We therefore sought to measure the relationship of network architecture to the impact of ongoing seizures on cognitive function in children.

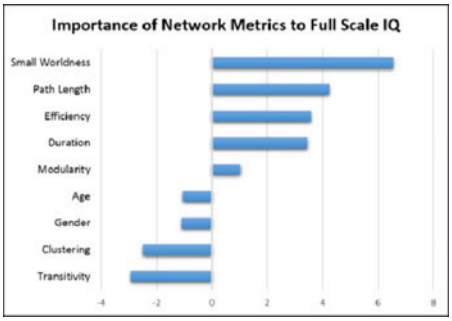

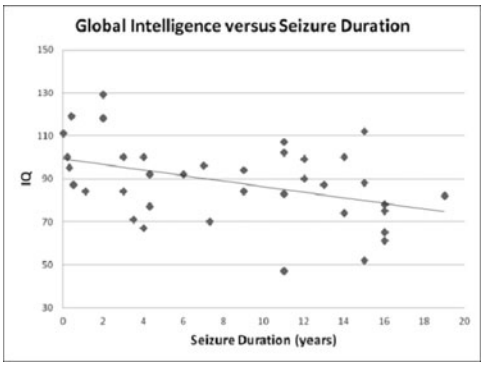

Methods & Materials: Patients were retrospectively identified with: 1. A diagnosis of localization related epilepsy; 2. Brain MRI including a resting state functional MRI sequence; 3. Full scale IQ measured (with age-appropriate version of Wechsler Intelligence Test) by a pediatric neuropsychologist. Resting-state time series were co-registered to a T1-weighted structural image. The cerebral cortex was parcellated into 400 gray matter network "nodes". The strength of a connection between two nodes was defined as the absolute value of the correlation between their BOLD time series. The following network properties were calculated: clustering coefficient, transitivity, modularity, path length, small worldness, and global efficiency. The relationship between seizure duration and IQ was assessed by linear regression. A machine learning algorithm measured the independent contribution of each metric to IQ after adjusting for the contribution of all other variables.

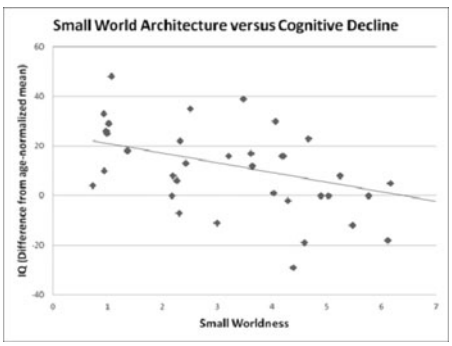

Results: 34 patients met criteria (age: 4-18 years). Seizure duration was associated with decreasing IQ (p<0.04; Figure 1). After accounting for seizure duration, brain network architecture remained strongly associated with IQ (Figure 2). In terms of fractional variance explained, network metrics captured approximately 77% of the overall effect of seizure duration on IQ. This finding is exemplified by small worldness which was inversely related to the degree of cognitive decline relative to age-defined norms (p<0.002; Figure 3).

Conclusions: These results provide further support for the idea that ongoing seizures contribute to cognitive decline in children. Metrics that quantify integration across the cerebral network have the potential to provide imaging markers of cognitive function in this setting.

Paper #: 093

High-resolution CT Angiography and Computational Fluid Dynamics for stroke risk assessment in a mouse model of pediatric cerebrovascular disease

Zbigniew Starosolski, PhD, *Pediatric Radiology, Texas Children's Hospital, Houston, TX, zastaros@texaschildrenshospital.org;* Shaolie Hossain, Travis Sanders, Dianna Milewicz, Ananth Annapragada, Ph.D.

Disclosures: Zbigniew Starosolski has indicated a relationship with Alzeca Biosciences, LLC. Ananth Annapragada has indicated a relationship with Alzeca LLC as a stockholder. All other authors have disclosed no financial interests, arrangements or affiliations in the context of this activity.

Purpose or Case Report: Mutations in the *ACTA2* gene coding for smooth-muscle a-actin lead to stenosis, occlusions and pathological straightening of cerebral arterial structures in the Circle of Willis (CoW) territory. We studied blood flow dynamics in the cerebrovascular anatomy of *ACTA2-/-* mice to understand the effect of vascular occlusions on stroke pathology.

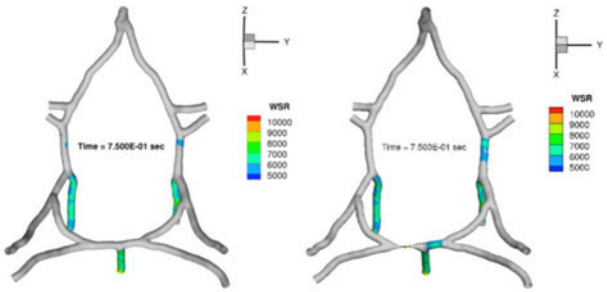

Fig. 1: WSR (s^{-1}) distribution at peak systole within the CoW of a Knockout ACTAT2 -/- mouse model with (right) and without occlusion (left) in the right SCA. Note, WSR values above the coagulation threshold (>5000 s^{-1}) are reported here.

Methods & Materials: All in vivo procedures were approved by the IACUC. Mice were imaged at 7+/-1 weeks of age, under anesthesia and head restraint to eliminate motion artifacts. A liposomal long circulating CT contrast agent (~120 nm particle size, iodine dose 2.2 mg/g was i.v. administered). Micro-CT angiographic images were collected using a Siemens Inveon scanner (70 kVp, 500 uA, 850 ms exposure). Image reconstruction with 19 μm isotropic voxels ensured identification and separation of intertwined arterial and venous structures. Segmentation of the vascular anatomy in the CoW territory was performed with Sculptor software, followed by manual selection of the arterial structures. The resulting geometry was processed through a vascular modeling pipeline to generate a 3D NURBS mesh, followed by computational fluid dynamics (CFD) analysis.

Results: Blood flow conditions were approximated by a pulsatile inflow, consistent with cardiac output. Symmetric bilateral flow was observed under normotensive conditions. Wall shear rate (WSR) distribution

pattern in the *ACTA2-/-* geometry was similar to that of the wild type, and remained essentially below the coagulation threshold of 5000 s^{-1}, suggesting that vessel straightening alone in the *ACTA2-/-* mouse is not sufficient to predict an increased stroke risk. Simulation of occlusion in the right SCA in the *ACTA2-/-* model Fig. 1 resulted in left dominant flow and critical WSR values in the left superior cerebellar artery (SCA) and left internal carotid artery, suggesting a higher probability of thrombus formation in vessels contralateral to the occlusion. Retrograde flow was also detected in the right posterior communicating artery, indicating sustained flow in the presence of the occlusion.
Conclusions: The liposomal blood pool contrast agent enables in-vivo high-resolution CTA, necessary for recognition and separation of cerebrovasculartur e. A careful study of *Acta2-/-* CTA revealed an increased incidence of obstructions and malformations in the SCA branch. CFD analysis of arterial structures indicates the locations of segments susceptible to stenosis, and potential stroke, a common outcome in patients with mutant *ACTA2*.

Paper #: 094

Variable Refocusing Flip Angle Single Shot Imaging For Faster Anesthesia-Free Brain MRI

Kristen Yeom, MD, Thomas Cullen, *Stanford University, Palo Alto, CA, cullen.tom@gmail.com;* Ufra Yousaf, Andreas Loening, Valentina Taviani, Michael Iv, Shreyas Vasanawala, MD/PhD

Disclosures: Shreyas Vasanawala has indicated a relationship with Arterys, stock/consultant and GE Healthcare, research collaboration. All other authors have disclosed no financial interests, arrangements or affiliations in the context of this activity.
Purpose or Case Report: Evaluation for hydrocephlaus and ventricular catheter placement is increasingly being performed with MRI to avoid ionizing radiation, particularly in patients who require serial imaging. Currently, fast pediatric brain MRI with conventional single shot fast spin echo (SSFSE) is limited by patient motion, relatively long scan times, poor signal to noise ratio, and reduced sensitivity to small lesions and blood products. The purpose of this study was to determine whether variable refocusing flip angles in single shot fast spin echo (vrfSSFSE) pediatric brain MRI can improve image quality, reduce interslice motion artifacts, and decrease scan times over conventional SSFSE.

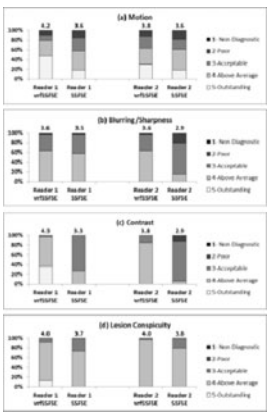

Methods & Materials: The refocusing flip angle train for SSFSE was modulated to minimize energy deposition while minimizing blurring and motion-related signal loss and integrated into our institution's protocol in April 2014. Subjects were scanned on a 3 T MR750 scanner (GE Healthcare, USA) with a receive-only 8-channel brain coil. With IRB approval, we retrospectively identified all children referred for anesthesia-free post-operative brain MRI who had both coronal vrfSSFSE and standard SSFSE. Image quality was scored by two readers independently in blinded, randomized order on four parameters: motion, blurring/sharpness, contrast, and lesion conspicuity on a five-point Likert scale. The distribution of scores for vrfSSFSE and SSFSE by both readers were interpreted by Box Whisker plots. Inter-observer agreements were analyzed.

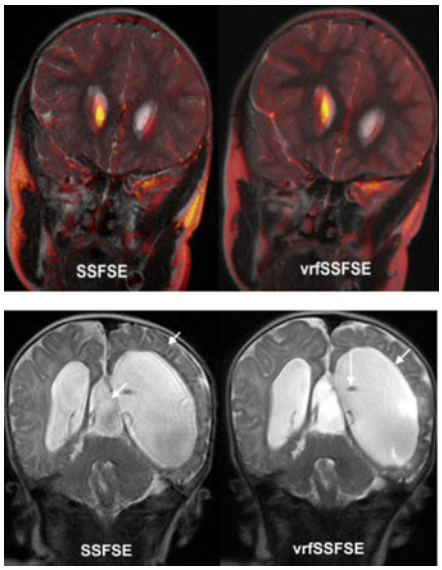

Results: Thirty-three patients with median age 4.9 years were identified. Both readers reported significantly improved contrast and lesion conspicuity with vrfSSFSE ($p<0.01$). One reader reported reduced motion artifacts with vrfSSFSE ($p<0.001$), while the other reader found the same level of motion on both sequences ($p=0.25$). Only one reader found significantly reduced blurring/sharpness with vrfSSFSE ($p<0.79$ for reader 1, $p<0.001$ for reader 2). Regarding scan time, the minimum TR for vfrSSFSE was 543+/-157, producing a nearly two-fold reduction in scan time over conventional SSFSE (TR=1115 +/-383).
Conclusions: Conventional SSFSE enables evaluation of hydrocephalus, ventricular morphology and catheter location without the use of ionizing radiation and sedation. When compared to conventional SSFSE, vrfSSFSE has significantly improved contrast and lesion conspicuity with an approximate two-fold reduction in scan time. vrfSSFE also shows potential in evaluating parenchymal masses and extra-axial collections.

Paper #: 095

Does size really matter? - Role of CT measurement in identification of otherwise normal "dwarf" cochlea in pediatric cochlear implant candidates

Nikita Nanwani, MD, *Topiwala national medical College, Mumbai, India, nikita.nanwani@gmail.com*

Disclosures: All authors have disclosed no financial interests, arrangements or affiliations in the context of this activity.
Purpose or Case Report: **Background:** In children with congenital sensorineural hearing loss (SNHL), a CT scan of the temporal bone is grossly normal to visual inspection in 75% of patients. In these patients,

the hearing loss is often attributed to radiologically undetectable abnormalities of the inner ear. However, subtle malformations like "dwarf" cochlea may be missed because visual inspection alone is insensitive for detection.

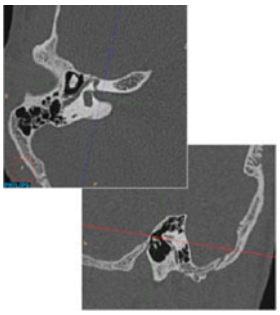

Aims and Objectives: 1. To establish the CT measurements of the normal cochlear height in Indian children
2. To evaluate the cochlear height in children with congenital SNHL who have "normal" findings at HRCT temporal bone
3. To determine radiological criteria of cochlear height correlated with SNHL.
Methods & Materials: Retrospective measurements of cochlear height were made on coronal temporal bone CT scans in a predefined reference plane on 30 ears without SNHL and 30 ears with SNHL having grossly normal temporal bone CT scans. The mean value +/- SD was calculated for both cohorts. Statistical analysis consisted of the nonparametric Wilcoxon rank sum test and Mann Whitney test using SPSS16 software.

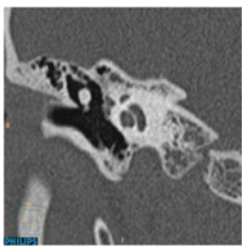

Results: Cochlear height was found to be significantly smaller in the SNHL group (4.16 +/- 0.38 mm) than in the control group (4.55+/- 0.30 mm, $p<0.05$), a size <3.9 mm being highly suggestive of SNHL (specificity-96%; PPV-90%). Dwarf cochlea (<3.9 mm) were identified in 9 ears which were not identified by visual inspection.

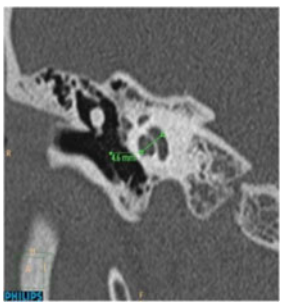

Conclusions: Routine measurement of cochlear height in conjunction with visual inspection of CT images, will increase recognition of dwarf cochlea. This will have an impact on the decision and prognosis of cochlear implant in children with dwarf cochllea.

Paper #: 096

Severe Nasomaxillary Hypoplasia on Prenatal US/MRI: An Important Marker for the Prenatal Diagnosis of Chondrodysplasia Punctata (CDP)

Anna Blask,MD, *Radiology, Children's National Medical Center, Washington, DC, ablask@childrensnational.org;* Eva Rubio, MD, Dorothy Bulas, MD

Disclosures: All authors have disclosed no financial interests, arrangements or affiliations in the context of this activity.
Purpose or Case Report: A new classification for CDP includes various etiologies such as SLE, warfarin and Binder syndrome. Our goal was to review prenatal findings in CDP and identify potential markers that can suggest the diagnosis.
Methods & Materials: A retrospective review of prenatal US and or MRI imaging in CDP between 2007 and 2015. Maternal history, postnatal imaging, phenotype and genetics were correlated with prenatal findings.
Results: 6 CDP cases with prenatal imaging, 9 US and 4 MRI, were identified. GA 19 -32 weeks. 5 had striking nasomaxillary hypoplasia, with small or absent nasal bone and flat or concave facial profile. The 6th fetus had a normal profile with symmetric limb shortening (5th %). A small nose with patent nares was confirmed postnatally in all five (Binder phenotype). Prenatally, 2 of these 5 had normal long bones, 2 had mildly short long bones (5th %) and 1/5 had isolated rhizomelic shortening (<5th %). Radiographs in 4 neonates showed stippled epiphyses, most conspicuous in the hands, feet, cervical and sacral spine, with minimal stippling in the long bones. Only 1 case had stippled epiphyses identified at the knees prenatally. 3/4 neonates had brachytelephalangic CDP with scattered stippling, small triangular distal phalanges of fingers /toes and scattered hypoplastic/broad phalanges, metacarpals and metatarsals by Xray. These hand and foot abnormalities were not well detected prenatally either by US or MR. Spine irregularity was questioned by prenatal US/MR in 2 cases. Postnatally 4 cases were confirmed to have stippled calcifications, cervicothoracic kyphosis and/or narrowing of the spinal canal. Fetal MR was useful in confirming abnormal facial profile and lack of fluid in the anterior nasopharynx in 4/4 MR cases. MR was also useful in demonstrating small fluid filled nostrils (1), small thorax (1), and spinal narrowing and/or kyphosis (2). All 6 cases survived, 2 with mild respiratory distress. CPD was X-linked recessive in 2, brachytelephalangic CPD in 3, and secondary to autoimmune disease in 1 (SLE).
Conclusions: CDP results from a diverse group of etiologies including metabolic, autoimmune and chromosomal and can have a variable outcome. Long bone shortening is not always present and hand/foot anomalies and stippled calcifications may be difficult to identify prenatally. A useful marker is severe midface hypoplasia. When the nose appears absent or severely flattened, CDP should be considered in the differential with close assessment of the spine, hands and feet.

Paper #: 097

Are there calcifications in the parenchyma of solid organs in children with meconium peritonitis?

Pablo Caro Dominguez, Fellow, *Diagnostic Imaging Department, The Hospital for Sick Children, University of Toronto, Toronto, ON, Canada, pablocaro82@hotmail.com;* Augusto Zani, Alan Daneman

Table 1. Surgical findings in the 30 children with meconium peritonitis who were treated surgically

Surgical Finding	Number patients
Idiopathic perforation	8
Ileal atresia	6
Jejunal atresia	5
Volvulus with perforation (no malrotation)	5
Ileal stenosis	1
Anorectal malformation with calcified meconium in the distal pouch	1
Multiple small bowel and colonic atresias	1
Doudenal atresia with trachea-esophageal fistula	1
Esophageal atresia with trachea-esophageal fistula	1
Multiple intestinal atresias with volvulus	1

Disclosures: All authors have disclosed no financial interests, arrangements or affiliations in the context of this activity.
Purpose or Case Report: To investigate if calcifications are present in the parenchyma of solids organs in children with meconium peritonitis.
Methods & Materials: A search of our PACS system in 15 years, between January 1999 and December 2014, revealed 48 children with meconium peritonitis (MP).
The clinical, imaging, medical, surgical and pathology reports were reviewed and the abdominal radiographs, fluoroscopic images and abdominal ultrasound (US) images were re-evaluated by a pediatric radiologist, a pediatric radiology fellow and a pediatric surgery fellow.

Table 2. Imaging findings in 48 children with meconium peritonitis

Imaging findings	Radiograph	Ultrasound	Upper GI	Contrast Enema
Calcification	Diffuse peritoneal	30	25	-
Meconium pseudocyst	8	13	-	-
Intraluminal	6	1	-	-
Parenchyma of solid organs	-	14	-	-
Scrotal	-	3	-	-
Obstruction	Proximal	1	11	-
Distal	9			
Gasless	3			
Free air	2	2	-	-
Ascites	5	5	-	-
Volvulus	-	1	-	1
Duodenal atresia	-	-	1	-
Jejunal atresia	-	-	1	-
Ileal atresia	-	-	-	3
Colonic atresia	-	-	-	1
Meconium Ileus	-	-	-	3

Results: 48 children (33 fetuses, 12 neonates, 3 infants, 26 males/22 females) were diagnosed with MP in this period. 30 children underwent surgery, 16 were managed conservatively and 2 died due to complications of severe prematurity. The surgical findings are detailed in Table 1. Five of them had cystic fibrosis (10%).
Radiographs were performed in 46 children and US in 41. Radiography and US were equally sensitive for the detection of calcifications. They were detected, in 37 of 46 children on radiography (80%) and in 33 of 41 on ultrasound (80%).
Three main types of calcifications were visualized on both abdominal radiographs and US: 1. Nodular or linear, diffuse along the peritoneum (image 1a), 2. Curvilinear, in the wall of a meconium pseudocyst and 3. Round, in the lumen of the bowel.
On US examination, 14 neonates had calcifications in the parenchyma of the solid organs (29%), 13 within the liver, predominantly in the periphery of the lobes (image 1b). One child had calcifications in the spleen and in the adrenals. None of these patients had clinical or laboratory evidence of infection. Imaging findings are detailed in table 2.

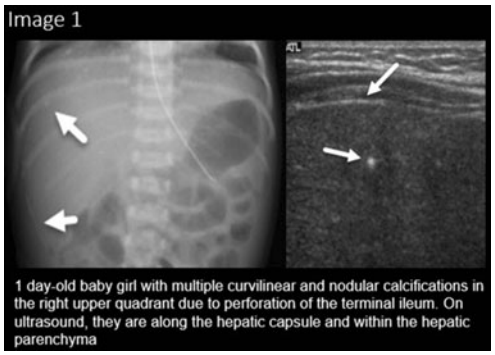

Conclusions: 29% of children who presented with meconium peritonitis in our Hospital in a period of 15 years had calcifications in solid organs (primarily the hepatic parenchyma) on US. The mechanism of intrahepatic calcifications in MP is uncertain, but may relate to intravenous passage of meconium from the bowel to the liver.
Calcifications in the liver should alert pediatric radiologists, surgeons and neonatologists to search for other evidence of meconium peritonitis in fetuses, newborns and infants.

Paper #: 098

Low intralesional T2 signal on fetal MRI: is it pathology-specific?

Ray Somcio, MD, *Pediatric Radiology, Texas Children's Hospital, Sugar Land, TX, rjsomcio@gmail.com;* Christopher Cassady, MD, Amy Mehollin-Ray, M.D., Darrell Cass, Claire Langston

Disclosures: All authors have disclosed no financial interests, arrangements or affiliations in the context of this activity.
Purpose or Case Report: Congenital lung malformations (CLM), a diverse group of anomalies, are increasingly common findings on prenatal screening. The natural history of each type of CLM is different: congenital cystadenomatoid malformation (CCAM) lesions have increased morbidity and a greater potential for surgical intervention compared with bronchial atresia spectrum lesions. Therefore, the ability to differentiate lesions by imaging significantly impacts management. We sought to understand whether low T2 signal inside the lesion had specificity for a pathologic type of CLM.
Methods & Materials: At a large pediatric tertiary-care hospital, we conducted a retrospective review of congenital lung malformations. Inclusion criteria included a prenatal MRI performed from 2002 to 2015, surgical resection, and pathologic diagnosis of the lung malformation. We recorded the MRI characteristics of the lung lesion, fetal

gestational age at time of MRI, and pathological diagnosis. The association of lung lesion signal characteristics with pathological diagnosis was analyzed with Fisher's exact test. Interobserver agreement was calculated using Cohen's kappa coefficient.

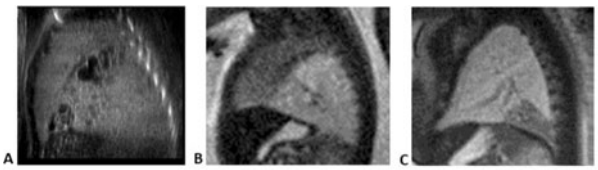

Figure 1. Sagittal images of a patient with segmental bronchial atresia of the left lower lobe. At 25 3/7 weeks gestational age, the lesion is hyperechoic and heterogeneous on ultrasound **(A)** and has high signal on T2-weighted SSFSE MRI **(B)**. At 35 weeks gestational age, the lesion is hypointense relative to normal lung parenchyma on T2-weighted SSFSE MRI **(C)**.

Results: A total of 104 patients with congenital lung lesions met the inclusion criteria. These included 82 primary bronchial atresia spectrum lesions (with or without systemic blood supply) and 42 other congenital lung lesions (CCAM, bronchogenic cyst, congenital lobar overinflation, and neoplasm) without bronchial atresia. Signal hypointense to normal lung on T2-weighted single shot fast spin echo (SSFSE) sequences was significantly more common in bronchial atresia spectrum lesions (20/82 patients, 24%) than lesions without bronchial atresia (1/42 patients, 2.4%) (p=0.002). The interobserver agreement of this signal was near perfect (kappa 0.92). All bronchial atresia spectrum lesions containing low signal were in patients with a gestational age greater than 32 weeks; in cases with multiple fetal MRIs, this finding was seen only after 32 weeks gestational age, indicating that the signal change evolved with time. The signal's overall sensitivity and specificity for bronchial atresia spectrum lesions was 24% and 98%, respectively.
Conclusions: Low signal on T2-weighted SSFSE sequences is a common and specific finding for bronchial atresia spectrum lesions on fetal MRI. In our experience, pure CCAM lesions do not show this finding. This signal characteristic is reassuring and supports a strategy of conservative management.

Paper #: 099

Correlation between maternal breakfast and fetal motion during fetal MRI

Christopher Yen, M.D., *Radiology, Baylor College of Medicine, Houston, TX, cjyen@bcm.edu;* Amy Mehollin-Ray, M.D., Felisa Bernardo, Wei Zhang, Christopher Cassady, MD

Table 1. Categorized questionnaire responses and MR scores

Category	Specific item	Number of patients with MR score:	P-value of Fischer's exact test		
1	2	3			
Beverages	Milk	8	26	5	0.04
Fruit juice	10	15	9	0.59	
Other sweetened	6	10	4	1.00	
Coffee (caffeinated)	8	13	7	0.80	
Soda (caffeinated)	2	2	4	0.14	
Tea	4	3	1	0.63	
Foods	Eggs	17	17	10	0.37
Cheese	14	22	7	0.82	
Meat	21	23	12	0.49	
(continued)					
Sweetened cereals	5	8	3	1.00	
Whole grains	7	16	7	0.54	
Major macronutrients	Protein	28	37	18	0.78
Carbohydrates	58	78	33	0.47	
State	Fat	44	44	23	0.03
	Non-fasting	62	90	39	0.92

Disclosures: All authors have disclosed no financial interests, arrangements or affiliations in the context of this activity.
Purpose or Case Report: Although ultrafast magnetic resonance imaging (MRI) sequences have significantly reduced scan time, motion of the fetus remains a major limitation in the diagnostic capability of fetal MRI. Based on anecdotal experience, some imaging centers have required mothers to fast prior to fetal MRI studies in an effort to reduce motion; however, there is no current literature that describes the effect of maternal diet on fetal activity. The objective of this study is to define associations between specific foods and beverages consumed prior to a fetal MRI study and the severity of fetal motion during the study.
Methods & Materials: As part of the check-in process on the morning of a scheduled MRI, patients were asked to recall the specific foods or drinks they had, if any, prior to arrival. A technologist with 9 years of fetal experience, blinded to the survey responses, then performed the MRI, at which time she rated the level of fetal activity (MR score) on a 3-point scale, in which: 1=much less motion than normal, 2=normal fetal motion, and 3=much more motion than normal. A total of 228 patient encounters from 9/2013 to 5/2015 were included in the study. Data was statistically analyzed using a Fisher's exact test using 2×3 contingency tables with p-values less than 0.05 considered significant.
Results: Questionnaire responses were categorized into beverages, foods, major macronutrient groups, and fasting/non-fasting. For example, a response of "sausage and biscuit with coffee" would count toward the items of coffee, meat, protein, carbohydrates, and fat. Statistical analysis compared an item to its complement (coffee drinkers vs. non coffee-drinkers). There were only two statistically significant associations - more patients who received an MR score of 2 consumed milk (p=0.04), and more patients who received an MR score of 1 had high fat in their meal (p=0.03). Otherwise, statistical analysis demonstrated that MR scores were not significantly affected by fasting state or any specific beverage or food (Table 1).
Conclusions: No specific food, beverage, or macronutrient was associated with a significant increase in fetal motion in this pilot study, although high-fat meals may correlate with decreased fetal motion. Additionally, fasting did not have a significant effect on fetal motion. Thus, for the purpose of minimizing fetal activity, it seems unnecessary for mothers to fast or avoid any specific foods or beverages (such as those containing caffeine or sugar) the day of an MRI study.

Paper #: 100

Derangement of the knee in patients with congenital longitudinal deficiencies of the lower limbs: MR findings

Maria Perez, Clinical Fellow, *Diagnostic Imaging, Hospital For Sick Kids, Toronto, ON, Canada, manuela.perez@sickkids.ca;* Simon Kelley, Jennifer Stimec

Disclosures: All authors have disclosed no financial interests, arrangements or affiliations in the context of this activity.
Purpose or Case Report: The purpose of this study was to present our experience with knee MR in patients with congental longitudinal deficiencies of the lower limbs (CLD), and to define and review the

osteochondral and extraosseous dysplastic changes that occur in the knee. Our hypothesis were that: (1) the patients with congenital longitudinal deficiencies of the lower limb invariably have associated defects of the osteochondral and/or soft tissues of the knee; (2) the changes vary and may not relate to the severity of the primary deficit.

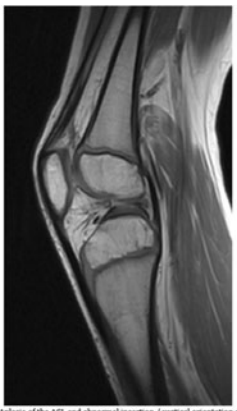

Figure 1: Aplasia of the ACL and abnormal insertion / vertical orientation of the PCL on a patient with PFFD. Sag PD.

Methods & Materials: We retrospectively reviewed the MR examinations of a group of children with varying types of CLD, including proximal focal femoral deficiency (PFFD), fibular hemimelia (FH) and tibial hemimelia (TH). We classified the primary deficits according to the pertinent classifications based on MR, and then registered the osseous and extraosseous knee findings, as well as the presence of other associated anomalies in the lower limbs. To asess for a relationship between the variables, we calculated the Pearson correlation coefficient.

Results: There were a total of 16 patients with CLD and MRI of the ipsilateral knee joint. Bilateral involvement in 3 patients yielded a total of 19 knees. The mean age at the time of the scan was 5 years 6 months (range 8 months to 14 years). 7 patients were male and 9 female.

Predominant fibular hemimelia was found in 5 patients and predominant PFFD in 9. There were 2 cases of tibial hemimelia. Shortening of the extremity varied according to the type of deficiency and age and ranged between 2 and 25 cm. The imaging findings related to the knee are documented in table 1.

Knee abnormalities were seen in all patients, with the most frequently affected extraosseous structure being the cruciate ligaments, which presented some degree of dysplasia in all patients. The most common associated osseous finding were varying degrees of shortening of other long bones and dysplastic distal femoral changes. The Pearson correlation coefficient was 0 in all categories, indicating no linear relationship between the severity of the primary deficit and the degree of the dysplastic knee changes.

Conclusions: Our experience indicates that all of the patients with CLD have associated abnormalities of the knee, and that this changes vary and are not strictly related to the severity of the primary deficit. Thus, imaging of the knee is recommended for guiding the ongoing orthopaedic management.

Nr	Diagnosis	Classif*	Osseous**	ACL	PCL	Ant tibial translation	Meniscus	Med Coret	Lat coret ***	BF tendon****	Extensor mechanism
1	FH	1b	2	Absent	Absent	No	Normal	Normal	2a	2a	Unremarkable
2	FH	2	2, 3	Absent	Vertical	Yes - 9 mm	Lat tear	Normal	2b	2b	Unremarkable
3	FH	2	2	Absent	Absent	Yes - 7 mm	Lat hypo	Normal	2a	2a	Unremarkable
4	FH	2	2,3	Absent	Vertical	No	Normal	Normal	2b	2b	Unremarkable
5	FH	2	2	Absent	Vertical	No	Normal	Normal	Absent	Absent	Unremarkable
6	PFFD	1	2	Absent	Absent	No	Normal	Normal	1	1	Absent
7	PFFD	1	2	Absent	Absent	No	Absent	Normal	1	1	Unremarkable
8	PFFD	2	1	Absent	Normal	No	Absent	Normal	1	1	Unremarkable
9	PFFD	2	2	Absent	Absent	No	Normal	Normal	1	1	Dislocation
10	PFFD	2	2	Absent	Absent	NA	Normal	Normal	1	1	Unremarkable
11	PFFD	3	2	Hypoplastic	Hypoplastic	Yes - 7mm	Normal	Normal	1	1	Unremarkable
12	PFFD	3	2	Absent	Absent	Yes	Normal	Normal	1	1	Unremarkable
13	PFFD	3	2	Absent	Absent	Yes	Normal	Normal	1	1	Unremarkable
14	PFFD	4	2	Absent	Normal	No	Discoid medial	Normal	1	1	Unremarkable
15	TH	1	1	Absent	Absent	NA	NA	NA	NA	1	Absent
16	TH	1	2	Absent	Absent	NA	NA	NA	NA	NA	Absent

* As per Achterman and Kalamchi in FH. Amputa in PFFD and Kamlamchi y Dawe for TH.
** 1 normal, 2 dysplastic changes, 3 OCD
*** 1 normal, 2 abnormal; a: joins BF tendon and tracks into leg, b: inserts in tibia
**** 1 normal, 2 abnormal; a: joins LCL and tracks into leg, b: inserts in tibia
NA: Not asessable

Table 1: Summary of osseous and extraosseous findings asessed around the knee.

Paper #: 101

Ultra-High Resolution Imaging of Utero-Placental Vasculature in a Rodent Model of Pregnancy

Zbigniew Starosolski, PhD, *Pediatric Radiology, Texas Children's Hospital, Houston, TX, zastaros@texaschildrenshospital.org;* Ketan Ghaghada, PhD, Haijun Gao, Igor Stupin, Saakshi Bhayana, Chandresh Patel, Chandrasekhar Yallampalli, Ananth Annapragada, Ph.D.

Disclosures: Zbigniew Starosolski has indicated a relationship with Alzeca Biosciences, LLC. All other authors have disclosed no financial interests, arrangements or affiliations in the context of this activity.

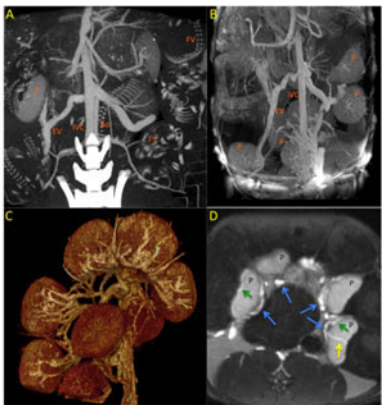

Figure 1. Ultra-high resolution imaging of maternal and utero-placental vasculature. (A) Coronal thick slab maximum intensity project (MIP) CT image demonstrating major maternal vessels including inferior vena cava (IVC), descending aorta (Ao), endometrial vessel (EV). The highly perfused placenta (P) is visualized as a uniformly opacified organ. In addition, the fetal vertebrate (FV) and skull (FS) are also demonstrated in the CT image. (B) Coronal MIP-MRA demonstrating similar details of maternal and placental vasculature along with multiple placentas (P). (C) 3D volume-rendered segmented CT image demonstrating the extensive vasculature architecture associated with multiple placentas. (D) Axial thick islab MIP-MR image demonstrating visualization the central vessel (yellow arrow) running through one of the placentas (P). Labyrinth vessels (green arrows) and maternal vessels (blue arrows) are also visible.

Purpose or Case Report: Non-invasive imaging of maternal and placental vasculature in rodent species is of interest to the pre-clinical study of clinically-relevant placental pathologies. In this work, we investigated the utility of high-resolution MR angiography (MRA) and CT angiography (CTA) acquired using placental non-permeable, long circulating blood-pool liposomal contrast agents in a pregnant rat model.

Methods & Materials: In vivo imaging studies were performed in Sprague Dawley rats under a protocol approved by the institutional animal care and use committee. 11-13 week old pregnant rats were used in the study. Imaging was performed between day 18 and day 21 of gestation. Ultra-high resolution CTA (36 μm isotropic resolution) was performed on a micro-CT scanner using the following scan parameters: 80 kVp, 0.5 mA, 360 projections, 850 ms X-ray exposure, 15 min scan time. CTA was performed using a long circulating liposomal-iodine contrast agent (110 mg I/mL) administered as an intravenous infusion via the tail vein at an iodine dose of 2.2 mg/g. MRA studies were performed on a 1 T permanent MRI scanner following administration of a liposomal-Gd contrast agent (0.2 mmol Gd/kg). A low field MR magnet was chosen since the liposomal-Gd agent has optimal T1 relaxivity (200, 000 $mM^{-1}.sec^{-1}$) at low field strength. MR images were acquired using a 3D-GRE sequence with the following scan parameters: TE=4 ms; TR=20 ms; flip angle: 50; Slice thickness: 0.5 mm, in-plane resolution=237 μm; NEX=4.

Results: The long circulating property of the liposomal contrast agent enabled exquisite visualization of maternal and placental vasculature (Fig 1A & B). Both the arterial and venous structures were visible including the endometrial vessels, uterine vessels and the central canal (Fig 1C & D). Furthermore, the inability of the liposomal agent to penetrate the placental barrier enabled selective visualization of the utero-placental circulation (Fig 1C & D).

Conclusions: The current study demonstrates the use of blood-pool liposomal contrast agents for interrogation of utero-placental vasculature.

Such non-invasive imaging techniques could greatly aid in the study of placental pathologies.

Paper #: 102

In vivo Profiling of Folate Receptor Expression in Rat Placenta Using MR Molecular Imaging

Ketan Ghaghada, PhD, *Texas Children's Hospital, Houston, TX, kbghagha@texaschildrens.org;* Zbigniew Starosolski, PhD, eric tanifum, Haijun Gao, Igor Stupin, Saakshi Bhayana, Chandresh Patel, Chandrasekhar Yallampalli, Ananth Annapragada, Ph.D.

Disclosures: Zbigniew Starosolski has indicated a relationship with Alzeca Biosciences, LLC. All other authors have disclosed no financial interests, arrangements or affiliations in the context of this activity.
Purpose or Case Report: Non-invasive imaging techniques for profiling the expression levels of placental vascular receptors are of interest in the study of fetal programming. In this work, we investigated the feasibility of a high T1 relaxivity nanoparticle Gd contrast agent (200,000 $mM^{-1}.sec^{-1}$) for MR molecular imaging of placenta. A folate-targeted liposomal-Gd contrast agent was fabricated and evaluated in vivo for MRI-based profiling of folate receptor (FR) expression in rat placenta.
Methods & Materials: Liposomal-Gd nanoparticles presenting folic acid ligands were fabricated. The liposomes were labeled with indocyanine green (ICG) to facilitate near-infrared (NIR) imaging. In vivo MRI studies were performed in pregnant rats under a protocol approved by the institutional animal care and use committee. Animals were divided into two groups: Group 1 animals were fed a normal diet (20% Casein) whereas Group 2 animals were fed a low-protein (6% Casein) diet throughout pregnancy. Imaging was performed on a 1 T permanent magnet using a T1w 3D-GRE. On E18.5 days, a pre-contrast scan was performed followed by i.v. administration of the targeted liposomal-Gd (0.15 mmol Gd/kg). Post-contrast scan were acquired immediately and at 72 h (E21.5 days) after administration of contrast agent. Subsequently, the animals were sacrificed, placentae extracted and imaged on NIR imaging system for ex vivo confirmation of folate receptor targeting.
Results: In both groups, MR images acquired at 72 h post-administration of targeted liposomal-Gd demonstrated higher signal intensity in the placenta compared to pre-contrast images. Rats fed a low protein diet demonstrated higher inter-placental variability in signal intensity compared to rats fed a normal diet, suggesting variability in FR expression. NIR imaging corroborated the MRI results, demonstrating the localization of folate-targeted liposomal-Gd in the placenta and inter-placental variability in FR distribution. In both the imaging techniques, the normal diet placentae had uniform distribution of the FR throughout the placenta, while the low protein placentae exhibited a preferential distribution towards the maternal decidua and the junction zone of the placenta.

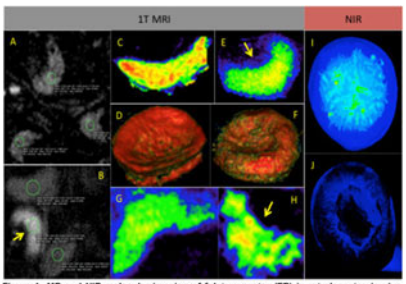

Figure 1. ***MR and NIR molecular imaging of folate receptor (FR) in rat placentae in vivo.*** Animals were injected with FR-targeted Liposomal-Gd on E18.5, and imaged by T1-MR at 1T, (where the relaxivity of the agent is maximal) at one hour and 72 hours post injection. (A) Rats fed normal diet have uniformly weak FR signal in placentae at E21.5 (B) Rats fed a low protein diet have much higher FR signal in some placentae (arrow). (C) and (D): Blood pool in placentae of low protein diet rats is heterogeneous and crescent shaped while (E) and (F): the FR is localized in a toroidal (donut) shape, away from the placental labyrinth (arrow in E). In contrast, the blood pool (G) and FR (H) in normal diet rats are uniform and practically co-distributed. Preferential distribution of the FR in low protein rats towards the maternal decidua is confirmed by ex vivo NIR images. The maternal decidual face (I) shows significant ICG signal while the fetal labyrinth face (J) shows very little.

Conclusions: This study demonstrates the profiling of receptor expression levels and receptor distribution in a rodent placenta using a molecularly targeted liposomal-Gd agent at low (1 T) field strength. To our knowledge this is the first demonstration of molecular imaging in the placenta without radioactive elements.

Paper #: 103

T1 weighted MRI of the fetus using 3D mDixon gradient echo.

Logan Dance, Patricia Cornejo, Amber Pokorney, Deepa R. Biyyam, Tuan Doa, Tammam Beydoun, Brian P. Keehn, Michael Peterson, Dianna M. Bardo, Mittun Patel.

Disclosures: All authors have disclosed no financial interests, arrangements or affiliations in the context of this activity.
Purpose or Case Report: The purpose of this poster is to demonstrate the clinical utility and superior image quality of the 3D mDixon gradient echo (GRE) sequence for fetal imaging. 3D mDIXON GRE when compared to eTHRIVE gradient echo sequence has a faster acquisition time with similar spatial resolution and improved fat saturation, characteristics which are ideal for imaging the moving fetus.
Methods & Materials: 9 fetal MRI examinations were performed utilizing both 3D mDIXON GRE and eTHRIVE to obtain T1 weighted images. Matching single best image of the rectum for both 3D mDIXON GRE and eTHRIVE were used for a direct side-by-side comparison. Using a four point scale with 1 being poor, 2 being fair, 3 being good and 4 being excellent, six pediatric radiologists rated the images in four categories: motion artifact, detail, contrast, and fat suppression. Reviewers then chose the image they preferred for each of the categories. Finally reviewers selected which image demonstrated the best overall image quality. The radiologists were blinded to which sequence they were rating. Select images will be shown to illustrate the clinical utility of 3D mDIXON GRE sequence.
Results: Reviewers clearly preferred mDIXON- GRE compared to eTHRIVE for all categories. For motion artifact, mDIXON- GRE sequence had a mean rating 2.67 and eTHRIVE sequence had a mean rating of 1.69, P value of<0.01. A total of 53 preferred mDixon over 1 for eThrive. For detail, mDIXON- GRE sequence had a mean rating 2.85 and eTHRIVE sequence had a mean rating of 1.7, P value of<0.01. A total of 52 preferred mDixon over 2 for eThrive. For contrast, mDIXON- GRE sequence had a mean rating 2.93 and eTHRIVE sequence had a mean rating of 1.91, P value of<0.01. A total of 53 preferred mDixon over 1 for eThrive. For fat suppression, mDIXON- GRE sequence had a mean rating 3.13 and eTHRIVE sequence had a mean rating of 2.04, P value of<0.01. A total of 53 preferred mDixon over 1 for eThrive. For overall image quality, mDIXON- GRE sequence was preferred 53 times and eTHRIVE sequence was preferred 1 time.
Conclusions: mDIXON- GRE sequence allows for high quality images to be obtained with a faster acquisition time, resulting in decreasing fetal motion artifact. Compared to our traditional eTHRIVE sequence, mDIXON- GRE sequence is both superior to and preferred over eTHRIVE sequence in fetal imaging.

Paper #: 104

Fetal Coloboma and its Associations

Alexis Rothenberg Maddocks, MD, *Radiology, The Children's Hospital of Philadelphia, Bryn Mawr, PA, Alexis.Rothenberg@gmail.com;* Beverly Coleman, Teresa Victoria, MD, PhD, Avrum Pollock, Tamara Feygin

Disclosures: All authors have disclosed no financial interests, arrangements or affiliations in the context of this activity.
Purpose or Case Report: Vitreous coloboma may present as an isolated finding or may be associated with an underlying systemic disorder. The purposes of this study include: 1. Description of fetal imaging appearance

of coloboma. 2. Assessment of spectrum of congenital disorders associated with fetal coloboma.

Methods & Materials: With IRB approval, retrospective selection of fetal orbital colobomata was performed using keywords "coloboma", "fetal". Cases were selected from fetal ultrasound and fetal MR imaging performed at our institution from 2008 to 2015 for suspected fetal anomalies on obstetric ultrasound. Available imaging in the selected cases was independently reviewed by 3 neuroradiologists, and 1 senior sonographer.

Results: Evaluation of MRI/US examinations and patient's charts revealed 11 patients with confirmed vitreous coloboma. Coloboma was diagnosed during work up of suspected fetal central nervous system anomalies. The indications for imaging were hydrocephalus, facial clefts or multiple congenital anomalies. The gestational age at the time of imaging was between 18 and and 30 weeks. The lesion appeared as a focal defect within the posterior globe resulting in outpouching of the vitreous fluid. Coloboma was bilateral in 2 cases and unilateral in 9. All colobomas were equally seen on fetal MRI and ultrasound. No single case of isolated coloboma was evident in our study. All cases were associated with a variety of underlying syndromes, including 3 cases of PHACES, 2 cases of CHARGE, 2 cases of Walker-Warburg, 2 cases of Aicardi, 1 case of Wolf- Hirschhorn syndromes and 1 case of unclassified multiple congenital anomalies.

Conclusions: Although identification of fetal coloboma during prenatal imaging is considered to be an unusual occurrence, it indicates a high potential for underlying systemic disorder. Presence of this lesion behooves careful search for associated birth defects arising simultaneously or those sharing the same progenitor cell.

Paper #: 105

Diagnostic Accuracy of Micro-CT for Fetal Heart Dissection (Comparison of Imaging To Autopsy)

J. Hutchinson, MRes MBBS, *Histopathology, Great Ormond Street Hospital, London, United Kingdom, ciaran.hutchinson@nhs.net;* Michael Ashworth, Andrew Ramsey, Will Mifsud, Claudio Lombardi, Neil Sebire, Owen Arthurs, FRCR, PhD

Disclosures: All authors have disclosed no financial interests, arrangements or affiliations in the context of this activity.

		Autopsy		Totals	
		POSITIVE (Abnormal)	NEGATIVE (Normal)	*n*	% (95% CI)
μCT	POSITIVE (Abnormal)	23	1	26 (20.6%)	PPV= 95.8 (79.8, 99.3)
μCT	NEGATIVE (Normal)	4	91	98 (77.8%)	NPV= 95.8 (89.7, 98.4)
TOTALn		27 (21.4%)	94 (74.6%)	126 (100%)	
		Sens 85.2 (67.5, 94.1)	Spec 98.9 (94.1, 99.8)	Agree=95.8 (90.5, 98.2)	

Purpose or Case Report: Congenital heart disease is common at perinatal autopsy; severe forms may be an indication for termination of pregnancy. Earlier terminations, smaller fetuses, maceration and imaging effects of feticide and poor post mortem MRI at low body weight / early gestation result in accurate diagnosis becoming increasingly challenging. Micro-CT can provide high resolution images (up to 3 μm) and has been used to non-invasively phenotype animal models of congenital heart disease. To date, it has not been systematically compared with fetal autopsy for diagnostic accuracy in humans. We hypothesised that micro-CT could provide useful diagnostic information in fetal congenital heart disease and compared it with the gold standard of autopsy.

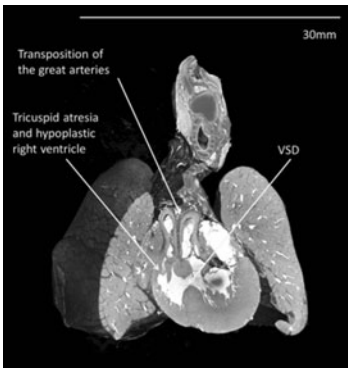

Methods & Materials: Six ex-vivo fetal hearts (17 - 23 weeks gestation; weight 1.1 g - 5.3 g) underwent micro-CT examination as part of an ethically approved research study. 21 indices to include atria, ventricles, outflow tracts, and coronary vasculature were evaluated for each case at both micro-CT and autopsy in a single-blinded fashion.

Results: All micro-CT scans provided excellent internal contrast. The correct overall diagnosis was made from micro-CT data in all cases. Overall agreement between micro-CT imaging and dissection was 114/119 (95.8 concordance (95%CI: 90.5, 98.2)), with only 7/126 indices that were classed as non-diagnostic at dissection or micro-CT examination. In this study, micro-CT had sensitivity of 85.2% (95%CI: 67.5, 94.1) and specificity of 98.9% (95%CI: 94.1, 99.8). Micro-CT was particularly useful at evaluating the myocardium when this was non-diagnostic at autopsy due to maceration.

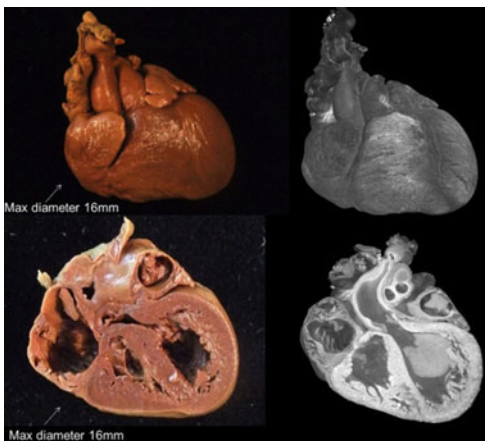

Conclusions: Micro-CT provides highly accurate early fetal diagnosis of complex congenital fetal heart disease at post mortem. This represents a significant advance in post-mortem imaging in early gestation fetuses.. Future studies should expand to include in-vivo postmortem evaluation and double-blinded comparison.

Paper #: 106

Prenatal Intestinal Volvulus About A Serie Of 12 Cases: The Snail Sign On Fetal Mri The Diagnosic Clue In 9 Cases

Olivier Prodhomme, MD, *Pediatric Radiology, Arnaud de Villeneuve Hospital, Montpellier, France, o-prodhomme@chu-montpellier.fr;* Magali Saguintaah, Jean-Michel Faure, Dominique Forgues, Catherine Baud, Julie Bolivar Perrin, Stephanie David, ikram taleb arrada, Alain Couture

Disclosures: All authors have disclosed no financial interests, arrangements or affiliations in the context of this activity.
Purpose or Case Report: To present 12 cases of fetal intestinal volvulus and their outcome. To discuss their etiologies. To describe a specific sign of volvulus on MRI. To discuss the contribution of MRI to the diagnosis and prognosis in comparison with ultrasonography.
Methods & Materials: Between 2006 and 2015, 12 cases of fetal intestinal volvulus were diagnosed in our institution. Inclusion criteria were a final diagnosis of fetal intestinal volvulus with correlation with both prenatal imaging (ultrasound and MRI). We retrospectively studied their clinical, ultrasonographic and MRI data. MRI was performed on a 1.5 T device with T1- and T2-weighted sequences in axial, coronal and sagittal planes.
Results: The term of diagnosis ranged from 22 to 33 weeks of gestation: 22WG (n=1), 26-29WG (n=5) and 31-33WG (n=6). The main clinical abnormality was a decrease in fetal mobility (n=8).
The volvulus was diagnosed on ultrasound in 4 cases by showing the whirlpool sign. It was suspected in 1 (bowel distension with hydrohydric level, ascitis). A hydrohydric level was recognized afterwards in 5 more cases.
The diagnosis was established on MRI in 10 cases, with:
- Snail sign in 9 cases: direct visualization of spiraled bowel loops, at best in coronal plane and on T1-W sequence (meconial hyper T1-W signal content)
- Hydrohydric level: n=4
Only one case was not diagnosed by prenatal imaging, neither prospectively nor retrospectively.
In all cases MRI allowed to evaluate the amount of normal bowel loops, not involved in the volvulus.
Associated abnormalities included: laparoschisis (n=1), cystic fibrosis (n=2), small bowel atresia (n=5), localized mesenteric fusion (n=2, in 2 twins). No midgut malrotation was present.
Two cases resolved spontaneously prenatally (after MRI (n=1), before MRI (n=1)). The outcome was favorable in 5 after neonatal surgery. One newborn died shortly after birth because of an associated huge meconial pseudocyst compromising the ventilation. Tow fetuses with cystic fibrosis were interrupted. The volvulus was confirmed in 9 cases by surgery or foetopathology.
Conclusions: Fetal intestinal volvulus is a rare pathology. MRI is a reliable tool for its diagnosis, allowing deciding the follow-up and the management. The snail sign is often present in our series and easy to assess. MRI helps to determine the amount of normal bowel and thereby the evaluation of prognosis. The prognosis seems good when the volvulus is segmental and without association with cystic fibrosis.

Paper #: 107
Training the Pediatric Interventional Radiologist

Claire Kaufman, MD, *Department of Radiology and Biomedical Imaging, Yale New Haven Hospital, New Haven, CT, claire.kaufman@gmail.com;* Charles James, MD, Roger Harned, MD, Derek Roebuck, Anne Marie Cahill, Bairbre Connolly, Josée Dubois, MD, Frank Morello, Robin Kaye, Manrita Sidhu

Disclosures: All authors have disclosed no financial interests, arrangements or affiliations in the context of this activity.

Training Type	Percent Completed
Radiology residency	97%
Pediatric radiology fellowship	40%
PIR fellowship	24%
Adult IR fellowship	63%
Pediatric residency	10%
Pediatric neuroradiology fellowship	4%
Adult neuroradiology fellowship	6%
Surgery residency	22%
Diagnostic (body) radiology fellowship	5%
Other	11%

Purpose or Case Report: Currently there is no standardized training pathway for pediatric interventional radiology (PIR). As a specialty it is unique from both pediatric diagnostic radiology and adult interventional radiology. The purpose of our study was to evaluate the present state of PIR training prior to the upcoming changes in interventional radiology training.
Methods & Materials: A 2-part online survey was sent to members of SPIR, SPR, SCORCH, and SIR. The first part was completed by all individuals and contained questions regarding training, certification, service coverage, and thoughts on the new IR residency. The second part focused on practice trends and was completed by one designated group leader. This included topics such as infrastructure, hiring, and service coverage.

Impact of new IR Residency on PIR	Number Individuals
Potentially increased training opportunities	41
Potentially decreased training opportunities	37
Increased awareness of PIR	46
Decreased awareness of PIR	33
Increased intereste in training in PIR	28
Decreased interest in training in PIR	32
Other	45

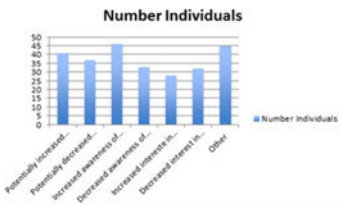

Results: There were 177 individual responses: 91 from SPIR, SPR, and SCORCH, and 86 from SIR. There were 88 service sites represented with 50 responses from SPIR, SPR, and SCORCH, and 38 responses from SIR. The majority of the responses were from the US (73%), with other countries represented including Canada, the UK, and Australia among to name a few. The majority (97%) of practitioners completed a radiology residency. Forty percent completed a pediatric radiology fellowship, 24% a pediatric IR fellowship, and 63% an adult IR fellowship (Table 1). The majority (80%) of respondents participated in teaching as part of their practice. Sedation can be a challenge for pediatric interventionalists. Only 38% (n=67) of individuals were taught how to administer pediatric sedation in their training. Subsequently only 37% (n=66) are currently PALS certified. Delivering bad news to families can be very difficult especially when dealing with children. Only 41% (n=71) practitioners have received formal training on how to deliver bad news to families. Despite this 69% (n=123) feel comfortable delivering bad news most of the time. Thirty five percent of respondents from the US feel that the new IR residency will be good for PIR while 28% are concerned it will be bad for PIR. The remainder is unsure of the effect the new residency will have. There were mixed responses explaining the impact of the new residency on PIR (Table 2, Graph 1).

Conclusions: There is no standard training pathway to pediatric interventional radiology. Training varies depending on the individual pathway to pediatric IR, and institution.

Paper #: 108

Case Controlled Analysis of Utility of Ultrasound Guidance during Bone Biopsies

Allen Acomb, MD, *Pediatric Radiology, Texas Children's Hospital, Houston, TX, adacomb@texaschildrens.org;* J. Kan, MD, Jose Hernandez, MD, Wei Zhang

Disclosures: All authors have disclosed no financial interests, arrangements or affiliations in the context of this activity.
Purpose or Case Report: Pediatric musculoskeletal bone tumors are frequently referred to our department for image guided biopsy for definitive pathologic diagnosis. Fluoroscopy and CT are conventional methods used for image guided biopsies. To our knowledge, the use of sonography to facilitate biopsy has not been evaluated. The purpose of this study is to determine utility of using sonographic guided bone biopsies as an adjunct to fluoroscopic and CT image guidance.

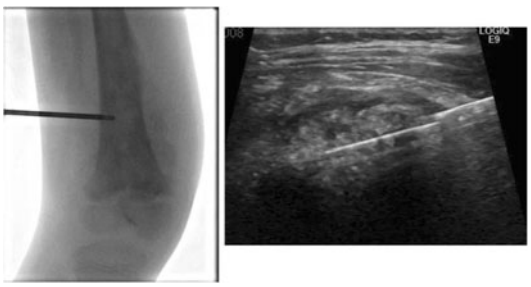

Methods & Materials: A case control retrospective analysis was obtained of all patients that underwent percutaneous bone biopsy from 9/25/13 to 9/24/15 using the keywords "bone biopsy". The study group (*N*=23, 69.5% male, mean age: 11 years) included all cases that had use of US for needle placement. The control group (*N*=26, 61.5% male mean age: 11 years) included cases that did not use US for needle placement. Procedural images and reports and pathology and clinical notes were reviewed. Data points consisted of demographics, sedation time, % of ultrasound guided biopsies requiring additional fluoroscopy or CT, fluoroscopy time, number of CT acquisitions, number of cases requiring repeat or open biopsy for definitive pathologic diagnosis and complication rate. Patients were categorized as neoplastic (e.g. any sarcoma or benign but locally recurring process such as an ABC) or benign (e.g. enchondroma).
Results: For the study population, 22 (95.8%) were neoplastic (top diagnosis osteosarcoma, *N*=8) and 1 benign. The control population, 19 (73.1%) were neoplastic (top diagnosis LCH, *N*=5), and 7 were benign (26.9%). For the study population, 17/23 (74%) ultrasound guided procedures required additional fluoroscopy *N*=12 (52.2%) or CT *N*=5 (21.7%). 6/23 (26.1%) biopsies were performed under ultrasound guidance alone. For study compared with control, average fluoroscopy time was lower (0.48 vs 3.7 min, *P*=0.0008), number of CT passes was lower (5.8 vs 10.5, *P*=0.05) and sedation time (77.6 vs 72.9 min, *P*=0.05) was higher. For all sarcomas in the study group, 3/10 (30%) were amenable to US guided biopsy alone; however, 1 required repeat biopsy for definitive diagnosis. For LCH cases in the study group, 1/4 (25%) were performed with US alone. The need for operative diagnosis or repeat biopsy for study and control group was similar (3/23 (13%) vs 2/26 (7.7%), *P*=0.655).
Conclusions: Percutaneous ultrasound guided biopsy in combination with either CT or fluoroscopy or used alone is safe and results in decreased radiation and minimal increase in the length of sedation.

Paper #: 109

Evaluation of MR Overlay on live fluoroscopy for pediatric percutaneous extremity biopsies of exclusively MR visible bone lesions in the Interventional Radiology suite

Sphoorti Shellikeri, Master's in Biomedical Engineering, *Radiology, Children's Hospital of Philadelphia, Philadelphia, PA, sphoortishellikeri@gmail.com;* Xiaowei Zhu, Randolph Setser, Ganesh Krishnamurthy, MD, DNB, Maricarmen Nazario, Marc Keller, M.D., Abhay Srinivasan, Seth Vatsky, Anne Marie Cahill

Disclosures: Randolph Setser, has indicated a relationship with Siemens Healthcare as an employee. All other authors have disclosed no financial interests, arrangements or affiliations in the context of this activity.

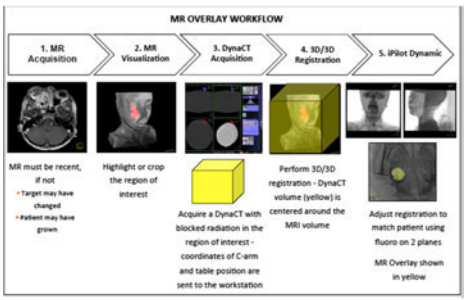

Purpose or Case Report: Bone marrow abnormalities are best visualized on MRI rather than CT/fluoroscopy. However, bone biopsy procedures are typically performed using conventional CT or more recently C-arm CT guidance. Lesions only visible on MRI require the operator to correlate with MRI images separately during the biopsy. This study describes our experience with a 3D MRI overlay technique on 2D fluoroscopy in the Interventional Radiology (IR) suite during pediatric percutaneous extremity bone biopsies of lesions that are only visible on MRI.
Methods & Materials: Pediatric patients presenting with extremity bone lesions, exclusively visible on MRI, from 2013 to 2015 were included in this IRB-approved prospective study. A C-arm CT is acquired without radiation at the beginning of each procedure and registered to a recent pre-procedural MRI using *syngo* InSpace 3D/3D fusion (Siemens) on a dedicated workstation. This sends the geometric coordinates of the C-arm and table position to the workstation. Final accurate registration is performed and the MRI is overlaid onto intraprocedural 2D fluoroscopy using *syngo* iPilot Dynamic (Siemens).
Mean procedure and fluoroscopic times were recorded. Effective radiation dose was estimated using PCXMC software (v2.0.1.3, Finland) with an age appropriate model and study specific techniques including kVp and DAP.

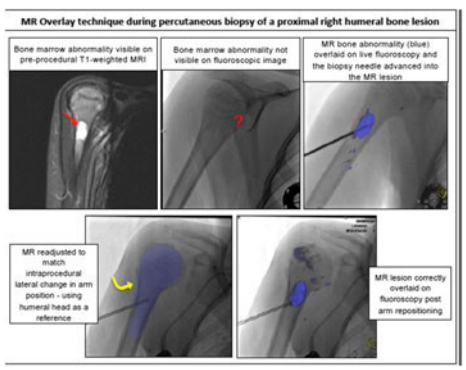

Results: Nine patients (6 F/3 M; mean age: 8 years) underwent MR Overlay assisted bone biopsies. All biopsies were diagnostic (4 neuroblastoma, 1 acute lymphoid leukemia, 1 osteomyelitis, 1 rhabdomyosarcoma, 1 healing fracture, 1 negative for leukemia and infection). The mean time interval between pre-procedural MRI and the intervention was 8 days. The mean procedure and fluoroscopic times were 68 ±39 min and 9±8 min. The mean effective radiation dose was 0.04 ±0.07 mSv (range: 0.00016-0.23 mSv). Minimal dose from an AP and lateral X-ray image was added during the final accurate registration.
MR Overlay was feasible even if the extremity was in a different orientation on the acquired MR than during the intervention. Further, any intraprocedural movement in patient's anatomy due to pressure from needle advancement could easily be adjusted for using iPilot Dynamic software.
Conclusions: In our experience 3D MRI Overlay on 2D intra-procedural fluoroscopy provides diagnostic pediatric bone biopsies of lesions exclusively visible on MRI, with low radiation dose in the IR suite. The use of this technology was not limited by intra-procedural changes in anatomic positioning of the biopsy site.

Paper #: 110

Diffusion Tensor Imaging in Pediatric Renal Transplants: Testing A Potential Non-Invasive Alternative to Biopsy

Yi Li, MD, *UCSF, San Francisco, CA, yi.li@ucsf.edu;* Marsha Lee, Pauline Worters, John MacKenzie, MD, Zoltan Laszik, Jesse Courtier, MD

Disclosures: Pauline Worters has indicated a relationship with GE Healthcare. John Mackenzie has indicated a relationship with General Electric Healthcare as a researcher. All other authors have disclosed no financial interests, arrangements or affiliations in the context of this activity.

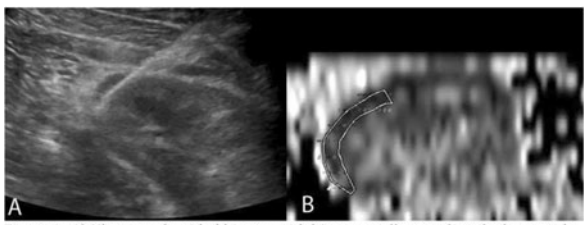

Figure 1. A) Ultrasound-guided biopsy, with biopsy needle sampling the lower pole cortex of a renal allograft. B) Axial reformatted FA map image through the lower pole of the renal allograft. Region of interest is drawn outlining the cortex in the lower pole, at the site of biopsy.

Purpose or Case Report: To compare renal cortical and medullary fractional anisotropy (FA) values with histopathologic Banff classification scores for renal transplant rejection in children.
Methods & Materials: Fourteen pediatric renal transplant recipients (mean age 15.7±2.9 years) were imaged on 3 T MRI, prior to ultrasound-guided renal transplant biopsy. Coronal echo-planar DTI sequence was performed using four b values (200, 400, 600, 800 s/mm^2). Each b-value was acquired separately with accompanying b=0 image. FA maps were created for each b value. Cortical and medullary FA values for each transplanted kidney were measured by defining regions of interest in the site of known biopsy. Allograft pathology was classified using the Banff system. Patients were grouped into two categories based on whether the outcomes of the biopsy changed subsequent clinical management. Mann Whitney U test was used to compare cortical and medullary FA values amongst patients whose biopsy results did and did not change clinical management. Pearson correlation coefficient was used to assess the relationship between the cortical and medullary FA values and several clinically relevant Banff scores: tubulitis (t), interstitial inflammation (i), tubular atrophy (ct), and interstitial fibrosis (ci).

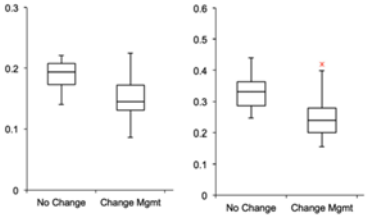

Figure 2. Fractional anisotropy (FA) values in renal allografts stratified into groups based on whether the concurrent biopsy changed clinical management. FA values in the medulla and cortex are both significantly different in these two groups. Lower FA values may indicate pathologically significant disease, which changes clinical management.

Results: The FA of the renal cortex in the region of biopsy, at b values 600 and 800, were significantly higher in the group in which biopsy results did not change clinical management (mean at b800=.189±.03, n=6) compared with the group in which results did change clinical management (mean at b800=.150±.04, n=8) (p<0.02 for b600 and p<0.008 for b800). Similarly, the FA of the renal medulla in the region of biopsy, at b values 400, 600 and 800, were significantly higher in the group in which biopsy results did not change clinical management (mean at b800=.335±.06, n=6) compared with the group in which results did change clinical management (mean at b800=.246±.07, n=8) (p<0.03 for b400, p<0.003 for b600, and p<0.001 for b800). Cortical FA at b800 and Banff t and i scores showed moderate correlation (R^2=0.37 and 0.45, respectively). Medullary FA at b800 and Banff t and i scores also showed moderate correlation (R^2=0.31 and 0.38, respectively).
Conclusions: DTI is a promising noninvasive technique for assessment of pediatric renal allografts, with potential for stratification of patients into categories in which biopsy results are or are not likely to affect clinical management, potentially sparing unnecessary renal allograft biopsies.

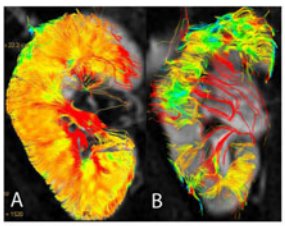

Figure 3. Tractography maps overlaid on an EPI image in (A) healthy and (B) diseased kidney demonstrates decreased number of fiber tracts in the diseased kidney.

Paper #: 111

Peripherally Inserted Central Catheters (PICC's) in Pediatric Patients: Variables Affecting the Central Tip Position

Ralph Gnannt, *Diagnostic Imaging, The Hospital for Sick Children, Toronto, ON, Canada, ralph.gnannt@sickkids.ca;* Bairbre Connolly, Avnesh Thakor

Disclosures: All authors have disclosed no financial interests, arrangements or affiliations in the context of this activity.
Purpose or Case Report: The position of the central tip of a peripherally inserted central catheter (PICC) is crucial; malposition can lead to malfunction of the line or life threating events. It is well known that arm movement affects the position of the central tip location of a PICC. The purpose of our study was to evaluate variables that impact this range of central tip movement that occurs with arm motion.
Methods & Materials: We included 112 consecutive pediatric patients (42 females, mean age 31 months ±13 months, mean weight 6.5 kg ±4.9 kg) in our study who underwent a PICC insertion. Inclusion criteria were patient who underwent upper limb PICC access, body weight <20 kg, available chest imaging with the arm in 90° abduction, 45°

abduction, 0° abduction, and an arm view marking the skin entry site relative to the shoulder. Variables evaluated were patient (gender, age, weight, and number of previous PICC's), line characteristics (material, single or double lumen, size, and length of the line) and insertion site characteristics (right or left arm, arm vein accessed, and distance between entrance site to growth plate of humeral head). Central tip movement was measured as rib spaces from baseline (i.e. insertion position with arm abducted 90°). A positive value indicated tip descent deeper into the SVC, a negative value indicated upward ascent.
Results: The overall range of central tip movement was -1 to +4 rib spaces, mean +0.9±0.7. A significant difference was seen in range of central tip movement with different PICC materials (silicone PICC's moved less than polyurethane) and vein accessed (PICC's in cephalic vein move less; $P<0.05$ each). Patient characteristics and remaining line characteristics did not influence the range of central tip movement of a PICC ($P>0.05$).
Conclusions: Confirmation that arm movement affects the central tip position of a PICC. Central tip movement is minimized using a silicone line and cephalic vein access. Interventional radiologists may consider these findings in their decision when inserting PICCs.

Paper #: 112

Ultrasound Guided Percutaneous Cholecystostomy Drains in Children: a Case Series

Ralph Gnannt, *Diagnostic Imaging, The Hospital for Sick Children, Toronto, ON, Canada, ralph.gnannt@sickkids.ca;* Dimitri Parra, Bairbre Connolly

Disclosures: All authors have disclosed no financial interests, arrangements or affiliations in the context of this activity.
Purpose or Case Report: Insertion of percutaneous cholecystostomy drain (PCD) in elderly and very ill patients is an established image guided intervention to drain a critically inflamed gallbladder. It may be performed directly or by a transhepatic route. It is associated with high morbidity and mortality. However, there is limited experience of PCD insertion in children. The purpose of this review was to examine the safety, efficacy and role of PCD in children.
Methods & Materials: Between December 2000 and June 2015, we identified 7 children who underwent PCD, using ultrasound and fluoroscopic guidance. Both direct and transhepatic routes were employed, using either a 22G Chiba needle, 0.018" wire, Neff set, dilator and drain, or 16/18G needle, 0.035" wire, dilator and drain. Integrity of drain positions were confirmed with contrast. Clinical indications, procedural complications, catheter dwell times and outcomes were analyzed.
Results: 7 patients (2F: 5M) aged 10.4 years (range 3.7- 17.1 year) underwent PCD under general anaesthesia. Underlying diagnoses included malignancy and immunosupression ($n=2$), congenital hepatic fibrosis with severe portal hypertension ($n=1$). 4/7 patients had calculous and 2/7 had acalcolous cholecystitis; 1/7 had tumoral obstruction (AML). The latter underwent both a PCD and a right intrahepatic biliary drain placement. 2/7 had hydrops of the gallbladder. The transhepatic route was used in 5/7 (71%) and direct access in 2/7. All purpose drains were placed, 8French ($n=5/7$) or 10Fr (2/7). All 7 procedures were technically successful; no bile leak occurred. Mean drainage time was 55 days (16 - 97 days). Late cholecystectomy was performed in 4/7 (57%). 3 patients (43%) died of their underlying disease, with a functioning drain in-situ.
Conclusions: This relatively large series of PCD in children indicate a high technical success and low complication rate. Peri-procedural mortality is lower than in adults. PCD insertion is feasible in children and should be considered, when the acutely ill child with an inflamed gallbladder is not fit for a surgical cholecystectomy.

Paper #: 113

Integration of *syngo* iGuide navigational software with C-arm CT images for percutaneous bone biopsies in the Interventional Radiology suite at a pediatric institution

Sphoorti Shellikeri, Master's in Biomedical Engineering, *Radiology, Children's Hospital of Philadelphia, Philadelphia, PA, sphoortishellikeri@gmail.com;* Xiaowei Zhu, Randolph Setser, Ganesh Krishnamurthy, MD, DNB, Maricarmen Nazario, Marc Keller, MD, Seth Vatsky, Abhay Srinivasan, Anne Marie Cahill

Disclosures: Randolph Setser has indicated a relationship with Siemens Healthcare as an employee. All other authors have disclosed no financial interests, arrangements or affiliations in the context of this activity.
Purpose or Case Report: Navigational software can be used to provide real-time fluoroscopic guidance during percutaneous interventions in the Interventional Radiology (IR) suite. Using 3D C-arm CT data, a path is drawn from the skin entry point to the target lesion. This path is transposed onto intraprocedural fluoroscopic images to guide the physician. This study describes our experience with *syngo* iGuide navigational software (Siemens Healthcare) for pediatric percutaneous bone biopsies in the IR suite and evaluates the diagnostic accuracy, mean effective radiation dose and procedure time.

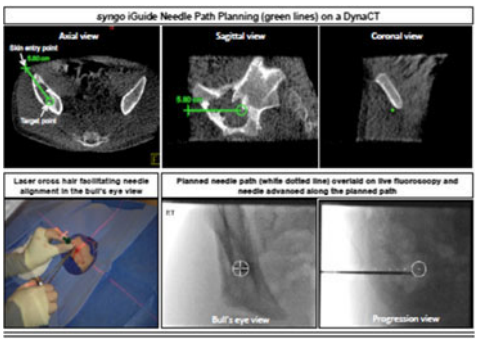

Methods & Materials: Pediatric patients with bone lesions identified by any of the following studies: X-ray, CT, PET-CT or MRI, but not accessible by ultrasound underwent biopsies in the IR suite between 2011 and 2015, under an IRB approved protocol. Depending on the anatomic detail required, different C-arm CT protocols were used: institution developed low-dose (0.1/0.17 μGy/projection), regular-dose (0.36 μGy/projection), or a combination of low/regular dose protocols. Effective radiation doses were estimated using PCXMC program (v2.0.1.3, STUK, Finland) and procedure times were evaluated.
Results: Twenty-three patients (10 F/13 M, mean age 10 year) underwent bone biopsies with iGuide guidance in the following anatomic regions: 12 pelvic, 7 lumbar, 4 lower-extremity. Low dose C-arm CT was used in 11/23 cases (6 pelvic, 2 lumbar, 3 extremity), regular dose in 9/23 (4 pelvic, 5 lumbar), and a combination of low/regular dose in 3/23 cases (2 pelvic, 1 extremity). The average number of C-arm CTs acquired per biopsy procedure was 3.6 (range 1-6; mode 3). Field-of-view was collimated for update DynaCT acquisitions (foot-head direction only).
22/23 (96%) bone biopsies were diagnostic. Overall, the mean effective radiation dose for all cases was 3.3±3.5 mSv. For cases using low-dose C-arm CT, the mean radiation dose was 1.4±2.0 mSv, 6.0±3.5 mSv for regular-dose, and 1.9±2.4 mSv for cases using combined low/regular dose C-arm CT. The mean effective radiation dose for pelvic cases was 3.5±2.9 mSv, 4.7±4.4 mSv for lumbar cases and 0.02±0.02 mSv for extremity cases. The mean procedure time was 91±36 min.
Conclusions: In our experience, iGuide technology in the IR suite provides real-time fluoroscopic needle guidance during bone biopsies in children and demonstrates good diagnostic accuracy. Patient radiation dose was controlled with the use of an institution developed low-dose

C-arm CT protocol and field-of-view collimation during DynaCT acquisition.

Paper #: 114

Placement of small caliber tunneled central lines via the internal jugular vein in children less than 2 years

Matthew Plunk, MD, *Texas Children's Hospital, Houston, TX, mxplunk@gmail.com;* Kamlesh Kukreja, Jose Hernandez, MD, Christopher Cassady, MD, Shireen Hayatghaibi, MPH, Daniel Ashton

Disclosures: All authors have disclosed no financial interests, arrangements or affiliations in the context of this activity.
Purpose or Case Report: The use of peripherally inserted central catheters [PICC] is common in children requiring long term central venous access but concerns remain about the sequelae of venous thrombosis particularly in young children. Accessing a larger diameter vessel, such as the internal jugular vein, may decrease this complication. We will describe our technique and outcomes for placing a tunneled PICC in the internal jugular vein in young children.
Methods & Materials: IRB approved retrospective review of a clinical and imaging database between 10/2012 and 7/2015 identified 69 tunneled jugular PICC's in 51 children (31 male and 20 female) younger than 2 years. All lines were placed in the interventional radiology suite under general anesthesia. A 21 G needle was utilized to access the internal jugular vein typically be a single stick technique. The right jugular was accessed in all but 9 cases. This was followed by an 0.018' glide wire to navigate to the SVC followed by tract dilation and PICC placement. Fisher's exact test was used to compare the frequency of complications between this group and a similar group who received upper extremity PICC's.
Results: The mean age was 292 days and mean time with line in place was 52.5 days. The most common indications were need for total parental nutrition [TPN] (28 lines), chemotherapy (16), & antimicrobial therapy (9). A 3 Fr single lumen PICC was the most common line placed. All lines were successfully placed without any immediate complications. On follow up, the most common complication was malposition with 13 occurrences (18.8%), infection (11.8%), malfunction (5.8%), thrombosis (4.3%), and bleeding (1.4%). There was a statistically significant higher malposition rate in the internal jugular group compared to the upper extremity PICC group (p=0.02) but no difference in infection rate (p=0.12).
Conclusions: Tunneled PICC's via the internal jugular vein in children less than 2 years were technically feasible without any immediate complications in our study. A higher incidence of malposition is likely related to a shorter intravascular length.

Paper #: 115

Davis Intubated Ureterotomy: Treatment of Ureteral Injury/ Transection

Richard Towbin, MD, *Phoenix Children's, Phoenix, AZ, rtowbin@phoenixchildrens.com;* David Aria, M.D., Carrie Schaefer, Tammam Beydoun, Robin Kaye

Disclosures: All authors have disclosed no financial interests, arrangements or affiliations in the context of this activity.
Purpose or Case Report: 15 year-old male presented with abdominal pain after sports injury. CT demonstrated active bleeding from a left perinephric mass confirmed to be a metastatic retroperitoneal paraganglioma with osseous metastases. Patient underwent open resection of the mass with renal sparing but subsequently developed left hydronephrosis with excretion of IV contrast into a dilated proximal ureter and large left urinoma without visualization of the distal ureter. Cystoscopy with retrograde pyelogram was performed demonstrating extravasation into the urinoma with a 3 cm distraction distance of the proximal left ureter. A Davis type intubated ureterotomy was performed. The cystoscopically-placed distal ureteral catheter was exchanged for a snare. From above, a wire was advanced, grasped, and retrieved via the urethra and a double-J ureteral stent placed across the ureteral defect. Healing occurred by secondary intention with smooth-muscle regeneration. After 6 weeks, a repeat retrograde pyelogram demonstrated complete healing of the ureteral defect with stenosis. The patient continues to be treated with a double-J left ureteral stent.

Paper #: 116

Intra-operative MRI guided, laparoscopic-assisted anorectoplasty in the treatment for imperforate anus

Damien Grattan-Smith, MBBS, *Children's Healthcare of Atlanta, Atlanta, GA, damien.grattansmith@mac.com;* George Raschbaum, John Bleacher, Joseph Williams, Stephen Little, Richard Jones

Disclosures: All authors have disclosed no financial interests, arrangements or affiliations in the context of this activity.
Purpose or Case Report: To evaluate the use of Intra-operative MRI Laparoscopically-Assisted Anorectoplasty (IMRI-LAARP) in children with imperforate anus.
Methods & Materials: Since July 2008, 27 children with imperforate anus underwent IMRI-LAARP. They were 24 boys and 3 girls. The average age at surgery was 7.2 months (range 4-18 months). Preoperative MRI was performed after dilute Gadolinium based contrast agent was instilled into the mucous fistula to document the anatomy of the anorectal malformation and the parasagittal and vertical muscle complex as well as to identify and localize rectovesical or rectourethral fistula. The spine was scrutinized for underlying dyraphism. The perineum was pierced with an MRI compatible 20G spinal needle at the central portion of the muscle complex as determined by a direct muscle stimulator. The needle was then advanced incrementally within the muscle complex as guided by intra-operative MRI until the levator floor was penetrated. LAARP was then completed using the 20 gauge needle as a guide for the pull-through procedure.
Results: There was a wide variation in the development and morphology of the parasagittal and vertical muscle complex. In all cases, the muscle cone described a unique arc extending anteriorly and then passing posteriorly. In most cases the diameter of the muscle cone measured less than 5 mm and there was significant variation in the course of the muscle complex. The intraoperative MRI was crucial in delineating the ideal course through the muscle complex as well as confiming needle placement centrally in all three planes. Follow-up MRI in 10 children demonstrated placement of the pulled-through segment in a central location through the length of the muscle complex. Early post-operative results have been very encouraging with most patients demonstrating nocturnal continence.
Conclusions: MRI-guided LAARP results in anatomically correct placement of the rectum within the parasagittal and vertical muscle complex. Early post-operative results suggest significant functional improvement when compared with traditional operative tecniques. Although the ultimate factors determing continence are complex and relate to the degree of spinal dysraphism and developmental morphology of the muscle complex, it seems logical that optimal results from LAARP will only be obtained if the pull-through is centered within the individual anorectal muscle complex.

Paper #: 117

CT-guided preoperative localisation of nonpalpable lung nodules in children

S Murthy Chennapragada, FRANZCR, *University of Sydney, Sydney, NSW, Australia, murthy.c@gmail.com;* David Lord

Disclosures: All authors have disclosed no financial interests, arrangements or affiliations in the context of this activity. Purpose or Case **Report**: To assess the utility of CT guided marking of small subpleural nonpalpable lung nodules for preoperative localisation prior to video-assisted thoracoscopy (VAT) and resection in children
Methods & Materials: A retrospective review of all patients that underwent CT guided lung nodule localisation prior to VATand resection. The following data were recorded: demographic details; primary diagnoses; technical details of the procedure; complications; surgical findings; histopathology results
Results: Between November 2006 and March 2014, 11 children (4.5 years-18 years; M:F=8:3) underwent 11 procedures. 9/11 nodules were marked with methylene blue tattoing and hook wire placement. 2/11 nodules were localised with methylene blue alone. 10/11 localisations were accurately identified at surgery; there was one technical failure due to methylene blue staining of the pleura due to spillage. There were no major complications relating to the procedures. All nodules were found at pathological examination of the resected lung. 6/12 (50%) nodules were benign lymph nodes/lymphoid aggregates. 2/12 were metastatic nodules; 3/12 were inflammatory nodules.
Conclusions: CT guided preoperative marking of lung nodules in children is safe, effective and accurate for localisation prior to VAT resection

Paper #: 118

Pre-Season versus Post-Season Quantitative MRI Assessment of the Elbow in Little League Baseball Players

Jeffrey Koning, MD, *University of California San Diego Department of Radiology, San Diego, CA, jlkoning@ucsd.edu;* Peter Kruk, Andrew Pennock, Andrew Pytiak, Phil Stearns, Tracey Bastrom, Jerry Dwek

Disclosures: All authors have disclosed no financial interests, arrangements or affiliations in the context of this activity.
Purpose or Case Report: Youth baseball has been associated with elbow pain and pathology leading to the implementation of throwing and pitching guidelines by governing bodies. The purpose of the current study was to compare baseline pre-season with post-season quantitative MRI measurements in the dominant arm elbows of Little League baseball players, and to correlate these findings with the players' throwing history and physical exams.
Methods & Materials: A prospective study of little league players age 10-13 years was performed. Players underwent dominant arm elbow MRI before and after one season, and non-dominant arm elbow MRI was performed as a control. The MRIs were read independently by two blinded, board-certified pediatric radiologists. Medial epicondyle (ME) physeal width, ulnar collateral ligament (UCL) width, and distance from the UCL to the ME physis were compared. All players underwent a physical exam and questionnaire addressing their playing history and elbow pain. Responses on the questionnaire and physical exam findings were correlated with MRI measurements.
Results: Twenty-six players were enrolled. Twenty (77%) players were right handed and 14 (54%) were a pitcher and/or catcher. Baseline UCL thickness in the dominant arm was greater than the non-dominant arm (1.3 mm vs 1.1 mm, $p<0.04$); however, baseline ME physeal width was similar between the dominant arm and non-dominant arm (1.5 mm vs 1.7 mm, $p=0.116$). One player (3.8%) suffered a UCL tear over the season. ME physeal width increased from pre to post-season (1.5 mm vs 2.3 mm, $p<0.001$). There was no change in UCL thickness (1.3 mm vs 1.4 mm, $p=0.407$) or distance from the UCL attachment to the ME physis (4.8 mm vs 4.4 mm, $p=0.071$) pre versus post-season. There was an increase in elbow extension to hyperextension on physical exam among all players pre versus post-season (1.3° vs -4.2°, $p<0.001$), and increased distance from the UCL attachment to the ME physis on MRI correlated with increased elbow extension ($R^2=0.65$, $p<0.001$). Player reported pain did not correlate with quantitative MRI measurements.
Conclusions: MRI abnormalities involving the medial elbow are common in Little League baseball players. Quantitative MRI detected post-season increased ME physeal width, although this change did not correlate with player reported elbow pain, which may indicate this physeal widening represents an occult physeal injury. Increased distance from the UCL attachment to the ME physis may represent a useful measure to predict development of elbow hyperextension.

Paper #: 119

Fetal, infant, and childhood growth and acetabular hip dysplasia at skeletal maturity: findings from a prospective study with follow-up from newborn to adult life

Francesco Sera, Karen Rosendahl, **Lene Laborie, MD PhD**, *UCL Institute of Child Health, London, United Kingdom, lenebj80@hotmail.com;* Trude Gundersen, Ingvild Engesæter, Lars Engesæter, Carol Dezateux

Disclosures: All authors have disclosed no financial interests, arrangements or affiliations in the context of this activity.
Purpose or Case Report: Obesity and tall stature at skeletal maturity are associated with an increased risk of hip joint replacement, suggesting that skeletal growth and maturation may influence hip joint structure and function in adult life potentially by increasing the risk of acetabular dysplasia. We examine associations between growth in early life and acetabular dysplasia at skeletal maturity in a unique prospective study with follow up from newborn to adult life.
Methods & Materials: We report data from a population-based prospective follow-up of a two-stage sample of 11,925 newborns recruited to a randomised study of ultrasound imaging to screen for developmental hip dysplasia. Of 4,507 invited 2,338 (51.9%) attended follow-up at age 18 years including an erect pelvic anteroposterior radiograph, 1,846 (79.0%) with at least one previous anthropometric measurement. Radiographic features of hip dysplasia included the acetabular depth-width ratio (ADR). Birth weight and length were obtained from the national birth registry and height and weight measured at ages 2, 4, and 7 years from child health clinic records. Body Mass Index (BMI) and sex and age-specific z-scores were calculated. Weighted multivariable regression models were used to evaluate associations between anthropometric distances and velocity z-scores at birth, 2, 4, 7 and 18 years and ADR at 18 years.
Results: For girls ($n=1079$) higher BMI at maturity was associated with a lower ADR (more acetabular dysplasia): regression coefficient (95%CI) -2.64 (-4.69; -0.59) for one BMI z-score increase. An interaction between birth weight and BMI at maturity ($p<0.05$) was observed, with the effect of BMI at maturity greater for girls of low birth weight. In multivariable analyses a one z-score increase in BMI between birth and 2 years and between 2 years and skeletal maturity were associated with a lower ADR: regression coefficients -3.77 (-6.66; -0.87) and -2.44 (-4.78; -0.10) respectively.
Conclusions: Body size growth in childhood is associated with radiologically-defined acetabular dysplasia at skeletal maturity in girls, especially in those of lower birth weight, suggesting an effect on skeletal maturation of early and late catch-up growth. These preliminary findings need independent replication in other populations however highlight the importance of a life course approach to understanding acetabular dysplasia.
Funding Arthritis Research UK ref. 18196; UK Medical Research Council ref GO400546. Western Norway Regional Health Authority.

Paper #: 120

Clinical Update On Rapid High Resolution Two-Point DIXON Turbo Spin Echo (TSE) With Conventional TSE On 3T MR Imaging of the Pediatric Knee in 50 patients

Bamidele Kammen, MD, *Diagnostic Imaging, UCSF Benioff Children's Hospital, Oakland, Oakland, CA, bkammen66@gmail.com;* Eric Padua, Sabiha P Karakas, MD, Ward Hagar, Lynne Neumayr, Ronald Cohen, Dave Hitt, Nirav Pandya, Taylor Chung, MD

Disclosures: All authors have disclosed no financial interests, arrangements or affiliations in the context of this activity.
Purpose or Case Report: Update on clinical performance of two-point DIXON TSE proton-density-weighted (PD) sequence compared with conventional TSE PD sequence with and without fat suppression in 50 pediatric knee MRI's.
Introduction\: Rapid two-point DIXON TSE sequence has recently become clinically available. In one DIXON acquisition, four image types can be generated. The water-only image is equivalent to fat suppression. The in-phase-water-and-fat image is equivalent to no fat suppression.
Methods & Materials: This is an IRB-approved retrospective study of 50 consecutive pediatric knee MR examinations for knee pain. PD DIXON TSE sequence and conventional PD TSE and PD TSE fat suppressed (PD TSE FS) sequences were acquired in the same imaging plane with identical spatial resolution. Two hundred sets of images (DIXON water-only, DIXON in-phase, PD TSE, PD TSE FS) were reviewed by three pediatric radiologists blinded to the imaging sequence for homogeneity of fat suppression, detection of intra- and extra-articular pathology, and characterization of susceptibility and vascular pulsation artifacts. Readings were tabulated irrespective of the reader in 2×2 tables that summarized concordance and discordance between PD and DIXON for each study. McNemar's test was used to determine the significance of discordance between the DIXON and PD techniques.
Results: PD DIXON and PD TSE with identical voxel size have comparable acquisition times. PD TSE FS sequences were completed in 5.5 to 6.5 min, PD TSE in 4.5 to 5.5 min and PD DIXON in 5 to 6 min. Water-only image PD DIXON sequence showed homogeneous fat suppression. PD DIXON performed equally with PD and PD FS and all sequences showed similar conspicuity of osseus, meniscal, and ligamentous lesions. DIXON demonstrated increased conspicuity of soft tissue abnormalities ($p<0.001$) and improved suppression of susceptibility artifact ($p<0.031$). Vascular artifacts were less pronounced on the PD FS images ($p<0.001$).
Conclusions: Rapid two-point DIXON TSE can replace conventional PD TSE and PD TSE FS to shorten the overall examination time for high resolution pediatric knee MR on 3 T while maintaining excellent intra-articular lesion conspicuity and improved extra-articular conspicuity of soft tissue pathology due to superior homogeneity of fat suppression. Vascular pulsation artifact is more prominent on DIXON images in the sagittal plane and future work on motion suppression for DIXON sequences is desirable. We have adopted DIXON in our routine imaging of the knee.

Paper #: 121

Fast Comprehensive Single Sequence 4D Pediatric Knee MRI

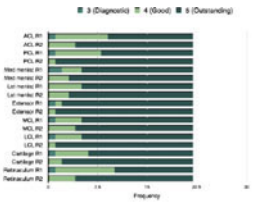

Frequency of ratings for each anatomic structure with T2Sh for both readers. No structures were given a rating of 1 (non-diagnostic) or 2 (limited) which are therefore not included.

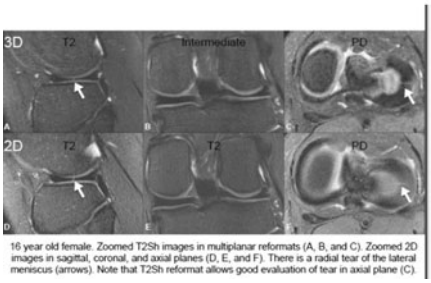

16 year old female. Zoomed T2Sh images in multiplanar reformats (A, B, and C). Zoomed 2D images in sagittal, coronal, and axial planes (D, E, and F). There is a radial tear of the lateral meniscus (arrows). Note that T2Sh reformat allows good evaluation of tear in axial plane (C).

Shanshan Bao, MD, *Radiology, Lucile Packard Children's Hospital Stanford, Palo Alto, CA, sbao10@stanford.edu;* Jonathan Tamir, Umar Tariq, Martin Uecker, Peng Lai, Michael Lustig, Shreyas Vasanawala, MD/PhD

Disclosures: Shreyas Vasanawala has indicated a relationship with Arterys, stock/consultant and GE Healthcare, research collaboration. All other authors have disclosed no financial interests, arrangements or affiliations in the context of this activity.
Purpose or Case Report: Volumetric variants of fast spin-echo (FSE) have been described to simplify and accelerate joint imaging, based on the ability to reformat into multiple planes. However in practice, elimination of standard 2D imaging has not been feasible due to blurring, likely due to very long echo trains required for volumetric imaging. This work evaluates a redesigned volumetric FSE acquisition which resamples k-space positions at multiple echo times to estimate and correct for T2 decay. This yields effectively a 4 dimensional acquisition, producing images of different T2 weighting, with scan time of about 7 min. We hypothesize that this technique, termed T2 shuffling (T2Sh) can suffice as a single sequence pediatric knee protocol.
Methods & Materials: With IRB approval, 22 consecutive children were scanned at 3 T (GE MR750) with a routine clinical knee MRI protocol and underwent imaging with T2Sh. Two radiologists evaluated each case on a multiplanar reformat capable workstation, first forming a diagnosis based solely on the T2Sh images, reconstructed at 3 effective echo times (proton density, intermediate, and T2-weighted). Findings were then compared to the official report and are concordant if all actionable structural derangements were identified. T2Sh image quality of 9 anatomic structures were evaluated on a scale of 1 (non-diagnostic) to 5 (outstanding). Relative quality of structure delineation of T2Sh and 2D sequences were also compared. A Wilcoxon rank-sum test assessed the null hypothesis that the relative quality of T2Sh structure delineation compared to conventional 2D is unchanged. Inter-observer agreement was evaluated with kappa statistics.

Reader 1	Reader 2
Avulsion of tibial spine	Avulsion of tibial spine
Joint body (2 cases)	Joint body (2 cases)
Patellar cartilage injury	Infrapatellar ligament edema
Lateral meniscus central tear	
Lateral meniscus saucerization	

Major missed findings on T2Sh for each reader, which were readily perceptible on T2Sh in retrospect. Contributory factors include level of experience as well as absence of clinical history and prior studies.

Results: Delineation of the 9 anatomic structures on T2Sh images was at least diagnostic in all cases for both readers. The mean ratings for delineation was between 4.5 and 4.9 for reader 1 and 4.8-5 for reader 2. Inter-observer agreement analysis was limited due to the distribution of ratings. There was no significant difference in quality of structure delineation between T2Sh and 2D except for the retinaculum for reader 1 ($p<0.05$), where 2D was preferred. Interpretations were concordant in 77% of cases for reader 1 and 82% for reader 2, with 95% CI of 63-97%. The missed findings were readily perceived in retrospect on T2Sh. Of note, interpretations were made without clinical history or comparison studies.
Conclusions: T2Sh yields high quality, multiplanar reformable, 4D images with potential for application as a single sequence pediatric knee protocol.

Reader 1	Reader 2
Avulsion of tibial spine	Avulsion of tibial spine
Joint body (2 cases)	Joint body (2 cases)
Patellar cartilage injury	Infrapatellar ligament edema
Lateral meniscus central tear	
Lateral meniscus saucerization	

Major missed findings on T2Sh for each reader, which were readily perceptible on T2Sh in retrospect. Contributory factors include level of experience as well as absence of clinical history and prior studies.

Paper #: 122

Arthroscopic and MRI discrepancies for chondral injuries of the knee in 329 children

Siddharth Jadhav, M.D., *Pediatric Radiology, Texas Children's Hospital, Houston, TX, spjadhav@texaschildrens.org;* Erica Schallert, MD, J. Kan, MD, Megan May, Scott McKay

Disclosures: All authors have disclosed no financial interests, arrangements or affiliations in the context of this activity.

Purpose or Case Report: Knee MRI is an established tool for evaluating internal derangement in adult patients but no large study has evaluated its utility in children. The purpose of this study is to evaluate discrepancy between MRI and arthroscopy relating to chondral pathology in 329 consecutive pediatric knee exams.

Methods & Materials: In this descriptive IRB approved HIPAA compliant study, a retrospective review of 329 consecutive knee arthroscopies between January 2014 and September 2015 at a large pediatric hospital was performed. Two pediatric orthopedic surgeons independently reported discrepancies between the pre-operative MRI report and their arthroscopy findings. The pre-operative MRI's of the patients with discrepant arthroscopic findings were reassessed by two pediatric musculoskeletal radiologists separately, blinded to arthroscopy findings. Any inter-reader discrepancies were settled by consensus review. Inclusion criteria was pediatric patients with knee arthroscopy performed at our institution between January 2014 and September 2015 with an internal pre-operative MRI on a 1.5 or 3 T magnet.

Results: Of the 329 knee arthroscopies, 257 (78.2%) surgical and MRI findings were concordant and 72 (21.9%) were discordant. Of these, 27.8% (20/72) were related to traumatic chondral pathology. These comprised 6.1% (20/329) of the arthroscopies. The majority 90%(18/20) of acute traumatic chondral injuries were false negatives. 80% (16/20) of discrepancies involved the lateral compartment, 10% (2/20) the medial compartment and 10% (2/20) the patella.

Conclusions: A large number of arthroscopy-knee MRI discrepancies relate to chondral injuries. MRI does not do particularly well in excluding the presence of traumatic chondral injury, especially in the lateral compartment of the knee. It is important to recognize this limitation of MRI in detecting chondral injuries of the knee in pediatric patients.

Paper #: 123

Bone Marrow Fat Content in 70 Adolescent Girls with Anorexia Nervosa: MRI/MRS Assessment

Kirsten Ecklund, M.D., *Radiology, Boston Children's Hospital, Boston, MA, kirsten.ecklund@childrens.harvard.edu;* Sridhar Vajapeyam, PhD, Robert Mulkern, PhD, Henry Feldman, Jennifer O'Donnell, Sokdina Keo, Catherine Gordon

Disclosures: All authors have disclosed no financial interests, arrangements or affiliations in the context of this activity.

Purpose or Case Report: Osteoporosis in girls with anorexia nervosa (AN) is associated with premature conversion of red to yellow marrow. Hormonal changes may lead to adipocyte over osteoblast differentiation in mesenchymal stem cells, resulting in increased marrow fat. We utilized knee MRI with T1 relaxometry and MRS in a large cohort of adolescents with AN to evaluate marrow fat content and to correlate it with age and disease severity.

Methods & Materials: We enrolled 70 girls with AN, age 11 - 18 years, mean 15.5 years, BMI 12.8 - 22.4 kg/m^2, mean 18.73 kg/m^2. IRB approval/informed assent and consent were obtained. All subjects underwent 3 T MRI of the knee with coronal T1W images, T1 relaxometry (T1R), and single-voxel proton MRS at 30, 60 msec TEs. T1 images were scored visually for red marrow (RM) content, designated as areas of low signal intensity. Metaphyses were graded: 0=homogeneous hyperintensity, no RM; 1=few hypointense signal striations, mild RM; 2=scattered hypointense areas, moderate RM; 3=more diffuse hypointense regions, extensive RM. Visual T1 score (VS), T1 relaxometry values, and MRS fat fractions were compared with age, BMI, and bone mineral density (BMD) as markers of disease severity. MRS included unsaturated fat index (UI), T2 water, olefinic, and methylene values.

Results: All measures of RM (VS, T1R, and MRS) declined significantly with age, $p<0.0008$. Relaxometry T1 values correlated with BMI and BMD negatively for girls ≤16 years (Pearson correlation r=-0.34, -0.44) and positively for those ≥17 years (r=0.47, 0.42). MRS identified a strong inverse correlation between T2 water and saturated fat fraction (methylene:water) at 60 ms, r=-0.85, $p<0.001$. No correlation was evident between UI and BMI or BMD. No relationship between marrow fat content and duration of disease could be identified.

Conclusions: The strong physiologic association between marrow fat content and age remains dominant even in patients with AN. The correlation between T1 and BMI, BMD for older girls suggests more marrow fat (↓T1) in those with more severe disease (↓BMI). The increased RM normally present in younger girls may obscure this effect. The strong correlation between T2 water and saturated fat has not previously been seen and may relate to restriction of water with increasing marrow fat. MR/MRS techniques can be used to qualitatively and quantitatively assess marrow fat content in patients with AN.

Paper #: 124

Does Pre-Operative Hip Location or Post-Operative Hip Abduction Angle Better Predict Perfusion Abnormalities on Post-Operative SPICA MRI after Closed Reduction for Developmental Dysplasia of the Hip?

Michael Rivlin, M.D., J. Kan, MD, Erica Schallert, MD, *Texas Children's Hospital, Houston, TX, ekschall@texaschildrens.org*, Siddharth Jadhav, M.D., Wei Zhang, Scott Rosenfeld

Disclosures: All authors have disclosed no financial interests, arrangements or affiliations in the context of this activity.

Table 1. Pre-operative hip location and percentage of femoral head enhancement after closed reduction.

	% Femoral head enhancement	Standard deviation
Hips dislocated on pre-operative imaging (N=19)	61%	44%
Hips in the socket on pre-operative imaging (N=17)	88%	22%
P value	0.0405	

Table 2. Relationship between average post-operative hip abduction angle and number of hips with abnormal (</= 50%) femoral head enhancement after closed reduction.

Average Post-Operative Hip Abduction Angle	Number of Hips with femoral head enhancement </= 50%	Number of Hips with femoral head enhancement >50%	Total
</=60°	4	12	16
>60°	5	15	20
P value=1.0			36

Purpose or Case Report: SPICA MRI with gadolinium is an established technique for postoperative determination of perfusion abnormalities of the capital femoral epiphysis after closed reduction of developmental dysplasia of the hip (DDH). When perfusion abnormalities are present, patients are at risk for developing epiphyseal osteonecrosis. The purpose of this study is to investigate the relative impact of two variables related to postoperative perfusion abnormality on SPICA MRI in patients with DDH: pre-operative hip location versus the degree of postoperative hip abduction.

Methods & Materials: Waiver of informed consent was obtained for this retrospective study. 18 patients with DDH (average age 11.7 months, range 4-36 months, 4:14 male:female) who underwent gadolinium enhanced SPICA MRI after closed hip reduction were identified between 07/25/2011 and 11/14/2014. A total of 36 individual hips were evaluated using a 1.5 T MRI. Pre-operative imaging of these 36 hips was reviewed, and the hip location was characterized as being 1) out of the socket (dislocated) or 2) in the socket (including normal, subluxed, and dysplastic hips). Hip abduction angle and percentage of femoral head volume perfused were calculated from post reduction contrast-enhanced SPICA MRI. Hip location on pre-operative radiographs and hip abduction angles after closed reduction were compared with the degree of femoral head perfusion via the Wilcoxon rank test and Fisher's exact test.

Results: Of the 19 dislocated hips on pre-op imaging, the mean volume of femoral head perfusion was 61%±44%. Of the 17 hips that were in the socket on pre-op imaging, the mean volume of femoral head perfusion was 88%±22% (P=0.04). For post-op hips that were abducted less than or equal to 60° on MRI, 4/16 (25%) demonstrated abnormal (less than or equal to 50%) femoral head perfusion compared with 5/20 (25%) hips that were abducted greater than 60° (P=1.0).

Conclusions: Hips that were out of the socket pre-operatively demonstrated a lower percentage of perfusion than those hips that were in the socket. The degree of post-op hip abduction did not correlate with perfusion abnormalities. Pre-operative hip location may be a more important factor in predicting post-reduction perfusion than post-op abduction angle. Patients whose hips are not dislocated may not require contrast enhanced MRI examination postoperatively.

Paper #: 125

Preliminary accuracy of 3D ultrasound diagnosis of infant hip dysplasia using indices of acetabular 3D shape and coverage

Abhilash Hareendranathan, Myles Mabee, Dornoosh Zonoobi, Alana Heath, Lucy Jamieson, Chad Diederichs, Adrienne Thompson, **Jacob Jaremko, MD, PhD**, *Radiology & Diagnostic Imaging, University of Alberta Hospital, Edmonton, AB, Canada, 1082085@gmail.com*

Disclosures: All authors have disclosed no financial interests, arrangements or affiliations in the context of this activity.

Purpose or Case Report: Developmental dysplasia of the hip (DDH), when severe, is usually clinically obvious as dislocated hips, but milder cases are easily missed clinically and lead to premature osteoarthritis. Image aided DDH diagnosis includes dynamic tests and static imaging such as Graf classification which quantifies the acetabular shape seen at two-dimensional ultrasound (2DUS). Relying upon a 2D image to quantify a 3D structure may miss or misidentify deformity, and increase inter-scan variability. 3D ultrasound (3DUS) is a promising alternative for more reliable DDH diagnosis. However, analysis of the data-rich 3DUS image set can be challenging. Here, we perform preliminary testing of the diagnostic accuracy of an automated method to detect DDH based on geometric features derived from 3D acetabular surface models.

Methods & Materials: With informed consent from parents, we added 3DUS to routine 2DUS scans in infants presenting to our tertiary radiology department for evaluation of hip dysplasia. We had 79 hips in infants aged 4-111 days (36 normal, 16 borderline, 27 dysplastic based on orthopedic surgeon assessment at time of scan, blinded to 3DUS). 3DUS hip volumes were obtained using a Philips 13VL5 13 MHz linear transducer, requiring 3.2 s per scan. For each 3DUS we performed graph-based semi-automated segmentation to produce 3D acetabular surface models, then calculated geometric features including the Automatic Alpha Angle (AA), Acetabular Contact Angle (ACA), Kurtosis (K), Skewness (S) and Convexity (C). Mean values of features obtained from surface models were used as inputs to train a "random forest" classifier to predict whether a hip was normal or dysplastic.

Results: Surface models were generated rapidly (user time <1 min) via semi-automated segmentation, and visually closely correlated with the actual acetabular contour. The random forest classifier correctly predicted 24/27 dysplastic hips and considered the other 3 borderline, with 5 false positive results; 47 normal hips were considered normal. Depending on how borderline results were treated, this gave 89-100% sensitivity and 90% specificity, 94-100% negative predictive value for hip dysplasia in a clinic population with high prevalence of DDH.

Conclusions: Dysplastic hips can be accurately detected by 3D ultrasound, after only seconds of scan time and 1 min of user post-processing time. Refinements including modelling the femoral head may further improve accuracy. This technique may soon be useful in clinical practice.

Paper #: 126

Acute inflammatory neck swelling in children: which patients benefit most from early ultrasound?

Farahnaz Golriz, M.D, *Radioloogy, Texas Children's Hospital, Houston, TX, fxgolriz@texaschildrens.org;* Andrea Cruz, Beth D'Amico, Alade Kiyetta, Lane Donnelly, MD, George Bisset, M.D.

Disclosures: All authors have disclosed no financial interests, arrangements or affiliations in the context of this activity.

Purpose or Case Report: To identify clinical factors predictive of early surgical drainage (within 24 h of admission) in children with acute inflammatory neck swelling with the aim of reducing the overuse of ultrasound (US) in management of pediatric neck swelling.

Methods & Materials: We retrospectively reviewed the medical records of children (0-18 years) who visited the emergency department between 2012 and 2014 with an inflammatory neck swelling and who underwent initial imaging work-up with neck US within 12 h of admission. Data collected included age, gender, duration of neck swelling, antibiotic use prior to admission, presence of fever, fluctuance, erythema and/or tenderness on examination, WBC count, and the result of neck US. Data were analyzed to determine the factors associated with early surgical drainage.

Results: 337 patients were included (median age 2.3y; 54% male). 34 (10%) underwent early surgical drainage. Among those, 26 patients had an US diagnosis of abscess or fluid collection; and in 8 patients, US was interpreted as early abscess or suppurative lymphadenitis. Factors associated with early surgical drainage included fluctuance (odds ratio [OR] 81; 95% confidence interval [CI], 16-400), age <2 years (OR, 4.7; CI, 2-10.7), neck swelling duration >2 days (OR, 4.9; CI, 2.6-13.6), and prior antibiotic use (OR, 3.1; CI, 1.5-6.4). Decision tree analyses demonstrated that children aged 2 years or younger, with neck swelling duration >2 days were at the highest risk (32%) of having an abscess or suppurative lymphadenitis in US which required early surgical drainage. In contrast, none of the 110 children older than 2 years of age with neck swelling less than 2 days underwent early surgical drainage, regardless of US findings.

Conclusions: In the absence of fluctuance on examination and prior treatment with antibiotics, the chance of early surgical drainage in children >2 years-old with neck swelling duration of <2 days is very low. This knowledge could help physicians in determining the need for performing early ultrasound versus an initial antibiotic therapy trial for management of pediatric inflammatory neck swelling.

Paper #: 127

An Evidence Based Medicine Approach to Paediatric Cervical Spine Trauma: Cervical Spine Plain Radiography Vs Computed Tomography

Maria McGill, *Radiology, Royal Victoria Hospital, Belfast, United Kingdom, mariaemcgill@yahoo.co.uk;* Anne Paterson

Disclosures: All authors have disclosed no financial interests, arrangements or affiliations in the context of this activity.
Purpose or Case Report: The Oxford Centre for Evidence Based Medicine (OCEBM) describes a '5-stage approach to evidence based medicine (EBM)'. Could this tool provide an EBM answer to a common radiological dilemma?
Methods & Materials: **Stage 1:** '*Ask an answerable question*'. 'In a child <8 years of age, presenting with cervical spine trauma, how does cervical spine plain radiography compare with computed tomography in terms of diagnostic sensitivity, specificity, radiation dose and cost-effectiveness?'
Stage 2: '*Search for best evidence*'. A MeSH- term search strategy was developed and evidence databases were interrogated. The level of evidence was assessed against DiCenso's 2009 6S hierarchy of evidence and the 2011 OCEBM Levels of Evidence.
Stage 3: '*Appraise evidence for validity*'. The evidence was appraised utilising critical appraisal tools such as Agree II, PRISMA and OCEBM Systematic Review Appraisal Sheet. A 'mini meta-analysis' was also undertaken.
Stage 4: '*Apply results in practice*'.
Stage 5: '*Assess performance*'.
Results: The highest level of evidence identified was NICE 2014 'Investigation for injuries to the cervical spine in children with head injury' guidelines which when assessed against the Agree II appraisal tool were found to be based on Level 5 evidence. The next highest level of evidence was a systematic review which didn't focus specifically on children aged <8 years. However using a 'reverse citation approach' a number of individual studies were identified, from which data specific to <8 years could be extracted. A mini meta-analysis was performed on this data however the validity of this meta-analysis was poor.
Conclusions: Based on currently available best evidence: In a paediatric population (<8 years) presenting with LOW RISK cervical spine trauma requiring radiology clearance cervical spine radiography provides a diagnostically sensitive, safe and cost-effective form of imaging when compared with cervical spine computed tomography as a reference standard.

Paper #: 128

What is the value of spine, hand and foot radiographs as part of the skeletal survey for diagnosing suspected physical child abuse?

Jessica Smith, Michael Paddock, MBBS, *University of Sheffield Medical School, Sheffield, United Kingdom, michael.paddock@doctors.org.uk;* Alan Sprigg, Isla Lang, Amaka Offiah, MBBS, PhD
Disclosures: All authors have disclosed no financial interests, arrangements or affiliations in the context of this activity.

Kappa	Strength of Agreement
≤0.20	Poor
0.21-0.40	Fair
0.41-0.60	Moderate
0.61-0.80	Good
0.81-1.00	Very good

Purpose or Case Report: Following Royal College of Radiologist and Royal College of Paediatrics and Child Health recommendations (2008), the UK skeletal survey (SS) comprises standard 20 radiographs performed in any child under the age of 2 years in suspected physical abuse, with follow up 10-14 days after initial SS.
Fractures of the hands, feet and spine are generally rare (≤1% in reported literature assessing SS). Current literature provides a spectrum of opinion: exclusion; selective imaging based on clinical suspicion; full SS in every case of suspected physical abuse. Our aim was to provide further evidence to inform future practice.

Grade	Definition	Example
0	No difference between surveys	
1	Difference is technical	Transverse vs oblique
2	Factual difference that would have no clinical impact	5 or 7 ribs, all of the same age
3	Factual difference that could have a clinical impact	Fracture not seen by all observers Fractures recorded to be different ages

Methods & Materials: PACS at our institution was interrogated over a 36-month period from November 2011. 119 individual SS were identified for analysis after inclusion criteria were applied: performed for suspected inflicted injury (non-accidental injury); follow up SS consisting of at least a chest radiograph; patient aged 3 years or less at time of imaging; antemortem.
Three consultant paediatric radiologists reviewed all SS. A random number sequencer assigned patient number, which also selected 40 random patients to repeat, to assess intra-rater reliability. Agreement was assessed using Cohen's kappa (Table 1).
Data was captured using Survey Monkey questionnaires including: the site, type, age. and confidence of fracture presence (scale 1 - 5); presence of underlying metabolic disease; whether abuse was a relevant diagnosis (scale 1 - 5) on both initial and follow up SS. Fracture prevalence and site were analysed. A consensus meeting was held between all readers in case of discrepancies and only included in final analysis if unity agreement. Grading rater discrepancies is outlined in Table 2. Patient notes were also reviewed where available.
Results: Fractures were the second most common presentation for suspected physical abuse (28%), bruising being the first. Thirty-three percent of patients were previously known to children's services. Likelihood of abuse was reported in 85 cases. Of these, 25% were thought to be highly likely or confirmed as physical abuse.
35% of SS had at least one fracture (median: 0, mode 0, range: 0-9). Skull fractures were the most common site (46% of positive SS). There were only 3 vertebral fractures (2.5%) with evidence of soft tissue injury, bruising and shaking: two diagnosed on initial SS, one on follow up SS. There were no hand or foot fractures.
Inter-rater reliability
Kappa (all 3 pairs) was calculated first, given that discrepancies have different levels of clinical importance. All were rated good (range 0.67 - 0.76) inclusive of all discrepancies. Discrepancies that would have had a clinical impact (grade 3) were all rated very good (range 0.84 - 0.88).
Mean kappa (Conger's method) inclusive of all discrepancies was good (0.72). When assessing grade 3 discrepancies only, agreement was very good (0.86), z-score -2.65, p-value 0.01.
Intra-rater reliability
Cohen's kappa was performed twice for each observer, once using all the repeat patients, then removing patients where repeats were noticed (distinctive artefact/fracture). There was little or no variation between kappa when obvious repeat patients were removed

(0.81 vs 0.88). Reliability was very good for all three observers, all variations testing ≥0.8.
Conclusions: From our cohort, there were only 3 spine fractures and no hand or foot fractures.
Lateral spine radiographs can be removed from SS provided: no clinical evidence of injury to this area (bruising, swelling); no signs of spinal cord damage or compression (provided thorough neurological examination performed); high quality AP radiographs have been performed. Hand and foot radiographs can be removed from SS provided no evidence of injury to these areas on physical examination.

Paper #: 129

Normal values for size of ovaries, testes, uterus, and breast buds at birth

Summer Kaplan, **M.D.**, *Radiology, The Children's Hospital of Philadelphia, Philadelphia, PA, kaplans2@email.chop.edu;* Christopher Edgar, Eileen Ford, Margaret Adgent, Joan Schall, David Umbach, Walter Rogan, Virginia Stallings, Kassa Darge, MD, PhD

Organ Size in the Neonate

	Number	Long Axis, cm			Volume, cm³		
	Subjects/Organs	Mean (SD*)	5th – 95th %-ile	CV†	Mean (SD)	5th – 95th %-ile	CV
Female							
Uterus‡	194/194	4.2 (0.6)	3.3 – 5.0	0.14	10.0 (3.5)	5.0 – 16.2	0.35
Ovaries‡	154/266	1.0 (0.3)	0.6 – 1.5	0.30	0.2 (0.2)	0.1 – 0.6	1.00
Breast Bud§	194/388	1.2 (0.4)	0.6 – 2.0	0.33	0.7 (0.5)	0.1 – 1.7	0.71
Male							
Testes¶	204/408	1.1 (0.1)	0.9 – 1.3	0.18	0.3 (0.1)	0.2 – 0.4	0.33
Lambert#	–	–	–	–	0.4 (0.1)	0.2 – 0.5	0.25
Breast Bud§	204/408	1.1 (0.4)	0.5 – 1.9	0.36	0.6 (0.5)	0.1 – 1.7	0.83

* SD = standard deviation

† CV = coefficient of variation: $SD/mean$

‡ Volume of cylinder with elliptical base: $2\pi \times \frac{L}{4} \times \frac{W}{2} \times \frac{D}{2}$; L = length (SAG diameter), W = width (TRV diameter), D = depth (AP diameter)

§ Volume of prolate ellipsoid: $\frac{4\pi}{3} \times \frac{L}{2} \times \frac{W}{2} \times \frac{D}{2}$

¶ Lambert volume: $0.71 \times L \times W \times D$

Disclosures: All authors have disclosed no financial interests, arrangements or affiliations in the context of this activity.
Purpose or Case Report: Hormonally-sensitive organs in the neonate can change size within days of birth as circulating maternal estrogen wanes. Although several reports document the size of these organs through infancy, few focus attention on the near-birth period. If clinical anomalies prompt ultrasound evaluation of these organs, reference size standards would aid clinical judgment. We describe the size of the uterus, ovaries, testes, and breast buds in healthy term neonates, and we compare our results to those from previous reports.
Methods & Materials: We prospectively examined ovaries, uterus, testes, and breast buds in 398 infants (194 females, 204 males) using ultrasound. We measured the largest diameter of these organs in the sagittal, transverse, and anterior-posterior planes. We estimated summary statistics for length of the long axis and for volume calculated from measured diameters. We evaluated size differences by laterality and sex.
Results: Normal values for the 5th - 95th percentile for length and volume, respectively, were: uterus, 3.3 - 5.0 cm and 5.0 - 16.2 cm^3; ovary, 0.6 - 1.5 cm and 0.1 - 0.6 cm^3; testis, 0.9 - 1.3 cm and 0.2 - 0.4 cm^3 (or 0.2 - 0.5 cm^3 Lambert volume); female breast bud, 0.6 - 1.5 cm and 0.1 - 0.6 cm^3; male breast bud, 0.5 - 1.9 cm and 0.1 - 1.7 cm^3. Breast buds were larger in females than males. Laterality differences were typically below the precision of clinical measurement.
Conclusions: Using our data from a large cohort together with published values, we provide guidelines for evaluating the size of reproductive organs within the first 3 days of life. We suggest that between-subject variability in measurements may arise largely from the compressibility of the organ, while variability across publications may arise in part from different volumetric models or populations.

Paper #: 130

Fetal Intracranial MRI in Complicated Monochorionic Multiple Gestations Undergoing In Utero Therapy

Sherelle Laifer-Narin, **Rama Ayyala**, **M.D.**, *Columbia University Medical Center, New York, NY, rsa2121@columbia.edu;* Russell Miller, Lynn Simpson

Disclosures: All authors have disclosed no financial interests, arrangements or affiliations in the context of this activity.
Purpose or Case Report: Monochorionic multiple gestations are at risk for specific complications as a result of uneven distribution of a common placenta or shared placental circulation, with examples including unequal placental sharing (UPS), twin-twin transfusion syndrome (TTTS), and single twin demise. Fetoscopic laser therapy and radiofrequency ablation (RFA) are procedures that are utilized for severe UPS and TTTS presentations, respectively. Fetal MRI has been utilized to assess for intracranial hemorrhage and/or ischemia in viable twins following these procedures. The purpose of this study is to determine the incidence of intracranial insults in this cohort of patients.
Methods & Materials: A retrospective review of fetal MRI performed between April 2008 and August 2015 for the indication of detecting intracranial abnormalities in monochoronic gestations that underwent laser or RFA therapy was performed. Imaging studies were reviewed by two radiologists. Information obtained included presence of intracranial hemorrhage or sequalae of prior hemorrhage, presence of acute ischemia or sequalae of prior ischemia, and any other intracranial abnormalities detected.
Results: A total of 70 cases were identified, 37 post laser treatment and 33 post RFA treatment. There was one set of monochorionic/diamniotic triplets in each group. The time interval range between the interventional procedure and fetal MRI was 3 days to 3 weeks. Gestational age at MRI ranged from 20 weeks to 23 5/7 weeks. A single case of unilateral germinal matrix hemorrhage (1/33) was identified in the cohort of cases that underwent RFA. No abnormalities were seen in the remainder of RFA survivors. 37 monochorionic gestations were assessed in the post-laser MRI group, with 13 fetuses (12 twins/1 triplet) excluded due to in utero demise. Within the subgroup of single fetal demise, there was a single case of unilateral germinal matrix hemorrhage (1/13). In 12/13 cases with single fetal demise (11 twins, 2 triplets) there were no abnormal MRI findings. In 24 post laser pregnancies without in utero demise, intracranial MRI was normal for 48 twins.
Conclusions: Fetal MRI demonstrated a low rate of neuroanatomical abnormalities in this cohort of fetuses who underwent in utero intervention for complications due to monochorionic status.

Paper #: 131

Sonography and Neuromotor Outcomes in Prematurity

Brendan Litt, **Darren Palathinkal**, **MD**, *Radiology, Queen's University, Kingston, ON, Canada, 13dmp3@queensu.ca;* Omar Islam, Denise Castro, Don Soboleski

Disclosures: All authors have disclosed no financial interests, arrangements or affiliations in the context of this activity.
Purpose or Case Report: This study aims to provide evidence supporting routine sonographic Doppler evaluation of the anterior cerebral artery in the prognostication of neurodevelopmental disorders in preterm infants. Although resistive indices have been used to provide prognostic value in term babies with a history of hypoxic ischemic encephalopathy, there is little data on the prognostic value in preterms with otherwise normal neurosonograms that demonstrate no classic structural change to the neuroaxis.

Methods & Materials: A retrospective chart review and clinical follow-up of 59 infants yielded a gestational age range from 24 weeks to 32 weeks 6 days. Resistive index (RI) and peak systolic flow velocity (pSV) in the anterior cerebral arteries (ACA) were recorded without and with gentle compression of the anterior fontanelle by ultrasound probe. Study includes infants in whom a transcranial ultrasound was performed within the first 14 days of life. Patients with structural abnormalities were excluded. Neurodevelopment was assessed in up to 5 years of clinical follow-up, with specific search for fine motor delay, gross motor delay, and cerebral palsy. Mann-Whitney U-test was used for analysis of non-parametric continuous variables, and Chi-squared test was used for analysis of categorical variables. A receiver operating characteristic analysis was performed using selected ACA RI cut-off values.
Results: In preterm infants with favourable neuromotor outcomes at 2-5 year follow-up, mean ACA RI was 0.724 and in infants with neurologic impairment ACA RI was 0.638. Resistive index was significantly lower in infants with unfavourable neuromotor outcomes ($p<0.01$). A cut-off ACA RI <0.70 had a sensitivity of 79% and a specificity of 64% for predicting long-term neuromotor delay/abnormality (2-tailed chi-squared=7.96, $p=0.0048$).
Conclusions: On neurosonography, resistive index values of 0.6 to 0.8 on have typically been regarded as within the normal range. Our study suggests that infants with resistive index values within the ACA within the lower end of this range were significantly more likely to have subsequent NDD despite an otherwise normal neurosonogram. We submit that an ACA RI of below 0.7 may help identify those preterm infants at risk for NDD and warrant closer clinical follow-up in the special infant clinic.

Paper #: 132

Experience with Institutional Imaging Guidelines for Intussusception at a Regional Children's Hospital: Compliance and Outcomes

Sarah Farley, **M.D.**, *Radiology, University of Washington, Seattle, WA, farley@uw.edu;* Randolph Otto, Ramesh Iyer, A. Luana Stanescu, MD, Marguerite Parisi, MD,MS

Disclosures: All authors have disclosed no financial interests, arrangements or affiliations in the context of this activity.
Purpose or Case Report: For quality assurance, we reviewed adherence to and outcomes from our existing institutional intussusception pathway, in which patients presenting to the Emergency Department (ED) with suspected intussusception are initially imaged with 2-3 view abdominal radiographs.
Methods & Materials: Patients were identified by querying imaging report texts from 7/2014-12/2014 for radiographs, ultrasound (US), and fluoroscopy with keyword "intussusception," age ≤5 years, and ED location. Imaging studies and medical records were reviewed to see if the imaging pathway was followed, identify alternative imaging diagnoses, and assess patient outcomes. The primary outcome was ileocolic intussusception confirmed on fluoroscopic enema.

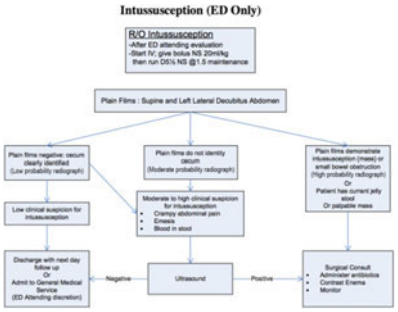

Results: 246 patients (155 male, 91 female) underwent 256 imaging workups for intussusception. Seventeen cases of ileocolic intussusception were found in 15 patients.
The radiography-first pathway was followed in 69.5% (178/256) of workups. These consisted of radiographs only (34.3%), radiographs + US (58.4%), radiographs + US + fluoroscopy (6.7%) in 12 intussusception cases, and radiographs + fluoroscopy (0.6%) in 1 intussusception case. Intussusception was confirmed in 7.3% (13/178) of pathway workups, including 0.8% (1/122) of workups with low probability radiographs, 18.5% (10/54) with moderate probability radiographs, and 100% (2/2) with high probability radiographs. Radiographic sensitivity was 92.3% and specificity was 73.7%. Low probability radiographs had NPV of 99.2% and moderate and high probability radiographs had PPV of 21.4%. Alternative diagnoses were found in 32.8% (20/61) of radiographs only workups and 29.8% (31/104) of radiographs + US workups.
The pathway was not followed, with US performed first in 30.5% (78/256) of workups. These consisted of US only (85.9%), US + radiographs (9.0%), US + radiographs + fluoroscopy (3.8%) in 3 intussusception cases, and US + fluoroscopy (1.3%) in 1 intussusception case. Intussusception was found in 5.1% (4/78) of first-line US exams (sensitivity: 100%, specificity: 100%, NPV: 100%, PPV: 100%). US found alternative diagnoses in 19.2% (15/78) of workups.
Conclusions: Similar rates of intussusception were found in the radiography-first pathway group and ultrasound-first group. More alternative imaging diagnoses were found in the pathway group. While test characteristics of ultrasound alone outperformed those of radiography alone for detecting ileocolic intussusception, first-line radiography had a high NPV and enabled selective use of ultrasound.

Paper #: 133

Reducing by three-quarter the surgical laparotomy rate for intussusception with the introduction of US-guided hydrostatic reduction

Daniel Solomon, **MD**, **MHA**, *Diagnostic Radiology, Addis Ababa University, Addis Ababa, Ethiopia, dzewdnehsolomon@yahoo.com;* Eyasu Wakjira, Samuel Sisay, Yocabel Gorfu, Tesfaye Kebede, Amezene Tadesse, Kassa Darge, MD, PhD

Disclosures: All authors have disclosed no financial interests, arrangements or affiliations in the context of this activity.
Purpose or Case Report: The management of intussusception (ISN) in children in Ethiopia, a developing country, has been exclusively surgical. Functional fluoroscopy units are rarely available. The use of ultrasound (US) for ISN reduction was not well-known. Following a CME course in which the utility and techniques of US-guided hydrostatic reduction for ISN were presented, we introduced this method in the main referral hospital of the country. The aim of this study was to assess the efficacy of US guided hydrostatic reduction of ISN as an initial non-surgical management option and to evaluate its impact on the rate of surgical intervention.
Methods & Materials: In this prospective, IRB-approved study from August 2014 to July 2015, all patients with positive US finding of ileocolic ISN were included. US including color Doppler was performed using a 7.5 MHz linear transducer. Following an informed written consent of the parents, US-guided hydrostatic reduction was attempted in those that fulfilled the inclusion criteria for reduction. The normal saline enema was performed using a Foley catheter with the balloon inflated. The on-call surgical resident was present during the procedure.
Results: During the 1-year study period 53 patients (43 males) with a mean age of 20 months were diagnosed on US with ISN. The median duration of symptoms at presentation was 30 h and included vomiting (98%), abdominal pain (96%) and bloody stools (62%). Six of the patients were excluded from hydrostatic reduction due to failure to meet the inclusion criteria. 4 of them had no flow on color Doppler US, 1 case presented after 5 days of onset of symptoms and the 6th case had a pathological lead point. US-guided hydrostatic reduction was attempted

in 47/53 and was successful in 41/47 (87%) of the patients. Overall, in 41/53 (77%) patients non-surgical management was successful. Out of the 6 cases with failed hydrostatic reduction 1 had a gangrenous bowel segment and 1 other an ileocolocolic ISN. There was a single case (2%) of bowel perforation during the procedure.
Conclusions: After the introduction of US-guided hydrostatic reduction of ISN in children, as the first non-surgical intervention for ISN in the country, the rate of surgical laparotomy in our hospital could be reduced from 100% to 23%. This US procedure resulted in successful reduction of ISN in 87% comparable to published reduction rates. The marked improvement gained in the care of children with ISN calls for a rapid widespread implementation of this method in the country.
After the introduction of US-guided hydrostatic reduction of ISN in children, as the first non-surgical intervention for ISN in the country, the rate of surgical laparotomy in our hospital could be reduced from 100% to 23%. This US procedure resulted in successful reduction of ISN in 87% comparable to published reduction rates. The marked improvement gained in the care of children with ISN calls for a rapid widespread implementation of this method in the country.

Paper #: 134

The usefulness of second time cranial ultrasonography in predicting the significant white matter injury of premature neonates

Byoung Hee Han, **Dr.**, *Radiology, Dankook University College of Medicine, Cheil General Hospital & Women's Healthcare Center, Seoul, Korea (the Republic of), ubf2931@msn.com;* Sun Young Ko, Yeon Kyung Lee

Disclosures: All authors have disclosed no financial interests, arrangements or affiliations in the context of this activity.
Purpose or Case Report: To determine the usefulness of the 2nd time cranial ultrasonography(US) taken 1 week after 1st US to predict the significant white matter injury in premature neonates below 32 weeks of gestational age.
Methods & Materials: Ninety-seven premature babies delivered below 32 weeks of gestational age had taken brain MRI on term-equivalent age. Among them, 91 babies who had taken first US below 1 week of age and taken follow-up US within 2 weeks (mean 7.3 days) were included in this study. They were divided by two groups according to the grading of periventricular echogenecity (PVE) - US Group 1: high PVE (grade 2 or more), US Group 2: low PVE (less than grade 2). We divided each group into two subgroups (1: low, 2: high PVE) according to the grade of PVE on 2nd times follow-up US. MRI findings were divided into two groups - group 1: normal to minimal periventricular leukomalacia (PVL), group 2: significant cystic or non-cavitary PVL. We evaluate that the grouping of 2nd times US is how much correlated with MRI grouping.
Results: Regardless of group 1 and 2 of first US, all the subgroup 2 babies (3 in group 1 and 13 in group 2) showed significant cavitary or noncavitary PVL (MR group 2). In case of subgroup 1, all 30 babies in US group 2 was MRI group 1 although 3 of 45 cases of subgroup 1 in US group 1 showed cavitary PVL on MRI (group 2).
Conclusions: The 2nd time cranial US taken 1 week after 1st US is useful to predict early the severity of the white matter injury.

Paper #: 135

Computer Aided Diagnosis (CAD4WHOKids) for WHO Endpoint Consolidation on Chest X-Ray in Children

Nasreen Mahomed, **MBBCh (Wits)**, **FC Rad (SA)**, **MMed (Wits)**, *University of Witwatersrand, Johannesburg, South Africa, nasreen.mahomed@wits.ac.za;* Bram Van Ginneken, Rick Philipsen R, Jamie Melendez, David Moore, Tanusha Sewchuran, Halvani Moodley, Shabier Madhi

Disclosures: All authors have disclosed no financial interests, arrangements or affiliations in the context of this activity.
Purpose or Case Report: **Introduction:** Pneumonia is the leading infectious cause of morbidity and mortality in children under 5 years globally, and the chest X-ray remains the most readily available and most common imaging modality for the assessment of childhood pneumonia. The number of radiologists in low income countries is limited. Standardization of chest X-ray interpretation in children is important to allow comparison of research between studies and to extrapolate results from different geographic areas. There is international need for the development of novel computer aided diagnosis (CAD) software for WHO standardized chest X-rays interpretation in children.
Objective: To determine the sensitivity and specificity of CAD (CAD4WHOKids) for WHO endpoint consolidation compared to a consensus human interpretation.

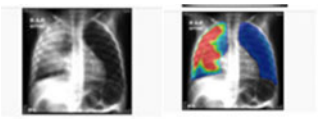

Fig 1a and 1b: 1a Frontal chest X-ray and 1b frontal chest X-ray colour heat map generated by the computer aided diagnosis software (CAD4WHOKids). Chest X-ray interpretation using computer aided diagnosis involved training and testing which was done in 10-fold cross validation. To obtain an image score on the test image, the 95th percentile score of the pixels was used. Example of a test image analysis using computer aided diagnosis textural analysis (fig 1b) demonstrates the area of WHO end-point consolidation correctly identified on the test image. The colour heat map generated demonstrates the area of WHO end point consolidation represented as red and blue representing normal lung fields.

Methods & Materials: This study is nested within the prospective PERCH study, South African site. Chest X-rays were independently evaluated by 3 radiologists (blinded to all clinical data) using modified WHO standardized chest X-ray interpretation criteria. The majority consensus was used as the final reading during the data analysis phase. CAD4WHOKids involved automatic lung field segmentation followed by manual inspection and correction, training, feature extraction and classification. In 858 interpretable chest X-rays, the areas of WHO endpoint consolidation and areas of other infiltrate were manually drawn to train CAD using a texture analysis system. Pixels in outlined regions were used as positive examples. Training and testing was done in 10-fold cross validation. Pixel data was filtered with Gaussian derivatives on multiple scales, extracting texture features to classify each region. To obtain an image score, the 95th percentile score of the pixels was used.
Results: For WHO endpoint consolidation versus normal chest X-rays (where normal chest X-rays were considered negative and chest X-rays with other infiltrate were excluded from the analysis), from the 651 chest X-rays used CAD4WHOKids generated a sensitivity was 82%, specificity of 80% and area under the ROC curve of 0.889. For WHO endpoint consolidation versus normal chest X-rays and other infiltrate (where normal chest X-rays and other infiltrate were considered negative), from the 858 chest X-rays used, CAD4WHOKids generated a sensitivity of 76%, specificity of 80% and area under the ROC curve of 0.858.
Conclusions: The results of the software CAD4WHOKids is promising for identifying WHO endpoint consolidation on chest X-ray in children. Further multicentre studies are required for validation of this software.

Paper #: 136

Magnetic Resonance Imaging of Congenital Lung Lesions

Christina Amaxopoulou, *Pediatric Radiology, University Children's Hospital, Zurich, Switzerland, camaxopulu@hotmail.com;* Ueli Möhrlen, Peter Bode, Christian Kellenberger

Disclosures: All authors have disclosed no financial interests, arrangements or affiliations in the context of this activity.
Purpose or Case Report: To evaluate the performance of magnetic resonance imaging (MRI) for assessment of congenital pulmonary malformations.
Methods & Materials: Retrospective review of consecutive lung MRI performed between 2013 and 2015 in 19 children (median age 0.4years, range 2 days -15 year) for suspected congenital lung anomalies with the detection of 20 lesions including congenital pulmonary airway malformation (*n*=9), sequestration (*n*=3), hybrid lesion (*n*=3), hypogenetic lung syndrome (*n*=2), congenital lobar hyperinflation (*n*=1), bronchogenic cyst (*n*=1) and bronchial atresia (*n*=1). Respiratory-gated fast spin echo and dynamic contrast enhanced images, obtained at 1.5 T during free breathing, were assessed for parenchymal, vascular and perfusion abnormalities. MRI findings were compared to those from computed tomography (CT) and to pathology following surgery, when available.
Results: Lung parenchyma of the 20 lesions was delineated as morphologically normal (*n*=3; 15%), solid (*n*=3; 15%), cystic (*n*=5; 25%), hyperinflated (*n*=2; 10%), or mixed (*n*=7; 35%). Mucus plugs were seen in 3 cases. Systemic arterial supply was evident in 8 cases and systemic or anomalous venous drainage in 4 cases. All parenchymal lesions showed altered perfusion, either as perfusion defect (*n*=12; 60%), delayed systemic perfusion (*n*=7; 35%) or both (*n*=1; 5%), which was helpful for lesion detection and characterisation in 8 cases (40%). Parenchymal findings were confirmed by CT in 8/8 cases. The type of congenital lung lesion was verified by intraaoperative and pathological findings in 15/15 cases. So far no correlation is availabe in 3 patients managed conservatively and in 2 patients awaiting surgery.
Conclusions: With a dedicated lung protocol, MRI is able to reliably delineate not only vascular but also parenchymal abnormalities. As complete characterisation of congenital lung lesions has become feasable, lung MRI should be considered as radiation free alternative to the current standard CT for postnatal evaluation of these lesions.

Paper #: 137

Chest X-Ray Findings in Children Hospitalized with WHO Defined Severe, Very Severe Pneumonia in a High HIV Prevalence Setting in the Era of Bacterial Conjugate Vaccines

Nasreen Mahomed, **MBBCh (Wits)**, **FC Rad (SA)**, **MMed (Wits)**, *Diagnostic Radiology, University of Witwatersrand, Johannesburg, South Africa, nasreen.mahomed@wits.ac.za;* David Moore, Tanusha Sewchuran, Halvani Moodley, Shabier Madhi

Disclosures: All authors have disclosed no financial interests, arrangements or affiliations in the context of this activity.
Purpose or Case Report: The chest X-ray remains the most readily available and commonest imaging modality for the assessment of childhood pneumonia, especially in resource limited countries. HIV has affected the epidemiology of childhood pneumonia, changing the profile of pathogens causing pneumonia, antimicrobial susceptibility and prognostic outcome. In the African setting, HIV- exposed-uninfected (HEU) infants have two to four times higher mortality compared to HIV-unexposed infants and pneumonia is an important cause. To date the impact of bacterial conjugate vaccines on chest X-ray findings in a high HIV prevalence setting in children hospitalized with pneumonia has not been described. Objectives: To describe and compare chest X-ray patterns in HIV-infected, HEU and HIV-unexposed children under 5 years hospitalized with WHO defined severe, very severe pneumonia.

Table 1 Summary of Chest X-ray findings in Children Stratified by HIV Status

Chest X-ray Pattern	HIV-infected N=108 (%)	HEU* N=284 (%)	HIV-unexposed N=428 (%)	HIV-infected vs HIV-unexposed OR (95% CI)	HEU vs HIV-unexposed OR (95% CI)
Airspace disease	65 (60)	91 (32)	163 (38)	2.5 (1.6-3.8)	0.8 (0.6-1.1)
Pleural disease	8 (7)	9 (3)	9 (2)	3.7 (1.4-9.9)	1.5 (0.6-3.9)
WHO end-point consolidation#	65 (60)	94 (33)	163 (38)	2.5 (1.6-3.8)	0.8 (0.6-1.1)
Other infiltrate only~	29 (27)	77 (27)	88 (21)	1.4 (0.9-2.3)	1.4 (1.0-2.0)
Chronic lung disease	5 (5)	4 (1)	5 (1)	4.1 (1.2-14.5)	1.2 (0.3-4.5)
Intrathoracic lymphadenopathy	18 (17)	41 (14)	68 (16)	1.1 (0.6-1.9)	0.9 (0.6-1.4)
Bilateral air trapping	21 (19)	42 (15)	60 (14)	1.5 (0.9-2.7)	1.1 (0.7-1.6)
Cardiomegaly	6 (6)	15 (5)	18 (4)	1.3 (0.5-3.5)	1.3 (0.6-2.6)
Normal^	7 (6)	81 (29)	123 (29)	5.8 (2.6-12.9)	1.0 (0.7-1.4)

*HEU HIV-exposed-uninfected
Airspace disease and/or pleural disease, may include other infiltrate only
~ other infiltrate without WHO end-point consolidation
^absence of airspace disease, pleural disease, other infiltrate, chronic lung disease, intrathoracic lymphadenopathy and bilateral air trapping

Methods & Materials: This study was nested within the prospective PERCH study, South African site. Children hospitalized with WHO defined severe, very severe pneumonia in Soweto, Johannesburg, were enrolled over 2 years (August 2011 to August 2013). Chest X-rays were interpreted by 3 radiologists independently, blinded to all clinical data, using modified WHO standardized chest X-ray interpretation criteria. The majority consensus reading was used during the data analysis phase.
Results: Interpretable chest X-rays were available in 858 (93%) of 920 children of 9.0 months mean age. Of these 108 (13%) were HIV- infected, 284 (33%) were HEU, 428 (50%) were HIV-unexposed and 38 (4%) of unknown HIV-exposure-status. The commonest finding was WHO end-point consolidation, prevalent among 60% of HIV-infected, 33% HEU and 38% HIV-unexposed children. WHO end-point consolidation was twice as common in HIV-infected (OR 2.5; 95% CI 1.6-3.8) compared with HIV-unexposed children. Pleural disease was four times as common in HIV-infected children (7%; OR 3.7; 95% CI 1 .4-9.9) compared to HIV-unexposed children (2%). Other infiltrate only was more common in HEU (27%; OR 1.4; 95% CI 1.0-2.0) compared with HIV-unexposed children (21%). Radiographic evidence of chronic lung disease (1-5%) and cardiomegaly (4-5%) were uncommon in all 3 groups, however chronic lung disease was 4.1-fold (95% CI: 1.2-14.5) more common in HIV-infected compared with HIV-unexposed children. Intrathoracic lymphadenopathy was prevalent in 14-17% of children and bilateral air trapping in 14-19% of children, with no significant difference between the 3 groups. The chest X-ray was more likely to be categorized as being "normal" among HIV-unexposed (29%; OR 5.8; 95% CI 2.6-12.9) compared to HIV-infected children (6%).
Conclusions: WHO end-point consolidation remains the commonest chest X-ray abnormality in HIV-infected, HEU and HIV-unexposed children under 5 years hospitalized for WHO-defined severe, very-severe pneumonia even in the era of routine HiB and PCV immunization. HIV-infected children were more likely to have WHO end-point consolidation and less likely to have normal chest X-rays compared with HIV-unexposed children. HEU children were more likely to have other infiltrate only compared with HIV-unexposed children. This supports literature that HIV exposure with or without infection causes increased susceptibility to bacterial infection and other opportunistic pathogens such as *pneumocystis jirovecii* pneumonia.

Paper #: 138

Diagnosis of secondary pulmonary lymphangiectasia in congenital heart disease: a novel role for chest ultrasound.

Christopher Lam, **MD**, *Diagnostic Imaging, The Hospital for Sick Children, Toronto, ON, Canada, christopherzlam@gmail.com;* Tanmay Bhamare, Tamadhir Gazzaz, Mike Seed

Table 1. Sensitivity, specificity, and likelihood ratios of ultrasound criteria for diagnosis of secondary pulmonary lymphangiectasia.

Criterion	Sensitivity (%)	Specificity (%)	Positive Likelihood Ratio	P-Value
Irregular lung surface	100.0 [69.2–100.0]	54.5 [23.4–83.3]	2.2 [1.2–4.2]	0.012
Subpleural cysts	90.0 [55.5–99.7]	45.5 [16.7–76.6]	1.7 [0.9–2.9]	0.149
Pleural effusion	20.0 [2.5–55.6]	100.0 [71.5–100.0]	NA	0.214
Subpleural cysts underlying surface irregularity	90.0 [55.5–99.7]	81.8 [48.2–97.7]	5.0 [1.4–17.6]	0.002

Brackets are 95% confidence intervals. NA = not applicable.

Table 2. Mortality of patients with and without secondary pulmonary lymphangiectasia.

6 deaths of 10 patients with secondary pulmonary lymphangiectasia[1]			
Underlying Condition	Age at Death (days)	Time from US to death (days)	Cause of Death
TAPVC	112	97	Respiratory failure, unable to extubate, weaned off ECMO
TAPVC	222	205	Cardiac arrest causing severe irreversible end-organ injury
TAPVC	367	366	Cardiopulmonary failure with poor prognosis, weaned off ECMO
HLHS	12	10	Stroke at birth, weaned off life support
HLHS	5	2	Cardiac arrest causing stroke
Cor Triatriatum	532	140	Upper airway obstruction in the setting of tracheostomy
1 death in 11 patients without pulmonary lymphangiectasia			
Underlying Condition	Age at Death (days)	Time from US to death (days)	Cause of Death
TAPVC	68	64	Unexpected death at home of unknown cause

Average follow-up time for alive patients was 31 months (range 4.5-59 months).
US = ultrasound. TAPVC = total anomalous pulmonary venous connection. HLHS = hypoplastic left heart syndrome. ECMO = extracorporeal membrane oxygenation.
[1]One of the ten patients was lost to follow-up

Disclosures: All authors have disclosed no financial interests, arrangements or affiliations in the context of this activity.

Purpose or Case Report: Secondary pulmonary lymphangiectasia (PL) is a rare complication of congenital heart disease (CHD), commonly due to pulmonary venous obstruction in hypoplastic left heart syndrome (HLHS) and total anomalous pulmonary venous connection (TAPVC). The diagnosis of secondary PL likely impacts prognosis and can potentially trigger aggressive therapy that may have a morbidity and mortality benefit. Secondary PL can be suggested by clinical or radiographic features, but definitive diagnosis is challenging and often requires lung biopsy. Preliminary observations at our institution suggest that PL may have a distinctive ultrasound (US) appearance. This study has two parts, 1) to investigate the role of chest US in the diagnosis of secondary PL, and 2) to compare the clinical course of CHD patients with and without secondary PL.

Methods & Materials: Chest US was performed on 21 inpatients with HLHS, TAPVC, or cor triatriatum. Clinically, 13 of these patients had obstructed pulmonary vein physiology (62% male, mean age 91 days old, range 1 - 430 days old), while 8 did not (63% male, mean age 111 days old, range 30 - 285 days old). The US presence of irregular lung surface, subpleural cysts, or pleural effusion was documented. When present, whether subpleural cysts were separate from or directly underlying lung surface irregularity was also assessed. The sensitivity, specificity, and likelihood ratio for each finding was determined in reference to the final diagnosis of secondary PL. Diagnosis of PL for reference standard was based on clinical course, other imaging, and biopsy when available. Clinical course for those with and without secondary PL were also compared.

Results: The 21 cases consisted of 9 HLHS, 10 TAPVC, 1 HLHS and TAPVC, and 1 cor triatriatum. 10 of the 21 patients had final clinical diagnosis of PL, all in the group with obstructive pulmonary venous physiology. Examples of chest US findings are shown in Fig 1. Diagnostic utility of US findings is summarized in Table 1. Statistically significant criteria include irregular lung surface (LR 2.2, 95% CI 1.2 - 4.2) and subpleural cysts underlying surface irregularity (LR 5.0, 95% CI 1.4 - 17.6). The diagnosis of secondary PL was associated with increased mortality (OR 20.0, 95% CI 1.7 - 238.6, p=0.017). Causes of mortality are described in Table 2.

Conclusions: Chest US plays a novel complementary role in the diagnosis of secondary pulmonary lymphangiectasia in CHD patients with pulmonary venous obstruction. These patients have worse prognosis.

Paper #: 139

Imaging Findings of Nuss Bar Migrations: A Retrospective Review

Lauren Binkovitz, *Mayo Clinic, Rochester, MN, bbinkovitz@gmail.com;* Larry Binkovitz, Benjamin Zendejas, Christopher Moir

Disclosures: All authors have disclosed no financial interests, arrangements or affiliations in the context of this activity.

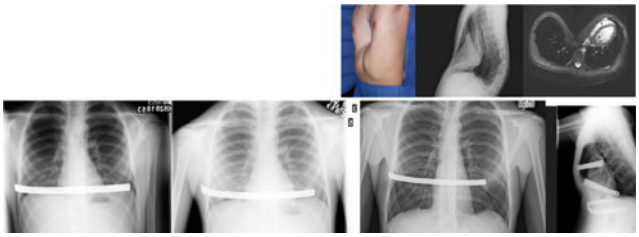

Purpose or Case Report: To assess the frequency and types of Nuss bar migrations/displacements following surgery for pectus excavatum deformity.
To illustrate the radiographic manifestations of Nuss bar migrations/displacements.
Methods & Materials: HIPPA-compliant and IRB approved retrospective review
Includes all patients who underwent a minimally invasive pectus excavatum repair at Mayo Clinic Rochester between April, 1998 to June, 2014.
Frequency and type of bar migrations/displacement were evaluated and recorded
All relevant imaging studies (radiographs, CTs and MRIs) were reviewed
Results: *N*=311 patients who underwent minimally invasive surgery for pectus excavatum deformity
Post-operative follow up for a mean of 3.8 years (0-16 years)
Bar migration was demonstrated in 23 patients (6%)
Nuss bar migration occurred: superiorly (*n*=6) inferior (*n*=4) lateral (*n*=4) rotary (*n*=3)
Single cases of lateral stabilizer bar displacement and of bar rotating about its long axis (flipping).
Miscellaneous/combination migrations were present in 4 cases.
Conclusions: Nuss bar migrations were present in a small number of patients and typically occurred soon after surgery. The radiographic manifestations of migration include superior and inferior displacement, lateral migration, and long or short axis rotation. Migration of lateral stabilizing bars can also be demonstrated radiographically. Radiologists should be familiar with these findings to expedite diagnosis and early repair.

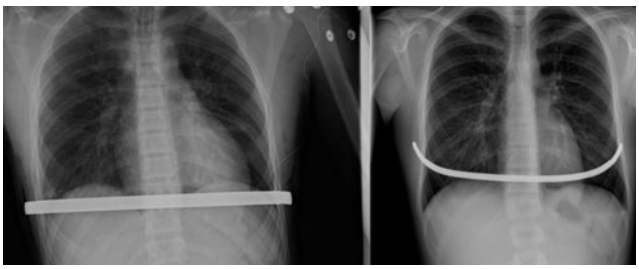

Paper #: 140

Thoracic CTA in Children with Hemoptysis: Imaging Findings and Implications for Appropriate Use

Arash Zandieh, **MD**, *Boston Children's Hospital, Boston, MA, zandieh.az@gmail.com;* Elizabeth Asch, David Zurakowski, Edward Lee

Disclosures:
Purpose or Case Report: To investigate imaging findings and determine appropriate utilization of thoracic CT angiography (CTA) in the pediatric patient with hemoptysis.
Methods & Materials: Following IRB approval, we retrospectively searched radiologic reports over the past 10 years (from January 2005 through October 2015) in order to identify pediatric patients (≤18 years old) at our institution who underwent thoracic CTA for the evaluation of hemoptysis. Thoracic CTA studies were evaluated by two pediatric radiologists for the presence of airspace disease, active pulmonary hemorrhage, arteriovenous malformation, and enlarged bronchial arteries or prominent aortopulmonary collaterals. The electronic medical record was reviewed for patient comorbidities (e.g. congenital heart disease, cystic fibrosis) and ultimate patient outcome. The decision for conventional angiogram with subsequent embolization procedure based on thoracic CTA findings was investigated.
Results: A total of 51 thoracic CTA examinations met search criteria, comprising 42 patients (22 females, 20 males; mean age 10.9; range 1 month to 18 years). Patient comorbidities included congenital heart disease in 9 patients (21.4%), laryngotracheal or pulmonary disease requiring tracheostomy in 5 patients (11.9%), cystic fibrosis in 4 patients (9.5%), metastatic lung disease in 3 patients (7.1%), and severe pulmonary hypertension in 1 patient (2.4%). All of these patients were hemodynamically stable at the time of thoracic CTA.
Among the 51 thoracic CTA studies, only 1 study (1.9%) had findings of active hemorrhage in a patient with severe pulmonary hypertension. Airspace disease was seen in 38 out of 51 studies (74.5%). No arteriovenous malformation was seen. A total of 18 studies (35.3%) showed enlarged bronchial arteries or significant aortopulmonary collaterals, in which 12 conventional angiograms (66.7%) were subsequently performed. A total of 11 of the 12 conventional angiograms (91.7%) underwent embolization.
Conclusions: Although thoracic CTA may have a limited role in detecting active hemorrhage in hemodynamically stable pediatric patients with hemoptysis, it can provide useful information regarding enlarged bronchial arteries or aortopulmonary collaterals, particularly when conventional angiography and embolization are anticipated.

Paper #: 141

Fifty shades of enhancement: timing of post gadolinium images strongly influences the degree of pathology on wrist MRI in children with Juvenile Idiopathic Arthritis.

Jasper Rieter, Laura Tanturri de Horatio, Charlotte Nusman, Lil-Sofie Ording Muller, Robert Hemke, Derk Avenarius, Mario Maas, **Karen Rosendahl**, *Academic Medical Center, Amsterdam, Netherlands, karen.rosendahl@helse-bergen.no*

Disclosures: All authors have disclosed no financial interests, arrangements or affiliations in the context of this activity.
Purpose or Case Report: Although early treatment with methotrexate and the biologics has reduced the morbidity in juvenile idiopathic arthritis (JIA), the observed long term side effects are concerning. This has necessitated accurate tools for monitoring treatment response, allowing for personalized therapy. Magnetic resonance imaging (MRI) has the potential to become such a tool. In contrast to adult rheumatoid arthritis, however, there is currently no standardized, validated and feasible assessment systems for the use of MRI in JIA, with the exception of knee-arthritis. The aim of the present study was to examine whether or not timing of post contrast images influences the MR-scoring of inflammatory change in children with JIA of the wrist.
Methods & Materials: Two post-contrast (Gd) 3D-GRE MRI sequences in 34 children with JIA (5 to 20 years of age; mean: 11 years) were analyzed. One acquired immediately after intravenous contrast injection, and an additional series obtained after approximately 10 min. The dataset was drawn from a prospective multi-centre project (Health-e-Child). We evaluated five locations in the wrist (the radioulnar (RU), radiocarpal (RC), mid-carpal (MC), 1st metacarpal and 2nd-5th metacarpal) for the following features: synovial enhancement (score 0-3), effusion (score 0-1) and overall inflammation (score 0-3). All the examinations were scored twice, in a blinded fashion, by en experienced paediatric radiologist; first based on the early post-contrast images and in a later session, based on the

late post-contrast images. The project was approved by the institutional Ethics' committees at OPBG, and written informed consent was obtained from all the patients or their caregivers.

Results: Mean time between early and late enhanced sequences was 6.4 min (range 5-14). Of the 170 locations scored, pathological contrast enhancement was seen in 100/170 when based on early postcontrast images vs. 131/170 when based on late postcontrast images. Fifty-two of the 170 locations (30.6%) received a higher synovial enhancement-score based on the late post-contrast images as compared to the early post-contrast images. 28 of the 52 locations were upgraded from score 0 to score 1, 21 locations from 1 to 2 and 3 locations from 0 to 2. Opposite, none of the locations received a lower score. As for the total inflammation scores, 60/170 locations received a higher total inflammation score based on the late post-contrast images. No statistically significant differences in effusion scores were seen.

Conclusions: A MRI-based scoring system for the presence and degree of synovitis should be based on a standardized MR-protocol, with a fixed interval between intravenous contrast injection and post-contrast images.

Paper #: 142

A Nanoparticle Contrast Agent Does Not Penetrate the Placental Barrier

Anil Shetty, Robia Pautler, Ketan Ghaghada, PhD, Zbigniew Starosolski, PhD, Rohan Bhavane, Igor Stupin, Saakshi Bhayana, Chandresh Patel, Chandrasekhar Yallampalli, Andrey Bednov, **Ananth Annapragada, Ph.D.**, *Baylor College of Medicine, Houston, TX, avannapr@texaschildrens.org*

Disclosures: Zbigniew Starosolski has indicated a relationship with Alzeca Biosciences, LLC. Rohan Bhavane has indicated a relationship with Sensulin LLC as a consulter and stockholder. All other authors have disclosed no financial interests, arrangements or affiliations in the context of this activity.

Purpose or Case Report: We hypothesized that a liposomal nanoparticle bearing gadolinium (Gd) chelates would not penetrate the placental barrier, and thus enable placental vascular imaging, with minimal (if any) exposure of the fetus to the contrast agent.

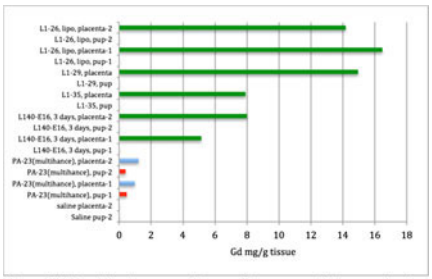

Figure 1. *Gd levels in placentae and fetuses, 1 hour post, and 3 day post imaging. Fetal Gd is only present when conventional Gd agent is used. Green: placental Gd, liposomal-Gd agent. Blue: placental Gd, Multihance. Red: fetal Gd. Gd levels measured by ICP-MS.*

Methods & Materials: To test the above hypothesis, we prepared such contrast agents and tested them in three models: (1) perfused human placentae representing normal pregnancy, gestational diabetes mellitus, and intrauterine growth restriction; (2) normal pregnant mice (3) pregnant rats under normal diet and low protein diet conditions. Fluorescent labeling of the lipids and ICP-MS analysis (for elemental Gd analysis) of perfusate and tissue was used to estimate barrier penetration by the liposomal contrast agent. In vivo MRI studies were performed on low field 1 T permanent MRI magnet and 9.4 T high field magnet. DCE-MRI studies were performed using T1w-GRE sequences.

Results: In the human perfused placentae, fetal side concentrations were less than 0.1% of the maternal side, less than the estimated leak in the perfusion model itself. In mice, the Gd detected in the fetus was below the detection limit of the ICP-MS methodology used (Figure 1). In contrast, conventional Gd chelates avidly penetrated the barrier and were readily detected on the fetal side (Figure 1). T1 weighted imaging in mice and rats exquisitely demonstrated the maternal placental vasculature, including the penetrating arteries, the placental labyrinth, the central arterial canal and the venous return (Figure 2). DCE-MRI studies demonstrated two zones within the placenta, the labyrinth zone that showed initial signal enhancement, and the proximal decidual zone that showed delayed signal enhancement. K_{trans} for the conventional agent was marginally lower than that for the liposomal agent, consistent with loss into the fetal compartment, while K_{ep} was substantially higher, consistent with rapid renal clearance of the conventional agent and extremely slow RES clearance of the liposomal agent.

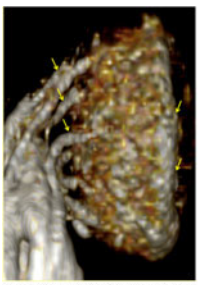

Figure 2. *High resolution imaging of vasculature in a single rat placenta. Liposomal-Gd contrast enhanced T1 weighted image using GRE FLASH on 9.4T MRI. Note the arterial supply (central), venous return (peripheral) and labyrinth (indicated by yellow arrows) on the maternal and fetal faces of the placenta respectively.*

Conclusions: The current study provides preliminary evidence for a liposomal-based Gd contrast agent with absence of placental barrier penetration. Extensive further testing of the agent to confirm maternal safety, and the lack of placental permeation is required before human use can be considered, but in the interim it offers a new tool for use in preclinical studies.

Paper #: 143

Utility of Gadolinium Use in the Imaging Follow-Up of Non-enhancing Primary CNS Neoplasms in Children

Brittany Albers, MD, *Radiology, Mayo Clinic Florida, Jacksonville, FL, albers.brittany@mayo.edu;* Chetan Shah

Disclosures: All other authors have disclosed no financial interests, arrangements or affiliations in the context of this activity.

Purpose or Case Report: Gadolinium based contrast agents (GBCAs) have been used for the evaluation of pediatric intracranial neoplasms since the 1980s. Excluding patients with renal failure, GBCAs are well tolerated and thought to be safe in pediatric populations. However, data has emerged that GBCAs used in routine clinical practice result in the deposition of gadolinium in the soft tissues even in patients with normal renal function. No studies have addressed deposition in pediatric brains. While no definite ill effect has yet been associated with this deposition, research is being done. With this in mind, our purpose was to retrospectively review the benefit of including GBCAs in the routine follow-up of primary pediatric intracranial neoplasms which did not initially enhance

Tumor Type	Age at Diagnosis	Pathology?	# F/U MRI with GBCA	Years of follow-up	Eventual Enhancement?
Anaplastic Astrocytoma	11.0	Yes	7	1.1	No
Astrocytoma (WHO II)	8.7	Yes	21	7.3	No
Astrocytoma (WHO II)	5.9	Yes	16	8.4	No
Astrocytoma (WHO II)	6.4	Yes	3	0.6	No
DNET	4.8	Yes	7	4.7	No
DNET	10.0	Yes	4	5.3	No
DNET	3.5	Yes	10	3.6	No
Oligodendrogtioma	9.7	Yes	11	9.2	No
Oligodendrogtioma	5.9	Yes	15	4.2	Yes**
Oligodendrogtioma	2.7	Yes	12	3.1	No
Brainstem Glioma	9.1	Yes	4	1.3	No
Brainstem Glioma	6.0	No	6	2.8	No
Brainstem Glioma	15.3	No	6	2.1	No
Brainstem Glioma	2.9	No	5	1.4	No
Teratoma	7.6	No	4	6.0	No
Tumor of Unknown Histopathology*	17.9	No	3	1.9	No
Tumor of Unknown Histopathology	15.0	No	3	3.1	No
Tumor of Unknown Histopathology	11.0	No	5	4.6	No
Tumor of Unknown Histopathology	12.8	no	2	0.7	No
Tumor of Unknown Histopathology	15.5	no	2	0.8	No
Tumor of Unknown Histopathology	8.3	No	4	2.8	No
Tumor of Unknown Histopathology	14.6	No	4	3.6	No
Tumor of Unknown Histopathology	0.4	No	3	0.8	No
Tumor of Unknown Histopathology	8.1	No	11	7.1	No
Tumor of Unknown Histopathology	7.7	No	9	8.6	No
Tumor of Unknown Histopathology	8.0	No	3	3.4	No
Tumor of Unknown Histopathology	10.1	No	3	1.3	No
Tumor of Unknown Histopathology	16.4	No	1	0.2	No
Tumor of Unknown Histopathology	13.9	No	3	1.6	No
Tumor of Unknown Histopathology	16.9	No	2	1.1	No

Table 1, 30 patients with initially non-enhancing primary intracranial nepolasms. * Tumors of Unknown Histopathology are those solitary CNS FLAIR hyperintense lesions with characteristics suggestive of low-grade glioma, but are in location that are either unsafe to biopsy or demonstrated no worrisome features so follow-up was recommended. None of the patients carry a diagnosis that renders them susceptible to

Methods & Materials: After obtaining IRB approval, we retrospectively reviewed 116 patients who were diagnosed and treated for primary intracranial neoplasm between 2001 and 2015. Thirty seven patients were identified with non-enhancing tumors, 7 were excluded due to lack of follow up imaging. We documented patient demographics, age at diagnosis, spectroscopy data, histopathology, and the number of follow up exams with GBCA, including the date of the most recent follow-up exams.

Results: Thirty patients are summarized in table 1. There were 11 girls and 19 boys with a median age at diagnosis of 8.9 years (0.4-17.9 years). Thirty patients received 189 MRIs with GBCAs. They received an average of 6.3 exams over an average of 3.4 years. A single patient developed a 2 mm nodule of enhancement along the resection margin 4 years following resection of an oligodendroglioma (Figure 1, attached). No other patient has developed enhancement or other evidence of recurrent / residual tumor.

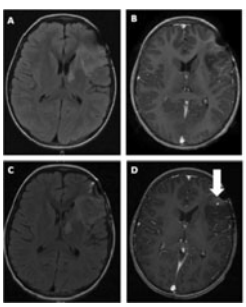

Figure 1.
A. Axial FLAIR December 2014.
B. Axial PG FS December 2014.
C. Axial FLAIR June 2015.
D. Axial PG FS June 2015.

Slight FLAIR abnormality (A) that was stable compared to prior (not shown) without any abnormal enhancement (B). Images obtained 6 months later show stable FLAIR appearance (C) with new 2 mm enhancing nodule (D, arrow).

Conclusions: Judicious use of GBCA in children, especially when numerous exams over many years are anticipated, is advised. Our preliminary results suggest that it may be feasible to omit GBCA from routine

follow-up in non-enhancing neoplasms which have been resected. Additional benefits include decreased exam time and decreased cost. The rate of call backs for further imaging with GBCA is expected to be low. Further research with evaluation of specific imaging parameters (scan time delay, type and dose of contrast, etc.) following contrast administration is warranted.

Paper #: 144

Safety of Gadoterate Meglumine in Over 1,600 Children Included In the Prospective Observational SECURE Study

Matthias Hackenbroch, *Radiology, University of Cologne, Köln, Germany, Matthias.hackenbroch@googlemail.com;* De Hua Chang, David Maintz

Disclosures: Matthias Hackenbroch has indicated a relationship.
All other authors have disclosed no financial interests, arrangements or affiliations in the context of this activity.
Purpose or Case Report: To assess the safety profile of gadoterate meglumine (DOTAREM®) in a broad patient population scheduled for contrast-enhanced Magnetic Resonance Imaging (MRI). Secondary objectives were to detect any case of Nephrogenic Systemic Fibrosis (NSF) suspicion and to collect efficacy data (image and diagnosis quality).
Methods & Materials: The SECURE study is a worldwide observational study including 35499 patients from 10 countries. Among them, 1631 patients less than 18 years old (4.6% of all patients) were included in 9 countries. MRI indication, risk factors and conditions of product administration were recorded for each patient. Adverse Events (AEs) occurring during MRI examination and usual follow-up were collected. A specific follow-up of at least 3 months was set up for patients with moderate to severe renal impairment in order to detect any case of NSF suspicion. Image quality was analyzed in a five point grading-scale (very poor, poor, fair, good and very good) and ability to come to diagnosis was assessed.
Results: The pediatric population of the SECURE study comprised 106 children (6.5%) less than 2 years, 815 (50.0%) in the 2-11 age class and 710 (43.5%) in the 12-17 age class, with a mean (± SD) age of 10.2 (±4.9) years. Pediatric patients were essentially recruited in India (47.8% of the total pediatric population), Germany (19.8%), and France (19.1%). The main MRI indication for the pediatric population was central nervous system (80.4%) and the most frequent pre-existing risk factors were nervous system disorders (16.6%), any stage of renal impairment (9.8%) and allergies (5.2%). Only one pediatric patient (0.06%) experienced one AE: vomiting of mild intensity. This AE occurred in a 2-year old child and was reported as non-serious and doubtfully related to gadoterate meglumine. No suspicion of NSF was reported during follow-up in patients with moderate to severe renal impairment. Good to very good image quality was obtained for more than 98% of the pediatric patients and diagnosis could be established for 99.6% of the cases.
Conclusions: The SECURE study confirmed the very good safety profile of gadoterate meglumine in a large pediatric population as well as its efficacy in terms of image and diagnosis quality in routine practice.

Paper #: 145

Evaluation of Potential Gadolinium Deposition in the Abdomen of Children Following Administration of Gadoxetate Disodium

John Roebel, *Cincinnati Children's, Cincinnati, OH, john.roebel@cchmc.org;* Jonathan Dillman, M.D., M.Sc., Bin Zhang, Alexander Towbin, MD

Disclosures: Alexander Towbin has indicated a relationship with Merge as a shareholder, Guerbet as anunrestricted grant/ consultant, Elsevier as an author and Applied Radiology as a consultant. Johnathan Dillman has indicated a relationship with Siemens Medical Solutions USA as a Primary Investigator. All other authors have disclosed no financial interests, arrangements or affiliations in the context of this activity.
Purpose or Case Report: Recently, there have been multiple reports of gadolinium deposition in the brain following contrast-enhanced MRI. These reports have shown a dose dependent effect related to the number of administrations of a gadolinium-based contrast agent. The purpose of this study was to determine if there is a relationship between precontrast T1-weighted signal intensity in abdominal organs and the lifetime total gadoxetate disodium dose in children.
Methods & Materials: Following IRB approval, we retrospectively identified all patients younger than 18 years of age in our department who had at least three MRI examinations with gadoxetate disodium before administration of a second gadolinium-based contrast agent. For all MRI examinations, precontrast T1-weighted 3D spoiled gradient recalled echo images were reviewed separately by two dedicated, fellowship-trained pediatric radiologists. Standardized circular regions of interest were drawn in various abdominal organs as well as in skeletal muscle and vertebral body. Linear mixed models were used to assess the relationship between the ratio of signal intensity in each abdominal organ (e.g., liver) to skeletal muscle and the lifetime total gadolinium dose (measured as cumulative dose/weight), adjusted for reviewer and random effects. All models were controlled for correlation between multiple measurements within each subject. A p-vale of <0.05 was considered significant.
Results: A total of 87 MRI examinations in 19 (11/19 female; mean age 9.5 years) patients were included in this study. The overall number of examinations per patient ranged from 3 to 10 (mean 4.6 examinations). Our results demonstrated a small but significant negative relationship between cumulative gadolinium dose and liver, pancreas, spleen, and renal cortex signal intensity ratios (p-values=0.035, 0.009, 0.010, and 0.022, respectively). There was no change in renal medulla and vertebral body signal intensity ratios with increasing cumulative gadolinium dose (p-values=0.22 and 0.15).
Conclusions: With increased cumulative lifetime dose of gadoxetate disodium in children, there is slightly decreased T1-weighted precontrast signal intensity within the liver, pancreas, spleen and renal cortex. These findings are surprising and suggest that another variable, such as iron deposition, may be present and confounding the data. Currently this data does not support the hypothesis that there is gadolinium deposition in abdominal organs after repeated administration of gadoxetate disodium.

Paper #: 146

NSsaFe study: Observational study on the incidence of nephrogenic systemic fibrosis in patients with renal impairment following gadoterate meglumine administration

Jeffrey Brown, *St. Louis University, St. Louis, MO, jjbrown@slu.edu*

Disclosures: All authors have disclosed no financial interests, arrangements or affiliations in the context of this activity.
Purpose or Case Report: To prospectively determine the incidence of Nephrogenic Systemic Fibrosis (NSF) after gadoterate meglumine (DOTAREM®) administration in the high-risk population of patients with renal impairment.
Methods & Materials: The NSsaFe study is a worldwide post-marketing study including hundreds of patients with moderate to severe and end stage renal impairment, scheduled to undergo a contrast-enhanced Magnetic Resonance Imaging (MRI) using gadoterate meglumine. Medical history, indication for MRI and renal function are recorded for each patient at inclusion. Adverse Events (AE) occurring during the MRI examination or the duration of usual follow-up post-gadoterate meglumine administration are recorded. Patients are then followed up over 2 years with 3 visits separated by at least 3 months in order to detect any occurrence of NSF.

Results: As of 6 October 2015, data from 540 patients (mean age: 69.6 years, range: 21-95; male: 58.5%) were analyzed. The population included 69.3% of moderate, 16.1% of severe, 12.0% of end stage renal insufficiency and 2.6% of kidney transplanted patients and the mean (±SD) eGFR was 37.6 (±15.7) ml/min/1.73 m^2 (range: 4.0-74.2). The main MRI indication was central nervous system (34.6%). A total of 369 patients attended the first follow-up visit (between 3 and 12 months after MRI), 231 patients attended the second (between 13 and 21 months after MRI) and 165 patients attended the third (between 22 and 27 months after MRI). No AEs related to the administration of gadoterate meglumine were reported. No cases of NSF have been observed.
Conclusions: This interim analysis confirms the excellent safety profile of gadoterate meglumine in the high-risk population of patients with renal impairment.

Paper #: 147

Arterial Spin Labeling: a normative value pediatric database

Priya Doerga, Matthias Wagner, Andrea Poretti, **Maarten Lequin**, *Plastic Surgery, Erasmus MC, Rotterdam, Netherlands, m.h.lequin@umcutrecht.nl;* Irene Mathijssen

Disclosures: All authors have disclosed no financial interests, arrangements or affiliations in the context of this activity.
Purpose or Case Report: Arterial spin labeling (ASL) is a magnetic resonance imaging (MRI) technique to quantify cerebral blood flow (CBF) without the use of a contrast agent. ASL has been shown to be useful in neurovascular disease, epilepsy and Alzheimer's disease among others. However not much ASL research has been done in the pediatric population, despite the advantages of ASL in this population, such as a shorter transit time and a higher cerebral blood flow than in the adult. In this study we want to create a reference database of the CBF in a healthy pediatric population, which could serve as a database of healthy controls for future research.
Methods & Materials: In this exploratory study, the ASL scans of 46 healthy children aged 0 to 4 years, were studied to create a CBF normative value database. The areas in which the CBF was studied included the cortex and white matter of the frontal, parietal, temporal and occipital lobe, deep gray matter and cerebellum. We used pseudo continuous ASL to assess the resting CBF. The ASL images were co-registered with the T1 and T2 weighted images. Post-processing and ASL measurements were done with GE AWserver.
Results: Multiple level analysis shows no significant differences between the left and right sides of the different structures that we measured. Significant differences were found between the four cerebral lobes and between the cortex, white and deep gray matter. A number of patients with syndromic craniosynostosis was compared to these normal controls. The patients with syndromic craniosynostosis showed a lower CBF in the cortex and white matter.
Conclusions: In this study we examined the CBF values in the brain, derived from ASL data from MRI's in healthy subjects. The values that were found are generally higher than the known data about CBF in adults derived from FDG-PET and SPECT. When used as a reference database the CBF in multiple patients groups, like craniosynostosis, can be assessed.

Paper #: 148

Amide Proton Transfer MRI Assessment of Brain Tumors: Preliminary Experience in Pediatric Patients

John Curran, **MD**, *Radiology and Medical Imaging, Phoenix Children's Hospital, Phoenix, AZ, jcurran@phoenixchildrens.com;* Houchun Hu, PhD, Amber Pokorney, Jonathan Chia, Richard Towbin, MD, Jochen Keupp

Disclosures: Jochen Keupp has indicated a relationship with Philips as an employee. All other authors have disclosed no financial interests, arrangements or affiliations in the context of this activity.
Purpose or Case Report: The purpose of this study is to evaluate the feasibility of non-Gadolinium (Gd)-contrast amide proton transfer (APT) MRI in assessing pediatric brain tumors. APT is a technique sensitive to amide proton groups, which are particularly prevalent in tumors.

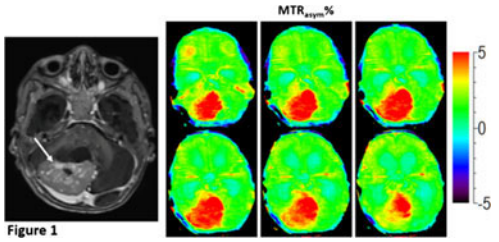

Figure 1

Methods & Materials: This pilot study was approved by our institutional review board and conducted on two 3 T Philips Ingenia MRI platforms with dual channel RF transmission and 32 channel head coils. Two patients underwent both APT MRI and standard brain MRI exams with Gd (Dotarem, Guerbet) contrast. The first patient was a 9-months old male with a lobulated right cerebellar hemisphere and vermian mass. The second patient was an 11-years old male with two intra-axial masses of metastatic Ewing's sarcoma, one in the right temporal lobe, the other in the right parietal lobe. APT MRI was performed immediately prior to tumor resection. For comparison, APT was also performed in pediatric patients (i.e., controls) without brain tumors. A pediatric neuroradiologist assessed the diagnostic utility of the APT data by comparing it to conventional T1, T2, and post-Gd images. Region-of-interest (ROIs) analysis was performed on the APT-weighted images to quantify the asymmetric magnetization transfer ratio (MTRasym), a recently reported potential biomarker of tumor activity and underlying tissue protein content. ROIs were drawn in tumor and healthy brain tissue for comparison. The APT technique was based on a 3D fast-spin-echo pulse sequence. The protocol consisted of 9-12 slices of 4.4 mm thickness, with a 180-220 mm field-of-view, an in-plane voxel size of 1.8×1.8 mm^2, and a TE/TR of 6.2 ms/5 s. APT scan time was 4-5 min. Additional technical details will be described in our presentation.

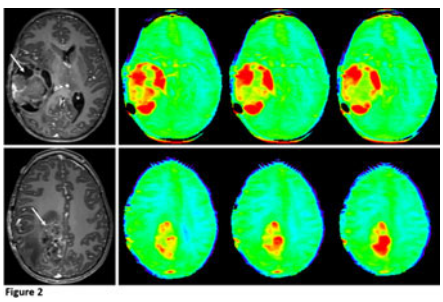
Figure 2

Results: Examples of APT-weighted images in patients with tumors are shown in Figures 1 and 2. The colorbar scale is the standard MTRasym metric. Post-Gd T1 images illustrate tumor enhancement (arrows). The figures show multiple APT slices to illustrate 3D coverage. Tumor APT signal measures in the 4-6% range, whereas from control data healthy gray matter signal is in the 1-3% range, and healthy white matter shows minimal signal. This study is ongoing as we further gain experience with APT.
Conclusions: Our preliminary experience with APT MRI in pediatric patients suggests promising clinical feasibility of APT in the assessment of Gd enhancing brain tumors. APT may eventually supplement or potentially supplant traditional Gadolinium-based imaging for brain tumor imaging.

Paper #: 149

The Diagnostic Yield of Head Ultrasound in Outpatient Infants Presenting with Benign Macrocrania

Alexa Stamler, *Gannon University, Erie, PA, stamler001@knights.gannon.edu;* Michael Rubin, MD, Lena Naffaa

Disclosures: All authors have disclosed no financial interests, arrangements or affiliations in the context of this activity.
Purpose or Case Report: Benign Macrocrania is a commonly encountered condition in the primary care outpatient setting referred for head US. Our purpose was to determine the frequency of head US findings that required a neurosurgical consultation and neurosurgical procedure for outpatients referred for benign macrocrania.
Methods & Materials: We performed a retrospective analysis from September 2011 until June 2015 on all outpatients referred to our US department for benign macrocrania. The US images and reports were reviewed along with follow-up imaging. In addition the electronic medical record was reviewed for the following: gender, referring physician specialty, first head circumference, head circumference closest to the time of the US, last known head circumference, neurologic issues, neurosurgical consultation, neurosurgical procedures, and clinical outcome.
Results: During the study period 326 outpatients underwent a head US for benign macrocrania. Eight patients were excluded for known abnormalities. Of the 318 remaining patients, 130 (40.8%) had a normal head ultrasound, 181 (56.9%) had benign enlargement of the subarachnoid spaces (BESS), and 7 (2.3%) had an abnormal head US that required a neurosurgical consultation. Of the 181 patients with BESS, 23 had follow up imaging with 22 having unchanged BESS or a normal head US and one a mild stable ventriculomegaly. Three patients (1%) that required a neurosurgical consultation had a mild stable ventriculomegaly. Four patients (1.3%) that had a neurosurgical consultation needed a neurosurgical procedure: a 6-week old with aquaductal stenosis, a 4 month-old with hydrocephalus, a 7 month-old with a malignant brain neoplasm, and a 4-month old with subdural hematomas from non-accidental trauma. Statistical analysis using the Kruskal Wallis Rank Sum Test and Fischer's Exact Test (Chi Square Test of Independence) demonstrated no statistically significant variable(s) that could differentiate the normal/BESS patients from the patients requiring a neurosurgical consultation.
Conclusions: With only 1.3% of outpatients undergoing Head US for benign macrocrania requiring a neurosurgical procedure we propose that short interval surveillance with head circumference and assessment for the development of neurologic abnormalities may be a more cost effective strategy then Head US.

Paper #: 150

Can MRI face the challenges of cerebellar mutism?

Anjali Sergeant, *Diagnostic Imaging, McMaster University, Mississauga, ON, Canada, anjali.sergeant@hotmail.com;* Adam Fleming, MD, JoAnn Duckworth, Brij Karmur, Forough Farrokhyar, Saleh Almenawer, Sheila Singh, Nina Stein, Pediatric Radiologist

Disclosures: All authors have disclosed no financial interests, arrangements or affiliations in the context of this activity.
Purpose or Case Report: To determine if there are surgical and/or MRI markers that increase risk for cerebellar mutism (CM) development in children after posterior fossa surgery for tumour resection.
Methods & Materials: Retrospective cohort-comparison study among patients diagnosed with childhood brain tumours from 2004 to 2015, extracted from the Pediatric Brain Tumour Study Group database. Patients were matched by age and tumour type. CM was defined as a significant lack of speech or loss of speech within 3 days post-operatively. Pre-surgical and first 48 h post surgical MRI images were reviewed. Clinical presentation, intraoperatory findings and acute post surgical complications were assessed. MRI findings including location of the tumor within the posterior fossa, presence of restricted diffusion and pattern of enhancement, presence of local infiltrative pattern or adjacent vasogenic edema, presence of CNS metastases or leptomeningeal enhacement and presumed imaging diagnosis are being investigated.
Results: 11/138 cases (8%) were identified with CM. 27/138 cases (19.5%) were diagnosed with posterior fossa medulloblastoma and 10 (37%) of these cases developed CM. 47/138 cases (34%) were diagnosed with posterior fossa pilocytic astrocytoma and only one case (2%) developed CM. There was no statistical difference on age and sex among the two groups. Preliminary results show that 10 (91%) patients with CM had tumour adherent to the floor of the fourth ventricle, compared to non-cases in which 5 patients (45%) had tumour invading the fourth ventricle. 9/11 (82%) of patients who developed CM had a gross total resection (GTR - defined by post-operative MRI), while only 4/11 (36%) of matched comparisons had a GTR. The mean size of tumour was not significant among the two groups. Further MRI data is being evaluated.
Conclusions: Review of the data reveals that the intra-operatory finding of tumor adherent to the floor of the 4th ventricle is potentially a risk factor to develop CM, as well as agressive surgeries in these cases. To our knowledge, this is a new described risk factor for development of post surgical CM in children with posterior fossa tumors. We hope that MRI analyses will be able to detect further imaging markers as well as predict the location of the tumor in relation to the 4th ventricle.

Paper #: 151

Can cranial Doppler ultrasound be used as a problem-solving tool in neonates with equivocal cerebral sinovenous thrombosis?

Li-tal Pratt, **MD**, *Tel Aviv Sourasky Medical Center, Tel Aviv, Israel, litalpratt@gmail.com;* Manohar Shroff, Helen Branson, Alan Daneman, Susan Blaser, Jose Jarrin, Elka Miller

Disclosures: All authors have disclosed no financial interests, arrangements or affiliations in the context of this activity.

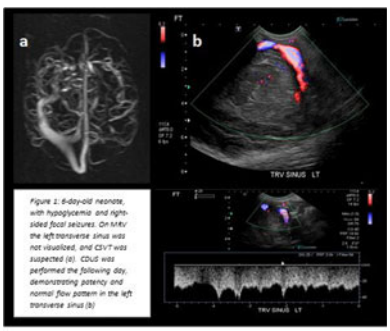

Figure 1: 6-day-old neonate, with hypoglycemia and right-sided focal seizures. On MRV the left transverse sinus was not visualized, and CSVT was suspected (a). CDUS was performed the following day, demonstrating patency and normal flow pattern in the left transverse sinus (b)

Purpose or Case Report: More than 40% of childhood cerebral sinovenous thromboses (CSVT) occur in neonates. Early detection provides an opportunity for treatment decisions, before complications occur. Diagnosis of CSVT in neonates can be challenging, even on cross-sectional imaging (CT, MRI). Cranial Doppler ultrasound (CDUS) was recently described as being highly specific for exclusion of CSVT in neonates. Our aim was to retrospectively evaluate CDUS as a problem-solving tool in neonates with indeterminate MRI/V neonatal CSVT.
Methods & Materials: Research ethics board approval was obtained to search for all neonatal unenhanced brain MRI/V performed between 2004 and 2014, which had CDUS done within a week apart. MRI findings equivocal for CSVT included: abnormal signal or diameter of a vein, and non-visualization or flow gaps on MRV sequences. CDUS was considered helpful when no clot was visualized on grey scale and normal

flow pattern was demonstrated (negative study), or when no venous flow was observed with or without clot visualization (positive study). Unhelpful CDUS included cases with partial assessment of the venous sinuses or slow-flow patterns.
Results: 75 neonates had both MRI/V and CDUS performed within a week apart. 59 neonates (16 preterms) had MRI findings non-conclusive for diagnosis of CSVT. The common indications for performing CDUS included non-visualization or flow-gaps involving: left transverse sinus (34/59, 58%, (figure 1a)), right transverse sinus (24/59, 41%), superior sagittal sinus (13/59, 22%), left sigmoid sinus (9/59, 15%), right sigmoid sinus (5/59, 8%) and straight sinus (6/59, 10%). CDUS was helpful (figure 1b) in 49 (83%), and positive in 9 cases (15%). In 6 cases (10%) CDUS was unable to visualize the veins in question, and in 4 cases (7%) only partial assessment was achieved (reasons for incomplete exam were technical factors: operator dependent, difficult access and limited window).
Conclusions: CDUS is a quick, non-invasive modality that can be readily used at bedside as part of the routine neonatal care as an adjuvant tool in cases of indeterminate CSVT on MRI scans. It can easily prove patency, providing flow pattern assessment, in common scenarios of anatomical variants, such as venous hypoplasia. The ability to characterize various sinovenous appearances and flow patterns is highly operator-dependent; however, the technique is simple, with only a short training required.

Paper #: 152

Incidence of Venous Sinus Thrombosis and Blunt Cerebrovascular Injury in Pediatric Temporal Bone Fracture

Nathan Webb, **M.D.**, *Radiology, University of Colorado, Aurora, CO, nathan.webb@ucdenver.edu;* David Mirsky, Laura Fenton, MD, John Maloney, Nicholas Stence, MD

Disclosures: All authors have disclosed no financial interests, arrangements or affiliations in the context of this activity.
Purpose or Case Report: The reported prevalence of blunt cerebrovas cular injury (BCVI) in children (15.4-25.8%) is higher than in adults (2.0-16.0%). The literature regarding trauma-induced venous sinus thrombosis (VST) is scant, but suggests a possible decreased likelihood in children compared to adults. Identified risk factors for VST include fractures that cross dural venous sinuses or the jugular bulb, and fractures of the petrous portion of the temporal bone, with incidence ranging from 22.4 to 34.9% in adults. This study aims to determine the prevalence of VST and BCVI in children who sustained temporal bone fractures (TBF) and underwent screening for vascular injury. At the time of this writing, this is the largest study undertaken to examine the incidence of trauma-induced VST in the pediatric population, and one of the largest to look at BCVI in children
Methods & Materials: This is a retrospective cohort study of pediatric patients (under 18 years of age) presenting to a large, tertiary care children's hospital over a 6-year period from 1/1/2009-12/31/2014. Using the keywords "temporal fracture," the authors searched through the imaging reports of multidetector computed tomography (CT) scans of the head performed at their institution during the specified time frame. The authors then searched the electronic medical record to determine what, if any, follow-up imaging was performed for those patients who sustained TBF. Follow-up magnetic resonance (MR), CT angiogram and CT venogram reports and images were reviewed for the presence or absence of VST and BCVI.
Results: 195 patients with TBF were identified. 77 patients (39.5%)received follow-up imaging to screen for VST or BCVI, based on the modified Denver criteria. 1 patient had VST, 1 patient had BCVI, and 1patient sustained both types of injury. 9 patients had indeterminate findings for vascular injury. Vascular injury was most common in fractures crossing the jugular bulb or sigmoid plate, occurring in 2/20 such fractures (10.0%). 2 patients suffered a stroke, both of whom had BCVI.
Conclusions: VST and BCVI are infrequent complications of blunt head trauma in the pediatric population, even in children with TBF. The incidence of VST in this study is lower than in previous studies in adults. Our incidence of BCVI is less than in earlier pediatric studies, and more consistent with previous findings in adults. The greatest risk factor for VST or BCVI identified in this study is fracture crossing the jugular bulb or sigmoid plate.

Paper #: 153

Evaluation of Arcuate Fascicules in Patients with Language Delay and Autism

Deniz Altinok, **MD**, *Children's Hospital of Michigan - Wayne State University, Detroit, MI, altinokd@yahoo.com;* Fidaa Wishah, Sheena Saleem

Disclosures: All authors have disclosed no financial interests, arrangements or affiliations in the context of this activity.
Purpose or Case Report: The arcuate fascicules (AF) is a major intrahemispheric association pathway, which is composed of arched fiber bundles connecting two cortical areas that play a major role in human language, Wernicke's (WA) and Broca's areas (BA).
There is a strong evidence to suggest an important contribution of AF to language function.
Patients with speech and language delay with or without Autism usually presented with unremarkable MRI of the brain. The purpose of this study is to evaluate the individual arcuate fascicules and compare it with the degree of speech impediment and correlate with MRI findings.
In contrast to the right AF whose presence is highly variable, the left AF has been consistently identified in normal subjects.

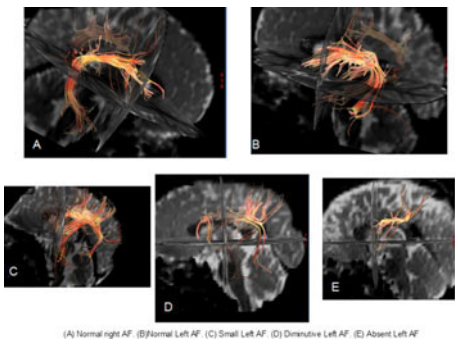

(A) Normal right AF. (B)Normal Left AF. (C) Small Left AF. (D) Diminutive Left AF. (E) Absent Left AF

Methods & Materials: This HIPAA-compliant study was approved by the local institutional review board.
A total of 81 patients were identified retrospectively with the following inclusion criteria:
Pediatric patients between 18 months and 12 years of age with mean of a 3.5 years.
Language development was characterized by a pediatric neurologist and was graded as mild, moderate and severe delay.
MRI of the brain performed at 3 T GE, including 55 Direction diffusion tensor tractography were evaluated by 2 different Pediatric Neuroradiologist.
Individual Arcuate fascicules were constructed and segmented and graded by deterministic tractography for all patients.
Results: Seventy five of 81 brain MRI were normal and 6 abnormal.
Fifty two of 81 diffusion tensor tractography studies of left arcuate fibers were abnormal..
Absent or significantly small left AF was strongly associated with language and speech delay. (p value 0.05), sensitivity 11%, specificity 100%, positive predictive value 100%.

Conclusions: 1. Patients with language and speech delay usually present with normal MRI of the brain but abnormal Diffusion Tensor tractography .
2. To accurately evaluate, DTI images should be obtained in every patient with speech and language delay.
3. Abnormal left arcuate fasciculus findings are strongly associated with language impairment

Paper #: 154

MRI Signal Intensity Characteristics of the Hemorrhagic Subdural Collections in Children

Marco Oriundo Verastegui, **Melissa Valdez Quintana**, **Pediatric Radiology Fellow**, *Medical Imaging, Children's Hospital of Eastern Ontario, Ottawa, ON, Canada;* Elka Miller, Jorge Davila, MD

Disclosures: All authors have disclosed no financial interests, arrangements or affiliations in the context of this activity.

Purpose or Case Report: The purpose of our study was to describe the MRI signal intensity (SI) characteristics of Hemorrhagic Subdural Collections (HSDC) according to time of original traumatic head injury in pediatric patients with dated and corroborated head injury.
Methods & Materials: Retrospective review. Inclusion criteria: 1) pediatric patients with known traumatic head injury that developed HSDC between January 2010 and December 2014, 2) known date of injury, 3) assessment with head 1.5 T MRI. Exclusion criteria: non-accidental head injury, excluded by the institution child abuse committee.
HSDC were classified according to the time of head injury in acute (0-3 days), early subacute (4-7 days), late subacute (8-21 days), and chronic (>21 days). SI of the homogenous subdural collections and the foci/sediment of the heterogeneous collections were compared with grey matter SI and classified as iso, high or low SI on T1WI, T2WI, FLAIR and DWI (b=0,1000) sequences by one pediatric radiologist and one pediatric neurorradiologist.
We also analyzed the signal intensity on T1WI and T2WI according to the time of injury and the mode, median and interquartile range (IQR) were calculated.
Institutional REB was approved before starting study.

Table N°1. Signal intensities (SI) characteristics of the hemorrhagic subdural collections on T1WI, T2WI, FLAIR and DWI sequences.

Stage	N	T1WI (n)	T2WI (n)	FLAIR (n) ±	DWI (n)[a]
Acute	3	High SI (2) Low SI (1)	Low SI (3)		
Early Subacate	9	High SI (6) Iso SI (2) Low SI (1)	Low SI (5) High SI (3) Iso SI (1)	Low SI (1) High SI (1)	Restriction (4)
Late Subacate	5	High SI (4) Iso SI (1)	Low SI (4) High SI (1)		Restriction (1)
Chronic	8	High SI (1) Low SI (7)	Low SI (1) High SI (7)	Low SI (2) High SI (2)	Restriction (2) No Restriction (3)

± FLAIR sequences were performed in 6SDH.
[a]DWI sequences were evaluated in 10 SDH
N.- Total number of SDH in each stage.
n.- number of SDH by signal intensity

Results: 13 cases reach the inclusion criteria (range of age: 3 days - 17 years). Mechanism of trauma included: delivery (2), fall of height (7) and motor vehicle accident (4). A total of 25 HSDC were reviewed, 11 homogeneous collections and 14 heterogenous collections.
According to the time of head injury we found 3 acute, 9 early subacute, 5 late subacute and 8 chronic HSDC. High variability of SI characteristic where seen in the different groups (results are summarized in table 1). The lower variability of SI was seen on chronic HSDC.
HSDC demonstrated T1WI low SI from 3 to 140 days (median: 56 days, IQR: 38-63 days) and T1 WI high SI from 3 to 39 days (median: 7 days, IQR: 6-11 days). They showed T2WI low SI from 3 to 106 days (median: 7 days; IQR 6-10 days) and T2WI high SI from 5 days to 140 days (median: 39 days; IQR 11-56 days).
Conclusions: There is overlapping of SI characteristics between the different stages of hemorrhagic subdural collections in pediatric population. Dating HSDC regarding its MRI SI characteristics is not accurate. Chronic HSDC have a tendency to show low SI on T1WI and high SI on T2WI, but these findings were also seen in subacute HSDC.

Paper #: 155

3 Tesla Multi-transmit Fetal Brain MRI: Preliminary Experience

Patricia Cornejo, **M.D**, *Pediatric Radiology, Phoenix Children's Hospital, Phoenix, AZ, pcornejo@phoenixchildrens.com;* Mittun Patel, Jonathan Chia, Houchun Hu, PhD, Amber Pokorney

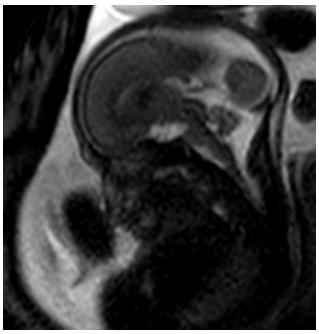

Disclosures: Johathan Chia has indicated a relationship with Philips Healthcare as an employee. All other authors have disclosed no financial interests, arrangements or affiliations in the context of this activity.
Purpose or Case Report: The objective of this work was to assess the diagnostic image quality of fetal brain MR images at 3 T using single-shot TSE images with and without the use of multi-transmit technology.
Methods & Materials: Ten fetuses with abnormal prenatal brain ultrasounds underwent non-Gadolinium contrast 3 T MRI evaluation between the second and third trimesters. All exams were performed according to a standardized protocol in a 3.0 T scanner (Ingenia; Phillips Medical Systems) with a 16 channel matrix coil. Fetal brain single-shot T2 weighted turbo-spin-echo images were obtained in sagittal plane with and without multi transmit technology (TR 4000 ms; TE 320 ms; voxel size 1×1.4×3 mm^3). Adding multi-transmit option to the pulse sequence does not require additional scan time.

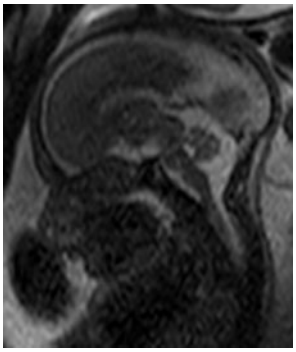

The diagnostic quality of the resultant images was independently assessed by 3 pediatric neuroradiologists in a blinded fashion. Each rater were shown non-multi transmit and multi-transmit images in a randomized manner without any text annotations or identifying information. The neuroradiologists were particularly asked to focus on the signal homogeneity of the amniotic fluid and the fetus in each image, and whether or not diagnostic confidence and visualization of fetal structures were superior in one image set versus the other. The rating was done on a 3-point scale (-1, 0, 1) with 0 representing equivalency between the non-multi-transmit and multi transmit results.
Results: One rater (13 years of experience) preferred the multi-transmit images for diagnostic quality in all ten cases. The second rater (20+ years of experience) preferred multi transmit images in 8 cases. In the remaining two cases, visualization of the fetus and overall image signal homogeneity was deemed similar between non-multi transmit and multi transmit images. The third reviewer preferred multi transmit images in 9 cases, and non-multi transmit images in the remaining case.
Conclusions: Our preliminary clinical experience demonstrates that routine fetal imaging at 3 T is possible and that multi-transmit RF parallel imaging should be employed to improve diagnostic image quality.

Paper #: 156

Twin Twin Transfusion Syndrome and Cerebral Pathology: A Comparison of Fetal MRI and Ultrasound

Beth Kline-Fath, MD, *Radiology, Cincinnati Children's Hospital Medical Center, Cincinnati, OH, Beth.Kline-Fath@cchmc.org;* Maria Calvo-Garcia, MD

Disclosures: All authors have disclosed no financial interests, arrangements or affiliations in the context of this activity.
Purpose or Case Report: Twin twin transfusion syndrome (TTTS), a complex condition which occurs due to unbalanced intertwin transfusion in monochorionic twin gestations, carries a significant risk of neurologic impairment. The purpose of this study is to determine the frequency of brain anomalies identified by fetal MRI in TTTS and correlate those with prenatal ultrasound (US).
Methods & Materials: This retrospective study was IRB approved. Prenatal imaging performed in monochorionic twin gestations were reviewed and placed in the study if a fetal MRI was performed and the criteria for TTTS was met, which included oligohydramnios in one twin sac and polyhydramnios in the other. The cerebral imaging findings were identified and correlated with prenatal US.
Results: 270 twin gestations met the criteria for TTTS. 32/270 (12%) pregnancies (mean gestational age 21 weeks) demonstrated cerebral findings on fetal MRI. A comparative US was available in all except 2/32 pregnancies. 24 donor twins had anomalies, 10 being cerebral malformations, 3 mild ventriculomegaly (VM) and 11 encephaloclastic in origin. The malformations included aqueductal stenosis (5), foreshortened vermis (2), anencephaly (1), alobar holoprosencephaly (1) and cloverleaf skull with enlarged extraaxial fluid space (EAFS)(1). 7 of these anomalies demonstrated cerebral abnormalities on US, including VM (4), anencephaly, holoprosencephaly and cloverleaf skull. In the two cases of mild VM, the ultrasound was interpreted as normal. The ischemic findings included diffuse parenchymal loss supratentorial (5), ischemia/edema (2), germinal matrix hemorrhage (4). In these 11 cases, 7 US were read as normal, 2 had no comparison, and 3 suggested mild VM. 12 recipients had abnormal findings. 9 of these were encephaloclastic with 6 germinal matrix hemorrhage (1 cerebellar), 1 parenchymal volume loss, 1 ischemic hemisphere and 1 multifocal cystic encephalomalacia. US was read as normal (7) or as VM in the 2 with volume loss. There were two cases of mild unilateral VM, 1 US read as normal and the other mild VM. 1 case of enlarged EAFS was normal via US. In total, 11/22 (50%) affected donors and 3/12 (25%) affected recipients with findings on fetal MRI were abnormal with US. Hypoxic ischemic abnormalities were not suggested via US in 14/18 cases (78%).
Conclusions: Fetal MRI identifies cerebral abnormalities in 12% of cases of TTTS, 7% (20/270) being encephaloclastic. MRI is more sensitive in the detection of hypoxic ischemic lesions than ultrasound in TTTS.

Paper #: 157

Assessment of Cerebral Perfusion in Infants with Hypoxic Ischemic Encephalopathy with Dynamic Color Doppler Sonography

Ricardo Faingold, MD, *Montreal Children's Hospital - McGill University Health Center, Montreal, QC, Canada, ricardo.faingold@gmail.com;* Guilherme Cassia, Chatchay Prempunpong, Christine Saint-Martin, Linda Morneault, Guilherme Sant'Anna

Disclosures: All authors have disclosed no financial interests, arrangements or affiliations in the context of this activity.
Purpose or Case Report: To evaluate the perfusion of the deep gray matter in infants with hypoxic ischemic encephalopathy(HIE) and to investigate the correlation between perfusion measurements and severity of disease with dynamic color Doppler sonography.
Methods & Materials: Prospective study with 3 groups of term infants with different levels of HIE at admission : mild, moderate and severe. A group of normal infants was studied for comparison. Head ultrasound (HUS) was performed between 24 and 36 h of life using standard technique.

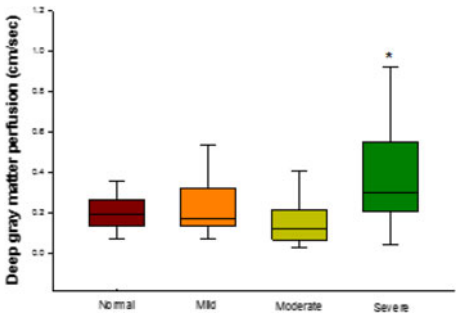

Measurements of cerebral perfusion were performed with an 11LW4 MHz linear array transducer to obtain DICOM color Doppler videos of blood flow in the deep gray matter (basal ganglia and thalami). The video images were analyzed using the *Pixelflux Chameleon* software, which allows automatic quantification of color Doppler data from a region of interest (ROI) by dynamically assessing color pixels and flow velocity (cm/s) during the heart cycle. Six videos of 3 s each were obtained for the ROI and used to calculate cerebral perfusion intensity (CPI).

The study was approved by the research ethics board, and informed consent was obtained from parents. Data was checked for outliers and the Shapiro-Wilk test for normality was applied. A linear regression model using cooling as interaction showed a p value<0.001. Thus, a *t-test* to compare Normal *vs* Mild (not cooled) and Moderate *vs* Severe (cooled) groups was performed. Data is presented as mean±standard error.

Results: A total of 66 term infants underwent HUS: Normal (n=17), Mild HIE (n=16), Moderate HIE (n=17), and Severe HIE (n=16). Infants with moderate and severe HIE were treated with therapeutic hypothermia. There was no significant difference on deep gray matter perfusion between Normal vs Mild infants (Figure). A statistically significant difference was observed between the Severe and Moderate HIE groups, with a much higher CPI noted in severely asphyxiated infants despite cooling treatment (p<.001). Interestingly, moderately asphyxiated infants had the lower perfusion values of all groups, likely secondary to the effect of therapeutic hypothermia.

Conclusions: A significantly increased perfusion of the deep gray matter using bedside HUS was observed in infants with severe HIE during treatment with therapeutic hypothermia. CPI measurements with dynamic color Doppler sonography has the potential to be used as a biomarker of disease severity and/or response to treatment in this population

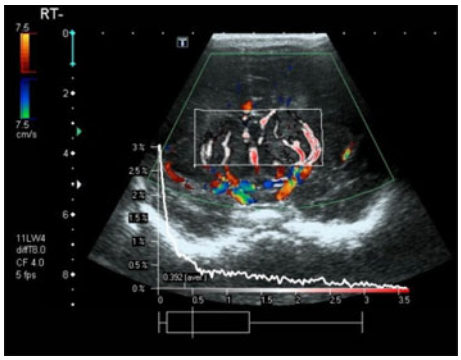

Paper #: 158

Pediatric Radiology: What Does it Take to get published?

Susan Shelmerdine, **FRCR MBBS BSc MRCS**, *Great Ormond Street Hospital, London, United Kingdom, susie_c_s@yahoo.co.uk;* Jeremy Lynch, Owen Arthurs, FRCR, PhD

Disclosures: All authors have disclosed no financial interests, arrangements or affiliations in the context of this activity.

Table 1
Table demonstrating th e APR and median impact factors (IF) of destination journals for studies according to country of origin of the first author. APR values were compared to the UK (index country) by Fisher's test.
***p** value statistically significant (<0.05)

Country	No. Abstract	No. Publications	Median IF	cAPR (%)	Relative 'Risk" Ratio	95% CI lower	95% CI upper	***P*** value
UK	53	12	2.56	0.23	1	NA	NA	NA
USA	366	153	2.53	0.42	1.85	1.00	3.40	0.049*
Canada	43	18	2.68	0.42	1.85	1.00	3.40	0.049*
France	38	15	2.78	0.39	1.74	0.92	3.29	0.105
Italy	30	6	1.65	0.20	0.88	0.37	2.11	1.000
Germany	17	7	1.81	0.41	1.82	0.85	3.87	0.208
Greece	12	3	1.65	0.25	1.10	0.37	3.31	1.000
Norway	11	7	2.80	0.64	2.81	1.44	5.49	0.012*
China	10	3	3.53	0.30	1.33	0.45	3.86	0.690
South Korea	9	5	2.36	0.56	2.45	1.14	5.29	0.099
Netherlands	8	6	3.08	0.75	3.31	1.75	6.27	0.006*
Israel	7	6	2.73	0.86	3.79	2.11	6.78	0.002*
South Africa	5	3	1.54	0.6	2.65	1.11	6.34	0.103
All other countries (15 countries)	68	18	1.56	0.26	1.17	0.62	2.21	0.676

Purpose or Case Report: To evaluate the abstract to publication rate (APR) for major pediatric radiology conferences, and identify predictive factors for publication success.

Methods & Materials: All Medline / PubMed database articles that originated from oral presentations at ESPR, SPR or IPR conferences 2010 - 2012 were evaluated. Published vs unpublished groups were compared, and "relative APR" was calculated by country. Multiple linear regression analyses were performed for publication and impact factor.

Results: Overall APR was 262/677 (38.7%), with no significant differences between prospective studies (71/176; 40%) or retrospective studies (191/497; 38%: p=0.65). The majority of articles were published in radiology specific journals (162/262; 62%), with overall median impact factor 2.29 (IQR 1.29, Range 0 - 18.03). Median study sample size in the

final published articles was 52 (IQR 102.5, range 1 - 6351), with 18 months median time from conference to publication. The best single predictor was number of abstract authors, although this accounted for only 10.4% variance in the data (95% CI 2.6, 18.1%; $p<0.01$). Using a multivariate model, abstract author number, first author country and pediatric subspecialty topic were the best predictors of successful conversion to publication.

Conclusions: 38.7% of pediatric radiology oral abstracts achieve publication after a period of at least 3 years from presentation. Studies with more authors, originating from certain countries and on certain subspecialty topics were more likely to get published.

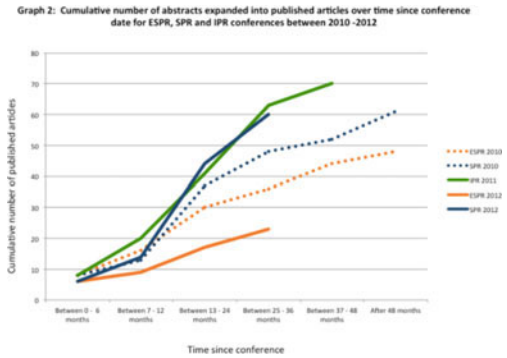

Paper #: 159

Visualization of altered pulmonary artery hemodynamics following TOF repair by 4D flow MRI

Julia Geiger, *Radiology, University Children's Hospital, Zurich, Switzerland, askja.julia@web.de;* Malek Makki, Emanuela Valsangiacomo-Büchel, Barbara Burkhardt, Kevin Johnson, Christian Kellenberger

Disclosures: Kevin Johnsom has indicated a relationship with GE Healthcare as a researcher. All other authors have disclosed no financial interests, arrangements or affiliations in the context of this activity.

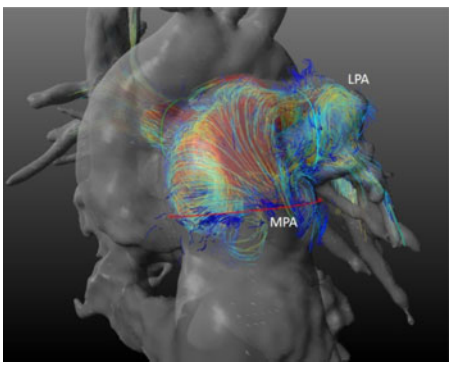

Purpose or Case Report: To evaluate hemodynamics of pulmonary arteries following repair of Tetralogy of Fallot (rTOF) in comparison to patients with normal cardiovascular anatomy using 4D flow MRI.

Methods & Materials: Prospectively ECG-gated, radially undersampled velocity-encoded time-resolved flow-sensitive MRI ("PC-VIPR": venc=200 cm/s, temporal resolution ~ 33-44 ms, isotropic voxels 1.4 mm^3) was performed in 18 rTOF patients (mean age 28±11 years, 7 female) and 11 patients with normal cardiovascular anatomy (age 24 ±11 years, 4 female) serving as control group. 3D hemodynamics in the main pulmonary artery (MPA), the right and left pulmonary artery (RPA, LPA) was visualized by color-coded particle traces according to the blood flow velocity and evaluated with regard to helices, vortices and backward flow in a consensus reading. Semi quantitative assessment with a 3-grade ranking scale was applied: 0=no helix/vortex/retrograde flow, 1=slight helix/vortex up to 360° rotation/slight retrograde flow, 2=severe helix/vortex more than 360° rotation/severe retrograde flow. Regurgitation fraction in the MPA and right to left blood flow ratios were assessed with retrospectively gated 2D PC sequences, and compared with independent t-tests between groups.

Results: RTOF patients revealed more systolic and diastolic helices in the RPA (14/18, mean grade 1.2) compared with the control group (6/11, 0.5) which usually showed a slight right-handed helix at the level of the bifurcation. Helices were less pronounced in the LPA (8/18, 0.6) in rTOF patients and only one control had a grade 1 helix. 2/18 rTOF patients showed vortices in the RPA (0.2) and 13/18 in the LPA (1.0) whereas none of the controls had any vortical flow. Increased flow turbulences were observed in the rTOF patients' MPA (11/18 helices, 0.9; 14/18 vortices, 1.3, figures 1 and 2). Retrograde flow was more frequent and severe in the LPA than in the RPA of rTOF patients (12/18, 1.1 vs. 8/18, 0.7) and highest in the MPA (13/18, 1.3). 5 patients without visual MPA retrograde flow had a 2D regurgitation fraction below 10%. RTOF patients had a mean regurgitation fraction in the MPA of 23%±17% vs. 0% in patients with normal anatomy. This was concordant with no detectable retrograde flow in visualization assessment. RPA/LPA ratio did not differ significantly between the two groups ($p=0.2$) but flow was slightly higher in the RPA in rTOF patients (59%/41%) vs. other patients (55%/45%).

Conclusions: Pulmonary flow analysis by 4D flow MRI reveals marked hemodynamic alterations in rTOF patients compared to patients with normal cardiovascular anatomy. There is a tendency to higher RPA helicity and pronounced LPA vorticity probably due to abnormal pulmonary artery geometry. Further analysis with regard to the type of surgical repair and potential correlation with the degree of pulmonary stenosis and insufficiency will be needed for better understanding of the observed flow patterns.

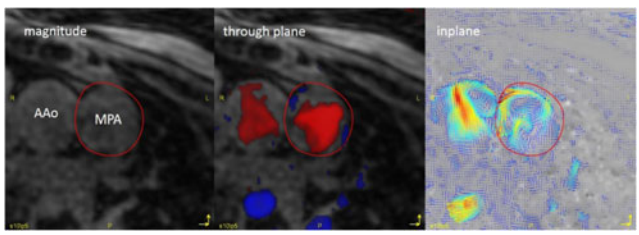

Paper #: 160

Flow-sensitive 4D MRI for the Follow-up of Pediatric Patients with Marfan Syndrome: Early Risk Stratification of Progressive Aortic Disease

Julia Geiger, *Radiology, University Children's Hospital, Zurich, Switzerland, askja.julia@web.de;* Kristina Gottfried, Daniel Hirtler, Julia Romberg, Brigitte Stiller

Disclosures: All authors have disclosed no financial interests, arrangements or affiliations in the context of this activity.

Purpose or Case Report: 4D flow MRI was performed to analyze aortic hemodynamics in patients with Marfan syndrome (MFS) to find suitable risk factors for early identification of high or low risk patients for cardiovascular complications.

Methods & Materials: Flow-sensitive 4D MRI (venc 200 cm/s, TE=2.4-3.7 ms, TR=4.8-6.1 ms, spatial resolution=(1.7-2.9) × (1.5-2.4) × (2.2-3.5) mm^3, temporal resolution=38.4-48.4 ms, field of view=210-270 mm

× 275-360 mm) of the thoracic aorta was performed twice (t1/t2) in 19 pediatric patients with MFS (mean age at t1: 12.7 +/- 3.6 years, t2: 16.2 +/- 4.3 years). Visualization of aortic flow was performed by 3D particle traces. Secondary flow patterns (helix and vortex flow) in the ascending aorta, aortic arch, and descending aorta were graded in three categories (blinded reading, 2 observers). Regional time-averaged absolute wall shear stress (WSS), peak flow velocity and oscillatory shear index (OSI) were assessed quantitatively at eight sites along the thoracic aorta. For statists, paired t-tests, Spearman's rank correlation coefficient and Cohen's kappa coefficient were applied.

Table

t_2	peak velocity	OSI	WSS	peak WSS
Z-Score<2 n=11	1.07±0.17 m/s	16.2±7.0%	0.23±0.07 N/m^2	0.45±0.22 N/m^2
Z-Score<2 n=8	1.12±±0.26 m/s	12.7±5.3%	0.26±0.10 N/m^2	0.55±0.28 N/m^2
p	0.15	<0.001	0.01	0.01

Results: The incidence of secondary flow patterns did not increase significantly between first (t1) and second (t2) examination (see figure: DAo vortex was present at t1 (left) and t2 (middle) with magnified vortex on the right). Aortic diameters decreased related to the patients' body surface area (aortic sinus: t1: 20.9±5.6 mm/m^2, t2: 18.9±4.0 mm/m^2, p=0.005). Peak flow velocity (t1: 1.19±0.17 m/s, t2: 1.09±0.21 m/s, p=< 0.001) and WSS (t1: 0.38±0.09 N/m2, t2: 0.24±0.08 N/m2, p<0.001) decreased, and OSI (t1: 9.11±5.44%, t2: 14.71±6.59%, p<0.001) increased significantly. A subgroup analysis by Z-scores demonstrated significantly higher WSS and lower OSI in patients with enlarged aortic diameters (Z-score >2, see table).
Conclusions: We detected no significant correlations between progress in WSS, OSI, flow patterns and aortic diameters, probably due to accelerated length growth rate during puberty and the current medication. Patients with larger aortic diameters seem to have a pro-atherogenic constellation. Further follow-up controls between the age of 20 and 30 years are mandatory to evaluate the critical life span for development of aneurysm and dissection. 4D flow MRI is a valuable tool to simultaneously analyze aortic diameters, flow and wall parameters in the follow-up of MFS patients.

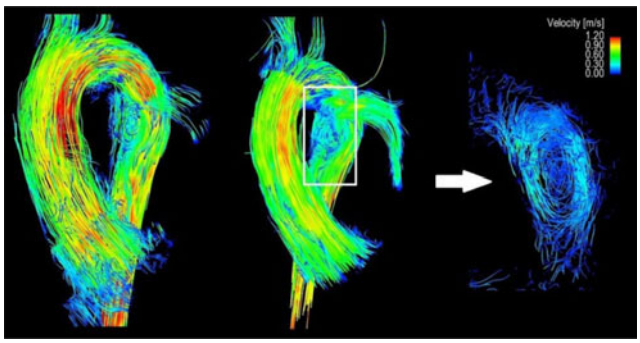

Paper #: 161

Serial Analysis of Aortic Hemodynamics in Patients with Repaired Aortic Coarctation by 4D flow MRI

Julia Geiger, *Radiology, University Children's Hospital, Zurich, Switzerland, askja.julia@web.de;* Julia Romberg, Daniel Hirtler, Kristina Gottfried, Brigitte Stiller

Disclosures: All authors have disclosed no financial interests, arrangements or affiliations in the context of this activity.
Purpose or Case Report: The aim of this study was to analyze the evolution of aortic hemodynamics in patients with repaired aortic coarctation (CoA) while aiming to detect specific characteristics of patients with coexistent bicuspid aortic valve (BAV).

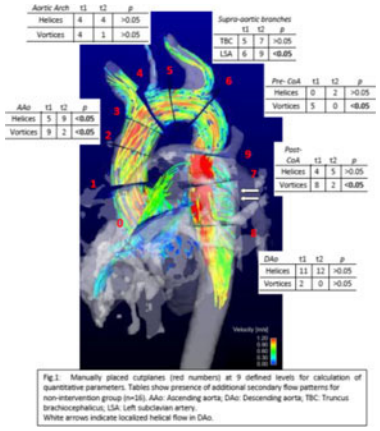

Methods & Materials: Two 4D flow MRI scans of the thoracic aorta (TE=2.4-2.7 ms, TR=4.8-5.0 ms, spatial resolution=(1.7-2.9) × (1.5-2.4) × (2.2-3.5) mm^3, temporal resolution=38.4-48.8 ms, field of view=210-270 mm × 275-360 mm, venc=200 cm/s) were performed in 28 CoA patients: mean age at first scan (t1) 14.6±7.9 years, at second scan (t2) 19.0±8.3 years. Wall shear stress (WSS), peak velocities and oscillatory shear index (OSI) were calculated at 9 defined levels of the thoracic aorta, and aortic diameters (ascending/descending aorta (AAo/DAo), arch, CoA) were measured. Blood flow visualization was performed by 3D particle traces. For statistical analysis, patients who underwent intervention (12/28) and patients with BAV (11/28) were evaluated separately.

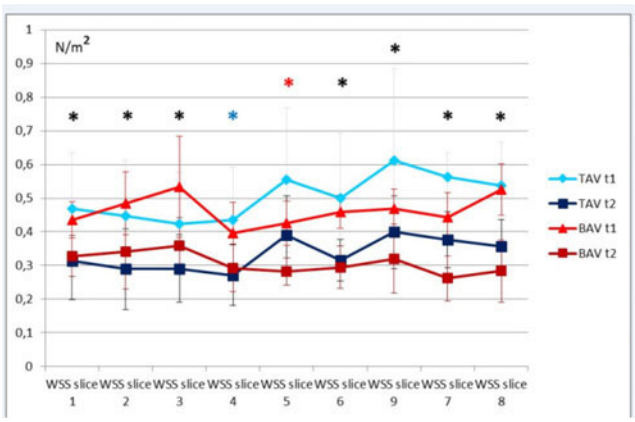

Results: Quantitative analysis showed an overall decrease in WSS (mean t1: 0.48±0.18 N/m^2, t2: 0.33±0.13 N/m^2; p<0.005) and an increase in OSI (t1: 7.16±4.05, t2: 9.98±4.76; p<0.05). The significant quantitative changes were even more pronounced in the group without intervention. AAo/DAo ratio decreased in all subgroups (t1: 1.44±0.29, t2: 1.34±0.18; p=0.017). Peak velocities decreased significantly in the AAo of all groups (t1: 1.42±0.37 m/s, t2: 1.27±0.37 m/s; p<0.001). BAV patients revealed lower OSI and higher WSS in the AAo (p>0.05, see figure 1) and lower peak velocities in the aortic arch, the CoA site and the DAo (p<0.05). The total number of secondary flow patterns decreased, whereas additional localized helices in the AAo increased (see figure 2).

Conclusions: In patients with repaired CoA, we noticed the normalization of aortic hemodynamics in the follow-up regardless of intervention. BAV patients showed specific characteristics in quantitative parameters and should be studied separately. 4D flow MRI permits the evaluation of qualitative and quantitative aortic changes in CoA patients over time that are not limited to the CoA site.

Paper #: 162

Feasibility of Non-Anesthesia Neonatal and Young Infant Cardiac Magnetic Resonance Imaging

Lillian Lai, **MD**, *Lucile Packard Children's Hospital, Stanford University, Radiology, Stanford, CA, lmlai@stanford.edu;* Joseph Cheng, Marcus Alley, Tao Zhang, Michael Lustig, Shreyas Vasanawala, MD/PhD

Disclosures: Tao Zhang has indicated a relationship with GE Healthcare as a research collaborator. Shreyas Vasanawala has indicated a relationship with Arterys, stock/consultant and GE Healthcare, research collaboration.
Joseph Cheng has indicated a relationship with GE Healthcare as a researcher. Marcus Alley had indicated a relationship with GE Medical Systems as a researcher and Arterys as a consultant. All other authors have disclosed no financial interests, arrangements or affiliations in the context of this activity.
Purpose or Case Report: We aim to evaluate the feasibility of anesthesia-free congenital heart magnetic resonance imaging (MRI) in neonates and young infants.
Methods & Materials: With IRB-approval, we retrospectively identified 17 consecutive neonates and young infants (1 day to 11 weeks old, median age of 3 days) who underwent a rapid two sequence (MRA and 4D-Flow) MRI protocol with intravenous ferumoxytol without sedation (n=13) or light sedation (n=4) between June 2014 and October 2015 for complex congenital heart disease (Table). Medical records were reviewed for clinical indication, ferumoxytol dose, medications, complications, whether any further diagnostic imaging was performed after MRI (including catheterization), and operative confirmation of MRI findings. Confidence interval of proportions assessed the likelihood of requiring additional diagnostic imaging test after MRI. A blinded reader scored the images on a five-point scale for overall image quality and delineation of various anatomical structures on MRA and 4D-Flow according to preset criteria. Wilcoxon-rank sum score was used to test the hypothesis that 4D-flow was superior to MRA in delineation of anatomical structures.

Patient Demographics

Age (days)	Weight (kg)	Heart rate (bpm)	Diagnosis
2	3	136	Heterotaxy, AV canal, arch hypoplasia
3	3.57	126	Heterotaxy, arch hypoplasia
3	3	122	D-TGA, single coronary artery, pulmonic stenosis
6	3.14	151	? Vascular ring
77	4.08	139	Heterotaxy with TAPVR
77	3.75	150	DORV with coarctation
1	2.54	127	Heterotaxy, DORV, AV canal, TAPVR
1	3.61	148	Hypoplastic left heart, TAPVR, coarctation
49	3.7	184	? Pulmonary vein stenosis
6	3.5	118	? Vascular ring
2	3.4	123	Heterotaxy, DORV, AV canal, TAPVR
1	3.56	147	Heterotaxy, DORV, AV canal, TAPVR, pulmonary stenosis
10	3.2	115	Tetralogy of Fallot with major aortopulmonary collaterals
2	3.43	154	? Loeys-Dietz, evaluate aneurysms and coarctation
2	3.25	136	Truncus
2	2.67	132	? Vascular ring
15	3.68	146	? Vascular ring

Results: One patient was scanned at 1.5 T (5.9%), and was the only subject requiring additional imaging, a CTA performed largely to assess for lung parenchymal disease, but in part also for further delineation of peripheral pulmonary arteries. The 80% confidence interval of the proportion of exams requiring further imaging was up to 13.2%. Out of 10 patients with operative confirmation, in only one patient, there was a minor discrepancy between the radiology report and operative procedure, with a small patent ductus arteriosus seen at surgery but not on MRI. 4D-Flow was significantly superior to MRA for the evaluation of systemic arteries (inclusive of coronary arteries), valves, ventricular trabeculae, and overall grade (Fig. 1). Mean scores for 4D Flow and MRA respectively were: systemic veins (4.9±0.2, 5±0), systemic arteries (3.8±0.8, 3±0) (p<0.05), pulmonary arteries (3.7 ±1.0, 3.4±0.6), pulmonary veins (4.5±0.8, 4.4±0.7), valves (4.1 ±0.8, 1.2±0.4) (p<0.05), ventricles (4.2±0.7, 3.4±0.5) (p<0.05), and overall score (4.1±0.6, 3.4±0.5) (p<0.05). An example is in Fig. 2.

Conclusions: Ferumoxytol-enhanced MRI without anesthesia is feasible for evaluation of complex congenital heart disease in neonates and young infants, with a low likelihood of need for additional diagnostic studies.

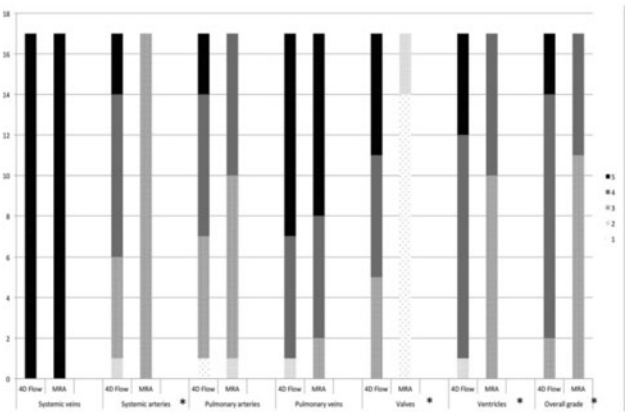

Figure 1: Side-by-side comparison of 4D-Flow versus MRA in the delineation of various anatomical structures. 4D-Flow was significantly superior to MRA for the evaluation of systemic arteries (inclusive of coronaries), valves, ventricular trabeculae, and overall grade (*p<0.05).

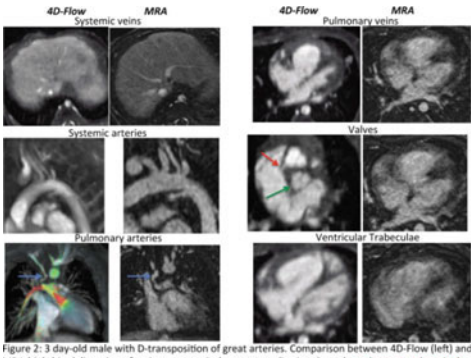

Figure 2: 3 day-old male with D-transposition of great arteries. Comparison between 4D-Flow (left) and MRA (right) in delineation of various anatomical structures. Depicted are the pulmonary valve, single-left-sided coronary artery, and right subclavian artery arising from right pulmonary artery.

Paper #: 163

Low Dose Dynamic CTA for Pulmonary Vein Obstruction in Children: A Technical Innovation

Pamela Deaver, **MD**, *Texas Children's Hospital, Houston, TX, pamela.deaver@gmail.com;* Prakash Masand, Siddharth Jadhav, M.D., Rajesh Krishnamurthy

Disclosures: All authors have disclosed no financial interests, arrangements or affiliations in the context of this activity.
Purpose or Case Report: Pulmonary venous pathology is a significant cause of morbidity in children, and decisions regarding intervention often hinge on whether obstructive physiology is present. The current standard for initial evaluation of these patients with single-phase CT angiography (CTA) is effective, but often compromised by: a) timing issues resulting in inadequate opacification of the obstructed pulmonary veins due to delayed filling and b) lack of functional information to assess severity or significance of anatomic narrowing. To overcome these pitfalls, we propose a novel low dose dynamic volumetric CTA (DVCTA) technique in this population.
Methods & Materials: In this IRB-approved study on patients referred to CT for suspected pulmonary vein stenosis, 7 patients (mean age: 13 months, range: 12 days-46 months) who underwent DVCTA and 2 patients who had cine pulmonary perfusion CT between March 2013 and October 2015 were retrospectively reviewed. Dynamics were obtained at 80 kVp and 20-30 mA a few seconds after brisk contrast injection via a lower extremity vein. The number of dynamics ranged from 7 to 15. Average effective doses were calculated based on ICRP 103 conversion. In patients with anatomic pulmonary vein stenosis, severity was assessed using qualitative differential flow and transit time analysis based on redistribution of pulmonary blood flow to normal segments, delayed wash in and washout, and poor parenchymal perfusion in affected segments.
Results: All studies were diagnostic, with first pass opacification of all the pulmonary veins and good image quality. Each dynamic resulted in effective dose of 0.26 +/- 0.05 mSv. A minimum of 7 dynamics were needed for optimal wash-in and wash-out analysis of normal and obstructed veins, which implies a cumulative dose of 1.84 mSv for a single dynamic CTA. This is comparable to the dose of a standard 64-slice ungated chest CT. Three patients had pulmonary vein stenosis with qualitative findings allowing objective grading of severity (Figures 1, 2). In one patient, there was anatomic moderate narrowing of a vertical vein draining the left upper lobe and lingula, with normal wash in-washout physiology, suggesting that the narrowing was not functionally significant. Remaining patients had normal morphology of the veins with normal transit.
Conclusions: Low-dose DVCTA is technically feasible, and offers the potential for timing independent opacification of the pulmonary veins by CT, and assessment of disease severity when pulmonary vein obstruction is present.

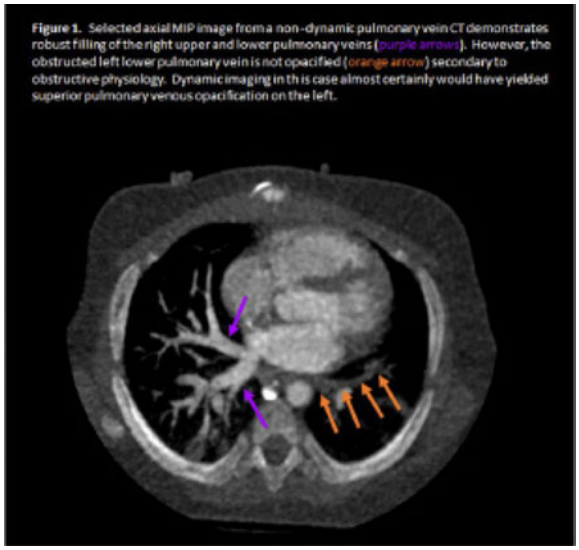
Figure 1. Selected axial MIP image from a non-dynamic pulmonary vein CT demonstrates robust filling of the right upper and lower pulmonary veins (purple arrows). However, the obstructed left lower pulmonary vein is not opacified (orange arrow) secondary to obstructive physiology. Dynamic imaging in this case almost certainly would have yielded superior pulmonary venous opacification on the left.

Paper #: 164

Peri-coronary fat sign on multidetector computed tomographic angiography (MDCTA): A new sign to determine presence and length of intramural course of anomalous aortic origin of the coronary artery (AAOCA)

Prakash Masand, **MD**, *Pediatric Radiology, Texas Children's Hospital, Houston, TX, drmasand@gmail.com;* Siddharth Jadhav, M.D., Silvana Molossi, Carlos Mery, Wei Zhang, Rajesh Krishnamurthy

Disclosures: All authors have disclosed no financial interests, arrangements or affiliations in the context of this activity.
Purpose or Case Report: To assess the diagnostic accuracy and inter-observer variability of the pericoronary fat sign on MDCTA, in determining the presence & length of intramural course of AAOCA, with surgical findings as the gold standard for comparison.
Methods & Materials: After IRB approval, diagnostic performance of MDCTA was evaluated in 25 consecutive patients who underwent surgery for AAOCA. A standardized protocol for volumetric MDCTA performance and interpretation in the setting of AAOCA was created. A new sign based on the absence of a complete cuff of pericoronary fat in the intramural segment, called 'pericoronary fat sign', was described, and compared to the oval versus round shape of the proximal coronary segment. Other pathologic variables in AAOCA, including type of AAOCA, radial location, height and shape of ostium, and presence of ostial stenosis were also assessed by 3 independent blinded readers using a numerical coded system. All targets were assessed similarly at surgery, the reference standard. Diagnostic performance of MDCTA was evaluated for each feature, and accuracy calculated on a per-target basis using weighted or unweighted kappa (range -1 to 1). Intra-class correlation coefficient analyzed the length of intramurality based on coronary vessel shape or lack pericoronary cuff of fat in the proximal course.

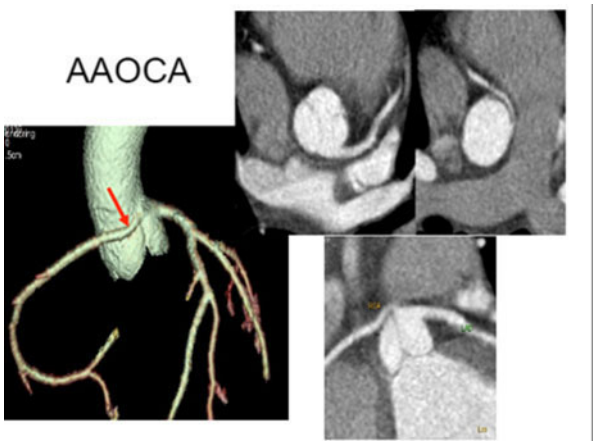

Results: MDCTA correctly identified AAOCA in all 25 coronaries. For the 3 readers, CTA had accuracy of 100% for detection of type of AAOCA, accuracy of 98%, 96%, and 92% respectively for detection of intramurality using the pericoronary fat sign, and 98%, 94%, and 92% respectively for detection of intramurality by vessel shape. The intra-class correlation coefficient for prediction of intramural length was 0.67, 0.75, and 0.81 respectively using pericoronary fat, and 0.69, 0.50, and 0.81 respectively using oval shape. Scatter plots with regression lines for length of intramurality based on pericoronary fat for the 3 readers, compared with surgery, is provided on figure 1.
Conclusions: The pericoronary fat sign on MDCTA evaluation of AAOCA, detected the presence of intramurality with high accuracy, and correlated with the length of intramurality with moderate accuracy, and may be used in conjunction with the shape of the proximal coronary to determine intramurality.

Paper #: 165

Cardiac catheterization (CC) compared with cardiac MRI (CMR) prior to second stage single ventricle (SV) palliation in low risk patients.

Christine Nelson, **MD**, *Department of Radiology, Texas Children's Hospital, Houston, TX, cn3@bcm.edu;* Pamela Deaver, MD, Luis De Leon, Dhaval Parekh, Shireen Hayatghaibi, MPH, Wei Zhang, Lauren Kane, Rajesh Krishnamurthy

Disclosures: All authors have disclosed no financial interests, arrangements or affiliations in the context of this activity.
Purpose or Case Report: CC or CMR are often used prior to second stage palliation for functional single ventricle patients. The study hypothesis is that CMR is a safer, less expensive, and an equally effective alternative to CC by comparing diagnostic accuracy, procedural morbidity and costs, operative morbidity, and clinical outcome between the two groups.
Methods & Materials: After IRB approval, a retrospective review of all patients undergoing a bidirectional Glenn at our institution from 2007 to 2014 was performed. A low-risk population, comprising 70% of all patients undergoing pre-Glenn evaluation, was isolated by excluding patients with severe atrioventricular regurgitation, severe ventricular dysfunction, aortic obstruction, pulmonary hypertension, pulmonary vein stenosis, or known large collaterals. Information was collected regarding clinical characteristics, diagnostic findings, procedural morbidity and costs, operative data, and post-operative morbidity and outcomes. End-points included specificity and negative predictive value of imaging findings, frequency of major or minor adverse events related to imaging, procedural costs, peri-operative complications, post-operative hospitalization duration, and clinical outcome, progression to cardiac transplant, or death. Continuous variables were compared via the Wilcoxon rank test, while categorical variables were compared via the Fisher's exact test.

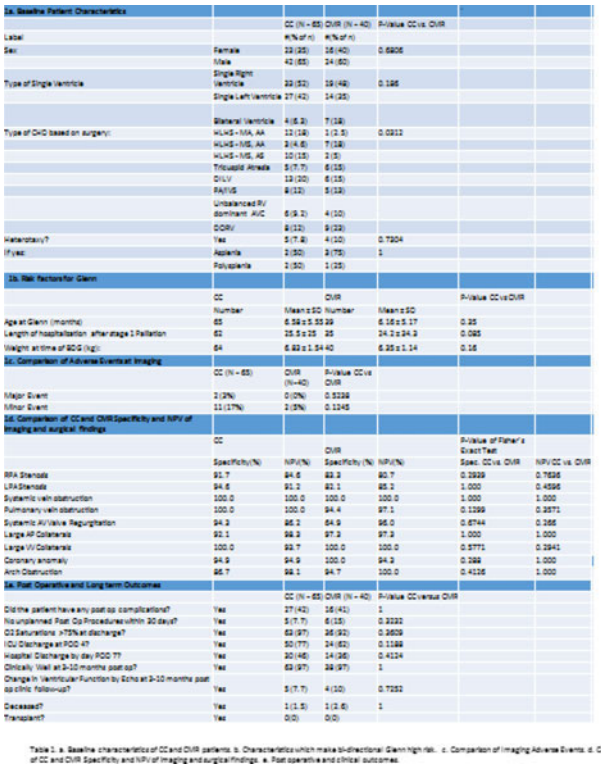

1a. Baseline Patient Characteristics						
		CC (N = 65)	CMR (N = 40)	P-Value CC vs. CMR		
Label		#(% of n)	#(% of n)			
Sex	Female	23 (35)	16 (40)	0.6806		
	Male	42 (65)	24 (60)			
Type of Single Ventricle	Single Right Ventricle	33 (52)	19 (48)	0.186		
	Single Left Ventricle	27 (42)	14 (35)			
	Bilateral Ventricle	4 (6.2)	7 (18)			
Type of CHD based on surgery:	HLHS – MA, AA	13 (18)	1 (2.5)	0.0312		
	HLHS – MS, AA	3 (4.6)	7 (18)			
	HLHS – MS, AS	10 (15)	2 (5)			
	Tricuspid Atresia	5 (7.7)	6 (15)			
	DILV	13 (20)	6 (15)			
	PAIVS	8 (12)	5 (13)			
	Unbalanced RV dominant AVC	6 (9.2)	4 (10)			
	DORV	8 (12)	9 (23)			
Heterotaxy?	Yes	5 (7.8)	4 (10)	0.7304		
If yes:	Asplenia	2 (50)	3 (75)	1		
	Polysplenia	2 (50)	1 (25)			
1b. Risk factors for Glenn						
	CC		CMR		P-Value CC vs CMR	
	Number	Mean ± SD	Number	Mean ± SD		
Age at Glenn (months)	65	6.58 ± 5.33.39		6.16 ± 5.17	0.35	
Length of hospitalization after stage 1 Palliation	62	25.5 ± 25	25	24.3 ± 24.3	0.095	
Weight at time of BDG (kg):	64	6.83 ± 1.54 40		6.35 ± 1.14	0.16	
1c. Comparison of Adverse Events at Imaging						
	CC (N = 65)	CMR (N=40)	P-Value CC vs CMR			
Major Event	3 (3%)	0 (0%)	0.5238			
Minor Event	11 (17%)	2 (5%)	0.1245			
1d. Comparison of CC and CMR Specificity and NPV of Imaging and surgical findings						
	CC		CMR		P-Value of Fisher's Exact Test	
	Specificity (%)	NPV (%)	Specificity (%)	NPV (%)	Spec. CC vs. CMR	NPV CC vs. CMR
RPA Stenosis	91.7	94.6	83.3	90.7	0.3939	0.7636
LPA Stenosis	94.6	91.3	93.1	95.3	1.000	0.4596
Systemic vein obstruction	100.0	100.0	100.0	100.0	1.000	1.000
Pulmonary vein obstruction	100.0	100.0	94.4	97.1	0.1299	0.3571
Systemic AV Valve Regurgitation	94.3	96.3	94.9	96.0	0.6744	0.366
Large AP Collaterals	93.1	98.3	97.3	97.3	1.000	1.000
Large VV Collaterals	100.0	93.7	100.0	100.0	0.5771	0.2941
Coronary anomaly	94.9	94.9	100.0	94.3	0.388	1.000
Arch Obstruction	96.7	98.1	94.7	100.0	0.4136	1.000
1e. Post Operative and Long term Outcomes						
		CC (N = 65)	CMR (N = 40)	P-Value CC versus CMR		
Did the patient have any post op complications?	Yes	27 (42)	16 (41)	1		
No unplanned Post Op Procedures within 30 days?	Yes	5 (7.7)	6 (15)	0.3332		
O2 Saturations >75% at discharge?	Yes	63 (97)	36 (92)	0.3659		
ICU Discharge at POD 4?	Yes	50 (77)	24 (62)	0.1186		
Hospital Discharge by day POD 7?	Yes	30 (46)	14 (36)	0.4124		
Clinically Well at 9-10 months post op?	Yes	63 (97)	38 (97)	1		
Change in Ventricular Function by Echo at 9-10 months post op clinic follow-up?	Yes	5 (7.7)	4 (10)	0.7252		
Deceased?	Yes	1 (1.5)	1 (2.6)	1		
Transplant?	Yes	0 (0)	0 (0)			

Table 1. a. Baseline characteristics of CC and CMR patients. b. Characteristics which make bi-directional Glenn high risk. c. Comparison of Imaging Adverse Events. d. Comparison of CC and CMR Specificity and NPV of imaging and surgical findings. e. Post operative and clinical outcomes.

Results: The total number of low risk patients undergoing pre-Glenn evaluation was 105, with 65 in the CC group and 40 in the CMR group. Both groups were similar in age, sex, type of SV, and prevalence of heterotaxy (Table 1a). Patient characteristics indicating a high risk Glenn procedure were similar in both groups (Table 1b). There was no significant difference in diagnostic specificity or negative predictive value for evaluation of the pulmonary arteries, pulmonary veins, aorta, systemic veins, atrioventricular valvular regurgitation or ventricular function (Table 1c). There was a higher incidence of major and minor adverse events with CC relative to CMR (Table 1d). There was no significant difference in bypass time, length of intubation, ICU duration, or hospital days after surgery, or in post operative morbidity (Table 1e). Procedural cost data is being gathered.
Conclusions: Low risk SV patients undergoing pre-Glenn evaluation by CMR or CC have similar diagnostic accuracy for major targets in SV, surgical morbidity and long term clinical outcomes, with a higher rate of procedural morbidity with CC compared to CMR.

Paper #: 166

Effect of Stage 3 Fontan Operation on Liver Stiffness in Children with Single Ventricle Physiology

Jonathan Dillman, **M.D.**, **M.Sc.**, *Cincinnati Children's Hospital Medical Center, Cincinnati, OH, jonathan.dillman@cchmc.org;* Frank DiPaola, Kurt Schumacher, Joshua Friedland-Little, Caren Goldberg

Disclosures: Johnathan Dillman has indicated a relationship with Siemens Medical Solutions USA as a Primary Investigator. All other authors have disclosed no financial interests, arrangements or affiliations in the context of this activity.

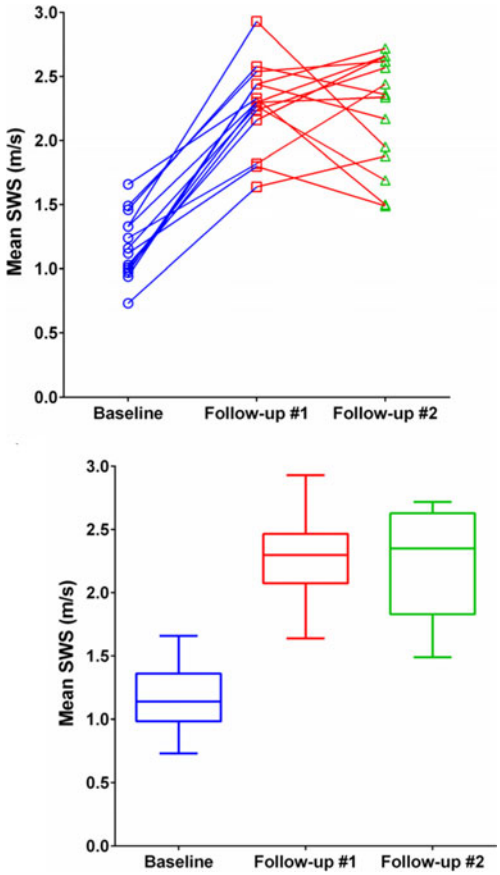

Purpose or Case Report: To determine the effect of Stage 3 Fontan operation on liver stiffness using ultrasound shear wave elastography in children with hypoplastic left heart syndrome/single ventricle physiology.

Methods & Materials: All children undergoing stage 3 Fontan operation for hypoplastic left heart syndrome/single ventricle physiology were approached between November 2014 and August 2015 at a single institution; 18 subjects were enrolled, and 14 subjects completed all study requirements. Eight ultrasound liver shear wave speed measurements (Acuson S3000 ultrasound system - Virtual Touch Quantification; Siemens Medical Solutions USA) were obtained from the central right hepatic lobe within the 4 week period prior to surgery, 2±1 days after surgery (follow-up time point #1), and within 1 days of planned hospital discharge (follow-up time point #2). Data were summarized as means and standard deviations. Change in mean liver shear wave speed over time was assessed using repeated measures one-way analysis of variance (ANOVA). Pairwise comparison of different time points also was performed using Tukey correction for multiple comparisons. A p-value <0.05 was considered statistically significant.

Results: **Results:** There were 5 girls and 9 boys. Mean age at the time of ultrasound prior to surgery was 35.1±10.6 months. Follow-up time point #1 was 2.4±1.0 days post-stage 3 palliation, while follow-up time point #2 was 7.3±1.5 days post-stage 3 palliation. There was a significant difference in mean shear wave speed between baseline and the two follow-up time points (p<0.0001). Mean liver shear wave speed at baseline was 1.18±0.26 m/s vs. 2.27±0.34 m/s at follow-up time point #1 (p<0.0001). Mean liver shear wave speed at baseline was 1.18±0.26 m/s vs. 2.22±0.44 m/s at follow-up time point #2 (p<0.0001). There was no difference in mean liver shear wave speed between follow-up time points #1 and #2 (p=0.92).

Conclusions: In children with hypoplastic left heart syndrome/single ventricle physiology, liver stiffness is normal prior to stage 3 Fontan palliation. There is a marked increase in liver stiffness immediately after stage 3 Fontan palliation that persists at the time of hospital discharge; it is uncertain if liver stiffness eventually returns to baseline (normal). Our results suggest that liver shear wave speed is potentially a confounded biomarker, as it can be significantly impacted by both liver congestion and fibrosis.

Paper #: 167

High Takeoff of Coronary Arteries: Incidental finding or Ischemic Predisposition?

Carol Ann Browning, MD, *Pediatric Radiology, University of Colorado, Aurora, CO, carol.browning@childrenscolorado.org;* Lorna Browne, James Jagger, David Mauchley, Jason Weinman, MD

Disclosures: All authors have disclosed no financial interests, arrangements or affiliations in the context of this activity.

Purpose or Case Report: Anomalous high takeoff of coronary arteries, defined as those originating above the sinotubular junction, have been reported to in less than 0.5% of the catheterized population with some considering it to be a benign normal variant. However case reports of this entity are scattered and opinions differ as to its clinical significance.

Methods & Materials: A retrospective review was conducted of 12 patients with the diagnosis of a high coronary artery origin on cardiac CT performed from November 2013 - September 2015. Coronary artery origin and course on CT were evaluated in each case with 2D, 3D and virtual angioscopic assessment. Relevant clinical and surgery history were recorded in each case.

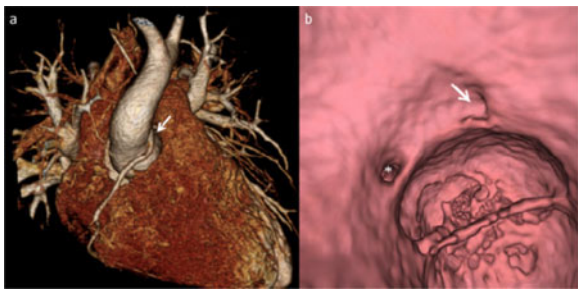

Results:

Patient ages ranged from 1 to 29 years at diagnosis. Anomalous high takeoff of the right coronary artery was involved in all. 1 patient had high takeoffs of both right and left coronary arteries. 10 patients demonstrated an interarterial course of which 7 underwent surgical correction. Six of the surgically corrected vessels were found to be intramural in location. The 2D and 3D morphological characteristics of these intramural courses included an elliptical orifice, proximal vertical descending course, narrowing, angle of origin of less than 30° and absences of epicardial fat. 3 patients (all interarterial and intramural) presented with exercise induced symptoms (chest pain/syncope). Nine patients were assymptomatic at presentation. Three of these had surgical correction of interarterial and intramural courses. One asymptomatic patient with a surgically corrected interarterial and intramural course had a first degree relative with a sudden cardiac death attributed to identical anomaly.

Conclusions: This data shows that interarterial and vertical descending intramural courses occur with relative frequency in patients with a high coronary origin, and that the virtual angioscopic appearance of the orifice was the most reliable CT morphological feature suggesting an intramural course.

Paper #: 168

Inter and Intra-Observer Variability in the Volumetry of Single Ventricle Hearts using a Standardized Approach to Segmentation on MRI

Nicholas Dodd, **BM**, *Radiology, Texas Children's Hospital, Houston, TX, nadodd@texaschildrens.org;* Ramkumar Krishnamurthy, Ph.D., Lamya Atweh, MD, Rajesh Krishnamurthy

Disclosures: All authors have disclosed no financial interests, arrangements or affiliations in the context of this activity.

Purpose or Case Report: Patients with single ventricle (SV) physiology after final palliation frequently undergo cardiac magnetic resonance imaging (CMRI) when echocardiography windows diminish or suggests ventricular dysfunction. The presence of complex and variable intracardiac anatomy has precluded development of semi-automated algorithms for volumetry of SV, and studies of reproducibility are scarce in this setting. We describe a standardized approach to segmentation of SV hearts that accounts for the diversity of morphology and evaluates the inter- and intra-observer variability of this approach.

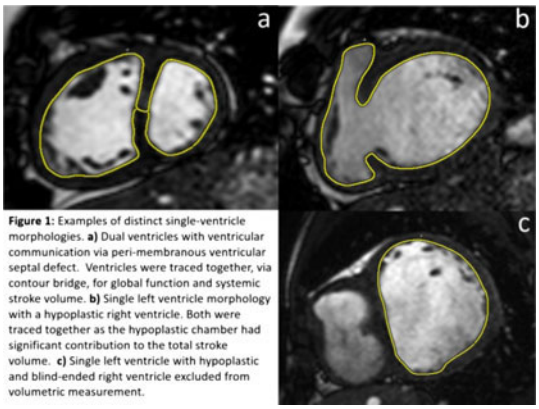

Figure 1: Examples of distinct single-ventricle morphologies. **a)** Dual ventricles with ventricular communication via peri-membranous ventricular septal defect. Ventricles were traced together, via contour bridge, for global function and systemic stroke volume. **b)** Single left ventricle morphology with a hypoplastic right ventricle. Both were traced together as the hypoplastic chamber had significant contribution to the total stroke volume. **c)** Single left ventricle with hypoplastic and blind-ended right ventricle excluded from volumetric measurement.

Methods & Materials: In 2013-14, 21 patients (9-17 years old) with SV physiology, status post total cavopulmonary connection (TCPC), and 9 healthy controls (8-17 years old) were prospectively recruited for CMRI. 2D cine SSFP short axis stacks were performed for volumetric analysis. SV hearts were classified as either single left ventricle (SLV), single right ventricle (SRV), or dual ventricles (DV). Each SV was treated as a single volume, and traced from apex to base, defined by bordering myocardium, and up to the aortic and atrioventricular valves, excluding septum (Figure 1). Non-contributing ventricular chambers without inflow or outflow were excluded. With two functional ventricular chambers, both were traced together as a single volume via a contour bridge across the ventricular septum (Figure 1). For normal controls only the left ventricles were traced. Segmentation and volumetry was performed independently by 2 blinded observers. One later repeated all measurements. Intraclass correlation coefficients (ICCs) were used to assess observer agreement levels and student t-tests to assess for differences between sample populations.

Table 1: Patient Population and Cardiac Measures Absolute Means ±Standards Deviation

	N	Age (years)	EDV (mL)	ESV (mL)	SV (mL)	EF (%)
SLV	7	13±3	166±89	93±78	73±19	49±12
SRV	8	11±1	108±25	55±16	53±11	49±5
DV	6	13±4	133±27	62±11	71±18	53±5
All SV (SLV+SRV+DV)	21	12±3	134±58	70±47	65±18	50±8*
Control	9	13±3	122±30	46±14	76±18	63±5

*Value significantly different from control mean ($p<0.05$)

Table 2: 2D SSFP Short Axis Volumetry Intraclass Correlation Coefficient

	Inter Observer				Intra Observer			
	EDV	ESV	SV	EF	EDV	ESV	SV	EF
Single Ventricle	0.95	0.98	0.87	0.88	>0.99	>0.99	0.98	0.98
Control	0.97	>0.99	0.98	>0.99	0.99	>0.99	>0.99	>0.99

Results: 7 patients were classified as SLV, 8 as SRV, and 6 as DV (Table 1). ICC results for intraobserver agreement (≥0.98, 95% CI: 0.96-1.00) and interobserver agreement (0.87-0.99, 95% CI: 0.72-0.99) were excellent for SV (Figure 3). There was no significant difference in observer variability between different SV morphology ($p>0.05$). Difference in inter-observer agreement was noted for end diastolic volume measurements between SV and normal LV with higher variability in SV ($p<0.03$; Table 2).

Conclusions: A standardized methodology for segmentation and volumetry that accounts for the spectrum of morphology encountered in SV physiology yields highly consistent results, minimizing user variance in an otherwise challenging patient population.

Paper #: 169

Post Mortem CT as an adjunct to radiographic skeletal survey in the assessment of sudden unexpected death in infancy and childhood

Nick Clarke, *Radiology, Royal Belfast Hospital for Sick Children, Belfast, United Kingdom, nickclarke77@gmail.com;* Anne Paterson

Disclosures: All authors have disclosed no financial interests, arrangements or affiliations in the context of this activity.

Purpose or Case Report: A full radiographic skeletal survey is obtained in all cases of sudden unexpected death in infancy (SUDI), in line with UK national guidelines, as these must all be viewed as the result of non-accidental injury (NAI) until proven otherwise. Routine radiographic skeletal survey for live children with suspected NAI includes follow-up chest radiographs, as acute rib fractures may be occult- but these are not possible in SUDI. A "chest sweep" is performed as part of the pathologists' post mortem but it is not routine practice for each rib to be individually assessed. Post-mortem chest CT was added to our SUDI imaging protocol 2008 to aid detection of occult rib fractures. We reviewed our practice of postmortem CT chest in cases of SUDI, to assess its efficacy.

Methods & Materials: We have maintained a prospective register of post-mortem CT chest examinations, to document the presence/absence or rib fractures, and if present, to describe the pattern of rib injury. Our register also includes relevant clinical information such as whether cardiopulmonary resuscitation (CPR) was attempted. Discrepancy between radiographic skeletal survey & CT chest was explored. Imaging results are made available to our pathology colleagues prior to their examination, in line with our hospital protocols; post-mortem findings are also recorded

Results: 66 post mortem CT examinations have been performed, with 82 rib fractures demonstrated in 16 cases. The sensitivity of radiographic skeletal survey for detection of these rib fractures was only 18.8%.

Two different patterns of injury emerged: following attempted CPR, rib anterior rib fractures in ribs 4-8 predominated, usually buckle fractures of the internal cortices, whereas with NAI, posterior rib fractures & "spike" fractures of the costochondral junction (CCJ) were seen more often. These patterns correlated well with post-mortem findings. 81.2% of rib fractures were felt consistent with CPR-related injury.
Conclusions: We feel that our data proves that the addition of CT chest to the routine post mortem radiographic skeletal survey in SUDI increases sensitivity for detection of rib fractures. We suggest that where feasible, that this should become routine practice for confirming or refuting suspected NAI in cases of SUDI. Our findings also support previous published studies, which have observed distinct patterns of injury associated with suspected NAI, and that these differ to those which occur after attempted CPR.

Paper #: 170

Diagnostic accuracy of perinatal post mortem magnetic resonance imaging: single reporter experience

Clare Ashwin, **J. Hutchinson**, *Radiology, Great Ormond Street Hospital, London, United Kingdom;* Neil Sebire, Owen Arthurs, FRCR, PhD

Disclosures: All authors have disclosed no financial interests, arrangements or affiliations in the context of this activity.
Purpose or Case Report: Post mortem magnetic resonance imaging is now an accepted part of the perinatal autopsy, with excellent agreement between PMMR and autopsy findings. However, in the largest study to date, each part of the PMMR was reported independently by expert specialist practitioners (e.g. the heart was reported by specialist paediatric cardiac radiologist etc.), which does not reflect every-day clinical conditions. The purpose of this paper was to report single reporter experience on a new dataset, from a paediatric radiologist who had trained on a large dataset.

Table 1: Overall diagnostic performance of PMMR vs. autopsy

PMMR	AUTOPSY		
	POSITIVE (abnormal)	NEGATIVE (normal)	Non Diagnostic
POSITIVE (abnormal)	93	5	18
NEGATIVE (normal)	8	27	0
Non Diagnostic	3	0	0
TOTAL	104	32	1

Methods & Materials: We performed PMMR on an unselected group of 150 fetuses and newborns <7 days of age, in an ethically approved study with parental consent. All scans were performed on 1.5 T (Avanto, Siemens Medical Solutions, Erlangen, Germany) MR scanner using a standardized protocol. All PMMR images were reported by one paediatric radiologist with 3 years PMMR reporting experience, blinded to any autopsy findings. Primary outcome was diagnostic accuracy, compared to autopsy findings.

Table 2: Overall diagnostic performance of PMMR vs. autopsy, by body system

(*n*=137)	ND	TP / FP	FN / TN	Sensitivity %	Specificity %	PPV (%)	NPV (%)	Concordance
Neuro	13	48/8	2/66	96.0% [86.5, 98.9]	89.5% [80.1, 94.4]	85.7% [74.3, 92.6]	97.1% [89.9, 99.2]	91.9% [85.8, 95.6]
Cardiac	4	8/5	3/117	72.7% [43.4, 90.3]	85.9% [90.8, 98.2]	61.5% [35.5, 82.3]	97.5% [92.9, 99.1]	94.0% [88.6, 96.9]
Chest	1	11/7	2/116	84.6% [57.8, 95.7]	94.3% [88.7, 97.2]	61.1% [38.6, 79.7]	98.3% [94.0, 99.5]	93.4% [87.9, 96.5]
Abdo	1	24/10	2/100	92.3% [75.9, 97.9]	90.9% [84.1, 95.0]	70.6% [53.8, 83.2]	98.0% [93.1. 99.5]	91.2% [85.2, 94.9]
MSK	0	25/1	12/99	67.6% [51.5, 80.4]	99.0% [94.6, 99.8]	96.2% [81.1, 99.3]	89.2% [82.0, 93.7]	90.5% [84.4, 94.4]
Overall (*n*=685)	19	116/31	21/498	84.7% [77.77, 89.8]	94.1% [91.8, 95.8]	78.9% [71.6, 84.7]	96.0% [93.9, 97.3]	92.2% [89.9, 94.0]
Overall (*n*=137)	4	93/5	8/27	92.1% [85.1, 95.9]	84.4% [68.2, 93.1]	94.9% [88.6, 97.8]	77.1% [61.0, 87.9]	90.2% [84.0, 94.2]

Results: PMMR was performed on 137 cases, with mean gestation 25.6 ±7.5 weeks, mean post mortem interval (death to PMMR) 8.7±3.9 days. 93/104 diagnoses made at autopsy were reported on PMMR (concordance 90.2%; 95% CI 84.0, 94.2; Table 1). Single reporter diagnostic accuracy for individual body systems (CNS, heart, chest, abdomen, and musculoskeletal system) was over 90% for all body systems, and over 92.2% overall (95% CI 89.9, 94.0; Table 2), with particularly high specificity and NPV, compared to autopsy findings.
Conclusions: This data suggests that PMMR can be performed by a single reporter following training on a large dataset, with high diagnostic accuracy that compares favorably with the reported literature. The high NPV may allow PMMR to be confidently used as a negative screening tool as part of the minimally-invasive autopsy procedure.

Paper #: 171

Incidence and location of abusive skeletal injuries in infants and children: does perpetrator handedness matter?

Stevan Kriss, *Kosair Children's Hospital, Louisville, KY, stevankriss2016@gmail.com;* Gina Bertocci, Angela Thompson, Melissa Currie, Vesna Kriss

Disclosures: All authors have disclosed no financial interests, arrangements or affiliations in the context of this activity.
Purpose or Case Report: Although a crucial component in the evaluation of abusive pediatric injury, radiographs offer no information as to perpetrator identity. This project evaluated the potential relevance that perpetrator handedness has on abusive skeletal injuries, particularly rib fractures. 85% of the general population is right-handed and tends to be at least 10% stronger with the dominant hand. While holding an infant/child facing toward the perpetrator, the right hand will encircle the left chest. Are abusive rib fractures randomly distributed (L/R) or is there a preponderance of LEFT sided fractures, suggesting relevance of perpetrator handedness?
Methods & Materials: Retrospective review was performed of a University Pediatric Forensic Medicine data base of documented abusive

skeletal injuries of children from 2008 to present with radiographic studies available to review. L/R side of fracture was recorded. Statistical T-test was performed.

Results: 81 children (53 males and 28 females) were identified as abused and having a rib fracture

Age of abused victims ranged from 1 to 48 months; average age was 5 months.

Total number of rib fractures was 368; 246 (67%) were left sided and 122 (33%) were right sided ($p<.0001$).

50 of 81 children had rib fractures only on one side; 35 (70%) left sided and 15 (30%) right sided.

31 of 81 children had rib fractures on both sides; 22 (71%) had more left sided predominant fractures while 2 (6.5%) had more right sided rib fractures. 7 (22.5%) of the children had the same number of rib fractures on both sides.

Summary of rib data reveals 57 of 81 children (70%) had only left sided or left predominant rib fractures. 17 children (21%) had only right or right predominant rib fractures. 7 children (9%) had the same number of rib fractures on both sides, $p<.0001$

There were 97 other abusive appendicular fractures besides ribs in these 81 children; 65 (67%) were left sided while 32 (33%) were right sided, $p<.0001$

Conclusions: Our study reveals a non-random distribution of abusive fractures with significantly increased left sided vs. right sided fractures in all cases, suggesting that perpetrator handedness may matter, potentially offering a clue as to perpetrator identity since right handed abusers are more likely to fracture left sided skeletal structures and vice versa. For the first time, radiographs might offer evidence to assist in perpetrator identity.

Future prospective study is planned to correlate documented perpetrator handedness with L/R side of abusive fractures.

Paper #: 172

Ischiofemoral impingement in children and adolescents: MRI evaluation

Erin Healey, *Nemours / A.I. duPont Hospital for Children, Wilmington, DE, ehealey@villanova.edu;* Heidi Kecskemethy, Arabinda Choudhary, Lauren Averill, MD

Disclosures: All authors have disclosed no financial interests, arrangements or affiliations in the context of this activity.

Purpose or Case Report: To describe the incidence of ischiofemoral impingement (IFI) on MRI of the hips or pelvis in children and adolescents with hip pain, and evaluate the utility of anatomic measurements that may assist in the diagnosis.

0–3 years

Measurement	Positive IFI n	(mm)	Negative IFI n	(mm)	*p*-value
IFS	2	6.5±0.7	18	14.8±3.5	0.0053**
QFS	2	4.5±0.7	18	10.2±2.8	0.0053**

4–7 years

Measurement	Positive IFI n	(mm)	Negative IFI n	(mm)	*p*-value
IFS	8	8.8±2.5	34	18.0±4.8	<0.0001****
QFS	8	6.5±1.5	34	13.8±4.3	0.0001****

(continued)

8–12 years

Measurement	Positive IFI n	(mm)	Negative IFI n	(mm)	*p*-value
IFS	9	13.9±4.6	67	22.3±5.9	<0.0001****
QFS	9	10.8±3.8	67	17.5±5.6	0.0004***

12+ years

Measurement	Positive IFI n	(mm)	Negative IFI n	(mm)	*p*-value
IFS	10	13.3±2.1	112	26.8±7.6	<0.0001****
QFS	10	7.8±1.4	112	21.7±7.3	<0.0001****

Methods & Materials: The electronic medical record was queried for MRI exams of the hips or pelvis acquired at a tertiary care children's health system for the indication of hip pain from January 2007 to June 2015. Studies were included if they contained axial T2 fat suppressed (T2FS) images of both hips. Exclusion criteria included: skeletal dysplasia, extensive soft tissue abnormality around the hip such as seen with severe trauma or infection, and metallic artifact obscuring the quadratus femoris muscle (QFM). Axial T2FS images were evaluated for the presence or absence of QFM edema and atrophy. Each hip was analyzed independently, and the presence of QFM edema was considered positive for the diagnosis of IFI. The ischiofemoral space (IFS) and quadratus femoris space (QFS) were measured for each hip. Images were also reviewed for other possible causes of hip pain.

Results: 130 MRI exams were included in the study, with 16 patients having QFM edema in at least one hip. The affected group included a preponderance of females (11 F, 5 M), while the negative group had essentially equal gender representation (58 F, 59 M). The mean age and age range were similar for both groups.

The 130 MRI exams yielded 260 hips for evaluation, with 29 hips (11%) showing QFM edema. 26/29 (90%) positive cases were bilateral. 4/29 (14%) also showed QFM atrophy. Positive and negative groups were segmented by age (0-3, 4-7, 8-12, and 13+ years) for measurement analysis. In all age groups, the IFS and QFS were significantly smaller in hips with IFI compared to negative hips (p-values 0.0053 to <0.0001) (Table 1). In general, the IFS and QFS measurements increased with age, although the positive IFI group plateaued between the 8-12 and 13+ years groups.

In the positive IFI group, alternative pain generators were seen in 4 of 29 hips, including 1 femoral neck stress fracture and 3 hip joint effusions.

Conclusions: The MRI features of IFI, including QFM edema and narrowed QFS and IFS, were seen in 11% of hips in children and adolescents undergoing MRI for the evaluation of hip pain, with a female predominance. These results mirror reports of IFI in the adult literature. Furthermore, our study showed most cases were bilateral. Future research is needed to determine the clinical significance of the MRI diagnosis of IFI.

Paper #: 173

Incorrect Diagnosis of Distal Radius Buckle Fractures in Children

Tal Laor, MD, *Department of Radiology, Cincinnati Children's Hospital, CIncinnati, OH, laor@cchmc.org;* Bernard TerreBlanche, Emily Eismann, Roger Cornwall, Kevin Little

Disclosures: All authors have disclosed no financial interests, arrangements or affiliations in the context of this activity.

Purpose or Case Report: Simple buckle fractures of the distal radius can be treated symptomatically with a splint with only rare complications, prompting recent transition from specialty to primary care. However, other more complex distal radius fractures may include buckling of the metadiaphysis as a radiologic feature, and pose risk for misdiagnosis as a simple buckle fracture. Improper diagnosis of distal radius fractures risks under-treatment and complications, such as redisplacement and growth arrest. The purpose of this study was to determine the accuracy of diagnosis of a buckle fracture by interpreting radiologists and treating clinicians at a tertiary pediatric institution.
Methods & Materials: Following IRB approval, hospital records over 6 months were used to identify children <18 years of age diagnosed with distal radius fracture on radiographs. Exclusion criteria included wrist surgery, systemic disease, multitrauma, arthropathy, and infection. For a diagnostic reference criterion, 3 blinded observers (2 pediatric upper extremity surgeons, 1 pediatric musculoskeletal radiologist) independently reviewed the radiographs to assess if the fracture was considered a buckle or not. Buckle fracture was defined as an incomplete distal radial metadiaphysal compression without cortical break, and normal bone morphology between the buckle and distal physis. Images with discrepant reads were reviewed together for consensus. Diagnostic accuracy of the original interpreting radiologist and treating clinician was determined by comparing their diagnoses to the reference criterion.
Results: 585 children (309 boys, 276 girls; ages 0.9-17.9, mean 8.8 years) met inclusion criteria. There were 142 buckle and 443 non-buckle fractures by expert review. Compared to the reference criterion, interpreting radiologists had a sensitivity of 81%, specificity of 79%, and positive predictive value of 56% for diagnosis of buckle fracture (207 diagnosed, 115 accurate). Treating clinicians had a sensitivity of 87%, specificity of 76%, and positive predictive value of 54% (229 diagnosed, 124 accurate). Thus, radiologists and treating clinicians improperly diagnosed more complex distal radius fractures (most often physeal fractures and fractures with complete cortical disruption) as simple buckle fractures in 92/443 and 105/443 patients, respectively.
Conclusions: Buckle fractures are over-diagnosed by both radiologists and clinicians. Unambiguous definitions for fracture types are necessary to limit misdiagnosis and potential under-treatment.

Paper #: 174

The Effect of Scapular Position on MRI Measurements of Glenohumeral Dysplasia Caused by Brachial Plexus Birth Palsy

Jill Stein, **MD**, *Department of Radiology, Cincinnati Children's Hospital, Cincinnati, OH, jill.stein2@cchmc.org;* Tal Laor, MD, Preston Carr, Andrew Zbojniewicz, Roger Cornwall

Disclosures: All authors have disclosed no financial interests, arrangements or affiliations in the context of this activity.
Purpose or Case Report: Brachial plexus birth palsy (BPBP) frequently causes glenohumeral dysplasia. Quantification of this dysplasia on MRI can guide and monitor the effect of therapeutic intervention. However, coronal scapular tilt on the thorax frequently is asymmetric between affected and unaffected sides and may affect standard dysplasia measurements prescribed perpendicular to the long axis of the body. Therefore, our purpose is to compare routine measurements of glenohumeral dysplasia obtained from standard axial images to those obtained from reformatted axial images aligned perpendicular to the scapular coronal plane ("corrected axial"), which correct for scapulothoracic position.

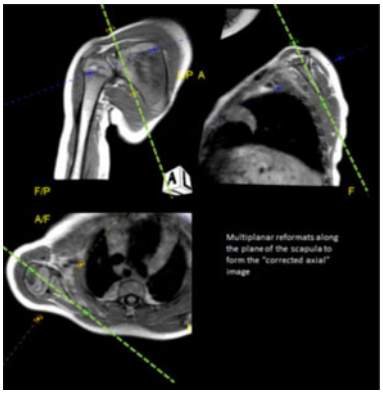

Methods & Materials: MRIs were analyzed from 19 BPBP patients (0.8-18, median 2.4 years) without prior surgery. Three radiologists measured glenoid version angle (GVA) and percentage of humeral head anterior to midscapular line (PHHA) on standard and corrected axial images of the affected and unaffected shoulders. Scapular tilt in the coronal plane was measured and averaged between the 3 readers. Measurements were compared between standard and corrected axial planes using paired t-tests. Effect of scapular tilt on the difference between standard and corrected GVA and PHHA measurements was assessed with linear regression. Interrater reliability was calculated using intraclass correlation coefficients.

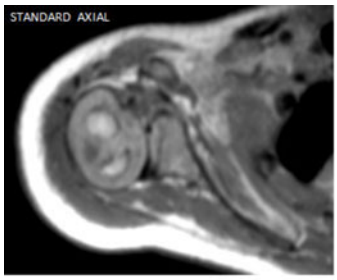

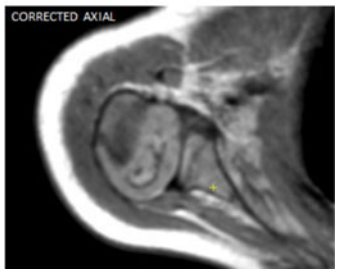

Results: GVA of the affected shoulder was significantly greater on standard than corrected images (p=0.002). Standard images overestimated glenoid retroversion on average 5° and up to 34°. PHHA of the affected shoulder was significantly less on standard than corrected images (p<0.001). Standard images overestimated humeral head posterior subluxation on average 5% and up to 33%. Increased scapular tilt of the affected shoulder significantly predicted increased discrepancy between standard and corrected measurements of GVA (p=0.03) but not PHHA. Unaffected shoulders showed no significant difference in GVA or PHHA measurements between standard and corrected axial planes. Interrater reliability ranged from fair to substantial and did not differ between standard and corrected planes.

Conclusions: Standard axial images of shoulders affected by BPBP overestimate severity of glenohumeral dysplasia, due at least in part to the variable position of the scapula on the thorax. Our study reveals the importance of, and offers a means to control for the confounding effect of scapular malposition in the quantification of glenohumeral dysplasia caused by BPBP.

Paper #: 175

Evaluation of Adductus Foot Deformations in Infants Using Ultrasound: A Longitudinal Study

Marie-Claude Miron, *CHU Sainte-Justine, Montréal, QC, Canada, marieclaudemiron@hotmail.com;* Guy Grimard, Anne-Laure Ménard, PhD

Disclosures: All authors have disclosed no financial interests, arrangements or affiliations in the context of this activity.
Purpose or Case Report: Among pediatric foot deformities, metatarsus adductus include simple metatarsus adductus (SMA) and skewfoot (SF). Although SF is a more complex deformation, it is clinically misdiagnosed with SMA, reducing its prevalence. Both deformities present similar clinical aspects, and cannot be identified using X-ray imaging in young children before bone (navicular) ossification around 4 years old. However, early diagnosis is critical to provide appropriate treatment. Ultrasound (US) technique identifies soft and bone structures; therefore it is able to differentiate SF and SMA in young children. This study aims at characterizing and quantifying displacements in both SMA and SF young patients using US.
Methods & Materials: Medical records and US findings of children under 4 years old with foot adductus deformities were retrospectively reviewed. Exclusion criteria were the presence of a chromosomal, neurological or syndromic abnormality. Clinical examinations assessed adductus rigidity and medial skinfold severity. On US images, three characteristic displacements were measured in SF patients: lateral subluxation of the first cuneiform on the navicular, and lateral and plantar displacements of the navicular over the talus. SMA is characterized by a single displacement, which is a lateral subluxation of the first cuneiform on the navicular was found and quantified. T-tests were performed to compare differences between clinical and US data of SF and SMA patients ($p<0.05$).
Results: 197 patients were included with 101 SF and 96 SMA. Clinically, SF had more rigid and severe deformations. The mean follow-up was 328 days (±296) for SF and 228 days (±198) for SMA ($p<0.05$). US showed lateral displacements of the 1st cuneiform over navicular of 22.5% (±6.2) (SF) versus 22.2% (±6.8) (SMA) ($p>0.05$). No differences were found between left and right feet. In SF, displacements of navicular over talus were found in two planes: a 19.0% (±10.0) plantar one and a 23.5% (±8.9) lateral one.
Conclusions: A single displacement was found in SMA. SF showed more rigid deformations requiring longer treatment to respectively correct plantar and lateral navicular over talus displacements, followed by 1st cuneiform over navicular displacement. US is a useful tool to characterise foot displacements and differentiate SF from SMA early in children before navicular ossification. Moreover, US could be used clinically not only as a diagnostic tool in patients with foot adductus deformations but also during follow-up.

Paper #: 176

Finite Element Analysis of the Classic Metaphyseal Lesion of Infant Abuse: Preliminary Experience

Andy Tsai, MD, PhD, *Radiology, Boston Children's Hospital, Boston, MA;* Brittany Coats, Paul Kleinman, MD

Disclosures: All authors have disclosed no financial interests, arrangements or affiliations in the context of this activity.

Purpose or Case Report: The classic metaphyseal lesion (CML) is highly associated with infant abuse, but the biomechanics responsible for this common injury have received little rigorous study. Radiologic/CT-pathologic correlates show that the distal tibial CML always involves the bone surface at the junction of the subperiosteal bone collar (SPBC) and cortex; the degree of planar extension across the medullary spongiosa is variable. A reasonable hypothesis is that the primary site of bone failure is in the cortex, then progressing centripetally into the medullary cavity. The purpose of this study was to use finite element analysis (FEA) to identify potential initial cortical failure sites of the distal tibial CML under multiple loading scenarios.

Fig. 1: Geometric Domain & Boundary Conditions

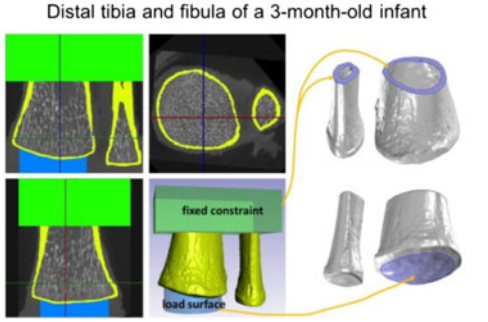

Methods & Materials: The normal left distal tibial and fibular cortices of a non-abused 3-month-old infant were segmented based on intensity threshold from 45 μm isotropic resolution micro-CT data. The resulting 3D model was used to generate a 3D tetrahedral mesh for FEA (Fig. 1). The cortices were modeled as elastic materials, characterized by Young's modulus and Poisson's ratio. The boundary conditions of this model were set to mimic forceful manipulation of the ankle in eight different load modalities: A fixed constraint was prescribed along the diaphyses, and various principal modes of mechanical stress (tension/compression, internal/external rotation, flexion/extension, and abduction/adduction) were created by applying a displacement along the distal tibial metaphyseal/epiphyseal margin (zone of provisional calcification).
Results: For most load types, the simulation demonstrated increased 1st principal strains along the region of the SPBC (e.g. Fig. 2). The degree and extent of these strains varied with the type of applied loads. Tension/compression provided uniform strain patterns at the SPBC and adjacent cortex; abduction/adduction and flexion/extension resulted in more localized areas of high strain aligned with thinner regions of the cortex. These strain patterns were not as evident with internal/external rotation loading.
Conclusions: The strain patterns generated in these modest FEA simulations suggest that the initial cortical bone failure point of the CML is at the SPBC–consistent with prior radiologic/CT-pathologic studies. Further FEA investigation of strain patterns will expand insights into the biomechanics of the CML, and can potentially clarify the type and magnitude of externally applied forces responsible for this strong indicator of infant abuse.

Fig. 2: First Principal Strain Under Compression

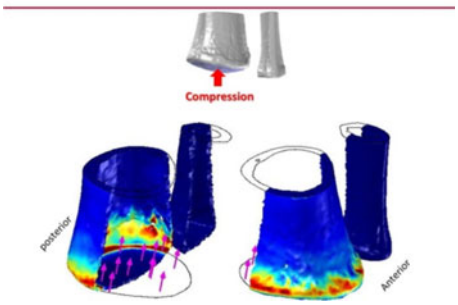

Paper #: 177

Extended Field of View MR Imaging for suspected Extended Field of View MR Imaging for suspected osteomyelitis in very young children: Is it useful?

Aaron Lindsay, *The Children's Hospital of Philadelphia, Department of Radiology, Philadelphia, PA, ajlindsay25@gmail.com;* Diego Jaramillo, MD, MPH, Jorge Delgado, Nancy Chauvin, MD

Disclosures: All authors have disclosed no financial interests, arrangements or affiliations in the context of this activity.
Purpose or Case Report: Osteomyelitis is a challenging diagnosis for clinicians, particularly in very young children in which occult, multifocal sites of infection or non-infectious pathologies may be present. A prompt diagnosis is crucial and MRI is the imaging of choice. At our institution, the MRI protocol in suspected osteomyelitis for children ≤5 y of age includes a limited whole body MRI with coronal fluid-sensitive sequences from neck to feet, regardless of the clinical site of concern. The purpose of this study is to determine if extended field of view (FOV) MRI contributed significant information in young children with suspected osteomyelitis.

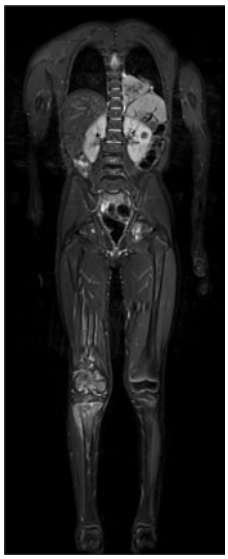

Methods & Materials: We conducted a retrospective study of children ≤5 y of age imaged for a clinical suspicion of osteomyelitis. MRI studies performed from Jan 2014 to Sept 2015 were queried using a search engine (Softek Illuminate®). All children underwent coronal fluid-sensitive STIR imaging from neck to feet. Subsequent multiplanar, multisequence imaging was performed focused to the abnormal sites depicted on survey imaging. Two radiologists recorded additional abnormalities seen on the survey series as well as the number of stations and acquisition times of the survey images. Imaging findings were correlated to the clinical outcome and statistical significance was calculated using the Fisher's exact test.
Results: We studied 54 subjects with a mean age of 2.1 y (range: 21 days - 5.6 years); 53.7% were boys. Osteomyelitis was depicted by MRI in 17 subjects (31.5%). Survey coronal fluid-sensitive imaging was accomplished by adding a single fluid-sensitive series in 1 child, 2 series in 34 children and 3 series in 19 children. Survey imaging added an average total of 7.3 min to the examination (range 2.5-19.3 min). Extended FOV imaging added significant information in 7/54 subjects (13.0%); 3 cases (5.5%) of infection and in 4 cases (7.4%) by suggesting alternative diagnoses: leukemia/lymphoma (n=2) [Figure 1], non-accidental trauma (n=1) and scurvy (n=1) [Table 1]. The Fisher's exact test showed that the number of added diagnoses by coronal STIR imaging was significant (p<0.05).

Conclusions: The addition of extended FOV MRI in young children with suspected osteomyelitis added important clinical information in 13% of subjects while only adding an average of 7.3 min to the examination. We believe that in children ≤5 y of age, the ease of covering the small body with coronal STIR imaging, combined with the relative high yield, supports the continuation of this practice.
Table 1. Subjects in which extended field of view MR imaging in young children added important clinical information

Subject	Age (years)	Presenting Symptom	Examination Ordered	MRI diagnosis	Final Diagnosis
1	1.3	Bilateral lower extremity weakness	Both legs	Osteomyelitis/ discitis at L3-L4	Vertebral osteomyelitis/ discitis
2	2.8	Right thigh pain	Right femur	Osteomyelitis/ discitis at L4-L5	Vertebral osteomyelitis/ discitis
3	1.5	Sickle cell disease, right arm pain	Right humerus	Right humerus osteomyelitis and elbow effusion, left humerus osteomyelitis with micro-abscesses, bone infarct vs osteomy-elitis in both legs	Right humerus osteomyelitis and septic arthritis, left humerus osteomyelitis
4	4.9	Right foot	Right Foot	Diffuse marrow infiltration, leukemia	Acute Lymphoblastic Leukemia
5	4.6	Right knee	Right knee	Distal right femoral a nd proximal tibial masses, marrow abnormalities within the left hemipelvis, sacrum, left proximal humerus paravertebral mass, bilateral renal massess c/w malignancy	Lymphoma
6	0.8	Right elbow swelling	Right elbow	Acute distal humeral fracture/physeal separation with healing fractures in the left tbia	Non-accidental trauma
7	4.5	Intermittent refusal to walk	Pelvis	Diffuse metaphyseal abnormalities suggestive of scurvy	Scurvy

Paper #: 178

Modern American Scurvy – Experience with Vitamin C Deficiency at a Large Children's Hospital

Farahnaz Golriz, M.D, *Radiology, Texas Children's Hospital, Houston, TX, fxgolriz@texaschildrens.org;* Lane Donnelly, MD, Sridevi Devaraj, Rajesh Krishnamurthy

Disclosures: All authors have disclosed no financial interests, arrangements or affiliations in the context of this activity.
Purpose or Case Report: Scurvy related to dietary deficiency has been a historic note for most US radiologists. When such cases arise, there can be a delay in diagnosis from lack of recognition of imaging findings. We present a review of cases of vitamin C deficiency (VCD) at a single institution.

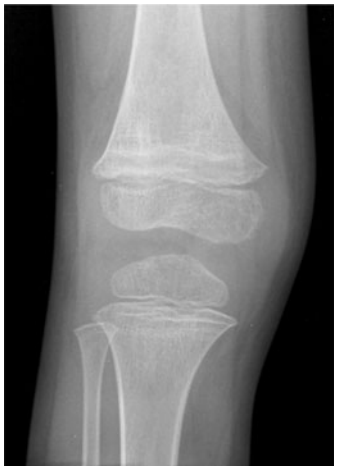

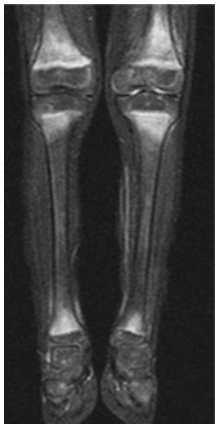

Methods & Materials: Cases of VCD were identified from a retrospective review of ascorbic acid deficiency tests over 2 years - Normal>28 mM, moderate deficiency 18 - 28 mM, and severe deficiency<18 mM. Identified cases were evaluated: clinical history, underlying medical condition, imaging studies obtained, and imaging findings.
Results: 25 children with VCD were identified - 15 severe and 10 moderate. 15 had underlying iron overload (sickle cell anemia, thalassemia). Other underlying conditions included neurologic disorders (3) [autism 2, developmental delay 1], bone marrow transplant / chemotherapy (3), neglect / failure to thrive (1), hereditary fructose deficiency (1), and HSP(1). No otherwise normal children with scurvy were identified. All of these children (except one) had multiple imaging studies, primarily related to their underlying conditions. 2 of these (autism, developmental delay), both with severe VCD, had extensive imaging work ups related to diffuse musculoskeletal pain and had delay in diagnosis. Imaging findings included ill-defined sclerotic and lucent metaphyseal bands (mainly at knee) (Fig 1) and on MRI diffuse increased T2-weighted signal and abnormal enhancement throughout the metaphysis of the lower extremities bilaterally (Fig. 2). In other patients, differentiation of imaging findings related to VCD as opposed to their underlying conditions was difficult. Many of these patients did have perceived osteopenia by radiography but not other findings usually attributed to scurvy.
Conclusions: VCD and scurvy occurs not uncommonly at quaternary children's hospitals. At risk populations include those with iron overload, neurologic conditions such as autism, and bone marrow transplant recipients. Scurvy in otherwise normal children was not identified. Imaging does not play a central role in the work up of VCD. However, metaphyseal changes seen on radiography or MRI in a child with diffuse musculoskeletal pain and an underlying at-risk condition should raise the possibility of scurvy and warrants testing for ascorbic acid levels. Targeted imaging when indicated should include radiographs of the knee or wide field of view MRI from the pelvis to knee.

Paper #: 179

Evaluation of Femoral Head Viability in the Post-Operative Pediatric Patient

Ashishkumar Parikh, MD, *Radiology, Vanderbilt Children's Hospital, Nashville, TN, ashishkumar.k.parikh@vanderbilt.edu;* Adam Bobbey, Eleby Washington, Holly Leshikar, Jonathan Schoenecker, Stephanie Spottswood, MD, MSPH

Disclosures: All authors have disclosed no financial interests, arrangements or affiliations in the context of this activity.
Purpose or Case Report: Avascular necrosis (AVN) is a well-known and devastating complication following surgical fixation for slipped capital femoral epiphyses (SCFE), femoral neck fractures and Legg-Calvé-Perthes (LCP) disease. When the surgically fixated femoral head exhibits ischemia, the orthopedist may prescribe measures to prevent development of AVN. The ability to evaluate femoral head vascularity is important to assess this risk of AVN. MRI and CT evaluation are hampered by metal-induced artifact from the surgical hardware, and CT cannot assess early vascular abnormalities leading to AVN. Nuclear medicine (NM) bone scans can determine the presence of femoral head perfusion and are not limited by the presence of metallic hardware. Our study describes the utility of NM bone scans in assessing femoral head perfusion in children who have undergone surgery for SCFE, femoral neck fractures and LCP disease.
Methods & Materials: We retrospectively evaluated NM bone scans of 20 children after surgical fixation for SCFE, femoral neck fracture, or LCP disease. 10 children had a diagnosis of SCFE, 6 had femoral neck fractures, and 4 had LCP disease. All children received a weight-based dose of Tc-99 m methylene diphosphonate (MDP), after which triple-phase bone scintigraphy was performed, including delayed pinhole magnification imaging of the hips. All of the children additionally underwent serial plain radiography of the pelvis, and several underwent pelvic CT and/or MRI examinations.
Bone scan images were evaluated for the presence of radiopharmaceutical activity in the femoral head, and were compared with plain radiographs,

CT and/or MRI of the pelvis. The gold standard for determining femoral head perfusion was the intra-operative appearance of the bone. Surrogates for femoral head viability in those who did not undergo repeat surgery included a normal imaging appearance of the femoral head and the child's return to normal function.
Results: 23 of 25 (92%) bone scans in 19 of 20 (95%) patients revealed findings consistent with the clinical outcomes and/or intraoperative appearance of the femoral head. 4 of 20 cases (20%) had AVN, and the remaining 16 of 20 (80%) demonstrated normal or increased perfusion post-operatively.
Conclusions: Our results demonstrate that scintigraphic evaluation of the post-operative pediatric hip containing metallic hardware is valuable for determining risk for femoral head AVN, a potential complication of SCFE, femoral neck fractures and LCP disease.

Paper #: 180

Comparative analysis of anterior and posterior contrast injection approaches for shoulder arthrograms

Theodore Gupton, MD, *Children's Hospital of Philadelphia, Philadelphia, PA, ted.gupton@gmail.com;* Jorge Delgado, Anne Marie Cahill, Nancy Chauvin, MD

Disclosures: All authors have disclosed no financial interests, arrangements or affiliations in the context of this activity.
Purpose or Case Report: Anterior approach glenohumeral joint injections are known to produce artifacts on shoulder MR arthrograms that confound shoulder pathology, particularly within the anterior joint stabilizers. Thus, some radiologists advocate a posterior approach. The purpose of this retrospective study was to compare capsular distention, extra articular contrast extravasation, post-injection pain, fluoroscopic time and radiation dose of fluoroscopically guided anterior and posterior glenohumeral joint contrast injections in children.

Parameter/Mean (STD)	Anterior Approach (*n*=67)	Posterior-Approach (*n*=67)	*p*-value
Age (Years)	15.98 (1.6)	15.99 (1.6)	0.66
Gender M/F	39/28	39/28	-
Weight (Kg)	73.11 (18.2)	72.32 (18.1)	0.86
Height (cm)	170 (10.2)	171 (11.8)	0.78
BMI	25.08 (5.7)	24.66 (4.5)	0.67

Methods & Materials: Injections performed from March 2011 to September 2015 were queried using a search engine (Softek Illuminate®). Sixty-seven subjects who underwent an anterior approach glenohumeral contrast injection with subsequent MR imaging and 67 age and gender matched subjects who underwent a posterior approach injection were evaluated. Two radiologists independently reviewed multiplanar T1-weighted fat suppressed MR shoulder arthrogram sequences. Capsular distention was designated as suboptimal (limited assessment of the intraarticular structures) or optimal. Degree of contrast extravasation was graded as per Table 2. The medical record was queried for documentation of post procedural pain. Total fluoroscopic time and skin radiation dose was recorded. Interrater reliability of capsular distention and contrast extravasation was calculated using de Cicchetti Kappa.
Results: There were no significant differences in age, gender, height, weight, or BMI between the two populations. The amount of contrast extravasation between both groups was not significantly different (p=0.538). Three anterior injections (4.5%) and 1 posterior (1.5%) were suboptimal, not statistically significant (p=0.955). Two anterior injection (3.0%) and 9 posterior injection subjects (13.4%) reported pain after the procedure, not statistically significant (p=0.252). There was no significant difference in fluoroscopy time: 1.1 min anterior and 1.3 min posterior (p=0.13). There was a significant difference in radiation skin dose: 0.7 mGy anterior and 1.1 mGy posterior (p=0.003). There was excellent agreement on degree of extravasation and capsular distention; de Cicchetti kappa values were 0.87 and 0.88 respectively.
Conclusions: Both techniques were technically successful and well tolerated. There was no difference in the fluoroscopy time for either approach. The dose was greater using the posterior approach, however not clinically significant, being well below the accepted threshold dose for deterministic effects.

Parameter/Median (range)		Anterior Approach (*n*=67)	Posterior Approach (*n*=67)	*p*-value
Failure of procedure		3/67	1/67	0.955
Presence of Pain		2/67	9/67	0.252
Fluoroscopy time (min)		1.1 (0.1-6.2)	1.3 (0.1-12.5)	0.13
Radiation (mGy)		0.7 (0.1-35	1.1 (0.1-192)	0.003*
Suboptimal Distention/Failure		4/67	1/67	0.96
Extravasation	None	41/67	37/67	0.538
	Small (contrast along the linear needle tract)	5/67	2/67	
	Moderate (contrast along muscle fiber striations measuring<5 cm in length	16/67	22/67	
	Large (contrast along striations measuring > 5 cm in length or pooling of contrast outside the joint)	5/67	6/67	

Paper #: 181

Endovascular management of portal venous complications after pediatric liver transplantation: a single center experience

Andrew Marsala, Parth Patel, Jose Hernandez, MD, *Baylor College of Medicine, Houston, TX, jahernan@texaschildrens.org;* sheena pimpalwar, MD, Daniel Ashton, Kamlesh Kukreja

Disclosures: All authors have disclosed no financial interests, arrangements or affiliations in the context of this activity.

Purpose or Case Report: To demonstrate the utility of endovascular techniques in the management of portal venous complications after pediatric liver transplantation.
Methods & Materials: An IRB-approved retrospective chart review was conducted on liver transplant patients who underwent portal vein catheterization at our institution between July 2009 to August 2015.
Results: 16 patients were identified who underwent 30 procedures, 25 of which (25/30, 83.3%) involved in an intervention. The most frequent indication for initial intervention was gastrointestinal hemorrhage (10/16, 62.5%). Other indications included hypersplenism, portal vein occlusion or stenosis and, in one patient, multiple intrahepatic portosystemic shunts resulting in persistent hyperammonemia. Roux limb varices were identified in 7 patients (7/16, 43.4%), 6 of whom presented with gastrointestinal hemorrhage (6/7, 85.7%). All 6 patients (6/6, 100%) who presented with hemorrhage underwent embolization. On initial intervention, portal vein occlusion was identified in 8 patients (8/16, 50%). Recanalization was attempted in 6 patients (6/8, 75%) and successful in just 3 patients (3/6, 50%). On initial intervention, portal vein stenosis was identified in 7 patients (7/16, 43.75%) and angioplasty performed in 6 patients (6/7, 85.7%). The portal venous system was accessed via a transsplenic approach in 15 cases (15/30, 50%), trans-hepatic approach in 14 cases (14/30, 46.7%) and both approaches in 1 case (1/30, 3.3%). Clinically significant hemorrhagic complications of access were not observed (0/30, 0%).
Conclusions: The management of post-liver transplant complications involving the portal vein is challenging and requires a diverse skillset. Percutaneous endovascular techniques can be of benefit, particularly in the management of gastrointestinal hemorrhage and portal vein stenosis, and, to a lesser degree, portal vein occlusion. Roux limb varices are frequently discovered in patients who present with hemorrhage. Trans-splenic access has proven safe, useful and is frequently necessary in the treatment of portal venous complications after pediatric liver transplantation.

Paper #: 182

The Role of Portal Venous Embolization as an Adjunct to Hepatectomy by Helping Prevent Post-Resection Liver Failure

Robin Kaye, *Phoenix Children's, Phoenix, AZ, rkaye@phoenixchildrens.com;* Carrie Schaefer, David Aria, M.D., Tammam Beydoun, Richard Towbin, MD

Disclosures: All authors have disclosed no financial interests, arrangements or affiliations in the context of this activity.
Purpose or Case Report: A 7 year-old previously healthy male presented with a palpable abdominal mass. CT revealed a large, heterogeneous right hepatic lobe mass. Biopsy confirmed a diagnosis of undifferentiated embryonal sarcoma and the patient was started on chemotherapy. After 4 rounds of chemotherapy (3 months), PET/CT demonstrated significant decrease in size and FDG-activity of the lesion. Given the excellent response, the patient became a candidate for surgical resection but there was concern for post-operative liver failure after right trisegmentectomy. The patient presented to IR for right portal vein embolization to induce left hepatic/caudate lobe hypertrophy prior to resection. Both the anterior and posterior divisions of the right portal vein were embolized with a combination of vascular coils, plugs, and embospheres. At 1-month follow-up, CT demonstrated approximately 17% left hepatic/caudate lobe hypertrophy (286 mL post-embolization vs. 245 mL pre-embolization) and further decrease in tumor size. The patient subsequently underwent right hepatectomy (segments 4, 5, 6, 7, and 8) and after 6 months, continues to be tumor free.
Conclusions: Portal Venous Embolization is effective as an adjunct to hepatectomy by promoting remnant liver hypertrophy.

Paper #: 183

Tract embolization for ultrasound-guided percutaneous liver biopsies in a pediatric population: Does what we use matter?

Heather Cleveland, BSRS, *Interventional Radiology, Texas Children's Hospital, Houston, TX, heclev7@yahoo.com;* Daniel Ashton, Shireen Hayatghaibi, MPH, Kamlesh Kukreja

Disclosures: All authors have disclosed no financial interests, arrangements or affiliations in the context of this activity.
Purpose or Case Report: A coaxial needle technique can be used to reduce the moderate risk of bleeding during a pediatric percutaneous liver biopsy by embolizing the tract with various embolic materials. We compare the complications after ultrasound-guided percutaneous liver biopsies with tract embolization between two embolic agents, Avitene™ (Microfibrillar Collagen Hemostat) and Gelfoam.
Methods & Materials: A retrospective cohort study was performed on ultrasound-guided liver biopsies with tract embolizations between 01/01/2013 to 07/30/2015. Patient data was acquired through electronic medical record and entered into a REDCap database. Complications were classified according to Society of Interventional Radiology (SIR) criteria by a pediatric interventional[1]. A Fisher's exact test was conducted to detect differences in complication rates between the two tract embolization groups.
Results: 363 liver biopsies were performed using a coaxial system with tract embolization by either Avitene™ or Gelfoam. All together there was 34 complications (9.4%). 29 (8%) were categorized as minor (grade A and B) and 5 (1.4%) were categorized as major (grade C and D) according to SIR criteria. 195 tracts were embolized with Avitene™ (54% of total biopsies) in which there were 26 (13%) complications. 23 (12%) of the Avitene™ complications were categorized as minor (grade A and B) and 3 (2%) as major (grade C and D). 168 were embolized with Gelfoam (46% of total biopsies) in which there were 8 (4.7%) complications. 6 (3.6%) of the Gelfoam complications were categorized as minor (grade A and B) and 2 (1.2%) as major (grade C and D). The majority of the minor complications were delayed abdominal pain and/or rash. The Fisher's exact test show use of Avitene™ has a statistically higher minor complication rate than Gelfoam (p=.004).
Conclusions: Based on a retrospective cohort of pediatric patients, tract embolization following percutaneous liver biopsy results in a low rate of major complications for both embolization agents, however more minor complications were detected with the use of Avitene.

Paper #: 184

Pediatric Outpatient Ultrasound-Guided Liver Biopsies: Does Decreasing Post-Biopsy Observation Period Time Impact Complication Rates?

Shireen Hayatghaibi, MPH, *Radiology, Texas Children's Hospital, Houston, TX, sehayatg@texaschildrens.org;* Daniel Ashton, Heather Cleveland, Kamlesh Kukreja

Disclosures: All authors have disclosed no financial interests, arrangements or affiliations in the context of this activity.
Purpose or Case Report: To measure the effect of decreasing post-biopsy observation on the rate of complications after outpatient ultrasound-guided liver biopsy in children.

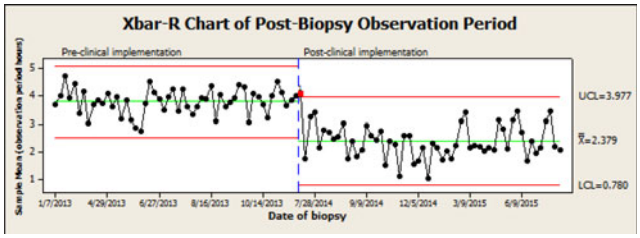

Methods & Materials: Pediatric patients who underwent an ultrasound-guided liver biopsy either before or after implementation of a revised clinical guideline that reduced the post-biopsy observation period from 4 h to 2 h were retrospectively identified from the electronic medical record. Relevant demographic, procedure note, post procedure note and follow-up information were entered into a REDCap database. Complications were categorized according to Society of Interventional Radiology (SIR) complication criteria by a pediatric interventional radiologist[1]. Complication rates for the two groups were compared using Fisher's exact test in Minitab.

Results: The final study population comprised 216 patients who underwent an outpatient ultrasound-guided liver biopsy between 01/01/2013 and 07/30/2015 (age range: 0 - 17 years, mean: 10.6 years). 104 biopsies were performed prior to implementation of the new clinical observation guideline (median [IQR] observation time: 3.93 [.72] hours). 112 biopsies were performed after shortening patient observation time (median [IQR] observation: 2.23 [.81] hours).

Overall, 15 complications were detected (6.9% of all biopsies) in 15 patients. 7 (46.5%) complications were categorized as SIR type A (minor) and 7 complications (46.5%) as type B (minor). There was no significant difference in overall complication rates between the long observation (9.6%) and short observation (3.6%) groups (p=0.097). Median (IQR=4.5 days) time of complication detection was 4.5 days. Only one patient experienced a complication within 24 h of the procedure (SIR type B; complication detected at 7 h). The remaining 14 (93%) complications occurred at least 24 h post-biopsy. Decreasing observation time saved patients an average of $1,072 dollars per procedure.

Conclusions: In a cohort of pediatric patients undergoing outpatient ultrasound guided liver biopsy, reducing the post-procedure observation period from 4 h to 2 h did not increase the rate of complications. All complications occurred 7 h or more post-biopsy.

Paper #: 185

Incidental splenic masses detected during MRI evaluation for iron overload in children

Rayan Ahyad, MBBS, SBR, *Department of Medical Imaging, University of Toronto; Department of Diagnostic Imaging, The Hospital for Sick Children, Toronto, ON, Canada, ahyadr@gmail.com;* Christopher Lam, MD, Omid Shearkhani, Oscar Navarro

Disclosures: All authors have disclosed no financial interests, arrangements or affiliations in the context of this activity.

Purpose or Case Report: Hemoglobinopathies are among the major hematological diseases that indirectly increase the risk for iron overload. Patients with these conditions can develop foci of preserved splenic tissue or extramedullary hematopoiesis that may present on imaging as single or multiple splenic masses. Our aim was to evaluate the incidence, imaging characteristics, and course of these incidental splenic masses detected during MRI evaluation for iron overload.

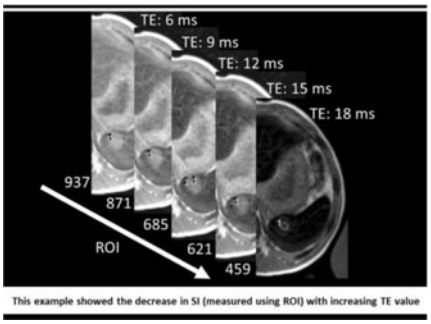

Methods & Materials: Retrospective review of all MRI studies performed for iron overload evaluation in a tertiary pediatric hospital between 2005 and 2015. The presence of focal splenic masses including number, size, signal characteristics and changes on follow-up scans was recorded. Patient's age, gender and diagnosis of underlying hematological disease were also documented.

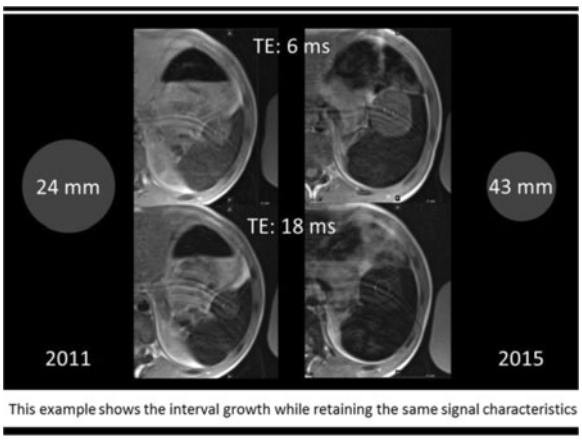

Results: There were 318 patients that had MRI for iron overload during this period, of which 27 (8.5%) had at least one splenic mass. Mean age was 10±4 years with male:female ratio of 2:5. Underlying hematological diseases included sickle cell disease in 23 patients (85%), thalassemia in three (11%), and inherited bone marrow failure syndrome in one (3.7%). In 24 patients (88%), the masses had high signal intensity relative to the spleen. Regardless of their signal intensity, progressive signal decrease of the masses with increasing time-to-echo (TE) value was noted in 26 patients (96%) [Fig 1]. Follow-up was performed in 21 patients (78%), which showed interval increase in size of the splenic masses in seven (33%) [Fig 2], stability in 12 (57%), and size decrease in two (9.5%).

Conclusions: Incidental splenic masses during MRI evaluation for iron overload are not uncommon in pediatric patients, most frequently in the setting of sickle cell disease. Most of these lesions show typical imaging features and are thought to represent preserved splenic tissue. These masses do not require further imaging even if they show increase in size on follow-up scans.

Paper #: 186

Limited Chest MRI for Detecting Intrathoracic Lymphadenopathy in Children with Suspected Pulmonary Tuberculosis

Tanyia Pillay, MBChB (WITS), FC Rad (Diag) SA, Dip Paeds Rad (UCT), *Department of Radiology, Chris Hani Baragwanath Hospital,*

University of the Witwatersrand, Eikenhof, South Africa; Savvas Andronikou, MBBCh, FCRad, FRCR, PhD, Heather Zar

Disclosures: All authors have disclosed no financial interests, arrangements or affiliations in the context of this activity.
Purpose or Case Report: The global burden of tuberculosis (TB) is considerable. TB remains the most common notifiable diaease in South Africa. The diagnosis of pulmonary TB in children is often difficult because of a non-specific clinical presentation, a non-uniform clinical approach, the questionable value of skin and sputum tests, the low yield of gastric aspirates and non-specific radiological signs. Plain chest radiographs have a low/moderate sensitivity and specificity for lymphadenopathy in children and have a wide inter-observer variabilty. CT has shown lymphadenopathy in up to 60% of cases that have a normal chest radiograph.
An imaging method for detecting intrathoracic TB lymphadenopathy that has a greater diagnostic accuracy than a chest radiograph, lower raditaion dosage than a CT and that does not require anaesthesia, is needed.
Limited Chest MRI may detect intrathoracic lymphadeopathy in unsedated children and may represent a "gold standard" diagnostic test for problem solving in suspected pulmonary TB in children.
Methods & Materials: Children (under 13 years of age) undergoing evaluation for suspected pulmonary TB at a tertiary referral paediatric practice at Red Cross War Memorial Children's Hospital in South Africa were referred for an MRI. These children had a suspicion of TB, on the basis of clinical findings.
TB was categorized as definite (culture confirmed), possible (clinical diagnosis) or not TB (alternative diagnosis and improvement without TB treatment).
Limited STIR and Diffusion Weighted MRI sequences were performed on a 1.5 T magnet in the corocnal plane and were only repeated in the axial plane if the patient was compliant. The maximum time allowed for each sequence was 10 min. MRI procedures that were not tolerated, as defined by continuous prolonged crying or movement artifact, were terminated and categorized as unsuccessful.
Results: Only 86% (62/72) of children tolerated the MRI.
95% (59/62) of children demonstrated lymphadenopathy and 74% (46/62) had low/intermediate signal lymphadenopathy on STIR.
Of the patients with culture confirmed TB, 95% (21/22) demonstrated lymphadenopathy on DWI and 82% (18/22) showed low/intermediate intensity lymphadenopathy on STIR.
Of the patients with clinical TB, 97% (33/34) showed lymphadenopathy on DWI imaging and 76% (26/34) showed low/intermediate lymphadenopathy on STIR.
All the patients who were considered not to have TB, still demonstrated lymphadenopathy on DWI imaging but only 33% (2/6) showed low/intermediate intensity lymphadenopthy on STIR.
Conclusions: Limited/"Fast" MRI chest is feasible for diagnosing lymphadenopathy in children without sedation at reduced cost and time. Differentiating TB from other causes of lung patholgy requires further study.

Paper #: 187

MR Imaging of Tumor Associated Macrophages In Pediatric Patients with Malignant Lymphomas and Sarcomas

Raphael Alford, MD, *Stanford, Palo Alto, CA, rapha@stanford.edu;* Maryam Aghighi, Anne Muehe, Samantha Holdsworth, Florette Hazard, Dita Gratzinger, Neyssa Marina, Sandra Luna-Fineman, Ranjana Advani, Heike Daldrup-Link

Disclosures: All authors have disclosed no financial interests, arrangements or affiliations in the context of this activity.
Purpose or Case Report: Tumor associated macrophages (TAM) are key components of the tumor microenvironment and play a role in the pathogenesis and progression of many tumors. TAM are becoming both a tracked clinical marker for tumor-associated inflammation and a target of immunotherapies. The aim of this study is the clinical translation of Magnetic Resonance (MR) Imaging for TAM detection in pediatric tumors through correlation of ferumoxytol tumor enhancement with macrophage content on histopathology.
Methods & Materials: This is a single center prospective clinical trial approved by our IRB and performed under an IND with the FDA. 12 pediatric patients and young adults with lymphoma (n=8) or sarcoma (n=4) and scheduled tumor surgery were recruited. FDA approved iron supplement Ferumoxytol was injected intravenously at a dose of 5 mg Fe/kg, 24-48 h prior to MRI. MR sequences included STIR, T1-weighted SPGR, multi-echo T2* FSPGR and eFGRE sequences. Histopathology evaluation was performed by 2 pathologists with prussian blue and immunohistochemistry stains for macrophage markers CD-68 and CD-163. The percent area covered by CD68+ or CD163+ macrophages was estimated using color thresholding followed by macrophage counts. A threefold approach was taken to evaluate the ability of MRI to image TAM: (1) In a pilot study of 3 patients who underwent pre and post contrast imaging, we confirmed tumor ferumoxytol enhancement. T2* values were correlated on postcontrast scans with TAM quantity on histopathology. (2) To determine if ferumoxytol-MRI can differentiate tumors with different TAM content, we compared T2* enhancement data of lymphomas and sarcomas. (3) To determine if ferumoxytol-MRI can differentiate tumor areas with different TAM content, we correlated T2* enhancement with regional TAM quantities of whole tumor specimen.
Results: (1) Significant iron oxide tumor enhancement was noted on postcontrast scans compared to precontrast scans (p=0.013). On immunohistochemistry there was a positive correlation between T2* and TAM quantity (Pearson r=.45, p<0.0001). (2) A significant difference in postcontrast T2* relaxation times was noted between lymphomas and sarcomas (p<0.05). (3) Tumor areas with variable T2* enhancement showed a positive correlation between T2* relaxation times and TAM quantities.
Conclusions: This is the first clinical translation of TAM detection in pediatric tumors with ferumoxytol-enhanced MR Imaging demonstrating a ferumoxytol tumor MR enhancement with macrophage content .

Paper #: 188

N-Myc Gene Amplification on Pediatric Neuroblastomas

Cinthia Cruz Romero, MD, *Abdominal Radiology, Massachusetts General Hospital, Boston, MA, ccruzromero@mgh.harvard.edu;* Michael Gee, MD, PhD

Disclosures: All authors have disclosed no financial interests, arrangements or affiliations in the context of this activity.
Purpose or Case Report: Neuroblastoma is the most common extracranial solid malignancy in childhood. N-Myc oncogene amplification is observed in up to 25% of neuroblastomas and is a risk factor associated with tumor progression and decreased survival. The purpose of this study is identify imaging features associated with N-Myc status in pediatric neuroblastomas.
Methods & Materials: IRB approved and HIPAA compliant retrospective study of consecutive patients who underwent contrast enhanced CT or MRI at time of the diagnosis with neuroblastoma between 2000 and 2015. Contrast enhanced CT and MRI were read in consensus by two radiologists blinded to tumor N-Myc status for presence or absence of intratumoral areas of non-enhancement, calcification, and hemorrhage, as well as lymphatic or hematogenous metastasis. Results of genetic testing for N-Myc amplification (NMA) were obtained from the electronic medical records and correlated to the imaging features using Fisher's exact test with statistical significance defined as p<0.05.
Results: Twenty-nine patients ranging from 0.01 to 17.7 years of age (mean 2.5 yrs); including 13 females and 16 males. Fifteen patients

(51%) were positive for NMA. Nine of 15(60%) patients with NMA also had a deletion of chromosome 1p demonstrating a significant correlation (OR:6 CI:0.9 to 38.6 p=0.05). Subjects with NMA neuroblastomas exhibited a significantly increased incidence (10/15; 67%) of lymphatic metastasis at time of diagnosis compared with non-NMYC amplified (5/14; 35%) tumors (p=0.01 OR:151.3 to 167.6). NMA neuroblastomas also exhibited significantly increased intratumoral hemorrhage (71%; p=0.04) and decreased calcification (80%; p=0.04) compared with non-MYCN amplified tumors. No significant correlation between pattern of enhancement and genotype was found.
Conclusions: N-myc amplified neuroblastomas are significantly associated with multiple distinct imaging features, including increased rates of lymphatic metastasis and intratumoral hemorrhage, as well as decreased intratumoral calcification, compared with non-MYCN amplified neuroblastomas. These results suggest a relationship between neuroblastoma genotype and imaging appearance and may be helpful for tracking potential changes in neuroblastoma gene expression over time and during therapy.

Paper #: 189

Streamlining PET/MRI Workflow in Pediatric Oncologic Imaging

Lillian Lai, MD, *Lucile Packard Children's Hospital, Stanford University, Radiology, Stanford, CA, lmlai@stanford.edu;* Anne Muehe, David Larson, Neyssa Marina, Ranjana Advani, Arun Rangaswami, Valentina Taviani, Samantha Holdsworth, Dawn Holley, Heike Daldrup-Link

Disclosures: All authors have disclosed no financial interests, arrangements or affiliations in the context of this activity.
Purpose or Case Report: Our goal is to streamline the workflow and improve patient satisfaction for whole-body staging PET/MRI in pediatric oncological patients using Lean and Six-Sigma strategies.
Methods & Materials: We prospectively evaluated the workflow of our new hybrid PET/MR imaging technique for whole-body staging in pediatric and young adult patients with solid cancers.
Utilizing Lean and Six-Sigma strategies and the Define, Measure, Analyze, Improve and Control (DMAIC) methodology, we detected areas of improvement. We identified processes contributing to inefficiencies before the scan (determining streamlined MR protocols based on primary malignancy), during the scan (fitting in the desired sequences into the PET-bed time), and after the scan (post-processing including fusing the MR and PET data, labeling series, and sending images to PACS workstation). We then proposed and applied interventions for the most frequent problems.
To track our progress, we documented the time of each individual step from the patient entering until exiting the PET-MR suite. We also generated a questionnaire for our patients modeled after a United Airlines post-flight customer satisfaction survey. Finally, we created a satisfaction survey for the PET/MR technologist, radiologist, and oncologist.

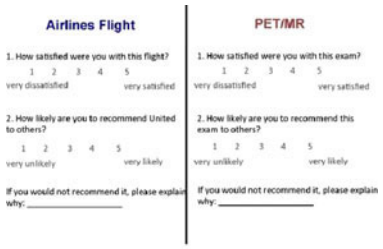

Figure 1: Example questions from a PET/MR patient satisfaction survey, modeled after an airlines flight satisfaction questionnaire.

Results: We improved workflows, developed streamlined MRI protocols, improved post-processing of imaging studies, and utilized patient waiting times for answering the questionnaire.
Scan time and time spent in the PET-MRI suite both decreased due to our interventions. For the initial scans, the average scan time was 1 h 45 min, and average time spent in the PET-MRI suite was 3 h 21 min. After time-saving interventions, the average scan time was 1 h 13 min, and average PET-MRI suite time was 2 h 38 min.
Initial studies had an average of 21561 images and poor PET/MR fusion, whereas later scans averaged 9707 images and had excellent fusion.
After applying the interventions, patient satisfaction increased. Perception of efficiency and ease of use improved among the technologists, radiologists, and oncologists with progressive scans. We continue our streamlining interventions to further improve time-efficiency and satisfaction of PET/MR procedures.
Conclusions: Optimization of PET/MRI workflow is possible using a strategic, streamlined, efficient approach and significantly improves patient satisfaction.

Paper #: 190

Association between carotid artery non invasive elastography and BMI as an indicator of early changes of cardiovascular diseases in children

Ramy El Jalbout, MD, *Radiology, CHU Sainte Justine, Montreal, QC, Canada, ramy.jalbout@yahoo.com;* Josée Dubois, Chantale Lapierre, Melanie Henderson, Marie-Hélène Roy-Cardinal, Guy Cloutier

Disclosures: All authors have disclosed no financial interests, arrangements or affiliations in the context of this activity.
Purpose or Case Report: 1- Describe the technique of Noninvasive vascular elastography (NIVE)
2- Explore the association between early vascular elastographic changes and obesity

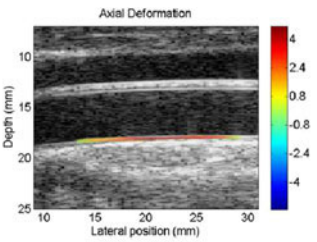

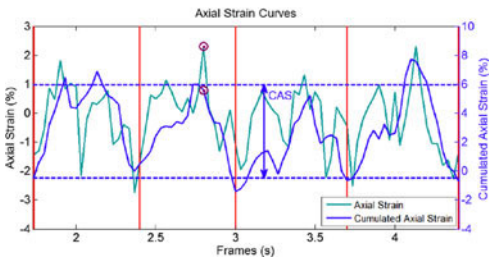

Methods & Materials: The QUebec Adipose and Lifestyle InvesTigation in Youth (QUALITY) study aims at evaluating the natural history of obesity in childhood and its cardiometabolic consequences. Children having at least one obese parent were recruited at 8 to 10 years of age (n=630). Data on 564 children are available for the present analyses; of these, we randomly selected 60 obese children (body mass index (BMI) ≥ the 85th percentile for age and sex) and 60 normal weight children (BMI<85th percentile). The ultrasonographic videos of the common carotid artery taken using radiofrequency-mode ultrasound were analysed. NIVE was then applied to the far away (relative to the transducer) segmented carotid artery vessel wall. Elastography results are expressed as maximal

shear strain magnitude (%) the cumulated axial strain (CAS) (%), cumulated axial translation (CAT) in mm, cumulated lateral translation (CLT) in mm and the ratio CAS over CAT. Outcomes were compared between the two groups using one-way ANOVA.

Results: Non invasive vascular elastography (NIVE) is an elastography technique that generates the axial, lateral and shear strain calculation using the Lagrangian Speckle method which takes into account the two dimensional strain tensor to calculate the Von Mises coefficient. This coefficient is not usually calculated with other elastography techniques. The ratio of cumulated axial strain over cumulated axial translation was higher in the non-obese group (mean=13.34±0.05) compared to the obese group (mean=9.54±0.05) (p<0.001). CAT was lower in the non-obese group (mean=0.51±0.17 versus mean=0.67 ±0.24 for the obese group) (p<0.001). The maximal shear strain value was higher in the obese group (0.52 versus 0.48 (p=0.04)). We found no difference in the CAS value between both groups (mean of 6.10±1.78 and 5.72±1.86 for the non-obese and obese groups respectively (p=0.192)), nor were the CLT values different between the groups, being 0.98±0.33 and 0.90±0.34 for the non-obese and obese groups (p=0.074).

Conclusions: These preliminary results suggest that elastography according to NIVE has the potential to detect early physical vascular changes at the level of the carotid vessel wall in overweight children.

Future studies are required to determine NIVE's potential as a screening tool in children at risk of cardiovascular disease.

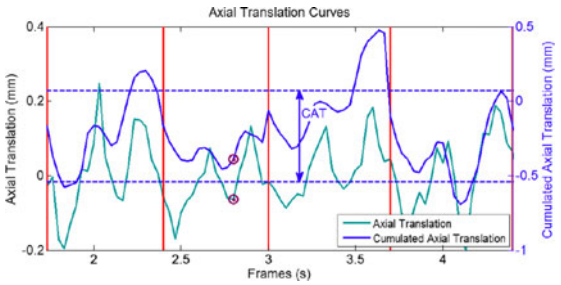

Paper #: 191

Free-breathing Reduced Field of View (ZOOM) Black Blood Imaging in Pediatric Cardiac MRI

Ramkumar Krishnamurthy, PhD, *Texas Children's Hospital, Houston, TX, rxkrish1@texaschildrens.org;* Cory Noel, MD, Prakash Masand, MD, Amol Pednekar, Rajesh Krishnamurthy

Disclosures: All authors have disclosed no financial interests, arrangements or affiliations in the context of this activity.

Purpose or Case Report: Double inversion recovery respiratory-triggered single shot Black Blood Turbo Spin Echo (BB-TSE) sequence is routinely used for assessment of morphology in pediatric cardiac MRI, when patients have compromised breath-holding capacity. Such images suffer from cardiac motion and T2 decay-related blurring, often yielding nondiagnostic images [1,2].

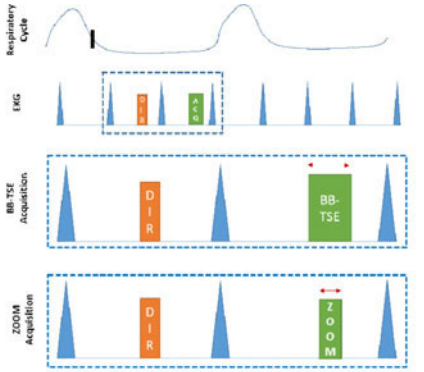

Figure 1: Schematic showing the respiratory triggered single-shot black blood – turbo spin echo (BB-TSE) and zoom acquisitions. Once the end-expiratory trigger is received from the respiratory bellow, scanning commences in which blood pool inversion happens with double inversion recovery sequence, and acquisition happens at the next RR interval, once blood pool is nulled. It is seen that the zoom acquisition time is significantly shorter than the BB-TSE sequence.

Hypothesis:

Using a reduced field of view imaging (Zoom) sequence, which has orthogonal placement of 90 and 180 RF pulses to reduce aliasing [1–3], scan times within a cardiac cycle can be shortened such that cardiac motion and T2 decay-related blurring can be reduced, yielding better image quality than BB-TSE in free-breathing patients.

Methods & Materials: This is an ongoing IRB approved prospective study. So far, 6 consecutive pediatric patients undergoing clinically indicated cardiac MRI, have been imaged with this protocol. After acquisition of initial survey sequences, axial stack of the thoracic region was acquired using a respiratory triggered single shot 1) BB-TSE sequence and 2) Zoom sequence, with identical imaging parameters: acquired voxel resolution of 1.5-2 * 1.5-2 *5-7 mm. TR=2 heart beats; TE ~=60 ms; SENSE=1.5 to 2. Three experienced observers compared two sets of anonymized and randomized images, and scored them on a scale of 1 - 5 (1 - non-diagnostic; 5 - excellent image quality) for 1) overall signal to noise ratio (SNR), 2) endocardial edge definition, and 3) blood pool nulling. Paired Student's t-test was used for comparison

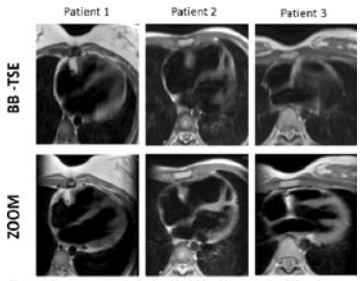

Figure 2: Representative single shot black blood images using TSE and zoom acquisitions are shown. It can be seen that there is superior edge definition and less blurring with zoom images – due to inherently lesser cardiac motion and decreased T2 decay.

Results: Both sequences were acquired successfully in all patients. There was a 42±6% reduction in scan time (within a cardiac cycle) using Zoom imaging. A consistent improvement in image quality was seen by all three observers in terms of SNR (3.3 vs 4.2), endocardial edge definition (3.4 vs 4.4), and blood pool nulling (3.0 vs 4.5) (figures 2, 3). Statistically significant improvement was observed for both SNR and endocardial edge definition (p<0.05) with Zoom imaging.

Conclusions: Zoom black blood imaging cuts scan time within a cardiac cycle by 42%, thereby reducing cardiac and T2 decay-related blurring, resulting in improved cardiovascular image quality in free-breathing children when compared to BB-TSE.

References:
1. Bueker et al., JMRI 1998;8:955–959
2. Hussain T, JMRI. 2011 Aug;34(2):279–85.
3. Muthupillai et al., 2010, 12(Suppl 1):O73

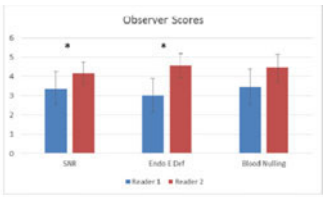

Figure 3: Average clinical scores from the three observers for BB-TSE and Zoom images. It was seen that zoom images consistently scored higher for SNR, endocardial edge definition and blood pool nulling. Statistical significance ($p < 0.05$) was reached for SNR and endocardial edge definition.

Paper #: 192

Image Quality Assessment of 3T MR Coronary Angiography (3D SSFP) In Patients Operated For Transposition of the Great Arteries with Three Qualitative Methods

L. Kathrine Suther, MD, *Oslo University Hospital, Department of Radiology and Nuclear Medicine, Pediatric Unit, Oslo, Norway;* Einar Hopp, MD, PhD, Henrik Brun, MD, PhD, Stig Larsen, PhD, Bac Nguyen, BSc, RT, Anders Høye Tomterstad, BSc, RT, Rolf Svendsmark, MSc, Bjarne Smevik, MD, Harald Lindberg, MD, PhD, Charlotte De Lange, MD, PhD

Disclosures: All authors have disclosed no financial interests, arrangements or affiliations in the context of this activity.
Purpose or Case Report: Patency of the coronary arteries after arterial switch operation (ASO) in patients with transposition of the great arteries (TGA) is a major concern due to cases of sudden cardiac death. Conventional coronary angiography is the current gold standard for visualization, but unfortunately with ionizing radiation. MR coronary angiography (MRA) without intravenous contrast media might be a possible alternative if the image quality and artery visualization is satisfactory.
This study compares three different methods of qualitative assessment of the image quality of 3 T MRA.
Methods & Materials: Twenty-four individuals, aged 10-15 years were examined. Twelve were former TGA patients corrected with ASO, and 12 were age-correlated healthy individuals. All individuals (n=24) had 3D steady-state free precession (SSFP) performed. Image quality of the coronary arteries at their origin was evaluated by two blinded radiologists using 3 different scales: a fixed point scale (FPS) from 1 to 4, a 10 cm non-figurative visual analogue scale (VAS) and a 10 cm figurative visual analogue scale (fVAS). Statistical analyses were performed determining Cohen's kappa coefficient (κ) for FPS and agreement index (AI) for VAS and fVAS.
Results: FPS showed an intra-observer κ value 0.5 for LAD, 0.44 for CX and 0.55 for RCA, but there was no significant positive agreement for LMS and no inter-observer agreement for any of the coronary artery origins.
Using VAS the intra-observer AI was 0.52 for both LAD and RCA, 0.12 for CX. The inter-observer AI could not be determined for LMS and LAD due to significant disagreement between the readers, but it was 0.24 for RCA.
With fVAS the intra-observer AI was 0.58 for LMS, 0.54 for LAD, 0.66 for CX and 0.72 for RCA. While the inter-observer AI was 0.97 for LMS, 0.42 for LAD, but AI for CX and RCA could not be determined due to significant disagreement between the readers.
Conclusions: Qualitative assessment of image quality of MR coronary angiography is challenging. Both FPS and VAS showed some intra-observer agreement, but nearly complete lack of inter-observer agreement. In general, fVAS partly improved both the intra- and inter-observer agreement. This may imply that qualitative evaluation may be better determined by the fVAS method. It could be that MRA with CM would show an even better agreement.

Paper #: 193

Optimizing contrast enhanced thoracoabdominal CT in children during extracorporeal membrane oxygenation (ECMO)

Marika Gullberg Lidegran, *Department of Paediatric Radiology, Astrid Lindgren Children's Hospital, Karolinska University Hospital, Stockholm, Sweden, marika.gullberg-lidegran@karolinska.se;* Lena Gordon Murkes, Björn Frenckner, Jonas Andersson Lindholm

Disclosures: All authors have disclosed no financial interests, arrangements or affiliations in the context of this activity.
Purpose or Case Report: To prospectively evaluate the quality and value of contrast enhanced (CE) chest and abdominal CT in children during ECMO, using a protocol for contrast medium administration adapted to the type of ECMO circuit, cannulation sites and clinical question.
Methods & Materials: All CE thoracoabdominal CT examinations in pediatric patients on ECMO during a 19 months period were included in the study. An updated protocol for iv contrast delivery was applied taking into account the type of ECMO circulation [venovenous (VV) or venoarterial (VA)], ECMO cannulation sites, preferred CT phase and the anatomy of interest.
For each examination a study protocol was completed. The ECMO intesivist recorded clinical information and ECMO technique, the radiologist at the CT department added information on CT technique and contrast administration. The following day a senior radiologist graded the quality of the scan and evaluated any added information from CT and impact on the treatment, in consensus with the ECMO intensivist.
Results: During the study time 37 CE thoracoabdominal CT examinations were performed in neonates and children on ECMO. Mean age was 3,9 years (2 d-17 y). Thirty scans were performed during VA and 7 during VV ECMO. Sixteen examinations included CTA of systemic arteries or pulmonary circulation.
In a majority of examinations (n=27) CT contrast was delivered to the membrane oxygenator with preserved ECMO flow. A peripheral or central venous access was utilized in the remaining10 examinations, with reduced ECMO flow during contrast injection. Among these were two CT pulmonary angiograms and four systemic CTA during VA ECMO.
Bolus tracking (BT) was used in all patients for timing of contrast material. In case of contrast delivery to the oxygenator, an estimated transit time through the ECMO circuit was used as guidance for start of BT, to reduce radiation dose.
Mean scan quality was graded 4,6 on a five grade scale. One examination, an abdominal CTA during VA ECMO with femoral artery cannulation, was initially non-diagnostic after contrast injection via a central venous line and had to be rescanned with injection to the oxygenator.

In 34 of the 37 examinations CT added new information and in 24 the CT findings affected the treatment.
Conclusions: High quality CE CT scans can reliably be performed in children on ECMO by adapting contrast medium delivery to the type of ECMO circulation, cannulation sites and anatomy of interest. The CT examinations frequently add important information affecting the treatment.

Paper #: 194

Lessons learned from patient-specific 3D printing of pulmonary atresia with major aortopulmonary collaterals (MAPCAS) for surgical planning

David Ezon, MD, *Radiology, Texas Children's Hospital, Houston, TX, ezon18@gmail.com;* Zbigniew Starosolski, PhD, Nicholas Dodd, BM, Jeffrey Heinle, Emmett Dean Mckenzie, Rajesh Krishnamurthy

Disclosures: Zbigniew Starosolski has indicated a relationship with Alzeca Biosciences, LLC. All other authors have disclosed no financial interests, arrangements or affiliations in the context of this activity.
Purpose or Case Report: To investigate the appropriate technique for 3D printing of pulmonary atresia with MAPCAS for surgical planning based on surgeon feedback.

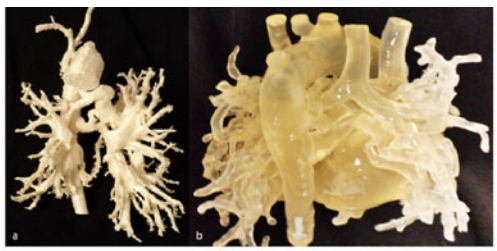

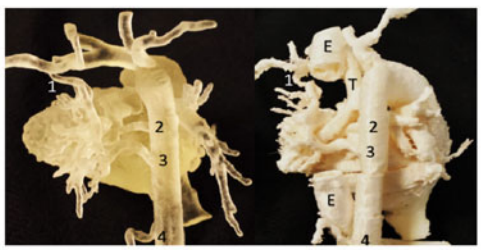

Figure 1: 2 3D printed models using a flexible, inexpensive technique (a), and a flexible expensive technique (b), both of which are affected by pulmonary venous contamination, and difficulty in distinguishing native pulmonary artery branches and MAPCAS from veins. 1a was printed after removal of the cardiac mass, while 1b retained the cardiac mass as well as the trachea for relationships.

Figure 2: Two 3D printed models of the same patient, an expensive flexible model on the left (a), and an inexpensive flexible model on the right (b). There are 4 major collaterals to the right lung, marked 1-4. 2a was printed without the trachea, while 2b was printed with the trachea (T) and esophagus (E), which has been partially resected to show the underlying anatomy. Although 2a has better structural detail, 2b allows determination of the relationship of the MAPCAS to the airway and esophagus. MAPCA 2 travels ventral to the right mainstem bronchus, MAPCA 3 travels posterior to the right mainstem bronchus and ventral to the esophagus, while MAPCA 4 travels posterior to the esophagus. These are useful landmarks for the surgeon during unifocalization.

Methods & Materials: After institutional IRB approval, the CT angiography scans of 6 patients with pulmonary atresia and MAPCAS were selected for 3D printing. Volumetric CTA data obtained on a Toshiba 320 detector CT was segmented on MIMICS to create 3D stl models and printed with 3 different techniques: an inexpensive rigid model, an inexpensive flexible model, and an expensive flexible model. Morphologic options included removal of the cardiac mass to better demonstrate the pulmonary vasculature, retention of the trachea on the print to demonstrate relationships, and segmentation of the pulmonary arterial structures and exclusion of pulmonary venous structures (Figure 1). The models were presented to 3 experienced pediatric cardiovascular surgeons for feedback on the models' realism, effectiveness for surgical planning and training, and patients' comprehension of disease, and their responses were evaluated with plotted questionnaires.
Results: Printed models of 6 patients were fabricated successfully. Surgeon feedback revealed the following preferences:
1. Importance of selective arterial phase of enhancement during CT acquisition in order to create a clean segment of the arterial tree without venous contamination. This is achievable by scanning during the first pass of contrast enhancement through the ascending aorta prior to left atrial opacification.
2. Demonstration of the hypoplastic mediastinal pulmonary arteries (PA).
3. Inclusion of the airway within the vascular model rather than as a separate print, to enable usage of the airway as an operative landmark for MAPCA location.
4. Flexible model that will allow distortion of the airway to show relationships of the MAPCAS to the carina and mainstem bronchi, and intraparenchymal distribution of MAPCAS versus native PA branches.
Based on this feedback, an optimal protocol for acquisition and printing of MAPCAS was instituted, with selective arterial phase imaging of the vasculature, and 3D printing performed with inexpensive flexible material with and without embedded airway information (Figure 2).
Conclusions: Generating 3D printed models of pulmonary atresia with MAPCAS with face and content validity is feasible with refinements to acquisition and fabrication based on surgeon preferences.
Legend for figures 1 and 2 on Figure 3.

ALTERNATE PAPER

Pediatric Alveolar Rhabdomyosarcomas: Genetic Influence on Imaging Features

Cinthia Cruz Romero, MD, Abdominal Radiology, Massachusetts General Hospital, Boston, MA, ccruzromero@mgh.harvard.edu; Michael Gee, MD, PhD

Disclosures: All authors have disclosed no financial interests, arrangements or affiliations in the context of this activity.
Purpose or Case Report: To identify imaging features associated with genetic alterations in pediatric alveolar rhabdomyosarcomas.
Methods & Materials: IRB approved and HIPAA compliant retrospective study of consecutive patients with biopsy proven alveolar rhabdomyosarcoma from 2000 to 2014. Contrast enhanced CT and MRI were blindly read in consensus by two radiologists for presence or absence of intratumoral areas of non- enhancement, hemorrhage, calcification and T2-weighted hypointensity, as well as lymphatic or hematogenous metastasis. Primary tumor long axis and location of the tumors were also recorded. Genetic testing results for the FKHR-PAX3/PAX7-gene rearrangement (FPR), which is known to be associated with alveolar rhabdomyosarcoma treatment response and clinical outcome, were obtained from the electronic medical record and associated with imaging features using Fisher's Exact Test with statistical significance at $p<0.05$.
Results: 10 female and 7 male subjects. FPR was present in 9/17(53%) cases (8 FKHR-PAX3 and 1 FKHR-PAX7). Areas of non-enhancement were found in 9/17(53%) and hemorrhage in 3/17(18%) cases overall. Ten tumors exhibited homogeneous T2-weighted hyperintensity, of which 7 (70%) carried a FPR ($p=0.03$ compared with non-FPR tumors); none of the other imaging features correlated with genotype. The mean diameter of FPR tumors (5.6+-1.5 cm) was significantly increased compared with non-FPR tumors (4.1+-1.8 cm) ($p=0.04$). Presence of lymphatic or hematogenous metastasis, as well as primary tumor location, did not significantly vary based on tumor genotype.

Conclusions: The FKHR-PAX rearrangement in the alveolar rhabdomyosarcoma histologic subtype is significantly correlated to T2-weighted homogeneous hyperintensity and increased tumor size compared with tumors lacking the rearrangement. These results suggest an association between alveolar rhabdomyosarcoma imaging appearance and treatment response/survival rate.

SCIENTIFIC PAPERS – RADIOGRAPHERS

(R) indicates a Radiographer Program Submission

Paper #: 01 (R)

A comparison of paediatric CT protocols and doses across Irish hospitals

Shane Foley, PhD, *Diagnostic Imaging, University College Dublin, Dublin, Ireland, shane.foley@ucd.ie;* Dara Murphy, Louise Rainford, PhD

Disclosures: All authors have disclosed no financial interests, arrangements or affiliations in the context of this activity.
Purpose or Case Report: To compare paediatric CT protocols and radiation doses across Irish CT departments using automatic dose management software.
Methods & Materials: Data was collected retrospectively for the 2014 calender year from all Irish radiology departments connected to the national PACS using automatic dose management software (eXposure, Radimetrics, Bayer Healthcare). All available data for paediatric patients (0-18 yrs) was collated and protocol data was analysed between sites, including scanner type, patient ages and paediatric categorisation. Mean CT doses (dose length product) were compared between sites.
Results: A total of 6976 CT dose reports were available from 25 sites across Ireland and included scanners with 6-128 row detectors and two dedicated paediatric centres. The dedicated paediatric centres conducted 28% of the total CT examinations with a median patient age of 9 in comparison to 15 years in general hospitals. The most common examinations being brain (57%), abdomen (6.5%), chest (4%), and chest/abdomen/pelvis (2%). Both paediatric centres used age based protocols for brain and weight for trunk examinations but this was replicated in only 61% and 13% of general hospitals, respectively. There was no consistency in age or weight categories used across centres. Paediatric centres had 16 brain protocols, in comparison to a mean of 5 for general centres. Mean doses between centres varied by a factor of 5 for CT brain.
Conclusions: Automated dose management software facilitates relatively easy review of CT doses and comparison of protocols between sites. There is an obvious need for optimisation for paediatric CT protocols nationwide.

Paper #: 02 (R)

Combined PET/Diagnostic CT exams as a means toward dose reduction in pediatric patients with lymphoma

Erica Gates, *Radiology, Cincinnati Children's Hospital Medical Center, Cincinnati, OH, Erica.Kremer@cchmc.org;* Zhihua Qi, Maureen O'Brien, Andrew Trout

Disclosures: Andrew Trout has indicated a relationship with Philips Healthcare, Advisory Board. All other authors have disclosed no financial interests, arrangements or affiliations in the context of this activity.
Purpose or Case Report: To reduce radiation exposure and provide a unified report for lymphoma patients undergoing both diagnostic CT (D-CT) and 18-F FDG-PET/CT exams, we have developed a program where the D-CT is used as the attenuation correction (AC)/localization CT for the PET exam and no additional AC-CT is performed. The purpose of this study was to review our experience developing a PET/D-CT program with attention to dose reduction through use of the combined exam.
Methods & Materials: All PET/D-CT exams performed between 10/2014 and 8/2015 were reviewed. The estimated total effective dose from each of these exams was compared to the total effective dose from previous separately acquired FDG-PET/AC-CT and D-CT exams in the same patient or, if not available, the institutional target dose for patients of similar weight. The total effective dose for each CT exam was calculated by summing the effective doses for each body segment (head/neck, chest, abdomen/pelvis), determined by multiplying Dose-Length-Product (DLP) values by an age- and anatomy-appropriate k factor. Total effective doses were analyzed by a paired t-test to determine whether there was a statistically significant reduction in effective dose through the use of the combined exam.
Results: 17 patients (median 14 years) underwent a total of 21 PET/D-CT exams during the study period. Prior separately performed D-CT exams and AC-CT exams were available in 9 patients (53%). Mean estimated effective dose was 8.5±3.1 mSv for the PET/D-CT exam and 9.5 ±3.5 mSv for separately acquired PET/AC-CT and D-CT exams with a mean dose savings of 1±2.2 mSv (95%CI: 0-2 mSv, $p<0.05$) for the PET/D-CT exam. Greatest dose savings (3.7-5 mSv) occurred in exams with larger targeted areas of D-CT imaging and when the lower legs were not imaged. 4/21 PET/D-CT examinations resulted in increased effective dose vs. combined PET/AC-CT+D-CT exams due to limitations in scanner dose prediction based on inclusion of the lower extremities in the imaged field of view. Subsequent optimization of technique has addressed this issue. A combined PET/D-CT exam has allowed creation of a report inclusive of all imaging elements of the Lugano criteria. Clinical reception of the PET/D-CT examination and associated report has been highly positive.
Conclusions: A combined FDG-PET/D-CT examination achieves dose savings over separately acquired PET/CT and D-CT exams and provides a more unified, clinically valuable report. Further dose savings can be achieved with technical modifications.

Paper #: 03 (R)

The impact of paediatric Computed Tomography tube current and tube voltage modulation intensity in organ dose and image quality

Marina Alves, Patrícia Fernandes, Dulce Costa, Graciano Paulo, **Joana Santos, PhD**, *Medical Imaging & Radiotherapy, IPC- Coimbra Health School, Portugal, joanasantos@estescoimbra.pt*

Disclosures: All authors have disclosed no financial interests, arrangements or affiliations in the context of this activity.
Purpose or Case Report: Taking into account that head and chest Computed Tomography (CT) examinations are the most frequently performed in paediatric the aim of this study is to analyse the impact of the different tube current and tube voltage modulation intensities in dose values and image quality.
Methods & Materials: Head and trunk CT examinations (n=22) were performed in a Siemens® Somatom Definition AS CT scanner (64 detector row) using a 5 years old paediatric anthropomorphic phantom (ATOM-705-CIRS). A three channel Patient Skin Dose (PSD Unfors) detector (right eye lens, the left mammary gland and gonads) was used to analyse the organ dose (μSv). The CT dose values in terms of CT Dose Index (CTDIvol - mGy) and Dose Length Product (DLP - mGy.cm) were directly collected on the CT scanner. Objective image analysis was based on the image noise measured in homogeneous regions of interest. Phantom quality control kit images were subjective analysed by 3 radiographers with more than 10 years of experience.
Results: The combination tube current and tube voltage modulations allowed examination dose reduction of 19% and 75% for head and trunk CT, respectively. The organ dose decreased 46% and 72% for the same procedures. No significant differences were founded for dose values and image noise using the different modulation intensities in head and trunk paediatric CT examinations.

Conclusions: Considering the results for dose values (examination and organ) and image quality, the average modulation intensity was considered the most suitable for head and trunk CT examinations.

Paper #: 04 (R)

Optimisation and establishment of Diagnostic Reference Levels in paediatric plain radiography

Graciano Paulo, *Medical Imaging & Radiotherapy, IPC- Coimbra Health School, Portugal, graciano@estescoimbra.pt;* Adriano Rodrigues, Eliseo Vaño

Disclosures: All authors have disclosed no financial interests, arrangements or affiliations in the context of this activity. Purpose or Case Report: This study aimed to propose Diagnostic Reference Levels (DRLs) in paediatric plain radiography and to optimise the most frequent paediatric plain radiography examinations in Portugal following an analysis and evaluation of current practice.
Methods & Materials: Anthropometric data (weight, patient height and thickness of the irradiated anatomy) was collected from 9,935 patients. National DRLs were calculated for the three most frequent X-ray procedures: chest AP/PA projection; abdomen AP projection; pelvis AP projection. Exposure factors and patient dose were collected prospectively. In order to analyse the relationship between exposure factors, the use of technical features and dose, experimental tests were made using two anthropomorphic phantoms: a) CIRS™ ATOM model 705®; height: 110 cm, weight: 19 kg and b) Kyoto kagaku™ model PBU-60®; height: 165 cm, weight: 50 kg. Objective image analysis was performed by analysing the variation of the mean value of the standard deviation, measured with OsiriX® software (Pixmeo, Switzerland). A Visual Grading Characteristic image quality evaluation was performed blindly by four paediatric radiologists, each with a minimum of 10 years of professional experience, using anatomical criteria scoring.
Results: A high heterogeneity of practice was found and the established Portuguese DRL values were higher than the most recent published data. The national DRLs (KAP_{P75}) established for Portugal are: CHEST: 13 mGy.cm^2, 19 mGy.cm^2, 60 mGy.cm^2, 134 mGy.cm^2, 94 mGy.cm^2; ABDOMEN: 25 mGy.cm^2, 84 mGy.cm^2, 140 mGy.cm^2, 442 mGy.cm^2, 1401 mGy.cm^2; PELVIS: 29 mGy.cm^2, 75 mGy.cm^2, 143 mGy.cm^2, 585 mGy.cm^2, 839 mGy.cm^2, respectively for age groups <1, 1-<5, 5-<10, 10-<16, 16-≤18.
Significant dose reduction was achieved through the implementation of an optimisation programme: an average reduction of 41% and 18% on KAP_{P75} and $ESAK_{P75}$, respectively for chest plain radiography; an average reduction of 58% and 53% on KAP_{P75} and $ESAK_{P75}$, respectively for abdomen plain radiography; and an average reduction of 47% and 48% on KAP_{P75} and $ESAK_{P75}$, respectively for pelvis plain radiography.
Conclusions: Portuguese DRLs for plain radiography were obtained for paediatric plain radiography (chest AP/PA, abdomen and pelvis). Experimental phantom tests identified adequate plain radiography exposure criteria, validated by objective and subjective image quality analysis. The implementation of the optimisation programme allowed a significant dose reduction to paediatric patients, without compromising image quality.

Paper #: 05 (R)

Establish and optimise dose levels for chest radiography in paediatric intensive care unit

Paula Lago, Graciano Paulo, Joana Santos, PhD, *Medical Imaging & Radiotherapy, IPC- Coimbra Health School, Portugal, joanasantos@estescoimbra.pt*
Disclosures: All authors have disclosed no financial interests, arrangements or affiliations in the context of this activity.
Purpose or Case Report: To perform radiographs in Paediatric Intensive Care Unit (PICU) special attention must be given to radiological protection in children considering their high radiosensitivity. This study aim to analyse the values of scattered radiation during chest radiography in the PICU and optimise the procedures to reduce exposure.
Methods & Materials: Quality control of the radiography portable equipment was made and the scattered radiation during bedside chest radiography (with and without protection between beds) was measured using RaySafe Xi equipment and Educational Direct Dosimeter (EDD), respectively. Exposure parameters and dose levels were collected during children chest radiographs to allow establishing DRLs. In order to optimise the procedure experimental test were performed in a newborn and 5 years old equivalent anthropomorphic phantoms. Image quality analyses based on CEC criteria was performed by 5 radiographers
Results: The scattered radiation during bedside chest radiography was completely reduced when shielding between beds (2 m) was used. The DRL for chest radiography was 1.17Gy.cm^2 for newborn and 4.2 Gy.cm^2 for 1 to 5 years old. Dose values were reduced 22% in phantom experimental tests without influence in image quality.
Conclusions: Shielding between beds should be used in order to eliminate the scattered radiation effects in other children. DRLs for chest radiography were established and optimised in the PICU.

Paper #: 06 (R)

Analysis of overexposed areas in paediatric plain radiography

Ana Pereira, Bárbara Poiares, Bruno Esteves, Joana Santos, PhD, **Graciano Paulo**, *Medical Imaging & Radiotherapy, IPC- Coimbra Health School, Portugal, graciano@estescoimbra.pt*

Disclosures: All authors have disclosed no financial interests, arrangements or affiliations in the context of this activity.
Purpose or Case Report: Compare the beam collimation with electronic collimation in chest, abdomen and pelvis paediatric plain radiographies, in order to quantify the over exposed areas. Analyse the impact of beam collimation in DAP values in paediatrics.
Methods & Materials: Retrospective analysis of exposure parameters, dose values and beam collimation (based on the irradiated detector area) of chest, abdomen and pelvis plain radiographies *Digital Imaging Archiving and Communication System* (DICOM) headers, available on *Picture Archiving and Communication System* (PACS). The electronic collimation and anatomic collimation (based on the European Guidelines in quality criteria) were directly measure on the image using the same calibrated workstation, and the areas were calculated. The impact of the reduction of 1 cm^2 beam collimation in DAP values was analysed using paediatric anthropomorphic phantoms.
Results: The exposure parameters and dose values of the chest, abdomen and pelvis radiographies (n=256), as expected, increased with the patient age, however this fact non-occurred for the beam collimation. Significant differences were founded for beam collimation and electronic collimation areas, with a 17% mean overexposed area. There were no significant differences from anatomic and electronic collimated areas. The variation of 1 cm^2 in beam collimation in paediatric anthropomorphic phantoms revealed an increased of 9% in DAP values.
Conclusions: In the majority of the exposures, radiographers electronic collimated according to the anatomic quality criteria instead of using beam collimation. Considering the impact of beam collimation in DAP values this collimation type must be used in order to reduce the dose values in children.

Paper #: 07 (R)

An Investigation of the current status of the Alliance for Radiation Safety in Paediatric Imaging (ARSPI) Back to Basics campaign in Paediatric Projection Radiography in Ireland

Saundra O Connor, BSc Diagnostic Radiography, *Diagnostic Imaging, University College Dublin, Killarney, Ireland, saundraoconnor@gmail.com;* Kate Matthews

Disclosures: All authors have disclosed no financial interests, arrangements or affiliations in the context of this activity.
Purpose or Case Report: Background: Projection radiography is the most common type of examination in diagnostic imaging. Literature recognises the associated dose burden particularly for paediatric patients. The Back to Basics campaign seeks to promote best practice in paediatric projection radiography internationally. The campaign promotes the use of objective tools to assist professional judgment regarding paediatric exposure and image appraisal.
Methods & Materials: Method: Opinions and practices of Irish radiographers regarding the advice within the Back to Basics campaign were investigated via a nationwide postal survey. The survey sample was selected at random by multi-stage stratified sampling, and radiographer respondents were from Irish hospitals of varying size and paediatric caseload.
Results: Results: 81% (n=58) of respondents were unaware of Back to Basics and only 4% (n=3) of respondents acknowledged that some answers were influenced by the campaign. The majority of respondents (78%) considered optimisation of equal importance for paediatric and adult patients. Despite recognised best practice, subjective visual assessment of patient size (89%, n=64 respondents) continues to supersede measurement of body thickness (7%, n=5 respondents). Only 25% (n=18) of respondents understand and use digital indicators appropriately. Good practice related to elements of the campaign was evident, but more consideration is needed of best use of lead protection, AEC and grid. No significant association was revealed between duration of clinical experience and knowledge of Back to Basics or implementation of campaign best practices
Conclusions: Conclusions: Further education regarding best practices in digital paediatric radiography is required in Ireland. This could be via greater promotion of Back to Basics material.

Paper #: 08 (R)

An investigation of how to improve recall and awareness of radiation dose levels associated with pediatric cardiovascular interventional procedures

Sorcha Mullen, *School of Medicine, University College Dublin, Dublin, Ireland;* Jonathan McNulty, Toni Buchanan, Veronica McGuire, Louise Rainford, PhD

Disclosures: All authors have disclosed no financial interests, arrangements or affiliations in the context of this activity.
Purpose or Case Report:
Staff awareness of pediatric cardiovascular (CV) interventional radiation dose is an essential element of radiation protection. This study tested a protocol involving real-time recall and review of procedural dose to evaluate its impact upon staffs' level of awareness of radiation dose for common procedures and to gain their feedback on the protocol applied in practice.
Methods & Materials: A pre-intervention survey (22 questions) was completed by radiographers (n=13) and cardiac clinicians (n=4) in the national pediatric center in Ireland offering specialized cardiac imaging services, to ascertain radiation awareness and recall levels. A "Record and Report" intervention was then implemented for a 2-week period. A poster portraying agreed local reference dose levels (DRLs) for the three most common pediatric CV interventional procedures was displayed at CV suite exposure console. Following each procedure, the radiographer verbally informed the cardiac clinician of the examination dose (DAP) and procedural time. The clinicians classified procedures as routine, slightly complex or complex. Verbal confirmation of whether the procedural dose was low, comparable or high when compared to displayed local DRLs was affirmed. A post- intervention survey determined the impact on recall and awareness of dose and sought opinion on the practical suitability of the protocol/intervention.
Results: The study's findings identified 37.5% of participants who completed the post-intervention survey stated increased awareness of dose levels, 12.5% reporting increased radiation safety culture in the CV suite. Post intervention 60% stated radiation dose responses closer to the provided reference values, compared to pre-intervention responses. Radiographers reported increases in dose discussion (60%), however no increase was reported amongst cardiac clinicians. Furthermore 50% reported that consideration of high, comparable or low dose had a positive impact on their practice and 37.5% stated they would make changes to enhance their own practice in the future.
Conclusions: Overall, cardiac clinicians and radiographers benefited from the "Record and Report" intervention. The findings identify emphasis should be placed on improving radiographer and clinician awareness of radiation dose and on their ability to recall locally administered doses. Positive responses were received from the participants and further investigation over an extended period of time is warranted.

Paper #: 09 (R)

Comparison of radiation dose between centers in the aim of establishing DRLs for commonly performed pediatric cardiac interventional procedures

Louise Rainford, PhD, *School of Medicine, University College Dublin, Dublin, Ireland, louise.rainford@ucd.ie;* Diego Catania, Liz Masterson, Clare Mc Claren, Shane Foley, PhD

Disclosures: All authors have disclosed no financial interests, arrangements or affiliations in the context of this activity.
Purpose or Case Report: There is limited published data on radiation doses in pediatric cardiac interventional radiology. Cases can be complex leading to large variations in examination techniques and when categorized by age or weight the sourcing of sufficient numbers on which to establish DRLs is difficult to achieve. This study collected pediatric cardiac interventional data to compare mean radiation doses for varied equipment models and to establish DRLs for frequently performed examinations.
Methods & Materials: Institutional permission was granted to access imaging records in the national Irish children's center and retrospective data (n=48 months) was collated for cardiac interventional procedures performed on a Siemens Bicor unit. Data was age categorized: 0 - <1, 1-<5, 5-<10, 10-<15 and >15-18 years and patient weights were recorded. Data was also attained from two specialized pediatric centers prospectively in London (UK) and Milan (Italy), these centers using newer imaging equipment: Siemens Artis and Philips Integris Allura respectively. Data for cardiac catheterization (CC), closure of patent ductus arteriosus (PDA) and atrial septal defect (ASD) procedures was recorded. A minimum of 10 examinations in each age category was deemed essential, 20+ cases preferred for DRL calculation, using the 75th percentile.
Results: Data from 600+ examinations was collated, the most common age group was the 1-<5 year category. CC recorded the greatest numbers. Large differences in mean radiation doses were noted between centers, up to 5 fold, which were statistically significant. DRLs for CC in the 1-<5 year category for the Irish, Italian and UK centers were 526.66 (n=50), 337.00 (n=20), 172.23 (n=26) mGycm^2 respectively (patient numbers in parenthesis).

Conclusions: Establishing DRLs in pediatric cardiac interventional radiology is difficult due to the limited number of patients presenting in each age category and should be restricted to the most common examinations. DRL establishment needs to consider equipment specifications involved in the imaging process.

Paper #: 10 (R)

Measurement of the density of bronchoceles in cystic fibrosis as an indicator of allergic broncho-pulmonary aspergillosis: preliminary study

Marie Baqué Juston, Aurelie Occelli, myriam guesmi, corinne boyer, **Beatrice Leloutre**, *Hopitaux Pediatrique de Nice CHU-Lenval, Nice, France, beatrice.leloutre@lenval.com;* Anne Geoffray

Disclosures: All authors have disclosed no financial interests, arrangements or affiliations in the context of this activity.
Purpose or Case Report: Allergic broncho-pulmonary aspergillosis (ABPA) is a severe and often under-diagnosed complication of cystic fibrosis. The diagnosis is multifactorial and includes clinical, biological and radiological criterias. The aim of the study was to determine whether the mucus content of bronchoceles in cystic fibrosis complicated with ABPA show a higher density than the mucus content of non-ABPA cystic fibrosis.
Methods & Materials: we studied retrospectively 32 CT scans from a pediatric population of cystic fibrosis patients. We measured the mucus attenuation in Hounsfield Units (HU) of all bronchoceles >5 mm in diameter. In patients showing multiple bronchoceles, only the highest density was recorded.
Results: We found bronchoceles > 5 mm in 13/32 patients. 5/13 patients had a positive diagnosis of ABPA.
The median value of all bronchoceles content was 31 UH (10-135), the median value of bronchoceles in ABPA was 98 UH (26-135), the median value of bronchoceles of patients without ABPA was 28 UH (10-36). In our population of patients, a treshold > 36 UH had a 80% sensibility and 100% specificity for the diagnosis of ABPA
Conclusions: CF complicated with ABPA show higher attenuation bronchoceles on chest CT scan. Systematic density measurements of bronchoceles could help to raise the difficult diagnosis of ABPA in patient suffering from cystic fibrosis. Larger series could confirm a treshold in UH which could become a new imaging criterion for the diagnosis of ABPA .

Paper #: 11 (R)

Clinically acceptable noise levels in paediatric chest and abdomen CT examinations

Michelle O'Connor, *School of Medicine, University College Dublin, Dublin 4, Ireland, michelle.oconnor@ucd.ie;* Shane Foley, PhD
Disclosures: All authors have disclosed no financial interests, arrangements or affiliations in the context of this activity.
Purpose or Case Report: Acceptable levels of noise on CT images for diagnostic purposes are lacking, especially in paediatrics. This research investigated current noise levels in chest and abdomen CT scans in two paediatric centres.
Methods & Materials: Following ethical permission, a random sample of 100 chest and abdomen CT scans were retrospectively collected from two paediatric hospitals, both with Philips 64slice Brilliance scanners and using weight based protocols (80- 120kVp, AEC, 64x0.625 mm collimation, pitch 0.891, iDose level 4). Patient size was calculated by measuring waist circumference (WC) at L3- L4 and chest circumference (CC) at the level of the nipples. Noise was measured by three experienced observers using identical sized regions of interest (ROI) in four homogenous locations of the body; Bladder, bronchus at level of carina, subcutaneous adipose tissue, and in air anterior to skin. Each measurement was performed on three sequential slices. Linear regression was carried out to assess patient size, age and clinical site as noise predictors.
Results: Patients ranged in age from 1 to 16 years (mean: 8) with mean WC 72.3 cm (range: 59-86 cm) and mean CC 57.1 cm (range: 46-71 cm). Mean[SF1] noise in the chest (centrally: 10.5HU, range 6-16HU and peripherally: 11.1HU, range 4-19HU) was significantly (p>0.05) higher than that in the abdomen (centrally: 9.4HU, range:4-14HU and peripherally: 10.3HU, range:4-16HU). No statistically significant linear dependence was found between mean noise in abdominal (F(3,96)=0.317, p=0.813) or chest (F(3,96)=1.044, p=0.377) regions based on age, patient size or hospital site. Inter- and intra-viewer reliability were excellent (ICC>0.98).
Conclusions: It is widely reported in literature that higher levels of noise are acceptable on CT scans of larger patients and more obese patients; however our findings show no significant difference in noise levels across patient age and size. Use of AEC results in consistent noise levels for paediatric trunk CT across patient ages and sizes suggesting that further individual optimization is possible according to clinical indications and patient size.

Paper #: 12 (R)

A comparison of manual, semi-automated and automated visceral adipose tissue quantification on paedatric abdominal CT examinations

Michelle O'Connor, *School of Medicine, University College Dublin, Dublin 4, Ireland, michelle.oconnor@ucd.ie;* Shane Foley, PhD
Marika Gullberg Lidegran, *Department of Paediatric Radiology, Astrid Lindgren Children's Hospital, Karolinska University Hospital, Stockholm, Sweden*, *marika.gullberg-lidegran@karolinska.se*; Lena Gordon Murkes, Björn Frenckner, Jonas Andersson Lindholm

Disclosures: All authors have disclosed no financial interests, arrangements or affiliations in the context of this activity.
Purpose or Case Report: Excessive visceral adipose tissue (VAT) is a significant risk factor for many obesity-related metabolic diseases. This research investigates the consistency and time efficiency of VAT quantification on paediatric abdomen CT scans using manual, semi-automated and automated methods.
Methods & Materials: Sixty abdomen CT datasets were retrieved from paediatric hospitals, via random sampling stratified according to age (0-5, 5-10 and 10-15 years) following ethical permission. All examinations were performed on a Phillips Brilliance 64 slice scanner using weight-based scanning protocols that incorporated automatic exposure control at 80 kVp for patients <40 kg, 100 kVp for 40-60 kg patients and 120 kVp for patients over 60 kg. Each scan included the entire abdomen from the diaphragm to the symphysis pubis. VAT was measured at each intervertebral level between T12 and S1 using ImageJ software by thresholding adipose tissue (-190 to -30HU) and then manually segmenting visceral from subcutaneous adipose tissue by tracing the inner boundary of the abdominal muscle wall. Automatic VAT quantification was performed using Terarecon software (Acquarius iNtuition). Semi-automated VAT quantification was performed using two steps; 1)automatic VAT quantification using Tererecon software; 2)manually editing VAT border to correct any segmentation error. All measurements were performed by two experienced observers. Ten duplicate scans were included to test intra-viewer reliability. Inter- and intra-viewer reliability were tested using Spearmans correlation. VAT measurements were correlated using Spearmans correlation. The mean time taken to perform each method was recorded.
Results: VAT volume quantification was very consistent for both manual and semi-automatic VAT quantification (rho>0.96, p<0.01). Inter- and intra-viewer reliability was excellent for all three methods (rho > 0.97, p 0.96, p<0.01). Automatic VAT quantification did not correlate to the

other methods and almost always overestimated VAT (96.67% of cases). Frequently encountered causes of VAT overestimation were identified and developed into learning points for future VAT quantification research. The mean time taken to quantify VAT automatically was 16 s, semi-automatically 68 s and manually 243 s

Conclusions: VAT quantification using a semi-automated approach is the recommended method in paediatric CT due to its high accuracy, reproducibility and time efficiency. Learning points have been developed to assist researchers in VAT quantification.

Paper #: 13 (R)

The practical considerations of research scanning using ARFI elastography: A healthy pediatric liver cohort investigation.

Therese Herlihy, McGee Allison, Louise Rainford, PhD, Marion Rowland, Billy Bourke, **Marion Maher**, **MSc**, *Diagnostic Imaging, University College Dublin (UCD), Dublin, Ireland, marion.maher@ucd.ie*

Disclosures: All authors have disclosed no financial interests, arrangements or affiliations in the context of this activity.

Purpose or Case Report: Acoustic Radiation Force Impulse imaging (ARFI) is an ultrasound-based quantitative elastography technology that can be used to determine liver elasticity and thus liver health. ARFI has been used in the evaluation of fibrotic liver parenchyma in the adult population but to date has not been widely used in the pediatric population. This study investigates the practical elements of scanning which must be considered when using ARFI elastography to scan the normal pediatric liver in order to obtain accurate and reproducible results.

Methods & Materials: Ethical approval was obtained and 103 pediatric patients ranging in age from 5 to 17 years volunteered to be scanned from a sports club: this research forming part of a larger national cystic fibrosis project. A Siemens Acuson S2000 HELX Ultrasound System was used and volunteers were scanned twice by two experienced sonographers, scanning consecutively (blinded). Each sonographer took ten AFRI measurements from the right lobe of liver, using an intercostal approach.

Results: The majority of children were scanned without issue however variations in age profile and body habitus influenced the scanning technique, patient position required for scanning and length of examination. Anatomical variations of liver position also affected scanning technique. Reproducibility and optimized scanning technique were inter-related.

Conclusions: The study identified practical considerations which must be taken into account when applied to ARFI elastography for pediatric populations. In order to obtain accurate ARFI values optimal ultrasound technique is critical and sonographers must be aware of challenges of performing ARFI on pediatric cohorts.

Paper #: 14 (R)

The Benefits of an Online MRI Safety Awareness Training Module in a Hospital Setting: "Just Log In"

Matthew Head, *Medical Imaging, Children's Hospital of Eastern Ontario, Ottawa, ON, Canada, mhead@cheo.on.ca;* Elka Miller, Cassandra Kapoor, Berry Smith, Salwa Akiki, Wendy Rabbie

Disclosures: All authors have disclosed no financial interests, arrangements or affiliations in the context of this activity.

Purpose or Case Report: MRI is often viewed as a "safe" practice as ionizing radiation is not involved; however, magnet safety is critical to ensure the safety of patients, families and staff. The MRI environment has potential hazards related to three main components: the strong static field, the pulsed gradient magnetic fields, and the pulsed radiofrequency (RF)[1]. In a pediatric environment, safety is a greater challenge as the size of the multidisciplinary team involved in a child's circle of care is greater than in an adult facility. Establishing effective pre-MRI screening policies and ensuring that all staff are up to date and trained to work within the MR area are two vital components of MR safety[1,2]. The aim of this project was to develop and implement a web-based MRI safety module to increase MRI safety awareness for staff and healthcare providers in our institution.

Supplement 1:

Table 1	Percentage of Staff Who Scored 100%	
	Pre-Test	Post-Test
Non-Clinical	23.0	95.5
Clinical	24.0	92.6
Physicians	22.5	94.6

Methods & Materials: A web-based MRI safety module was designed and implemented through the Online Learning Centre at our pediatric institution. The module included MR safety guidelines from the ACR guidance document on MR safe practices and the Reference Manual for Magnetic Resonance Safety, Implants, and Devices[3,4]. To validate the effectiveness of the module, hospital staff completed pre and post assessments. Hospital staff included non-clinical, clinical, and physicians. A pre-assessment was presented to hospital staff before taking the module and the post-assessment occurred immediately after the module was completed. Both assessments had 10 identical questions.

Results: Data was collected from 243 hospital staff (non-clinical (n=74), clinical (n=129), and physician (n=40)). In the pre-assessment, 23.5% (n=57) of hospital staff scored 100% and after taking the module, 97.8% (n=220) of hospital staff scored 100% in the post-assessment. The results were similar between all staff (Table 1). A McNemar Test showed that 5/10 questions were highly statistically significant (p<0.001), 3/10 questions were statistically significant (p<0.05) and 2/10 questions were not statistically significant (p<0.1) in learning between the pre-assessment and post-assessment.

Conclusions: Implementation of a web-based MRI safety module in our institution was an effective tool to create awareness of safety risks in the MRI area. It was evident that hospital staff are under informed about the risks and safety hazards in the MRI environment. These results can help other MR facilities to implement initiatives for MR safety or to improve their pre-existing MR safety program.

Supplemental 2:

1. Dempsey MF, Condon B, Hadley DM. MRI Safety Review. Seminars in Ultrasound, CT, and MRI, 23(5):392–401.
2. Sawer-Glover AM, Shellock FG. Pre-MRI procedure screening: recommendations and safety considerations for biomedical implants and devices. JMRI 12:92–106, 2000.
3. Kanal E, *Barkovich AJ, Bell C,* et al. *ACR guidance document for safe MR practices: 2007*. AJR Am J Roentgenol 2007;188: 1447–1474.
4. Shellock FG. Reference Manual for Magnetic Resonance Safety, Implants, and Devices: 2012 ed. Los Angeles, CA: Biomedical Research Publishing Group, 2011.

Paper #: 15 (R)

Disclosure of radiation risks in paediatric CT- radiographer's practice and viewpoint.

Marie-Louise Butler, *University College Dublin, Dublin 4, Ireland, marielouise.butler@ucd.ie;* Kelly Foley-Friel, Louise Rainford, PhD

Disclosures: All authors have disclosed no financial interests, arrangements or affiliations in the context of this activity.

Purpose or Case Report: Communicating the benefits and risks of Computed tomography (CT) with parents will allow an informed decision to be made in the child's best interest. This study established current practice surrounding radiographers' disclosure of radiation risks to parents prior to paediatric CT examinations and investigated radiographer's opinions on how and when the risks should be disclosed.
Methods & Materials: Questionnaires (n=60) were disseminated to the specialised national paediatric centres (n=3) in Ireland and three regional hospitals that perform both adult and paediatric examinations. Topics that were examined included current practice of informing parents about radiation risks in paediatric CT and radiographers' opinions and viewpoint on discussing radiation risks. Comparisons between other risk disclosure was surveyed, as were the presence of departmental protocols.
Results: Radiographers do not routinely disclose radiation risks to parents, despite over 50% of radiographers' opinion stating that parents wish to be informed of them. 20% of respondents indicated routinely informing parents of radiation risks in paediatric CT, whilst 90% inform of scan duration and 95% inform about equipment movements. A distinct lack of departmental protocols relating to risk disclosure was evident. 60% or respondents stated this responsibility lies with the radiographer and referring clinician.
Conclusions: The current study identifies that there is a lack of understanding and consistency in dealing with risk disclosure in paediatric CT. Radiographer's viewpoints indicate that education and protocol should be put in place.

Paper #: 16 (R)

Non-Contrast Dynamic Angiography with Arterial Spin Labeling: Preliminary Experience in Children With CINEMA

Amber Pokorney, *Radiology and Medical Imaging, Phoenix Children's Hospital, Phoenix, AZ, apokorney@phoenixchildrens.com;* Niccolo Stefani, Houchun Hu, PhD, Jonathan Chia, Richard Towbin, MD, Jeffrey Miller

Disclosures: Niccolo Stefani has indicated a relationship with Philips as an employee. Johathan Chia has indicated a relationship with Philips Healthcare as an employee. All other authors have disclosed no financial interests, arrangements or affiliations in the context of this activity.
Purpose or Case Report: With increasing concerns over possible Gadolinium deposition in the brain from contrast-enhanced MRI exams, the purpose of this study was to evaluate a 3D non-contrast dynamic angiography MRI technique based on arterial spin labeling (ASL) called CINEMA (Contrast inherent INflow Enhanced Multi phase Angio) to assess the arterial neurovasculature in pediatric patients.
Methods & Materials: All studies were performed on two identical 3 Tesla MRI platforms (Ingenia, Philips) using 13- and 32-channel head coil arrays. In the past 6 months, CINEMA has been successfully implemented in over 40 patients, ranging in age from newborns to teenagers. The CINEMA variant evaluated in this work was based on a pulsed ASL technique and had a scan time of 7 min. Briefly, the approach acquires paired control and labeled data sets. The latter contain blood signals that have been previously inverted (i.e., labeled) by radiofrequency (RF) pulses. Multi-phase dynamic data are acquired by varying the start time of data acquisition from the time of RF inversion (i.e., label delay). Subtraction of labeled and control (non-labeled) data sets at each dynamic phase suppresses static tissues and yields an arterial-only image. Our protocol utilized a 3D segmented gradient echo EPI readout. Eighty axial slices were acquired with a resolution of $1.2\times1.3\times0.8$ mm^3. Twelve dynamic phases were acquired, starting with a label delay of 200 ms, followed by 120 ms intervals. In addition to CINEMA, 3D time-of-flight (TOF) with a resolution of $0.6\times0.8\times0.7$ mm^3 were acquired.
Results: Figures 1 and 2 illustrate exemplary results in a 7 years old and a 13 months old, respectively. Both males are Moyamoya patients and axial TOF projections demonstrate compromised anterior and middle cerebral arteries on the left and right sides, respectively. The first four and eight CINEMA dynamics corroborate these finding, illustrating delayed arterial filling on the affected side through the coronal projections. Figure 3 illustrates an exemplary result in a 1 day old boy who presented with seizures, showing all 12 dynamics in the axial and sagittal projections of an otherwise normal angiogram.
Conclusions: Our preliminary study demonstrates the robustness and clinical utility of non-contrast CINEMA in pediatric neurovascular imaging. The technique is particularly useful in assessing patients with Moyamoya disease and supplements TOF imaging. Further evaluation in patients with seizures, strokes, brain tumors, and arterial-venous malformations is warranted.

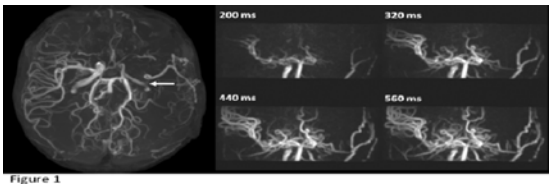

Figure 1

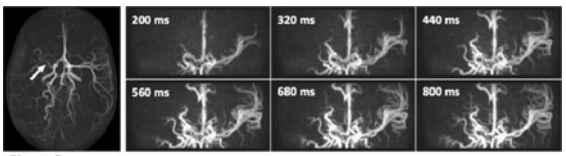

Figure 2

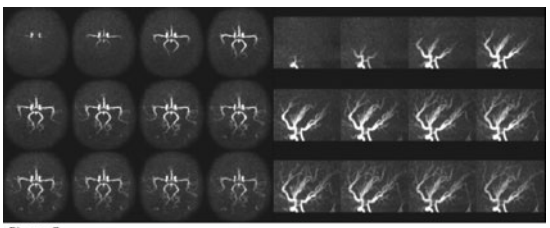
Figure 3

Paper #: 17 (R)

An investigation of radiology practitioners' and radiographers' opinion of benefit-risk communication and parental consent for pediatric imaging procedures

Jonathan Loui Portelli, Radiography, Jonathan McNulty, Paul Bezzina, **Louise Rainford, PhD**, *Department of Radiography, University of Malta, Msida, Malta, louise.rainford@ucd.ie*

Disclosures: All authors have disclosed no financial interests, arrangements or affiliations in the context of this activity.
Purpose or Case Report: To investigate radiology practitioners' and radiographers' opinion of benefit-risk communication and parental consent for pediatric imaging procedures.
Methods & Materials: Institutional ethical approval was attained. A prospective cross-sectional survey was completed amongst radiology practitioners and radiographers at the primary pediatric referral center in Malta. The participants were asked a series of closed and open ended questions to gain an insight into radiology practitioners' and radiographers' opinions and practices of benefit-risk communication and consent in pediatric imaging. Survey themes included: whether parents/guardians should be informed of the potential risks and/or benefits; what type of information, if any, they would generally provide to pediatric patients and their parents/ guardians in

such circumstances; their confidence in conveyance of benefit-risk information; professionals responsible for benefit-risk communication; current consent practice and any concerns commonly expressed by parents/guardians.
Results: Completed questionnaires (n =112) provided a response rate of 66.7%. Only 17% of participants felt that they had received education/training in benefit-risk communication. Despite the fact that nearly all participants believed that parents/guardians should be provided with benefit-risk information, not everyone did so in practice, and only 36.7% were highly confident in their abilities to portray such information. Nonetheless, in their practice, parental consent was generally sought and obtained by 89% of participants. Responses also revealed that parents' concern about the radiation risks associated with pediatric imaging is real, and several participants had encountered situations whereby parents refused to pursue with an imaging examination requested for their child.
Conclusions: The findings highlight the need for educational institutions and professional associations to address a possible gap in education and/or training of radiology practitioners and radiographers with respect to benefit-risk communication. Knowledge and the development of effective communication skills should help radiology practitioners and radiographers foster improved benefit-risk dialogues with all those concerned.

Paper #: 18 (R)

Improving the Operational Efficiency of Pediatric MR Suites; A multi-year journey

Laura Gruber, *Lurie Children's Hospital, Chicago, IL, LGruber@luriechildrens.org*

Disclosures: All authors have disclosed no financial interests, arrangements or affiliations in the context of this activity.
Purpose or Case Report: Pediatric MR is one of the most complex modalities within the imaging department. Creating a productive, efficient, safe and rewarding environment within the pediatric hospital can be challenging and takes a strategic plan to accomplish the goal. Complicated exams covering every body part, long studies many of which require anesthesia, care coordination with other units in the hospital (IR, OR, critical care, emergencies) and safety issues make scheduling difficult. Our hospital had many issues which led to dissatisfaction of the customers, inaccurate ordering practices, errors in scheduling, failed sedations, unpredictable inpatient volumes and poor staff morale. Each of these issues had an effect on revenue with open scanner time and a several week backlog waiting for an appointment.
Methods & Materials: The solutions we undertook have taken over 3 years and continue to be improved upon. We partnered with the Anesthesia team to take over sedation/anesthesia services at the acute care hospital for which they actively participate in the process of ownership and set goals to reduce the failure rate. We engaged a consultant to initiate LEAN principles and methodology for process improvement in scheduling, template design, streamline workflows, real-time visual tracking boards, all with staff actively participating throughout the process.
Results: Appointments are scheduled based on the patient's needs, review of prior history, provider order requests for sedation/anesthesia and answers to order questions. Improved the patient engagement scores; "I was able to schedule an appointment when I expected."
Anesthesia appointment backlog went from an average of 45 days to 14 days for routine outpatient exams. Urgent requests are completed within 7 days from time of order, stats are completed same day.
In house coverage is now 24/7, 365 to increase outpatient appointments and care for in-patients after prime hours.
Conclusions: Partnering with anesthesia and developing a team approach with constant surveillance has led to our success of increasing volume, improving the turn around time from order to completion, increasing patient satisfaction and improving staff morale. This is a continued effort to keep this under control and constant "tweeks" to the process will continue to occur in response to the changing healthcare marketplace.

Paper #: 19 (R)

An investigation of the challenges of continuing professional development in the "specialist" field of pediatric radiography

Jennifer Grehan, BSc MSc, *Diagnostic Imaging, School of Medicine, University College Dublin, Dublin, Ireland, jennifer.grehan@ucd.ie;* Marie-Louise Butler, Clare Simcock, Liz Masterson, Sara McGeough, Jason Last, Louise Rainford, PhD

Disclosures: All authors have disclosed no financial interests, arrangements or affiliations in the context of this activity.
Purpose or Case Report: CPD is a mandatory condition of state registration in the UK, Ireland and parts of mainland Europe. For those working in specialist areas of radiography the need to source CPD relevant to their scopes of practice has always been an issue. One area of pseudo specialism in diagnostic radiography which has particular struggles is pediatric radiography. This small scale study investigated the opinions of radiographers in the UK and Ireland working in dedicated pediatric hospitals around satisfaction with specialized CPD provision, self-perception and barriers to specialization in this area.
Methods & Materials: An online questionnaire containing four sections covering: demographics and CPD experience, clinical roles and perception was distributed via clinical Radiography managers in three pediatric centers in the UK and Ireland. Radiographers opinion was captured through the use of closed and open questions.
Results: Out of a possible 63 responses, 37 were received (58%). Radiographers characterized by length of qualification were well represented: 0-5 to 30+ years (mode=0-5 years); the majority of respondents (51%) ranked themselves as pediatric radiographer first and diagnostic radiographer second.
Over 67% of respondents considered CPD either to be important, very important or critical. While the majority had undertaken CPD activities in the area of pediatric radiography outside their place of work (62%), almost 30% stated that these offerings never met their expectations. Likewise there was a low satisfaction level (94% dissatisfied) with the pediatric radiography specific CPD options available. Respondents identified strongly (73%) that pediatric radiography should be considered a specialist skills base.
Conclusions: This study identified dedicated pediatric radiographers' desire to see and undertake more specialized CPD offerings. An overall positive perception towards CPD was noted however barriers to pediatric radiography gaining specialist status were identified and will require careful consideration.

CASE REPORT, EDUCATIONAL REPORT AND SCIENTIFIC POSTERS

Authors are listed in the order provided. An author listed in bold identifies the presenting author.

Poster #: CR-001

Wandering Liver: A Rare Cause of Acute Abdominal Pain In Children

Simone Sala, *AOU S. Anna, Ferrara, Italy, dott.sala@gmail.com;* Edoardo Raimondi, Caterina Albieri, Marco Cirillo

Disclosures: All authors have disclosed no financial interests, arrangements or affiliations in the context of this activity.

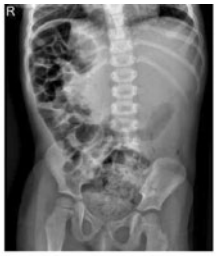

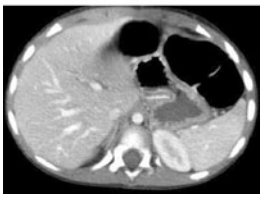

Purpose or Case Report: Wandering liver (WL) is a rare entity consisting of excessive mobility of the liver due to irregular hepatic fixation. We report a case of WL in a 3-year-old girl, who was referred to our department with acute abdominal pain and recurrent episodes of vomiting. Laboratory tests showed only leukocytosis. In order to define possible causes of acute abdomen an US scan of the abdomen was performed which revealed a left-sided liver, confirmed by abdominal X-ray that showed hyperlucent right upper quadrant by the presence of bowel air (Fig. 1); the hepatic shadow was seen in the midline left abdomen. As patient symptoms persisted, 24 h after the admission a new abdominal X-ray and US scan were performed; return of the liver in normal right position was observed. Barium X-rays of the gastrointestinal tract excluded a congenital malrotation. A supine abdominal CT showed the liver normally occupying the right hypochondrium (Fig. 2); subsequently, left decubitus CT scan showed hepatic migration across the midline to the left (Fig. 3). The patient's symptoms resolved in the next few hours so she was conservatively managed and was discharged a few days later. The first documented case of wandering liver was presented by Heister in 1754 and few cases have been described ever since. The clinical presentation of wandering liver is variable and non specific. WL is often an asymptomatic condition diagnosed incidentally, although in more than 75% of cases colonic obstruction coexists. It has been reported that the cause of wandering liver is related to abnormalities of the suspensory apparatus of the liver. Such abnormalities permit excessive mobility of the liver in the transverse plane. Surgical treatment is usually reserved for symptomatic patients. In our case the patient was managed conservatively due to the lack of evidence of intestinal obstruction and the prompt relief of the symptoms, probably favored by the supine position for an extended period and return of the liver in the right abdomen. Detection of WL is difficult but it is essential in order to avoid misdiagnosis and unnecessary imaging procedures. In our experience any evidence of abnormal positioning of the liver should be investigated with serial imaging in the lateral decubitus position, mainly in children with unexplained causes of abdominal pain.

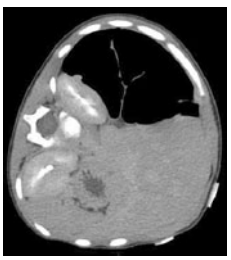

Poster #: CR-002

Case Series: Krabbe Disease – An Unusual Presentation of Optic Nerve Enlargement

Disclosures: All authors have disclosed no financial interests, arrangements or affiliations in the context of this activity.

Maria Kaloianova, MBBCh, *Diagnostic Radiology, University of the Witwatersrand, Johannesburg, South Africa, Johannesburg, South Africa, mkaloianova@gmail.com;* Jaishree Naidoo, Heather Thomson, Louisa Bhengu

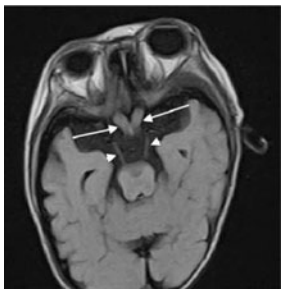

Purpose or Case Report: Krabbe disease is an autosomal recessive leukodystrophy that presents clinically with regression of milestones, excessive irritability and inconsolable crying. The pathologic basis of the disease is due to abnormal myelin metabolism resulting from a deficiency in the galactocerebrosidase enzyme with subsequent white matter destruction.

Although optic atrophy is a classic presentation of Krabbe disease, we report two patients who are biological brothers presenting with optic nerve enlargement in addition to other typical MR imaging features of Krabbe disease, thereby confounding the initial diagnosis.

Krabbe disease, also known as globoid cell leukodystrophy, is a lysosomal function disorder which ultimately results in demyelination and dysmyelination of white matter.

Worldwide incidence of Krabbe disease has been shown to be 1 in 100, 000-200,000, with 1 in 150,000 live births reported in Europe (1, 2). The incidence in the South African population has not been well established.

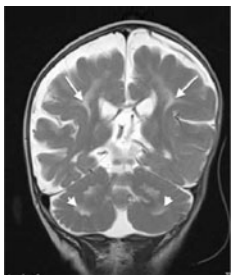

Case Report 1:

Patient 1 presented in February 2012 to the paediatric neurodevelopmental clinic at 7 months of age with excessive inconsolable crying, regression of milestones, numerous café au lait macules and large eyes. Birth history was non-contributory.

MRI of the brain was done, demonstrating hypertrophy of the optic nerves and multiple other cranial nerves bilaterally (see figure 1).

High signal intensities were noted within the white matter of the brachium pontis, cerebellar dentate nuclei and corona radiata with a significant background of cortical and white matter atrophy (see figure 2).

Patient 1 died at 1 year of age with a provisional diagnosis of Neurofibromatosis I (NFI). No specific tests for Krabbe disease were performed prior to his death.
Case Report 2:
Patient 2 presented in November 2014 at 5 months of age with regression of milestones, excessive crying which was difficult to soothe, numerous café au lait macules, large eyes and a relative macrocephaly. Birth history was non-contributory and the child developed normally up until 3 months of age.
Blood tests for amino acids and organic acids, as well as liver and renal functions were normal. CSF lactate and glycine levels were also normal. Specific enzyme testing for Krabbe disease was performed for patient 2 in Philadelphia, United States. Results revealed the galactocerebrosidase enzyme value to be very low (0.07). This is in the range of patients affected with Krabbe disease.
Patient 2 died shortly after the diagnosis of Krabbe disease was confirmed.
MRI brain scan of patient 2 demonstrated markedly hypertrophied optic nerves (see figures 3 and 4). Increased T2 and T2 Flair signal intensities of the white matter of the brachium pontis and the cerebellar dentate nuclei (see figure 5). The midbrain, pons and cerebellum also demonstrated increased T2 and T2 Flair signal intensities with a significant background of cortical and white matter atrophy (see figure 6).
PLEASE NOTE: the discussion related to Krabbe disease in this case review has not been included here due to charachter limitations. In addition, 6 images in total will be included should this case report be accepted for presentaton.
Conclusions: Optic atrophy is one of the clinical presenting features of Krabbe disease. However, in rare cases as we report, optic nerve enlargement may be an association. Considering the higher prevalence of Neurofibromatosis-I, one can easily be misled by these imaging features into making the diagnosis.
The early awareness of neuroimaging findings in Krabbe disease together with a suggestive clinical presentation will allow for timely management and genetic counseling to parents.

Poster #: CR-003

No Laughing Matter - A Rare, but Significant Complication from Entonox Use

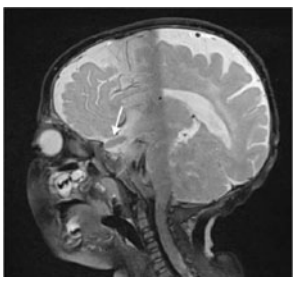

Sunit Davda, MBBS, **Akif Hussein**, *Radiology, Royal London Hospital, London, United Kingdom, akif.hussein@bartshealth.nhs.uk;* Ashok Adams, Anant Krishnan, Amit Roy

Disclosures: All authors have disclosed no financial interests, arrangements or affiliations in the context of this activity.
Purpose or Case Report: We report the case of a 14 year old male who presented to our Emergency Department with a 2 weeks history of worsening neurological symptoms including decreased subjective sensation, fingertip paraesthesia, and unilateral leg weakness, requiring assitance with stairs. Initial MRI evaluation revealed what appeared to be a longitudinally extensive transverse myelitis centred on the cervical region; however a follow-up MRI 1 month subsequently (undertaken on account of persistent symptoms) demonstrated long-segment spinal cord swelling and intrinsic signal change apparently confined to the dorsal columnar segments. After correlation with the clinical team, a history of recreational Entonox use for recurrent episodes of chest pain was elicited. With prolonged exposure, the nitrous oxide component of Enotnox can cause inactivation of vitamin B12. Following discussion serum vitamin B12 and folate levels were obtained, demonstrating deficiency in both. Thus in rare cases, Entonox use can lead to subacute combined degeneration of the cord, as demonstrated in our patient.
Recreational Entonox use is on the rise and recognition of its relevance in a history is important as it can be associated with significant morbidity, as our case highlights. By utilising a multidisciplinary approach and recognising this rare, yet important diagnosis, we were able to guide patient management.

Poster #: CR-004

Filamin A (FLNA) Mutation – A Newcomer to the Childhood Interstitial Lung Disease Classification (ChILD)

Susan Shelmerdine, FRCR MBBS BSc MRCS, *Great Ormond Street Hospital, London, United Kingdom, susie_c_s@yahoo.co.uk;* Thomas Semple, MBBS, BSc, Helen Spencer, Anjay Pillai, Catherine Owens

Disclosures: All authors have disclosed no financial interests, arrangements or affiliations in the context of this activity.
Purpose or Case Report: To evaluate the radiographic and CT appearances of filamin A (FLNA) mutation related lung disease and review the available medical literature regarding this new entity.

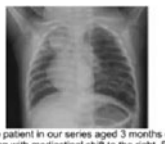

Figure 1: A chest radiograph of one patient in our series aged 3 months old demonstrates hyperinflation and hyper lucency within the left lung with mediastinal shift to the right. Fine interstitial thickening and septations are noted in the left lower zone.

Methods & Materials: Interstitial lung disease (ILD) in infants represents a rare and heterogenous group of disorders, distinct from those occurring in adults. In recent years filamin A (FLNA) mutation related lung disease has been recognized as a new entity within the ChILD classification scheme. A well-known association already exists between FLNA mutation and disorders of neuronal migration, vascular function and skeletal development however pulmonary manifestations are only now becoming evident, and are important as they significantly contribute to morbidity and mortality.
Fewer than 10 cases have been described in the literature with radiographic features mimicking those of congenital lobar over inflation. In some cases treatment has involved either lobar resection or lung transplantation. Given the progressive nature of this disease and potentially fatal outcomes, we present our own case series of four patients with confirmed FLNA mutation and associated pulmonary manifestations. We also outline the radiological features and clinical course of these patients and their management, with the aim of raising diagnostic awareness and improving early identification of this rare entity.

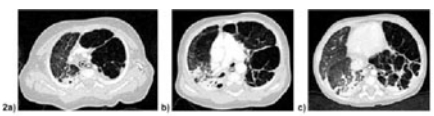

Figures 2a -c: Axial contrast enhanced chest CT images of the same patient aged 5 months old. Images a, b and c reflect changes within the upper, middle and lower zones respectively. There is ongoing left lung hyperinflation and septal thickening. Dependent changes with consolidation are also seen in the right upper and lower lobes.

Poster #: CR-005

Fetal MRI with Post Mortem MRI Correlation in a Case Report of VECTERL and OHVIRA Syndromes

Nucharin Supakul, *Radiology, Ramathibodi Hospital, Mahidol University, Bangkok, Thailand, nucharinsupakul@gmail.com*

Disclosures: All authors have disclosed no financial interests, arrangements or affiliations in the context of this activity.
Purpose or Case Report: To demonstrate an unusual association of VECTERL and uterus didelphys with obstructed hemivagina and ipsilateral renal agenesis (OHVIRA) syndromes in fetal MRI with post mortem MRI correlation.

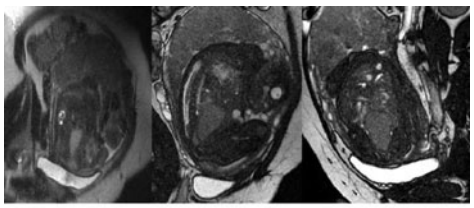

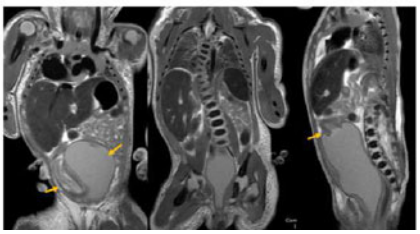

Methods & Materials: 35-year-old female, 31 weeks pregnant, with severe oligohydramnios. The prenatal US was limited to evaluate both kidneys. Fetal MRI was requested before termination of pregnancy.
Results: Fetal MRI showed multiple cystic lesions in the right kidney (MCDK) in the right renal fossa. The left kidney was not identified. There was a large T1hypo/T2isointense globular-shaped lesion in the pelvic cavity, anterior to the rectum, likely turbid-fluid filled in the vagina (hydro/ hydrometrocalpos). Severe fetal lungs hypoplasia was noted. Findings were suggestive of possible OHVIRA syndrome.
Termination of pregnancy was obtained due to multiple anomalies with severe fetal lung hypoplasia. Post mortem MRI was obtained.
Post mortem MRI showed baby girl with OHVIRA syndrome. MCDK of the right kidney is also noted, associated with large ASD, double SVCS, thoracic dextroscoliosis with T9 hemivertebra, suggestive of VACTERL syndrome.
Conclusions: OHVIRA Syndrome is a rare congenital anomaly of the female genital tract, sometimes referred to as Herlyn-Werner-Wunderlich syndrome (HWW). It occurs due to arrest of the midline fusion of the Mullerian and Wolffian ducts, either completely or incompletely. Incidence of Mullerian duct anomalies ranges from 0.8% to 4%. The true incidence of the OHVIRA syndrome is unknown, estimated 0.1-3.5% of all Mullerian anomalies. Most of the patients are usually diagnosed at puberty after menarche due to recurrent severe dysmenorrhea and/or chronic pelvic pain.
VACTERL is an association of congenital malformation, characterized by the presences of at least three of the following: vertebral defects, anal atresia, cardiac defects, tracheo-esophageal fistula, renal and limb anomalities. The etiology is unknown. Diagnosis is based on the clinical presentation at birth. Antenatal diagnosis can be challenging.
The association between OHVIRA and VACTERL syndromes has never been published. This is the first case report of OHVIRA and VACTERL syndromes association.
We will demonstrate embryological development of the Mullerian and Wolffian ducts to help understanding spectrum of the anomalies in OHVIRA syndrome as well as imaging checklists in fetal MRI in diagnosis of OHVIRA and VACTERAL anomalies.

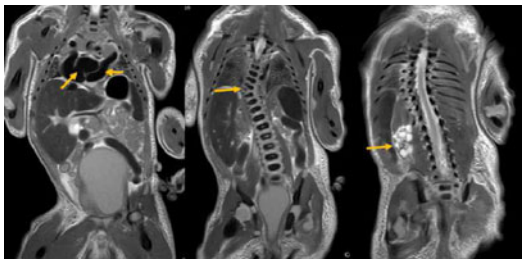

Poster #: CR-006

Congenital Portosystemic Venous Shunts: Intrahepatic and Extrahepatic Anatomical Variants

Domen Plut, Radiologist, *Department of Radiology, University Medical Centre Ljubljana, Ljubljana, Slovenia, plut.domen@gmail.com;* Ziva Zupancic, Senja Mali Brajovic, Tomaz Kljucevsek, Mojca Tomazic, Mojca Glusic, Matjaz Homan

Disclosures: All authors have disclosed no financial interests, arrangements or affiliations in the context of this activity.
Purpose or Case Report: Congenital portosystemic venous shunts (CPVS) are rare vascular abnormalities in which the portal blood drains into a systemic vein. They are results of embryogenetic alterations during the complex development of the portal system in early gestational period. Anatomically they are classified into two groups; extrahepatic and intrahepatic. Extrahepatic shunts were first described in 1793 by Abernethy and are thus also called Abernethy malformations. Presentation of CPVS can be highly variable and consequences severe.
CASE1:
An 8 year old boy was admitted to our hospital due to severe abdominal pain. Doppler ultrasound (US) revealed an abnormal intrahepatic tubular vascular structure. The computed tomography angiography (CTA) confirmed a direct vascular connection between the left portal vein and the dilated left hepatic vein. The right portal vein was small in size, indicating main portal blood flow through the left side bypassing the liver. The treatment for this intrahepatic CPVS was embolization of the shunt. The boy has been well since the procedure.
CASE2:
A routine medical check-up in a 14 year old girl discovered abnormal liver function tests. Abdominal US showed a huge mass in the right lobe of the liver and a big mass of similar structure in the epigastrium. Portal vein was not identified. CTA showed a short main portal vein connected directly to the inferior vena cava, consistent with the Abernethy malformation. The big mass in the epigastrium was shown to be a tumor in the caudate lobe of the liver. Focal nodular hyperplasia (FNH) was considered for liver lesions due to the imaging findings and known association with the Abernethy malformation. Biopsy confirmed the diagnosis. The girl is currently waiting for liver transplantation, as it is the treatment of choice for this extrahepatic CPVS.
Conclusions: CPVSs are rare vascular abnormalities with less than 400 cases reported in the literature. The first imaging method for the evaluation is usually the US. A thorough inspection of the portal venous system with Doppler is necessary and is often diagnostic. A CTA is the method of choice to confirm the diagnosis and to define the precise anatomical variant of the shunt. The precise anatomical definition of the shunt is important because different variants require different treatment to prevent damage and complications. Early diagnosis of CPVS is important because consequences of CPVS are severe.

Poster #: CR-007

Non-Invasive Phenotyping of Mouse Embryos Using Micro-CT: Implications for Perinatal Autopsy Imaging

J. Hutchinson, MRes MBBS, *Histopathology, Great Ormond Street Hospital, London, United Kingdom, ciaran.hutchinson@nhs.net;* Maria Peltzer, Maurice Darding, Henning Walczak, Neil Sebire, Owen Arthurs, FRCR, PhD

Disclosures: All authors have disclosed no financial interests, arrangements or affiliations in the context of this activity.
Purpose or Case Report: Retention of embryonic tissue for teaching and research has become complex for medicolegal reasons following numerous organ retention issues. Virtual datasets of embryos would allow anatomical diagnosis and are both less controversial and simpler to obtain and store. Several imaging techniques are now available (High field MRI and micro-CT) which alleviate the need to dissect the tissue to create serial sections, thus maintaining tissue integrity.
We present a series of images from phenotypically normal and abnormal mouse embryos (length 4-5 mm) obtained using micro-CT. Three mouse embryos were immersed in potassium triiodide for 24 h prior to being individually immobilised using non-nutrient agar. Images were acquired using a Nikon XTH225 micro-CT scanner, reconstructed using proprietary software and post-processed using VG StudioMAX.
Excellent internal contrast was demonstrated in all specimens, with all organ systems delineated. Excellent views of normal central nervous system, respiratory system, cardiovascular system, genitourinary and digestive tract systems were also obtained at micrometer resolution. Specific abnormalities identified include a possible VSD (0.24 mm), exencephaly and foreface disruption.
Micro-CT technology can be used to create datasets of embryos at high resolution (up to 3.7 micrometers achieved), which can then be re-dissected, 3D printed or indefinitely stored and could provide a solution to current issues affecting the use of embryonic tissue for diagnosis, teaching and research.

Poster #: CR-008

Micro-CT in Perinatal Autopsy: Changing Diagnoses at Early Gestation

J. Hutchinson, MRes, MBBS, *Histopathology, Great Ormond Street Hospital, London, United Kingdom, ciaran.hutchinson@nhs.net;* Ian Haig, Neil Sebire, Owen Arthurs, FRCR, PhD

Disclosures: All authors have disclosed no financial interests, arrangements or affiliations in the context of this activity.
Purpose or Case Report: Autopsy examination of early miscarriages (<20 weeks' gestation) can be technically challenging, with an associated error rate due to small size. Imaging is increasingly used to guide the autopsy process and post mortem MRI (PMMRI) at 1.5 T shows excellent correlation with autopsy findings over 18gw / 500 g bodyweight, however, its diagnostic accuracy is reduced below these thresholds. We have evaluated the use of Micro-CT, which has been used in animal imaging and industry for many years. We present a radiological / pathological correlation of a case from the first clinical use of micro-CT in perinatal autopsy practice, under an ethically approved study with full consent.
A termination of pregnancy was performed at approximately 14gw for presumed sacrococcygeal teratoma. Standard CT and 1.5 T PMMRI was non-diagnostic for every organ system. Following immersion of the fetus in potassium triiodide and formalin for 48 h, a micro-CT scan was performed using a Nikon XTH225 micro-CT scanner, reconstructed using proprietary software (CT Pro 3D, Nikon Metrology) and post-processed using VG Studio MAX (Volume Graphics GmbH).
Views of all organ systems were obtained that were used to guide subsequent unblinded autopsy. Micro-CT demonstrated multiple abnormalities, including amniotic membranes in contact with the fetal skin, multiple disruptions of the abdomen and limbs, and externalisation of internal organs including the kidneys and liver. These were confirmed at the subsequent autopsy and a final diagnosis of ADAM complex (amniotic deformity, adhesions, mutilations) was made.
This case report demonstrates the potential of micro-CT to provide detailed PM imaging of entire fetuses whilst maintaining tissue integrity, allowing pre-autopsy identification of multiple congenital abnormalities in cases where 1.5 T PMMRI and standard CT fail to achieve diagnostic resolutions.

Poster #: CR-009

Embolization of Intraosseous Hemangioma of the Maxilla in an Early Infant: A Case Report

Young-Youn Choi, MD, PhD, *Chonnam National Univeristy Medical School & Hospital, Gwangju, Korea (the Republic of), yychoi@jnu.ac.kr*

Disclosures: All authors have disclosed no financial interests, arrangements or affiliations in the context of this activity.

Purpose or Case Report: Hemangioma occurs mainly in soft tissue but rarely be shown in bone. It is benign vascular bone tumors that account for 1% of all primary bone tumors. It is also called hamartoma because it is proliferating tumor originated from bone tissue. Most prevalent sites of intraosseous hemangioma are vertebrae and skull. Within the calvarium, the parietal bone is most commonly involved followed by the frontal bone. Within the facial skeleton, the mandible, maxilla, and nasal bones are involved. Hemangioma of the maxilla is very rare in newborn period. We experienced a neonatal case of intraosseous hemangioma of the right maxilla treated with embolization in an early infant period.
Methods & Materials: Eleven day old male baby was visited outpatient clinic because of non-tender, non-pulsatory hard swelling of right maxillary area since birth. There were no specific family or pregnancy history and it was not noted by antenatal ultrasonography. The baby (gestational age 39^{+2}, weeks, birth weight 3,960 g) was delivered by C-section from a 33 year old nulliparous mother because of fetal distress and massive vaginal bleeding. On physical examination, right hemifacial bony hyperplasia and right maxillary buccal gingiva and Bohn's nodule were noted. Family history and maternal history were non-specific. Laboratory examinations were non-specific. On 10 days of life, facial CT showed a 3×3×2.5 cm, osteolytic soft tissue mass with some internal calcification looks like honeycomb or sunburst appearance of bone lesion in right maxilla suggesting intraosseous hemangioma with nonspecific enlarged cervical lymph node. On 24 days of life, facial MRI showed a 2.9×2.8×2.5 cm, homogeneously enhancing soft tissue mass in right maxilla with flow voids in the mass suggesting intraosseous hemangioma. At 3 months of age, brain CT showed no abnormal density lesion in brain parenchyma and no midline shifting or hydrocephalus. CT angiography showed right internal maxillary artery is the main feeder of right maxillary mass. At 4 months of age, internal and external carotid angiographies with embolization were performed.
Results: Follow up at 6 months of age, growth and development were normal with no further change of hemangioma size.
Conclusions: Total surgical excision is the preferred method of treatment for intraosseous hemangiomas with reconstruction. But, in young infant, initial choice of treatment is embolization to prevent further proliferation of vascular tumor.

Poster #: CR-010

Radiologic Findings of Van Den Ende-Gupta Syndrome (VDEGS): A Case Report

Young-Youn Choi, MD, PhD, *Chonnam Univeristy Medical School & Hospital, Gwangju, Korea (the Republic of), yychoi@jnu.ac.kr*

Disclosures: All authors have disclosed no financial interests, arrangements or affiliations in the context of this activity.
Purpose or Case Report: Van Den Ende-Gupta syndrome (VDEGS) is an extremely rare autosomal recessive disorder with mutation of SCARF2. It is characterized by distinctive craniofacial and skeletal manifestations include blepharophimosis, a narrow nose, malar hypoplasia, deformed ears, an everted lower lip, flexion contractures, camptodactyly, arachnodactyly and dolichostenomelia, while development and intelligence are normal. It needs a regular follow-up with orthopedics because of joint contracture deformity and scoliosis.
Methods & Materials: A female baby was born at 40^{+2} gestational weeks with birth weight 2,580 g (<10 percentile), length 47 cm (10-25 percentile), and head circumference 34.5 cm (50-75 percentile). The baby was delivered vaginally from a nulliparous mother. Pregnancy and family histories were nonspecific. Her parents were not consanguineous marriage. Apgar score was 9 at 1 min, 10 at 10 min. Craniofacal characteristics were inverted triangle face, micrognathia, asymmetric face (left face hypoplasia), a narrow nose, relatively short neck with torticollis, blepharophimosis, down slant eye, blue sclera, low-set and hypoplastic ears. Multiple joint contractures (both elbows, fingers, hips and knees), arachnodactyly, camptodactyly, club foot, umbilical hernia, and sacral dimple were noted.
Results: Infantogram and skeletal X-ray showed long slender bones with multiple joint contractures. Cardiac, renal and pelvic sonographic findings were non-specific. Eye and ear examination showed microcornea with shallow anterior chamber and referred hearing test. Chromosomal microarray was non-specific and diagnostic exome sequencing test confirmed autosomal recessive disorder of VDEGS with SCARF2 mutation transmitted by heterozygotic carrier parents. Follow up at 4 months of age, body weight was 5.0 kg(<3 percentile), length 61.7 cm (25-50 percentile), and head circumference 41.0 cm (50-75 percentile), and development was normal.
Conclusions: We report a characteristic radiologic finding of VDEGS patient confirmed by diagnostic exome sequencing who was born to parents with heterozygous carrier. This is the first report in Korea.

Poster #: CR-011

Antenatal and Postnatal Imaging Of Hallermann-Streiff Syndrome: Two Cases

Young-Youn Choi, MD, PhD, *Chonnam Univeristy Medical School & Hospital, Gwangju, Korea (the Republic of), yychoi@jnu.ac.kr*

Disclosures: All authors have disclosed no financial interests, arrangements or affiliations in the context of this activity.
Purpose or Case Report: Hallermann-Streiff syndrome (HSS) is a very rare congenital disorder associated with characteristic head and face abnormalities include bird-like face, hypotrichosis, atrophy of skin, dental abnormalities, proportionate nanism, and many ophthalmic disorders. Many patients die during infancy because of life-threatening complications, such as respiratory and cardiac problems.
Methods & Materials: Case 1. Male baby (gestational age 36^{+6} weeks, birth weight 2,100 g) was transferred to NICU due to intrauterine growth restriction (IUGR) and abnormal looking face. Family history and maternal history were non-specific. Micro- and brachycephaly with left parietal cephalhematoma, 4 cm sized large anterior fontanel with wide separation of sutures, sparse hair, prominent forehead, microophthalmia with cataract, beak like nose tip, blue colored skin around the nose, low set ear, retro-, and micrognathia, three natal teeth, small mouth, and chubby cheek, small testis and both simian hands with pointed finger were shown.
Case 2. Female baby (geatational age 32^{+6} weeks, birth weight 1,750 g) was admitted due to respiratory distress and dysmorphic feature compatible with HSS.
Results: Case 1. Antenatal ultrasonography at 36 weeks of gestation, short and thin long bones, prominent forehead, and small nose with chubby cheek were noted. Postnatal radiologic studies showed thin tubular bones, small and flatted vertebral bodies, and pathologic fracture of left proximal radius. Skull X-ray and cranial CT showed widely opened fontanelle with sutures, flattened parietal bone, midfacial hypoplasia and left parietal cephalhematoma without other intracranial abnormalities. Chromosomal microarray was non-specific. Follow up 9 months of age, he showed failure to thrive and delayed motor development.
Case 2. Antenatal ultrasonography at 29 weeks of gestation, short long bone and IUGR were noted. Postnatal radiologic studies showed thin clavicle, ribs, vertebrae and tubular bone (hands and feet), and pathologic fractures of both proximal radius. On day 43 of life, head and neck CT showed widely opended fontanelle, thin parietal bone and maxillary hypoplasia, scanty subcutaneous fat tissue. Chromosomal microarray was non-specific. The patient was died on 49 days of life due to cardiorespiratory failure.
Conclusions: HSS can be diagnosed by characteristic clinical feature with antenatal ultrasonography and postnatal radiologic findings.

Poster #: CR-012

Ductus Arteriosus Calcification: A Literature Review

Mark Chopra, *Radiology, Great Ormond Street Hospital, London, United Kingdom, mark.chopra@gosh.nhs.uk;* Hannah Barrett, J. Hutchinson, Liina Kiho, Owen Arthurs, FRCR, PhD

Disclosures: All authors have disclosed no financial interests, arrangements or affiliations in the context of this activity.
Purpose or Case Report: Ductus Arteriosus calcification is a poorly comprehended pathology occasionally reported on chest radiographs, more commonly on CT. The purpose of this educational abstract is to present the concepts surrounding ductal arteriosus (DA) calcification and reviews the literature to date.
We retrospectively searched the main medical literature (PubMed, MEDLINE, CINAHL and Google scholar databases) using the following keywords: “ductus arteriosus”, “ligamentum arteriosum”, “calcification”, “ductal”, “patent ductus arteriosus”, “children”, “paediatric”. Articles regarding ductus arteriosus calcification were further evaluated for citations.
Sixteen articles were found which dated back over nearly a century. Of these eight concerned a paediatric population and very few had histological confirmation. The majority highlighted that ductal calcification is more prevalent than previously thought. Ductal calcification was initially reported on the chest roentgen-ray in 1931 by Weiss. The increasing prevalence has been compounded by the use of the greater spatial resolution offered by modern CT scanners. A study in 2012 showed up to a third of children have ductal calcification on CT, with peak incidence is towards the end of the first decade in girls. There is conflicting opinion regarding the pathophysiology of ductal calcification, which may be either ductal aneurysmal thrombus regression, or more likely ligamentum arteriosum intimal and medial wall calcification.
This literature review illustrates the general paucity of histological data and suggests that the autopsy evidence favours intimal and medial wall calcification.

Evidence Table

First Author Name	Study Type	Sample size	Calcification Frequency	Findings	Comment	Histological confirmation
Proisy, 201 5	Retrospective CT/ autopsy	69 children	60.9% (children under 2 years)	No correlation between age and calcification .	Mean age if present was 9 months	Yes
Hong, 2012	Retrospective CT/ XR review	476 children for XR and 508 for CT	XR 3.6% CT 37.8%	Calcification is more common than previously reported but does not reach statistical significance	Peaks 6 -10 years, Low prevalence after 30 years	No
Ampanozi, 2010	Autopsy	1 adult	-	Mural calcification in 65 year old male	-	Yes
Lucas, 2000	Case reports and XR	1 case report of 7 year old girl	-	Large calcified ductal aneurysm (pulmonary and aortic mouths)	-	No
Beluffi, 1998	Retrospective CXR review	38476 children	0.83%	Uncertain clinical significance. Female more prevalent. Disappears eventually	Peak between 4-6 years and 7-12 months, 6 months - 8 years after	No
Wimpfheimer , 1996	Retrospective CT review	402 adults	48% (6% ligament alone)	Punctate type DA calcification most common. Increases with age and atherosclerosis	-	No
Bonhoeffer , 1992	Retrospective review	21 adults (ranging from 19 -62 years)	33.3%	PDA umbrella closure is feasible in the calcified PDA	-	No
Bisceglia, 1991	Retrospective CT review	53 children (5 month – 14 years)	13.2%	CT calcification is more common than XR and should not be confused with mediastinal calcifications	Few months - several years	No
Currarino , 1970	Literature review	75 children	-	Presence can be used against patency of DA. Relatively common finding and probably disappears	Peak between 2-5 years	No
Furuse , 1968	Case report and comment	24 year female	-	Surgical manipulation of calcified DA	-	No
Ruskin and Samuel , 1950	Case reports XR	4 females aged 29 -42 year old	-	Unable to determinate exact location. Consider differentials	-	No
Child and Mckenzie, 1945	Case series XR/ Autopsy	4 infants aged 5 -21 months	-	One patient was incidental autopsy finding	-	Yes
Keye and Shapiro, 1943	Autopsy series	57 adults	10.%% (but only 1 solitary to the duct)	At 17 years, the normal expectation of life was halved if the ductus was patent. 42% subacute bacterial endocarditis	-	Unknown
Jager and Wollenman , 1942	Histological case series	71 cases from fetus to 80 years	Occasional	Calcification seen in intimal layer. Degenerative changes were more marked in the elderly	-	Yes
Graham , 1940	Case series	2 adult case reports	-	Ductal aneurysm calcifies	-	Unknown

Poster #: CR-013

Ductus Arteriosus Calcification: Histopathological Correlation in 2 Case

Mark Chopra, *Radiology, Great Ormond Street Hospital, London, United Kingdom, mark.chopra@gosh.nhs.uk;* Hannah Barrett, J. Hutchinson, Liina Kiho, Owen Arthurs, FRCR, PhD

Disclosures: All authors have disclosed no financial interests, arrangements or affiliations in the context of this activity.

Purpose or Case Report: Ductus Arteriosus calcification is a relatively common, typically unreported feature on plain film radiography. The more recent literature quotes a prevalence on unenhanced CT of between 37 and 61% of children and a peak at the age of 6-10 years. Adult studies have shown that calcification of the ligamentum arteriosum can occur alone or be associated with atherosclerotic and/or granulomatous calcification. We report two cases in whom they were identified as incidental findings on forensic post mortem CT, for whom we obtained histological confirmation.

Case 1: An 8 month old child who died in non-suspicious circumstances had incidental ductal arteriosus calcification reported on post mortem CT, following unremarkable skeletal survey. Intimal mural calcification was reported on histology at autopsy.

Case 2: A 19 month old child who died of aspiration underwent full skeletal survey and PMCT as part of the pre-autopsy imaging assessment. The skeletal survey revealed incidental ductus arteriosus calcification, initially reported as PDA clip, with correlation at CT. Intimal and medial mural calcification was reported on histology at autopsy.

These cases showed that ductal calcification was intimal and medial in nature. This is consistent with the current literature regarding mural calcification rather than thrombus regression calcification.

Poster #: CR-014

PHACE Syndrome: MRI of Intracranial Anomalies Associated with PHACE Syndrome - A series of 3 Patients

Ehab Hamouda, Consultant, *KK Women's and Children's Hospital, Singapore, Singapore, hamodaehab@hotmail.com;* Achint Gupta, MBBS, FRCR, M.Med(Radiology), Ahmed Sharaf

Disclosures: All authors have disclosed no financial interests, arrangements or affiliations in the context of this activity.
Purpose or Case Report: PHACE syndrome (P: posterior fossa malformations, H: haemangioma, A: arterial anomalies, C: coarctation of the aorta and cardiac defects, E: eye abnormalities, S: sternal defects) is one of the neurocutaneous disorders. It describes a constellation of abnormalities that can occur in association with segmental craniofacial infantile haemangioma, which is the hallmark of this syndrome. Intracranial anomalies are the most common extracutaneous feature of PHACE syndrome. Typical intracranial malformations include posterior fossa malformations like Dandy-Walker complex and cerebellar hemispheric hypoplasia ipsilateral to the hemangioma, arterial anomalies like agenesis, aneurysms, arterial kinking or coiling, Moyamoya-like collateralization and persistent embryonic arteries. Less frequent findings include cortical dysplasia and cortical migration anomalies, dysplasia of the corpus callosum, intracranial capillary hemangiomas and arachnoid cysts.
We present 3 cases which we think significantly contribute to the growing recognition of relatively unique intracranial associations that are likely important for the diagnosis of PHACE syndrome.

Poster #: CR-015

Post-Traumatic Cystic Lesion Following a Distal Radial Fracture; A Case Report

Ehab Hamouda, Consultant, *KK Women's and Children's Hospital, Singapore, Singapore, hamodaehab@hotmail.com;* Achint Gupta, MBBS, FRCR, M.Med(Radiology), Viswanath Anand Chidambaram, Guo Rui Lee

Disclosures: All authors have disclosed no financial interests, arrangements or affiliations in the context of this activity.
Purpose or Case Report: Post-traumatic osseous cystic lesions are a rare complication in children. An etiology of intramedullary fat seepage thorough the damaged bone cortex and its entrapment within the subperiosteum has been proposed. These lesions run a benign course and usually resolve spontaneously. The presence of fatty marrow gives it a distinct appearance which aids in its diagnosis and differentiation from other bone lesions.
This case demonstrates a fat-fluid level within the subperiosteal cystic lesion in MRI and this is a typical feature of post-traumatic cystic lesion in a child. Recognition of this feature allows for a confident diagnosis, cutting down on unnecessary, potentially invasive investigations.

Poster #: CR-016

Wilms' Tumor Arising in Horseshoe Kidney; Report of Two Cases

Simone Sala, *Radiology, AOU S. Anna di Ferrara, Ferrara, Italy, dott.sala@gmail.com;* Marco Cirillo, Edoardo Raimondi, Matteo Bassi
Disclosures: All authors have disclosed no financial interests, arrangements or affiliations in the context of this activity.
Purpose or Case Report: The incidence of upper genitourinary anomalies in children has been reported up to 4-6% and the association of cryptorchidism, hypospadias, double collecting system or fused kidney with Wilms' tumor is well known. Horseshoe kidney is a rare anomaly of fusion occurring between 4th and 6th weeks of gestation. The association of Wilms' tumor with horseshoe kidney is uncommon, with limited cases described. The incidence varies from 0.4% to 0.9% of all Wilms' tumor. Rare variants of Wilms' tumor like extrarenal teratoid tumor have also been described in children with horseshoe kidney. We describe two cases of Wilms' tumor arising from horseshoe kidney, detected on US and later confirmed on CE-CT with low-dose imaging protocol. Both cases underwent surgical resection of the abnormal kidney and the diagnosis of Wilms'tumor was confirmed on microscopic examination of the excised tumor. In presence of kidney abnormalities imaging surveillance and follow-up evaluation is mandatory in order to grant an early detection of neoplastic evolution.
In our experience, multislice CT allows complete preoperative evaluation of this rare condition mainly using multiplanar reconstructions and may facilitate surgery.

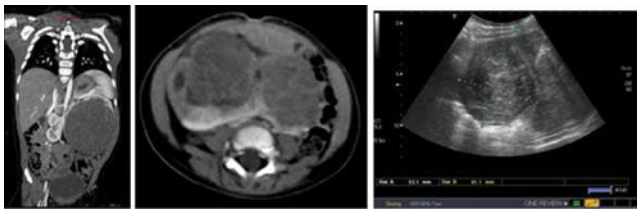

Poster #: CR-017

Gastrointestinal Stromal Tumors (GIST) our Experience

Daniela Carmona, Jose Erripa, Juliana Lostra, Ana Rizzi, Esteban Dardanelli, **Slvia Moguillansky**, Universitary, *Imaging, Hospital Garrahan, Vicente Lopez, Argentina, smoguil@yahoo.com;* Jose Lipsich

Disclosures: All authors have disclosed no financial interests, arrangements or affiliations in the context of this activity.
Purpose or Case Report: Gastrointestinal stromal tumors (GIST) in children are not well characterized, different adult rare entity. It corresponds to a heterogeneous group of lesions for correct classification requires histological, immunohistochemical evaluation and in some cases also adds to the cytogenetic diagnosis. We describe the findings of pediatric GIST.
Methods & Materials: Descriptive, retrospective and observational study. Review of medical records of five patients of both sexes diagnosed with GIST between January 2007 to July 2015 in our hospital.
With an age range from 12 to17 years of age (mean 13 years). They were evaluated clinical findings ultrasound, tomographic, surgical and pathological.
Results: The predominant symptoms were abdominal pain (n=4) 3 of them, and one recurrent acute enterorrhagia (n=1), hematemesis (n=1) and incidental (n=1). The 80% (n=4) patients had stomach commitment, 40% (n=2) of the small intestine and 20% (n=1), colon. At diagnosis 60% had intraabdominal dissemination (peritoneum, liver and pancreas). No significant differences between genders (1.5/1) were demonstrated.
Sonographic evaluation showed solid lesions, and poor vascularization hypoechoic (n=4), MSCT of abdomen with oral contrast and solid images showed EV, lobulated contours, hypodense, with heterogeneous enhancement without nodal involvement in 100% cases (n=5).
GISTs are KIT(CD117)-positive. One of them also showed deletion of exon 11 of the KIT gene linked to familial predisposition to the disease. Only in one case tumor recurrence was observed, with positive findings on PET-scan and poor response to treatment with monoclonal antibodies (imatinib)
Conclusions: These tumors are, in most cases, slow growth and intraabdominal dissemination at diagnosis. The most frequently affected organ was the stomach. The ultrasound was a sensitive method, both at

diagnosis, and monitoring of these patients given the good correlation obtained with CT findings

Poster #: CR-018

Case Report: Aortic and Iliac Dissection

M Cecilia Vargas, Silvina Crido, Karina Quintero, Jose Alonso, Ana Rizzi, J Pibernous, Jose Lipsich, **Slvia Moguillansky**, Universitary, *Imaging, Hospital Garrahan, Vicente Lopez, Argentina, smoguil@yahoo.com*

Disclosures: All authors have disclosed no financial interests, arrangements or affiliations in the context of this activity.
Purpose or Case Report: Aortic dissection in children is often associated with congenital heart disease (bicuspid aortic valve or aortic coarctation), collagenopathies or serious injuries. It rarely arises as a differential diagnosis in the presence of thoracic or abdominal pain in an apparently healthy child. Early diagnosis and treatment is crucial to their survival.
Our purpose is describe the clinical and images characteristics that allowed to diagnose .
Methods & Materials: We present a 14 year old patient, who consulted in their hometown due to abdominal pain, marked asthenia since 3 months and arterial hypertension. Patient's history included chronic renal failure (left kidney uretero hydronephrosis and right kidney hypoplasia), dilated cardiomyopathy, and poorly controlled hypertension. It is referred to our hospital for study and treatment.
Results: Abdominal ultrasound showed at color Doppler examination aliasing flow in the abdominal aorta and both iliac arteries, and waves with different flow velocities within the same inner diameter of vessel. With the evidence of vascular pathology CT angiography was performed showing abdominal aorta and both iliac arteries dissection type III-B (DeBakey-Stanford classification). Treatment is performed by hemodynamic department by placing aorto- bi iliac stent.
Conclusions: Aortic dissection has a very low incidence in the pediatric population. It should be suspected in the presence of intense chest or abdominal pain, depending on the location of the dissection, hypertension and predisposing pathology .
The imaging methods allow a definitive diagnosis and treatment.

Poster #: CR-019

Horseshoe Lung With an Extremely Hypoplastic Right Lung Mimics Right Pulmonary Agenesis on Fetal MRI

Yoshihiro Tanaka, *Radiology, Nagoya City University Graduate School of Medical Sciences, Nagoya-city Aichi, Japan, yoshi.t4416@gmail.com;* Motoo Nakagawa, Yoshiyuki Ozawa, Yuta Shibamoto

Disclosures: All authors have disclosed no financial interests, arrangements or affiliations in the context of this activity.
Purpose or Case Report: The case was a fetus in a 29-year-old mother (gravida 3, para 1). At 29 weeks of gestation, she was referred to our hospital due to abnormality of fetal heart sounds. On fetal MRI, the right pulmonary agenesis was suspected. A 3.5-kg baby girl was born at 41 weeks and 1 day of gestational ages by cesarean section with Apgar scores of 6 and 9 at 1 and 5 min respectively. Her respiratory status was stable under administration of 30% oxygen in an incubator.
Methods & Materials: To examine her pulmonary and cardiovascular system, contrast-enhanced CT was performed at 1 day old. The mediastinum was deviated to the right side, and almost occupied the entire right thoracic cavity. The significant small right lung was found at the base and posterior part of the right thoracic cavity. The right lung parenchyma was fused with the left lower lobe of the lung between the heart and esophagus. The very small pulmonary artery arose from the trunk of the pulmonary artery and reached the right hypoplastic lung parenchyma. The very small pulmonary vein which flowed to the left atrium from the right hypoplastic lung was also found. The bronchus which deviated to the right hypoplastic lung was indistinct.
Results: The pulmonary agenesis, aplasia and hypoplasia are defined as follows. 1) The pulmonary agenesis: complete absence of lung parenchyma, bronchus, and pulmonary vasculature. 2) The pulmonary aplasia: blind-ending rudimentary bronchus is present, without lung parenchyma or pulmonary vasculature. 3) The pulmonary hypoplasia: the bronchus and rudimentary lung are present; however, the airways, alveoli, and pulmonary vessels are decreased in size and number. In our case, right pulmonary agenesis was suspected on fetal MRI, but contrast-enhanced CT revealed very small right lung parenchyma found at the base of the right thoracic cavity afterbirth. Because this hypoplastic right lung had a very small pulmonary artery and vein, we considered that it was an extremely hypoplastic right lung. Moreover, this hypoplastic lung was fused with the left lower lobe of the lung. Horseshoe lung usually involves unilateral lung hypoplasia which is almost always on the right side. Therefore, we considered diagnosis of our case was not right lung agenesis but horseshoe lung with extremely hypoplastic right lung.
Conclusions: Our case suggests that horseshoe lung and pulmonary agenesis may be included in the spectrum of the same anomaly.

Poster #: CR-020

MRI Diagnosis of Leukodystrophy with Vanishing White Matter with Corpus Callosum Involvement

Liam Lorentz, *Radiology, University of the Witwatersrand, Johannesburg, South Africa, liam.lorentz@gmail.com*

Disclosures: All authors have disclosed no financial interests, arrangements or affiliations in the context of this activity.
Purpose or Case Report: Introduction

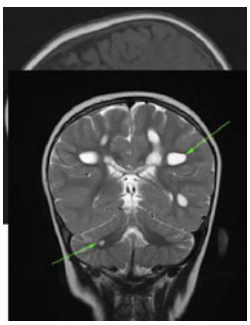

Leukodystrophy with vanishing white matter (VWM), previously known as childhood ataxia with central hypomyelination (CACH) is considered one of the most prevalent inherited white matter disorders.Clinical history
We report a 20 month old male with a 2 week history of right hemiplegia and ataxic gait. Infant is well grown with no previous medical or familial history of note. Normal development and unremarkable birth history.
MRI findings
Brain MRI demonstrates multiple T2 hyperintense periventricular deep white matter cavitating lesions with cortical sparing (fig 2, top arrow). These lesions were of CSF signal intensity on FLAIR and demonstrated differential water content; central hypointensity with peripheral hyperintesity (fig 3). There is no restricted diffusion centrally, however, the peripheral areas that are hyperintense on FLAIR were restricting. The temporal lobes are unaffected. Single, non-enhancing cerebellar white matter hyperintensity (non-cystic) within right hemisphere (fig 2, bottom arrow); no cerebellar or brainstem atrophy. White matter involvement of

the corpus callosum with outer rim sparing (fig 1). There is no hydrocephalus and no basal ganglia involvement.
Conclusions: MRI diagnosis with typical symptomology of Leukodystrophy with VWM is well documented. Biochemical markers have limited use and genetic studies are not mandatory for diagnostic purposes. Despite a common mutation, phenotypic variation is common. Rarefraction and cystic degeneration of white matter is obligatory with involvement of the corpus callosum, sparing the outer rim is suggestive of the diagnosis.

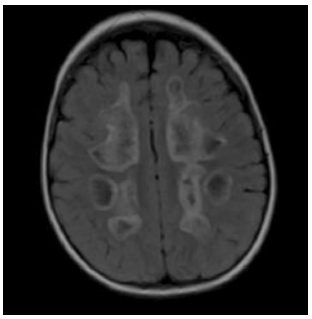

Poster #: CR-021

Oral Cavity Teratoma Diagnosed By Fetal MRI – From Common Radiological and Surgical Point of View

Blanka Prosova, Resident, *Radiology, Faculty Hospital Motol, Prague, Czech Republic, b.pros@centrum.cz*

Disclosures: All authors have disclosed no financial interests, arrangements or affiliations in the context of this activity.
Purpose or Case Report: We present a case of expansion in the oral cavity, referred from routine antenatal ultrasound screening to fetal MRI in 24th gestational week for extension of diagnostic information concerning predominantly the character of tissue and relationship to adjacent structures. The aim of the presentation, which includes two fetal MRI and one MR performed immediately postnatal, is to specify which details could be obtain by evaluating the fetal MRI in such type of diagnoses and what is their practical application for influencing the outcome of the baby. Orofaryngeal teratomas are exceedingly rare and despite their usual benign histopathology they are potentially lethal due to airway obstruction. Complete surgical resection is the guiding principle of usually urgent postnatal management. The role of imaging method and MRI, with its tissue contrast, is the best method of the choice, is to establish the level of the airway compression, to specify the extent of the lesion for facilitating the postnatal planning, including the approach for resection. We emphasized some question the radiologist could be asked by involved surgeon, especially concerning the tongue involvement, as this factor definitely influenced the quality of life.

Poster #: CR-022

Beyond Toddler Fractures - Spondylodiscitis as a Rare Cause Of An Infant That Refuses To Walk

Norbert Utz, *Pediatric Radiology, HELIOS Klinikum Krefeld, Krefeld, Germany, norbert.utz@gmx.de;* Ilona Daumer, Marcus Katoh

Disclosures: All authors have disclosed no financial interests, arrangements or affiliations in the context of this activity.
Purpose or Case Report: To present two rare cases of spondylodiscitis of the infant age group who refused to walk and stand. Both had no fever and showed only mild laboratory signs of infection with slight CRP and ESR elevation without leukocytosis.
Methods & Materials: The clinical, laboratory and imaging data of two infants (girl and boy, 30 and 18 months of age, respectively) with spondylodiscitis are presented. Both underwent sonography of the hips and the knee joints, radiographs of the hip and leg as well as MRI scan of the lumbar spine and the pelvis.
Results: Initial CRP and ESR were 36/21 mg/l and 44/70 mm respectively after the first hour. Both had no fever and no leukocytosis. All blood cultures during the course were negative.
Sonography ruled out effusion of the hip and knee joint. Radiographs of the hip and the knee were unremarkable with no evidence of a toddler fracture. The MRI scan of the lumbar spine showed signs of spondylodiscitis at the level of L4/S1 with reduction of the disc height, increased contrast enhancement of the adjacent vertebra as well as a small prevertebral soft tissue abscess in both cases.
Onset of symptoms to final diagnosis took 5 and 6 weeks, respectively. Both were treated with intravenous antibiotics for 3 weeks without complications. No needle biopsy for pathogen isolation was performed.
Conclusions: Spondylodiscitis in infants is uncommon to rare and can present with subtle and unspecific signs and symptoms. It can mimic typical diseases of that age like coxitis fugax or a toddler fracture.
These unspecific clinical findings can lead to delayed diagnosis. In the literature a delay in up to 3 months is described in 50% of the cases.
An awareness of this rare diagnosis in this age group can shorten the diagnostic process especially if laboratory findings show signs of an infection.

Poster #: CR-023

Paediatric MR Enterography under General Anaesthetic: Our Experience

Mark Chopra, *Radiology, Great Ormond Street Hospital, London, United Kingdom, mark.chopra@gosh.nhs.uk;* Tom Watson, Øystein Olsen

Disclosures: All authors have disclosed no financial interests, arrangements or affiliations in the context of this activity.
Purpose or Case Report: The incidence of paediatric inflammatory bowel disease (pIBD) is increasing. MR enterography (MRE) is increasingly recognised as the gold standard imaging technique for the small bowel in IBD. The advantages of MRE include the lack of ionising radiation and greater soft tissue definition. It also allows functional information from diffusion sequences and is used for IBD diagnosis, monitoring of disease activity and complications such as abscess, stricture or fistula. Extra-intestinal manifestations can also be identified.
Younger children often need a general anaesthetic (GA) in order to undergo MRI. Excellent distension of the small bowel loops on MRE is essential to aid accurate assessment. As the child cannot drink a large volume of fluid prior to anaesthetic induction, fluid distension is facilitated through insertion of a nasojejunal tube and instillation of fluid via the tube whilst under GA. We present our institutional practice from a large paediatric hospital for performing MR enterography under GA in young children.
A retrospective study of our Radiology Information Service (RIS) was undertaken to identify children under the age of 10 years who underwent MRE under GA between 2010 and 2015. The anaesthetic charts of these children were obtained and the anaesthetic duration / complications were recorded. The imaging was reviewed to evaluate the MRI quality, degree of distension and report finding. The MR protocol and sequence optimisation will also be discussed.
12 patients were included in the study, aged from 23 months to 10 years. The length of GA time ranged from 110 to 185 min (average 142 min) and no significant adverse effects were described. The mean fluoroscopy radiation dosage for NJ insertion was low (8 micrograys) and the success rate was high (91%).
All completed studies were reviewed and oral contrast reached the terminal ileum in 100%. Bowel distension was rated as good or excellent in all cases.

Our institutional experience has shown that MRE under GA with nasojejunal tube enteroclysis is feasible and can safely produce high quality, diagnostic imaging in the young paediatric patient.

Poster #: CR-024

Pictorial Review of Paediatric Pulmonary Hydatid Disease in South Africa

Tanyia Pillay, MBChB (WITS), FC Rad (Diag) SA, Dip Paeds Rad (UCT), *Department of Radiology, Chris Hani Baragwanath Hospital, University of the Witwatersrand, Eikenhof, South Africa;* Charl Verwey, Jacinta Adrigwe

Disclosures: All authors have disclosed no financial interests, arrangements or affiliations in the context of this activity.
Purpose or Case Report: Pulmonary hydatid disease is more common in paediatric than in adult patients, and affects males more commonly than females. Concurrent liver and lung disease is present in 6% of cases.
Hydatid disease is caused by a parasite, echinococcus granulosus. Disease in humans is a result of faeco-oral contamination from ingestion of parasitic eggs contained in dog faeces. Pulmonary hydatid cysts results from either transdiaphragmatic or haemtogenous spread, with cysts being bilateral in 20% and multiple in 30% of patients.
Clinical symptoms are usually due to the mass effect of the cysts. Children are usually asymptomatic but may present with coughing, shortness of breath, chest pain or haemoptysis.
Diagnosis is usually suspected by the characteristic findings on plain chest radiograph and a positive serological test. CT and MRI are used for a better definition and delineation of the diease extent, particulary for surgical planning. Definitive diagnosis is made by histological analysis of the cyst.
Children diagnosed with pulmonary hydatid should have an abdominal ultrasound, and if neurological symptoms are present, a CT or MRI of the brain. Siblings living with the affected child should have a screening chest radiograph and an abdominal ultrasound.
Results: Cysts may vary in number and morphology depending on the stage of the growth. Uncomplicated cysts are usually well defined, round homogenous masses with a lower lobe predominance. The "Meniscus" or "Crescent" sign is seen when air appears between the pericyst and laminated membrane. The "Onion peel" sign is when there is air between the pericyst and the endocyst. Complete separation of the endocyst from the pericyst results in the "Water-Lily" sign in which the endocyst floats within the partially fluid-filled cystic cavity.
Conclusions: The disease may affect any part of the body and may present with a variety of radiological features. Paediatric pulmonary hydatid disease shoud be considered as a differential diagnosis in a child with a rounded opacity in the lung with associated lower respiratory tract symptoms, particularly in areas where hydatid is endemic.

Poster #: CR-025

Imaging Findings of Abdominal Basidobolomycosis in Immunocompetent Children: The Omani Experience

Asya Al-Busaidi, MD, *Radiology, Oman Medical Speciality Board, Al-Khoudh, Oman, asya.b@hotmail.com;* Saud Al-Shabibi

Disclosures: All authors have disclosed no financial interests, arrangements or affiliations in the context of this activity.
Purpose or Case Report: During the past 1 year we encountered three previously healthy children ages 10,8 and 2 years respectively who presented with localized colicky abdominal pain of few days duration. All three patients had eosinophilia, one of whom had an associated fever and a high white blood cell count. Firm tender masses were palpated in the right side of their abdomens.
Their abdominal ultrasounds showed well defined hypoechoic masses with central components of gaseous artefacts, indicating bowel loop involvement. Computed tomography then done, showed aneurysmal dilatation with mural circumferential thickening of the ascending colon. The affected bowel loops were attenuating, showed perilesional fat stranding and multiple mesenteric lymph nodes some of which showed signs of necrosis. Neoplastic and infectious causes were therefore entertained.
Gastrointestinal lymphoma would show such aneuryusmal dilatation with mural thickening. However 50% of these affects the ileo-caecal segment. Moreover, our patients did not exhibit any symptoms or laboratory findings suggestive of a malignant process.
The presence of necrotic lymph nodes geared towards tuberculosis. However, again this is most commonly seen in the ileocecal segment. Since the patients were not septic and had high eosinophil count, atypical infections were considered. Having come across some reported cases of basidobolomycosis from the Arabian peninsula we therefore put this diagnosis at the top of our differentials.
The patients underwent hemicolectomies and were all confirmed histologically to have characteristic features of basidobolomycosis. In retrospective review of the patients' files we did observe that they were all from the coastal region of Oman.
The main objectives of this report is to draw the attention that such rare fungal infections are not uncommon in our country and the region and to enlighten the importance of a broad systematic approach when considering the various aetiological causes of focal bowel thickening including rare diseases that may be endemic in certain areas.

Poster #: CR-026

Purely Cystic Sacrococcygeal Teratoma; Imaging Findings

Mine Aslan, MD, *Istanbul University, Cerrahpasa Medical School, Istanbul, Turkey, mineus_77@yahoo.com;* Hatice Arioz Habibi, Ayse Kalyoncu Ucar, Yesim Namdar, Ibrahim Adaletli, Sebuh Kurugoglu

Disclosures: All authors have disclosed no financial interests, arrangements or affiliations in the context of this activity.

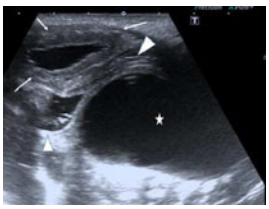

Purpose or Case Report: Sacrococcygeal teratoma (SCT) is one of the most common tumors of the newborn. SCT is seen frequently in the presacral region and in forms of solid or mixed solid and cystic masses. Only 10-15% of all sacrococcygeal teratomas are in pure cystic form. Here, in this case, we aimed to present sonographic and magnetic resonance images (MRI) of a newborn with pelvic cystic mass and bilateral hydronephrosis that were seen on prenatal ultrasonography.
An operation was planned for 2 days of age girl patient for cystic pelvic mass and bilateral hydronephrosis detected by prenatal sonography during the third trimester. On her abdominal X-ray radiography, there was no bowel gas at the midline pelvis. The patient was referred to the sonography unit with the suspicion of a duplication cyst. Abdominal sonography revealed bilateral hydroureteronephrosis, bladder wall thickening, and a 75×55×32 mm pure cystic mass located between the rectum and bladder. The mass had a fine septa at the inferior site. Abdominal MRI showed that the mass had no connection with the spinal canal or solid component. The patient was operated and the diagnosis of purely cystic sacrococcygeal teratoma was confirmed histopathologically.

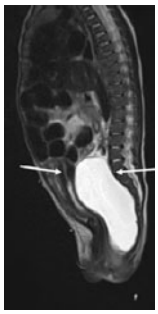

Anterior meningocele, tail gut cyst, rectal duplication cyst, and cystic sacrococcygeal teratomas are common lesions of the presacral region diagnosed in the prenatal or antenatal period. Sacrococcygeal teratoma should be kept in mind in patients with presacral cystic mass in the neoatal period and radiologic methods are helpful for displaying the extent and content of a cystic mass.

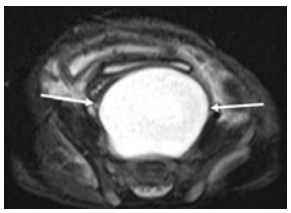

Poster #: CR-027
Imaging Findings of Wolman Disease

Mine Aslan, MD, *Istanbul University, Cerrahpasa Medical School, Istanbul, Turkey, mineus_77@yahoo.com;* Ayse Kalyoncu Ucar, Hatice Arioz Habibi, Yesim Namdar, Sebuh Kurugoglu, Ibrahim Adaletli

Disclosures: All authors have disclosed no financial interests, arrangements or affiliations in the context of this activity.

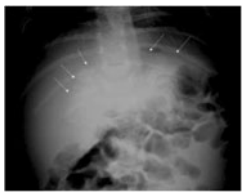

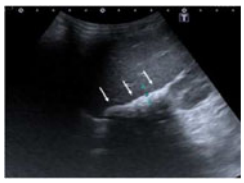

Purpose or Case Report: Wolman disease is a rare autosomal recessive inherited disease characterized by storage of cholesterol esters and triglycerides in lysosomes due to a deficiency of lysosomal acid lipase. Clinical signs such as persistent vomiting, diarrhea, hepatosplenomegaly, growth retardation and liver dysfunction occur in the first weeks of life. Most cases die in the first year of life. Here, we aim to present radiological findings of Wolman disease.

An asymptomatic girl 2 months of age was admitted to the pediatric genetic disease service with the history of Wolman disease in two brothers who had died in the neonatal period. Abdominal X-ray imaging displayed calcification of the bilateral adrenal gland regions. Hepatosplenomegaly and bilateral adrenal gland posterior acoustic shadowing due to calcifications were revealed by abdominal sonography. Magnetic resonance imaging showed enlarged hypointense adrenal glands in all sequences and hepatosplenomegaly. The lysosomal acid lipase levels were low compatible with Wolman disease.
Multimodality radiologic imaging methods should be performed to display hepatosplenomegaly, hepatosteatosis, bilateral adrenal gland enlargement and calcification in Wolman disease.

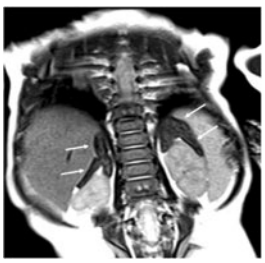

Poster #: CR-028

Hemihypertrophy Syndromes

Breege Gilmartin, MB BCh BAO, *Medical Imaging, The Royal Children's Hospital, Melbourne, Australia, Melbourne, VIC, Australia, breege.gilmartin@rch.org.au;* Karen Atkin

Disclosures: All authors have disclosed no financial interests, arrangements or affiliations in the context of this activity.
Purpose or Case Report: To give an overview of hemihypertrophy syndromes, to discuss the latest established aetiology/pathophysiology, to emphasise the importance of careful evaluation of imaging findings in this heterogeneous group of disorders and to outline the latest screening recommendations in an appropriate subset of patients.
Methods & Materials: Hemihypertrophy can be considered a spectrum which ranges from asymmetric enlargement of a limb or one side of the body compared with the contralateral limb or side beyond the limits of normal variation to focal gigantism or macrodactyly which causes enlargement of the digits or portion of an extremity. We focus our talk on defining, describing and illustrating some of the more commonly encountered conditions.
Results: We outline a number of syndromes including Beckwith Wiedemann: a hemihypertophy syndrome associated with macroglossia, enlarged abdominal organs, umbilical hernia and an increased predilection for development of embryonal cell tumours especially Wilm's tumour and Klippel-Trenaunay: a triad of hemihypertophy, port-wine stain, and anomalous veins and Diffuse Lipomatosis which demonstrates a diffuse increase in adipose tissue.
Conclusions: Knowledge of, and the ability to differentiate, these relatively uncommonly encountered lesions is important because young children who have hemihypertrophy may have increased risk of malignant intra-abdominal embryonal tumors, such as Wilm's tumor or hepatoblastoma and, as such, require close follow-up screening.

Poster #: CR-029

Teenage Boy with Cerebriform Testicular Adrenal Rest Tumors

Scott Willard, MD, *McLane Children's - Baylor Scott & White, Temple, TX, mendocinos@yahoo.com;* Krista Birkemeier, MD

Disclosures: All authors have disclosed no financial interests, arrangements or affiliations in the context of this activity.

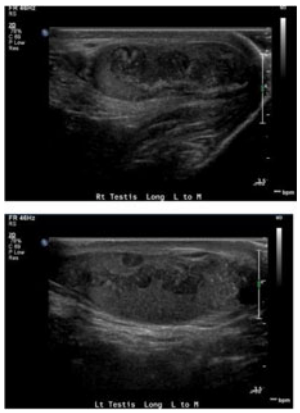

Purpose or Case Report: We present the case of a 14 year old Asian male with a history of poorly controlled congenital adrenal hyperplasia (CAH) and growing testicular adrenal rest tumors. While on high dose steroid therapy, the lesions decreased in size from 1.1×1.0 cm to 0.5×0.8 cm. However, they subsequently increased in size, measuring 2 to 3 cm in length when the patient was not compliant with the steroid regimen due to Cushingoid side effects. The masses were bilateral, symmetric, and located at the mediastinum testis, all findings consistent with testicular adrenal rest tumors as opposed to Leydig tumor. With growth, they coalesced to form undulating masses with hyperechoic and hypoechoic layers mimicking the cerebrum, an appearance more typically seen in the adrenal glands at initial diagnosis of CAH. Current practice guidelines in much of the developed world typically result in early diagnosis and advanced therapy, making testicular adrenal rest tumors of this size and appearance unique.

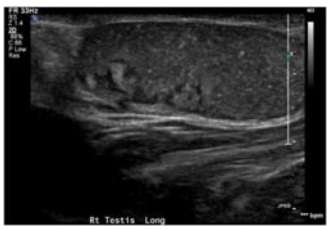

Poster #: CR-030

IMAGe Syndrome – A Case Report

Gerald Drocton, MD, *Diagnostic Radiology, University of Kansas-Wichita, Wichita, KS;* Debbie Dobbs-Desilet, Shobana Kubendran, Kamran Ali, Adam Zarchan, Jurgen Spranger, Bradley Schaefer

Disclosures: All authors have disclosed no financial interests, arrangements or affiliations in the context of this activity.
Purpose or Case Report: We present a case of IMAGe syndrome in a newborn patient and review the associated abnormalities with emphasis on the radiologic findings.
IMAGe syndrome is an acronym for the major findings of intrauterine growth restriction (IUGR), metaphyseal dysplasia, adrenal hypoplasia congenital (AHC) and genitourinary abnormalities. Image syndrome is caused by a CDKN1C mutation only if the mutation is present on a maternally inherited copy of the gene.
The clinical features of AHC and IUGR with or without a family history of IMAGe syndrome are highly suggestive of the diagnosis. The skeletal findings may include metaphyseal and/or epiphyseal dysplasia, osteopenia, gracile long bones, mesomelia, and delayed bone age. Genital abnormalities are common in males and include unilateral or bilateral cryptorchidism and hypospadias. Facial features include mild frontal bossing, flat or broad nasal bridge, and small or low set ears.
A Caucasian male was born at 38 weeks gestation to nonconsanguineous healthy parents. Prenatal ultrasound imaging demonstrated IUGR. The infant was small for gestational age with a birth weight of 2390 grams (4.5 percentile). On clinical exam, the patient demonstrated simian creases, hypospadias, and undescended testicles. Phenotypically, the patient demonstrated findings more severe than hypochondroplasia but less prominent than achondroplasia. Facial features included micrognatia, a high-arched palate, and mild frontal bossing. The skeletal findings on imaging consisted of thin gracile ribs, markedly delayed bone maturation, and irregular distal femoral metaphyseal margins. The distal femoral metaphyses also demonstrated a celery stalk appearance. Pelvic findings included triangular ischia, unossified pubic bones, and irregular acetabular roofs. The case is particularly unique in that the patient also presented with rhizomelia of the bilateral humeri; a finding which has not been previously described with IMAGe syndrome to the authors' knowledge. The patient experienced episodes of hyponatremia, hyperkalemia, and decreased cortisol levels consistent with primary adrenal insufficiency. Genetic testing detected a mutation in the CDKN1C gene. The patient's mother was detected to carry the same mutation, thereby confirming the inheritance pattern and confirming the diagnosis of IMAGe syndrome in the patient.
IMAGe syndrome is rare. Only 25 individuals with a clinical and/or molecular diagnosis have been reported to date.

Poster #: CR-031

Subserosal Cyst of the Urinary Bladder in A Male Neonate

Megan Daghfal, M.D., *Diagnostic Radiology, University of Illinois College of Medicine at Peoria, Peoria, IL, mdaghf1@gmail.com;* Craig Mitchell, D.O., Churphena Reid

Disclosures: All authors have disclosed no financial interests, arrangements or affiliations in the context of this activity.
Purpose or Case Report: We report the case of a previously unreported subserosal cyst of the urinary bladder in a male neonate. Prenatal sonography revealed a cystic structure in the fetal bladder that was presumed to be a ureterocele. Renal and bladder sonography at 11 days-of-age revealed a 9 mm thin-walled simple cyst within a decompressed urinary bladder. The kidneys were sonographically normal. A VCUG performed the same day revealed an ovoid-shaped filling defect along the posterior-superior bladder wall. The bladder was otherwise normal. There was no vesicoureteral reflux, but a prostatic utricle filled with contrast. Cystoscopy performed at 3 months of age revealed single ureteral orifices bilaterally and no ureterocele. A dome-like lesion measuring approximately 1 cm in size was visualized along the posterior bladder wall. Sonography of the bladder performed earlier on the same day as cystoscopy once again revealed a thin-walled anechoic cyst within the posterior bladder wall. At 7 months of age, the infant underwent cystoscopic surgical excision of the bladder lesion as well as orchiopexy for an undescended testicle. The results of histopathologic analysis revealed a benign subserosal cyst with an epithelial lining and an entrapped duct. A review of the literature revealed only two previously reported cases of subserosal bladder cyst, both in adults. The natural history of these cysts is unknown. However, given the benign sonographic and histopathologic appearance of these lesions, we propose that these cysts can be safely followed with interval sonography.

Poster #: CR-032

A Swing, a Miss, and an MRI: A Case of Batter's Shoulder in a Young Athlete

Sandra Allbery, MD, *Children's Hospital and Medical Center, Omaha, NE, sallbery@childrensomaha.org;* Andria Powers, Terri Love, Lisa Wheelock

Disclosures: All authors have disclosed no financial interests, arrangements or affiliations in the context of this activity.

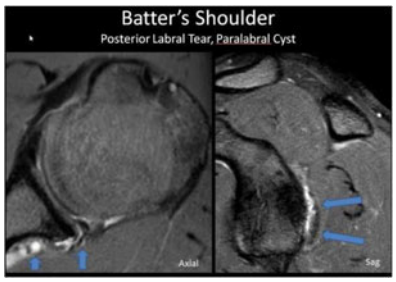

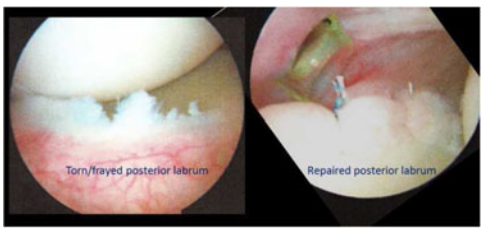

Purpose or Case Report: We present a case of an 18YO male high school baseball player with acute onset posterior pain in his non-throwing left shoulder, the leading shoulder in his batting swing. Pain began on a missed attempt at hitting an outside pitch. The pain only occurred when he was batting and resulted in subsequent loss of batting power and accuracy. Patient was asymptomatic when he was not batting. Prior to the acute event, patient had low grade pain in this location during intermittent at bats. Physical exam showed 1-2+ left shoulder posterior instability and mildly asymmetric left less than right shoulder strength. He had negative Neer, Whipple, Speed's, and Hawkin's tests. MRI left shoulder showed posterior labral tear with paralabral cyst. Patient underwent laparoscopic posterior labral repair with placement of four anchoring sutures and Bankart reconstruction. He did well post-operatively, returning to preinjury strength and range of motion in 4 months and returning to play in 6 months.

Batter's shoulder is a rare condition recently recognized in the orthopedic literature and has not been reported to our knowledge in the radiologic literature. Although the adolescent/young adult spectrum of shoulder injuries in the throwing arm have been well described, injury types and mechanisms involving the non-throwing arm are not commonly known. The mechanics of hitting places considerable stress on the leading shoulder. Biomechanics studies by Welch CM et al. show that as the hitter slides forward, the force applied by the front foot equals 123% of body weight and the hip segment rotates to a maximum speed of 714 degrees/second. This is followed by maximum shoulder segment velocity of 937 degrees/second and maximum linear bat velocity of 31 m/second. During a missed pitch, these forces are magnified due to lack of a counterforce against the dynamic posterior pulling force on the lead shoulder. Athletes with labral tear of the leading shoulder during batting (Batter's shoulder) have a better prognosis than throwing arm labral tear, with approximately 90% returning to previous level of play.

This exhibit will display biomechanics, pre-operative and post-operative MRIs, and intra-operative laparoscopic images of Batter's Shoulder.

Poster #: CR-033

Atretic Cephalocele: Prenatal and Postnatal Imaging Features

Heidi Lewis, MD, *Radiology, University of South Florida, Tampa, FL, HLewis1@health.usf.edu;* Jennifer Kucera, MD, MS

Disclosures: All authors have disclosed no financial interests, arrangements or affiliations in the context of this activity.

Purpose or Case Report: Atretic cephalocele is a rare type of neural tube defect that occurs in the parietal or occipital scalp. Most cases present postnatally with a scalp nodule which may also have associated skin and hair abnormalities. We will present a case of atretic cephalocele diagnosed with fetal MRI as well as two additional cases of postnatally diagnosed atretic cephalocele in different patients.

A 26 week gestational age male fetus was found to have ventriculomegaly on routine OB ultrasound and was referred to maternal fetal medicine. Further ultrasound imaging demonstrated features suspicious for a posterior fossa encephalocele. A fetal MRI was then performed which demonstrated imaging findings consistent with an atretic cephalocele.

The imaging findings associated with atretic cephalocele including embryologic positioning of the straight sinus, the "spinning top" appearance of the tentorial incisura, and the "cigar shaped" CSF tract in the interhemispheric fissure will be illustrated in the exhibit using both fetal and postnatal MRI. Although the exact embryological development of atretic cephaloceles is not completely understood, the proposed mechanisms will be discussed. A brief summary of the associated syndromes and clinical outcomes reported in the literature will be presented.

Atretic cephalocele is a rare condition that is usually diagnosed postnatally with several characteristic imaging findings. These same abnormalities can also be seen on fetal MRI which can lead to an earlier diagnosis and more appropriate family counseling.

Poster #: CR-034

Unique Case of a Giant Fibrous Hamartoma of Infancy with Differing Prenatal and Postnatal MRI Appearance

Scott Willard, MD, *Radiology, Baylor Scott & White, Temple, TX, mendocinos@yahoo.com;* Krista Birkemeier, MD

Disclosures: All authors have disclosed no financial interests, arrangements or affiliations in the context of this activity.

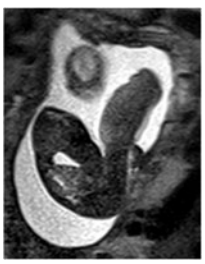

Purpose or Case Report: Prenatal screening ultrasound at 18 weeks gestation identified homogeneous enlargement of the distal left leg. There was relative increased blood flow by Doppler, but the bone lengths were symmetric. There were no cysts and no amniotic bands. MRI was performed at 21 weeks gestation for further characterization. MRI demonstrated a lobulated, infiltrative, asymmetric soft tissue signal intensity thickening extending from the knee to the dorsum of the foot. There was no fat content appreciable on T1 or T2 fat saturated images. Given these findings, a vascular soft tissue mass such as kaposiform hemangioendothelioma was the primary differential consideration, with other fibrous tumors considered less likely. Follow up ultrasounds demonstrated commensurate growth of the lesion with the child. At scheduled cesarean delivery, the otherwise healthy female infant had a leg mass that measured 14 cm, extending from the knee to the dorsum of the foot, as seen on prenatal imaging. The skin overlying the lesion was thick and redundant with hypertrichosis. Postnatal MRI was performed on day 2, unexpectedly showing extensive fat signal, along with edema

signal and enhancement of the muscle, fat, and thickened skin. There was no abnormal vascularity and no focal mass. There was mild tibial bowing. Incisional biopsy was performed on day 6, with pathologic diagnosis of spindle cell tumor suggestive of fibrous hamartoma of infancy (FHI).

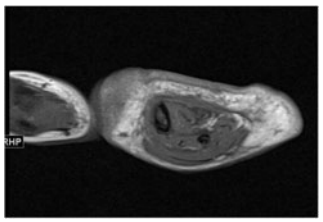

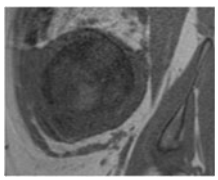

This apparent case of FHI is an atypical presentation, with interesting imaging implications. FHI is usually smaller (3-5 cm), more common in males (2.4:1), and only rarely involves the lower extremities distal to the knee (0.5% of cases). Only 23% of FHI are present at birth. To our knowledge, there are no case reports describing the fetal MRI appearance of this entity. Hamartomatous lesions and macrodystrophia lipomatosa had been excluded from the differential diagnosis due to the lack of fat signal intensity on fetal MRI. However, the fetus was imaged in early second trimester and normal subcutaneous fat is usually not visible on MRI until late in the second trimester. This case raises questions regarding the timing of appearance of fat in this lesion. As a result, we recommend that fat containing lesions not be excluded on the basis of absence of fat in early fetal MRI. Repeat MR imaging of musculoskeletal tumors in the third trimester to re-assess content may be useful.

Poster #: CR-035

A Rare Cause of Spinal Canal Stenosis in a Child with Neurofibromatosis Type I

Alan Chen, *University of South Florida College of Medicine, Tampa, FL, amchen2107@gmail.com;* Jennifer Kucera, MD, MS

Disclosures: All authors have disclosed no financial interests, arrangements or affiliations in the context of this activity.
Purpose or Case Report: A 10-year-old female with neurofibromatosis type 1 and severe dysplastic scoliosis, presented with a 2-month history of difficulty ambulating due to lower back pain. The patient did not have neurological symptoms. An MRI of the thoracolumbar spine demonstrated subluxation of the right tenth and eleventh ribs through the neural foramina, causing mass effect on the thecal sac, but at T9-T10 without abnormal cord signal or cord compression. Several clusters of neurofibromas were present along the right ribs and paravertebral soft tissues at these levels. CT evaluation was performed for greater osseous definition, which confirmed the findings. The patient underwent complex posterior spine fusion and segmental spinal instrumentation, which included T9-T10 thoracoplasty, rib resections, and multiple Ponte osteotomies.
Cases of rib head protrusion into the central canal in the setting of dystrophic scoliosis have been documented in only a limited sample of case reports. The angulated short-segment curvature in dystrophic scoliosis causes vertebral body rotation, foraminal enlargement, spindling of transverse process, and penciling of the apical ribs. These changes can alter the articulation of the rib along the spinous process. The enlarged foramina also create a space into which a rib may displace. As a result, in most reported cases, the subluxed ribs were on the convex apex of the curve in the mid-to-lower thoracic region. The risk of cord injury makes complete depiction of the anatomy crucial for surgical management.

Poster #: CR-036

Imaging Review of Hypophosphatasia: A Rare, but Important Metabolic Disorder with Characteristic Radiographic Features

Ashish Parikh, MD, *Vanderbilt, Nashville, TN, ashishckt@gmail.com;* Yu Luo, MD, PhD, Stephanie Spottswood, MD, MSPH

Disclosures: All authors have disclosed no financial interests, arrangements or affiliations in the context of this activity.
Purpose or Case Report: First described by Rathbun in 1948, hypophosphatasia is an inherited metabolic disorder arising from the deficient activity of the tissue-nonspecific isoenzyme of alkaline phosphatase. There are several different types and varying clinical presentations of hypophosphatasia, characterized according to their age of onset by Fraser in 1957. In addition, the severity of the radiographic findings is inversely correlated with the age of presentation, with older patients presenting with less severe forms of the disease. Classically, the radiographic findings resemble rickets/osteomalacia, but in the presence of normal Vitamin D metabolism. Additional findings associated with hypophosphatasia are Bowdler spurs, which are transverse bony spurs in the radius, fibula and ulna and central lucencies or "punched out" lesions in the metaphysis, particularly of the knee (Case 1). In this case series of 3 patients, these characteristic radiographic features as depicted on skeletal surveys, along with their clinical manifestations, diagnostic criteria, management, treatment, and prognosis will be discussed. In particular, the evolution of radiographic changes with treatment in one patient will be assessed (Case 2).

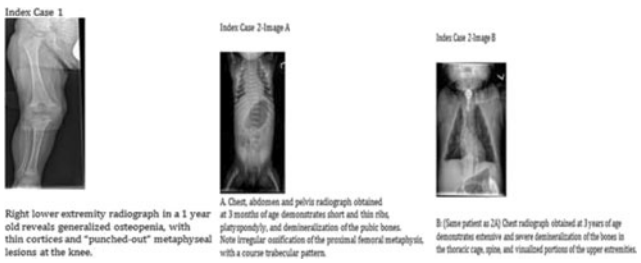

Poster #: CR-037

Spinal Dysraphism with Peritoneal Communication

Carlos Gimenez, M.D., *Radiology, Ochsner Clinic Foundation, New Orleans, LA, cgimenez@ochsner.org;* Noah Emerson, Maria Camila Barrera Arango, Andrew Matthews

Disclosures: All authors have disclosed no financial interests, arrangements or affiliations in the context of this activity.

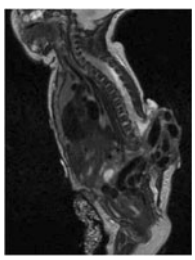

Purpose or Case Report: Spinal dysraphism is a broad term used to describe congenital abnormalities of the spine and spinal cord that demonstrate a multifactorial etiology including both genetic and environmental factors. Spina bifida is a subtype of spinal dysraphism that is often described as the most common congenital CNS malformation with an estimated incidence of 1 in 1000-2000 live births. Among the various ways of categorizing these disorders, the open and closed designation is one of the most accepted ones. Open defects correspond to those cases in which there is an overlying skin defect that allows neural tissue to be exposed to the environment while closed defects are covered by intact skin. We present a case of a 10 month old patient with an extreme form of open spinal dysraphism consisting of a myelomeningocele with associated peritoneal communication that allowed bowel and other abdominal contents to protrude into the defect.

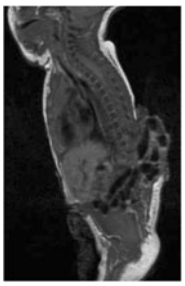

Poster #: CR-038

Focal Fatty Infiltration of the Liver as a Possible Rare Side Effect of Gabapentin: Case Report of a 14 Year Old Female Developing Abdominal Symptoms Following Initiation of Treatment

Ravi Sharma, MD, *Radiology, Integris Baptist Medical Center, Oklahoma City, OK, rav.sharma03@gmail.com;* David Bohn, Neal Sharma, Richard Stanford

Disclosures: All authors have disclosed no financial interests, arrangements or affiliations in the context of this activity.
Purpose or Case Report: Several possible etiologies for focal hepatic steatosis have been explored to date, and in this case of a 14 year old female patient, the hepatotoxic side effect of Gabapentin was clinically addressed as a possible, very rare culprit. There is extremely limited data on the hepatotoxic effects of gabapentin and only a few individual case reports of liver injury from gabapentin have ever been published. The patient was started on Gabapentin by her ENT physician for ear pain approximately 3 months prior to her imaging workup. Since starting the medication, she had developed symptoms of nausea, vomiting, and right upper quadrant abdominal pain. Her physician referred her for radiologic evaluation of her abdominal symptoms.
Methods & Materials: The patient's imaging workup was initially performed with sonographic evaluation of the right upper quadrant of the abdomen. A same day HIDA scan was performed immediately following the ultrasound. An MRI of the abdomen with contrast the following day was obtained on a 1.5 T Siemens scanner.
Results: The ultrasound demonstrated a normal gallbladder and three hyperechoic solid lesions within the left liver measuring up to 3.8 cm. The liver itself was normal in size and noncirrhotic in appearance. The HIDA nuclear medicine scan was normal. The MRI demonstrated intralesional fat characteristics of mildly increased precontrast T1 signal and signal dropout on the out of phase images within all three of the hepatic lesions. There was no enhancement or other suspicious features, and traversing, nondisplaced portal and hepatic veins were visualized through these lesions. The patient had been taking 100 mg Gabapentin 1-2 capsules PO TID, and following review of clinical symptoms and imaging findings by her pediatric GI and behavioral specialist physicians, she began tapering off the medication completely.
Conclusions: Focal hepatic steatosis may appear as multiple nodular areas in atypical locations producing a pseudotumor appearance and can pose a diagnostic challenge, especially with more atypical presentations as seen in this patient. Although not as common as the diffuse form, the focal form has a significant prevalence in the pediatric population and the natural history and possible etiologies are not yet fully understood. Additionally, this case demonstrates how the judicial use of MRI may help clarify challenging pediatric patient cases in a manner that upholds the principles of ALARA.

Poster #: CR-039

Vascular Head and Neck Lesions: Utility of Time resolved MRA

Eleza Golden, MD, *Radiology, Emory University, Atlanta, GA, eorenst@emory.edu;* Nadja Kadom, MD

Disclosures: All authors have disclosed no financial interests, arrangements or affiliations in the context of this activity.

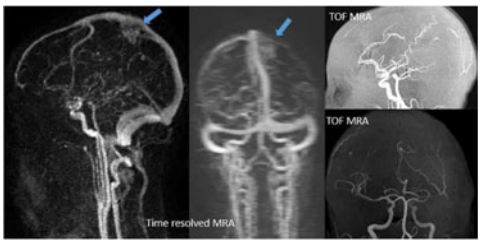

Purpose or Case Report: On conventional MRI pediatric vasoproliferative neoplasms or vascular malformations may demonstrate similar features including T2 hyperintensity and enhancement. Hemangiomas can appear similar to vascular malformations when there are large feeding vessels.
Our objective is to illustrate typical imaging findings of vasolproliferative neoplasms and vascular malformations of the head and neck on conventional MRI and the benefits of time resolved MRA to further distinguish between high and slow flow lesions

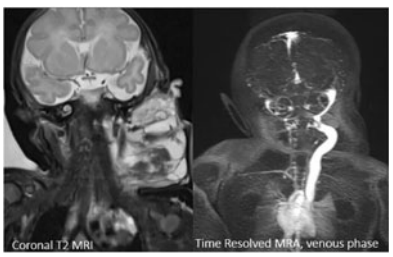

Methods & Materials: We performed a retrospective review to identify patients with vascular lesions of the head and neck seen at our tertiary care facility. We selected a total of five patients to illustrate the typical imaging findings of a hemangioma, arteriovenous malformation (AVM), arteriovenous fistula (AVF), venous malformation, and lymphatic malformation.
For each entity we present conventional MRI images, conventional MRA/MRV, and multiple time points of time resolved MRA. Time resolved MRA was performed by sampling lower spatial frequencies more often than higher spatial frequencies. After an initial pre-contrast mask, images are obtained over multiple time points during flow of contrast through arterial, capillary, and venous phases for a minimum of 15 phases.
Results: Time-resolved MRA is a useful tool to help distinguish types of vascular lesions. Spatial resolution is sacrificed in lieu of improved temporal resolution. On time resolved MRA, hemangiomas demonstrate

avid, homogeneous, early arterial enhancement (Case 1). The arterial phase may show prominent feeding vessels, but there should not be draining veins. AVMs and AVFs, on the other hand, demonstrate enhancement of both the feeding arteries and draining veins during the early arterial phase (Case 2, Case 3). Tortuous neovascularity during the arterial phase is suggestive of an alternative diagnosis of another solid tumor. Venous malformations demonstrate no enhancement in the early arterial phase and usually show patchy areas of enhancement, possible puddling of contrast, and enlarged draining and surrounding veins in the venous phase (Case 4). Lymphatic malformations show no or very limited enhancement during time-resolved MRA (Case 5).
Conclusions: Using case examples, we illustrate the typical imaging appearance on time resolved MRA of commonly encountered vascular lesions of the head and neck.

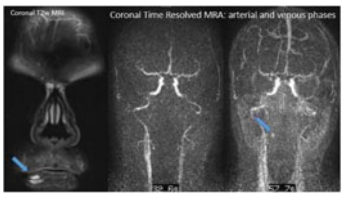

Poster #: CR-040

Case Report of a 4-year-old with Myositis Ossificans secondary to Non-accidental Trauma

Vasant Garg, MD, *Radiology, University Hospital Case Medical Center, Cleveland, OH, Vasant.Garg@UHHospitals.org;* Sasan Partovi, MD, Pauravi Vasavada, Dayna Weinert, Sheila Berlin, Lolita McDavid, Carlos Sivit
Disclosures: All authors have disclosed no financial interests, arrangements or affiliations in the context of this activity.

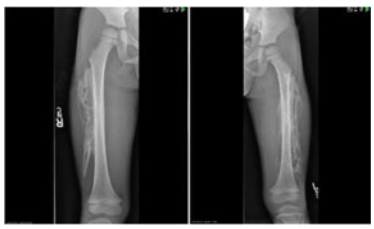

Purpose or Case Report: We present a rare Case Report Exhibit of a 4-year child with myositis ossificans secondary to non-accidental trauma. The child presented to the ER complaining of a headache. Head CT was unremarkable. However, initial physical examination revealed numerous bruises over the lower abdomen and thighs including belt marks. The patient also demonstrated restricted range of motion. A skeletal survey showed multiple remote fracture deformities and myositis ossificans extending the length of both femurs. Although myositis ossificans frequently occurs in athletes who sustain blunt injury, this unfortunate case occurred secondary to non-accidental trauma and specifically the caregiver intentionally standing on the patient's legs. Pediatric radiologists should be mindful of non-accidental trauma as a potential cause of myositis ossificans, especially in very young children and when multifocal.
Methods & Materials: We are presenting a Case Report Exhibit. Our presentation will not contain a "Methods and Materials" section.
Results: We are presenting a Case Report Exhibit. Our presentation will not contain a "Results" section.
Conclusions: Please see "Purpose or Case Report" above.

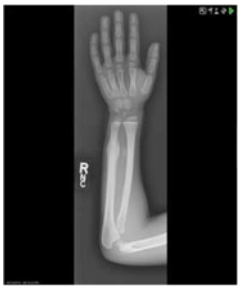

Poster #: CR-041

Wernicke's Encephalopathy in the Pediatric Patient

Angela Beavers, MD, *Radiology, UNMC, Omaha, NE, angela.beavers@unmc.edu;* Sandra Allbery, MD

Disclosures: All authors have disclosed no financial interests, arrangements or affiliations in the context of this activity.
Purpose or Case Report: Wernicke's encephalopathy, traditionally a clinical diagnosis, may present a diagnostic conundrum, particularly those cases that do not present with the clinical triad of ataxia, ocular abnormalities, and mental status changes. MR imaging is often employed in the work-up of patients with altered mental status, and although the imaging findings of Wernicke's encephalopathy are non-specific, suggestion of the diagnosis on imaging in conjunction with clinical findings can enable treatment of a potentially reversible encephalopathy, which may otherwise result in significant morbidity and mortality if the diagnosis is delayed or missed. A case is presented with MR images characteristic of Wernicke's encephalopathy, in which the patient had clinical resolution of her symptoms following thiamine administration. The patient in this case had short gut syndrome complicated by sepsis, which likely contributed to her thiamine deficiency. Given the underdiagnosis of Wernicke's encephalopathy in the pediatric population and the general safety of intravenous thiamine, being able to suggest the diagnosis based on MR imaging can potentially significantly influence patient outcomes.

Poster #: CR-042

Management of Congenital Portosystemic Shunts in Children with Stent

Josée Dubois, MD, *Medical Imaging, CHU Ste-Justine, Montreal, QC, Canada, josee-dubois@ssss.gouv.qc.ca;* Frederic Thomas-Chausse, Rafik Ghali, Gilles Soulez

Disclosures: All authors have disclosed no financial interests, arrangements or affiliations in the context of this activity.
Purpose or Case Report: Congenital portosystemic shunt is a rare vascular malformation that leads to severe complications. Two types are described: extrahepatic and intrahepatic. Extrahepatic shunt is represented by a direct communication of the portal trunk, or one of its branches of origin, to the inferior vena cava, or one of its branches.
We present two cases of extrahepatic shunt treated with stent-graft placement.
Case 1: Two y.o. male with cutaneous telangiectasias and liver calcifications on abdominal ultrasound. An extrahepatic portosystemic shunt was detected on color Doppler examination.
MR and catheter angiography revealed a large fistula between the main portal vein and the suprarenal inferior vena cava. The fistula was closed by deploying a balloon expandable stent-graft in the retrohepatic inferior vena cava. Five years later, the liver function was normalized and no complication was observed.

Case 2: Thirteen years old male referred for three hepatic lesions and an extrahepatic portosystemic shunt.
MR and angiography revealed a large fistula between the left portal vein and the inferior vena cava. It was closed by deploying a custom self-expandable stent-graft (Zenith, Cook Medical, Bloomington, IN) in the inferior vena cava. At 5 years follow-up, the patient is asymptomatic with a resolution of the liver lesions.
Conclusions: Stent-graft placement in inferior vena cava to close large extrahepatic portosystemic shunt is an alternative to open surgery, especially when the fistula cannot be occluded by coil or amplatzer plugs.

Poster #: CR-043

Postoperative Intussusception on MRI: A Case Report and Review of the Literature

Jane Kim, M.D., *University of Maryland Medical Center, Baltimore, MD, janekim80@gmail.com;* Jeannie Chun, Wendy Kim, MD, Cara Morin, Narendra Shet, MD

Disclosures: All authors have disclosed no financial interests, arrangements or affiliations in the context of this activity.
Purpose or Case Report: Postoperative intussusception is a rare complication with a reported rate of 0.01-0.25% in children following laparotomy, accounting for 5-10% of postoperative bowel obstruction. We present a case of a 6-month-old infant with increasing abdominal fullness over several weeks who was found to have a large left renal mass. Following surgical resection of an atypical cellular form of Congenital Mesoblastic Nephroma, the patient developed abdominal distension and was presumed to have a postoperative ileus. Due to unexplained persistent hypertension following surgery, MR Angiogram of the Abdomen was performed to evaluate the renal arteries. On this MR exam, a right lower quadrant ileocolic intussusception was identified. Air enema intussusception reduction attempt was unsuccessful, and laparotomy was performed with successful reduction. We review the literature on pediatric postoperative intussusception including the variety of initial surgical operations, clinical symptoms, intussusception type, treatment, and patient outcomes.
Conclusions: Intussusception is a rare but important complication to recognize following surgery in children, usually presenting with atypical symptoms, and should be considered in cases with postoperative bowel obstruction.

Poster #: CR-044

Imaging of the Thoracic Inlet in Morquio A Syndrome

Lauren Averill, MD, *Nemours / A.I. duPont Hospital for Children, Wilmington, DE, laverill@nemours.org;* Shunji Tomatsu, Mary Theroux

Disclosures: All authors have disclosed no financial interests, arrangements or affiliations in the context of this activity.
Purpose or Case Report: Morquio A syndrome is an autosomal recessive lysosomal storage disorder characterized by skeletal dysplasia and progressive disability due to orthopedic complications, spinal cord compression and airway compromise. Although the bony changes and cervical spine instability have been well described in the radiology literature, the importance of imaging the airway in these patients has received scant attention. The purpose of this poster is to illustrate the progressive abnormality of the thoracic inlet and trachea seen in children and young adults with Morquio A syndrome.
The interplay of pectus carinatum, hypertrophied clavicular heads and upper thoracic kyphosis leads to bony narrowing of the thoracic inlet. Furthermore, glycosaminoglycan deposition degrades the structural integrity of the tracheal wall, creating a twisted and floppy airway. Additional crowding by a crossing tortuous right brachiocephalic artery and sometimes the thyroid gland contribute to progressive narrowing of the trachea at the thoracic inlet. Imbalance of growth between the skeleton and the airway and blood vessels may also play a role.
We present a series of patients with Morqiuo A syndrome, with multimodality imaging depicting the complex anatomy of the thoracic inlet contributing to airway compromise. Radiographs of the neck, chest or spine can suggest airway narrowing with a tilted hourglass shape of the trachea seen in the frontal projection; lateral views, though, are often limited. MRI of the cervical spine, frequently acquired to evaluate the craniocervical junction, also allows for assessment of the thoracic inlet including the trachea and crossing right brachiocephalic artery. CT angiogram of the chest can more clearly delineate vascular, bony and airway relationships in individuals with declining respiratory function or unexpected airway difficulty during anesthetic management. Three dimensional rendering and airway fly-through techniques may help guide anesthetic care and, in extreme cases, airway reconstruction. The imaging features of the thoracic inlet in this group of Morquio A patients are correlated with clinical phenotype, pulmonary function tests, and bronchoscopy when available.

Poster #: CR-045

Synchronous Gastric and Ileal Trichobezoars Causing Small Bowel Obstruction

Denise Castro, *The Hospital for Sick Children, University of Toronto, Toronto, ON, Canada, denisecastro22@gmail.com;* Cecília Silva, Isabela Paranhos, Andréa Lira, Josélia Fonseca, Rafaela Ribeiro

Disclosures: All authors have disclosed no financial interests, arrangements or affiliations in the context of this activity.
Purpose or Case Report: A 10-year-old girl presented with 18-h history of crampy periumbilical pain, associated with three episodes of nonbilious vomiting and anorexia over the past few days. She denied fever and had a normal bowel movement 1 day before admission. She had no medical history and was not on any medication. Her social development and school performance were both unremarkable. On physical examination, the abdomen was distended, tender in the periumbilical area, with normal bowel sounds and no peritoneal signs.
The abdominal radiograph showed air-fluid levels with distended small bowel loops and a large heterogeneous mass conforming to the shape of the stomach and a possible distended loop with mottled gas pattern in the mid pelvis, to the left of the midline. Six hours later, while in the hospital, the patient developed bilious vomiting and a computed tomography (CT) showed a mottled air-containing large mass within the stomach and a second smaller similar appearing mass within a segment of small bowel in the left lower quadrant, with diffuse distension of small bowel loops and multiple air-fluid levels proximal to it, in keeping with small bowel obstruction (SBO). The patient admitted to trichotillomania and trichophagia and a patch of alopecia was noted in the left parietal scalp. She was sent to the operating room where a supraumbilical vertical midline incision was made and a large obstructing trichobezoar completely filling the gastric lumen was removed through a transverse gastrotomy. The small bowel was inspected and a palpable, obstructing smaller trichobezoar was removed from the jejunum, approximately 1 meter from the pylorus.
Trichobezoars form after the ingestion of large amounts of hair, often over many years. Although trichotillomania affects about 1% of the population, only one third have trichophagia and just 1% of these individuals eat enough hair to require surgical intervention, making trichobezoars very uncommon in clinical practice. They are usually single and seen in the stomach, but in 5% of cases more then one bezoar is found. SBO occurs in fewer than 10% of patients with trichobezoar.

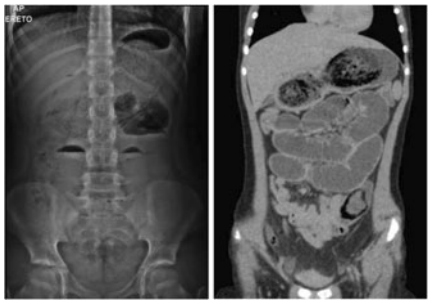

Plain radiographs are usually the initial imaging tool for diagnosis of SBO. CT can be helpful in determining the presence of obstruction in clinically suspected cases with equivocal plain radiographs, and determining the site and cause of obstruction, including trichobezoars.
Poster #: CR-046

The Natural History of Pectus Excavatum: An Unusual Illustration of Deformity Progression

Kathryn Henault, MD, *Radiology, Hartford Hospital, Burlington, CT, henaultk@gmail.com;* Douglas Moote, Brendan Campbell

Disclosures: All authors have disclosed no financial interests, arrangements or affiliations in the context of this activity.
Purpose or Case Report: Pectus excavatum is a deformity that affects 1-in-1000 children and causes 80% of all chest wall abnormalities. Although usually mild at a young age, it rapidly progresses during puberty requiring dedicated interval monitoring to assess the need for surgical intervention. This sudden acceleration is not without a physiological and psychological impact. Prior to surgery, the patient's cardiopulmonary status is assessed. In addition, the patient's psychological welfare should be monitored, given the known link of pectus excavatum with poor body image and social isolation.

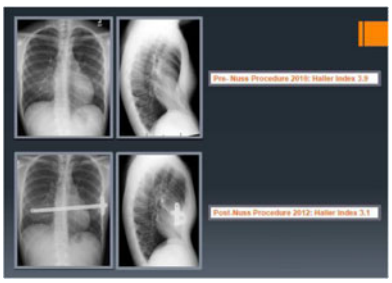

The Haller Index is the standard measurement to assess the severity of the pectus deformity. A calculated index of > 3.25 is a generally accepted marker of disease and the need for surgical correction. This number represents a ratio between the distance from the posterior sternum to the anterior spine and the widest transverse diameter of the chest wall.
There has been an evolution of treatment strategies since this deformity was first recognized. In the 16th century medical management consisted of fresh air and breathing exercises; in the early 20th century, treatment swung to the other end of the spectrum with radical surgery involving excision of the anterior chest wall. Since then, surgical procedures have advanced to the current minimally invasive standard of care that incorporates the malleability of the chest wall using reconfiguration and bracing. Bilateral chest wall incisions are made and a subcutaneous substernal tunnel is created. With this procedure in mind, the pre-pubertal patients (11-14 years) are the optimal age for surgical correction - providing the opportunity for the quickest recovery and excellent results.
This clinical case report is a unique look into the progression of pectus excavaum. The diagnosis was made by a radiologist through sequential abdominal CT scans performed to evaluate for recurrent disease for her Stage II Wilms Tumor. She was subsequently referred to a pediatric surgeon at the age of 12 for surveillance monitoring. Over the course of 2 years (2007-2009) the patient received biannually thoracic CT scans with progressively larger Haller Indices. Given the widening index and a new presentation of shortness of breath at the age of 14, the Nuss procedure was performed with an immediate improvement to the deformity. The bar remained in place for 2 years, and was successfully removed with only a mild pectus deformity remaining.

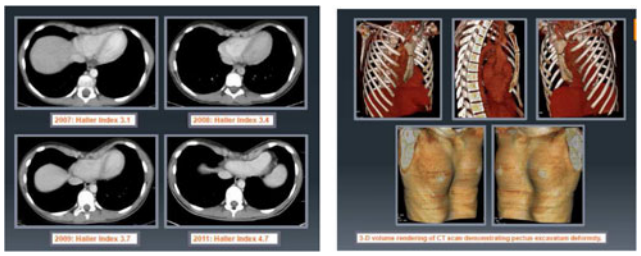

Poster #: CR-047

Fibroepithelial Stromal Polyp of the Vagina In An Infant- Clinical, Radiologic And Histologic Findings

Jared Green, MD, *Medical Imaging, Ann & Robert H. Lurie Children's Hospital of Chicago, Chicago, IL, jrgreen@luriechildrens.org;* Alok Jaju, Jamie Richard

Disclosures: All authors have disclosed no financial interests, arrangements or affiliations in the context of this activity.
Purpose or Case Report: A 17-month-old female presented with a 1-month history of abnormal soft tissue protruding from the vaginal introitus. The patient's past medical history was significant for hemi-hypertrophy of the left lower extremity. Physical examination demonstrated normal external genitalia, with pink solid tissue protruding from the vagina posterior aspect, and mild associated white fluid discharge. Laboratory analysis revelaed a normal CBC, serum HCG and AFP.
An ultrasound examination of the pelvis demonstrated a heterogeneous echogenicity soft tissue mass with scant internal vascularity centered in the vagina and cervix, measuring approximately 4.0×2.3×2.5 cm.
The patient's clinical and imaging findings were most concerning for malignancy, namely vaginal rhabdomyosarcoma, so consultation was requested from Pediatric Surgery and Oncology. As a result of these consultations, the patient was scheduled for vaginoscopy with biopsy under general anesthesia, as well as surgical port placement due to the high suspicion for malignancy. Also to be performed under the same anesthetic was a CT examination of the chest and MR examination of the pelvis.
Vaginoscopy revealed a "pebbly appearance" of the vaginal walls, which also reportedly "felt thickened" on digital exam. Multiple surgical biopsy specimens were obtained from the visibly abnormal areas.
MR examination immediately post biopsy showed circumferential mural thickening of the cervix and vagina, with a more prominent area of soft tissue thickening at the level of the vaginal introitus. The areas of mural thickening appeared T1 and T2 signal isointense with mild post-contrast enhancement and no evidence of abnormal restricted diffusion. No focal mass was identified. CT examination of the chest was normal.
Histopathologic analysis revealed a benign lesion composed of a relatively small number of spindle cells embedded in a loose fibrous stroma. No significant numbers of mitoses or atypia were observed, including in the

lining squamous epithelium. These features were most consistent with a fibroepithelial stromal polyp.
In light of the pathology findings, the port implant was removed, and the patient has since undergone surveillance vaginoscopy examinations.
This case illustrates MRI findings of a rare benign condition which may mimic vaginal rhabdomyosarcoma on the basis of clinical and ultrasound findings. MRI demonstrating an absence of aggressive features may help to suggest this rare differential consideration.

Poster #: CR-048

Traumatic Aortic Injury in the Setting of Radiolucent Foreign Body

Pamela Deaver, MD, *Texas Children's Hospital, Houston, TX, pamela.deaver@gmail.com;* Prakash Masand

Disclosures: All authors have disclosed no financial interests, arrangements or affiliations in the context of this activity.
Purpose or Case Report: In a child with escalating hemoptysis, negative TB testing, and history of penetrating thoracic trauma, chronic inflammation and

vascular injury as a result of radiolucent foreign body should be considered.
Methods & Materials: A previously healthy 8.5 year old female presented with 10 months of escalating hemoptysis, prompting admission to an outside facility.
18 months prior to the onset of hemoptysis, the patient was playing hide and seek among pine trees, which resulted in wooden pine needles penetrating her anterior chest. Her parents removed part of one, but they felt it broke off and brought her to the ER, where she underwent bedside and subsequently surgical exploration of the anterior chest wall. No foreign body was identified. Radiography revealed no radiopaque foreign body.
She underwent multiple tests for TB, with all results negative. She was empirically started on 4 drug TB therapy given radiographic findings of chronic consolidation in the right upper lobe. Laboratory data was otherwise significant for anemia.
Results: She underwent CTA at our institution, which revealed pseudoaneurysm of the ascending aorta with a subtle linear filling defect at this level. There was adjacent soft tissue thickening in the mediastinum and consolidation within the anterior right upper lobe. Associated lymphadenopathy was also noted. Right bronchial artery hypertrophy was also present.
These findings in combination were suspicious for traumatic injury to the ascending aorta with pseudoaneurysm formation, either as a consequence of radiolucent foreign body or chronic inflammatory state secondary to foreign body in adjacent lung parenchyma with formation of a mycotic aneurysm.
Preoperatively, the patient went to angiography for embolization of the right bronchial artery and diagnostic aortogram to confirm the CT findings.
At surgery, a 5 cm wooden pine needle was recovered from the patient's right upper lobe, and the aortic pseudoaneurysm was repaired with a pericardial patch.
Treatment for TB was ceased.
Conclusions: Wooden and other radiolucent foreign bodies are an important cause of morbidity in children. Although traumatic aortic injury is rare, the diagnosis could have been made more promptly with a high level of suscpicion paired with the knowledge that radiography may not reveal radiolucent foreign bodies. Sonography is of benefit in other areas, though aerated lung in the chest makes imaging for thoracic radiolucent foreign body challenging. CT or MR angiography should be considered in these patients.

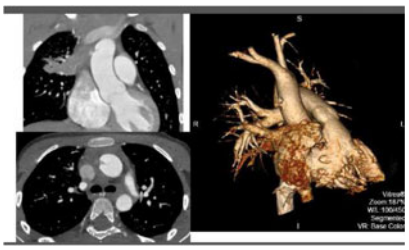

Poster #: CR-049

Brown Fat Necrosis with Calcifications in the Newborn: Risk Factors, Radiographic Findings, and Clinical Course

Eleza Golden, MD, *Radiology, Emory University, Atlanta, GA, eorenst@emory.edu;* Stephen Simoneaux, Paula Dickson, M.D.

Disclosures: All authors have disclosed no financial interests, arrangements or affiliations in the context of this activity.
Purpose or Case Report: To describe the radiographic appearance of subclinical calcified brown fat necrosis and to delineate the associated clinical and laboratory findings. While brown fat necrosis has been described in infants with underlying cardiac disease treated with prostaglandins, we emphasize hypotension from cardiac or respiratory arrest as a primary risk factor.
Methods & Materials: PACS was searched using keywords "soft tissue calcification" and "chest." The clinical record was searched for history of cardiac surgery, bypass, ECMO, prostaglandin use, hypoxia, age when calcifications were first detected, location, resolution, and associated hypercalcemia, thrombocytopenia, and elevated triglycerides. Renal results were evaluated for nephrocalcinosis.
Results: 5 patients were found. 3 were premature. None had skin lesions on exam. All had underlying congenital heart disease and experienced cardiac and/or respiratory arrest with hypotension between 1 week and 6 weeks before soft tissue calcifications were detected. Single ventricle physiology was the most common lesion (1 tricuspid atresia, 2 hypoplastic left heart syndrome). 3 received prostaglandin therapy. Soft tissue calcifications occurred bilaterally in areas of brown fat in the cervical, supraclavicular, and peri-scapular soft tissues and axilla. 2 patients had resolution by 9 weeks and 5 months. Hypercalcemia was present in 3 (60%), thrombocytopenia in 2 (40%), and elevated triglycerides in all 5 (100%). Renal ultrasound was performed in all patients with 1 with nephrocalcinosis.
Conclusions: Brown fat necrosis is subclinical, diagnosed on plain film, and likely self-limited. It may be a marker of prior systemic stress. It has previously been described in term infants with congenital heart disease treated with prostaglandins. Rather than medication related, it may be related to hypoxic/ischemic insult and occurs in both term and premature infants with underlying cardiac disease who experience cardiac or respiratory arrest with hypotension. Similar to other studies, several patients demonstrated mild hypercalcemia, thrombocytopenia, and all had elevated triglycerides. However, other studies have suggested that severe hypercalcemia can occur up to 6 months of age and the radiologist can help identify patients that need to be followed. Additionally, renal ultrasound should be considered to evaluate for nephrocalcinosis.

	Age (weeks)	Age at first appearance of calcifications (weeks)	Location (bilateral)	Resolution	Cardiac Risk factors	Hypercalcemia (mg/dL)	thrombocytopenia	Elevated Triglycerides (mg/dL)
1	35	6	axilla	unknown	Trisomy 18, large VSD, multiple apneic episodes	Yes 11.1	no	Yes 224
2	36	8	Cervical, supraclavicular, perscapular abdomen	Yes by 5 months of age	Tricuspid atresia, cardiac arrest and ECMO	yes 12.3	yes	Yes 520
3	32	24 days	Around the clavicles	unknown	HLHS, bypass, and induced hypothermia	no	no	Yes 171
4	39	3	Cervical, supraclavicular, perscapular abdomen	unknown	HLHS, bypass, required ECMO	yes 11.3	yes	Yes 447
5	39	5	Anterior chect wall, cervical, axilla	Yes by 9 weeks	None	no		Yes 81

- HLHS=hypoplastic left heart syndrome

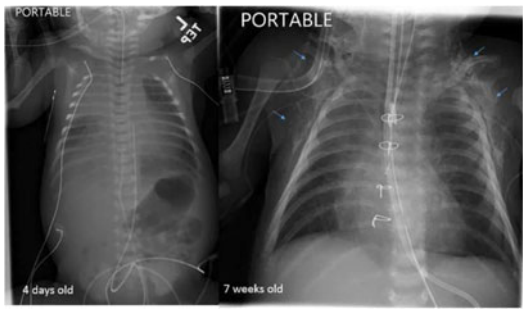

Poster #: CR-050

Pediatric Colonic Volvulus–The Role of CT in Diagnosis and Definitive Management

Aditi Hendi, M.D., *Thomas Jefferson University Hospital, Philadelphia, PA, aditi.hendi@jefferson.edu;* Mary Harty, Leslie Grissom

Disclosures: All authors have disclosed no financial interests, arrangements or affiliations in the context of this activity.

Purpose or Case Report: Pediatric colonic volvulus is very rare with 40% mortality, making diagnosis time-sensitive. Surgeons rely on imaging confirmation, but sensitivity of plain film is low and contrast enema is contraindicated in patients with acute abdomen. Alternatively, CT is a safe, sensitive modality and aids in pre-operative planning. We identified 11 patients over 10 years with colonic volvulus, of which 5 are chosen to describe the role of CT in work-up.

Case 1: A 12 yo male with Prune-Belly Syndrome and prior abdominal surgery presents with a day of abdominal distention. Radiography was initially concerning for small bowel obstruction. He deteriorated and the next day CT showed necrotic, distended colon in the midline. Exploratory laparotomy 24 h after presentation revealed volvulus and necrosis of the mid transverse colon, and partial colectomy was performed.

Case 2: A 17 yo female with cerebral palsy, mental retardation and prior abdominal surgery presents with a day of abdominal distension. Radiography was concerning for volvulus. Barium enema confirmed cecal volvulus but did not decompress the bowel. Rectal tube trial was also unsuccessful. Exploratory laparotomy 2 h after presentation revealed 720° cecal volvulus and ileocecectomy was performed.

Case 3: A 4 yo female with chronic constipation presented with 12 h of severe abdominal pain. Radiography was initially concerning for small bowel obstruction, but CT showed transverse colonic volvulus. Four hours after presentation, the transverse colonic volvulus was detorsed and bowel was preserved during laparotomy.

Case 4: A 10 yo male with chronic constipation presented with severe abdominal pain. Radiography was nonspecific but CT showed fecal impaction and cecal volvulus. Exploratory laparotomy 6 h after presentation confirmed cecal volvulus, which was detorsed and partial cecectomy was performed.

Case 5: A 15 yo male with Goldenhar syndrome, chronic constipation and prior abdominal surgery presents with a day of severe abdominal pain. CT showed cecal volvulus, reduction of which was unsuccessful with contrast enema. During exploratory laparotomy 12 h after presentation, a 720° cecal volvulus was detorsed and bowel was preserved.

Conclusions: Imaging work-up of colonic volvulus depends on the clinical stability and needs of the patient. CT should be considered in patients with acute abdomen, perhaps before conservative management, as it minimizes time to diagnosis, possibly facilitating bowel preservation.

Poster #: CR-051

Preaortic Iliac Confluence - Rare or Often Overlooked Anatomical Variant

Patrick Bacon, MD, *Radiology, Children's Mercy Hospital, Kansas City, Kansas City, MO, pnbacon@cmh.edu*

Disclosures: All authors have disclosed no financial interests, arrangements or affiliations in the context of this activity.

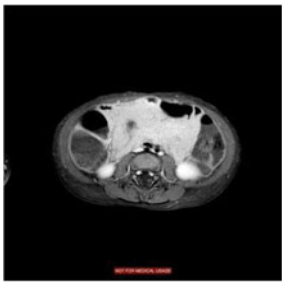

Purpose or Case Report: Congenital anomalies of the inferior vena cava (IVC) may easily be overlooked and present difficulties during abdominal and intravascular surgeries. Being aware of even the less common of these anatomical variations is essential. We present two cases of preaortic iliac confluence found incidentaly within the last year. The preaortic iliac confluence is described as a very rare variant with less than 50 reported cases within the last century. Also known as marsupial vena cava, it is a congenital anomaly of the development of the IVC in which the IVC is located anterior to the aortic bifurcation or the right common iliac artery. Both of the cases presented here coincide with additional congenital abnormalities which suggests an error of early embryogenesis may play a role in the development of this variant. Both of these cases were not identified on initial CT or MRI studies. It is possible that this variant is more common than previously thought but is often overlooked because of a lack of awareness of it's existance. Imaging findings on CT, with and without contrast, and MRI will be reviewed.

Poster #: CR-052

Rectosigmoid Venous Malformation Presenting with Longstanding Hematochezia and Anemia

Jonathan Berger, **Anna Thomas, MD,** *Le Bonheur Children's Hospital & UTHSC, Memphis, TN, annakthomasmd@gmail.com;* Clint Teague

Disclosures: All authors have disclosed no financial interests, arrangements or affiliations in the context of this activity.

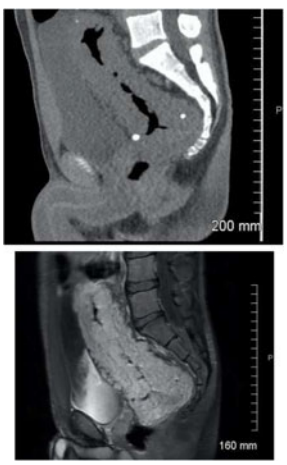

Purpose or Case Report: * To present a rare case of rectosigmoid venous malformation in a 15-year old male patient without Klippel Trenaunay Syndrome.
* To review common syndromic and nonsyndromic causes of pediatric lower gastrointestinal bleeding with presentation of relevant imaging.
* To discuss the classic imaging features and various treatment options for colorectal venous malformations.
Methods & Materials: While preserving anonymity, we will present the imaging and clinical findings of a teenager with colorectal venous malformation who came to our institution with a 2 year history of anemia and intermittent hematochezia. This patient had an extensive workup including Meckel's scan, upper endoscopy, colonoscopy, CT, and MRI. This patient had imaging features classic for a large venous malformation confined to the rectosigmoid and did not meet the clinical criteria for Klippel Trenaunay syndrome. Although there have been older reported cases of colorectal cavernous hemangiomas (a misnomer and term no longer preferred) without associated vascular malformation syndromes, nonsyndromic colorectal venous malformations are rarely reported.
We have also performed an extensive medical literature search for colorectal venous malformations, and syndromic and nonsyndromic causes of lower gastrointestinal bleeding in pediatric patients.
Results: We will present a case of colorectal venous malformation with lower gastrointestinal bleeding that had a delayed diagnosis. We will review the clinical and imaging features of colorectal venous malformations. We will also review other common causes of lower gastrointestinal bleeding in the pediatric patient with presentation of relevant imaging where applicable.
Conclusions: Colorectal venous malformations are an under recognized cause of gastrointestinal bleeding in the pediatric patient and therefore the diagnosis is often delayed resulting in patient morbidity. While colorectal venous malformations are often seen in the setting of vascular malformations syndromes such as Klippel Trenaunay, nonsyndromic colorectal venous malformations can occur. We hope that this case report will provide an educational review and increase awareness of lower gastrointestinal bleeding from underlying vascular malformations.

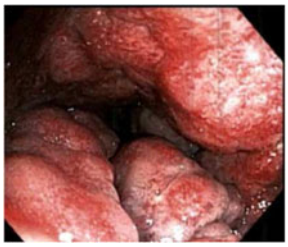

Poster #: CR-053

Imaging Characteristics of Large Hepatic Masses in the Adolescent Population

Jeffrey Gnerre, M.D., *Radiology, Westchester Medical Center, Valhalla, NY, gnerrej@wcmc.com;* Angela Tong, Jason Jimenez-Ocasio, Leslie LeCompte

Disclosures: All authors have disclosed no financial interests, arrangements or affiliations in the context of this activity.
Purpose or Case Report: Cancer is the most common cause of disease-related mortality for adolescent patients, 13-19 years of age. Primary liver neoplasms are relatively uncommon entities in this population accounting for 0.5-2.0% of all neoplasms as per the current literature. The most common primary liver malignancy in adolescent patients is hepatoblastoma, which accounts for approximately two thirds of liver tumors. Benign tumors of the liver in the adolescent population include adenomas, focal nodular hyperplasia, hamartomas, and vascular tumors.

Hepatic neoplasms in adolescent patients are typically not detected clinically until they reach a large size. While there are many exceptions, these patients generally have normal liver function as well as normal growth and development. In this case series, we examine the imaging characteristics across multiple modalities of several large primary hepatic neoplasms in the adolescent population encompassing both benign and malignant as well as common and uncommon entities. We will also review how the underlying pathophysiology of these neoplasms relates to their imaging appearances. Cross-sectional imaging with MRI or CT, similar to evaluation in adult patients, is considered the best method of evaluating the character and extent of hepatic masses. However, initial workup usually includes plain film x-ray or ultrasound. Benign and malignant hepatic neoplasms in the adolescent population share many similar radiographic features, and therefore, knowledge of these entities and their imaging appearances is essential in order to develop an appropriate differential diagnosis.

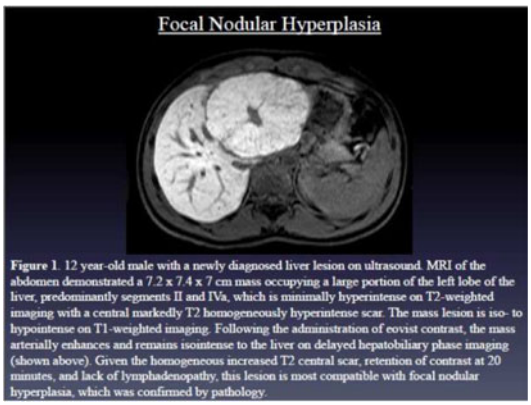

Figure 1. 12 year-old male with a newly diagnosed liver lesion on ultrasound. MRI of the abdomen demonstrated a 7.2 x 7.4 x 7 cm mass occupying a large portion of the left lobe of the liver, predominantly segments II and IVa, which is minimally hyperintense on T2-weighted imaging with a central markedly T2 homogeneously hyperintense scar. The mass lesion is iso- to hypointense on T1-weighted imaging. Following the administration of eovist contrast, the mass arterially enhances and remains isointense to the liver on delayed hepatobiliary phase imaging (shown above). Given the homogeneous increased T2 central scar, retention of contrast at 20 minutes, and lack of lymphadenopathy, this lesion is most compatible with focal nodular hyperplasia, which was confirmed by pathology.

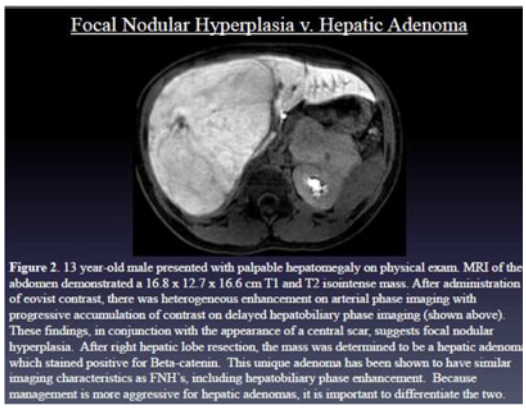

Figure 2. 13 year-old male presented with palpable hepatomegaly on physical exam. MRI of the abdomen demonstrated a 16.8 x 12.7 x 16.6 cm T1 and T2 isointense mass. After administration of eovist contrast, there was heterogeneous enhancement on arterial phase imaging with progressive accumulation of contrast on delayed hepatobiliary phase imaging (shown above). These findings, in conjunction with the appearance of a central scar, suggests focal nodular hyperplasia. After right hepatic lobe resection, the mass was determined to be a hepatic adenoma which stained positive for Beta-catenin. This unique adenoma has been shown to have similar imaging characteristics as FNH's, including hepatobiliary phase enhancement. Because management is more aggressive for hepatic adenomas, it is important to differentiate the two.

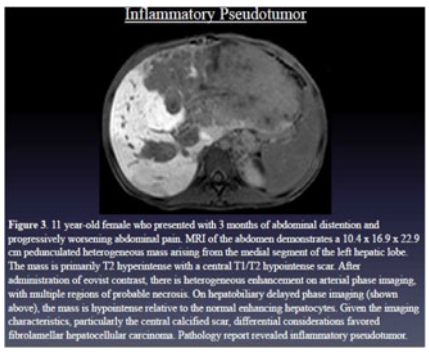

Figure 3. 11 year-old female who presented with 3 months of abdominal distention and progressively worsening abdominal pain. MRI of the abdomen demonstrates a 10.4 x 16.9 x 22.9 cm pedunculated heterogeneous mass arising from the medial segment of the left hepatic lobe. The mass is primarily T2 hyperintense with a central T1/T2 hypointense scar. After administration of eovist contrast, there is heterogeneous enhancement on arterial phase imaging, with multiple regions of probable necrosis. On hepatobiliary delayed phase imaging (shown above), the mass is hypointense relative to the normal enhancing hepatocytes. Given the imaging characteristics, particularly the central calcified scar, differential considerations favored fibrolamellar hepatocellular carcinoma. Pathology report revealed inflammatory pseudotumor.

Poster #: CR-054

Congenital Glioblastoma Multiforme: A Unique Case Report of a Rare Intracranial Tumor

Kathryn Henault, MD, *Radiology, Hartford Hospital, Burlington, CT, henaultk@gmail.com;* Paul Kanev, Michael O'Loughlin

Disclosures: All authors have disclosed no financial interests, arrangements or affiliations in the context of this activity.

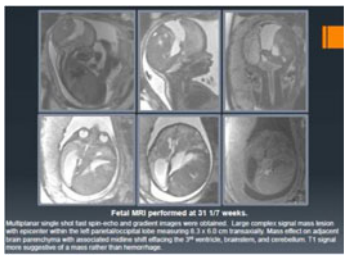

Purpose or Case Report: Congenital glioblastoma multiforme (cGBM) is the rarest type of congenital brain tumors, constituting approximately 3.5% of cases according to the latest literature, with roughly 60 cases published worldwide. This specific presentation can be defined as 'definitely congenital', based on the 1964 classification of congenital tumors by Solitare and Krigman. The case report discusses the clinical presentation, radiologic and histologic findings, treatment, and prognosis of cGBM.

The tumor was first detected on an ultrasound at 31 weeks gestation, performed for a clinical diagnosis of mild oligohydramnios, revealing an unexpected large intracranial lesion. Prior to this finding, the pregnancy course was uneventful - the fetus was naturally conceived by a 30-year-old G2P1001 without history of infection, radiation, or trauma. No concerning maternal past medical history or use of drugs/alcohol during pregnancy. No family history of CNS malignancy was documented. MRI performed at 31 3/7 weeks confirmed a large complex cystic and solid mass lesion, bigger than previously measured on the aforementioned ultrasound, with mixed T1 and T2 signal within the left parietal/occipital lobe. Findings were concerning for a mass lesion, specifically a GBM given the size and complex signal characteristics. A second ultrasound preformed 12 days later showed even further growth, raising suspicion for a rapidly enlarging tumor. A pediatric neurosurgeon and maternal fetal medicine team following the patient had preemptively decided to deliver the fetus at 36 weeks due to increasing macrocephaly, with a plan for postnatal biopsy to establish pathology before a definitive treatment plan was ascertained. Unfortunately the mother presented to the clinic at 33 1/7 weeks with no fetal movement and an ultrasound confirmed intrauterine demise. After a classic Cesarean section, an autopsy confirmed a diagnosis of cGBM. No other congenital abnormalities were revealed.

Although fetal brain tumors are exceedingly rare, it is imperative to diagnose them in-utero due to potential prenatal and postnatal complications. Comorbidities such as polyhydramnios, spontaneous intracranial hemorrhage, dystocia during delivery, and immediate postnatal heart failure should be continually evaluated for. Knowledge of an intracranial mass will allow providers to appropriately plan the mood of delivery and immediate postnatal course with necessary specialists available for immediate intervention.

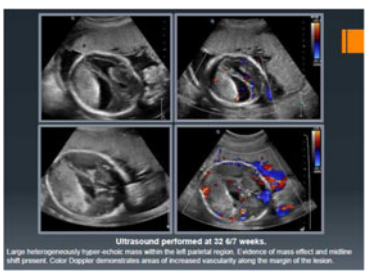

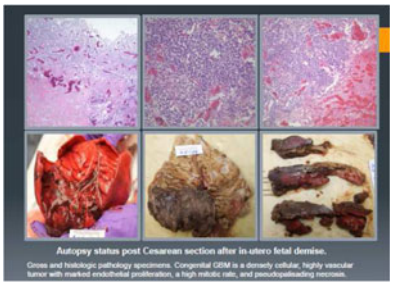

Poster #: CR-055

Radiographic Manifestations of DICER1 Mutation Mosaicism

Ruri Lee, *Radiology, Westchester Medical Center, Valhalla, NY, ruri.rachel@gmail.com;* Perry Gerard, Claudio Sandoval, MD

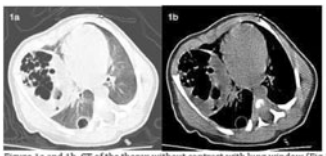

Figure 1a and 1b. CT of the thorax without contrast with lung window (Fig 1a) and soft tissue window (Fig 1b) shows a large multicystic lesion in the right middle lobe.

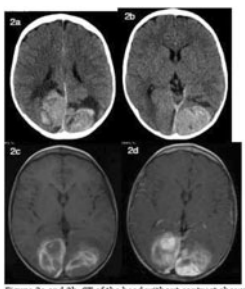

Figure 2a and 2b. CT of the head without contrast shows predominantly hyperdense lesions in the bilateral parieto-occipital lobes, reflecting hemorrhagic metastases.

Figure 2c and 2d. MRI of the brain without and with contrast. T1 pre- (Fig 2c) and post-contrast (Fig 2d) sequences show corresponding T1 hyperintensity and avid enhancement within the metastatic lesions.

Disclosures: All authors have disclosed no financial interests, arrangements or affiliations in the context of this activity.

Purpose or Case Report: DICER1 is an RNA endoribonuclease that plays a role in the biogenesis of microRNAs (miRNAs). These miRNAs regulate gene expression by suppressing the translation of messenger RNA (mRNA) into proteins. Dysfunction of this mRNA suppression can result in oncogenic transformation. Patients with germ-line mutations of the DICER1 gene are predisposed to the development of certain organ-based childhood neoplasms such as pleuropulmonary blastoma (PPB), cystic nephroma (CN), nasal chondromesenchymal hamartoma (NCMH), and other rare tumors.

Our case report describes a patient who presented with multiple primary tumors consistent with DICER1 syndrome but tested negative for germ-line DICER1 mutation. Somatic DICER1 mutation with resultant mosaicism resulting in this phenotypic presentation has been recently described (de Kock et al. J Med Genet 2015); however, this DICER1 mosaicism is an extremely rare phenomenon with very few cases reported in literature. Here we describe the radiographic manifestations of a patient with such mosaicism of DICER1.

Our patient was initially diagnosed with pulmonary cystic lesions on prenatal ultrasound. Initial non-contrast CT of the thorax was performed on the first day of life and showed cystic lesions in both the right middle and lower lobes. A predominant lesion in the right middle lobe contained multiple cystic and possibly solid components (Figure 1). The patient subsequently underwent right middle lobe cyst resection with a final pathologic diagnosis of Type I PPB.

At 9 months of age, the patient experienced repeated episodes of intussusception. Colonoscopy showed multiple polyps that were removed and returned benign pathology. At 2 years of age, the patient was diagnosed with Type II PPB. MRI of the brain was performed at that time, which showed large hemorrhagic metastases in the brain (Figure 2). He underwent multiple brain mass resections as well as chemotherapy, radiation therapy, and stem cell transplant. Additionally, he was diagnosed with NCMH at 8 years of age.

Although our patient presented with multiple primary tumors that are characteristic of DICER1 germ-line mutation, genetic testing for germ-line DICER1 mutation yielded negative results. As this case illustrates, for patients presenting with this constellation of radiographic findings and pathologic diagnoses of characteristic rare organ-based neoplasms, further genetic testing for somatic DICER1 mutation mosaicism is necessary.

Poster #: CR-056

CT and Upper GI Findings of Esophageal Bronchi in Infants

Gabrielle Colleran, MD, MB BCh BAO, FFR RCSI, *Radiology, Boston Children's Hospital, Brookline, MA, gabrielle.colleran@childrens.harvard.edu;* Edward Lee, David Rea, Clare Brenner

Disclosures: All authors have disclosed no financial interests, arrangements or affiliations in the context of this activity.

Purpose or Case Report: Esophageal bronchi are a rare form of communicating bronchopulmonary foregut malformations (CBPFM) that can be seen in association with esophageal atresia.

Esophageal bronchi are rare but important causes of an opaque hemithorax on chest radiograph. This is especially pertinent in the setting of esophageal atresia (EA) and tracheo-esophageal fistula (TEF) and VACTERL (vertebral defects, anal atresia, cardiac defects, tracheo-esophageal fistula, renal anomalies, and limb abnormalities) anomalies as these conditions are associated with a higher incidence of esophageal bronchi.

The purpose of this case report series is describe the pertinent radiological features in four patients with esophageal bronchi.

Methods & Materials: A literature review was performed to evaluate the various approaches to imaging the infant with a suspected bronchial anomaly.

The radiological features with emphasis on CT and UGI findings of esophageal bronchi in four neonatal patients are described.

Results: Consolidation and atelectasis in conjunction with a low volume hemithorax and an abnormal carina or anomalous vascular anatomy suggest the possibility of an esophageal bronchus or an esophageal lung on CT.

Three of the four cases described occurred in the context of associated VACTERL anomalies. 2 of the 4 had EA and TEF.

None of the cases had a prenatal diagnosis but neither was the prenatal imaging normal. All demonstrated non-specific findings: two displayed polyhydramnios and two had intrauterine growth restriction.

CT Thorax is increasingly useful for establishing the diagnosis, confirmation of UGI findings and for assessment of parenchymal damage due to recurrent aspiration and infection.

Conclusions: The radiologist has a key role in guiding the multidisciplinary approach to the diagnosis and treatment of children with suspected bronchial anomaly.

Consolidation and atelectasis in conjunction with a low volume hemithorax, ipsilateral mediastinal shift and an abnormal carina or anomalous vascular anatomy suggest the possibility of an esophageal bronchus or an esophageal lung on CT.

While esophageal bronchi are a rare cause of a white hemithorax, CT and UGI imaging play key roles in its diagnosis.

Familiarity with this diagnostic approach and prompt consideration of this diagnostic entity is of great clinical importance as early diagnosis, prior to the development of aspiration pneumonia, may allow consideration to parenchymal sparing surgery as opposed to pneumonectomy.

Poster #: CR-057

Vaginal Ewing Sarcoma: An Uncommon Clinical Entity in Pediatric Patients

Nathan Cross, **A. Luana Stanescu, MD,** *University of Washington, Seattle, WA, stanescu@u.washington.edu;* Erin Rudzinski, MD, Doug Hawkins, MD, Marguerite Parisi, MD; MS

Disclosures: All authors have disclosed no financial interests, arrangements or affiliations in the context of this activity.

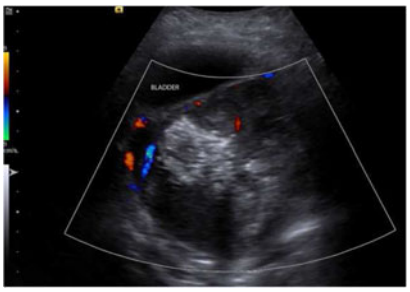

Purpose or Case Report: Ewing sarcoma is the second most common malignancy of bone with an incidence of approximately 200 cases per year in the United States in children under 20. Extraosseous Ewing sarcoma originating in the vagina is rare, with only 8 cases reported to date in the literature. These highly aggressive tumors require a more intensive treatment regimen compared to other vaginal masses like rhabdomyosarcoma. While the imaging findings are non-specific, awareness of this clinical entity can facilitate early diagnosis and appropriate treatment, which may improve prognosis.
Methods & Materials: We present two cases occurring in teenagers, one of them being the youngest case reported so far. Clinical data, imaging studies and pathology reports were reviewed. Both patients underwent chemotherapy, followed by surgery or surgery and radiation.
Results: Both our cases demonstrate a heterogeneous appearance on ultrasound and MR imaging, more conspicuous in the first case where a larger mass with extensive calcifications and areas of necrosis was present. Minimal necrosis and no definite calcifications characterized the second case, possibly due to the smaller size of the mass. Neither of these lesions demonstrated significant Doppler color flow, although a few serpentine flow voids were noted on MR in the second case. Both lesions showed restricted diffusion and heterogeneous contrast enhancement on MRI. FDG avidity of the primary lesions as well as metastatic lesions was noted.
Conclusions: Ewing sarcoma, including classical Ewing sarcoma of the bone and primitive neuroectodermal tumors arising in bone or extraosseous primary sites, is a highly aggressive childhood neoplasm. We describe the spectrum of multimodality imaging appearances of Ewing sarcoma at this unusual primary site. Since imaging is not definitive, a well structured differential diagnosis for a pediatric or adolescent patient with an aggressive pelvic (extra-ovarian) lesion should include: rhabdomyosarcoma, extraskeletal Ewing sarcoma, synovial sarcoma, malignant melanoma, and less frequently carcinoma. While biopsy is key in confirming the diagnosis, imaging remains critical in defining the extent of disease, in evaluating response to treatment and in the detection of recurrent/metastatic disease. Awareness of vaginal Ewing tumors may facilitate prompt diagnosis and lead to a different surgical approach than the more commonly encountered vaginal rhabdomyosarcoma.

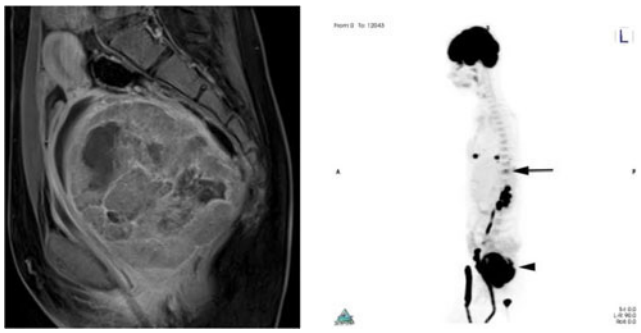

Poster #: CR-058

Canal of Nuck Hernia: A Case Series

Sarah Abdulla, Sameh Tadros, **Judy Squires, M.D.,** *University of Pittsburgh School of Medicine, Pittsburgh, PA, joodysquires@gmail.com*

Disclosures: All authors have disclosed no financial interests, arrangements or affiliations in the context of this activity.
Purpose or Case Report: The female anatomic equivalent of the male processus vaginalis is the canal of Nuck. The canal is formed from a small peritoneal protuberance from the round ligament that extends through the inguinal ring, into the inguinal canal, and terminates in the labia majora. Obliteration of the canal occurs in a superior to inferior direction and usually completes within the first year of life. Non-closure results in a persistent canal of Nuck. Very rarely herniation of abdominal and pelvic contents into the canal of Nuck can occur, much less commonly in females than in the male equivalent. Hernias can present at any age but are most common in children. Recognition of this entity is especially important in cases of ovarian herniation due to the risk of incarceration.
We will provide a review normal anatomy, potential canal contents, the imaging appearance on ultrasound, CT, as well as MRI, and discuss differential diagnosis using cases of canal of Nuck hernia in 4 patients aged 22 days though 17 years.

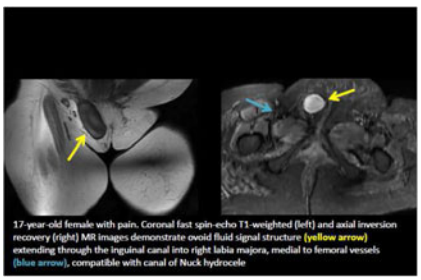

Poster #: CR-059

Leptomeningeal Dissemination at Initial Presentation of Gliomas in Children? What Does It Mean?

Nina Stein, Pediatric Radiologist, **Brij Karmur,** *Diagnostic Imaging, McMaster University, Mississauga, ON, Canada, brijkarmur@gmail.com;* Sheila Singh, Adam Fleming, MD

Disclosures: All authors have disclosed no financial interests, arrangements or affiliations in the context of this activity.

Purpose or Case Report: Leptomeningeal dissemination (LD) is a common occurrence in primary central nervous system tumours. The most common tumours that develop LD are medulloblastoma, germ cell tumours, and glial tumours. However, in gliomas, this occurrence is rare. It has been reported that only 2-5% of children with low-grade gliomas present with LD. Retrospective review of the Pediatric Brain Tumour Study Group database revealed 4 cases of gliomas with leptomeningeal enhancement at initial presentation: 2 cases of pilocytic astrocytoma, 1 case of glioblastoma multiform in the cervical spinal cord and 1 case of diffuse intrinsic pontine glioma. The presence of LD at initial presentation of gliomas usually indicates poor prognosis, even in cases of pilocytic astrocytoma. Therapeutics also become a chalenge in face of such a rare and diffuse finding. Differential diagnosis should be made imaging wise with possible infectious/inflammatory process giving LD and focal lesions simulating tumors. Identification of LD at initial diagnosis is of major importance for treatment options and prognostication of gliomas in children.

Poster #: CR-060

Asymptomatic Spontaneous Pneumoperitoneum and Pneumatosis Intestinalis in Anorexia Nervosa

Guy-Anne Massé-Bouillé, *Pediatrics, Hôpital Sainte-Justine, Montréal, QC, Canada, guyanne.m@gmail.com;* Danielle Taddeo, Olivier Jamoulle, Jean-Yves Frappier, Jean Wilkins, Marie-Claude Miron

Disclosures: All authors have disclosed no financial interests, arrangements or affiliations in the context of this activity.

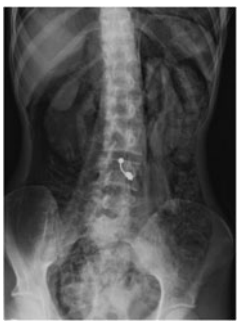

Purpose or Case Report: Anorexia nervosa is a condition with a wide range of presenting signs and symptoms. Our report describes an adolescent suffering from restrictive anorexia nervosa (no purging) who presented with a Body Mass Index (BMI) of 9,73 kg/m^2 and asymptomatic spontaneous subcutaneous emphysema, pneumomediastinum, pneumoperitoneum and pneumatosis intestinalis. History revealed fatigue, lower limbs weakness, jaw pain and swollen neck over the last few weeks but no abdominal complaints. She was successfully managed with supportive care and progressive enteral nutrition leading to a favourable outcome with significant weight gain (BMI of 12,1 kg/m^2 at discharge). Her clinical course was complicated by refeeding syndrome and Rotavirus gastroenteritis leading to a pre-shock state. We hypothesize that her clinical presentation was attributable to severe chronic undernourishment. Previous reports support the theory that severe undernourishment can lead to altered interstitial wall composition, which could result in migration of air through weakened alveolar or intestinal wall. This case is of interest given that spontaneous pneumoperitoneum and pneumatosis intestinalis have rarely been described in association with anorexia nervosa, especially in an asymptomatic patient. In addition, her favorable outcome suggests that these patients can effectively be managed with conservative care.

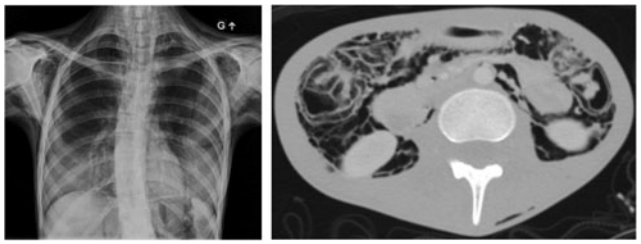

Poster #: CR-061

Terror-Tomas: Unusual Cases of Pediatric Germ Cell Tumors

Julia Singer, *Pediatrics, New York Medical College, Valhalla, NY, julia_singer@nymc.edu;* Jessica Bodea, Perry Gerard, Claudio Sandoval, MD

Disclosures: All authors have disclosed no financial interests, arrangements or affiliations in the context of this activity.

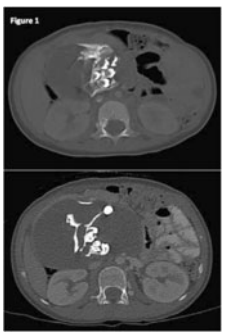

Purpose or Case Report: Germ cell tumors (GCT) comprise benign and malignant neoplasms arising from variation of normal differentiation of totipotent primordial germ cells. Pediatric GCT are rare, representing 3% of all malignant pediatric tumors with an estimated incidence of 0.9/100.000 children up to 15 years of age. Germ cell tumors are located in the gonads, sacrococcygeal region, retroperitoneum, anterior mediastinum and pineal gland. Herein we describe a case of fetus in fetu and maternal-fetal choriocarcinoma.

Methods & Materials: A clinical and radiographic review of 2 unusual pediatric GCT cases.

Results: Case 1 - Fetus in fetu - 7-month-old boy presented with non-bilious emesis and abdominal mass. Abdominal computed tomography showed a mass with cystic and solid components and bone. Laparotomy revealed a mass containing ribs and skull, and because of a shared blood supply was deemed unresectable. Postoperative serial computed tomographic evaluations showed dental eruptions (Figure 1). The mass was never resected and he remains alive and well 9 years post-biopsy.

Case 2 - Maternal-fetal choriocarcinoma - 32-year-old women presented with left shoulder pain and difficulty breathing during the 9th month of gestation. After delivery of a healthy appearing boy, she was diagnosed with stage 4 choriocarcinoma. Computed tomography of the chest revealed multiple lung nodules (Figure 2A). Concurrently, her 1-month-old baby boy was diagnosed with gestational choriocarcinoma. Computed tomography of the liver demonstrated a large heterogeneous hypervascular mass within the left hepatic lobe, situated between the middle and left hepatic veins (Figure 2B). Computerized tomography of the chest revealed peripheral nodular opacities in both lungs, and of the brain and orbits showed hemorrhage in the choroid of the right globe posteriorly and medially. Mother and infant were treated with cisplatin,

etoposide and bleomycin and had normalization of serum βHCG. Figure 3A and 3B reveal interval tumor responses. The mother and boy remain alive without any evidence of disease on physical examination and serum tumor marker, and the boy has no vision in the right eye and wears hearing aids.

Conclusions: Despite the unusual rarity of our cases they provide us with an opportunity to educate and fascinate our colleagues.

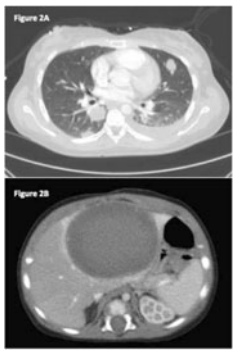

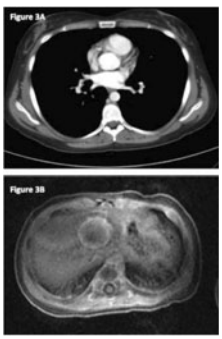

Poster #: CR-062

Anterior Bowing of the Intra-Thoracic Trachea: A Sign of Radiolucent Esophageal Foreign Body; a Report of 2 Cases

Mostafa Youssfi, MD, *Radiology, Phoenix Children's Hospital, Phoenix, AZ, myoussfi@phoenixchildrens.com*

Disclosures: All authors have disclosed no financial interests, arrangements or affiliations in the context of this activity.

Purpose or Case Report: Esophageal radiolucent foreign bodies can be overlooked in infants since the symptoms are usually non-specific. Chest X-Rays are often the initial diagnostic tool. The lateral view is key since it may reveal anterior bowing and/or focal narrowing of the intra-thoracic trachea which should alert the radiologist to the possibility of radiolucent esophageal foreign body and the need for an Esophagram. We present two cases that illustrate the importance of this radiographic finding.

Poster #: CR-063

Multimodal Imaging Findings in Children with PRES

Jonathan McGovern, MD, *Children's Hospital of Pittsburgh of UPMC - Department of Radiology, Pittsburgh, PA, mcgovernj@upmc.edu;* Giulio Zuccoli, Rakesh Goyal

Disclosures: All authors have disclosed no financial interests, arrangements or affiliations in the context of this activity.

Purpose or Case Report: To evaluate multimodal magnetic resonance imaging (MRI) characteristics in pediatric patients diagnosed with posterior reversible encephalopathy syndrome (PRES).

Table: Salient Clinical Features

	Age, y	Gender	Diagnosis	Clinical Presentation	BP max prior to imaging	Risk factors
Patient 1	7.4	MM	Acute lymphoplastic leukemia. Status-post intrathecal chemotherapy.	New onset seizure.	145/99	Hypertension, intrathecal methotrexate
Patient 2	4.3	F	Severe aplastic anemia. Status-post BMT	Tonic posturing, high ICP.	225/93	Hypertension cyclosporine A.
Patient 3	22.1	M	Hirschsprung's disease, status-post bowel transplanr admitted with transplant rejection.	New onset seizures, altered mental status.	142/92	Tacrolimus, hypertension
Patient 4	16.4	F	Sickle cell disease. Status-post BMT	GVHD. Fever. Hypertension. Abnormal gaze.	145/96	Hypertension, tacrolimus
Patient 5	8.6	F	Acute lymphoblastic leukemia. Status-post BMT	Fever. Altered mental status. Hypertension. Seizure	160/111	Hypertension, tacrolimus, microangiopathy, low serum magnesium.

Abbreviations: BMT=bone marrow; GVHD=graft-versus-host-disease; ICP=intracranial pressure

Methods & Materials: A retrospective case series of five pediatric patients diagnosed with PRES based on clinical presentation and imaging findings is presented. Maximum blood pressure prior to imaging, presenting symptoms, and suspected etiology were recorded. MRI sequences included T1-weighted, T2-weighted, fluid attenuated inversion recovery (FLAIR), diffusion weighted (DWI) and apparent diffusion coefficient (ADC) maps, susceptibility weighted angiography (SWAN), and arterial spin labeling (ASL). Each study was reviewed by a pediatric neuroradiologist. Regions of interest were evaluated across multiple sequences to correlate regions of vasogenic edema with perfusion abnormalities and microhemorrhage.

Results: Clinical characteristics are summarized in the Table. All patients were found to have hyperintense FLAIR signal

abnormalities in the occipital and parietal cortices, however, two patients had lesions in the temporal lobes and one patient had frontal lobe involvement. Correlating ASL signal, from which regional cerebral blood flow can be derived, with FLAIR signal abnormality yielded mixed results: Patient 1 demonstrated hyperperfusion in all areas of FLAIR signal abnormality, Patient 2 demonstrated hyperperfusion in most areas of FLAIR signal abnormality, however, also had hypoperfusion in an occipital lesion, Patient 3 demonstrated minimal FLAIR signal abnormality but extensive cortical hypoperfusion, Patient 4 demonstrated marked cortical hypoperfusion associated with areas of FLAIR signal abnormality, and Patient 5 demonstrated both intense hypoperfusion and hyperperfusion associated with hyperintense occipital FLAIR signal. In all patients, perfusion defects were found in areas of cerebral cortex that appeared normal on FLAIR sequences and ADC maps.

Conclusions: PRES is diagnosed based on both clinical presentation and imaging findings. The pattern of T2/FLAIR hyperintense lesions associated with vasogenic edema affecting primarily the occipital and posterior parietal cortex has been well-described in the pediatric population. However, perfusion defects in PRES have not been clearly described in children. This retrospective case series suggests that either hypo- or hyperperfusion defects identified on ASL imaging may be a more sensitive indicator of PRES than FLAIR or ADC abnormalities.

Poster #: CR-064

Bilateral Optic Nerve Aplasia: A Case Report and Review of Imaging Features, Associated Abnormalities and Genetics

Kuan-Chi Lai, *Department of Pediatrics, UCLA Medical Center, Los Angeles, CA, kuan-chilai@mednet.ucla.edu;* Julian Martinez-Agosto, Soni Chawla, Brian Zipser, M.D.

Disclosures: All authors have disclosed no financial interests, arrangements or affiliations in the context of this activity.

Purpose or Case Report: Optic nerve aplasia (ONA) is a very rare developmental anomaly characterized by absence of optic nerve, retinal ganglion, and optic nerve vessels. The majority of reported ONA cases are unilateral. The rarer cases of bilateral ONA are often associated with additional brain anomalies. ONA is considered distinct from optic nerve hypoplasia. Both environmental and genetic factors have been hypothesized to contribute to ONA, and several genetic mutations have been identified, including PAX6, OTX2, CYP26A1, or CYP26C1. We report a case of bilateral ONA in an otherwise healthy infant with mild hypoplasia of the corpus callosum without dysplasia, and macrocephaly.

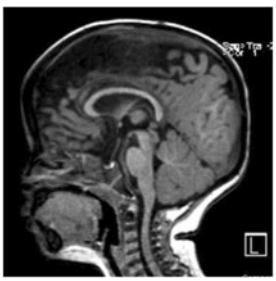

A 13-month-old male presented for evaluation of macrocephaly and global developmental delay that was attributed to cortical blindness. He was born full-term without complications, however mother felt no fetal movement for 1 week prior to delivery. Abnormal roving eye movements were noted since the early neonatal period. There was no family history of any congenital diseases. Examination revealed conjugate non-purposeful rapid eye movements without nystagmus, bilateral lens opacification, and absence of the pupillary light response, startle reflex, and red reflex. The remainder of the physical exam was normal.

MRI of the brain and obits demonstrated absence of the bilateral optic nerves, optic chiasm, and the optic tracts. The globes were normal in size and appearance, although with the right minimally larger than the left. The corpus callosum was relatively thin, but intact, suggesting mild hypoplasia without dysplasia. In contrast to the majority of reported bilateral ONA cases that have associated CNS anomalies (polymicrogyria, corpus callosum agenesis, hypopituitarism, hydrocephalus, microphthalmus), our patient was only noted to have macrocephaly and mild hypoplasia of the corpus callosum. No other brain structural abnormalities were present. Initial genetics evaluation with a microarray was normal, therefore further testing with exome sequencing is planned. We report an extremely rare case of bilateral ONA in an otherwise healthy infant and review the literature for the associated radiologic and genetic findings.

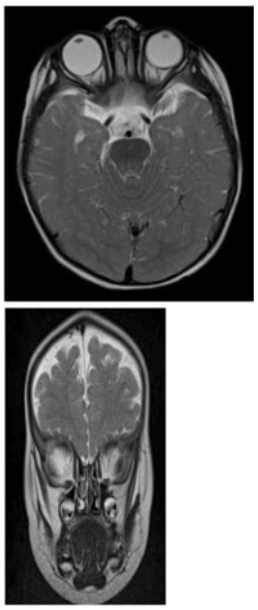

Poster #: CR-065

Characteristic Imaging Features of Epithelioid Hemangioendothelioma, a Rare Multisystem Vascular Tumor

Caroline Lacroix, MD, *Diagnostic Imaging, The Hospital for Sick Children, Toronto, ON, Canada, caroline.lacroix@sickkids.ca;* Rayan Ahyad, MBBS, SBR, Abha Gupta, Govind Chavhan, MD

Disclosures: All authors have disclosed no financial interests, arrangements or affiliations in the context of this activity.

Purpose or Case Report: Epithelioid hemangioendothelioma (EHE) is a rare vascular tumor, of low malignant potential. It is typically seen in adults, but it can also less frequently affect children.

Because of its multisystem involvement, it can present in various ways both clinically and on imaging. It can present with multiple hepatic lesions and/or with multinodular lung disease simulating interstitial lung

disease, infectious disease and metastatic disease among others. Multifocal bone involvement is another presentation of EHE.

One of the radiologist's daily practice challenges is that rare diseases can have significant overlap of imaging features with more frequent diagnoses (that sometimes present with atypical features). It is therefore of high relevance to know the classical and unique imaging features and signature of rare entities such as epithelioid hemangioendothelioma, in order to raise clinical suspicion when needed to direct appropriate diagnostic work-up. Our goal is to present a case of EHE, discuss possible clinical presentations and illustrate classical imaging findings. An overview of clinical implications of this diagnosis and of the available treatment options will also be provided.

Combining multisystem affection and characteristic imaging features, especially MRI features of liver lesions, radiologist can help to make early diagnosis of EHE that is rarely seen in children.

Poster #: CR-066

Superior Mesenteric Vein Varix: Who came first, the Egg or the Chicken?

Nina Stein, Pediatric Radiologist, **Fahran Ahmed,** *Diagnostic Imaging, McMaster University, Mississauga, ON, Canada, ahmedfar@hhsc.ca*

Disclosures: All authors have disclosed no financial interests, arrangements or affiliations in the context of this activity.

Purpose or Case Report: We present a radiologic case of a teenager with portal, inferior mesenteric, superior mesenteric, and splenic vein thromboses presenting with acute abdominal pain and treated conservatively with anticoagulation therapy. Ultrasound and computed tomography were done at the acute presentation and follow up magnetic resonance images were performed. One year of anticoagulation therapy correlated with almost complete resolution of splanchnic thrombosis; however, the superior mesenteric vein continues to remain severely dilated close to the confluence on subsequent annual imaging. The initial imaging also diagnosed multiple phlebolith in the pelvis. We suspect this is a congenital malformation of the porto-splanchnic circulation presenting with acute thrombosis. Differential is variceal dilatation as sequela of extensive thrombosis.

Poster #: CR-067

Prenatal and Postnatal Imaging of Epignathus (Oral Teratoma) with Lateral Skull Base and Intracranial Extension

David Leake, MD, *Radiology, Dell Children's Medical Center of Central Texas, Austin, TX, leakedmd@ausrad.com*

Disclosures: All authors have disclosed no financial interests, arrangements or affiliations in the context of this activity.

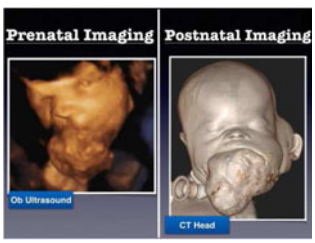

Purpose or Case Report: The purpose of this case report is to describe a rare case of epignathus (oral teratoma) with lateral skull base and intracranial extension. A 29-year-old G4P1122 female was referred to our institutuion after third trimester ultrasound and fetal MRI revealed a 34 week fetus with oral mass. There was extension intracranially through the lateral skull base. The complex mass showed cystic, solid, and fatty components. Polyhydramnios was also demonstrated. The prenatal imaging was crucial in planning the delivery of the fetus using EXIT procedure. Postnatal MRI Head and Neck, CT Head and Neck, CTA Head and Neck were helpful in guiding surgical resection of the oral, skull base, and intracranial mass. Emphasis will be made on the value of imaging to guide the management of this extremely difficult and rare case.

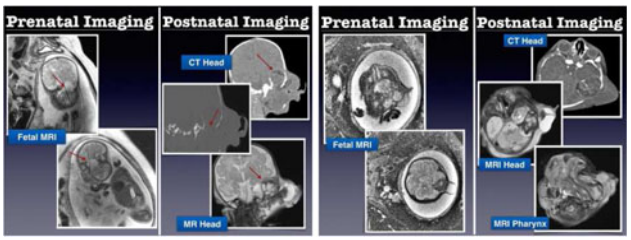

Poster #: CR-068

Currarino's Triad - 2 Cases with Classic Findings

Kelly Wepking, *University of Wisconsin School of Medicine and Public Health, Madison, WI, kwepking@uwhealth.org;* Kara Gill, Erica Riedesel, MD

Disclosures: All authors have disclosed no financial interests, arrangements or affiliations in the context of this activity.

Purpose or Case Report: Currarino's Syndrome (CS) is a unique form of caudal regression syndrome characterized by triad of sacral dysplasia, anorectal malformation, and presacral mass. Additional congenital malformations of the genitourinary tract and spine may be present.

Currarino's Syndrome has a variety of clinical presentations - from asymptomatic to severe chronic constipation - depending on associated malformations. Early identification and adequate treatment prevents eventual serious complications.

Plain radiograph of the sacrum is the first diagnostic step. Ultrasound or pelvic/spinal MRI is used to better evaluate for presacral mass. Fluoroscopic enema studies may be used for further evaluation of anorectal malformation. Additional imaging of the GU tract with US and VCUG is suggested due to risk for associated GU anomaly or vesicoureteral reflux.

We present two cases of Currarino's Syndrome which demonstrate classic imaging findings on plain film radiograph, ultrasound, and MRI.

Case 1 presented in infancy with severe chronic constipation. Abdominal radiograph demonstrated classic "scimitar" sacrum. Fluoroscopic enema demonstrated high grade anal stenosis. US and MRI of the spine and sacrum revealed large anterior sacral meningocele.

Case 2 presented at birth with imperforate anus. Abdominal radiograph demonstrated classic "scimitar" sacrum. MRI of the spine and sacrum revealed small anterior sacral meningocele. Additional GU anomalies were discovered including vesicoureteral reflux and uterine didelphis.

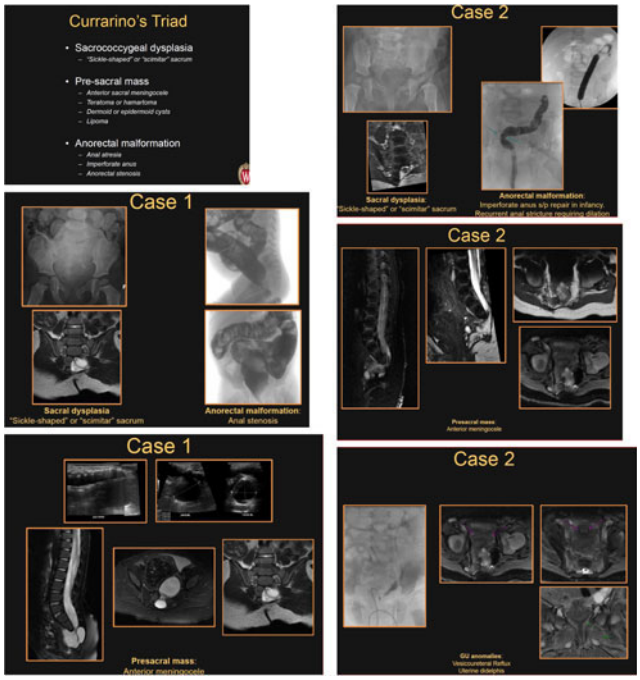

Poster #: CR-069

Traumatic Sternal Segment Dislocation in a 3-year-old Girl

Nicolas Murray, Françoise Rypens, Jean-Sébastien Trudel, Marie-Andrée Cantin, **Marie-Claude Miron, Associate Professor,** *CHU de Quebec, Quebec, QC, Canada, marieclaudemiron@hotmail.com*

Disclosures: All authors have disclosed no financial interests, arrangements or affiliations in the context of this activity.

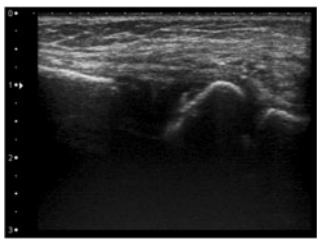

Purpose or Case Report: Traumatic lesions to the sternum are uncommon, especially in the pediatric population. Sternal fractures require significant force to occur due to the greater thorax elasticity in children compared to adults. Sternal segment dislocation is extremely rare with only 13 cases reported in the literature. We report a case of traumatic sternal segment dislocation in a 3-year-old girl.

After falling on a pole, a 3-year-old girl presented chest pain increased by Valsalva and low-grade fever for few days. Her parents brought her to the hospital when she experienced a painful thoracic crisis with the development of a presternal lump. Ultrasonography showed an acoustic shadowing calcified mass representing the first sternal segment being dislocated and rotated at almost 90 degrees. CT showed dislocation with horizontal alignment of the first sternal segment and an undisplaced fracture line in the middle of this segment. There was soft tissue swelling but no repercussion on mediastinal structures. A bone scintigraphy was ordered to exclude any infectious process surimposed and was normal. Conservative management was elected. X-rays 2 months later showed partial remodeling of the sternum. Ten months after the initial trauma, patient remained asymptomatic. CT showed partial osteolysis of the first sternal segment compatible with osteonecrosis.

The main cause of sternal dislocation is direct trauma to chest wall. The sternal body is composed of 4 segments which begin to ossify early in childhood. The manubrium is rigidly attached to both the first ribs and clavicles, providing relative elasticity of other sternal segments. The first sternal segment is the most common dislocated segment. Patient usually presents with limited chest pain and anterior chest wall deformation. The diagnosis of sternal segment dislocation is based on history and physical exam. Imaging studies are useful to confirm the diagnosis. The sternal segment may be minimally dislocated initially, but can continue its rotation for about 2 weeks. Fragment gain stability at 90 degrees rotation. According to the review of the 13 published cases, both operative and conservative treatments show similar outcome.

Conclusions: Sternal segment dislocation in childhood is rare. Successful conservative management with remodeled sternal segment within few months may suggest that operative management may be reserved for severe or persistent symptoms.

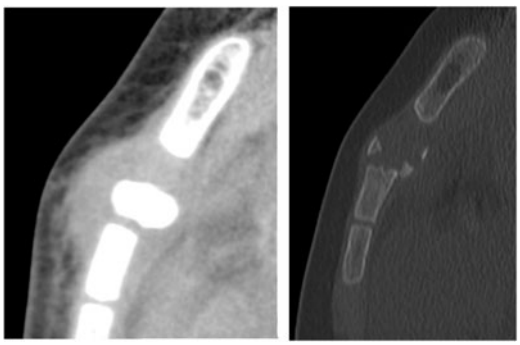

Poster #: CR-070

A Multidisciplinary Approach to Management of a Rare Congenital Adrenal Mass

Sean Bowman, **Austin Trinh**, *Loma Linda University Children's Hospital, Loma Linda, CA, atrinh@llu.edu;* Smyrna Tuburan, MD

Disclosures: All authors have disclosed no financial interests, arrangements or affiliations in the context of this activity.

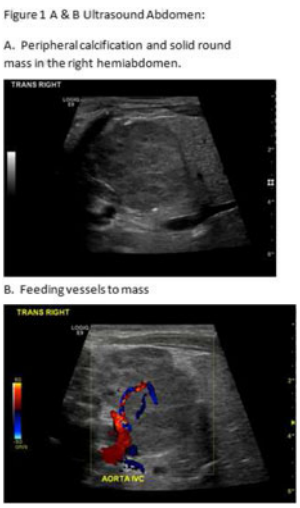

Purpose or Case Report: A 4 day old female, born at term without complications and with reported proper prenatal care was referred to a tertiary care center after her parents were notified of an abnormal 17-OHP on newborn screening. Work-up for suspected congenital adrenal hyperplasia was initiated. An abdominal ultrasound showed a 2.8×3.6×3.7 cm heterogeneously hypoechoic right suprarenal mass with peripheral calcification and large feeding vessels. An MRI abdomen was then obtained, which showed a round circumscribed 3.6×3.5×3.4 cm T1 hypointense and T2 iso-hyperintense heterogeneously enhancing mass. The radiologist raised the suspicion for an adrenocortical tumor, with neuroblastoma or teratoma as less likely etiologies. An MIBG scan was then obtained, revealing absence of activity in the region of the known mass, further supporting the diagnosis of an adrenocortical
of neural crest origin. IR then performed an ultrasound guided biopsy of the right adrenal mass. Pathology reported features consistent with an adrenal cortical neoplasm and without features of neuroblastoma. Due to concern for potential aggressive behavior, pathology recommended complete surgical excision. There is a paucity of literature secondary to the extremely low incidence of congenital adrenal cortical neoplasms. Therefore, a multidisciplinary committee, which included pediatric surgery and radiology, was held. The consensus was that the mass would be best treated by, and is amenable to, surgical excision. At 28 days old, the patient underwent an open right adrenalectomy. Pathology confirmed an adrenal cortical neoplasm of uncertain malignant potential. The postoperative course was without complications. Per pediatric hematology-oncology recommendations, a nuclear medicine whole body bone scan was obtained and demonstrated no osteoblastic metastasis. The patient was discharged and will continue to follow up with hematology-oncology and endocrinology as an outpatient. As illustrated above, the early and correct identification of a potentially aggressive neoplasm by radiology accelerated the treatment course, allowing for potentially curative interventions. This case demonstrates the necessity for multidisciplinary management to include both diagnostic and interventional radiologists and to communicate an appropriate range of differential diagnoses, regardless of incidence.

Figure 2: MIBG: Photopenic region of known mass

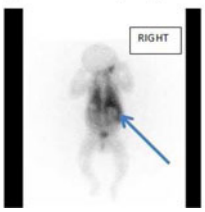

Poster #: CR-071

Hepatic AVMs: Old Dogs, New Tricks

Carrie Schaefer, *Phoenix Children's, Phoenix, AZ, cschaefer@phoenixchildrens.com;* David Aria, M.D., Tammam Beydoun, D.O., Robin Kaye, Richard Towbin, MD

Disclosures: All authors have disclosed no financial interests, arrangements or affiliations in the context of this activity.
Purpose or Case Report: In 2014, 3 patients including a 28-week preemie, 18 day-old neonate, and 11 month-old infant, were treated for large hepatic AVMs. Symptoms included CHF in both the 890-gram preemie and neonate and no symptoms in the infant with imaging revealing extensive shunting. Embolization of the AVMs was performed using various agents, entry sites, and arterial and venous techniques. Agents utilized included detachable and non-detachable coils and vascular plugs. Both direct puncture and intra-vascular techniques, including the use of the umbilical artery, were utilized. Immediate hospital course and short-term clinical and radiographic follow-up was conducted.
Technical success was achieved in all 3 patients without immediate complications. The two symptomatic patients improved clinically on short-term follow up with resolution of the preemie's and neonate's CHF, confirmed on post-embolization imaging. Conventional angiography demonstrated complete resolution of the AVM in the infant.

Poster #: CR-072

Clinical Dilemma of Developmental Delay, Atypical Brain Imaging Findings and Borderline Elevated NAA in Two Cases

Vikas Yadav, MD, *Radiology, Christian Medical College, Vellore, India, vkyadav77@yahoo.co.in;* Sniya Sudhakar, Maya Thomas, Gautham Arunachal

Disclosures: All authors have disclosed no financial interests, arrangements or affiliations in the context of this activity.
Purpose or Case Report: A 1-year-old boy with uneventful perinatal history, non-consanguineous parentage presented with global developmental delay. Family history was not contributory. There was no history suggestive of visual or hearing loss, seizures, bladder and bowel involvement or extrapyramidal symptoms. On examination, Head size was large for age with hyper pigmented nevi over right arm. There was delay involving language, motor and cognition. CNS examination revealed stance ataxia with generalized hypotonia. No obvious organomegaly was noted on abdominal examination.
MRI done in August 2014 showed signal abnormality in dorsal brainstem, dentate nuclei, bilateral thalami and basal ganglia. Gyri appeared swollen with subcortical U fiber involvement. Central white matter was spared. MRS revealed elevated borderline elevation of NAA and lactate. CT did not reveal any obvious calcification in these areas.
Based on these findings differential diagnosis of mitochondrial etiology and L2 hydroxyglutaric aciduria were considered. However, urine tests for routine organic acids were negative.
Literature search revealed findings fitting into Canavan variant disease. Consequently, urine examination showed elevated N acetyl aspartate. The ASPA gene mutation was confirmed on genetic testing.
Another case showed similar clinical presentation. However head size was normal in second case. Imaging findings were similar in nature. Genetic mutation confirmed the diagnosis.
Recognition of the Canavan Variant is important, as most of the cases would be diagnosed as mitochondrial (Leigh's/ LBSL) or L2 hydroxyglutaric aciduria initially. This pattern recognition lead to correct genetic testing and diagnosis.

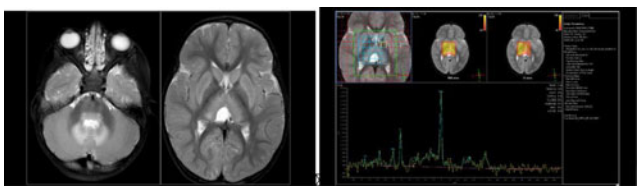

Poster #: CR-073

Postnatal Spontaneous Resolution of CPAM in a Neonate

Melissa Valdez Quintana, Pediatric Radiologist, *Diagnostic Imaging, Instituto Nacional de Salud del Niño San Borja, Lima, Peru;* Carlos Ugas, Doris Katekaru Tokeshi, Irma Matos Rojas, Physician, Edgar Delgado

Disclosures: All authors have disclosed no financial interests, arrangements or affiliations in the context of this activity.
Purpose or Case Report: We report a case of a term neonate who shortly after birth developed respiratory distress and left-sided

pneumothorax. The pneumothorax was drained by a chest tube and the patient was referred to our institution. On day 17 of life a chest Xray and chest CT were performed demonstrating a multiloculated cystic lesion compromising the left upper lobe, most likely representing congenital pulmonary airway malformation (CPAM) type II (Figure 1). No abnormal systemic vessels were identified. At that time the patient was diagnosed with B influenza infection and the surgical intervention was deferred. Over the next several days the patient demonstrated improvement of the respiratory distress and progressive decrease of supplementary oxygen need. On day 25 of life the patient presented significant clinical improvement and, at physical examination, breath sounds were found on the left hemithorax. A follow-up chest xray demonstrated spontaneous resolution of the prior visualized cystic lesion that was confirmed with a chest CT (Figure 2).

Postnatal spontaneous resolution of CPAM have been reported in only few cases, with resolution of the malformation in few months or years. Although we do not have pathologic confirmation, we postulate that our case represent CPAM type II that resolved spontaneously before the first month of life. The management of CPAM diagnosed during the neonatal period remains controversial, some authors recommend postpone surgical intervention in asymptomatic neonates and in patients with prompt resolution of respiratory distress without other significant anomalies.

Our case illustrates the possibility of spontaneous resolution of CPAM and adds to the few reported cases that recommend conservative treatment.

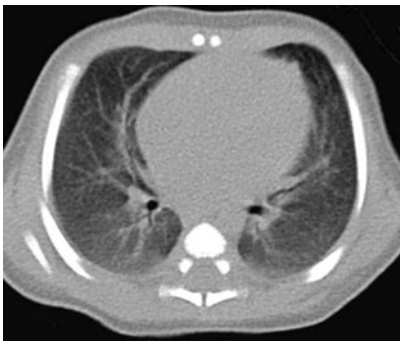

Poster #: CR-074

Atypical Appearance of a Rare Pediatric Tumor: Juvenile Granulosa Cell Tumor of the Testis

Carly Harvey, *University of Nebraksa Medical Center, Omaha, NE;* Sandra Allbery, MD, Andria Powers

Disclosures: All authors have disclosed no financial interests, arrangements or affiliations in the context of this activity.

Purpose or Case Report: Juvenile Granulosa Cell Tumor of the Testis is a rare testicular tumor that falls within the category of stromal cord neoplasms. There have been less than 50 cases described in the literature with all cases being described as having a cystic component (1, 2). We present a case of a 6 month old boy presenting with unilateral scrotal swelling. Ultrasound evaluation revealed an entirely solid, hypervascular, intratesticular mass. Alpha-fetoprotein levels were negative. At surgery, radical orchiectomy was performed and pathology revealed a Juvenille Granulosa Cell Tumor.

Testicular tumors arising in the neonatal and prepubescent period are a unique set of tumors distinct from their adult counterparts. In this younger age group, germ cell tumors predominate. Of the germ cell tumors, Yolk Sac tumors are the main tumor of clinical significant, and the reason why alpha-fetoprotein is such a relevant marker (3). Stromal cell tumors account for only a small percentage of testicular tumors within this age group. When they do occur, Juvenile Granulosa Cell Tumors (JGC) predominate, particularly if the child is under 1 year of age, with this tumor type being the most common testicular tumor present at birth (3, 4). JGC tumors are associated with genetic and structural anomalies of the Y chromosome, ambiguous genitalia, and contralateral undescended testis. One of their defining pathologic characteristics is positive staining with Inhibin (3).To date there are no cases of metastatic JGC tumors. In all reported cases, Sonographic evaluation demonstrates a grossly multicystic tumor (2). The adult variant of Granulosa Cell tumors can appear as a solid mass with little or no cystic component and carries the risk of metastasis of approximately 20% (2). Surgical management of testicular JGC tumors has largely been radical orchiectomy but, some studies have shown tumor sparing excision to be curative in cases with salvageable testicular parenchyma (2). This finding highlights the importance of including stromal cell tumors, particularly JGC, in the differential for solid appearing testicular masses in the neonate. With more reported cases of JGC tumors of the testes, surgical management could include a more conservative approach. Although JGC tumor of the testis is not known to be malignant, given the atypical features of this tumor and similarities with its more malignant adult counterpart, close surveillance is warranted to ensure benign course.

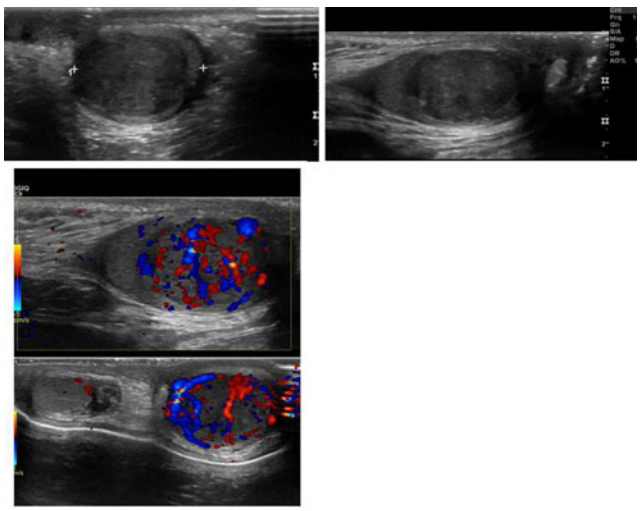

Poster #: CR-075

Imaging Appearance of Crayons

Aaron McAllister, MD, MS, *Radiology, Cincinnati Children's Hospital, Cincinnati, OH, aaron.mcallister@cchmc.org;* Neil Lall

Disclosures: All authors have disclosed no financial interests, arrangements or affiliations in the context of this activity.

Purpose or Case Report: An 18 month old male presents with fever and green discharge from the right external auditory canal. A temporal bone CT demonstrated an 8 mm cylinderical structure 3 cm in length isointense to muscle with linear central hypoattenuation. An MRI demonstrated a cylindrical signal void on all sequences performed; including T1, T2, and FLAIR sequences; within the masticator space corresponding to the foreign body on CT, although the dimensions appeared slightly larger. There was considerable surrounding edema with findings

consistent with osteomyelitis of the mandible with right mastoid and middle ear effusions. In the operating room a small opening on the buccal mucosa was identified and a 3 cm green crayon fragment was removed. Upon further questioning the mother reports the child running with a green crayon, and tripping approximately 3 weeks prior to presentation. The child was treated with IV antibiotics following foreign body removal and is recovering well.

Given the common understanding of a crayon as a solid stick of parafin wax, the imaging appearance as a foreign body on CT and MRI was unexpected. On CT the overall density was isointense to soft tissues and demonstrated a central linear area of hypoattenuation. The central hypoattenuation corresponds to a central air channel in some crayons by the method of manufacture. On MRI the low signal with apparent blooming is related to the pigments. In modern crayons these pigments are transition metal compounds. Iron oxide complexes are the most important and are responsible for the yellow, orange, red, brown, and black color families and their various permutations and mixtures. Other transition metal compounds such as titanium dioxide for white, and copper for blue are also used. Pigments make up to 10% of a crayon. In our case of a green crayon, the iron oxide particles responsible for the yellow portion of the green would explain the abscence of signal on routine MRI sequences with apparent blooming. Understanding the appearance of crayons can help positively identify them as foreign bodies, and may help identify small retained fragments.

Poster #: CR-076

Right Aortic Arch with Isolated Left Subclavian Artery

Carolina Weitz, Resident, Francisca Leiter, MD, *Clínica Santa María, Santiago, Chile, francisca.leiter@gmail.com;* Jose Arce, Hugo Figueroa

Disclosures: All authors have disclosed no financial interests, arrangements or affiliations in the context of this activity.

Purpose or Case Report: The right aortic arch (RAA) is a relatively frequent congenital anomaly, occurring in approximately 0.05% of the general population. It is classified into three types, according to the branching pattern of the aortic arch vessels: a RAA with an aberrant left subclavian artery, an RAA with mirror image branching and RRA with an isolated left subclavian artery.

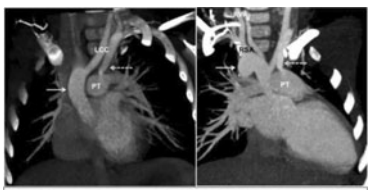

Figure 1. Volume rendered reconstruction of chest CT. Showing: right aortic arch (white arrow), right subclavian artery (RSA), right vertebral artery (RVA), left common carotid (LCC), left isolated subclavian (white dashed arrow) and pulmonary artery (PT).

The RRA with an isolated left subclavian artery is the least common type of the aortic arch anomalies, with a prevalence of 0.8%. It occurs when the left subclavian artery losses its connection with the aorta, arising from the ipsilateral pulmonary artery through a left ductus arteriosus, which may be either patent or closed. If the ductus arteriosus is patent, a shunt between the pulmonary and the systemic circulation is established which leads to the congenital subclavian steal phenomenon. The latter is clinically manifested by asymmetric pulse, blood pressure meassurement and size between the upper extremities. This phenomenon will not manifest clinically if there are accompanying cardiac anomalies which balance the preassures of the pulmonary and systemic circulation, which occurs in approximately in 60% of cases.

The diagnosis of this anomaly can be established by invasive arteriography or CT angiography, where late retrograde opacification of the left subclavian artery from the left vertebral artery is observed, with no connection with the aortic arch. The treatment of this anomaly is surgical or endovascular in the presence of symptoms of subclavian steal syndrome. We present a case report of a 5 year old female patient with history of a right aortic arch and patent ductus arteriosus with clinically significant hemodynamic effect. On physical examination, there was important asymmetry in pulse palpation, blood pressure readings and size of the upper extremities, which motivated invasive angiographic study which confirmed a right aortic arch, a permeable ductus arteriosus with filiform flow, as well as an isolated subclavian artery with steal phenomenon and direct communication with the main pulmonary artery, leading to significant left heart overload. CT angiography of head and neck was consistent with these findings. Surgical management consisted in reimplantation of the left subclavian artery into the left common carotid artery with favorable clinical outcome.

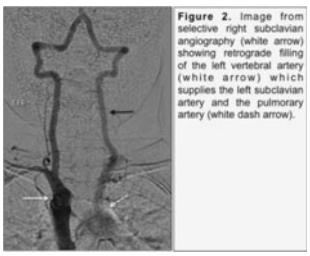

Figure 2. Image from selective right subclavian angiography (white arrow) showing retrograde filling of the left vertebral artery (white arrow) which supplies the left subclavian artery and the pulmorary artery (white dash arrow).

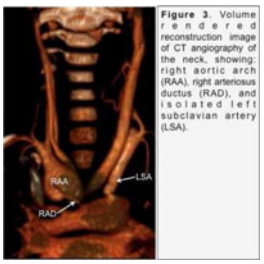

Figure 3. Volume rendered reconstruction image of CT angiography of the neck, showing: right aortic arch (RAA), right arteriosus ductus (RAD), and isolated left subclavian artery (LSA).

Poster #: CR-077

Imaging of Alveolar Capillary Dysplasia with Misalignment of Pulmonary Veins

Jaspreet Singh, *Loma Linda University Children's Hospital, Loma Linda, CA, jassingh@llu.edu;* Smyrna Tuburan, MD

Disclosures: All authors have disclosed no financial interests, arrangements or affiliations in the context of this activity.

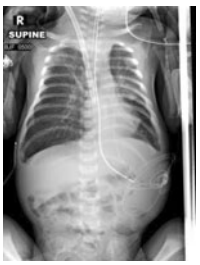

Purpose or Case Report: We report the case of a neonatal male with alveolar capillary dysplasia with misalignment of the pulmonary veins (ACD/MPV). ACD/MPV is a rare, fatal disorder of the

development of the alveolar vasculature. In this disorder, alveolar capillaries are reduced in number and are improperly located within the walls of the alveoli impeding oxygen exchange. In addition to alveolar capillary abnormalities, there are other associated abnormalities with the cardiovascular, gastrointestinal tract, and genitourinary systems. In this report, we describe the case of a term male neonate with a prenatal diagnosis of hypoplastic left heart who developed respiratory distress shortly after birth. The patient required prolonged ECMO and underwent evaluation with CT angiography of the chest. CT findings included diffuse bilateral interstitial thickening with enhancing airspace disease scattered in the left lung. The respiratory distress continued to be unresponsive to treatment, with difficulty weaning ECMO and respiratory support. Life support was withdrawn on day 30. Pathologic examination at autopsy demonstrated ACD/MPV. Our case adds to the limited literature available in describing imaging findings of ACD/MPV and support for early diagnosis with lung biopsy as it can prevent aggressive futile interventions.

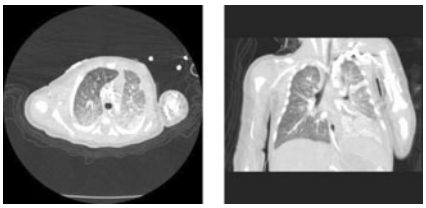

Poster #: CR-078

ROHHAD What? (Rapid Onset Obesity with Hypothalamic Dysregulation, Hypoventilation and Autonomic Dysregulation)

Preet Sandhu, *Le Bonheur Children's Hospital, Memphis, TN, drpreetkiran@gmail.com;* Jignesh Shah

Disclosures: All authors have disclosed no financial interests, arrangements or affiliations in the context of this activity.
Purpose or Case Report: We present a case of a rare entity, ROHHAD syndrome. A 2 year and 11 month old previously healthy caucasian girl was seen at an outside hospital, and was noticed to have hypothermia (90-93 degree F), bradycardia (heart rate of 30), and decreased blood oxygen saturation (40%). She was transferred to our emergency room. Past medical history was positive for viral meningitis in infancy, and asthma. Additional history of sudden weight gain since 1 ½ years of age was noted. Concern for ROHHAD syndrome, a rare entity was raised in light of sudden weight gain, and signs of autonomic dysfunction. Computed Tomography (CT) and Magnetic Resonance Imaging (MRI) of the brain were performed, which were positive for mild parenchymal volume loss. CT of the abdomen was performed which showed multiple enhancing left perinephric and paraspinal masses, concerning for neural crest tumors. Iodine-123-Meta-iodobenzylguanidine (MIBG) scan was performed which was positive. Urine Homovanillic and Vanillylmandelic acid/g creatinine were elevated. Patient underwent resection of left perinephric masses and pathology showed neuroblastoma with intermixed Ganglioneuroblastoma elements.
ROHHAD is a rare disease and only 100 cases have been reported. Anatomic malformations of Autonomic nervous system including tumors of neural crest origin occur in 40% of cases. Term ROHHADNET- Rapid Onset obesity with Hypothalamic Dysregulation, Hypoventilation and Autonomic Dysregulation and neuroendocrine tumors has been used to describe these cases.

Poster #: CR-079

A Rare Case of Plague Complicated By Meningitis, Pneumonia, and Osteomyelitis

Aaron Jen, BA, *UCLA David Geffen School of Medicine, Los Angeles, CA, ajen@mednet.ucla.edu;* Paul Iskander, MD, Shahnaz Ghahremani, MD

Disclosures: All authors have disclosed no financial interests, arrangements or affiliations in the context of this activity.
Purpose or Case Report: A 14 year-old previously healthy male presented to the emergency department with weakness, fever, diarrhea, lateral right eye deviation and transient vision loss, following a week of headaches and dizziness. The symptoms began following a recent camping trip to Yosemite National Park with friends, where distant contact with squirrels and several bug bites were noted. The initial physical examination revealed additional photophobia, limited neck flexion secondary to pain, and a raised, non-tender soft tissue mass over the anterior right shin. Soon after admission, the patient developed pain in the right hip and left leg and significant lower extremity weakness. A chest X-ray demonstrated left lower lobe consolidation, a left upper lobe lung nodule, and a right upper lobe lung nodule. MRI showed multifocal osteomyelitis and multiple intraosseous, intramuscular and soft tissue abscesses. Contrast-enhanced CT angiogram demonstrated septic emboli, scarring, and atelectasis within the left lower lung with a small hydropneumothorax. Lucent lesions were also noticed in the T3-T6 vertebral bodies with increased prominence of the paravertebral soft tissue. A lumbar puncture was found consistent with bacterial meningitis. A blood culture, CSF culture, and culture of abscess fluid from the right hip were all found to be PCR positive for *Yersinia pestis,* and the patient was placed on a treatment regimen of ciprofloxacin, gentamicin, and tetracycline.
Discussion: Plague, colloquial known as the Black Death, is a zoonosis caused by the gram-negative bacterium *Yersinia pestis* and endemic to the Western United States and developing countries. In the modern day, plague is typically found in infected rodents and spread to humans through fleas. Three forms of plague are reported in humans: bubonic, septicemic, and pneumonic. Our patient's presented primary septicemic plague complicated by secondary pneumonia, meningitis, and osteomyelitis. Notably, Yersinia osteomyelitis has been reported only once in the historical literature, and was likely underappreciated before the advent of MRI. This case presentation will highlight the unique imaging manifestations of the patient's disseminated disease.

Poster #: CR-080

Evolution of Intramedullary Cystic Bone Lesions in a Patient with Congenital Generalized Lipodystrophy

Stephen Miller, MD, *Radiology, LeBonheur Children's Hospital, Memphis, TN, sfmjoker1@yahoo.com;* Jeffrey Scrugham, MD, Eniko Pivnick

Disclosures: All authors have disclosed no financial interests, arrangements or affiliations in the context of this activity.
Purpose or Case Report: Congenital generalized lipodystrophy, also known as Berardinelli-Seip syndrome, is a rare autosomal recessive disorder associated with osteosclerosis and cystic intramedullary bone

lesions. However, the transition from generalized osteosclerosis in the young patient to the development of cystic intramedullary bone lesions in areas converting from red to yellow marrow in the growing child has not been previously described. We present a young man with congenital generalized lipodystrophy, followed in our clinic from age 5 years through age 14 years, and document the development over time of dramatic cystic lesions within previously sclerotic long bones. The location of these intramedullary bone cysts appears to mirror the transition of red (hematopoietic) to yellow (fatty) marrow in the maturing child. Recognition of this pattern may affect recommended physical activity and subsequent orthopedic management.

Poster #: EDU-001

A Pictorial Review of Imaging Findings in Paediatric Post-transplant Lymphoproliferative Disorder

Neelika Kirihetti Liyanage, MBBS, *Royal Children's Hospital Melbourne, Parkville, VIC, Australia, neelikaliyanage@yahoo.com;* Surekha Kumbla

Disclosures: All authors have disclosed no financial interests, arrangements or affiliations in the context of this activity.

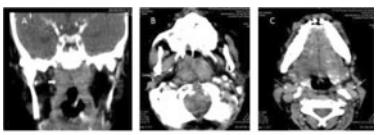

Figure 1: Contrast enhanced (CE) CT scan of the paranasal sinuses of a 8-year-old boy diagnosed of PTLD post bone marrow transplant. Coronal (A) and axial (B) images demonstrating diffuse enlargement of the Waldeyer's ring. Axial CE CT neck (C) showing bilateral cervical adenopathy.

Purpose or Case Report: Post-transplant lymphoproliferative disorder (PTLD) is an important cause of morbidity and mortality which affects transplant recipients of solid organs and allogenic bone marrow transplants. Paediatric recipients of organs that require high levels of immunosuppression are the most susceptible population. Incidence and the frequency of PTLD in paediatric age group is consistently higher than it is in adults. There is insufficient recent literature on imaging features of PTLD in the paediatric age group.

Our purpose is to illustrate multi-modality imaging characteristics of PTLD affecting different organs and systems in a cohort of paediatric patients with biopsy proven PTLD.

Methods & Materials: We retrospectively reviewed imaging studies of children diagnosed of PTLD in our institution following solid organ and bone marrow transplantation over a period of 10 years.

Results: Imaging findings: Imaging features of PTLD are multiple and complex and can affect nearly any organ or system. It can involve the allograft or other nodal or extra nodal sites. Most patients present with enlarged lymph nodes masses.

Involvement of the Waldeyer's ring, pharyngeal and palatine tonsils and cervical adenopathy are common manifestations of head and neck disease Gastrointestinal tract disease manifest as bowel wall thickening, intussusception and abdominal lymphadenopathy.

Solid organ involvement manifest as focal lesions, infiltration and organ enlargement.

Conclusions: PTLD remains an important treatment associated complication in paediatric transplant recipients. As imaging plays a vital role in the diagnosis and surveillance, familiarity with imaging features of PTLD is paramount for early diagnosis and management of these patients.

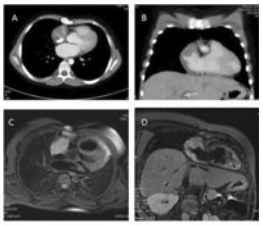

Figure 2: CECT scan, axial(A), coronal(B) images and T2 cardiac MR scan axial(C) and coronal(D) views showing a large soft tissue mass involving the right atrial free wall in a post cardiac transplant patient with cardiac lymphomatous infiltration.

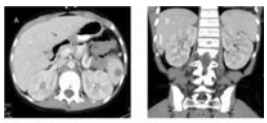

Figure 3 CECT scan of a patient diagnosed of PTLD post bone marrow transplant. Axial view(A) showing a hypo dense lesion in the spleen and coronal view(B) showing multiple lesions left kidney and liver(arrow).

Poster #: EDU-002

Chest radiographic findings in congenital heart disease –comparison with CT images-

Motoo Nakagawa, *Radiology, Nagoya City University Graduate School of Medical Sciences, Nagoya, Japan, lmloltlolol@gmail.com;* Yoshiyuki Ozawa, Yoshihiro Tanaka, Yuta Shibamoto

Disclosures: All authors have disclosed no financial interests, arrangements or affiliations in the context of this activity.

Purpose or Case Report: Characteristic chest radiographic findings of patients with congenital heart disease have been reported for some decades ago. For beginner, it may be hard to detect these findings and to understand reasons why these findings depict. Recently, radiologists can interpret specific findings of congenital heart disease because technique of CT have been developed.

Methods & Materials: This poster provide the overview of chest radiographic findings of congenital heart disease and explain these findings using images obtained by dual-source CT with ECG-triggered high-pitch spiral acquisition (Flash Spiral Cardio mode).

Results: 1) Boot-shaped heart (Coeur en Sabot): This finding is commonly seen in tetralogy of Fallot. Combination of elevated cardiac apex due to enlarged right ventricle and concave the pulmonary artery segment makes this overall configuration. 2) Egg-on-side: This appearance is seen in complete transposition of the great arteries (TGA). In complete TGA, because pulmonary trunk and outflow tract is right side and ascending aorta is located anterior and rightward of the pulmonary trunk, convexity of left pulmonary segment is flattened. 3) Snowman configuration: it suggests total anomalous pulmonary venous connection to the innominate vein. The vertical vein forms left sides of snowman's head. The enlarged heart forms lower part. This sign is rarely seen in infancy with complete TGA. 4) Box-shaped heart: Though size of the left atrium is normal, left cardiac contour is shelved because the right atrium and right ventricle is extremely enlarged. The aorta is small and contour of the pulmonary trunk is obscured. The combination of these features produce the box-shaped heart configuration.

Conclusions: Radiologist should be familiar with characteristic signs of chext radiographs. Reviewing the CT images of patients with congenital heart disease helps us to understand these findings.

Poster #: EDU-003

Contrast Enhanced Ultrasound (CEUS) in the Follow Up of Pediatric Intra-Abdominal Visceral Organ Injury - Findings from a Level One Major Trauma Centre

Sunit Davda, MBBS, *Radiology, Royal London Hospital, London, United Kingdom, sunit.davda@bartshealth.nhs.uk;* Jimmy Kyaw Tun, Ounali Jaffer, Anoushka Ljutikov

Disclosures: All authors have disclosed no financial interests, arrangements or affiliations in the context of this activity.
Purpose or Case Report: Contrast Enhanced Ultrasound (CEUS) has a proven utility in the adult population. It is a safe, accurate and easily accessible technique of pathology assessment. Within the Pediatric cohort, CEUS offers a significant advantage as it potentially negates the need for repetitive radiation exposure resultant of multiple CT examinations.
Methods & Materials: As a Level One Major Trauma Centre in London, we have been examining the use of this under utilized technique in our pediatric trauma population. This case series will demonstrate how CEUS has played an integral part in management decisions of our pediatric patients with liver, splenic and renal trauma within a multidisciplinary setting.
Results: The findings on CEUS directly determined: the need for arterial embolisation; the detection of secondary complications, such as pseudoaneurysm with repeat studies to ensure resolution; as well as facilitate safer discharges as an endpoint of conservative management.
Conclusions: CEUS offers a reliable and effective method of follow-up of the solid abdominal organ injury in the pediatric population, and has the added benefit of allowing safe repeated examinations as it eliminates radiation dose concerns.

Poster #: EDU-004

Imaging and Reporting Considerations for Skeletal Manifestations of Inflicted Injury in Infants and Young Children: a Pictorial Review

Michael Paddock, MBBS, *Academic Unit of Radiology, University of Sheffield, Sheffield, United Kingdom, michael.paddock@doctors.org.uk;* Amaka Offiah, MBBS, PhD, Alan Sprigg

Disclosures: All authors have disclosed no financial interests, arrangements or affiliations in the context of this activity.
Purpose or Case Report: Recognising the skeletal manifestations of inflicted injury (II) in infants and young children is of crucial importance. There are specific fracture patterns that are highly suspicious of II and common differential diagnoses with which radiologists should be familiar.
Methods & Materials: The radiologist's role is to detect findings suggestive of physical abuse, differentiating from other underlying pathologies/normal variants.
Skeletal survey (SS) can detect occult bony injuries and identify underlying medical conditions predisposing to fracturing (metabolic disorder/skeletal dysplasia). Follow-up imaging (approximately 14 days) improves the sensitivity of initial SS, identifies fractures not previously seen due to interval healing, and can assist in dating injuries.
Results: Specific fracture patterns: in a non-ambulant infant, any fracture may be suspicious for physical abuse if the history is inappropriate. Due attention and consideration should be given to the mechanism of injury including whether the history correlates with the radiological findings.
Classic metaphyseal lesion (CML): in the correct clinical context is almost pathognomonic of II. Shearing mechanism/torsional force across metaphyses result in cumulative microfractures of immature bone that rarely occur during 'normal' handling. 'Bucket handle' and 'corner' fractures are descriptive terms given to CMLs.
Posterior rib fractures have strong correlation with II. Follow-up chest radiography should be performed in all cases of suspected abuse given that rib fractures are more easily identified as healing callus develops.
Long bone fractures in non-ambulant infants are always suspicious of II.
Undisplaced hairline tibial spiral fracture in an ambulant child ("toddler's fracture", common accidental injury) if present in isolation is not suggestive of physical abuse.
Fractures in unusual locations: Scapula, sternum, spinous process (3 S's) are uncommon but almost diagnostic of II as significant force (high energy) is required. Whilst uncommon, metacarpal, metatarsal and vertebral fractures are occasionally identified reinforcing the need to perform dedicated imaging of these areas as part of the SS.
Dating fractures: difficult and subjective but there are recognised stages of fracture healing.
Acute long bone, rib arc fractures: no periosteal reaction with/without soft tissue swelling, likely sustained in preceding 14 days, most will heal completely by 3 months.
Healing metaphyseal, costochondral fractures: usually less than 4 weeks old, heal completely by 4-6 weeks.
Vertebral, skull fractures: cannot be reliably dated; soft tissue (scalp) swelling over skull fracture suggests acute (less than 2 weeks) injury.
Abusive head trauma: unexplained/suspicious head injury requires a full SS to detect occult skeletal injury and vice versa.
Differential diagnoses must be considered before diagnosing II.
Osteogenesis imperfecta: congenital disorders of collagen type 1 production affecting bone and connective tissue. With propensity to fracture, the subtypes and corresponding clinical characteristics are extensive.
Rickets: results from undermineralisation of bone with resultant growth plate abnormalities in vitamin D deficient children, including widening and irregularity of the metaphyses with cupping, flaring and fraying.
Birth trauma: beyond 3 months, any birth related injury should have healed.
What to do:
Radiologists play a key role in the detection of II. Failure to instigate child protection measures may result in an infant being exposed to further (potentially fatal) injury if allowed to remain in an abusive environment.
It is best practice for any imaging performed in suspected II to be reported by two different suitable experienced radiologists to minimise errors.
Conclusions: The diagnosis of child abuse is complex, to which imaging plays a large and important role.

Poster #: EDU-005

Demystifying Iterative Reconstruction in Pediatric Chest CT

Sunit Davda, MBBS, *Radiology, Royal London Hospital, London, United Kingdom, sunit.davda@bartshealth.nhs.uk;* Mohammed Rashid Aktar, Kirsteen McDonald, Emma Cheasty, Jonathan Colledge

Disclosures: All authors have disclosed no financial interests, arrangements or affiliations in the context of this activity.
Purpose or Case Report: Iterative reconstruction is an evolving reconstruction technique in CT that has so far been associated with a typical image appearance that many radiologists are still unfamiliar with. This educational presentation aims to demystify the technique by demonstrating the origin of the alteration in image quality and providing readers with an insight as to its benefits.
Methods & Materials: Examples of iterative reconstruction and filtered back projection images at both high and low doses are compared using

image processing techniques and plot profiles across lung structures and abnormal interstitium as well as phantom structures.
Results: We will demonstrate that with iterative reconstruction image quality is preserved, specifically acutance relating to structures within the lungs. Filtered back projection will be shown to have high acutance noise creating the impression of overall high acutance/ sharpness in the image without actually improving diagnostic quality.
Conclusions: Iterative reconstruction in pediatric CT imaging preserves acutance and sharpness, maintaining high diagnostic quality whilst having the added benefits of low noise and lower doses in the radiosensitive pediatric population

Poster #: EDU-006 – ***Withdrawn***

Poster #: EDU-007

Chest CT with Iterative Reconstuction Technique in Youngest Children - Review of Pathology And Dose Consideration

Marzena Barczuk, *Department of Pediatric Radiology, Pediatric Hospital, Warszawa, Poland, marz.barczuk@gmail.com;* Danuta Roik, Zofia Ostapska, Agnieszka Biejat, Michal Brzewski

Disclosures: All authors have disclosed no financial interests, arrangements or affiliations in the context of this activity.

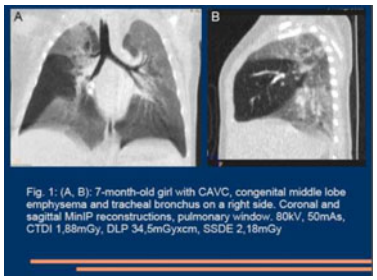

Purpose or Case Report: Computed tomography with its excellent spatial and temporal resolution remains valuable diagnostic modality in pediatrics. On the other hand there has been increasing attention placed on the radiation risks associated with CT imaging, especially in children.
In recent years many advances in CT hardware and software, for example automatic exposure control tools and iterative reconstruction techniques allowed for the reduction of applied radiation dose while maintaining image quality.
The aim of our educational exhibit is:
- to present optimal protocols for chest CT in the youngest age group of children, scanned according to body weight protocols (0-10 kg; 10-30 kg) with assessment of image quality and dose indices (CTDIvol and DLP; SSDE)
- to present pictorial review of the pediatric chest pathologies in low dose chest CT
Methods & Materials: We reviewed our database for chest CT performed in youngest group of children (aged 0-5 years), according to body weight protocols (0-10 kg and 10-30 kg), examined with iterative reconstruction technique iDose; 64-slice scanner Philips Brillance. Scans were performed to confirm or exclude suspected congenital malformations of lungs, heart and great vessels, chest wall and diaphragm and in patients with acquired pulmonary conditions, such as infections and BPD.
CTDIvol and DLP for 16-cm phantom were obtained to estimate radiation dose and SSDE was calculated.
Evaluation of image quality in lowest dose exams were performed addressing to the most important factors which influence the quality. Potential space for further optimization was established.

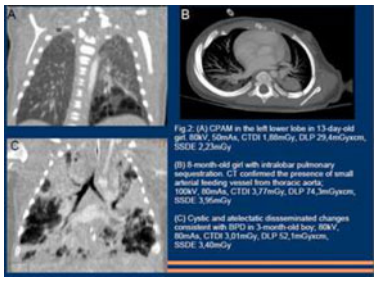

Results: Spectrum of pathologies examined with the lowest dose included:
- congenital pulmonary airway malformation (Fig. 2)
- pulmonary hypoplasia in patients with congenital diaphragmatic hernia
- congenital bronchial abnormalities (Fig. 1)
- pulmonary sequestration (Fig. 2)
- pulmonary infections; BPD as a complications of RDS (Fig. 2)
- abnormalities of the aortic arch: right-sided aortic arch, vascular rings, coartaction of aorta (Fig. 3)
Dose indices for the lowest dose scans ranged: CTDIvol 1,88 - 3,9 mGy; DLP 29,4 - 62.1mGyxcm; SSDE 2,18 - 3,95 mGy.
Lowest dose indices were obtained in examination performed in children in pre-operative evaluation of heart and great vessels with no adverse influence on image quality.
Conclusions: Chest pathologies can be properly visualized in small children using iterative CT reconstruction technique with appropriate quality of scans at a reduced dose with no influence on observer performance.
Our experience in chest CT in the youngest group of patients enhances the need for futher optimalization of CT protocols.

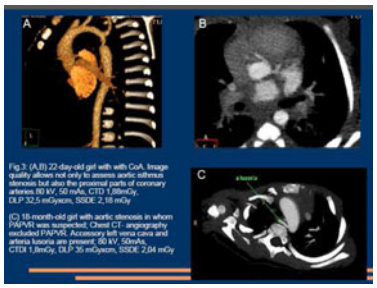

Poster #: EDU-008

A ChILD of our time – ***A Comprehensive Overview of 21st Century Childhood Interstitial Lung Disease Imaging (ChILD)***

Thomas Semple, MBBS, BSc, *Great Ormond Street Hospital, London, United Kingdom, tsemple@doctors.org.uk;* Michael Ashworth, Paul Aurora, Catherine Owens

Disclosures: All authors have disclosed no financial interests, arrangements or affiliations in the context of this activity.
Purpose or Case Report: To review the CT features of childhood interstitial lung diseases (ChILD).

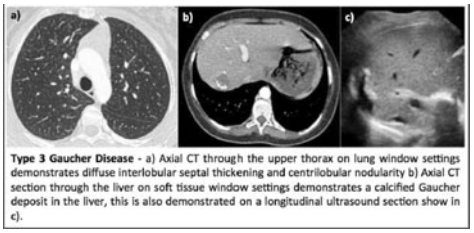

Type 3 Gaucher Disease - a) Axial CT through the upper thorax on lung window settings demonstrates diffuse interlobular septal thickening and centrilobular nodularity b) Axial CT section through the liver on soft tissue window settings demonstrates a calcified Gaucher deposit in the liver, this is also demonstrated on a longitudinal ultrasound section show in c).

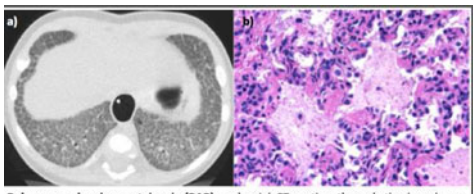

Pulmonary alveolar proteinosis (PAP) – a) axial CT section through the lung bases demonstrating diffuse inter- and intra-lobular septal thickening (the 'crazy-paving' appearance). b) H&E staining demonstrates alveolar septal thickening with proteinacious material (bright pink) filling the alveolar spaces. This patient was found to have a surfactant protein (ABCA3) dysfunction mutation.

Methods & Materials: We illustrate specific examples of ChILD from our patient cohort at a large national childrens hospital alongside their histopathology, in order to demonstrate CT features of interstitial lung disease within the paediatric population.

Results: Although rare, interstitial lung disease in the paediatric population is very different from that seen in adulthood and infers significant morbidity and mortality.

Imaging plays a crucial role in the assessment of these patients, sometimes demonstrating features consistent with individual pathological diagnoses, demonstrating the distribution and extent of disease and guiding any subsequent biopsy.

We review techniques in paediatric thoracic CT and illustrate the specific disorders below.

Childhood interstitial lung diseases (ChILD) can be divided into 2 groups:

1) Conditions more prevalent in infancy - diffuse developmental disorders (we present images of congenital alveolar dysplasia), lung growth abnormalities (cystic lung disease in trisomy 21 and filamin A protein deficiency related lung disease), conditions of unknown aetiology (neuroendocrine hyperplasia of infancy - NEHI) and surfactant dysfunction mutations (pulmonary alveolar proteinosis in ABCA3 dysfunction).

2) Conditions not specific to infancy - Normal host (constrictive obliterative bronchiolitis), immunocompromised host (Lymphocytic interstitial pneumonitis - LIP and pleuroparenchymal fibroelastosis - PPFE), disorders relating to systemic processes (Gaucher disease, Niemann-Pick and Langerhan's cell histiocytosis) and masqueraders of ChILD (pulmonary lymphangiectasia and pulmonary veno-occlusive disease).

Conclusions: Childhood interstitial lung disease comprises a rare and diverse group of conditions. Imaging and histological correlation is crucial in the investigation and management of these patients and offers fascinating insights into these unusual conditions.

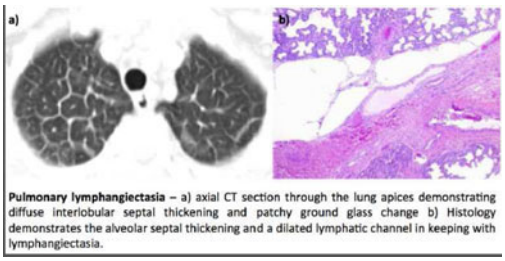

Pulmonary lymphangiectasia – a) axial CT section through the lung apices demonstrating diffuse interlobular septal thickening and patchy ground glass change b) Histology demonstrates the alveolar septal thickening and a dilated lymphatic channel in keeping with lymphangiectasia.

Poster #: EDU-009

CT Dose Measurement and Dose Reduction Techniques in Cardiac and Cardiovascular CT – ***What you really need to know…***

Thomas Semple, MBBS, BSc, *The Royal Brompton Hospital, London, United Kingdom, tsemple@doctors.org.uk;* Rebecca Schofield, Ricardo Petraco Da Cunha, Catherine Owens, E Nicol, Lawrence King, I Castellano

Disclosures: All authors have disclosed no financial interests, arrangements or affiliations in the context of this activity.

Purpose or Case Report: To review the basics of CT dose calculation, in particular the nuances of dose calculation / estimation in cardiac CT and the many and varied methods of dose reduction in cardiac and cardiovascular CT.

Methods & Materials: We summarise the main themes covered in the CT physics portion of our advanced cardiovascular CT fellowship program.

Results: There is increasing evidence from recent studies that medical radiation exposures during childhood are associated with increased risks of subsequent malignancies, however, CT imaging can play a key role in the assessment of the heart and coronary and great vessels in neonates and young children who are too unwell or anatomically complicated for adequate assessment via echocardiography or cardiac MRI.

Measures of dose: We explain the difference between absorbed and effective dose, define CTDIvol and how this is measured, define DLP and the significance of patient weight and height on effective dose achieved per unit DLP, and define size-specific dose estimates and how these might be useful for understanding paediatric CT doses.

We explain the origin of the conversion factors used to estimate effective dose from DLP and the significance of historic use of a standard chest CT conversion factor approximately half the more recently calculated cardiac CT specific conversion factor and the significance this has on reported dose in the literature.

Dose reduction techniques: Topics discussed include:

1) Optimization of tube voltage (kV) and current (mA) and the benefit of lowering the kV to increase the conspicuity of contrast medium.

2) Adaptive dose control and the effects of automatic exposure controls on end doses achieved.

3) High pitch and dual source scanning

4) The effect of iterative reconstruction on image quality and the potential for lower diagnostic doses

5) Modes of ECG gating (retrospective gating with and without ECG controlled dose modulation, prospective gating in end-diastolic and end-systolic phases and ultra-high pitch single shot acquisitions (FLASH)

Conclusions: There have been significant advances over the past 5-10 years in dose reduction, but a basic understanding of CT physics and dose calculation is vital in realising the potential of these techniques and in assessing future innovations. It is important that we as imaging experts are able to clearly explain to our referrers and patients, the risks associated with CT, the benefits of CT in the correct situation and the measures taken to reduce dose to as low as is reasonable achievable.

Poster #: EDU-010

Pictorial Review of Chest X-ray Findings in HIV-infected Children

Nasreen Mahomed, MBBCh (Wits), FC Rad (SA), MMed (Wits), *Diagnostic Radiology, University of Witwatersrand, Johannesburg, South Africa, nasreen.mahomed@wits.ac.za*

Disclosures: All authors have disclosed no financial interests, arrangements or affiliations in the context of this activity.

Purpose or Case Report: Abstract: HIV is a global pandemic. According to the UNAIDS Report on the Global Aids Epidemic 2013, approximately 3.3 million children under the age of 15 years are living with HIV infection globally. Sub-Saharan Africa has the highest burden of disease with 2.9 million of HIV-infected children. HIV has affected the epidemiology of childhood pneumonia, changing the spectrum of pathogens, antimicrobial susceptibility of bacteria and prognostic outcome. More than 70% of HIV-infected children will suffer at least one episode of a pulmonary infection in the course of their illness. The pneumococcal conjugate vaccine (PCV) demonstrated vaccine efficacy of 20% in HIV-uninfected children and 13% in HIV-infected children in South African using WHO standardized chest X-ray interpretation criteria. The chest X-ray remains the most readily available and the commonest imaging modality for childhood pneumonia. A combination of clinical findings with pattern recognition on chest X-ray narrows the differential diagnosis. We present a pictorial review of chest X-ray findings in HIV-infected children due to infectious causes: pulmonary TB, bacterial pneumonia, *Pneumocystis jiroveci* pneumonia, viral pneumonia and non- infectious causes: immune reconstitution inflammatory syndrome (IRIS), lymphocytic interstitial pneumonia (LIP) and lymphoma.

Poster #: EDU-011

Enteral Feeding Tubes - Tips, Tricks and Pitfalls

Sunit Davda, MBBS, Radiology, Royal London Hospital, London, United Kingdom, sunit.davda@bartshealth.nhs.uk; Farrukh Arfeen, Charlotte Roberts, Sam Chippington, Kirsteen McDonald

Disclosures: All authors have disclosed no financial interests, arrangements or affiliations in the context of this activity.
Purpose or Case Report: Enteral feeding tubes are increasingly being requested and utilized. Furthermore there are now a wide variety of enteral tubes available. This educational exhibit will provide a review of the different types of enteral feeding tubes used in the pediatric population as well as useful hints and tips for pediatric radiologists, general radiologists and clinicians alike.
Methods & Materials: Using cases from our experience within a Tertiary Pediatric Surgical and Pediatric Gastroenterology centre, we will provide a comprehensive pictorial review of enteral feeding tubes and the kit required for tube placement; including a description of techniques used for challenging cases and commonly encountered pitfalls.
Results: This educational exhibit will provide the reader with confidence in the insertion, maintenance and management of complications in children with feeding tubes.
Conclusions: Pediatric enteral feeding tubes are increasingly encountered by radiologists. This illustrative review will provide the reader with confidence in the various techniques undertaken and how to cope with difficulties that may arise.

Poster #: EDU-012

Multifocal Bone Marrow Lesions in Children: MRI Findings

Maria Raissaki, *Department of Radiology, University Hospital of Heraklion, Heraklion, Greece, mraissaki@yahoo.gr;* Stelios Demetriou, Christos Skiadas, Kostas Spanakis, Maria Stratigaki, Nikos Katzilakis, Eftichia Stiakaki, Apostolos Karantanas

Disclosures: All authors have disclosed no financial interests, arrangements or affiliations in the context of this activity.

Purpose or Case Report: There are various conditions or diseases that may cause multiple bone marrow lesions in children or adolescents. Radiographically, lytic lesions may become apparent after loss of >50% of bone mineral content. Scintigraphy requires osteoblastic activity and is not specific. MRI has been increasingly employed for the investigation of diseases that involve the skeleton and for further delineation of radiographic findings in symptomatic children.
Purpose: To describe the MRI findings of entities resulting in multiple bone marrow lesions in children and provide a wide differential diagnosis.
Methods & Materials: MRI scans and records of children examined during the last 4 years for symptoms relevant to the musculoskeletal system or as further diagnostic workup of conditions that affect the bones were retrieved. All scans with more than one focal bone marrow lesion in a single bone or with polyostotic involvement were included. Final diagnosis was based on histological diagnosis and/or clinical evolution following conservative therapy.
Results: Diagnoses included: Metastatic diseases, LCH, lymphoma, CRMO, multifocal osteomyelitis, polyostotic fibrous dysplasia, multifocal Ewing's Sarcoma, multifocal osteosarcoma, bone infarcts, bilateral Perthe's disease, multiple stress fractures/reactions, multiple exostoses, multiple enchondromatosis syndrome, multifocal osteochondritis dissecans, bone marrow reconversion or hyperplasia, post radiation changes.
Parameters that were considered useful for the pre-biopsy diagnosis included radiographic appearances, known history, athletic activity/physiotherapy, synchronous or metachronous lesions, zone of transition, signal intensity, bilaterality or laterality with regard to midline as well as location in the bone (cortex or medulla, diaphysis, metaphysis or epiphysis).
Conclusions: MRI may significantly contribute to the diagnosis of conditions that cause multifocal bone marrow lesions in children. The differential diagnosis is wide and includes both malignant and benign entities.

Poster #: EDU-013

Abdominal Fluid-Containing Masses of the Newborn: All You Need to Know

Costanza Bruno, *radiplogy, policlinico gb rossi, Verona, Italy, costanza_bruno@libero.it;* Salvatore Minniti

Disclosures: All authors have disclosed no financial interests, arrangements or affiliations in the context of this activity.

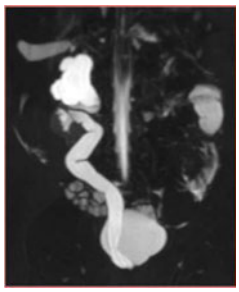

Purpose or Case Report: To offer a complete overview of the diagnostic hypotheses of the various fluid-containing masses which can be found in the neonatal abdomen.
Methods & Materials: The abdominal fluid-containing masses of the newborn can be divided into newly-formed masses (ovarian cysts, gastroenteric duplication cysts, choledocal cysts, cystic teratomas and renal cysts) and dilation of pre-existing hollow structures, these latter being either normal viscera (stomach, renal pelvis, ureter, bladder, uterine cavity) dilated because of a downstream obstacle or persistent embryological remnants as observed in cloacal and urogenital sinus malformations.

Results: For each abnormality drawings, schemes (also illustrating embryological origin when needed), the radiological images (ultrasound, magnetic resonance, contrast enema and voiding cystourethrography) necessary to a full description and when useful surgical findings are provided.
Conclusions: The finding of a fluid-containing mass is not a rare event in the evaluation of the neonatal abdomen. General radiologists should be confident with the main imaging findings in order to choose the pathway leading to a correct diagnosis

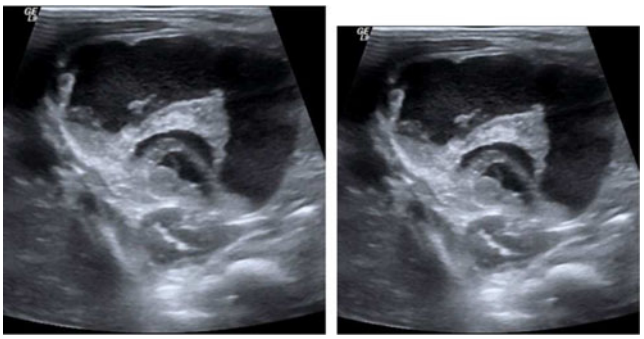

Poster #: EDU-014 – ***Withdrawn***

Poster #: EDU-015

Intussusception in Children: Sonographic Approach and Impact in the Management

Catherine Baud, *Pediatric Radiology, Hôpital Arnaud de Villeneuve, Montpellier, France, c-baud@chu-montpellier.fr;* Magali Saguintaah, Julie Bolivar Perrin, Stephanie David, Alain Couture, Olivier Prodhomme, MD

Disclosures: All authors have disclosed no financial interests, arrangements or affiliations in the context of this activity.
Purpose or Case Report:
1. To describe intussusception US aspect
2. To diagnose the different anatomic forms
3. To detect a leadpoint at the intussusceptum apex
4. To provide sonographic prognostic criteria
5. To recognize benign small bowel intussusception
6. To desmontrate US impact in the therapeutic management

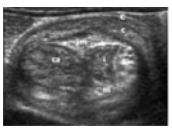

Ileocecocolic intussusception in axial scan: the center is composed of the ileum (i) next to the cecum (ca) surrounded by the hyperechoic mesentery (m). The outer ring is formed by the receiving (C) and the returning (c) limbs of the colon.

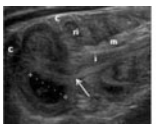

Ileoileocolic intussusception in longitudinal scan: the returning limb of the ileum (ri) has a characteristic coiled spring aspect due to the presence of folds perpendicular to the entering ileum (i) dragging its mesentery (m). A segment of blind-ending, thick-walled bowel containing some fluid (crosses) corresponding to a Meckel diverticulum, projects from the apex of the entering ileum (arrow) into the receiving colon (C).

Methods & Materials: 451 intussusceptions diagnosed with sonography over a 13-year period, were studied for US pattern, anatomic type, lead point at the intussusceptum apex, trapped fluid within the intussusceptum, associated small bowel occlusion, and treatment by sucessful therapeutic enema or surgery with information about bowel compromise and pathological findings.
Results: 1. Intussusception US features with anatomic correlation
2. Characteristic US findings in ileocolic, ileoileocolic, small bowel and colocolic types
3. US appearance of leadpoints: Meckel's diverticulum, cystic duplication, Burkitt lymphoma, and polyp
4. Risk criteria: trapped fluid within the intussusceptum and small bowel obstruction. No risk criterion: absence of ischemia. Both criteria: high risk of bowel compromise increasing with fluid amount
5. Benign small bowel intussusceptions: very frequent, small, peristaltic, with thin layers, no leadpoint, no bowel obstruction and spontaneous reduction
6. Enema therapy: to reduce idiopathic ileo(ileo)colic and colocolic forms. US: to guide hydrostatic enema, to assess reduction or recurrence. Surgery: in cases with bowel compromise, with leadpoint and in pathological small bowel intussusception. Chemotherapy: to produce spontaneous reduction in proven disseminated Burkitt lymphoma.
Conclusions: US diagnosis of anatomic form, of risk criteria and of a leadpoint permits to guide therapeutic management. The idiopathic ileocolic intussusception due to lymphoid hyperplasia, by far the most common form, must almost always be reduced by enema. Surgery shoud be required only in cases with pathological leadpoint and/or with bowel compromise (almost exclusively in ileoileocolic form). In contrast, pathological small bowel intussusception is very rare, secondary or associated with a predisposing condition, produces small bowel occlusion and almost always requires surgery. Colocolic intussusception is exceptional, easily reduced by enema but it will recur if the leadpoint is not removed.

Poster #: EDU-016

Obstruction, Flow, and Function as Relating to Functional Renal Imaging

André Eichenberger, MD, BSEE, *Radiology, Children's University Hospital Zürich, Zürich, Switzerland, aceichenberger@gmail.com*

Disclosures: All authors have disclosed no financial interests, arrangements or affiliations in the context of this activity.
Purpose or Case Report: A theory is developed that describes the mechanism by which functional renal imaging (FRI) assigns a property called "function" to an obstructed kidney. The theory elucidates the association between obstruction, flow, and function.
Background: There are three common beliefs held about FRI: 1) obstruction reduces flow; 2) flow is an appropriate measure of renal function; and 3) renal function measured by FRI positively correlates with flow. According to the Patlak method, tracer amount is estimated by integration over time of the product of flow and tracer density. Curiously, FRI measures neither tracer density nor flow within tubular structures. The disparity between the theoretical Patlak method and applied FRI results in an ambiguous assessment of flow and renal function.
Methods & Materials: The kidney is modeled as an autoregulated and partially collapsed elastic tubular structure equivalent to a Starling resistor. FRI is modeled semi-quantitatively to illustrate the dependency of function on both renal volume and flow. Additionally, obstruction is equated to ureteral resistance. The theory predicts that during steady state excretion function is a measure only of volume. Moreover, during transient hyperexcretion, function is a measure of volume as well as a measure of variable flow.
Results: During steady state conditions, no correlation is found between obstruction and flow, as well as no correlation between function

and flow. During increasing pelvic pressure, flow is greater in an obstructed than in a non-obstructed kidney. The arbitrary measurement of function is the result of indeterminate flow and ureteral resistance. A re-interpretation of data acquired by both MR Urography and scintigraphy verifies that, on average, ureteral resistance uniquely determines function.
Conclusions: Function is a measure only of obstruction. Neither flow nor function evaluates the true performance of an autoregulated kidney. Functional imaging is based on misconceptions - functional imaging muddles the definitions of obstruction, flow and function. Clinical evaluations of obstructive uropathy may be misguided. The use of FRI should be reconsidered.

Poster #: EDU-017

Biliary Atresia: Comprehensive Pre-Transplantation Evaluation Checklists

Nucharin Supakul, *Radiology, Ramathibodi Hospital, Mahidol University, Bangkok, Thailand, nucharinsupakul@gmail.com*

Disclosures: All authors have disclosed no financial interests, arrangements or affiliations in the context of this activity.
Purpose or Case Report: To summarize our experience using Computed Tomography Angiography (CTA) of the liver as an imaging tool for preliving donor liver transplantation (LDLT) evaluation in biliary atresia (BA) patients. This pictorial review will illustrate and discuss several aspects of imaging techniques and the important findings that clinician need to know before LDLT.
Key imaging findings for vascular anatomy/collateral vessels will be made, emphasizing what clinicians need to know. Correlation with intraoperative findings will also be provided.

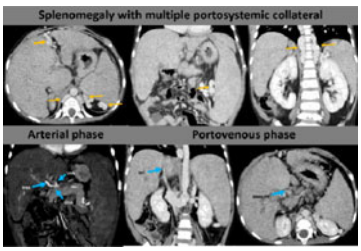

Methods & Materials: Using our radiology database, a retrospective review of CTA liver studies in BA patients from 2001 to 2015 was performed. A hundred CTA studies were reviewed with intraoperative LDLT finding correlation. We will demonstrates the optimal imaging techniques including CT parameters, amount of contrast and delayed scan time.
Imaging checklists for both vascular anatomy/collateral vessels and potential intra/post-operative complications will be demonstrated.
Results: BA is one of the most common indication for LDLT, especially in Asian population. Details of pre LDLT of vascular anatomy/collateral vessels are crucial for safe and successful transplantation. CTA liver plays an important role to demonstrate vascular anatomy, portosystemic collateral pathway and potential complications. Awareness of the anatomical variations and potential post-operative complications is essential for the radiologist to generate a meaningful report to help surgeon preparing before LDLT. It is also mandatory for the radiologist to be aware of the surgeon's perspective.
The optimal CT parameter are not only based on patient's body weight but also the maximum abdominal thickness. Due to portal hypertension and portosystemic collaterals, amount of IV contrast should be given more than 2 ml/kg but not exceed 4 ml/kg to get a better opacification of hepatic vessels. Further evaluation with Doppler US is recommended in selected case for better visualization of the vascular structure.
Conclusions: CT is a comprehensive non-invasive assessment of pre LDLT. Awareness of the anatomical variations and collateral vessels as well as potential intra/post-operative complications is important for the radiologist to generate a meaningful report.
To achieve a successful LDLT programs, radiologist should be an integral part of the team and is present during transplant planning discussions.

Poster #: EDU-018

Odontoid Osteomyelitis in Two Children and Review of the Literature

Julien Aguet, *Department of Diagnostic, Interventional and Paediatric Radiology, University Children's Hospital, Bern, Switzerland, julien.aguet@icloud.com;* Petra Zimmermann, Enno Stranzinger

Disclosures: All authors have disclosed no financial interests, arrangements or affiliations in the context of this activity.
Purpose or Case Report: Odontoid osteomyelitis is a rare disease in children. As the condition is not commonly known, children are frequently initially misdiagnosed with torticollis and treated symptomatically, leading to delayed diagnosis. We present two illustrative cases of odontoid osteomyelitis and a literature review summarizing clinical presentation, risk factors, diagnostic methods, radiological findings and therapies of all previously reported cases.
Methods & Materials: A literature review was performed using Medline, Embase and Web of Science (1950 to September 2015) using the search terms 'odontoid osteomyelitis' or 'osteomyelitis odontoid peg' or 'dens osteomyelitis' or 'vertebral osteomyelitis'. References were hand-searched for additional articles. Only cases of patients with odontoid osteomyelitis and sufficiently detailed description of clinical presentation, diagnostic methods and therapies were included.
Results: In the cases reviewed, the mean age at presentation was 23 months (range 1 - 84). Children usually presented in good general condition with no fever. Most common radiological findings include bone destruction of the odontoid and prevertebral soft tissue swelling on computed tomography (CT). Magnetic resonance imaging (MRI) can show edematous signal alterations within the odontoid and adjacent joint spaces as well as enhancing abscesses in surrounding soft tissues. The most common symptoms were reduced head movement or neck stiffness. While the white blood cell count (WBC) or C-reactive protein (CRP) was normal or only mildly elevated, the erythrocyte sedimentation rate (ESR) was commonly elevated. Even though the mean duration from the initial presentation to the time of the diagnosis was 27 days (range 0 - 90), patients showed a favourable outcome either under antibiotic treatment only or additional surgical intervention.
Conclusions: Odontoid osteomyelitis should be considered in children presenting with decreased head movement and an elevated ESR, especially without improvement under anti-inflammatory therapy. History of a trauma may be misleading. Even MRI- and CT- findings may be subtle and difficult to differentiate from non-ossified cartilaginous parts of the atlas and axis, variants of synchondroses, and osseous gaps. In most cases plain radiographs are not reliable enough. Thus evaluation should include CT or MRI. A delay in diagnosis may lead to destruction of the vertebral bodies, subluxation of the atlanto-axial joint or cervical cord compression.

Poster #: EDU-019 – ***Withdrawn***

Poster #: EDU-020

Pontine Stroke in a Child with Neurofibromatosis 2 (NF-2)

Norbert Utz, *Pediatric Radiology, HELIOS Klinikum Krefeld, Krefeld, Germany, norbert.utz@gmx.de;* Ilona Daumer, Marcus Katoh

Disclosures: All authors have disclosed no financial interests, arrangements or affiliations in the context of this activity.
Purpose or Case Report: To present a very rare case of a pontine stroke in a 13-year-old boy with NF-2.
Methods & Materials: 13-year-old boy with clinically proven neurofibromatosis type 2 (bilateral acusticus schwannoma, meningeoma of the cavernous sinus, schwannoma of the cauda equina), who developed a left-sided brachium pontis stroke. Clinical, laboratory and imaging findings (MRI, MRA, angiography) are presented and discussed.
Results: The patient was referred for sudden onset of dizziness and vertigo. He presented an ataxic gait pattern and complained in addition about a reduced hearing ability on the left side.
MRI revealed the known bilateral acustic schwannoma and a lesion in the right cavernous sinus presumed to be a meningioma.
In addition a lesion of the left brachium pontis with intense restriction of diffusion in the DWI was seen initially interpreted as a glioma.
Biopsy was performed that showed thickening of the vessel wall of the small vessels indicative of vasculopathy. No tumor cells or signs of inflammation could be observed.
Intense coagulation work-up including protein C, protein S, homocystein, anticardiolipid antibodies were unremarkable. MR-angiography and conventional angiography could not detect any vascular pathology.
Conclusions: Childhood stroke -although rare- is a well known complications of NF-1 but not of NF-2.
Until now there are only 3 case reports about childhood stroke in NF-2. Two of these describe an infratentorial location as in our case.
Our pathologic specimen revealed changes of the vessel wall that could be an expression of a vasculopathy although the imaging findings of the larger vessels do not support this assumption.

Poster #: EDU-021

Beyond the Sacral Dimple: Imaging Approach of the Lumbrosacral Spine in Neonates and Children

Evangelia Manopoulou, *Radiology, Mitera Hospital, Athens, Greece, evimanopoulou@gmail.com;* George Magganas, Christina Meleti, Spyros Yarmenitis, Panagiotis Tagalakis, Georgia Papaioannou

Disclosures: All authors have disclosed no financial interests, arrangements or affiliations in the context of this activity.
Purpose or Case Report: Our objective is to demonstrate the value of imaging exploration of the lumbar spine and sacrococcygeal region in neonates and young children, when certain clinical indications exist.
Methods & Materials: Complicated sacral dimples, pigmented lesions, sacral soft tissue masses and hairy patches indicated detailed exploration of the lumbrosacral spine in neonates, infants and children who were referred to our institution. Additionally, in certain cases spinal findings were incidental.
Ultrasound was the modality of choice in evaluating the neonatal lumbrosacral spine.
MRI on the other hand, is valuable not only in diagnosing spinal dysraphism spectrum in infants and children, but also in presurgical planning.
Results: A variety of anomalies with a range of clinical significance are presented, such as: filum cyst, tethered cord (with low-lying conus medullaris), spinal lipoma (+/- syrinx), lipomyelomeningocele, caudal regression syndrome and diastematomyelia.
Conclusions: Imaging evaluation of the lumbrosacral spine, in the presence of complex skin lesions and findings, usually reveals associated anomalies of the spinal dysraphism spectrum.

Poster #: EDU-022

An Algorithmic Approach to a Pancreatic Mass in a Child

Nasreen Mahomed, *Diagnostic Radiology, University of Witwatersrand, Johannesburg, South Africa, nasreen.mahomed@wits.ac.za*
Disclosures: All authors have disclosed no financial interests, arrangements or affiliations in the context of this activity.
Purpose or Case Report: Pancreatic tumours are a rare and unusual entity in pediatric patients accounting for less than 0.2% of malignant paediatric deaths. The limited number of cases and the diversity of histopathologic subtypes have made it difficult to predict prognosis which differs significantly from adults. In general, pancreatic tumours that occur in children are well circumscribed and partially encapsulated. Their relatively soft nature and encapsulated rather than infiltrative growth pattern allow them to become large prior to clinical presentation. Owing to their large size, central necrosis is common.
Causes of pancreatic masses in children are usually benign and include pancreatic pseudocyst, congenital pancreatic cyst, dermoid cyst, hydatid cyst, islet cell tumours, lymphangioma, pancreatic hemangioendothelioma and cystadenomas. Causes of malignant pancreatic masses in children (which are rare) include pancreatoblastoma, lymphoma, neuroblastoma, solid-pseudopapillary tumour and rhabdomyosarcoma.
We present an algorithmic approach to a pancreatic mass in a child, describing the common imaging features in each of the benign and malignant causes of pancreatic mass in a child with radiologic cases. We also report a very rare case of a pancreatic kaposiform hemangioendothelioma in an 8 month old boy who presented with Kasabach Merritt syndrome.

Poster #: EDU-023

Sounds Good: Practical Guide for Good Ultrasound Examination after Pediatric Liver Transplantation

Shunsuke Nosaka, MD, *Radiology, National Center for Child Health and Development, Setagaya-ku, Japan, nosaka-s@ncchd.go.jp*

Disclosures: All authors have disclosed no financial interests, arrangements or affiliations in the context of this activity.
Purpose or Case Report: It is well known that ultrasound is a powerful imaging tool for pediatric patients after liver transplantation. With proper use, ultrasound provides static as well as dynamic information of the transplanted liver. The purpose of this educational exhibit is to demonstrate the way of good ultrasound examination after pediatric liver transplantation.
Methods & Materials: Methods of this exhibit include the demonstration of the technical aspect of routine ultrasound examination after pediatric liver transplantation including tips and pitfalls.
Materials are provided by personal experience of more than 2,000 ultrasound examinations during recent 10 years since introduction of pediatric liver transplantation program at author's institution. Majority of the patients are the recipients of a left lateral segment from living-donor liver transplantation. A small number of deceased donor liver transplantation recipients are also included.
Results: Routine postoperative ultrasound examination includes vascular analysis by means of color-coded imaging, and evaluation of liver parenchyma, intrahepatic bile duct, localized fluid collection surrounding the transplanted liver, pleural effusion, intraperitoneal fluid collection, and intestinal peristalsis and intestinal wall thickness. In regard to the evaluation of the vascular structure, RI and peak systolic velocity of the hepatic artery, mean velocity and flow volume of the portal vein, and maximum

velocity of the hepatic vein are measured and recorded. Demonstration of the hepatic artery is sometimes technically demanding for example it located behind the portal vein. Careful evaluation of the vascular structure is mandate for early detection of their complications.
Conclusions: With high quality ultrasound examination after pediatric liver transplantation, precise selection of the candidate for further diagnostic test such as CT and/or MR imaging will be conducted. Accurate ultrasound result sounds good to transplant surgeon for prompt action in regard to therapeutic intervention.

Poster #: EDU-024

Early Onset Infantile Inflammatory Bowel Disease

John Adu, BSc, MBChB, *Radiology, Great Ormond Street Hospital, London, United Kingdom, john.adu@bartshealth.nhs.uk;* Tom Watson

Disclosures: All authors have disclosed no financial interests, arrangements or affiliations in the context of this activity.
Purpose or Case Report: The inflammatory bowel diseases (IBD), Crohn's disease (CD) and ulcerative colitis (UC) are multifaceted disorders as a consequence of complex interplay between genetic, environmental and immunological factors, leading to a dysregulated immune response of the host intestinal bacteria. In children both the mucosal immune system and the intestinal microflora are still developing. Taken together, it seems that patients with early onset IBD (EO-IBD) are a unique subset within IBD with particular gene defects, phenotypic appearance, drug responsiveness and immune pathology.
Imaging plays a key role in the diagnosis and follow-up of EO-IBD, with MRI enterography being the gold standard in modern IBD practice, largely because of its ability to provide excellent spatial resolution without ionising radiation. EO-IBD can also be elegantly demonstrated on ultrasound and can be used a complimentary imaging tool in both the diagnostic workup and follow up imaging.
The aims of this educational exhibit are to:
(i) Provide a pictorial review of the key imaging finding of EO-IBD as demonstrated on MRI and ultrasound.
(ii) Review the imaging techniques and protocols for MR enterography as applied to EO-IBD.
(iii) Discuss the role of genetic mutations and innate immune defects in the pathophysiology of EO-IBD.
Methods & Materials: Images provided are from retrospective review over a 10 year period (2005 - 2015) of confirmed cases of EO-IBD who were managed at our institution.
Results: N/A.
Conclusions: EO-IBD is a distinct subtype of IBD and differs from later onset and adult IBD with regards to genetics, disease location and responsiveness to treatment. Paediatric radiologists must have a solid knowledge and understanding of the optimum imaging techniques and protocols to facilitate diagnosis, and also be familiar with the key imaging findings and disease distribution in EO-IBD.

Poster #: EDU-025

MRI of the Neonatal and Pediatric Orbit

Georgia Papaioannou, Director, *Pediatric Radiology, Mitera Hospital, Athens, Greece, gpapaio@hotmail.com;* Evangelia Manopoulou, Irene Vraka, George Magganas, Spyros Yarmenitis, John Zambelis, Nikolaos Kritikos

Disclosures: All authors have disclosed no financial interests, arrangements or affiliations in the context of this activity.
Purpose or Case Report: To illustrate a spectrum of MRI findings of the orbital anomalies and pathologies in the neonates and children.
Methods & Materials: Normal MRI orbital anatomy will be analyzed. MRI findings in orbital pathological entities (congenital, inflammatory, neoplastic) will be discussed and illustrated.
Conclusions: A pictorial essay of the pediatric MR orbital imaging of the normal and the abnormal.

Poster #: EDU-026

Lumps and Bumps of the Head and Neck in Neonates, Infants and Children: Spectrum of Imaging Findings

Georgia Papaioannou, Director, *Pediatric Radiology, Mitera Hospital, Athens, Greece, gpapaio@hotmail.com;* Panagiotis Tagalakis, Christina Meleti, Evangelia Manopoulou, Spyros Yarmenitis, Nikolaos Kritikos

Disclosures: All authors have disclosed no financial interests, arrangements or affiliations in the context of this activity.
Purpose or Case Report: To illustrate the findings of multimodality imaging exploration of the lumps and bumps in the pediatric neck and head.
Methods & Materials: Population includes neonates, infants and children referred to our department for the investigation of a palpable lump in the head and the neck. Ultrasound was the investigation of choice which resulted in the diagnosis in the majority of the cases. Complex pathologies required further exploration with MRI to set the final diagnosis and organize surgical planning.
Results: Typical imaging features of these entities (sternomastoid tumor of infancy, lymphadenopathy, infections and abscesses, vascular dysplasias, inclusion cysts, congenital cysts, thyroid gland pathologies, dental pathologies, benign and malignant tumors) investigated with ultrasound and/ or MRI are presented in detail.
Conclusions: Imaging investigation of lumps and bumps in the pediatric head and neck is usually straight forward with ultrasound; however complex pathologies may require more detailed investigation with MRI.

Poster #: EDU-027

Trampoline Injuries: One Giant Leap Can Lead to One Small Step; Reviewing Proximal Tibial Metaphyseal Fractures

Jane McEniery, *Medical Imaging Nuclear Medicine, Lady Cilento Children's Hospital, Brisbane, QLD, Australia, janeymceniery@gmail.com*

Disclosures: All authors have disclosed no financial interests, arrangements or affiliations in the context of this activity.
Purpose or Case Report: Trampoline-related injuries in children are a common cause for presentation to the Emergency Department, and their incidence is increasing. Injuries to the lower limb are the most common. Transverse fractures of the proximal tibial metaphysis are a well-described classic fracture. These fractures may be subtle, only diagnosed at the time of follow up x rays. When reviewed at Radiology Quality Assurance meetings, these missed fractures were perceptible on the original imaging. We sought to examine the characteristics of fractures that were missed, and elucidate measures that could improve diagnostic accuracy.
Methods & Materials: All patients who received conventional x rays of the lower limb for trampoline-related injuries at the Mater Children's Hospital during the 6 year period January 2009 - December 2014 were reviewed. Patient demographics included gender and age. The referring department and mechanism of injury was determined from the request form. The regions x rayed and the views

obtained were noted. All imaging was reviewed to assess for fracture and for any complications such as non union or angulation. Where fractures were present, reports were reviewed to determine the timing of fracture diagnosis. The fractures were classied as to bone, location (diaphysis, metaphysis), involvement of growth plate, and type: complete/incomplete. Particular attention was paid to those fractures within the proximal tibial metaphysis.
Results: 250 patients (102 male, 148 female) underwent x rays of the lower limb for trampoline-related injuries. The vast majority (242) were referred by the Emergency Department, the remainder from primary care or outpatient clinics. The average age was 3.6 years (range 1 - 15 years). Fractures were present in 45% patients. Of these, 62% were located in the proximal tibial metaphysis. While the majority were diagnosed at the time of original injury, in our series, 10% were not. These fractures were subsequently diagnosed at the time of first follow up x ray. The fractures that were missed were subtle: either undisplaced linear fractures of the "hairline" variety or incomplete, buckle type fractures. The buckle fractures that were not perceived commonly occurred in a region of overlap between the proximal tibia and fibula on the AP projection. When femoral x rays were also performed at the time of injury, this improved conspicuity of proximal tibial fractures, particularly those of the buckle type. There were no complications of non union or significant angulation, with mean follow up duration of 4.7 weeks.
Conclusions: Trampoline-related injuries are increasing in frequency, despite measures to improve product design and safety standards. The proximal tibial metaphysis is the classic site of trampoline fracture, however these may be subtle. Delayed diagnosis has obvious implications on patient management. In our review, the most commonly missed fracture types were undisplaced linear and buckle fractures, particularly those with isolated angulation of the lateral tibia. Buckle fractures often occurred in a region of overlap between the proximal tibia and fibula on the AP projection. When x rays of the femur are also performed, re-assessment of the tibia is recommended, as this view may result in increased conspicuity of proximal tibial fractures compared with images of the tibia/fibula alone, due to differences in centring of the x ray beam. Windowing of images may improve conspicuity of subtle, undisplaced linear fractures. In order to reduce delayed diagnosis, the proximal tibial metaphysis should be an area of review when reporting x rays for patients with trampoline injuries. Specific attention to any region of overlap of the proximal tibia/fibula on the AP projection and re-assessment of the proximal tibia on any femur x rays (if these were also performed) can improve diagnostic accuracy.

Poster #: EDU-028

Traumatic Solid Abdominal Organ Injury in the Paediatric Population – What You Need to Know and What You Need to Look Out for

John Adu, BSc, MBChB, *Royal London Hospital, London, United Kingdom, john.adu@bartshealth.nhs.uk;* Kirsteen McDonald

Disclosures: All authors have disclosed no financial interests, arrangements or affiliations in the context of this activity.
Purpose or Case Report: In a child the abdominal organs are more at risk from blunt injury, the reasons for this include the fact that the organs are relatively more anterior and inferior and lie inferior to the ribs rather than behind them as in an adult. Additionally, paediatric ribs are cartilaginous and so although rib fractures are less likely, compressive injuries secondary to the relative elasticity of the rib cage are far more common. The computed tomography (CT) features of abdominal visceral injury include lacerations, subcapsular or parenchymal haematomas, active haemorrhage, and vascular injuries, all of which the radiologists must be familiar with. Although there is an increasing trend toward non-operative management of abdominal solid organ injury, radiologists must also be aware of the key imaging features that suggest the need for surgical or interventional radiology input.
Based on our experience as one of the largest Level 1 trauma centres in Europe, the aims of this educational exhibit are to:
(i) Provide a pictorial review the spectrum of findings in blunt injury to the liver, kidneys and spleen as demonstrated on CT.
(ii) Discuss the role of Interventional Radiology in cases of associated vascular injury.
Methods & Materials: The Trauma Audit Research Network (TARN) was searched to produce a list of paediatric patients (<16 years of age) who had imaging performed in our institution institution following trauma. This generated a list of paediatric patients that had sustained liver, renal or spleninc trauma. Images were then reviewed using our local Pictures Archiving and Communications System.
Results: N/A.
Conclusions: CT accurately depicts various patterns of abdominal visceral injuries and other associated surgically important findings. Knowledge of the CT findings of visceral injury is vital for both radiologists and surgeons for optimum patient care. In particular, radiologists must be vigilant for the key imaging features that necessitate surgery or interventional radiology input.

Poster #: EDU-029 – *Withdrawn*

Poster #: EDU-030

Everything the Radiologist Needs to know about Scoliosis Surgery

Alaa Alsharief, *Pediatric Radiology, Dalhousie University, Halifax, NS, Canada, a.alsharief@hotmail.com;* R. El-Hawary, P. Schmit

Disclosures: All authors have disclosed no financial interests, arrangements or affiliations in the context of this activity.
Purpose or Case Report: To review the radiological findings of different orthopaedic implants and techniques used to treat Adolescent Idiopathic Scoliosis (AIS) and Early Onset Scoliosis (EOS).
To present the imaging findings of their most frequent post-operative complications.
Methods & Materials: We retrospectively reviewed and selected the most didactic post surgical spinal imaging of patients treated at our institution for AIS and EOS to document and to present the historical steps of AIS and EOS surgical treatments.
Results: Post-operative imaging after Harrington rods, Luque rods, Luque-Galveston implants and segmental pedicle screw for AIS will be presented along with the related post-operative complications as pseudoarthrosis, implant failure, spinal infection and altered biomechanics.
Regarding EOS, the guiding principles used for AIS could not apply to a growing spine as they would impede on lung development. So, other devices have been developed to correct the curve and to allow spinal growth. These include VEPTR (requiring repetitive surgeries) and MAGEC (with a magnetic locking/unlocking system). Other more recent ones are SHILLA and thoracoscopic anterior spinal tether which allow guided growth of the spine without repetitive interventions.
Conclusions: Knowledge of the different procedures and implants used in the treatment of AIS and EOS, the rationale behind the different techniques and their expected post-operative complications allows the radiologist to easily assess post-operative radiological findings, provide insightful follow up, and ensure better communication with the orthopaedic surgeons.

Poster #: EDU-031

Mayer-Rokitansky-Kuster-Hauser Syndrome; Spectrum of Presentation and the Utility of Daignosis Using US and MRI

Tahani Alturkistani, *RAdiology, Children's National Medical Center, Hyattsville, MD, drtoti3@gmail.com;* Terry Levin, MD, Jessica Kurian, Fernanda Mazzariol

Disclosures: All authors have disclosed no financial interests, arrangements or affiliations in the context of this activity.
Purpose or Case Report: 1. To review the embryology of female genital system.
2. To define Mayer-Rokitansky-Küster-Hauser syndrome (MRKH) and atypical MRKH, also called MURCS (Müllerian aplasia, unilateral renal agenesis and anomalies of the cervico-thoracic somites).
3. To discuss the imaging findings and clinical management of classic MRKH and contrast it to MURCS.
4. To discuss the rare association of MRKH and MURCS with gonadal dysgenesis/agenesis. US and MR were evaluated to determine efficacy of identifying adnexae.

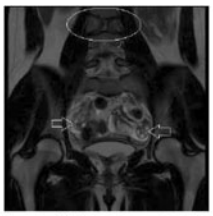

Coronal T2-weighted MRI in an 18-year old with MURCS. Both ovaries are normal (yellow arrows). Note the associated hemivertebrae in the lower lumbar spine (yellow circle).

Methods & Materials: A retrospective review (2000-2015) of diagnosed cases of MRKH/MURCS was performed using Montage search engine. The medical records of these patients were reviewed. Chromosomal abnormalities, physical examination findings and the identification of associated abnormalities including cardiac, renal, and skeletal anomalies were recorded. Sonographic and MR examinations were also reviewed. Images were evaluated for type of uterine anomaly as well as the presence or absence of ovarian, skeletal, cardiac or renal anomalies. In patients with abnormal ovaries, MR images were evaluated to determine the most reliable method to locate ovarian tissue.
Results: Eight patients were identified with MRKH or MURCS. Two had MRKH with normal ovaries, one had MRKH with complete gonadal agenesis, three had MURCS with normal ovaries, and two had MURCS, one with a streak gonad and the other with bilateral ovarian agenesis. Of the patients with MURCS, two had renal anomalies (solitary kidney and horseshoe pelvic kidney), and two had skeletal anomalies.
All patients were karyotypically female 46xx with two cases of 46xx with chromosomal deletion and one 46xx with chromosomal duplication.
In all patients, MRI was more accurate in delineating the extent of Müllerian dysgenesis and in confirming the presence or absence of normal gonadal tissue.
Conclusions: MRKH and MURCS, both related syndromes which occur secondary to a type 1 Müllerian agenesis/dysgenesis affecting the uterus and upper third of vagina in phenotypically and karyotypically females may present with normal, absent or dysplastic ovaries.
Identification of streak or ectopic gonads is essential in this patient population as early treatment with hormonal replacement therapy will allow these patients to develop secondary sexual characteristics.
MRI is superior to ultrasound in characterizing the degree of mullerian agenesis/dysgenesis as well as in identifying and locating gonadal tissue.

Poster #: EDU-032

Computed Tomography of Pediatric Penetrating Trauma: Optimizing Image Acquisition and Interpretation

Tahani Alturkistani, *Children's National Medical Center, Washington, DC, drtoti3@gmail.com;* Bernard Goldwasser, Einat Blumfield, Mark Liszewski, Benjamin Taragin

Disclosures: All authors have disclosed no financial interests, arrangements or affiliations in the context of this activity.

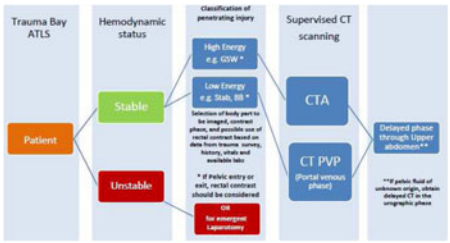

Purpose or Case Report: 1) To understand penetrating injury in pediatric patients and how the child's body habitus is more susceptible to multi organ injury than that of adult.
2) To explain the role of computed tomography (CT) in a pediatric penetrating trauma triage algorithm.
3) To discuss optimization of CT protocols in pediatric trauma patients based on the mechanism of injury with attention to radiation dose reduction.
4) To review the imaging findings in penetrating injuries to the chest, abdomen and pelvis.
Methods & Materials: Retrospective review of penetrating trauma cases in pediatric patients, 0-21 years of age, was performed. The cases were from two hospitals in New York metro area (level 1 and level 2 trauma centers).
Injuries were divided into high energy injury, such as gun shot, and low energy injury, such as stabbing. Injuries to the superficial soft tissues, musculoskeletal system, spine, head, and neck were excluded. Injuries of interest involve the chest, abdomen and pelvis, including vascular injuries are included as well. History and mechanism of injury, image findings as well as CT protocols were recorded.
Results: 18 cases of pediatric penetrating trauma were identified. 10 cases were classified as low energy and 8 were high energy injuries. Injuries involved solid organs such as the liver and spleen as well as hollow organs such as the colon and rectum. All were hemodynamically stable and underwent contrast enhanced CT imaging. All injuries were well delineated although imaging protocols varied depending on the mechanism of injury and suspected organ injured.
Conclusions: Penetrating trauma is a cause of severe injury in children. By utilizing optimized CT protocols, radiologists can achieve excellent image quality while reducing dose and making potentially life saving diagnoses.

Poster #: EDU-033

Congenital Chest Lesions: A Pictorial Review

Kimberly Funaro, MD, *Radiology, University of South Florida, Riverview, FL, kfunaro@health.usf.edu;* Jennifer Kucera, MD, MS

Disclosures: All authors have disclosed no financial interests, arrangements or affiliations in the context of this activity.

Purpose or Case Report: Congenital chest lesions encompass a wide array of pathology with overlapping imaging characteristics. With prenatal ultrasound and MRI, more congenital chest lesions are being detected sooner, and it is important for radiologists to be familiar with their imaging findings for both diagnostic and prognostic purposes. This educational exhibit reviews the spectrum of pediatric congenital chest lesions and their key imaging findings.
Methods & Materials: Congenital chest lesions detailed in this exhibit are illustrated using radiography, CT, ultrasound, and MRI, including fetal imaging. The abnormalities are described with an emphasis on the key imaging features to distinguish each entity.
Results: The range of congenital chest abnormalities is broad and encompasses a spectrum of normal to abnormal vasculature with normal to abnormal lung. This pictorial review presents the most commonly encountered lesions and their imaging findings. Additional chest lesions which do not fit into the designated categories of bronchopulmonary foregut malformations or vascular anomalies will also be discussed separately.
1. Normal vasculature-abnormal lung: Pulmonary aplasia/agenesis, bronchial atresia, congenital lobar hyperinflation, bronchogenic cyst, congenital pulmonary airway malformation (types I-III), tracheoesophageal fistula, combination lesions
2. Abnormal vasculature-abnormal lung: Sequestration (intralobar and extralobar), scimitar syndrome
3. Abnormal vasculature-normal lung: Pulmonary arteriovenous malformation, pulmonary sling
4. Other chest pathology: Congenital diaphragmatic hernia
Conclusions: Neonatal chest lesions are commonly encountered by the radiologist, and an understanding of their pre- and postnatal imaging features is necessary for accurate diagnosis to guide proper treatment. By grouping these lesions using the above the categories, congenital chest lesions can be more easily approached and diagnosed by the radiologist, leading to optimal patient care.

Poster #: EDU-034

Congenital Bone Anomalies: Part I-Upper Extremity

Ali Al-Saraf, *Radiology, University of Chicago, Chicago, IL, ali1987@sbcglobal.net;* Seng Ong

Disclosures: All authors have disclosed no financial interests, arrangements or affiliations in the context of this activity.
Purpose or Case Report: Congenital anomalies of bone are many and can be difficult to approach. In addition, it is important to recognize that while some of these anomalies occur sporadically or in isolation, others are inherited or associated with systemic conditions/syndromes that require further assessment, diagnostic testing, and proper referral.
In this two-part exhibit, congenital bone anomalies of the upper and lower extremities will be reviewed. The first part of the exhibit will cover upper extremity anomalies while the second part will focus on the lower extremity. The purpose is multifold: 1. To illustrate the wide spectrum of congenital bone anomalies based on classic clinical presentation and demographics. 2. Highlight key imaging characteristics across multiple modalities to allow for accurate differentiation between the various congenital bone anomalies of the extremities. 3. Guide the viewer to proper workup and referral for these entities.

Methods & Materials: Patients with congenital upper extremity bone anomalies encountered in our institution were reviewed and selected for illustration. Clinical presentation as well as key imaging findings unique to each of these conditions will be highlighted to allow for efficient and accurate differentiation.
Results: In the first part of this exhibit, multiple entities encompassing upper extremity congenital bone anomalies are succinctly characterized. These include: Radial Deficiency, Ulnar Deficiency, Constriction/Amniotic Bands, Carpal Fusion, Radioulnar Synostosis, Kirner Deformity, Delta Phalanx, Clinodactyly, and Camptodactyly.
Conclusions: Congenital bone anomalies require an appropriate diagnosis as well as proper communication and, if warranted, referral. Through this exhibit, the process will be simplified for the radiologist to reaching the correct diagnosis and to implement the appropriate workup.

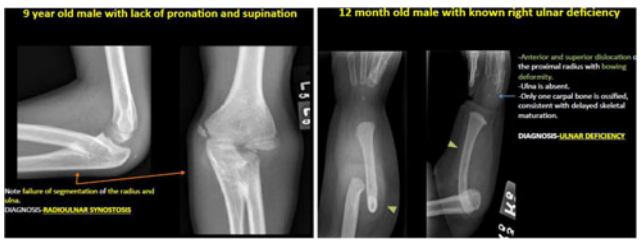

Poster #: EDU-035

Holes in the Dome: MR imaging of late presenting and recurrent diaphragmatic defects in children

Wendy Kim, MD, *Department of Radiology, University of Maryland Medical Center, Baltimore, MD;* Jesse Courtier, MD, Cara Morin, Narendra Shet, MD, Eric Strauch, Jane Kim, M.D.

Disclosures: All authors have disclosed no financial interests, arrangements or affiliations in the context of this activity.
Purpose or Case Report: Late-presenting or recurrent diaphragmatic defects can pose a diagnostic challenge due to varying clinical presentations. Current diagnostic approaches include plain film radiograph for initial assessment, with other imaging modalities such as fluoroscopy, ultrasound, CT and MRI mainly employed for troubleshooting. As a radiation-free modality, MRI can provide a more definitive diagnosis in particular cases due to its ability to visualize discontinuity of the diaphragm (distinguishing it from eventration), hernia contents, defect location and size.
In this exhibit, we will:
1. Review the normal appearance of the diaphragm.

2. Share our institutional MRI protocol for optimal evaluation of the diaphragm, including use of CINE steady state free precession sequences and use of negative slice spacing in T2 weighted images.
3. Discuss important postnatal MR imaging findings of late presenting and recurrent diaphragmatic hernias in children.
4. Describe potential diagnostic pitfalls in the imaging of the diaphragm.
Methods & Materials: We present MRI cases performed for suspicion of late presenting and recurrent diaphragmatic hernias at two academic pediatric hospitals. Representative cases were selected to demonstrate a variety of hernia types and contents, which were correlated with other available imaging modalities, clinical course and intraoperative findings.
Results: Select MRI cases of different hernia types including late presenting Bochdalek and Morgagni hernias, acquired hiatal hernias, and recurrent congenital diaphragmatic hernias are reviewed with relevant discussion of the imaging findings and correlation with intraoperative findings.
Conclusions: MRI can be a useful diagnostic tool in the assessment of late presenting or recurrent diaphragmatic hernias.

Poster #: EDU-036

Tight Spaces: A Review of Clinical Findings and Imaging Features of Compression Syndromes

Ingy Sleman, MD, *Radiology, Montefiore Medical Center, Bayonne, NJ, ingyhanna@gmail.com;* Benjamin Taragin, Jessica Kurian

Disclosures: All authors have disclosed no financial interests, arrangements or affiliations in the context of this activity.

Purpose or Case Report: Compression syndrome is the entrapment of any vessel or luminal structure by another vessel. These are often due to an underlying anatomic anomaly or variant. Though seen in young and healthy individuals, compression syndromes may have severe clinical outcomes including arterial ischemia, embolism, early satiety, hypertension, weight loss, dyspnea, venous stasis and thrombosis. The purpose of this educational exhibit is to familiarize radiologists and clinicians alike with the clinical presentation, best diagnostic imaging modalities and characteristic imaging features for the diagnosis of compression syndromes in the pediatric population.
Methods & Materials: We will review the clinical presentation, imaging techniques and features of compression syndromes in which a vessel compresses another vessel such as May-Thurner Syndrome (left common iliac vein compression syndrome) and Nutcracker Syndrome (renal vein entrapment syndrome) as well as those in which a nonvascular structure compresses a vessel as in Paget-Schroetter Syndrome (effort thrombosis) and popliteal artery entrapment. We will also discuss compression syndromes in which vessels compress luminal structures such as innominate artery compression syndrome, superior mesenteric artery syndrome, and uretero-pelvic junction obstruction.
Conclusions: Compression syndromes often occur in young, healthy individuals and may present with a variety of subtle and non-specific symptoms. Often the unusual clinical presentation and imaging features must be correlated to diagnose compression syndromes. It is important to familiarize clinicians and radiologists with these entities, as prompt diagnosis and treatment can prevent any long term morbidity or sequelae.

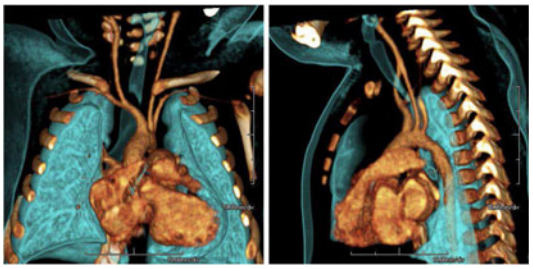

Poster #: EDU-037

Review of Nonmalignant Inguinal Masses in Pediatric Patients

Shannon Farmakis, MD, *St. Louis University School of Medicine, St. Louis, MO, farmakis@slu.edu;* Geetika Khanna

Disclosures: All authors have disclosed no financial interests, arrangements or affiliations in the context of this activity.

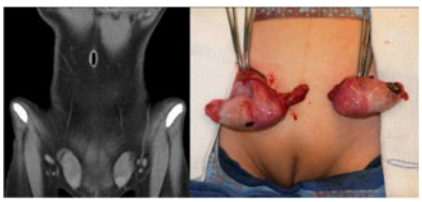

Purpose or Case Report: Located at the border between the abdomen and the groin, the inguinal region can be a cause for consternation for the practicing radiologist. The inguinal canal can be a site for pathology secondary to abdominal or scrotal pathology. Though lymphadenitis is the most common cause of an inguinal mass in a child, a variety of conditions can result in an inguinal mass.
The purpose of our poster is to review the imaging appearance and differential diagnosis of various potential causes of nonmalignant inguinal masses in children.

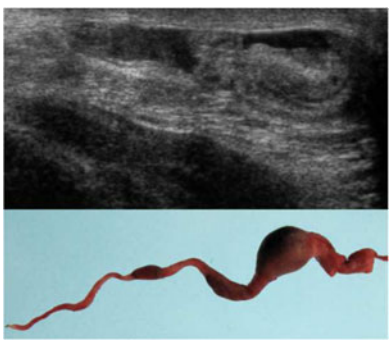

Methods & Materials: Our cases will be derived from the archives of two tertiary level childrens' hospitals We present a pictorial essay reviewing the embryology, anatomy, and nonmalignant pathologies that can present as an inguinal mass in pediatric patients.
Results: Our poster will be organized as follows:
1. Normal anatomy of the inguinal region.
2. Normal embryology of the inguinal region.
3. Benign pathologies with emphasis on imaging findings and differential diagnosis:
a. Inflammatory: Lymphadenitis/abscesses
b. Congenital: Hydrocele, funicular cyst, meconium peritonitis.
Hernia–including bowel/omentum, ovaries, uterine, bladder
c. Gonadal: undescended testicle (including androgen insensitivity), retractile testis, ovotestis
d. Vascular: varicocele, pseudoaneurysm, hematomas
Conclusions: Non-malignant conditions affecting the inguinal canal can be normal variants, congenital anomalies, vascular abnormalities, and infectious or inflammatory processes. The inguinal region requires careful attention to avoid misdiagnosis.

Poster #: EDU-038

Pediatric Orbital Abnormalities: A Pictorial Review

Heidi Lewis, MD, *Radiology, University of South Florida, Tampa, FL, HLewis1@health.usf.edu;* Jennifer Kucera, MD, MS

Disclosures: All authors have disclosed no financial interests, arrangements or affiliations in the context of this activity.
Purpose or Case Report: The pediatric orbit presents a wide spectrum of possible abnormalities which differ significantly from those seen in adults. Evaluation of the various pediatric orbital abnormalities depends on radiologic assessment with different imaging techniques to aid in diagnosis. The purpose of this exhibit is to describe and differentiate the more commonly encountered pediatric orbital abnormalities using a multimodality approach.
Methods & Materials: Orbital abnormalities detailed in the exhibit are illustrated using CT, MRI and ultrasound. The abnormalities are described with emphasis on the specific imaging characteristics which help distinguish each abnormality.
Results: The pictorial review will be divided into three broad categories: congenital, inflammatory and neoplastic abnormalities. A brief review of the anatomy of the pediatric orbit will be provided, with the focus of the exhibit on the most common orbital abnormalities encountered in the pediatric population. The following abnormalities will be discussed: 1. Congenital abnormalities: coloboma, persistent hyperplastic primary vitreous, dacrocystocele, hemangioma, dermoid/epidermoid, and fibrous dysplasia. 2. Inflammatory processes: orbital cellulitis, inflammatory pseudotumor, and dacrocystitis. 3. Neoplastic lesions: optic nerve glioma, leukemia/lymphoma, metastatic disease, and rhabdomyosarcoma.
Conclusions: The pediatric orbit can be affected by a wide variety of potential abnormalities. Recognition of the imaging appearance of the many different pediatric orbital abnormalities is important to aid in prompt diagnosis and to help guide treatment.

Poster #: EDU-039

Unique Challenges of CT Angiography with ECMO

Nathan Hull, M.D., *Department of Radiology, Mayo Clinic, Rochester, MN, hull.nathan@mayo.edu;* Tiffany Robb, Phillip Young

Disclosures: All authors have disclosed no financial interests, arrangements or affiliations in the context of this activity.
Purpose or Case Report: This poster will review the complexities and challenges of performing CTA on pediatric patients on ECMO and provide practical suggestions for performing these exams.
Methods & Materials: Illustrative case examples and sample calculations will be used to discuss the complexities of these exams including the basics of ECMO and associated altered hemodynamic flow, safety issues with CT table excursion and contrast injection, contrast dosing and scan time, and coordination with critical care providers and perfusionists.
Results: After review of this poster, the reader should have an improved understanding of the unique challenges when performing CTA on pediatric patients on ECMO.
Conclusions: Performing CT angiography on pediatric patients with ECMO can be very challenging. It requires an understanding of the patient's underlying anatomy and pathology, the flow dynamics of ECMO, as well as coordination with critical care providers and perfusionists to successfully perform these exams.

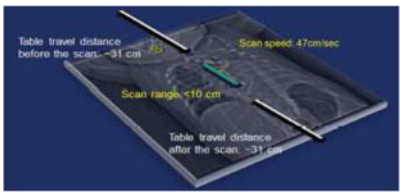

Poster #: EDU-040

Duplication of the Pituitary Gland: A Review of Embryology and the Theories of Pathogenesis

Judith Gadde, DO, *University of Wisconsin Hospital & Clinics, Fitchburg, WI, jgadde@uwhealth.org;* Susan Rebsamen, Tabassum Kennedy

Disclosures: All authors have disclosed no financial interests, arrangements or affiliations in the context of this activity.
Purpose or Case Report: 1. To briefly review the embryology and anatomy of the pituitary gland.
2. To illustrate the imaging spectrum of duplication of the pituitary gland through an example, to include often associated anomalies such as thickening of the hypothalamus and a palatal teratoma.
3. To review the theories of pathogenesis leading to duplication of the pituitary gland.
Methods & Materials: All CT and MR imaging included for embryologic or anatomic correlation was performed at our instutition. Any graphic illustrations will be appropriately cited from the literature as necessary. The example case of duplication of the pituitary gland was both performed at our institution, as well as at outside institutions as mentioned.
Results: The embryology and anatomy of the pituitary gland will be briefly reviewed via graphic illustrations, as well as CT and MR imaging. An example of pituitary gland duplication from our institution will be described. Further description of the potential anomalies associated with duplication of the pituitary gland will be discussed. The theories of pathogenesis to include anomalies of notochord formation leading to pituitary gland duplication will also be reviewed.
Conclusions: Duplication of the pituitary gland is a relatively rare finding that can also have various associated anomalies. Understanding the embryology of the pituitary gland, as well as the pathogenesis specificaly associated with duplication of the gland, is important. Pediatric radiologists and pediatric neuroradiologists should be familiar with this rare entity and the associated imaging spectrum in order to target imaging studies appropriately to look for any additional associated findings.

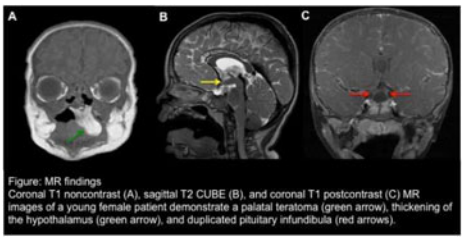

Figure: MR findings
Coronal T1 noncontrast (A), sagittal T2 CUBE (B), and coronal T1 postcontrast (C) MR images of a young female patient demonstrate a palatal teratoma (green arrow), thickening of the hypothalamus (green arrow), and duplicated pituitary infundibula (red arrows).

Poster #: EDU-041

Imaging in the Diagnosis of Pediatric Urolithiasis

Gabrielle Colleran, MD, MB BCh BAO, FFR RCSI, *Radiology, Boston Children's Hospital, Brookline, MA, gabrielle.colleran@childrens.harvard.edu;* Michael Callahan, MD, Jeanne Chow

Disclosures: All authors have disclosed no financial interests, arrangements or affiliations in the context of this activity.
Purpose or Case Report: Pediatric urolithiasis is an important and increasingly prevalent cause of pediatric morbidity and hospital admission. Ultrasound is the recommended primary imaging modality for suspected urolithiasis in children and this view is endorsed by all of the largest pediatric and urological societies.
There is however widespread use of CT as a first line study for abdominal pain in many institutions involved in pediatric care, many of whom are free standing hospitals delivering predominantly adult care.
The purpose of this educational review is to outline the state-of-the-art imaging modalities and methods for diagnosing urolithiasis in children and to suggest an imaging algorithm for best practice.
Methods & Materials: A literature review was performed to identify the best practice use of the various imaging modalities in the diagnosis of urolithiasis with emphasis on methods to optimize ultrasound sensitivity and advances in CT technology.
Representative urolithiasis cases were identified from our departmental databases, with images selected to illustrate the various teaching points.
Results: A best practice algorithm for imaging of the pediatric patient with suspected urolithiasis is suggested, starting with US as the initial imaging modality.
Recent advances in CT technology enable a significant reduction in dose, while maintaining diagnostic sensitivity and specificity. Indications for CT where US is inconclusive will be discussed with consideration of radiation exposure and optimized protocols.
The use of dual-energy CT for renal stone spectral analysis is also discussed with case examples.
Conclusions: The pediatric radiologist plays a key role in ensuring that the appropriate imaging modality is performed in the setting of suspected pediatric urolithiasis.
Our proposed imaging algorithm starts with ultrasound, and describes the optimal technique and indications for the use of CT.
Since most hospitals use adult protocols where CT is the first evaluation tool for urolithiasis, there needs to be improved communication with a greater collaborative approach between pediatric and general radiology departments so that pediatric patients undergo the appropriate imaging evaluation.

Poster #: EDU-042

Venous Malformations: Untangling their Common and Unusual Presentations with State-Of-The-Art MRI

Nicole Hughes, *Radiology & Biomedical Imaging, UCSF, San Francisco, CA, nicole.hughes@ucsf.edu;* Andrew Phelps, MD, Anna Meyer, Jesse Courtier, MD, John MacKenzie, MD, Matthew Zapala, MD,PhD

Disclosures: All authors have disclosed no financial interests, arrangements or affiliations in the context of this activity.
Purpose or Case Report: Accurate diagnosis of venous malformations can be challenging, and confidently diagnosing them is important for accurate treatment. A thorough understanding of the etiology, imaging appearance, and important mimickers of venous malformations is critical for the radiologist to provide an accurate assessment for the clinician.

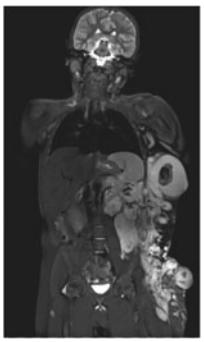

Methods & Materials: Using multiple case examples from our teaching file over the past 15 years, this exhibit will allow viewers to:
1. Review relevant developmental etiologies for venous malformations.
2. Learn optimal MR imaging technique for assessment of venous malformations, including use of blood-pool contrast agents and whole body MRI.
3. Understand most common imaging characteristics of venous malformations.
4. Discuss important mimics and imaging pitfalls in diagnosing venous malformations.
5. Learn the "must describe" features when reporting venous malformations.
6. Test the reader's knowledge with a brief quiz.
Results: This educational review will present the wide range of image features of venous malformations. The frequency of these features encountered in our patient population will emphasize the most useful imaging findings for appropriate diagnosis. The performance and utility of routine MRI, and advanced MRI such as blood-pool contrast agents and whole body imaging will be discussed. Case examples will be provided in addition to self-assessment questions.
Conclusions: Venous malformations are commonly encountered in pediatric imaging. This educational exhibit provides a review of MRI protocols and characteristic imaging patterns from our clinical database over the past 15 years. An in depth knowledge of the characteristic MRI findings, in addition to the MRI techniques available and their utility, will assist in concise diagnosis. If key MRI findings are present, the radiologist can confidently diagnose venous malformations. Furthermore, the radiologist's expertise can aid the clinical team involved in the patient's care.

Poster #: EDU-043

Strategies to Reduce Anesthesia Exposure for Magnetic Resonance Imaging: A review and update.

Anh-vu Ngo, MD, *Anh-Vu Ngo, Seattle Children's Hospital, Bellevue, WA, ango@uw.edu;* Randolph Otto

Disclosures: All authors have disclosed no financial interests, arrangements or affiliations in the context of this activity.
Purpose or Case Report: 1. To review clinical strategies for reducing the anesthesia exposure for magnetic resonance imaging exams.

2. To review magnetic resonance imaging protocols to reduce examination time.
Methods & Materials: Content Organization:
- Background information: Recent anesthesia literature suggests there are likely detrimental long term, dose dependent effects on cognitive and behavioral outcomes in infants and young children. Increased magnetic resonance imaging utilization requires better strategies to reduce such exposure.
- Preclinical strategies: Exam selection and appropriateness. Patient selection, predominantly depending on age. Selection amongst anxiolytics, sedation, and general anesthesia. Child life assessments and education prior to exams.
- Clinical strategies: Sleep deprivation, feed, swaddle, and scan in infants. Child life specialists participation in exams. Breathing instruction and exercises. Distraction techniques.
- Environmental optimization: Various themed suites and machines from different vendors.
- Protocols: Coil selection. Quiet gradients. Respiratory triggering. Radial motion averaging/correction. Signal averaging. Fast imaging. Differents ways to fill k-space, such as non-cartesian (radial), simultaneous multi-slice, and undersampling techniques.
- Protocol examples for specific exams and sample cases.
Conclusions: The major teaching points of this exhibit are:
1. Reiterate the potential long term effects of early anesthesia exposure.
2. Review the clinical strategies to avoid and reduce anesthesia exposure for magnetic resonance imaging examinations.
3. Provide specific protocol examples to reduce examination length.

Poster #: EDU-044

What they never teach us: Unusual Tumors and Tumor-Like Conditions in Scrotal Ultrasound

Marta Tijerin Bueno, Fellow, *Sickkids Hospital for Sick Children/ University of Toronto, Toronto, ON, Canada, tijerinradiologist@gmail.com;* Claudia Martinez-Rios, MD, Alan Daneman, Alejandro De La Puente Gregorio, Oscar Navarro

Disclosures: All authors have disclosed no financial interests, arrangements or affiliations in the context of this activity.

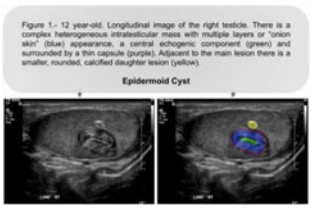

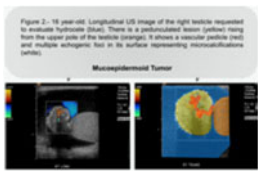

Purpose or Case Report: To review unusual sonographic findings of tumors and tumor-like conditions one can encounter in pediatric scrotal ultrasound and to design a diagnostic algorithm that can be useful with the challenges of differential diagnosis in this situation.
Methods & Materials: Retrospective review of scrotal ultrasound examinations performed in our institution, a tertiary pediatric hospital, between 2000 and 2015. Cases of unusual tumoral pathology or atypical sonographic presentation of common scrotal tumors and tumor-like conditions were selected and grouped according to certain imaging features, which included location of lesion (intra or extratesticular), texture (homogenous or heterogeneous), presence of cystic areas, fat and/or calcifications, and degree of vascularity on Doppler interrogation. Patient information collected included patient's age. Histopathology report of these tumors was reviewed whenever available.
Results: Categorization of the lesions based on patient's age and sonographic features allowed creation of a systematic approach to scrotal tumoral conditions that helped in the differential diagnosis.
Conclusions: A systematic approach to unusual tumor and tumor-like conditions found in scrotal ultrasound is our advice to face what they never teach us.

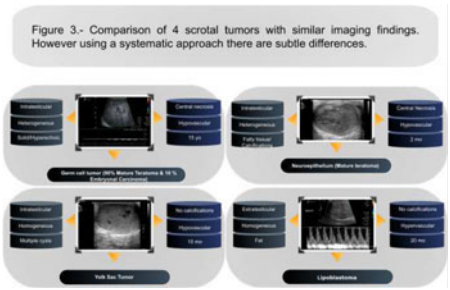
Figure 3.- Comparison of 4 scrotal tumors with similar imaging findings. However using a systematic approach there are subtle differences.

Poster #: EDU-045

Ollier's Disease: A Pictorial Review of MRI Findings

Eleza Golden, MD, *Radiology, Emory University, Atlanta, GA, eorenst@emory.edu;* Kiery Braithwaite, Kelley Marshall

Disclosures: All authors have disclosed no financial interests, arrangements or affiliations in the context of this activity.
Purpose or Case Report: To characterize the typical findings of Ollier's disease on MRI.

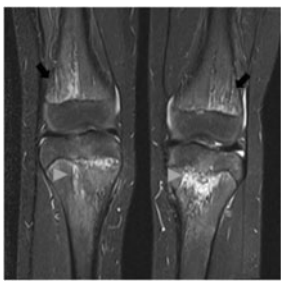

Methods & Materials: We performed a retrospective review of MRI scans of patients diagnosed with Ollier's disease at our institution from 2003 to 2015. The MRIs were reviewed by two pediatric radiologists and a pediatric radiology fellow. Specific characteristics evaluated included lesion morphology, appearance of the underlying bone with presence or absence of striated cartilaginous columns, multiplicity of lesions, lesion location, signal characteristics, and post contrast appearance. Additional patient data collected included age and symptoms at presentation, age at first imaging, was a skeletal survey performed, change in lesions over time, and pathology results.
Results: A total of 9 patients were identified. One patient was excluded due to discordant pathology results demonstrating multiple osteochondromas. Of the 8 patients included, 100% had metaphyseal lesions, 88% diaphyseal, and only 25% had lesions in the epiphysis. In patients with bilateral lesions, one side predominated. Right sided lesions occurred more frequently than left. All

patients had lesions that were T1 dark, T2 bright, expansile, and enhanced post contrast. Enhancement was predominantly solid although some patients had lesions with peripheral enhancement. 88% of patients had striated bones with tubular T1 dark, T2 bright columns extending from the physes into the metaphysis representing cartilaginous columns.
Conclusions: We illustrate the common MRI findings in Ollier's disease in a series of 8 patients. Our findings demonstrate that MRI is a useful adjunct to plain radiographs and CT in lesion characterization and detection in a disease that is primarily diagnosed by imaging.

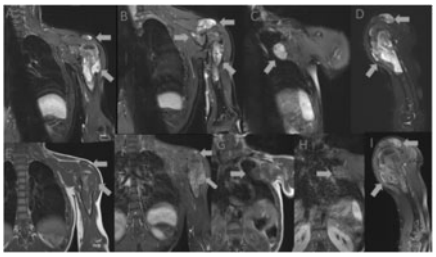

Poster #: EDU-046

Don't be a Dweeb, Use DWIBS in Pediatric Body Imaging

Monica Epelman, MD, *Radiology, Nemours Children's Hospital, Orlando, FL, monica_epelman@hotmail.com;* David Dinan, Thang Ngo, Craig Johnson, Fabiola Weber-Guzman, Tushar Chandra, Daniel Podberesky

Disclosures: Daniel Podberesky has indicated a relationship with Philips Healthcare. All other authors have disclosed no financial interests, arrangements or affiliations in the context of this activity.
Purpose or Case Report: The purpose of this exhibit is:
-To discuss the role of DWIBS (diffusion-weighted whole body imaging with background body signal suppression) in the evaluation of pediatric body imaging pathology and to identify common indications for its use
-To review normal DWIBS findings in various body organs and to understand imaging pitfalls
-To provide examples of pathological conditions seen on DWIBS

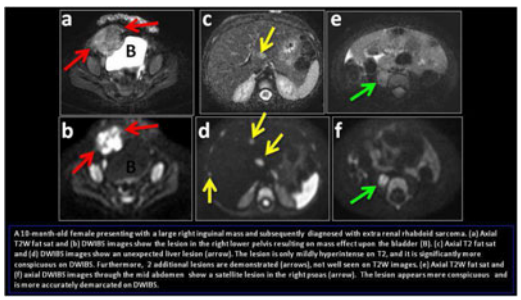

A 18-month-old female presenting with a large right inguinal mass and subsequently diagnosed with extra renal rhabdoid sarcoma. (a) Axial T2W fat sat and (b) DWIBS images show the lesion in the right lower pelvis resulting an mass effect upon the bladder (B). (c) Axial T2 fat sat and (d) DWIBS images show an unexpected liver lesion (arrow). The lesion is only mildly hyperintense on T2, and it is significantly more conspicuous on DWIBS. Furthermore, 2 additional lesions are demonstrated (arrows), not well seen on T2W images. (e) Axial T2W fat sat and (f) axial DWIBS images through the mid abdomen show a satellite lesion in the right psoas (arrow). The lesion appears more conspicuous and is more accurately demarcated on DWIBS.

Methods & Materials: We present cases in which DWIBS was used as part of a body MR study performed at our institution over the last 3 years.
Results: Several cases from our institution are presented to illustrate normal and abnormal findings of DWIBS imaging in children. Pitfalls will be emphasized. Technical aspects of DWIBS and the current role of the method in pediatric body imaging will be discussed.
Conclusions: DWIBS is a promising imaging technique increasingly being used in pediatric patients. The feasibility of free breathing and its relative short scan duration makes it ideal for pediatric patients. DWIBS sequence is performed with heavy diffusion weighting (b=1000 sec/mm^2) and fat suppression using an inversion or chemical shift-selective pre-pulse, such as STIR. Multiple thin axial slices with a high number of signal averages are acquired during free breathing, which is a unique feature making it ideal for its use in children. The axial source DW images may be reconstructed in the coronal plane and the gray scale may be inverted to resemble PET images. This is convenient for analyzing the distribution of primary lesions and their metastases. On DWIBS images there is suppression of background tissues with visualization of only those structures and lesions with low diffusion values. DWIBS aids in neoplasm detection, as these have restricted diffusion and characteristically display high signal with high b-values. DWIBS is also playing an expanding role in the detection of inflammatory processes, in the assessment of multifocal infection and abscess formation, and in monitoring response to treatment.

Poster #: EDU-047

Imaging Update in Takayasu's Arteritis

Mary-Louise Greer, MBBS, *Diagnostic Imaging, The Hospital for Sick Children/University of Toronto, Toronto, ON, Canada, marylouisegreer@yahoo.com;* Lars Grosse-Wortmann

Disclosures: All authors have disclosed no financial interests, arrangements or affiliations in the context of this activity.
Purpose or Case Report: Takayasu's arteritis (TA) is one of the most common childhood vasculitides, primarily involving large and, to a lesser extent, medium sized arteries. The aorta and pulmonary arteries are most frequently affected. Historically, diagnosis depended on typical fluoroscopic angiographic features, in conjunction with a number of clinical and hematologic criteria. Increasingly, a range of imaging modalities is used in initial diagnosis as well as for monitoring disease progression and treatment response. The purpose of this educational exhibit is to provide an update on the current role of imaging in TA, defining disease extent and activity, as well as highlighting end organ complications.

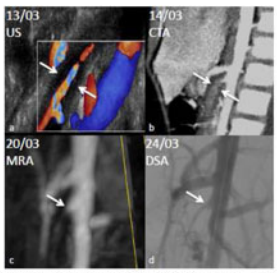

Figure 1. 5-year-old female with one month history of abdominal pain diagnosed with Takayasu's arteritis. Sagittal images from (a) abdominal ultrasound with colour Doppler, (b) CT Angiogram, (c) MR Angiogram maximum intensity projection and (d) Digital Subtraction Angiogram all show superior mesenteric artery narrowing, with mural thickening best seen here on (a) US and (b) CTA.

Methods & Materials: Utility and limitations of ultrasound (US), computed tomographic angiography (CTA), magnetic resonance angiography (MRA), and digital subtraction angiography (DSA) are discussed. Technical considerations for image optimization in children and adolescents are considered, based on literature review and the authors' experience in pediatric cardiovascular and body imaging. The imaging characteristics of TA across these modalities are illustrated through several cases.

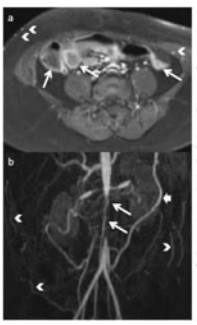

Figure 2. Same patient with non-responsive Takayasu's arteritis one year later, now with bowel ischemia from almost total superior mesenteric artery and abdominal aortic occlusion seen on abdominal MRA.

(a) Axial post contrast fat suppressed T1 turbo spin echo weighted image shows thick walled appendix, small and large bowel loops with mucosal enhancement (long arrows).

(b) Coronal MRA shows aortic and superior mesenteric artery high-grade stenoses (long arrows) with inferior mesenteric artery (short arrow) and abdominal wall collateral vessels (arrowheads in a & b).

Results: Primary manifestations of TA depend on disease chronicity. Mural and perivascular thickening and enhancement are signs of acute disease and can be seen on CTA with its high spatial resolution. Arterial narrowing and occlusion, observed both acutely and with chronic TA are well demonstrated by DSA, CTA and MRA. MRA's superior contrast resolution further aids distinction of active from inactive disease, avoiding ionizing radiation, as does US. MRA and US can also demonstrate altered flow dynamics. US depicts lumen, mural and perimural changes, although with small field of view; US contrast agents are increasingly used for wall enhancement. (Figure 1) End organ complications can involve the heart, lungs, bowel or solid abdominal organs. Imaging choice and related findings depend upon the clinical presentation, such as US or MRA for suspected bowel ischemia with wall thickening and mucosal enhancement. (Figure 2)
Conclusions: The range of modalities now utilized in TA evaluation has expanded. Comprehensive knowledge of the role of each helps ensure the most suitable technique is applied to resolve the clinical question during disease evolution, while minimizing risk. Distinguishing active from inactive disease and recognizing complications guide care for patients with TA.

Poster #: EDU-048

Oh, the places you'll gonads! An imaged-based review of misdirected and misplaced reproductive tissue in pediatric patients

Thomas Cullen, *Stanford University, Palo Alto, CA, cullen.tom@gmail.com;* Jayne Seekins, Safwan Halabi

Disclosures: All authors have disclosed no financial interests, arrangements or affiliations in the context of this activity.

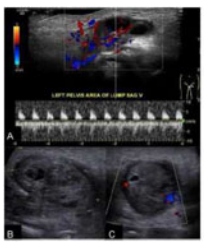

Figure 1: Herniated ovaries. A) 2 month old female with left groin mass. US with color Doppler demonstrates ovarian tissue within the canal of Nuck. Vascularity is preserved. B) 3 month old female with tender right groin mass. Grayscale and color Doppler ultrasound images demonstrate an enlarged ovary with heterogeneous stroma. Doppler showed no evidence of flow. An infarcted ovary was removed during surgical exploration.

Purpose or Case Report: The development and migration of reproductive organs is a complex process that is often poorly understood. Abnormally located testes and ovaries may reflect an incidental transient finding or underlying/pending pathology. Cryptorchidism is the most common genitourinary anomaly in males with associated increased risk of infertility and malignancy. Ectopic testes (outside the normal line of descent) have been reported within the perineum, penis, and femoral canal, representing a rare- but important entity to recognize and diagnose. Abnormally positioned ovaries- either in the midline pelvis or within the canal of Nuck- may mimic tumors or reflect underlying vascular compromise of the tissue.
This educational exhibit will present a case-based review of the normal migration and anatomic position of gonadal tissue, as well as common and uncommon aberrant locations. In addition, this exhibit will highlight imaging strategies, including appropriate modalities and techniques. A brief discussion of current concepts in management will also be provided.
Conclusions: It is imperative that pediatric radiologists have a comprehensive understanding of the normal migration, appearance, and location of reproductive organs. A detailed knowledge of potential aberrant locations and their associated sequela is also essential to ensure appropriate imaging, clinical management and improved patient outcomes.

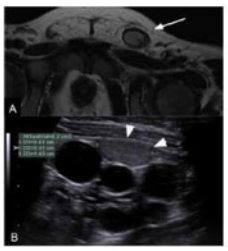

Figure 2: Cryptorchidism and testicular ectopia. A) 4 year old male with absent left testicle on physical exam. Axial T2W sequence demonstrates normal appearing testicle in the left inguinal canal (arrow). B) Non-palpable right testis in a 3 month old male. Ultrasound evaluation of the abdomen demonstrates the right testicle adjacent to a multicystic dysplastic kidney (arrowheads).

Poster #: EDU-049

MRI Sedation Education for Referring Physicians

Stacey Langford, MD, *Radiology, Children's Hospital of Pittsburgh of UPMC, Pittsburgh, PA, stace1212@gmail.com;* Erika Hess, Carolyn Lenhart, Kathleen Kapsin

Disclosures: All authors have disclosed no financial interests, arrangements or affiliations in the context of this activity.
Purpose or Case Report: Some negative patient and family experiences at our institution relating to sedation MRI examinations were thouroughly investigated. While causes of negative experiences varied, multiple patients arrived with misconceptions and unrealistic expectations regarding their examination, particularly relating to issues of MR safety, MR incompatibility, and use of sedation. Some of these misconceptions were found to be derived from interactions with referring physicians. As our institution already has multiple practices in place for preparing and educating our sedation MRI patients and families, we instead targetted the education of our referring physicians with a comprehensive sedation MRI packet complete with additional resources for both physicians and patients.
Methods & Materials: First, a letter to our referring physicians was generated describing our goal to educate them and in turn their patients regarding sedation MRI. Then, a comprehensive information sheet was created describing what a patient and familiy can expect before, during, and after a sedation MRI at our institution. Sources for this information included observations from our nursing and sedation staff, MRI technologists, department child life specialist, patient schedulers, radiologists, patient experiences from Press-Ganey surveys, and department administration. This information was converted into a more concise version in an easy to read Frequently Asked Questions (FAQ) brochure. Elements regarding types and levels of sedation, scheduling, dietary restrictions, and MRI incompatible materials was included in these documents. Finally, a list of helpful telephone numbers and websites was provided. With each education packet, a link to a survey regarding the usefulness and impact of the education material was included.
Results: Survey data collection is ongoing, and overall response rate is low.
Conclusions: A comprehensive sedation MRI education packet was created for our referring physicians to improve understanding of sedation, MR safety, and MRI compatibility. It is our hope that these efforts, aimed at our most frequent referrers, will diminish perpetuation of misinformation and improve patient and family preparation for sedation MRI. We also anticipate that by increasing referring physician knowledge understanding of this type of procedure, we will improve their preprocedural consultations with families and lead to most appropriate use of this exam. http://www.chp.edu/our-services/radiology

Poster #: EDU-050

Sterile Pyogenic Arthritis Pyoderma Gangrenosum, and Acne (PAPA) Syndrome: Musculoskeletal Imaging Findings and Common Differential Diagnosis in Children

Claudia Martinez-Rios, MD, *The Hospital for Sick Children, Toronto, ON, Canada, claudia.martinez-rios@sickkids.ca;* Mehul Jariwala, Kerri Highmore, Karen Watanabe Duffy, Ronald Laxer, Jennifer Stimec

Disclosures: All authors have disclosed no financial interests, arrangements or affiliations in the context of this activity.

Purpose or Case Report: Sterile pyogenic arthritis, pyoderma gangrenosum, and acne (PAPA syndrome) is a rare autosomal dominant inherited entity due to a missense mutation in the proline serine threonine phosphatase-interacting protein 1 (PSTPIP1/CD2BP1) gene, characterized by typical recurrent episodes of sterile pyogenic arthritis, either spontaneous or following a trauma, and skin manifestations characterized by pyoderma gangrenosum and acne. The articular manifestation is seen in the first decade of life, where most of the initial episodes are treated as septic arthritis. Cutaneous manifestations appear in early adulthood. Although uncommon, the potential therapeutic and clinical implications due to the rapidly destructive nature of PAPA syndrome warrant a prompt diagnosis. We present two unrelated pediatric patients from different institutions with genetically confirmed PAPA syndrome. The purpose of this study was to illustrate the musculoskeletal radiologic spectrum of findings of PAPA syndrome, and to discuss the differential diagnostic entities commonly seen in children. A second objective was to review the clinical and laboratory findings that allow diagnosis of PAPA syndrome

Methods & Materials: Patients' consent were obtained. We reviewed the imaging features of PAPA syndrome in different imaging modalities including plain radiograph, ultrasound, and magnetic resonance imaging, and we included representative cases of more common musculoskeletal diagnostic entities that present with similar imaging and clinical features in children

Results: Many of the imaging features seen in PAPA syndrome overlap with other clinical conditions including septic arthritis, osteomyelitis and juvenile idiopathic arthritis, including joint effusion, synovial thickening and extensive soft tissue swelling

Conclusions: PAPA syndrome would not be suspected initially based on imaging appearance alone, but should be considered in cases of recurrent septic arthritis or in those demonstrating skin manifestations. Radiologists familiarization with the syndrome may allow them to recognize the condition earlier in its course

Poster #: EDU-051

Pediatric Oncologic Emergencies: Must know Diagnoses

T Shawn Sato, **Lillian Lai, MD**, *Lucile Packard Children's Hospital, Stanford 8484 University, Palo Alto, CA, lmlai@stanford.edu;* Yutaka Sato, MD

Disclosures: All authors have disclosed no financial interests, arrangements or affiliations in the context of this activity.

Purpose or Case Report: Review the unique features of pediatric oncologic emergencies using case review of neurological, spinal, thoracic and abdominal pathologies, covering complications due to the malignancy or its treatment.

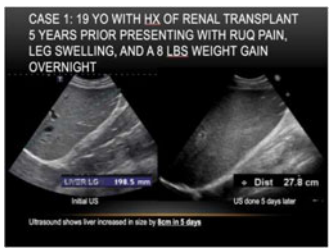

Methods & Materials: 1. Review mechanisms of pediatric oncologic emergencies

2. Emphasize differences of children versus adults making children prone to certain emergencies

3. Review pros/cons of different imaging modalities to assess for emergencies in children (i.e. attempt ultrasound over CT due to radiation, sedation with MRI)

Conclusions: After reviewing this presentation we hope to arm physicians with knowledge of expected oncologic emergencies in pediatric-specific malignancies and the best imaging modalities to assess for these complications. We also hope to help physicians make accurate diagnoses and formulate timely treatment strategies to treat children with these life-threatening diseases.

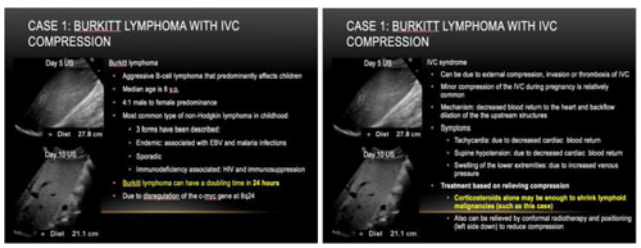

Poster #: EDU-052

Three-Dimensional Ultrasonography of the Neonatal Brain

Jessica Kurian, *Montefiore Medical Center, Bronx, NY, jkurian@montefiore.org;* Mark Liszewski, William Gomes, Thomas Hoffman, Benjamin Taragin

Disclosures: All authors have disclosed no financial interests, arrangements or affiliations in the context of this activity.

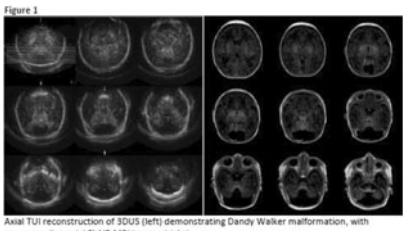
Figure 1
Axial TUI reconstruction of 3DUS (left) demonstrating Dandy Walker malformation, with corresponding axial FLAIR MRI images (right).

Purpose or Case Report: The purpose of this exhibit is to describe 3D ultrasonography (3DUS) of the head in neonates. Traditionally, 2D ultrasonography has been used for evaluation of the neonatal brain. 3DUS is a more recent advanced technique in which a volume of tissue is scanned in a single acquisition, and the 3D data set is subsequently manipulated using specialized software. This exhibit reviews current literature relating to 3DUS, demonstrates basic technical aspects of 3DUS, describes 3DUS of normal brain, and illustrates 3DUS features of acquired and congenital neonatal brain disorders.
Methods & Materials: Our method for performing 3DUS of the neonatal head will be reviewed, including description of scanning technique and systematic demonstration of post-processing. Photographs and videos will be used to depict acquisition and reconstruction methods. A variety of cases, including normal brains and pathologic conditions will be used to illustrate these techniques. Comparison of 3DUS to CT and MRI will be provided when available.
Results: 3DUS allows rapid scanning of the entire brain as a volume of tissue using a single sweep. This data can be stored for later analysis, thereby reducing the scan time required at the bedside. Both grayscale and color Doppler 3DUS can be performed. Post-processing methods include multiplanar reformatting, tomographic ultrasound images (TUI), and volumetric reconstruction. Image rendering modes include minimum and maximum, transparency, and surface modes. Unlike 2D neurosonography, brain anatomy can be displayed in orientations other than the original scan plane; three planes can be viewed simultaneously. Data can be reconstructed into axial slices similar to CT and MRI, facilitating comparison between modalities. Volumetric images can be created, including surface and shell displays, and numerical volume analysis. The entities presented with 3DUS will include germinal matrix and intraventricular hemorrhage, parenchymal hemorrhage/infarct, periventricular leukoencephalomalacia, hydrocephalus, and structural malformations.
Conclusions: 3DUS has been shown to provide useful diagnostic information in multiple clinical applications. Our preliminary experience indicates that 3DUS may also be a powerful technique for evaluation of the neonatal brain. 3DUS decreases scan time, allows evaluation of brain anatomy in three dimensions, and allows ventricular volume analysis in hydrocephalus. Reconstruction of data in the axial plane allows comparison with CT and MRI.

Figure 2

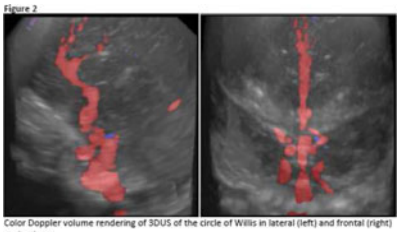

Color Doppler volume rendering of 3DUS of the circle of Willis in lateral (left) and frontal (right) projections.

Figure 3

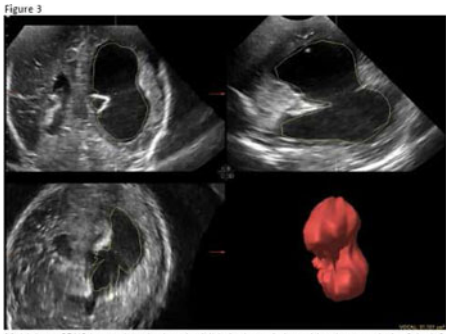

Multiplanar 3DUS (coronal, sagittal, and axial) in hydrocephalus, with volume analysis of the left lateral ventricle (shell display and VOCAL volume calculation, bottom right).

Poster #: EDU-053

Blastomycosis in Pediatric Population - Meeting "The Great Mimicker"

Katya Rozovsky, MD, *Department of Diagnostic Imaging, Child Health, Health Sciences Centre, University of Manitoba, Winnipeg, MB, Canada, katro70@yahoo.com;* Rick Higgins, Hayley Moffatt, Jens Wrogemann, Faisal Al-Somali, Elka Miller, Lina Alqublan, Martin Bunge

Disclosures: All authors have disclosed no financial interests, arrangements or affiliations in the context of this activity.

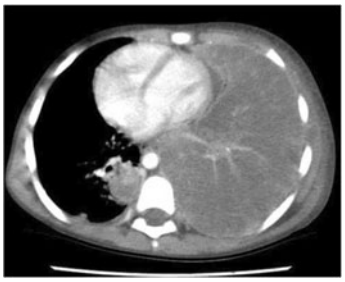

Purpose or Case Report: Blastomycosis is a rare granulomatous fungal infection, endemic to Canada and Midwest of the North America. The clinical features of blastomycosis are extremely variable, since the disease may involve any organ or system. Pediatric blastomycosis is uncommon, and the diagnosis is often delayed, which results in severe and disseminated disease by the time of diagnosis. Imaging studies plays an important role in the diagnosis and management of pediatric patients with blastomycosis.
The purpose of our educational exhibit is to describe the imaging features of pulmonary and extrapulmonary blastomycosis in the pediatric population.
Methods & Materials: We present a pictorial review discussing the imaging findings and characteristics of the varying presentations of pulmonary and extrapulmonary blastomycosis in children aged 2 months to 17 years, emphasizing the most unusual and challenging for diagnosis.
Our presentation includes different patterns of pulmonary blastomycosis, which can mimic bacterial pneumonia, a mass lesion, interstitial disease or pulmonary TB. We present challenging cases of skeletal involvement with scoliosis and bony destruction, which can mimic a malignant process or bacterial osteomyelitis/discitis. Our cases of CNS involvement of blastomycosis include: mass-like brain lesion, brain abscess, spinal inflammatory mass and a very unusual case of a pituitary mass lesion with involvement of the hypothalamo-hypophyseal axis, leptomeningial spread and ventriculitis.

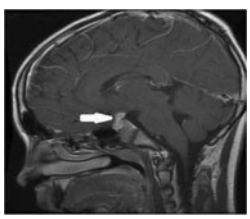

Results: The most challenging for imaging assessment are cases of extrapulmonary presentation of blastomycosis in young children, especially in the absence of a history of a prior infectious exposure.
Conclusions: In order to provide the correct and prompt diagnosis of this rare type of infection the pediatric radiologist should be familiar with the different and multiple imaging manifestations of blastomycosis.

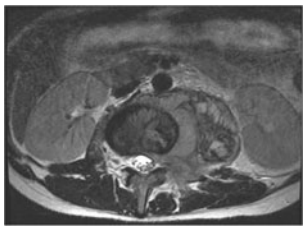

Poster #: EDU-054

Testicular Versus Spermatic Cord Torsion: What's in a Name?

Boris Sinayuk, MD, *Radiology, Rhode Island Hospital - Brown University, Providence, RI, bsinayuk@lifespan.org;* David Swenson, MD, Thaddeus Herliczek, Michael Wallach, John Cassese

Disclosures: All authors have disclosed no financial interests, arrangements or affiliations in the context of this activity.
Purpose or Case Report: 1. Highlight recent literature on ultrasound (US) imaging of the spermatic cord for testicular torsion.
2. Present illustrative cases of testicular torsion from our institution that demonstrate the spectrum of US findings, highlighting the importance of evaluating the spermatic cord and how relying solely on grayscale US and doppler of the testicle itself can be misleading in the setting of torsion.
3. Encourage real-time US evaluation of the spermatic cord in all suspected cases of testicular torsion.

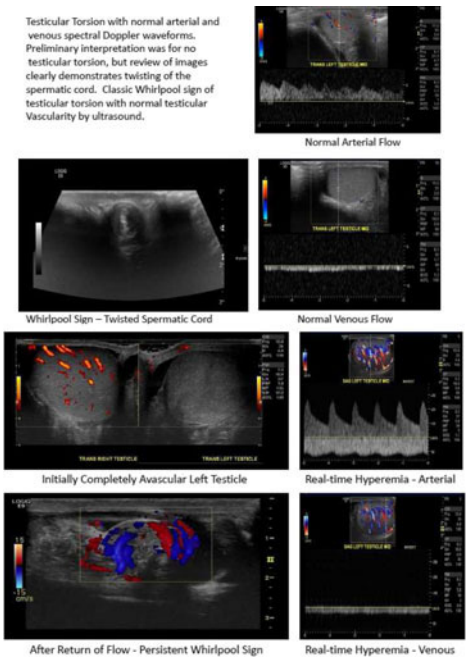

Methods & Materials: Draw on over 611 pediatric scrotal ultrasound examinations performed at our instution between 09/01/2014 and 08/31/2015 to highlight the variety of grayscale and Doppler imaging findings in the setting of surgically confirmed testicular torsion.
Results: Select cases of testicular torsion will demonstrate the wide variety in the imaging presentation of torsion. For example:
1. Classic testicular torsion with stromal edema, lack of vascular flow, and "whirlpool" sign of the twisted spermatic cord.
2. Normal grayscale and Doppler in the setting of torsion. Only findings are a small hydrocele and subtle twisting of the spermatic cord.
3. Normal grayscale and Doppler in the setting of torsion, but edematrous, hypervascular epididymis. Clear twisting of the spermatic cord.
4. Initial edematous, avascular testicle with twisted spermatic cord. During real-time exam there is sudden testicular hyperemia, despite persistent twisting of cord, proving that a hyperemic testicle can still be torsed. This must be distinguished from epididymo-orchitis.
5. Single patient with 5 scrotal US exams over 2 months, with varying interpretations suggesting either torsion-detorsion with reactive hyperemia or epidydimitis/orchitis. Initially treated infection. After several weeks of improved symptoms, the patient returned with recurrent pain, and US showed normal grayscale and Dopple evaluation of the testicle, but tight spermatic cord twisting throughout the lower inguinal canal. Found to be 900 degrees torsed in operation room.
Conclusions: While historically the US diagnosis of testicular torsion has focused on grayscale and Doppler evaluation of testicular parenchyma, direct imaging of the spermatic cord itself is critical for assessing torsion, and should be the standard of care.

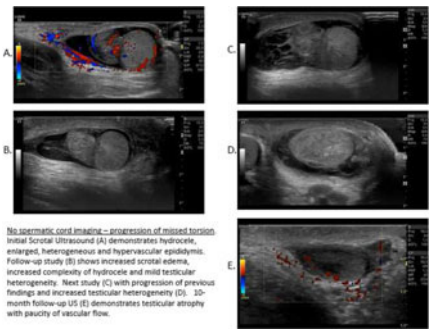

Poster #: EDU-055

The Duplicated Collecting System of the Urinary Tract: Embryology, Radiologic Appearances, and Clinical Considerations

Ryne Didier, *Boston Children's Hospital, Boston, MA, didierr@ohsu.edu;* Jeanne Chow, Neha Kwatra, MD, Robert Lebowitz

Disclosures: All authors have disclosed no financial interests, arrangements or affiliations in the context of this activity.

Purpose or Case Report: Duplicated collecting systems can be associated with vesicoureteral reflux, urinary obstruction, ureteroceles, incontinence, and renal parenchymal scarring which can result in decreased renal function, therefore, early identification by radiologists and clinicians is crucial. The purpose of this educational exhibit is to review the embryology, highlight the imaging manifestations, and discuss the clinical ramifications of duplicated renal collecting systems in the pediatric population.
Methods & Materials: Imaging studies performed in the evaluation of patients with renal collecting system duplication at our institution were retrospectively reviewed. Representative images were selected to depict the varied appearances of duplicated urinary tract anomalies as seen by ultrasonography, voiding cystourethrography (VCUG), computed tomography, Dimercaptosuccinic acid (DMSA) renal cortical scintigraphy, and magnetic resonance urography (MRU).
Results: 1. Basic embryologic development of the urinary tract was reviewed to contextualize the spectrum of duplicated urinary tracts.

2. The salient imaging features of duplicated urinary tract collecting systems and associated anomalies were illustrated by each imaging modality with special attention to subtle diagnostic clues and potential pitfalls.
3. The potential complications and clinical management of patients with duplicated urinary tracts were discussed to provide perspective and guidance in regards to radiologic interpretation and reporting.
Conclusions: By understanding the embryology, varied radiologic appearances, and clinical persepctives, the radiologist can promptly recognize duplication anomalies of the pediatric urinary tract and the commonly associated complications.

Poster #: EDU-056

Current and Emerging Applications of Pediatric Gastrointestinal Tract Sonography

Heather Gale, MD, *Pediatric Radiology, Massachusetts General Hospital, Quincy, MA, heather.imsande@gmail.com;* Michael Gee, Sjirk Westra, Edward Lee, Katherine Nimkin

Disclosures: All authors have disclosed no financial interests, arrangements or affiliations in the context of this activity.

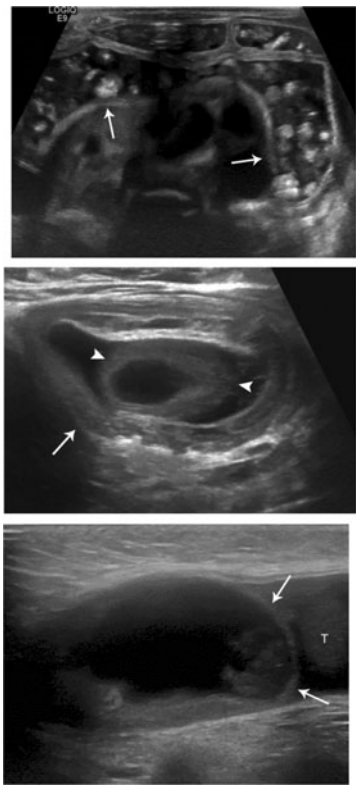

Purpose or Case Report: To review up-to-date imaging techniques, normal sonographic anatomy, and characteristic sonographic features of disorders affecting the gastrointestinal tract in children.
Methods & Materials: We performed a literature review on gastrointestinal ultrasound imaging indications, techniques, and findings in children. We included cases and experience from our institution to summarize diagnostic pearls and pitfalls for pediatric gastrointestinal pathology. We review congenital, acquired, infectious, inflammatory, neoplastic, and vascular disorders, as well as foreign body ingestion.
Results: Ultrasound is an ideal imaging modality in children because it is a real-time, non-invasive, relatively low cost examination without ionizing radiation that requires no sedation. Ultrasound of the bowel is typically a targeted examination, designed to answer a specific question, and common indications include evaluation for appendicitis, intussusception, and pyloric stenosis. Other indications include evaluation of prenatally detected congenital abnormalities, confirmation of suspected hernia, and problem solving in the patient with necrotizing enterocolitis. Unsuspected bowel abnormalities may be found during screening for non-specific abdominal pain, including foreign body, tumor, infection, or bowel hematoma. A more comprehensive examination of the entire bowel can be used to evaluate inflammatory bowel disease and celiac disease in children.
Recent improvements in ultrasound technology, including high-resolution linear probes (12-15 MHz) and harmonic and panoramic imaging, improve image quality. Color Doppler evaluation can detect increased perfusion in inflamed loops of bowel. Ultrasound cine clips document bowel motility, and graded compression assesses compressibility and improves resolution by displacing air from the bowel lumen. Oral administration of non-carbonated fluid 30 min prior to the examination will reduce air in the bowel. Small-intestine intravenous contrast enhanced ultrasound and enteric contrast bowel distention are other promising newer techniques for bowel evaluation.
Conclusions: Ultrasound is the often the initial modality detecting abnormalities of the gastrointestinal tract in children, either as part of a targeted examination at the site of symptoms or as an incidental finding. Radiologists interpreting ultrasound examinations in children should be familiar with the sonographic appearance of both the normal and abnormal gastrointestinal tract.

Poster #: EDU-057

Updated Concepts in Pediatric Epilepsy Imaging

Douglas Drumsta, MD, *Emory University, Atlanta, GA, ddrumst@emory.edu;* Nadja Kadom

Disclosures: All authors have disclosed no financial interests, arrangements or affiliations in the context of this activity.
Purpose or Case Report: Within the last several years there have been updates and changes to the clinical terminology in epilepsy, as well as the histopathologic classification of hippocampal sclerosis and focal cortical dysplasia. The purpose of this exhibit is to review these changes and illustrate them with corresponding MR examples.
Methods & Materials: This exhibit provides three updates:
1. Summary of recent changes to the terminology of epilepsy types that are commonly provided as an imaging indication.
2. An illustrated review of the new histopathology classification system for focal cortical dysplasia types I-III on pediatric MRI imaging.
3. An illustrated review of the new histopathology classification system for three hippocampal sclerosis subtypes using MRI imaging.
Results: The new classification system of epilepsy eliminates neonatal seizures as a separate entity, simplifies abscence seizures, adds epileptic spasms, removes the distinction between focal seizures and adds myoclonic atonic seizures. The etiology of seizures is now classified as genetic, structural/metabolic and unknown etiology as opposed to idiopathic, symptomatic and cryptogenic. Other terminology that has changed includes the addition of self-limited, pharmacoresponsive, evolving to bilateral and focal seizures.
New to the focal cortical dysplasia classification is the addition of FCD type III which is subdivided into type type IIIa, IIIb, IIIc, and IIId as follows:
Type IIIa: FCD type II with hippocampal sclerosis.
Type IIIb: FCD type II with a glial or glioneuronal tumor.
Type IIIc: FCD type II with a vascular malformation.
Type IIId: FCD type II with an acquired lesion.
Also new, are the subtypes of hippocampal sclerosis. Type 1 is the classic hippocampal sclerosis associated with diffuse segmental volume loss of the hippocampus. Type 2 is when cell loss is isolated to the CA1 segment.

Type 3 is when the cell loss is isolated to the dentate gyrus and CA4 segment.
Conclusions: At the end of the exhibit, the viewer will be familiar with the new histopathologic and clinical epilepsy classification system and will be able to classify brain MRI findings in pediatric epilepsy patients according to these classifications.

Poster #: EDU-058

Ultrasound-guided Shoulder Injection for MR Arthrography: Our Experience

Lincoln Wong, MD, *Pediatric Radiology, Children's Hospital and Medical Center, Omaha, NE, liwong@childrensomaha.org;* Andria Powers
Disclosures: All authors have disclosed no financial interests, arrangements or affiliations in the context of this activity.
Purpose or Case Report: MR shoulder arthrography is a frequently ordered study in the pediatric population for shoulder symptoms relating to sports injuries. The traditional technique for injecting contrast into the shoulder joint has been with fluoroscopy. Following principles of ALARA, we set out to find ways to reduce or eliminate radiation from the procedure. Ultrasound has been utilized increasingly for diagnosing musculoskeletal pathology and is a well-established technique in the adult population to guide joint injection of medication. This educational exhibit aims to discuss how we implemented this technique at our hospital, outline tips and pitfalls we learned along the way, and discuss benefits and drawbacks with the procedure.
Methods & Materials: We reviewed the current literature about joint ultrasound techniques and utilization. Radiation dose using fluoroscopy will be compared to radiation dose using our ultrasound technique. Our experience performing ultrasound-guided shoulder joint injection in the pediatric population will be discussed utilizing case examples.
Results: By using ultrasound over fluoroscopy for injecting contrast into the shoulder joint in our pediatric patient population, we were able to reduce radiation exposure normally associated with MR shoulder arthrogram examinations.
Conclusions: Ultrasound-guided injection of contrast into the shoulder joint for MR shoulder arthrography is a viable alternative over fluoroscopy to reduce radiation, especially in the pediatric patient population.

Poster #: EDU-059

Tubo Ovarian Abscess in Non-sexually Active Girls: A Case Review

Dana Jackson, Sharon Gould, MD, *Medical Imaging, Nemours/AIDHC, Wilmington, DE, sgould@nemours.org;* Kirk Reichard, Monica Epelman

Disclosures: All authors have disclosed no financial interests, arrangements or affiliations in the context of this activity.
Purpose or Case Report: Tubo-ovarian abscesses are uncommon and are usually associated with pelvic inflammatory disease secondary to sexually transmitted disease; however, there has been a small number of reported cases occurring in non-sexually active girls. A series of six virginal girls with tubo-ovarian abscesses is presented for discussion of the clinical circumstances, imaging findings and diagnostic difficulties encountered in this uncommon diagnosis.
Methods & Materials: The PACS database was queried for the words "tubo-ovarian abscess" resulting in finding of 5 cases between August 2011 and 2015. An additional case from this time period was retrieved from the teaching file of one investigator (SG). The charts and imaging studies of each patient were reviewed.
Results: Six girls were found with imaging or surgical documentation of tubo-ovarian abscess. The patients ranged in age from 8 to 15 years old at time of presentation and each denied ever engaging in oral, vaginal or anal sexual intercourse. Five of six cases were associated with appendicitis. Two of these cases were associated with acute ruptured appendicitis. The other three cases occurred in patients with prior ruptured appendicitis with recent appendectomy 2-3 weeks prior to presentation. The sixth case was felt to be due to poor hygiene with resulting ascending E. coli infection. Four of six abscesses were correctly diagnosed by imaging alone. Ultrasound, computed tomography, and magnetic resonance imaging were helpful in making the diagnosis, and the imaging findings are described. Two cases were not diagnosed until laparoscopy performed for complex adnexal mass/cyst thought to be of ovarian origin, but abscess was not included in the preoperative differential diagnosis.
Conclusions: Tubo-ovarian abscess is an uncommon diagnosis, but should be included in the differential diagnosis of a complex adnexal mass even in non-sexually active girls. Correct diagnosis by imaging can be difficult given the number of more common potential causes of complex adnexal masses and the reluctance to suggest this diagnosis without a history of sexual activity. However, a delay in diagnosis can result in chronic pelvic pain and increased risk of infertility. Further evaluation for a ruptured appendix should ensue in a girl with a tubo-ovarian abscess who denies sexual activity.

Poster #: EDU-060

Lymphoscintigraphy in Children: Pictorial Review

Hisham Dahmoush, *Boston Children's Hospital, Brookline, MA, dahmoushh@gmail.com;* Frederick Grant, Neha Kwatra, MD

Disclosures: All authors have disclosed no financial interests, arrangements or affiliations in the context of this activity.
Purpose or Case Report: Lymphoscintigraphy is a minimally invasive first-line imaging technique for the evaluation and management of primary and secondary lymphedema, detection of chylous leaks, and sentinel lymph node mapping. This exhibit will provide an illustrated review of the technique, clinical indications, characteristic imaging findings, and pitfalls in interpretation of lymphoscintigraphic studies in children.

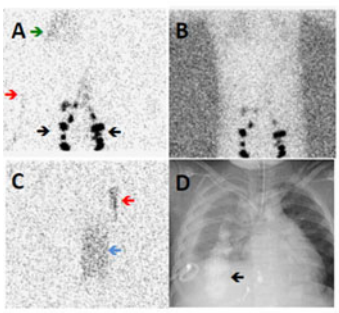

Figure 1. 9 year-old girl with persistent chylous pleural effusion and ascites after multivisceral organ transplant

Anterior emission (A) and transmission (B) images and posterior emission (C) image of the torso, 150 minutes after injection of ^{99m}Tc sulfur colloid in the feet. Normal inguinal and pelvic nodes are seen bilaterally (Black arrows in A). Abnormal tracer accumulation in the right thoracic cavity (Green arrow), in the right pigtail drainage catheter (Red arrows) and collecting bag (Blue arrow).
Delayed image from corresponding lymphangiogram (D) shows contrast extravasation in the right thoracic cavity (Black arrow in D) and right pleural effusion.

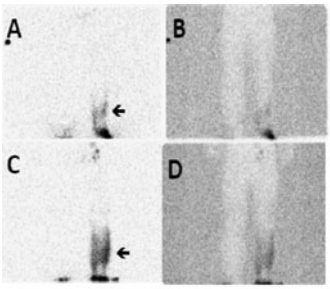

Figure 2. Two year-old girl with bilateral lower extremity swelling since birth, greater on the right

Anterior emission (A & C) and transmission (B & D) images 1 and 4 hours after injection of ^{99m}Tc sulfur colloid in the feet show absence of proximal tracer transit in the right lower extremity as well as delayed tracer transit and dermal backflow (Arrows in A & C) in the left lower extremity indicating bilateral lymphatic dysfunction consistent with primary lymphedema

Methods & Materials: Lymphoscintigraphy is routinely performed with a dual-head gamma camera after intradermal injection of small amount of radiolabelled colloidal particles (typically filtered ^{99m}Tc sulfur colloid). Injections are placed in the dorsum of the feet or hands for evaluation of lymphedema and peritumorally for sentinel node studies. Sequential anterior and posterior planar or whole body images are typically obtained within the first 15 min, at 45-60 min, and 120 min with a parallel hole, high-resolution collimator. Delayed imaging may be necessary in many cases. All 92 lymphoscintigraphy procedures performed at our institution between January 2005 to September 2015 in patients 18 years or younger were reviewed in PACS and representative examples were selected for the exhibit.
Results: 1. Primary lymphedema due to congenital lymphatic aplasia or hypoplasia is a more common cause of lymphedema in children and adolescents as compared to secondary lymphedema. Absent visualization of regional lymph nodes, delayed or asymmetric transit of lymph flow, collateral lymphatic channels, and dermal backflow are the key imaging findings in lymphedema.
2. Lymphoscintigraphy is utilized in the assessment of chylous pleural effusion, pericardial effusion, or ascites.
3. Lymphoscintigraphy is essential to sentinel lymph node biopsy, which is used in children with melanoma and sarcomas, such as synovial cell sarcoma and rhabdomyosarcoma.
Conclusions: Lymphoscintigraphy is a simple, reliable and inexpensive diagnostic tool for the functional assessment of lymphatic transit. It usually does not require sedation and the radiation dose to the child is minimal. In the pediatric population, lymphoscintigraphy is most commonly utilized to confirm or exclude lymphatic dysfunction as the cause of a swollen extremity. Pediatric radiologists may guide clinical decisions based on their knowledge and expertise in performing and interpreting lymphoscintigraphic studies.

Poster #: EDU-061

Pediatric Bladder Masses: What the Radiologist Needs To Know

Emily Edwards, *UCSF Benioff Children's Hospital, San Francisco, CA, famousamose@gmail.com;* Matthew Zapala, MD, PhD, Hillary Copp, MD, MS, John MacKenzie, MD, Andrew Phelps, MD, Jesse Courtier, MD

Disclosures: All authors have disclosed no financial interests, arrangements or affiliations in the context of this activity.

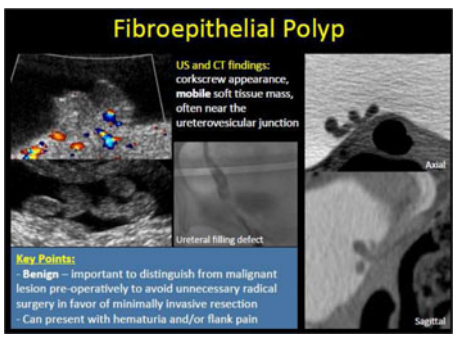

Purpose or Case Report: Bladder masses are periodically encountered in the pediatric population, yet there are few resources to guide appropriate imaging assessment of pediatric bladder masses. A pediatric bladder mass may be encountered in a wide variety of clinical settings, ranging from investigation of a specific symptom or laboratory abnormality to an incidental finding during routine evaluation. Familiarity with the spectrum of benign and neoplastic processes that may give rise to pediatric bladder masses increases the likelihood of timely and accurate diagnosis and management.
Methods & Materials: A literature review was performed and salient cases were collected. The information provided in this educational exhibit will allow the reader to do the following:
1. Review the overall incidence of bladder pathology in pediatric patients
2. Learn the optimal imaging assessment of bladder lesions in children including the role of fluoroscopy, US, CT and MRI
3. Understand the imaging features of common benign bladder lesions
4. Understand the imaging features of common malignant bladder neoplasms
5. Discuss potential pitfalls in bladder imaging in children, including post-operative assessment following vesicoureteral reflux or bladder augmentation surgeries
6. Briefly describe common surgical and non-surgical management approaches to bladder masses in children
Results: Ultrasound is the first-line modality for imaging bladder lesions in the pediatric population, with CT and MRI serving as useful adjuncts for further evaluation when a potential neoplastic process is suspected.
Conclusions: Imaging plays an important role in the evaluation and management of pediatric bladder masses, as characteristic imaging features can help guide appropriate management decisions.

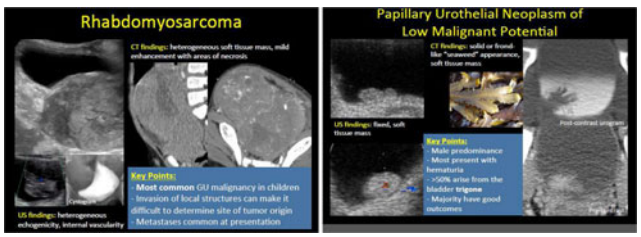

Poster #: EDU-062

Can 3T Fetal MRI Improve Resolution of Brain Structures?

Gema Priego, Fellowship, *Pediatric Radiology Deparment, Children's Hospital Eastern Ontario, Ottawa, ON, Canada;* Julie Hurteau-Miller, Lucia Fontalvo, Elka Miller

Disclosures: All authors have disclosed no financial interests, arrangements or affiliations in the context of this activity.
Purpose or Case Report: Describe the anatomy and regional difference in brain maturation of various brain structures comparing 3 and 1.5 Tesla fetal MRI.
Methods & Materials: 1. Technique and optimization of 3T fetal MRI
2. Description of the sulcation and different layers of the brain maturation as well as other brain structures on 3T fetal MRI
3. Qualitative comparison of 3 and 1.5 Tesla fetal MRI with age matched fetuses
4. Conclusion
Results: Higher field magnetic resonance has already been used to improve spatial resolution of normal structures in other areas of imaging. This educational exhibit will summarize the advantages and disadvantages of normal brain fetal anatomy performed on a 3 Tesla in comparison with age matched fetuses performed on a 1. 5 Tesla magnet.
Conclusions: Fetal MRI has become an essential technique in the prenatal diagnosis of fetuses with a high risk of structural disorders. Knowledge

of the normal fetal anatomy in MRI is advantageous to improve the prenatal assessment.

Poster #: EDU-063

An Interactive Animated Computer Generated Module of Hip Pathology in Children; A Prototype for Radiology Resident Education

Steven Benitez, *Radiology, Montefiore Medical Center, Mamaroneck, NY, stbenite@montefiore.org;* Terry Levin, MD

Disclosures: All authors have disclosed no financial interests, arrangements or affiliations in the context of this activity.
Purpose or Case Report: With the expansion of the internet and the development of new media tools, learning methods among medical students and residents in all specialties particularly Radiology have changed. While didactic lectures and personal interaction with mentors each play an important part in education, self learning via a variety of internet sources has gained a significant role and has come to replace the use of standard textbooks. Existing online modules are minimally interactive and present radiographic images concurrently with text. In most, users use the cursor to hover over the image in order to display the abnormality.

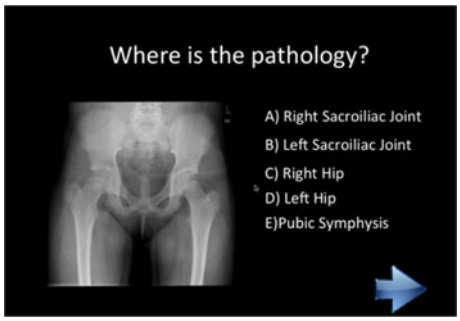

Methods & Materials: We present an interactive module on the imaging of hip pathology in children in which radiology residents are shown an image and led through a series of questions based on their response to the preceding question. The images are accompanied by appropriate clinical information, are supplemented with audio, graphics and animation and require viewer engagement to proceed. Topics covered included congenital hip dysplasia, slipped capital femoral epiphysis, and Legg-Calve-Perthes disease.
Results: The learning module is user friendly and engaging and allows for viewer trial and error in order to guide the viewer to the correct diagnosis. Its multisensory and interactive approach fully engages the learner. The format of this module can be used to create interactive learning modules for alternative topics in pediatric radiology.
Conclusions: Interactive media driven educational tools may act as an effective supplement to didactic lectures in radiology resident and medical student education.

Poster #: EDU-064

Ultrasound of the Neonatal Spine

Kathleen Gebarski, MD, *Pediatric Radiology, U of Michigan, Ann Arbor, MI, kgebarsk@umich.edu;* Stephen Gebarski

Disclosures: All authors have disclosed no financial interests, arrangements or affiliations in the context of this activity.
Purpose or Case Report: Sonography of the neonatal spine can be challenging and difficult to interpret. We composed a pictorial guide of a wide variety of variants and diseases for education and reference.
Methods & Materials: Illustrative cases including terminal ventricle, sacral dimple with tract, filum terminale lipoma, cauda equina cyst, tethered cord, meningomyelocele, lipomyelomenigocele, syrinx, diastematomyelia, and sacrococcygeal teratoma were chosen from the last 10 years of neonatal sonography at our institution. MRI and pathologic correlation are included.
Results: Reviewing these cases provides sonographic experience of a wide variety of neonatal spinal disease and improves the accuracy of interpretation.
Conclusions: A pictorial review of a wide variety of diseases diagnosed with neonatal spinal sonography improves the accuracy of interpretation.

Poster #: EDU-065

Sonography of the Posterior Fossa in Infants

Kathleen Gebarski, MD, *Pediatric Radiology, U of Michigan, Ann Arbor, MI, kgebarsk@umich.edu;* Stephen Gebarski

Disclosures: All authors have disclosed no financial interests, arrangements or affiliations in the context of this activity.
Purpose or Case Report: Sonography of the posterior fossa in infants can be challenging and difficult to interpret. Use of posterior fontanelle, mastoid and squamous temporal bone acoustic windows has improved the visualization of the posterior fossa in infants. We provide a 10 year experience of posterior fossa sonography to improve familiarity with a wide variety of diseases of the posterior fossa.
Methods & Materials: A review of findings from 10 years experience with these windows from our institution is provided with illustrative cases of a variety of posterior fossa disease in infants with MRI and pathologic correlation.
Results: Reviewing these cases provides sonographic experience with a wide variety of posterior fossa diseases in infants and improves the accuracy of interpretation.
Conclusions: A review of sonography of a wide variety of diseases in the posterior fossa with use of posterior fontanelle, mastoid and squamous temporal bone acoustic windows in infants improves the accuracy of interpretation.

Poster #: EDU-066

Spectrum of MRI Findings in Evaluation of Fetal Teratoma

Sherelle Laifer-Narin, Sejal Patel, Rama Ayyala, M.D., *Columbia University Medical Center, New York, NY, rsa2121@columbia.edu;* Stuart Bentley-Hibbert, Elizabeth Hecht, Jeffrey Newhouse

Disclosures: All authors have disclosed no financial interests, arrangements or affiliations in the context of this activity.
Purpose or Case Report: Teratoma is one of the most common fetal tumors that is diagnosed on prenatal imaging. Various sites and organs can be involved, and therefore it is important to be aware of the imaging findings on fetal MRI. Imaging not only aids in prompt diagnosis, but also directs obstetrical care and provides vital information for counseling. The purpose of this exhibit is to review key anatomic, pathologic, and imaging characteristics of fetal teratomas.
Methods & Materials: A retrospective review of the fetal database was performed to identify patients with presumed prenatal diagnosis of fetal teratomas. Patients included in this review are those with postnatal pathological confirmation of the diagnosis.
Results: The key anatomy and pathology of fetal teratomas will be briefly reviewed followed by the optimal technique of fetal MRI imaging to evaluate these lesions. A spectrum of fetal teratoma cases will be

presented, including intracranial, oropharyngeal, intra-abdominal, sacrococcygeal, as well as a rare form of a parasitic twin.
Conclusions: Teratoma is one of the most common prenatally diagnosed masses, therefore fetal MRI plays a crucial role in the diagnosis of this entity. Not only does MRI allow for characterization of the mass, but also allows evaluation of associated findings such as airway patency, amniotic fluid quantification, and presence of hydrops, which can play a vital role in management. It is important for radiologists to familiarize themselves with the spectrum of findings in order to provide a prompt diagnosis to ultimately guide prenatal and postnatal care.

Poster #: EDU-067

Congenital Bone Anomalies: Part II-Lower Extremity

Ali Al-Saraf, *Radiology, University of Chicago, Chicago, IL, ali1987@sbcglobal.net;* Seng Ong

Disclosures: All authors have disclosed no financial interests, arrangements or affiliations in the context of this activity.
Purpose or Case Report: In the second part of this exhibit, congenital bone anomalies of the lower extremity will be identified and reviewed. Through this exhibit, the reader will be able to: 1. Define the most common entities encompassing congenital lower extremity bone anomalies based on classic clinical presentation and demographics. 2. Highlight key multi-modality imaging characteristics to accurately differentiate between the various congenital bone anomalies of the lower extremity.

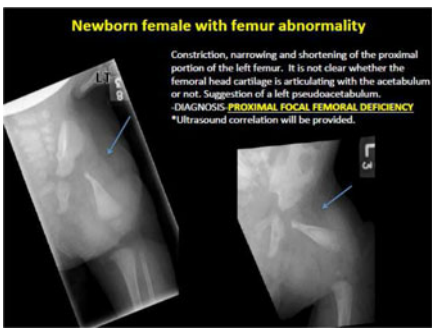

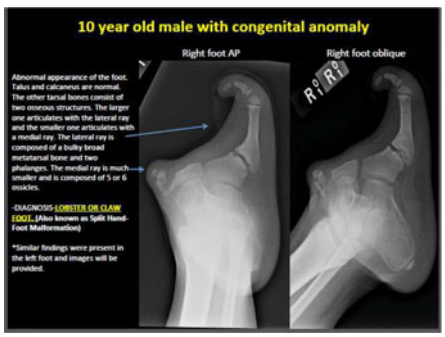

Methods & Materials: Patients with congenital lower extremity bone anomalies encountered in our institution were reviewed and selected to highlight pertinent clinical and radiologic features that are associated with each anomaly. Key imaging findings unique to each of these conditions will be highlighted.
Results: Multiple congenital bone anomalies of the lower extremity will be described based on clinical presentation and key imaging characteristics. These entities include: Proximal Focal Femoral Deficiency, Fibular Hemimelia, Tibial Hemimelia, Tarsal Coalition, Femoral Duplication, Achondroplasia, Split Hand-Foot Malformation, Coxa Valga, Tibial Bowing, Constriction/Amniotic Bands, and Developmental Dysplasia of the Hip.
Conclusions: The goal of this two-part exhibit is to highlight key imaging findings unique to each of these conditions to allow for efficient and accurate differentiation. This will provide a high yield approach to simplifying the diagnosis based on clinical presentation, demographics and imaging findings.

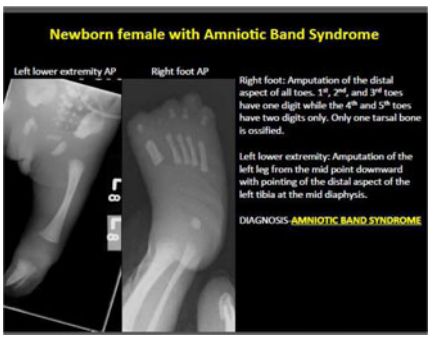

Poster #: EDU-068

Soccer Injuries in Youth: What the Radiologist Needs to Know

Kamaldine Oudjhane, MD MSc, *Hospital for Sick Children University of Toronto, Toronto, ON, Canada, kamaldine.oudjhane@sickkids.ca;* Ahmed Alzahrani

Disclosures: All authors have disclosed no financial interests, arrangements or affiliations in the context of this activity.

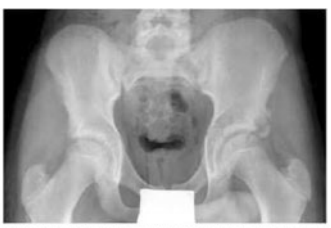
Fig1: 15-year-old male, soccer player experienced leg snap and pain while kicking soccer ball. Pelvis radiograph : Avulsion injury at the left anterior inferior iliac spine

Purpose or Case Report: Soccer practice is steadily increasing in the world and brings its statistics of injuries, most of them acute and minor. There is a better understanding of the epidemiology and biomechanics in the genesis of such injuries. This electronic presentation on soccer injuries in children outlines the following: 1. Review of epidemiology and biomechanics factors (equipment, athletic skills, contact sport). 2. Mechanisms of injury: headings, avulsion, contusion, fracture, twisting knee injury, overuse). 3. Imaging characteristics at various sites of injury.
Methods & Materials: A retrospective search of PACS was performed on imaging studies at our institution for the past 10 years on children who presented with soccer injuries. Selection of illustrative cases was made depicting the different locations of the body injuries as well as the imaging features by various imaging modalities.
Results: Comprehension of the genesis of soccer injuries in children is facilitated by knowledge of epidemiology and biomechanics factors (equipment factors: Indoor/outdoor, surface, shoes, ball size, goalie post) as well as of technical factors (athletic skills, contact

sport). Specific parts of the body are involved: soft tissues, ligaments and joints, apophyses, menisci, head, face, spine and trunk. Injury mechanisms include: headings, avulsion, contusion, sprain, fracture, twisting knee injury, overuse. Use of ultrasound is appropriate for joints, ligaments, soft tissues, radiographs are indicated for bones, CT/MRI for head/face, spine as well as for pelvis, knee, ankle. The knee is mostly involved with ACL tears in female players and collateral ligament trauma in males.
Conclusions: A practical approach in imaging assessment relies in appreciation of the degree of severity of injuries, with the reasoned use of various imaging modalities. Head injuries severity documented by imaging prompts preventive measures related to goal post. Prevalence of lower limb trauma is linked to technical factors (field, ball size, shoe type).

Poster #: EDU-069

MRI Evaluation of Bone and Soft Tissue Lesions Using a 3D mDIXON FFE Technique

Michael Peterson, MD, *Phoenix Children's Hospital, Phoenix, AZ, mpeterson23@gmail.com;* Mittun Patel, MD, Logan Dance, MD, Brian Keehn, DO, Amber Pokorney, Craig Barnes

Disclosures: All authors have disclosed no financial interests, arrangements or affiliations in the context of this activity.
Purpose or Case Report: The objective of this work was to determine whether a 3D gradient echo-based mDIXON T1-weighted sequence can replace a TSE-based mDIXON sequence in the evaluation of bone and musculoskeletal soft tissue lesions.

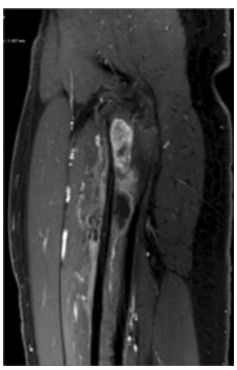

Methods & Materials: 17 cases were reviewed in which patients had either a bone or soft tissue lesion and imaging was obtained using the classic mDixon- TSE sequences and the new mDixon- FFE sequences. The mDixon- FFE technique is a volumetric 3D sequence which can provide reformats in all 3 planes. In addition it uses a 7 peak model for shimming which provides better homogeneity on fat saturated images. Cases were reviewed by fellows and attending radiologists for image quality and lesion delineation. Age ranges for patients with bone lesions was between 7 years and 14 years old. Bone lesions included Desmoid, Ewing's Sarcoma, Aneurymsal Bone Cyst, and Osteoid Osteoma among others. Age ranges for patients with soft tissue lesions varied between 8 months and 14 years old. Soft tissue lesions included abscess, myositis, fasciitis, venous malformation, and sebaceous cyst among others.
Results: It was widely agreed that the mDixon- FFE sequence provided superior lesion delineation and image quality as compared to the mDixon- TSE sequence.

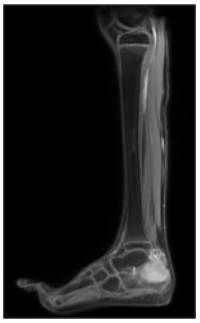

Conclusions: Our preliminary study demonstrates that the mDixon- FFE sequence is superior to the mDixon- TSE sequence and should be considered as a replacement in evaluation of bone and MSK soft tissue lesions. It has superior resolution, shorter scan time, better image quality, smaller slices, and is a volumetric 3D sequence allowing for multiplanar reformatted images. While our reviewers agree that the overall image quality is superior with the gradient echo sequence our pictoral essay will show numerous examples of our gradient mDixon and our TSE mDixon with numerous different osseous and soft tissue lesions.

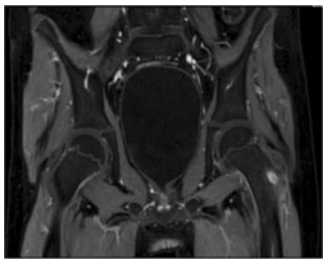

Poster #: EDU-070

A Literature Review on Brain Gadolinium Deposition

Michael Rozenfeld, DO, *Medical Imaging, Ann & Robert H. Lurie Children's Hospital of Chicago, Chicago, IL, mikerozenfeld@gmail.com;* Sebastian Garcia, Paige Nelson, Delilah Burrowes

Disclosures: All authors have disclosed no financial interests, arrangements or affiliations in the context of this activity.
Purpose or Case Report: Gadolinium based contrast agents (GBCAs) are widely used in medical imaging with 10 million annual doses given in the US alone. There is a very low 0.03% risk of serious adverse reactions. GBCAs were thought entirely safe until 2006 when reports of nephrogenic system fibrosis (NSF) surfaced. NSF was nearly eliminated by 2009 through careful screening and reducing dosage. In 2014, it was reported that GBCAs may deposit in the brains of patients. The purpose of this review is to examine the literature to date.
Methods & Materials: Every article on brain gadolinium deposition to date was reviewed and compiled for this presentation.
Results: Brain gadolinium deposition is seen in patients with normal renal function. It is associated with both the number of gadolonium dose administrations as well as the overall dose of gadolinium. It is not associated with the mean interval between gadolinium administrations, patient age, sex, creatinine level, or history of chemotherapy or radiotherapy. Of the regions of the brain examined, the most gadolinium deposition is noted in the dentate nuclei. There is a significant risk of gadolinium deposition in the brain after ≥ 4 doses or ≥ 77 ml.

Conclusions: While it is now fairly certain that gadolinium does deposit within the brains of patients with normal renal function, the clinical implications of this are currently unknown. In addition, there is very little data in children. Further studies are needed

Poster #: EDU-071

MRI Findings of Classic Radiographic "Don't touch lesions"

Brian Keehn, DO, *Radiology, Phoenix Children's Hospital, Phoenix, AZ, bkeehn@atsu.edu;* Mittun Patel, MD, Michael Peterson, MD, Logan Dance, MD, Deepa Biyyam, MD, Amber Pokorney, Craig Barnes

Disclosures: All authors have disclosed no financial interests, arrangements or affiliations in the context of this activity.
Purpose or Case Report: Radiologists have classically been taught the imaging findings of skeletal "Don't touch lesions" on radiographs. The radiologist's goal is to best characterize these boney lesions and avoid tissue biopsy, especially since some bone lesions are misleading when viewed histologically, with nonaggressive lesions appearing aggressive. Many of these classical "Don't touch lesions" are now being further evaluated with contrast enhanced magnetic resonance imaging (MRI). MRI findings of these radiographically classical lesions are not as well understood by radiologists with less MRI experience. We will provide an education exhibit to display MRI and corresponding radiographic appearances of characteristic "Don't touch lesions".

Poster #: EDU-072

Pancreatic Lesions in Pediatric Patients at MRI

Zeeshaan Bhatti, MD, *University of Michigan, Ann Arbor, MI, zsbhatti@med.umich.edu;* Edward Richer, MD

Disclosures: All authors have disclosed no financial interests, arrangements or affiliations in the context of this activity.
Purpose or Case Report: Pancreatic tumors are very rare in the pediatric population, with a reported incidence of 1.8 cases per 1,000,000 children in the United States. Several case reviews in the literature from large referral centers have yielded relatively few cases of pancreatic neoplasm. The most commonly reported pancreatic tumors include solid pseudopapillary epithelial neoplasm (SPEN), pancreatoblastoma, and neuroendocrine tumors. Other, more commonly encountered pancreatic abnormalities include trauma and pancreatitis. Given their rarity, the imaging characteristics of pancreatic lesions at MRI may be unfamiliar. The purpose of this exhibit is to present the typical imaging appearance of various pancreatic lesions in children.
Methods & Materials: IRB approval was obtained for this pictorial review. Illustrative cases of pancreatic lesions were obtained through review of the radiology information system.
Results: Several illustrative examples of pediatric pancreatic lesions will be highlighted, including cases of primary tumor, metastasis, and tumor-mimickers. Relevant clinical features will be incorporated in this review. Finally, the differential diagnosis of pancreatic lesions based on specific imaging features will be discussed, including cystic lesions, enlargement, atrophy, fatty replacement, and solid masses.
Conclusions: After viewing this presentation, the pediatric radiologist should be more familiar with the MRI appearance of pediatric pancreatic lesions and be able to provide a focused differential diagnosis based on the imaging characteristics.

Poster #: EDU-073

Imaging Genitourinary Catheters: The Good, the Bad, and the Ugly

Sheryl Tulin-Silver, *Radiology, Boston Children's Hospital, Boston, MA, sheryl.tulin-silver@childrens.harvard.edu;* Horacio Padua, Richard Yu, Jeanne Chow

Disclosures: All authors have disclosed no financial interests, arrangements or affiliations in the context of this activity.
Purpose or Case Report: The purpose of this educational exhibit is to review radiography, fluoroscopy, computed tomography (CT), and ultrasound (US) imaging appearance of commonly placed genitourinary catheters. The imaging findings associated with appropriately positioned catheters as well as misplaced and displaced catheters are described.
Methods & Materials: Imaging studies were retrospectively reviewed for patients with genitourinary catheters evaluated in the diagnostic radiology or interventional radiology departments at our tertiary care pediatric institution from September 2013 through August 2015. Some of the genitourinary catheters were placed at our institution and others were referred for evaluation after catheter placement at outside institutions. A literature review was performed in addition to the review of departmental cases. Imaging was selected for appropriately positioned catheters in patients with normal anatomy and those with congenital or postsurgical anatomical variants. Imaging was also selected for misplaced and displaced catheters in order to describe key findings in recognizing malpositioned catheters.
Results: Imaging findings are presented for a variety of genitourinary catheters, including nephrostomy tube, double-J ureteral stent, kidney internal splint stent (KISS) stent, Malecot catheter, Foley catheter, and feeding tube bladder catheter.
Conclusions: Genitourinary catheters have diverse imaging appearances, especially in patients with congenital anatomical variants and postsurgical changes. It is important for diagnostic radiologists to be familiar with normal and abnormal positions of a variety of genitourinary catheters as displacement may be first recognized on diagnostic imaging studies.

Poster #: EDU-074

Low Dose C-arm CT: Interventional Radiology Applications at a Pediatric Institution

Michael Acord, MD, *The Children's Hospital of Philadelphia, Philadelphia, PA, acordm@email.chop.edu;* Sphoorti Shellikeri, Master's in Biomedical Engineering, Seth Vatsky, Maricarmen Nazario, Abhay Srinivasan, Ganesh Krishnamurthy, MD, DNB, Marc Keller, MD, Anne Marie Cahill

Disclosures: All other authors have disclosed no financial interests, arrangements or affiliations in the context of this activity.
Purpose or Case Report: Low dose C-arm Computed Tomography (CT), is a technology that uses flat panel detectors to acquire real-time 3D images during an interventional radiology (IR) procedure to assist with anatomic localization and procedural mapping. This study describes our low dose protocol and applications of its use at a pediatric institution.
Methods & Materials: A retrospective study performed between October 2007 and August 2015 of procedures utilizing our low dose protocol (5sDR/8sDR, 248/396 projection images/acquisition and 0.1-0.17μGy/projection dose at the detector with 0.3/0.6/0.9 mm Cu filtration.) Cases were categorized by procedure type and then average patient age and C-arm CT and total dose area product (DAP) were calculated.

Results: 237 cases utilized C-arm CT with our low dose protocol. Results by each procedure type are listed in Table 1. The most common procedures were temporomandibular (TMJ) and sacroiliac (SI) joint injection (55%) and sclerotherapy (33%). C-arm CT was used in cases of difficult percutaneous access in less common applications such as cecostomy and gastrostomy placement, lumbar puncture and thoracentesis. C-arm CT accounted for between 11% and 88% of the total procedural DAP.
Conclusions: Low dose C-arm CT has multiple applications within pediatric IR and may be considered as an adjunctive imaging technique in a variety of procedures, particularly when percutaneous access is challenging.

	N (%)	Age (y) mean ±SE	C-Arm CT DAP (mGy-cm2) mean ±SE	% of total DAP
TMJ and SI joint injection	131 (55-%)	12.4±0.4	26.1±7.9	88%
Sclerotherapy	78 (33-%)	10.6±0.9	69.1±23.8	45%
Bone and soft tissue biopsy	26 (11-%)	10.9±1.0	771.5±229.1	80%
Arterial embolization	5 (2%)	9.8±2.2	197.1±77.4	11%
Thoracentesis	3 (1%)	0.5±0.25	73.2±58.2	65%
Cecostomy	2 (0.-8%)	8.3±0.7	169.6±33.2	65%
Primary gastrostomy	2 (0.-8%)	6.0±5.7	225.5±215.6	41%
Other**	8 (3%)	9.5±3.7	219.3±94.5	55%

Table 1
*Lumbar puncture, abscess drainage, sialography, lymphangiogram, and foreign body removal

Poster #: EDU-075

Ultrasound Artifacts: Where have all the Shadows gone?

Michael Baad, MD, *Radiology, University of Chicago, Chicago, IL, mike.baad@gmail.com;* Adrian Sanchez, Kevin Little, Ingrid Reiser, Zheng Feng Lu, Kate Feinstein

Disclosures: All authors have disclosed no financial interests, arrangements or affiliations in the context of this activity.
Purpose or Case Report: 1. Discuss benefits and limitations of different sonographic techniques
2. Provide phantom studies and clinical examples to demonstrate the effect of altering imaging parameters and sonographic techniques on both desired and undesired artifacts
3. Increase awareness of common errors in technique and provide recommendations to tailor the exam to the specific imaging question
Methods & Materials: Ultrasound is of critical importance in pediatric imaging. Recent advances, including harmonic imaging and spatial compounding, are now commonly utilized to improve overall image quality. Additionally, modern ultrasound units are equipped with features such as altering the speed of sound, 3D and large FOV. While these techniques offer many benefits, they may come at a cost, including reduction of desired artifacts, such as acoustic shadowing and enhancement. For this educational exhibit, we have constructed a phantom made of gelatin containing patient kidney stones and mimics of cysts. The effect of different imaging techniques on image quality and common artifacts are illustrated with the phantom and compared with clinical examples.
Results: Spatial compounding has been shown to reduce noise and speckle while increasing contrast and margin definition. This will be demonstrated on phantom and clinical examples, along with examples of its effect on ring down artifact, shadowing, edge shadowing and posterior enhancement. This is of clinical importance, as some of these desired artifacts are either less discernible or result in a different appearance with spatial compounding. The benefits of harmonic imaging will be shown, such as improved spatial resolution, decreased reverberation and increased contrast. Examples of the effect of harmonic imaging on shadowing, posterior enhancement and penetration will then be discussed and demonstrated. On newer units, resolution can be optimized by adjusting the speed of sound to match the imaged object. This will be demonstrated in phantom and clinical examples. As well, the effect of these imaging techniques and focal zone placement on twinkling artifact in color Doppler will be illustrated.
Conclusions: Ultrasound advances have led to increased image quality and a reduction in image artifacts. However, some of these artifacts are often desired and critical for diagnosis. An understanding of the effect of various sonographic techniques and parameters on both wanted and unwanted artifacts is critical to proper incorporation of these techniques into routine practice.

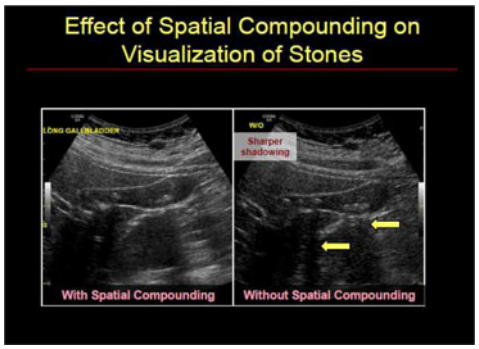

Poster #: EDU-076

Fat Gone Wrong: A Review of Pathological Fat in the Pediatric Abdomen and Pelvis

Jaclyn Thiessen, MD, *Diagnostic Radiology, Oregon Health and Science University, Portland, OR, thiessen@ohsu.edu;* Ryan Moore, Kelli Schmitz, Petra Vajtai, Katharine Hopkins, MD

Disclosures: All authors have disclosed no financial interests, arrangements or affiliations in the context of this activity.
Purpose or Case Report: Fat, like any other organ or tissue, can cause both disease and symptomatology. In the pediatric abdomen and pelvis, fat may be involved by a number of conditions, ranging from symptomatic to occult, self-limited to progressive, benign to malignant. This is a review of multimodality cross-sectional imaging findings associated with abdominopelvic fat pathology in children.
Methods & Materials: Case material from our hospital teaching file is used to illustrate a spectrum of diseases involving fat in the pediatric abdomen and pelvis as they manifest on ultrasound, CT, and MRI. Emphasis is placed on imaging features that differentiate these processes from each other and the role that cross-sectional imaging plays in guiding therapy.
Results: Entities discussed include obesity, steatosis, trauma, vascular compromise (epiploic appendagitis, segmental omental torsion/infarct, and omental herniation), primary neoplasia (lipoblastoma, lipoblastomatosis, and lipoma), secondary neoplasia, and patterns of secondary inflammation or fat necrosis (such as from pancreatitis, appendicitis, Meckel's

diverticulitis, and inflammatory bowel disease). Fat-containing tumors such as dermoid, teratoma, and angiomyolipoma are also reviewed.
Conclusions: Recognition and differentiation of these pathologies involving fat by the pediatric radiologist will allow for appropriate diagnosis and treatment.

Poster #: EDU-077

Posterior Fossa Tumors in Children: An Educational Review

Candace Scace, *St. Christopher's Hospital for Children, Philadelphia, PA, candace.scace@gmail.com*

Disclosures: All authors have disclosed no financial interests, arrangements or affiliations in the context of this activity.
Purpose or Case Report: Brain tumors are the most common solid tumor of childhood and the leading cause of death among all childhood cancers. Because many pediatric brain tumors occur infratentorially, it is important for the radiologist to recognize and distinguish both classic and more rare tumors that can present within this region. The purpose of this presentation is to review the imaging findings associated with the most common posterior fossa tumors in children, discuss their differentiating features, and expand upon this differential by including imaging characteristics of less common, but equally important neoplasms occuring within the posterior fossa.
Methods & Materials: A retrospective review of pediatric brain tumors was performed at St. Christopher's Hospital for Children. A series of cases with identified infratentorial tumors were collected for review and presentation.
Results: Neuroradiologic examinations of children with identified posterior fossa tumors were collected for review. The classic and distinguishing imaging characteristics of the most common pediatric infratentorial tumors are presented, including juvenile pilocytic astrocytoma, brainstem glioma, medulloblastoma, and ependymoma. Additionally discussed are less common neoplasms including atypical teratoid rhabdoid tumor (ATRT), hemangioblastoma, vestibular schwannoma, and cerebellopontine angle epidermoid/dermoid.
Conclusions: Brain tumors, particularly within the infratentorial region, cause significant morbidity and mortality in the pediatric population. Knowledge of distinguishing characteristics of both common and more rare posterior fossa tumors can aid the radiologist in an accurate and clinically relevant diagnosis.

Poster #: EDU-078

Thyme to Respect the Thymus

Lillian Lai, MD, *Lucile Packard Children's Hospital, Stanford University, Palo Alto, CA, lmlai@stanford.edu;* Safwan Halabi, Kristen Yeom, MD, Richard Barth, Jayne Seekins

Disclosures:
Purpose or Case Report: The pediatric thymus is a constant but confusing, dynamic entity. The goal of this educational exhibit is to illustrate the range of appearances of the normal thymus and to identify key imaging features that can help pediatric radiologists differentiate normal thymic tissue from neoplastic conditions and other mimics.
Methods & Materials: We retrospectively collected cases of varied appearances of the normal thymus across different modalities and patient ages, including normal thymic variants, ectopic thymic tissue, and non-neoplastic thymic conditions such as rebound hyperplasia. Imaging modalities included ultrasound, CT, and MRI. Clinical data, operative reports, and pathology reports were correlated with imaging findings.
Results: A pictorial review of varied appearances of the normal thymus will be presented. Cases will include absence of the thymus in a fetal MRI in a fetus with diGeorge syndrome, ectopic thymic tissue in the neck, ectopic thymic tissue in the supraclavicular region, and rebound thymic hyperplasia. The characteristic imaging features of the thymus will be reviewed across different modalities. We will also review the embryology, anatomy, and dynamic physiology of the thymus.
Conclusions: After reviewing this exhibit, the reader will become familiarized with varied imaging appearances of the pediatric thymus across different modalities, patient ages, and various clinical situations. Recognizing the varied appearances of the thymus is essential to avoid unnecessary imaging or invasive procedures.

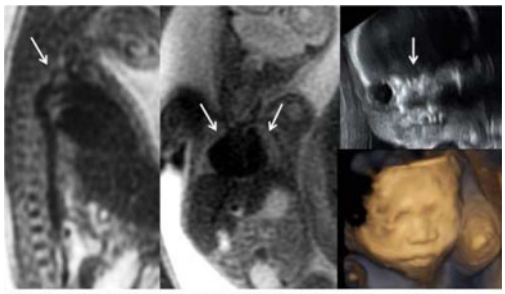

Figure 1: Thymic hypoplasia/aplasia in a 23-week gestational age fetus. Patient also had an interrupted aortic arch, hypotelorism, and midface hypoplasia. Amniocentesis revealed a deletion at 22q11.21 consistent with DiGeorge syndrome.

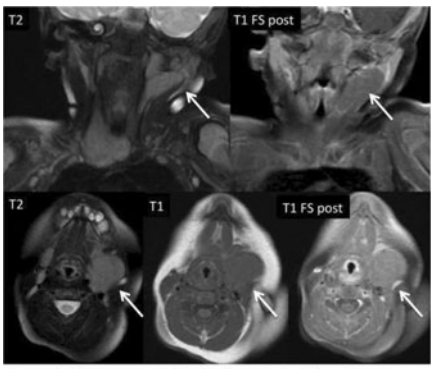

Figure 2: Biopsy-proven thymic tissue in the left neck (paracervical, submandibular, and carotid spaces) of a 3 month-old boy.

Poster #: EDU-079

Clinical Importance of Joint Evaluation by the Ultrasonography in the Pediatric Patients with Haemophilia

Chihiro Tani, *Hiroshima University Hospital, Hiroshima, Japan, ctani620@gmail.com;* Yuko Nakashima, Shinji Kume, Makoto Iida, Masao Kobayashi, Kazuo Awai

Disclosures: All authors have disclosed no financial interests, arrangements or affiliations in the context of this activity.
Purpose or Case Report: Haemophilic arthropathy is caused by recurrent bleeding into joint. The first bleeding episodes usually occurs in knee and ankles between 1 year and 3 years old. In the pediatric patients with haemophilia, it is important to detect the joint damage as soon as possible because appropriate prophylaxis is provided. Ultrasonography is increasingly used for joint assessment recently. The purpose of this study is to present clinical importance of joint evaluation by the ultrasonography in the pediatric patients with haemophilia.
Methods & Materials: We reviewed the 38 patients (median age 10.5 years, range 2-28 years) with haemophilia who underwent both ultrasonography and radiograph of bilateral knee and ankles in 2015. We compared ultrasonography findings with radiographic findings. In addition, we performed MRI in 4 patients and compared ultrasonography findings with MRI findings.
Results: Over all, 152 joints were evaluated. 11 of 152 joints were pointed out the abnormal findings by joint radiograph. The abnormal findings

that could be pointed out by joint radiograph were as follows: joint space narrowing, osteophyte, subchondral bone irregularity. On the other hand, in joint ultrasonography, the abnormal findings were pointed out in 31 of 152 joints. The abnormal findings that could be pointed out by joint ultrasonography were as follows: intraarticular effusion or hematoma, synovial thickening, cartilage thinning, cartilage surface irregularity, subchondral bone irregularity, osteophyte. The joint ultrasonography is superior in evaluation of cartilage, synovium and intraarticular fluid than joint radiograph. In addition, the ultrasonography can evaluate bone surface including osteophyte and the subchondral bone. In 4 patients underwent MRI, the abnormal findings on MRI could be detected easily and clearly also on a joint ultrasonography. Although MRI is very useful for assessment of haemophilic arthropathy, use of MRI is limited because very of its high cost and time-consuming examinations, and requirement of sedation in small children. Compared with MRI, ultrasonography is easily available and can evaluate multiple joints without sedation.
Conclusions: In the pediatric patients with haemophilia, ultrasonography is the most useful modality as screening to detect initial intraarticular abnormalities to lead to haemophilic arthropathy.

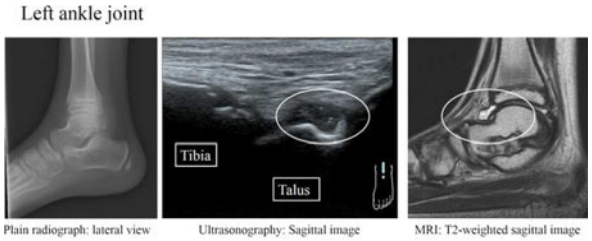

Intraarticular fluid effusion is depicted by ultrasonography and MRI (circle).

Irregularity of the subchondral bone of the left knee joint (circle).

Poster #: EDU-080

Beyond Achondroplasia: Radiographic Findings and Differential Diagnoses of Type 2 Collagen Disorders

Shawn Parnell, MD, *Radiology, Seattle Children's Hospital, Seattle, WA, shawn.parnell@seattlechildrens.org*

Disclosures: All authors have disclosed no financial interests, arrangements or affiliations in the context of this activity.
Purpose or Case Report: The skeletal dysplasias are a large diverse group of several hundred disorders which are marked by abnormal bone and cartilage growth with resultant short stature. Dysplasias have been divided into larger groups according to common radiographic and/or genetic mutations. The purpose of this educational exhibit is to highlight one of these major groups, which are characterized by mutations of type 2 collagen.
Methods & Materials: This exhibit will provide examples of several different disorders of type 2 collagen, highlighting clinical and radiographic features. There will also be discussion of other common skeletal dysplasias which have similar features to the type 2 collagenopathies.
Results: The observer will become more familiar with the spectrum of disorders characterized by type 2 collagen disorders, to include the lethal hypochondrogenesis and achondrogenesis type 2, moderately severe Kneist dysplasia, spondyloepiphyseal dysplasia congenita (SEDC), spondyloepimetaphyseal dysplasia (SEMD) Strudwick type, and milder forms such as Stickler syndrome. Radiographic and clinical features of type 2 collagen disorders will be contrasted with mucopolysaccharidoses such as Morquio syndrome and metatropic dysplasia, both of which can share a similar radiographic appearances.
Conclusions: As the skeletal dysplasias are a large diverse set of entities, the radiologist may be overwhelmed by the sheer number of disorders to be mastered. Previous educational exhibits have reviewed common radiographic features and nomenclature to be used in the interpretation of skeletal surveys for skeletal dysplasias, highlighting commonly encountered dysplasias over a wide range of categories. This exhibit will allow the observer to become more familiar with one of the more common groups within the skeletal dysplasias, those characterized by mutations in type 2 collagen.

Poster #: EDU-081

Gadolinium-based Contrast Agent Use in the Follow-up of Pediatric Primary Intracranial Neoplasms

Brittany Albers, MD, *Radiology, Mayo Clinic Florida, Jacksonville, FL, albers.brittany@mayo.edu;* Chetan Shah

Disclosures: All authors have disclosed no financial interests, arrangements or affiliations in the context of this activity.
Purpose or Case Report: Gadolinium based contrast agents have been used in pediatric neuroradiology for years and are thought to be safe when administered appropriately. However, it has been discovered that gadolinium used in routine clinical practice results in gadolinium deposition in the even in patients with normal renal function. No studies have addressed gadolinium deposition in the soft tissues of pediatric patients or its potential ill-effects. The potential for harm may exist. We reviewed our gadolinium use in the follow up of pediatric primary intracranial neoplasms.
Methods & Materials: After IRB approval, we retrospectively reviewed data from 96 patients with initial imaging between 2001 and 2015, who had been diagnosed with a primary intracranial neoplasm either by histopathology or widely accepted imaging appearance. We gathered patient demographics, tumor, and data related to contrast enhanced MRIs (CE-MRI). We noted whether or not the original tumor enhanced.
Results: Overall, 96 patients (46 girls, 50 boys) received 851 contrast enhanced MRIs. They ranged in age from 0.1 to 18.8 years at the time of the first CE-MRI. They received an average of 7.9 (range 0-31) follow-up CE-MRIs over an average of 3.3 years (range 0-14.1). Number of cases with age, exam, and follow-up data is presented in table 1. The trend was for enhancing lesions to receive for more exams for longer time, the difference was not statistically significant (table 2). A summary of solitary FLAIR hyperintense non-enhancing lesions is presented in table 3.
Conclusions: Children are undergoing a very large number of CE-MRIs for follow-up of primary intracranial neoplasms. The data did not take patient death into account, so we did not evaluate the significance of tumor grade or prognosis on follow up. Alternatively, lower grade neoplasms have an excellent prognosis and these children may have many years of imaging follow-up. Many patients likely "graduated" from our institution during the study time, which could lead to underrepresentation of their true follow up. Neoplasms which did not initially enhance continued to receive contrast for follow up exams. Whether or not this is necessary is yet to be determined, and is the focus of some of our on-going research. In light of new evidence of gadolinium deposition in the tissue, perhaps more care could be taken in protocolling exams for follow-up. Non-enhancing neoplasms and postoperative follow -up MRIs without recent change would be excellent opportunities to reduce contrast administration.
Table 1

Tumor Type	# Patients	% with Histopathology	% Initially Enhancing	Median Age at DX (range), yrs	Average # F/U MRI w/ God, (range)	Average Years of F/U, (range)
Pilocytic Astrocytoma	19	100	100	8.9 (2.0-17.1)	10.8 (1-31)	4.5 (0.7-12.4)
Pilomyxoid Astrocytoma	2	100	100	3.5 (1.7-5.4)	9.5 (5-14)	2.1 (0.8-3.4)
Other WHO II Astrocytomas	8	100	50	8.4 (1.0-16.4)	10.4 (3-21)	4.6 (0.6-11.8)
Brainstem Gliomas	9	0	33.3	6.9 (0.6-17.7)	5.9 (0-18)	2.8 (0–9.2)
Tumor of Unknown Histology*	20	0	10	11.2 (0.1-17.9)	4.3 (0-22)	2.9 (0-14.1)
Pleamorphic Xanthoastrocytoma	1	100	100	3	9	3.8
Anaplastic Astrocytoma	5	100	80	9.6(5.9-17.0)	7 (4-13)	1.8 (0.4-6.1)
GBM	1	100	100	14.9	11	2.1
Oligodendroglioma	3	100	0	5.9 (2.7-9.8)	12.7 (11-15)	5.5 (3.1-9.2)
Ependymoma	3	100	100	15.3 (1.3-18.8)	7.3 (5-10)	2.6 (0.6-6.4)
Choroid Plenus Carcinoma	2	100	100	2.4 (0.8-1.4)	6 (1-11)	1.6 (0-3.1)
Choroid Plexus Papilloma	1	100	0	1.3	2	0.3
Ganglioglioma	3	100	100	9.1 (7.5-12.3)	14.7 (9-18)	4.9 (3.0-5.8)
DNET	5	100	66.7	4.9 (3.5-14.8)	9 (4-18)	4.3 (1.9–6.0)
Medulloblastoma	6	100	100	5.4 (3.2-7.6)	7 (2-15)	1.8 (0.1-4.3)
PNET	1	100	100	2.8	2	0.9
Mixed High-Grade	1	100	100	9.8	16	4.9
Hemangioendothelioma	1	100	100	13.4	11	3.0
Germinoma	1	100	100	10.8	6	0.9
Teratoma	2	100	100	8.4 (7.6-9.6)	2 (0-4)	3 (0-6)
AVM	2	100	100	12.3 (8-16.6)	5.5 (5-6)	1.2 (0.8-1.6)

Table 1 shows data distributed by tumor type. *Tumor of Unknown Histology reflects solitary FLAIR hyperintense lesions that are not amenable to biopsy due to anatomic location. These patients have no known malignancy otherwise, and are therefore not prone to metastatic lesions. No patients had identifiable neurocutaneous conditions that could have accounted for the lesion.

Table 2

	Enhancing Tumors (n=59)	Non-enhancing Tumors (n=37)	p-value
Median age at Diagnosis	7.5	8.9	0.46
Average # F/U MRI	5.2	9.6	0.50
Average Years F/U	2.8	3.6	0.46

Table 2 shows that although the trend was for initially enhancing tumors to receive more exams over a longer follow-up time, the difference was not statistically significant. We found that tumors' enhancement pattern was typical for the tumor type, without significant outliers. For example, all pilocytic astrocytomas, ependymomas, and gangliogliomas enhanced, and none of the oligodendrogliomas enhanced.

Table 3

Patient	Lesion Location	Lesion Size (axial plane), mm
1	Left frontal white matter	8×6
2	Left frontal white matter	11×5
3	Right thalamus	9×8
4	Left temporal white matter	15×6
5	Left temporal white matter	12×11
6	Right parietal white matter	10×5
7	Right globus pallidus	3×5
8	LEft cerebral peduncle	7×5
9	Vermis	15×13
10	Left midbrain	6×4
11	Right medulla	9×9
12	Right parietal white matter	8×4
13	Left cerebellum	10×9
14	Left corona radiata	11×7
15	Right occipital white matter	4×3
16	Left middle cerebellar peduncle	5×3
17	Left frontal white matter	6×5
18	Right globus pallidus	6×6
19	Right cerebral peduncle	19×12
20	Right parietal white matter*	13×11

Table 3 summarizes tumors of unknown histopathology by location and size. Many were not amenable to biopsy, or were thought to be completely unrelated to patient symptoms. One patient* had severe metabolic disease with limited life expectancy, therefore no biopsy was performed.

Poster #: EDU-082

MRI for Evaluation of Acute Pelvic Pain in Girls: A Case Review

Dana Jackson, Sharon Gould, MD, *Medical Imaging, Nemours/AIDHC, Wilmington, DE, sgould@nemours.org;* Arabinda Choudhary, Monica Epelman

Disclosures: All authors have disclosed no financial interests, arrangements or affiliations in the context of this activity.
Purpose or Case Report: Acute onset pelvic pain in a pubertal girl has many possible etiologies. Reproductive, urinary and gastrointestinal pathology all can underlie acute onset pelvic pain in this age group and may have similar presentations. We present a series of six cases in which MRI was utilized for further evaluation of US findings and either confirmed the need for surgical intervention, or established the cause of pain and eliminated the need for surgery.
Methods & Materials: Both focused MRI for evaluation of appendicitis and dedicated, brief pelvic MRI protocols are utilized in our institution for further investigation of pelvic/right lower quadrant pain and abnormal pelvic ultrasound findings. Six cases are presented culled from our teaching file that demonstrate the utility of MRI in clarifying pelvic pathology in the emergent setting.
Results: MRI evaluation of the appendix can confirm or eliminate a diagnosis of appendicitis. In addition, the high soft tissue contrast inherent in MRI can detect intra-ovarian pathology such as hemorrhagic or corpus luteum cysts. Diffusion weighted imaging and contrast are helpful in identifying ovarian torsion. These studies can be performed in most instances in less than 30 min.
Conclusions: The most worrisome potential etiologies of acute pelvic pain are those requiring emergent surgery: acute appendicitis, ovarian torsion, and ectopic pregnancy. Since pregnancy can be established prior to imaging, and, if present, warrants ultrasound, this entity is not be discussed here. Given the need for timely evaluation, an organized approach to the imaging work up is needed for efficient diagnosis and to avoid unnecessary radiation exposure. Our institution utilizes pelvic and/or appendiceal ultrasound followed by tailored MRI if the ultrasound findings are inconclusive or do not fit the clinical diagnosis. Further imaging evaluation prior to discharge or laparoscopy can direct appropriate management eliminating unnecessary radiation and surgery.

Poster #: EDU-083

Intracranial imaging findings in late Hemorrhagic Disease of Newborn

Vikas Yadav, MD, *Radiology, Christian Medical College, Vellore, India, vkyadav77@yahoo.co.in;* Parthasarathy Ealai

Disclosures: All authors have disclosed no financial interests, arrangements or affiliations in the context of this activity.
Purpose or Case Report: To delineate the spectrum of intra cranial imaging findings in infants with late hemorrhagic disease of newborn (late HDN)
Methods & Materials: A retrospective study of infants from January 2003 to February 2014, fulfilling the criteria of late HDN with CNS symptoms was done. None of them had history of vitamin k injection at birth. They were evaluated for the pattern and location of the bleed, infarcts, cerebral edema and mass effect. Hematological parameters were noted in all infants. Condition at the time of discharge and follow up imaging findings were also noted.
Results: Out of 24 infants (20 males and 4 females), 16 presented with intracranial bleed only, while 8 had bleed involving both CNS and other sites. Among intracranial hemorrhage 22 subdural hemorrhage, 19 subarachnoid hemorrhage, 8 parenchymal, and 5 intraventricular hemorrhage pattern were observed. Temporal lobe is the commonest parenchymal location, followed by frontal lobe. Combination pattern of hemorrhage (19 infants) was commoner than single location hemorrhage, most common being subdural hemorrhage and subarachnoid hemorrhage. Infarcts were seen in 10 infants and significant midline shift in 11 infants. Seventeen were discharged in stable condition. Seven were discharged against medical advice in view of poor prognosis. Two underwent surgery, of which one recovered completely. 7 infants had follow up imaging, of which 5 showed cystic encephalomalacia and 2 had subdural hygroma
Conclusions: This study shows the various findings in a potentially preventable cause of intracranial bleed. In some parts of world, infants still suffer from this disease due to various factors related to maternal, neonatal and socio-economic conditions. Vitamin K dose at birth can prevent catastrophic neurological complications in these infants.

Poster #: EDU-084

Ultrasound Guided Muscle Injection of Botulinum Toxin A in Children: How We Do It

Ralph Gnannt, Bairbre Connolly, Darcy Fehlings, Walid Mubarak, *Diagnostic Imaging, The Hospital for Sick Children, Toronto, ON, Canada, walid.mubarak@sickkids.ca;* Dimitri Parra

Disclosures: All authors have disclosed no financial interests, arrangements or affiliations in the context of this activity.
Purpose or Case Report: The purpose of this educational poster is to describe and illustrate our technique to perform Ultrasound Guided Botulinum Toxin A muscle injections in children. We explain the pre-procedural preparation including clinical assessment, injection planning and obtaining informed consent. Intra-procedure we describe limb positioning and preparation on the procedure table; showing and explaining in detail the equipment that we use. We illustrate muscle schematics with ultrasound correlation. The identification of different muscle groups on ultrasound is the main goal of this educational poster. Additionally, we will provide technical tips and potential pitfalls, which an interventional radiologist may encounter performing this procedure. The post-procedural management will wrap up our educational poster.

Poster #: EDU-085

Special Delivery: Spectrum Liver Abnormalities on Fetal Ultrasound and MRI

Ibrahim Hakim, *Stanford University School of Medicine, Stanford, CA, ishakim@stanford.edu;* Safwan Halabi

Disclosures: All authors have disclosed no financial interests, arrangements or affiliations in the context of this activity.
Purpose or Case Report: Fetal MRI (FMR) has been particularly helpful in the evaluation of abnormalities observed on antenatal ultrasound (US). In this educational exhibit, the aim is to present the spectrum of liver abnormalities encountered in the fetus with US and FMR imaging. The most common entities encountered in utero include hemochromatosis, cystic lesions, hepatoblastoma, hemangioma, and metastatic disease. Antenatal identification of liver abnormalities contributes to accurate diagnosis and recognition of complications, ultimately guiding delivery, postnatal imaging, therapeutic planning, and treatment.
Methods & Materials: This retrospective analysis identifies fetal liver abnormalities from antenatal imaging studies of pregnant women at our tertiary care institution. These women were referred to the Perinatal

Diagnostic Center for fetal abnormalities which include entities such as hemochromatosis, cystic lesions, hepatoblastoma, hemangioma, and metastatic disease. We identified key imaging findings of these fetal liver abnormalities present on US and FMR. Postnatal imaging is also presented as a correlate to the prenatal imaging findings.
Results: In fetuses with hemochromatosis, FMR demonstrates an abnormal hyperintense liver signal suggestive of iron overload. US of simple cysts reveals a hypoechoic well circumscribed mass and FMR reveals well-defined water-attenuated lesions without enhancement; T1-weighted scans reveal a low-intensity lesion while T2-weighted images reveal a high-intensity lesion. Hepatoblastoma presents on US as a heterogeneous mass with coarse calcifications and an osseous matrix; T2 weighted FMR images show a large, well-circumscribed heterogeneous mass lesion. Hepatic hemangioma appears as a focal well-demarcated mass of heterogeneous echogenicity and enlarged hepatic vessels; on FMR it presents as hepatomegaly with masses T2 hyperintense to the liver parenchyma. Neuroblastoma metastasizes most often to the liver in the fetus and neonate followed by leukemia and renal tumors.
Conclusions: US and FMR are valuable imaging modalities for characterizing various fetal liver abnormalities including hemochromatosis, cystic lesions, hepatoblastoma, hemangioma, and metastatic disease in the fetal liver. Management may be limited by the gestational age and maturity of the fetus but better knowledge of the appearance of these lesions can help guide delivery planning, postnatal therapeutic planning and may lead to improved neonatal outcomes.

Poster #: EDU-086

Man's Best Friend? Not Always
A Review of Craniofacial Injury in the Setting of Dog Bites

Kriti Gwal, MD, *Children's Hospital of Philadelphia, Cherry Hill, NJ, kritigwal@gmail.com;* Karuna Shekdar

Disclosures: All authors have disclosed no financial interests, arrangements or affiliations in the context of this activity.
Purpose or Case Report: To describe the imaging spectrum of injuries in children who had suffered dog bites to the craniofacial region evaluated with radiographs and/or helical Computed Tomographic (CT) scans.
Methods & Materials: This retrospective descriptive study reviewed radiographs and/or helical CT scans of patients listed as having been bitten by dogs in the craniofacial region presenting between 2000 and 2015. Depending on the extent of the bite/injury site, the evaluation included non-contrast head CT alone or with CT of the orbits, face, temporal and neck regions. Suspected penetrating vascular injury was evaluated with CT angiography.
Results: A total of 48 children presented to the emergency room with dog bite injuries between 2000 and 2015. The patients ranged from 5 months to 12 years. 36 (75%) of the patients had a CT scan and 12 (25%) had radiographs, with 9 (19%) of the patients having had both performed. The spectrum of injuries included cutaneous abrasions, lacerations of the scalp, face and neck, and orbital or periorbital injuries. In 7 (15%) of the cases, the injuries resulted in fractures. 13 (27%) of the children suffered other complications due to the attack, including intracranial extension, hemorrhage, cellulitis, intra-orbital involvement, dental injury and vascular injury.
Conclusions: In younger children, craniofacial injuries from dog bites are more common. Soft tissue lacerations were the most common injuries. Infants and young children are especially at risk for fractures and intracranial injuries from dog bites due to their small stature and thin skull. Imaging of craniofacial injuries particularly with CT scans can assess the extent of the injury and potential complications, and provide crucial information to the emergency physicians, neuro-surgeons and plastic surgeons in planning immediate treatment.

Poster #: EDU-087

The faces of Juvenile Paracoccidioidomycosis

Fernanda Braojos, MD, *Radiology, Hospital da Criança e Maternidade de São José do Rio Preto, São José do Rio Preto, Brazil, ferdcb@hotmail.com;* Mariana Cardoso, Elaine Arruda, Letícia Bueno, Pedro Henrique Cação, Marcia Catelan, Antonio Souza

Disclosures: All authors have disclosed no financial interests, arrangements or affiliations in the context of this activity.
Purpose or Case Report: This education exhibit aims to:
Provide a concise overview of the imaging aspects of the paracoccicidioidomycosis in childhood
Illustrate and discuss the main radiological findings of these endemic mycotic infection in Brazil

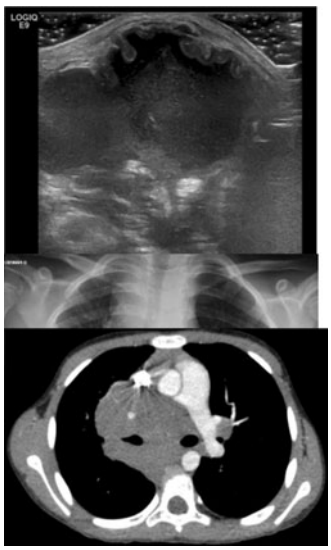

Methods & Materials: We searched at the Hospital da Criança e Maternidade de São José do Rio Preto electronic medical records and reviewed the radiology picture archiving, including all available imaging exams (radiograph, CT scans, MRI, and ultrasound) between 2013 and 2015. Excisional node biopsy was used as a confirmatory diagnosis.
Results: Five patients (1 girl and 4 boys) in the last 2 years were diagnosed with paracoccicidioidomycosis in our tertiary hospital, with ages between 4 and 25 years. At the initial analyses of the images none of the radiologist suggested the hypothesis of paracoccicidioidomycosis. In fact, in 4 cases the suggested diagnose were lymphoma like disease; one case systemic tuberculosis and the other one pneumonia.
Conclusions: Paracoccicidioidomycosis is a fungical granulomatous disease caused by *Paracoccidioides brasiliensis,* which is considered the most important systemic mycosis in Latin America and is endemic in Brazil.
Inhalation of the fungus is the most common form of disease transmission; however traumatic inoculation can also occur.
Although the infection is mostly acquired between 10 years and 20 years of age, clinical manifestations and progression to disease are not common in this group. This is why nearly 95% of the cases occur in adults as a chronic disease, manifested by mucosal and pulmonary involvement. Children, adolescents and young adults (under 30 years of age) are generally affected by an acute or subacute form, know as juvenile paracoccicidioidomycosis with a rapid course and marked involvement of the reticuloendothelial system, without mucosal lesions. The imaging findings in juvenile form are generalized lymphadenopathy and hepatoesplenomegaly.

The diagnosis is based upon fungus microscopic visualization and/or culture, and sorologic testing. Imaging methods are very helpful to identify the structures involvement, however, there are no specific pattern of this disease.
In the absence of therapy mortality rates are high, making the suspicion essential for the satisfactory prognosis of the disease. The objective of this educational review is awareness radiologists that a lymphoproliferative aspect of a systemic or localized disease in endemic areas can represent a paracoccicidioidomycosis infection.

Poster #: EDU-088

How to Differentiate between Normal Variants and Child Abuse on Skeletal Survey

Misun Hwang, MD, *Radiology, Children's Hospital of Philadelphia, Philadelphia, PA, mshwang1@gmail.com;* Sabah Servaes

Disclosures: All authors have disclosed no financial interests, arrangements or affiliations in the context of this activity.
Purpose or Case Report: Many normal variants in the skeletal survey can be misconceived as signs of child abuse. Accurate differentiation between the two is crucial in subjecting only the perpetrators to trial. The present exhibit educates on the radiographic signs and techniques that can help differentiate between normal variants and child abuse on the skeletal survey.

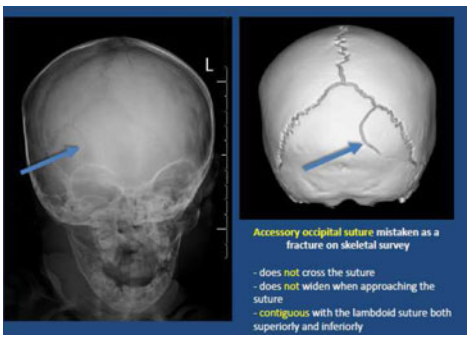

Methods & Materials: All publications on the topic to date were compiled to create a list of normal variants that simulate child abuse on the skeletal survey. For the purpose of this exhibit, normal variants are categorized into the three categories: skull, appendicular skeleton, and axial skeleton. Common normal variants in each of the three categories are described. Key characteristic radiographic features that can differentiate these normal variants from child abuse are also examined.
Results: Skull suture variants particularly in the parietal and occipital bones are oftentimes erroneously interpreted as fractures. Radiographic findings of normal skull sutures include zigzag pattern with sclerotic borders, absence of diastasis, bilateral and symmetric appearance, absence of soft tissue swelling. Calvarial fractures on the other hand are lucent with nonsclerotic edges, typically unilateral, widen when approaching the suture, and sometimes cross the suture.
Normal metaphyseal variants including step-off, beak, spur, and fragmentation mimic child abuse. Differentiation of metaphyseal findings can be difficult but the awareness of normal variants, acquisition of AP and lateral coned views, and follow up radiographs are all important.
The notable anatomical variants of the spine include normal synchondrosis, ossification centers, intersegmental clefts, anterior wedging of up to 3 mm particularly at C3, and pseudoxubluxation at the C2-C3 level. Anatomical variants of the cervical spine can be differentiated by the knowledge of normal variants, technique or position dependent changes, preservation of the posterior cervical line, and absence of prevertebral soft tissue thickening.
Conclusions: Differentiation between normal variants and child abuse on the skeletal survey requires knowledge of the normal variants and key radiographic features that favor one from another. Since the final report generated by radiologists directly impacts the management of suspected cases of child abuse, proper education on this topic is of utmost clinical importance.

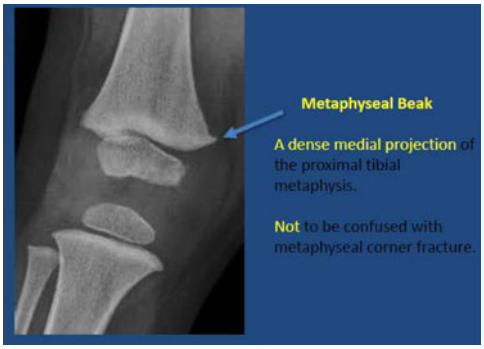

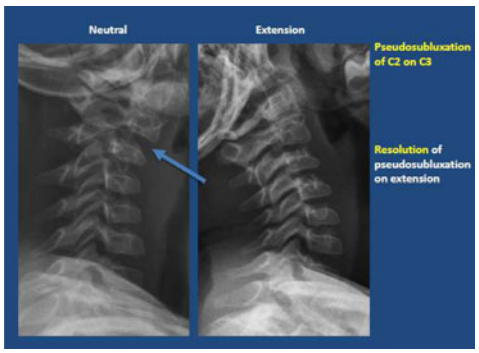

Poster #: EDU-089 – ***Withdrawn***

Poster #: EDU-090

Art and Architecture, Form and Function: Importance of Cardiac Micro-Structure in Congenital Heart Disease

Richard Southard, Erik Ellsworth, Tabitha Moe, Robyn Augustyn, Marrit Thorkelson, **Dianna Bardo, M D,** *Phoenix Children's Hospital, Phoenix, AZ, dmebmd@gmail.com*

Disclosures: All authors have disclosed no financial interests, arrangements or affiliations in the context of this activity.
Purpose or Case Report: The structure of the heart is more complex than 4 major chambers, 4 major valves, venous inflow and arterial outflow.
Muscular and soft tissue ridges, perforated membranes, tissue flaps, electrical pathways, external grooves, endocardial surface characteristics, and a core architecture structured of fibrous tissue and embryonic tissue remnants form distinguishing anatomic landmarks. These structures provide insight into cardiac development, serve physiologic purpose, define structural and functional elements, as well as offer prognostic information.
Specific details of cardiac anatomy may not be recognized on cardiac MR and CT examinations. Structural anomalies that affect cardiac function and anatomic or physiologic relationships may be abnormal in hearts with congenital malformations. The fine structural details of the heart are typically not part of an imagers

search pattern and are therefore overlooked or underreported. Each minute structure and anatomic characteristic provides clues to errors in cardiac formation and may provide clinically relevant diagnostic information. After palliation of CHD defining anatomic structure may be lost, displaced, interrupted or even restored.

Important processes, corresponding anatomic landmarks, and effects of malformation in defining congenital heart disease anatomy, physiology and functional variation from normal include basal structures such as the central fibrous body of the heart, atrial structures including the crista terminalis, the sinus venarum, and eustacian valve, and ventricular structures such as the crista supraventricularis.

Each structure is described along with its normal location, anatomy functional and physiologic importance, the effect of congenital malformation, and imaging findings as in the example of the central fibrous body (table 1).

Minute cardiac anatomy will be shown in illustration as well as in CT and MR images (figure 1).

CARDIAC ANATOMIC STRUCTURE & NORMAL ANATOMY	CHD DIAGNOSIS	ANATOMIC MANIFESTATION OF ABNORMAL CARDIAC STRUCTURE	PHYSIOLOGIC OR FUNCTIONAL MANIFESTATION OF ABNORMAL CARDIAC STRUCTURE
BASE OF THE HEART			
CENTRAL FIBROUS BODY	ACHD		
Dense fibrous tissue which forms attachment for the mitral, tricuspid and aortic valves		Fibrous mitral and tricuspid valve rings are discontinuous	Morphology of the mitral and tricuspid valve rings and valve are disrupted - may be balanced or unbalanced
The central fibrous body extends into the interventricular and atrioventricular membranous septum - normal atrial myocardium is contiguous with ventricular myocardium via fibro-fatty tissues of the central fibrous body at the AV junction and AV valve rings		Atrial myocardium is contiguous to ventricular myocardium via fibro-fatty tissues at the AV junction and AV valve rings	Septal defects allow mixing of blood from left to right and right to left - electrical pathways between atrioventricular node and bundle of His are disrupted, manifests with subsequent arrhythmia

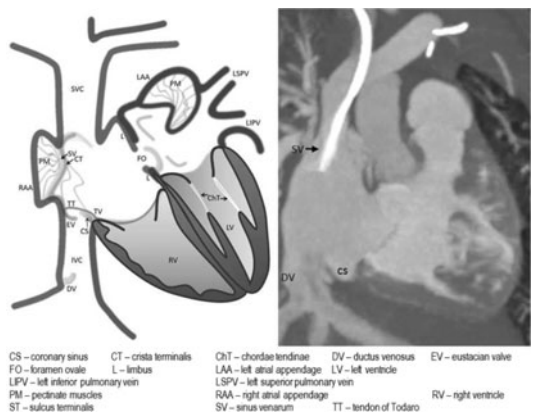

Poster #: EDU-091

Sonographic Findings in Pediatric Liver Transplant: A Must Know Summary for Radiology Residents and Fellows

Claudia Martinez-Rios, MD, *Diagnostic Imaging, The Hospital for Sick Children, Toronto, ON, Canada, claudia.martinez-rios@sickkids.ca;* Marta Tijerin Bueno, Fellow, Tahani Ahmad, MD, Kamaldine Oudjhane, MD MSc, Oscar Navarro

Disclosures: All authors have disclosed no financial interests, arrangements or affiliations in the context of this activity.

Purpose or Case Report: Pediatric liver transplant (PLT) is an established treatment for many hepatic conditions in children. In recent years there has been a significant increase in the number of PTL associated with an improved survival. In children however, due to the complex surgical procedures and peculiar hemodynamic physiology there is also an increased risk for vascular and biliary complications. High resolution ultrasonography (US) is the modality of choice to evaluate and monitor the evolution of pediatric liver graft. This exhibit intends to illustrate fellows and residents with the US characteristics of the normal hepatic anatomy, the normal early and late US appearances of the graft, and the US features of complications that may compromise graft's survival.

Methods & Materials: This exhibit starts with a quiz. Same questions are again asked at the end of the presentation, and it is our expectation that the reader will be able to answer them. Then we briefly describe the common indications of liver transplant in children, types of transplants and surgical approaches in children. We define the gray scale and Doppler US features of the normal liver, and the normal graft, including the hepatic artery (HA) velocities and the normal resistive indexes (RI) of day 1 and 3 post-transplant. We also describe the common vascular and biliary complications with its sonographic features and representative examples. Finally, we include illustrative cases of other extra-hepatic complications including collections, arterio-venous fistulae, and post-transplant lymphoproliferative disease and we provide a "take home" summary of the exhibit.

Results: The most common complications in PTL are biliary-related and include anastomotic leak, strictures, bleeding, or infection. Common vascular complications are hepatic artery, portal or hepatic veins stenosis, and thrombosis. Hepatic artery RI<0.5 with low systolic velocities (<50 cm/

sec), monotonic hepatic veins flow with low hepatic vein velocity (<25 cm/sec), and absent or low portal venous flow (<30 cm/sec), warrant further assessment.

Conclusions: Fellows and residents must be aware of the normal sonographic features of the liver, the early and late postoperative features of the pediatric liver transplant to be able to recognize potential complications. Although, there is no yet established definitive cut off Doppler values to predict graft status in children, recognition of abnormal arterial and venous velocities or spectrum warrant further assessment.

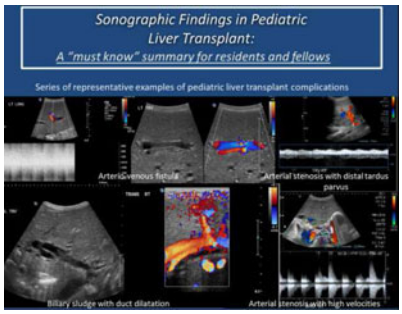

Poster #: EDU-092

Evaluating Types of Childhood Hydroceles with Ultrasound, Maneuvers and Urologic Management

Kathleen Boyer, *Tripler Army Medical Center, Aiea, HI, kmboyer2281@gmail.com;* Jonathan Wood, Leah McMann, Veronica Rooks

Disclosures: All authors have disclosed no financial interests, arrangements or affiliations in the context of this activity.

Purpose or Case Report: This educational exhibit will present the importance and utility of utilizing ultrasound and various sonographic-imaging techniques to investigate and clarify the different types of pediatric hydroceles. It will convey the necessity for specifying the type of hydrocele in order to implement the best management protocols.

Methods & Materials: Hydroceles are one of the most common causes for young males to present with painless scrotal swelling. Persistence of the processus vaginalis results in a hydrocele. In rare instances female infants are born with a patent processus vaginalis, termed the canal of Nuck. Through this canal they can develop hydroceles and hernias similar to their male counterparts.

Representative sonographic cases will be used to demonstrate the various types of hydroceles, including simple testicular hydroceles, funicular and encysted spermatic cord hydroceles, as well as female canal of Nuck hydroceles. The cases presented will further demonstrate how various ultrasound techniques such as using supine versus upright positioning, application of probe pressure against the fluid collection and demonstration of color Doppler imaging, can elucidate the specific type of hydrocele. The importance of classifying hydroceles will be exemplified by brief commentary on urologic treatment for each variation of hydrocele.

Results: The exhibit displays the various sonographic techniques and the representative hydrocele images. The sonographic findings for each hydrocele is explained. Lastly, the importance of employing various sonographic methods to unveil the exact type of hydrocele is illustrated by correlation with the urologic treatment protocol.

Conclusions: Ultrasonography is a useful tool to utilize when diagnosing and classifying hydroceles. Various maneuvers like use of minimal compression, upright examination versus supine, as well as color Doppler imaging are employed for differentiating the types of hydroceles seen in both males and females. The importance of being able to describe the fluid collection and its route assists clinicians in determining treatment options. Truly understanding the specific type of hydrocele, can save some children from unnecessary surgical procedures.

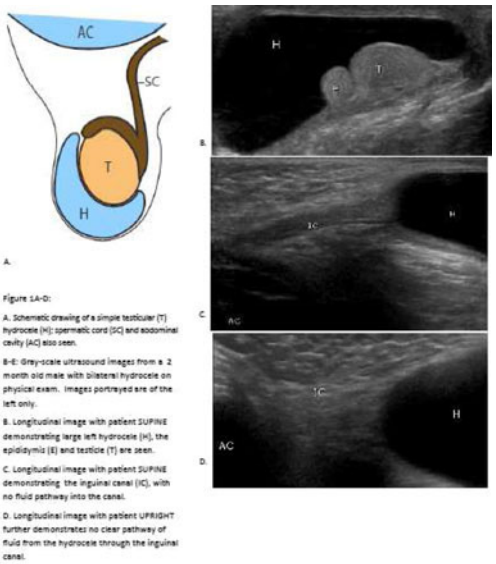

Figure 1A-D:

A. Schematic drawing of a simple testicular (T) hydrocele (H); spermatic cord (SC) and abdominal cavity (AC) also seen.

B-E: Grey-scale ultrasound images from a 2 month old male with bilateral hydrocele on physical exam. Images portrayed are of the left only.

B. Longitudinal image with patient SUPINE demonstrating large left hydrocele (H), the epididymis (E) and testicle (T) are seen.

C. Longitudinal image with patient SUPINE demonstrating the inguinal canal (IC), with no fluid pathway into the canal.

D. Longitudinal image with patient UPRIGHT further demonstrates no clear pathway of fluid from the hydrocele through the inguinal canal.

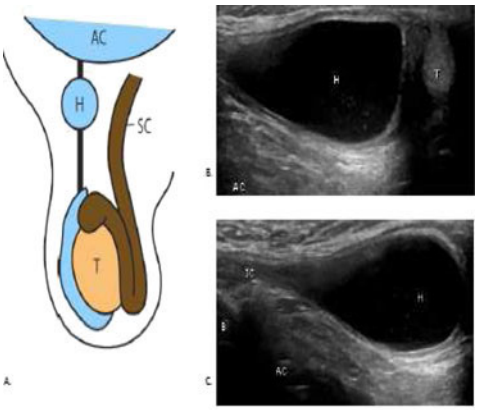

Figure 2A-C:

A. Schematic drawing of an encysted spermatic cord (SC) hydrocele (H); testicle (T) and abdominal cavity (AC) also seen.

B-C: Grey-scale ultrasound images from a 2 year old male presenting with a right inguinal mass.

B : Longitudinal image with patient supine demonstrating right side hydrocele (H) in the spermatic cord, displacing the testicle (T) inferiorly; abdominal cavity (AC) is seen.

C: Longitudinal image with patient supine with application of gentle pressure. Hydrocele fluid is not reducible into through inguinal canal (IC) in to the abdominal cavity; portion of bowel (B) is seen.

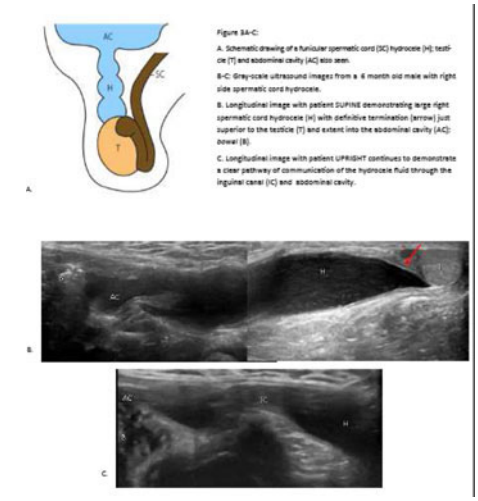

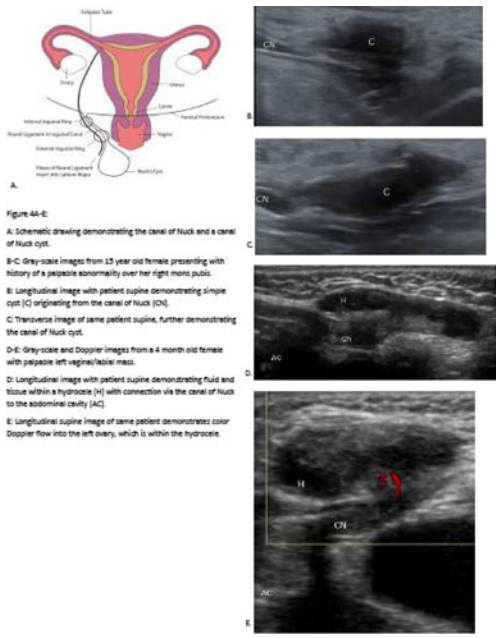

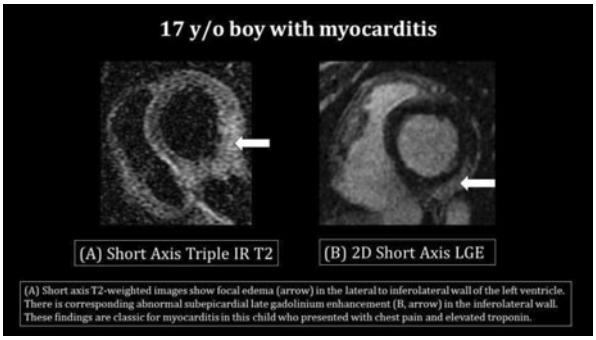

Poster #: EDU-093

Pediatric Cardiomyopathy: A Pictorial Review

Evan Zucker, M.D., *Massachusetts General Hospital, Boston, MA, zucker@post.harvard.edu*

Disclosures: All authors have disclosed no financial interests, arrangements or affiliations in the context of this activity.

Purpose or Case Report: Cardiomyopathy is rare in children but associated with significant morbidity and mortality when symptomatic. It also comprises a large proportion of cardiac MR imaging referrals in typical pediatric radiology practice. The purpose of this educational exhibit is to review the major types of cardiomyopathy in children, focusing on cardiac MRI.

Methods & Materials: Background information (prevalence, demographics) is discussed. An approach to imaging and cardiac MRI protocols are offered. The major types of cardiomyopathy are detailed, including dilated, hypertrophic, restrictive, and unclassified. Within these categories, disorders discussed include myocarditis, Duchenne muscular dystrophy, and anthracycline toxicity (dilated); hypertrophic cardiomyopathy (HCM); Fabry disease (restrictive); and arrhythmogenic right ventricular cardiomyopathy (ARVC), left ventricular non-compaction (LVNC), and Friedreich's ataxia (unclassified). MRI as well as clinical features of each entity are highlighted.

Results: Most cardiomyopathies in children are dilated. Within this group, myocarditis followed by neuromuscular disease is the most common identifiable cause. HCM is the second-most common type in children but comprises a disproportionate number of cardiac MRI referrals; the role for MRI in this disorder is well established, including assessment of wall thickness, systolic anterior motion of the mitral valve (SAM), left ventricular outflow tract obstruction, and fibrosis. Restrictive disease is rare. Within the unclassified category, ARVC and LVNC have well-defined cardiac MR criteria. Common to many cardiomyopathies is subepicardial to mid-myocardial abnormal late gadolinium enhancement (LGE) with an inferolateral predominance and variable systolic dysfunction. Quantitative imaging findings that assist in diagnosis include the Lake Louise criteria for myocarditis, wall thickness cutoffs for HCM, the 2010 Revised Task Force Criteria for ARVC, and the non-compacted to compacted (NC/C) ratio for LVNC. While increasingly detected in asymptomatic children with strong family history, cardiomyopathy when symptomatic commonly progresses to cardiac transplant or death.

Conclusions: Cardiomyopathies in children are uncommon and heterogeneous disorders, often with a genetic basis. MRI allows earlier detection compared to other modalities, offering important prognostic information and facilitating prompt initiation of cardioprotective medications. Future directions include targeted imaging markers and personalized therapies.

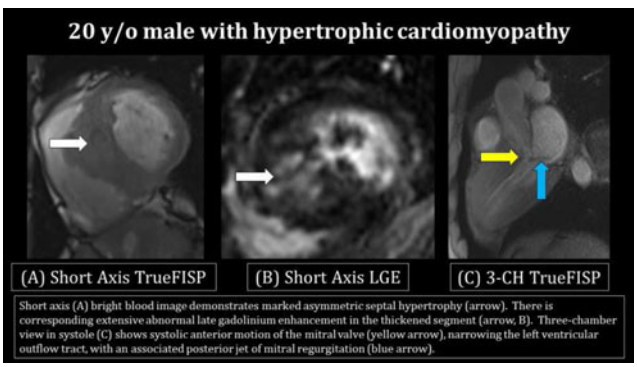

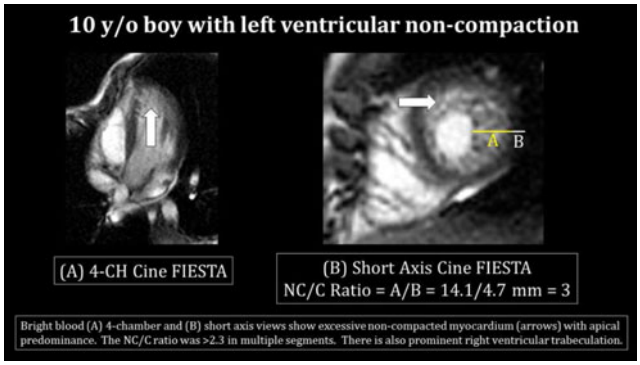

Poster #: EDU-094

Pediatric Imaging and Intervention: Classic Diagnostic Cases and Their Management

Terrence Metz, MD, *Children's Hospital of Michigan, Detroit, MI, terrencemetz@gmail.com;* Edward Richer, MD, Ranjith Vellody

Disclosures: All authors have disclosed no financial interests, arrangements or affiliations in the context of this activity.
Purpose or Case Report: To present nine classic pediatric diagnostic imaging cases and their subsequent interventional managements in order to emphasize the interventionalist's role in caring for the child and educate the pediatric radiologist to guide further care.
Methods & Materials: Nine separate pediatric radiology diagnoses and their associated interventional procedures were selected from patients presenting to two tertiary care children's hospitals. Cases include perforated appendicitis/abscess and drainage, fibromuscular dysplasia and renal angiography/angioplasty, osteoid osteoma and radiofrequency ablation, biliary atresia and liver biopsy, venolymphatic malformation and sclerotherapy, osteomyelitis and bone biopsy/PICC placement, ureteropelvic junction obstruction and percutaneous nephrostomy, neonatal ischemia/encephalopathy and percutaneous gastrostomy tube placement, and portosystemic shunt and venous occlusion.
Results: Nine common pediatric imaging diagnoses and their associated interventional procedures are presented with imaging figures and discussion emphasizing imaging findings and interventional technique/methodology.
Conclusions: As pediatric interventional radiology continues to play a more common and prominent role in the care of children, it is important to be aware of the common pediatric-specific interventional radiology procedures and their associated imaging diagnoses. Recognizing the imaging findings is essential for initial diagnosis and understanding the associated interventional management is important when guiding further care with the referring clinician.

Poster #: EDU-095

Soft Tissue Vascular Malformations: What the Radiologist Needs to Know

Joshua Chern, D.O., *Radiology, St. Christopher's Hospital for Children, Philadelphia, PA, chernjs@gmail.com;* Mea Mallon, Jaqueline Urbine, Archana Malik, Faaiza Kazmi, Erica Poletto, Eric Faerber

Disclosures: All authors have disclosed no financial interests, arrangements or affiliations in the context of this activity.
Purpose or Case Report: Soft tissue vascular malformations encompass a wide variety of lesions throughout the body. Appropriate treatment for these lesions is dependant on accurate classification and diagnosis. Unfortunately, inappropriate nomenclature and description by the radiologist can lead to confusion and possibly mismanagement.
Methods & Materials: A retrospective review of patients with known vascular malformations seen over the past 10 years at a small urban children's hospital was performed. Medical records and radiologic studies were correlated with clinical history and where available, surgical findings. A selection of cases with important radiologic findings was identified and used for an imaging review.
Results: A multimodality review of the imaging findings seen with various soft tissue vascular malformations will be provided. Additionally, there will be a review of the International Society for the Study of Vascular Anomalies (ISSVA) classification system, which is widely used by various subspecialists to classify these lesions. Examples of various vascular tumors, low-flow, and high-flow vascular malformations will be provided.
Conclusions: Vascular malformations and tumors are a complex group of lesions which can be daunting for the radiologist to describe and accurately diagnose. Due to the varying treatment for these lesions, accurate diagnosis is paramount. For this reason, pediatric radiologists should be familiar with the radiologic appearance and classification of these lesions.

Poster #: EDU-096

The Pediatric Thyroid: What to do With Those Nodules?

Deepa Biyyam, MD, *Radiology, Phoenix Children's Hospital, Phoenix, AZ, dbiyyam@phoenixchildrens.com;* Mittun Patel, Logan Dance, MD, Tuan Dao, MD, Mostafa Youssfi, MD, Richard Towbin, MD

Disclosures: All authors have disclosed no financial interests, arrangements or affiliations in the context of this activity.
Purpose or Case Report: After reviewing the exhibit, participants will be able to recognize suspicious and non-suspicious ultrasound (US) features of pediatric thyroid nodules which will help to triage nodules that need a biopsy.
Methods & Materials: The exhibit will illustrate the imaging findings of benign nodules such as adenomatoid/ hyperplastic nodule, colloid nodule, chronic lymphocytic thyroiditis and follicular adenoma as well as malignant lesions such as papillary carcinoma, follicular carcinoma, medullary carcinoma, lymphoma and metastasis. The role of thyroid elastography to differentiate benign from malignant thyroid nodules will be briefly discussed.
Recently published management guidelines for children with thyroid nodules and differentiated thyroid cancer by the American Thyroid Association Guidelines Task Force will be briefly discussed.
Results: US features suggestive of a benign nodule include nodule with a uniform halo, predominantly cystic composition, and avascularity.
US features highly suspicious for malignancy include micro-calcifications, extension beyond the thyroid margin, taller-than-wide shape in the transverse plane, marked hypoechogenicity and associated enlarged cervical lymph nodes.
Less specific US features that may raise suspicion include lack of a halo, ill-defined or irregular margin, solid composition and increased central vascularity.
Conclusions: Although relatively rare in children, radiologists are likely to encounter thyroid nodules in routine clinical practice, whether incidentally or during imaging workup for a palpable nodule or abnormal thyroid function test. It is often challenging to determine which nodules are malignant. This presentation will help the radiologist identify suspicious and non-suspicious US features of pediatric thyroid nodules helping to appropriately triage nodules that need biopsy.

Poster #: EDU-097

Congenital Anomalies of the GI Tract

Orrie Close, MD, Judy Squires, M.D., *University of Pittsburgh School of Medicine, Pittsburgh, PA, joodysquires@gmail.com*

Disclosures: All authors have disclosed no financial interests, arrangements or affiliations in the context of this activity.
Purpose or Case Report: There are numerous congenital anomalies of the gastrointestinal tract with varying frequency. Some anomalies are life-threatening and require prompt diagnosis with immediate treatment. Evaluation of patients with these anomalies can be complex, sometimes requiring multiple imaging modalities for accurate diagnoses and timely treatment. It is therefore essential for radiologists to have a firm understanding of specific imaging features. The purpose of this exhibit is to review common and uncommon congenital anomalies of the gastrointestinal tract, including clinical and imaging features as well as treatment options.

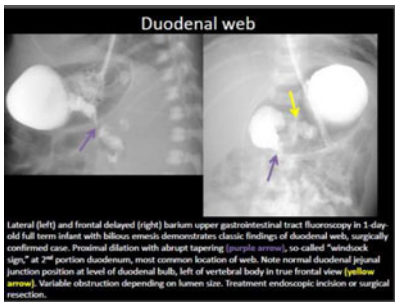

Methods & Materials: A single institution retrospective review was conducted to identify pediatric patients with congenital abnormalities of the gastrointestinal tract. Each patient's imaging studies were correlated with pathology results, surgical findings, and clinical course.
Results: Embryologic development, relevant anatomy, as well as imaging features associated with congenital gastrointestinal anomalies are presented. Common pitfalls leading to delayed diagnosis and treatment of these anomalies are addressed. A broad range of cases is presented including, esophageal atresia with and without fistula, esophageal rings/slings, malrotation with and without midgut volvulus, duodenal web, duodenal, jejunal, and ileal atresia, gastroschisis, Hirschpsrung disease, meconium ileus, microcolon, and anorectal malformations. Cased-based examples are supplemented with a review of the current literature.
Conclusions: Many embryologic abnormalities can affect the gastrointestinal tract, which have important implications for patient care including treatment and prognosis in the pediatric population. Knowledge of normal alimentary development and characteristic imaging findings of congenital malformations can aid radiologists in delivering timely and accurate diagnoses, enabling appropriate interventions that have maximal benefit to patients.

Poster #: EDU-098

Necrotizing Enterocolitis: An Image Intense Review of the Radiologic Findings

Joshua Chern, D.O., *Radiology, St. Christopher's Hospital for Children, Philadelphia, PA, chernjs@gmail.com;* Archana Malik, Mea Mallon, Jaqueline Urbine, Erica Poletto, Faaiza Kazmi, Eric Faerber

Disclosures: All authors have disclosed no financial interests, arrangements or affiliations in the context of this activity.
Purpose or Case Report: Necrotizing Enterocolitis (NEC) is a potentially fatal disease that is commonly encountered in pediatric hospitals. Early diagnosis is of utmost importance, and thus, radiologists must be aware of the varied imaging findings seen in association with NEC and its complications.
Methods & Materials: A retrospecitve review of patients who were known to have necrotizing enterocolitis over the last 2 years at an urban children's hospital was performed. Medical records and radiologic studies were correlated with clinical history and where available; surgical findings. A selection of cases with important radiographic findings was identified and used for an imaging review.
Results: An in depth review of the pertinent imaging findings in necrotizing enterocolitis will be provided. Special attention will be paid toward the plain radiographic findings in NEC as this remains the gold standard in the diagnosis and management of this patient population. Examples of pneumatosis intestinalis, portal venous gas, pneumoperitoneum, and post-NEC stricture will be demonstrated. Additionally, ultrasound will be shown to be an adjunct examination in the evaluation of necrotizing enterocolitis.
Conclusions: Necrotizing enterocolitis is a disease of unknown etiology affecting primarily low birth weight and preterm infants which may manifest many different imaging features. It is of critical importance that the radiologist be able to identify not only the initial presentation of necrotizing enterocolitis, but also the complications.

Poster #: EDU-099

Fetal MR Imaging with Postnatal Imaging Correlation: A Pictorial Review

Judit Machnitz, resident, *Pediatric Radiology, St. Christopher's Hospital for Children, Cherry Hill, NJ, jmchntz@yahoo.com;* Faaiza Kazmi, M.D., Mea Mallon, Erica Poletto, Archana Malik, Jaqueline Urbine

Disclosures: All authors have disclosed no financial interests, arrangements or affiliations in the context of this activity.
Purpose or Case Report: Fetal MR imaging plays a continuously increasing role as an adjunct to routine prenatal ultrasound examinations in confirming and clarifying prenatal abnormalities, usually at an earlier gestational age. It also has a critical role in parental counseling, prenatal and postnatal surgical planning, and delivery method. Our pictorial review demonstrates a variety of common and less typical congenital pathology.
Methods & Materials: In conjunction with our Regional Fetal Evaluation Center, we retrospectively identified patients who underwent a fetal MRI examination and then correlated their fetal MR imaging findings with their infant's postnatal follow up radiological studies.
Results: Our review illustrates a wide spectrum of abnormalities including pathology involving the brain, spine, chest, abdomen, pelvis, and musculoskeletal soft tissues.
Conclusions: Fetal MRI plays a critical and complimentary role in early and precise diagnosis of congenital abnormalities aiding in parental counseling as well as appropriate and timely prenatal and postnatal care.

Poster #: EDU-100

Cecostomy tubes: A practical Approach for the Radiologist

Amaya Basta, MD, *Diagnostic Radiology, Oregon Health & Science University, Portland, OR, basta@ohsu.edu;* Petra Vajtai, Katharine Hopkins, MD, Kelli Schmitz

Disclosures: All authors have disclosed no financial interests, arrangements or affiliations in the context of this activity.

Purpose or Case Report: Cecostomy tubes are not uncommonly encountered in a busy pediatric radiology practice but can pose a challenge to the unfamiliar. These devices provide access to the colon for routine antegrade enemas to promote bowel regularity and continence, most commonly in children with spinal dysraphism. This educational exhibit will describe the typical routine for cecostomy tube exchange, characterized by the Seldinger technique, and describe interesting cases of more difficult exchanges and complications, including different scenarios of broken and malpositioned tubes, and a practical approach to management of these challenges. After viewing this exhibit, the radiologist should be armed with several strategies for approaching both routine and complicated cecostomy tube exchanges.

Poster #: EDU-101

Imaging of Renal Trauma in Children

Ryan Moore, *Diagnostic Radiology, Oregon Health & Science University, Portland, OR, moorry@oshu.edu;* Amaya Basta, MD, Kelli Schmitz, Katharine Hopkins, MD, Petra Vajtai

Disclosures: All authors have disclosed no financial interests, arrangements or affiliations in the context of this activity.
Purpose or Case Report: Renal trauma is not uncommon in the pediatric population and can be seen in a wide variety of settings, from minor sports-related injuries to serious motor vehicle accidents. The imaging appearance is as varied as the etiology of injuries, ranging from minor parenchymal defects to avulsion of the vascular pedicle. Our educational poster aims at exploring a variety of injuries of the kidney in children, including chronic subcapsular hematoma, different severities of laceration, renal rupture without and with urine extravasation, injuries to the ureter, trauma involving kidneys with congenital anomalies, and trauma in an undiagnosed Wilms' tumor. Because renal trauma can present with many different faces, we aim to highlight essential diagnostic pearls as well as some unusual factors which may predispose the kidney to injury.

Poster #: EDU-102

Radiologic Examination of Devices in the Pediatric Population

David Skelton, *Radiology, Children's Mercy Hospital, Kansas City, MO, dts3m4@mail.umkc.edu;* Patrick Bacon, MD, Daniel Davignon

Disclosures: All authors have disclosed no financial interests, arrangements or affiliations in the context of this activity.
Purpose or Case Report: The purpose is for participants to become familiar with devices that are commonly and uncommonly used in the pediatric population. They will learn the proper location and configuration of these devices, which will be useful throughout their professional career. Being able to recognize subtle abnormalities that can occur with these devices is important for radiologists, and being aware of basic information of these devices can help other physicians when they become exposed to them in their career.
Methods & Materials: Several images of various pediatric devices and interventions were obtained at Children's Mercy Hospital in Kansas City, MO. Most images are from plain film x-ray, although there are some supplemental images obtained from MRI and CT. All images are obtained from patients under the age of 18.
Results: Key devices included in the presentation are: umbilical catheters, vertical expanding prosthetic titanium rib (VEPTR), Nuss bar, Codman-Hakin valve, Vagal nerve stimulator, Atrial Septal defect (ASD) closure devices and others. In some instances, images of proper and improper placement will be included. Textual information will supplement the images and highlight key information included in the presentation. The pathophysiology involved in several interventions will be included to provide background information regarding the purpose of the device.
Conclusions: Participants will learn the indications and goals of therapy of several pediatric devices, as well as the purpose of radiologic imaging in monitoring the patient's medical course in acute and chronic settings. Several complications can also occur as a result of these devices, and participants will learn how to utilize radiologic images in monitoring for their occurrence.
At the completion of the presentation, participants should be able to recognize various pediatric devices in plain film images and apply the process of examining these images for placement, functionality and complication monitoring.

Poster #: EDU-103

A Web 2.0 Approach for Assessing and Reporting Pediatric Bone Age Studies

Patrick Do, M.D., *Radiology, Santa Clara Valley Medical Center, Fremont, CA, patrickdo@gmail.com;* Priya Krishnarao, MD

Disclosures: All authors have disclosed no financial interests, arrangements or affiliations in the context of this activity.
Purpose or Case Report: Assessing and reporting pediatric bone age is a subjective and often tedious multi-step process. The typical reporting workflow at our institution requires perusing a hardcopy of a bone age atlas to find an image matching the PACS screen, finding reference values in a table, and performing rote arithmetic to determine the progress of skeletal maturity.

Methods & Materials: We developed and implemented a website with an atlas of reference images and a dynamic report generator, using HyperText Markup Language (HTML), Cascading Style Sheets (CSS), JavaScript, jQuery, and additional open source web development tools. Data and images were obtained from the commonly used Greulich and Pyle (G&P) reference atlas as well as our institution. This website is universally accessible and does not require any special hardware, software, or storage media.
Using this website, interpreting radiologists simply select the patient's sex and date of birth, then use the mouse to scroll through reference images. A standardized structured report is dynamically generated for use in a radiology reporting system.
Results: This method of assessing and reporting pediatric bone age was implemented in our radiology department and found widespread acceptance, with nearly all users noting increased accuracy and efficiency based on a survey following several months of implementation. 14 of 14 (100%) users indicated increased

accuracy, 14 of 14 (100%) indicated increased efficiency, and 9 of 10 surveyed residents (90%) indicated improved resident-attending concordance following implementation. Furthermore, blinded retrospective comparison of this web-based method with the traditional method across 50 studies showed a 96% concordance within 6 months estimated bone age.
Conclusions: Modern web development technology tools can help improve quality and efficiency in many domains of radiology, such as assessing and reporting pediatric bone age, by streamlining and automating workflow.

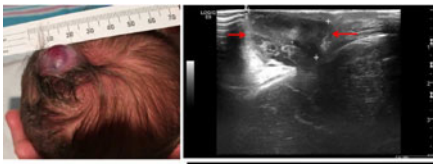

Soft tissue mass on posterior occiput seen on gross photo (above) with central echogenic debris (above right, red arrows) and peripheral color Doppler flow on US (right) consistent with an atretic posterior meningocele.

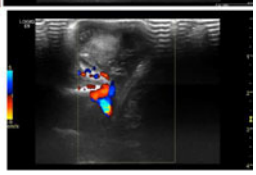

Poster #: EDU-104

Persistence of the Falcine Sinus: Embryology, Variants, and Associated Anomalies on Imaging

Disclosures: All authors have disclosed no financial interests, arrangements or affiliations in the context of this activity.
Jaren Meldrum, MD, *Radiology, Tripler Army Medical Center, Kaneohe, HI, jtm121@gmail.com;* Jonathan Wood, Veronica Rooks
Purpose or Case Report: The purpose of this exhibit is to provide radiologists at various levels of training with a concise and comprehensive illustrated review of anomalies associated with persistence of the falcine sinus. The exhibit will rely on literature review, illustrations, and multimodality imaging from patients with persistent falcine sinus associations.
Methods & Materials: 1. Review the relevant anatomy and embryology of the cerebral venous system, focusing on the falcine sinus.
2. Review common normal anatomic variants of the cerebral venous system.
3. For each of the following anomalies associated with persistence of the falcine sinus, characterize the anomaly, presentation, imaging findings, work up, treatment, and prognosis:
-medial prosencephalic vein (vein of Galen) malformation with fetal MRI
-atretic occipito-parietal meningocele
-agenesis of the corpus callosum
-acrocephalosyndactyly (Apert syndrome)
-osteogenesis imperfecta
-Chiari malformation Type II
-bifid cranium
-absent or dysplastic tentorium cerebelli
-bilateral giant parietal foramina
-sinus thrombosis associated with falcine sinus
Results: Example cases:
- 2mo M with 7q11.23 micro deletion and developmental delay presented with leaking atretic parietal meningocele.
- 21mo F with median prosencephalic vein malformation requiring embolization.
- 3mo M with persistent falcine sinus and thrombosed superior sagittal sinus requiring recanalization.
Conclusions: The falcine sinus is a normal embryological structure within the falx cerebri, which drains the cerebral venous system to the superior sagittal sinus. Though it typically involutes after birth, a persistent falcine sinus may be associated with a number of anomalies. Understanding normal anatomic variants as well as the anomalies associated with persistence of the falcine sinus is important to ensure proper work up, diagnosis, and treatment of associated pathology.

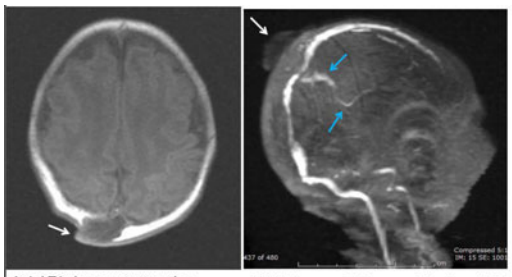

Axial T1 demonstrates the meningocele (white arrow) immediately posterior to the superior sagittal sinus.

MRV demonstrates persistent vertical falcine vein (blue arrows) extending superiorly to the atretic meningocele (white arrow).

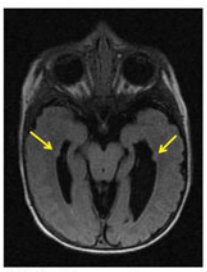

Bilateral temporal heterotopic grey matter nodules (yellow arrows) on axial FLAIR sequence.

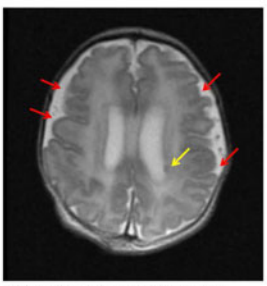

Axial T2 demonstrates diffuse cortical dysgyria (red arrows) and left posterior heterotopic grey matter nodules (yellow arrow).

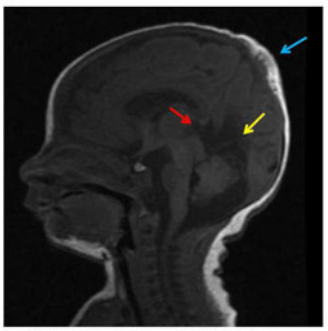

Sagittal T1 shows prominence of the superior cerebellar cistern (yellow arrow). Superior peaking of the posterior tentorium is noted with a prominent peri-pineal recess. Atretic meningocele visualized (blue arrow).

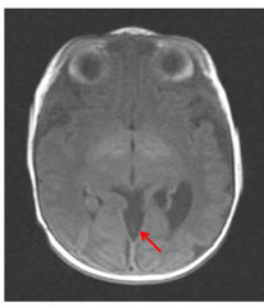

Axial T1 image demonstrates superior peaking of the posterior tentorium with a spinning top configuration (red arrow) of the tentorial incisura.

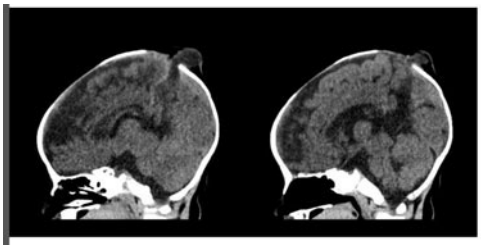

Sagittal midline CT demonstrates the calvarial defect cranium bifidum with atretic posterior meningocele.

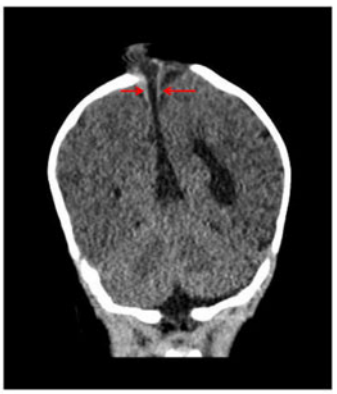

Coronal CT demonstrates fenestration of the superior sagittal sinus (red arrows) at the atretic parietal meningocele.

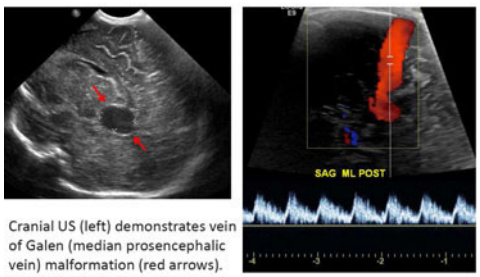

Cranial US (left) demonstrates vein of Galen (median prosencephalic vein) malformation (red arrows). Arterialized color Doppler waveform noted in persistent falcine sinus (right).

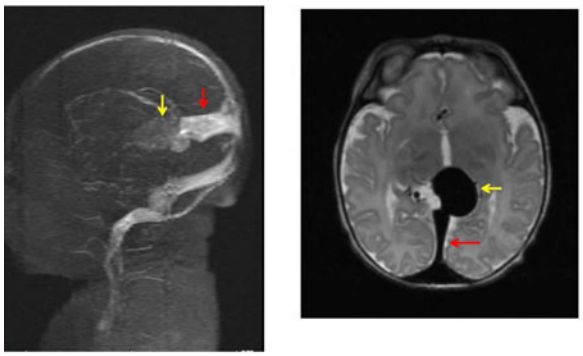

MRV (left) and axial MR (right) demonstrating a persistent falcine sinus (red arrows) draining the medial prosencephalic vein (yellow arrows).

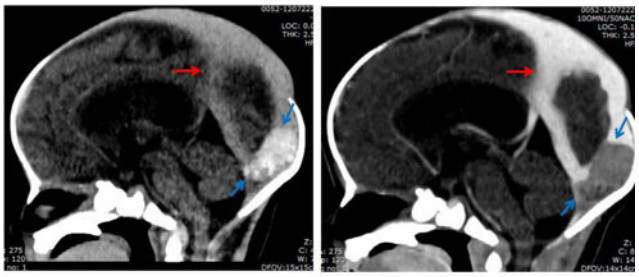

Sagittal CT without contrast (left) and with contrast (right) demonstrate persistent falcine sinus (red arrows) and superior sagittal sinus leading to torcular thrombus (blue arrows), likely formed due to irregular flow dynamics.

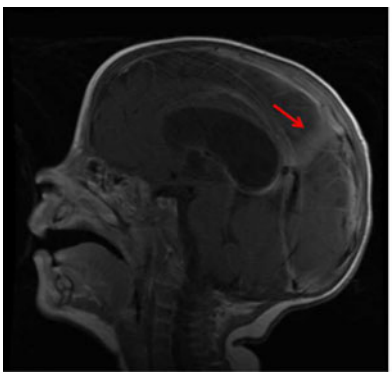

Sagittal T1 MR post-gadolinium shows interval resolution of thrombus post-recanalization. There is persistent but decreased size and flow in falcine sinus (red arrow).

Poster #: EDU-105

Making Change at Scale: The World Federation of Pediatric Imaging (WFPI)

Amanda Dehaye, *World Federation of Pediatric Imaging, Chicago, IL, wfpi.office@gmail.com;* Cicero Silva, M.D., Kassa Darge, Sanjay Prabhu, Savvas Andronikou, Bernard Laya, Brian Coley, MD, Ines Boechat, MD

Disclosures: Brian Coley has indicated a relationship with Elsevier as an editor. All other authors have disclosed no financial interests, arrangements or affiliations in the context of this activity.
Purpose or Case Report: Created in 2011, WFPI has spent the last 5 years overcoming geographic, temporal, cultural and linguistic distances to define its added value in the global imaging arena. Have the efforts been worth it?
Methods & Materials: WFPI's member organizations and members of the Society of Pediatric Radiology (SPR) were asked to consider WFPI's priorities, projects and structure. The responses were tied into WFPI's output and strategic approach.
Results: Members of regional societies and 273 individual members of SPR provided feedback. The results provided WFPI's leadership with guidance on member support, dissent and future strategies. The large majority felt that WFPI's inclusive set-up, networking and aim of providing a united front to address the challenges in global pediatric imaging should be pursued. Attracting external funding is a challenge. Intrinsic initiatives run by member societies are important to maintain; WFPI can play a critical role in global dissemination of tools, "lessons learnt" and give recognition by an international pediatric radiology body. Highest ranking priorities include global imaging safety, online education and advocacy. WFPI partnered with the Image Gently Alliance to promote efficient and effective use of resources; consolidation and expansion to regional initiatives elsewhere is now a must. WFPI offers educational web pages, social media and an online video library (11 videos posted to date, viewed over 5000 times) launched with SPR in 2015. Advocacy underpins WFPI's work, encompassing WHO/IAEA workshops, RAD-AID conferences, WFUMB and ACR outreach committees and IDoR 2015. To avoid resource duplication WFPI adopts a "bolt on" approach, actively engaging with other organizations to leverage pre-existing resources and infrastructure. Examples: Imaging the World in Malawi/Uganda and RAD-AID in Laos/Ghana, ACR educational courses in Haiti, telereading and field manuals for MSF and partnership with the CHOP/USA fellowship program in Ethiopia.
Conclusions: WFPI members and most SPR respondent members believe that WFPI "is the right way to go". It has taken time to mould but international organizations must continuously morph. Consisted of expert professionals, WFPI seeks to create tools and generate resources for leverage by multiple groups and use where the need/desire arises. This choice is relevant and impactful and has the chance to make change at scale.

Poster #: EDU-106

Pediatric Renal Tumors and Associated Clinical Syndromes

Catherine Evans, *Cedars-Sinai Medical Center, Los Angeles, CA;* Allen Ardestani, MD, PhD, Christopher Watterson, MD, Snehalkumar Patel

Disclosures: All authors have disclosed no financial interests, arrangements or affiliations in the context of this activity.
Purpose or Case Report: The objectives of this educational exhibit are (1) To review the radiologic appearance of pediatric renal tumors in multiple imaging modalities, (2) To review the demographic and clinical contexts in which pediatric renal tumors occur, and (3) To survey various syndromes classically associated with pediatric renal tumors.
Methods & Materials: A variety of cases representing a spectrum of pediatric renal tumors were collected from two teaching institutions. Radiologic features of these renal lesions were identified across multiple imaging modalities and closely correlated with available clinical information and pathology results. The clinical syndromes and conditions most commonly associated with these renal tumors are also presented with radiological and clinical correlation.
Results: Examples of a wide range of pediatric renal tumors will be presented including:
Benign lesions:
Multicystic dysplastic kidney
Polycystic kidney diseases
Multilocular cystic nephroma
Nephroblastomatosis
Mesoblastic nephroma
Angiomyolipoma
Ossifying renal tumor of infancy
Malignant lesions:
Wilms tumor (with differentiating features from neuroblastoma)
Clear cell sarcoma
Renal cell carcinoma
Rhabdoid tumor
Lymphoma
Rhabdomyosarcoma
Metastases
Rare lesions
Associated syndromes and clinical conditions:
Tuberous sclerosis
Von Hippel-Lindau
WAGR
Beckwith-Wiedmann
Sickle cell disease
Neurofibromatosis
Bloom syndrome
Birt-Hogg-Dube
Conclusions: The differential diagnosis of pediatric renal tumors includes a vast array of congenital and acquired tumors, both malignant and benign. The distinctive radiologic appearances of many of these tumors can aid significantly in accurate diagnosis of these lesions. Familiarity with features common to associated clinical syndromes may also provide a valuable tool to radiologists in the diagnosis of pediatric renal tumors.

Poster #: EDU-107

Anatomic – Pathophysiologic Correlates of Pulmonary Haemorrhage in Children – Relating the Physiology to the Anatomy

Caroline Lacroix, MD, *Diagnostic Imaging, The Hospital for Sick Children, Toronto, ON, Canada, caroline.lacroix@sickkids.ca;* Rayan Ahyad, MBBS, SBR, David Manson

Disclosures: All authors have disclosed no financial interests, arrangements or affiliations in the context of this activity.
Purpose or Case Report: Pulmonary haemorrhage in children is a non-specific response to a number of varying insults. Many of these insults favour particular anatomic foci along the pulmonary and bronchial

arterial trees respectively. Although recent years have seen an emerging interest in the understanding and classification of pulmonary vasculitides, this pathophysiology represents only one subset of the causes of pulmonary haemorrhage in children. Our purpose is to review the imaging and pathophysiologic manifestations of varying causes of pulmonary haemorrhage according to the anatomic region of susceptibilities in the pulmonary arterial and bronchial artery trees.
We aim to provide a perspective of imaging manifestations of the pathophysiologies of pulmonary haemorrhage displayed schematically according to their relative anatomic areas of susceptibility. We aim to focus on useful constellations or associated findings that will serve to help the reader differentiate amongst entities that often have otherwise similar imaging presentation.
Conclusions: Pulmonary haemorrhage can present in paediatric patients of all ages. Understanding of the main pathophysiologic mechanisms that can occur in different subsets of patients can help radiologists to provide a more targeted differential diagnosis to guide clinical teams and to direct further imaging recommendations in some cases.

Poster #: EDU-108

Blunt Bowel Trauma: What the Pediatric Radiologist Should Know

Nupur Verma, MD, Pratik Patel, MD, Dhanashree Rajderkar, MD, *Radiology, University of Florida, Gainesville, FL, drdhana1@gmail.com*

Disclosures: All authors have disclosed no financial interests, arrangements or affiliations in the context of this activity.
Purpose or Case Report: Accidents remain a top cause of morbidity and mortality in pediatric patient. Assessment for blunt trauma to the abdomen is difficult in the trauma patient and findings of bowel injury can be subtly or confounded by visceral injuries. The most specific finding of free air in blunt hollow visceral organ is often minimally present, or entirely unseen. The pediatric radiologist must be familiarity with the more often seen and less specific secondary signs on CT, including free fluid, bowel wall thickening, and mesenteric contusion injury. We present, by case example, bowel injuries in the traumatic pediatric patient and their management and outcomes, while addressing common pearls and pitfalls. As many of these patients do well with non-operative treatment the radiologist must also be familiar with findings that would allow such option, to appropriately advice referring providers and manage potential re-image of the pediatric patient.

Poster #: EDU-109

Pediatric Thyroid Cancer: Common Sonographic Appearances and Pitfalls

Claudia Martinez-Rios, MD, *Diagnostic Imaging, The Hospital for Sick Children, Toronto, ON, Canada, claudia.martinez-rios@sickkids.ca;* Lydia Bajno, Alan Daneman, Rahim Moineddin, Danielle CM van der Kaay, Jonathan Wasserman

Disclosures: All authors have disclosed no financial interests, arrangements or affiliations in the context of this activity.
Purpose or Case Report: High-resolution ultrasonography (US) is a valuable and accessible imaging tool to assess and characterize the thyroid gland in children. Pediatric thyroid nodules are infrequent. However, the incidence of thyroid carcinoma in children is near twice the adult population, where the risk of malignancy is up to 15%. Children also have an increased risk for recurrence (39%) as compared to adults, justifying further work and a more aggressive approach. Prompt recognition of the common and uncommon sonographic features of thyroid cancer in children will allow radiologist to identify this malignancy in early stages of the disease, expediting appropriate treatment improving the standard of patient care. The purpose of this exhibit is to 1. To illustrate the spectrum of sonographic findings of thyroid cancer in a pediatric population. 2. To describe the typical sonographic characteristics of malignant thyroid nodules in children. 3. To identify the uncommon features of pediatric thyroid cancer. 4. To describe an appropriate approach to deal with uncertain diagnosis.

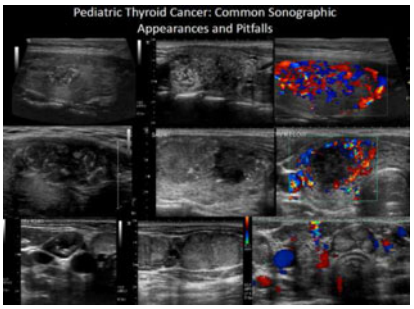

Poster #: EDU-110

A Pictorial Review of the Manifestations of Sickle Cell Disease Involving the Central Nervous System

Joshua Chern, DO, *Radiology, St. Christopher's Hospital for Children, Philadelphia, PA, chernjs@gmail.com;* Jaqueline Urbine, Mea Mallon, Faaiza Kazmi, Archana Malik, Erica Poletto, Eric Faerber

Disclosures: All authors have disclosed no financial interests, arrangements or affiliations in the context of this activity.
Purpose or Case Report: Sickle cell disease is a common inherited disorder due to a structural abnormality in hemoglobin affecting the shape of the red blood cells. There are a variety of manifestations of this disease affecting a multitude of different organ systems. Some of the complications with the highest morbidity are those involving the central nervous system, and thus, the radiologist plays a pivotal role in the clinical management of these patients. It is important for the radiologist to understand the disease process, the radiologic manifestations, and the screening modalities available.
Methods & Materials: A retrospective review of patients with sickle cell disease that presented to an urban children's hospital over the past 15 years was performed. Medical records and imaging findings were correlated with clinical history. A variety of cases with interesting and classic radiographic findings was selected for an imaging review.
Results: A review of the imaging findings in sickle cell disease will be provided, with particular attention to those involving the brain and spine. CT, MRI, and ultrasound examinations will be shown which demonstrate important findings associated with sickle cell disease.
Conclusions: Sickle cell disease is a common disorder that presents in childhood in a multitude of ways. Because of the morbidity and mortality associated with this disease, the radiologist should be familiar with the disease process along with the various imaging manifestations of it.

Poster #: EDU-111

Prenatal Imaging Appearance of Congenital Vertical Talus and its Associated Anomalies

Disclosures: All authors have disclosed no financial interests, arrangements or affiliations in the context of this activity.

Nimisha Mehta, MD, *Children's National Medical Center, Washington DC, DC, nimisha.kapadia@gmail.com;* Dorothy Bulas, Anna Blask, MD, Eva Rubio

Purpose or Case Report: To describe the prenatal imaging appearance of Congenital Vertical Talus (CVT) by US and MRI and detail the associated anomalies and outcome. The postnatal imaging appearance will also be discussed.

Methods & Materials: Using our radiology database, we performed a retrospective review of fetal US and MRI from 2006 to 2015. Cases of CVT were identified and associated findings as well as outcomes were assessed.

Results: 24 prenatal cases of CVT were identified. Both by US and MRI, CVT demonstrated a distinct appearance with a protuberant heel and dorsiflexion of the forefoot. This resulted in a convex contour of the plantar surface of the foot. In contrast, congenital talipes equinovarus (CTE) has a distinctive varus angulation to the foot, resulting in visualization of the tibia in the same plane. A significant number of concurrent anomalies were identified in the CVT cases, including brain and/or spinal anomalies (23/24, 96%), aneuploidy (5/24, 21%), and limb anomalies (13/24, 54%).

Conclusions: Congenital vertical talus has a distinct prenatal appearance that can be identified by US and MRI. It is associated with a high risk of additional fetal anomalies and there were no cases of isolated CVT in our series. It is important to distinguish CVT from CTE, which can often be an isolated finding. Identification of CVT through its classic dorsiflexion, convex plantar surface and prominent calcaneus should prompt a thorough search for additional anomalies prenatally. Fetal MRI is a helpful adjunct when this abnormality is present, particularly for identification of brain and spine malformations. Complete characterization of fetal anomalies allows for comprehensive family counseling.

Poster #: EDU-112

Sonographic Characterization of Pediatric Calvarial and Scalp Lesions

Kathryn Milks, MD, *Radiology, Nationwide Children's Hospital, Columbus, OH, ks.mueller@gmail.com*

Disclosures: All authors have disclosed no financial interests, arrangements or affiliations in the context of this activity.

Purpose or Case Report: The calvarium and overlying scalp is a uniquely changing entity in childhood that presents a dynamic source of pathologies in early life as the child grows and the sutures fuse. Various "lumps and bumps," both symptomatic and not, may be discovered by the parents or detected by pediatricians. Although some may be diagnosed clinically, others may require imaging for diagnosis. Ultrasound offers a simple and often definitive alternative to CT and MRI for evaluation of calvarial lesions, avoiding unnecessary radiation and expense; however, it requires a sonologist with thorough understanding of the various calvarial and scalp entities. The purpose of this exhibit is to describe the progression of calvarial and scalp lesions encountered from the neonatal period through young adulthood.

Methods & Materials: Normal development of the skull and overlying scalp is presented from birth through fusion of the sutures and scalp maturation. Concomitant common calvarial pathology at various ages is described with supplemental sonographic images.

Results: Knowledge of the growth and development of the skull and superficial soft tissues is fundamental to the accurate interpretation of findings therein. Ultimately, the age of the patient dictates the differential diagnosis of calvarial lesions and their manifestations on ultrasound.

Conclusions: This presentation highlights the various lesions encountered on sonographic evaluation of the head in a chronologic manner, with parallel description of the skull and scalp maturation, whereby the reader can formulate a reasonable differential at each stage of development.

Poster #: EDU-113

Still a Puzzle- Pediatric Post Transplant Lymphoproliferative Disorder (PTLD). Atypical cases of PTLD- an Educational Experience

Naziya Samreen, MD, Priya Sharma, MD, Ibrahim Tuna, Dhanashree Rajderkar, MD, *Radiology, University of Florida, Gainesville, FL, drdhana1@gmail.com*

Disclosures: All authors have disclosed no financial interests, arrangements or affiliations in the context of this activity.

Purpose or Case Report: 1. To establish the role of imaging in diagnosing the atypical/unexpected cases of post transplant lymphoproliferative disorder in Pediatric population.

2. To review the role of Radiology Imaging in staging, treatment monitoring and predicting the prognosis in Pediatric PTLD.

Methods & Materials: We did a retrospective analysis of some of the atypical presentations-both clinical and radiological in the patients of PTLD. We will present the case scenarios and share the established guidelines to approach the management of such patients.

Results: PTLD is a well-recognized complication following organ transplantation ranging from abnormal lymphoid hyperplasias to frank neoplasias. The clinical presentation is not specific, and almost any organ can be affected. The disease may involve the lymph nodes or may be extra nodal. It could present as a limited disease or could be widespread. Early diagnosis is associated with a better prognosis and disease extent is an important prognostic factor that may affect therapy. The median time of onset is almost 5 years after transplantation in adult population, which is not necessarily true in the pediatric population. Treatment monitoring is equally important for initiating the patient management. Detection of the extra nodal disease is more challenging on the conventional imaging.

We would present atypical presentations of the pathologically proven PTLD in patients who had undergone various organ transplants including heart, lung,renal and liver. We would evaluate the change in patient management influenced by imaging. We would determine if there are any confounding factors of post treatment inflammatory changes in determining the response to the therapy.

Conclusions: Presentation in the pediatric age group is varied. There is potential threat of missing this malignant pathology. Radiology plays an important role in establishing early diagnosis in patients of PTLD. Crucial steps and a meticulous approach can improve the management and survival of the pediatric patients of PTLD.

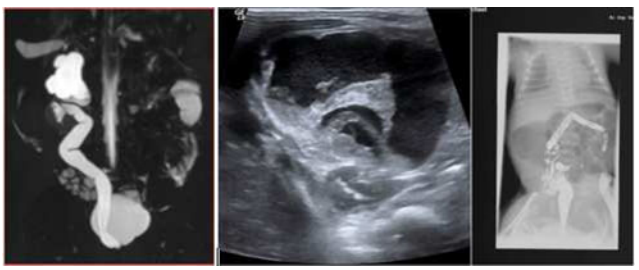

Poster #: EDU-114

Cornstarch Kids: Imaging of Glycogen Storage Diseases in Pediatric Patients

Priya Sharma, MD, *University of Florida Gainesville, Gainesville, FL, priya.sharmamd@gmail.com;* Dhanashree Rajderkar, MD

Disclosures: All authors have disclosed no financial interests, arrangements or affiliations in the context of this activity.

Purpose or Case Report: Learning Objectives: This educational exhibit will review glycogen storage diseases and the imaging findings of these disease processes using a multimodality approach. We will also review

complications and discuss the treatment and role of imaging as a measure of treatment response.
Methods & Materials: Background: Glycogen storage diseases (GSD) are a unique set of inherited disorders that affect glycogen metabolism. To date, more than 12 types of GSD are recognized and are sub-divided by enzyme deficiency and affected tissue. These autosomal recessive conditions affect 1 in 50-100,000 births. The University of Florida in Gainesville is home to the largest clinical research program for GSD in the world and provides care for pediatric patients with GSD from over 30 countries.
Results: Imaging Findings: Depending on the exact enzymatic deficiency these patients can present with unique manifestations of the disease process on various imaging modalities. Types I, III, and IX compromise 80% of the hepatic GSD. Hepatic adenoma formation is often seen in Type I GSD. This can be complicated by malignant transformation into the hepatocellular carcinoma. Renal enlargement and nephrocalcinosis can be seen as well. Apart from the propensity to develop recurrent or chronic bacterial infections patients with type Ib disease are clinically and metabolically indistinguishable from type Ia disease. Those with type Ib can often also manifest with delayed bone maturation and demonstrate a variety of findings on radiography. Patients with type IIIa disease can manifest cardiomyopathy often assessed on cardiac MRI (magnetic resonance imaging). Neuromuscular manifestations are a mainstay of more rare subtypes. Osseous manifestations are also appreciated in many types of glycogen storage disease subtypes.
We will use a series of cases to demonstrate the typical imaging findings associated with various types of glycogen storage diseases and their complications. We will also demonstrate how imaging can be used as a measurement of treatment response. We will provide examples using a multimodality approach with radiography, US (ultrasound), CT (computed tomography) and MRI (magnetic resonance imaging).
Conclusions: Glycogen storage diseases offer an interesting variety of multimodality imaging findings. Accurate recognition of these findings allows the pediatric radiologist to alert the referring physician to complications and help guide treatment for this unique group of patients.

Poster #: EDU-115

Congenital Pulmonary Arterial Anomalies: Swinging Beyond the Sling

Leslie Hirsig, Nupur Verma, MD, Priya Sharma, MD, Dhanashree Rajderkar, MD, *Radiology, University of Florida, Gainesville, FL, drdhana1@gmail.com*

Disclosures: All authors have disclosed no financial interests, arrangements or affiliations in the context of this activity.
Purpose or Case Report: Congenital and childhood findings of pulmonary artery anomalies are uncommon but not infrequently encountered by referral centers. We present by case examples anomalies of pulmonary arterial vasculature, and discuss their clinical presentation, associated cardiothoracic anomalies, and overall prognosis.
Methods & Materials: We did a retrospective data collection on the examples of the congenital pulmonary anamolies, other than the well known condition called 'Pulmonary Slings'.
Results: Some of the examples we encountered in our referral center for the congenital heart disease are-
1. Aberrant origin of the pulmonary artery from the aorta.
2. Origin of branch vessels from the aorta.
3. Congenital absence of the pulmonary artery
4. Pulmonary artery aneurysm
5. Arteriovenous malformations
6. Type I and II truncus arteriosus
7. Idiopathic pulmonary hypertension in the pediatric patient.
Conclusions: There is familiarity with pulmonary slings, but other less common anatomical variants of the pulmonary arteries are also important to recognize and understand. Prompt identification by the pediatric radiologist is essential in guiding medical or surgical management of the patient, and in some instances plays a key role in avoiding potential cardiopulmonary compromise.

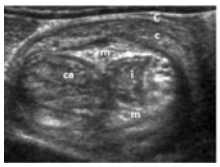

Ileocecocolic intussusception in axial scan: the center is composed of the ileum (i) next to the cecum (ca) surrounded by the hyperechoic mesentery (m). The outer ring is formed by the receiving (C) and the returning (c) limbs of the colon.

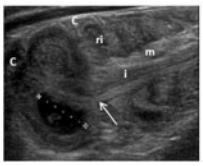

Ileoileocolic intussusception in longitudinal scan: the returning limb of the ileum (ri) has a characteristic coiled spring aspect due to the presence of folds perpendicular to the entering ileum (i) dragging its mesentery (m). A segment of blind-ending, thick-walled bowel containing some fluid (crosses) corresponding to a Meckel diverticulum, projects from the apex of the entering ileum (arrow) into the receiving colon (C).

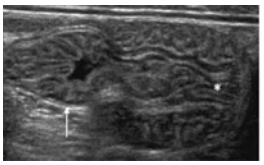

Transient small bowel intussusception: longitudinal scan shows a short, peristaltic intussusception with thin bowel layers, well-visible folds, no leadpoint at the apex (*) and no small bowel obstruction (arrow).

Poster #: EDU-116

Spectrum of Fascinating Benign Bony Lesions-A Complete Review of Multifocal Bony Benign Lesions in Pediatric Age Group

Nicholas Bates, **Tarik Nurkic, MD,** Priya Sharma, MD, Dhanashree Rajderkar, MD, *Radiology, University of Florida, Gainesville, FL, drdhana1@gmail.com*

Disclosures: All authors have disclosed no financial interests, arrangements or affiliations in the context of this activity.
Purpose or Case Report: There are many recognized causes of benign bony lesions in pediatric age group. Some of the lesions are commonly encountered, and some of them are very rare. The purpose of our exhibit is to illustrate a complete spectrum of the benign bony pathologies including 'Donot touch lesions'.
Methods & Materials: A retrospective study was done to evaluate the frequency of multifocal bony lesions found in the pediatric age group. Depending upon the imaging findings on different modalities, an approach was developed to characterize them further and make recommendation for further evaluation. Many of these lesions have characteristic appearance, and do not need any follow up. Unnecessary investigations can be potentially avoided in such cases.
Results: Some of the bony lesions encountered during our study were-
Fibrous dysplasia,
CRMO
TB
Hydatid
EG
Sarcoidosis
Hemosiderosis
Myelofibrosis
Hematopoietic Hyperplasia
Mastocytosis
Renal Osteodystrophy
Lipomas

Hemangiomas
TS
Bone infarcts
Storage disorders
Spondyloarthropathy
Histiocytic fibroms
Fibroosseous tumors

Conclusions: Benign bony lesions can be congenital or acquired. The acquired conditions could be infectious, inflammatory or neoplastic. Characterizing these lesions utlizing appropriate radiology modality is the key to the successful management.

Poster #: EDU-117

Mending a Broken Little Heart: Multimodality Imaging Findings of Hypoplastic Left Heart Syndrome and its Repair

Priya Sharma, MD, *University of Florida Gainesville, Gainesville, FL, priya.sharmamd@gmail.com;* Dhanashree Rajderkar, MD

Disclosures: All authors have disclosed no financial interests, arrangements or affiliations in the context of this activity.

Purpose or Case Report: In this exhibit we will review the multimodality imaging findings in patients with HLHS using chest radiography (CXR), computed tomography (CT) and magnetic resonance imaging (MRI). We will discuss the physiologic basis for the radiologic findings of HLHS, describe the palliative surgical procedures to correct HLHS and their complications.

Methods & Materials: Background: Hypoplastic left heart syndrome (HLHS) consists of a spectrum of cardiac abnormalities characterized by hypoplasia of the left ventricle and ascending aorta. HLHS comprises 1.2 -1.5% of all congenital heart defects with an annual incidence of 0.16-0.36 per 1000 live births. Without surgical correction HLHS is uniformly fatal. Before the availability of surgical correction HLHS accounted for 25% of all neonatal cardiac deaths. Through revolutionary surgical work, a series of reconstructive palliation techniques have been developed allowing those infants to survive into childhood. The pediatric radiologist now sees a larger population of HLHS patients making it imperative to understand the imaging of these palliative techniques.

Results: Imaging Findings: In a neonate exhibiting early clinical signs of distress the chest radiograph is often the first imaging study ordered.

Cross sectional imaging such as CT and MRI are useful, not only for characterizing anatomy but for surgical planning and decision making. The surgical palliation of HLHS consists of 3 stages aimed at constructing separate, nonobstructed pulmonary and systemic vascular circulations with systemic flow returning passively to the lungs and a single ventricle providing systemic blood flow. The first stage, known at the Norwood Procedure consists of a creation of a "neo-aorta," atrial septectomy, patent ductus arteriosus (PDA) ligation and the formation of a controlled source of pulmonary blood flow through a Blalock-Taussig shunt (BTS) or Sano modification. The second stage results in the creation of a bidirectional superior cavopulmonary connection using a bidirectional Glenn shunt and ligation of previously created BTS. The third stage is the Fontan operation which reroutes the systemic venous return from the inferior vena cava directly to the lungs through a conduit resulting in bypassing the single functional ventricle.

Conclusions: The pre- and post-surgical imaging features of hypoplastic left heart syndrome are complex and cross -sectional imaging can assist the radiologist in understanding surgical palliative repairs as well as identifying potential complications.

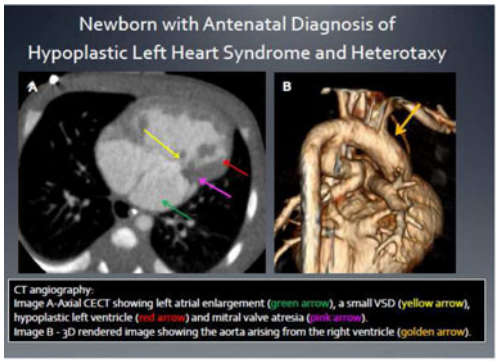

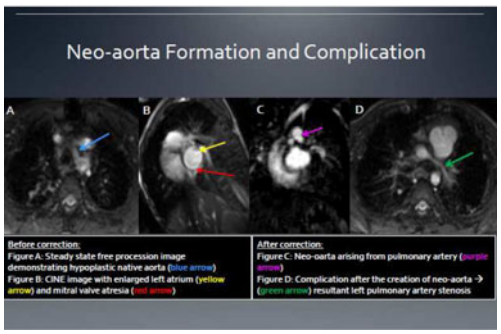

Poster #: EDU-118

Forgive and Don't Forget: A Review of Pediatric Splenic Lesions and an Algorithm on Approaching Non-cystic Splenic Lesions

Priya Sharma, MD, *University of Florida Gainesville, Gainesville, FL, priya.sharmamd@gmail.com;* Yvonne Estrin, Daphne Loubriel, MD, Dhanashree Rajderkar, MD

Disclosures: All authors have disclosed no financial interests, arrangements or affiliations in the context of this activity.

Purpose or Case Report: Learning Objective: This educational exhibit will review a variety of pediatric splenic lesions and their appearance on various specific multimodality imaging finding as seen on ultrasound, computed tomography (CT), and magnetic resonance imaging (MRI). This exhibit will also review an algorithm to approaching non-cystic splenic lesions in pediatrics.

Methods & Materials: Background: The spleen is often termed the "forgotten organ". The Spleen is involved in many pathologic processes in infants and children. These may be part of systemic illness or may be isolated to the spleen. This educational exhibit will review many benign and malignant non-cystic lesions of the spleen as well as give an overview of the normal spleen at different ages.

Splenic lesions are most often detected on imaging incidentally and are referred to as "incidentalomas". It is often difficult to distinguish whether non-cystic incidentalomas are benign or malignant solely on the basis of imaging characteristics. MRI is the most useful modality in aiding the radiologist in making a definitive diagnosis and providing reassurance. This will evade seeking a histologic diagnosis, which is especially important considering the relatively low rates of invasive cancers in the pediatric population. This education exhibit will also provide an algorithm to help make a definitive diagnosis when diagnosing non-cystic splenic lesions.

Results: Imaging Findings:
Congenital Anomalies of the Spleen:
Polysplenia
Asplenia

Wandering Spleen
Malignant Neoplasms:
Lymphoma
Angiosarcoma
Metastatic lesions
Benign Neoplasms:
Hemangiomas
Lymphangiomas
Hamartomas
Peliosis
Non-neoplastic Lesions of the Spleen
Sarcoidosis and Granulomatous Diseases
Infection
Extra-medullary Hematopoiesis
Splenomegaly
Trauma
Algorithm for Non-cystic Splenic Lesions:
The Usefulness of MRI and An Approach to Non-cystic Lesions
Conclusions: Although primary and secondary neoplasms in the spleen are infrequently encountered, the spleen should not be forgotten.

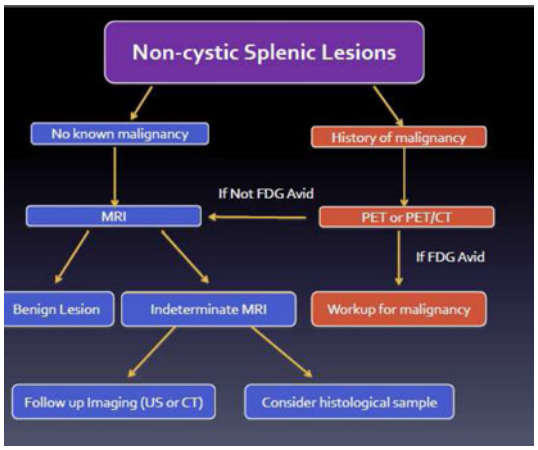

Poster #: EDU-119

Adventures in the Adnexa: Elucidating the Uncertainties of Atypical Pediatric Ovarian Neoplasms

Priya Sharma, MD, *University of Florida Gainesville, Gainesville, FL, priya.sharmamd@gmail.com;* Daphne Loubriel, MD, Yvonne Estrin, Dhanashree Rajderkar, MD

Disclosures: All authors have disclosed no financial interests, arrangements or affiliations in the context of this activity.
Purpose or Case Report: Learning objectives: This educational exhibit will review atypical ovarian neoplasms in the pediatric population. We will discuss the epidemiology, clinical presentation, multimodality imaging findings as seen on ultrasound (US), computed tomography (CT), magnetic resonance imaging (MRI) and positron emission tomography/computed tomography (PET/CT) of these rare adnexal entities.
Methods & Materials: Background: Although relatively rare in the pediatric population, ovarian neoplasms are the most common genital neoplasm occurring in childhood. These lesions may or may not be symptomatic and often may present as an incidental imaging findings. Atypical ovarian lesions, if not diagnosed and treated in a timely manner, may have significant impact on the patient's fertility and can even be fatal. Therefore, recognition of their imaging appearance is of the utmost importance for the practicing radiologist. Imaging, in combination with tumor markers, has had a significant impact on management of ovarian neoplasms, allowing for more conservative approaches and positive outcomes.
Results: Imaging findings: We will review the imaging features of following atypical pediatric ovarian neoplasms using a multi-modality case based approach.
Primary:
Sex cord-stromal tumors
Germ cell tumors
Gonadoblastoma
Germ cell sex cord-stromal tumor of nongonadoblastoma type
Mesothelial tumors
Inflammatory myofibroblastic tumor
Gestational trophoblastic disease
Soft tissue tumors not specific to the ovaries
Lymphomas/Leukemias
Rhabdomyosarcoma
Secondary:
Metastatic tumors
Conclusions: Identifying and characterizing ovarian neoplasms in the pediatric population can be challenging and often presents a diagnostic dilemma. However, by using a multi-modality approach the pediatric radiologist can use key imaging features to elucidate the diagnosis and guide referring clinicians.

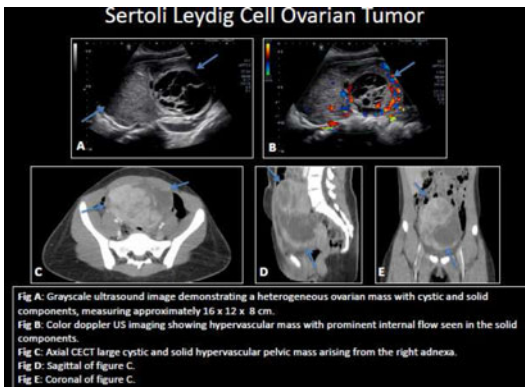

Poster #: EDU-120

Ventriculostomy Simulation Using Patient-specific ventricular anatomy, 3D Printing, and Hydrogel Casting

Justin Ryan, *Phoenix Children's, Phoenix, AZ, jryan1@phoenixchildrens.com;* Stephen Pophal, David Aria, M.D., Richard Towbin, MD

Disclosures: All authors have disclosed no financial interests, arrangements or affiliations in the context of this activity.
Purpose or Case Report: Educational simulators provide a means for students and experts to learn and refinesurgical skills. Our objective was to develop a cost-effective, patient-derived medical simulacrum for cerebral lateral ventriculostomy.
Methods & Materials: A cost-effective patient-derived medical simulacrum was developed for placement of an external lateral ventriculostomy. Elastomeric and gel casting techniques were used to achieve realistic brain geometry and material properties. 3D printing technology was leveraged to develop accurate cranial properties and dimensions. An economical, gravity-driven pump was developed to provide normal and abnormal ventricular pressures. A small pilot study was performed to gauge simulation efficacy using a technology acceptance model.

Results: An accurate geometric representation of the brain was developed with independent lateral cerebral ventricular chambers. A gravity-driven pump pressurized the ventricular cavities to physiologic values. A qualitative study illustrated that the simulation has potential as an educational tool to train medical professionals in the ventriculostomy procedure.
Conclusions: The ventricular simulacrum can improve learning in a medical education environment. Rapid prototyping and multi-material casting techniques can produce patient-derived models for costeffective and realistic surgical training scenarios.

Poster #: EDU-121

The Utility of 3D Printing in in Assisting Transcatheter Aortic Valve Replacement (TAVR)

Disclosures: All authors have disclosed no financial interests, arrangements or affiliations in the context of this activity.

Justin Ryan, *Phoenix Children's, Phoenix, AZ, jryan1@phoenixchildrens.com;* Stephen Pophal, David Aria, M.D., Richard Towbin, MD

Purpose or Case Report: Transcatheter Aortic Valve Replacement (TAVR) is widely becoming an accepted therapy for aortic stenosis. In the last 10 years, estimates place the deployment of TAVRs as high as 50,000 worldwide. Differences in size and morphology of the aortic root and surrounding anatomy are important considerations in determining which TAVR to deploy. 3D printing based off of patient images can be leveraged to create models for patient-specific surgical planning purposes.

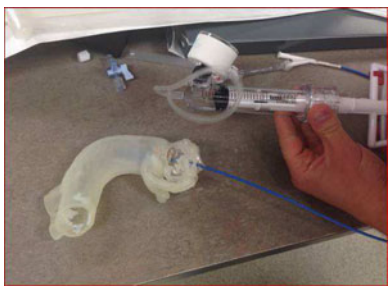

Methods & Materials: An 82 year old female was diagnosed with severe aortic stenosis. Traditional measurements based on CT were inconclusive on size of TAVR for deployment. The decision was made to print an aortic model in a compliant medium with calcifications in a non-compliant medium. TAVR devices were deployed in the model to assist with device determination.
Results: The multi-material, 3D print of the patient's diseased aortic anatomy allowed physicians to perform two mock interventions on the patient-specific model with different TAVR specifications. From the results of the patient-specific, simulated TAVR deployment and information traditionally available through conventional imaging, the clinicians selected the larger available TAVR device for future deployment in the patient.
Conclusions: This case study and modelling process yield compelling results for pre-interventional planning in regards to TAVR deployment. Specifically, representing the two tissue types, lumen and sclerosis, was an achievement through new 3D printing techniques. Integration of this rapidly developing technology within cardiovascular centers is recommended for further study and validation.

Poster #: EDU-122

Contrast-enhanced Voiding Urosonography (Cevus) in an Academic Pediatric Hospital Setting: Lessons Learned in the First Year

Gabrielle Colleran, MD, MB BCh BAO, FFR RCSI, *Radiology, Boston Children's Hospital, Brookline, MA, gabrielle.colleran@childrens.harvard.edu;* Carol Barnewolt, MD, Jeanne Chow, MD, Harriet Paltiel, MDCM

Disclosures: All authors have disclosed no financial interests, arrangements or affiliations in the context of this activity.

Figure 2: Transverse view of bladder during filling phase of ce-VUS showing bilateral distal hydroureter, without reflux, concordant with VCUG.

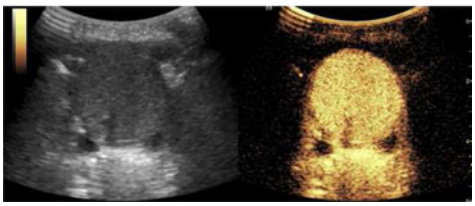

Purpose or Case Report: Fluoroscopic voiding cystourethrography (VCUG) and radionuclide cystography (RNC) are conventional techniques used for the diagnosis of vesicoureteral reflux (VUR) in children. Contrast-enhanced voiding urosonography (ceVUS) is a radiation-free alternative to the traditional VCUG. ceVUS has gained acceptance in Europe, but has not yet been widely adopted in the USA.
The purpose of this educational review is to describe our initial experience with ceVUS using the second generation US contrast agent Optison™, with a focus on optimization of examination technique, utility in the depiction of a variety of pathological entities, and a discussion of potential pitfalls.
Methods & Materials: Using our experience with 80 ceVUS studies, performed as a paired exam with VCUG [42 girls and 38 boys, age range 2 days to 10 years (mean age 11 months, median 3 months)], we summarize our observations, including both successful and unsuccessful approaches.
Results: Excluding bladder catheterization, ceVUS takes 5-6 min on average. Excessive bowel gas makes the exam more challenging and "practice" sonographic views of the kidneys and bladder prior to instillation of contrast are helpful. As with VCUG, careful attention to exclusion of air from connecting tubing and complete bladder emptying prior to contrast instillation is key. If one is facile with sonography and VCUG, the technique is easily learned. Examples of VUR, intrarenal reflux, ectopic ureterocele, ureteral duplication, posterior urethral valves, and spinning top urethra will be discussed. Interpretive challenges, including vaginal reflux, gas in the bowel and visible intrarenal vessels will also be addressed.
Conclusions: The high-sensitivity, safety, and ease of performance of ceVUS has the potential to largely replace conventional fluoroscopic VCUG for diagnosis of VUR which requires exposure to ionizing radiation.

Figure 1 (parts a, b, and c).
A. High-grade reflux with IRR on VCUG.

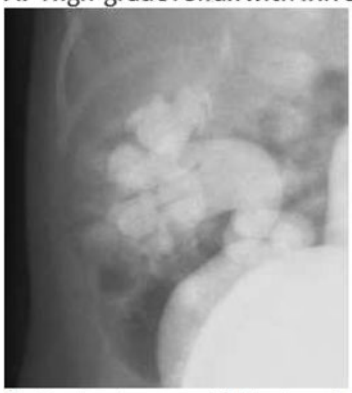

B. Early phase ce-VUS, showing reflux into the pelvicalyceal system in the same patient.

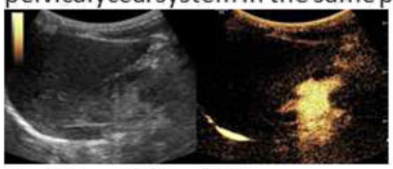

C. After voiding, IRR is seen on ce-VUS.

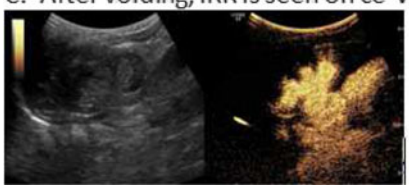

Fig 3. Normal appearance of male urethra on transperineal scan during ce-VUS (a) as correlated with VCUG, with the image turned to mimic the orientation on ce-VUS (b).

3 a

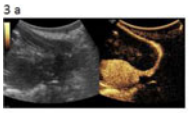

3 b

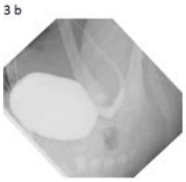

Poster #: EDU-123

Novel Applications to Functional, Molecular and Clinical Imaging Surveillance

Claudia Martinez-Rios, MD, *Radiology, The Hospital for Sick Children, Toronto, ON, Canada, claudia.martinez-rios@sickkids.ca;* David Malkin, Reza Vali, Amer Shammas, Marta Tijerin Bueno, Fellow, Mary-Louise Greer, MBBS, Andrea Doria

Disclosures: All authors have disclosed no financial interests, arrangements or affiliations in the context of this activity.

Purpose or Case Report: Whole-body (WB) magnetic resonance (MR) imaging in children is of special interest because it is radiation free and can be used to evaluate systemic conditions, exploiting the advantage of the superior soft-tissue contrast provided by MR imaging. An important clinical application of whole-body MR imaging in children is its use for screening of oncologic conditions, tumor characterization, and staging. However, the list of non-oncologic applications of WB MRI has recently expanded to include the evaluation of numerous multisystemic conditions.

This is a pictorial review of different oncologic applications of WB MRI including cancer predisposition syndromes, solid neoplasias and lymphomas, as well as of non-oncologic applications of WB MRI including chronic recurrent osteomyelitis (CRMO), enthesitis related arthritis (ERA), vascular malformations and benign tumors. In this review we discuss the advantages and challenges of conventional and functional MRI sequences including the use of diffusion weighted imaging (DWI), color-encoded DWI enhanced with iron supplement Ferumoxytol as blood pool contrast agent, as well as the advantages and disadvantages of the recently introduced WB positron emission tomography (PET)/MRI.

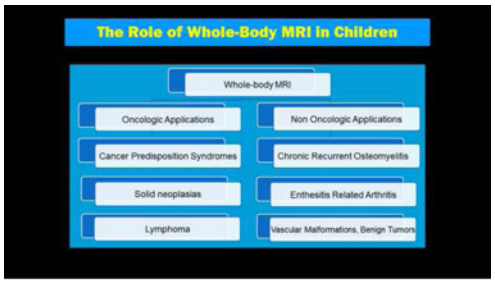

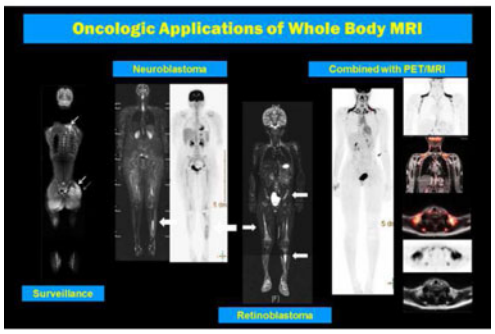

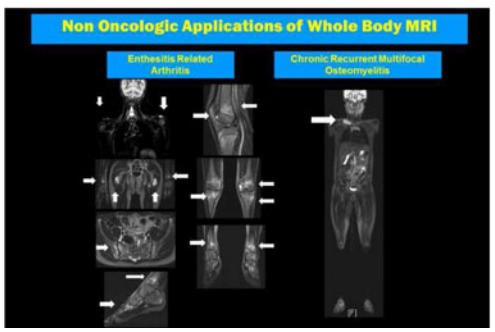

Poster #: EDU-124

Take (AIM)^2 at the Pediatric Acute Abdomen

Patrick Pan, MD, *Radiology, University of California, Los Angeles, Los Angeles, CA, ppan@mednet.ucla.edu;* Antoinette Roth, Soni Chawla, MD

Disclosures: All authors have disclosed no financial interests, arrangements or affiliations in the context of this activity.

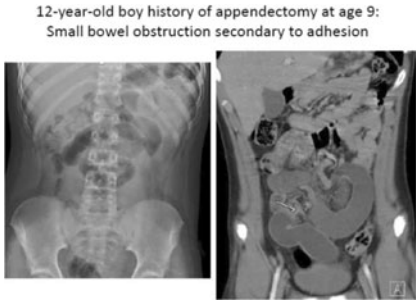

Purpose or Case Report: Acute abdomen is one of the most common presentations encountered in any pediatric emergency department. This educational exhibit refreshes reader with the most common causes of acute abdomen encountered in the pediatric population through a simple mnemonic (AIM)[2] which includes Appendicitis, Adhesions, Intussusception, Incarcerated inguinal hernia, Meckel's diverticulum and Mal-rotation with midgut volvulus. Initial abdominal radiographs and confirmatory ultrasound and/or cross-sectional images including CT and MRI will be presented.

There will be emphasis on "Image Gently" principles in keeping with minimum radiation exposure to our most vulnerable pediatric population. The best use of available diagnostic modality with the least or no radiation is suggested for given pathologies and clinical scenarios in pediatric patients. Also, appropriateness criteria for the diagnostic studies will be reviewed in our exhibit.

Plain films may reveal an abnormal bowel gas pattern, which may suggest an underlying pathology. Use of ultrasound as part of the initial evaluation is advocated in many situations because it may be quickly performed at bedside and repeated as needed without harmful ionizing radiation. In certain cases, ultrasound examination may be confirmatory.

CT is best used when the initial tests are unrevealing, or when the patient is acutely deteriorating. CT has proven to save lives of children by allowing prompt and accurate evaluation. Minimizing radiation exposure while maintaining diagnostic accuracy remains an ongoing effort of the entire care team, including the radiologists, radiology technologists and the referring physicians.

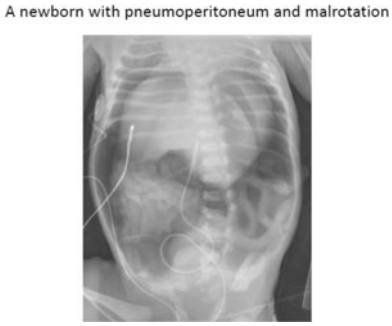

Poster #: EDU-125

The Biliary Atresia/Splenic Malformation Syndrome – A Pictorial Review

Ellen Patrick, MD, MEd, *Children's Healthcare of Atlanta, Egleston. Emory, Atlanta, GA, ellen.patrick@choa.org;* Paula Dickson, MD, Adina Alazraki, MD, Rene Romero

Disclosures: All authors have disclosed no financial interests, arrangements or affiliations in the context of this activity.

Purpose or Case Report: Ninety percent of biliary atresia cases occur with no associated anomalies. Ten percent of cases of biliary atresia are considered syndromic, occurring in association with a variety of congenital anomalies including heterotaxy, polysplenia, asplenia, congenital cardiac defects, intestinal malrotation, interrupted IVC, hepatic artery anomalies, and portal vein anomalies, including pre-duodenal portal vein. The incidence of hepatopulmonary syndrome is also increased in this group. Images from CT, MR, radiography, nuclear medicine, ultrasound and fluoroscopy will illustrate the variety of imaging appearances of the biliary atresia/splenic malformation syndrome.

Methods & Materials: After obtaining approval from our Institutional Review Board we retrospectively reviewed the imaging and clinical presentation of 16 pediatric patients with biliary atresia and splenic malformations.

Conclusions: Pediatric radiologists should be aware of the association of biliary atresia and splenic malformations, and should be suspicious for biliary atresia in the presence of liver malfunction or jaundice in patients with splenic abnormalities. Additional structural abnormalities such as malrotation and vascular anomalies should be investigated as they may complicate surgical interventions such as Kasai procedure or liver transplant.

Poster #: EDU-126

Fear of the Unknown: Get to Know the Complications of Hematopoietic Cell Transplant (HCT)

Yachao Zhang, MD, *Radiology, Westchester Medical Center, Valhalla, NY, yachao.zhang@wmchealth.org;* Kevin McNerney, MD, Perry Gerard, Leslie LeCompte

Disclosures: All authors have disclosed no financial interests, arrangements or affiliations in the context of this activity.

Purpose or Case Report: Review the time course of early and late complications of hematopoietic cell transplant (HCT).

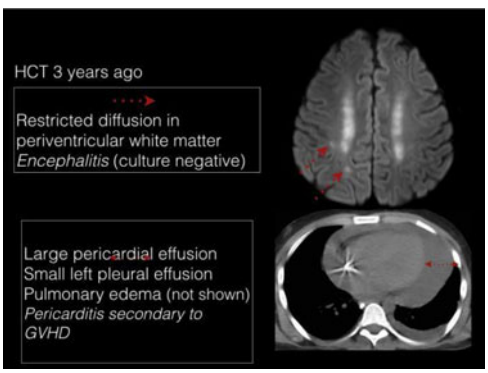

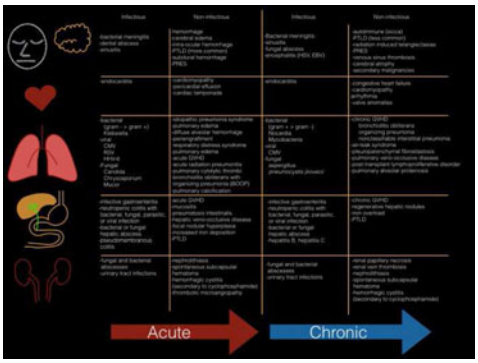

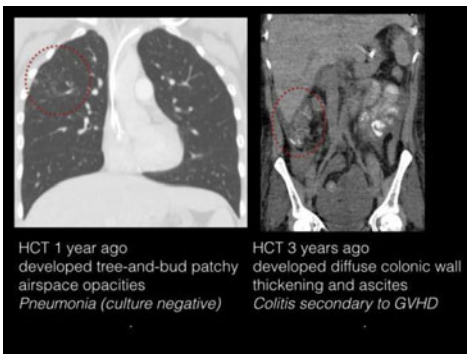

Assess and compare the infectious and non-infectious complications of HCT secondary to immunosuppression and treatment-related toxicity.
Review the imaging pearls in diagnosing non-infectious complications post HCT pediatric patients with case examples.
Methods & Materials: A head-to-toe comprehensive review of the diagnostic pearls of infectious and non-infectious post-HCT complications among pediatric patients through literature search and case based learning utilizing multimodal imaging examples including radiograph, ultrasound, CT and MRI. Diagrams and flow charts are employed to facilitate review of the time-wise complications of HCT secondary to immunosuppression and treatment-related toxicity.
Results: CNS/Head and neck:
Infectious (I): meningitis/encephalitis, dental abscess, sinusitis
Sterile (S): CVA, subdural hemorrhage, PTLD, autoimmune (i.e. Sicca)
Lung:
I: sino-pulmonary infection, bacterial, viral (HSV, CMV, PCP, RSV) and fungal pneumonia
S: acute/chronic graft versus host disease, idiopathic pneumonia syndrome, pulmonary edema, diffuse alveolar hemorrhage, engraftment syndrome, pulmonary cytolytic thrombi, air-leak syndrome, pleuroparenchymal fibroelastosis, venoocclusive disease, PTLD
Cardiovascular:
I: endocarditis
S: CHF, cardiomyopathy, pericardial effusion
GI:
I: infectious colitis (bacterial/fungal/viral), bacterial or fungal abscesses of liver
S: neutropenic colitis, venoocclusive disease of the liver/spleen (aute, chronic, medication toxicity), PTLD
GU:
I: bacterial/fungal renal abscess
S: hemolytic uremic syndrome, papillary necrosis, renal vein thrombosis, hemorrhagic cystitis, renal papillary necrosis, nephrolithiasis
Conclusions: As hematopoietic stem cell transplantation becomes widely available in both large academic centers and smaller community hospitals, radiologists must be familiar with both its infectious and non-infectious complications. While most infectious etiologies may be clinically identified with culture and exam, the non-infectious causes can be confusing and complex. Imaging findings are essential in identifying the cause in combination with the appropriate clinical context. A working knowledge of the time course of these complications, clinical context in which they occur, and characteristic appearance on imaging will aid the radiologist in the diagnosis of these conditions.

Poster #: EDU-127

Pilocytic Astrocytoma: Pictorial Review of MRI Imaging Features, the Classic and the Atypical

Irit Maianski, MD, *IWK Health centre, Halifax, NS, Canada, irit.maianski@iwk.nshealth.ca;* Tahani Ahmad, Naeem Khan

Disclosures: All authors have disclosed no financial interests, arrangements or affiliations in the context of this activity.
Purpose or Case Report: The purpose of this pictorial review is
* To illustrate the classic MRI characteristics of PA in common and less typical locations in both standard advanced MRI sequences. Special attention to MR Spectroscopy will be provided
* To outline the less specific imaging features
* To discuss the relevant differential diagnosis according to tumor location
Methods & Materials: Pilocytic Astrocytoma (PA) is the most common pediatric glial tumor, typically located in he posterior fossa with predilection to the cerebellum. Other common locations are along the hypothalamic pituitary axis, optic nerves and chiasm. The association with neurofibromatosis (NF1) is well established, known to affect mainly the optic pathways. Supratentorial and spinal cord location are not often seen in pediatric population.
The classic radiologic appearance of cystic lesion with avidly enhancing mural nodule makes potential easy diagnosis. Nevertheless, less specific features are also known and include necrotic mass, hemorrhagic change, predominantly solid lesion, aggressive local invasion and leptomeningeal spread.
The treatment of choice is surgical resection providing excellent outcome. Chemotherapy and radiotherapy are reserved for compromising tumor location and disseminated disease.
Results: This presentation will demonstrate the imaging features of PA in the posterior fossa, pituitary axis and optic pathways as well as less common imaging characteristics and locations like brain stem, cerebral hemispheres and with leptomeningeal dissemination.
Relevant differential options including high grade glioma, germ cell tumours and hemangioblastoma will be discussed.
Conclusions: PA is a common pediatric CNS tumor and usually easily diagnosed with the classis imaging features of cystic mass with enhancing mural nodule. Familiarity with the spectrum of imaging characteristics will facilitate diagnosis and appropriate treatment option.

Poster #: EDU-128

Hepatic Sinusoidal Obstruction Syndrome (SOS) - Review of Ultrasound and Doppler Findings

Matthew Shore, *University of Wisconsin School of Medicine and Public Health, Madison, WI, MShore@uwhealth.org;* Erica Riedesel, MD

Disclosures: All authors have disclosed no financial interests, arrangements or affiliations in the context of this activity.
Purpose or Case Report: Hepatic sinusoidal obstruction syndrome (SOS) - previously termed hepatic veno-occlusive disease (VOD) - is a serious cause of acute liver failure in patients undergoing hematopoietic cell transplantation (HCT).
Hepatic SOS results from injury to the hepatic venous endothelium during intensive myelopablative chemotherapy or radiation therapy prior to HCT. Endothelial injury eventually leads to fibrous obliteration of the terminal hepatic venules with sinusoidal obstruction, hepatocyte necrosis, and hemorrhage, typically seen in the first 3-6 weeks post-transplant.
Early identification of this disease process is critical given high incidence of multi-organ failure and significant morbidity and mortality. Ultrasound is extremely valuable in accurate early diagnosis as imaging findings often precede clinical signs of disease. Spectrum of findings on gray-scale ultrasound includes hepatomegaly, heterogeneous hepatic parenchymal echotexture, ascites, and gallbladder wall thickening. Findings on Doppler ultrasound - increased mean hepatic artery resistive index (RI) and decreased or reversed portal venous flow - are highly sensitivie for hepatic SOS.
In this education exhibit we will review the epidemiology and pathophysiology of hepatic sinusoidal obstruction syndreom (SOS) and discuss imaging findings that aid in accurate diagnosis. Special attention will be given to Doppler ultrasound findings and additional diagnostic information provided by B-flow Doppler ultrasound.

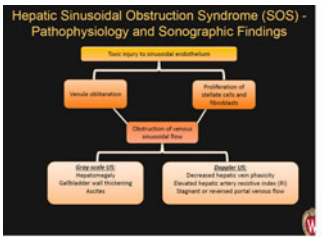

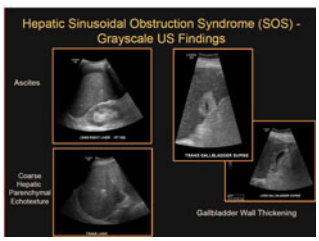

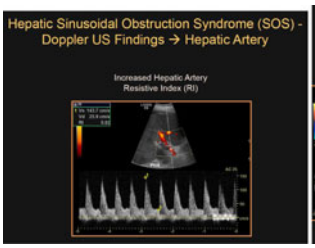

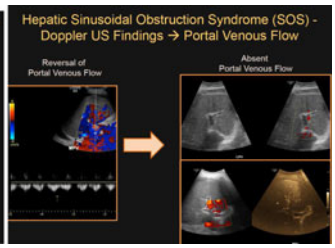

Poster #: EDU-129

Look at Those Peepers: Imaging Review of Pediatric Proptosis

Crysela Smith, MD, *Radiology, University of Washington, Seattle, WA, cmsmith2@uw.edu;* Dinesh Sundarakumar, MD, Kenneth Maravilla

Disclosures: All authors have disclosed no financial interests, arrangements or affiliations in the context of this activity.
Purpose or Case Report: Imaging description of causes for Pediatric Proptosis
Methods & Materials: Discuss the role of imaging in investigation of proptosis in pediatric patients, correlating etiology and anatomical compartments.

Location	Benign	Malignant
Ocular	Macroophthalmos,	Retinoblastoma
Extraconal	Benign lacrymal gland tumors	Metastasis, Lymphoma, Meningioma
Intraconal	Dysthyroid ophthalmopathy, pseudotumor,	Rhabdomyosarcoma
Trans-compartmental	Vascular malformations, Infantile hemangioma, Plexiform neurofibroma, pseudotumor	Leukemic deposits
Osseous	Dermoid inclusion cyst, fibrous dysplasia, juvenile ossifying fibroma	Osteosarcoma, Neuroblastoma metastasis, Eosinophilic granuloma
Infectious/Inflammatory	Retrobulbar cellulitis/ abscess	
Developmental	Congenital proptosis, Shprintzen-Goldberg craniosynostosis syndrome, Craniofacial dysostosis/Crouzon	
Vascular	Carotid artery-cavernous sinus fistula, Cavernous sinus thrombosis, Orbital varix.	

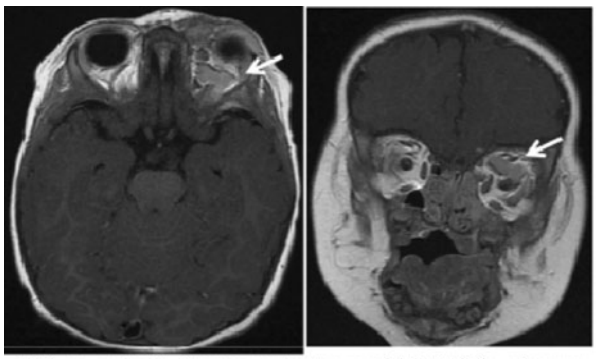

T1W w contrast , T1W w contrast coronal MR: Mildly enhancing retrobulbar mixed venous malformation causing left-proptosis.

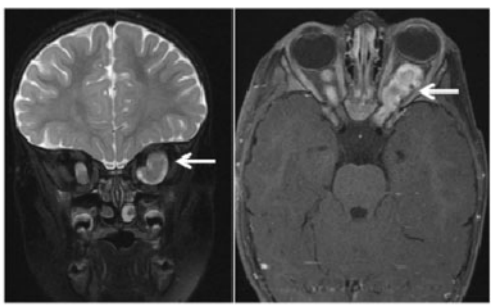

Optic nerve glioma causing left-sided proptosis.T2W coronal, T1W FS w contrast MR, fusiform T1W iso mildly hypointense, T2W hyperintense intensely enhancing mass involving both optic nerves, left greater than right.

Results: Proptosis in children is caused by a spectrum of etiologies often different from those encountered in the adult population. Imaging is important in determining the etiology and planning treatment. Clinical characterization of proptosis (uni- or bilateral, axial or extra axial displacement, visual acuity etc.) provides valuable information, is often helpful in image interpretation. True proptosis must be distinguished from pseudo proptosis (i.e., relative disparity in the globe size and the orbital space). Proptosis then can occur secondary to developmentally reduced orbit size, or mass effect associated with a normal size orbit, displacing the globe.
Pediatric pathologies causing globe displacement in the setting of normal orbit size include infectious and non-infectious inflammatory conditions, such as dysthyroid orbitopathy, pseudotumor, developmental conditions such as dermoid, vascular malformations and hamartoma; these benign causes for proptosis constitute 85% of all cases in the pediatric population. Retinoblastoma, the most common pediatric intraocular tumor and rhabdomyosarcoma are the most common malignant causes for proptosis which are unique

for the pediatric population. Other neoplastic causes of proptosis include metastasis from neuroblastoma, granulocytic sarcoma from acute myelogenous leukemia optic nerve glioma- juvenile pilocytic astrocytomas. These conditions differ in terms of their treatment and in the eventual visual outcome. An imaging algorithm based on the anatomical compartment, helpful in determining the origin of the lesion is delineated in the exhibit. Lesions are discussed including specific imaging characteristics that help in arriving at the accurate diagnosis.
Conclusions: Imaging plays an important role in defining the cause of proptosis in the pediatric patient; characterization of which guides treatment with the goal of minimizing the impact on vision and health of pediatric patients.

Poster #: EDU-130

Imaging of Pediatric Supporting Lines and Tubes

Anand Majmudar, MD, *Radiology, Lebonheur Children's Hospital, UTHSC, Memphis, TN, amajmuda@uthsc.edu;* Vijay Pandey

Disclosures: All authors have disclosed no financial interests, arrangements or affiliations in the context of this activity.
Purpose or Case Report: 1) To identify the correct radiographic position of pediatric support lines and tubes.
2) To review abnormal placement of the lines and tubes as well as their anatomic consideration.
3) To review potential complication of incorrectly positioned lines.
Methods & Materials: 1) Retrospective evaluation of the cases with incorrectly positioned lines and tubes in a pediatric tertiary care hospital.
2) Review of available types of support lines and tubes as well as their normal position on radiograph.
3) Review of their abnormal position and complications arising due to abnormal position.
Results: 1) Deviation from the normal position of support lines and tubes help indicate their abnormal placement and also sometimes abnormal anatomy of the organs involved.
2) Incorrect positioning of lines and tubes can result in life threatening complications. Imaging is of tremendous help in this context.
Conclusions: A systematic approach and knowledge of the radiographic features of the common pediatric indwelling tubes and lines is of the utmost importance to prevent harmful positioning of such devices.

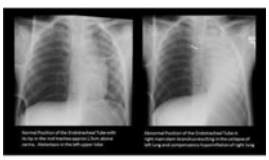

Fig-1

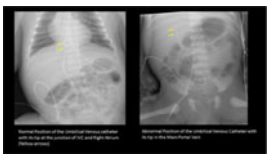

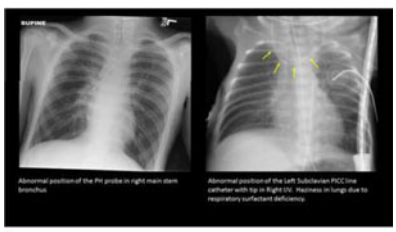

Fig-3

Poster #: EDU-131

Finding the Right Spot: Imaging Evaluation of Focal Cortical Dysplasia in Pediatric Epilepsy

Crysela Smith, MD, *Radiology, University of Washington, Seattle, WA, cmsmith2@uw.edu;* Dinesh Sundarakumar, MD, Kenneth Maravilla

Disclosures: All authors have disclosed no financial interests, arrangements or affiliations in the context of this activity.
Purpose or Case Report: Imaging features and evaluation of focal cortical dysplasias (FCDs).
Methods & Materials: Discuss the role of imaging in investigation of focal cortical dysplasias in epileptic pediatric patients.
Results: FCDs are an important cause for medication refractory focal seizures in the pediatric population. FCDs are characterized by abnormal cortical architecture and gray-white matter junction differentiation. Extensive preoperative electrophysiological investigations such as electroencephalography (EEG) and functional magnetic resonance imaging (fMRI) are performed to guide electrode implantation and map out surgical treatment of the epileptogenic focus. Despite considerable progress in the preoperative investigatory techniques, FCD-related epilepsy remains difficult to diagnose and treat. The comprehensive three-tiered International League Against Epilepsy (ILAE) classification system of FCD is used to distinguish this diverse clinicopathological entity. This exhibit will describe the MRI and PET imaging features of various types of FCDs based on the above mentioned classification system. Limitations of current imaging techniques in identification of FCD and reasons for discrepant imaging and electrophysiological studies will also be described.
Conclusions: Imaging plays an important role in defining the cause for focal epilepsy in the pediatric patient, the characterization of which guides treatment with the goal of a seizure-free life after surgery.

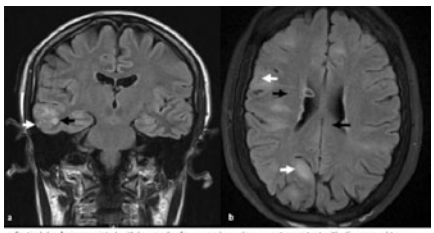

a Cortical dysplasia associated with low grade glioneuronal neoplasm, most consistent with glioneuronal tumor. Coronal FLAIR image in a 22-year-old female demonstrates an ill-defined multicystic lesion in the lateral right temporal lobe representing a glioneuronal neoplasm (black arrow). There is extensive cortical thickening and abnormal FLAIR hyperintensity in the lateral temporal lobe representing type III cortical dysplasia (white arrow). b Cortical dysplasia associated with Tuberous Sclerosis. Axial FLAIR image in a 10-year-old female demonstrates multiple subependymal nodules (black arrows) and multifocal cortical thickening with abnormal FLAIR hyperintensity representing Type III cortical dysplasia (white arrows).

Table: ILAE classification system for Focal Cortical Dysplasia

Type	Subtypes		
Isolated Type II FCD	FCD Ia: abnormal radial (vertical) cortical architecture	FCD Ib: abnormal tangential (horizontal) cortical lamination	FCD Ic: abnormal radial and tangential cortical architecture
Isolated Type II FCD	FCD Ia: with dysmorphic neurons	FCD IIb: with dysmorphic neurons and balloon cells	
Associated FCD type III	FCD IIIa: cortical lamination abnormalities in the temporal lobe associated with HS	FCD IIIb: cortical lamination abnormalities adjacent to a glial or glioneuronal tumor	FCD IIIc and d: cortical lamination abnormalities adjacent to vascular malformation or acquired lesions

Poster #: EDU-132

Society for Pediatric Radiology Member Attitudes toward International Outreach and the World Federation of Pediatric Imaging – 5 Years Later

Amanda Dehaye, Richard Barth, Jennifer Boylan, MA, Brian Coley, MD, *World Federation of Pediatric Imaging, Chicago, IL, brian.coley@cchmc.org*

Disclosures: Brian Coley has indicated a relationship with Elsevier as an editor. All other authors have disclosed no financial interests, arrangements or affiliations in the context of this activity.

Purpose or Case Report: Five years ago, the Society for Pediatric Radiology (SPR) supported the founding of the World Federation of Pediatric Imaging (WFPI). In order to guide future activities, SPR members were surveyed about their views on international outreach in general and the activities of WFPI specifically.

Methods & Materials: SPR members were electronically surveyed in March 2014. 3 questions out of 66 pertained to SPR international activities and WFPI. Respondents could choose 5 responses ranging from strongly approve/very important to strongly disapprove/very unimportant. Free text comments were also collected.

Results: 273 SPR members responded (23% response rate: 85% complete, 15% partial).

Seventy-nine percent of SPR members strongly approved or approved of the question "Is WFPI being something SPR should continue to pursue". Eighty-three percent strongly approved or approved the statement "should WFPI unite pediatric imaging societies around the world" while 77% strongly approved or approved that SPR should increase its involvement in other societies' international work.Sixty-four percent strongly approved or approved of SPR's involvement in intrinsic international outreach efforts.

Eighty-eight percent considered spreading child imaging safety work globally as very important or important. Eighty-seven percent felt it is very important or important to provide affordable online education worldwide. Eighty-eight percent consider advocacy as very important or important and 86% consider it very important or important to produce imaging guidelines on pediatric topics. Onsite teaching and teleradiology scored 73% and 71% very important or important respectively. Lowest in importance at 55% was initiating international research.

Free text comments underscored reservations about added value, resources and a non-domestic focus.

WFPI work to date aligns with SPR member priorities and wishes. There has been work on safety in partnership with the Image Gently campaign. Providing freely accessible online education has been initiated with SPR. WFPI has engaged in advocacy and direct patient care with the WHO, ACR, RAD-AID, WFUMB, IAEA, Imaging the World and MSF.

Conclusions: Most responding SPR members are supportive of international outreach efforts and see value in WFPI and its goals. There is alignment between SPR member priorities and WFPI activities. WFPI, an international extension of SPR/ESPR/SLARP/AOSPR/ASPI and other societies, should continue to advocate for pediatric imaging globally and to partner with like-minded organizations to leverage resources and impact.

Poster #: EDU-133

Gastro-intestinal Emergencies & Malformations in a Neonate-Revisited!

Dhanashree Rajderkar, MD, *Radiology, University of Florida, Gainesville, FL, drdhana1@gmail.com;* Priya Sharma, MD, Nupur Verma, MD

Disclosures: All authors have disclosed no financial interests, arrangements or affiliations in the context of this activity.

Purpose or Case Report: GI Emergencies and congenital malformation in the neonate are variable in their presentation and can be seen from the hypo-pharynx to the anus. The pediatric radiologist often plays a key role in diagnosis and planning of early surgical management.

Methods & Materials: We exhibit a case review of GI anomalies frequent encountered in pediatric radiology, including presentation on radiograph and fluoroscopy. We discuss prenatal diagnosis, with fetal ultrasound or MR, when applicable.

Results: We discuss the clinical presentation and imaging examples of GI emergencies in the new born, cases include:

Tracheoesophageal fistula
Duodenal web
Malrotaion
Midgut volvulus
Omphaloceles and gastroschisis
Meconium plug,
Meconium ileus with or without perforation
Ileal,duodenal, and colonic atresia
Hirschsprung's disease
Congenital small left colon
Anal atresia

Conclusions: It is vital to recognize GI malformations in the neonatal period. Many of these conditions are corrected in the first few weeks of life and some, such as midgut volvulus and meconium ileus, may present catastrophically. Some may need radiology guidance for diagnosing additional associations like in patients of omphalocele may need additional radiology imaging versus meconium ileus may need genetic testing.

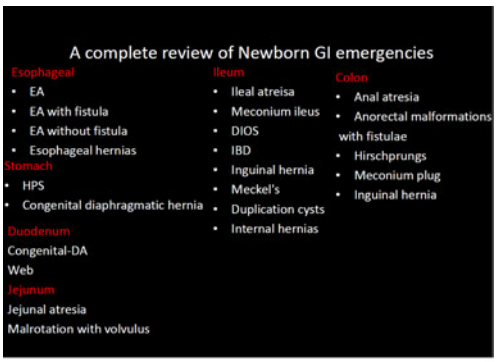

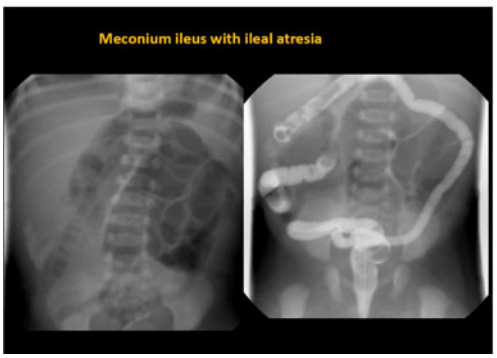

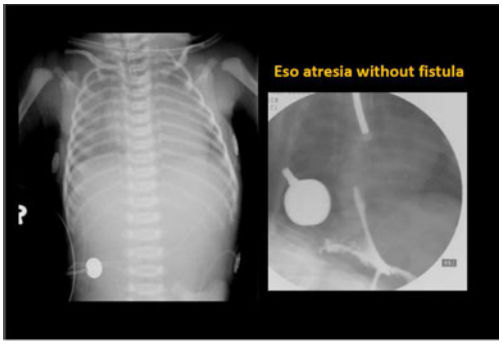
Eso atresia without fistula

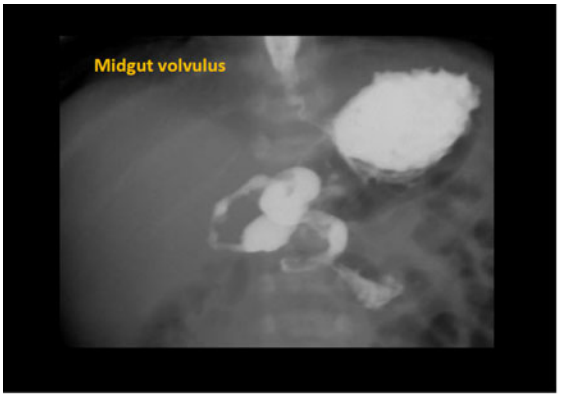
Midgut volvulus

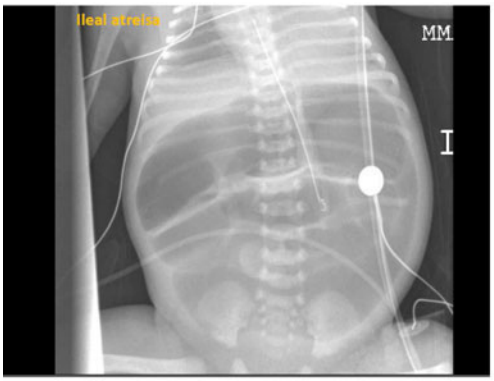
Ileal atresia
MM

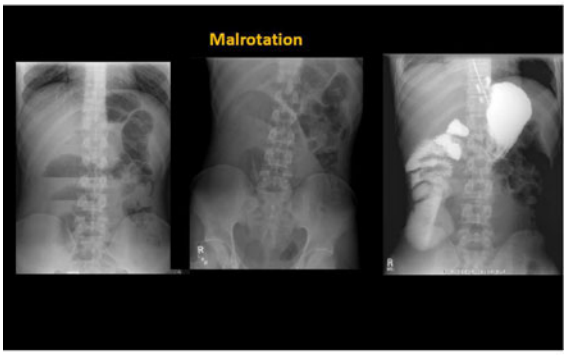
Malrotation

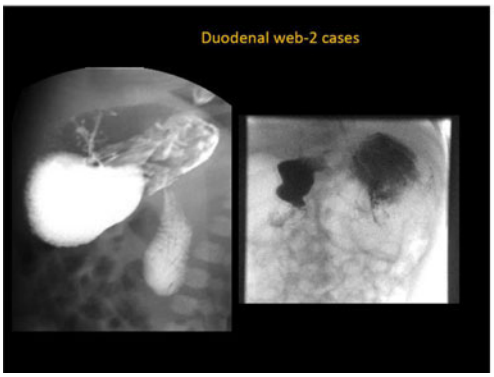
Duodenal web-2 cases

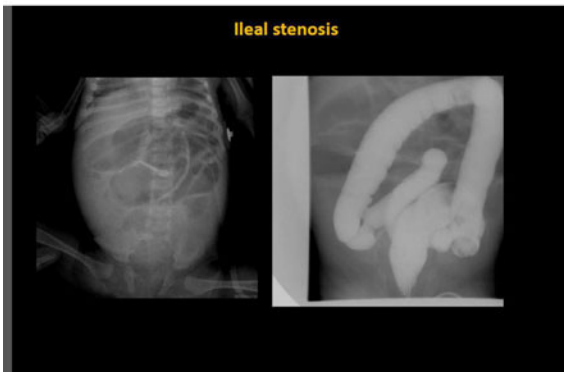
Ileal stenosis

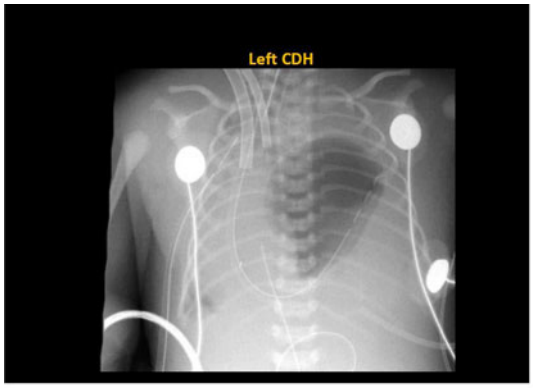

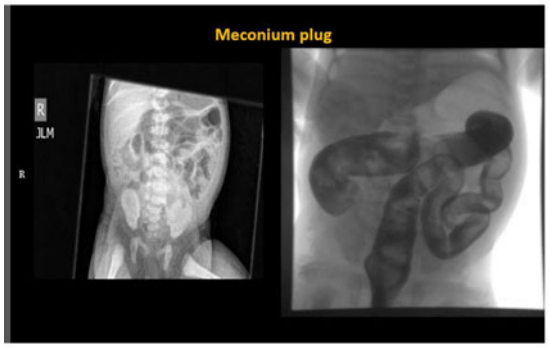

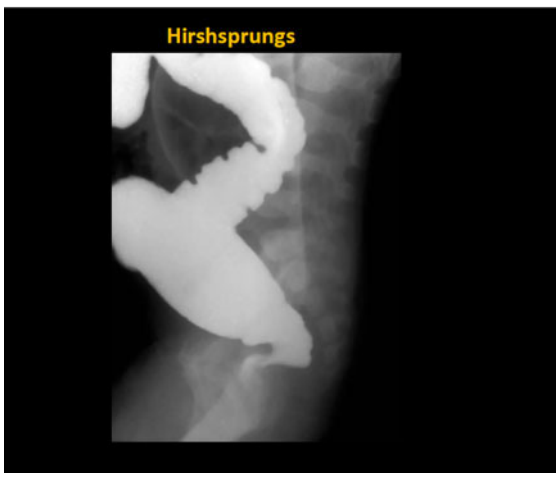

Poster #: EDU-134

International Outreach in Pediatric Radiology Education: The CHOP Program in Ethiopia

Kassa Darge, MD, PhD, *University of Pennsylvania, Dept. of Radiology, The Children's Hospital of Philadelphia, Philadelphia, PA, darge@email.chop.edu;* Anne Marie Cahill, Diego Jaramillo, MD, MPH, Marc Keller, MD, Soroosh Mahboubi, Andrew Mong, MD, Sabah Servaes, Karuna Shekdar, Teresa Victoria, MD, PhD, Chris Tomlinson, Tequam Debebe, Yocabel Gorfu, Daniel Zewdneh, Alemayehu Bedane, Tesfaye Kebede, Pooja Renjen, Ines Boechat, MD, Amanda Dehaye, Janet Reid, MD, FRCPC

Disclosures: Janet Reid has indicated a relationship with Oxford University as an editor. All other authors have disclosed no financial interests, arrangements or affiliations in the context of this activity.

Purpose or Case Report: Pediatric radiology focuses on appropriate and safe diagnostic imaging and intervention in children of all ages. In Ethiopia, a sub-Saharan developing country in East Africa, almost 60% of the population is in the pediatric age group. In the main referral general hospital of the country children make up 48% of the patient population. Currently, there is no pediatric radiologist in the country. The aim of this presentation is to describe the undertakings of the International Outreach in Pediatric Radiology Education Program in Ethiopia of the Department of Radiology, The Children's Hospital of Philadelphia (CHOP), which is aiming to improve the existing situation. This program is carried out under the auspices of the World Federation of Pediatric Imaging (WFPI).

Methods & Materials: The outreach program was started in 2008 with 2 main partners in Ethiopia. The first one is the Department of Radiology, Faculty of Medicine, Addis Ababa University in the capital city. Here we support the pediatric part of the residency training and have started a pediatric radiology fellowship program. The other partner is the Radiological Society of Ethiopia (RSE) collaborating on the annual national continuing medical education (CME) course in pediatric radiology.

Results: The pediatric part of the residency program is enhanced by on-site lectures and bedside teaching sessions by regularly visiting professors from CHOP and external partners of this outreach program. For the fellowship program a 2-year curriculum was developed and accredited by the Addis Ababa University. The focus is on teaching the teachers in academic institutions and enabling them to subspecialize in pediatric imaging. The fellowship is carried out by a combination of remote and on-site learning. Currently, 2 staff radiologists from the Department of Radiology are enrolled in the program and will be completing the fellowship by the end of 2016. The CME course in pediatric radiology covering a wide range of topics is a 1-day annual event with faculty both from CHOP and our external partners. The course has been successfully conducted every year for the past 5 years. The number of participants has almost doubled from 80 to over 150 with some 90% of the radiologists in the country taking part. The program is enhanced by the networking and exposure provided by the WFPI.

Conclusions: The CHOP International Outreach in Pediatric Radiology Education program in Ethiopia is an exemplary and successful undertaking of advancing pediatric imaging worldwide.

http://wfpiweb.org/EDUCATION/WFPIEducationalInitiatives/Ethiopia.aspx
http://wfpiweb.org/Portals/7/Education/Pediatric%20Radiology%20Curriculum_Addis%20Ababa%20University-CHOP_2014_KD.pdf

Poster #: EDU-135

Ultrasound Evaluation of Pediatric Elbow Disorders with Multimodality Correlation

Adebunmi Adeyiga, *CNMC, Herndon, VA, badeyiga@gmail.com;* Anjum Bandarkar

Disclosures: All authors have disclosed no financial interests, arrangements or affiliations in the context of this activity.

Purpose or Case Report: 1. Review focused elbow ultrasound technique for pediatric patients

2. Review normal pediatric elbow anatomy by ultrasound

3. Present a spectrum of pediatric elbow disorders evaluated by ultrasound and demonstrate correlative findings on radiography, arthrography and MRI.

Methods & Materials: We retrospectively reviewed cases of elbow ultrasound at our institution in patients referred for elbow pain,

swelling and decreased movement. Clinical presentations and imaging findings were recorded, with an emphasis on sonographic features. Correlation was made with other available imaging modalities and surgical/pathologic findings. Normal sonographic anatomy of the pediatric elbow was studied using two healthy volunteers, ages 6 and 9 years.
Results: Patients referred for elbow ultrasound ranged in age from 1 day to 19 years. The spectrum of elbow disorders evaluated by ultrasound included soft tissue infection and soft tissue abscess, osteomyelitis and subperiosteal abscess, septic arthritis, juvenile arthritis, hemophilic arthropathy, trauma, and congenital dislocation. Key ultrasound findings of each case were highlighted and compared with findings of alternative imaging modalities, as well as results of surgical and pathologic assessments.
Conclusions: Ultrasound is a powerful tool in the assessment of pediatric elbow disorders that enables a detailed and real-time assessment without the use of ionizing radiation. A review of normal elbow anatomy by ultrasound is pertinent to the effective utilization of this tool in pathologic states

Poster #: EDU-136

STIRing the CRMO Pot: Whole Body MRI

Manish Baja, M.D., *Pediatric Radiology, University of Iowa Hospitals and Clinics, Iowacity, IA, mbj_rnt@hotmail.com;* T Shawn Sato, Yutaka Sato, MD, Simon Kao, Polly Ferguson

Disclosures: All authors have disclosed no financial interests, arrangements or affiliations in the context of this activity.
Purpose or Case Report: This educational exhibit aims to :
1. Discuss the pathogenesis of Chronic Recurrent Multifocal Osteomyelitis (CRMO) with enumeration of Diagnostic Clinical Criteria
2. Describe pertinent findings on whole body Short tau Inversion Recovery (STIR) MR Imaging.
3. Illustrate evolution of MR findings on follow up imaging.
4. Identify common imaging differentials to be considered and pitfalls to be avoided
Methods & Materials: All patients with a diagnosis of CRMO presenting to pediatric radiology department at our institute who have undergone whole body STIR MRI are retrospectively evaluated for pertinent imaging findings. The information will be used to create an educational exhibit organized as under:
Etiopathogenesis (Derangement of Primitive Immune System)
Characterstic sites of Involvement (Mandible, medial clavicle, around knee, pelvis)
Pros and Cons of different imaging modalities used.
Role of follow up imaging to elucidate temporal course of disease.
Results: Chronic Recurrent Multifocal osteomyelitis(CRMO) is an important clinical-radiological entity characterized by multifocal inflammatory lesions involving skeleton in Pediatric/Adolescent age-group. Though increasingly recognized, this entity is usually a diagnosis of exclusion. However, characterstic sites of involvement on imaging and characteristic clinical course of waxing and waning multifocal lesions in temporal course of disease can help narrow the diagnosis.
Conclusions: 1. CRMO is an important clinicoradiological entity, given its characterstic clinical and excellent outcome with appropriate management.
2. Diagnosis of CRMO can be made by referring clinicians' high index of clinical suspicion and radiologists' thorough knowledge of findings of CRMO on imaging.
3. A knowledge of characteristic sites of involvement and waxing and vaning pattern of involvement seen on whole body STIR MRI can help pinpoint the diagnosis and guide management for CRMO

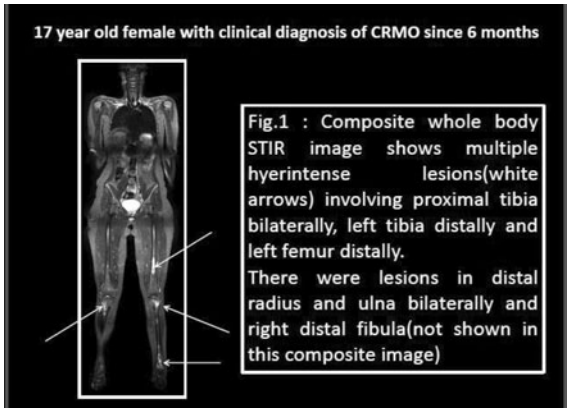

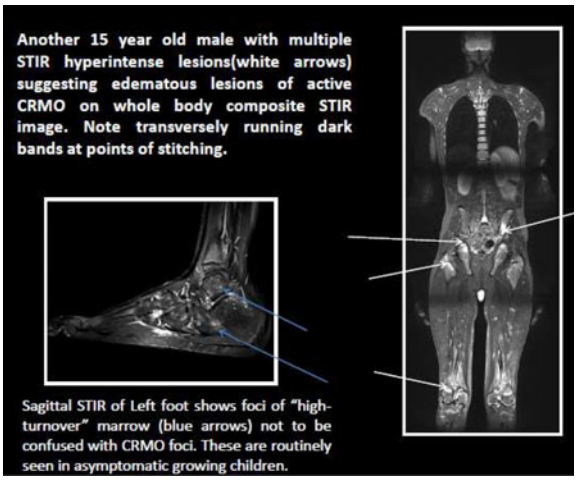

Poster #: EDU-137

Comprehensive Content and Learning Management System: Focused Multifaceted Learning for Pediatric Radiology

Janet Reid, MD, FRCPC, *Children's Hospital of Philadelphia, Philadelphia, PA, reidj@email.chop.edu;* Trupti Gandhi, Parvez Kazmi, Sudha Anupindi, Michael Francavilla, MD, Lisa States

Disclosures: Janet Reid has indicated a relationship with Oxford University as an editor. All other authors have disclosed no financial interests, arrangements or affiliations in the context of this activity.
Purpose or Case Report: Learning at point of care has become the norm. There is endless unfiltered radiology educational material available on the internet. Radiology trainees and educators need a filtered high quality engine available at point of care to enable efficient and effective learning and teaching.
Methods & Materials: This presentation will include a complete pictorial display of all of the facets of a content and learning management system complete with detailed annotation and illustration to explain the role for each component.
Results: This learning resource is built on a Microsoft platform connected to a SQL-server based learning management system. Components of the program include: links to an array of established and vetted online resources, library complete with e-texts and atlases, teaching files, recorded lectures, video-based skills tutorials, fellows' and residents' orientation materials, subspecialty "corners" (fetal, MSK etc.), reference articles,

required reading, imaging protocols, case of the day, educator's toolkit, virtual rounding platform for ICU, and administrative corner. An internal search engine allows easy access within the firewall to the university library and improves search efficiency in removing the reliance on unfiltered searches through the usual browsers.
Conclusions: This electronic Education platform provides efficient and effective access to high quality learning and teaching resources at point of care for trainees and radiologists in pediatric radiology.

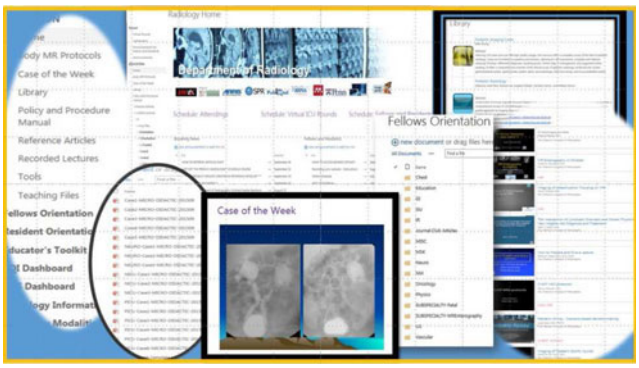

Poster #: EDU-138

Role of Imaging in Respiratory Distress in Neonates

Vijay Pande, MD, *Pediatric Radiology, University of Tenessee Health Science Center, Memphis, TN, vpande@uthsc.edu;* Anand Majmudar, MD

Disclosures: All authors have disclosed no financial interests, arrangements or affiliations in the context of this activity.
Purpose or Case Report: 1) To make the reader aware of imaging features in neonatal respiratory disterss.
2) Multimodality imaging of infants with respiratory distress.
3) Role of antenatal imaging, especially fetal MRI in multidisciplinary approach in management of respiratory disorders of infants.
Methods & Materials: We retrospectively evaluated imaging studies in neonates with respiratory distress in radiology department in a tertiary care pediatric hospital.
Also we prospectively followed neonates who had abnormalities detected on fetal MRI affecting respiratory system. We specifically evaluated how the antenatal imaging affected the management and outcomes.
Results: Causes of neonatal respiratory distress can be divided into those amiable to medical management and those treated surgically.
Common medical causes are: Respiratory distress syndrome secondary surfactant deficiency from prematurity, transient tachyapnoea of newborn, meconium aspiration syndrome, pulmonary hypoplasia and sepsis.
Common surgical causes of neonatal respiratory distress are: Congenital diaphragmatic hernia, congenital pulmonary airway malformations, tracheo-esophageal fistulas, pulmonary sequestration and congenital lobar emphysema.
Most of these surgical causes can be detected and accurately characterized by antenatal imaging by ultrasound and fetal MRI.
Conclusions: Imaging plays a pivotal role in diagnosis, stratification and managment of causes for neonatal respiratory distress.
Fetal MRI plays a crucial role in detection of anomalies affecting the fetal respiratory system and thus helps in planning refferal to higher centers for a multidisciplinary managemnet approach.

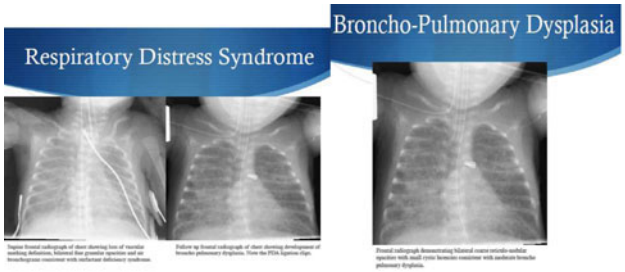

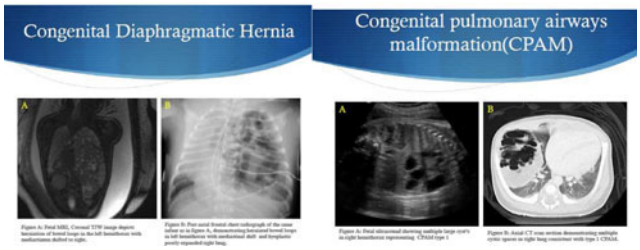

Poster #: EDU-139

Pelvic Retroperitoneal Masses in children: What Does the Radiologist Need to Know?

Jignesh Shah, *Pediatric Imaging, Le Bonheur Children Hospital, Memphis, TN, jigs82rad@gmail.com;* Saurabh Gupta, Preet Sandhu, Harris Cohen

Disclosures: All authors have disclosed no financial interests, arrangements or affiliations in the context of this activity.
Purpose or Case Report: 1. To discuss anatomy and development of pelvic retroperitoneal structures
2. To discuss etiologies and pathogenesis of pelvic retroperitoneal masses in children
3. To review multimodality imaging features with implications on management
Methods & Materials: Anatomy and development of pelvic retroperitoneal structures; etiologies and pathogenesis of pediatric pelvic retroperitoneal masses; imaging features of various pelvic retroperitoneal masses in children including but not limited to cystic masses such as cystic sacrococcygeal teratoma, tailgut cyst, anterior sacral meningocele, lymphangioma, rectal duplication cyst, hemato/hydrocolpos; vascular lesions such as seen in Klippel-Trénaunay-Weber Syndrome; fat containing masses such as lipoblastoma; malignancies such as sarcoma, ewing's sarcoma, desmoplastic small round cell tumor, lymphoma, mesenchymal chondrosarcoma; neurogenic tumors such as neuroblastoma; extension from primary bone tumor involving sacrum; discuss implications of imaging on management.
Conclusions: The pelvic retroperitoneal space is a complex anatomic region that may be affected by a wide variety of masses in children. CT and MR imaging play a central role in the evaluation of primary lesions that occur in this region. Knowledge of the normal anatomy and familiarity with the imaging features and clinical manifestations of these lesions are important for determining the type of mass or narrowing the differential diagnosis, as well as for defining the extent of the mass, an especially important surgical consideration.

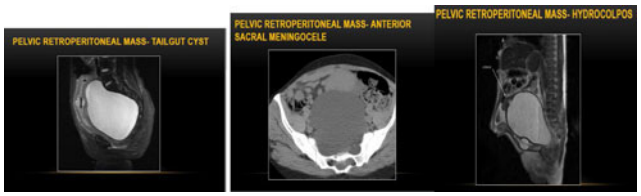

Poster #: EDU-140

Dose Reduction in Pediatric Nuclear Medicine with Emphasis on Appropriate Administered Activities

Michael Gelfand, MD, *Children's Hospital, Cincinnati, OH, michael.gelfand@cchmc.org;* S. Treves

Disclosures: All authors have disclosed no financial interests, arrangements or affiliations in the context of this activity.
Purpose or Case Report: The North American and European administered activity recommendations will be reviewed and compared in this educational exhibit.
Methods & Materials: The joint efforts of European and North American work groups have created consensus documents that suggest appropriate administered activities for pediatric nucear medicine studies.
Results: Administered activities in single photon imaging and positron emission tomography have been reduced and standardized through joint efforts in Europe (the EANM Paediatric Dose Card in 2007 and 2008 and the North American Consensus Guidelines in 2011). Differences between the European and North American recommendations were harmonized through international efforts in 2014. Dose recommendations for additional radiopharmaceuticals have been addressed in 2015 for brain, cardiovascular and thyroid applications. Other contributors have created smartphone applications that are based on the recommended administered activities.
In addition to a review and comparison of the North American and European administered activity recommendations, other dose reduction techniques that can be applied in planar and hybrid imaging will be discussed.
Conclusions: Recommendations for administered activities in pediatric nuclear medicine are available from European and North American sources.

Poster #: EDU-141

Imaging of Multifocal Liver Lesions in Children with Malignancy and/or Immunosuppression

Khaldoun Koujok, MD, *Medical Imaging, Children's Hospital of Eastern Ontario, Ottawa, ON, Canada, kkoujok@cheo.on.ca;* Ahmed Bilal, FRCR, Nishard Abdeen, MD

Disclosures: All authors have disclosed no financial interests, arrangements or affiliations in the context of this activity.
Purpose or Case Report: The purpose of this educational exhibit is to demonstrate the imaging characteristics of several conditions that cause multifocal liver lesions in children that are immunocompromised, have a history of malignancy, or being treated for a malignancy using a radiological multi-modality method.
Methods & Materials: Multiple hepatic lesions are not uncommon findings in children that are immunocompromised, have a history of malignancy, or being treated for a malignancy. It is a challenge for the radiologist to differentiate between several causes such as metastases, fungal/bacterial infections, lymphoproliferative disease, multiple focal nodular hyperplasia, hepatic hemangiomas, and extra medullary hematopoietic marrow.
Many of these conditions have very similar findings on imaging, requiring percutaneous needle or open biopsy for an accurate diagnosis. However, it is possible sometimes to make the diagnosis, or at least narrow it down, depending on imaging characteristics and the clinical presentation.
We are going to present several cases of patients with multiple hepatic lesions as seen on ultrasound, CT, MRI, and Nuclear Medicine (PET CT, HIDA scan). The radiologic appearances of lesions in each modality will be discussed. Imaging findings were correlated with clinical, laboratory, and pathologic information.
Results: In this exhibit, we will present cases of hepatic metastases (neuroblastoma, Wilm's tumor, etc.), fungal/bacterial microabscesses, lymphoproliferative disease, multiple focal nodular hyperplasia, hepatic hemangiomas, and extra medullary hematopoietic marrow. All of these cases were in children that have previous treated malignancy, being treated for malignancy, recently diagnosed with malignancy but not treated yet, or immunocompromised. All of these patients have serial imaging using different modalities.
Conclusions: It is essential for radiologists to be able to recognize the imaging characteristics of multifocal liver lesions in children that are immunocompromised, have a history of malignancy, or being treated for a malignancy. The viewer will be familiar with these imaging characteristics and how to approach the imaging studies and what to look for.

Poster #: EDU-142

Pictorial Review: Median Arcuate Ligament Syndrome

Paul Lewis, MD, *Radiology, Children's National Medical Center, Washington, DC, spencer251@gmail.com;* Anjum Bandarkar, Dorothy Bulas, MD, Timothy Kane

Disclosures: All authors have disclosed no financial interests, arrangements or affiliations in the context of this activity.
Purpose or Case Report: Background: Median Arcuate Ligament Syndrome (MALS) has a long and controversial past. Currently a diagnosis of exclusion, MALS is considered in patients suffering from functional abdominal pain who have typically had extensive prior workups. More common in slender, young women, MALS patients classically present with postprandial epigastric pain, nausea, weight loss, and occasional diarrhea. Since it was first described in 1963, debate has continued as to the pathophysiology of the disease with authors disagreeing whether symptoms are due to mesenteric ischemia and vascular steal phenomenon or compression of the celiac plexus and resulting neuropathy. The association with Postural Orthostatic Tachycardia Syndrome (POTS) in the pediatric population adds further speculation to the exact etiology.
Surgical treatment for MALS is becoming more common, particularly in the pediatric population. Recent technical advances in ultrasound and cross sectional imaging have led to an increased role of diagnostic radiologists in the diagnosis of MALS. Imaging provides an objective measurement in a sea of subjective complaints, with the results often dictating whether surgery is even considered.
Methods & Materials: Since February 2013, over 70 pediatric patients at our institution have had surgical treatment for MALS. We will provide a pictorial review based on our experiences.
Results: We will present a review of MAL anatomy, a summary of the current theories of the pathophysiology, a pictorial explanation of the pertinent findings, and a discussion of what we believe to be the ideal imaging techniques and significant values in pediatric patients based on both our experiences and the most recent literature.
Conclusions: As surgical intervention for MALS becomes more common, it is important for radiologists to be aware of the evolving techniques for for its evaluation.

Poster #: EDU-143 – ***Withdrawn***

Poster #: EDU-144

Radiological Features in Patients with Short Stature Homeobox-Containing (SHOX) Gene Deficiency

Maria Perez, Clinical Fellow, *Diagnostic Imaging, Hospital for Sick Kids, Toronto, ON, Canada, manuela.perez@sickkids.ca;* Oscar Navarro

Disclosures: All authors have disclosed no financial interests, arrangements or affiliations in the context of this activity.
Purpose or Case Report: The objective of this poster is to expose the classical radiological signs associated to SHOX gene insufficiency, giving emphasis to those features that can be visualized in the hand and wrist.
Methods & Materials: Human growth is a multifactorial trait in which genetic factors play a crucial role in the individual's final height and linear limb development. Short stature is defined as height that is more than 2 standard deviations below the mean for age and gender. It is one of the most common reasons for referral to paediatric endocrinologists, and a very important clue in its assessment is determining if it is disproportionate or not. SHOX gene haploinsufficiency (short stature homeobox), discovered in 1997, is an important cause of disproportionate short stature with a very varied fenotype, and has been found to be the molecular basis of the abnormal limb development and short stature seen in a number of diseases such as Turner syndrome and the discondrosteosis. Its clinical expression is more frequent and severe in women, and it tends to manifest and worsen during puberty, which is likely due to its complex interaction with estrogen at the level of the physis. The early recognition of its radiological manifestations can be very important to suggest the directed study of this patients and their siblings, some of which may benefit from therapy with GH.
Results: Several constitutional osseous diseases (including over 100 skeletal dysplasias) are diagnosed postnatally. Most have familar history of short stature or minor skeletal malformations, and the moderate forms may be suspected only based upon mild disproportion of the osseous segments. The recommendations regarding the radiologic studies for short stature patients vary, but there is a general consensus that every child with a suspected disproportion should get a complete skeletal survey.
Conclusions: SHOX gene abnormalities have proven to be the cause of short stature in several of this diseases. A lot of its radiological characteristics can be seen in the AP view of the hand indicated for bone age study, and recognition of these early features, sometimes very subtle, may be pivotal for the diagnosis.

Poster #: EDU-145

Go with the Flow: Characterization of GU Anomalies

Yachao Zhang, MD, *Radiology, Westchester Medical Center, Valhalla, NY, yachao.zhang@wmchealth.org;* Kevin McNerney, MD, Adele Brudnicki

Disclosures: All authors have disclosed no financial interests, arrangements or affiliations in the context of this activity.
Purpose or Case Report: Demonstrate an effective visual learning method by utilizing simple graphics/diagrams with matching real-time case examples including fluoroscopy and ultrasound imaging findings of GU anomalies.
Review the categories of congenital GU anomalies including posterior urethral valves, urachal anomalies and inguinal hernia/hydrocele.
Review the embryology, clinical manifestations and management of these GU anomalies.
Methods & Materials: A comprehensive review of typing of GU anomalies utilizing simple graphics with matching real-time case examples from our institutions.
Review the fluoroscopy and ultrasound techniques and imaging pearls for evaluation of GU anomalies.
Literature review of the embryology, anatomy, clinical manifestations and management of common GU anomalies.
Results: The typing and categorization of posterior valves, urachal anomalies and hydroceles are illustrated via case examples and simple graphics. Embryology, clinical manifestations, anatomy and management of these GU anomalies are reviewed.
Conclusions: Simple graphics is an effective learning tool to organize common GU anomalies.
Despite of the advancement in high resolution imaging, the basic fluoroscopy and ultrasound techniques are simple and effective tools of evaluating GU anomalies with low or no radiation. Therefore, it is essential that residents master the technical and imaging aspects of fluoscopy and ultrasound during residency training.

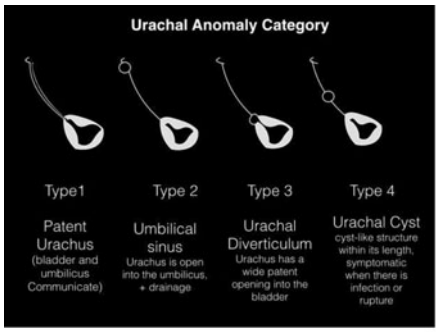

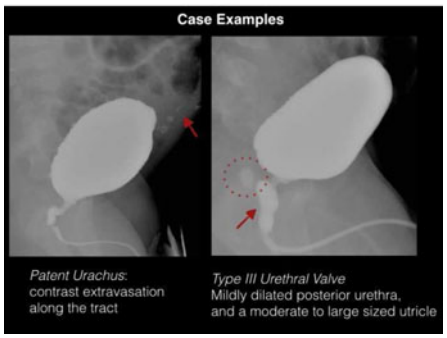

Poster #: SCI-001

Fetal Tracheal Length Estimation from Post Mortem Magnetic Resonance Imaging

Raksa Tupprasoot, Dean Langan, Mike Sury, **Owen Arthurs, FRCR, PhD,** *Radiology, Great Ormond Street Hospital, London, United Kingdom, owen.arthurs@gosh.nhs.uk*

Disclosures: All authors have disclosed no financial interests, arrangements or affiliations in the context of this activity.
Purpose or Case Report: Endotracheal or nasotracheal intubation can be difficult in preterm infants in an intensive care environment, with a high rate of endobronchial tube placement. We measured tracheal length and diameter in a population of post mortem fetuses to define the relationship between gestational age or body weight and tracheal size, in order to see whether this could help future tube selection or correct placement.

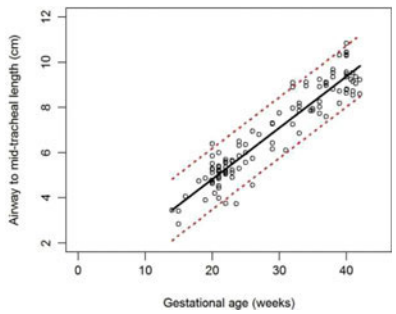

Methods & Materials: Written informed consent was obtained for all patients for clinical pre-autopsy PMMR as part of our institution's clinical post mortem assessment. T_2 weighted isotropic PMMR sequences of the head and chest were retrospectively reconstructed into 3D MPR datasets to identify the airway. We excluded only cases in which the airway was either abnormal, or image quality was inadequate to permit measurements.
We measured trachea length (defined as from mouth to carina; TL), oropharyngeal length (mouth to glottis; OL) and tracheal diameter (internal minimum luminal diameter; TD). Mid-tracheal length was calculated from TL and OL. 20 random datasets were repeated to give a measure of intra-observer and inter-observer variability. Linear regression analysis was performed in SPSS.
Results: 117 cases were analysed, with mean age 27.5±8.3 weeks gestation. We found a good linear relationship between tracheal length and gestational age (TL=0.28 GEST+0.14; R^2=0.91), and mid-tracheal length and gestational age (MTL=0.23 GEST+0.29; R^2=0.94). Tracheal diameter was more difficult to measure, particularly on small fetuses, with poorer linear relationship of TD=0.009 GEST -0.05 (R^2=0.52).
Conclusions: The linear relationship between TL, TD and gestation may help intensive care practitioners to appropriately size and more correctly place endotracheal tube in preterm infants.

Poster #: SCI-002

Paediatric patients with sudden vision impairment – An overview of MRI findings –

Luciana Porto, *Frankfurt University, Frankfurt, Germany, luciana.porto@kgu.de*

Disclosures: All authors have disclosed no financial interests, arrangements or affiliations in the context of this activity.
Purpose or Case Report: Sudden visual impairment in children occurs sporadically, but when present needs urgent attention. Optimal management strategies and timely recognition are required. Often psychogenic disorders are the cause in school-age children; but this is a diagnosis of exclusion. Therefore, MRI plays an important role in ruling out pathology along the optic pathways or helping with the diagnosis of underlying life threatening diseases, such as hydrocephalus or intracranial mass. The purpose of this study was first to evaluate non-traumatic (tumoural and non-tumoural) causes of acute vision impairment; and second, to assess if conventional neuroimaging is helpful children with sudden visual impairment.
Methods & Materials: We retrospectively analysed the MRI scans and clinical findings of 95 children (47 male, 48 female; mean age: 12.5 years, range: from 2 to 17 years) who presented symptoms of monocular or bilateral acute vision impairment.
Results: Patients with acute visual impairment were usually older than 7 years. In 40% of the patients a correlation between the MRI findings and the clinical symptoms was found. The most common causes of visual impairment were: infectious diseases (16%), migraine (12%), autoimmune diseases (11%), optic nerve neuritis with unknown aetiology (8%), neoplasms (8%), idiopathic intracranial hypertension (5%) and orthostatic hypotension (4%). Still, in 23% of the patients the cause remained unclear.
Conclusions: Acute vision impairment is frequently caused by infectious diseases, migraine, autoimmune diseases or tumours in children. Despite the increased recognition of the different causes of the visual impairment with MRI; our analyses suggest that in most part of the paediatric patients the cause for acute visual impairment remains unclear.

Poster #: SCI-003

MR Cholangiography for the Diagnosis of Biliary Atresia in Infants with Jaundice

Mu Sook Lee, assist professor, *Diagnostic Radiology, Jeju National University Hospital, Jejusi, Korea (the Republic of), musuki.lee@gmail.com;* Mi-Jung Lee, Myung-Joon Kim, Hyun Joo Shin, MD

Disclosures: All authors have disclosed no financial interests, arrangements or affiliations in the context of this activity.
Purpose or Case Report: To evaluate the diagnostic value of preoperative MR cholangiography (MRCP) for the diagnosis of biliary atresia in infants with jaundice.
Methods & Materials: We retrospectively reviewed MRCP performed in infants with jaundice for last 2 years at our hospital. We measured the maximum diameter of periportal signal change (MR triangular cord) on axial T1-WIs and axial and sagittal T2-WIs. The diameter of hepatic artery and portal vein and the spleen length was also measured. We also evaluated the visibility of common bile duct and the abnormality of gallbladder. On DWI, we measured ADC value in the homogeneous parenchyma of liver and spleen in each patient. We compared the initial chemistry levels and MR findings between the infants diagnosed with biliary atresia (BA group) and the infants with non-surgical etiology (non-BA group).
Results: Totally 29 infants were included with 17 in the BA group and 12 in the non-BA group. The mean age at the time of MRCP was 7 weeks with the range of 1-12 weeks. On chemistry, only the level of gamma-glutamyltranspeptidase was different between the two groups (median, 316 vs. 98 IU/L in BA vs. non-BA group; p<0.001). On MRCP findings, MR triangular cord was thicker in the BA group than in the non-BA group on all the axial T1-WIs (median, 4.2 vs. 3.1 mm; p=0.004), axial T2-WIs (median, 4.3 vs. 2.9 mm; p=0.011), and coronal T2-WIs (median, 5.0 vs. 2.8 mm; p<0.001). Portal vein was larger in the BA group (median, 4.7 vs. 4.0 mm; p=0.030). Common bile duct was visualized only in one infant (1/17, 6%) in the BA group and all 12 infant (12/12, 100%) in the non-BA group (p<0.001). Gallbladder was abnormal in 16 infants (16/17, 94%) in the BA group and no infants in the non-BA group (p<0.001). The BA group had lower ADC value of liver (median, 0.975 vs. 1.200; p=0.008). However, the ADC value of spleen or spleen size was not different between the two groups.
Conclusions: MRCP demonstrated thicker MR triangular cord on both T1- and T2-WIs, larger portal vein size, non-visualized common bile duct, abnormal gallbladder, and decreased ADC value of liver in infants with biliary atresia which showed the possibility of utility of MRCP for the diagnosis of biliary atresiain infants with jaundice.

Poster #: SCI-004

Visibility of Transient Fetal Compartements on Brain MRI of Preterm and Term Born Infants at Term Equivalent Age: A New MRI Assessment Tool for Estimation of Cerebral Maturity?

Lana Vasung, MD, PhD, *Division of Development and Growth, Department of Pediatrics, University of Geneva, Geneve, Switzerland, lana.vasung@gmail.com;* Cristina Borradori Tolsa, Sylviane Hanquinet, Petra Huppi, Laura Merlini

Disclosures: All authors have disclosed no financial interests, arrangements or affiliations in the context of this activity.
Purpose or Case Report: A spatio-temporal delay in maturation and reorganization of transient fetal compartements, such as subplate zone, Von Monakow segments of white matter, crossroad areas and migrating cell bands, seems to be linked to abnormal brain growth and radial vulnerability(Kostovic et al. 2014) in preterm born infants (PT). The aim of our study was to test the MRI visibility of these transient fetal structures and eventually to compare their appearance patterns in two group of infants: term borns and PT at term equivalent age.
Methods & Materials: Two readers retrospectively reviewed 3D T2 weighted MRI images of 13 term born neonates (mean age=40.1±0.7 GW) and 14 PT (mean age=28.1±2.2 GW) that were acquired on a 3 T Siemens system at term equivalent age. The following was assessed: MRI characteristics of subplate (0=not detectable, 1="patchy" appearance, 2=hyperintense and narrow), von Monakow segments of white matter (0=not discernable, 1=hyperintense, 2=hypointense), presence of crossroads (1=not visible, 2=visible) and presence of migrating glial cells bands (1=visible, 2=not visible). Agreement and reproducibility between readers and visibility difference in the 2 groups

were assessed for each structure by a Cohen Kappa statistic system. Appropriate statistical test (Fischer or *Mann-Whitney U test)* were used.
Results: Inter-observer reliability was high (K=0.8) for detection of subplate, von Monakow segments of white matter and crossroads aspect and perfect (K=1) for presence of migrating glial cells bands. Term born neonates display more mature pattern of subplate zone (Figure 1:red arrows) in frontal and occipital regions (seen as T2 hyperintense narrow band) while in PT this zone had a « patchy » appearance (Table 1). Compared to term borns, PT showed immature (T2 hyperintense) von Monakow segments II and III in frontal, central and occipital regions (Table 1; Figure 1: II-III). C1, C4 and C6 crossroads were visible in majority of term borns, while only C2 and C5 were visible in PT (Figure 2: white arrows). Migrating glial cells bands were equally visible in the two groups.
Conclusions: Fetal transient cerebral structures can be visualized in MRI studies in term and PT babies. Our results suggest that reorganisation of transient fetal compartments is altered in PT (Figure 1, 2). Therefore, these parameters could be in the future included in a new scoring system and further studies are needed to understand if they can be reliable marker for prediction of cognitive and motor development of PT.

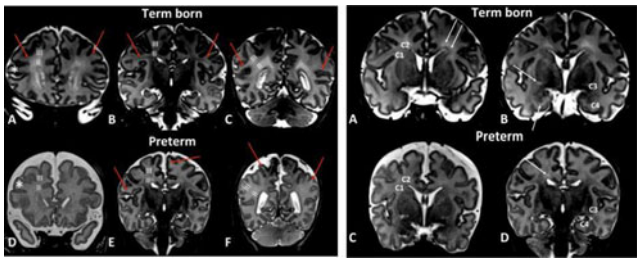

Table 1. Significant differences in MRI signs and T2 properties of transient fetal compartments between prematurely born infants and term born controls.

Crossroads *(T2 hyper intensity of crossroad)*	Prematurely born	Term borns	*p*
C1	50%	92.3%	0.033
C2	78.6%	100%	
C4	14.3%	69.2%	0.006
C6	7.1%	61.5%	0.004
Subplate maturation score			
Frontal	0.5±0.5	1.7±0.5	U=14, *p<0.01*
Central	1.7±0.5	2±0	U=65, *p=0.04*
Occipital	0.8±0.5	1.9±0.3	U=12, *p<0.01*
SUM	3.1±0.9	5.6±0.6	U=4, *p<0.01*
Maturation score of Von Monakow segments			
Segment II frontal	0.7±0.5	1.1±0.3	U=60, *p=0.03*
Segment III frontal	0.9±0.8	1.9±0.3	U=24, *p=< 0.01*
Segment III central	1.6±0.5	2±0	U=58, *p=0.02*
Segment III occipital	1.1±0.5	2±0	U=13, *p=< 0.01*
SUM	12.5±1.6	15.1 ±1.3	U=19.5, *p=< 0.01*

Poster #: SCI-005

Can The Brain Computed Tomography Be Justified In Pediatric Brain Trauma Patients, Under 2 Years?

Sun Kyoung You, M.D., *Radiology, Chungnam National University Hospital, Daejeon, Korea (the Republic of), sunkyou@cnuh.co.kr;* So Mi Lee, Hyun-Hae Cho

Disclosures: All authors have disclosed no financial interests, arrangements or affiliations in the context of this activity.
Purpose or Case Report: To investigate of imaging findings of brain computed tomography (CT) and demographic findings of children with head trauma under 2 years.
Methods & Materials: Seventy-seven patients younger than 2 years who visited emergency department of our institution with head trauma between Mar 2014-Feb 2015, were included in our study (M:F=39:38, mean age=14.31±5.77 months, age range, 0.8-23.8 months). A retrospective review of clinical information and imaging findings of CT scan was performed.
Results: Incidence of brain CT findings were as follows; no acute pathologic findings (*n*=44, 57.1%), isolated scalp swelling or hematoma (*n*=17, 22.1%), skull fracture (*n*=9, 11.7%), skull fracture with EDH (*n*=6) or SDH (*n*=1) (*n*=7, 9.1%). Of 22 patients younger than 12 months, 7 showed skull fracture (31.8%). Of 55 patients between 12 and 24 months, 9 showed skull fracture (16.3%). The most common mechanism of injury was fall from height/fall down stairs (22/33, 66.6%) followed by walked or ran into stationary object (6/33, 18.1%) and fall to ground (5/33, 15.1%). Also, fall from height was the most common injury mechanism in children with skull fracture with/without hemorrhage (13/16, 81.2%). No one did not require surgical treatment until discharge and during follow-up.
Conclusions: No clinically important traumatic brain injury was observed under 2 years in our study. Considering exposure of radiation from brain CT, a careful neurological examination should be performed before brain CT. However, when we face children under 12 months with head trauma, we have to consider the presence of skull fracture with/without hemorrhage.

Poster #: SCI-006

Local experience in utilization of EOS biplanar X-ray imaging system in Asian paediatric patients

Kenneth Cheung, MBBS, *Department of Radiology, Queen Mary Hospital Hong Kong, Hong Kong, Hong Kong, knnth.c@gmail.com;* Damian Lau, Wendy Lam

Disclosures: All authors have disclosed no financial interests, arrangements or affiliations in the context of this activity.
Purpose or Case Report: Our hospital is a local tertiary referral centre for paediatric spinal deformities. Patients were traditionally imaged with digital radiography and secondary digital stitching of images. Repeated imaging is routinely required for monitoring of disease progression.
EOS biplanar X-ray imaging unit is a novel system utilizing slot-scanning technology to acquire high-quality full-length images of patients in an upright weight-bearing position. The EOS system is now commonly used in Western countries. However, studies describing utilization in Asian population has not been published, according to our understanding. This study aims to describe our local experience, in particular lower radiation dose requirements when compared with default settings.
Methods & Materials: Comparison was made with the standard digital radiography system (Discovery XR650 Digital Radiography System, GE Healthcare, Milwaukee, WI) and biplanar X-ray unit (EOS, EOS

imaging, Paris, France), on entrance surface doses and dose area products with respect to patient body height and weight.
Spinal imaging quality was also assessed by paediatric radiologists and paediatric orthopaedic surgeons.
Results: Significant dose reduction can be achieved with EOS imaging system, with satisfactory spinal image quality.
(Conventional imaging mean total dose: 19.09 $dGycm^2$; EOS imaging (lowdose protocol) mean total dose: 662.65 $mGycm^2$; EOS imaging (microdose protocol) mean total dose: 61$mGycm^2$)
Patient throughput is comparable with traditional imaging techniques.
Asian paediatric patients required less radiation dose for image acquisition when compared with default settings optimized for Caucasian population, likely due to thinner body builds with lower body mass indices.
Conclusions: EOS system is a useful imaging tool for paediatric spinal deformities, with significant dose reduction when compared with conventional imaging techniques. Full-length images in upright weight-bearing position can also be acquired.
Tailor-made imaging protocols for Asian population are suggested for further dose reduction and optimization of image quality.
Further studies in characterization of normal geometrical values of the paediatric spine in Asian population are required for accurate utilization of the EOS 3D system.

Poster #: SCI-007

Fetal petrous bone and olfactive bulbs and sulci: a 97 cases prospective study with a 3D high resolution T2 TRUFISP MRI. Contribution to the prenatal diagnosis of CHARGE syndrome

Magali Saguintaah, *Pediatric Radiology, Chu Montpellier, Montpellier Cedex 5, France, m-saguintaah@chu-montpellier.fr;* Alain Couture, ikram taleb arrada, Julie Bolivar Perrin, Catherine Baud, Stephanie David, Olivier Prodhomme, MD

Disclosures: All authors have disclosed no financial interests, arrangements or affiliations in the context of this activity.
Purpose or Case Report: To present a MRI technic to explore the fetal petrous bone (3D high resolution MRI) and choanae, olfactory bulbs and sulci (3D whole brain sequence). To present the clinical applications in fetal detection of CHARGE syndrome. To remind the major diagnostic criteria of CHARGE syndrome.
Methods & Materials: In 2012-2013, 97 fetuses between 27 weeks and 37 weeks of gestation were prospectively explored after maternal informed consent, in addition to the usual brain exploration, with a 3D high resolution T2 sequence with 1.4 mm scans centered on the petrous bones, and a 3D T2 TRUFISP sequence with 1.5 mm scans on the whole brain. The cochlea, vestibule, semicircular canals, choanae, olfactory bulbs and sulci were analyzed.
These anatomical structures, as well as ocular globes, vermis and thymus were studied in 4 fetuses with US suspected CHARGE syndrome.
Results: The cochlea, anterior and lateral semicircular canals were identified in 95.8% of cases. In 4 cases motion artefacts prevented from a good analysis. Olfactory bulbs and sulci were correctly visualized in 94%. Choanae were always visible.
4 fetuses were referred for suspicion of CHARGE syndrome. The US abnormality were a cardiac malformation (3), external ears abnormalities (2), labiopalatine cleft (1), thymic hypoplasia (1).
MRI was performed at 26 weeks to 32 weeks of gestation and showed
3 colobomas
4 absent semicircular canals
3 absent olfactory bulbs and sulci
1 bilateral choanal atresia
2 vermis hypoplasia
2 thymic hypoplasia
CHARGE syndrome was confirmed in all cases. 2 pregnancies were interrupted. 1 baby survived 8 weeks. 1 is 23 months old with multiple impairments.
Conclusions: Antenatal diagnosis of CHARGE syndrome is challenging because of the poor specificity of minor criteria (cardiac, limb, genital, oesophagal, urinary tract and central nervous system malformations, facial cleft) and the high difficulty to assess some of the major criteria: semicircular canal agenesis, arrhinencephalia, coloboma, choanal atresia. The 3D high resolution T2 TRUFISP MRI, as performed in our institution, provides a high sensitive tool to image these anatomical structures and thereby assess the diagnosis. Thymic and vermis hypoplasia are minor criteria that should lead to a petrous bone MRI exploration.
Given the severity of the malformations association in CHARGE syndrome, prenatal diagnostic is useful to help parents counselling and/or interrupt the pregnancy.

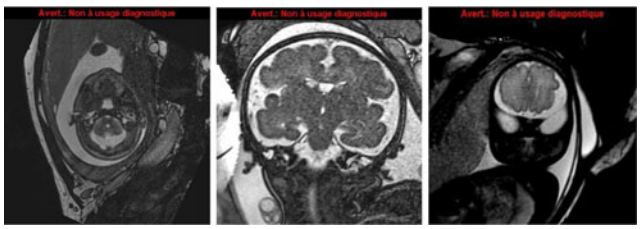

Poster #: SCI-008

Minimal Hepatic Encephalopathy Detected by Brain MRI/ Spectroscopy in Children with Chronic Liver Disease and/or Porto-Systemic Shunting

Sylviane Hanquinet, *Department of Pediatric Radiology, University Children's Hospital of Geneva, Geneva, Switzerland, Sylviane. Hanquinet-Ginter@hcuge.ch;* Claire Morice, Laura Merlini, Vladimir Cousin, Valérie McLin, Mehrak Anooshiravani

Disclosures: All authors have disclosed no financial interests, arrangements or affiliations in the context of this activity.
Purpose or Case Report: The diagnosis of hepatic encephalopathy is mainly detected by neuropsychological tests. These tests, however, do not always apply depending on the status of the child (age, social and cultural environment) and are therefore not reliable for subtle changes. We propose to detect minimal hepatic encephalopathy (minHE) in children with chronic liver disease and/or porto-systemic shunting, using MRI with Diffusion-weighted (ADC) and ^{1}H- spectroscopy in the globus pallidum.
Methods & Materials: Our cohort includes 44 patients (mean age: 120 months ±58): 14 biliary atresia with Kasai operation, 7 hepatic transplant, 7 portal cavernoma, 4 sclerosing cholangitis, 3 cystic fibrosis, 2 Wilson disease, 2 undeterminate cirrhosis, 1 alpha 1 antitryspsin deficiency, 1 congenital hemochromatosis,1 hemolysis-urémia syndrome, 1 Alagille syndrome, 1 tricho-hepato-enteric syndrome. Among them, 8 had a surgical mesenteric-caval shunt at the time of the study and 8 had two MRI.
Fifty-two brain MRI was performed on a 1.5 T magnet to examine T1-weighted / ADC images in pallidi. The cho/Cr, mI/Cr, Glx/Cr ratios were calculated and compared with 25 healthy controls. The relation to serum bilirubin, albumin, ammonium and behavioral changes was analyzed.
Results: Among all MR findings only T1-weighted signal (ROI) and mI/Cr ratio in the pallidi differred significantly between patients and healthy controls (p<0.001). MRI of subjects were divided into 3 groups according to the pallidum T1 signal: normal (n=15), grey (n=15), hyperintense (n=22). There was a significant difference in mI/Cr between healthy and T1 hyperintense subjects (p <0.001) and between normal intensity

and hyperintense subjects (p=0.02). ADC values did not differ significantly between the three groups. There was no correlation with ammonium, bilirubin or behavioral changes. Serum albumin was lower in the hyperintense group when compared to the grey-signal group (p=0.02)
Conclusions: Children with chronic liver disease and/or portosystemic shunting present brain MR patterns compatible with minHE. Serum ammonia and bilirubin concentrations are not predictive of these changes and neuropsychological tests may be difficult to interpret. MR findings may explain neurocognitive difficulties observed in these patients. MRI/spectroscopy should be performed in the initial neurological work up followed by adapted psychological tests. Early diagnosis and treatment is essential in the preservation of brain function in the growing child.

Poster #: SCI-009 – ***Withdrawn***

Poster #: SCI-010

Characteristics of Children with Craniosynostosis and the Possibility of Diagnosing By Ultrasound

Goran Djuricic, *Pediatric radiology, University Children's Hospital, Belgrade, Belgrade, Serbia, gorandjuricic@gmail.com;* Rasa Medovic, Ivana Dasic, Polina Pavicevic, MD,PHD, Dubravka Furtula, Tijana Radovic
Disclosures: All authors have disclosed no financial interests, arrangements or affiliations in the context of this activity.
Purpose or Case Report: Craniosynostosis is the premature fusion of one or more cranial sutures, leading to deformed head shape, increased intracranial pressure and restricted brain growth. The most reliable diagnostic method to use is computed tomography (3D-CT). Aim of this study was to present the characteristics of children with craniosynostosis and to compare US findings with 3D-CT as "gold standard".
Methods & Materials: Cross-sectional study was performed on 225 children suspected of craniosynostosis. All the children were examined using US evaluation of cranial sutures and 3D-CT at the University children's hospital, Belgrade, in the 3-year period. We analysed: gender, age, number of births, gestation week on birth (GW), body weight on birth (BW), difficult delivery (forceps, vacuum), presence of the syndromes, circumference of the head, size of the large fontanelle and head shape. Statistical analysis was done in SPSS 20.0.
Results: Craniosynostosis was confirmed by 3D-CT in 197 (87%) cases, with M:F ratio being 2:1. Diagnosis was confirmed in the period between 5th and 6th month of age in 24% cases and in 3% newborns. 47% patients were firstborns. Mean value of GW was 37,5±2,6 and mean BW was 3026±765 g. In 8% of cases the delivery was completed with forceps or vacuum. There were no children with syndromic craniosynostosis. Mean value of the head circumference was 35±2,5 cm, and mean size of the large fontanelle was 1,1±0,2×0,7±0,1 cm. 40% patients had dolihocephaly. Brachycephaly was present in 22%, plagiocephaly and trigoncephaly in 18% and 17% cases. The most frequent was sagittal (24%) and metopic (21%) craniosynostosis individually, followed by bicoronal and bilambdoid in 16%, while the most rare was the combination of sagittal and bicoronal fusion in 2% cases. In 42% of cases the existence of craniosynostosis was confirmed by US, from which 68% had sagittal craniosynostosis, individually or in combination with the other fusions. Bicoronal and bilambdoid fusions were not recognized at US.
Conclusions: In our cohort children with craniosynostosis was in most cases male, firstborns, with a slightly smaller head circumference and large fontanelle, with dolihocephalic head shape and sagittal or metopic fusion. In addition to the 3D-CT, US evaluation of cranial sutures can be used, especially in the case of sagittal stenosis. Thus it can be avoided unnecessary radiation of children.

Poster #: SCI-011

Comparison of Postmortem Ultrasound and X-Ray with Autopsy in Fetal Death: Retrospective Study of 169 Cases

Olivier Prodhomme, MD, *Pediatric Radiology, Arnaud de Villeneuve Hospital, Montpellier, France, o-prodhomme@chu-montpellier.fr;* Catherine Baud, Magali Saguintaah, Julie Bolivar Perrin, Stephanie David, ikram taleb arrada, Alain Couture

Disclosures: All authors have disclosed no financial interests, arrangements or affiliations in the context of this activity.
Purpose or Case Report: To present the technique and the images obtain by postmortem ultrasound in the particular setting of fetal death and discuss its abilities and limitations.
To compare the diagnostic yields of joint analysis of ultrasound and X-Ray compared to autopsy in the setting of fetal death.
Methods & Materials: Retrospective study of postmortem fetal ultrasounds performed between January 2009 and December 2013 in addition to X-Ray in the work-up for cases of fetal death. Inclusion criteria were a complete anatomical ultrasound study and the availability the foetopathology report. Cases with autopsy refusals were excluded. When cases of TOP were included, antenatal imaging data (US, CT and/or MRI) were available. All scans were performed by a senior pediatric radiologist. Foetopahtology was performed by senior foetopathologists and pathologists aware of fetal medicine.
Results: We collected 169 patients. The gestational age was 27 weeks +/- 6 days [15-38WG]. The population consisted mainly of fetuses originating from TOP (164/169 [97%]). Only 5 cases involved in utero fetal deaths (IUFD). Half (49.2%) of the conditions involved were cerebral.
The duration of the exam was about 10-15 min.
Complete concordance between the findings of postmortem imaging and autopsy was observed in 81% [137/169] of cases.
Conclusions: Ultrasound allows a comprehensive post-mortem study complementary to standard X-Rays. In fetal deaths situations, ultrasound is much more relevant than in any other postmortem conditions. Ultrasound, although less effective than MRI, shows a benefit/drawback balance that proves very interesting, especially in the youngest fetuses. Besides it is more available and realistic to use it in a systematic practice.

Poster #: SCI-012

Variations of Lower Spine and Ribs: Possible Pitfalls in Spinal Ultrasonography

Yoshiyuki Tsutsumi, *Radiology, National Center for Child Health and Development, Tokyo, Japan, tsutsumi-y@ncchd.go.jp;* Reiko Okamoto, Mikiko Miyasaka, Osamu Miyazaki, Masaya Ishii, Ayako Muto, Haruka Okada, Hiroko Hara, Shunsuke Nosaka, MD

Disclosures: All authors have disclosed no financial interests, arrangements or affiliations in the context of this activity.
Purpose or Case Report: To assess the level of the conus medullaris using spinal ultrasonography, bony landmarks such as the lowest ribs, the most caudal ossification center (MCOC) of the vertebral body, and angulation in the lumbosacral region are used. However, determining the level of the conus medullaris is sometimes difficult because of the variations of these landmarks.
Purpose of this study was to analyze the variation of these landmarks. However, it is difficult to evaluate these variations using ultrasonography, because this method allows a narrow field of view. To supplement this limitation, we tried to evaluate these landmarks retrospectively using (1) whole spine CT or (2) lumbosacral CT in combination with chest radiography.

Methods & Materials: Patients aged less than 4 months who underwent spine CT for at least the lumbosacral region at our institution were included. Patients with vertebral segmentaion anomalies, severe vertebral deformity, known bone dysplasias, and sacrococcygeal teratomas were excluded.

In patients who underwent whole spine CT, MCOC were counted down from the C2 on sagittal reformatted CT images. In patients who did not undergo whole spine CT, chest radiograph was referred and MCOC were counted down from the 12th thoracic spine or equivalent vertebra. Angulation of the spine in the lumbosacral region was determined similarly. We also correlated the level of the landmarks using full spine MRI. The number of ribs was counted using 3D reconstructed imaging and chest radiography.

Results: A total of 155 CT studies (99 patients) were included in this study. Whole spine CT was performed in 31 studies, and only caudal to the lower thoracic vertebrae were scanned in 124 studies. About 10% of the patients did not have 12 pairs of ribs. MCOC was located at the S5 (or S5 equivalent) in 42% of patients aged less than 1 month. MCOC tends to be more caudally located with age. The angulation in the lumbosacral region was formed by the 24th and 25th vertebra from the C1 in 97% of patients.

Conclusions: It might be difficult to determine the level of the conus medullaris using a single anatomical landmark, and a combination of the multiple landmarks might result in more precise level determination. Knowledge about the variations in the lumbosacral spine and ribs might be useful for evaluating the level of the conus medullaris in a spinal ultrasonography.

Poster #: SCI-013

Patient-Related Factors Affecting Radiation Dose for Pediatric Abdominal CT

Ji Eun Park, Fellow, *Radiology, Seoul National University Children's Hospital, Seoul, Korea (the Republic of), zerocool-je@hanmail.net;* Young Hun Choi, Jung-Eun Cheon, Woo Sun Kim, In-One Kim, Hyun Suk Cho

Disclosures: All authors have disclosed no financial interests, arrangements or affiliations in the context of this activity.

Purpose or Case Report: The use of pediatric abdominal CT has been increasing rapidly. However increased radiation exposure is a public health concern for children because of children are more sensitive to radiation than adults. The purpose of this study is to estimate which patient-related factors affect radiation dose, to pediatric patients undergoing abdominal CT

Methods & Materials: The data evaluated had been recorded for 434 pediatric abdominal CT between November 2013 and May 2015. Of these exams, 284 (153 boys, 131 girls; mean age 7.1±4.8 years) were included in this study and retrospectively reviewed. The patients were divided according to their age (0-2, 3-5, 6-10 and 11-15 years old) at the time of performing abdominal CT and we calculated the size-specific dose estimates (SSDE). In each age groups, the patients who have the highest 25% of SSDE value were classified as Group 1 and the patients who have the lowest 75% of SSDE value were classified as Group 2. The age, BMI, arm positioning (both arms up, both arms at sides, right arm up, and left arm up), leg positioning (both legs down, both legs at sides, right left down, and left down) and patient centering (distance between data collection center and reconstruction target center) were evaluated and compared between two groups. The factors influencing increased radiation dose were evaluated by univariate and a multivariate logistic regression model

Results: Seventy patients included in Group 1 and 214 patients included in Group 2. The average of SSDE was statistically significant differences between the two groups (5.68±2.39 in Group 1 and 3.80±1.47 in Group 2, $P<0.001$). BMI was statistically significantly higher in the Group 1 than Group 2 ($P<0.001$). In 12 cases (17%) and 6 cases (2%) in Group 1 and 2 respectively, both or one arms were at sides. Statistically significant differences in arm positioning were found between the two groups ($P<0.001$). Age, leg positioning and patient centering did not show significant differences between two groups. Arm positioning and BMI were significant risk factors for an increased radiation dose, as confirmed by univariate and multivariate analyses

Conclusions: Children have the higher radio-sensitivity compared with adults. For children, it is important to reduce the radiation dose. We evaluate the patient-related factors affecting radiation dose for pediatric abdominal CT. The patient BMI and arm positioning are important factors of radiation dose for pediatrics

Poster #: SCI-014

Optimizing Thresholds for Computed Tomography Angiography in Young Children Considered Varying Hounsfield Units at Different Tube Voltages

Eszter Nagy, *Department of Radiology, Division of Pediatric Radiology, Medical University Graz, Graz, Austria, eszter.nagy@medunigraz.at;* Robert Marterer, Sebastian Tschauner, Franz Lindbichler, Erich Sorantin

Disclosures: All authors have disclosed no financial interests, arrangements or affiliations in the context of this activity.

Purpose or Case Report: Children have up to 10 times higher sensitivity to ionising radiation, therefore dose reduction is still a hot topic in paediatric computed tomography (CT). One of the most effective dose reduction tools is decreasing tube voltage. Because of the exponential relationship between radiation dose and peak kilovoltage, tube voltage should be adjusted according to age. Since Hounsfield units (HU) are depending on the radiation dose, different computed tomography angiography (CTA) thresholds for different tube voltages should be considered.

This study was designed to demonstrate the alteration of HU depending on varied tube voltage and furthermore to consider the necessity of consequently modified CTA threshold values.

Methods & Materials: Nine different samples (water, air, fat, and six samples with different concentration of contrast agent) were included in a phantom, which was scanned with three different tube voltages (120 kV, 100 kV, 80 kV). The same radiation dose (10.4 DLP) was obtained in every scans, therefore the relevant parameters were corresponding modified. HU of different samples were measured in all scans and afterward compared to each other. Measurements at 120 kV were served as reference.

Results: Compared to reference values HU has changed at 100 kV and at 80 kV up to 18.79% and 50.42%, respectively. The lower tube voltage is associated with increased HU.

Corresponding to these data there was found also increased (up to 17.13% at 100 kV and up to 47.08% at 80 kV) HU according the CTA thresholds (100-400 HU).

Conclusions: Decreased tube voltage from 120 kV to 100 kV or to 80 kV is followed by alteration in CT Hounsfield units. Therefore CTA thresholds should be adapted to tube voltage.

Poster #: SCI-015 – ***Withdrawn***

Poster #: SCI-016

Imaging and Clinical features of Congenital Neuroblastoma: Special focus on a cystic type

Sook Min Hwang, *Radiology, Samsung Medical Center, Seoul, Korea (the Republic of), okanagan@naver.com;* So-Young Yoo, Ji Hye Kim, Tae Yeon Jeon, MD

Disclosures: All authors have disclosed no financial interests, arrangements or affiliations in the context of this activity.
Purpose or Case Report: Neuroblastoma (NB) is the most common malignancy in neonate and infancy, and, furthermore, growing use of prenatal US has led to increased detection of congenital NB. This study aims to evaluate imaging assessment and clinical features of congenital NB with a special focus on cystic NB.
Methods & Materials: A total of 53 cases (M:F 24:29, mean age 1.27 months) with surgically confirmed congenital NB in a single tertiary center was enrolled. We reviewed imaging features including location, cystic vs non-cystic and presence of metastasis. We also evaluated clinical features including outcome.
Results: Out of 53, 28 tumors (53%) were detected prenatally and, in the remaining, the most common presentation was abdominal distension. The location was as following; adrenal gland (n=41, 77%), mediastinum (n=6, 11.3%), extraadrenal retroperitoneum (n=5, 9.4%), chest wall (n=1, 1.8%). Out of 41 adrenal NB, 41% (n=17) appeared cystic as a complex cyst (n=16) or a purely cystic type (n=1) based on US findings and all of cystic tumor were detected prenatally. All of tumors in the other sites were solid. In terms of imaging modality for initial diagnosis, US (n=53) followed by CT (n=47) or MR (n=10) was performed. In cystic NB (n=17), there was no additional diagnostic information by CT/MR compared with US. All of metastasis (IVS n=8, IV n=7) were noted in non-cystic NB including liver (n=12), lymph node (n=3), and bone marrow (n=1). Out of 53, 9 were n-myc amplified tumors (16.8%) and among them, 3 tumors were cystic NB (17.6%). Most of the cases (n=49, 92.4%) showed good outcome without relapse for mean 59.6 month follow-up.
Conclusions: Congenital NB often appears as a prenatally detected adrenal cystic lesion with overall good prognosis. US seems to be the only imaging tool needed in the cystic type.

Poster #: SCI-017

Structured Reporting in Hypoxic-Ischemic Encephalopathy – Initial Experiences

Andrea Lakatos, *MR Research Center, Semmelweis University, Miskolc, Hungary, drea820317@gmail.com;* Marton Kolossvary, Miklos Szabo, Mate Kiss, Gyula Gyebnar, Zsolt Bagyura, Lajos Rudolf Kozak

Disclosures: All authors have disclosed no financial interests, arrangements or affiliations in the context of this activity.
Purpose or Case Report: The radiology report is a tool to communicate information to the referring physician and record data for follow-up or research purposes. With structured reporting templates information becomes uniform, comprehensive and easily manageable. In collaboration with neonatologists and information technologists we developed a structured MRI reporting template for neonatal hypoxic-ischemic encephalopathy (HIE).
Methods & Materials: A systematic reporting template (iSORT for HIE) was developed based on the literature data and the retrospective analysis of 50 term neonates with the clinical diagnosis of asphyxia. MRI studies were performed with a Philips Achieva 3 T MR scanner between 2007 and 2014. The key findings on T1-, T2-, T2*/SWI, diffusion weighted MR images and single voxel MR-spectroscopy were evaluated. The proposed reporting system, iSORT for HIE is an "easy walk through" template in a web-based framework, which we initially started using in research.
Results: The iSORT outline follows a tree structure, directs focus on the most characteristic imaging findings seen in neonatal HIE. Although the full reporting template consists of about 500 questions, only the relevant headings and subheadings are to be filled as the report progresses. The first section is composed of patient data and the technical aspects of the MRI examination. The second part records signal intensity changes in nested anatomic landmarks. We created a third section with an objective and semi-objective scaling system, to evaluate neonates with a baseline MRI study and a 2-year follow-up neurologic examination.
Conclusions: Here we introduced iSORT for HIE, a novel structured reporting template for MRI examinations. Getting used to the iSORT system, the data recording is faster and the information is more detailed compared to a conventional report. The search for a particular term is easily achievable with only a mouse-click input. Besides the benefits in research, the template is useful in the everyday clinical practice by reducing interpretation ambiguity. Hence it may have a direct positive impact on patient care.

Poster #: SCI-018

Vessel Flexibility Index as a Potential New Marker for Cardio-Vascular Disease - A Pilot Study

Eszter Nagy, *Department of Radiology, Division of Pediatric Radiology, Medical University Graz, Graz, Austria, eszter.nagy@medunigraz.at;* Clarina Wieser, Jana Windhaber, Kristina Kogler, Monika Steinberger, Erich Sorantin

Disclosures: All authors have disclosed no financial interests, arrangements or affiliations in the context of this activity.
Purpose or Case Report: Morphological and functional carotid artery alteration can occur already in youth ages, essentially in presence of cardiovascular risk factors. Studies have showed that sonographic assessment of carotid artery (CA) Intima-Media Thickness (IMT) serves as prognostic factors for cardio-vascular disease also in youth patient population. As functional changes occur earlier than vessel wall morphological changes, this might be indicated by a decrease in vessel elasticity prior to the increase of IMT. This hypothesis indicates to use an early functional parameter for cardiovascular risk assessment.
This study was designed to assess and evaluate IMT as well as CA vessel elasticity in three groups, in young sportsmen and youth volunteers without any cardio-vascular risk factors (CV-RF) comparing to youth volunteers with CV-RF.
Methods & Materials: 60 subjects (14-35 years) were enrolled: 27 sportsmen, 16 youth volunteers with and 17 without CV-RF respectively. IMT was determined by B-Mode-US. Vessel elasticity was characterized by vessel flexibility index (VFI): minimal (Min) and maximal (Max) CA cross-sectional area values were obtained with B-Mode sonography during the cardiac cycle and afterward VFI was calculated on the following way: VFI=(Min*100)/Max.
Results: Mean and SD values for IMT were in volunteers without and with CV-RF and in sportsmen 0.42±0.04 mm; 0.48±0.06 mm; and 0.27 mm±0.05 mm respectively.
Mean and SD values VFI was found in volunteers without and with CV-RF and in sportsmen 21.53±3.94%; 17.7%±3.5%; and 27.05%±4.15% respectively.
For IMT and VFI significant differences (p<0.05) were found between volunteers without and with CV-RF, percentage difference was found 14.6% and 21.6% respectively.
Conclusions: VFI and IMT were able to discriminate between all groups, but VFI scored better than IMT (bigger percentage difference). Therefore VFI could serve as a more sensitive parameter characterising cardio-vascular risk, but to prove this statement more data is needed.

Poster #: SCI-019

Right Ventricular Function Assessed by Cardiac MRI: Impact of Right Branch Bundle Block on the Evaluation of Axial Plane Volume Measurements

Eszter Nagy, *Department of Radiology, Division of Pediatric Radiology, Medical University Graz, Graz, Austria, eszter.nagy@medunigraz.at;* Robert Marterer, Sebastian Tschauner, Gernot Grangl, Erich Sorantin

Disclosures: All authors have disclosed no financial interests, arrangements or affiliations in the context of this activity.
Purpose or Case Report: Right ventricular (RV) function represents a prognostic marker in patients with congenital heart defects (CHD), essentially in patients with right bundle branch block (RBBB). Due to the limitations of echocardiographic ventricle volume assessment, cardiac magnetic resonance imaging (CMR) is nowadays the method of choice in the follow-up of these patients.
In a recently published study it has been shown that delayed RV contraction due to RBBB should be taken into account when performing CMR volumetric assessment with short axis plane method.
Since recent recommendations suggest axial plane volume measurements, therefore current work was designed to assess the impact of RBBB on cardiac volumetric parameters evaluated with the axial plane method.
Methods & Materials: 38 patients (aged 25.9±11.9 years) with Tetralogy of Fallot and RBBB were enrolled in this retrospective study. With post-processing CMR images RV end-systolic volume (ESV) and end-diastolic volume (EDV) were measured with axial plane method twice: once neglecting RBBB (group I) and once considering RBBB (group II). Consequently, RV stroke volume (SV) and RV ejection fraction (EF) were calculated separately for each group and then compared with each other. All of the measurements were obtained separately by two observers, one with many years, one with just a few experiences. Inter-observer agreement was also calculated regarding the RV volumetric data of all patients.
Results: A delayed RV contraction due to RBBB has been found. Therefore, RV-ESV of group I was 10.68%±5.08 higher compared to group II. Accordingly RV-SV and RV-EF were 19.1%±12.3 higher in group II. All of these differences were statistically significant ($p<0.001$). With considering RBBB EF shifted from reduced (<50%) to normal (≥50%) in 8% of the cases. A substantial intra-observer agreement ($\kappa=0.68$; 95% CI: 0.57-0.78) was found between the two observer regarding the right ventricle measurements.
Conclusions: Results confirm that delayed RV contraction due to RBBB should be also considered at CMR based volume measurements with axial plane method. Ignoring RV physiology in RBBB patients leads to underestimation of RV performance parameters respectively RV function.

Poster #: SCI-020

Radiological Characterization of Congenital Lower Gastrointestinal Tract Abnormalities in Children

Ana Coma, *Hospital Vall d'hebrón, Barcelona, Spain, acoma@vhebron.net;* Goya Enriquez, Pilar Garcia - Peña, Ignasi Barber, MD, Amparo Castellote, Joan Carles Carreno, Elida Vazquez, MD

Disclosures: All authors have disclosed no financial interests, arrangements or affiliations in the context of this activity.
Purpose or Case Report: To review common and uncommon congenital lesions affecting the lower gastrointestinal tract in children.
To illustrate the radiologic features of these conditions using various imaging techniques.
To provide tips to avoid potential diagnostic errors.
Methods & Materials: Congenital abnormalities of the lower gastrointestinal tract (GI) are relatively common in children and present in a wide range of clinical settings. In most patients, the clinical symptoms appear at birth, whereas in others, the manifestations appear later. They may be an incidental finding or present with an acute onset in neonates, infants, older children, and even in adults.
Radiological examination is essential to suggest the diagnosis. Although abdominal radiography and contrast gastrointestinal examination can provide the diagnosis, imaging features may be challenging. Exquisite ultrasonography technique, Computed Tomography CT and Magnetic resonance imaging (MRI) may be helpful in selected cases.
Results: The clinical presentation, imaging features, and diagnostic approach for congenital lower GI tract abnormalities are discussed. Associated abnormalities are reviewed.
Conclusions: Radiologists have an important role in the diagnosis of congenital upper gastrointestinal tract abnormalities, although the imaging features may be challenging.
Awareness of these common and uncommon abnormalities and its associations will guide radiological investigation and lead to an accurate diagnosis, which may be crucial for prompt, adequate treatment of conditions that are life-threatening in some cases.

Poster #: SCI-021

Role of Diffusion-Weighted MRI in Differentiation of Wilms Tumor and Neuroblastoma

Mine Aslan, MD, *Istanbul University, Cerrahpasa Medical School, Istanbul, Turkey, mineus_77@yahoo.com;* Hatice Arioz Habibi, Ayse Kalyoncu Ucar, Evrim Ozmen, Ahmet Aslan, Selim Bakan, Onur Yildirim, Sebuh Kurugoglu, Ibrahim Adaletli

Disclosures: All authors have disclosed no financial interests, arrangements or affiliations in the context of this activity.
Purpose or Case Report: The diagnosis of Wilms tumor and adrenal gland neuroblastoma can be challenging, even with imaging methods such as computed tomography and magnetic resonance imaging (MRI). This study aimed to show the utility of diffusion weighted MRI (DW-MRI) in the differentiation of neuroblastoma and Wilms tumor.
Methods & Materials: Eleven histopathologically diagnosed tumors (7 neuroblastoma and 4 Wilms tumor) were evaluated in 11 patients retrospectively. The patients were scanned on a 1.5 Tesla magnetic resonance scanner (Siemens Avanto 1.5 T Magnetom, Siemens AG Medical Solutions, Erlangen, Germany) and DW-MRI was performed with b-values of 50, 400, and 800 s/mm^2 for all patients. The apparent diffusion coefficient (ADC) values (mm^2/s) of the tumors were evaluated by means of region-of-interest (ROI) measurements on a workstation (Syngo Via Console, software version 2.0, Siemens AG Medical Solutions, Erlangen, Germany). T2-weighted axial images were used as a reference to avoid measurements from cystic, necrotic and hemorrhagic areas of the tumors. The mean age (months), size (cm), and ADC values were compared with each other. Receiver operating characteristic analysis was performed to obtain the optimal cut-off value. Statistical significance was set as $p<0.05$.
Results: The mean size was 14.37±4.6 cm for Wilms tumor and 8.17 ±3.45 cm for neuroblastoma. The mean age was 62.5±16.29 months for Wilms tumor, and 28.5±17.43 months for neuroblastoma ($p=0.017$). The mean ADC was $0.607\times10^{-3}\pm0.148\times10^{-3}$ mm^2/s for neuroblastoma and $0.829\times10^{-3}\pm0.89\times10^{-3}$ mm^2/s for Wilms tumor ($p=0.013$). A cut-off ADC value of ≥ 0.733 for differentiating Wilms tumor from neuroblastoma had a sensitivity of 100%, specificity of 85.7%, positive predictive value of 87.4%, and negative predictive value of 100%.
Conclusions: Although the numbers of tumors were relatively small in this study, the mean ADC value of Wilms tumor was significantly higher than the mean ADC value of neuroblastoma. This finding could be helpful when the detection of the mass origin is challenging, and DW-MRI should be added to abdominal MRI protocols in patients with suspected Wilms tumor or neuroblastoma.

Poster #: SCI-022

Diffusion Tensor Imaging in Evaluation of Muscles in Patients with Congenital Muscular Torticollis: A Pilot Study

Hyun Gi Kim, *Department of Radiology, Ajou University School of Medicine, Suwon, Korea (the Republic of), catharina315@aumc.ac.kr*

Disclosures: All authors have disclosed no financial interests, arrangements or affiliations in the context of this activity.

Purpose or Case Report: Congenital muscular torticollis (CMT) is a common disorder of the musculoskeletal system in neonates and infants. Most CMT patients can be treated with stretching exercise but some patients with do not response to the treatment. Diffusion tensor imaging (DTI) is an emerging tool to measure and evaluate skeletal muscle injury. Our aim was to evaluate whether DTI has potential to show the difference in the affected muscle in CMT patients.
Methods & Materials: Six CMT patients (22.3±30.8 months) for whom conservative management was not successful were selected by a clinician and were evaluated using DTI. Fractional anisotropy (FA) and mean diffusivity (MD) of the involved sternocleidomastoid (SCM) muscle were compared with that of the intact SCM muscle on the other side.
Results: The mean FA value of the involved SCM muscles was significantly higher than that of the intact SCM muscles (0.437±0.051 vs. 0.364 ±0.022, P=0.009). The mean MD value of the involved SCM muscles was not significantly different to that of intact SCM muscles (0.155 ±0.019 vs. 0.155±0.018, P=.979).
Conclusions: DTI measures of FA values were significantly higher in the involved SCM muscles in patients with CMT. This may reflect the subtle change in the involved muscle which may progress in later stages and become fibrotic. Further studies correlating the DTI values with clinical outcome are needed.

Poster #: SCI-023

Three-dimensional, T1-weighted Gradient-Echo Imaging of the Brain with a Radial Sampling of *K-Space*: An Alternative Technique to Reduce Motion Artifacts in Breathless Children

Ji Eun Park, Fellow, *Radiology, Seoul National University Children's Hospital, Seoul, Korea (the Republic of), zerocool-je@hanmail.net;* Young Hun Choi, Jung-Eun Cheon, Woo Sun Kim, In-One Kim, Hyun Suk Cho

Disclosures: All authors have disclosed no financial interests, arrangements or affiliations in the context of this activity.
Purpose or Case Report: Brain MRI in children is often limited by motion artifacts. Radial k-space sampling techniques have been shown to reduce motion artifacts.
To compare a contrast-enhanced radial volumetric interpolated brain examination (radial VIBE) sequence with a magnetization-prepared rapid acquisition gradient echo (MP-RAGE) sequence in pediatric brain MR imaging.
Methods & Materials: Twenty consecutive children underwent post-contrast brain MR examinations with axial radial VIBE and MP-RAGE. For qualitative assessment, we retrospectively scored motion and vascular pulsation artifacts, lesion conspicuity, vascular enhancement and overall image quality. For quantitative analysis, signal variations and signal-to-noise ratios (SNRs) of the gray and white matters for each sequence were calculated.
Results: Motion and pulsation artifacts were significant reduced in radial VIBE than MP-RAGE (score 1.8±0.8 vs. 1.0±0, 1.9±0.6 vs. 1.0±0 respectively, P<0.05). Lesion conspicuity and vascular enhancement scores were similar between the both sequences (P=0.06 and P=0.1, respectively). Overall image quality scores were also similar for both sequences (P=0.57). However, in children showing motion artifacts, radial VIBE showed better overall image quality compared to MP RAGE (score 2.9 ±0.5 vs. 3.5±0.4, P<0.05). The radial VIBE was associated with diminished signal variations, while SNRs of the gray and white matters were significantly higher in MP-RAGE SNR.
Conclusions: The radial VIBE reduced motion and pulsation artifacts in pediatric brain imaging and overall image quality was improved with radial VIBE in children with motions. Therefore, the radial k-space sampling technique could be a good alternative to MP-RAGE for the brain MR imaging of restless children.

Poster #: SCI-024

Intrauterine Repair of Open Neural Tube Defects: Prenatal and Postnatal Magnetic Resonance Imaging Considerations

Elida Vazquez, MD, *Pediatric Radiology, Hospital Universitari Vall d'Hebron, Barcelona, Spain, evazquez@vhebron.net;* Ignacio Delgado, Angel Sanchez-Montañez, Ignasi Barber, MD

Disclosures: All authors have disclosed no financial interests, arrangements or affiliations in the context of this activity.
Purpose or Case Report: Open spinal dysraphism occurs as a consequence of failed neurulation during embryological development and includes two subtypes, myelomeningocele and myelocele. Intrauterine fetal repair can result in reversal of the associated Chiari II malformation and is now considered a treatment option.
The main imaging method for prenatal detection, management, and monitoring of open neural tube defects is US, but MRI is essential for the preoperative assessment, indications and workup for fetal surgery, and postnatal follow-up. This prospective study describes the contribution of MRI in this clinical scenario.
Methods & Materials: Fourteen fetuses underwent prenatal closure of myelomeningocele (9) or myelocele (5) over the last 5 years. Gestational age was below 27 weeks (19-26 weeks). The first 7 fetuses underwent surgery using a conventional laparotomic approach, whereas a fetoscopic approach was used in the last 7 fetuses.
Prenatal MR images were obtained on a 1.5 T system (Avanto; Siemens, Erlangen, Germany), using a phased array abdominal coil. Axial, sagittal, and coronal HASTE, T1 fast low-angle shot (GRE), axial T2 GRE, and axial DWI sequences were part of the routine examination of the fetal spine and brain. Fetal sedation was not used. All cases were examined at least 3 times by MR imaging: preoperatively, immediately after prenatal surgery, and postnatally. All MR images were interpreted by at least 2 experienced pediatric neuroradiologists.
Results: The assignment of lesion level, verification of Chiari II, and ventricular size were similar by prenatal US and MRI. The main contribution of prenatal MRI was to confirm or exclude the indication for surgery.
During postoperative prenatal MRI some relevant parameters were analyzed, including posterior fossa size and lower cerebellar position,

visualization of the 4th ventricle and CSF posterior fossa spaces, improvements in ventricular size, and presence or not of adequate coverage of the neural defect. Confirmation of this last factor was the most challenging task for MRI.

Postnatal MRI can clarify patch-related fistula, need for VP shunt, and postnatal Chiari status.

Conclusions: Recent advances in fetal repair of open neural defects, such as earlier closure in gestation and development of less invasive approaches, require parallel improvements in the fetal MRI technique.

The information provided by MR imaging beyond US findings makes MR essential in the workup and follow-up of intrauterine repair of open neural tube defects.

CASE EXAMPLE 1

Prenatal pre-closure MRI

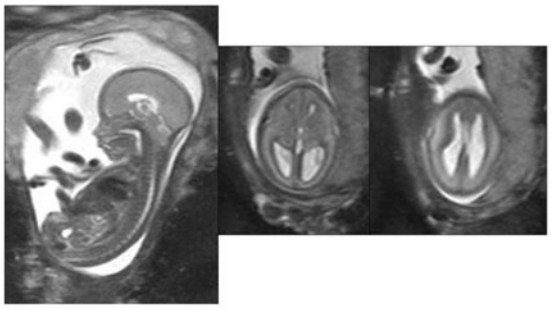

Prenatal post-closure MRI

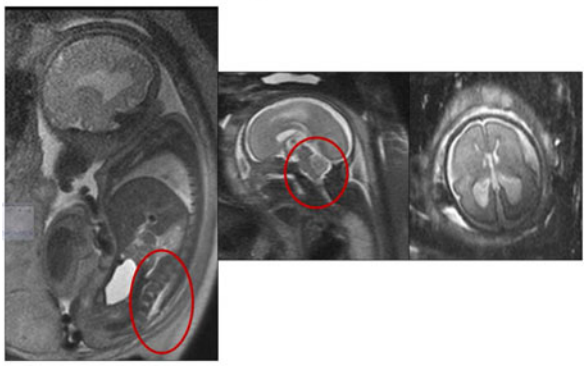

Postnatal MRI

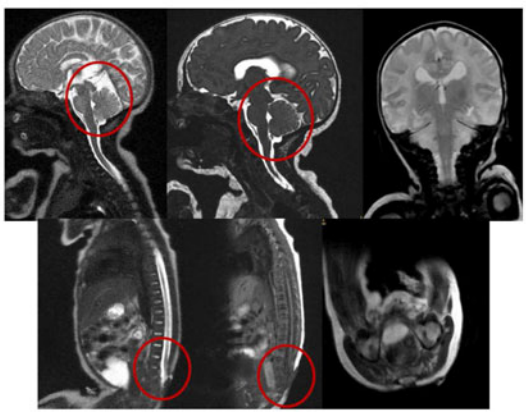

CASE EXAMPLE 2

Prenatal pre-closure MRI

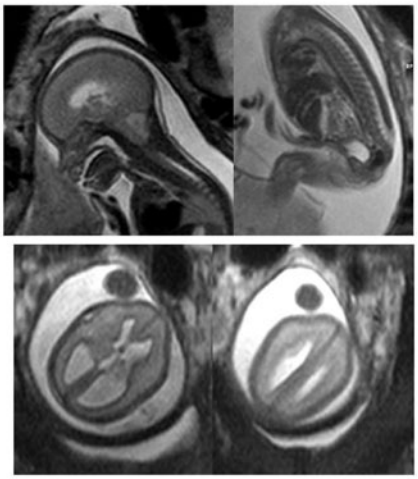

Prenatal post-closure MRI

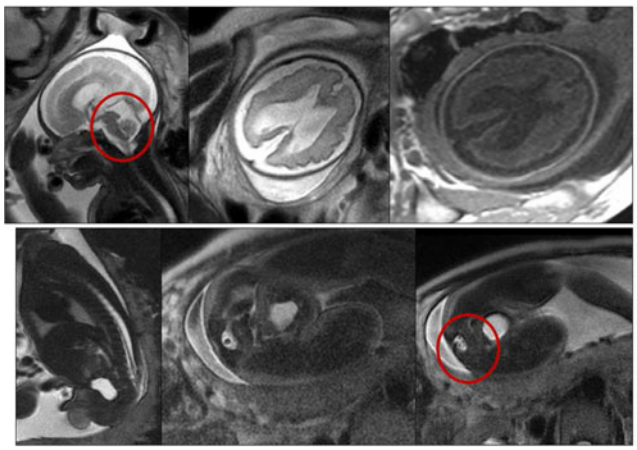

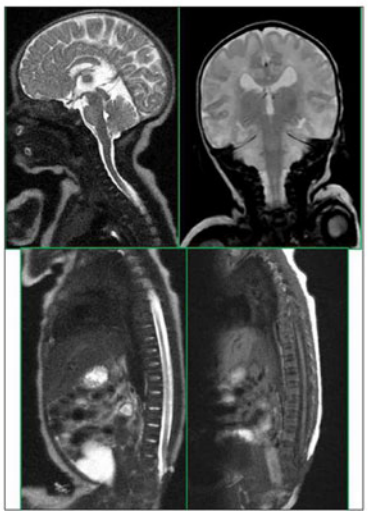

Poster #: SCI-025 – ***Withdrawn***

Poster #: SCI-026 – ***Withdrawn***

Poster #: SCI-027

Serum Biochemical Markers to Predict Radiologic Metabolic Bone Disease in Preterm Infant

Sun Kyoung You, MD, *Radiology, Chungnam National University Hospital, Daejeon, Korea (the Republic of), sunkyou@cnuh.co.kr;* So Mi Lee, Hyun-Hae Cho

Disclosures: All authors have disclosed no financial interests, arrangements or affiliations in the context of this activity.
Purpose or Case Report: To assess the relationship between radiographic findings and biochemical markers, such as serum alkaline phosphatase (ALP), used for screening of metabolic bone disease (MBD) in preterm infants.
Methods & Materials: Preterm infants who underwent serial wrist radiographs and biochemical studies in our neonatal intensive care unit between January and November 2014 were studied. Retrospective review of biochemical studies and wrist radiographs was performed. Patients were subdivided into four groups according to MBD severity by the wrist radiographs for the first analysis and into two groups according to presence of MBD for the second analysis.
Results: Twenty-seven (61.3%) and 6 (13.6%) of 44 infants had very low and extremely low birth weight, respectively. The highest ALP after serial follow up (ALP-h) and before first wrist radiograph (ALP-hb) was measured on average at 6.6 weeks and 5.5 weeks, respectively, after birth. The ALP during the first wrist radiograph (ALP-s), ALP-h, and ALP-hb were significantly different between Grades 0 and 3 (p=0.004). At second analysis, ALP-h, the ALP-hb, and serum phosphorous during the first radiograph (P-s) were significantly different between MBD presence and absence groups (p<0.0125). Specificity of ALP-h/ALP-hb, with a cut-off value of 503.5 IU/L, in detecting radiographic change (76.9%) was higher than that of P-s (54.8%).
Conclusions: ALP-h/ALP-hb level in 5-6 week-old preterm neonates is a predictor of MBD. Further studies are required to distinguish normal neonates from neonates with mild MBD.

Poster #: SCI-028

Ultrasound Performance in Diagnosis of Abnormal Neck Masses in Children

Gabrielle Laurindo Mariano De Oliviera, Resident, *Instituto Nacional de Pediatría, Ciudad de México, Mexico, glaurindo@hotmail.com;* Víctor García Gallegos, Humberto Cobián Machuca

Disclosures: All authors have disclosed no financial interests, arrangements or affiliations in the context of this activity.
Purpose or Case Report: The presence of abnormal masses in the neck of children always represents a diagnostic challenge. Ultrasound can provide useful information about the origin of an inflammatory mass in the neck and is effective in differentiating solid from cystic lesions. The aim of this study was to evaluate the diagnostic performance of ultrasound in the characterization of abnormal neck masses of the pediatric population.
Methods & Materials: In this observational, cross-sectional study neck ultrasound was performed in 56 children presenting with abnormal neck mass. In 33 patients computed tomography (CT) was also obtained. Patients were categorized into three diagnostic groups: lymphadenopathy, abscess, and miscellaneous masses. The gold standard was a combination of histopathological findings collected during surgery and clinical evolution during medical treatment.
Results: The median age was 6.35 years, and 57.1% were girls. The final diagnosis was lymphadenopathy in 26 (46.4%) patients, abscess in 10 (17.8%) and miscellaneous masses in 19 (33.9%). In one patient it was not possible to reach the final diagnosis. The first clinical diagnostic impression was correct in 32 (57.1%) cases, while ultrasound examination hit in 48 (85.7%) cases. For the correct diagnosis of adenopathies, ultrasound showed sensitivity (Sn), specificity (Sp), positive (PPV) and negative (NPV) predictive value of 98%, 94%, 95%, and 98%; respectively. For abscess, ultrasound exhibited Sn, Sp, PPV and NPV of 95%, 93%, 75%, and 99%; respectively. For miscellaneous neck masses Sn, Sp, PPV and NPV were 79%, 97%, 94%, and 90%; respectively. Notably, ultrasound showed a higher accuracy than CT (as shown by the ROC curve) in the correct identification of adenopathies (90% vs 82% respectively), abscess (93% vs 63% respectively) and miscellaneous masses (83% vs 67% respectively).
Conclusions: Our findings suggest that ultrasound should be the initial imaging approach in assessing abnormal neck masses in children.

Poster #: SCI-029

Adaptive Statistical Iterative Reconstruction (ASIR) Use for Radiation Dose Reduction in Pediatric Lower Extremity CT Scan: Impact on Diagnostic Image Quality

Amisha Shah, MD, *Radiology, Children's Hospital of Pittsburgh of UPMC, Pittsburgh, PA, shaha3@upmc.edu;* Mitchell Rees, Erica Kar, Kimberly Bolton, Ashok Panigrahy, Vince Lee

Disclosures: All authors have disclosed no financial interests, arrangements or affiliations in the context of this activity.
Purpose or Case Report: To evaluate the effect of different levels of adaptive statistical iterative reconstruction (ASIR) in pediatric lower extremity CT scan to compare the radiation dose, objective imaging parameters and subjective diagnostic image quality ratings.
Methods & Materials: This HIPPA-compliant, quality improvement study was approved for IRB-exempt status. The study cohort included 91 pediatric patients who underwent CT scan of the lower extremity, defined as a CT of the thigh, knee, leg, ankle or foot. The control group consisted of 37 patients who were scanned with a standard CT protocol using 0% ASIR and 100% FBP. The other group of patients was imaged on a CT scanner equipped with ASIR software. Out of the second group 20 patients were scanned with 30% ASIR and 70% FBP, and 34 patients were scanned with 40% ASIR and 60% FBP.
Objective imaging parameters obtained on all studies included signal-to-noise ratio (SNR) within bone versus air and contrast-to-noise ratio (CNR) between bone and muscle versus air. All measurements were made using standardized regions of interest (1-1.5 cm^2) on images of 1.25 mm slice thickness. Computed tomography dose index (CTDI) and dose-length product (DLP) were recorded for each study as estimates of radiation dose.
Two pediatric radiologists who were blinded to the level of ASIR made subjective ratings on each study with agreement. The categories of rating included image noise, image sharpness, diagnostic acceptability and artifacts.
The objective data was analyzed by linear regression and the subjective data from the readers was analyzed by Logistic regression that compared the level of ASIR to the image quality ratings of each category.
Results: We found significant radiation dose reduction with higher levels of ASIR, indicated by decrease in CTDI (p-value 0.0046) and DLP (p<0.001). With increased ASIR levels, subjective noise level decreased (p<0.0001) and signal-to-noise ratio increased (p-value 0.0006). As the ASIR level increased, however, the image sharpness and diagnostic acceptability decreased on subjective assessment by readers (p<0.0001 and p-value 0.0100 respectively) compared to standard CT protocols studies.

Conclusions: Pediatric lower extremity CT performed at 30% and 40% ASIR levels significantly reduced the radiation dose and perceived noise level with improved signal to noise ratio (SNR) compared to standard CT scan. The subjective image sharpness and diagnostic acceptability, however, significantly decreased as the ASIR level increased.

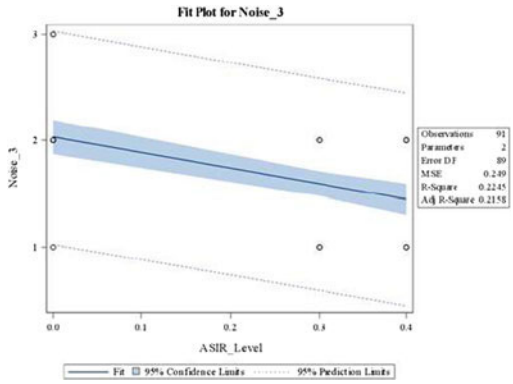

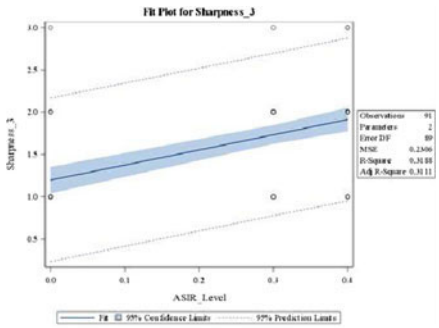

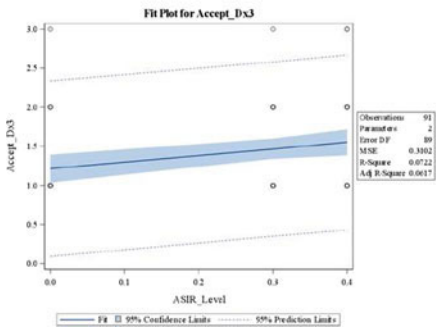

Score	Subjective Image Noise	Subjective Image sharpness	Diagnostic acceptability	Artifacts
1	Too little Noise	Structures are will defined with sharp contours	Acceptable	No artifacts
2	Appropriate Noise	Contours are not fully sharp but structures are defined	Acceptable with reservations	Minor artifacts
3	Noisy but permits evaluation	Structures can be seen and contours are barely sharp enough	Only acceptable under limited conditions	Major artifacts but interpretable
4	Too much noise so that no information is gathered	Though structures can be visualized, contours are blurred and images are insufficient for diagnostic reporting	Unacceptable	Artifacts make image interpretation impossible

Poster #: SCI-030

A Double Balloon Catheter for the Treatment of Intussusception, Follow Up

Cephus Simmons, MRS, RRA, *Radiology, Medical University of South Carolina, Mount Pleasant, SC, simmonce@musc.edu*

Disclosures: All authors have disclosed no financial interests, arrangements or affiliations in the context of this activity.
Purpose or Case Report: To identify the regulatory process for an innovative device that will create an airtight seal around the anus during anintussusception reduction procedure

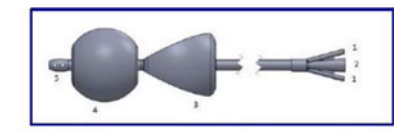

Product Description

1. Ports for balloon inflation with a one-way luer lock valve
2. Port for insufflating air or fluid
3. Proximal (external) balloon with a maximal capacity of 50 mL
4. Distal (internal) balloon with a maximal capacity of 70 mL
5. Catheter tip with an end hole and four side holes

Methods & Materials: After the conclusion of the animal laboratory study to identify the shape and size of the balloons, utility patent applications were submitted. The testing required by the FDA was conducted. They include the benchtop testing and a feasibility animal testing. Multiple different tests were conducted to evaluate the durability, reliability, and efficiency of the product. These tests evaluate the flow rate through the central lumen, the balloon inflation/deflation rate, product continuity, and burst rate of the balloons. A minimum of 5 catheters were utilized for each test.

A feasibility test was performed. This involved utilizing an anesthetized pig. The Cephus Catheter was inserted per rectum and the internal balloon was inflated under fluoroscopic guidance. The external balloon was inflated to until a seal was created. A dye was then introduced into the rectum through the central lumen. The colon was then insufflated with air. Fluoroscopic images were obtained of the distended colon. Additional, photos were taken at the rectum to record any leakage of dye.
Results: Twelve benchtop tests were performed on the catheter and identified that it was functional, durable, and safe. The feasibility test yielded a moderate rate for bowel distention and identified the absence of leakage around the anus.
Conclusions: The study identified that the catheter is functional, durable and safe for used on human. It also identified that the catheter creates an air tight seal around the anus. Therefore, the innovative device will improve the process of intussusception reduction. Upon FDA approval, the product will be used in a risk analysis clinical trial.

Poster #: SCI-031

CT and MRI Findings in Branchial Apparatus Anomalies: What the surgeon needs to know

Melissa Neveu, MD, *Ann & Robert H. Lurie Children's Hospital of Chicago, Chicago, IL, mneveu@luriechildrens.org;* Alok Jaju, Maura Ryan, MD, John Maddalozzo

Disclosures: All authors have disclosed no financial interests, arrangements or affiliations in the context of this activity.
Purpose or Case Report: Branchial apparatus anomalies (BAA) due to aberrations in the development and involution of the branchial apparatus can present as a cyst, fistula, or sinus tract. Definitive treatment for a BAA is complete surgical excision. The embryology of BAA has been well described, but few reports in the published literature discuss optimally imaging these patients. The purpose of this study is to describe the CT and MR imaging findings of BAA, and to correlate the imaging findings with surgery and pathology results. The goal is to develop a standardized imaging approach and search pattern specific to each subtype of BAA that would answer the most pertinent clinical questions for surgical planning.
Methods & Materials: All patients less than 18 years of age with proven BAA by surgical or pathology findings and preoperative CT or MR imaging performed between January 1, 2006 and February 28, 2015 were identified by searching our electronic medical records. Two observers (1 pediatric neuroradiologist, 1 pediatric radiology fellow) recorded the imaging findings, including anomaly type, size, extent and the presence of a cyst, fistula or sinus tract. The findings were correlated with clinic notes, operative reports, and pathology results.
Results: Fifty patients with surgically proven BAA and preoperative CT or MRI were identified. Of these, 19 had a first BAA, 18 had second BAA, and 13 had a third or fourth BAA. A total of 33 contrast enhanced CT and 25 MRI were reviewed, with 8 patients having both a CT and a MRI. CT was 88% sensitive and MRI was 96% sensitive for the detection of BAA. For all BAA, 72% (26 of 36) of fistulas were identified preoperatively, with 58% (14 of 24) identified on CT and 93% (14 of 15) identified on MRI. Approximately 53% of patients with a first BAA had involvement of the parotid gland, with 100% of cases identified on CT (3 of 3) and 57% identified on MRI (4 of 7). For third and fourth BAAs, 8 patients had thyroid gland involvement with 100% of cases detected on both CT and MRI, and 7 had pyriform sinus involvement with 100% of cases detected on CT (4 of 4) and 80% of cases detected on MRI (4 of 5).
Conclusions: Preoperative imaging provides vital information for surgical planning by defining the type and extent of BAA. CT and MRI are both sensitive for the detection of a BAA and determining involvement of adjacent head/neck structures. Overall, MRI is more sensitive for determining the presence of a fistula or sinus tract, although CT fistulagram can be valuable in selected cases.

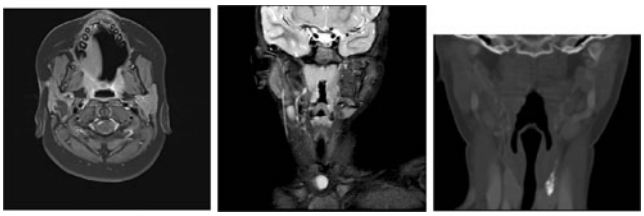

Poster #: SCI-032

Assessment of Cerebral Blood Flow in Children with a 3D Pseudocontinuous Arterial Spin Labeling Sequence Using Spiral MRI: a Diamox Study

Amber Pokorney, *Phoenix Children's Hosptial, Phoenix, AZ, apokorney@phoenixchildrens.com;* Houchun Hu, PhD, Jim Pipe, Zhiqiang Li, Jeffrey Miller

Disclosures: All authors have disclosed no financial interests, arrangements or affiliations in the context of this activity.
Purpose or Case Report: To assess cerebral blood flow (CBF) in pediatric patients before and after an acetazolamide (Diamox) challenge using a 3D pseudo-continuous arterial spin labeling (pCASL) pulse sequence with a spiral-in/out k-space trajectory.
Methods & Materials: Exams were performed on a 3 T Ingenia MR platform from Philips Healthcare, utilizing a 32-channel head array. Four patients have been studied: Patient 1-an 8y old girl with Moyamoya disease, Patient 2-a 14y boy with neurofibromatosis 1 migraines, Patient 3-a 21y old girl with an optic glioma, and Patient 4-a 13 months male with suspected Moyamoya Disease.

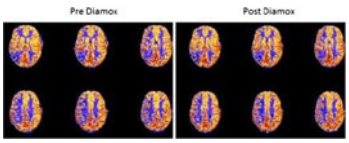

Diamox dosages were 490 mg, 800 mg, 780 mg, and 142 mg, respectively, for the four patients. pCASL was performed twice, immediately before and 15 min after Diamox injection. Spiral raw data were reconstructed offline and quantitative CBF maps were generated. White and gray matters voxels were extracted using FSL and Matlab software and a CBF histogram of the whole-brain was computed.
Results: In Patient 1, time-of-flight (TOF) angiography demonstrated impaired flow in both the right middle cerebral (MCA) and internal carotid arteries (ICA). The Moyamoya patient exhibited very little CBF change in response to Diamox (pre- CBF average: 59.5 ml/100 g/min, post- CBF average: 59.4 ml/100 g/min), suggesting limited CBF reserve. In Patient 2, the response to Diamox was moderate, with mean CBF increasing from 42.7 to 56.0 ml/100 g/min. TOF confirms a marked narrowing of the right MCA, and dynamic susceptibility contrast imaging further corroborates decreased CBF in the affected brain parenchyma. Patient 3 exhibited significant flow voids in the right distal MCA and ICA. The patient demonstrated significant increase in CBF in response to Diamox, from 28.9 to 49.8 ml/100 g/min. Patient 4 exhibited a 12% increase in CBF after Diamox administration. pCASL results corroborate TOF findings of narrowed MCA, ICA, and anterior cerebral artery.
Conclusions: 3D spiral pCASL provides a clinically useful quantitative approach to assess CBF in pediatric patients.

Poster #: SCI-033

Giant Hepatic Regenerative Nodules in Pediatric Patients with Alagille Syndrome: US and MRI Findings

Jordan Rapp, MD, *Temple University Hospital, Philadelphia, PA, jrapp24@gmail.com;* Sudha Anupindi, Richard Bellah

Disclosures: All authors have disclosed no financial interests, arrangements or affiliations in the context of this activity.
Purpose or Case Report: To describe ultrasound (US) and magnetic resonance imaging (MRI) findings of giant hepatic regenerative nodules (GHRN) in pediatric patients with Alagille Syndrome (AS).
Methods & Materials: In a retrospective review over a 12 year period of hepatic masses in patients with AS, we found six patients with large hepatic masses, each of whom had US and MRI studies. Imaging and medical records were then analyzed.
Results: Our study revealed 3 males and 3 females, mean age of 8.8 years (range 1.4 - 25.9 years). All patients had imaging findings showing varying degrees of chronic liver disease and portal hypertension. In the setting of cirrhosis, large hepatic masses, which ranged from 6.4 cm to 11.8 cm in size, were also identified. On US, all masses were isoechoic to adjacent liver, and splayed portal vessels; large segments of the portal veins (PV) and hepatic veins (HV) were also noted to course through the center of several masses. On MRI, 5/6 masses were slightly low to isointense in signal intensity (SI) on T1W and low SI on T2W images. One GHRN showed increased SI on T1. Post-contrast with conventional gadolinium chelates, the enhancement pattern of the masses followed that of adjacent liver. In one case where Eovist was given, the mass enhanced similar to the adjacent liver. Similar to US, PV branches were seen centrally. In 4/6 cases with DWI sequences, GHRN did not restrict. Four patients had pathologic correlation demonstrating benign hepatic nodules with preserved ductal architecture.
Conclusions: Patients with AS can develop cirrhosis which puts them at high risk of developing primary hepatic neoplasms. Among our group of AS patients from over a 12-year period, GHRN were the only hepatic masses we identified. Strikingly large in size, with distinct US and MRI features, recognition and discrimination of these lesions from malignant tumors, such as hepatocellular carcinoma, is important to avoid unnecessary intervention.

Poster #: SCI-034

MRI Evaluation of Vascular Malformations Using a 3D mDIXON Gradient Echo Technique

Logan Dance, MD, *Phoenix Children's Hospital, Phoenix, AZ, logandance@gmail.com;* Brian Keehn, D.O., Mittun Patel, M.D., Amber Pokorney, Michael Peterson, M.D., David Aria, M.D., Craig Barnes, Smita Bailey, MD

Disclosures: All authors have disclosed no financial interests, arrangements or affiliations in the context of this activity.
Purpose or Case Report: 3D mDIXON Gradient Echo (GRE) technical superiority has already been established: improved fat saturation, faster acquisition time, high spatial resolution, and volumetric data acquisition allowing for a comprehensive multiplanar and 3D post-contrast evaluation of vessels and soft tissue lesions. Vascular malformation imaging requires large field of view images that can adversely affect fat saturation, is frequently performed with a non-sedated patient resulting in motion artifact, and requires higher spatial resolution to better characterize a lesion and evaluate lesion extent. Additionally the interventional radiologists at our institution prefer 3D post-contrast imaging to assist in treatment planning. We believe that this sequence is well suited for vascular malformation MRI imaging. The primary purpose is to illustrate the clinical utility and superior image quality of the 3D mDIXON GRE sequence over more conventional mDIXON TSE sequence through a series of cases of a variety of vascular malformations in different body regions. The secondary purpose of this presentation is to validate the clinical superiority of this sequence through a blinded reviewer comparison to the more conventional mDIXON TSE sequence.
Methods & Materials: 25 sequential vascular malformation MRI examinations were performed which included postcontrast mDIXON TSE and postcontrast mDIXON GRE sequences. Matching single best image representative of pathology with the same plane of imaging for both mDIXON sequences was used for a direct side-by-side comparison. Six independent blinded reviewers rated image quality in four categories: fat suppression, contrast, motion artifact, and detail. Reviewers then chose the sequence they preferred for each of the categories as well as overall quality. Select cases will be shown to illustrate the image quality and clinical utility of the mDIXON GRE sequence.
Results: Reviewers preferred the mDIXON GRE sequence to the mDIXON TSE sequence for fat suppression (48 votes versus 12 votes), contrast (40 v. 20), motion artifact (51 v. 9), detail (37 v. 23), and overall image quality (48 v. 12).
Conclusions: The mDIXON GRE sequence is technically and clinically superior to mDIXON TSE for the evaluation of vascular malformations. In addition to decreasing scanning time, there was an increase in image quality and ability to obtain 3D reformatted images of vasculature and pathology.

Poster #: SCI-035

Alternative Etiologies for Abdominopelvic Pain in Pediatric Patients Undergoing MRI after Indeterminate Ultrasound for Clinically Suspected Appendicitis

Claudia Cartagena, *Diagnostic Imaging, Alpert Medical School of Brown University/Rhode Island Hospital, Providence, RI;* Thaddeus Herliczek, Elizabeth Dibble, MD, David Swenson, M.D.

Disclosures: All authors have disclosed no financial interests, arrangements or affiliations in the context of this activity.
Purpose or Case Report: To describe the spectrum and incidence of alternative etiologies for lower abdominal and pelvic pain identified on magnetic resonance imaging (MRI) following indeterminate appendix ultrasound (US) in pediatric patients.
Methods & Materials: In this IRB-approved, HIPAA compliant retrospective study, we reviewed the radiology database for all pediatric patients who underwent appendix MRI after indeterminate appendix US between 1/1/2011 and 8/31/2014. When etiologies other than appendicitis were identified for acute lower abdominal and pelvic pain, they were categorized as follows: (1) gynecologic, (2) non-appendix gastrointestinal, (3) urinary tract, (4) hepatobiliary, and (5) musculoskeletal.
Results: We identified 276 patients (4-17 years of age) who underwent appendix MRI after indeterminate appendix US. 55 (19.9%) patients were diagnosed with appendicitis on MRI and were therefore excluded from the analysis. 221 (80.1%) patients' MRI examinations were negative for appendicitis. 159 (71.9%) of these patients had no alternative etiology for abdominopelvic pain identified on MRI. 63 (28.5%) patients' MRI examinations revealed alternative causes for their symptoms. Gynecologic etiologies were found in 27 (42.9%) cases: e.g., ovarian or paratubal cysts (n=19) and adnexal torsion (n=2). Non-appendix gastrointestinal abnormalities were seen in 26 (41.3%) cases: e.g., regional enteritis or colitis (n=18) and epiploic appendagitis (4). Urinary tract pathology was identified in 6 (9.5%) cases: e.g., pyelonephritis (n=2) and urolithiasis (n=2). Hepatobiliary abnormalities were found in 3 (4.8%) cases: e.g., cholelithiasis (n=1) and choledocholithiasis (n=1). Finally, a musculoskeletal cause of pain was identified in 1 (1.6%) patient: a rectus muscle strain.
Conclusions: MRI performed after indeterminate appendix US in children with acute lower abdominal pain provides an alternative diagnosis in approximately one-in-four patients. Pathologies evident on MRI involve

multiple organ systems and are of varying clinical urgency from simple muscle strain to emergent adnexal torsion.

Poster #: SCI-036

What are the Short-Term Effects of Physical Activity on the Cartilage of Healthy Adolescent Boys? Preliminary Functional Imaging Perspective

Humayun Ahmed, MSc., *Diagnostic Imaging, The Hospital for Sick Children, Toronto, ON, Canada, humayun_21@hotmail.com;* Kuan Chung Wang, Marshall Sussman, Afsaneh Amirabadi, Rahim Moineddin, Greg Wells, Carina Man, Victor Blanchette, Andrea Doria

Disclosures: All authors have disclosed no financial interests, arrangements or affiliations in the context of this activity.
Purpose or Case Report: 1. To determine short-term interval changes in T2 maps of knee cartilage of healthy boys before and after a 2-min knee-squat exercise at 1.5 T and 3 T MRI; 2. To determine interval changes in T2 maps pre-exercise at 1.5 T vs. 3 T, and post-exercise at 1.5 T vs. 3 T; 3. To determine interval changes pre- and post-exercise among minimal-, moderate-, and high-activity subjects at 1.5 T and 3 T; and 4. To determine inter- and intra-reader reliability of 1.5 and 3 T values.
Methods & Materials: 13 healthy boys (ages: 12-19) with different (8 moderate/high and 5 minimal) World Health Organization-recommended levels of physical activity were asked to follow a knee-squat protocol under supervision. Their knees were scanned at 1.5 T and 3 T pre- and post-exercise. T2 maps at TE=13,19, 28 ms were obtained. 8 ROIs (weight-bearing [WB], non-weight-bearing [NWB], and whole areas) of femurs and tibias were analysed using MATLAB software. Qualitative analysis of gray-scale representations of T2 maps was performed.
Results: At 1.5 T, in both medial and lateral ROIs, there were no significant differences observed between pre- and post-exercise T2 values. At 3 T, there were significant differences between pre- and post-exercise T2 values in the lateral proximal tibia (P=0.02), but not in other ROIs. At 1.5 T and 3 T, there were significant differences between pre-exercise values in medial femoral and tibial ROIs (P=0.03, 0.002, 0.0002), and between post-exercise values in medial femoral and tibial ROIs (P=0.006, 0.02, 0.001) and lateral femoral and tibial ROIs (P=0.01, 0.017, 0.04, 0.0017, 0.0046). Intra-reader reliability of T2 maps was mostly excellent (ICC=0.76 - 0.99), and inter-reader reliability, mostly ranged from moderate to excellent (ICC=0.51-0.99). No significant differences were observed at any ROIs between pre- and post-exercise T2 values in minimal- vs. moderate- vs. high-activity participants.
Conclusions: Exercise does not have a short-term effect on the direction of cartilage fibers as represented by T2 maps, regardless of weekly activity levels. This suggests that short-term exercise may not deform cartilage significantly in vivo. Further investigation is needed to determine the long-term effects of exercise on the direction of collagen fibers as this information could direct safe integration of exercise into arthropathic treatment regimens.

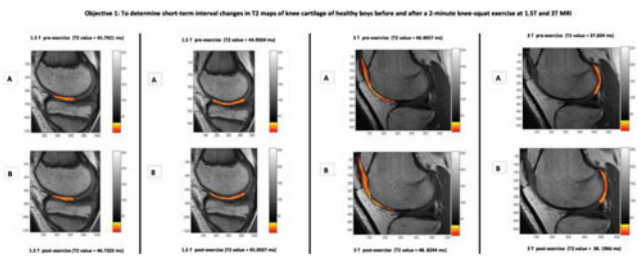

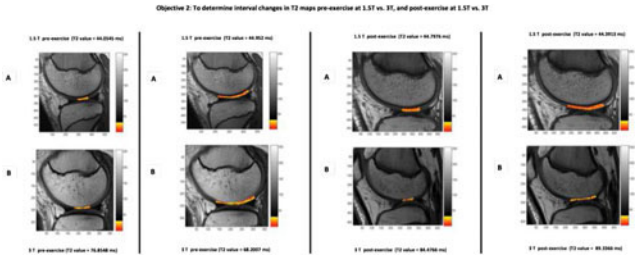

Poster #: SCI-037

CT Risk Disclosure in the Emergency Department – A Practice in Evolution

Karen Thomas, MD, *Department of Diagnostic Imaging, Hospital for Sick Children, Toronto, ON, Canada, karen.thomas@sickkids.ca;* Jennifer Marin, Angela Mills, Kathy Boutis

Disclosures: All authors have disclosed no financial interests, arrangements or affiliations in the context of this activity.
Purpose or Case Report: Awareness of the need for benefit:risk assessment prior to imaging studies has increased dramatically over the past decade, but the impact of this on the disclosure practice of Emergency Department (ED) Physicians is not known. Our aim was to assess ED physician practice and attitudes towards CT radiation risk disclosure for stable patients.
Methods & Materials: Electronic Survey of all USA and Canadian Emergency Medicine Residency Program Directors and Associate/Assistant Directors.
Results: Response rate was 51% (276/545), with most (83%) respondents stating that their routine practice included at least some pediatric patients. Reported rates of discussion (almost always or most of the time) of potential radiation risks with stable patients and their families were inversely related to patient age (>65 yrs 5%, 41-65 years 21%, 19-40 years 50%, 0-18 years 76%). Discussion was most likely if there was discordance in family vs physician perception of need for CT, or if the patient/family directly asked for information. Factors most relevant to the decision not to discuss risk were the lower risk in the elderly or patients with reduced life expectancy, time pressure and concern that refusal might compromise patient care. 43% of respondents correctly identified the future excess cancer mortality risk associated with Head CT, and 83% were aware that the risk is higher in children. Most respondents (84%) would favour verbal informed discussion over written informed consent if risk disclosure became standard of care. Familiarity with Image Gently and Image Wisely Campaigns was only moderate compared to clinical campaigns such as Choosing Wisely. Although 57% of respondents now feel comfortable (extremely or very) in discussing CT risks with patients and their families, most would appreciate further educational tools.
Conclusions: Our survey suggests that risk disclosure and discussion is becoming a more frequent part of routine ED care for patients undergoing CT. Most ED physicians are aware of the greater potential risk in younger patients, and this is reflected in a higher rate of discussion with pediatric and young adult patients/families. Opportunities to improve patient care through collaboration and dissemination of knowledge between Diagnostic Imaging and the Emergency Department exist.

Poster #: SCI-038

Diagnostic Pathway for Imaging Acute Appendicitis in Children

Tahani Ahmad, MD, *IWK Health Center, Halifax, NS, Canada, tahani1523@yahoo.com*

Disclosures: All authors have disclosed no financial interests, arrangements or affiliations in the context of this activity.
Purpose or Case Report: To assess the validity and appropriatness of the diagnostic pathway that suggests clinical evaluation, primary use of US and staged limited CT for evaluation of children with suspected appendicitis
Methods & Materials: Retrospective review of the electronic medical records of 206 consecutive children who presented to our ER department with acute abdominal pain and underwent US examination for suspected appendicitis. The imaging findings, management plan, and surgical outcome, if surgery was contemplated, were reviewed. The diagnostic accuracy of US was calculated. The number of CT scans performed and the negative appendectomy rate were also analyzed.
Results: Of the 206 suspected appendicitis cases 68 (33%) had acute appendicitis (AA) at surgery. The appendix was identified on an initial US in 161 (78%) patients (66 (41%) normal, 68 (42.2%) inflamed and 27 (16.8%) equivocal). CT scan was performed in 4 equivocal cases (2 positive and 2 negative). Surgical confirmation of AA was seen in 57/58 positive sonographic studies with one false positive.
In 45/206 children (20%) the appendix was not identified on the first US. US was repeated in 11/45 cases. The appendix was seen in 10/11 cases (7 normal and 3 inflamed) and was not delineated in 1 case which was inflamed at surgery. Only 5/45 CT scans were performed.
Overall, a normal appendix was visualized in 47% (66/138) of children on primary US and in 59% (82/138) on further imaging (US or CT or both). An inflamed appendix was not depicted in 11.7% of cases on initial US and the non-detection rate dropped markedly to 1.5% after second US and/or CT. The US was repeated in 24 patients (11.6%), while CT was performed in 9 cases (4.3%). The ratio of US to CT in our cohort was 23:1. US demonstrated a sensitivity of 93.2%, specificity of 94.1%, PPV of 92.1%, NPV of 94.9% and accuracy of 93.7%. The negative appendectomy rate was 2.7%.
Conclusions: US proved reasonably accurate in diagnosing acute appendicitis and should be validated as the primary imaging modality in children with suspected appendicitis. The diagnostic strategy of repeating the US in equivocal cases and limiting the use of CT scans to cases were US fails to identify the appendix or remains equivocal despite a second examination, results in reasonable negative appendectomy rate and offers the opportunity to substantially reduce radiation.

Poster #: SCI-039

Validation of a Novel Scoring System, the Radiographic Global Impression of Change (RGI-C) Scale, for Assessing Skeletal Manifestations of Hypophosphatasia in Infants and Children

William McAlister, MD, *Mallinckrodt Institute of Radiology at St. Louis Children's Hospital, St. Louis, MO, mcalisterw@mir.wustl.edu;* Kenji Fujita, Scott Moseley, David Thompson, Michael Whyte
Disclosures: All authors have disclosed no financial interests, arrangements or affiliations in the context of this activity.
Purpose or Case Report: Hypophosphatasia (HPP) is the rare inherited metabolic bone disease caused by loss-of-function mutations in the tissue nonspecific alkaline phosphatase (TNSALP) gene. Resultant TNSALP deficiency leads to extracellular excess of inorganic pyrophosphate, an inhibitor of bone mineralization. Rickets in infants and children has distinctive radiographic features. Here, we report the validity and reproducibility of a novel scoring system to quantify HPP-specific radiographic changes in pediatric patients (pts).
Methods & Materials: The Radiographic Global Impression of Change (RGI-C) is a 7-point ordinal scale (-3=severe worsening; 0=no change; +3=near/complete healing) designed to provide a comprehensive evaluation of skeletal health in pediatric pts with HPP. Sequential radiographic studies (chest [<5 years of age only], knees, and wrists) are assessed for improvement or worsening using age-specific (< or ≥5 years of age) hallmarks of HPP developed by expert consensus. Features common to both age groups include metadiaphyseal sclerosis, apparent physeal widening, and metaphyseal radiolucencies and/or fraying. Age-specific features include gracile and/or absent bones and chest deformity for pts <5 years, and osteopenia, "popcorn calcification," and physeal corner defects for pts ≥5 years. Inter- and intrarater agreements for 6 raters across 3 treatment studies were assessed using intraclass correlation coefficients (ICC) and weighted kappa coefficients (KC). Concurrent validity was assessed via correlation between RGI-C scores and simultaneous changes from baseline in: 1) Rickets Severity Scale (RSS)[1]; 2) Pediatric Outcomes Data Collection Instrument (PODCI) Global Function scale; 3) Child Health Assessment Questionnaire (CHAQ) Disability Index; 4) 6 Minute Walk Test (6MWT); and 5) height z- scores, in children ≥5 years.
Results: ICC revealed moderate-to-good interrater agreement for pts <5 years (0.65, 227 radiographs; $P<0.0001$) and pts ≥5 years (0.57, 136 radiographs; $P<0.0001$). Most raters achieved substantial ($n=4$, KC >0.6) or almost perfect ($n=4$, KC>0.8) intrarater agreement ($n=1$, moderate agreement, KC>0.5). The linear regressions revealed significant correlations with RSS, PODCI Global Function, CHAQ Disability Index, 6MWT, and height z-scores (Table 1).
Conclusions: The RGI-C scale is a reproducible and valid measure for assessing over time clinically important changes in skeletal manifestations of HPP in pediatric pts.
1. Thacher TD, et al. *J Trop Pediatr* 2000;46:132–9.
Table 1. Correlations betwee RGI-C and changes from baseline in other clinical outcomes in HPP patients

Measure	Number of data points	Pearson correlation (r)	*P*-value
Rickets Severity Scale	135	-0.664	<0.0001
PODCI Global Function	84	0.595	<0.0001
CHAQ Disability Index	84	-0.589	<0.0001
6 Minute Walk Test	100	0.284	0.0043
Height Z-score	108	0.261	0.0065

Poster #: SCI-040

Differences of Placental ADC Measurements in Fetuses with and without CNS Abnormalities

Melissa Valdez Quintana, Pediatric Radiology Fellow, *Diagnostic Imaging, Children's Hospital of Eastern Ontario, Ottawa, ON, Canada;* Pablo Caro Dominguez, Fellow, David Grynspan, Julie Hurteau-Miller, Jorge Davila, MD, Felipe Moretti, Elka Miller
Disclosures: All authors have disclosed no financial interests, arrangements or affiliations in the context of this activity.
Purpose or Case Report: Diffusion weighted images (DWI) have the potential to provide valuable information on the diffusion and perfusion properties of the human placenta and therefore has the capability for detection of early developmental fetal anomalies. The purpose of this study was to determine if DWI of the placenta demonstrates differences between fetuses with and without central nervous system (CNS) abnormalities.
Methods & Materials: After REB approval was obtained, 1.5 T Fetal MRI of 57 singleton pregnancies (mean gestational age 21 weeks 5 days)

were retrospectively analyzed, 39 with CNS morphologic abnormalities and 18 controls without morphologic abnormalities. On DWI (b values 0-1000 s/mm^2) the slice that displaced the largest surface of placenta was selected and the apparent diffusion coefficient (ADC) maps were reconstructed. Two ADC quantification methods were performed 1) manually outline the entire surface of the placenta and, 2) 3 regions of interest (ROI) of 79 mm2, in both borders and center of the placenta. Measurements were compared with the presence or absence of CNS fetal abnormalities. Wilcoxon tests were used.

Results: There was significant discrepancy between the two ADC quantification methods (p<0.0001). The ROI measurement method demonstrated significant correlation (p=0.002) between low ADC and presence of fetal CNS abnormalities compared to controls. However, with the manually outlined method, there was a lack of significant association between low ADC and CNS abnormalities (p=0.1).

Conclusions: The quantification of DWI of the placenta in fetal MRI suggests that the presence of fetal CNS abnormalities is associated with restricted diffusion and reduced ADC values of the placenta using the ROI ADC quantification method. Therefore in the pathologic placenta, DWI and ADC mapping have the potential to quantify early changes, even in the absence of gross structures anomalies. The differences between the two ADC quantification methods suggest inhomogeneity of the ADC values with the large ROI.

Placental DWI has a promising role on the evaluation of early placental anomalies and could have an impact in prediction of CNS fetal abnormalities.

Poster #: SCI-041

Simulation Evaluation: PACS Based Radiology Simulator for Resident Examination

Kevin O'Brien, MD, *Radiology, University of Chicago Hospitals, Chicago, IL, kobrienmd@gmail.com;* Seng Ong

Disclosures: All authors have disclosed no financial interests, arrangements or affiliations in the context of this activity.

Purpose or Case Report: We intended to develop and test a PACS based radiology simulation program as an objective tool to evaluate residents. We utilized the simulator as the pediatric "end of rotation" (EOR) exam and compared it to our institution's traditional EOR review. We hypothesized that a simulator evaluation tool would better identify areas for residents to improve, create a clear gradient of resident performance, or identify a struggling resident.

Methods & Materials: The simulator we employed was developed internally and very closely approximates the appearance and functionality of the PACS in use at the hospital. The simulation cases are real cases that have been wiped of all patient identifiers. The simulator contains the entire study, closely mimicking the true PACS environment. Each resident was given the same 12 cases with a 1 h time limit. Residents were instructed to provide a preliminary report for the study and complete as many studies as possible within 1 h. Four senior residents took the simulation EOR exam: 2 PGY-5 residents and 2 PGY-4 residents. Three junior residents took the simulation EOR exam: 3 PGY-2 residents. The attending evaluator compared the preliminary report provided by the resident to the findings and impression of the final report for that study. A grading system was devised: correct, incorrect, and not attempted. A passing score was set as percentage correct greater than 60%. Our institution's traditional EOR exam, where a resident takes a number of cases from Powerpoint slides one on one with the attending evaluator, was compared to the simulator. The traditional EOR exam is subjectively scored as pass/fail.

Results: All residents completed 12 cases in the allotted time. The percentage correct ranged from 67% to 92% with a mean score of 83% and standard deviation of 8%. All residents passed the simulator exam. The senior residents' scores ranged from 83% to 92% with a mean of 87.5% and standard deviation of 5%. The junior residents' scores ranged from 67% to 83% with a mean of 78% and standard deviation of 9%. The case most missed by junior residents: VCUG demonstrating a posterior urethral valve. The case most missed by the senior residents: normal elbow radiograph with multiple ossifications.

Conclusions: The simulator provided objective data allowing the evaluator to develop a clear distribution of resident performance as well as identify areas needing improvement. We demonstrated that the PACS based simulator is a superior evaluation tool for an EOR exam.

Poster #: SCI-042

Cross-Modality Validation of 3D Ultrasound for Developmental Dysplasia of the Hip

Chad Diederichs, Alana Heath, Myles Mabee, Abhilash Hareendranathan, Dornoosh Zonoobi, Adrienne Thompson, Jacob Jaremko, MD, PhD, *Department of Radiology and Diagnostic Imaging, University of Alberta Hospital, Edmonton, AB, Canada, 1082085@gmail.com*

Disclosures: All authors have disclosed no financial interests, arrangements or affiliations in the context of this activity.

Purpose or Case Report: Developmental dysplasia of the hip (DDH) is a common congenital problem affecting up to 3% of the the population. If untreated, DDH may lead to hip dislocation and premature osteoarthritis. Current DDH diagnosis is highly operator-dependent as it relies on 2D ultrasound. 3D ultrasound offers more complete, and potentially more reliable, imaging of infant hip geometry. However, it is unclear whether 3D ultrasound images, noisy with artifacts and reconstructed by proprietary algorithms from non-parallel beams, give accurate 3D shape information. We sought to validate the fidelity of acetabular surface models obtained by 3D ultrasound by comparison with those obtained concurrently from MRI.

Methods & Materials: 3D ultrasound and MRI scans were performed on the same day in 20 infants aged 0-6 months old. Coronal 3D MEDIC images (1 mm slice thickness) were obtained in a 1.5 T Siemens scanner. 3D ultrasound was performed using a Philips VL13-5 probe. Acetabular surface models were generated for 40 hips from both MRI and 3D ultrasound data sets using semi-automated tracing software. Three observers traced the MRI and 3D ultrasound bony surfaces to assess the inter-observer variability in surface model generation. To evaluate the inter-modality variation between the models, the root mean square (RMS) distances between 3D ultrasound and MRI models were calculated using Amira software. This involved an initial manual transformation to align 3D ultrasound and MRI surfaces, followed by an automated iterative closest point rigid registration to minimize RMS distances between the two surfaces. Registrations were repeated on a subset of surface models to determine the reproducibility of the RMS distance calculations in Amira.

Results: Inter-modality variability was minimal on inspection and was confirmed with a mean RMS distance of 0.4+/-0.3 mm. A 95%

confidence interval for the mean RMS distances was <1 mm for all comparison sets. Intra- and inter-observer mean RMS distances were significantly smaller for 3DUS than for MRI ($P<0.05$).

Conclusions: Acetabular geometry was reproduced by 3D ultrasound surface models within 1 mm of the corresponding 3D MRI surface model, and the 3DUS models were more reliable. This validates the fidelity of 3D ultrasound modelling and encourages future use of 3D ultrasound in assessing infant acetabulum anatomy, which may be useful to detect and monitor treatment of hip dysplasia.

Poster #: SCI-043

Trends and Characteristics of Pediatric Radiology Research: 2006 - 2015

Caroline Lacroix, MD, *Diagnostic Imaging, The Hospital for Sick Children, Toronto, ON, Canada, caroline.lacroix@sickkids.ca;* Susan Shelmerdine, FRCR MBBS BSc MRCS, Govind Chavhan, MD

Disclosures: All authors have disclosed no financial interests, arrangements or affiliations in the context of this activity.

Purpose or Case Report: To determine the characteristics and trends of original research articles published in Pediatric Radiology over the last 10 years.

Methods & Materials: This was a retrospective bibliometric analysis not involving human subjects.

All original research articles published in the July issues of the Pediatric Radiology journal between 2006 and 2015 were evaluated. Case reports, editorials and pictorial reviews were excluded from analysis.

Information regarding sample size, study design, declared funding, number of authors, author country and gender were examined and analysed for trend over time using the Pearson correlation test. Descriptive statistics were used to illustrate total numbers of articles analysing a particular subspecialty area, radiology modality and study design.

Results: In total 80 articles were analysed, with 10 (13%) articles analysing data from multicentre sources, 40 (50%) with multicentre investigators, 22 (28%) prospective in study design and 9 (11%) with declared funding. The most common pediatric subspecialty topics included gastrointestinal (18, 23%), musculoskeletal (16, 20%) and neuroradiology (11, 14%). Studies assessing a combination of various modalities were most common (23, 29%), along with those utilising CT (19, 24%) and MRI (16, 20%).

There was a significantly positive trend towards number of original research articles being published ($r=0.72$, $p=0.02$), first authors originating from United States ($r=0.69$, $p=0.03$) and a negative trend towards total number of authors ($r=-0.65$, $p=0.04$).

There was a positive but not statistically significant trend towards last authors originating from United States ($r=0.48$, $p=0.16$), studies relating to interventional radiology ($r=0.40$, $p=0.25$) and the use of statistical analysis tests ($r=0.46$, $p=0.18$). A negative but not significant trend was seen for the female gender of last authors ($r=-0.42$, $p=0.23$).

There was no trend in study sample sizes, prospective study design, those involving multicentre investigators, using multicentre data, those with declared funding or female gender of first author.

Conclusions: Characteristics of Pediatric Radiology journal research articles over time have been described. This information may be helpful in recognizing current limitations or pitfalls of our published research work and in steering the future directions of research in our specialty, informing prospective researchers and editorial staff.

Table 1:

Table demonstrating trends in various original research article characteristics over time.

Table 2:

	2006	2007	2008	2009	2010	2011	2012	2013	2014	2015	F Value	P value
Total articles, n	5	8	5	7	10	8	9	8	11	9	0.72	0.0
Median author number, n	6	7	4	5	6	5	5	5	4	4	-0.65	0.04
Median sample size, n	65	95.5	12	98	67	118.5	41	78	24	62	-0.17	0.64
Multicentre Investigators, n(%)	3 (60)	4 (50)	0	3 (43)	4 (40)	5 (63)	6 (67)	5 (63)	8 (73)	2 (22)	0.18	1.00
Multicentre Data, n (%)	2(40)	0	0	0	2 (20)	2 (25)	0	2 (25)	1 (9)	1 (11)	-0.09	0.80
Female first author, n (%)	1 (20)	5 (63)	2 (40)	3 (43)	6 (60)	3 (38)	4 (44)	4 (50)	5 (45)	3 (33)	0.05	0.89
Female last author, n (%)	2 (40)	3 (38)	1 (20)	2 (29)	3 (30)	4 (50)	4 (44)	3 (38)	2 (18)	0	-0.42	0.23
First author from United States, n (%)	1 (20)	1 (13)	0	3 (43)	6 (60)	4 (50)	5 (56)	3 (38)	5 (45)	5 (56)	0.69	0.03
Last author from United States, n (%)	2 (40)	1 (13)	0	3 (43)	6 (60)	6 (75)	5 (56)	3 (38)	6 (55)	4 (44)	0.48	0.16
First author radiologist, n (%)	4 (80)	4 (50)	5 (100)	6 (86)	6 (60)	8 (100)	7 (78)	7 (88)	7 (64)	8 (89)	0.14	0.70
Last author radiologist, n (%)	1 (20)	4 (50)	4 (80)	5 (71)	6 (60)	4 (50)	5 (56)	7 (88)	8 (73)	5 (56)	0.44	0.20
Interventional Radiology articles, n (%)	0	0	0	0	0	2 (25)	1 (11)	1 (13)	1 (9)	0	0.40	0.25
Number of prospective studies, n (%)	0	4 (50)	0	2 (29)	3 (30)	4 (50)	4 (44)	2 (25)	2 (18)	1 (11)	0.07	0.85
Statistical analysis, n (%)	3 (60)	5 (63)	0	5 (71)	5 (50)	6 (75)	5 (56)	5 (63)	9 (82)	7 (78)	0.46	0.18
Declared funding, n (%)	0	1 (13)	0	0	2 (20)	3 (38)	2 (22)	0	0	1 (11)	0.14	0.70

Table demonstrating the different pediatric radiology subspecialties and imaging modalities represented in the articles published.

	2006	2007	2008	2009	2010	2011	2012	2013	2014	2015	Total (n, %)
Pediatric Radiology Subspecialty											
Gastrointestinal	0	1	1	2	2	1	4	1	5	1	18 (23)
Musculoskeletal	1	0	1	1	3	1	2	4	0	3	16 (20)
Neuroradiology	2	2	1	0	1	0	1	0	2	2	11 (14)
Genltourinary	1	4	1	0	0	0	0	0	0	0	6 (8)
Radiation Dosage	0	0	0	1	1	2	0	1	0	1	6 (8)
Chest	0	0	0	2	1	0	0	1	1	0	5 (6)
Cardiac	1	1	0	0	0	1	0	1	1	0	5 (6)
Head and Neck	0	0	1	0	0	0	0	0	1	2	4 (5)
Fetal	0	0	0	0	1	1	1	0	0	0	3 (4)
Other	0	0	0	0	1	2	0	0	0	0	3 (4)
Vascular	0	0	0	0	0	0	1	0	1	0	2 (3)
Education	0	0	0	1	0	0	0	0	0	0	1 (1)
Imaging Modality Utilized											
Combination	0	7	4	1	1	2	3	3	1	1	23 (29)
CT	1	0	1	4	2	4	1	1	4	1	19 (24)
MRI	1	0	0	0	4	2	2	2	3	2	16 (20)
Ultrasound	2	1	0	0	1	0	1	0	2	2	9 (11)
Radiography	1	0	0	1	1	0	1	1	0	2	7 (9)
Interventional Radiology	0	0	0	0	0	0	0	1	1	0	2 (3)
Other, N/A	0	0	0	1	1	0	0	0	0	0	2 (3)
Fluoroscopy	0	0	0	0	0	0	1	0	0	0	1 (1)
Nuclear/Functional Imaging	0	0	0	0	0	0	0	0	0	1	1 (1)

Poster #: SCI-044

Differences in Characteristics between General Medical, Radiology and Pediatric Radiology Research Studies

Susan Shelmerdine, FRCR MBBS BSc MRCS, *The Hospital For Sick Children, Toronto, ON, Canada, susie_c_s@yahoo.co.uk;* Caroline Lacroix, MD, Govind Chavhan, MD, Andrea Doria

Disclosures: All authors have disclosed no financial interests, arrangements or affiliations in the context of this activity.

Purpose or Case Report: 1) Determine differences in characteristics of studies published within high impact radiology and medical journals journals in comparison to a Pediatric Radiology journal.

2) Outline factors that may have contributed to differences in quality of design of studies and components that could be incorporated into the design of future pediatric radiology research studies in order to improve their quality.

Methods & Materials: Original research articles published within the May - July 2015 issues of JAMA (2014 impact factor [IF], 35.3), Radiology (2014 IF, 6.9) and Pediatric Radiology (2014 IF, 1.6) journals were evaluated for study characteristics (research design, sample size, funding), author details (academic degrees, gender of first/senior authors) and institution (country, type of centre). Case reports, editorials and pictorial reviews were excluded from analysis.

'Oxford Centre for Evidence-Based Medicine' levels of evidence were used to grade the design quality of the published articles. The chi squared test was used to compare number of study characteristics between the three groups. Descriptive statistics were used to differentiate study design and author details.

Results: 148 articles were analysed (35 JAMA, 80 Radiology, 33 Pediatric Radiology). There was a significant difference in the number of prospective studies among the 3 groups (17(48.6%) vs. 42 (52.5%) vs. 6 (18.2%) respectively, p-value=0.003), in number of studies with declared funding (32 (91.4%) vs. 48 (60%) vs. 6 (18.2%), p-value <0.0001) and in number of studies that used multicentre data (33 (94.3%) vs. 12 (15%) vs. 5 (15.2%), p-value <0001).

The median (range) sample sizes were 4513 (7 - 68,374,904), 100 (3 - 124,000,000) and 56 (7 - 3834) respectively. There were more systematic reviews and randomised controlled trials within JAMA (14, 40%) compared to within Radiology (1, 1.3%) and Pediatric Radiology (0, 0%). No radiology-related studies were published in JAMA during the period of investigation.

Conclusions: Fewer radiology studies than general medical studies are systematic reviews or randomised controlled trials, the hierarchically highest quality research designs. Pediatric radiology studies have smaller sample sizes compared with adult radiology and clinical studies, are less likely to be prospective or include multicentre data, likely due to lack of external funding support for most studies. Increased awareness of these factors may be helpful in guiding future pediatric radiology research.

Table 1:

Differences in characteristics between original research articles published within JAMA, Radiology and Pediatric Radiology journals over a 3 month period from May to July 2015.

	JAMA	%	Radiology	%	Pediatric Radiology	%
Total articles:	35		80		33	
Prospective Studies:	17	48.6	42	52.5	6	18.2
Median Sample Size:	4513		100		56	
Upper quartile:	61728.3		168		3834	
Lower quartile:	443.8		36		39.5	
IQR:	61284.5		132		109	
Minimum sample size:	7		3		7	
Maximum sample size:	68374904		124000000		3834	
Study Types:						
Observational	1	2.9	26	32.5	11	33.3
Case Series	0	0.0	6	7.5	1	3.0
Cross sectional	3	8.6	0	0.0	3	9.1
Case Control	0	0.0	15	18.8	5	15.2
Cohort with nested case control	2	5.7	0	0.0	0	0.0
Cohort	13	37.1	21	26.3	5	15.2
Preclinical	2	5.7	11	13.8	5	15.2
Meta-analysis/ Systematic Review	4	11.4	0	0.0	0	0.0
RCT	10	28.6	1	1.3	0	0.0
Drug Trials:	7	20.0	2	2.5	1	3.0
Funding:	32	91.4	48	60.0	6	18.2
Funding source:						
Government	22	68.8	31	64.6	2	33.3
Private	6	18.8	8	16.7	1	16.7
Both	4	12.5	9	18.8	3	50.0
Statistics Used:	33	94.3	77	96.3		
Multicentre Data:	33	94.3	12	15.0	5	15.2
Multicentre Investigators:	35	100.0	54	67.5	16	48.5
Median author number:	10		8		5	
First author female:	9	25.7	24	30.0	12	36.4
First author country = USA:	21	60.0	26	32.5	19	57.6
Last author female:	12	34.3	11	13.8	9	27.3
Last author country = USA:	21	60.0	29	36.3	20	60.6

Poster #: SCI-045

Imaging Review of DICER1 Syndrome: A Single Centre Experience

Marta Tijerin Bueno, Fellow, *Hospital for Sick Children/University of Toronto, Toronto, ON, Canada, tijerinradiologist@gmail.com;* Alejandro De La Puente Gregorio, Claudia Martinez-Rios, MD, David Malkin, Mary-Louise Greer, MBBS

Disclosures: All authors have disclosed no financial interests, arrangements or affiliations in the context of this activity.

Purpose or Case Report: To determine the spectrum of abnormalities associated with DICER1 syndrome.

To review imaging studies performed in oncologic staging and surveillance.

To delineate the screening protocol used in those with positive genetic testing.

Methods & Materials: This research ethics board approved retrospective study evaluated genetically confirmed or suspected DICER1 pediatric patients referred to our tertiary institution between 2004 and 2015.

Patients with tumors such as pleuropulmonary blastoma (PPB) or pineoblastoma (PNB) in isolation with no other features of DICER1 spectrum were excluded.

Modality type and timing was captured and imaging analyzed to determine what related to staging; to treatment e.g. screening for infection, line insertions; and to cancer predisposition screening.

Results: There were 12 patients (5 male and 7 female) with mean age at presentation of 4.6 years (range 14 days to 8 years). We included all patients with a confirmed genetic diagnosis (10) and strong clinical history (2) whose parents did not consent to genetic testing.

During the study period, our patients underwent 619 imaging studies (139 x-rays, 186 ultrasounds, 99 CTs and 195 MRIs). This included oncologic staging and follow-up, and surveillance imaging, some elements suspended during active cancer treatment.

The screening protocol for additional tumors in those with known malignancies, and at risk for neoplasia but with no known tumors, started as early as 14 days old, the youngest age at first malignancy being 1 year.

Screening initially consisted of a chest x-ray, abdominal and neck ultrasound and dedicated brain MRI. Novel technique whole body MRI was introduced during the study period, performed simultaneous to the brain MRI, substituting the chest x-ray, to minimize ionizing radiation.

DICER1 related pathology included malignant lesions in 75% of patients: 4 PPB, 2 PNB, 2 ovarian sex cord stromal tumors and 1 renal sarcoma. No patient had > 1 malignancy during the study period.

Benign lesions in 83% of patients included: 2 cystic nephromas, 3 thyroid nodules, 3 thyroid cysts, 1 renal cyst and 1 pineal cyst.

Two subjects, confirmed with DICER1, who were relatives of index cases, had no tumors.

Conclusions: Given the high incidence of neoplasia in DICER1 and early age at first presentation, early screening of at risk patients is critical, as is awareness of the types of DICER1-related tumors.

The current DICER1 screening protocol used in our institution includes an abdominal and neck ultrasound, and whole body and brain MRI.

Subject	Imaging Findings
1	- pineoblastoma - thyroid nodules
2	- cystic nephroma - pineal cyst
3	- no findings
4	- pleuropulmonary blastoma - thyroid cysts
5	- renal high grade sarcoma
6	- ovarian juvenile granulosa cell tumor
7	- cystic nephroma - thyroid cysts - ovarian embryonal rhabdomyosarcoma
8	- no findings
9	- pleuropulmonary blastoma - thyroid nodules and cysts
10	- pineoblastoma - thyroid nodules - renal cysts
11	- pleuropulmonary blastoma
12	- pleuropulmonary blastoma

Figure 1. Spectrum of DICER1-related pathology, benign and malignant, in patient cohort.

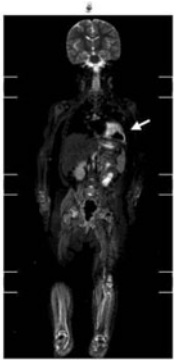

Figure 2. 23-month-old female presented with developmental delay. Genetic testing was DICER1 positive. First surveillance study performed was a Whole Body MRI using coronal STIR with fat suppression demonstrated a complex solid and cystic mass in the left hemithorax, confirmed to be a pleuropulmonary blastoma on surgical pathology.

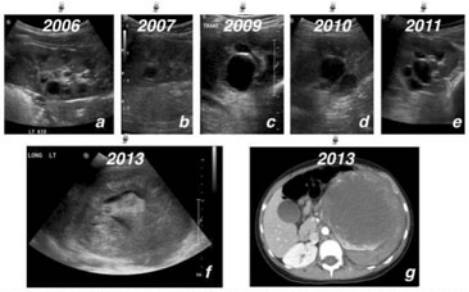

Figure 3. Sonographic images (a-f) of sequential abdominal ultrasounds performed as a screening in a 2 year-old female with a renal cyst followed since 2006. The cystic lesion was increasing in size and getting more complex, finally becoming a large renal sarcoma at the age of 8 seen in (g) axial enhanced abdominal CT.

Poster #: SCI-046

Multimodality Imaging Features of Massive Ovarian Edema in Children

Hisham Dahmoush, *Department of Radiology, The Children's Hospital of Philadelphia, Philadelphia, PA, dahmoushh@gmail.com;* Nancy Chauvin, MD

Disclosures: All authors have disclosed no financial interests, arrangements or affiliations in the context of this activity.

Purpose or Case Report: Massive ovarian edema (MOE) is a rare benign condition that affects childbearing women including girls. MOE is thought to result from intermittent or partial torsion of the ovary compromising the venous and lymphatic drainage but with preserved arterial supply. The clinical features of MOE are nonspecific and can simulate tumors, frequently resulting in oopherectomy. Fertility-sparing surgery may be undertaken if the diagnosis is considered prospectively and intraoperatively with a wedge biopsy, avoiding unnecessary resection of the affected ovary. We present clinical presentations and imaging features that should alert pediatric radiologists to the diagnosis of MOE.

Methods & Materials: The Institutional Review Board approved the research protocol. A list of radiology and pathology reports performed from January 2005 to November 2014 containing the words "Massive Ovarian Edema" in patients 18 years or younger were populated using a search engine (Softek Illuminate®). Two radiologists retrospectively reviewed the clinical presentation, imaging findings, and operative reports of patients who had confirmed massive ovarian edema on histopathology.

Results: We identified five subjects, mean age 12.5 years (range 9.6-14.3 years) with the diagnosis of massive ovarian edema at pathology. Presenting symptom, side, imaging appearance, preoperative diagnosis and intraoperative findings are detailed in Table 1. Common imaging findings included: ovarian enlargement with edema of the stroma, peripheral placed follicles with preservation of blood flow, MR: isointense signal on T1WI and markedly hyperintense signal on T2WI (Figure 1), preservation of color Doppler flow by ultrasound (Figure 2) and CT Hounsfield units below 40. The uterus was deviated to the affected side in all cases. 2/5 cases had small to moderate amount of free pelvic fluid. At pathology, the mean ovarian volume was 560 mL (range 108-1361).

Conclusions: While the clinical presentation of MOE is non-specific, an enlarged ovary with stromal edema, peripherally placed follicles and preservation of blood flow could suggest MOE and wedge biopsy should be considered intraoperatively to avoid unnecessary removal of the ovary in girls.

Subject	Age (Y)	Presenting symptom	Side	Imaging appearance	Size of ovary on imaging	Intraoperative findings	Ovarian volume (cc)
1	9.6	Pain	Right	US: Mass with mulitple cysts. Vascularity seen within a pedicle of the mass CT: Mass in the left cul de sac (HU:less than 40) posterior to the uterus. The uterus deviated to the right. Edema in the right fallopian tube. No free fluid	5×5.59×7 cm	Torsion	108
2	13.8	Virilization	Left	US: Mass with mulitple cysts. Vascularity seen within a pedicle of the mass CT: Mass in the right cul de sac (HU:less than 30) posterior to the uterus. The uterus deviated to the left. Edema in the left fallopian tube. No free fluid	13.1×7.7×7.1 cm	Ovaria mass	375
3	12.7	Pain	Right	US: Mass with multiple cysts. Vascularity seen within a pedicle of the mass CT: Mass in the right cul de sac (HU: less than 30) posterior to the uterus. The uterus deviated to the left. Edema in the left fallopian tube. No free fluid	13.1×7.7×7.1 cm	Ovarian mass	375
4	12.3	Mass	Left	MRI: Isointense T1WI and markedly hyperintense T2WI compared to muscle. Striated enhancement	16.2×13.6×6.5 cm	Ovarian mass	749
5	14.3	Virilization & Abdominal distention	Left	CT: Midline mass superior to the uterus. Dilated fluid-filled serpiginius left fallopian tube. Pedicle seen MRI: Isointense T1WI and heterogeneous markedly hyperintense T2WI compared to muscle. Mild homogeneous enhancement of the stroma. Rim enhancement of the cysts walls. NO solid enhancing nodules enhancement	7.7×16.9×20 cm	Torsion and ovarian mass	1361

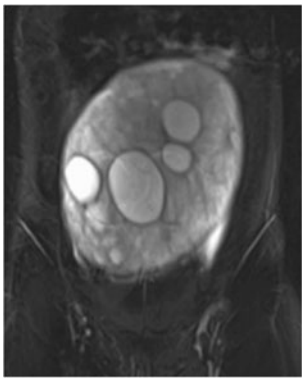

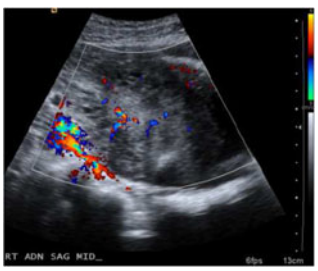

Poster #: SCI-047

3D Gradient Echo mDIXON MRI in Pediatric Osteomyelitis: Initial Experience

Tammam Beydoun, *Phoenix Children's Hosptial, Phoenix, AZ, tbeydoun@phoenixchildrens.com;* Amber Pokorney, Brian Keehn, Houchun Hu, PhD, Mittun Patel, Craig Barnes

Disclosures: All authors have disclosed no financial interests, arrangements or affiliations in the context of this activity.
Purpose or Case Report: To compare image quality ratings between 3D gradient echo mDIXON (GRE) vs. 2D turbo-spin-echo mDIXON (TSE) in pediatric patients with osteomyelitis.
Methods & Materials: Twenty patients were included in this study. They were imaged with both 3D GRE and 2D TSE after Gadolinium contrast injection. All exams were performed on 3 Tesla Philips Ingenia platforms. All images were retrospectively and independently reviewed by two board certified pediatric body radiologists to compare the conspicuity of lesion borders and quality of fat suppression. The following rating scale was used. -1: GRE superior to TSE, 0: GRE similar to TSE, and 1: TSE superior to GRE. Each radiologist also commented on whether the new GRE approach was "acceptable" or "unacceptable" for diagnostic use.
Results: 10 female and 10 male patients (average age: 11 years, range: 6 months to 17 years) were involved. No 3D GRE images were deemed unacceptable for diagnostic use by either radiologist. For delineation of lesion borders and fat suppression, Radiologist 1 (attending) preferred GRE over TSE in 12 cases, while Radiologist 2 (fellow) preferred GRE in 15 cases. The attending radiologist deemed GRE and TSE similar in 5 cases, while TSE was preferred in the remaining 3 cases. Radiologist 2 preferred TSE in 5 cases.
Conclusions: 3D GRE mDIXON demonstrates clinically acceptable image quality with higher spatial resolution (0.8×0.8×0.8 mm^3) and less

scan time (0:52) than 2D TSE mDIXON (0.9×0.9×2.5 mm^3, 3:51) in a cohort of pediatric patients undergoing osteomyelitis imaging. 3D GRE mDIXON is a viable replacement to 2D mDIXON TSE and may be especially useful in uncooperative patients.

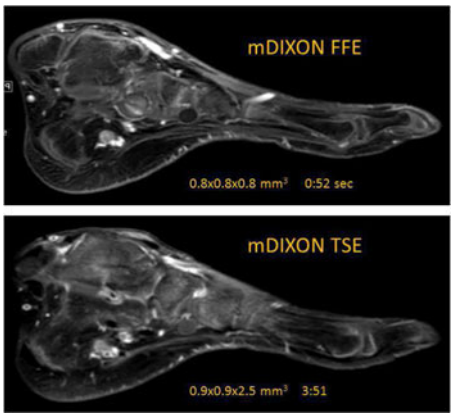

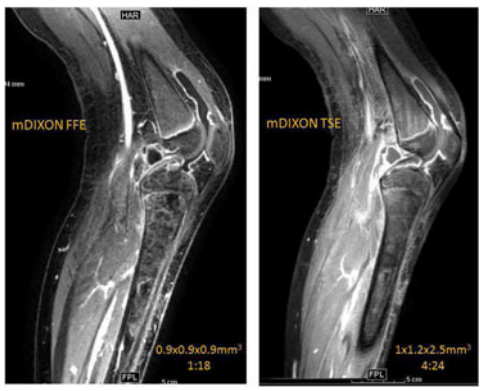

Poster #: SCI-048

The Proximal Pulmonary Arteries in Infants with Shunt Dependent Pulmonary Blood Flow: How Do Computed Tomography and Transthoracic Echocardiography Compare?

Daniel Ehrmann, MD, *Children's Hospital Colorado/University of Colorado, Aurora, CO, daniel.ehrmann@childrenscolorado.org;* Lorna Browne, Brian Fonseca, Adel Younoszai, Michael DiMaria

Disclosures: All authors have disclosed no financial interests, arrangements or affiliations in the context of this activity.
Purpose or Case Report: Infants with one functional cardiac ventricle undergo operations that yield unobstructed systemic outflow and a controlled source of pulmonary blood flow, often starting with the Norwood operation with Blalock-Taussig (BT) shunt. Infants with shunt dependent pulmonary blood flow are at risk for developing proximal pulmonary artery (PA) stenoses, which may result in morbidity and mortality. Echocardiography (TTE) is the primary means of surveillance for PA narrowing, but is limited by acoustic windows, operator experience and patient cooperation. Computed tomography (CT) offers high spatial resolution, rapid acquisition and relatively low radiation exposure. To date, there have been no studies comparing TTE and CT-derived measurements of the proximal PA anatomy in this high-risk population.
Methods & Materials: A retrospective chart review identified infants with shunt dependent pulmonary blood flow that had both TTE and CT performed less than 14 days apart between 1/1/2010 and 9/15/2015. TTE images were reviewed to measure proximal right (RPA) and left PA (LPA) diameters. CT measurements of the proximal RPA and LPA were made using multi-planar reconstruction. Statistics included calculation of PA Z-scores, linear and intra-class correlation (ICC) coefficients and Bland-Altman plots.
Results: Twenty two pairs of studies were analyzed. Sixty percent had Hypoplastic Left Heart Syndrome and 60% had a BT shunt. Analysis of all proximal PA data had moderate linear correlation and agreement (R=0.55, p=0.0003, ICC=0.65, Fig. 1A), though the RPA showed both stronger correlation and agreement (R=0.72, p=0.0005, ICC=0.73, Fig. 2A) than the LPA (R=0.41, p=0.07, ICC=0.60, Fig. 2B). CT detected missed PA stenoses (Z-score<-2) in 4 cases on the left compared to 1 on the right. There was significant variation but no systematic bias over the range of PA diameters by Bland-Altman analysis (Fig. 1B). The median radiation dose was 0.3 mGy (CTDI vol).
Conclusions: In this study of infants with shunt dependent pulmonary blood flow, TTE measurements of proximal PA diameter had only moderate correlation and agreement with CT measurements. RPA diameter was more accurately determined by TTE than LPA diameter using CT as the gold standard, with missed LPA stenosis identified more commonly by CT. In this population at high-risk for circulatory failure due to PA obstruction, a rapid, low-radiation CT may be warranted routinely to prevent missed PA stenosis.

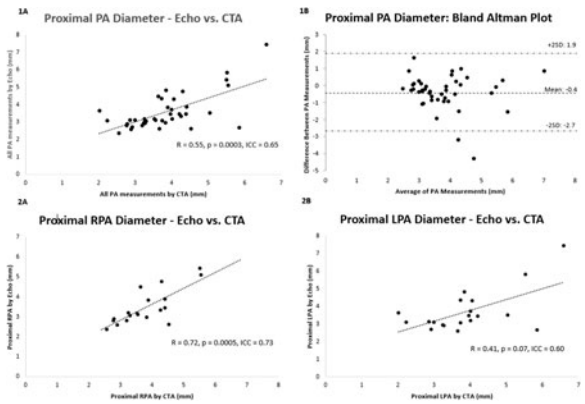

Poster #: SCI-049

Reliability of the Lung Head Ratio Measurements in Congenital Diaphragmatic Hernia Made With Ultrasound as Compared with Fetal MR

Raphael Alford, MD, *Pediatric Radiology, Stanford, Alice Ln, CA, rapha@stanford.edu;* Erika Rubesova, MD, Safwan Halabi, Yair Blumenfeld, Susan Hintz, Richard Barth

Disclosures: All authors have disclosed no financial interests, arrangements or affiliations in the context of this activity.
Purpose or Case Report: The purpose of this study is to determine the reliability of sonographic (US) lung measurements compared with Fetal MR in fetuses with congenital diaphragmatic hernia. The sonographic lung head ratio (LHR) is a widely used prognostic tool in CDH, but can be difficult to obtain due to shifted mediastinum and fetal position. To our knowledge, comparison of MRI measured LHR with US has not been previously reported.

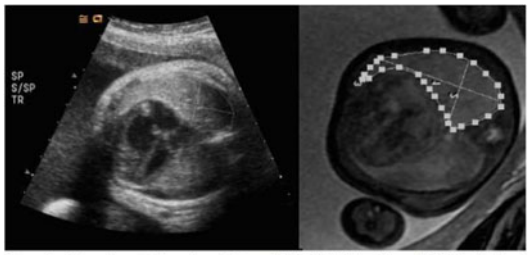

Figure 1: 33 week gestational age fetus with left CDH by US and MRI. Both images depict the longest diameter and area methods measuring the lung opposite the the hernia on at the level of the 4 chamber view.

Methods & Materials: A retrospective review was performed of 40 subjects with a prenatal diagnosis of CDH, who underwent MRI and US on the same day. On both US and MRI the LHR was obtained using both the longest perpendicular diameter method and the method of tracing the lung area on the 4-chamber heart view. Three radiologists with expertise in prenatal imaging performed the measurements. Interobserver agreement was calculated. A paired samples t test was used to detect differences between US LHR and MRI LHR.

Results: Eight subjects were excluded due to lack of head circumference measurement. There were 6 right and 26 left CDHs. There was a high degree of interobserver agreement with lung area tracing on both ultrasound and MRI (correlations of 0.86 and 0.96 respectively). Inter-observer correlation was lower with the longest diameter method (0.82). US consistently underestimated lung area as compared to MRI ($p<0.0001$), by a mean of 70 mm^2 (±137) by longest diameter method and by a mean of 147 mm^2 (±263) by tracing method. All methods of LHR measurement significantly correlated with total lung volume: US LHR by longest diameter $p<0.014$, US LHR by area $p<0.047$, MRI LHR by longest diameter and area both with p <0.0001. US LHR measurements by longest diameter correlate more strongly to total lung volume than do US LHR measurements by area (z=0.34).

Conclusions: The difficulty of obtaining an accurate US lung area measurement in fetuses with congenital diaphragmatic hernia may result in underestimation of the LHR and influence the prognostic assessment. Although ultrasound measurements by longest diameter are not as reproducible, the measurement correlates better with MRI measured total lung volume. Increased agreement between observers with MRI over ultrasound suggests MRI as a better gold standard of measurement.

Poster #: SCI-050

The Aortic Isthmus after Complex Arch Reconstruction in Infants with Single Ventricle Physiology: How does Transthoracic Echocardiography Compare to a Computed Tomography Gold Standard?

Daniel Ehrmann, MD, *Pediatrics, University of Colorado/Children's Hospital Colorado, Aurora, CO, daniel.ehrmann@childrenscolorado.org;* Michael DiMaria, Brian Fonseca, Adel Younoszai, Lorna Browne

Disclosures: All authors have disclosed no financial interests, arrangements or affiliations in the context of this activity.

Purpose or Case Report: Infants with one functional cardiac ventricle often undergo the Norwood procedure which seeks to create unobstructed outflow from the single ventricle to aorta using a complex aortic arch reconstruction. The distal region of the patch used to fashion the neo-aorta terminates near the aortic isthmus, and represents an area of extensive challenge and manipulation for cardiothoracic surgeons. Re-coarctation in this region is common after the Norwood procedure and may be linked with longer-term morbidity and mortality. Echocardiography (TTE) is the primary means of surveillance of the aortic isthmus, though measurements are often difficult due to poor acoustic windows and lack of patient cooperation. To date, there have been no studies that assess how accurately TTE measures the aortic isthmus relative to a computed tomography (CT) derived gold standard.

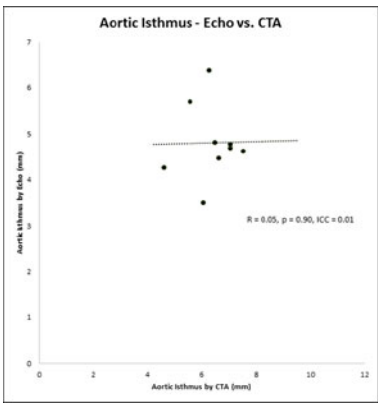

Methods & Materials: A retrospective chart review identified infants with single ventricle physiology status post Norwood procedure that had both TTE and CT performed less than 14 days apart between 1/1/2010 and 9/15/2015. TTE images were reviewed in order to measure the aortic isthmus using the suprasternal notch window. CT measurements of the aortic isthmus were made using multi-planar reconstruction. The relationship between TTE and CT measurements were assessed by linear and intra-class correlation (ICC) coefficients.

Results: 22 pairs of studies met inclusion criteria over the study period. TTE was unable to identify and measure the aortic isthmus in 13 cases (60%). Of the remaining 9 cases, 66% had Hypoplastic Left Heart Syndrome and 56% had a BT shunt. Compared to CT measurements, TTE measurements of the aortic isthmus had extremely poor linear correlation and agreement (R=0.05, p=0.90, ICC=0.01, figure). There were no aortic interventions required. The median radiation dose received was 0.3 mGy (CTDI vol).

Conclusions: In this study of infants with single ventricle physiology status post Norwood procedure, TTE-derived measurements of the aortic isthmus were challenging to obtain and poorly reflective of the true isthmus diameter using CT as a gold standard. Further studies are needed to determine the impact of poor linear correlation and agreement on morbidity and mortality. In this high-risk population for aortic arch obstruction after the Norwood procedure, CT may be a more accurate and timely modality for routine surveillance or imaging upon clinical concern of re-coarctation.

Poster #: SCI-051

Comparison between Ultrasound and MRI Measurements of Fetal Intracranial Volume

Jaladhar Neelavalli, PhD, Edgar Hernandez-Andrade, Swati Mody, MD, *Wayne State University, Detroit, MI, smody@dmc.org;* Brijesh Yadav, Maria Kabrera, Pavan Jella, Lami Yeo, Ewart Haacke, Sonia Hassan, Roberto Romero

Disclosures: All authors have disclosed no financial interests, arrangements or affiliations in the context of this activity.

Purpose or Case Report: Fetal intracranial volume is one of the most important parameters used in assessing normal fetal growth. Based on volumetric ultrasound (US), Virtual Organ Computer-Aided-anaLysis (VOCAL™) is a commonly used technique for such measurement. Magnetic resonance imaging (MRI) offers better soft tissue contrast for fetal brain imaging and is considered as one of the best tools for tissue volumetry, and as a standard for comparison. In this work we compare fetal intracranial volumes measured from MRI with those obtained from VOCAL™ measurements in the same fetuses.

Methods & Materials: Forty Nine fetuses from uncomplicated pregnancies at a median gestational age 31 weeks (1st quartile=27.1, 3rd quartile=35.6, range=20-39) were evaluated. Intracranial volumetric US was performed using a Voluson E-8 (GE Healthcare, Milwaukee, WI, USA) system and the VOCAL™ tool using a rotational method with 30° separation between each image. Volume calculation was performed by delineating the intracranial perimeter in each of the 12 images obtained from the US volume. Fetal MRI was performed on a 3.0 T Siemens Verio system within 1 week of the US assessment. HASTE (Half-Fourier Acquisition Single-shot Turbo spin Echo imaging) images of the fetal brain were acquired in 3 orthogonal orientations. MRI images were systematically assessed by an experienced pediatric neuro radiologist for fetal motion and artifacts and image volumes suitable for intracranial volumetry were selected. Intracranial (IC) volume assessment was carried out through manual tracing. The correlation between volumes obtained from US and MRI was estimated using Pearson's (R) and determination coefficients (R^2), and their association using linear regression.

Results: Excellent correlation (R^2=0.98; p<0.05) between MRI and US fetal intracranial volumes was found with the equation relating the US and MRI volumes as Y=0.73X. MRI-IC volumes were slightly larger than those measured from US. A quadratic increase in the MRI-IC volumes as a function of gestational age was observed, in good agreement with previously published reports.

Conclusions: MRI and US measures of fetal intracranial volumes are in close agreement with each other. The increased volume estimation by MRI may be important to consider while interpreting fetal intracranial volumes in absolute terms.

Poster #: SCI-052

Is Ovarian Medialization a Useful Finding in the Setting of Torsion?

Jeffrey Otjen, MD, *Radiology, Seattle Childrens Hospital, Seattle, WA, Jeffrey.otjen@seattlechildrens.org;* A. Luana Stanescu, MD, Marguerite Parisi, MD, MS

Disclosures: All authors have disclosed no financial interests, arrangements or affiliations in the context of this activity.

Purpose or Case Report: Ovarian torsion in pediatrics is challenging to diagnose, both clinically and radiologically. Ultrasound is most commonly used to evaluate for this process, though there are no sonographic findings that are pathognomonic. One sonographic finding that has been infrequently reported in the literature is medialization of the ovary (defined as the ovary at or crossing the midline of the uterus), as the adnexal structures are drawn inwards by the twisted broad ligament. Knowledge of this finding in addition to the other more classic findings of torsion can be an important clue to the diagnosis. This study evaluates the presence of ovarian medialization in a large number of cases of known torsion.

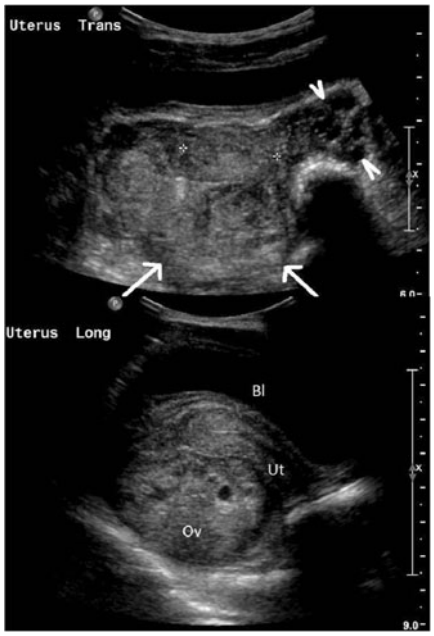

Methods & Materials: All cases of ovarian torsion at a large standalone children's hospital were identified retrospectively by queries of a radiology database and a hospital wide ICD code database after IRB approval. 103 cases were included between 2005 and 2014. Imaging for each case was reviewed and presence or absence of medialization was recorded. Other imaging features were also evaluated, including ovary size and size ratio (compared to the contralateral side), Doppler vascular flow, follicular pattern, associated mass, and free fluid. Percentage of positive findings for each was calculated. Comparison to values in the literature were performed.

Results: Ovarian medialization was present in 60/103 patients. No contralateral (non-torsed) ovaries were found to be medialized. Other findings associated with torsion show similar frequency compared to that in the literature.

Conclusions: Ovarian medialization occurs in the majority of cases of torsion, though is not sensitive enough to exclude torsion as a solitary finding. Increased awareness of medialization, used in conjunction with other more well known findings along with the clinical scenario will aid in efficiently diagnosing torsion.

Poster #: SCI-053

Focal Nodular Hyperplasia in Pediatric Patients on Hepatobiliary Phase MRI After Gadoxetate Disodium Administration

Eric Hu, *Department of Radiology - Section of Pediatric Radiology, University of Michigan - C.S. Mott Children's Hospital, Ann Arbor, MI, erhu@med.umich.edu;* Edward Richer, MD, Peter Strouse, MD, FACR, Ethan Smith, MD

Disclosures: All authors have disclosed no financial interests, arrangements or affiliations in the context of this activity.

Purpose or Case Report: Focal nodular hyperplasia (FNH) is a benign lesion. Gadoxetate disodium (Eovist), a hepatocyte specific contrast agent, is becoming more widely used in pediatric MR imaging. FNH is composed of hepatocytes and should demonstrate homogeneous enhancement on the hepatobiliary phase of imaging; however, in clinical practice a variety of enhancement

patterns have been observed. The purpose of this study is to document the features of FNH on hepatobiliary phase MRI in pediatric patients.
Methods & Materials: Institutional review board approval was obtained. Radiology records were searched for pediatric (<18 years) MRI examinations performed with gadoxetate disodium between 9/2010 and 9/2015 containing at least one the following terms: "focal nodular hyperplasia" or "FNH". Clinical records were reviewed for the following: demographics; malignancy/chemotherapy; non-cancer related liver disease; liver surgery/biopsy. The most recent MRI was reviewed independently by 2 fellowship trained pediatric radiologists. Only the arterial phase and delayed hepatobiliary phase (20 min) axial images were evaluated. For the largest (or only) lesion in each patient, the following was recorded based on the hepatobiliary phase images: lesion size, location and number; central scar; enhancement pattern. Descriptive statistics were used.
Results: 18 patients (12 girls) met inclusion criteria (mean age 13.7 years; range=4-17). 7 patients had prior malignancy/chemotherapy; 3 had non-cancer related liver disease. 11 patients had solitary lesions; 7 patients had multiple lesions. 57% (4/7) of cancer patients and 100% (3/3) of liver disease patients had multiple lesions. Mean lesion size was as follows: all patients=2.6 cm (range 0.9-11.8 cm); cancer patients=2.2 cm; liver disease patients=1.8 cm; sporadic=3.3 cm. 22.2% (4/18) of lesions had a central scar. Hepatobiliary phase enhancement patterns for the largest lesion in each patient were as follows: 39% (7/18) heterogeneous; 33% (6/18) homogeneous; 28% (5/18) peripheral; 0% (0/18) central. Cancer patients most frequently had homogeneous enhancement (57%; 4/7); sporadic lesions most frequently had heterogeneous enhancement (50%; 4/8); liver disease patients were split between the observed enhancement patterns (1 each).
Conclusions: FNH has a variety of enhancement patterns on hepatobiliary phase Eovist MRI. Across all patients, the most common enhancement pattern was heterogeneous, although in cancer patients the majority of lesions enhanced homogeneously.

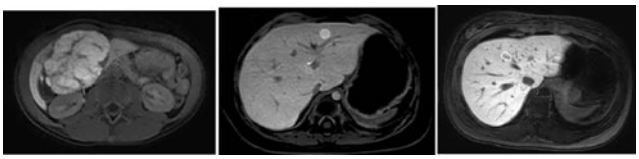

Poster #: SCI-054

Don't put your fingers on that!

Nina Stein, Pediatric Radiologist, Marylin Kereliuk, Michael Schmidt, *Diagnostic Imaging, McMaster University, Mississauga, ON, Canada, michaeldavidschmidt@gmail.com*

Disclosures: All authors have disclosed no financial interests, arrangements or affiliations in the context of this activity.
Purpose or Case Report: Following the ALARA principle, the amount of radiation exposure to those working with x ray technology should be minimized as much as possible. The aim of this study was to access the prevalence of extraneous adult finger(s) in portable NICU chest x ray studies.
Methods & Materials: Retrospective review of 100 portable NICU chest x ray studies was performed after REB approval. Studies available from January 2012 to May 2012 were assessed. The studies were classified as positive or negative for the presence of extraneous adult fingers.
Results: 73/100 were one view studies and 27/100 two view studies making a total of 127 views reviewed. 10/127 (7.9%) views or 10/100 (10%) studies had adult fingers in the films.
Conclusions: The prevalence of 10% of adult fingers in NICU chest films is somewhat high compared to the literature. A group from University of Saskatoon has published 57% reduction in their initial prevalence of 13% after educational activities with hospital staff. We attempt to decrease our rate with similar methodology. Educational material is being created and formal training with review sessions are being organized for radiology and NICU staff. We expect to publish our preliminary results on the second phase of this project after implementation of the educational material in the department. Our goal is to decrease our rate in at least 57%.

Poster #: SCI-055

Simulation Workshop for Medical Emergencies and Patient Safety Concerns in Pediatric Radiology

Elaine Ng, *The Hospital for Sick Children, Toronto, ON, Canada, elaine.ng@sickkids.ca;* Darlene Murray, Oscar Navarro, Jennifer Stimec

Disclosures: All authors have disclosed no financial interests, arrangements or affiliations in the context of this activity.
Purpose or Case Report: Simulation-based education allows for experiential learning to practice and reinforce the CanMEDS roles[1] (as medical expert, communicator and collaborator) in the management of rare events such as medical emergencies in Pediatric Radiology and situations related to patient safety (such as disclosure of adverse events and discussions related to consent). Our objective was to create a simulation workshop to address these education gaps and to determine feasibility, acceptance and educational value as perceived by the participants.
Methods & Materials: The Quality Management Department approved this project. All pediatric radiology trainees who recently started in the general division were invited to participate. The workshop consisted of six time-based stations to address these situations: initial management of anaphylaxis, delivery of basic life support skills, handover of care, safe injection of contrast agents, informed consent, disclosure of adverse events, and triage of cases including selection of protocols for imaging. Checklists were used for scoring. Each trainee received brief personalized feedback at each station. A group debrief and facilitated teaching concluded the workshop. A mixed method approach was used for evaluation including a questionnaire on satisfaction, a 1-min paper[2] and group discussions on perceptions and lessons learned.
Results: Five trainees and five facilitators participated in the workshop. Most trainees ranked "strongly agree" or "agree" on a 5-point Likert scale on questions on satisfaction. They had variable comfort level and experience with the topics covered and simulation-based education. The workshop was considered "pertinent", "really good", "it was…an eye opener…good to get feedback" and more than once different stations were stated as "the most useful station and helpful" and "they were fair". Additional comments included "it was easy because it was a simulation, but real life… would be different" with "different comfort level".
Conclusions: This time-based simulation workshop was resource-intensive but it covered multiple intrinsic roles that are difficult to teach in daily clinical practice. This novel type of teaching and learning was acceptable to our Pediatric Radiology trainees. It was useful to practice by reinforcing the management of medical emergencies and patient safety concerns. It encouraged reflection of their own learning and revealed education gaps. The format may also contribute to the future development of a competency-based curriculum.
References
1. http://www.royalcollege.ca/portal/page/portal/rc/common/documents/canmeds/framework/canmeds2015_framework_series_IV_e.pdf
2. Angelo, T; Cross, P. Minute paper. Retrieved from http://www.writing.ucsb.edu/faculty/dean/Upload2021-W08/minpapercat–ChrisComments.pdf

Poster #: SCI-056

Improving the Diagnosis of Obstructive Hydronephrosis in Children using the Functional Analysis of the Magnetic Resonance Urography Scan (fMRU)

Sandra Bareño, Lizbet Pérez-Marrero, Staff, Isabel Fuentealba, Georgette Pose, Gloria Soto, *Imágenes, Clínica Alemana de Santiago, Santiago, Chile, gloria.soto@gmail.com;* Claudio Silva, Cesar Salinas

Disclosures: All authors have disclosed no financial interests, arrangements or affiliations in the context of this activity.
Purpose or Case Report: To determine the cause of obstructive hydronephrosis using fMRU in pediatric patients with inconclusive conventional studies.
Methods & Materials: A prospective, non-experimental, exploratory study in pediatric patients with moderate to severe hydronephrosis for whom conventional studies were inconclusive to determine obstruction as a cause was performed.
Patients included did not have renal impairment nor vesicoureteral reflux.
fMRU was performed with a 1.5 T device and our protocol included both morphological and functional studies before and after gadolinium injection.
For functional analysis we used Khrichenko and Darge Software, available at http://www.CHOP-fMRU.com.
Image analysis was performed by two radiologists and the final diagnosis was made by consensus.
The results of fMRU were correlated with surgical findings in the cases that underwent surgery and patients were followed for a period of 1 year after surgery.
Results: 10 patients were included in the study with a total of 20 renal units analyzed. 12 units had hydronephrosis, 8 moderate and 4 severe. 8 renal units were normal.
The fMRU was able to determine that 11 cases were obstructive hydronephrosis and one was inconclusive. Also, it was possible to determine if the obstructive systems were unbalanced or not. Regarding the level of obstruction, ureteropelvic junction stenosis was the most frequent finding. Those findings were certificated during surgery.
Differential renal function was estimated in 9 patients with good correlation when compared to nuclear medicine scans.
All the cases that underwent surgery improved the hydronephrosis and they are in good conditions 1 year later.
Conclusions: fMRI is a good method to asses obstruction as a cause of hydronephrosis in cases where conventional studies are inconclusive.
fMRU provides all the information needed to make clinical decisions without the use of ionizing radiation. Its disadvantage is the requirement for anesthesia and / or sedation in young children.

Poster #: SCI-057

A Study of Radiological Features of Healing in Infant Long Bone Fractures

Christopher Warner, *University of Colorado, Aurora, CO, christopher.warner@ucdenver.edu;* Sabine Maguire, Angie Miller, Laszlo Trefan, Michael Fadell, M.D.

Disclosures: All authors have disclosed no financial interests, arrangements or affiliations in the context of this activity.
Purpose or Case Report: Fractures are a common manifestation of physical child abuse, and when present can have considerable bearing on the legal process. Although the timing of skeletal injury and healing is of great importance in forensic cases, the dating of fractures in the age group in which fractures from physical abuse most frequently occur is largely based on the radiologist's personal experience as opposed to primary research. A full understanding of the radiological features of healing in infant fractures will enhance the assessment of fracture dating in cases where the time of injury is unknown, such as suspected abuse. The objective of this study was to describe the timing of fracture healing in infants using previously defined radiographic signs of fracture healing.
Methods & Materials: We completed a retrospective cross-sectional time-series study of long bone fractures in infants from 2006 to 2013. After exclusion criteria were applied a total of 100 digital images were available for review from 51 infants. Utilizing published criteria for dating fractures, the presence or absence of four pre-defined features of healing were scored: periosteal reaction, callus, bridging, and remodeling. Three radiologists independently scored radiographs with a 3 point scale, marking each feature as present, absent, or equivocal. Statistical analysis using free marginal kappa was conducted.
Results: The level of agreement between the three radiologists was high (0.77-0.95) reinforcing the validity of the observations. Features of healing were first seen at 7, 9, 15, and 51 days for periosteal reaction, callus, bridging, and remodeling respectively. The peak periods, defined as 'data tabulated to identify the earliest agreed recording, peak prevalence intervals (present in >40% of images), and last agreed recording of each feature, were as follows: periosteal reaction 7-130 days, callus 9-26 days, bridging 15-67 days, and remodeling 51-130 days (Fig. 1).
Conclusions: Features of fracture healing develop in a logical progression with periosteal reaction developing first, followed by callus formation, then bridging callus, and finally remodeling. This study builds on prior research in this area, and provides additional supportive evidence when determining whether a given fracture is consistent with a proposed time frame, especially in assessing cases in which non-accidental trauma is a consideration.

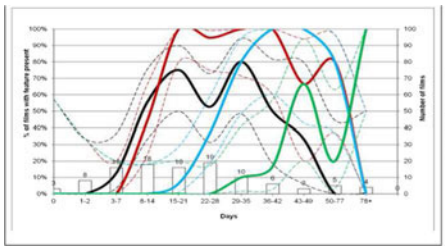

Figure 1: Periosteal Reaction (black), Callus (red), Bridging (blue), and Remodelling (green) - as defined by the percentage of agreement between observers of the presence of finding (solid line) with the 95% lower and upper confidence intervals (dashed lines)

Poster #: SCI-058

Challenges of Point Of Care Ultrasound (POC-US) in Evaluating Hemophilic Arthropathy – Preliminary Experience

Magdy Mohamed Ezzelarab Soliman, *The Hospital for Sick Children (SICKKIDS), Toronto, ON, Canada, magdy.soliman@sunnybrook.ca;* Vanessa Bouskill, Arun Mohanta, Ningning Zhang, Alex Zhou, Jose Jarrin, Ai hua Huo, Runhui Wu, Yun Peng, Andrea Doria

Disclosures: All authors have disclosed no financial interests, arrangements or affiliations in the context of this activity.
Purpose or Case Report: POC-US aims at shortening the scanning and interpretation time being easy to use by clinicians and allied health professionals at the time of patients' physical examination. Our purposes are: 1. To compare POC-US to detailed US and MRI in evaluating hemophilic arthropathy. 2. To point out limitations of POC-US that can decrease its accuracy. 3. To propose strategies to refine protocols.
Methods & Materials: 7 knees, 8 ankles and 7 elbows of 23 hemophilic boys (7-18 years; median, 13) followed at Beijing Children's Hospital, China underwent POC-US (performed by a nurse trained in POC-US), detailed gray scale/color Doppler US (5-17 MHz linear probes, performed by experienced sonographers), 3 T MRI (PD, Gradient Echo, T2 fat sat and WATSc) and physical examination. (Hemophilia Joint Health Score [HJHS] performed by a physiotherapist). Scoring of US and MRI images was achieved by consensus by a panel of experienced imagers based on International Prophylaxis Study Group systems.
Results: Median HJHS scores were 10.5/7/10.5 for knees, ankles, elbows. Whereas synovial hypertrophy and hemosiderin were diagnosed

in 19 (83%) cases by MRI and detailed US, respectively. they were missed (false-negatives, FN) in 8/23 (35%) and 5/23 (22%) cases by POC-US. Mild to moderate joint effusion was detected in 6/23 (26%) cases by both MRI and detailed US, and in 4/23 (17%) by POC-US. One false-positive (FP) case was misdiagnosed by POC-US when mild effusion was mis-interpreted as hemosiderin.

Detection of osteochondral changes was limited by POC-US: out of 17/23 (74%) cases with cartilage loss and erosions diagnosed by MRI and detailed US, POC US missed 4 and 7 cases (FN), respectively.

Conclusions: Diagnostic accuracy of POC for assessing hemophilic arthropathy is overall limited. Challenges of POC-US include limited imaging planes, focused training, lack of optimized technical parameters and difficulties for interpreting a reduced number of images. Adding imaging planes, color Doppler, increasing level of training and availability of images are suggested ways to improve the accuracy of the technique.

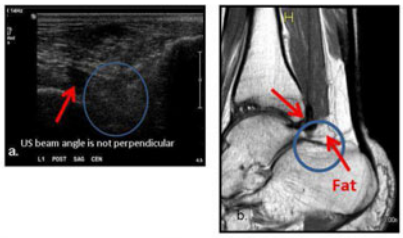

Fig.1 16 years old boy with moderate hemophilic arthropathy and recurrent left ankle bleed (a) Sagittal posterior point of care ultrasound image (POC-US) image of the left ankle joint shows a hypoechoic area (arrow) considered to represent hemosiderin and an echogenic area (circled) reported as synovial hypertrophy.

(b) Corresponding sagittal proton density MR image shows normal posterior ankle fat signal (circled).

There is no synovial hypertrophy. Small volume dark hemosiderin was confirmed over the distal tibia. Limited operator experience, technical errors and few imaging planes in POC US can contribute to false-positive and false-negative results.

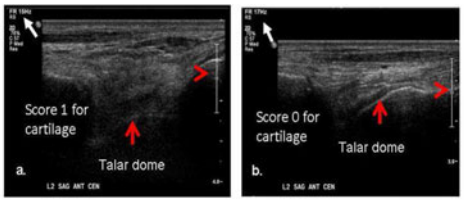

Fig.2 7 years old girl with mild hemophilic arthropathy of right ankle.

(a) Sagittal anterior POC US image of the right ankle considered attenuation of the articular cartilage over the talar dome (red arrow, score 1, articular cartilage changes). The examination was performed by a health care professional who received short-US training.

(b) Same ankle examined by a board certified sonographer shows normal uniform thickness of the hypoechoic articular cartilage (red arrow, score 0). Adjusting depth, focal zone (red arrowheads) and frequency (white arrow above) are technical demands for proper US examination which require high level of US training.

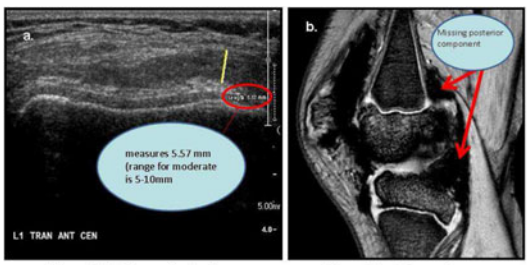

Hemosiderin Score: Moderate Hemosiderin Score: Severe

Fig.3 8 years old boy with severe hemophilic arthropathy of the left knee.

(a) Axial anterior POC US image of the knee joint shows hypoechoic hemosiderin in the suprapattelar recess (yellow line) reported as moderate amount.

(b) Corresponding sagittal gradient-echo MR image shows additional intra-articular hemosiderin posterior in the knee joint (red arrows). Limited imaging planes in POC US may lead to underestimation of findings and consequently, to false-negative results concerning intra-articular hemosiderin deposits.

Poster #: SCI-059

Assessment of Radiology Resident Performance in Neonatal Head Ultrasound after Implementation of a Novel Brain Phantom Training Model

Kedar Patil, Medical Doctorate, *Diagnostic Imaging, McGill University Health Centre, McGill University, Montreal, QC, Canada;* Natalia Gorelik, MD, Zonah Kumalo, Lionel Bure, Pedro Albuquerque, Ricardo Faingold

Disclosures: All authors have disclosed no financial interests, arrangements or affiliations in the context of this activity.

Purpose or Case Report: There is no standardized evidence-based neonatal head ultrasound (HUS) training guidelines within the literature. Simulation models have previously shown to improve resident proficiency in performing ultrasound-guided procedures. We developed an ultrasound-compatible neonatal brain phantom from polyvinyl alcohol cryogel (Figure 1) with the relevant cross-sectional anatomy.

The purpose of this study was to determine whether resident performance in HUS improves with the use of this novel brain phantom training model.

Methods & Materials: In this retrospective blinded study, 10 junior diagnostic imaging residents, with at least 1-year of general radiology training, performed HUS at the beginning of their pediatric radiology rotation. Each resident received a detailed protocol sheet and then passively observed an ultrasound technologist perform a complete HUS on a neonatal patient. All residents also receive routine teaching with our brain phantom model. There were two different groups. In Group A, five residents independently performed one HUS exam, subsequently received training using the phantom-simulation model, and then performed a post-training HUS exam. In Group B, five residents received phantom-simulation model training prior to their first HUS exam. Three experienced pediatric radiologists reviewed the ultrasound images of each HUS exam for proficiency of image-acquisition, using a validated scoring system, and blinded to each other's results. Statistical analysis was performed using a paired two-way repeated measures ANOVA.

Results: Residents who initially trained with the phantom training model performed significantly better than those residents who did not (p=0.012). There was also a statistically significant improvement in performance when comparing the same residents pre and post-phantom training (p=0.004).

Conclusions: Our novel HUS phantom training model significantly improves radiology resident performance and appears to be beneficial in the radiology residency-training curriculum.

Poster #: SCI-060

Prenatal MRI and US findings of small bowel obstruction: Imaging Clues and Postnatal Outcomes

Eva Rubio, MD, *Children's National Medical Center, Washington, DC, rubioeva@yahoo.com;* Anna Blask, MD, Dorothy Bulas, Andrea Badillo

Disclosures: All authors have disclosed no financial interests, arrangements or affiliations in the context of this activity.

Purpose or Case Report: Differentiating levels of small bowel obstruction in the fetus and predicting the outcome remain challenging. Our goal is to characterize imaging details which suggest the level of obstruction or a potentially complex postnatal course.
Methods & Materials: A retrospective review of prenatal cases of small bowel obstruction imaged with MRI and US from 2005 to 2015 was conducted. Prenatal and postnatal imaging, surgical findings and long term outcomes were reviewed.
Results: 12 cases were identified, with 91% survival. Intraoperative and long term outcomes were available for 10. One fetus expired at 26 weeks and underwent autopsy. One fetus is not yet born. Gestational age at evaluation ranged from 25 to 36 weeks. 9/12 (75%) had polyhydramnios. 8/10 (80%) liveborn fetuses delivered prematurely. The level of obstruction was confirmed intraoperatively as jejunal in 9/11 (82%), ileal in 2/11 (18%). In 8/11 (73%) evaluated postnatally, intraoperative or autopsy findings were complex: multiple atresias (3), perforation (3), volvulus (1) and multiple anomalies including anal atresia (1). Cystic fibrosis (CF) was confirmed in 3/12 (25%). Fetal MRI signal characteristics of dilated small bowel loops correlated with obstruction level confirmed postnatally: in 5/11 low T1w dilated bowel loops corresponded to jejunal atresia, in 2/11 intermediate T1w signal bowel loops corresponded to distal jejunal atresia or complex perforation, and in 4/11 bright T1w signal in dilated bowel loops corresponded to CF, ileal atresia or concomitant anal atresia. The colon on T1w imaging was abnormally faint in all cases. Imaging of the rectum was similar in 8 cases of jejunal or ileal atresia irrespective of obstruction level, with adequate meconium distension. However, an abnormal paucity of rectal filling was noted in all cases of CF and in 1 case with concomitant high anal atresia. 3/11 (27%) developed short gut syndrome, 1 of which had perforation prenatally. The 2 postnatal cases of CF have had no further gastrointestinal complications.
Conclusions: Prenatal jejunal-ileal obstruction can have a variable outcome dependent on etiology, coexisting abnormalities such as CF and number of atresias. Complications may include volvulus, perforation, and preterm delivery. Fetal MRI is useful in the more complex atresias for assessment of meconium distribution within the small bowel, colon and rectosigmoid.

Poster #: SCI-061

Colonic Volvulus in Children and Adolescents: A Review of 11 Cases

Aditi Hendi, MD, *Radiology, Thomas Jefferson University Hospital, Philadelphia, PA, aditi.hendi@jefferson.edu;* Mary Harty, Leslie Grissom

Disclosures: All authors have disclosed no financial interests, arrangements or affiliations in the context of this activity.
Purpose or Case Report: Colonic volvulus in the pediatric population is very rare with 40% mortality making timely diagnosis imperative. Radiologists should operate with a high degree of clinical suspicion in patients with risk factors for large bowel volvulus. Recognition of colonic volvulus on plain film, contrast enema and CT is paramount to work-up and definitive management. This case series is the largest from any single institution and describes the clinical course and imaging findings in cases of volvulus, with the goal of familiarizing the radiologist with the appearance of this disease entity on several imaging modalities.
Methods & Materials: An IRB-approved 10-year retrospective review of 11 pediatric patients with colonic volvulus was done. Imaging findings suggestive of volvulus in each case were identified, including featureless or dilated colon on plain film, lack of contrast passage on enema and beaked colon or twisting of mesocolon on CT. Imaging results were correlated with initial clinical presentation and final surgical or colonoscopic diagnosis.

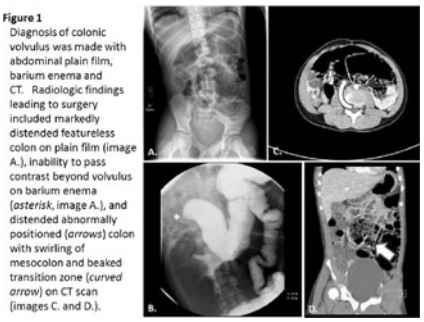

Figure 1
Diagnosis of colonic volvulus was made with abdominal plain film, barium enema and CT. Radiologic findings leading to surgery included markedly distended featureless colon on plain film (image A.), inability to pass contrast beyond volvulus on barium enema (*asterisk*, image A.), and distended abnormally positioned (*arrows*) colon with swirling of mesocolon and beaked transition zone (*curved arrow*) on CT scan (images C. and D.).

Results: Eleven cases of large bowel volvulus in patients aged 3 months to 18 years were reviewed. Five had volvulus of the sigmoid, 3 of the cecum and 3 of transverse colon. Ten of 11 patients had a history of chronic constipation, 4 had prior abdominal surgeries, and 5 patients had either a neurologic condition or mental retardation limiting communication. Patients who underwent CT or contrast enema had earlier diagnosis, whereas those who received plain films required additional imaging for confirmation. Diagnosis of volvulus by imaging was reached in 6/9 patients who had plain film, 3/3 who had contrast enema and 9/9 who had CTs. Location of volvulus on CT and contrast enema corresponded with surgical or colonoscopic findings in 100% of cases, but only 22% of plain film findings were accurate for identifying the segment of colon involved in volvulus. At laparotomy, 5 out of 11 patients underwent partial colectomy of which 2 were found to have necrotic bowel. The remaining 6 had volvulus detorsion and bowel was preserved.
Conclusions: Plain film is a good screening modality when clinical presentation and risk factors raise suspicion for pediatric colonic volvulus. Further imaging by contrast enema or CT should be recommended, depending on stability of the patient. Familiarity with imaging findings of large bowel volvulus can improve detection of this disease entity, aiding in timely management of these patients.

Poster #: SCI-062

Prevalence of Knee MRI Findings in Patients with Acute Versus Nonacute Knee Pain in the Sports Medicine Setting

Sean Oneill, MD, *Radiology, Ann and Robert Lurie Children's Hospital, Chicago, IL, ONEILLSM@GMAIL.COM;* Rebecca Carl, Cynthia LaBella, Jonathan Samet, MD

Disclosures: All authors have disclosed no financial interests, arrangements or affiliations in the context of this activity.
Purpose or Case Report: Depending on the age of the patient, knee MRI may be a daunting exam. Physicians may have a higher threshold to order MRI in the pediatric setting compared to the adult setting. Few if any studies are available which attempt to predict the prevalence of MRI findings based on the patient's presenting history in the sports medicine setting. Our objective was to determine the prevalence of knee pathology using MRI in two groups of pediatric patients: those with an acute event, and those with knee pain without history of acute event.
Methods & Materials: A database of patients who were seen at a tertiary care center non-surgical sports medicine was accessed. This study included those who presented with knee pain, had a knee MRI, and had been categorized by a sports medicine physician into acute or nonacute/overuse groups. A consensus read between a fellowship-trained musculoskeletal radiologist and a pediatric radiology fellow was performed for each MRI using a structured reporting system. Follow-up MRIs on the same knee were excluded.
Results: A total of 26 knee MRIs performed on patients with acute pain (average age 14.7 years, range 11-26 years) and 26 MRIs in those with nonacute pain (average age 12.8 years, range 7-17 years) were reviewed. Significantly more knees with imaging findings of patellofemoral instability were seen in the acute group (50%) versus nonacute group (15%), $p<0.05$. The acute group included more bone contusions (58% vs 4%, $p<0.0001$) and soft tissue edema (27% vs 0%, $p<0.01$). More Baker's cysts were seen in the nonacute group (27% vs 4% in acute), $p<0.05$. Prevalence of extensor mechanism abnormalities such as patellar and quadriceps tendinopathy and Osgood-Schlatter disease was 15% in the acute and 27% in the nonacute groups. Prevalence of MCL injury in the acute vs nonacute groups was 11% vs 0%, cartilage injury was 35% vs 11%, and osteochondritis dessicans was 0% vs 11%. Prevalence of cruciate ligament injury, meniscal injury, and lateral collateral ligament complex injury was low in both groups (<4%).
Conclusions: In the sports medicine setting, patients with acute injury are more likely to have patellofemoral instability, bone contusions, and soft tissue edema than those with a nonacute presentation. Patients with a nonacute presentation are more likely to have Baker's cysts. The prevalence of ligamentous and meniscal injury was low in this nonsurgical setting.

Poster #: SCI-063

Clinical Utility of Dual-Energy X-Ray Absorptiometry for Assessment of Fractures in Pediatric Osteogenesis Imperfecta: Evidence-Based Knowledge Synthesis

Daniel Yacoub, *The Hospital for Sick Children, Toronto, ON, Canada, yacoub.daniel@gmail.com;* Kuan Chung Wang, Prakeshkumar Shah, Rahim Moineddin, Andrea Doria

Disclosures: All authors have disclosed no financial interests, arrangements or affiliations in the context of this activity.
Purpose or Case Report: Increased fracture risk is a complication that occurs in the context of primary bone diseases such as osteogenesis imperfecta (OI). Despite being considered as the reference-standard, the use of dual-energy X-ray absorptiometry (DXA) to evaluate fragility fractures in OI has not been validated by prior systemic review. Identifying patients at greatest risk for bone fragility fractures and determining skeletal health markers that can monitor bone mass concerning response to bone-active treatments are important issues for clinicians. In this systematic review we assessed the clinical utility of DXA for evaluating osteoporotic bone in OI pediatric patients according to the U.S. Preventive Services Task Force guidelines.
Methods & Materials: We retrieved articles that assessed abnormal bone quality in patients of mean age ≤18 years (MEDLINE and EMBASE, 1946-2015). Evidence was accrued for concurrent and predictive validity, and responsiveness of DXA according to the questions: (1) Is DXA a good predictor and/or indicator of bone fragility fracture risk in patients with OI? (2) Is DXA responsive to an intervention (bone-active treatment, e.g. bisphosphonate, calcitriol, exercise) in OI patients? Two reviewers independently evaluated articles' quality of reporting and methodological quality using Standards for Reporting of Diagnostic Accuracy and Quality Assessment of Diagnostic Accuracy Studies tools.
Results: Out of 162 retrieved references we included 18 studies (778 patients; 357 reported boys and 315 girls; age range, 0-18 years). The mean quality of reporting score was "moderate" (77.8% of articles); the mean methodological quality score was "high" (81.4%). For the proposed questions, conflicting evidence exists in the literature to support DXA's ability to diagnose fracture in patients with OI (Grade C) and insufficient evidence is available to make a recommendation regarding the value of DXA for prediction of future fractures (Grade I). Nevertheless, fair recommendation exists for the use of lumbar spine bone mineral density to assess the effect of bisphosphonates on bone health (Grade B). Gaps in the literature included lack of information concerning effects of different statistical adjustment applications during measurement differences between OI subtypes.
Conclusions: DXA-based measurements can respond to bisphosphonate interventions (fair evidence), however insufficient evidence exists to support other clinimetric properties of this technique.
Levels of evidence and recommendations according to the guidelines of the U.S. Preventive Services Task Force's (USPSTF) recommendation guidelines

Maneuver (Fig. 1)	Focus Area (1, 2, or 3)	Evidence	USPSTF categorization	Recommendations
Concurrent validity of DXA to diagnose fracture (1)	1	Two studies reported poor diagnostic ability of changes in BMD measured by DXA for diagnosis of vertebral compression fractures. Two studies reported significant correlation and adequate diagnostic ability of ability of aLSBMD.	Four cross-sectional studies, four retrospective cohort studies; Level II-2 (*n*=4)	Grade C: Conflicting evidence in the literature.
Predictive ability of DXA to predict future fracture (3)	3	One study investigated the predictive ability for future fracture. It reported adequate prediction of BMD using lifetime fracture rate. The following 4 gaps were noted: (i) predictive value for peripheral vs. vertebral fracture; (ii) difference between single time-point measurement vs. multitime point in measurements; (iii) choice of region of interest; (iv) difference between area vs. volumetric measurement	Retrospective cross-sectional and cohort case study; Level II-2 (*n*=1)	Grade I: Insufficient evidence in terms of both quantity and quality
Responsiveness of DXA to intervention (2)	1	Fifteen studies investigated the responsiveness of DXA measurements to bisphosphonate therapy, Overall, aLSBMD was reported to be responsive to intervention. The following 2 gaps were noted: (i) difference/choice between areal or volumetric measurements; (ii) the choice of region of interest	Three experimental non-randomized control trials, one open label uncontrolled study, five prospective cohort studies, one retrospective cohort study, one case controlled prospective cohort, three randomized control trials, and one double blind RCT; Level II-1 (*n*=4), II-2 (*n*=8), I (*n*=3)	Grade B: Fair recommendations was made against the use of DXA measurement to detect bisphosphonate therapy.
3				

Abbreviations: DXA, dual-energy absorptiometry; aLSBMD, areal lumbar spine bone mineral density; aTBBMD, areal total body bone mineral density; aFBMD, femoral neck bone mineral density; vLSBMD, volumetric lumbar spine bone density; LSBMC, lumbar spine bone mineral content
Note: Focus Area 1 represents areas in the existing literature that have enough knowledge (in quantity and quality) to be synthesized; Focus Area 2 represents areas that are too heterogeneous or scarce to provide clinically useful informations and that require further standardization of imaging and research methods; Focus Area 3 represents gaps in the literature.

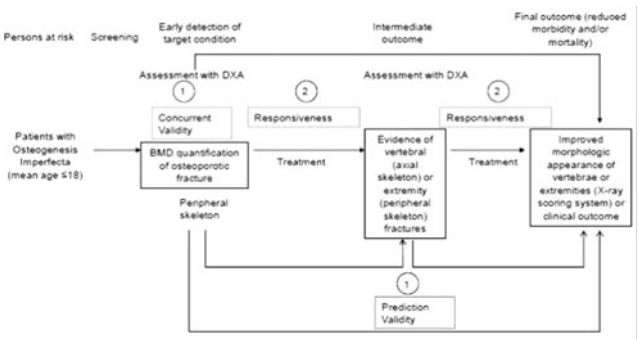

Poster #: SCI-064

Diagnostic Accuracy of MR Enterography Detecting Mucosal Healing in Pediatric Crohn's Disease

Jorge Davila, MD, *Children's Hospital of Eastern Ontario, Ottawa, ON, Canada, jdavila@cheo.on.ca;* Kerri Highmore, Elka Miller

Disclosures: All authors have disclosed no financial interests, arrangements or affiliations in the context of this activity.
Purpose or Case Report: The objective of this prospective study was to determine the accuracy of MR Enterography (MRE) in the assessment of mucosal healing in patients with Pediatric Crohn's Disease (PCD) after starting treatment. MARIA and Clermont scores are MRE scores that were originally developed in adult population for the assessment of severity of Crohn's Disease (CD) in correlation to Crohn's Disease Endoscopic Index of Severity (CDEIS). MARIA score has shown close correlation to disease severity of colonic CD and Clermont score has shown close correlation to terminal ileum disease. A few reports have shown correlation of mucosal heling when assess by MRE scores and CDEIS in Adult population, but not work is available in pediatrics.
Methods & Materials: 16 patients with PCD underwent ileocolonoscopy (IC) and immediately after MR Enterography (MRE) at the time of diagnosis or when biological treatment

was going to be started (time 1). Each patient had a 12-week follow up with IC and MRE (time 2), in the same settings as was performed at time 1. MRE included multiphase fiesta, 3 planes SSFSE, 2 planes DWI b1000 and pre-contrast and post-contrast dynamic multiphase T1-fat sat weighted sequences. Endoscopic activity was evaluated based in the Short Endoscopic Score for CD (SES-CD). MRE scores were calculated based in the independent readings performed by two experimented Pediatric Radiologists who were blinded to the SES-CD. The assessment of the terminal ileum (TI) was separated from the large bowel that was divided in 6 segments. ICC for Maria and Clermont scores were calculated as well as ROC when compare with SES-CD. Correlation of the variation of MRE scores and variation of SES-CD between T1 and T2 where calculated for the assessment of mucosal healing.

Results: ICC in the TI was 0.33 for MARIA and 0.34 for Clermont. ICC in colon were 0.16-0.87 for MARIA and 0.27 - 0.96 for Clermont. No significant correlation was found between SES-CD and MRE scores in the colon. Spearman coefficient in the TI was 0.54 (p: 0.0039) for MARIA and SES-CD and 0.50 (p:0.0039) for SES-CD and Clermont. Spearman coefficient in the TI for assessing interval healing changes for MARIA was 0.47 (p: 0.069) and for Clermont was 0.48 (p:0.062).

Conclusions: Developed MRE severity scores are only valid for the assessment PCD in the terminal ileum. Assessment for mucosal healing is close to be significant, further recalculation in the ponderation of values for both scores may be beneficial for adequate assessment of healing in pediatric population.

Poster #: SCI-065

Breast Imaging in the Pediatric Population: Pitfalls and Practices

Cory Pfeifer, MD, Jeannie Kwon, Kristi Oatis, MD, *Radiology, University of Texas Southwestern Medical Center, Dallas, TX, Kristi@doatis.com*

Disclosures: All authors have disclosed no financial interests, arrangements or affiliations in the context of this activity.

Purpose or Case Report: The purpose of this exhibition is to outline practice patterns among breast imaging in the pediatric population while identifying barriers to execution of standard breast imaging practices in pediatric patients.

Methods & Materials: All breast ultrasounds in patients aged 18 years or younger performed at our facility (n=1214, 1037 female and 178 male) over the preceding 4 year period were reviewed following removal of identifiable information. All reports were studied with respect to class (inpatient, outpatient, or emergency), patient age, sex, indication, findings, recommendations, reporting verbiage, and recommendations.

Results: Of the 1214, exams, 914 (75%) were ordered in the outpatient setting. Imaging features of breast buds were described in 158 patients (13%). A diagnosis of gynecomastia was assigned to 66 male (37%) patients. BI-RADS designations were assigned in 28 examinations (2%) with 11 of these denoted as BI-RADS 1, 1 as BI-RADS 2, and 18 as BI-RADS 3 with most BI-RADS 3 lesions showing characteristics of fibroadenoma. No designations of BI-RADS 4 or BI-RADS 5 were applied. A diagnosis of fibroadenoma was provided in 198 (16%) of the reports with 6 of these lesions assigned a notation that Pseudoangiomatous stromal hyperplasia (PASH) cannot be excluded. Biopsy was discussed in 20 cases (1.6%), all of which in reference to previously diagnosed or probable fibroadenomas. Lymph nodes were described in 37 (3%) of ultrasounds. In 26 impressions (2%), follow-up at designated women's imaging centers was recommended, however, follow-up at such centers proved to be difficult given payment models for pediatric patients and differences in preferences among surgeons and referring clinicians.

Conclusions: Breast ultrasounds in the pediatric population rarely show concerning features, nonetheless, pediatric radiologists are often faced with making recommendations regarding breast findings in children. Despite the availability of BI-RADS designations for breast ultrasounds, pediatric radiologists do not frequently assign them. Reasons for this may include a lack of a reimbursable follow-up mechanism, inability of designated women's imaging centers to accommodate pediatric patients, and conflicting practice habits of pediatric surgeons. Given the high likelihood of benignity in the pediatric population, further study is suggested to define distinct practice parameters for pediatric breast imaging.

Poster #: SCI-066

Development of an Objective Scoring System to Assess Resident Proficiency at Performing Head Ultrasound in Infants

Natalia Gorelik, MD, *Montreal Children's Hospital, McGill University Health Center, Montreal, QC, Canada, natalia.gorelik@mail.mcgill.ca;* Zonah Khumalo, FC Rad Diag, Christine Saint-Martin, Lionel Bure, Ricardo Faingold

Disclosures: All authors have disclosed no financial interests, arrangements or affiliations in the context of this activity.

Purpose or Case Report: Our study aims to test for validity a recently developed scoring system for the assessment of resident proficiency at performing a head ultrasound (HUS) examination in infants.

Methods & Materials: A scoring system, which includes the most important elements in technique and relevant anatomic structures, was designed by 4 senior pediatric radiologists. Face and content validity were obtained by consensus.

Using the scoring system, 10 HUS examinations performed by residents (5 junior and 5 senior) and 10 HUS examinations performed by experienced ultrasound technologists were retrospectively graded by 3 senior pediatric radiologists. To test the scoring system for construct validity, the average scores of the technologists vs. residents and of the junior vs. senior residents were compared using the two-way analysis of variance test.

Results: The maximum score was 36. The mean score was 33.3 for the technologists and 28.6 for the residents. The senior residents scored, on average, higher (31.6) than the juniors (25.6). There is a significant statistical difference between the technologists' and residents' scores (p=009) as well as between the junior and senior residents' scores (p=0.035). The inter-rater variability is moderate (0.5).

Conclusions: The scoring system demonstrates validity for assessing proficiency at performing HUS examinations. The use of in-training evaluation provides the opportunity for a critical appraisal of the resident's competency and allows for timely corrective action through formative feedback. The scoring system will subsequently be used to evaluate the effects of a newly introduced brain phantom simulation on HUS training.

Scoring System (By Gorelik and Faingold)
Assessment of Resident Performance at Head Ultrasound

Date: _____
Name of Resident: _____
Year of Residency: _____
Name of Evaluator: _____

	unsatisfactory	needs improvement	satisfactory
	0	1	2
Scanning Technique			
Chose appropriate transducer (sector/vector then linear)			
Use multiple focal zones - ensure enough depth to visualize the cerebellum			
Acquire a sufficient quantity of images (minimum of 28): - 10 coronal and 10 sagittal with sector probe - 2 coronal and 4 sagittal with linear probe - 2 pulse + Color Doppler (pericalosal artery and superior sagittal sinus), if relevant			
Obtain centered and straight images (interhemispheric fissure is midline and perpendicular)			
Appropriate orientation (left side of image represents patient's right side on the coronal view or the anterior of the brain on the sagittal view)			
Label images accordingly with the side and the anatomical site			
Tilt probe about 10 degrees for parasagittal acquisition of caudothalamic groove to temporal lobes			
Recognize common artifact and use strategies to reduce them			
Anatomy			
Coronal View			
- frontal lobe and frontal horns of the lateral ventricles			
- septum pellucidum, corpus callosum, and portions of the frontal, parietal, and temporal lobes			
- caudothalamic groove and basal ganglia			
- bodies of the lateral ventricles, periventricular white matter			
- posterior portions of the temporal lobes, occipital lobes, fourth ventricle, cerebellum, and cisterna magna			
Sagittal View			
- Midline Sagittal View			
- corpus callosum, cavum septum pellucidum and cavum vergae extension (if present), third ventricle, fourth ventricle, vermis of the cerebellum			
- Parasagittal View			
- caudothalamic groove			
- lateral ventricle with occipital horn and its choroid plexus			
- periventricular white matter			
- sylvian fissure			
Total Score			**/36**

Comments:

Poster #: SCI-067

The Utility of CT and/or MRI in the Management of Benign Macrocrania

M. Edward Haws, MD, PhD, Luke Linscott, MD, *Child Neurology, Cincinnati Children's Hospital Medical Center, Hebron, KY, Luke.Linscott@cchmc.org;* Cameron Thomas, Beth Kline-Fath, MD

Disclosures: All authors have disclosed no financial interests, arrangements or affiliations in the context of this activity.
Purpose or Case Report: Benign macrocrania (BM) is primarily diagnosed by ultrasound (US). Many children with BM have developmental delay which triggers neurosurgical evaluation and CT or MR brain imaging due to concerns for communicating hydrocephalus. The purpose of this study was to determine if CT and/or MR imaging changed the diagnosis or management in those children whose primary complaint was macrocephaly with or without developmental delay.
Methods & Materials: IRB approval was obtained for this retrospective study. The radiology database was searched to identify patients diagnosed with BM via head US between 2006 and 2013. Those with follow up CT or MR imaging were identified and compared to initial US studies to identify change in diagnosis. Chart review was performed to determine the neurologic and clinical status of each patient and the consequent clinical management.
Results: Initial search identified 467 patients (68.6% male) with a head US and diagnosis of BM (mean age of 6.47 +/- 2.43 months). In this group, 81 (17.5%) went on to have head CT or MR imaging done. 2/81 (2%) had neurological findings with additional significant findings on MRI. 6/79 (7%) had a stable diagnosis of BM with incidental findings including Chiari I (3), small subdural bleeds (2), arachnoid cyst (1), frontal bone dermoid (1) and nonspecific white matter disease (1), stable over two studies. None of these cases resulted in a change in management. 64.6% of all patients had neurosurgical evaluations, none requiring intervention for communicating hydrocephalus. Of the 177 infants with available developmental follow up records, 94 (53.1%) had speech, fine motor or gross motor delay. At the time of the last available clinical follow up 58/94 (61.7%) still showed some delay (average age at last follow-up was 38.0 +/- 2.0 months).
Conclusions: Our study suggests that patients diagnosed with BM with or without developmental delay and without other focal neurological findings do not require subsequent brain CT/MR imaging or neurosurgical evaluation. Routine developmental surveillance by primary care providers with referral to appropriate developmental therapy services is the best clinical management. This change in practice would decrease costs incurred by unnecessary imaging, would free up clinic appointments for neurosurgeons, and avoid risks associated with radiation and sedation.

Poster #: SCI-068

Fetal MRI: The Role of the Radiologist and Importance of the Consultation Following the Exam

Eleza Golden, MD, *Radiology, Emory University, Atlanta, GA, eorenst@emory.edu;* Adina Alazraki, MD, Sarah Milla, MD, Nilesh Desai

Disclosures: All authors have disclosed no financial interests, arrangements or affiliations in the context of this activity.
Purpose or Case Report: Prior studies have suggested that patients undergoing fetal MRI have a high level of anxiety, while other studies have indicated that patients have a limited understanding of the role of the radiologist in patient care. Further, many patients would prefer to learn their results immediately after the examination rather than wait to meet with their obstetrician. Our objective is to assess patient perception of what fetal MRI is and the role of the radiologist.
Methods & Materials: A voluntary anonymous survey consisting of 12 questions before and 5 questions after fetal MRI and consultation with a pediatric radiologist was administered to patients referred for fetal MRI at a tertiary care children's hospital from July-August 2015. A total of 21 patients participated. 2 patients did not complete the second half of the survey.
Results: Prior to the consultation, 17 (81%) of the women surveyed believed a radiologist should discuss what to expect prior to the MRI, 18 (86%) believed a radiologist alone or in conjunction with their obstetrician should discuss the results and 19 (90%) the prognosis after the fetal MRI was completed. When asked when was an acceptable time to receive results, 17 (81%) wanted results immediately after the MRI, and 20 (95%)

would rather receive results right away from the radiologist rather than wait to hear the results from their obstetrician. Of the 19 women who completed the survey after consultation with a pediatric radiologist, all (100%) felt it was very important for the radiologist to be involved in their consultation/care, and 18 (95%) felt the consultation was very helpful to understand the results of the fetal MRI. Moreover, 18 (95%) reported being very satisfied with the consultation, and 19 (100%) replied that it was necessary to consult with the radiologist regarding their results.
Conclusions: Our preliminary data suggests that the majority of patients undergoing fetal MRI prefer the radiologist be involved and prefer to hear the results expediently. The results of the survey highlight the importance of immediate consultation by a radiologist to our fetal MRI patients.

Poster #: SCI-069

Low Dose Imaging of Neonates with Congenital Cardiovascular Disease: Initial Experience with FLASH Computed Tomography Angiography (CTA)

Aarti Luhar, MD, *Radiology, UCLA, Los Angeles, CA, aluhar@mednet.ucla.edu;* Dan Vu, Nathan Holmes, Pierangelo Renella

Disclosures: All authors have disclosed no financial interests, arrangements or affiliations in the context of this activity.
Purpose or Case Report: Computed Tomography Angiography (CTA) is a valuable non-invasive tool for assessment of congenital heart disease in neonates. Though it requires less radiation, contrast and sedation than catheter angiography, which is the current standard of care, traditional CTA can still necessitate significant radiation dose, sedation, breath-holding and/or low heart-rates to achieve diagnostic studies. In this frequently imaged neonatal patient population, it is imperative to minimize cumulative radiation to limit the lifetime risk of cancer. At our institution, we have successfully used a new fast-acquisition FLASH CTA protocol to achieve high quality imaging of neonates with complex congenital heart disease with minimal radiation dose and without sedation.
Methods & Materials: Nineteen neonatal patients with complex congenital heart disease who required pre-surgical imaging underwent FLASH CTA from 8/2010-9/2015. Two of these patients had repeat examinations, for a total of 21 studies. At time of examination, the patients ranged in age from 1 to 30 days (median 7 days) and weighed 1.3-4.1 kg (median 3.7 kg) at the time of imaging. In all cases, imaging was performed on a dual source Siemens CT machine, the Somatom Definition Flash, using the FLASH protocol. Images were acquired from the thoracic inlet to top of the abdomen. Images interpretation was performed by experienced radiologists and cardiologists. All examinations were performed awake with free breathing and without sedation.
Results: All 21 examinations were considered diagnostic quality by the interpreting physician. Radiation dose ranged from 0.2 to 3.4 mGy (CTDi) and 3-33 mGy-cm (DLP). In fact, as the protocol was refined over time, radiation dose decreased: for the 14 examinations done in 2014-2015, the radiation dose ranged from 0.2 to 0.7 mGy (CTDI) and 3.0-14.0 mGy-cm (DLP). No adverse events or complications were associated with the examinations.
Conclusions: Our experience suggests that FLASH CTA offers diagnostic image quality with low radiation dose and no need for sedation in neonates with congenital heart disease.

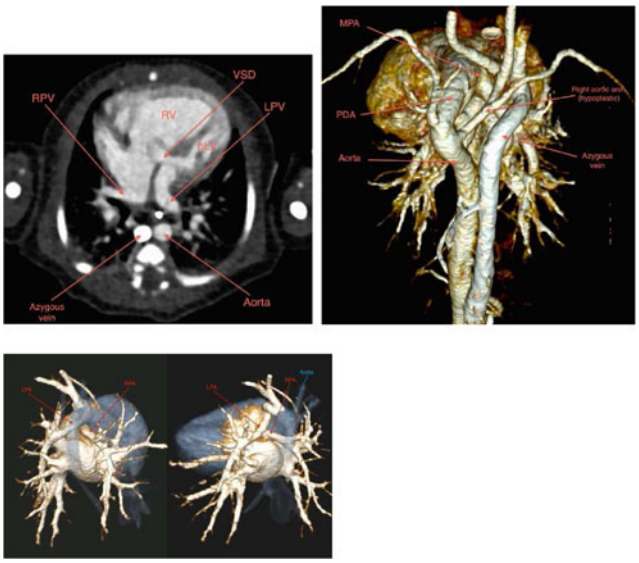

Poster #: SCI-070

Bone age assessment with conventional ultrasonography in healthy infants from 24 to 44 months of age

Monica Daneff, *Fundacion Científica del Sur, Lomas de Zamora, Argentina, monicadaneff@hotmail.com;* Claudia Casalis, Claudio Bruno, Didier Bruno

Disclosures: All authors have disclosed no financial interests, arrangements or affiliations in the context of this activity.
Purpose or Case Report: Radiographic bone age determination is part of the routine evaluation of suspected growth disorders. Simplicity and low cost are its major advantages but ionizing radiation should be taken into consideration. Conventional ultrasonography (US) has proven effective to identify ossification centers of the hand and wrist between 0 and 24 months of age. It may become an innocuous follow-up tool for patients with growth disorders. We aimed to asses the chronological US emergence of the ossification centers of the hand and wrist in healthy infants between 2 and 4 years of age.
Methods & Materials: Cross-sectional study of healthy patients aged between 24 and 44 months (n=96, girls n=47). After written parental consent, all patients underwent US evaluation of the left hand and wrist to identify and measure the different bone nuclei. For statistical analyses, patients were divided in 3 age ranges: 24-29 months, 30-35 and 36 or over.
Results: Size-for-age relation showed linear increase of the measured nuclei. Girls showed an earlier emergence of the evaluated nuclei and a trend to a greater size than age-range-matched boys, less significantly with age progression. Between 24 and 29 m, all patients had their Hamate, Capitate and distal epiphysis of the radius nuclei present. The second metacarpophalangeal joint (index finger) followed in order of emergence, fully present in girls and in almost every boy (p=ns) between 24 and 29 m. The proximal epiphysis of the first metacarpal bone (thumb) followed in order of appearance almost at the same time with the triquetrum, in accordance with the radiographic atlas. The nucleus of the Thumb was present significantly earlier in girls during the first age-range (OR 27.4, 95%CI: 3.28, 229.7 p<0.001). Between 30 and 36 m of age, sign-test showed it should be present in girls (p=0.016) and not necessarily in boys (Sign-test p=0.69). After 36 m of age it was present in all the patients. Girls showed a trend to earlier emergence of the Triquetrum, becoming more frequent with age progression but not fully present over 36 months of age. Lunate nucleus was absent in both groups between 24 and 29 m (Sign-Test p<0.001 for both). After 36 m it could be either present or absent in girls, but most likely absent in boys (Z`Sign test for boys p=0.02).

Conclusions: Conventional US allows proper identification of the ossification centers of the hand and wrist and may become an innocuous follow-up tool for patients with growth disorders.

Age (months)	Boys (*n*=49)	Girls (*n*=47)
24	16	18
25	1	2
26	1	2
27	0	1
28	3	5
29	4	2
30	1	1
31	1	0
32	0	1
33	4	1
35	1	3
36	11	9
38	1	0
39	0	1
40	1	0
42	1	2
43	1	0
44	0	1
Mean age (SD)*	29.6 (6)	30.3 (5.8)
Median age	28	29
Kurtosis	-0.74	-1.143
Skewness	0.71	0.363
95% CI	27.9, 31.3	28.5, 32
*p=0.534		

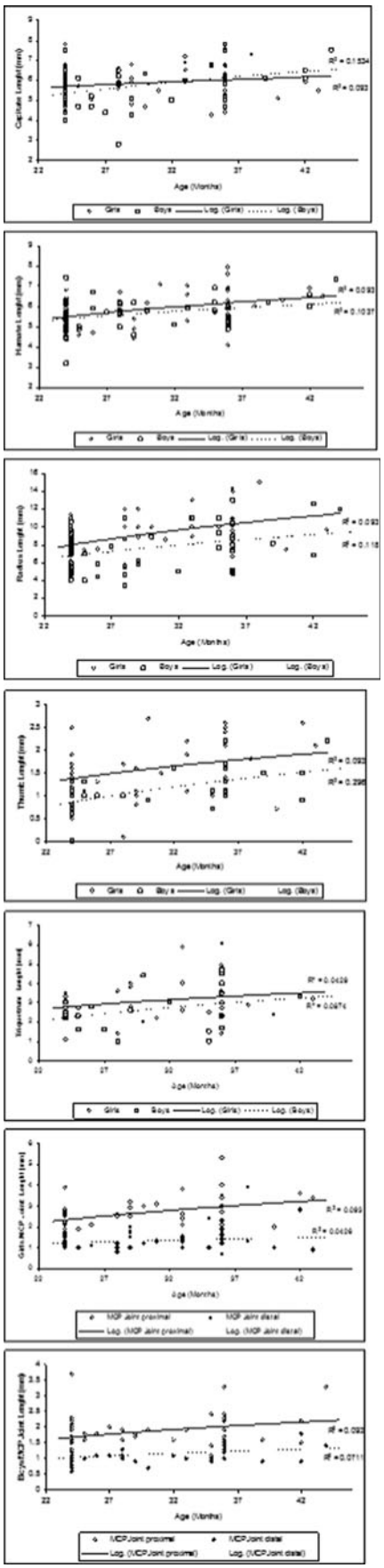

Poster #: SCI-071

Comparison of Hand versus Mechanical Administration of IV Contrast for CT Pulmonary Angiography in Pediatric Patients

Matthew Zapala, MD,PhD, *Boston Children's Hospital, Boston, MA, mzapala@hotmail.com;* David Zurakowski, Edward Lee

Disclosures: All authors have disclosed no financial interests, arrangements or affiliations in the context of this activity.
Purpose or Case Report: To compare hand versus mechanical administration of intravenous (IV) contrast on the quality of CT pulmonary angiography in the pediatric population.
Methods & Materials: A retrospective IRB approved review of the electronic medical records was performed to identify pediatric patients (≤18 years) with CT pulmonary angiography performed between September 2012 and March 2015. The information obtained included method of contrast administration (hand versus mechanical), IV size/gauge, IV site, amount and type of contrast administered, and rate of administration (ml/sec). Both qualitative and quantitative evaluation of the CT image quality was performed by two pediatric radiologists independently. Analysis of variance using the F-test compared contrast enhancement within the pulmonary arteries in hand versus mechanical administration of IV contrast adjusting for age.
Results: 148 consecutive pediatric patients (77 males, 71 females; mean age 11.1 years, range 8 days old to 17.9 years) were identified during the study period. 29 patients (19.6%, 1.4 years ±1.8 years; range 8 days to 8.1 years) had hand administration of contrast and 119 patients (80.4%, 13.5 years, ±3.9 years, range 1.2-17.9 years)had mechanical administration of contrast. The contrast enhancement of the pulmonary arteries was not significantly different between the two IV contrast administration methods at the main pulmonary artery (385±141 versus 296 ±109, p=0.313), right pulmonary artery (385±141 versus 291 ±104, p=0.364) and left pulmonary artery (395±149 versus 288 ±102, p=0.241) adjusting for age.
Conclusions: Diagnostic quality CT pulmonary angiography can be achieved using hand administration of IV contrast in infants and young pediatric patients less than 5 years old.

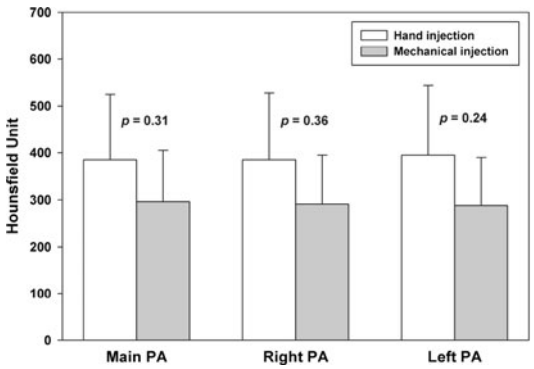

Poster #: SCI-072 - ***Withdrawn***

Poster #: SCI-073 - ***Withdrawn***

Poster #: SCI-074 - ***Withdrawn***

Poster #: SCI-075

Neonatal and Infantile Ovarian Torsion: A Spectrum of Imaging Findings with Pathologic Correlation in a Large Series of Patients

A. Luana Stanescu, MD, *Radiology, Seattle Children's Hospital, Seattle, WA, stanescu@u.washington.edu;* Jeffrey Otjen, MD, Marguerite Parisi, MD, MS

Disclosures: All authors have disclosed no financial interests, arrangements or affiliations in the context of this activity.
Purpose or Case Report: Ovarian torsion is rare in neonates and infants. Clinical diagnosis is challenging in the setting of lack of specific symptoms and the limitations in assessing pain in infants. Torsed ovaries in this patient population are also a diagnostic dilemma on imaging. In this study we reviewed the spectrum of imaging findings with pathologic correlation in a large series of patients.
Methods & Materials: This was an IRB-approved HIPAA compliant retrospective study. All cases of ovarian torsion at a large standalone children's hospital were identified by queries of a radiology database and a hospital wide ICD code database. Out of a total number of 103 cases of ovarian torsion found between 2005 and 2014, imaging and clinic-pathologic data of 15 patients under 1 year of age diagnosed with ovarian torsion were reviewed. The age range was 0-10 months, with 14 out of the 15 patients being aged 0-4 months at the time of diagnosis.
Results: Four patients had an abdominal mass detected by prenatal ultrasound. Ten patients underwent exploratory laparotomy, while 4 were followed up to resolution with serial ultrasounds for complex cystic lesions presumed to represent torsed in-utero ovaries between 6 and 22 months after initial exam. One patient is still undergoing serial ultrasounds.
Ultrasound findings included large cysts with layering echogenic debris and no adjacent ovarian tissue in 10 patients, one hemorrhagic cyst with lace-like reticular echoes, 2 solid avascular masses and 2 small simple ovarian cysts surrounded by ovarian tissue. The large cysts with echogenic debris were found to represent largely necrotic and fibrotic tissue with foci of hemorrhage, granulation changes and dystrophic calcifications at pathology, with no viable ovarian tissue, consistent with remote torsion. Two of these lesions were mobile in the abdomen, consistent with autoamputation. The solid lesions corresponded to necrotic tissue and old blood with extensive calcification, also consistent with remote torsion. The 2 patients with small cysts had pathologic features of acute ovarian torsion.
Conclusions: We present a spectrum of imaging findings in neonatal and infantile ovarian torsion. Increased awareness can help in diagnosing and differentiating from other benign and malignant abdominal masses encountered in this patient population. In our series of patients, large cysts with layering echogenic debris represented the most common imaging finding, however solid lesions may also be encountered.

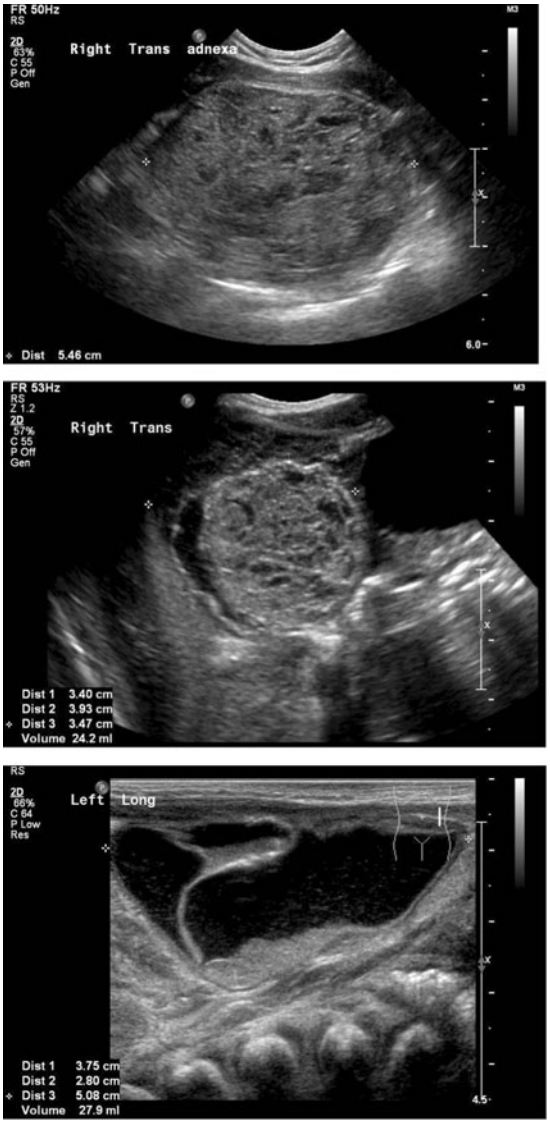

Poster #: SCI-076

Ultrasound Diagnosis of Median Arcuate Ligament Syndrome (MALS): A Single Institutional Experience

Anjum Bandarkar, *CNMC, Herndon, VA, anjumnb@gmail.com;* Hansel Otero, MD

Disclosures: All authors have disclosed no financial interests, arrangements or affiliations in the context of this activity.

Purpose or Case Report: The Median Arcuate Ligament Syndrome (MALS) is a diagnosis of exclusion. It is a condition characterized by abdominal pain due to compression of celiac artery by the median arcuate ligament.
1. The purpose of this study is to review a single institutional experience in screening and diagnosing MALS in the pediatric population with emphasis on the diagnostic accuracy of ultrasound (US) Doppler against additional imaging and follow up.
2. We also describe our technical approach of performing Doppler US in suspected MALS and various diagnostic criteria.
Methods & Materials: We retrospectively reviewed all patients referred for Doppler ultrasound examination of the celiac artery for suspected MALS between February 2013 and August 2015. Sonographic images, reports, subsequent imaging, surgeries and plans for follow up were recorded. The ultrasound studies were classified as positive or negative based on whether the diagnosis of MALS was made or not. Subsequent imaging and clinical follow up are described and diagnostic accuracy of ultrasound is calculated. Detailed step-by-step sonographic approach and Doppler US protocol are discussed.
Results: 74 patients (61F:13M; 6-20 years, mean 14.9 years) were selected all of whom presented with chronic abdominal pain and symptoms of POTS. US evidence of MALS was found in 27 patients (36.5%); 16 of these 27 patients (74%) underwent further imaging with CT (n=10) or MRI (n=6); and 11 patients had no further imaging. 14/16 patients had confirmatory CT (n=9) or MR (n=5). 2/16 were false positives where the US showed features of MALS but the CT/MR showed a normal celiac trunk. 4/11 who received no further imaging went directly to surgery (where MALS was confirmed), 3/11 were lost to follow up and the remaining 4/11 are currently either on conservative management or awaiting surgery.
47 (63.5%) patients had no evidence of MALS on US. 5 of these patients got additional imaging (CT n=4, MR n=1) due to severity of symptoms. 42 patients were managed conservatively. The specificity of US was 96%, sensitivity was 100%. There were no false negative cases. Our practice considered all US negative cases as true negative, hence accuracy was 90.5%.
Conclusions: Doppler US is a highly accurate screening and diagnostic tool for suspected MALS in children. Cross-sectional imaging confirmation is frequently performed but may not be necessary when the diagnosis is obvious on US exam. Following a standard Doppler US protocol is key to obtaining high sensitivity and specificity.

Poster #: SCI-077

Frequency of Abdominal Injuries in Children with Suspected Non-Accidental Trauma

Mark Heitzmann, DO, *Radiology, Children's National Medical Center, Poolesville, MD, heitzmanndo@gmail.com;* Eglal Shalaby-Rana, Katherine Deye

Disclosures: All authors have disclosed no financial interests, arrangements or affiliations in the context of this activity.
Purpose or Case Report: Abdominal injuries account for a relatively small percentage of non-accidental trauma. Previous estimates range from 0.5% to 11%. Despite this, abdominal injuries are the second leading cause of death in non-accidental trauma after head injury. Our objective

is to assess the prevalence of abdominal injuries in the setting of suspected non-accidental trauma within a large urban children's medical center.
Methods & Materials: After IRB approval, from a database of nearly 3000 patients who were assessed for possible abuse from 1997 to 2012, 177 children with suspected non-accidental trauma who obtained both an abdominal CT and skeletal survey were identified. 3 patients diagnosed with systemic disease (tuberous sclerosis, neuroblastoma, and hepatoblastoma) were excluded. The resulting database consisted of 174 patients. All imaging studies including CT abdomen, CT brain and skeletal surveys were reviewed.
Results: Of the 174 patients, 72 were girls and 102 boys with age range from 1 to 139 months, mean age of 18 months. Thirty patients (17%) were found to have abdominal organ injuries, to include visceral, hollow organ, and vascular injuries.
These 30 patients were 21 boys, 9 girls with age range 1 month to 72 months, (mean age 29 months). Injuries included 22 liver (73%), 3 bowel (10%), 3 pancreatic (10%), 3 adrenal (10%), 1 renal (3%), 1 splenic (3%), 1 bladder (3%), and 1 aortic tear (3%). 13 of the 30 patients (43%) had intracranial injuries. 16 of the 30 patients (53%) had concurrent skeletal injuries, most commonly rib fractures (13/16, or 81%).
A separate group of 34 of the 174 patients (20%), 22 boys, 12 girls with age range 1 to 130 months (mean 21 months) had nonspecific abdominal CT findings including intraperitoneal fluid and equivocal abdominal organ injuries. 21 of these patients (62%) had intracranial injuries and 20 (59%) had skeletal injuries.
Conclusions: Abdominal organ injuries appear to be more common than previously reported in the literature. These findings support diligent screening for abdominal injuries in patients with suspected non-accidental trauma. Abdominal injuries are frequently accompanied by intracranial as well as skeletal injuries. A subgroup of patients with nonspecific/equivocal abdominal CT findings also had a high prevalence of associated intracranial and skeletal injuries; this group may warrant additional scrutiny.

Poster #: SCI-078

Imaging the Peritumoral Zone of Pediatric Brain Tumors Using Diffusion Tensor Imaging: The Good, the Bad, and the Ugly

Farhan Ahmed, *McMaster University Medical Centre, Hamilton, ON, Canada, maassoci@hotmail.com;* Nishard Abdeen, MD

Disclosures: All authors have disclosed no financial interests, arrangements or affiliations in the context of this activity.
Purpose or Case Report: The purpose of this exhibit is to ilustrate how the DTI color map can characterize the peritumoral zone in pediatric brain tumors, which is of potential benefit in preoperative planning.
Methods & Materials: Brain tumour cases at a pediatric teaching hospital were reviewed with repect to the DTI color map. Three categories of peritumoral zone were defined. One category was the dispalcement of white matter tracts by the tumor (the good) without destruction. The second was destruction of the white matter tracts (the bad), while the third category was infiltration of the white matter tracts by tumor (the ugly). Each category was illustarted with numerous examples, covering with common and uncommon pediatric brain tumors.
Results: Tumors with displacement of the white matter tracts (the good) included medulloblastoma, ependymoma, meningioma, and oligodendroglioma. Tumors with destroyed white matte tracts included anaplastic ependymoma, glioblastoma multiforme, and atypical teratoid rhabdoid tumour ("the bad"). Tumors with infiltrated white matter tracts were optic nerve glioma, brainstem glioma, pilocytic astrocytoma, diffuse infiltrative pontine glioma ("the ugly").
Conclusions: Color maps from DTI are useful in defining the relationship of tumor to adjacent white matter tracts and can help guide surgical planning.

Poster #: SCI-079

Quantitative MR Assessment of the Fetal Posterior Fossa: Reproducibility, Reference Ranges and Diagnostic Performance

Luís Goncalves, MD, *Oakland University William Beaumont School of Medicine, Rochester, MI, luis.goncalves@beaumont.edu;* Shilpa Jain, Ananth Krishnan, Zhou Yuxiang, David Bloom, Wesley Lee, Roberto Romero

Disclosures: All authors have disclosed no financial interests, arrangements or affiliations in the context of this activity.
Purpose or Case Report: To develop reference ranges for cerebellum and posterior fossa measurements by fetal MRI and to investigate the reproducibility and diagnostic performance of quantitative MR parameters for the differentiation of fetal posterior fossa abnormalities.
Methods & Materials: We systematically evaluated the posterior fossa of normal fetuses by MRI, including presence of fastigial point (FP), visualization of cerebellar vermis (CV) fissures, tegmento-vermian (TV) angle, proportion of CV above/below the fastigium-declive live, CV anteroposterior (AP) diameter, CV height, CV area, transverse cerebellar diameter and cisterna magna (CM) diameter. Measurements were performed on sagittal and axial 2-3 mm T2 HASTE (Half-Fourier Acquisition Single-shot Turbo Spin Echo) sequences. Regression analysis was performed and normal reference ranges constructed for each parameter. Intra- and interobserver reliability, repeatability, and agreement were evaluated by intra-class correlation coefficient (ICC), Bland-Altman plots and kappa statistics. Cases of posterior fossa anomalies were evaluated using these parameters.
Results: 116 normal fetuses and 13 fetuses with posterior fossa abnormalities were examined by fetal MRI between July 2005 and September 2015. Technically acceptable sagittal images of the CV were available for 95 of the 116 fetuses (81.8%). Intra- and inter-rater agreement were almost perfect (kappa>0.80) for identification of the FP, primary and prepyramidal CV fissures. Intra- and inter-rater reliabilities were excellent (ICC>0.75) for CV area, AP and CC diameters, and pons AP diameter. Reliability was poor for the proportion of CV above/below the fastigium-declive line. TV angles were significantly different among the13 abnormal cases: Dandy-Walker malformation (DWM) (n=3, 55-82.6 degrees), Blake's pouch cyst (BPC) (n=5, 22.3-41.8 degrees), mega cisterna magna (MCM) (n=4, 0-22.3 degrees), and arachnoid cyst (AC) (n=1, 1 degree) (Kruskal-Wallis test p=0.0001) (Figure 1). DWM cases were also more likely to have CV area and AP diameter<5th percentile for gestational age (Figures 2 and 3). In addition, FP and primary cerebellar fissure were not visualized in DWM.
Conclusions: Reference values for quantitative evaluation of posterior fossa may help differentiate among DWM, BPC, AC, and MCM. DWM is characterized by lack of visualization of the FP and primary CV fissure, large TV angle, as well as CV AP diameter and CV area below the 5th percentile for gestational age.

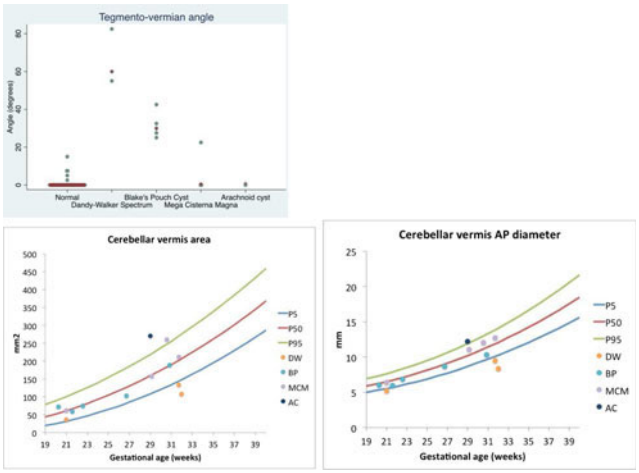

Poster #: SCI-080

Pediatric Biofeedback During Non-sedated MRI: Initial Experiences

Raphael Alford, MD, *Pediatric Radiology, Stanford, Alice Ln, CA, rapha@stanford.edu;* Shreyan Jain, Joseph Cheng, Tao Zhang, Shreyas Vasanawala, MD/PhD

Disclosures: Tao Zhang has indicated a relationship with GE Healthcare as a research collaborator. Shreyas Vasanawala has indicated a relationship with Arterys, stock/consultant and GE Healthcare, research collaboration. Joseph Cheng has indicated a relationship with GE Healthcare as a researcher. All other authors have disclosed no financial interests, arrangements or affiliations in the context of this activity.

Purpose or Case Report: The purpose of this study is to develop a method of training pediatric patients in effective breathing during magnetic resonance imaging (MRI).

Methods & Materials: An Arduino microcontroller was adapted to digitize pressure changes in a respiratory bellows and configured to wirelessly communicate with an iPad. An application was then developed for the iPad to display visually the breathing pattern. Through inspiration and expiration, the patient can control the displayed breathing waveform, with the goal following a sinusoidal path for regular breathing and a straight path for breath holding (Fig 1). An MRI-compatible video goggle system was adapted to enable mirroring of display of the iPad screen, thus enabling the patient is able to see his or her breathing pattern through video goggles during the exam. Pediatric subjects referred for MRI of the torso were recruited with informed consent. Respiratory information was recorded during an initial free-breathing sequence without visual feedback, and was subsequently recorded for an identical sequence with feedback. Waveforms were analyzed for regularity. A 3D radiofrequency spoiled gradient recalled echo T1 weighted fat suppressed sequence was adapted to provide three dimensional motion navigators to assess regularity of motion with and without feedback.

Results: Eight subjects were recruited, aged 7 to 24 years old. Although subjectively there was a broadening of the period and amplitude of respiration during visual feedback (Fig. 2), these metrics were not significantly different ($p<0.53$ and $p<0.9$ respectively). Comparison of images with and without feedback demonstrated similar image quality (Fig. 3).

Conclusions: Real-time respiratory feedback is feasible but may not be effective in regularizing breathing pattern or improving image quality.

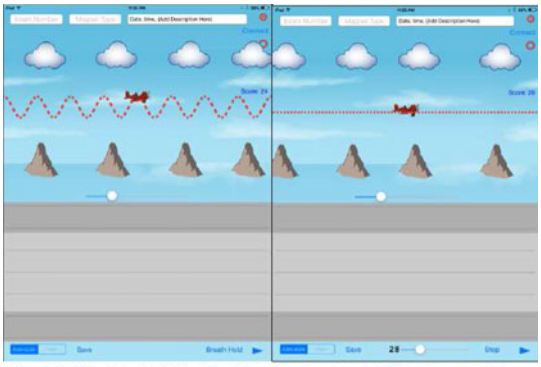

Figure 1: A) Non breath hold guide. Damaging the plane by hitting the mountains or clouds resets the players score. B) Breath hold guide.

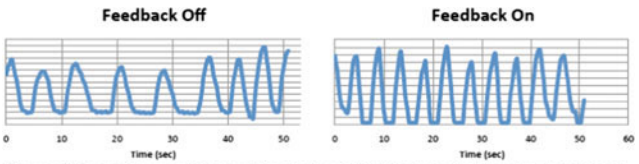

Figure 2: Example waveforms without visual feedback and with visual feedback.

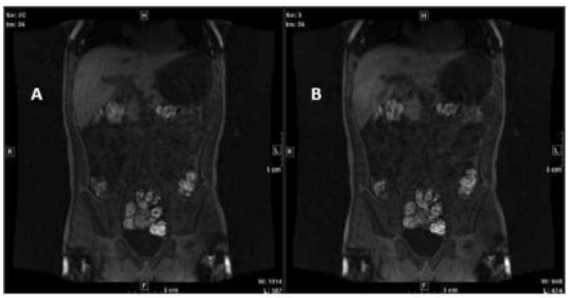

Figure 3: Example images without (A) and with (B) respiratory feedback.

Poster #: SCI-081

The Role of Functional MR Urography in Diagnosing Calyceal Diverticula

Harutyun Haroyan, M.D., *Radiology, Children's Hospital of Philadelphia, Philadelphia, PA, harut81@gmail.com;* Aikaterini Ntoulia, MD, PhD, Dmitry Khrichenko, Richard Bellah, Christopher Long, Kassa Darge, MD, PhD

Disclosures: All authors have disclosed no financial interests, arrangements or affiliations in the context of this activity.

Purpose or Case Report: Calyceal diverticula (CD) are rare lesions which are difficult to differentiate from renal cysts. Cross sectional examination with excretory imaging facilitates diagnosis in a noninvasive fashion. Functional MR urography (fMRU) provides comprehensive morphological, functional and excretory assessment of the kidney with CD. We aim to describe the findings of CD in fMRU.

Methods & Materials: The fMRU records over a 5-year period were reviewed for patients with CD. The following characteristics of the CD were determined: location, diameter, contour, signal characteristics and timing and pattern of contrast filling. Of the involved kidney the calyceal

transit time (CTT), volumetric (vDRF) and Patlak (pDRF) differential renal functions were evaluated. The functional parameters were compared to the contralateral side. Renal ultrasound (US) was utilized to determine the presence of calcifications in the CD or its wall.
Results: A total of 16 patients, 9 males and 7 females (mean age 9 y 4 m [1y7m-17y8m]) were identified to have 19 CD. 1 patient had 2 CD, 1 patient had 3 CD. Diagnosis was confirmed surgically in 10 patients by retrograde pyelogram. 13 CD were located in the upper pole (7=right, 6=left), 5 were located in the interpolar area, 1 in the lower pole. The average diameter was 3.0 cm (0.8-6.4 cm). Sixteen were simple, 2 contained a single septa and 1 was a complex lesion. The contour of the CD was smooth in 12, lobulated in 5 and irregular in 2. No calcifications were seen on accompanying US. 15 CD (78.9%) demonstrated filling with contrast (7 complete, 4 partial, 4 minimal). 4 (20.1%) CD never filled. The average time from the injection of contrast to the beginning of opacification was 44.4 min (4.6 min-150.5 min). The 6 CD with complete filling demonstrated very early opacification (average 4.3 min), but one was delayed (150.5 min). The 4 CD that had minimal filling showed it late (mean 96.7 min). 4 CD that never were imaged on average for only 22.8 min (17.1 min-27.0 min) without any delayed images. There were no significant differences in CTT, vDRF and pDRF in affected versus contralateral kidneys.
Conclusions: fMRU is a potent tool for evaluation of CD, differentiating a calyceal diverticulum from a simple cyst. A third of the CD are contrasted within a few minutes. In the absence of early contrast filling of the CD delayed post-contrast images are necessary. Majority of CD are located in the upper poles. The presence of CD does not affect renal functional parameters as calculated from the fMRU.

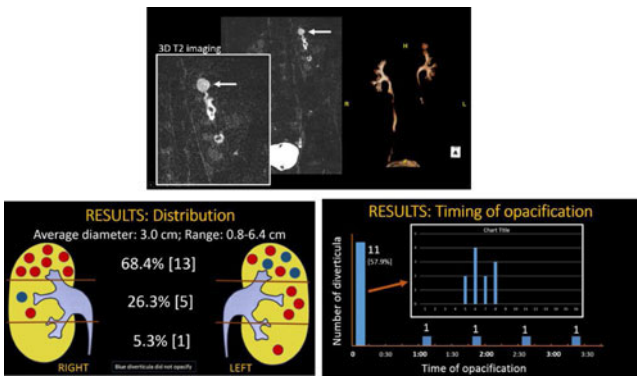

Poster #: SCI-082

Improving the Sensitivity and Specificity of CT to Diagnose Tracheomalacia at the Work Station

Prasnjeet Das, Robert Thomen, Sarah Halula, Jason Woods, **Robert Fleck, MD**, *Radiology MLC 5031, Cincinnati Children's Hospital Medical Center, Cincinnati, OH, robert.fleck@cchmc.org*

Disclosures: All authors have disclosed no financial interests, arrangements or affiliations in the context of this activity.
Purpose or Case Report: CT is often performed and advocated in patients with risk factors for or symptoms of tracheomalacia (TM). However, TM is traditionally defined as a 50% decrease in the cross-sectional area of the airway during a forced expiratory maneuver. This basis for detecting TBM was never meant for use in CT and leads to the under diagnosis of TM in young children by CT and typically requires inspiratory/expiratory CT (IECT). Additionally, some pictures archiving systems do not have tools to measure area. The aim of this investigation is to show that TM is under diagnosed by IECT relative to bronchoscopy and to develop a "view box" parameter to improve sensitivity while maintaining specificity in identifying the trachea as normal or affected by TM.
Methods & Materials: Patients were identified from electronic medical records that had both an IECT and bronchoscopy. The narrowest segment of the trachea was measured in the shortest transverse dimension and longest transverse dimension on both inspiratory and expiratory CT. The radiology and bronchoscopy reports were abstracted for presence and severity of reported TM.
Results: 280 patients were identified, of which 103 had TM on bronchoscopy. IECT reported TM in 20 for a sensitivity of 19.4% and specificity of 99.4%. The negative predictive value (NPV) of these clinical reads of IECT was 95% but the positive predictive value (PPV) was 68%. The ratio of anterior-posterior diameter of the normal trachea, regardless the phase of respiration, ranges from 0.8 to 1.1 (prior presentation). Using a cut-off ratio of 0.7, regardless of inspiratory phase, results in a sensitivity of 91.3% and specificity of 91.2%. The negative predictive value using this ratio is 94.5% and the positive predictive value increased to 85.8%. Using expiratory CT images alone and a cut-off ratio of 0.6, results in 93.2% sensitivity and 97.2% specificity with PPV and NPV of 95% and 96%, respectively.
Conclusions: The current clinical paradigm for identifying TM by CT has poor sensitivity and only identifies patients a small fraction of TM compared to bronchoscopy. Applying a simple ratio of two measures, short axis to long axis, acquired at the viewing station can allow us to more accurately and consistently differentiate normal tracheas from tracheas affected by TM. A ratio of 0.7 is adequately accurate if only inspiratory images, or an unknown phase of respiration, are available. Images obtained during expiration are even more accurate when a ratio of 0.6 is applied.

Poster #: SCI-083

Is Subjective Assessment of the Pylorus as Accurate as Formal Measurement in Diagnosis of Hypertrophic Pyloric Stenosis?

Edward Richer, MD, *University of Michigan, Ann Arbor, MI, richerej@gmail.com;* Ramon Sanchez

Disclosures: All authors have disclosed no financial interests, arrangements or affiliations in the context of this activity.
Purpose or Case Report: Hypertrophic pyloric stenosis (HPS) is a frequent cause of vomiting in young infants, with an incidence of 1.5-4 per 1000 live births, depending on demographic group. The gold standard diagnostic test is abdominal ultrasound targeting the pylorus, and the measurement thresholds for determining an abnormal pylorus are well established. The objective of this study was to assess whether visual, subjective assessment of the pylorus was as accurate in diagnosing HPS as traditional formal measurements.
Methods & Materials: IRB approval was obtained for this retrospective study. All abdominal ultrasounds performed at our institution for evaluation for HPS from August 2014 to August 2015 were obtained through review of the radiology information system. The exams were formatted such that no indelible measurements were present on the images, and were then reviewed by two experienced pediatric radiologists (ER, RS). The ultrasounds were categorized as positive, negative, or equivocal for HPS based solely on the visual appearance of the pylorus. One author (ER) then recorded the formal pylorus measurements obtained for each study. Results were compared to the reference standard of the surgical report in positive cases, and were considered to be truly negative if the patient did not undergo surgery or present for repeat ultrasound within 1 week.
Results: Subjective assessment of the pylorus without obtaining formal measurements was highly accurate in the diagnosis of HPS, with an accuracy of greater than 95%. There was also a high degree of inter-rater agreement.
Conclusions: Qualitative evaluation of the pylorus is as accurate in diagnosis of HPS as traditional formal measurements. While pediatric surgeons will likely continue to require formal measurements before taking a patient to surgery, the knowledge that the study "looks positive" can add a

layer of diagnostic confidence for the radiologist, and potentially increase efficiency in busy practices. Additionally, pyloric measurements can sometimes be inaccurate, if images are obtained in oblique rather than orthogonal planes, or if the incorrect anatomic structure is measured, such as the antrum or duodenum rather than the pylorus.

Poster #: SCI-084 - ***Withdrawn***

Poster #: SCI-085 - ***Withdrawn***

Poster #: SCI-086

Evaluation of Pediatric Tracheobronchial Anomalies with congenital heart disease using Three-dimensional Turbo Field Echo Magnetic Resonance Imaging Sequence

Yumin Zhong, *Diagnostic Imaging Center, Shanghai Children's Medical Center, Shanghai, China, zyumin2002@163.com;* Aimin Sun, Wei Gao

Disclosures: All authors have disclosed no financial interests, arrangements or affiliations in the context of this activity.
Purpose or Case Report: Tracheobronchial anomalies including tracheobronchial stenosis, tracheal bronchus, cardiacbronchus and bronchial isomerism are common in congenital heart disease. Cardiovascular anomaly is the principal extrinsic lesion causing tracheobronchial stenosis. MRI has the advantage of being non-ionizing and providing excellent soft tissue contrast for the diagnosis of congenital heart disease and tracheobronchial anomalies
Purpose: To define diagnostic accuracy of three-dimensional turbo field echo (3D-TFE) to detect tracheobronchial anomalies in patients with congenital heart disease
Methods & Materials: Sixty-eight patients with congenital heart disease from December 1, 2013 to September 31, 2014 were retrospectively reviewed. Cardiac MR was performed to provide further preoperative information about anatomy and function. In 68 patients, age ranged from 1.4 months to 134 months; the median age was 10.4 months. A 3D-TFE and 3D Balanced turbo field echo (3D B-TFE) sequences were performed on all patients to evaluate tracheobronchial anatomy. All patients also underwent multi-slice computed tomography (MSCT) either before or after MRI. Inter-modality agreement for tracheobronchial anomaly findings was tested by the kappa coefficient and the sensitivity, specificity of 3D-TFE for the detection of tracheobronchial anomalies were evaluated
Results: Among the 68 cases, 35 cases had a normal tracheobronchial tree, 33 had tracheobronchial anomalies (1 had situs inversus bronchus, 3 had bronchial isomerism, 8 had tracheal bronchus and 25 had tracheobronchial stenosis). The predominant causes of tracheobronchial stenosis were double aortic arch, right aortic arch with mirror- image branching, right aortic arch with left aberrant subclavian artery and posterior patent ductus arteriosus (PDA) or ligament, left pulmonary artery sling enlarged left atrium. There was excellent inter-modality agreement between 3D-TFE and MSCT for the detection of tracheobronchial anomalies. The sensitivity and specificity of 3D-TFE were 90% and 84%.
Conclusions: 3D-TFE is a useful MRI sequence for demonstrating the tracheobronchial tree and diagnosing tracheobronchial anomalies in congenital heart disease. MRI can supply helpful information for preoperative strategies.

Poster #: SCI-087

Championing radiation Safety in Africa: The AFROSAFE Campaign

Gladys Mwango, Department of Diagnostic Imaging and Radiation Medicine, University of Nairobi College of Health Sciences Schoolof Medicine, Nairobi, Kenya gmwango@yahoo.com; Rose A. Nyabanda, Michael G. Kawooya

Disclosures: All authors have disclosed no financial interests, arrangements or affiliations in the context of this activity.
Purpose or Case Report: Radiation safety is a critical component in pediatric imaging. In Africa, radiation-safety is championed by the AFROSAFE campaign under the umbrella of the African Society of Radiology (ASR). AFROSAFE was launched on 17th February, 2015 during the 8th biennial Pan African Congress of Radiology and Imaging (PACORI) which was held in Nairobi, Kenya. The mission of AFROSAFE is to ensure favorable benefit-risk ratio in theuse of ionizing radiation in medicine through encouraging adherence to safety standards and guidelines as per the "Bonn Call for Action". Through this Campaign, all the radiation health workers of Africa have agreed to unite with the common goal of identifying and addressing issues arising from radiation protection in medicine.
This is an educational poster that outlines the signifcant Milestones AFROSAFE has achieved 1 year later, the pertinent issues, challenges and success.
Methods & Materials: Six key strategic objectives have been identified which include developing DRLs and Imaging referral guidelines. The AFROSAFE Implementation Tool Matrix was launched on 5th November 2015 in an event to celebrate the International Day of Radiology. A key strategy in the implementation of AFROSAFE is to the formulationof national steering committees in each African country as well as the development of the AFROSAFE website, anessential resource-tool for relevant data facilitating the expansion of key networks. National AFROSAFE chaptershave been launched in Kenya and Uganda with the election of national AFROSAFE champions. Also planned is thelaunch of French and Portuguese-speaking chapters.
Results: AFROSAFE has grown to become a legitimate radiation-safety campaign with representation in several fora such as PACORI 2015, ASR 2015, the World Health Assembly Side-event (WHA 68), Global summit for Radiology Quality and Safety 2015, IAEA workshops in Kenya and Egypt and ECR 2016. Collaborations and partnerships with global agencies such as IAEA, WHO, governments and other radiation-safety campaigns like EuroSafe and Image Gently have been instrumental in establishing AFROSAFE.
Conclusions: Creation of AFROSAFE has stimulated radiation safety awareness in the continent leading to thedevelopment of national and regional chapters.

Poster #: SCI-088

Validation of the TIRADS Classification in Children and Adolescents

Andres Retamal Caro, Lizbet Pérez-Marrero, Eleonora Horvath, Claudio Silva, Paula Rojas

Disclosures: All authors have disclosed no financial interests, arrangements or affiliations in the context of this activity.
Purpose or Case Report: To determine the percentage of malignancy for the different TIRADS categories and theultrasound patterns in children and adolescents.To calculate the interobserver variability in the use of TIRADS classification in this group.
Methods & Materials: Retrospective observational study. All pediatric and adolescent patients who underwent to athyroid fine needle aspiration (FNA) in our institution between 2007 and 2014 were included.
Three blind radiologists evaluated independently the images and classified the ultrasound pattern and TIRADS foreach nodule. The gold standard was the FNA result. This result was correlated with TIRADS and the sonographic patterns. The risk of malignancy for each TIRADS categories and for different ultrasound pattern was estimated and comparedwith known adult risk. Interobserver variability was assessed using kappa coefficient test.

Results: 107 patients and 112 nodules were analyzed. Patients age was between 6 years and 21 years old.
The average nodules size was 15 mm. According to FNA results 56% were malignant and 44% benign.
According to TIRADS clasification 3% were TIRADS 2, 6% TIRADS 3, 66% TIRADS 4 and 25% TIRADS 5. The percentage of malignancy in different TIRADS categories was 0% for TIRADS 2 and 3, 50% for TIRADS 4 and93% for TIRADS 5. Results were similar to known adult risk, except in TIRADS 3, whose known risk is less than 5%. The risk of malignancy of each sonographic patterns were concordant with adults results. The kappa value was 0.85 which indicated high interobserver agreement.
Conclusions: We found good correlation between the percentage of malignancy of different TIRADS categories andsonographic patterns. According to our results we can suggest that TIRADS classification is applicable in children and adolescents. Our results are similar to adults.It is important that pediatrics radiologists be aware of TIRADS categories and utrasound patterns to improve the diagnosis of thyroid nodules.

CASE REPORT, EDUCATIONAL REPORT AND SCIENTIFIC POSTERS - RADIOGRAPHERS

(R) indicates a Radiographer Program Submission

Poster #: CR-01 (R)

A Diffuse Form of Neurofibromatosis of the Bladder in a New Born: Radiological Presentation of A Case

Beatrice Leloutre, *Hopitaux Pediatrique de Nice CHU-Lenval, Nice, France, beatrice.leloutre@lenval.com;* Corinne Boyer, Carole Leroux, Aurelie Occelli, Myriam Guesmi, Marie Baqué Juston

Disclosures: All authors have disclosed no financial interests, arrangements or affiliations in the context of this activity.
Purpose or Case Report: Objective: to report an unsual presentation of neurofibromatosis involving the genito-urinary tract. Bladder involvement was the initial presentation of a Von Recklinghausen disease in a new born for whom the family disease was initially unknown by the medical staff.
Methods & Materials: We report an exceptional case of a new born girl who presented with antenatal left hydronephrosis on ultrasound at 36 weeks LMP (last menstrual period). Post natal US and MRI performed the first month of life revealed a diffuse nodular bladder thickening, progressing on the follow up examinations and showing trigone involvement with bilateral uretero- hydronephrosis. Cystoscopy revealed a nodular thickening of the bladder wall, hiding both ureteral ostia. Bilateral nephrostomy and secondarily left ureterostomy have been performed. Bladder biopsy diagnosed a plexiform neurinoma.
Results: At 6 month old, the child does not suffer from secondary localization but shows delayed growth. She is medically treated by a drug on trial. Surgical indication has not been decides yet. Retrospectively, family research revealed that many members are suffering from neurofibromatosis (grand father, father, 2 brothers, uncle and aunt)
Conclusions: Unique teaching point: in neonatal period the first diagnosis to raise when there is a nodular thickening of the bladder wall is rhabdomyosarcoma. Plexiform neurofibroma is a very rare diferential diagnosis. The incidence of Von Recklinghausen is 1 in 3000 living births, howeverurinary manifestations are rare, and exceptional in neonatal period.

Poster #: CR-02 (R)

Vitamin K Deficiency with Intracranial Hemorrhage: Let's Check the Gallbladder

Stephanie Biscaye, Marco Albertario, Myriam Guesmi, Beatrice Leloutre, *Hopitaux Pediatrique de Nice CHU-Lenval, Nice, France, beatrice.leloutre@lenval.com;* Aurelie Occelli, Corinne Boyer

Disclosures: All authors have disclosed no financial interests, arrangements or affiliations in the context of this activity.
Purpose or Case Report: the aim of the study is to report the importance of the link between intracranial bleeding (ICB) and biliary atresia in neonates. Nowadays, the incidence of bleeding secondary to vitamin K deficiency has well-decreased, thanks to systematic vitamin K prophylaxis in neonates. However, ICB remains a severe complication of Vitamine K deficiency, with a high mortality rate and possible neurological disabilities.
Biliary atresia (BA) is a life-threatening condition in neonates, commonly diagnosed in the first 2 months of life, based on jaundice, cholestasis, pale-colored stools and dark urine. Occasionally, BA can be revealed later (25 to 65 days after birth), with severe symptoms such as intracranial, nasal or gastrointestinal bleedings.
Results: A 2 month-old boy was admitted in the emergency department with anorexia, vomiting, lethargy, and impaired consciousness, without fever. He also was slightly jaundiced with normal stools. He was born full-term and breastfed with a vitamin K supplementation as recommended. The examination revealed a 3-cm hematoma in the lumbar area and a bulging fontanelle. Cerebral CT-scan and MRI were performed rapidly and showed subdural hemorrhages and a frontal right intraparenchymal hematoma. Laboratory tests reflected anemia, cholestasis and coagulation disorder with deficiency of vitamin K-dependent factors. Surgical evacuation of intracranial hemorrhage was performed after intravenous vitamin K. An abdominal ultrasound showed afterwards an atrophic gallbladder, compatible with the diagnosis of BA without other ultrasonography signs of BA. Patient's stools and urine became respectively pale-colored and dark but only after the onset of neurological bleeding symptoms
The child was then rapidly transferred to another pediatric hospital, in order to perform a Kasaï intervention. The surgery went well but was complicated a few weeks later by a cytomegalovirus infection and a cholangitis.
Conclusions: BA should be strongly considered in infants up to 2 month old, presenting with a sudden tendency to bleed, especially when vitamin K-dependent factors are decreased. The presentation of BA can be atypical and revealed primarily by neurological symptoms, without any modification of stools or urine. ICB can be severe and life-threatening, hence the necessity of knowing these atypical presentations of BA.

Poster #: CR-03 (R) - ***Withdrawn***

Poster #: CR-04 (R)

Dermoid Cyst Imaging in the Central Nervous System

Irma Matos Rojas, Physician, *Instituto Nacional de Salud del Niño - San Borja, Lima, Peru, aracellymatos@yahoo.es;* Claudia Lazarte, Radiologist, Larry Alpaca Rodriguez

Disclosures: All authors have disclosed no financial interests, arrangements or affiliations in the context of this activity.
Purpose or Case Report: Three cases of dermoid cyst will be described with different clinical presentation and location. MRI and CT finding will be reviewed and correlated with pathological finding.
The first case is a 7 year- old child, with suspected diagnosis of stroke which MRI shows a midline posterior fossa tumor with fine occipital dermal sinus, better visualized in CT. The second case is 1 year- old enfant with delayed psychomotor development, a dimple with lock of hair and dorsal hemangioma, which MRI shows a dermal sinus at D4 - D5 level which continues with an intra and extramedullary mass. The last case is 2 year- old child

postoperated of mielomeningocele at birth that has neurogenic blader and Chiari II with a cyst mass at conus and low spinal cord insertion.
Conclusions: Intracranial dermoid cyst are uncommon. The typical MRI finding are hypointense T1 and hyperintense T2 signal that not enhance after contrast administration but can be hyperintense on T1 becouse of high lipid content.
Congenital dermal sinuses can occur anywhere along the craniospinal axis and dermoid cyst of posterior fossa associated with dermal sinus are rare. Dermal sinus is a defect in neural tube closure that occurs during the fifth week of embryonic development, characterized by tract lined coated by epithelium dural extending toward the skin surface within the central nervous system.
Spinal dermoid cyst are benig tumors that results from congenital or adquired ectodermal inclusion. These tumor account 0,8-1,1% of all primary spinal tumors, the majority in the extramedullary lumbosacral region and can be associated with low spinal cord insertion and dermal sinus.
Pathological finding show cystic structure with pearly white content, presence of hair shafts, hair follicle and sebaceous glands.

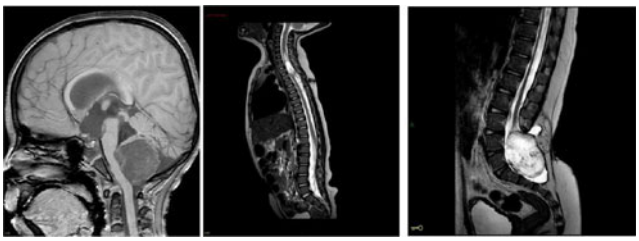

Poster #: CR-05 (R) - *Withdrawn*

Poster #: CR-06 (R)

OEIS Complex with Horseshoe Kidney

Irma Matos Rojas, Physician, *Instituto Nacional de Salud del Niño - San Borja, Lima, Peru, aracellymatos@yahoo.es;* Doris Katekaru Tokeshi

Disclosures: All authors have disclosed no financial interests, arrangements or affiliations in the context of this activity.
Purpose or Case Report: OEIS complex is the most severe end of the expectrum of the exstrophy - epispadias complex. It is characterized by omphalocele, extrophy, imperforate anus and spinal defects and is often associated with other malformations on chest, abdomen genitourinary, skeletal and neurologic. The incidence of OEIS complex is very rare, estimated to occur in 0, 5-1 per 200, 000 live births.
We present a case of OEIS complex associated with horseshoe kidney. The baby was delivered by vaginal delivery (GA 39 weeks). Present normal male kariotype.
On physical examination there were omphalocele with herniation of a segment of the large bowel, cloacal exstrophy with two hemi bladders, imperforate anus and spina bifida. No external genitalia were identified on physical examination but bilateral cryptorchidism was observed in pelvic MRI
Renal ultrasound show hoershoe kidney with left pelvic ectasia that was confirmed on abdominal MRI and urotomography. Spinal ultrasound and MRI show lipomyelomenigocele and low spinal cord insertion. Also the baby has sacral segmentation defects and congenital hip subluxation.

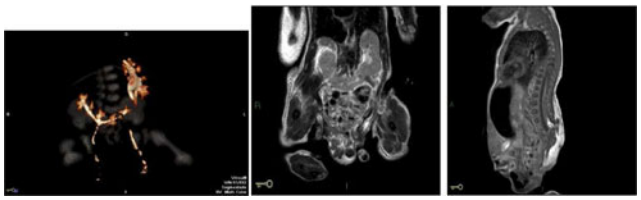

Poster #: CR-07 (R)

Complete Septate Uterus and Longitudinal Vaginal Septum Combined with Atresia of the Lower Vagina: Case Report With Review Of Imaging And Embryology

Matt Frank, MD, *Radiology, CHI CUMC, Omaha, NE, mrfrank71@gmail.com;* Jeb List, Katherine Harris

Disclosures: All authors have disclosed no financial interests, arrangements or affiliations in the context of this activity.
Purpose or Case Report: 12 year old female presented with history of ureteral re-implantation and severe pelvic pain for a month. Pelvic ultrasound showed a bi-lobed hypoechoic mass in the pelvis markedly distended with internal intermediate and low level echoes and septations suggestive of hematometrocolpos thought to be secondary to imperforate hymen. Subsequent MRI evaluation of the pelvis demonstrated a complete septate uterus with longitudinal vaginal septum, atresia of the lower 1/3 of the vagina, and hematocolpos. The patient was placed on Lupron and referred for reconstructive surgery.
Methods & Materials: Complete septate uterus and longitudinal vaginal septum combined with atresia of the lower third of the vagina is a rare congenital anomaly representing a combination of a Mullerian duct anomaly and failure of the primitive urogenital sinus to develop.
Conclusions: Through this case we will discuss the embryology and imaging findings of septate uterus and vagina and vaginal atresia with review of the literature.

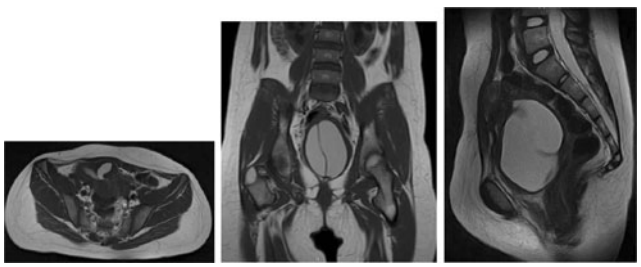

Poster #: EDU-01 (R)

Tips & Tricks for Dose Reduction in Pediatric Imaging

Kimberly Bauer, AAS, (RT), (R), *Medical Imaging, Anne and Robert H. Lurie Children's Hospital, Palos Heights, IL, kibauer@luriechildrens.org*

Disclosures: All authors have disclosed no financial interests, arrangements or affiliations in the context of this activity.
Purpose or Case Report: Since children are more susceptible to the potential effects of ionizing radiation, every opportunity to lower pediatric radiation dose will be explored.
Methods & Materials: Literature from Journals of the American Society of Radiologic Technoligists; recommendations from the FDA, recommendations from Pediatric Radiologists, IAEA (International Atomic Energy Agency), Image Gently
Results: The ALARA principle to reduce the risk to a minimum by strict adherence to justification and optimization; modern recommendations for

dose reduction when possible such as use (higher kvp, lower mas; short exposure times; high DQE digital systems; avoid unnecessary repeat exposures or duplicate examinations; encourage alternate exams that use less or no radiation exposure when possible; back to basics "Image Gently" which recommends measuring the body parts using calipers; posistion the patient properly; avoid using grids; collimate; shield gonads and breasts whenever possible; use AEC only when appropriate; use "child-size" techniques; center properly; immobilize; use proper distance selection; use PA instead of AP when possible; if possible, purchase equipment designed for use with pediatric patients; use pediatric protocols and technique charts; justify x-ray imaging exams by determining if the examination is needed to answer a clinical question; check the patient's medical imaging history to avoid duplicate exams; communication with the physician and imaging team ensures the patient receives the appropriate exam; if using fluoroscopy use pulsed or last-image hold to decrease dose.
Conclusions: Since children are more radiosensitive the adults, a variety of methods are used to reduce the risk. The individual risk from a necessary imaging exam is quite small when compared to the benefit of aiding an accurate diagnosis. If the x-ray prodecure is medically necessary then the medical benefit will alwasys exceed the cancer risk. The decision of whether an exam is justified needs to be made by the child's physician based on the medical needs of that particular child and the information the exam could provide. All exams must be justified and optimized.

Poster #: EDU-02 (R)

Simulation Based Training Utlizing Female Pediatric Vagina Simulator Model

Michelle Garza, AS, *Medical Imaging, Ann and Robert H. Lurie Children's Hospital of Chicago, Orland Park, IL, mgarza@luriechildrens.org;* Merima Karastanovic, Ellen O'Brien, Katherine Naselli Adamski

Disclosures: All authors have disclosed no financial interests, arrangements or affiliations in the context of this activity.
Purpose or Case Report: The purpose of this education is to provide direct practical experience using a simulator to Radiographers on catheterizing the female pediatric patient. The simulator will allow the Radiographer to develop the skills and techniques required for the procedure without exposing patients to unnecessary risks.
Methods & Materials: The simulator model was created to add a life like component to our catheterizing training module. The educational benefits of the simulator included repeated practice, removed patient risk, opportunity to evaluate trainees. We trained new staff the proper technique for catheterizing the female pediatric patient while using the simulator. The simulator was created with very small female infant anatomy. While using the simulator the staff was able to get an realistic feel of the urethra while placing the tube in a non-intimidating environment.
Results: The results of the staff utilizing the simulator as a training tool improved our outcome of successful catheterizations on actual pediatric female patients. The staff gained additional confidence with the repeated practice while using the simulator. Based on the results of our learning experience we have now adapted the simulator as one of our evaluation methods for new hires. The new hires before catheterizing their first patient they must successfully complete multiple skill based simulations.
Conclusions: Pediatric hospitals should include a female pediatric catheterization simulator to their existing training modules for catheterizing.

Poster #: EDU-03 (R)

Intraoperative MRI (iMRI) Needle Guidance for Rectal Pull-through Procedures

Scott Weisel, *MRI, Children's Healthcare of Atlanta at Scottish Rite, Senoia, GA, scott.weisel@choa.org*
Disclosures: All authors have disclosed no financial interests, arrangements or affiliations in the context of this activity.
Purpose or Case Report: IMRI is utilized for surgical guidance in patients with an imperforate anus. It helps for visualizing the muscle tracts as a road map for a successful pull-through procedure via needle guidance. IMRI allows the surgeon a unique perspective of the patient's anatomy in real time and identifies potential issues that may require additional interventions during the procedure.
Methods & Materials: Clinical patients were selected based on diagnosis of imperforate anus and pediatric age. The procedure scheduling required coordinating so that the appropriate surgical team, the interventional radiologist and two MRI technologists were present. An MRI safe needle was used for guidance. The needle was placed and manipulated by an interventional radiologist. One of the MRI technologist serves as an MR safety officer, as three or more clinicians may enter and exit the MRI suite several times during the procedure. This technologist also assists the interventional radiologist, who is gowned and gloved during the procedure. The second MRI technologist is tasked with imaging and manipulating the acquired images, as directed by the interventional radiologist.
Results: Approximately 60 rectal pull-through procedures with iMRI guidance have been performed at this institution since 2007. The iMRI method takes between 30 and 45 min, including preparation of the OR suite for MRI. Surgical outcomes compare favorably to other methods, such as fluoroscopy or ultrasound guided procedures.
Conclusions: MRI guidance in the operating room for rectal pull-through procedures affords the surgeon a navigational edge. Surgeons report improved visibility compared to ultrasound and fluoroscopy guided procedures. iMRI eliminates the need for radiation exposure compared to fluoroscopy guidance. IMRI requires staffing with two MRI technologists during the procedure to assure a safe MRI environment and to help surgeons and interventional radiologists with the use image guidance.

Poster #: EDU-04 (R)

Transitioning from Computed Radiography to Digital Radiography in Pediatric Imaging

Disclosures: All authors have disclosed no financial interests, arrangements or affiliations in the context of this activity.

Nikki Butler, BMSc, RT(R)(QM), *Radiology, Children's Healthcare of Atlanta, Atlanta, GA, nikki.butler@choa.org;* Dana Brinson

Purpose or Case Report: In a Radiology Department that solely cares for pediatric patients, transitioning from computed radiography (CR) to digital radiography (DR) was a challenge. The software for the DR system is designed for imaging adults and has limited pediatric processing features. In the CR system, technologists would manually adjust the imaging technique to child appropriate values based on a technique chart and the usage of a vast array of processing tools. With DR, these charts and processing tools became obsolete. In addition, for the DR wireless

flat panel detector to process the image correctly, 4% of the surface area must be exposed to radiation; a challenge in pediatric imaging. Therefore in order to achieve significant reduction in radiation exposure with DR equipment, extensive staff education, algorithm and technique chart modification is required.
Methods & Materials: A pedaitric radiology interdisciplinary team was established, including radiologic technologists, radiologists, quality analysts, an educator, the DR vendor application specialist, and the organization's Radiation Safety Officer. The team utilized resources from Image Gently, the ASRT s White Paper *Best Practices in Digital Radiography*, and the American Association of Physicists in Medicine's *Report of Task Group 116*, as well as, vendor recommendations to provide education, formulate custom algorithms designed to compensate for limited image processing tools, adjust for lack of surface area exposure and transition the obsolete technique chart into a useful standardized version. Efforts were made for establishing a process to analyze images being repeated by technologists and for creating a method giving radiologists the ability to provide feedback on images through a modification to our coding system.
Results: The implementation of a standardized technique chart for DR utilized in a pediatric setting resulted in a reduction of radiation exposure and the development of custom algorithms. The custom technique chart, shown to be effective, is being utilized by the equipment vendor as a resource and educational tool during new equipment installations. Effectiveness is continuously monitored for trends through the established educational code and repeat analysis by the interdisciplinary team.
Conclusions: Having optimized image quality and successfully reduced radiation exposure, which directly effects patient safety, Children's Healthcare of Atlanta Radiology Departments will continue to utilize standardized best practices for DR.

Poster #: EDU-05 (R)

Portable Imaging on Infants W/ Underlying Specialty Surfaces

Judy Le, *Medical Imaging, Lurie Children's Hospital of Chicago, Oaklawn, IL*

Disclosures: All authors have disclosed no financial interests, arrangements or affiliations in the context of this activity.
Purpose or Case Report: The goal of this study is to educate Radiographers on varies specialty surfaces that are often under critical care patients and how they affect image quality on portable x-rays. By understanding which items cause image artifacts, radiographers can reduce the amount of repeated images and thus, decrease dose to patients.
Methods & Materials: We retrospectively reviewed portable images on infants lying on a hypothermia blanket, z-flo pillow, or delta foam that were not removed for their exam. We also compared those images with others where all underlying objects were removed prior to imaging. Included were images acquired on 10 infants from the CCU/NICU under the age of 12 months using a portable x-ray machine set with a manual technique of 60-70 kvp with a mAs of 1. Images were assessed by radiologist to determine whether objects created artifacts that impacted diagnostic interpretation.
Results: Images with infants lying on a delta foam resulted in no artifacts. Hypothermia blankets resulted in a "honey comb" like artifact and must be removed prior to imaging unless prohibited by patient condition. Imaging through z-flos did not disrupt viewing of cannulas or lines but did affect viewing of lung detail.
Conclusions: Critical patients can be imaged while lying on delta foams without impacting diagnostic read. Hypothermia blankets and z-flo pillows must be moved prior to imaging unless prohibited by physician due to patient condition. Any images obtained without removal of a specialty surface should be properly documented.

Poster #: EDU-06 (R)

Improving Lead Integrity Testing and Tracking

Barbara Karl, *Ann & Robert H. Lurie Children's of Chicago, Chicago, IL, bkarl@luriechildrens.org;* Ellen Gray, Christina Sammet, PhD, DABR

Disclosures: All authors have disclosed no financial interests, arrangements or affiliations in the context of this activity.
Purpose or Case Report: The goal of this study is to develop a program to increase the level of understanding for the annual lead testing, what is deemed as acceptable versus unacceptable for lead integrity and more efficient tracking/documentation measures.
Methods & Materials: An educational power point was created to standardize acceptable cracks and pinpoint holes for the technologists. This has aided the process so that technologists have a clear understanding of pass, fail or second review. The process for tracking and documenting lead annually changed from a paper tracking, with handwritten descriptors, to a single database for data entry utilizing metal ID tags and grommets. Colored zip ties change annually to document which lead has been tested.
Results: Centralized database for documentation of annual lead checks with a standardized numbering system, eliminates duplicate checks (labor expense)
Easier record accessibility for the Joint Commission review (old method required manual count for totals)
Easier method of tracking missing or disposed of lead via central database (unaccounted for lead decreased significantly)
Better implementation process for newly purchased lead being brought into the Institution
Easier visibility for current year's lead check by color coded zip ties
Staff can readily identify lead that has not been checked based on the color of the zip tie. The lead can then be imaged and recorded to central database
Conclusions: The results of this study indicate that annual testing of lead is more consistent between staff after education and a centralized database for tracking has been implemented. Tracking of lead has also transitioned from a subjective labeling system to a consistent tag system with sequential numbers
Staff is now aware of what constitutes disposing of lead versus a second review.
Post staff education resulted in a universal understanding of what size cracks are not acceptable.
Staff is empowered to make a decision on lead integrity
This has improved how lead integrity is tracked (increase in lead disposal after education)

Lead at Lurie Childrens Facilities	2013	2015
Total # of Lead pieces	883	704
Total # of unaccounted for lead	136	2
Total # of duplicated lead checks	42	0
Total # of disposed lead	41	54

Poster #: EDU-07 (R)

Imaging the ECMO patient in CT: High Risk, Low Volume

Barbara Karl, *Medical Imaging, Ann & Robert H. Lurie Children's of Chicago, Oak Lawn, IL, bkarl@luriechildrens.org;* Christina Sammet, PhD, DABR, Andrada Popescu, MD, Cynthia Rigsby, MD

Disclourses: Cynthia Rigsby has indicated a relationship with Siemens as a researcher. All other authors have disclosed no financial interests, arrangements or affiliations in the context of this activity.

Purpose or Case Report: The goal of this education exhibit is to develop an imaging strategy to safely image the patient on extracorporeal membrane oxygenation (ECMO) within the CT department focusing on scan protocols, define table movement required for high pitch table movement, communication and necessary emergency supplies.
Methods & Materials: At our institution the ECMO patients are only imaged on our main scanner due to the speed when using the hi-speed mode and spiral imaging. Also taken into account, is the size of the room which can accommodate the increased staff presence, as well as any additional equipment (ECMO circuit, IV pumps, CT power injector). Transporting the patient from cardiac intensive care unit to the CT scanner suite requires a high degree of communication between the CT technologist, staff and the ECMO team. Educational materials will be provided to the technologists and a flow chart created for communication and needs (scan time, IV required, roles). The main risk of imaging patients on ECMO by CT is decannulation, particularly on fast scanners when utilizing spiral imaging and/ or high pitch/fast scan mode. One of the methods to ensure patient safety is to create a worksheet with the CT table movement for fast scans, based on the protocol pitch, that would allow the technologists to safely move the patient in and out of the scanner, accounting for the significant table ramp up and ramp down when utilizing a high table pitch (fast scan). This will create awareness for the techs and it will ensure that all lines willreach the full table travel distance for the desired examination.
Results: Results of this education and training will ensure that the ECMO patient can be safely transported to the CT suite and imaged safely within the CT department while decreasing the risk of complications.
Conclusions: CT staff is better prepared to image the ECMO patient regardless of what type of scan the child was having. The communication and role definition became more effective and concise which resulted in the safe arrival and imaging of the patient. Staff is now able to determine maximum table movement in and out based on a vendor specific chart created for the scanner.

Poster #: EDU-08 (R)

Anomalous Pulmonary Venous Return: Pictoral Review

Irma Matos Rojas, Physician, *Instituto Nacional de Salud del Niño - San Borja, Lima, Peru, aracellymatos@yahoo.es;* Carlos Ugas, Radiologist, Marlin Megue Huamani, Licenciado, Doris Katekaru Tokeshi, Claudia Lazarte, Radiologist, Melissa Valdez Quintana, Pediatric Radiologist, Larry Alpaca Rodriguez, Alvina Casamayor, Medico Radiologa Intervencionista

Disclosures: All authors have disclosed no financial interests, arrangements or affiliations in the context of this activity.
Purpose or Case Report: The purpose of this exhibit is to review imagings findings of anomalous pulmonary venous return on angiotomography and describe anomalies associated.
Magnetic resonance (MR) imaging and computed tomography (CT) are used in diagnostic and follow - up the congenital vein anomalies. CT provides superior spatial resolution and short time but there is exposure to ionizing radiation. However in many hospital there are only the possibility of obtain CT imaging in neonates and infant.
The total anomalous pulmonary venous return (TAPVR) is the result of failure of the common pulmonary vein to connect to the left atrium with persistence of the primitive splanchnic connections of the pulmonary veins. There are four categories: supracardiac, cardiac, infracardiac and mixed.
The partial anomalous pulmonary venous return (PAPVR) occurs when some but not all segments of the developing lung failed to establish connections with the common pulmonary vein.
Methods & Materials: A retrospective review of CT scan of patients with the diagnosis of anomalous pulmonary venous return was performed in a pediatric reference institute from January 2014 though October 2015.
Results: We found 29 patients with the diagnosis of anomalous pulmonary venous return, 6 were excluded for having postoperative changes. The average age was 17,8 months (11 days - 7 years). We found slight predominance of females patients (52%). TAPVR was found in 78%, and the majority of the patients had supracardiac TAPVR (56% of TAPVR) as describe literature. We also found infracardiac TAPVR, intracardiac TAPVR, mixed TAPVR, intracardiac PAPVR and scimitar syndrome. CT findings of these entities will be collected and widely described.
The more anomalies associated were atrial septal defect (52%), ductus venosus (30%) and heterotaxy (23%). Other anomalies found are ventricular septal defect, double outlet RV/LV, atrioventricular canal, estenosis / atresia of the pulmonary artery, aberrant subclavian artery. Also we found transposition of the great arteries, aortic coartation, and others.
Conclusions: There are a variety of anomalous pulmonary venous return and abnormalities associated. Knowledge of these entities can help the radiologists to differentiate between these venous congenital anomalies for timely and accurate diagnosis.

Poster #: EDU-09 (R)

Becoming a Pediatric Diagnostic Imaging Center of Excellence

Rebecca Clavijo, MS, *Radiology, Children's Healthcare of Atlanta, Cumming, GA, lynn.clavijo@choa.org*

Disclosures: All authors have disclosed no financial interests, arrangements or affiliations in the context of this activity.
Purpose or Case Report: It has become challenging for pediatric imaging centers to keep up with the various national requirements regarding quality of patient care and safety issued by the Joint Commission and others. The American College of Radiology's *Diagnostic Imaging Center of Excellence* program provides an avenue for pediatric radiology departments to demonstrate their qualifications of personnel, policies and procedures, equipment specifications, quality assurance activities, patient safety, image quality and the quality of patient care.
Methods & Materials: The American College of Radiology developed the Diagnostic Imaging Center of Excellence award as a way to provide "comprehensive assessment of the medical imaging facility, including structure and outcomes". Award requirements are 1) Participation in the ACR's Dose Index Registry (DIR), 2) Contribution to the General Radiology Improvement Database (GRID) and 3) Site visit by an ACR team. The DIR requires submitting CT dose information for benchmarking. GRID data include patient wait times, report turnaround times, digital radiography repeat rates, biopsy success rates and others. Facilities must meet requirements in categories such as radiation safety, medication management, quality management, and patient records.
Results: We achieved buy in from all stakeholders, including radiologists, physicists, management and staff. Information technology set up systems for data retrieval. We performed a SWOT (strengths, weaknesses, opportunities & threats) analysis: Our policies, marketing materials, quality data, job descriptions and meeting minutes demonstrated compliance but we also identified areas for improvement, such as availability of appropriateness criteria information for referring physicians. The ACR site visit team, consisting of a radiologic technologist, radiologist, and physicist, reviewed evidence of compliance and made suggestions that were implemented.
Conclusions: The Diagnostic Imaging Center of Excellence award was granted and has been used to distinguish the department as one

dedicated to excellence in imaging with patient safety as a top priority. Participation in national registries allows benchmarking with other facilities and is a way to ensure appropriate metrics are in place. The process of reviewing each element of compliance required thorough review of services and expanded the quality program into new areas. Participation also ensured compliance with Joint Commission standards.

Poster #: EDU-10 (R)

BENIGN TUMORS AFFECTING THE SYNOVIAL TISSUE OF THE KNEE IN CHILDREN

Maria Orozco, *Diagnostico Por Imagenes, Hospital Nacional De Pediatria J.P. Garrahan, Buenos Aires, Argentina, eugeorozco79@gmail.com;* Monica Bravo, Medico de Staff, Vivian Gonseski, Guillermo Arias, Juliana Lostra, Julio Kaplan, Jose Lipsich

Disclosures: All authors have disclosed no financial interests, arrangements or affiliations in the context of this activity.
Purpose or Case Report: Intraarticular masses may be classified into infectious granulomatous diseases (tuberculous arthritis or due to coccidioidomycosis), deposition diseases (gout, amyloid arthropathy), tumors or benign synovial proliferation processes (synovial chondromatosis, pigmented villonodular synovitis, lipoma arborescens, synovial hemangioma), vascular malformations and malignant tumors (chondrosarcoma, sarcoma, or synovial metastasis).
Intraarticular masses are rare in children and their diagnosis poses a challenge for radiologists, who must be aware of the specific features of different imaging studies to make an adequate diagnosis.
OBJECTIVES: To describe the typical imaging findings, mainly on magnetic resonance imaging (MRI), that allow us to make the differential diagnosis in children with painful chronic benign tumors (chronic synovitis) of the knee.
Methods & Materials: We conducted a descriptive and retrospective study, collecting the radiologic and clinical findings and data on the treatment, pathology diagnosis, and outcome of patients with chronic sinovitis of the knee seen at our hospital.
We present 4 prepubertal patients with a similar symptomatology, two of whom with a history of trauma, whose diagnoses were differential among them, but whose MRIs were typical: Pigmented villonodular synovitis, synovial hemangioma, synovial chondromatosis, and lipoma arborescens.
Conclusions: Benign synovial tumors are rare in childhood.
The knee is one of the most commonly affected joints.
The signs and symptoms of these pathologies are very similar, consisting of pain, increased joint size, limitation of movement that may lead to a joint block: All signs and symptoms of chronic synovitis.
In all cases, MRI is the imaging method of choice due to its superiority in showing the morphology of intra- and extraarticular structures, the extent of the lesion, and the nature of its contents (fat, hemosiderin, calcifications), distinguishing the typical features of different benign synovial tumors.
The diagnosis is confirmed by pathology studies.

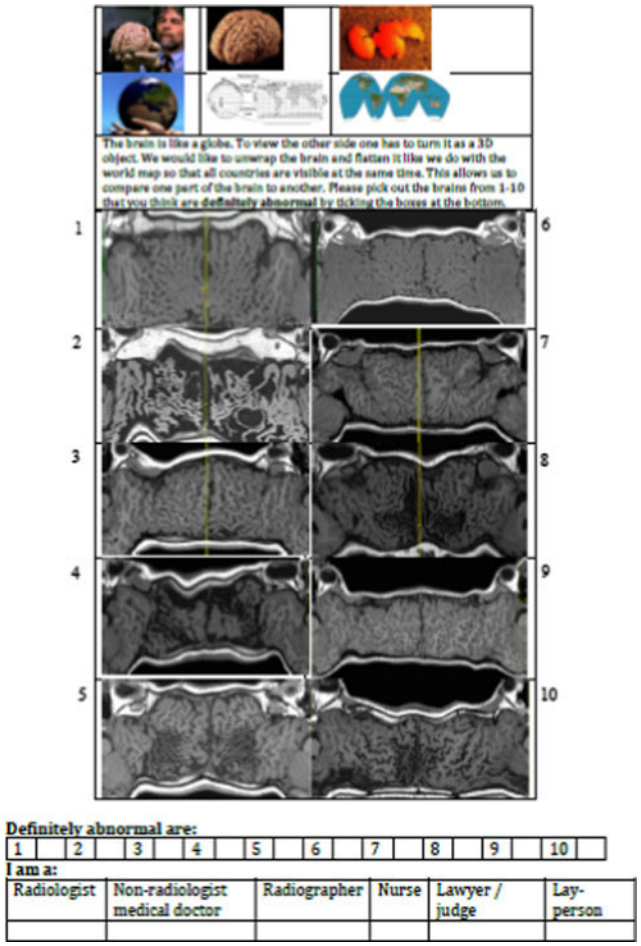

Poster #: EDU-11 (R) - *Withdrawn*

Poster #: EDU-12 (R) - *Withdrawn*

Poster #: EDU-13 (R)

Infections in Pediatric Patients with Hematologic Malignancy and Aplastic Anemia

Irma Matos Rojas, Physician, *Instituto Nacional de Salud del Niño - San Borja, Lima, Peru, aracellymatos@yahoo.es;* Claudia Lazarte, Radiologist, Doris Katekaru Tokeshi, Carlos Ugas, Radiologist, Melissa Valdez Quintana, Pediatric Radiologist, Alvina Casamayor, Medico Radiologa Intervencionista

Disclosures: All authors have disclosed no financial interests, arrangements or affiliations in the context of this activity.
Purpose or Case Report: Significant progress in improving outcome for patients with oncohematological diseases are attributed to intensive chemotherapy, bone marrow transplantation, platelet transfusions, development of new imaging techniques, new antimicrobials and others. All these advances increase the survival of these patients which in turn increases the frequent of risk of infections that are substantial cause of morbidity and mortality in these patients.

The purpose of this exhibit is to show the spectrum of infections in these patients; describe the imaging finding according to the etiology and associated factors.
There are a number of factors that need to be considered in order to interpret abnormalities seen on radiology as the type of hematological disease, stage of the hematological disease, treatment phase, profile of immunodeficiency, treatment for infection received, patient history and clinical signs. For example, according to type of immunosuppression there are different spectrum of infections but leukemia affect all types of immunosuppression that include neutropenia, T cell defect and B cell defect.
Methods & Materials: The medical records of patients with hematologic malignancy and aplastic anemia in a pediatric reference institute, with microbiological diagnosis or laboratory and clinics findings highly compatible with an etiologic agent will be collected and correlated with different imaging modalities available in these patients.
Conclusions: Different imaging techniques like X ray, CT, MRI and ultrasound have become a crucial aspect in the diagnosis of infectious disease among patients with hematological malignancies and aplastic anemia. There are some radiological signs associated to specific infections, but it is not easy and not is possible to make etiological diagnosis based solely on analyzing imaging in these patients. We need the various factors associated to make a precise diagnosis.

Poster #: EDU-14 (R)

Cranial Ultrasound Imaging

Jaclyn Harding, *Ultrasound, Children's Hospital of Orange County, Aliso Viejo, CA, jackierharding@gmail.com*

Disclosures: All authors have disclosed no financial interests, arrangements or affiliations in the context of this activity.
Purpose or Case Report: The purpose of this exhibit is to educate sonographers on proper technique when performing cranial ultrasounds as well as present abnormalities they may encounter. I will present detailed scenarios when scanning pediatric heads which will discuss proper parameters including proper orders, technique, transducers, and limitations of patients. Age appropriate scanning will be addressed in order to ensure an adequate, diagnostic, and meaningful study. Normal and abnormal anatomy and pathology will be addressed and discussed. Patient positioning and transducer placement will be reviewed.
Methods & Materials: In our institution, multiple images are obtained for a complete and comprehensive cranial ultrasound. Images are obtained through the anterior, posterior, and mastoid fontanelles. Different types of transducers are used to provide detailed information of the brain echotexture, ventricles, cerebellum, and extra axial space. I will present multiple images demonstrating normal anatomy and abnormal findings such has intracranial hemorrhage, PVL, agenesis of the corpus collosum or cavum septum pellucidum, infarction, ventriculitis, porencephalic cysts, and more.
Results: Often times, subtle abnormalities can be overlooked when cranial ultrasounds are performed. This presentation will give sonographers useful information regarding the importance of utilizing the proper transducer and recognizing normal anatomy and abnormal findings. This will in turn greatly assist the Radiologist in interpreting these studies.
Conclusions: Utilizing the proper transducers and technique will improve the diagnostic value of cranial ultrasounds. Understanding the normal and abnormal findings will greatly assist the Radiologist in interpreting the studies.

Poster #: EDU-15 (R)

Portable CT in a Pediatric ICU Setting

Renee Ahmed, BA, AMSc, *CT Scan - Radiology, Children's Healthcare of Atlanta at Egleston, Atlanta, GA, renee.ahmed@choa.org;* Stephen Simoneaux, Paula Dickson, M.D.

Disclosures: All authors have disclosed no financial interests, arrangements or affiliations in the context of this activity.
Purpose or Case Report: The objective is to describe the use of portable CT in neonatal, cardiac, and pediatric intensive care unit patients. Challenges of use, types of scans performed, and typical patients will be described.
Methods & Materials: The records were searched to determine the number of scans performed each month on the Neurologica Ceretom scanner. Types of patients are described along with the patient condition that precluded travel to the department. Also, we describe the technical challenges of performing the imaging in the unit setting, including patients on extracorporeal membrane oxygenation. Guidelines for which patients get a portable scan are also discussed.
Results: The scanner is an 8-slice scanner, and produces good scan quality. A task force of critical care physicians, radiologists, and CT technologists worked together to establish guidelines for determining which cases will most benefit from the use of the portable scanner. An assessment of the acuity of the patient will dictate whether the mobile unit is necessary. We can scan any body part of patients younger than 2, and head CTs on older patients. On average, 7 portable scans are done each month on patients with critical airways, those on ECMO, or too critical to leave the unit setting. The main difficulty is the initial setup of the scanner which requires two technologists and the cooperation of the unit staff.
Conclusions: Portable CT provides an excellent option for patients unable to travel to the CT department for a traditional scan. The use of the scanner does entail technical challenges in the setup of the gantry and requires two technologists and the unit staff assistance.

Poster #: SCI-01 (R)

Dynamic Volume Imaging by MDCT in Pediatric Patients with Tracheobronchial Stenosis

Shuji Abe, *Radiology, Osaka Medical Center and Research Institute for Maternal and Child Health, Izumi, Japan, sytm1962ipod@gmail.com;* Makoto Shimada, Yuki Abe, Masanori Nishikawa, Masahide Tominaga, Hidetoshi
Yatake, Koichi Yabunaka, Toshizo Katsuda

Disclosures: All authors have disclosed no financial interests, arrangements or affiliations in the context of this activity.
Purpose or Case Report: The 320-row multidetector computed tomography (MDCT) enables the scanning of a maximum length of 160 mm by volume scanning (VS). Dynamic volume scanning (DVS) with MDCT enables the development of a 4D dynamic image.
The 3D findings of tracheobronchial imaging in children who cannot control their breathing fail to reveal the phase of breathing in which the image was taken, which affects the accuracy of the diagnosis of tracheobronchial stenosis. Imaging by 4D-DVS enables the accurate observation of the tracheal dynamics in association with the respiratory kinetics, thus revealing the mechanism of the former. Furthermore, 4D-DVS would enable the imaging of the cardiac blood vessels by a contrast study simultaneously with the imaging of the stenosed area.

We assessed the efficacy of the 4D-DVS imaging technique in the diagnosis of pediatric tracheobronchial stenosis.

Methods & Materials: The study included 28 pediatric patients who underwent tracheobronchial imaging by 4D-DVS between January 1, 2013 and September 28, 2015 (age: 0 - 3 years old, median age: 1 year). All examinations were performed using a 320-row MDCT. The designated scan area was from the larynx to the bronchus or the lower end of the chest. Depending on the physique of the patient, the scanning length was set between 80 mm and 160 mm. The scanning parameters were: 80 kV tube voltage, CT-AEC tube current, 160 - 320×0.5 mm collimation, 0.35 - 1.0 s rotation time, and 0.5-mm reconstruction interval.

The efficacy of 4D-DVS was assessed by evaluating the findings of the tracheal dynamic imaging. The dynamic images were evaluated for the visualization of the constriction causing the tracheobronchial stenosis, and the 3D visualization of the breathing dynamics. The exposure dose of the DVS was determined from the dose length product (DLP)value of the dynamic tracheal scan.

Results: Of the 28 patients who underwent dynamic CT scanning, 19 patients were diagnosed with tracheobronchial stenosis. In 11 of the 19 patients, the stenoses were associated with respiratory kinetic images. Additionally, a ring-sling complex was identified in two of six patients who underwent contrast imaging simultaneously with DVS. The radiation dose of the DVS was higher than that of VS.

Conclusions: DVS is an effective technique for the diagnosis of tracheobronchial stenosis associated with the breathing dynamics. However, it is necessary to be cautious about the high radiation dosages in DVS.

Poster #: SCI-02 (R)

Voiding Cystourethrography (VCUG) in Children; a Hospital-Based Survey

Annette Schjerven, *Pediatric Radiology, Haukeland University Hospital, Bergen, Norway, annette.irene.schjerven@helse-bergen.no;* Kristine Fasmer, Stein Magnus Aukland

Disclosures: All authors have disclosed no financial interests, arrangements or affiliations in the context of this activity.

Purpose or Case Report: Despite the development of new methods for the detection of Vesico Urethral Reflux (VUR), Voiding Cystourethrography (VCUG) still plays an important role in pediatric uroradiology. However, the use seems to have changed over time. International guidelines exist and the main indication is the Ultrasonography (US) finding of hydronephrosis, indicating a high grade VUR or, in boys, to exclude Posterior Urethral Valve (PUV). VUR is a common condition found in 30-40% of children with UTI. Our department performs VCUG according to the guidelines given by the ESUR subgroup for Pediatric Uroradiology. Haukeland University Hospital (HUS) serve a population of 300,000 people. At the Section of Pediatric Radiology, we observed a decrease in the use of VCUG. We therefore did a systematic review of all VCUGs performed at our department during 2013 and 2014, focusing in detail on the age group 1 year or less. We aim to be true to the image gently policy, maintaining the ALARA principle, keeping the radiation doses as low as reasonably possible.

Methods & Materials: We performed a total of 94 VCUGs over a 2-year period, where 47 children were 0-1 year old. The collected data include clinical indication, age and gender, referring institution and results of the examination. In addition, the radiation dose was registered from the x-ray equipment as DAP values in $mGycm^2$. The Monte-Carlo Simulating Program (PCXMC) was used to present the collected DAP values as estimated effective doses (mSv).

Results: 47 VCUGs (22 girls and 25 boys) were performed on children 0-1 year old during 2013 and 2014. 72% were below 7 months of age at time of examination. Age distribution and reason for referral are presented in figures 1 and 2. 98% were referred from a pediatrician at HUS. 57% of the VCUGSs were reported as normal and VUR was the most common pathological finding, found in 40% (fig. 3). The mean DAP dose was 98 $mGycm^2$. Figure 4 presents the simulated estimated effective doses in mSv.

Conclusions: VCUG is still an important examination and we performed 94 VCUGs during 2013-2014. Nearly all 47 patients in the group 0-1 year of age, were referred from a pediatrician at our hospital. UTI was the most common reason for referral. Pathology was found in 43% of the cases and VUR grades 3, 4 and 5 were the most common pathological findings. The mean DAP dose when findings were normal, was 99,4 $mGycm^2$, and 100.4 $mGycm^2$ in cases with pathological findings.

2016 Author index by Abstract

Abadeh, Aryan	Paper #: 079	Canada
Abdeen, Nishard	Poster #: EDU-141, Poster #: SCI-078	Canada
Abdulla, Sarah	Poster #: CR-058	United States
Abe, Shuji	Poster #: SCI-01 (R)	Japan
Abe, Yuki	Poster #: SCI-01 (R)	Japan
Abu-El-Haija, Maisam	Paper #: 001	United States
Acomb, Allen D.	Paper #: 108	United States
Acord, Michael	Poster #: EDU-074	United States
Adaletli, Ibrahim	Poster #: CR-026, Poster #: CR-027, Poster #: SCI-021	Turkey
Adams, Ashok	Poster #: CR-003	United Kingdom
Adeb, Melkamu	Paper #: 053	United States
Adeyiga, Adebunmi	Poster #: EDU-135	United States
Adgent, Margaret	Paper #: 129	United States
Adu, John	Poster #: EDU-024, Poster #: EDU-028	United Kingdom
Advani, Ranjana	Paper #: 019, Paper #: 187, Paper #: 189	United States
Adzick, N S.	Paper #: 039	United States
Agarwal, Ritesh	Paper #: 086	India
Aghighi, Maryam	Paper #: 187	United States
Aguet, Julien	Poster #: EDU-018	Switzerland
Ahmad, Tahani	Paper #: 013, Poster #: EDU-091, Poster #: EDU-127, Poster #: SCI-038	Canada
Ahmed, Fahran	Poster #: CR-066	Canada
Ahmed, Farhan	Poster #: SCI-078	Canada
Ahmed, Humayun	Poster #: SCI-036	Canada
Ahmed, Omar	Paper #: 072	United States
Ahmed, Renee	Poster #: EDU-15 (R)	United States
Ahyad, Rayan A.	Paper #: 185, Poster #: CR-065, Poster #: EDU-107	Canada
Akiki, Salwa	Paper #: 14 (R)	Canada
Aktar, Mohammed Rashid	Poster #: EDU-005	United Kingdom
Al-Aswad, Nadine	Paper #: 080	Canada
Alazraki, Adina	Poster #: EDU-125, Poster #: SCI-068	United States
Albers, Brittany	Paper #: 143, Poster #: EDU-081	United States
Albertario, Marco	Poster #: CR-02 (R)	France
Albieri, Caterina	Poster #: CR-001	Italy
Albuquerque, Pedro	Poster #: SCI-059	Canada
Al-Busaidi, Asya S.	Poster #: CR-025	Oman
Alford, Raphael	Paper #: 187, Poster #: SCI-049, Poster #: SCI-080	United States
Ali, Kamran	Poster #: CR-030	United States
Allbery, Sandra M.	Poster #: CR-032, Poster #: CR-041, Poster #: CR-074	United States
Alley, Marcus T.	Paper #: 162	United States
Allison, McGee	Paper #: 13 (R)	Ireland
Almenawer, Saleh	Paper #: 150	Canada
Alonso, Jose	Poster #: CR-018	Argentina
Alpaca Rodriguez, Larry M.	Poster #: CR-04 (R), Poster #: EDU-08 (R)	Peru
Alqublan, Lina	Poster #: EDU-053	Canada
Alsabban, Zehour	Paper #: 002	Canada
Al-Saraf, Ali A.	Poster #: EDU-034, Poster #: EDU-067	United States
Al-Shabibi, Saud	Poster #: CR-025	Oman
Alsharief, Alaa N.	Poster #: EDU-030	Canada

Al-Somali, Faisal	Poster #: EDU-053	Canada
Altinok, Deniz	Paper #: 153	United States
Alturkistani, Tahani	Poster #: EDU-031, Poster #: EDU-032	United States
Alves, Marina	Paper #: 03 (R)	Portugal
Alzahrani, Ahmed	Poster #: EDU-068	Canada
Amaxopoulou, Christina	Paper #: 136	Switzerland
Amirabadi, Afsaneh	Poster #: SCI-036	Canada
Anand, Rama		India
Andersson Lindholm, Jonas	Paper #: 193	Sweden
Andronikou, Savvas	Paper #: 029, Paper #: 090, Paper #: 186, Poster #: EDU-105	United Kingdom
Annapragada, Ananth	Paper #: 093, Paper #: 101, Paper #: 102, Paper #: 142	United States
Anooshiravani, Mehrak	Poster #: SCI-008	Switzerland
Anupindi, Sudha A.	Paper #: 003, Paper #: 060, Paper #: 067, Poster #: EDU-137, Poster #: SCI-033	United States
Applegate, Kimberly E.	Paper #: 068	United States
Arce, Jose D.	Poster #: CR-076	Chile
Ardestani, Allen	Poster #: EDU-106	United States
Arfeen, Farrukh	Poster #: EDU-011	United Kingdom
Aria, David J.	Paper #: 115, Paper #: 182, Poster #: CR-071, Poster #: EDU-120, Poster #: EDU-121, Poster #: SCI-034	United States
Arias, Guillermo	Poster #: EDU-10 (R)	Argentina
Arioz Habibi, Hatice	Poster #: CR-026, Poster #: CR-027, Poster #: SCI-021	Turkey
Arruda, Elaine C.	Poster #: EDU-087	Brazil
Arthurs, Owen J.	Paper #: 023, Paper #: 105, Paper #: 158, Paper #: 170, Poster #: CR-007, Poster #: CR-008, Poster #: CR-012, Poster #: CR-013, Poster #: SCI-001	United Kingdom
Arunachal, Gautham	Poster #: CR-072	India
Asch, Elizabeth	Paper #: 140	United States
Ashton, Daniel	Paper #: 114, Paper #: 181, Paper #: 183, Paper #: 184	United States
Ashwin, Clare	Paper #: 170	United Kingdom
Ashworth, Michael	Paper #: 105, Poster #: EDU-008	United Kingdom
Aslan, Ahmet	Poster #: SCI-021	Turkey
Aslan, Mine	Poster #: CR-026, Poster #: CR-027, Poster #: SCI-021	Turkey
Athur, Sarah	Paper #: 029	United Kingdom
Atkin, Karen	Poster #: CR-028	Australia
Atweh, Lamya A.	Paper #: 168	United States
Augustyn, Robyn	Poster #: EDU-090	United States
Aukland, Stein Magnus	Poster #: SCI-02 (R)	Norway
Aurora, Paul	Poster #: EDU-008	United Kingdom
Avenarius, Derk	Paper #: 141	Norway
Averill, Lauren W.	Paper #: 172, Poster #: CR-044	United States
Avitzur, Yaron	Paper #: 013	Canada
Awai, Kazuo	Poster #: EDU-079	Japan
Ayyala, Rama	Paper #: 130, Poster #: EDU-066	United States
Baad, Michael	Paper #: 073, Poster #: EDU-075	United States
Babb, James	Paper #: 046	United States
Back, Susan	Paper #: 054	United States
Bacon, Patrick	Poster #: CR-051, Poster #: EDU-102	United States
Badillo, Andrea	Poster #: SCI-060	United States
Bagade, Swapnil	Paper #: 007	United States
Bagrosky, Brian M.	Paper #: 014	United States
Bagyura, Zsolt	Poster #: SCI-017	Hungary
Baheti, Akshay D.	Paper #: 016	United States
Bailey, Smita S.	Poster #: SCI-034	United States
Baja, Manish	Poster #: EDU-136	United States
Bajno, Lydia	Paper #: 025, Poster #: EDU-109	Canada
Bakan, Selim	Poster #: SCI-021	Turkey
Bandarkar, Anjum	Poster #: EDU-135, Poster #: EDU-142, Poster #: SCI-076	United States
Bao, Shanshan	Paper #: 121	United States
Baqué Juston, Marie	Paper #: 10 (R), Poster #: CR-01 (R)	France
Barber, Ignasi	Poster #: SCI-020, Poster #: SCI-024	Spain
Barczuk, Marzena	Poster #: EDU-007	Poland
Bardo, Dianna M.	Paper #: 103, Poster #: EDU-090	United States
Bareño, Sandra	Poster #: SCI-056	Chile
Barnes, Craig E.		United States

	Poster #: EDU-069, Poster #: EDU-071, Poster #: SCI-034, Poster #: SCI-047	
Barnewolt, Carol E.	Paper #: 055, Poster #: EDU-122	United States
Barrett, Hannah	Poster #: CR-012, Poster #: CR-013	United Kingdom
Barth, Richard	Paper #: 043, Poster #: EDU-078, Poster #: EDU-132, Poster #: SCI-049	United States
Bassi, Matteo	Poster #: CR-016	Italy
Basta, Amaya M.	Poster #: EDU-100, Poster #: EDU-101	United States
Bastrom, Tracey	Paper #: 118	United States
Bates, Nicholas	Poster #: EDU-116	United States
Batool, Saima	Paper #: 078	Canada
Baud, Catherine	Paper #: 106, Poster #: EDU-015, Poster #: SCI-007, Poster #: SCI-011	France
Bauer, Kimberly	Poster #: EDU-01 (R)	United States
Beavers, Angela J.	Poster #: CR-041	United States
Bedane, Alemayehu	Poster #: EDU-134	Ethiopia
Bednov, Andrey	Paper #: 142	United States
Bedoya, Maria A.	Paper #: 051, Paper #: 057	United States
Beishuizen, Auke	Paper #: 026	Netherlands
Bellah, Richard	Paper #: 054, Poster #: SCI-033, Poster #: SCI-081	United States
Benitez, Steven	Poster #: EDU-063	United States
Bentley-Hibbert, Stuart	Poster #: EDU-066	United States
Berger, Jonathan R.	Poster #: CR-052	United States
Berlin, Sheila	Poster #: CR-040	United States
Bernardo, Felisa	Paper #: 099	United States
Bertocci, Gina	Paper #: 171	United States
Beydoun, Tammam	Paper #: 103, Paper #: 115, Paper #: 182, Poster #: CR-071, Poster #: SCI-047	United States
Beyene, Joseph	Paper #: 079	Canada
Bezzina, Paul	Paper #: 17 (R)	Malta
Bhamare, Tanmay	Paper #: 138	Canada
Bhandal, Samarjeet	Paper #: 078	Canada
Bhatia, Anmol	Paper #: 086	India
Bhatti, Zeeshaan	Poster #: EDU-072	United States
Bhavane, Rohan	Paper #: 142	United States
Bhayana, Saakshi	Paper #: 101, Paper #: 102, Paper #: 142	United States
Bhengu, Louisa	Poster #: CR-002	South Africa
Biejat, Agnieszka	Poster #: EDU-007	Poland
Biko, David M.	Paper #: 003	United States
Bilal, Ahmed	Poster #: EDU-141	Canada
Binkovitz, Larry A.	Paper #: 139	United States
Binkovitz, Lauren	Paper #: 139	United States
Birkemeier, Krista L.	Poster #: CR-029, Poster #: CR-034	United States
Biscaye, Stephanie	Poster #: CR-02 (R)	France
Bisset, George S.	Paper #: 056, Paper #: 126	United States
Biyyam, Deepa R.	Paper #: 103, Poster #: EDU-071, Poster #: EDU-096	United States
Blanchette, Victor	Poster #: SCI-036	Canada
Blaser, Susan	Paper #: 151	Canada
Blask, Anna R.	Paper #: 096, Poster #: EDU-111, Poster #: SCI-060	United States
Bleacher, John	Paper #: 116	United States
Blitman, Netta	Paper #: 031	United States
Bloom, David	Poster #: SCI-079	United States
Blough, Kiara L.	Paper #: 040	United States
Blumenfeld, Yair	Poster #: SCI-049	United States
Blumfield, Einat	Poster #: EDU-032	United States
Bobbey, Adam	Paper #: 179	United States
Bode, Peter	Paper #: 136	Switzerland
Bodea, Jessica	Poster #: CR-061	United States
Boechat, Ines	Poster #: EDU-105, Poster #: EDU-134	United States
Bohn, David	Poster #: CR-038	United States
Bolivar Perrin, Julie	Paper #: 106, Poster #: EDU-015, Poster #: SCI-007, Poster #: SCI-011	France
Bolton, Kimberly	Poster #: SCI-029	United States
Borradori Tolsa, Cristina	Poster #: SCI-004	Switzerland
Botwin, Ariel L.	Paper #: 064	United States
Bourke, Billy	Paper #: 13 (R)	Ireland
Bouskill, Vanessa	Poster #: SCI-058	Canada

Boutis, Kathy	Poster #: SCI-037	Canada
Bove, Kevin E.	Paper #: 045	United States
Bowman, Sean	Poster #: CR-070	United States
Boyer, Corinne	Paper #: 10 (R), Poster #: CR-01 (R), Poster #: CR-02 (R)	France
Boyer, Kathleen	Poster #: EDU-092	United States
Boylan, Jennifer	Poster #: EDU-132	United States
Braithwaite, Kiery	Poster #: EDU-045	United States
Branson, Helen	Paper #: 151	Canada
Braojos, Fernanda d.	Poster #: EDU-087	Brazil
Bravo, Monica G.	Poster #: EDU-029, Poster #: EDU-10 (R)	Argentina
Breen, Micheal A.	Paper #: 061	United States
Brenner, Clare	Poster #: CR-056	Ireland
Brinson, Dana	Poster #: EDU-04 (R)	United States
Brody, Alan S.	Paper #: 085	United States
Brown, Jeffrey	Paper #: 146	United States
Browne, Lorna	Paper #: 087, Paper #: 167, Poster #: SCI-048, Poster #: SCI-050	United States
Browning, Carol Ann T.	Paper #: 167	United States
Brudnicki, Adele	Poster #: EDU-145	United States
Brun, Henrik	Paper #: 192	Norway
Bruno, Claudio H.	Poster #: SCI-070	Argentina
Bruno, Costanza	Paper #: 047, Poster #: EDU-013	Italy
Bruno, Didier A.	Poster #: SCI-070	Argentina
Brzewski, Michal	Poster #: EDU-007	Poland
Buchanan, Toni	Paper #: 08 (R)	Ireland
Bueno, Letícia F.	Poster #: EDU-087	Brazil
Bulas, Dorothy	Paper #: 096, Poster #: EDU-111, Poster #: EDU-142, Poster #: SCI-060	United States
Bunge, Martin	Poster #: EDU-053	Canada
Bure, Lionel	Poster #: SCI-059, Poster #: SCI-066	Canada
Burkhardt, Barbara	Paper #: 159	Switzerland
Burrowes, Delilah	Poster #: EDU-070	United States
Butler, Marie-Louise	Paper #: 15 (R), Paper #: 19 (R)	Ireland
Butler, Nikki	Poster #: EDU-04 (R)	United States
Cação, Pedro Henrique M.	Poster #: EDU-087	Brazil
Cahill, Anne Marie	Paper #: 107, Paper #: 109, Paper #: 113, Paper #: 180, Poster #: EDU-074, Poster #: EDU-134	United States
Callahan, Michael J.	Poster #: EDU-041	United States
Calvo-Garcia, Maria A.	Paper #: 156	United States
Campbell, Brendan	Poster #: CR-046	United States
Canning, Douglas	Paper #: 054	United States
Cantin, Marie-Andrée	Poster #: CR-069	Canada
Cardoso, Mariana R.	Poster #: EDU-087	Brazil
Carl, Rebecca	Poster #: SCI-062	United States
Carman, Nicholas	Paper #: 002	Canada
Carmichael, James	Paper #: 049	United Kingdom
Carmona, Daniela	Poster #: CR-017	Argentina
Caro Dominguez, Pablo	Paper #: 017, Paper #: 097, Poster #: SCI-040	Canada
Carr, Preston	Paper #: 174	United States
Carreno, Joan Carles	Poster #: SCI-020	Spain
Carson, Robert H.	Paper #: 051	United States
Carstens, Billie	Paper #: 014	United States
Cartagena, Claudia	Paper #: 076, Poster #: SCI-035	United States
Caruso, Paul	Paper #: 074	United States
Casalis, Claudia	Poster #: SCI-070	Argentina
Casamayor, Alvina E.	Poster #: EDU-08 (R), Poster #: EDU-13 (R)	Peru
Cass, Darrell	Paper #: 098	United States
Cassady, Christopher	Paper #: 040, Paper #: 098, Paper #: 099, Paper #: 114	United States
Cassese, John A.	Poster #: EDU-054	United States
Cassia, Guilherme	Paper #: 157	Canada
Castellano, I	Paper #: 033, Poster #: EDU-009	United Kingdom
Castellote, Amparo	Poster #: SCI-020	Spain
Castro, Denise A.	Paper #: 131, Poster #: CR-045	Canada
Catania, Diego	Paper #: 09 (R)	Italy
Catelan, Marcia W.	Poster #: EDU-087	Brazil
Cermeño, Claudia	Poster #: EDU-029	Argentina

Chacko, Anith	Paper #: 069, Paper #: 090	United Kingdom
Chandra, Tushar	Poster #: EDU-046	United States
Chang, De Hua	Paper #: 144	Germany
Chapieski, Mary L.	Paper #: 091, Paper #: 092	United States
Chapman, Teresa	Paper #: 016	United States
Chauvin, Nancy	Paper #: 177, Paper #: 180, Poster #: SCI-046	United States
Chavhan, Govind	Paper #: 013, Paper #: 017, Poster #: CR-065, Poster #: SCI-043, Poster #: SCI-044	Canada
Chawla, Soni C.	Poster #: CR-064, Poster #: EDU-124	United States
Cheasty, Emma	Poster #: EDU-005	United Kingdom
Chen, Alan M.	Poster #: CR-035	United States
Cheng, Joseph Y.	Paper #: 162, Poster #: SCI-080	United States
Chennapragada, S Murthy	Paper #: 117	Australia
Cheon, Jung-Eun	Poster #: SCI-013, Poster #: SCI-023	Korea (the Republic of)
Cherian, Shirley S.	Paper #: 056	United States
Chern, Joshua S.	Poster #: EDU-095, Poster #: EDU-098, Poster #: EDU-110	United States
Chernyak, Victoria	Paper #: 028	United States
Cheung, Kenneth K.	Paper #: 042, Poster #: SCI-006	Hong Kong
Chia, Jonathan	Paper #: 148, Paper #: 155, Paper #: 16 (R)	United States
Chidambaram, Viswanath Anand	Poster #: CR-015	Singapore
Chikwava, Kudakwashe	Paper #: 045	United States
Chippington, Sam	Poster #: EDU-011	United Kingdom
Cho, Hyun-Hae	Poster #: SCI-005, Poster #: SCI-027	Korea (the Republic of)
Cho, Hyun Suk	Poster #: SCI-013, Poster #: SCI-023	Korea (the Republic of)
Choi, Young Hun	Poster #: SCI-013, Poster #: SCI-023	Korea (the Republic of)
Choi, Young-Youn	Poster #: CR-009, Poster #: CR-010, Poster #: CR-011	Korea (the Republic of)
Chopra, Mark	Poster #: CR-012, Poster #: CR-013, Poster #: CR-023	United Kingdom
Choudhary, Arabinda K.	Paper #: 172, Poster #: EDU-082	United States
Choudhury, Subhasis R.		India
Chow, Jeanne S.	Paper #: 045, Paper #: 050, Poster #: EDU-041, Poster #: EDU-055, Poster #: EDU-073, Poster #: EDU-122	United States
Chu, Zili D.	Paper #: 036, Paper #: 091, Paper #: 092	United States
Chua, Kimberly	Paper #: 056	United States
Chun, Jeannie Y.	Poster #: CR-043	United States
Chung, Taylor	Paper #: 120	United States
Church, Peter	Paper #: 002	Canada
Cirillo, Marco	Poster #: CR-001, Poster #: CR-016	Italy
Clancy, John P.	Paper #: 085	United States
Clarke, Nick	Paper #: 169	United Kingdom
Clavijo, Rebecca L.	Poster #: EDU-09 (R)	United States
Cleveland, Heather	Paper #: 183, Paper #: 184	United States
Cleveland, Zackary	Paper #: 085	United States
Close, Orrie	Poster #: EDU-097	United States
Cloutier, Guy	Paper #: 190	Canada
Coats, Brittany	Paper #: 176	United States
Cobián Machuca, Humberto	Poster #: SCI-028	Mexico
Cohen, Harris L.	Poster #: EDU-139	United States
Cohen, Ronald A.	Paper #: 120	United States
Coleman, Beverly G.	Paper #: 039, Paper #: 104	United States
Coley, Brian	Poster #: EDU-105, Poster #: EDU-132	United States
Collado, Laura	Poster #: EDU-12 (R)	Argentina
Colledge, Jonathan	Poster #: EDU-005	United Kingdom
Colleran, Gabrielle C.	Poster #: CR-056, Poster #: EDU-041, Poster #: EDU-122	United States
Collins, Heather	Paper #: 005	United States
Coma, Ana	Poster #: SCI-020	Spain
Connolly, Bairbre L.	Paper #: 107, Paper #: 111, Paper #: 112, Poster #: EDU-084	Canada
Copp, Hillary	Poster #: EDU-061	United States
Cornejo, Patricia	Paper #: 103, Paper #: 155	United States
Cornwall, Roger	Paper #: 173, Paper #: 174	United States
Costa, Dulce	Paper #: 03 (R)	Portugal
Courtier, Jesse	Paper #: 110, Poster #: EDU-035, Poster #: EDU-042, Poster #: EDU-061	United States
Cousin, Vladimir	Poster #: SCI-008	Switzerland
Couture, Alain	Paper #: 106, Poster #: EDU-015, Poster #: SCI-007, Poster #: SCI-011	France
Crido, Silvina	Poster #: CR-018, Poster #: EDU-029	Argentina
Cross, Nathan M.	Poster #: CR-057	United States

Crowder, Lauren	Paper #: 058, Paper #: 077	United States
Cruz, Andrea T.	Paper #: 126	United States
Cruz Romero, Cinthia	, Paper #: 188	United States
Cullen, Thomas M.	Paper #: 043, Paper #: 094, Poster #: EDU-048	United States
Curran, John	Paper #: 148	United States
Currie, Melissa	Paper #: 171	United States
D'Amico, Beth	Paper #: 126	United States
Daghfal, Megan M.	Poster #: CR-031	United States
Dahmoush, Hisham	Poster #: EDU-060, Poster #: SCI-046	United States
Daldrup-Link, Heike	Paper #: 019, Paper #: 187, Paper #: 189	United States
Dal Soglio, Dorothée	Paper #: 044	Canada
Dance, Logan	Paper #: 103, Poster #: EDU-069, Poster #: EDU-071, Poster #: EDU-096, Poster #: SCI-034	United States
Daneff, Monica	Poster #: SCI-070	Argentina
Daneman, Alan	Paper #: 025, Paper #: 097, Paper #: 151, Poster #: EDU-044, Poster #: EDU-109	Canada
Dao, Tuan	Poster #: EDU-096	United States
Dardanelli, Esteban	Poster #: CR-017, Poster #: EDU-029	Argentina
Darding, Maurice	Poster #: CR-007	United Kingdom
Darge, Kassa	Paper #: 009, Paper #: 045, Paper #: 051, Paper #: 053, Paper #: 054, Paper #: 129, Paper #: 133, Poster #: EDU-105, Poster #: EDU-134, Poster #: SCI-081	United States
Das, Prasnjeet	Poster #: SCI-082	United States
Dasic, Ivana	Poster #: SCI-010	Serbia
Daumer, Ilona	Poster #: CR-022, Poster #: EDU-020	Germany
Davda, Sunit	Poster #: CR-003, Poster #: EDU-003, Poster #: EDU-005, Poster #: EDU-011	United Kingdom
Davenport, Matthew	Paper #: 004	United States
David, Stephanie	Paper #: 106, Poster #: EDU-015, Poster #: SCI-007, Poster #: SCI-011	France
Davignon, Daniel	Poster #: EDU-102	United States
Davila, Jorge	Paper #: 154, Poster #: SCI-040, Poster #: SCI-064	Canada
Davis, Angela		United States
Daw, Stephen	Paper #: 023, Paper #: 024	United Kingdom
de Alarcon, Alessandro	Paper #: 032	United States
Deaver, Pamela	Paper #: 035, Paper #: 163, Paper #: 165, Poster #: CR-048	United States
Debebe, Tequam	Poster #: EDU-134	Ethiopia
Dehaye, Amanda	Poster #: EDU-105, Poster #: EDU-132, Poster #: EDU-134	United States
de Lange, Charlotte	Paper #: 026	Norway
De Lange, Charlotte	Paper #: 192	Norway
De La Puente Gregorio, Alejandro	Paper #: 018, Poster #: EDU-044, Poster #: SCI-045	Spain
De Leon, Luis	Paper #: 035, Paper #: 165	United States
Delgado, Edgar	Poster #: CR-073	Peru
Delgado, Ignacio	Poster #: SCI-024	Spain
Delgado, Jorge	Paper #: 051, Paper #: 057, Paper #: 177, Paper #: 180	United States
Demetriou, Stelios	Poster #: EDU-012	Greece
Desai, Nilesh	Poster #: SCI-068	United States
Devaraj, Sridevi	Paper #: 178	United States
Deye, Katherine P.	Poster #: SCI-077	United States
Dezateux, Carol	Paper #: 119	United Kingdom
Dibble, Elizabeth H.	Paper #: 076, Poster #: SCI-035	United States
Dickson, Paula	Poster #: CR-049, Poster #: EDU-125, Poster #: EDU-15 (R)	United States
Didier, Ryne A.	Poster #: EDU-055	United States
Diederichs, Chad	Paper #: 125, Poster #: SCI-042	Canada
Dillman, Jonathan R.	Paper #: 004, Paper #: 010, Paper #: 011, Paper #: 012, Paper #: 045, Paper #: 145, Paper #: 166	United States
DiMaria, Michael	Poster #: SCI-048, Poster #: SCI-050	United States
Dinan, David	Poster #: EDU-046	United States
DiPaola, Frank	Paper #: 166	United States
DiPietro, Michael	Paper #: 004	United States
Djuricic, Goran	Poster #: SCI-010	Serbia
Do, Patrick	Poster #: EDU-103	United States
Doa, Tuan	Paper #: 103	United States
Dobbs-Desilet, Debbie	Poster #: CR-030	United States
Dodd, Alexander	Paper #: 008	United States
Dodd, Nicholas A.	Paper #: 168, Paper #: 194	United States
Doerga, Priya	Paper #: 147	Netherlands

Donnelly, Lane F.	Paper #: 030, Paper #: 056, Paper #: 126, Paper #: 178	United States
Doria, Andrea S.	Paper #: 079, Paper #: 080, Poster #: EDU-123, Poster #: SCI-036, Poster #: SCI-044, Poster #: SCI-058, Poster #: SCI-063	Canada
Drocton, Gerald T.	Poster #: CR-030	United States
Drumsta, Douglas	Poster #: EDU-057	United States
Dubois, Josée	Paper #: 044, Paper #: 107, Paper #: 190, Poster #: CR-042	Canada
Duckworth, JoAnn	Paper #: 150	Canada
Dwek, Jerry R.	Paper #: 118	United States
Ealai, Parthasarathy	Poster #: EDU-083	India
Ecklund, Kirsten	Paper #: 123	United States
Edgar, Christopher J.	Paper #: 065, Paper #: 067, Paper #: 129	United States
Edwards, Andrew	Paper #: 041	Australia
Edwards, Emily A.	Poster #: EDU-061	United States
Ehman, Richard L.	Paper #: 010	United States
Ehrmann, Daniel	Poster #: SCI-048, Poster #: SCI-050	United States
Eichenberger, André C.	Paper #: 052	Switzerland
Eismann, Emily	Paper #: 173	United States
El-Hawary, R.	Poster #: EDU-030	Canada
El Jalbout, Ramy	Paper #: 190	Canada
Ellsworth, Erik	Poster #: EDU-090	United States
Eng, Kevin A.	Paper #: 079	Canada
Engesæter, Ingvild	Paper #: 119	Norway
Engesæter, Lars	Paper #: 119	Norway
Enriquez, Goya	Poster #: SCI-020	Spain
Epelman, Monica	Poster #: EDU-046, Poster #: EDU-059, Poster #: EDU-082	United States
Erdfarb, Amichai	Paper #: 066	United States
Erripa, Jose	Poster #: CR-017	Argentina
Esteves, Bruno	Paper #: 06 (R)	Portugal
Estrin, Yvonne	Poster #: EDU-118, Poster #: EDU-119	United States
Evans, Catherine	Poster #: EDU-106	United States
Ezon, David	Paper #: 194	United States
Fadell, Michael	Poster #: SCI-057	United States
Faerber, Eric	Poster #: EDU-095, Poster #: EDU-098, Poster #: EDU-110	United States
Faingold, Ricardo	Paper #: 157, Poster #: SCI-059, Poster #: SCI-066	Canada
Farley, Sarah A.	Paper #: 132	United States
Farmakis, Shannon	Poster #: EDU-037	United States
Farrokhyar, Forough	Paper #: 150	Canada
Fasmer, Kristine E.	Poster #: SCI-02 (R)	Norway
Faure, Jean-Michel	Paper #: 106	France
Fay, Jill	Paper #: 028	United States
Fazeli, Soudabeh	Paper #: 004	United States
Fefferman, Nancy R.	Paper #: 046	United States
Feinstein, Kate A.	Paper #: 073, Poster #: EDU-075	United States
Feldman, Henry	Paper #: 123	United States
Felice, Marc A.	Paper #: 065, Paper #: 067	United States
Fenton, Laura Z.	Paper #: 014, Paper #: 152	United States
Ferguson, Polly	Poster #: EDU-136	United States
Fernandes, Patrícia	Paper #: 03 (R)	Portugal
Feygin, Tamara	Paper #: 104	United States
Figueroa, Hugo	Poster #: CR-076	Chile
Flake, Alan W.	Paper #: 039	United States
Fleck, Robert J.	Poster #: SCI-082	United States
Fleming, Adam J.	Paper #: 150, Poster #: CR-059	Canada
Foley, Shane J.	Paper #: 01 (R), Paper #: 09 (R), Paper #: 11 (R), Paper #: 12 (R)	Ireland
Foley-Friel, Kelly	Paper #: 15 (R)	Ireland
Fonseca, Brian	Poster #: SCI-048, Poster #: SCI-050	United States
Fonseca, Josélia N.	Poster #: CR-045	Brazil
Fontalvo, Lucia	Poster #: EDU-062	Canada
Ford, Eileen	Paper #: 129	United States
Forgues, Dominique	Paper #: 106	France
Fortner, Gail	Paper #: 006	United States
Francavilla, Michael	Paper #: 060, Paper #: 065, Poster #: EDU-137	United States
Frank, Matt	Poster #: CR-07 (R)	United States
Frappier, Jean-Yves	Poster #: CR-060	Canada
Frenckner, Björn	Paper #: 193	Sweden

Friedland-Little, Joshua	Paper #: 166	United States
Fuentealba, Isabel	Poster #: SCI-056	Chile
Fujita, Kenji P.	Poster #: SCI-039	United States
Funaro, Kimberly	Poster #: EDU-033	United States
Furtula, Dubravka	Poster #: SCI-010	Serbia
Gadde, Judith	Poster #: EDU-040	United States
Galambos, Csaba	Paper #: 087	United States
Gale, Heather I.	Poster #: EDU-056	United States
Gandhi, Trupti	Paper #: 060, Poster #: EDU-137	United States
Gao, Haijun	Paper #: 101, Paper #: 102	United States
Gao, Wei	Paper #: 034, Paper #: 038, Paper #: 084, Poster #: SCI-086	China
Garcia, Jacquelyn R.	Paper #: 040	United States
Garcia, Sebastian	Poster #: EDU-070	United States
García Gallegos, Víctor M.	Poster #: SCI-028	Mexico
Garcia - Peña, Pilar	Poster #: SCI-020	Spain
Garel, Laurent	Paper #: 044	Canada
Garg, Vasant	Poster #: CR-040	United States
Garza, Michelle	Poster #: EDU-02 (R)	United States
Gates, Erica L.	Paper #: 02 (R)	United States
Gazzaz, Tamadhir	Paper #: 138	Canada
Gebarski, Kathleen S.	Poster #: EDU-064, Poster #: EDU-065	United States
Gebarski, Stephen S.	Poster #: EDU-064, Poster #: EDU-065	United States
Gee, Michael S.	, Paper #: 064, Paper #: 070, Paper #: 071, Paper #: 074, Paper #: 083, Paper #: 188, Poster #: EDU-056	United States
Geiger, Julia	Paper #: 159, Paper #: 160, Paper #: 161	Switzerland
Gelfand, Michael J.	Poster #: EDU-140	United States
Geoffray, Anne	Paper #: 10 (R)	France
Gerard, Perry	Poster #: CR-055, Poster #: CR-061, Poster #: EDU-126	United States
Ghaghada, Ketan B.	Paper #: 101, Paper #: 102, Paper #: 142	United States
Ghahremani, Shahnaz	Poster #: CR-079	United States
Ghali, Rafik	Poster #: CR-042	Canada
Giannoni, Carla	Paper #: 072	United States
Gill, Kara	Poster #: CR-068	United States
Gilmartin, Breege	Poster #: CR-028	Australia
Gimenez, Carlos R.		United States
Glaser, Kevin J.	Paper #: 010	United States
Glusic, Mojca	Poster #: CR-006	Slovenia
Gnannt, Ralph	Paper #: 111, Paper #: 112, Poster #: EDU-084	Canada
Gnerre, Jeffrey M.	Poster #: CR-053	United States
Goebel, Juliane	Paper #: 015	Germany
Goel, Ishan		India
Goergen, Stacy	Paper #: 041	Australia
Goldberg, Caren	Paper #: 166	United States
Golden, Eleza T.	Poster #: CR-039, Poster #: CR-049, Poster #: EDU-045, Poster #: SCI-068	United States
Goldwasser, Bernard	Poster #: EDU-032	United States
Golriz, Farahnaz	Paper #: 030, Paper #: 037, Paper #: 072, Paper #: 091, Paper #: 092, Paper #: 126, Paper #: 178	United States
Gomes, William	Poster #: EDU-052	United States
Goncalves, Luís F.	Poster #: SCI-079	United States
Gonseski, Vivian C.	Poster #: EDU-10 (R)	Argentina
Goode, Chris	Paper #: 006	United States
Gordon, Catherine	Paper #: 123	United States
Gordon Murkes, Lena	Paper #: 193	Sweden
Gorelik, Natalia	Poster #: SCI-059, Poster #: SCI-066	Canada
Gorfu, Yocabel	Paper #: 133, Poster #: EDU-134	Ethiopia
Gottfried, Kristina	Paper #: 160, Paper #: 161	Germany
Gould, Sharon	Poster #: EDU-059, Poster #: EDU-082	United States
Goyal, Rakesh	Poster #: CR-063	United States
Granata, Claudio	Paper #: 026	Italy
Grangl, Gernot	Poster #: SCI-019	Austria
Grant, Frederick D.	Paper #: 050, Poster #: EDU-060	United States
Grant, Ronald	Paper #: 022	Canada
Grattan-Smith, Damien	Paper #: 116	United States
Gratzinger, Dita	Paper #: 187	United States

Gray, Ellen	Poster #: EDU-06 (R)	United States
Green, Jared	Poster #: CR-047	United States
Greer, Mary-Louise C.	Paper #: 002, Paper #: 018, Paper #: 022, Poster #: EDU-047, Poster #: EDU-123, Poster #: SCI-045	Canada
Greffe, Brian	Paper #: 014	United States
Grehan, Jennifer M.	Paper #: 19 (R)	Ireland
Griffiths, Anne	Paper #: 002	Canada
Grimard, Guy	Paper #: 175	Canada
Grissom, Leslie	Poster #: CR-050, Poster #: SCI-061	United States
Grosse-Wortmann, Lars	Poster #: EDU-047	Canada
Gruber, Laura	Paper #: 18 (R)	United States
Grynspan, David	Poster #: SCI-040	Canada
Guesmi, Myriam	Paper #: 10 (R), Poster #: CR-01 (R), Poster #: CR-02 (R)	France
Guillerman, R. P.	Paper #: 030, Paper #: 072	United States
Gullberg Lidegran, Marika	Paper #: 193	Sweden
Gundersen, Trude	Paper #: 119	Norway
Gupta, Abha A.	Poster #: CR-065	Canada
Gupta, Achint	Poster #: CR-014, Poster #: CR-015	Singapore
Gupta, Priya	Paper #: 078	Canada
Gupta, Saurabh	Poster #: EDU-139	United States
Gupton, Theodore B.	Paper #: 180	United States
Gwal, Kriti	Poster #: EDU-086	United States
Gyebnar, Gyula	Poster #: SCI-017	Hungary
Haacke, Ewart	Poster #: SCI-051	United States
Hackenbroch, Matthias	Paper #: 144	Germany
Hagar, Ward	Paper #: 120	United States
Haig, Ian	Poster #: CR-008	United Kingdom
Hakim, Ibrahim	Poster #: EDU-085	United States
Halabi, Safwan	Poster #: EDU-048, Poster #: EDU-078, Poster #: EDU-085, Poster #: SCI-049	United States
Halula, Sarah	Poster #: SCI-082	United States
Hamouda, Ehab S.	Poster #: CR-014, Poster #: CR-015	Singapore
Han, Byoung Hee	Paper #: 134	Korea (the Republic of)
Hankins, Jane S.	Paper #: 006	United States
Hanquinet, Sylviane	Poster #: SCI-004, Poster #: SCI-008	Switzerland
Hara, Hiroko	Poster #: SCI-012	Japan
Harding, Jaclyn	Poster #: EDU-14 (R)	United States
Hareendranathan, Abhilash	Paper #: 125, Poster #: SCI-042	Canada
Harned, Roger K.	Paper #: 107	United States
Haroyan, Harutyun	Poster #: SCI-081	United States
Harris, Katherine	Poster #: CR-07 (R)	United States
Hart, Catherine	Paper #: 032	United States
Hartung, Erum A.	Paper #: 009	United States
Harty, Mary	Poster #: CR-050, Poster #: SCI-061	United States
Harvey, Carly	Poster #: CR-074	United States
Hassan, Sonia	Poster #: SCI-051	United States
Hawkins, Doug	Poster #: CR-057	United States
Haws, M Edward	Poster #: SCI-067	United States
Hayatghaibi, Shireen	Paper #: 035, Paper #: 114, Paper #: 165, Paper #: 183, Paper #: 184	United States
Hazard, Florette K.	Paper #: 187	United States
Head, Matthew	Paper #: 14 (R)	Canada
Healey, Erin B.	Paper #: 172	United States
Heath, Alana	Paper #: 125, Poster #: SCI-042	Canada
Hecht, Elizabeth	Poster #: EDU-066	United States
Hedrick, Holly H.	Paper #: 039	United States
Heider, Amer	Paper #: 045	United States
Heinle, Jeffrey	Paper #: 194	United States
Heitzmann, Mark D.	Poster #: SCI-077	United States
Hemke, Robert	Paper #: 141	Netherlands
Henault, Kathryn	Poster #: CR-046, Poster #: CR-054	United States
Henderson, Melanie	Paper #: 190	Canada
Hendi, Aditi	Poster #: CR-050, Poster #: SCI-061	United States
Heo, Moonseong	Paper #: 031	United States
Herliczek, Thaddeus W.	Paper #: 076, Poster #: EDU-054, Poster #: SCI-035	United States

Herlihy, Therese	Paper #: 13 (R)	Ireland
Hernandez, Jose A.	Paper #: 108, Paper #: 114, Paper #: 181	United States
Hernandez-Andrade, Edgar	Poster #: SCI-051	United States
Hess, Erika	Poster #: EDU-049	United States
Hicks, John	Paper #: 030, Paper #: 045	United States
Higgins, Rick	Poster #: EDU-053	Canada
Highmore, Kerri	Poster #: EDU-050, Poster #: SCI-064	Canada
Hillenbrand, Claudia M.	Paper #: 006	United States
Hintz, Susan	Poster #: SCI-049	United States
Hirsig, Leslie	Poster #: EDU-115	United States
Hirtler, Daniel	Paper #: 160, Paper #: 161	Germany
Hitt, Dave	Paper #: 120	United States
Hoffman, Thomas	Poster #: EDU-052	United States
Ho-Fung, Victor	Paper #: 057	United States
Holdsworth, Samantha	Paper #: 019, Paper #: 187, Paper #: 189	United States
Holley, Dawn	Paper #: 189	United States
Holmes, Nathan	Poster #: SCI-069	United States
Homan, Matjaz	Poster #: CR-006	Slovenia
Hopkins, Katharine	Poster #: EDU-076, Poster #: EDU-100, Poster #: EDU-101	United States
Hopp, Einar	Paper #: 192	Norway
Horvath, Eleonora	Poster #: SCI-088	Chile
Hosmer, Andrew	Paper #: 055	United States
Hossain, Shaolie S.	Paper #: 093	United States
Hu, Eric	Poster #: SCI-053	United States
Hu, Houchun H.	Paper #: 148, Paper #: 155, Paper #: 16 (R), Poster #: SCI-032, Poster #: SCI-047	United States
Hughes, Nicole	Poster #: EDU-042	United States
Hull, Nathan	Poster #: EDU-039	United States
Humphries, Paul D.	Paper #: 023, Paper #: 024	United Kingdom
Huo, Ai hua	Poster #: SCI-058	China
Huppi, Petra	Poster #: SCI-004	Switzerland
Hurteau-Miller, Julie	Poster #: EDU-062, Poster #: SCI-040	Canada
Hussein, Akif	Poster #: CR-003	United Kingdom
Hutchinson, J. C.	Paper #: 105, Paper #: 170, Poster #: CR-007, Poster #: CR-008, Poster #: CR-012, Poster #: CR-013	United Kingdom
Hwang, Misun	Poster #: EDU-088	United States
Hwang, Sook Min	Paper #: 027, Poster #: SCI-016	Korea (the Republic of)
Iida, Makoto	Poster #: EDU-079	Japan
IP, Janice J.	Paper #: 042	Hong Kong
Ishii, Masaya	Poster #: SCI-012	Japan
Iskander, Paul J.	Poster #: CR-079	United States
Islam, Omar	Paper #: 131	Canada
Iv, Michael	Paper #: 094	United States
Iyer, Ramesh	Paper #: 132	United States
Jackson, Dana R.	Poster #: EDU-059, Poster #: EDU-082	United States
Jacot, Jeffrey	Paper #: 036	United States
Jadhav, Siddharth P.	Paper #: 037, Paper #: 122, Paper #: 124, Paper #: 163, Paper #: 164	United States
Jaffer, Ounali	Poster #: EDU-003	United Kingdom
Jagger, James	Paper #: 167	United States
Jain, Shilpa	Poster #: SCI-079	United States
Jain, Shreyan	Poster #: SCI-080	United States
Jaju, Alok	Poster #: CR-047, Poster #: SCI-031	United States
James, Charles	Paper #: 107	United States
Jamieson, Lucy	Paper #: 125	Canada
Jamoulle, Olivier	Poster #: CR-060	Canada
Jaramillo, Diego	Paper #: 043, Paper #: 054, Paper #: 177, Poster #: EDU-134	United States
Jaremko, Jacob L.	Paper #: 125, Poster #: SCI-042	Canada
Jariwala, Mehul	Poster #: EDU-050	Canada
Jarrin, Jose	Paper #: 151, Poster #: SCI-058	Canada
Jella, Pavan	Poster #: SCI-051	United States
Jen, Aaron	Poster #: CR-079	United States
Jeon, Tae Yeon	Paper #: 027, Poster #: SCI-016	Korea (the Republic of)
Jeong, Woo Kyoung	Paper #: 027	Korea (the Republic of)
Jimenez-Ocasio, Jason	Poster #: CR-053	United States
Johnson, Ann	Paper #: 039, Paper #: 051	United States

Johnson, Craig	Poster #: EDU-046	United States
Johnson, Kevin	Paper #: 159	United States
Jones, Richard	Paper #: 116	United States
Joshi, Madalsa	Paper #: 011, Paper #: 012	United States
Kabrera, Maria	Poster #: SCI-051	United States
Kadom, Nadja	Poster #: CR-039, Poster #: EDU-057	United States
Kaloianova, Maria	Poster #: CR-002	South Africa
Kalra, Mannudeep	Paper #: 083	United States
Kalyoncu Ucar, Ayse	Poster #: CR-026, Poster #: CR-027, Poster #: SCI-021	Turkey
Kammen, Bamidele F.	Paper #: 120	United States
Kan, J. H.	Paper #: 108, Paper #: 122, Paper #: 124	United States
Kane, Lauren	Paper #: 035, Paper #: 165	United States
Kane, Timothy D.	Poster #: EDU-142	United States
Kanev, Paul	Poster #: CR-054	United States
Kao, Simon	Poster #: EDU-136	United States
Kaplan, Julio S.	Poster #: EDU-10 (R)	Argentina
Kaplan, Summer	Paper #: 065, Paper #: 067, Paper #: 129	United States
Kapoor, Cassandra	Paper #: 14 (R)	Canada
Kapsin, Kathleen	Poster #: EDU-049	United States
Kar, Erica	Poster #: SCI-029	United States
Karakas, Sabiha P	Paper #: 120	United States
Karantanas, Apostolos	Poster #: EDU-012	Greece
Karastanovic, Merima	Poster #: EDU-02 (R)	United States
Karl, Barbara A.	Poster #: EDU-06 (R), Poster #: EDU-07 (R)	United States
Karmur, Brij	Paper #: 150, Poster #: CR-059	Canada
Katekaru Tokeshi, Doris A.	Poster #: CR-06 (R), Poster #: CR-073, Poster #: EDU-08 (R), Poster #: EDU-13 (R)	Peru
Katoh, Marcus	Poster #: CR-022, Poster #: EDU-020	Germany
Katsuda, Toshizo	Poster #: SCI-01 (R)	Japan
Katzilakis, Nikos	Poster #: EDU-012	Greece
Kaufman, Claire	Paper #: 107	United States
Kawooya, Michael G.	Poster #: SCI-087	Uganda
Kaye, Robin	Paper #: 107, Paper #: 115, Paper #: 182, Poster #: CR-071	United States
Kazmi, Faaiza	Poster #: EDU-095, Poster #: EDU-098, Poster #: EDU-099, Poster #: EDU-110	United States
Kazmi, Parvez	Paper #: 060, Poster #: EDU-137	United States
Kebede, Tesfaye	Paper #: 133, Poster #: EDU-134	Ethiopia
Kecskemethy, Heidi	Paper #: 172	United States
Keehn, Brian P.	Paper #: 103, Poster #: EDU-069, Poster #: EDU-071, Poster #: SCI-034, Poster #: SCI-047	United States
Kellenberger, Christian J.	Paper #: 136, Paper #: 159	Switzerland
Keller, Marc S.	Paper #: 109, Paper #: 113, Poster #: EDU-074, Poster #: EDU-134	United States
Kelley, Simon	Paper #: 100	Canada
Kennedy, Tabassum	Poster #: EDU-040	United States
Keo, Sokdina B.	Paper #: 123	United States
Kereliuk, Marylin	Poster #: SCI-054	Canada
Kerwood, Joanne	Paper #: 054	United States
Keupp, Jochen	Paper #: 148	Germany
Khan, Naeem	Poster #: EDU-127	Canada
Khandelwal, Niranjan	Paper #: 086	India
Khanna, Geetika	Paper #: 007, Poster #: EDU-037	United States
Khrichenko, Dmitry	Paper #: 051, Paper #: 053, Poster #: SCI-081	United States
Khumalo, Zonah	Poster #: SCI-066	Canada
Kiho, Liina	Poster #: CR-012, Poster #: CR-013	United Kingdom
Kim, Hyun Gi	Poster #: SCI-022	Korea (the Republic of)
Kim, In-One	Poster #: SCI-013, Poster #: SCI-023	Korea (the Republic of)
Kim, Jane	Poster #: CR-043, Poster #: EDU-035	United States
Kim, Ji Hye	Paper #: 027, Poster #: SCI-016	Korea (the Republic of)
Kim, Myung-Joon	Poster #: SCI-003	Korea (the Republic of)
Kim, Tammy	Paper #: 068	United States
Kim, Wendy	Poster #: CR-043, Poster #: EDU-035	United States
Kim, Woo Sun	Poster #: SCI-013, Poster #: SCI-023	Korea (the Republic of)
King, Lawrence	Poster #: EDU-009	United Kingdom
King, Nathan	Paper #: 057	United States
King, Sebastian	Paper #: 002	Canada

Kinner, Sonja	Paper #: 015	Germany
Kirihetti Liyanage, Neelika S.	Poster #: EDU-001	Australia
Kiss, Mate	Poster #: SCI-017	Hungary
Kiyetta, Alade H.	Paper #: 126	United States
Kleinman, Paul K.	Paper #: 061, Paper #: 176	United States
Kline-Fath, Beth M.	Paper #: 156, Poster #: SCI-067	United States
Kljucevsek, Tomaz	Poster #: CR-006	Slovenia
Ko, Lee-yuen	Paper #: 042	Hong Kong
Ko, Sun Young	Paper #: 134	Korea (the Republic of)
Kobayashi, Masao	Poster #: EDU-079	Japan
Kogler, Kristina	Poster #: SCI-018	Austria
Kohli, Rohit	Paper #: 011, Paper #: 012	United States
Kolossvary, Marton	Poster #: SCI-017	Hungary
Koning, Jeffrey L.	Paper #: 118	United States
Koroll, Alex G.	Paper #: 056	United States
Koujok, Khaldoun	Poster #: EDU-141	Canada
Kozak, Lajos Rudolf	Poster #: SCI-017	Hungary
Krafft, Axel J.	Paper #: 006	United States
Krishnamurthy, Ganesh	Paper #: 109, Paper #: 113, Poster #: EDU-074	United States
Krishnamurthy, Rajesh	Paper #: 035, Paper #: 036, Paper #: 037, Paper #: 163, Paper #: 164, Paper #: 165, Paper #: 168, Paper #: 178, Paper #: 191, Paper #: 194	United States
Krishnamurthy, Ramkumar	Paper #: 036, Paper #: 168, Paper #: 191, Poster #: SCI-084	United States
Krishnan, Anant	Poster #: CR-003	United Kingdom
Krishnan, Ananth	Poster #: SCI-079	United States
Krishnarao, Priya M.	Poster #: EDU-103	United States
Kriss, Stevan	Paper #: 171	United States
Kriss, Vesna M.	Paper #: 171	United States
Kritikos, Nikolaos	Poster #: EDU-025, Poster #: EDU-026	Greece
Kruk, Peter G.	Paper #: 118	United States
Kubendran, Shobana	Poster #: CR-030	United States
Kucera, Jennifer N.	Poster #: CR-033, Poster #: CR-035, Poster #: EDU-033, Poster #: EDU-038	United States
Kukreja, Kamlesh	Paper #: 114, Paper #: 181, Paper #: 183, Paper #: 184	United States
Kumalo, Zonah	Poster #: SCI-059	Canada
Kumbla, Surekha	Poster #: EDU-001	Australia
Kume, Shinji	Poster #: EDU-079	Japan
Kurian, Jessica	Poster #: EDU-031, Poster #: EDU-036, Poster #: EDU-052	United States
Kurugoglu, Sebuh	Poster #: CR-026, Poster #: CR-027, Poster #: SCI-021	Turkey
Kwatra, Neha	Poster #: EDU-055, Poster #: EDU-060	United States
Kwee, Thomas C.	Paper #: 026	Netherlands
Kwon, Jeannie	Poster #: SCI-065	United States
Kyaw Tun, Jimmy	Poster #: EDU-003	United Kingdom
LaBella, Cynthia	Poster #: SCI-062	United States
Laborie, Lene B.	Paper #: 119	Norway
Lacroix, Caroline	Poster #: CR-065, Poster #: EDU-107, Poster #: SCI-043, Poster #: SCI-044	Canada
Lago, Paula	Paper #: 05 (R)	Portugal
Lai, Kuan-Chi	Poster #: CR-064	United States
Lai, Lillian	Paper #: 019, Paper #: 162, Paper #: 189, Poster #: EDU-051, Poster #: EDU-078	United States
Lai, Peng	Paper #: 121	United States
Laifer-Narin, Sherelle L.	Paper #: 130, Poster #: EDU-066	United States
Lakatos, Andrea	Poster #: SCI-017	Hungary
Lala, Shailee	Paper #: 046	United States
Lall, Neil	Poster #: CR-075	United States
Lam, Christopher Z.	Paper #: 138, Paper #: 185	Canada
Lam, Wendy W.	Paper #: 042, Poster #: SCI-006	Hong Kong
Lang, Isla	Paper #: 128	United Kingdom
Langan, Dean	Poster #: SCI-001	United Kingdom
Langer, Jacob	Paper #: 002	Canada
Langford, Stacey	Poster #: EDU-049	United States
Langston, Claire	Paper #: 098	United States
Laor, Tal	Paper #: 173, Paper #: 174	United States
Lapierre, Chantale	Paper #: 044, Paper #: 190	Canada
Larsen, Stig	Paper #: 192	Norway

Larson, David	Paper #: 189	United States
Last, Jason	Paper #: 19 (R)	Ireland
Laszik, Zoltan	Paper #: 110	United States
Lau, Damian S.	Poster #: SCI-006	Hong Kong
Laurindo Mariano De Oliviera, Gabrielle	Poster #: SCI-028	Mexico
Law, Martin W.	Paper #: 042	Hong Kong
Laxer, Ronald	Poster #: EDU-050	Canada
Laya, Bernard	Poster #: EDU-105	Philippines
Lazarte, Claudia I.	Paper #: 088, Poster #: CR-04 (R), Poster #: EDU-08 (R), Poster #: EDU-13 (R)	Peru
Lazarus, Matthew S.	Paper #: 066	United States
Lazoura, O	Paper #: 033	United Kingdom
Le, Judy	Poster #: EDU-05 (R)	United States
Leake, David	Poster #: CR-067	United States
Lebowitz, Robert L.	Poster #: EDU-055	United States
LeCompte, Leslie	Paper #: 053, Poster #: CR-053, Poster #: EDU-126	United States
Lee, Edward Y.	Paper #: 086, Paper #: 140, Poster #: CR-056, Poster #: EDU-056, Poster #: SCI-071	United States
Lee, Guo Rui	Poster #: CR-015	Singapore
Lee, Kwanseop	Paper #: 075	Korea (the Republic of)
Lee, Marsha M.	Paper #: 110	United States
Lee, Mi-Jung	Poster #: SCI-003	Korea (the Republic of)
Lee, Mu Sook	Poster #: SCI-003	Korea (the Republic of)
Lee, Ruri	Poster #: CR-055	United States
Lee, So Mi	Poster #: SCI-005, Poster #: SCI-027	Korea (the Republic of)
Lee, Vince	Poster #: SCI-029	United States
Lee, Wesley	Poster #: SCI-079	United States
Lee, Yeon Kyung	Paper #: 134	Korea (the Republic of)
Lee, Yvonne	Paper #: 079	Canada
Leiter, Francisca H.	Poster #: CR-076	Chile
Leloutre, Beatrice	Paper #: 10 (R), Poster #: CR-01 (R), Poster #: CR-02 (R)	France
Lenhart, Carolyn	Poster #: EDU-049	United States
Lequin, Maarten	Paper #: 147	Netherlands
Leroux, Carole	Poster #: CR-01 (R)	France
Leshikar, Holly B.	Paper #: 179	United States
Leung, Daniel H.	Paper #: 008	United States
Levin, Terry L.	Paper #: 066, Poster #: EDU-031, Poster #: EDU-063	United States
Lewis, Heidi	Poster #: CR-033, Poster #: EDU-038	United States
Lewis, Paul S.	Poster #: EDU-142	United States
Li, Xiang	Paper #: 071	United States
Li, Yi	Paper #: 110	United States
Li, Zhiqiang	Poster #: SCI-032	United States
Ligocki, Carolina	Paper #: 079	Canada
Lin, Tom	Paper #: 032	United States
Lindberg, Harald L.	Paper #: 192	Norway
Lindbichler, Franz	Poster #: SCI-014	Austria
Lindsay, Aaron	Paper #: 177	United States
Linscott, Luke	Poster #: SCI-067	United States
Lio, Elizabeth S.	Paper #: 014	United States
Lipsich, Jose	Poster #: CR-017, Poster #: CR-018, Poster #: CR-03 (R), Poster #: EDU-029, Poster #: EDU-10 (R)	Argentina
Lira, Andréa F.	Poster #: CR-045	Brazil
List, Jeb	Poster #: CR-07 (R)	United States
Liszewski, Mark	Paper #: 031, Poster #: EDU-032, Poster #: EDU-052	United States
Litt, Brendan	Paper #: 131	Canada
Little, Kevin	Paper #: 073, Paper #: 173, Poster #: EDU-075	United States
Little, Stephen	Paper #: 116	United States
Littooij, Annemieke	Paper #: 021, Paper #: 026	Netherlands
Liu, Bob	Paper #: 071	United States
Ljutikov, Anoushka	Poster #: EDU-003	United Kingdom
Lo, Ryan	Paper #: 002	Canada
Loeffler, Ralf B.	Paper #: 006	United States
Loening, Andreas	Paper #: 094	United States
Lombardi, Claudio	Paper #: 105	Italy

Long, Christopher	Poster #: SCI-081	United States
Lord, David	Paper #: 117	Australia
Lorentz, Liam	Poster #: CR-020	South Africa
Lorenzo, Armando	Paper #: 022	Canada
Lostra, Juliana	Poster #: CR-017, Poster #: EDU-10 (R)	Argentina
Loubriel, Daphne M.	Poster #: EDU-118, Poster #: EDU-119	United States
Love, Terri	Poster #: CR-032	United States
Lovell, Mark	Paper #: 014	United States
Lu, Zheng Feng	Paper #: 073, Poster #: EDU-075	United States
Luhar, Aarti P.	Poster #: SCI-069	United States
Luna-Fineman, Sandra	Paper #: 187	United States
Luo, Yu	Poster #: CR-036	United States
Lustig, Michael	Paper #: 121, Paper #: 162	United States
Lynch, Jeremy	Paper #: 158	United Kingdom
Maas, Mario	Paper #: 141	Netherlands
Mabee, Myles	Paper #: 125, Poster #: SCI-042	Canada
Machnitz, Judit	Poster #: EDU-099	United States
MacKenzie, John D.	Paper #: 110, Poster #: EDU-042, Poster #: EDU-061	United States
Maddalozzo, John P.	Poster #: SCI-031	United States
Madhi, Shabier	Paper #: 082, Paper #: 135, Paper #: 137	South Africa
Magganas, George	Poster #: EDU-021, Poster #: EDU-025	Greece
Magill, Dennise	Paper #: 065, Paper #: 067	United States
Maguire, Sabine	Poster #: SCI-057	United Kingdom
Mahboubi, Soroosh	Poster #: EDU-134	United States
Maher, Marion	Paper #: 13 (R)	Ireland
Mahomed, Nasreen	Paper #: 082, Paper #: 135, Paper #: 137, Poster #: EDU-010, Poster #: EDU-022	South Africa
Maianski, Irit	Poster #: EDU-127	Canada
Maintz, David	Paper #: 144	Germany
Majmudar, Anand	Poster #: EDU-130, Poster #: EDU-138	United States
Makki, Malek	Paper #: 159	Switzerland
Mali Brajovic, Senja	Poster #: CR-006	Slovenia
Malik, Archana	Poster #: EDU-095, Poster #: EDU-098, Poster #: EDU-099, Poster #: EDU-110	United States
Malkin, David	Paper #: 018, Poster #: EDU-123, Poster #: SCI-045	Canada
Mallon, Mea	Poster #: EDU-095, Poster #: EDU-098, Poster #: EDU-099, Poster #: EDU-110	United States
Maloney, John A.	Paper #: 152	United States
Man, Carina	Poster #: SCI-036	Canada
Manopoulou, Evangelia	Poster #: EDU-021, Poster #: EDU-025, Poster #: EDU-026	Greece
Manson, David E.	Poster #: EDU-107	Canada
Maravilla, Kenneth	Poster #: EDU-129, Poster #: EDU-131	United States
Marin, Jennifer	Poster #: SCI-037	United States
Marina, Neyssa	Paper #: 019, Paper #: 187, Paper #: 189	United States
Marsala, Andrew	Paper #: 181	United States
Marshall, Kelley	Poster #: EDU-045	United States
Marterer, Robert	Paper #: 048, Poster #: SCI-014, Poster #: SCI-019	Austria
Martin, James	Paper #: 081	United States
Martinez-Agosto, Julian A.	Poster #: CR-064	United States
Martinez-Rios, Claudia	Paper #: 018, Paper #: 022, Paper #: 025, Paper #: 080, Poster #: EDU-044, Poster #: EDU-050, Poster #: EDU-091, Poster #: EDU-109, Poster #: EDU-123, Poster #: SCI-045	Canada
Masand, Prakash M.	Paper #: 037, Paper #: 163, Paper #: 164, Paper #: 191, Poster #: CR-048	United States
Massé-Bouillé, Guy-Anne	Poster #: CR-060	Canada
Masterson, Liz	Paper #: 09 (R), Paper #: 19 (R)	Ireland
Mathijssen, Irene	Paper #: 147	Netherlands
Mathison, David	Paper #: 081	United States
Matos Rojas, Irma A.	Poster #: CR-04 (R), Poster #: CR-06 (R), Poster #: EDU-08 (R), Poster #: EDU-13 (R)	Peru
Matthews, Andrew	Poster #: CR-037	United States
Matthews, Kate	Paper #: 07 (R)	Ireland
Mauchley, David	Paper #: 167	United States
May, Megan M.	Paper #: 122	United States
Mazzariol, Fernanda	Poster #: EDU-031	United States

McAlister, William H.	Poster #: SCI-039	United States
McAllister, Aaron	Poster #: CR-075	United States
McCarville, Beth	Paper #: 006	United States
Mc Claren, Clare	Paper #: 09 (R)	United Kingdom
McDavid, Lolita	Poster #: CR-040	United States
McDonald, Kirsteen	Poster #: EDU-005, Poster #: EDU-011, Poster #: EDU-028	United Kingdom
McEniery, Jane	Poster #: EDU-027	Australia
McGeough, Sara	Paper #: 19 (R)	Ireland
McGill, Maria	Paper #: 127	United Kingdom
McGovern, Jonathan	Poster #: CR-063	United States
McGuire, Veronica	Paper #: 08 (R)	Ireland
McKay, Scott	Paper #: 122	United States
Mckenzie, Emmett Dean	Paper #: 194	United States
McKinney, Jennifer	Paper #: 080	Canada
McLin, Valérie	Poster #: SCI-008	Switzerland
McMann, Leah	Poster #: EDU-092	United States
McNamara, Erin	Paper #: 045	United States
McNerney, Kevin O.	Poster #: EDU-126, Poster #: EDU-145	United States
McNulty, Jonathan P.	Paper #: 08 (R), Paper #: 17 (R)	Ireland
Medovic, Rasa	Poster #: SCI-010	Serbia
Megue Huamani, Marlin V.	Poster #: EDU-08 (R)	Peru
Mehollin-Ray, Amy R.	Paper #: 040, Paper #: 098, Paper #: 099	United States
Mehta, Nimisha	Poster #: EDU-111	United States
Meldrum, Jaren T.	Poster #: EDU-104	United States
Melendez, Jamie	Paper #: 135	Netherlands
Meleti, Christina	Poster #: EDU-021, Poster #: EDU-026	Greece
Ménard, Anne-Laure	Paper #: 175	Canada
Menezes, Leon	Paper #: 024	United Kingdom
Merlini, Laura	Poster #: SCI-004, Poster #: SCI-008	Switzerland
Mery, Carlos	Paper #: 164	United States
Metz, Terrence	Poster #: EDU-094	United States
Meyer, Anna	Poster #: EDU-042	United States
Meyers, Mariana L.	Paper #: 040	United States
Mifsud, Will	Paper #: 105	United Kingdom
Milewicz, Dianna	Paper #: 093	United States
Milks, Kathryn S.	Poster #: EDU-112	United States
Milla, Sarah S.	Paper #: 068, Poster #: SCI-068	United States
Miller, Angie	Poster #: SCI-057	United States
Miller, Elka	Paper #: 14 (R), Paper #: 151, Paper #: 154, Poster #: EDU-053, Poster #: EDU-062, Poster #: SCI-040, Poster #: SCI-064	Canada
Miller, Jeffrey	Paper #: 16 (R), Poster #: SCI-032	United States
Miller, Russell	Paper #: 130	United States
Miller, Stephen	Poster #: CR-080	United States
Mills, Angela	Poster #: SCI-037	United States
Minniti, Salvatore	Paper #: 047, Poster #: EDU-013	Italy
Miron, Marie-Claude	Paper #: 175, Poster #: CR-060, Poster #: CR-069	Canada
Mirsky, David M.	Paper #: 152	United States
Mitchell, Craig S.	Poster #: CR-031	United States
Miyasaka, Mikiko	Poster #: SCI-012	Japan
Miyazaki, Osamu	Poster #: SCI-012	Japan
Mody, Swati	Poster #: SCI-051	United States
Moe, Tabitha	Poster #: EDU-090	United States
Moffatt, Hayley	Poster #: EDU-053	Canada
Moguillansky, Silvia	Poster #: CR-017, Poster #: CR-018, Poster #: EDU-029	Argentina
Mohamed Ezzelarab Soliman, Magdy	Poster #: SCI-058	Canada
Mohanta, Arun	Poster #: SCI-058	Canada
Möhrlen, Ueli	Paper #: 136	Switzerland
Moineddin, Rahim	Paper #: 002, Paper #: 013, Paper #: 022, Paper #: 025, Paper #: 079, Poster #: EDU-109, Poster #: SCI-036, Poster #: SCI-063	Canada
Moir, Christopher	Paper #: 139	United States
Molossi, Silvana	Paper #: 164	United States
Mong, Andrew	Poster #: EDU-134	United States
Moodley, Halvani	Paper #: 082, Paper #: 135, Paper #: 137	South Africa
Moore, Alaina E.	Paper #: 062	United States

Moore, David	Paper #: 082, Paper #: 135, Paper #: 137	South Africa
Moore, Ryan	Poster #: EDU-076, Poster #: EDU-101	United States
Moote, Douglas	Poster #: CR-046	United States
Morello, Frank	Paper #: 107	United States
Moretti, Felipe	Poster #: SCI-040	Canada
Morgan, Trudy	Paper #: 054	United States
Morice, Claire	Poster #: SCI-008	Switzerland
Morin, Cara	Poster #: CR-043, Poster #: EDU-035	United States
Morneault, Linda	Paper #: 157	Canada
Morrone, Kerry	Paper #: 031	United States
Moseley, Scott	Poster #: SCI-039	United States
Mubarak, Walid	Poster #: EDU-084	Canada
Muehe, Anne	Paper #: 019, Paper #: 187, Paper #: 189	United States
Mulkern, Robert	Paper #: 123	United States
Mullan, Paul	Paper #: 081	United States
Mullen, Sorcha	Paper #: 08 (R)	Ireland
Munden, Martha M.	Paper #: 008, Paper #: 045, Paper #: 062	United States
Murphy, Dara	Paper #: 01 (R)	Ireland
Murray, Darlene	Poster #: SCI-055	Canada
Murray, Nicolas	Poster #: CR-069	Canada
Muto, Ayako	Poster #: SCI-012	Japan
Mwango, Gladys	Poster #: SCI-087	Kenya
Naffaa, Lena	Paper #: 149	United States
Nagy, Eszter	Poster #: SCI-014, Poster #: SCI-018, Poster #: SCI-019	Austria
Naidoo, Jaishree	Poster #: CR-002	South Africa
Nakagawa, Motoo	Poster #: CR-019, Poster #: EDU-002	Japan
Nakashima, Yuko	Poster #: EDU-079	Japan
Namdar, Yesim	Poster #: CR-026, Poster #: CR-027	Turkey
Nanwani, Nikita J.	Paper #: 095	India
Narula, Mahender K.		India
Naselli Adamski, Katherine	Poster #: EDU-02 (R)	United States
Navarro, Oscar M.	Paper #: 045, Paper #: 185, Poster #: EDU-044, Poster #: EDU-091, Poster #: EDU-144, Poster #: SCI-055	Canada
Nazario, Maricarmen	Paper #: 109, Paper #: 113, Poster #: EDU-074	United States
Neelavalli, Jaladhar	Poster #: SCI-051	United States
Nelson, Christine	Paper #: 035, Paper #: 165	United States
Nelson, Paige	Poster #: EDU-070	United States
Nerriman, Deena	Paper #: 024	United Kingdom
Neumayr, Lynne	Paper #: 120	United States
Neveu, Melissa L.	Poster #: SCI-031	United States
Newhouse, Jeffrey	Poster #: EDU-066	United States
Ng, Elaine	Poster #: SCI-055	Canada
Ngo, Anh-vu	Poster #: EDU-043	United States
Ngo, Thang	Poster #: EDU-046	United States
Nguyen, Bac	Paper #: 192	Norway
Nguyen, HaiThuy N.	Paper #: 085	United States
Nicol, E	Paper #: 033, Poster #: EDU-009	United Kingdom
Nievelstein, Rutger A.	Paper #: 026	Netherlands
Nimkin, Katherine	Paper #: 070, Paper #: 083, Poster #: EDU-056	United States
Nishikawa, Masanori	Poster #: SCI-01 (R)	Japan
Noel, Cory	Paper #: 036, Paper #: 191	United States
Nororis, Eduardo	Paper #: 066	United States
Nosaka, Shunsuke	Poster #: EDU-023, Poster #: SCI-012	Japan
Ntoulia, Aikaterini	Paper #: 053, Paper #: 054, Poster #: SCI-081	United States
Nurkic, Tarik	Poster #: EDU-116	United States
Nusman, Charlotte	Paper #: 141	Netherlands
Nyabanda, Rose A.	Poster #: SCI-087	Kenya
O'Brien, Ellen K.	Poster #: EDU-02 (R)	United States
O'Brien, Kevin	Poster #: SCI-041	United States
O'Brien, Maureen M.	Paper #: 02 (R)	United States
O'Connor, Michelle	Paper #: 11 (R), Paper #: 12 (R)	Ireland
O'Donnell, Jennifer	Paper #: 123	United States
O'Loughlin, Michael	Poster #: CR-054	United States
Oatis, Kristi	Poster #: SCI-065	United States
Occelli, Aurelie	Paper #: 10 (R), Poster #: CR-01 (R), Poster #: CR-02 (R)	France

O Connor, Saundra	Paper #: 07 (R)	Ireland
Offiah, Amaka	Paper #: 128, Poster #: EDU-004	United Kingdom
Okada, Haruka	Poster #: SCI-012	Japan
Okamoto, Reiko	Poster #: SCI-012	Japan
Olsen, Øystein E.	Paper #: 021, Poster #: CR-023	United Kingdom
Oneill, Sean	Poster #: SCI-062	United States
Ong, Seng	Poster #: EDU-034, Poster #: EDU-067, Poster #: SCI-041	United States
Ording Muller, Lil-Sofie	Paper #: 141	Norway
Oriundo Verastegui, Marco A.	Paper #: 154	Canada
Orozco, Maria E.	Poster #: EDU-10 (R)	Argentina
Orth, Robert C.	Paper #: 030	United States
Ortiz, Clara	Paper #: 078	Canada
Ostapska, Zofia	Poster #: EDU-007	Poland
Otero, Hansel J.	Paper #: 058, Paper #: 077, Paper #: 081, Poster #: SCI-076	United States
Otjen, Jeffrey P.	Poster #: SCI-052, Poster #: SCI-075	United States
Otrakji, Alexi	Paper #: 083	United States
Otto, Randolph	Paper #: 132, Poster #: EDU-043	United States
Oudjhane, Kamaldine	Paper #: 013, Poster #: EDU-068, Poster #: EDU-091	Canada
Owens, Catherine	Paper #: 033, Poster #: CR-004, Poster #: EDU-008, Poster #: EDU-009	United Kingdom
Ozawa, Yoshiyuki	Poster #: CR-019, Poster #: EDU-002	Japan
Ozkan, Mehmet	Paper #: 048	Turkey
Ozmen, Evrim	Poster #: SCI-021	Turkey
Paddock, Michael	Paper #: 128, Poster #: EDU-004	United Kingdom
Padley, SPG	Paper #: 033	United Kingdom
Padua, Eric M.	Paper #: 120	United States
Padua, Horacio	Poster #: EDU-073	United States
Palathinkal, Darren M.	Paper #: 131	Canada
Paldino, Michael J.	Paper #: 091, Paper #: 092	United States
Paltiel, Harriet J.	Poster #: EDU-122	United States
Pan, Patrick	Poster #: EDU-124	United States
Pande, Vijay S.	Poster #: EDU-138	United States
Pandey, Vijay	Poster #: EDU-130	United States
Pandya, Nirav	Paper #: 120	United States
Panigrahy, Ashok	Poster #: SCI-029	United States
Papaioannou, Georgia	Poster #: EDU-021, Poster #: EDU-025, Poster #: EDU-026	Greece
Paranhos, Isabela R.	Poster #: CR-045	Brazil
Parekh, Dhaval	Paper #: 035, Paper #: 165	United States
Parikh, Ashish	Poster #: CR-036	United States
Parikh, Ashishkumar K.	Paper #: 179	United States
Parisi, Marguerite T.	Paper #: 132, Poster #: CR-057, Poster #: SCI-052, Poster #: SCI-075	United States
Park, Ji Eun	Poster #: SCI-013, Poster #: SCI-023	Korea (the Republic of)
Parnell, Shawn	Poster #: EDU-080	United States
Parra, Dimitri	Paper #: 112, Poster #: EDU-084	Canada
Partovi, Sasan	Poster #: CR-040	United States
Patel, Chandresh	Paper #: 101, Paper #: 102, Paper #: 142	United States
Patel, Mittun	Paper #: 103, Paper #: 155, Poster #: EDU-069, Poster #: EDU-071, Poster #: EDU-096, Poster #: SCI-034, Poster #: SCI-047	United States
Patel, Parth	Paper #: 181	United States
Patel, Pratik	Poster #: EDU-108	United States
Patel, Sejal N.	Poster #: EDU-066	United States
Patel, Snehalkumar	Poster #: EDU-106	United States
Paterson, Anne	Paper #: 127, Paper #: 169	United Kingdom
Patil, Kedar	Poster #: SCI-059	Canada
Patrick, Ellen	Poster #: EDU-125	United States
Paulo, Graciano	Paper #: 03 (R), Paper #: 04 (R), Paper #: 05 (R), Paper #: 06 (R)	Portugal
Pautler, Robia	Paper #: 142	United States
Pavicevic, Polina	Poster #: SCI-010	Serbia
Pawley, Barbara K.	Paper #: 063	United States
Pednekar, Amol	Paper #: 191, Poster #: SCI-084	United States
Peltzer, Maria	Poster #: CR-007	United Kingdom
Peng, Yun	Poster #: SCI-058	China
Pennock, Andrew T.	Paper #: 118	United States
Pentiuk, Scott	Paper #: 032	United States
Peranteau, William H.	Paper #: 039	United States
Pereira, Ana	Paper #: 06 (R)	Portugal

Perez, Maria M.	Paper #: 100, Poster #: EDU-144	Canada
Pérez-Marrero, Lizbet	Poster #: SCI-056, Poster #: SCI-088	Chile
Perez-Rossello, Jeannette M.	Paper #: 061	United States
Peterson, Michael	Paper #: 103, Poster #: EDU-069, Poster #: EDU-071, Poster #: SCI-034	United States
Petraco Da Cunha, Ricardo	Poster #: EDU-009	United Kingdom
Pfeifer, Cory	Poster #: SCI-065	United States
Phelps, Andrew	Poster #: EDU-042, Poster #: EDU-061	United States
Philipsen R, Rick	Paper #: 135	Netherlands
Pibernous, J	Poster #: CR-018	Argentina
Pillai, Anjay	Poster #: CR-004	United Kingdom
Pillay, Tanyia	Paper #: 186	South Africa
pimpalwar, sheena	Paper #: 181	United States
Pinkney, Lynne	Paper #: 046	United States
Pipe, Jim	Poster #: SCI-032	United States
Pivnick, Eniko	Poster #: CR-080	United States
Plunk, Matthew R.	Paper #: 114	United States
Plut, Domen	Poster #: CR-006	Slovenia
Podberesky, Daniel J.	Paper #: 011, Paper #: 012, Poster #: EDU-046	United States
Poiares, Bárbara	Paper #: 06 (R)	Portugal
Pokorney, Amber	Paper #: 103, Paper #: 148, Paper #: 155, Paper #: 16 (R), Poster #: EDU-069, Poster #: EDU-071, Poster #: SCI-032, Poster #: SCI-034, Poster #: SCI-047	United States
Poletto, Erica	Poster #: EDU-095, Poster #: EDU-098, Poster #: EDU-099, Poster #: EDU-110	United States
Pollock, Avrum	Paper #: 104	United States
Popescu, Andrada R.	Poster #: EDU-07 (R)	United States
Pophal, Stephen	Poster #: EDU-120, Poster #: EDU-121	United States
Poretti, Andrea	Paper #: 147	United States
Portelli, Jonathan Loui	Paper #: 17 (R)	Malta
Porto, Luciana	Poster #: SCI-002	Germany
Pose, Georgette	Poster #: SCI-056	Chile
Powers, Andria	Poster #: CR-032, Poster #: CR-074, Poster #: EDU-058	United States
poznick, laura	Paper #: 054	United States
Prabhu, Sanjay	Paper #: 055, Poster #: EDU-105	United States
Pratt, Li-tal	Paper #: 151	Israel
Prempunpong, Chatchay	Paper #: 157	Canada
Price, Gemma	Paper #: 023	United Kingdom
Priego, Gema	Poster #: EDU-062	Canada
Prodhomme, Olivier	Paper #: 106, Poster #: EDU-015, Poster #: SCI-007, Poster #: SCI-011	France
Prosova, Blanka	Poster #: CR-021	Czech Republic
Pugmire, Brian S.	Paper #: 032	United States
Pytiak, Andrew	Paper #: 118	United States
Qi, Zhihua	Paper #: 02 (R)	United States
Quintero, Karina	Poster #: CR-018	Argentina
Quon, Andrew	Paper #: 019	United States
Rabbie, Wendy	Paper #: 14 (R)	Canada
Radovic, Tijana	Poster #: SCI-010	Serbia
Raimondi, Edoardo	Poster #: CR-001, Poster #: CR-016	Italy
Rainford, Louise A.	Paper #: 01 (R), Paper #: 08 (R), Paper #: 09 (R), Paper #: 13 (R), Paper #: 15 (R), Paper #: 17 (R), Paper #: 19 (R)	Ireland
Raissaki, Maria	Poster #: EDU-012	Greece
Rajderkar, Dhanashree A.	Poster #: EDU-108, Poster #: EDU-113, Poster #: EDU-114, Poster #: EDU-115, Poster #: EDU-116, Poster #: EDU-117, Poster #: EDU-118, Poster #: EDU-119, Poster #: EDU-133	United States
Ramirez, Raul	Paper #: 045	United States
Ramsey, Andrew	Paper #: 105	United Kingdom
Rangaswami, Arun	Paper #: 019, Paper #: 189	United States
Rao, Anil G.	Paper #: 005	United States
Rapp, Jordan B.	Poster #: SCI-033	United States
Raschbaum, George	Paper #: 116	United States
Rea, David	Poster #: CR-056	Ireland
Rebsamen, Susan	Poster #: EDU-040	United States
Rees, Mitchell	Poster #: SCI-029	United States
Reichard, Kirk	Poster #: EDU-059	United States
Reid, Churphena A.	Poster #: CR-031	United States

Reid, Janet R.	Paper #: 054, Paper #: 057, Paper #: 060, Poster #: EDU-134, Poster #: EDU-137	United States
Reiser, Ingrid	Paper #: 073, Poster #: EDU-075	United States
Renella, Pierangelo	Poster #: SCI-069	United States
Renjen, Pooja	Poster #: EDU-134	United States
Retamal Caro, Andres	Poster #: SCI-088	Chile
Ribeiro, Rafaela C.	Poster #: CR-045	Brazil
Richard, Jamie	Poster #: CR-047	United States
Richer, Edward	Paper #: 063, Poster #: EDU-072, Poster #: EDU-094, Poster #: SCI-053, Poster #: SCI-083	United States
Riedesel, Erica	Poster #: CR-068, Poster #: EDU-128	United States
Rieter, Jasper	Paper #: 141	Netherlands
Rigsby, Cynthia K.	Poster #: EDU-07 (R)	United States
Rincon, Sandra P.	Paper #: 074	United States
Rivlin, Michael J.	Paper #: 124	United States
Rizzi, Ana M.	Poster #: CR-017, Poster #: CR-018	Argentina
Robb, Tiffany	Poster #: EDU-039	United States
Roberts, Charlotte	Poster #: EDU-011	United Kingdom
Robinson, Alice	Paper #: 041	Australia
Rodrigues, Adriano	Paper #: 04 (R)	Portugal
Roebel, John	Paper #: 145	United States
Roebuck, Derek	Paper #: 107	United Kingdom
Rogan, Walter	Paper #: 129	United States
Roik, Danuta	Poster #: EDU-007	Poland
Rojas, Paula	Poster #: SCI-088	Chile
Romberg, Julia	Paper #: 160, Paper #: 161	Germany
Romero, Rene	Poster #: EDU-125	United States
Romero, Roberto	Poster #: SCI-051, Poster #: SCI-079	United States
Rooks, Veronica	Poster #: EDU-092, Poster #: EDU-104	United States
Rosenbaum, Daniel	Paper #: 003	United States
Rosendahl, Karen	Paper #: 119, Paper #: 141	Norway
Rosenfeld, Scott	Paper #: 124	United States
Rostad, Bradley S.	Paper #: 068	United States
Roth, Antoinette	Poster #: EDU-124	United States
Rothan, Sarah M.	Paper #: 045	United States
Rothenberg Maddocks, Alexis B.	Paper #: 020, Paper #: 104	United States
Rowland, Marion	Paper #: 13 (R)	Ireland
Roy, Amit	Poster #: CR-003	United Kingdom
Roy-Cardinal, Marie-Hélène	Paper #: 190	Canada
Rozenfeld, Michael	Poster #: EDU-070	United States
Rozovsky, Katya	Poster #: EDU-053	Canada
Rubens, M	Paper #: 033	United Kingdom
Rubesova, Erika	Paper #: 043, Poster #: SCI-049	United States
Rubin, Michael	Paper #: 149	United States
Rubio, Eva I.	Paper #: 096, Poster #: EDU-111, Poster #: SCI-060	United States
Rudzinski, Erin	Poster #: CR-057	United States
Ryan, Justin	Poster #: EDU-120, Poster #: EDU-121	United States
Ryan, Maura	Poster #: SCI-031	United States
Rypens, Françoise	Paper #: 044, Poster #: CR-069	Canada
Sagar, Pallavi	Paper #: 070, Paper #: 083	United States
Saguintaah, Magali	Paper #: 106, Poster #: EDU-015, Poster #: SCI-007, Poster #: SCI-011	France
Saint-Martin, Christine	Paper #: 157, Poster #: SCI-066	Canada
Sala, Simone	Poster #: CR-001, Poster #: CR-016	Italy
Saleem, Sheena	Paper #: 153	United States
Salinas, Cesar	Poster #: SCI-056	Chile
Samet, Jonathan	Poster #: SCI-062	United States
Sammet, Christina L.	Poster #: EDU-06 (R), Poster #: EDU-07 (R)	United States
Samreen, Naziya	Poster #: EDU-113	United States
Sanchez, Adrian A.	Paper #: 073, Poster #: EDU-075	United States
Sanchez, Ramon	Paper #: 004, Poster #: SCI-083	United States
Sanchez-Montañez, Angel	Poster #: SCI-024	Spain
Sanchez Salinas, Alicia C.		Argentina
Sanchez Salinas, Paola		Argentina
Sanders, Travis	Paper #: 093	United States

Sandhu, Preet K.	Poster #: CR-078, Poster #: EDU-139	United States
Sandoval, Claudio	Poster #: CR-055, Poster #: CR-061	United States
Sant'Anna, Guilherme	Paper #: 157	Canada
Santos, Joana	Paper #: 03 (R), Paper #: 05 (R), Paper #: 06 (R)	Portugal
Sasser, Hampton	Paper #: 005	United States
Sato, T Shawn	Poster #: EDU-051, Poster #: EDU-136	United States
Sato, Yutaka	Poster #: EDU-051, Poster #: EDU-136	United States
Saxena, Akshay K.	Paper #: 086	India
Scace, Candace	Poster #: EDU-077	United States
Schaefer, Bradley	Poster #: CR-030	United States
Schaefer, Carrie	Paper #: 115, Paper #: 182, Poster #: CR-071	United States
Schall, Joan	Paper #: 129	United States
Schallert, Erica K.	Paper #: 122, Paper #: 124	United States
Schemuth, Haemi P.	Paper #: 015	Germany
Schjerven, Annette I.	Poster #: SCI-02 (R)	Norway
Schmidt, Michael	Poster #: SCI-054	Canada
Schmit, P.	Poster #: EDU-030	Canada
Schmitz, Kelli	Poster #: EDU-076, Poster #: EDU-100, Poster #: EDU-101	United States
Schoenecker, Jonathan G.	Paper #: 179	United States
Schofield, Rebecca	Poster #: EDU-009	United Kingdom
Schuh, Suzanne	Paper #: 079, Paper #: 080	Canada
Schulz, Noah	Paper #: 055	United States
Schumacher, Kurt	Paper #: 166	United States
Schwartz, Carly	Paper #: 031	United States
Schweiger, Bernd	Paper #: 015	Germany
Scrugham, Jeffrey	Poster #: CR-080	United States
Sebire, Neil	Paper #: 021, Paper #: 105, Paper #: 170, Poster #: CR-007, Poster #: CR-008	United Kingdom
Seed, Mike	Paper #: 138	Canada
Seekins, Jayne	Poster #: EDU-048, Poster #: EDU-078	United States
Semple, Thomas R.	Paper #: 023, Paper #: 033, Poster #: CR-004, Poster #: EDU-008, Poster #: EDU-009	United Kingdom
Sera, Francesco	Paper #: 119	United Kingdom
Serai, Suraj D.	Paper #: 010, Paper #: 011, Paper #: 012	United States
Sergeant, Anjali	Paper #: 150	Canada
Servaes, Sabah	Paper #: 057, Poster #: EDU-088, Poster #: EDU-134	United States
Setser, Randolph	Paper #: 109, Paper #: 113	United States
Sewchuran, Tanusha	Paper #: 082, Paper #: 135, Paper #: 137	South Africa
Shah, Amisha	Poster #: SCI-029	United States
Shah, Chetan	Paper #: 143, Poster #: EDU-081	United States
Shah, Jignesh	Poster #: CR-078, Poster #: EDU-139, Poster #: EDU-143	United States
Shah, Prakeshkumar	Poster #: SCI-063	Canada
Shailam, Randheer	Paper #: 064, Paper #: 070, Paper #: 083	United States
Shalaby-Rana, Eglal	Poster #: SCI-077	United States
Shammas, Amer	Poster #: EDU-123	Canada
Sharaf, Ahmed F.	Poster #: CR-014	Singapore
Sharma, Neal	Poster #: CR-038	United States
Sharma, Priya G.	Poster #: EDU-113, Poster #: EDU-114, Poster #: EDU-115, Poster #: EDU-116, Poster #: EDU-117, Poster #: EDU-118, Poster #: EDU-119, Poster #: EDU-133	United States
Sharma, Ravi	Poster #: CR-038	United States
Shearkhani, Omid	Paper #: 185	Canada
Shekdar, Karuna	Paper #: 020, Poster #: EDU-086, Poster #: EDU-134	United States
Shellikeri, Sphoorti	Paper #: 109, Paper #: 113, Poster #: EDU-074	United States
Shelmerdine, Susan C.	Paper #: 158, Poster #: CR-004, Poster #: SCI-043, Poster #: SCI-044	United Kingdom
Shergill, Arvind	Paper #: 080	Canada
Shet, Narendra	Poster #: CR-043, Poster #: EDU-035	United States
Shetty, Anil	Paper #: 142	United States
Shibamoto, Yuta	Poster #: CR-019, Poster #: EDU-002	Japan
Shimada, Makoto	Poster #: SCI-01 (R)	Japan
Shin, Hyun Joo	Poster #: SCI-003	Korea (the Republic of)
Shore, Matthew	Poster #: EDU-128	United States
Shroff, Manohar	Paper #: 151	Canada
Sidhu, Manrita	Paper #: 107	United States
Silva, Cecília P.	Poster #: CR-045	Brazil

Silva, Cicero T.	Poster #: EDU-105	United States
Silva, Claudio	Poster #: SCI-056, Poster #: SCI-088	Chile
Simcock, Clare	Paper #: 19 (R)	United Kingdom
Simmons, Cephus E.	Poster #: SCI-030	United States
Simoneaux, Stephen	Paper #: 059, Poster #: CR-049, Poster #: EDU-15 (R)	United States
Simpson, Ewan	Paper #: 069, Paper #: 090	United Kingdom
Simpson, Lynn L.	Paper #: 130	United States
Sinayuk, Boris	Poster #: EDU-054	United States
Singer, Julia	Poster #: CR-061	United States
Singh, Dhruv	Paper #: 074	United States
Singh, Jaspreet	Poster #: CR-077	United States
Singh, Meenu	Paper #: 086	India
Singh, Sarabjeet	Paper #: 070, Paper #: 071, Paper #: 074	United States
Singh, Sheila	Paper #: 150, Poster #: CR-059	Canada
Sirin, Selma	Paper #: 015	Germany
Sisay, Samuel	Paper #: 133	Ethiopia
Sivit, Carlos	Poster #: CR-040	United States
Skelton, David	Poster #: EDU-102	United States
Skiadas, Christos	Poster #: EDU-012	Greece
Sleman, Ingy H.	Poster #: EDU-036	United States
Smevik, Bjarne	Paper #: 192	Norway
Smith, Berry	Paper #: 14 (R)	Canada
Smith, Crysela M.	Poster #: EDU-129, Poster #: EDU-131	United States
Smith, Ethan A.	Paper #: 004, Poster #: SCI-053	United States
Smith, Jessica	Paper #: 128	United Kingdom
Soboleski, Don A.	Paper #: 131	Canada
Sodhi, Kushaljit S.	Paper #: 086	India
Solomon, Daniel Z.	Paper #: 133	Ethiopia
Somcio, Ray	Paper #: 098	United States
Somers, Gino	Paper #: 022, Paper #: 045	Canada
Song, Ruitian	Paper #: 006	United States
Sorantin, Erich	Poster #: SCI-014, Poster #: SCI-018, Poster #: SCI-019	Austria
Soto, Gloria	Poster #: SCI-056	Chile
Soulez, Gilles	Poster #: CR-042	Canada
Southard, Richard	Poster #: EDU-090	United States
Souza, Antonio S.	Poster #: EDU-087	Brazil
Spanakis, Kostas	Poster #: EDU-012	Greece
Spencer, Helen	Poster #: CR-004	United Kingdom
Spottswood, Stephanie E.	Paper #: 179, Poster #: CR-036	United States
Spranger, Jurgen	Poster #: CR-030	United States
Sprigg, Alan	Paper #: 128, Poster #: EDU-004	United Kingdom
Squires, Judy H.	Poster #: CR-058, Poster #: EDU-097	United States
Sriharan, M	Paper #: 033	United Kingdom
Srinivasan, Abhay	Paper #: 109, Paper #: 113, Poster #: EDU-074	United States
Srivaths, Keshav S.	Paper #: 037	United States
Stallings, Virginia	Paper #: 129	United States
Stamler, Alexa	Paper #: 149	United States
Stanescu, A. Luana	Paper #: 016, Paper #: 132, Poster #: CR-057, Poster #: SCI-052, Poster #: SCI-075	United States
Stanford, Richard	Poster #: CR-038	United States
Starosolski, Zbigniew A.	Paper #: 093, Paper #: 101, Paper #: 102, Paper #: 142, Paper #: 194	United States
States, Lisa	Paper #: 020, Paper #: 060, Poster #: EDU-137	United States
Stearns, Phil	Paper #: 118	United States
Stefani, Niccolo	Paper #: 16 (R)	United States
Stein, Jill M.	Paper #: 174	United States
Stein, Nina	Paper #: 150, Poster #: CR-059, Poster #: CR-066, Poster #: SCI-054	Canada
Steinberger, Monika	Poster #: SCI-018	Austria
Stence, Nicholas V.	Paper #: 152	United States
Stiakaki, Eftichia	Poster #: EDU-012	Greece
Stiller, Brigitte	Paper #: 160, Paper #: 161	Germany
Stimec, Jennifer	Paper #: 100, Poster #: EDU-050, Poster #: SCI-055	Canada
Stout, Markus	Paper #: 064	United States
Stranzinger, Enno	Poster #: EDU-018	Switzerland
Stratigaki, Maria	Poster #: EDU-012	Greece
Strauch, Eric	Poster #: EDU-035	United States

Strouse, Peter	Poster #: SCI-053	United States
Strubel, Naomi	Paper #: 046	United States
Stupin, Igor V.	Paper #: 101, Paper #: 102, Paper #: 142	United States
Sudhakar, Sniya	Poster #: CR-072	India
Sun, Aimin	Paper #: 034, Paper #: 038, Paper #: 084, Poster #: SCI-086	China
Suncion-Loescher, Viky	Paper #: 088	United States
Sundarakumar, Dinesh K.	Poster #: EDU-129, Poster #: EDU-131	United States
Sung, Lillian	Paper #: 080	Canada
Supakul, Nucharin	Poster #: CR-005, Poster #: EDU-017	Thailand
Sury, Mike	Poster #: SCI-001	United Kingdom
Sussman, Marshall	Poster #: SCI-036	Canada
Suther, L. Kathrine R.	Paper #: 192	Norway
Svendsmark, Rolf	Paper #: 192	Norway
Swenson, David W.	Paper #: 076, Poster #: EDU-054, Poster #: SCI-035	United States
Szabo, Miklos	Poster #: SCI-017	Hungary
Tabari, Azadeh	Paper #: 070, Paper #: 071, Paper #: 074	United States
Taddeo, Danielle	Poster #: CR-060	Canada
Tadesse, Amezene	Paper #: 133	Ethiopia
Tadros, Sameh	Poster #: CR-058	United States
Tagalakis, Panagiotis	Poster #: EDU-021, Poster #: EDU-026	Greece
taleb arrada, ikram	Paper #: 106, Poster #: SCI-007, Poster #: SCI-011	France
Tamir, Jonathan I.	Paper #: 121	United States
Tanaka, Yoshihiro	Poster #: CR-019, Poster #: EDU-002	Japan
Tani, Chihiro	Poster #: EDU-079	Japan
tanifum, eric	Paper #: 102	United States
Tanturri de Horatio, Laura	Paper #: 141	Italy
Taragin, Benjamin H.	Paper #: 028, Paper #: 031, Paper #: 066, Poster #: EDU-032, Poster #: EDU-036, Poster #: EDU-052	United States
Tariq, Umar	Paper #: 121	United States
Taviani, Valentina	Paper #: 019, Paper #: 094, Paper #: 189	United States
Teague, Clint T.	Poster #: CR-052	United States
Teoh, Mark	Paper #: 041	Australia
TerreBlanche, Bernard	Paper #: 173	United States
Thai, Jade	Paper #: 069, Paper #: 090	United Kingdom
Thakor, Avnesh	Paper #: 111, Poster #: EDU-084	Canada
Thankachan, Sam	Paper #: 056	United States
Theroux, Mary	Poster #: CR-044	United States
Thiessen, Jaclyn E.	Poster #: EDU-076	United States
Thomas, Anna K.	Poster #: CR-052	United States
Thomas, Cameron W.	Poster #: SCI-067	United States
Thomas, Karen	Paper #: 080, Poster #: SCI-037	Canada
Thomas, Maya	Poster #: CR-072	India
Thomas-Chausse, Frederic	Poster #: CR-042	Canada
Thomen, Robert	Poster #: SCI-082	United States
Thompson, Adrienne	Paper #: 125, Poster #: SCI-042	Canada
Thompson, Angela	Paper #: 171	United States
Thompson, David	Poster #: SCI-039	United States
Thomson, Graham	Paper #: 078	Canada
Thomson, Heather	Poster #: CR-002	South Africa
Thorkelson, Marrit	Poster #: EDU-090	United States
Tijerin Bueno, Marta	Paper #: 018, Paper #: 022, Paper #: 045, Poster #: EDU-044, Poster #: EDU-091, Poster #: EDU-123, Poster #: SCI-045	Canada
Tipirneni-Sajja, Aaryani	Paper #: 006	United States
Tomatsu, Shunji	Poster #: CR-044	United States
Tomazic, Mojca	Poster #: CR-006	Slovenia
Tominaga, Masahide	Poster #: SCI-01 (R)	Japan
Tomlinson, Chris	Poster #: EDU-134	United States
Tomterstad, Anders Høye	Paper #: 192	Norway
Tong, Angela	Poster #: CR-053	United States
Towbin, Alexander J.	Paper #: 011, Paper #: 012, Paper #: 145	United States
Towbin, Richard	Paper #: 115, Paper #: 148, Paper #: 16 (R), Paper #: 182, Poster #: CR-071, Poster #: EDU-096, Poster #: EDU-120, Poster #: EDU-121	United States
Trefan, Laszlo	Poster #: SCI-057	United Kingdom
Treves, S. T.	Poster #: EDU-140	United States
Trinh, Austin	Poster #: CR-070	United States

Trout, Andrew	Paper #: 001, Paper #: 010, Paper #: 011, Paper #: 012, Paper #: 02 (R), Paper #: 032, Paper #: 045	United States
Trudel, Jean-Sébastien	Poster #: CR-069	Canada
Tsai, Andy	Paper #: 050, Paper #: 055, Paper #: 176	United States
Tschauner, Sebastian	Paper #: 048, Poster #: SCI-014, Poster #: SCI-019	Austria
Tsutsumi, Yoshiyuki	Poster #: SCI-012	Japan
Tuburan, Smyrna	Poster #: CR-070, Poster #: CR-077	United States
Tulin-Silver, Sheryl	Poster #: EDU-073	United States
Tuna, Ibrahim	Poster #: EDU-113	United States
Tupprasoot, Raksa	Poster #: SCI-001	United Kingdom
Uecker, Martin	Paper #: 121	Germany
Ugas, Carlos F.	Paper #: 088, Poster #: CR-073, Poster #: EDU-08 (R), Poster #: EDU-13 (R)	Peru
Umbach, David	Paper #: 129	United States
Urbine, Jaqueline	Poster #: EDU-095, Poster #: EDU-098, Poster #: EDU-099, Poster #: EDU-110	United States
Urquia, Arlen	Paper #: 049	United Kingdom
Utz, Norbert G.	Poster #: CR-022, Poster #: EDU-020	Germany
Vajapeyam, Sridhar	Paper #: 123	United States
Vajtai, Petra	Poster #: EDU-076, Poster #: EDU-100, Poster #: EDU-101	United States
Valdez Quintana, Melissa K.	Paper #: 154, Poster #: CR-073, Poster #: EDU-08 (R), Poster #: EDU-13 (R), Poster #: SCI-040	Peru
Vali, Reza	Poster #: EDU-123	Canada
Valsangiacomo-Büchel, Emanuela	Paper #: 159	Switzerland
van der Kaay, Danielle CM	Paper #: 025, Poster #: EDU-109	Netherlands
Van Ginneken, Bram	Paper #: 135	Netherlands
Vaño, Eliseo	Paper #: 04 (R)	Spain
Vargas, M Cecilia	Poster #: CR-018	Argentina
Vasanawala, Shreyas S.	Paper #: 094, Paper #: 121, Paper #: 162, Poster #: SCI-080	United States
Vasavada, Pauravi	Poster #: CR-040	United States
Vasung, Lana	Poster #: SCI-004	Switzerland
Vatsky, Seth	Paper #: 109, Paper #: 113, Poster #: EDU-074	United States
Vazquez, Elida	Poster #: SCI-020, Poster #: SCI-024	Spain
Vedajallam, Schadie	Paper #: 069, Paper #: 090	United Kingdom
Vellody, Ranjith	Poster #: EDU-094	United States
Verbeke, Jonathan I.	Paper #: 026	Netherlands
Verma, Nupur	Poster #: EDU-108, Poster #: EDU-115, Poster #: EDU-133	United States
Victoria, Teresa	Paper #: 039, Paper #: 104, Poster #: EDU-134	United States
Vraka, Irene	Poster #: EDU-025	Greece
Vu, Dan	Poster #: SCI-069	United States
Vukadinovic, Vojkan		Serbia
Waelti, Stephan	Paper #: 044	Canada
Wagner, Matthias	Paper #: 147	United States
Wakjira, Eyasu	Paper #: 133	Ethiopia
Walczak, Henning	Poster #: CR-007	United Kingdom
Wallach, Michael T.	Poster #: EDU-054	United States
Wallihan, Daniel B.	Paper #: 001	United States
Walters, Thomas D.	Paper #: 002	Canada
Wang, Kuan Chung	Poster #: SCI-036, Poster #: SCI-063	Canada
Warner, Christopher	Poster #: SCI-057	United States
Washington, Eleby R.	Paper #: 179	United States
Wasserman, Jonathan	Paper #: 025, Poster #: EDU-109	Canada
Watanabe Duffy, Karen	Poster #: EDU-050	Canada
Watson, Tom	Poster #: CR-023, Poster #: EDU-024	United Kingdom
Watterson, Christopher T.	Poster #: EDU-106	United States
Webb, Nathan R.	Paper #: 152	United States
Weber-Guzman, Fabiola	Poster #: EDU-046	United States
Weinert, Dayna	Poster #: CR-040	United States
Weinman, Jason P.	Paper #: 087, Paper #: 167	United States
Weinstock, Peter	Paper #: 055	United States
Weisel, Scott	Poster #: EDU-03 (R)	United States
Weiss, Dana	Paper #: 053	United States
Weitz, Carolina	Poster #: CR-076	Chile
Wells, Greg	Poster #: SCI-036	Canada
Wepking, Kelly N.	Poster #: CR-068	United States

Westra, Sjirk	Paper #: 070, Paper #: 071, Paper #: 083, Poster #: EDU-056	United States
Wheelock, Lisa	Poster #: CR-032	United States
White, Christina	Paper #: 087	United States
Whyte, Michael P.	Poster #: SCI-039	United States
Wieselthaler, Nicky	Paper #: 089	South Africa
Wieser, Clarina	Poster #: SCI-018	Austria
Wilejto, Marta	Paper #: 022	Canada
Wilkins, Jean	Poster #: CR-060	Canada
Willard, Scott	Poster #: CR-029, Poster #: CR-034	United States
Williams, Joseph P.	Paper #: 116	United States
Windhaber, Jana	Poster #: SCI-018	Austria
Wishah, Fidaa	Paper #: 153	United States
Wong, Katherine	Paper #: 043	United States
Wong, Lincoln M.	Poster #: EDU-058	United States
Wood, Jonathan	Poster #: EDU-092, Poster #: EDU-104	United States
Woods, Jason C.	Paper #: 085, Poster #: SCI-082	United States
Worters, Pauline W.	Paper #: 110	United States
Wrogemann, Jens	Poster #: EDU-053	Canada
Wu, Runhui	Poster #: SCI-058	China
Xanthakos, Stavra	Paper #: 011, Paper #: 012	United States
Yabunaka, Koichi	Poster #: SCI-01 (R)	Japan
Yacoub, Daniel	Poster #: SCI-063	Canada
Yadav, Brijesh	Poster #: SCI-051	United States
Yadav, Vikas K.	Poster #: CR-072, Poster #: EDU-083	India
Yallampalli, Chandrasekhar	Paper #: 101, Paper #: 102, Paper #: 142	United States
Yang, Kai	Paper #: 071	United States
Yarmenitis, Spyros	Poster #: EDU-021, Poster #: EDU-025, Poster #: EDU-026	Greece
Yatake, Hidetoshi	Poster #: SCI-01 (R)	Japan
Yen, Christopher J.	Paper #: 099	United States
Yeo, Lami	Poster #: SCI-051	United States
Yeom, Kristen	Paper #: 094, Poster #: EDU-078	United States
Yildirim, Onur	Poster #: SCI-021	Turkey
Yildirim, Utku	Paper #: 048	Turkey
Yonekura, Reimi	Paper #: 055	United States
Yoo, So-Young	Paper #: 027, Poster #: SCI-016	Korea (the Republic of)
You, Sun Kyoung	Poster #: SCI-005, Poster #: SCI-027	Korea (the Republic of)
Young, Phillip	Poster #: EDU-039	United States
Younoszai, Adel	Poster #: SCI-048, Poster #: SCI-050	United States
Yousaf, Ufra	Paper #: 094	United States
Youssfi, Mostafa	Poster #: CR-062, Poster #: EDU-096	United States
Yu, Richard	Poster #: EDU-073	United States
Yuxiang, Zhou	Poster #: SCI-079	United States
Zambelis, John	Poster #: EDU-025	Greece
Zandieh, Arash R.	Paper #: 140	United States
Zani, Augusto	Paper #: 097	Canada
Zapala, Matthew A.	Poster #: EDU-042, Poster #: EDU-061, Poster #: SCI-071	United States
Zar, Heather	Paper #: 186	South Africa
Zarchan, Adam	Poster #: CR-030	United States
Zbojniewicz, Andrew M.	Paper #: 174	United States
Zendejas, Benjamin	Paper #: 139	United States
Zennaro, Floriana	Paper #: 026	Italy
Zewdneh, Daniel	Poster #: EDU-134	Ethiopia
Zhang, Bin	Paper #: 045, Paper #: 145	United States
Zhang, Ningning	Poster #: SCI-058	China
Zhang, Tao	Paper #: 162, Poster #: SCI-080	United States
Zhang, Wei	Paper #: 008, Paper #: 030, Paper #: 035, Paper #: 037, Paper #: 040, Paper #: 072, Paper #: 091, Paper #: 092, Paper #: 099, Paper #: 108, Paper #: 124, Paper #: 164, Paper #: 165	United States
Zhang, Yachao	Poster #: EDU-126, Poster #: EDU-145	United States
Zhong, Yumin	Paper #: 034, Paper #: 038, Paper #: 084, Poster #: SCI-086	China
Zhou, Alex	Poster #: SCI-058	Canada
Zhu, Xiaowei	Paper #: 065, Paper #: 067, Paper #: 109, Paper #: 113	United States
Zimmermann, Petra	Poster #: EDU-018	Switzerland
Zipser, Brian D.	Poster #: CR-064	United States
Zonoobi, Dornoosh	Paper #: 125, Poster #: SCI-042	Canada

Zuccoli, Giulio	Poster #: CR-063	United States
Zucker, Evan J.	Poster #: EDU-093	United States
Zupancic, Ziva	Poster #: CR-006	Slovenia
Zurakowski, David	Paper #: 140, Poster #: SCI-071	United States

2016 Keywwod Index by Abstract

Q

R